THE RELATIONSHIP BETWEEN NEURAL CIRCUITRY AND BIOMECHANICAL ACTION

EDITED BY: Redha Taiar, Mario Bernardo-Filho, Borja Sañudo and Yury Ivanenko

PUBLISHED IN: Frontiers in Human Neuroscience, Frontiers in Physiology, Frontiers in Bioengineering and Biotechnology and Frontiers in Sports and Active Living

frontiers Research Topics

ISSN 1664-8714
ISBN 978-2-88974-579-1
DOI 10.3389/978-2-88974-579-1

About Frontiers

Frontiers is more than just an open-access publisher of scholarly articles: it is a pioneering approach to the world of academia, radically improving the way scholarly research is managed. The grand vision of Frontiers is a world where all people have an equal opportunity to seek, share and generate knowledge. Frontiers provides immediate and permanent online open access to all its publications, but this alone is not enough to realize our grand goals.

Frontiers Journal Series

The Frontiers Journal Series is a multi-tier and interdisciplinary set of open-access, online journals, promising a paradigm shift from the current review, selection and dissemination processes in academic publishing. All Frontiers journals are driven by researchers for researchers; therefore, they constitute a service to the scholarly community. At the same time, the Frontiers Journal Series operates on a revolutionary invention, the tiered publishing system, initially addressing specific communities of scholars, and gradually climbing up to broader public understanding, thus serving the interests of the lay society, too.

Dedication to Quality

Each Frontiers article is a landmark of the highest quality, thanks to genuinely collaborative interactions between authors and review editors, who include some of the world's best academicians. Research must be certified by peers before entering a stream of knowledge that may eventually reach the public - and shape society; therefore, Frontiers only applies the most rigorous and unbiased reviews.
Frontiers revolutionizes research publishing by freely delivering the most outstanding research, evaluated with no bias from both the academic and social point of view. By applying the most advanced information technologies, Frontiers is catapulting scholarly publishing into a new generation.

What are Frontiers Research Topics?

Frontiers Research Topics are very popular trademarks of the Frontiers Journals Series: they are collections of at least ten articles, all centered on a particular subject. With their unique mix of varied contributions from Original Research to Review Articles, Frontiers Research Topics unify the most influential researchers, the latest key findings and historical advances in a hot research area! Find out more on how to host your own Frontiers Research Topic or contribute to one as an author by contacting the Frontiers Editorial Office: frontiersin.org/about/contact

THE RELATIONSHIP BETWEEN NEURAL CIRCUITRY AND BIOMECHANICAL ACTION

Topic Editors:
Redha Taiar, Université de Reims Champagne-Ardenne, France
Mario Bernardo-Filho, Rio de Janeiro State University, Brazil
Borja Sañudo, Independent Researcher, Spain
Yury Ivanenko, Santa Lucia Foundation (IRCCS), Italy

Citation: Taiar, R., Bernardo-Filho, M., Sañudo, B., Ivanenko, Y., eds. (2022). The Relationship Between Neural Circuitry and Biomechanical Action. Lausanne: Frontiers Media SA. doi: 10.3389/978-2-88974-579-1

Table of Contents

frontiers in Human Neuroscience

EDITORIAL
published: 03 February 2022
doi: 10.3389/fnhum.2022.838028

Editorial: The Relationship Between Neural Circuitry and Biomechanical Action

Redha Taiar[1], *Mario Bernardo-Filho*[2], *Borja Sañudo*[3] *and Yury Ivanenko*[4]*

[1] MATIM, Université de Reims Champagne-Ardenne Reims, Reims, France, [2] Laboratório de Vibrações Mecânicas e Práticas Integrativas (LAVIMPI), Instituto de Biologia Roberto Alcântara Gomes and Policlínica Piquet Carneiro, Universidade do Estado do Rio de Janeiro, Rio de Janeiro, Brazil, [3] Department of Physical Education and Sport, University of Seville, Seville, Spain, [4] Laboratory of Neuromotor Physiology, IRCCS Fondazione Santa Lucia, Rome, Italy

Keywords: neuromechanics and control of physical behavior, musculoskeletal and neuromuscular biomechanics, rehabilitation in neuro-biomechanics, neuromechanical analysis in sport medicine, neuromuscular training

Editorial on the Research Topic

The Relationship Between Neural Circuitry and Biomechanical Action

In this Research Topic the relationship between neural circuity and biomechanical action of the musculoskeletal system is addressed. Biomechanics studies the complexity of the human behavior including dynamic motion models (i.e., balance and gait), consequently biomechanics and neural control of movement are interrelated. The control of different body segments is required by neurological and biomechanical management of human movement that can be coordinated in multiple ways to perform a defined task. To control a movement of a target in a task, the individual can use an infinite number of segmented trajectories that remain under the control of several actuators (muscles). This is all based on different types of sensory information sources that the individual is receiving. Comprehending how an individual's central nervous system directs all different levels of redundancy and how it manages to propose an optimal solution to perform the procedure remains a scientific challenge. Various studies have been developed to add information in better understanding of all this complex relationship between the coordination of neural circuitry and biomechanical action in the musculoskeletal system. Coordination is one of the central concepts in human movement science, especially in the field of biomechanics and motor control. Biomechanics is a field that aims to identify the function of elements (e.g., muscles, joint movements) involved in achieving motor tasks. This identification is expected to provide information on improving movement and making it safer. Nevertheless, because the musculoskeletal system is highly interconnected and integrated, it is almost impossible to identify the function of each element in isolation during a whole-body movement.

The aim of this Research Topic was to summarize the most important neuro-biomechanical parameters influencing human performance related to the health sciences and sports in individuals with different ages and with various clinical conditions. Besides the information acquired from clinical interventions or experimental models, mathematical point of view, understanding this interaction means solving systems of under-determined equations (i.e., systems that have more unknowns than equations), and therefore an infinity of solutions are possible. Moreover, the use of several tools is also relevant to access information related to the mechanism involved with neural circuits and responses associated with movements.

The collection of articles in this Research Topic covers a range of issues such as conceptual frameworks, neuromechanical assessment and analysis, neuromodulation designs, coordination, and biomechanics relating to training. Studies involving populations with Spinal Cord Injury

OPEN ACCESS

Edited and reviewed by:
Julie Duque,
Catholic University of Louvain, Belgium

***Correspondence:**
Yury Ivanenko
y.ivanenko@hsantalucia.it

Specialty section:
This article was submitted to Motor Neuroscience, a section of the journal Frontiers in Human Neuroscience

Received: *17 December 2021*
Accepted: *12 January 2022*
Published: *03 February 2022*

Citation:
Taiar R, Bernardo-Filho M, Sañudo B and Ivanenko Y (2022) Editorial: The Relationship Between Neural Circuitry and Biomechanical Action. Front. Hum. Neurosci. 16:838028. doi: 10.3389/fnhum.2022.838028

individuals, Parkinson's Disease, Stroke, Autism Spectrum Disorder, infants and healthy adults are presented and different strategies were used to access biological responses. This Research Topic includes 26 contributions (3 reviews, 1 mini review, 2 systematic reviews, 1 perspective, 1 opinion paper, 17 original articles, and 1 case report) that are summarized below in 4 thematic categories: (i) reviews and perspectives, (ii) neuromechanical assessments, (iii) coordination assessments, and (iv) biomechanics related to neuromuscular training and neuroplasticity in rehabilitation and sport.

REVIEWS AND PERSPECTIVES

Several articles present and discuss available evidence, conceptual frameworks, and fundamental questions concerning the relationship between neural circuits and biomechanical action from different perspectives, including motor development, basic control mechanisms and clinical applications.

Dewolf et al. discuss the relationship between neural circuitries and changing biomechanics from the developmental point of view. The authors review neural and biomechanical mechanisms underlying walking and running gaits, their development in early childhood, biomechanical determinants, differentiating features, and the neuromechanical underpinnings of early gait maturation. They also consider the neuromuscular maturation time frame of gaits resulting from active practice and the underlying plasticity of development. Bridging connections between movement mechanics and neural control of movement could have profound clinical implications for technological solutions to better understand locomotor development and to diagnose early motor deficits. In particular, in a perspective article, Gygax et al. present converging recent knowledge in neuroscience and biomechanics to outline the relationships between maturing neuronal network, behavior, and neurodevelopmental disorders. The authors argue that developmental gait biomechanics might appear as a possible motor phenotype and biomarker to be correlated to neuronal network maturation, in normal and atypical developmental trajectories—-such as autism spectrum disorder.

In the context of the interrelationship between biomechanics and neural control of movement, Kimura et al. consider coordination as a multidisciplinary concept for accurate interpretation of data and theory development. By comprehensively providing multiple perspectives on coordination from computational and ecological perspectives, and the meaning of this term, this review article intends to promote coordination studies in biomechanics and neural control. In the context of neuromechanical functioning of different body segments, Geroza and Lombardi review the multiple roles that emerged for bone tissue as the principal mechanosensitive organ. Particularly, its high innervation, sensitivity to mechanical stimuli, the endocrine function, the capability to sense and integrate different stimuli and to send signals to other tissues, allow the adaptation of the affected bony segment to the changing environment and its communication with the CNS. As exercise effectively modifies the release of osteokines, it has been hypothesized that some of the beneficial effects of physical activities on brain functions may be associated with such a bone-to-brain communication for the treatment of neurodegenerative diseases.

Several articles discuss the use of neuromodulation tools to access biomechanical responses, the underlying neural mechanisms, and related clinical interventions. In a mini review article, Wang and Choi review the physiological and pathophysiological roles of basal ganglia and cortical oscillations, as well as their interactions, in specific biomechanical manifestations of pathological gait. In particular, the authors consider the functioning of the brain network for the control of gait in Parkinson's disease (PD), where specific patterns of abnormal oscillatory synchronization in the basal ganglia thalamocortical network are associated with specific signs and symptoms. They also discuss potential therapies aimed at restoring gait impairments through modulation of the brain network in PD. Two systematic reviews included in the Research Topic assess the current knowledge of the effect of transcranial stimulation. Xiao et al. review the literature on the effect of transcranial direct current stimulation (tDCS) on the physical performance of the foot and ankle of healthy adults and discuss the underlying neurophysiological mechanisms through which cortical activities influence the neuromechanical management. tDCS may induce remarkable improvements in the physical performance, including vibratory and tactile threshold of the foot sole, toe pinch force, ankle choice reaction time, accuracy index of ankle tracking, and ankle range of motion, compared to sham. Fan et al. review the literature on the effect of repetitive transcranial magnetic stimulation (rTMS) in inducing neuroplastic changes and promoting brain function restoration in stroke patients for the treatment of lower-limb motor dysfunction and improving the neuro-biomechanical parameters of gait. Finally, in an opinion article, Moshonkina et al. review the literature and discuss a promising approach of non-invasive strategy for spinal neuromodulation (scTS) to control human locomotion that might be effective for neuromuscular control of postural and locomotor function in post-stroke subjects and in individuals with spinal cord injury (SCI). The authors introduce a strategy of spinal neuromodulation using the continuous stimulation to activate the locomotor networks in combination with rhythmic targeted activation of flexor and extensor motor pools of leg muscles in different phases of step cycle in accordance with the biomechanical function of these muscles.

NEUROMECHANICAL ASSESSMENTS

Neuromechanical assessments represent a powerful tool to investigate the relationships between neural circuitry and biomechanical action. Grooms et al. report a kinetically-instrumented neuroimaging evaluation of neural correlates of force control using fMRI. The authors document that knee extension and flexion force-matching tasks increase BOLD signal among cerebellar, sensorimotor, and visual-processing regions, and reveal some unique activation strategies depending on whether engaging knee extension or flexion. They argue that a

neuroimaging-compatible force control paradigm may serve as a method to investigate how pathologies affect lower extremity neuromuscular function. Martino et al. examine associations between biomechanical outcomes and clinical leg rigidity score in people with Parkinson's disease (PD) by recording kinematic data and electromyographic signals during the pendulum test. The results suggest that the biomechanical assessment of the pendulum test can objectively quantify parkinsonian leg rigidity and be associated with a history of falls. Different mechanisms that contribute to resting and activated rigidity can play an important functional role in balance impairments and be used for neuromechanical assessments.

Several studies consider the anatomical, functional and behavioral factors for neuromechanical assessments. Nobue et al. examine the relationship between nerve conduction velocity (NCV) and nerve size in healthy subjects using supramaximal electric stimulation and peripheral nerve ultrasonography. The results show that the NCV, nerve cross-sectional area (nCSA), and circumference of the ulnar and tibial nerves were higher and greater in the lower limbs than in the upper limbs. The results also suggest that NCV does not depend on the nCSA sizes or upper and lower limb circumference and thus they indicate the existence of limb-specific NCV but not nCSA developments. Knothe Tate et al. address the need to image and analyse cellular connectivity across length and time scales through development of technological approaches that incorporate cross length scale (nm to m) structural data, acquired *via* multi-beam scanning electron microscopy, with machine learning and information transfer using network modeling approaches. Cells constitute biological materials of living organisms that exhibit "smart" stimuli-responsive and adaptive behavior, including changes in cellular connectivity and tissue remodeling by cells. The authors discuss the implications of the outlined approach for neuromechanics and the control of physical behavior and neuromuscular training, and for understanding the cellular underpinnings of diseases. Weinman et al. report the influence of various behavioral factors on long-latency (involving cortical areas) responses to perturbations. They examine the effect and interaction of such factors as background muscle torque, perturbation direction, perturbation velocity and task instruction, and argue about feedback processes in the CNS to control interactions with the environment. Recenti et al. use a novel multimetric system to study the physiology associated with motion sickness and sickness and to evaluate the associated postural control disturbances. The multimetric system was based on using a mechanical moving platform, virtual reality, EMG, EEG and heart rate recordings. The feature importance analysis showed that muscle parameters are the most relevant, and for EEG analysis, beta wave results were the most important. The present work serves as the first step in identifying the key neurophysiological factors that differentiate those who suffer from motion sickness from those who do not.

The role of biomechanical factors is also described in assessing grasping, speech and postural control. Nataraj and Sanford describe how modifications in the display of a computer trace can co-modulate agency (perception of control) and performance of grasp on rigid and compliant surfaces. Agency and performance of grasp can be co-modulated across varying modes of control, especially for compliant grasp actions. The implications of this work are cognition-centered device interfaces for the rehabilitation of grasp after neurotraumas while considering whether the grasp interaction is rigid or compliant. Gómez et al. assess performance, neuromotor (EMG) activity, and distributions of the kinematic and acoustic velocities extracted from the speech signal during the utterance of a diadochokinetic exercise to characterize Hypokinetic Dysarthria in participants with PD. The regression results show the relationships between EMG and dynamic and acoustic estimates, significant cross-correlations between articulation kinematics, and suggest that kinematic distributions derived from acoustic analysis may be useful biomarkers toward characterizing Hypokinetic Dysarthria in neuromotor disorders. Lhomond et al. examine whether the brain uses an internal model of physical laws (gravitational and inertial forces) to help estimate body equilibrium when tactile inputs from the foot sole are depressed by carrying extra weight. To this end they analyzed EEG characteristics and neural responses to tactile stimulation of the foot sole and compared them in Judoka athletes with non-athlete participants and dancers. They show smaller amplitudes of P1N1 somatosensory cortical potential in the Load compared to the No Load condition in both non-athletes and dancers. This decrease in neural response to tactile stimulation was associated with greater postural oscillations. Along with improved postural reactions evoked by a translation of the support surface in Judokas, the results suggest that an internal model stored in the right PPC can optimize predictive mechanisms in situations with high balance constraints.

COORDINATION ASSESSMENTS

Even the simplest movement engages many brain structures and necessitates not only activation but also inhibition of relevant neural circuits since the same motoneurons and interneurons participate in a huge repertoire of possible motor actions. For the complex movements, coordination is an important concept with which the CNS must deal when controlling multiple muscles and multiple degrees of freedom. A number of articles in this Research Topic explore coordination assessments to get insights into the relationship between neural control and biomechanics of movement involving multiple body segments.

Four articles address the issue of coordination patterns of human gait. Stetter et al. assess modularity in motor control by analyzing kinematic synergies across varying locomotor tasks: straight-line walking, walking a 90° spin turn, and walking upstairs. Covariation of joint motions can be analyzed and interpreted in the context of kinematic synergies relating to the control mechanisms underlying human motor behavior. The findings further support the idea that movements can be performed efficiently through a flexible combination of a lower number of control-relevant variables. Bach et al. assess multi-muscle coordination in children of different age (2–9 yrs) by evaluating muscle synergies that were proposed to reflect the presence of a common neural input to multiple muscles.

By analyzing the activation patterns of 15 bilateral leg, trunk, and arm muscles, ground reaction forces, and kinematics of walking and running, including the "walk-run strategy" in pre-schoolers, the authors investigated the development of different gait control. In particular, the findings suggest that the increase in the number of muscle synergies in older children can be related to motor learning and exploration. Krajewski et al. examine the complexity and stability of the state of the locomotor control system by analyzing motor variability using a goal equivalent manifold approach. They assess the interactive effects of load magnitude and locomotion pattern on motor variability, stride regulation and gait complexity during 1-min trials of running and forced marching in healthy young adult women. Reduction in "good" variability as load increases and load-related decrease of gait complexity are interpreted as important characteristics and changes in the locomotor system function. Unni et al. investigate disruptions in the coordination pattern during an involuntary stopping of gait in late-stage PD patients, known as freezing of gait. They use a neuromechanical model of gait to infer the causes of both the observed variability and freezing in PD. The model reveals that the opposing forces generated by the plantar flexors of the swing and stance leg can induce freezing, as well as other gait abnormalities near freezing such as a reduction in step length, and irregular walking patterns. The study by Maeda et al. explores the eye-head coordination mechanisms by analyzing the effects of high frequency noisy vestibular electrical stimulation delivered by electrodes placed on mastoid processes. The coordination of eye–head movements was measured by eye-tracking and a motion capture system. The authors report that this stimulation can reduce the lag time between eye and head movement and improve coordination, contributing to a clear retinal image and argue that this technique could be applied as a form of vestibulo-ocular reflex (VOR) training for patients with vestibular hypofunction.

BIOMECHANICS RELATED TO NEUROMUSCULAR TRAINING AND NEUROPLASTICITY IN REHABILITATION AND SPORT

Several studies report and analyse the effects of training in rehabilitation and sport and the benefits of using neuromechanical outcomes and correlations for their assessment. The study by Simis et al. looked for a neurophysiological biomarker for functional recovery after robotic-assisted gait training in individuals with incomplete SCI. Functional impairments and improvements in balance and walking performance following rehabilitation therapy were correlated with the change in cortical activity measured by EEG. The results suggest that the EEG alpha/theta ratio may be a potential surrogate marker of functional improvement during rehabilitation. In a case report, Momeni et al. evaluate the biomechanical, neural, and functional outcomes of neuromuscular electrical stimulation (ES) in a supine position and combined with stand training using a body weight support system in an individual with spinal cord injury (SCI). The post test of ES alone showed gains in trunk independence with a decrease in lower limb muscle activation, while ES combined with stand training showed gains in trunk independence and increased muscle activation in trunk and lower limb muscles during the treadmill stepping paradigm. The results of the study illustrate the importance of loading during the stimulation for neural and mechanical gains. Huang et al. show the effectiveness of in-bed wearable elbow robot training in improving biomechanical and clinical outcomes in patients with early and late subacute stroke. Based on muscle strength recovery curve, the results also suggest that patients with severe upper limb motor impairment may benefit more from the robot training compared to those with moderate impairment. Purdom et al. report the effect of accumulated competition training stress on neuromuscular function and the incidence of increased injury risk in uninjured female athletes. They tested mobility/stability, leg length symmetry, and vertical power at three different points throughout the competitive season. The results show that competition stress affected neuromuscular function without affecting maximal power, which negatively affected stability.

Taken together, the articles compiled in this Research Topic demonstrate the growth of interest to using neuromechanical assessments for understanding the relationship between neural circuitry and biomechanical action. These works also show the importance of investigating the pathophysiology underlying these relationships to better develop assessments of impaired motor function and its restoration in patients with neurological disorders.

AUTHOR CONTRIBUTIONS

All authors listed have made a substantial, direct, and intellectual contribution to the work and approved it for publication.

FUNDING

This work was supported by *Conselho Nacional de Desenvolvimento Científico e Tecnológico (CNPq)* and *Fundação de Amparo á Pesquisa do Estado do Rio de Janeiro (FAPERJ)*, Brazil and the Italian Ministry of Health (Ricerca Corrente, IRCCS Fondazione Santa Lucia, Ricerca finalizzata RF-2019-12370232).

ACKNOWLEDGMENTS

We would like to thank all authors and reviewers for their contributions to this Research Topic. The editors also thank Frontiers team for professional help with this Research Topic.

this article, or claim that may be made by its manufacturer, is not guaranteed or endorsed by the publisher.

frontiers in Bioengineering and Biotechnology

REVIEW
published: 19 May 2020
doi: 10.3389/fbioe.2020.00473

Emergence of Different Gaits in Infancy: Relationship Between Developing Neural Circuitries and Changing Biomechanics

Arthur Henri Dewolf[1]*, *Francesca Sylos-Labini*[2], *Germana Cappellini*[2,3], *Francesco Lacquaniti*[1,2] and *Yury Ivanenko*[2]

[1] Department of Systems Medicine and Center of Space Biomedicine, University of Rome Tor Vergata, Rome, Italy, [2] Laboratory of Neuromotor Physiology, IRCCS Santa Lucia Foundation, Rome, Italy, [3] Department of Pediatric Neurorehabilitation, IRCCS Santa Lucia Foundation, Rome, Italy

How does gait-specific pattern generation evolve in early infancy? The idea that neural and biomechanical mechanisms underlying mature walking and running differ to some extent and involve distinct spinal and supraspinal neural circuits is supported by various studies. Here we consider the issue of human gaits from the developmental point of view, from neonate stepping to adult mature gaits. While differentiating features of the walk and run are clearly distinct in adults, the gradual and progressive developmental bifurcation between the different gaits suggests considerable sharing of circuitry. Gaits development and their biomechanical determinants also depend on maturation of the musculoskeletal system. This review outlines the possible overlap in the neural and biomechanical control of walking and running in infancy, supporting the idea that gaits may be built starting from common, likely phylogenetically conserved elements. Bridging connections between movement mechanics and neural control of locomotion could have profound clinical implications for technological solutions to understand better locomotor development and to diagnose early motor deficits. We also consider the neuromuscular maturation time frame of gaits resulting from active practice of locomotion, underlying plasticity of development.

Keywords: early development, human bipedal locomotion, gait transitions, biomechanical gait determinants, neural control of different gaits, infants

OPEN ACCESS

Edited by:
Yih-Kuen Jan,
University of Illinois at Urbana-Champaign, United States

Reviewed by:
Nadia Dominici,
VU University Amsterdam, Netherlands
Boris Prilutsky,
Georgia Institute of Technology, United States

***Correspondence:**
Arthur Henri Dewolf
arthur.dewolf@uclouvain.be

Specialty section:
This article was submitted to Biomechanics, a section of the journal Frontiers in Bioengineering and Biotechnology

Received: *19 February 2020*
Accepted: *23 April 2020*
Published: *19 May 2020*

Citation:
Dewolf AH, Sylos-Labini F, Cappellini G, Lacquaniti F and Ivanenko Y (2020) Emergence of Different Gaits in Infancy: Relationship Between Developing Neural Circuitries and Changing Biomechanics. Front. Bioeng. Biotechnol. 8:473. doi: 10.3389/fbioe.2020.00473

INTRODUCTION

What are the general characteristics of maturation of gait-specific pattern generation circuitries? Even though humans start to walk significantly later than most animals (Garwicz et al., 2009), stepping-like responses can be evoked in human neonates. These steps are very irregular and typically disappear few weeks after birth and reappear later when they evolve into intentional locomotion (Forssberg, 1985; Thelen and Cooke, 1987). Recent advances in biotechnology along with reduced physical size of electromechanical systems has enabled to unveil new information about the locomotor output of the stepping behavior (Zhu et al., 2015; Redd et al., 2019; Airaksinen et al., 2020). By comparing this stepping behavior with adult walking, it has been shown that the primitive muscular control patterns observed in neonates are highly preserved and recombined

during development, supporting the idea that this early stepping is a precursor to adult walking (Dominici et al., 2011; Sylos-Labini, La Scaleia, Cappellini, Fabiano, Picone, Keshishian, 2020), in spite of noticeable differences with mature gait (Forssberg, 1985; Ivanenko et al., 2013a; Yang et al., 2015). The infants also show the elements of quadrupedal coordination during stepping (La Scaleia et al., 2018), swimming (McGraw, 1939), or crawling (Patrick et al., 2012; Forma et al., 2019). However, the developmental path from the neonate behaviors to adult running gaits is still unknown.

While the specific features of the walk and run are clearly distinct in adults, there is little evidence for such distinct walking and running patterns at the onset of independent locomotion. Instead, the characteristics of gaits show gradual and progressive values during growth (Whitall and Getchell, 1995). In other words, the locomotor patterns in young children do not fall nicely into a classic category like walking or running (Vasudevan et al., 2016), but such distinction is stretched out over developmental time. Here, we argue that these two different modes of locomotion most likely evolved from similar circuitry, and represent a specific kind of developmental bifurcation with different maturational rates.

In the first sections, we briefly highlight the main features of the two modes of mature human locomotion and neurophysiological and biomechanical considerations for the control of different animal gaits. Next, we consider recent findings on the process of development of neural network, and the absence of clear distinction in infant stepping. In a final section, we discuss common elements of organization with different modes of locomotion, and how early motor experience during development may shape motor properties in different environmental contexts including early gait impairments in infancy.

THE TWO MODES OF HUMAN LOCOMOTION

Among a vast variety of possible ways of locomotion, humans generally prefer just two, categorized into walking and running (Cavagna et al., 1988). Mature walking gait can be caricatured by the hip joint swinging over a relatively straight leg, whereas mature running gait can be seen as a bounce off compliant leg followed by parabolic flight (**Figure 1**). Few variables clearly distinguish features of walking and running gait and represent the essence of these commonly produced behavioral patterns (called *collective variables*). Once identified, the process that underlies changes in locomotor behavior across the lifespan may be studied.

One key parameter to discriminate forms of locomotion has traditionally been the difference observed in the spatiotemporal features, specifically the relative timing of the feet contacts with the ground (**Figure 1**, lower panels). Indeed, periods of single support intersperse with periods of double support during walking and with periods of flights during running. Accordingly, walking and running are operationally distinguished based on the presence (running) or absence (walking) of an aerial phase during which neither foot is in contact with the ground. Therefore, the existence or absence of a flight phase is one well-accepted collective variable.

Another distinguishing feature between adult walking and running is the path of the center of mass (COM) of the body (**Figure 1**, upper panels). The basis for this approach is the work of Cavagna and co-workers (Cavagna et al., 1988), who showed that major characteristics that serve as signatures for human running and walking are the interaction between the forward and the vertical displacement of the center of mass of the body (COM). In walking, the COM reaches its lowest point when its forward velocity is maximal; this behavior characterizes a pendulum-like energy exchange between potential and kinetic energy. In running, the COM reaches its lowest point when its forward velocity is minimal; this behavior characterizes a storage-release of elastic energy. These mechanisms were defined as the "inverted pendulum" mechanism in walking, and the "pogo-stick bouncing" in running (**Figure 1**).

The trajectory of the COM in space in turn depends on the combined rotation of lower-limb segments (Lacquaniti et al., 1999, 2002; Dewolf et al., 2018). During both running and walking, the behavior of the COM is the result of a gait-dependent control of phase relationship between the lower-limb segments (Kao et al., 2000; Ivanenko et al., 2007a), also a distinguishing feature of gaits.

NEUROPHYSIOLOGICAL CONSIDERATIONS FOR THE CONTROL OF DIFFERENT GAITS

It is known that such gait coordination results from interplay between the activity of spinal central pattern generators (CPGs), sensory signals originating in the limbs and supraspinal signals (Grillner, 1981; Büschges et al., 1995). There are at least two conceptual models on how the locomotor circuitry may be organized (for a more comprehensive overview of hypotheses on CPG organization, see, for example, Duysens et al., 2013; Rybak et al., 2015; Kiehn, 2016; Minassian et al., 2017; Grillner and El Manira, 2020). One model considers a set of unit CPGs controlling specific groups of muscles (Grillner and El Manira, 2020). Another model consists of a two-layered CPG organization with one rhythm-generating circuit and another one for downstream control of muscle activity and coordination of different gaits (walk, trot, and gallop) (McCrea and Rybak, 2008; Danner et al., 2017).

Several studies on animals have shown that the CPG circuits reside mainly in the ventral aspect of the spinal cord (Kiehn, 2016; Grillner and El Manira, 2020), and are involved in changing the mode of locomotion. While the intensity of supraspinal inputs may determine the speed and mode of locomotion, the spinal circuitry is able to implement specific coordination patterns for different gaits. A classical physiological study on decerebrated cat stepping on a treadmill showed that increasing the strength of electrical stimulation of the mesencephalic locomotor region can make the gait changes from a slow walk to trot and finally gallop (Shik et al., 1966; Shik and Orlovsky, 1976). Another

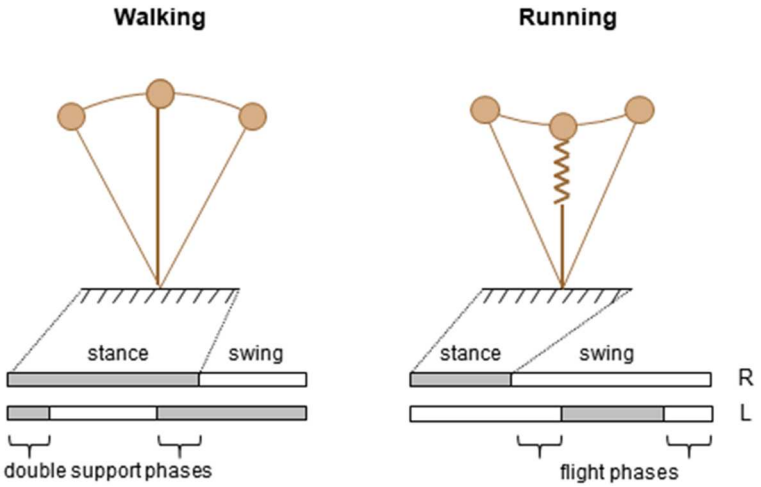

FIGURE 1 | Schematic representation of two modes of human locomotion during stance phase.

example of gait-related spinal control can be obtained during fictive swimming in the lamprey: varying the concentration of neurotransmitter applied to the lamprey spinal cord produces changes in the intersegmental coordination (Matsushima and Grillner, 1992). In humans, by using mental imagery of locomotion in fMRI, Jahn et al. (2008) have suggested that the supraspinal network of quadrupeds is conserved in both walking and running gaits, despite the transition to bipedalism. The similarities of the basic organization of supraspinal locomotor control for gait and speed regulation in humans and cats (Drew et al., 2004) suggest similar gait-related spinal circuitries across mammals. In sum, it is worth stressing that the neural mechanisms for the control of different gaits involve both shared and specific neural circuits. **Figure 2** illustrates examples of such gait-dependent changes in spinal locomotor controllers.

Using electrophysiological, pharmacological, or neuroanatomical approaches in invertebrates and vertebrates, the identification of the spinal interneurons and investigation of the locomotor output provided important insights into the gait-dependent organization of CPGs and how these functional circuits are formed during development. An example of developmental process can be observed during the Xenopus metamorphosis (**Figure 2A**). Limb and tail muscle coordination switches from pro-metamorphosis to metamorphic climax, suggesting that the neural network is progressively reshaped to allow the transformation from aquatic swimming to ground stepping (Rauscent et al., 2006). Such plasticity results from both a dynamic reconfiguration of spinal circuitry and the involvement of new circuitry (Combes et al., 2004). Studies focused on the patterns of recruitment of interneurons in the spinal motor system of zebrafish led to principles underlying the reorganization of spinal circuitry (Fetcho and McLean, 2010). The neurons producing fast movements are established early and, as the zebrafish develops, interneurons responsible for low frequency movements are progressively added (**Figure 2B**). At the end of development, the neurons producing slow, intermediate, or fast movements can be recruited either separately or combined sequentially to increase the locomotor speed (McLean et al., 2008; Grillner and El Manira, 2020). Studies on gait-related spinal circuits in mice demonstrated intriguing similarities with the zebrafish spinal cord (McLean et al., 2008; Fetcho and McLean, 2010). For example, in both species, V1 interneurons are critical for setting the speed of locomotion, and sequential V2a recruitment is observed with increasing speed (Ausborn et al., 2012). However, a major difference is that as they speed up, mice (as the great majority of terrestrial quadrupedal mammals) change their gait from walk to trot and to gallop (**Figure 2C**), and the inter-limb coordination switches from alternation during both walking and trotting to synchrony during galloping. Such gait-dependent left–right rhythmicity and coordination recruitments are mediated by speed-dependent spinal interneurons (**Figure 2C**). According to the unit-burst generator organization, spinal interneurons coordinate the activity of "excitatory core burst generators" dedicated to coordination of hip, knee and ankle flexor, and extensor motor output of each limb (Grillner and Jessell, 2009; Grillner and El Manira, 2020), which can be combined to produce various gait patterns (Catavitello et al., 2015; **Figure 2D**). One alternative concept of the CPG organization includes a separation of the networks for rhythm generation and motoneuron excitation. According to this hypothesis, the rhythm generating circuit would set the rhythm for one limb, and then interneurons would activate a certain set of motoneurons and inhibit others depending on gaits (Lafreniere-Roula and McCrea, 2005; Shevtsova and Rybak, 2016; Danner et al., 2017; Ausborn et al., 2018). Both approaches emphasize gait-specific coupling of elements of pattern generation circuitries, mediated by speed-dependent spinal interneurons.

Another way to get insight into CPG functioning for different gaits is to look at the spatiotemporal organization of the total locomotor output and multi-muscle activity patterns in particular. In dogs as in several other animal species

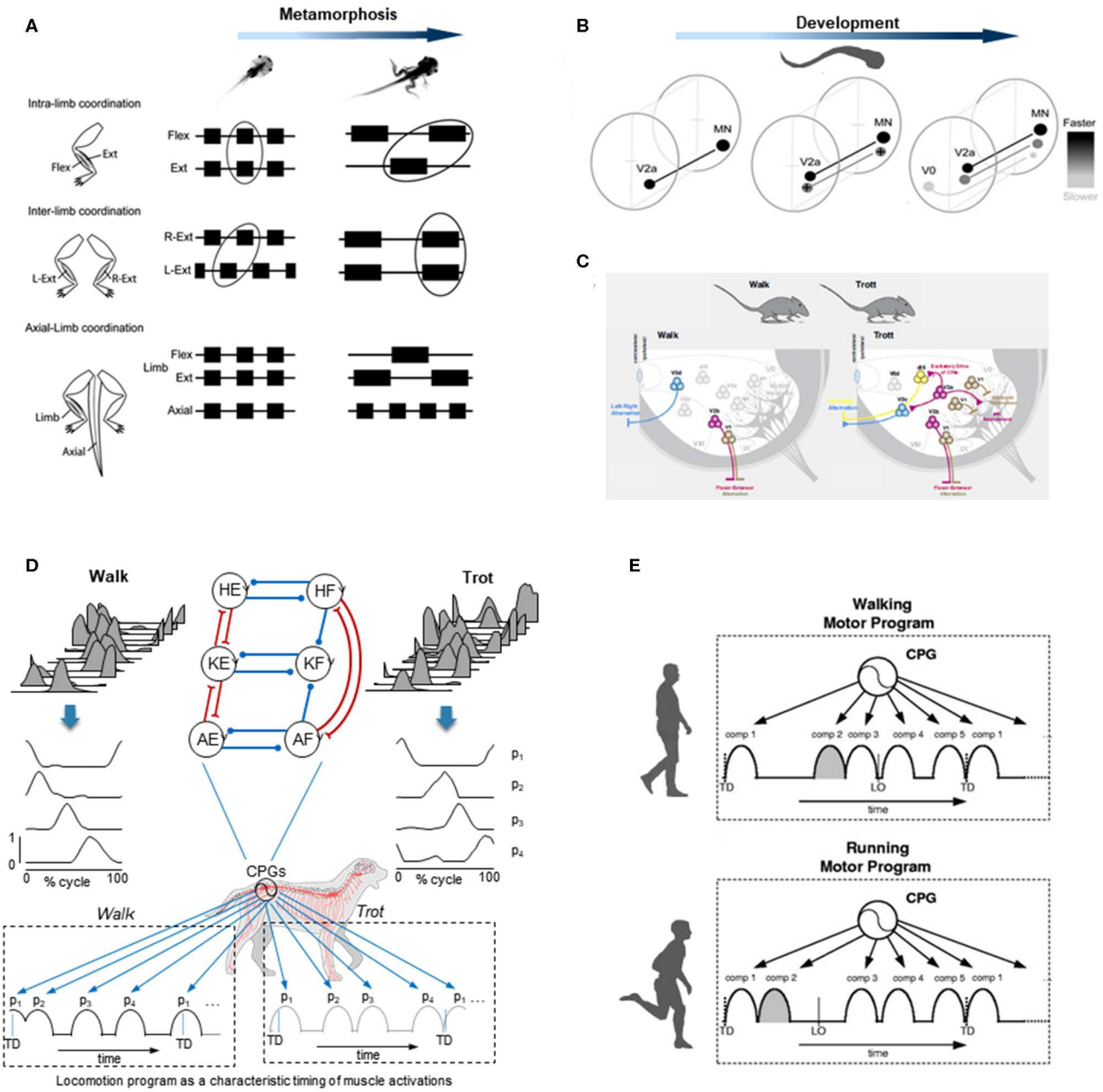

FIGURE 2 | Examples of gait-specific changes in spinal locomotor controllers. **(A)** changes in coordination between extensor, flexor, and axial muscle bursts during Xenopus metamorphosis (modified from Rauscent et al., 2006 with permission from Elsevier). **(B)** schematic summary of changes in the development and recruitment of spinal circuitry in larval Zebrafish: neurons responsible for progressively slower movements in larvae are added as zebrafish develop (modified from Fetcho and McLean, 2010 with permission). **(C)** distinct spinal interneurons circuits drive different gaits in mice (modified from Deska-Gauthier and Zhang, 2019 with permission from Elsevier). **(D)** locomotion program as a characteristic timing of muscle activations during walk (*left*) and trot (*right*) in dogs. *From top to bottom:* averaged hindlimb EMG data, basic activation patterns (p1-p4) obtained by decomposing muscle activity and a schematic sequence of activation patterns for each gait (modified from Catavitello et al., 2015). Schematic representation of the unit burst generator CPG model is also plotted on the top (circles are interneurons controlling hip (H), knee (K), and ankle (A) extensors (E) and flexors (F), excitatory and inhibitory connections are represented by lines ending with forks or circles, respectively) (redrawn from Grillner and El Manira, 2020). **(E)** locomotion motor program as a sequence of activation pulses for walking and running in humans (modified from Cappellini et al., 2006).

including humans, muscle activity patterns (**Figure 2D**) can be decomposed into a set of four basic temporal patterns that account for ∼90% of total variance (Dominici et al., 2011; Catavitello et al., 2015). These basic temporal patterns have specific timings during a gait cycle (**Figure 2D**), consistent with "drive pulse" rhythmic elements in the spinal circuitry of zebrafishes, frogs, or mice (Rauscent et al., 2006; Fetcho and McLean, 2010; Giszter et al., 2010). The specific timing

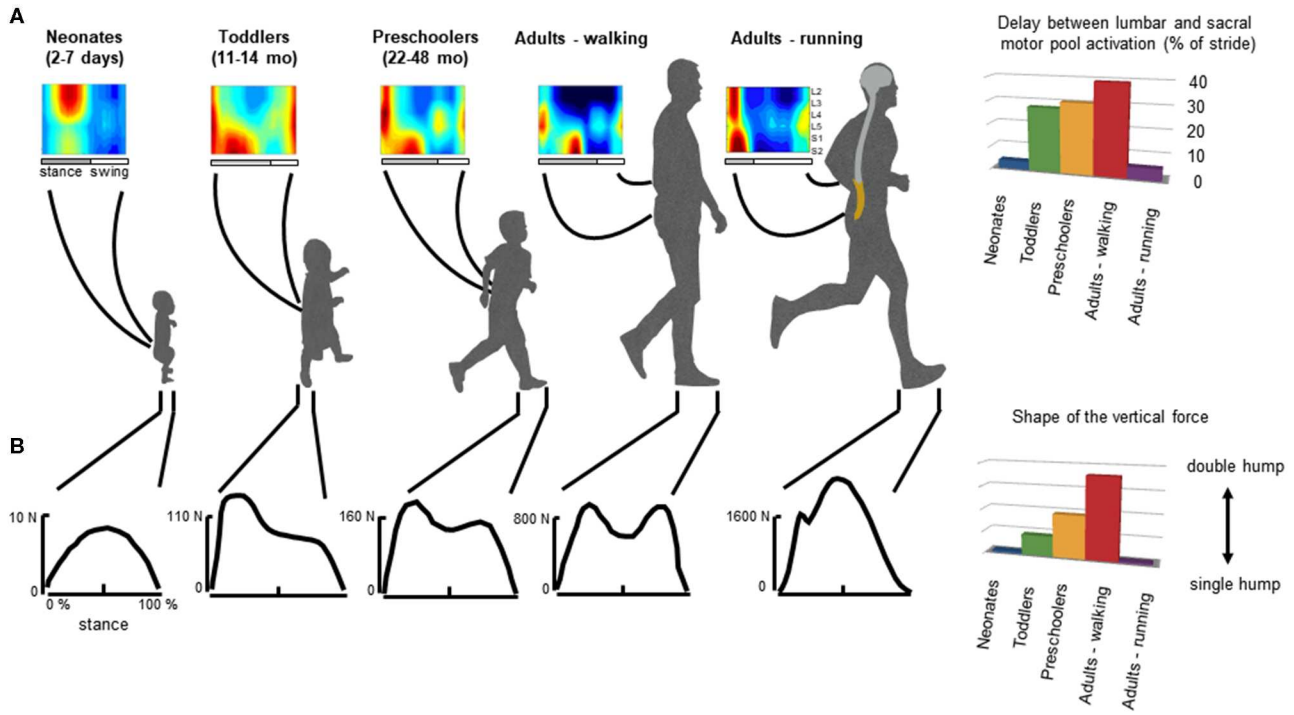

FIGURE 3 | General features of gait patterns from neonate to adult. **(A)** spatiotemporal maps of motoneuron activity of the lumbosacral enlargement in neonates, toddlers, preschoolers, and adults walking and running, and the delay between the maximum activation of lumbar and sacral motor pools (data from Ivanenko et al., 2013a for stepping, and Cappellini et al., 2010 for running). **(B)** typical vertical loading force during stepping in neonates, toddlers, preschoolers, and adults walking and running, and the characteristic force profile evaluated using an adapted ratio of the coefficients of Fourier series (Hallemans et al., 2006a) providing a description of the main features of the shape of the ground reaction force: when the ratio is nil the force curve has a single hump whereas when the ratio increases, the force curve tends to have a double hump shape.

of each basic temporal pattern differs between different gaits to produce various intra- and inter-limb coordination, as it does for human walking and running (Cappellini et al., 2006; **Figure 2E**). In both running and walking, the muscles activated by each basic temporal pattern are roughly similar, suggesting some degree of commonality (Cappellini et al., 2006). However, differences are also noticeable (Santuz et al., 2019), such as the number of modules that show mode-dependent modulation, with additional patterns detected during running as compared to walking (Yokoyama et al., 2016). Recent data from vertebrates indicates that the structure of the basic patterns extracted from EMGs may originate from spinal interneuronal networks (Caggiano et al., 2016; Takei et al., 2017). It is therefore plausible that the functioning of gait-related spinal circuits is reflected in the mode-dependent modulation of basic activation patterns. The mode-dependency in the neural networks underlying human locomotion is consistent with the speed control mechanism of vertebrate CPGs, providing indirect evidence for phylogenetically conserved neural circuits of locomotion (Grillner and Jessell, 2009; Yokoyama et al., 2016). The idea that neural mechanisms underlying walking and running are partly independent in adulthood is further supported by previous studies showing that newly acquired locomotor patterns at slow speed rarely transfer to fast speed movements (Vasudevan and Bastian, 2010; Ogawa et al., 2012, 2015). Taken together, these observations might reflect the fact that, even though there are shared neural circuits for different gaits, in adults there is no simple scaling of motoneuron and interneuron activity from walking to running, but the involvement of somewhat different neural circuits.

In addition to examples illustrated in **Figure 2**, there are also other important aspects related to the maturation rates of gait-specific pattern generation networks. There might be different rates of maturation in different animals; for instance, the development of spinal interneurons observed in zebrafish (**Figure 2B**) may not necessarily apply to other species. Nevertheless, increasing evidence suggests a similar developmental pattern of neurons in vertebrates (Cepeda-Nieto et al., 2005; Fetcho and McLean, 2010). Interestingly, it has been shown that walking and running in non-human bipeds do not mature at the same rate, with a running pattern relatively mature earlier in life in chicks (Muir et al., 1996). The fact that chicks can innately run almost as well as an adult may suggest that, as in zebrafish, the interneurons mainly involved in the production of fast movement are developed early. Humans have a relatively long period of gait development (Garwicz et al., 2009) and, in the following sections, we will specifically consider the organization and maturation of gait patterns in humans.

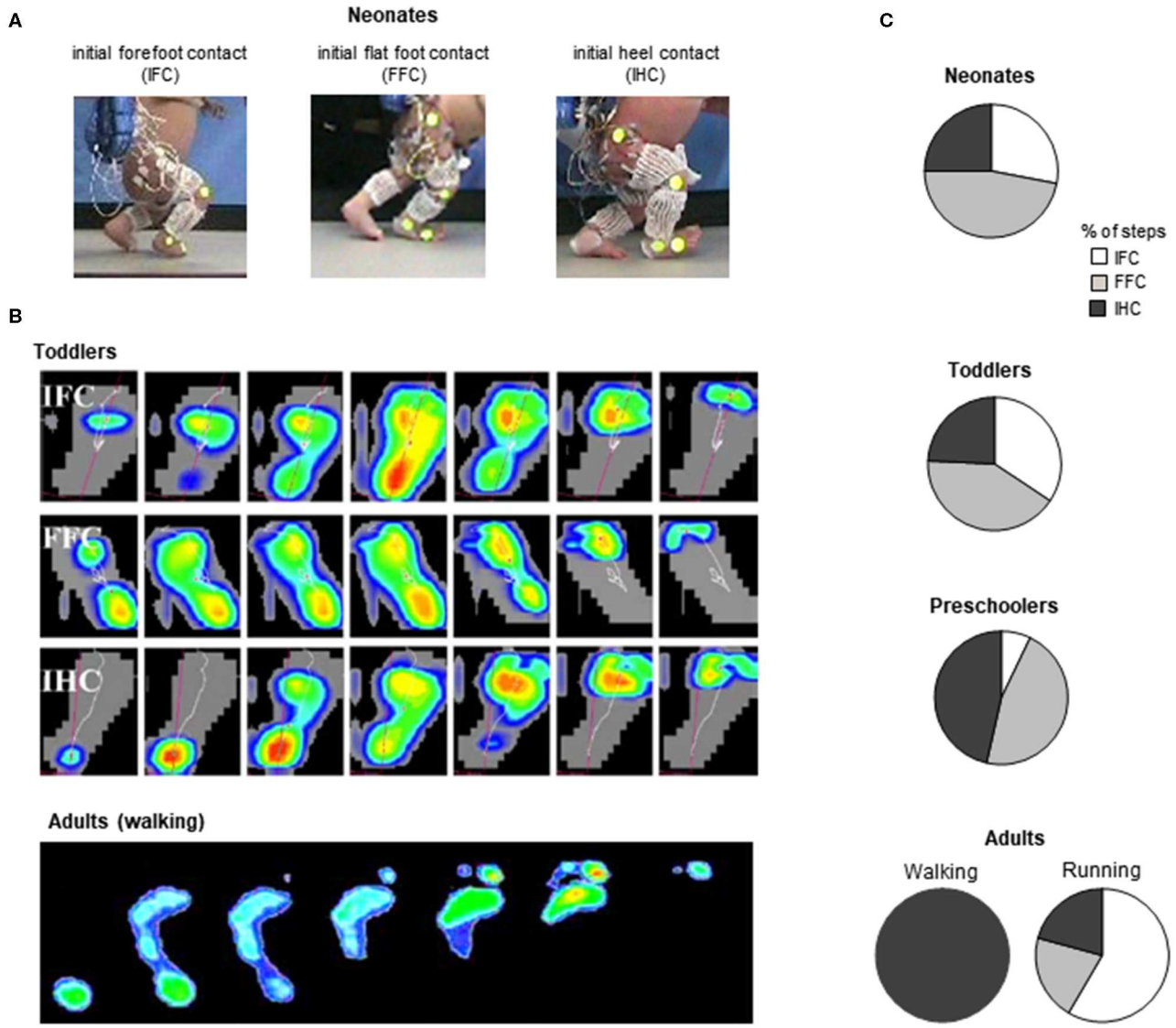

FIGURE 4 | General foot placement characteristics during stepping. **(A)** examples of initial forefoot (IFC), flat foot (FFC), and heel (IHC) contacts in three neonates (adapted from Sylos-Labini et al., 2017). **(B)** from top to bottom: three different foot-contact patterns in toddlers (IFC, FFC, and IHC) and plantar pressure prints (left foot) of a typical adult "heel-to-toe" rolling pattern during the stance phase (redrawn from Hallemans et al., 2006b with permission from Elsevier). **(C)** percent of steps with different types of touchdown contacts for stepping in neonates (from Sylos-Labini et al., 2017), toddlers and preschoolers (from Hallemans et al., 2006b) and adult walking and running (from Larson, 2014).

GENERAL FEATURES AND MATURATION OF GAIT PATTERNS FROM NEONATE TO ADULT

The CPGs in vertebrates emerged during evolution from a common ancestral circuit (Grillner and Jessell, 2009; Kiehn, 2016) and it has been suggested that, in humans, locomotor modules evolved from similar circuitry (Dominici et al., 2011; Yokoyama et al., 2016). In humans, when EMG activity patterns are mapped onto the spinal cord in approximate rostrocaudal locations of the motoneuron (MN) pools, the activation of MNs tends to occur in bursts (**Figure 3**) that can be associated with the major kinetic or kinematic events of the gait cycle in a gait-specific manner (Ivanenko et al., 2008a; Cappellini et al., 2010; La Scaleia et al., 2014; Yokoyama et al., 2017; Dewolf et al., 2019a). In particular, the sacral activation timing is clearly gait-dependent (Ivanenko et al., 2008a). It is worth stressing that these gait-specific features undergo functional reorganization during development from the neonate to the adult.

In adults, during walking the COM vaults over a relatively stiff limb with the heel well in front of the hip at the beginning of stance, and the heel lift with a maintained toe contact at the end of stance. One of the direct consequences of such heel-to-toe roll-over pattern is that the extension of distal joints is

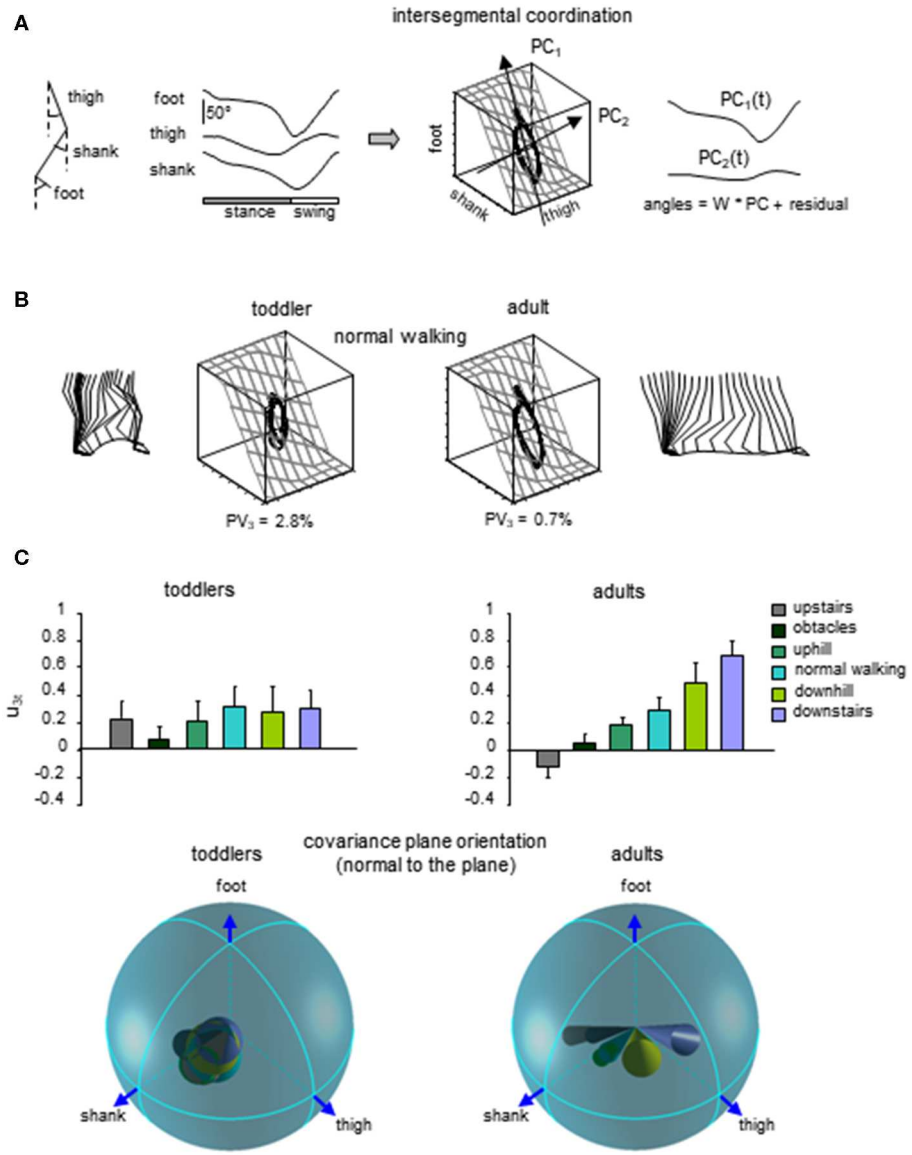

FIGURE 5 | Lack of adaptability of the intersegmental coordination to different locomotor conditions in toddlers. **(A)** intersegmental coordination assessed by principal component analysis (PCA) of limb segment elevation angles during walking. From left to right: thigh, shank, and foot elevation angles (relative to the vertical), corresponding 3D trajectory in segment angle space along with the interpolated plane and the directions of PC_1 and PC_2, and two principal components that account for ∼99% of variance of three elevation angles in adults (modified from Ivanenko et al., 2008b). **(B)** examples of gait loops and interpolation planes during walking in one toddler and one adult. Stick diagrams for one stride are also shown. Percent of variance explained by the third PC (PV_3) is indicated, and reflects the deviation from planarity. **(C)** changes in the orientation of the covariance plane during walking over different surfaces in adults and a lack of these adaptations in toddlers. Upper panels: projection of the normal to the covariance plane onto the thigh axis (u_{3t}, mean + SD). Lower panels: spatial distribution of the normal to the plane (u_3, the angles of cones correspond to 2 spherical angular dispersions) for each condition (modified from Dominici et al., 2010).

delayed relative to proximal joints, leading to the typical double-hump shape (so-called ≪m − pattern≫) of the vertical ground reaction force (**Figure 3**, bottom panel), characterized by Fourier analysis (based on the relationship between the shape of the force and the ratios of the coefficients of the Fourier series, Alexander and Jayes, 1980; Hallemans et al., 2006b). In addition, separate lumbar and sacral activations are observed: muscle activations intervene close to the apexes of the m-pattern to re-excite the inverted-pendulum oscillations of the system (Ivanenko et al., 2008a; Lacquaniti et al., 2012; Dewolf et al., 2019a). Conversely, during running with the center of mass rebounding on compliant spring legs, the vertical force exerted on the ground presents a single-hump shape (Nilsson and Thorstensson, 1989; Dewolf et al., 2016), and both the lumbar and sacral activations intervene close to the apexes of the ground reaction force (Ivanenko et al., 2008a; Cappellini et al., 2010; Yokoyama et al., 2017) (**Figure 3**).

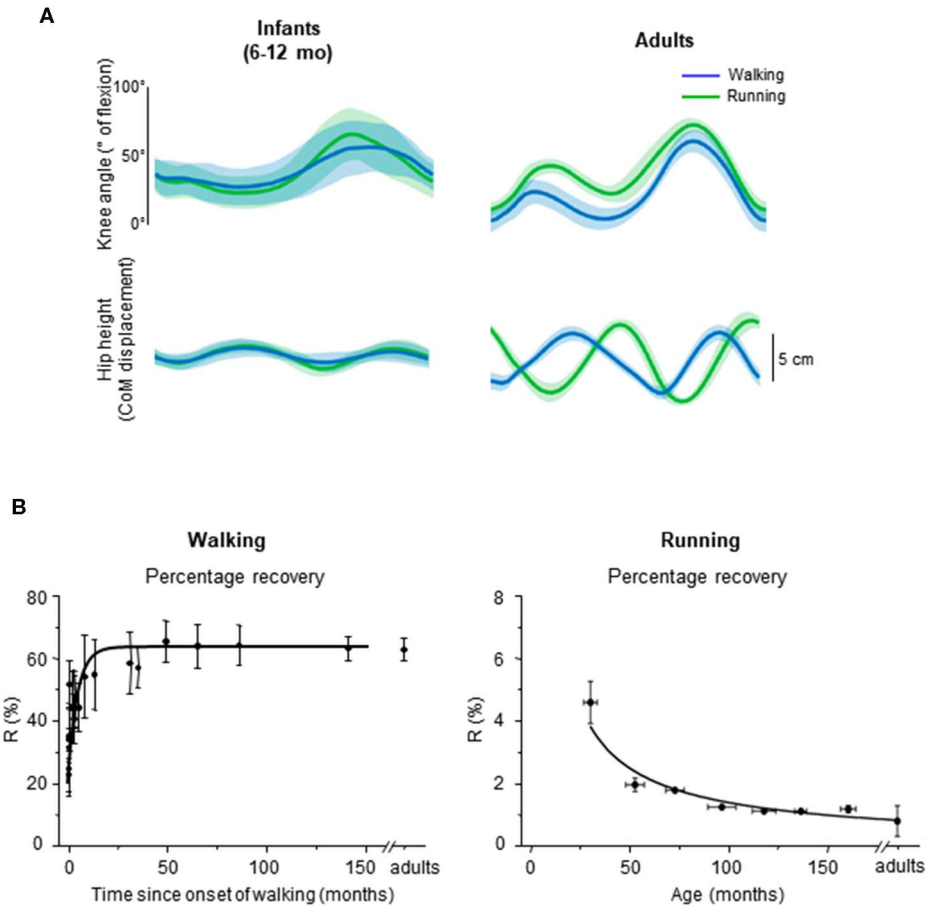

FIGURE 6 | Emergence of walking and running gait features during development. **(A)** comparison between knee angle (top) and hip vertical trajectory (bottom) in infants and adults, adapted from Vasudevan et al. (2016). Walking (blue) and running (green) gaits were defined based on the presence of double support period or flight phase, respectively. Note similar kinematic patterns in infants and distinct patterns in adults for both gaits. **(B)** percentage of recovery of mechanical energy (*R*%) during walking as a function of the time after the onset of independent walking (left) (adapted from Ivanenko et al., 2004), and *R*% during running as a function of age (data from Schepens et al., 1998). During walking, a greater *R*% reflects a potentially better pendular energy exchange whereas during running, a smaller *R*% reflects a potentially better elastic energy exchange.

In neonates, stepping lacks these specific features of adult heel-to-toe roll-over walking pattern (Forssberg, 1985; Dominici et al., 2011), and the foot placement characteristics in neonates showed wide variations (**Figure 4A**, Sylos-Labini et al., 2017). Three major footfall patterns were identified with the initial heel, midfoot, and forefoot contacts, respectively (**Figure 4C**). However, even when the neonates demonstrated a heel initial contact, the general features of gait patterns markedly differed relatively to adult. Indeed, the two peaks in the vertical ground reaction force and the associated MNs bursts were lacking. Instead, the vertical force exerted on the ground (neonates are generally able to support ∼30% of their weight) presents a single-hump shape, even if some influences of the manual body weight support on the ground reaction force cannot be excluded (Forssberg, 1985; Sylos-Labini et al., 2017). However, when adults walk with a body weight support system, the kinetic events defining the "m-pattern" (i.e., the early stance peak of vertical force, the mid-stance interval, and the late stance peak) are recognizable in the force profiles up to 75% of body weight support (Ivanenko et al., 2002). In addition, during stance, antigravity leg muscles tend to be co-activated with a quasi-sinusoidal waveform, corresponding to the single-hump shape of the force, independently of the level of body weight support (Sylos-Labini, La Scaleia, Cappellini, Fabiano, Picone, Keshishian, 2020). In turn, a quasi-synchronous lumbar and sacral activations is observed (**Figure 3A**), corresponding to the single peak of vertical force (Ivanenko et al., 2013a).

Throughout the development, a progressively greater occurrence of initial heel contacts is observed during walking (**Figure 4B**) (Bertsch et al., 2004; Hallemans et al., 2006b), along with maturation of the control of foot trajectory (Forssberg, 1985; Dominici et al., 2007) and intersegmental coordination (**Figure 5B**) Cheron et al., 2001; Ivanenko et al., 2004; Dominici et al., 2011. Meanwhile, the timing and amplitude of muscle activities are gradually tuned to the mechanical behavior

(Okamoto et al., 2003; Dominici et al., 2011; Teulier et al., 2012; Sylos-Labini, La Scaleia, Cappellini, Fabiano, Picone, Keshishian, 2020; Cheung et al. under review). The muscle activations are progressively shaped to produce the desynchronized joint extension, and the lumbar and sacral loci of activation become more dissociated (**Figure 3**) with shorter activation durations (Ivanenko et al., 2013a; Cappellini et al., 2016).

The progressive emergence of mature gait suggests that these patterns result from the neural maturation of central pathways, as well as a better integration of central commands with sensory signals (Yang et al., 1998). In adults, various cerebral cortices are involved in the control of locomotion (Leyton and Sherrington, 1917; Drew, 1988; Fukuyama et al., 1997), with some of them predominantly participating in the control of running rather than walking (Suzuki et al., 2004; Jahn et al., 2008). Neonates have most likely weak descending input (Yang and Gorassini, 2006). Indeed, many structures of the central nervous system are not mature at birth. For example, corticospinal tract axons become progressively myelinated only during the first 2–3 years of life (Richardson, 1982; Brody et al., 1987; Kinney and Volpe, 2018). While the involvement and the functionality of supraspinal structures for gait control have been little investigated in infants (see however Petersen et al., 2010), one can hypothesize that features of mature gaits are progressively added with the maturation and the gradual integration of supraspinal, intraspinal, and sensory control. In summary, the collective variables of mature patterns are not fully implemented at birth (**Figures 3**, **4**, **5B**), raising questions about complete innateness of gait-specific circuitry differentiation (Grillner and Wallén, 2004).

LACK OF GAIT TRANSITION IN INFANTS

Another evidence for the lack of differentiation between the two gaits in early infancy is the absence of clear gait transition events. Indeed, an essential criterion for gait distinction has been formulated by defining a gait as "a pattern of locomotion characteristic of a limited range of speeds described by quantities of which one or more change discontinuously at transitions to other gaits" (Alexander, 1989). Adults spontaneously walk at slow speeds and run at faster speeds, so that transitions from one gait to another generally occur when speeding up or slowing down and when one gait mode tends to become energetically more efficient than the other one. Despite small variations depending on walking conditions (De Smet et al., 2009; Van Caekenberghe et al., 2010), a spontaneous transition from walk to run occurs around 2 m/s (Van Caekenberghe et al., 2010; Ganley et al., 2011; Segers et al., 2013) and is typically abrupt (Raynor et al., 2002; Segers et al., 2013). In particular, the gait transition is marked by a discontinuous change in intralimb coordination (Saibene and Minetti, 2003; Ivanenko et al., 2011). This modification of coordination is related to the shift from the relatively straight leg of walking to the compliant spring leg behavior of running. This difference in support leg length during stance is clearly reflected by the trajectory of the hip and the knee joint angle (**Figure 6A**, right panels).

In infants, Vasudevan et al. (2016) analyzed the hip trajectory and knee joint angle during supported stepping on a treadmill in a large range of speeds (from 0.06 to 2.36 m/s; i.e., even above adult spontaneous walk to run transition). As speed increased, a period of flight started appearing, which suggests that infants switched from walk to run. However, when comparing the hip trajectory and knee joint angular motion during gait without (slow speeds) and with (fast speeds) flight phases, the authors did not find an altered intralimb coordination or a modified hip trajectory in a manner that would suggest adult-like gait transition (**Figure 6A**, left panels).

It is unlikely that the smoothness of gait transitions and the lack of differentiation between gaits are attributed to experimental conditions, such as partial body weight support in infants. In adults, a lack of abrupt changes was observed with a simulated lower level of gravity (Ivanenko et al., 2011; Sylos-Labini et al., 2011), supporting the idea that loading conditions may be a major trigger of the transition to running (Segers et al., 2013). To record infant stepping on a treadmill (Vasudevan et al., 2016), infants were manually supported (∼55% of their weight were supported, on average). Therefore, these authors also compared adults with 50% body weight support and observed that changes in intralimb coordination at the walk-to-run transition in adults remained. While body weight support may affect the abruptness of the walk-to-run transition, it does not completely eliminate signs of gait transition. The fact that the infants do not display distinct intralimb coordination and COM trajectory across a large range of speeds (**Figure 6A**) suggests that the gait-related neural circuitries are not mature yet.

BIOMECHANICAL FACTORS AND DEVELOPMENT

In addition to above-mentioned maturation of the neural circuitries, biomechanical factors also play a role in locomotor development (Thelen, 1995; Adolph and Robinson, 2015; Adolph et al., 2018). In humans as in other animals, locomotion behavior in its different forms arises from the closed-loop interaction between the neural output, the physical dynamics of the mechanical system (inertia, viscoelastic properties of muscles and tendons and body size) and the ability to adjust the movement to the external environment (Taga, 1995; Hatsopoulos, 1996; Aoi and Tsuchiya, 2006).

First, some influences on gait patterns in infants might be expected due to differences in the anthropometry, shape, and mass distribution across different body segments, all parameters changing considerably during the entire course of development through adult age. This implies a continuous update of the neural commands to take into account the changing mechanical factors. Different mass distribution across body segments in infants and, in turn, the location of the COM, induces modifications of balance (Druelle et al., 2016), which potentially affects the emerging locomotor behavior (Clark et al., 1988). The shape of the body, bone morphology (Shefelbine et al., 2002; Cowgill et al., 2010; Raichlen et al., 2015), and foot structure (Maier, 1961; Bosch et al., 2007; Price et al., 2018) in infants are different from

adults, and they also change with limb loading and locomotor experience during development. In particular, a child's foot goes through significant developmental changes in shape and soft tissues of the foot sole, e.g., the presence of a fat pad underneath the foot plantar surface in infants and slow ossification of intrinsic foot bones during the first years after birth (Maier, 1961; Gould et al., 1989; Bertsch et al., 2004). These latter factors are especially important since the spring-like longitudinal arch is a unique feature of the human foot, an essential evolutionary adaptation to the "bouncing" mechanism of running (Holowka and Lieberman, 2018; Venkadesan, Yawar, Eng, Dias, Singh, Tommasini, 2020). Therefore, different foot functions might be expected in infants as compared to spring-like behavior of the adult foot (Wager and Challis, 2016; Kelly et al., 2018).

Second, there might also be important peripheral contributors to the lack of adult-like locomotor patterns in early infancy, in particular due to slower and weaker muscles. For instance, based on the principle of dynamically similar locomotion (taking into account the differences in body proportions by comparing adults and infants moving at the same Froude number, Cavagna et al., 1983; Alexander, 1989; Schepens et al., 2004, neonates would be expected to show walk-to-run transition at ∼2 km/h (since their limb is about 6 times shorter), which would correspond to ∼0.25 s stride duration. Significantly wider muscle activation bursts in infants (Dominici et al., 2011; Cappellini et al., 2016; Sylos-Labini, La Scaleia, Cappellini, Fabiano, Picone, Keshishian, 2020) would further compromise the control of such short running cycles. Furthermore, given that skeletal muscles are substantially slower in neonates due to the absence of fast fibers at birth (Denny-Brown and Sherrington, 1929; Buller et al., 1960), it would be problematic for them to accurately control such short gait cycles. In fact, even during stepping, the stride duration in neonates (∼2–5 s) is considerably longer than in adults (∼1 s) (Ivanenko et al., 2013a). Even in older (11–13 yrs) children, muscle contraction time is ∼50% longer than in adults (Dayanidhi et al., 2013), and running requires faster limb oscillations due to shorter limbs (Schepens et al., 1998), which might possibly explain why children also display a third gait mode—"skipping"—requiring slower limb oscillations (Minetti, 1998). In addition, muscle strength also increases during development (Bäckman et al., 1989), and the deviation from adult gaits in infancy may also be related to adaptive strategies for limiting the muscle activation demands (Hubel and Usherwood, 2015).

Finally, a lack of gait-specific circuitry differentiation might also be associated with a general lack of adaptability to biomechanical constrains in infants. A key example of the closed-loop interaction between the development of neural commands and biomechanics is the emergence of multi-segmental coordinative law (Lacquaniti et al., 1999). Such a kinematic covariation between limb segment rotations has been uncovered in human walking and running (Borghese et al., 1996; Bianchi et al., 1998; Ivanenko et al., 2007a). Each segment oscillates back and forth relative to the vertical with a similar waveform, time-shifted across different segments (**Figure 5A**). The lower limb segment angles do not evolve independently of each other, but they are tightly coupled (Borghese et al., 1996). Indeed, when the angles are plotted one vs. the others, they co-vary along a plane, describing a characteristic loop over each stride (**Figure 5A**). The specific shape and orientation of the plane reflects the phase relationship between segments and therefore the timing of the intersegmental coordination (Barliya et al., 2009). Such coordination of limb segments can be described by statistical methods using principal component analysis (PCA). The two first principal components (PC1 & PC2) lie on the plane of angular covariation and describe the global form of the gait loop, whereas the third one (PC3) is orthogonal to the plane (Borghese et al., 1996). The percentage of variance accounted for by PC1 and PC2 reflect the shape of the gait loop, whereas the variance accounted for by PC3 reflects the planarity of the loop. At the onset of unsupported walking, a significant deviation from planarity is observed for the child (Cheron et al., 2001). Also, the gait loop was less elongated than in adults, and the variance accounted by PC1 (Ivanenko et al., 2004) was smaller than in adults, most likely due to a higher foot lift during swing phase (Dominici et al., 2007; Ivanenko et al., 2007a). Even if the intersegmental coordination in toddlers rapidly evolves toward the adult shape and planarity with experience (Cheron et al., 2001; Ivanenko et al., 2004; Dominici et al., 2011), when toddlers step on different support surface, they do not adapt their intersegmental coordination as adults do. Instead, they keep constant phase relationships (**Figure 5C**, Dominici et al., 2010). Since the changes in planar covariation are thought to reflect the ability to adapt to different gait conditions (Bianchi et al., 1998; Martino et al., 2014; Dewolf et al., 2018), such as walking and running (Ivanenko et al., 2007a), the lack of changes observed in toddlers suggest a reduced flexibility of gait (Dominici et al., 2010), and potentially the absence of distinct gait patterns at the onset of independent locomotion.

EMERGENCE OF DIFFERENT MODES OF LOCOMOTION DURING GROWTH

"During the second year of life, toddler's locomotion is neither walking, nor running, but something not yet differentiated"

Bernstein (1947)

First emphasized by Bernstein (1947), the above-considered observations are consistent with the idea that locomotor patterns in infants are immature and lack adaptive features. Indeed, with walking experience, the gait-specific collective variables progressively become close to the values obtained in adults (Whitall and Getchell, 1995). For instance, despite millions of years of bipedal evolution, at the onset of independent walking the pendulum-like mechanism of walking and the bouncing mechanism of running deviate significantly from those of adults (**Figure 6B**) (Ivanenko et al., 2004, 2007b; Legramandi et al., 2013). During running, a flight phase progressively occurs and increases as the vertical push provided by muscles increases with age (Legramandi et al., 2013). These changes with aging are concomitant with an enhancing of the elastic bounce that characterizes adult running gait (Schepens et al., 1998), as the percentage of pendular COM energy exchange decreases (**Figure 6B**). During walking, toddlers at the onset

of unsupported locomotion fail to demonstrate a prominent pendular energy exchange (Cheron et al., 2001; Ivanenko et al., 2004, 2007b) as well as an adult-like heel-to-toe roll-over pattern (**Figure 4**). With walking experience, the hip trajectory and the pendulum-like exchange of energy progressively evolve toward mature values (**Figure 6B**) (Ivanenko et al., 2004; Schepens et al., 2004; Van de Walle et al., 2010). At the same time, the foot-contact pattern shows a trend from initial forefoot to initial heel contact (**Figure 4C**), and the vertical force waveform slowly evolves toward a double-hump shape (**Figure 3**) (Hallemans et al., 2006b).

The gradual evolution of gaits after the onset of independent locomotion supports the idea that the original spinal networks are still used, but that gait-specific neural circuits mature progressively during development. Interestingly, the modification of intralimb coordination, vertical force, and spinal motor pools during walking in elderly adults suggests that aging causes a regression of the locomotor pattern: the ability to adapt the intersegmental coordination to speeds is reduced (Dewolf et al., 2019b), the second apex of the m-pattern progressively decreases (Meurisse et al., 2019), while the burst of sacral motor pools occurs earlier during the step cycle (Monaco et al., 2010). Even if far less attention has been devoted to the development of running skills, running most likely evolves from the same original spinal networks, and also requires maturation and experience. During growth, the older the child, the closer the waveform to the adult. It is interesting to note that, as in walking, these trends slowly reverse during the course of the life (Cavagna et al., 2008).

While the involvement of gait-dependent spinal interneurons has been emphasized above, the lack of evidence for distinct walking and running patterns in infants and the progressive developmental bifurcation between the different forms of gait suggest a sharing of circuitry before the full maturation of the brain and its descending inputs. In humans, the maturation of walking corresponds to maintenance of primitive patterns with superimposition of additional patterns (Dominici et al., 2011; Sylos-Labini, La Scaleia, Cappellini, Fabiano, Picone, Keshishian, 2020), and the maturation of running may also involve fine-tuning and reshaping of these primitive patterns (Cheung et al. under review). In adults, despite diverse biomechanical demands of running and walking, few patterns of muscle activation are also shared (Cappellini et al., 2006; Yokoyama et al., 2016), indirectly supporting a common neural origin for the two gait forms in infancy.

Such maturation is probably a process in which environmental signals act to bring about the characteristics of adult-like walking (Forssberg, 1992). This is supported by the fact that independent stepping acts as a functional trigger of gait maturation (Ivanenko et al., 2004; Yang et al., 2015), and Earth's gravity has a significant impact on early development of motor functions (Cheron et al., 2001; Ivanenko et al., 2007b). It is indeed well-documented that the interaction with the environment influences the development of motor networks. For example, early exposure of animals to altered gravitational field (hypo- or hyper-gravity) affects their mature motor performance (Sondag et al., 1997; Walton, 1998; Wubbels and de Jong, 2000; Walton et al., 2005; Bojados et al., 2013). Of particular interest, hyper-gravity reduces the postnatal development of descending inputs to the spinal cord (Brocard et al., 2003), suggesting that gravity has a critical role to shape the maturation of gait-specific pattern generation circuitries. When adult humans are exposed to microgravity, they start to rely more on skipping (a potential vestigium of gallop) or running gait (Pavei et al., 2015; Lacquaniti et al., 2017). It is therefore plausible that, if humans were even born on the Moon, modification of the chronology of the emergence of gait during development (and even novel locomotor behaviors) would occur, starting from the same inborn motor primitives.

The interactions with the environment that shape the emergence of gait is conceivable, because stepping development in infants highlights strong plasticity. For example, Patrick et al. (2014) showed that the interlimb coordination can be manipulated with a 4-week training, indicating experience-dependent learning at a young age (<10 months). In animals, early motor experience influences the muscle typology (Serradj and Jamon, 2016). Such impact of training procedures suggests that experience is required for normal development of locomotor behavior and that motor output in adults could be optimized by appropriate training during a defined period of motor development (Walton et al., 1992; Muir and Chu, 2002; Serradj and Jamon, 2016). Accordingly, human infants undergoing daily stepping exercise exhibit an earlier onset of independent walk than untrained infants (Zelazo et al., 1972; Yang et al., 1998).

As in animals, it is plausible that the two modes of locomotion and their corresponding neural circuits have different maturation rate. While the running pattern of chicks seems mature earlier in life (Muir et al., 1996), the current coarse picture of the development of running patterns in infants needs to be refined at different developmental stages, providing important insights into the process of skills acquisition. Even if the patterns of innate stepping differs from the efficient running adult gait, several parameters bear a striking resemblance to the mature running patterns (**Figures 3**, **4C**), such as the vertical force, the motoneuron activity of the lumbosacral enlargement, diverse foot contact strategies and knee flexed throughout stance (Yang et al., 2015; Vasudevan et al., 2016; Sylos-Labini et al., 2017). A hypothetical innateness of some features characteristic of adult running is also compatible with the evaluation of the evolution of the human body form. Indeed, Rolian et al. (2009) suggest that the modern human forefoot proportions might be part of a suite of adaptations selected especially for running gait that evolved in the genus Homo around 2 million years ago (Bramble and Lieberman, 2004; Venkadesan, Yawar, Eng, Dias, Singh, Tommasini, 2020). Hypotheses of innate behavior should always be taken in a relative terms, since any behavior is modified by experience (Grillner and Wallén, 2004; Vanden Hole et al., 2017).

CONCLUDING REMARKS

The emergence of adult-like walking and running patterns results from the evolution of multiple subsystems of the developing child, involving both neural and biomechanical

factors (Thelen and Ulrich, 1991). While the locomotor output of stepping neonates has been widely compared to the adult walking, its comparison with adult running patterns needs to be explored further to unravel some of the mysteries surrounding the progressive bifurcation of the locomotor networks at different developmental stages. The delayed onset of running in children may be related to environmental and musculoskeletal factors and a limited ability to adapt to biomechanical constrains in infants (Thelen, 1995). The findings we reviewed in this article point to a partial overlap in the neural and biomechanical control of walking and running in infancy, suggesting that different forms of gait are built starting from common, likely phylogenetically conserved elements.

Gaining insights into the maturation and differentiation of human gaits may also provide important clinical implications. For instance, while the rehabilitative protocols in children with cerebral palsy usually focus on walking training, early running training may also be beneficial, and improve walking gait (Lewis, 2017). Indeed, many studies have examined how children with cerebral palsy manage to walk, but few have investigated running, which may be even more stable than walking in these children (Iosa et al., 2013). There may also be critical developmental windows during which specific experiences have a greater effect on the early developmental process and differentiation of locomotor behaviors than at other times (Ivanenko et al., 2013b; Yang et al., 2013). Taking advantage of newly available biotechnological approaches and techniques (Zhu et al., 2015; Chung et al., 2019; Redd et al., 2019; Xu et al., 2019; Airaksinen et al., 2020) for both advanced neurophysiological pediatric recordings and rehabilitation training in the sensitive period for maturation (e.g., using biofeedback or neuromodulation) would help to diagnose and assess early motor deficits and to determine the activity-based intervention for infants with developmental disorders.

AUTHOR CONTRIBUTIONS

All authors listed have made a substantial, direct and intellectual contribution to the work, and approved it for publication.

FUNDING

This work was supported by the Italian Ministry of Health (Ricerca Corrente, IRCCS Fondazione Santa Lucia), the Italian Space Agency (grant I/006/06/0 and grant 2019-11-U.0) and the Italian University Ministry (PRIN grant 2017C BF8NJ_005).

REFERENCES

Adolph, K. E., Hoch, J. E., and Cole, W. G. (2018). Development (of walking): 15 suggestions. *Trends Cogn. Sci.* 22, 699–711. doi: 10.1016/j.tics.2018.05.010

Adolph, K. E., and Robinson, S. R. (2015). "Motor development," in *Handbook of Child Psychology and Developmental Science: Cognitive Processes*, eds L. S. Liben, U. Müller, and R. M. Lerner (John Wiley & Sons Inc.), 113–157.

Airaksinen, M., Räsänen, O., Ilén, E., Häyrinen, T., Kivi, A., Marchi, V., et al. (2020). Automatic posture and movement tracking of infants with wearable movement sensors. *Sci. Rep*. 10:169. doi: 10.1038/s41598-019-56862-5

Alexander, R. M. (1989). Optimization and gaits in the locomotion of vertebrates. *Physiol. Rev.* 69, 1199–1227. doi: 10.1152/physrev.1989.69.4.1199

Alexander, R. M., and Jayes, A. S. (1980). Fourier analysis of forces exerted in walking and running. *J Biomech* 13, 383–390. doi: 10.1016/0021-9290(80)90019-6

Aoi, S., and Tsuchiya, K. (2006). Bifurcation and chaos of a simple walking model driven by a rhythmic signal. *Int. J. Non Linear Mechan.* 41, 438–446. doi: 10.1016/j.ijnonlinmec.2005.09.001

Ausborn, J., Mahmood, R., and El Manira, A. (2012). Decoding the rules of recruitment of excitatory interneurons in the adult zebrafish locomotor network. *Proc. Natl. Acad. Sci. U.S.A.* 109, E3631–E3639. doi: 10.1073/pnas.1216256110

Ausborn, J., Snyder, A. C., Shevtsova, N. A., Rybak, I. A., and Rubin, J. E. (2018). State-dependent rhythmogenesis and frequency control in a half-center locomotor CPG. *J. Neurophysiol.* 119, 96–117. doi: 10.1152/jn.00550.2017

Bäckman, E., Odenrick, P., Henriksson, K. G., and Ledin, T. (1989). Isometric muscle force and anthropometric values in normal children aged between 3.5 and 15 years. *Scand. J. Rehabil. Med.* 21, 105–114

Barliya, A., Omlor, L., Giese, M. A., and Flash, T. (2009). An analytical formulation of the law of intersegmental coordination during human locomotion. *Exp. Brain Res.* 193, 371–385. doi: 10.1007/s00221-008-1633-0

Bernstein, N. A. (1947). *O Postroenii Dvizhenii (On the Construction of Movements, in Russian)*. Moscow: Medgriz.

Bertsch, C., Unger, H., Winkelmann, W., and Rosenbaum, D. (2004). Evaluation of early walking patterns from plantar pressure distribution measurements. First year results of 42 children. *Gait. Posture* 19, 235–242. doi: 10.1016/S0966-6362(03)00064-X

Bianchi, L., Angelini, D., Orani, G. P., and Lacquaniti, F. (1998). Kinematic coordination in human gait: relation to mechanical energy cost. *J. Neurophysiol.* 79, 2155–2170

Bojados, M., Herbin, M.arc., and Jamon, M. (2013). Kinematics of treadmill locomotion in mice raised in hypergravity. *Behav. Brain Res.* 244, 48–57. doi: 10.1016/j.bbr.2013.01.017

Borghese, N. A., Bianchi, L., and Lacquaniti, F. (1996). Kinematic determinants of human locomotion. *J. Physiol. 494,* 863–879

Bosch, K., Gerss, J., and Rosenbaum, D. (2007). Preliminary normative values for foot loading parameters of the developing child. *Gait. Posture* 26, 238–247. doi: 10.1016/j.gaitpost.2006.09.014

Bramble, D. M., and Lieberman, D. E. (2004). Endurance running and the evolution of Homo. *Nature* 432, 345–352. doi: 10.1038/nature03052

Brocard, F., Clarac, F., and Vinay, L. (2003). Gravity influences the development of inputs from the brain to lumbar motoneurons in the rat. *Neuroreport* 14, 1697–1700. doi: 10.1097/00001756-200309150-00008

Brody, B. A., Kinney, H. C., Kloman, A. S., and Gilles, F. H. (1987). Sequence of central nervous system myelination in human infancy. *I.* an *autopsy study of myelination. J. Neuropathol. Exp. Neurol.* 46, 283–301. doi: 10.1097/00005072-198705000-00005

Buller, A. J., Eccles, J. C., and Eccles, R. M. (1960). Differentiation of fast and slow muscles in the cat hind limb. *J. Physiol.* 150, 399–416.

Büschges, A., Schmitz, J., and Bässler, U. (1995). Rhythmic patterns in the thoracic nerve cord of the stick insect induced by *pilocarpine*. *J. Exp. Biol.* 198, 435–456.

Caggiano, V., Cheung, V. C. K., and Bizzi, E. (2016). An optogenetic demonstration of motor modularity in the mammalian spinal cord. *Sci. Rep.* 6:35185. doi: 10.1038/srep35185

Cappellini, G., Ivanenko, Y. P., Dominici, N., Poppele, R. E., and Lacquaniti, F. (2010). Migration of motor pool activity in the spinal cord reflects body mechanics in human locomotion. *J. Neurophysiol.* 104, 3064–3073. doi: 10.1152/jn.00318.2010

Cappellini, G., Ivanenko, Y. P., Martino, G., MacLellan, M. J., Sacco, A., Morelli, D., et al. (2016). Immature spinal locomotor output in

children with cerebral palsy. *Front. Physiol.* 7:478. doi: 10.3389/fphys.2016.00478

Cappellini, G., Ivanenko, Y. P., Poppele, R. E., and Lacquaniti, F. (2006). Motor patterns in human walking and running. *J. Neurophysiol.* 95, 3426–3437

Catavitello, G., Ivanenko, Y. P., and Lacquaniti, F. (2015). Planar covariation of hindlimb and forelimb elevation angles during terrestrial and aquatic locomotion of dogs. *PLoS ONE.* 10:e0133936. doi: 10.1371/journal.pone.0133936

Cavagna, G. A., Franzetti, P., and Fuchimoto, T. (1983). The mechanics of walking in children. *J. Physiol. 343*, 323–339.

Cavagna, G. A., Franzetti, P., Heglund, N. C., and Willems, P. (1988). The determinants of the step frequency in running, trotting and hopping in man and other vertebrates. *J. Physiol. 399*, 81–92.

Cavagna, G. A., Legramandi, M. A., and Peyré-Tartaruga, L. A. (2008). Old men running: mechanical work and elastic bounce. *Proc. R. Soc. B* 275, 411–418. doi: 10.1098/rspb.2007.1288

Cepeda-Nieto, A. C., Pfaff, S. L., and Varela-Echavarría, A. (2005). Homeodomain transcription factors in the development of subsets of hindbrain reticulospinal neurons. *Mol. Cell. Neurosci.* 28, 30–41. doi: 10.1016/j.mcn.2004.06.016

Cheron, G., Bouillot, E., Dan, B., Bengoetxea, A., Draye, J. P., and Lacquaniti, F. (2001). Development of a kinematic coordination pattern in toddler locomotion: planar covariation. *Exp. Brain Res.* 137, 455–466. doi: 10.1007/s002210000663

Chung, H. U., Kim, B. H., Lee, J. Y., Lee, J., Xie, Z., Ibler, E. M., et al. (2019). Binodal, wireless epidermal electronic systems with in-sensor analytics for neonatal intensive care. *Science* 363:eaau0780. doi: 10.1126/science.aau0780

Clark, J. E., Whitall, J., and Phillips, S. J. (1988). Human interlimb coordination: the first 6 months of independent walking. *Dev. Psychobiol.* 21, 445–456. doi: 10.1002/dev.420210504

Combes, D., Merrywest, S. D., Simmers, J., and Sillar, K. T. (2004). Developmental segregation of spinal networks driving axial- and hindlimb-based locomotion in metamorphosing Xenopus laevis. *J. Physiol.* 559, 17–24. doi: 10.1113/jphysiol.2004.069542

Cowgill, L. W., Warrener, A., Pontzer, H., and Ocobock, C. (2010). Waddling and toddling: the biomechanical effects of an immature gait. *Am. J. Phys. Anthropol.* 143, 52–61. doi: 10.1002/ajpa.21289

Danner, S. M., Shevtsova, N. A., Frigon, A., and Rybak, I. A. (2017). Computational modeling of spinal circuits controlling limb coordination and gaits in quadrupeds. *Elife* 6:e31050. doi: 10.7554/eLife.31050

Dayanidhi, S., Kutch, J. J., and Valero-Cuevas, F. J. (2013). Decrease in muscle contraction time complements neural maturation in the development of dynamic manipulation. *J. Neurosci.* 33, 15050–15055. doi: 10.1523/JNEUROSCI.1968-13.2013

De Smet, K., Malcolm, P., Lenoir, M., Segers, V., and De Clercq, D. (2009). Effects of optic flow on spontaneous overground walk-to-run transition. *Exp. Brain Res.* 193, 501–508. doi: 10.1007/s00221-008-1648-6

Denny-Brown, D. E., and Sherrington, C. S. (1929). The histological features of striped muscle in relation to its functional activity. *Proc. R. Soc. London. Series B* 104, 371–411. doi: 10.1098/rspb.1929.0014

Deska-Gauthier, D., and Zhang, Y. (2019). The functional diversity of spinal interneurons and locomotor control. *Curr. Opin. Physiol.* 8, 99–108. doi: 10.1016/j.cophys.2019.01.005

Dewolf, A. H., Ivanenko, Y., Zelik, K. E., Lacquaniti, F., and Willems, P. A. (2018). Kinematic patterns while walking on a slope at different speeds. *J. Appl. Physiol.* 125, 642–653. doi: 10.1152/japplphysiol.01020.2017

Dewolf, A. H., Ivanenko, Y. P., Zelik, K. E., Lacquaniti, F., and Willems, P. A. (2019a). Differential activation of lumbar and sacral motor pools during walking at different speeds and slopes. *J. Neurophysiol.* 122, 872–887. doi: 10.1152/jn.00167.2019

Dewolf, A. H., Meurisse, G. M., Schepens, B., and Willems, P. A. (2019b). Effect of walking speed on the intersegmental coordination of lower-limb segments in elderly adults. *Gait. Posture* 70, 156–161. doi: 10.1016/j.gaitpost.2019.03.001

Dewolf, A. H., Peñailillo, L. E., and Willems, P. A. (2016). The rebound of the body during uphill and downhill running at different speeds. *J. Exp. Biol.* 219, 2276–2288. doi: 10.1242/jeb.142976

Dominici, N., Ivanenko, Y. P., Cappellini, G., d'Avella, A., Mondì, V., Cicchese, M., et al. (2011). Locomotor primitives in newborn babies and their development. *Science* 334, 997–999. doi: 10.1126/science.1210617

Dominici, N., Ivanenko, Y. P., Cappellini, G., Zampagni, M. L., and Lacquaniti, F. (2010). Kinematic strategies in newly walking toddlers stepping over different support surfaces. *J. Neurophysiol.* 103, 1673–1684. doi: 10.1152/jn.00945.2009

Dominici, N., Ivanenko, Y. P., and Lacquaniti, F. (2007). Control of foot trajectory in walking toddlers: adaptation to load changes. *J. Neurophysiol.* 97, 2790–2801. doi: 10.1152/jn.00262.2006

Drew, T. (1988). Motor cortical cell discharge during voluntary gait modification. *Brain Res.* 457, 181–187. doi: 10.1016/0006-8993(88)90073-X

Drew, T., Prentice, S., and Schepens, B. (2004). Cortical and brainstem control of locomotion. *Prog. Brain Res.* 143, 251–261. doi: 10.1016/S0079-6123(03)43025-2

Druelle, F., Aerts, P., and Berillon, G. (2016). Effect of body mass distribution on the ontogeny of positional behaviors in non-human primates: Longitudinal follow-up of infant captive olive baboons (Papio anubis). *Am. J. Primatol.* 78, 1201–1221. doi: 10.1002/ajp.22575

Duysens, J., De Groote, F., and Jonkers, I. (2013). The flexion synergy, mother of all synergies and father of new models of gait. *Front. Comput. Neurosci.* 7:14. doi: 10.3389/fncom.2013.00014

Fetcho, J. R., and McLean, D. L. (2010). Some principles of organization of spinal neurons underlying locomotion in zebrafish and their implications. *Ann. N.Y. Acad. Sci.* 1198, 94–104. doi: 10.1111/j.1749-6632.2010.05539.x

Forma, V., Anderson, D. I., Provasi, J., Soyez, E., Martial, M., Huet, V., et al. (2019). What does prone skateboarding in the newborn tell us about the ontogeny of human locomotion? *Child. Dev.* 90, 1286–1302. doi: 10.1111/cdev.13251

Forssberg, H. (1985). Ontogeny of human locomotor control. I. Infant stepping, supported locomotion and transition to independent locomotion. *Exp. Brain Res.* 57, 480–493.

Forssberg, H. (1992). Evolution of plantigrade gait: is there a neuronal correlate? *Dev. Med. Child Neurol.* 34, 920–925. doi: 10.1111/j.1469-8749.1992.tb11391.x

Fukuyama, H., Ouchi, Y., Matsuzaki, S., Nagahama, Y., Yamauchi, H., Ogawa, M., et al. (1997). Brain functional activity during gait in normal subjects: a SPECT study. *Neurosci. Lett.* 228, 183–186. doi: 10.1016/S0304-3940(97)00381-9

Ganley, K. J., Stock, A., Herman, R. M., Santello, M., and Willis, W. T. (2011). Fuel oxidation at the walk-to-run-transition in humans. *Metabolism* 60, 609–616. doi: 10.1016/j.metabol.2010.06.007

Garwicz, M., Christensson, M., and Psouni, E. (2009). A unifying model for timing of walking onset in humans and other mammals. *Proc. Natl. Acad. Sci. U.S.A.* 106, 21889–21893. doi: 10.1073/pnas.0905777106

Giszter, S. F., Hart, C. B., and Silfies, S. P. (2010). Spinal cord modularity: evolution, development, and optimization and the possible relevance to low back pain in man. *Exp. Brain Res.* 200, 283–306. doi: 10.1007/s00221-009-2016-x

Gould, N., Moreland, M., Alvarez, R., Trevino, S., and Fenwick, J. (1989). Development of the child's arch. *Foot Ankle.* 9, 241–245. doi: 10.1177/107110078900900506

Grillner, S. (1981). "Control of locomotion in bipeds, tetrapods and fish," in *Handbook of Physiology: Section 1: The Nervous System,* Vol. 2*, Part.1 Motor Control*, eds B. Vernon, J. M. Brookhart, and V. B. Mountcastle (Bethesda, MD: Brooks), 1179–1236.

Grillner, S., and El Manira, A. (2020). Current principles of motor control, with special reference to vertebrate locomotion. *Physiol. Rev.* 100, 271–320. doi: 10.1152/physrev.00015.2019

Grillner, S., and Jessell, T. (2009). Measured Motion: Searching for Simplicity in Spinal Locomotor Networks. *Curr. Opin. Neurobiol.* 19, 572–586. doi: 10.1016/j.conb.2009.10.011

Grillner, S., and Wallén, P. (2004). Innate versus learned movements–a false dichotomy? *Prog. Brain Res.* 143, 3–12. doi: 10.1016/s0079-6123(03)43001-x

Hallemans, A., De Clercq, D., and Aerts, P. (2006a). Changes in 3D joint dynamics during the first 5 months after the onset of independent walking: a longitudinal follow-up study. *Gait. Posture* 24, 270–279. doi: 10.1016/j.gaitpost.2005.10.003

Hallemans, A., De Clercq, D., Van Dongen, S., and Aerts, P. (2006b). Changes in foot-function parameters during the first 5 months after the onset of independent walking: a longitudinal follow-up study. *Gait. Posture* 23, 142–148. doi: 10.1016/j.gaitpost.2005.01.003

Hatsopoulos, N. G. (1996). Coupling the neural and physical dynamics in rhythmic movements. *Neural Comput.* 8, 567–581. doi: 10.1162/neco.1996.8.3.567

Holowka, N. B., and Lieberman, D. E. (2018). Rethinking the evolution of the human foot: insights from experimental research. *J. Exp. Biol.* 221. doi: 10.1242/jeb.174425

Hubel, T. Y., and Usherwood, J. R. (2015). Children and adults minimise activated muscle volume by selecting gait parameters that balance gross mechanical power and work demands. *J. Exp. Biol.* 218, 2830–2839. doi: 10.1242/jeb.122135

Iosa, M., Morelli, D., Marro, T., Paolucci, S., and Fusco, A. (2013). Ability and stability of running and walking in children with cerebral palsy. *Neuropediatrics* 44, 147–154. doi: 10.1055/s-0033-1336016

Ivanenko, Y. P., Cappellini, G., Dominici, N., Poppele, R. E., and Lacquaniti, F. (2007a). Modular control of limb movements during human locomotion. *J. Neurosci.* 27, 11149–11161. doi: 10.1523/JNEUROSCI.2644-07.2007

Ivanenko, Y. P., Cappellini, G., Poppele, R. E., and Lacquaniti, F. (2008a). Spatiotemporal organization of alpha-motoneuron activity in the human spinal cord during different gaits and gait transitions. *Eur. J. Neurosci.* 27, 3351–3368. doi: 10.1111/j.1460-9568.2008.06289.x

Ivanenko, Y. P., d'Avella, A., Poppele, R. E., and Lacquaniti, F. (2008b). On the origin of planar covariation of elevation angles during human locomotion. *J. Neurophysiol.* 99, 1890–1898. doi: 10.1152/jn.01308.2007

Ivanenko, Y. P., Dominici, N., Cappellini, G., Dan, B., Cheron, G., and Lacquaniti, F. (2004). Development of pendulum mechanism and kinematic coordination from the first unsupported steps in toddlers. *J. Exp. Biol.* 207, 3797–3810. doi: 10.1242/jeb.01214

Ivanenko, Y. P., Dominici, N., Cappellini, G., Paolo, A. D., Giannini, C., Poppele, R. E., et al. (2013a). Changes in the spinal segmental motor output for stepping during development from infant to adult. *J. Neurosci.* 33, 3025–3036. doi: 10.1523/JNEUROSCI.2722-12.2013

Ivanenko, Y. P., Dominici, N., and Lacquaniti, F. (2007b). Development of independent walking in toddlers. *Exerc. Sport Sci. Rev.* 35, 67–73. doi: 10.1249/JES.0b013e31803eafa8

Ivanenko, Y. P., Grasso, R., Macellari, V., and Lacquaniti, F. (2002). Control of foot trajectory in human locomotion: role of ground contact forces in simulated reduced gravity. *J. Neurophysiol.* 87, 3070–3089. doi: 10.1152/jn.2002.87.6.3070

Ivanenko, Y. P., Sylos Labini, F., Cappellini, G., Macellari, V., McIntyre, J., and Lacquaniti, F. (2011). Gait transitions in simulated reduced gravity. *J. Appl. Physiol.* 110, 781–788. doi: 10.1152/japplphysiol.00799.2010

Ivanenko, Y. P., Wright, W. G., St George, R. J., and Gurfinkel, V. S. (2013b). Trunk orientation, stability, and quadrupedalism. *Front. Neurol.* 4:20. doi: 10.3389/fneur.2013.00020

Jahn, K., Deutschländer, A., Stephan, T., Kalla, R., Hüfner, K., Wagner, J., et al. (2008). Supraspinal locomotor control in quadrupeds and humans. *Prog. Brain Res.* 171 353–362. doi: 10.1016/S0079-6123(08)0 06523

Kao, J. C., Payne, V. G., Thomas, J. R., Martin, P. E., and Ringenbach, S. (2000). Intralimb coordination during walking and running. *J.Hum. Movement Stud.* 39, 105–113

Kelly, L. A., Cresswell, A. G., and Farris, D. J. (2018). The energetic behaviour of the human foot across a range of running speeds. *Sci. Rep.* 8:10576. doi: 10.1038/s41598-018-28946-1

Kiehn, O. (2016). Decoding the organization of spinal circuits that control locomotion. *Nat. Rev. Neurosci.* 17, 224–238. doi: 10.1038/nrn.2016.9

Kinney, H. C., and Volpe, J. J. (2018). "Chapter 8 - myelination events," in Volpe's Neurology of the Newborn, 6th edn, eds J. J. Volpe, T. E. Inder, B. T. Darras, L. S. de Vries, A. J. du Plessis, J. J. Neil, and J. M. Perlman (Amsterdam: Elsevier), 176–188.

La Scaleia, V., Ivanenko, Y., Fabiano, A., Sylos-Labini, F., Cappellini, G., Picone, S., et al. (2018). Early manifestation of arm-leg coordination during stepping on a surface in human neonates. *Exp. Brain Res.* 236, 1105–1115. doi: 10.1007/s00221-018-5201-y

La Scaleia, V., Ivanenko, Y. P., Zelik, K. E., and Lacquaniti, F. (2014). Spinal motor outputs during step-to-step transitions of diverse human gaits. *Front. Hum Neurosci.* 8:305. doi: 10.3389/fnhum.2014.00305

Lacquaniti, F., Grasso, R., and Zago, M. (1999). Motor patterns in walking. *Physiology* 14, 168–174.

Lacquaniti, F., Ivanenko, Y. P., Sylos-Labini, F., La Scaleia, V., La Scaleia, B., Willems, P. A., et al. (2017). Human locomotion in hypogravity: from basic research to clinical applications. *Front. Physiol.* 8:893. doi: 10.3389/fphys.2017.00893

Lacquaniti, F., Ivanenko, Y. P., and Zago, M. (2002). Kinematic control of walking. *Arch. Ital. Biol.* 140, 263−272. doi: 10.4449/aib.v140i4.485

Lacquaniti, F., Ivanenko, Y. P., and Zago, M. (2012). Patterned control of human locomotion. *J. Physiol.* 590, 2189–2199. doi: 10.1113/jphysiol.2011.215137

Lafreniere-Roula, M., and McCrea, D. A. (2005). Deletions of rhythmic motoneuron activity during fictive locomotion and scratch provide clues to the organization of the mammalian central pattern generator. *J. Neurophysiol.* 94, 1120–1132. doi: 10.1152/jn.00216.2005

Larson, P. (2014). Comparison of foot strike patterns of barefoot and minimally shod runners in a recreational road race. *J. Sport Health Sci.* 3, 137–142. doi: 10.1016/j.jshs.2014.03.003

Legramandi, M. A., Schepens, B., and Cavagna, G. A. (2013). Running humans attain optimal elastic bounce in their teens. *Sci. Rep.* 3:1310. doi: 10.1038/srep01310

Lewis, J. (2017). A Progressive running program for an adolescent with cerebral palsy. *Pediatr. Phys. Ther.* 29, E12–E16. doi: 10.1097/PEP.0000000000000429

Leyton, A. S. F., and Sherrington, C. S. (1917). Observations on the excitable cortex of the chimpanzee, orang-utan, and gorilla. *Quart. J. Exp. Physiol.* 11, 135–222. doi: 10.1113/expphysiol.1917.sp000240

Maier, E. (1961). [Longitudinal measurement research on the maturation of the child's foot]. *Monatsschr. Kinderheilkd.* 109, 222–226.

Martino, G., Ivanenko, Y. P., Serrao, M., Ranavolo, A., d'Avella, A., Draicchio, F., et al. (2014). Locomotor patterns in cerebellar ataxia. *J. Neurophysiol.* 112, 2810–2821. doi: 10.1152/jn.00275.2014

Matsushima, T., and Grillner, S. (1992). Neural mechanisms of intersegmental coordination in lamprey: local excitability changes modify the phase coupling along the spinal cord. *J. Neurophys.* 67, 373–388. doi: 10.1152/jn.1992.67.2.373

McCrea, D. A., and Rybak, I. A. (2008). Organization of mammalian locomotor rhythm and pattern generation. *Brain Res. Rev.* 57, 134–146. doi: 10.1016/j.brainresrev.2007.08.006

McGraw, M. B. (1939). Swimming behavior of the human infant. *J. Pediatr.* 15, 485–490. doi: 10.1016/S0022-3476(39)80003-8

McLean, D. L., Masino, M. A., Koh, I. Y. Y., Lindquist, W. B., and Fetcho, J. R. (2008). Continuous shifts in the active set of spinal interneurons during changes in locomotor speed. *Nat. Neurosci.* 11, 1419–1429. doi: 10.1038/nn.2225

Meurisse, G. M., Bastien, G. J., and Schepens, B. (2019). Effect of age and speed on the step-to-step transition phase during walking. *J. Biomechan.* 83, 253–259. doi: 10.1016/j.jbiomech.2018.12.001

Minassian, K., Hofstoetter, U. S., Dzeladini, F., Guertin, P. A., and Ijspeert, A. (2017). The human central pattern generator for locomotion: does it exist and contribute to walking? *Neuroscientist* 23, 649–663. doi: 10.1177/1073858417699790

Minetti, A. E. (1998). The biomechanics of skipping gaits: a third locomotion paradigm? *Proc. Biol. Sci.* 265, 1227–1235. doi: 10.1098/rspb.199 8.0424

Monaco, V., Ghionzoli, A., and Micera, S. (2010). Age-related modifications of muscle synergies and spinal cord activity during locomotion. *J. Neurophysiol.* 104, 2092–2102. doi: 10.1152/jn.00525.2009

Muir, G. D., and Chu, T. K. (2002). Posthatching locomotor experience alters locomotor development in chicks. *J. Neurophys.* 88, 117–123. doi: 10.1152/jn.2002.88.1.117

Muir, G. D., Gosline, J. M., and Steeves, J. D. (1996). Ontogeny of bipedal locomotion: walking and running in the chick. *J. Physiol.* 493, 589–601

Nilsson, J., and Thorstensson, A. (1989). Ground reaction forces at different speeds of human walking and running. *Acta Physiol. Scand.* 136, 217–227. doi: 10.1111/j.1748-1716.1989.tb08655.x

Ogawa, T., Kawashima, N., Obata, H., Kanosue, K., and Nakazawa, K. (2015). Mode-dependent control of human walking and running as revealed by split-belt locomotor adaptation. *J. Exp. Biol.* 218, 3192–3198. doi: 10.1242/jeb.120865

Ogawa, T., Kawashima, N., Ogata, T., and Nakazawa, K. (2012). Limited transfer of newly acquired movement patterns across walking and running in humans. *PLoS ONE* 7:e46349. doi: 10.1371/journal.pone.0046349

Okamoto, T., Okamoto, K., and Andrew, P. D. (2003). Electromyographic developmental changes in one individual from newborn stepping to mature walking. *Gait. Posture* 17, 18–27. doi: 10.1016/s0966-6362(02)00049-8

Patrick, S., Noah, J., and Yang, J. (2012). Developmental constraints of quadrupedal coordination across crawling styles in human infants. *J Neurophysiol.* 107, 3050–3061. doi: 10.1152/jn.00029.2012

Patrick, S. K., Musselman, K. E., Tajino, J., Ou, H.-C., Bastian, A. J., and Yang, J. F. (2014). Prior experience but not size of error improves motor learning on the split-belt treadmill in young children. *PLoS ONE* 9:e93349. doi: 10.1371/journal.pone.0093349

Pavei, G., Biancardi, C. M., and Minetti, A. E. (2015). Skipping vs. running as the bipedal gait of choice in hypogravity. *J. Appl. Physiol.* 119, 93–100. doi: 10.1152/japplphysiol.01021.2014

Petersen, T. H., Kliim-Due, M., Farmer, S. F., and Nielsen, J. B. (2010). Childhood development of common drive to a human leg muscle during ankle dorsiflexion and gait. *J. Physiol.* 588, 4387–4400. doi: 10.1113/jphysiol.2010.195735

Price, C., Morrison, S. C., Hashmi, F., Phethean, J., and Nester, C. (2018). Biomechanics of the infant foot during the transition to independent walking: a narrative review. *Gait. Posture* 59, 140–146. doi: 10.1016/j.gaitpost.2017.09.005

Raichlen, D. A., Gordon, A. D., Foster, A. D., Webber, J. T., Sukhdeo, S. M., Scott, R. S., et al. (2015). An ontogenetic framework linking locomotion and trabecular bone architecture with applications for reconstructing hominin life history. *J. Hum. Evol.* 81, 1–12. doi: 10.1016/j.jhevol.2015.01.003

Rauscent, A., Le Ray, D., Cabirol-Pol, M.-J., Sillar, K. T., Simmers, J., and Combes, D. (2006). Development and neuromodulation of spinal locomotor networks in the metamorphosing frog. *J. Physiol.* 100, 317–327. doi: 10.1016/j.jphysparis.2007.05.009

Raynor, A. J., Yi, C. J., Abernethy, B., and Jong, Q. J. (2002). Are transitions in human gait determined by mechanical, kinetic or energetic factors? *Hum. Movement Sci.* 21, 785–805. doi: 10.1016/S0167-9457(02)00180-X

Redd, C. B., Barber, L. A., Boyd, R. N., Varnfield, M., and Karunanithi, M. K. (2019). Development of a wearable sensor network for quantification of infant general movements for the diagnosis of cerebral palsy. *Conf. Proc. IEEE Eng. Med. Biol. Soc.* 2019, 7134–7139. doi: 10.1109/EMBC.2019.8857377

Richardson, E. J. (1982). "Myelination in the human central nervous system," in *Histology and histopathology of the nervous system,* eds W. Haymaker, R. D. Adams (*Springfield, IL): Thomas),* 146–73

Rolian, C., Lieberman, D. E., Hamill, J., Scott, J. W., and Werbel, W. (2009). Walking, running and the evolution of short toes in humans. *J. Exp. Biol.* 212, 713–721. doi: 10.1242/jeb.019885

Rybak, I. A., Dougherty, K. J., and Shevtsova, N. A. (2015). Organization of the mammalian locomotor cpg: review of computational model and circuit architectures based on genetically identified spinal interneurons(1,2,3). *eNeuro* 2:0069-15. doi: 10.1523/ENEURO.0069-15.2015

Saibene, F., and Minetti, A. E. (2003). Biomechanical and physiological aspects of legged locomotion in humans. *Eur. J. Appl. Physiol.* 88, 297–316. doi: 10.1007/s00421-002-0654-9

Santuz, A., Brüll, L., Ekizos, A., Schroll, A., Eckardt, N., Kibele, A., et al. (2019). Neuromotor dynamics of human locomotion in challenging settings. *iScience* 23:100796. doi: 10.1016/j.isci.2019.100796

Schepens, B., Bastien, G. J., Heglund, N. C., and Willems, P. A. (2004). Mechanical work and muscular efficiency in walking children. *J. Exp. Biol.* 207, 587–596. doi: 10.1242/jeb.00793

Schepens, B., Willems, P. A., and Cavagna, G. A. (1998). The mechanics of running in children. *J. Physiol.* 509, 927–940. doi: 10.1111/j.1469-7793.1998.927bm.x

Segers, V., Smet, K. D., Caekenberghe, I. V., Aerts, P., and Clercq, D. D. (2013). Biomechanics of spontaneous overground walk-to-run transition. *J. Exp. Biol.* 216, 3047–3054. doi: 10.1242/jeb.087015

Serradj, N., and Jamon, M. (2016). Postnatal training of 129/Sv mice confirms the long-term influence of early exercising on the motor properties of mice. *Behav. Brain Res.* 310, 126–134. doi: 10.1016/j.bbr.2016.04.035

Shefelbine, S. J., Tardieu, C., and Carter, D. R. (2002). Development of the femoral bicondylar angle in hominid bipedalism. *Bone* 30, 765–770. doi: 10.1016/S8756-3282(02)00700-7

Shevtsova, N. A., and Rybak, I. A. (2016). Organization of flexor-extensor interactions in the mammalian spinal cord: insights from computational modelling. *J. Physiol.* 594, 6117–6131. doi: 10.1113/JP272437

Shik, M. L., and Orlovsky, G. N. (1976). Neurophysiology of locomotor automatism. *Physiol. Rev.* 56, 465–501.

Shik, M. L., Severin, F. V., and Orlovski,i, G. N. (1966). Control of walking and running by means of electric stimulation of the midbrain. *Biofizika* 11, 659–666.

Sondag, H. N., de Jong, H. A., and Oosterveld, W. J. (1997). Altered Behaviour in Hamsters Conceived and Born in Hypergravity. *Brain Res. Bull.* 43, 289–294. doi: 10.1016/S0361-9230(97)00008-7

Suzuki, M., Miyai, I., Ono, T., Oda, I., Konishi, I., Kochiyama, T., et al. (2004). Prefrontal and premotor cortices are involved in adapting walking and running speed on the treadmill: an optical imaging study. *NeuroImage* 23, 1020–1026. doi: 10.1016/j.neuroimage.2004.07.002

Sylos-Labini, F., Ivanenko, Y. P., Cappellini, G., Gravano, S., and Lacquaniti, F. (2011). Smooth changes in the EMG patterns during gait transitions under body weight unloading. *J. Neurophysiol.* 106, 1525–1536. doi: 10.1152/jn.00160.2011

Sylos-Labini, F., La Scaleia, V., Cappellini, G., Fabiano, A., Picone, S., Keshishian, E. S., et al. (2020). Distinct locomotor precursors in newborn babies. *Proc. Natl. Acad. Sci. U.S.A.* 117, 9604–9612. doi: 10.1073/pnas.1920984117

Sylos-Labini, F., Magnani, S., Cappellini, G., La Scaleia, V., Fabiano, A., Picone, S., et al. (2017). Foot Placement Characteristics and Plantar Pressure Distribution Patterns during Stepping on Ground in Neonates. *Front. Physiol.* 8:784. doi: 10.3389/fphys.2017.00784

Taga, G. (1995). A model of the neuro-musculo-skeletal system for human locomotion. *II Real-time adaptability under various constraints. Biol. Cybern.* 73, 113–121. doi: 10.1007/bf00204049

Takei, T., Confais, J., Tomatsu, S., Oya, T., and Seki, K. (2017). Neural basis for hand muscle synergies in the primate spinal cord. *Proc. Natl. Acad. Sci. U.S.A.* 114, 8643–8648. doi: 10.1073/pnas.1704328114

Teulier, C., Sansom, J. K., Muraszko, K., and Ulrich, B. D. (2012). Longitudinal changes in muscle activity during infants' treadmill stepping. *J. Neurophys.* 108, 853–862. doi: 10.1152/jn.01037.2011

Thelen, E. (1995). Motor development: a new synthesis. *Am. Psychol.* 50, 79–95. doi: 10.1037/0003-066X.50.2.79

Thelen, E., and Cooke, D. W. (1987). Relationship between newborn stepping and later walking: a new interpretation. *Dev. Med. Child. Neurol.* 29, 380–393

Thelen, E., and Ulrich, B. D. (1991). Hidden skills: a dynamic systems analysis of treadmill stepping during the first year. *Monogr. Soc. Res. Child. Dev. 56, 1–98*

Van Caekenberghe, I., De Smet, K., Segers, V., and De Clercq, D. (2010). Overground vs. *treadmill walk-to-run transition. Gait. Posture* 31, 420–428. doi: 10.1016/j.gaitpost.2010.01.011

Van de Walle, P., Desloovere, K., Truijen, S., Gosselink, R., Aerts, P., and Hallemans, A. (2010). Age-related changes in mechanical and metabolic energy during typical gait. *Gait. Posture* 31, 495–501. doi: 10.1016/j.gaitpost.2010.02.008

Vanden Hole, C., Goyens, J., Prims, S., Fransen, E., Ayuso Hernando, M., Van Cruchten, S., et al. (2017). How innate is locomotion in precocial animals? A study on the early development of spatio-temporal gait variables and gait symmetry in piglets. *J. Exp. Biol.* 220, 2706–2716. doi: 10.1242/jeb.157693

Vasudevan, E. V., Patrick, S. K., and Yang, J. F. (2016). Gait transitions in human infants: coping with extremes of treadmill speed. *PLoS ONE.* 11:e0148124. doi: 10.1371/journal.pone.0148124

Vasudevan, E. V. L., and Bastian, A. J. (2010). Split-Belt treadmill adaptation shows different functional networks for fast and slow human walking. *J. Neurophysiol.* 103, 183–191. doi: 10.1152/jn.00501.2009

Venkadesan, M., Yawar, A., Eng, C. M., Dias, M. A., Singh, D. K., Tommasini, S. M., et al. (2020). Stiffness of the human foot and evolution of the transverse arch. *Nature* 579, 97–100. doi: 10.1038/s41586-020-2053-y

Wager, J. C., and Challis, J. H. (2016). Elastic energy within the human plantar aponeurosis contributes to arch shortening during the push-off phase of running. *J. Biomech.* 49, 704–709. doi: 10.1016/j.jbiomech.2016.02.023

Walton, K. (1998). Postnatal development under conditions of simulated weightlessness and space flight. *Brain Res. Rev.* 28, 25–34. doi: 10.1016/S0165-0173(98)00023-X

Walton, K. D., Harding, S., Anschel, D., Harris, Y. T., and Llinás, R. (2005). The effects of microgravity on the development of surface righting in rats. *J. Physiol.* 565, 593–608. doi: 10.1113/jphysiol.2004.074385

Walton, K. D., Lieberman, D., Llinás, A., Begin, M., and Llinás, R. R. (1992). Identification of a critical period for motor development in neonatal rats. *Neuroscience* 51, 763–767. doi: 10.1016/0306-4522(92)90517-6

Whitall, J., and Getchell, N. (1995). From walking to running: applying a dynamical systems approach to the development of locomotor skills. *Child Dev.* 66, 1541–1553

Wubbels, R. J., and de Jong, H. A. A. (2000). Vestibular-induced behaviour of rats born and raised in hypergravity. *Brain Res. Bull.* 52, 349–356. doi: 10.1016/S0361-9230(00)00279-3

Xu, S., Jayaraman, A., and Rogers, J. A. (2019). Skin sensors are the future of health care. *Nature* 571, 319–321. doi: 10.1038/d41586-019-02143-0

Yang, J. F., and Gorassini, M. (2006). Spinal and brain control of human walking: Implications for retraining of walking. *Neuroscientist* 12, 379–389. doi: 10.1177/1073858406292151

Yang, J. F., Livingstone, D., Brunton, K., Kim, D., Lopetinsky, B., Roy, F., et al. (2013). Training to enhance walking in children with cerebral palsy: are we missing the window of opportunity? *Semin. Pediatr. Neurol.* 20, 106–115. doi: 10.1016/j.spen.2013.06.011

Yang, J. F., Mitton, M., Musselman, K. E., Patrick, S. K., and Tajino, J. (2015). Characteristics of the developing human locomotor system: similarities to other mammals. *Dev. Psychobiol.* 57, 397–408. doi: 10.1002/dev.21289

Yang, J. F., Stephens, M. J., and Vishram, R. (1998). Infant stepping: a method to study the sensory control of human walking. *J. Physiol. 507*, 927–937

Yokoyama, H., Ogawa, T., Kawashima, N., Shinya, M., and Nakazawa, K. (2016). Distinct sets of locomotor modules control the speed and modes of human locomotion. *Sci. Rep.* 6:36275. doi: 10.1038/srep36275

Yokoyama, H., Ogawa, T., Shinya, M., Kawashima, N., and Nakazawa, K. (2017). Speed dependency in α-motoneuron activity and locomotor modules in human locomotion: indirect evidence for phylogenetically conserved spinal circuits. *Proc. Biol. Sci.* 284:20170290. doi: 10.1098/rspb.2017.0290

Zelazo, P. R., Zelazo, N. A., and Kolb, S. (1972). "Walking" in the newborn. *Science* 176, 314–315.

Zhu, Z., Liu, T., Li, G., Li, T., and Inoue, Y. (2015). Wearable Sensor Systems for Infants. *Sensors* 15, 3721–3749. doi: 10.3390/s150203721

Conflict of Interest: The authors declare that the research was conducted in the absence of any commercial or financial relationships that could be construed as a potential conflict of interest.

frontiers in Bioengineering and Biotechnology

ORIGINAL RESEARCH
published: 16 September 2020
doi: 10.3389/fbioe.2020.582219

Load Magnitude and Locomotion Pattern Alter Locomotor System Function in Healthy Young Adult Women

Kellen T. Krajewski[1], Dennis E. Dever[1], Camille C. Johnson[2], Qi Mi[1], Richard J. Simpson[3], Scott M. Graham[4], Gavin L. Moir[5], Nizam U. Ahamed[1], Shawn D. Flanagan[1], William J. Anderst[2] and Chris Connaboy[1]*

[1] Neuromuscular Research Laboratory and Warrior Human Performance Research Center, Department of Sports Medicine and Nutrition, University of Pittsburgh, Pittsburgh, PA, United States, [2] Biodynamics Laboratory, Department of Orthopedic Surgery, University of Pittsburgh, Pittsburgh, PA, United States, [3] Department of Nutritional Sciences, University of Arizona, Tucson, AZ, United States, [4] School of Applied Sciences, Edinburgh Napier University, Edinburgh, United Kingdom, [5] Exercise Science Department, East Stroudsburg University, East Stroudsburg, PA, United States

OPEN ACCESS

Edited by:
Yury Ivanenko, Santa Lucia Foundation (IRCCS), Italy

Reviewed by:
Shunta Togo, The University of Electro-Communications, Japan
Francesco Travascio, University of Miami, United States

***Correspondence:**
Kellen T. Krajewski
ktk20@pitt.edu

Specialty section:
This article was submitted to Biomechanics, a section of the journal Frontiers in Bioengineering and Biotechnology

Received: *10 July 2020*
Accepted: *19 August 2020*
Published: *16 September 2020*

Citation:
Krajewski KT, Dever DE, Johnson CC, Mi Q, Simpson RJ, Graham SM, Moir GL, Ahamed NU, Flanagan SD, Anderst WJ and Connaboy C (2020) Load Magnitude and Locomotion Pattern Alter Locomotor System Function in Healthy Young Adult Women. Front. Bioeng. Biotechnol. 8:582219. doi: 10.3389/fbioe.2020.582219

Introduction: During cyclical steady state ambulation, such as walking, variability in stride intervals can indicate the state of the system. In order to define locomotor system function, observed variability in motor patterns, stride regulation and gait complexity must be assessed in the presence of a perturbation. Common perturbations, especially for military populations, are load carriage and an imposed locomotion pattern known as forced marching (FM). We examined the interactive effects of load magnitude and locomotion pattern on motor variability, stride regulation and gait complexity during bipedal ambulation in recruit-aged females.

Methods: Eleven healthy physically active females (18–30 years) completed 1-min trials of running and FM at three load conditions: no additional weight/bodyweight (BW), an additional 25% of BW (BW + 25%), and an additional 45% of BW (BW + 45%). A goal equivalent manifold (GEM) approach was used to assess motor variability yielding relative variability (RV; ratio of "good" to "bad" variability) and detrended fluctuation analysis (DFA) to determine gait complexity on stride length (SL) and stride time (ST) parameters. DFA was also used on GEM outcomes to calculate stride regulation.

Results: There was a main effect of load (p = 0.01) on RV; as load increased, RV decreased. There was a main effect of locomotion (p = 0.01), with FM exhibiting greater RV than running. Strides were regulated more tightly and corrected quicker at BW + 45% compared ($p < 0.05$) to BW. Stride regulation was greater for FM compared to running. There was a main effect of load for gait complexity (p = 0.002); as load increased gait complexity decreased, likewise FM had less (p = 0.02) gait complexity than running.

Discussion: This study is the first to employ a GEM approach and a complexity analysis to gait tasks under load carriage. Reduction in "good" variability as load increases potentially exposes anatomical structures to repetitive site-specific loading.

Furthermore, load carriage magnitudes of BW + 45% potentially destabilize the system making individuals less adaptable to additional perturbations. This is further evidenced by the decrease in gait complexity, which all participants demonstrated values similarly observed in neurologically impaired populations during the BW + 45% load condition.

Keywords: complexity, motor variability, load carriage, motor control, regulation, biomechanics, gait

INTRODUCTION

Bipedal ambulation requires the complex integration of multisensory information (optical, somatic and vestibular) that is used to coordinate actions within specific environments in order to achieve goal-directed movement (Alexander, 1992; Warren et al., 2001; Bent et al., 2004a; Pandy and Andriacchi, 2010; Matthis et al., 2017). Perceptions of continuously obtained multisensory information yield opportunities to act (affordances) resulting in a perception-action coupling, with a specific movements success predicated on the modulation (tuning and weighting) of the afferent signals that provide (or fail to) appropriate affordances for the task (Gibson, 1966, 1979; Hollands and Marple-Horvat, 1996; Warren et al., 2001; Bent et al., 2004a,b; Rossignol et al., 2006; Peters et al., 2017). In conjunction with sensory "reafference," feedforward mechanisms stimulate coordinative structures or muscle synergies that produce a desired movement that achieves a locomotion task goal (Kim et al., 2011; Bizzi and Cheung, 2013; Minassian et al., 2017). Collectively, the reciprocal cooperation of feedback (afferent) and feedforward (efferent) subcomponents executing a locomotion task is known as the locomotor system. The function of the locomotor system reflects the emergent properties of the organization of the degrees of freedom during locomotor tasks, with specific macroscopic pattern of organization being influenced by the confluence of cost functions (i.e., metabolic efficiency and energy dampening), task, organism (including feedback and feedforward processes) and environmental constraints (i.e., gravity, uneven terrain) (Turvey, 1990; Newell and Vaillancourt, 2001; Davids et al., 2003; Sánchez et al., 2016; Caballero et al., 2019; Shafizadeh et al., 2019). Optimal locomotor system function is represented by biomechanical output that is both stable and adaptive to perturbation (Davids et al., 2003; West and Scafetta, 2003; Cusumano and Dingwell, 2013; Seifert et al., 2013). A common perturbation to bipedal locomotion, especially in military populations, is load carriage, especially "combat load" magnitudes of 20–30 kg (Taylor et al., 2016; Krajewski et al., 2020). How the locomotor system accommodates increasing load magnitudes to successfully execute locomotion task goals still remain unclear (LaFiandra et al., 2003; Attwells et al., 2006; Walsh et al., 2018). Thus, measuring the responses of biomechanical variables to the perturbation of additional loading during locomotory tasks provides valuable insight to the global functional state of the locomotor system.

Variability in the observed movement patterns (motor variability) represents the observed variation in a movement solution, when attempting to accomplish the same goal/task, such as using different segment coupling patterns to perform a step (Bernstein, 1967; Latash et al., 2002, 2010; Latash, 2016). The multitude of joints and muscles in the lower extremity lead to a large number of degrees of freedom that lends itself to equifinality; infinite number of movement solutions to accomplish the same task (Bernstein, 1967; Gelfand and Latash, 1998; Latash et al., 2010). A goal equivalent manifold (GEM; equifinality technique) approach seeks to quantify the "good" (plotted tangential to the GEM [δ_T]) versus "bad" (plotted perpendicular to the GEM [δ_P]) motor variability to further discriminate optimal performance (known as relative variability [the ratio of "good" motor variability to "bad" motor variability]) (Dingwell et al., 2010; Cusumano and Dingwell, 2013; Sedighi and Nussbaum, 2019). Recent theories have demonstrated that motor variability not only leverages equifinality, making the system more adaptable and stable to perturbation (i.e., overcoming varying terrain or recovering from a slip/trip) (Cusumano and Dingwell, 2013; Dingwell et al., 2017), it also has other cost function benefits (Gates and Dingwell, 2008). Specifically, by capitalizing on a larger workspace (greater relative variability) of movement patterns to perform steady-state (constant locomotion velocity) behaviors, energy can be dispersed through more supportive, anatomical structures, whereas limited motor variability (lower relative variability) may lead to site-specific mechanical overloading (cumulative mechanical stress) that can result in musculoskeletal injury (MSI) (Baida et al., 2018; Nordin and Dufek, 2019). Likewise, motor variability can distribute positive mechanical workloads across a greater number of muscle fibers improving metabolic efficiency by reducing the fatigue of a specific subset of muscle fibers (Gates and Dingwell, 2008).

Regulation of cyclical movements during steady-state behavior such as corrections of stride-to-stride fluctuations further elucidates the state of the locomotor system (Cusumano and Dingwell, 2013). Stride regulation is determined by statistical persistence assessment [alpha coefficients (Dingwell et al., 2017)] of deviations tangential (good variability) [δ_T] and orthogonal (bad variability) [δ_P] to the goal manifold (Dingwell et al., 2017). A seminal investigation by Dingwell et al. (2017) demonstrated that elderly individuals classified as low risk fallers and healthy young adults had the same amount of relative variability (ratio of "good" to "bad" motor variability) and used similar stride regulation strategies indicative of a minimal intervention principle ($\delta_T\alpha > 1$; $\delta_P\alpha < 0.5$) (Dingwell et al., 2017). Furthermore, it was suggested that changes in stride-regulation strategy to an absolute position control (POS) model [$\delta_T\alpha$ and $\delta_P\alpha < 0.5$] (Cusumano and Dingwell, 2013) may be the determinant of fall risk (Dingwell et al., 2017). The latter finding was determined with computational modeling (based on a minimum intervention principle) and is still theoretical at this point (Dingwell et al., 2017), but the use of a POS

regulation strategy may indicate perception heavily tuned on their exact position, neglecting/overpowering other important information which will impact affordances perception. In the case of military personnel, especially infantry, load carriage is only one perturbation that must be overcome in addition to uneven terrain, enemy threats and decision making. Thus, the quantification of regulation strategy of the system used for stride to stride fluctuations acts as an indirect assessment of the perception-action loop function namely: (i) the ability to (re)calibrate information-action in a dynamic environment, (ii) (re)weighting the relative importance of information sources as they become available, and (iii) modulate based on the relative importance in relation to the successful maintenance of a functionally useful action-response (Cusumano and Dingwell, 2013; Roerdink et al., 2019).

Components of the locomotor system operate/evolve over different time scales and configure in a *heterarchical* organization when functioning optimally (Bak et al., 1987; Turvey, 1990; Bak and Paczuski, 1995; Newell and Vaillancourt, 2001; Davids et al., 2003; Van Orden et al., 2003). A heterarchical organization of a dynamical system is considered to be complex (interaction of many independent subcomponents that yield an emergent behavior) and a perturbation of one subcomponent is less likely to affect the system globally (West and Shlesinger, 1989; Bak and Paczuski, 1995; Marks-Tarlow, 1999; Torre et al., 2007; Torre and Balasubramaniam, 2009). Thus quantification of system complexity indicates the state of dynamical system health (Iyengar et al., 1996; Gisiger, 2001; Goldberger et al., 2005; Hausdorff, 2007; Van Orden et al., 2009; Nourrit-Lucas et al., 2015; Torre et al., 2019) through non-linear signal processing techniques to determine the fractal structure of a time-series, which exhibits self-similarity at different time scales (Stadnitski, 2012). These fractals display long-range correlations, or learning behavior of current iterations from previous iterations (Hausdorff et al., 1995). Time-series structures of gait dynamics (stride length [S_L] and stride time [S_T]) that yield long range correlations (pink noise) have been linked to healthy functioning adults (Hausdorff et al., 1997, 1999; Hausdorff, 2007; Delignières and Torre, 2009; Ducharme et al., 2018); however, very strong long-range correlations exhibit over-regularity (brown noise) (Gisiger, 2001). Signals that are completely stochastic (white noise) demonstrate no correlation between strides and have been associated with individuals suffering central neurological impairment (Hausdorff et al., 1997; Hausdorff, 2009; Moon et al., 2016). Moreover, white noise has also been observed when imposing a frequency on cyclical steady-state behavior (Terrier et al., 2005; Terrier and Dériaz, 2012; Hunt et al., 2014; Ducharme et al., 2018; Roerdink et al., 2019). Interestingly, warfighters are encouraged to utilize a walking pattern during a velocity that exceeds the gait transition velocity (GTV), colloquially known as forced marching (FM) that is an unnatural (imposed frequency) gait. Little is known how load magnitude, especially military relevant loads (20–60 kg) (Taylor et al., 2016), and this imposed locomotion affect gait complexity in healthy individuals.

To date a load magnitude perturbation is evidenced only in terms of increased mechanical [greater ground reaction forces (GRF) (Birrell et al., 2007; Seay et al., 2014b) and joint kinetics (Knapik et al., 2004; Seay et al., 2014a,b; Liew et al., 2016; Willy et al., 2016, 2019; Lenton et al., 2019; Loverro et al., 2019; Wills et al., 2019; Krajewski et al., 2020)] and physiological [increased heart rate and ratings of perceived exertion (Simpson et al., 2010, 2011, 2017; Huang and Kuo, 2014)] demands compared to unloaded bipedal ambulation. The majority of these studies consisted of male dominated samples, leaving females underrepresented in load carriage research (Loverro et al., 2019). In addition, females are at twice the risk of MSI (Molloy et al., 2020), with a high incidence (∼78%) of MSI observed during basic combat training (recruits), the majority (30–64%) of those MSI suffered during load carriage conditioning in basic training (Jensen et al., 2019; Lovalekar et al., 2020) suggesting that individuals with little to no experience with load carriage tasks are of greater interest. However, there is a paucity of information regarding the effects of load carriage on motor control (LaFiandra et al., 2003; Attwells et al., 2006; Walsh et al., 2018). Importantly, previous work has focused on average behavior of spatiotemporal gait parameters (LaFiandra et al., 2003; Attwells et al., 2006) and have yet to elucidate key features of a healthy locomotor system such as motor variability, stride to stride regulation and the complexity of the system. Therefore, the purpose of this investigation was to determine the interactive effects of load magnitude and locomotion pattern on motor variability, stride regulation and gait complexity during bipedal ambulation in recruit aged females. It is hypothesized, based on an affordance-based control theory (Davids et al., 2003; Mukherjee and Yentes, 2018) that as load increases and the use of an unnatural (imposed) locomotion (FM) will constrain the locomotor system decreasing the number of affordances available which will be reflected by the reduction in relative variability (the ratio of "good" motor variability to "bad" motor variability). Likewise, increases in load and utilization of FM will lead to stricter regulation strategies. Lastly, individuals gait complexity will decrease as load increases and during the execution of the FM locomotion pattern.

MATERIALS AND METHODS

Ethics Statement

All participants were read and signed informed consent that has been approved by the Institutional Review Board (IRB) of The University of Pittsburgh. They were notified of potential risks and benefits associated with participation in the study.

Subjects and Protocol

Eleven healthy, recreationally active young adult females (see **Table 1** for participant characteristics) participated in this study. Recreationally active was defined as engaging in moderate physical activity a minimum of two times a week for at least 30 min, similar to comparable recruits. Moreover, women novice to load carriage and forced marching were chosen to represent a female recruit population, replicating initial exposure to load carriage tasks. Subjects were screened to exclude individuals who reported spine and lower extremity musculoskeletal injury, neurological disorder or pregnant.

TABLE 1 | Subject Characteristics and exercise status.

ID	Age (yr)	Wt (kg)	Ht (m)	BF%	Ses/Wk	Min/Ses	Min/Wk	Modes of exercise	LC Exp	CC
S1	27	56.5	1.57	21.2	4	45	180	running, boxing, cycling	N	S*
S2	27	62.4	1.69	32.8	3	90	270	running, rowing	N	O†
S3	21	62.1	1.57	31.7	3–5	30	90–150	running, walking	N	I
S4	21	50.8	1.53	23.1	6	90	540	cardio, weightlifting	Rec	O
S5	24	47.6	1.55	7.8	6	60–90	360–540	running, cycling, swimming	Rec	O†
S6	28	72.6	1.65	40.4	2–3	45	90–135	elliptical, yoga, hiking, kayaking	N	S
S7	25	70.6	1.68	34.4	3–5	30–40	90–200	running, calisthenics	N	O†
S8	24	60.9	1.64	33.8	3–5	60	180–300	running, cycling, pilates, zumba, weightlifting	N	O†
S9	24	52.9	1.64	14.5	5–6	60–90	300–540	running, weightlifting	Mil	S
S10	25	54.4	1.63	30.3	5	60	300	running, weightlifting, soccer	N	S*
S11	24	81.0	1.72	21.8	6	40	240	running, swimming	Rec	O†
Mn	24.5	61.1	1.6	26.5	4.5	58.6		-	-	-

*Wt = Weight; Ht = Height. Ses = Sessions; Wk = Week; Min = Minutes. BF% = Body fat percentage. LC Exp = Load Carriage Experience; Rec = Recreational; Mil = Military; N = None. CC = Complexity Classification (at baseline); S = Suboptimal; O = Optimal; I = Impaired. Mn = Mean; * = Observed improvements in complexity classification from baseline (FMBW, RN + 25% and FM + 25% conditions only); † = Maintained optimal complexity classification (FMBW and RN + 25% conditions only).*

The procedures for this investigation have been previously described in detail (Krajewski et al., 2020). Briefly, participants ran (RN) and forced marched (FM) on a instrumented split-belt treadmill (Bertec Corporation, Columbus, OH, United States) for 1 min at three different loaded conditions: Bodyweight (BW), plus an additional 25% of BW (BW + 25%), and plus an additional 45% of BW (BW + 45%) [which represents 20–30 kg "combat" loads in average young adult females (Taylor et al., 2016)] at 10% above their GTV (BW: 2.08 ± 0.25 m/s; BW + 25%: 2.02 ± 0.22 m/s; BW + 45%: 1.93 ± 0.23 m/s). All participants wore provided combat boots (Speed 3.0 Boot, 5.11 Tactical, Irvine, CA, United States) to control for influences of footwear on kinematics (Telfer et al., 2017) and loaded conditions were executed with an anterior-posterior loaded weight vest (Short Plus Style Vest, MIR, United States) to control for effects of center of mass (COM) location (Seay et al., 2014a; Loverro et al., 2019). All trials were randomized by load condition and then by locomotion pattern. Participants were given up to 5 min between each trial to control for effects of fatigue. During RN trials, participants were instructed to move "naturally" or how they felt most comfortable to maintain treadmill velocity. For FM trials, participants were instructed to maintain a walking gait regardless of the treadmill velocity. Each trial yielded ∼130 strides (120–180) dependent on the locomotion pattern and velocity. Prior to familiarization and data collection, participants filled out an activity questionnaire and body composition was assessed with dual energy X-ray absorptiometry (DXA) [Lunar iDXA, General Electric, Boston, MA, United States].

Data Collection and Processing

Three retro-reflective markers were placed on each boot (calcaneus, 1st and 5th metatarsophalangeal [MTP] joints) [see **Figure 1** for subject experimental set up]. Kinematic data was collected via 12 infrared cameras (Vicon Motion Systems Ltd., Oxford, United Kingdom) sampling at 100 Hz. Kinetic data was collected via an instrumented split-belt treadmill sampling at 1000 Hz that was synchronized with the motion analysis system. Using the Vicon Nexus® 2.0 software (Vicon Motion Systems Ltd., Oxford, United Kingdom), a custom labeling template was created for the marker configuration used in the study. Once all static and motion trials were reconstructed, the labeling template was used to auto label the static trials captured for each load condition (BW, BW + 25% and BW + 45%) which were then used to auto label their respective motion trials (RN and FM). Gap filling methods in Nexus 2.0 were used to correct any breaks in trajectory data due to marker occlusion. Data was then exported, and post processed in Visual 3D (C-Motion Inc., Germantown, MD, United States). Further analysis [GEM decomposition and Detrended Fluctuation Analysis (Atlas Collaboration et al., 2014)] was conducted with custom Matlab^{TM} 2019a (Mathworks, Inc., Natick, MA, United States) scripts. Kinematic and kinetic data were filtered with a second order Butterworth low-pass filter (cut-off frequencies of 6 Hz and 40 Hz for the kinematic and kinetic signals, respectively). Heel strike was defined as the time when vertical component of the ground reaction force exceeded a 50N threshold.

The following variables were calculated: Stride length (S_L) was computed as the distance covered from heel strike to ipsilateral heel strike; Stride time (S_T) was computed as the time elapsed from heel strike to ipsilateral heel strike; Stride speed (S_S) was computed as the quotient of S_L/S_T; Velocity (v) was computed as the average S_S over all *n* strides of a time-series. Average values (Means), standard deviations (SD) and DFA scaling exponents (α-value) were calculated for S_L, S_T and S_S across all trials.

Goal Equivalent Manifold Decomposition

Methods utilized for GEM decomposition have been described in detail by Dingwell et al. (2010). However, to further elaborate

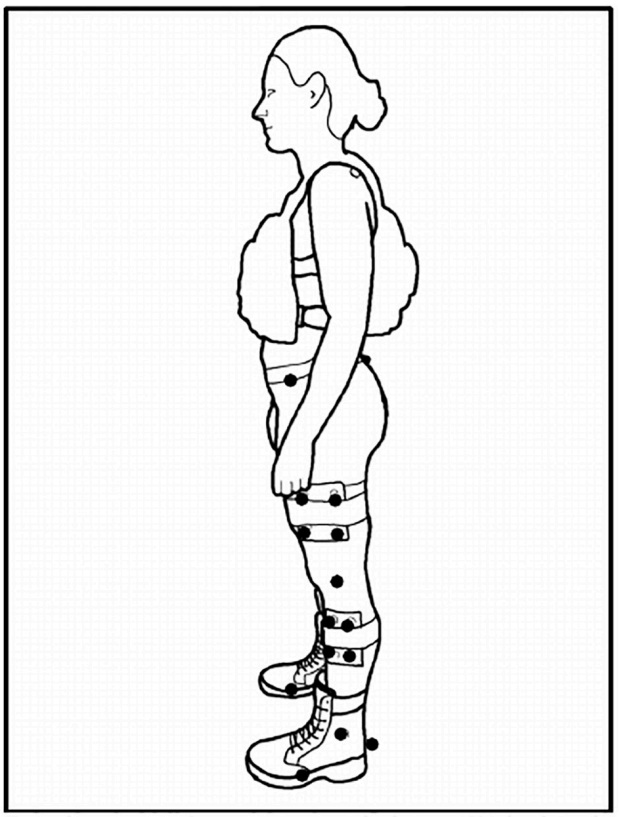

FIGURE 1 | Subject Set-Up. Exemplar set up of a participant with their +45% load in the anterior-posterior weight vest. Solid dots represent retroreflective markers. Markers at the medial/lateral epicondyles (knee) and medial/lateral malleoli (ankle) removed after static calibration trial capture. Markers at the calcaneus and 1st/5th metatarsophalangeal (MTP) joints defined the foot segment.

the process: firstly, S_L and S_T time-series for each trial was normalized to unit variance [dividing by its own standard deviation]. A specific operating point was computed for S_T as Eq. (1):

$$S_T^* = \ < S_T >_n \tag{1}$$

Where <■> represents the average across all *n* strides of the time series. The specific operating point for S_L was computed as Eq. (2):

$$S_L^* = vS_T^* \tag{2}$$

Here *v* represents the velocity of the treadmill for that specific trial. The new centered operating point was then computed as Eqs. (3) and (4):

$$S_{Tn}^{'} = S_{T_n} - S_T^* \tag{3}$$

and

$$S_{L_n}^{'} = S_{L_n} - S_L^* \tag{4}$$

Lastly, deviations tangential to the goal manifold were represented as δ_T and deviations perpendicular to the goal manifold were represented as δ_P. These deviations were calculated with a linear coordinate transformation as Eq. (5):

$$\begin{bmatrix} \delta_T \\ \delta_P \end{bmatrix} = \frac{1}{\sqrt{1+v^2}} \begin{bmatrix} 1 & v \\ -v & 1 \end{bmatrix} \begin{bmatrix} S_{T_n}^{'} \\ S_{L_n}^{'} \end{bmatrix} \tag{5}$$

Where, the σ of δ_T and δ_P were determined for each load and locomotion condition. Relative variability was calculated as the ratio between $\sigma\delta_T/\sigma\delta_P$. Therefore, a relative variability magnitude of 1 represents equal amounts of "good" versus "bad" variability; <1 represents more "bad" variability; and >1 represents more "good" variability. Additionally, DFA scaling exponents (α) were computed for δ_T and δ_P. Scaling exponents for δ_T and δ_P are interpreted as follows: $\alpha < 0.5$ represents anti-persistence (alteration in one direction more likely followed by an alteration in opposite direction); $\alpha > 0.5$ represents statistical persistence (alteration in one direction more likely followed by an alteration in same direction); and $\alpha = 0.5$ represents uncorrelated (alteration in one direction has same likelihood of being followed by alteration in either direction) (Dingwell et al., 2010, 2017).

Complexity Analysis

Complexity analysis was executed utilizing fractal methods, specifically DFA (Peng et al., 1993; Hausdorff et al., 1995; Delignières et al., 2006; Stadnitski, 2012) on S_L and S_T gait variables (∼130 consecutive strides). Refer to the aforementioned references for greater detail but briefly: DFA creates a one-dimensional signal $x(i)$, i = 1,. . ., L, where x is the initial signal of size L, and an integrated signal (x) is calculated according to the Eq. (6):

$$Y\left(k\right) = \sum_{i=1}^{k} (B\left(i\right) - B_{avg}) \tag{6}$$

where B_{avg} is the mean value of the signal (B = signal value at specific time point). The unified time series Y is then divided into segments (boxes that don't overlap) of length l, and the linear approximation Y_l is then obtained through a least-squares fit of each segment separately (trend of each section).

The mean fluctuation (root mean square) of the incorporated and detrended time-series is computed using Eq. (7):

$$F\left(l\right) = \sqrt{\frac{1}{L}\sum_{k=1}^{L} \left(Y\left(k\right) - Y_l\left(k\right)\right)^2} \tag{7}$$

The aforementioned calculations are repeated for a range of l. The goal of this analysis is to identify the relation between $F(l)$ and the size of segment l because this relationship serves as an indicator of a scaling phenomenon. In general, $F(l)$ increases with increases in the range of segment l. A double plot logarithmic graph (log ($F(l)$ vs log_l) is then formed, and this graph is used to acquire the scaling exponent (α). A linear dependency implies the existence of self-fluctuations, and $F(l)$ which is the slope of line outlines the scaling α exponent, which increases with l based on a power law, as detailed in Eq. (6):

$$F\left(l\right) - \ l^{\alpha} => \ log\left(\left(F\left(l\right)\right) - \ \alpha \ \times \ log\ \left(l\right)\right. \tag{8}$$

DFA ultimately yields a scaling exponent (α) which represent the correlational structure of the signal. White noise (uncorrelated

or completely stochastic) is represented as $\alpha = 0.5$; Pink noise (positive long-range correlations) is represented as $\alpha = 1.0$; Brown noise (persistent long-range correlations or too much regularity) is represented as $\alpha = 1.5$ (Peng et al., 1995). Classifications based upon a range of α were employed to provide greater clarity as values are rarely the exact values listed above. "Suboptimal self-organization" was represented by $\alpha < 0.75$; "Optimal self-organization" was represented by $\alpha = 0.75 - 1.30$; "Impaired self-organization" was represented by $\alpha > 1.30$. These values were based upon previously established ranges that classified populations (healthy, elderly, and impaired) as either white, pink or brown noise (Hausdorff et al., 1996, 1997, 1999; Ravi et al., 2020). The values attained during the RN with BW condition was considered the baseline because it is the natural locomotion pattern used 10% above GTV and unperturbed by an external load (no added load carriage). Change classifications were then determined for each individual (change from the baseline condition) as either "positive change" in complexity ("Suboptimal self-organization" or "Impaired self-organization" to "Optimal self-organization"), "negative change" ("Optimal self-organization" to "Suboptimal self-organization" or "Impaired self-organization"), "no change positive" ("Optimal self-organization" to "Optimal self-organization") and "no change negative" ("Suboptimal self-organization" or "Impaired self-organization" to "Suboptimal self-organization" or "Impaired self-organization").

Statistical Analysis

Descriptive statistics (mean and SD) were reported for all the variables. In order to determine interactive effects of load and locomotion on relative variability and gait complexity a two-way repeated measure analysis of variance (RMANOVA) for Load × Locomotion (3 × 2) was conducted separately. Additionally, to further elucidate findings regarding relative variability, tangential and perpendicular variability were assessed within locomotion pattern with a 3 × 2 (Load × Direction) RMANOVA. If interactions were significant, simple main effects were performed (paired *t*-tests for locomotion/direction stratified by load and RMANOVA for load stratified by locomotion/direction). If no significant interaction was observed, only main effects were analyzed. *Post hoc* analysis using Bonferroni-corrected pairwise comparisons were conducted when necessary.

To determine interactive effects of load and locomotion on stride regulation a three-way Load × Locomotion × Direction (3 × 2 × 2) RMANOVA was conducted on DFA scaling exponents of δ_T and δ_P. If a significant three-way interaction was observed then two-way RMANOVAs were conducted for load by locomotion (3 × 2), load by direction (3 × 2) and locomotion by direction (2 × 2). If a two-way interaction was observed, then simple main effects were analyzed (RMANOVA for load and paired *t*-tests for locomotion and direction). If no significant two-way interaction was observed, only main effects were analyzed. *Post hoc* analysis using Bonferroni-corrected pairwise comparisons were conducted when necessary. Lastly, if no significant three-way interaction was observed, only main effects were analyzed. *Post hoc* analysis using Bonferroni-corrected pairwise comparisons were conducted when necessary.

Partial eta squared (η^2_P) was calculated as a measure of effect size given the within-subject design (Bakeman, 2005; Richardson, 2011), with magnitudes of effect interpreted as: 0.01–0.085 (small effect); 0.09–0.24 (moderate effect); and > 0.25 (large effect) (Cohen et al., 2003). Additionally, frequencies of complexity classifications and change classifications are reported to qualitatively examine individual responses. The alpha level was set at 0.05 ($p \leq 0.05$).

RESULTS

Relative Variability

See **Table 2** for mean and SD of all GEM related outcomes. There was no significant interaction between load and locomotion for relative variability of motor control ($F_{2,20} = 0.167$, $p = 0.85$, $\eta^2_P = 0.02$). Load had a significant influence on relative variability reducing the number of successful or "good" movement solutions, exemplified as relative variability magnitude decreasing as load magnitude increased confirmed by the main effect of load ($F_{2,20} = 5.50$, $p = 0.01$, $\eta^2_P = 0.36$); with *post hoc* analysis revealing BW + 45% (1.28 ± 0.05) being significantly ($p = 0.02$) less than BW (1.55 ± 0.07). Additionally, FM demonstrated a more relative variability compared to running indicated by the main effect of locomotion ($F_{1,10} = 8.90$, $p = 0.01$, $\eta^2_P = 0.47$) with estimated marginal means for FM (1.53 ± 0.08) being greater than RN (1.27 ± 0.04).

The interaction between load and direction during RN was not statistically significant ($F_{2,20} = 2.33$, $p = 0.12$, $\eta^2_p = 0.19$). There was no significant main effect of load ($F_{2,20} = 3.05$, $p = 0.07$, $\eta^2_p = 0.23$). While not significant, as load increased mean tangential ("good") variability decreased (BW = 1.13 ± 0.10, BW + 25% = 1.10 ± 0.06, BW + 45% = 1.06 ± 0.07) and mean perpendicular ("bad") variability increased (BW = 0.84 ± 0.13, BW + 25% = 0.88 ± 0.08, BW + 45% = 0.94 ± 0.08). However, regardless of load, tangential variability was always greater evidenced by the main effect of direction ($F_{1,10} = 60.91$, $p < 0.001$, $\eta^2_p = 0.86$), with estimated marginal means revealing variability along the tangential (1.10 ± 0.01) was greater than along the perpendicular (0.88 ± 0.02).

There was no significant interaction between load and direction for FM ($F_{2,20} = 1.79$, $p = 0.19$, $\eta^2_p = 0.15$). There was no main effect of load ($F_{2,20} = 2.75$, $p = 0.09$, $\eta^2_p = 0.22$). While not significant, as load increased mean tangential ("good") variability decreased slightly (BW = 1.20 ± 0.08, BW + 25% = 1.15 ± 0.08, BW + 45% = 1.15 ± 0.06) and mean perpendicular ("bad") variability increased (BW = 0.74 ± 0.013, BW + 25% = 0.81 ± 0.12, BW + 45% = 0.81 ± 08). Lastly, regardless of load, tangential variability was always greater than perpendicular variability indicated by the main effect of direction ($F_{1,10} = 90.10$, $p < 0.001$, $\eta^2_p = 0.90$), with estimated marginal means revealing tangential variability (1.17 ± 0.02) was greater than perpendicular variability (0.79 ± 0.02). See

TABLE 2 | GEM outcomes (mean ± standard deviation).

	Run			Forced marching		
Variable	**BW**	**+25%**	**+45%**	**BW**	**+25%**	**+45%**
S_L	1.52 ± 0.20	1.48 ± 0.17	1.38 ± 0.15	1.70 ± 0.14	1.63 ± 0.13	1.54 ± 0.12
S_T	0.74 ± 0.04	0.75 ± 0.03	0.74 ± 0.04	0.84 ± 0.05	0.82 ± 0.05	0.83 ± 0.07
RV	1.41 ± 0.33	1.27 ± 0.18	1.14 ± 0.17	1.69 ± 0.40	1.47 ± 0.37	1.42 ± 0.23
δ_T (V)	1.13 ± 0.09	1.10 ± 0.06	1.05 ± 0.07	1.20 ± 0.08	1.15 ± 0.09	1.15 ± 0.06
δ_P (V)	0.83 ± 0.13	0.88 ± 0.08	0.94 ± 0.08	0.74 ± 0.13	0.81 ± 0.13	0.82 ± 0.09
δ_T (α)	0.91 ± 0.29	0.55 ± 0.41	0.35 ± 0.51	0.57 ± 0.38	0.43 ± 0.40	0.09 ± 0.38
δ_P (α)	0.68 ± 0.22	0.39 ± 0.30	−0.01 ± 0.51	0.21 ± 0.43	0.11 ± 0.40	−0.21 ± 0.36

S_L = Stride Length (meters); S_T = Stride Time (seconds). RV = Relative Variability ($\sigma\delta_T/\sigma\delta_P$). δ_T (V) = Tangential variability; δ_P (V) = Perpendicular variability. δ_T (α) = Tangential coordinate scaling exponent; δ_P (α) = Perpendicular coordinate scaling exponent. BW = Body Weight (no additional load).

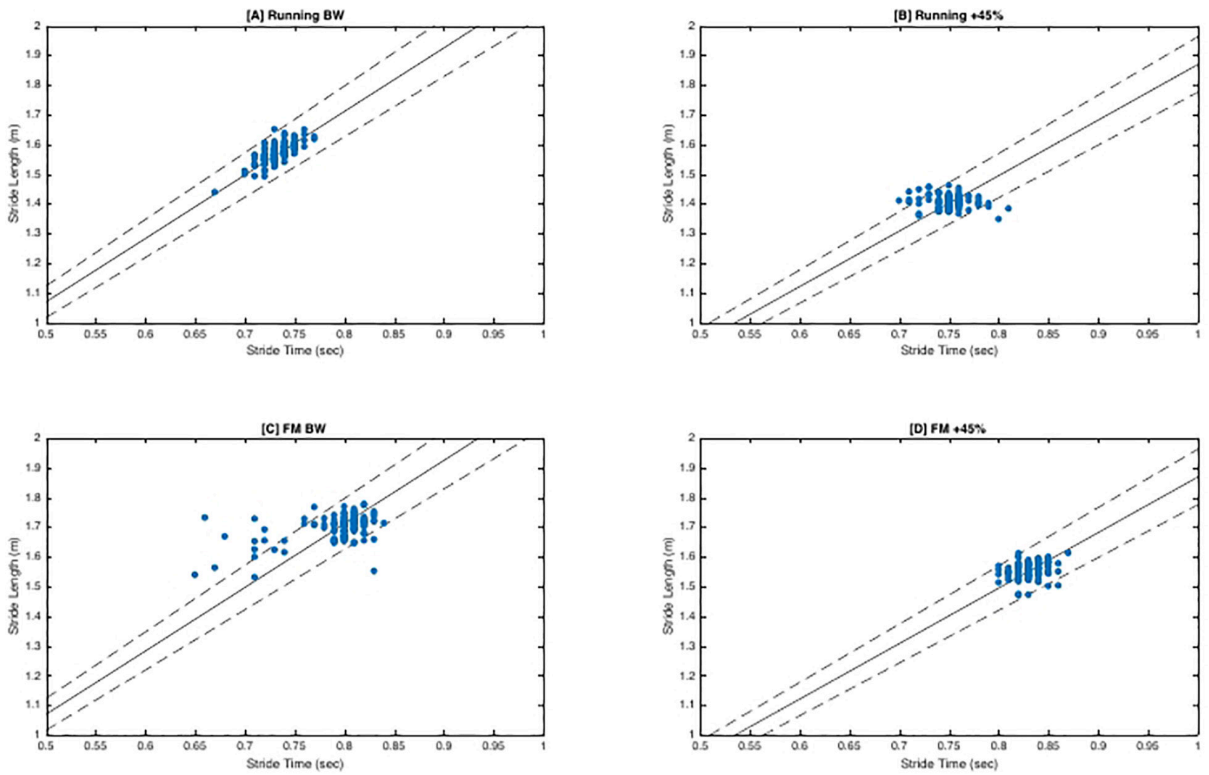

FIGURE 2 | Goal Equivalent Manifold (GEM) Exemplar Plots. Exemplar plots (S4) represent a time series of consecutive strides (∼156 strides). Solid dots represent the different combinations of SL and ST for each stride. The solid line represents the goal manifold, which in this case is the velocity of the treadmill. Therefore, the assumed goal of the participant is to maintain horizontal velocity so they do not drift off the end of the treadmill belt. The dashed lines superior and inferior to the solid line represent the ±5% error of the goal manifold. Dots that are tangential (along the solid goal manifold) are variations that still achieve the task goal ('good' variability). Dots that are perpendicular to the solid goal manifold line are variations that fail to achieve the goal manifold. Perpendicular coordinates will result in the participant moving forward or backward on the treadmill belt. (A,B) demonstrate more tangential variability as indicated by the larger spread along the goal manifold. Conversely, (C,D) exhibit a much tighter formation indicative of less variation and stricter stride regulation. Furthermore, in contrast of (A), (C) exhibits more stride variants that lie beyond the ±5% error range. Not surprisingly, this participant had complexity classifications of 'optimal' and 'suboptimal' for (A,C) respectively.

Figure 2 for exemplar plots of S_L and S_T combinations along the goal manifold.

Scaling Exponents (α): S_T & S_p

See **Table 2** for all means and SD of scaling exponents. There was no significant 3-way interaction between load, locomotion and direction ($F_{2,20}$ = 1.96, p = 0.17, η^2_p = 0.16). As load increased control of stride-to-stride fluctuations became more strict (and therefore corrected more quickly) evidenced by the main effect of load ($F_{2,20}$ = 8.87, p = 0.002, η^2_p = 0.47), with *post hoc* analysis revealing that BW (0.6 ± 0.08) was significantly (p = 0.02) greater than BW + 45% (0.04 ± 0.11). Additionally, running exhibited less control of stride-to-stride fluctuations indicated by the main effect of locomotion ($F_{1,10}$ = 8.57, p = 0.02,

η^2_p = 0.46), with estimated marginal means revealing that running (0.46 ± 0.07) was greater than FM (0.19 ± 0.08). Lastly, "bad" variations (perpendicular to the goal manifold) were controlled and corrected more quickly than "good" variations (tangential to goal manifold) as evidenced by the main effect of direction ($F_{1,10}$ = 67.12, $p < 0.001$, η^2_p = 0.87), with estimated marginal means revealing that persistence along the tangential (0.47 ± 0.06) was greater than the perpendicular (0.18 ± 0.07).

Complexity Analysis (α): S_L, S_T

See **Table 3** for mean and SD of scaling exponents. There was no significant interaction between load and locomotion for S_L ($F_{2,20}$ = 0.03, p = 0.97, η^2_p = 0.003). As load magnitude increased, gait complexity decreased independent of locomotion pattern as evidence by the main effect of load ($F_{2,20}$ = 8.74, p = 0.002, η^2_p = 0.4 = 7), with *post hoc* pairwise comparisons revealing BW (0.69 ± 0.06) was significantly (p = 0.02) greater than BW + 45% (0.1 ± 0.16). Additionally, FM reduced gait complexity compared to running independent of load magnitude indicated by the main effect of locomotion ($F_{1,10}$ = 7.59, p = 0.02, η^2_p = 0.43), with estimated marginal means revealed running (0.59 ± 0.06) was greater than FM (0.23 ± 0.13).

There was no significant interaction between load and locomotion for S_T ($F_{2,20}$ = 0.43, p = 0.36, eta = 0.10). The increase in load magnitude decreased gait complexity independent of locomotion pattern as evidenced by the main effect of load ($F_{2,20}$ = 6.52, p = 0.007, η^2_p = 0.40), with *post hoc* analysis revealing that BW (0.67 ± 0.10) was greater (p = 0.03) than BW + 45% (−0.10 ± 0.19). Lastly, FM reduced gait complexity compared to running independent of load magnitude as indicated by the main effect of locomotion ($F_{1,10}$ = 9.66, $p < 0.001$, η^2_p = 0.75), with estimated marginal means revealing running (0.76 ± 0.11) was greater than FM (−0.003 ± 0.15).

See **Table 3** for frequency of observed complexity classifications by condition and **Figure 3** for the frequency of each classification change of all conditions combined. For S_L and S_T 43.64% and 49.09% of the observed changes from baseline were negative changes ("Optimal self-organization" to "Suboptimal' or 'Impaired." Only two participants demonstrated a positive change with 63% of those occurrences accounted for by one participant. Positive change classifications only occurred at the BW + 25% load condition and not the BW + 45%. Two of the participants with positive changes from baseline reported having prior experience in a multitude of exercise modalities that would improve lower limb muscular endurance and anaerobic conditioning (see **Table 1**). For S_L only 10.91% of changes were classified as "no change positive" with 58% of the occurrences accounted for by two individuals. Both individuals performed a greater variety of exercise modalities including resistance training and trained more frequently and for longer periods of time. Lastly, only a single subject demonstrated an "Impaired" classification at baseline (RN at BW). This participant trained for the shortest durations (30 min maximum) only 2–3 times a week (see **Table 1** for more detailed characteristics).

DISCUSSION

The objectives of this investigation were to determine the interactive effects of load magnitude and locomotion pattern on motor variability, stride-to-stride control/regulation and complexity. Load magnitude significantly altered relative variability independent of locomotion pattern evidenced by the significant main effect of load. As load increased relative variability decreased with BW + 45% (1.28σ) having 21% less relative variability compared to BW (1.55σ), suggesting individuals are better able to leverage either the system degeneracy, or indeed, redundancy of coordinative patterns employed to execute a stride during unloaded bipedal ambulatory tasks. The higher relative variability ratios are achieved by a greater variance tangential the goal manifold ("good" variability) and a reduction in variance perpendicular to the goal manifold ("bad" variability) [see **Figure 2**]. Importantly, these findings alone do not necessarily indicate more stable performance (task execution), but that during unloaded conditions there is a greater workspace of solutions that can be utilized to accomplish the goal task (maintain velocity). Coupled with the observed complexity scaling exponents ∼1 for S_L/S_T at BW and BW + 25% load conditions suggest that individuals display an optimally organized locomotor system fully leveraging

TABLE 3 | Complexity outcomes (mean ± standard deviation) and class frequency (# of occurrences).

		Run			Forced marching		
Variable		**BW**	**+25%**	**+45%**	**BW**	**+25%**	**+45%**
S_L (α)		0.88 ± 0.31	0.63 ± 0.26	0.27 ± 0.63	0.49 ± 0.42	0.27 ± 0.46	−0.07 ± 0.55
S_T (α)		1.04 ± 0.50	1.09 ± 1.02	0.15 ± 0.54	0.29 ± 0.62	0.04 ± 0.53	−0.34 ± 0.59
'O'	S_L	6	4	2	4	3	0
	S_T	6	1	2	1	1	0
'S'	S_L	4	7	9	7	8	11
	S_T	2	6	9	9	10	11
'I'	S_L	1	0	0	0	0	0
	S_T	3	4	0	1	0	0

S_L = Stride Length; S_T = Stride Time. α = alpha coefficient derived from detrended fluctuation analysis. White Noise = 0.5 ('Suboptimal self-organization' ['S'] represented as < 0.75). Pink Noise = 1 ('Optimal self-organization' ['O'] represented as 0.75 – 1.30). Brown Noise = 1.5 ('Impaired self-organization' ['I'] represented as >1.30).

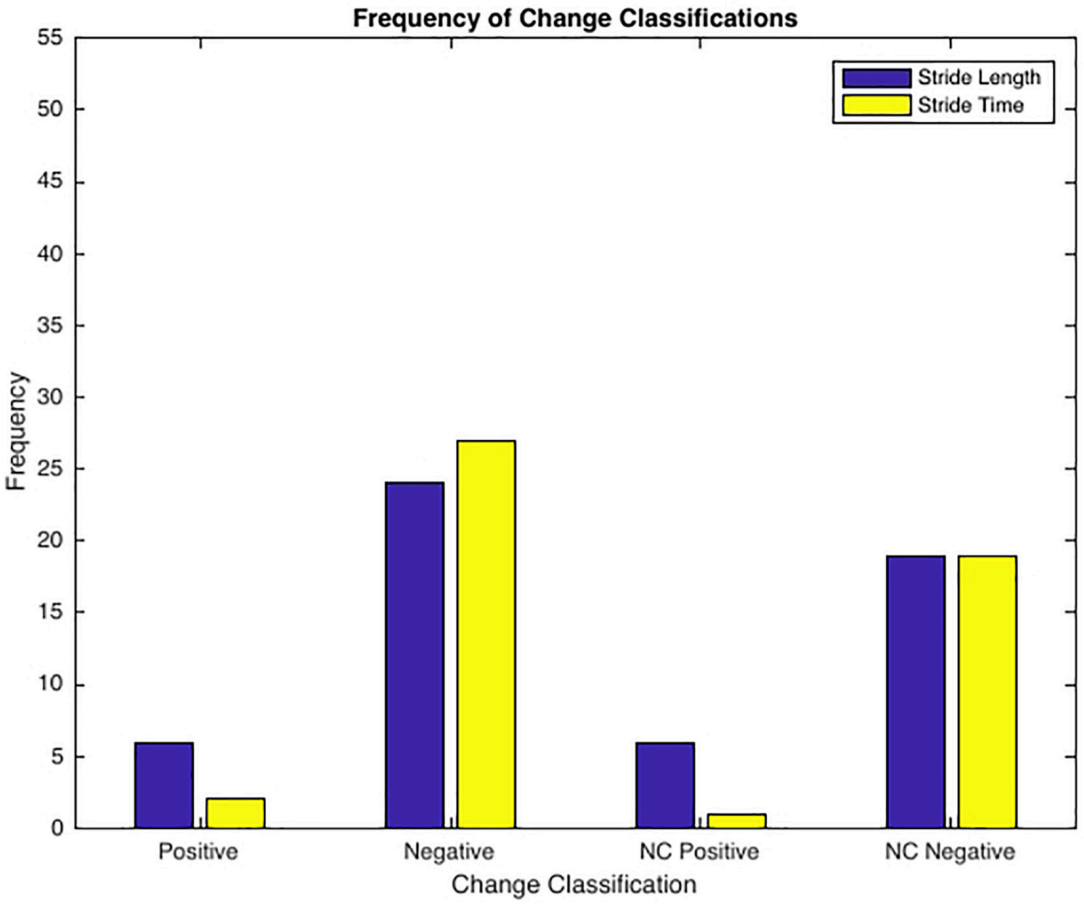

FIGURE 3 | Frequency of Change Classifications. Positive Change = 'Suboptimal' to 'Optimal' or 'Impaired' to 'Optimal' (only 2 subjects, 50% of incidences 1 subject); Negative Change = 'Optimal' to 'Suboptimal' or 'Optimal' to 'Impaired'; No Change Positive = 'Optimal' to 'Optimal' (2 subjects accounted for 59% of all incidences); No Change Negative = 'Suboptimal' to 'Suboptimal', 'Suboptimal' to 'Impaired', 'Impaired' to 'Impaired', or 'Impaired' to 'Suboptimal'.

equifinality. Furthermore, the lack of significant differences between BW and BW + 25% load conditions indicates that the latter load condition is insufficient to impose a constraint on the locomotor system that results in altered motor variability. At BW + 45%, the locomotor system has a diminished ability to leverage "good" motor variability. The lack of observed "good" variability, may limit energy dispersion across multiple structures up the kinetic chain when energy is highest [due to increased forces from load (Birrell et al., 2007; Lloyd, 2010; Liew et al., 2016; Willy et al., 2016, 2019; Krajewski et al., 2020)] increasing cumulative mechanic stress MSI risk (Nordin and Dufek, 2019; Baggaley et al., 2020).

Contrary to the proposed hypothesis, the FM (RV = 1.52) resulted in 19.6% greater relative variability than running (RV = 1.27). However, this finding alone should be interpreted with caution; the greater variability simply denotes a larger set of motor solutions observed for FM compared to running. Similar observations were made by Black et al. (2007) demonstrating greater motor variability in adolescents with down syndrome compared to aged-matched neurotypical adolescents, indicating that during unperturbed steady-state gait, those with down-syndrome needed to utilize their full movement solution potential in order to maintain velocity (Black et al., 2007). In addition, Black et al. (2007) demonstrated that the greater motor variability exhibited during unperturbed gait suggested a locomotor system operating closer to the action boundaries that would be more likely to fail (fall) with additional pertubrations (Black et al., 2007). Thus, greater relative variability alone may not indicate more task performance stability or motor-system health. In females during FM there is a greater contribution of frontal plane moments (adduction/abduction) to knee total joint moment, indicative of potentially deleterious movements (Krajewski et al., 2020). Although a greater range of movement solutions were utilized during FM compared to running, they may have included more movement solutions that while successful in executing the goal task (maintaining velocity), are maladaptive/deleterious with respect to joint/tissue health (Zabala et al., 2013; Asay et al., 2018; Baggaley et al., 2020; Krajewski et al., 2020). Future work should focus on elucidating the movement pattern structures (segment couplings)

in more detail, which coincide with relative variability, its magnitude and structure.

Additionally, the unfamiliarity of the task for this sample (they had little to no experience with FM) may have demonstrated a greater exploration of state-space as a consequence of learning to perform this locomotion pattern (Newell and Vaillancourt, 2001; Pacheco and Newell, 2017). The greater relative variability exhibited by FM compared to running may be indicative of a locomotor system trying to adapt to improve mechanical efficiency or reduce pain sensations associated with each stride. By obstructing the natural bifurcation of locomotion (participants executing FM at a velocity 10% above their GTV), the system is in search of an order parameter (segment coupling pattern) that adheres to cost function (decrease metabolic cost/increase mechanical efficiency) of the task control parameter (horizontal velocity) (McGinnis and Newell, 1982; Newell and Vaillancourt, 2001; Davids et al., 2003; Caballero et al., 2019; Shafizadeh et al., 2019). Consequently, the observed complexity for FM was $\alpha = 0.11$ ("suboptimal"), supporting the notion that the observed greater relative variability in FM compared to running, represented a state-space exploratory behavior. In conjunction with the low system complexity, the locomotor system is less stable to additional perturbations. Whilst imposed locomotion (FM) and load carriage are themselves perturbations dynamic military environments present even more perturbations (uneven terrain, enemy threats, orders from local commanders). If motor learning occupies a large percentage of the system workspace, it potentially results in the failure to identify external perturbations [due to competition over feedback/feedforward resources (Woollacott and Shumway-Cook, 2002; Al-Yahya et al., 2011; De Sanctis et al., 2014)] making the locomotor system less stable and more susceptible to failure (slips/trips/falls, identification of threats). Future research should compare novice and experienced individuals with load carriage to determine if there is a difference in relative variability and complexity while completing ambulatory tasks with load.

Stride-to-stride regulation demonstrated less control for unloaded conditions as evidenced by the main effect of load ($p = 0.002$). The BW + 45% load condition exhibited ($\delta_T\alpha = 0.22$, $\delta_p\alpha = -0.11$) significantly more regulation than BW ($\delta_T\alpha = 0.74$, $\delta_p\alpha = 0.45$). Alpha coefficient (α) values less than.5 indicate statistical anti-persistence, representing much stricter control because the subsequent stride variation is more likely to be the opposite composition (combination of S_L and S_T) than the previous. Thus, movements were corrected much quicker and more often with the addition of substantial (BW + 45%) load carriage independent of locomotion pattern. Moreover, the main effect of direction ($p < 0.001$) exhibited more strict regulation perpendicular to the manifold ("bad" variability) compared to tangential ("good" variability) [see **Table 1** for δ_T (α) and δ_p (α) means]. The combination of less control of "good" variability and more control of "bad" variability [resembling an ideal minimum intervention principle (MIP) model [$\delta_T\alpha > 1$; $\delta_p\alpha < 0.5$] (Cusumano and Dingwell, 2013)] is indicative of a stride-regulation strategy of a healthy system recognizing movement variations that impede the execution of the task goal (maintain velocity). Further, the "system controller" minimally intervenes, minimizing control effort theoretically freeing up system capacity for other components of the locomotor system (Cusumano and Dingwell, 2013). In fact, the BW results ($\delta_T\alpha = 0.74$, $\delta_p\alpha = 0.45$) of this investigation were similar to stride regulation findings of healthy adults ($\delta_T\alpha = \sim0.90$, $\delta_p\alpha = \sim0.42$) by Dingwell et al. (2017). If the individual were unhealthy, a failure to properly regulate "bad" motor variability potentially results in them unable to successfully execute the task. However, as load increased both $\delta_T\alpha$ and $\delta_p\alpha$ decreased indicating a change in stride-regulation strategy that reflected an absolute position control (POS) model [$\delta_T\alpha$ and $\delta_p\alpha < 0.5$] (Cusumano and Dingwell, 2013), postulating that maximal control effort was used thus reducing the capacity of other locomotor system components (Cusumano and Dingwell, 2013).

Locomotion pattern also affected stride-to-stride regulation independent of load, with FM ($\delta_T\alpha = 0.36$, $\delta_p\alpha = 0.04$) demonstrating stricter control compared to running ($\delta_T\alpha = 0.60$, $\delta_p\alpha = 0.35$). Even "good" motor variability ($\delta_T\alpha$) was tightly regulated for FM evidenced by the $\delta_T\alpha < 0.5$. Once again, the stride-regulation strategy utilized for FM at all load conditions more closely mimicked that of a POS model (Cusumano and Dingwell, 2013). A stricter regulation of stride-to-stride intervals coupled with greater relative variability of FM at BW + 45% compared to RN BW + 45% may further evidence the participant learning by exploring state-space and freezing/unlocking different degrees of freedom quickly (Bernstein, 1967; Sporns and Edelman, 1993; Newell and Vaillancourt, 2001). Thus in response to the load and imposed locomotion perturbations a structural reorganization of the locomotor system occurs, with potentially greater reliance on supraspinal input that disrupt feed forward mechanisms of gait (further supported by the observed $\alpha < 0.5$ for FM of S_L and S_T) due to the competition over feedback/feedforward resources (Woollacott and Shumway-Cook, 2002; Al-Yahya et al., 2011; De Sanctis et al., 2014). It is likely that the perturbations associated with FM and load elicit more system capacity dedicated to control in a relatively unperturbed state (walking on a treadmill) potentially overpowering other system components important to navigating dynamic environments. This may have important consequences to military populations, as loaded ambulatory tasks are often undertaken in dynamic circumstances requiring the integration of multiple information sources to understand the context within which the action takes place, i.e., quickly navigating across an open area of the battle space while aiming and firing a weapon.

When assessing complexity of gait dynamics (S_L and S_T) there was a main effect of load ($p = 0.002$ and $p = 0.007$), with complexity decreasing as load increased. The BW + 45% condition ($S_L\alpha = 0.1$; $S_T\alpha = -0.1$) exhibited significant less complexity than BW ($S_L\alpha = 0.69$; $S_T\alpha = 0.67$). Whilst, group mean comparison demonstrated a decrease in complexity, the group mean for BW still represents a "suboptimal" organization ($\alpha < 0.75$) (Hausdorff et al., 1997; Hausdorff, 2007). However, when observing the individual results, eight of the participants had "optimal" complexity or.75 $< \alpha <$ 1.30 during BW load conditions (see **Tables 1**, **3**). Moreover, only five participants had "optimal" complexity for BW + 25% and every participant

exhibited "suboptimal" complexity for the BW + 45% load condition. "Optimal" complexity or scaling exponents (α) ∼1 represent long-range correlations (pink noise) that is indicative of skilled performance and utilization of prior stride information (i.e., proprioceptive) to influence future strides (Hausdorff et al., 1996, 1997; Delignières and Torre, 2009; Nourrit-Lucas et al., 2015). Likewise, the fractal structure of "optimal" represents an independence of fluctuations at different time scales meaning a perturbation of one system component will not likely affect the global system (locomotor system as a whole) (West and Shlesinger, 1989; Bak and Paczuski, 1995; Marks-Tarlow, 1999; Torre et al., 2007). Therefore, the data observed within the present study indicates that a load carriage magnitude of at least BW + 45% reduces the system stability and adaptability, predisposing the system to failure (falling) in the presence of additional perturbations (i.e., increased fall risk with uneven terrain) in females with limited/no load carriage experience. Importantly, BW + 45% for this female sample was 26.6 ± 4.7kg, which represents a typical combat load (20 kg) (Taylor et al., 2016), a load used during operations that will bombard individuals with perturbations (terrain obstacles[debris], enemy threats, officer commands/questions) that if not actioned correctly could result in serious MSI or death. The latter suggests the need for further research to determine if experience/training with load carriage improves system complexity that can better handle additional adaptations.

In addition to a main effect of load, locomotion patterns also affected the complexity of S_L and S_T ($p = 0.02$ and $p < 0.001$, respectively). As hypothesized, the natural locomotion pattern running ($S_L\alpha = 0.59$; $S_T\alpha = 0.76$), exhibited greater complexity than FM ($S_L\alpha = 0.23$; $S_T\alpha < -0.01$). Considering that running is the extant locomotion observed at a velocity exceeding GTV, it is not surprising more participants (seven) had "optimal" complexity during RN conditions (BW and BW + 25% only). Five of the participants did have "optimal" complexity for FM but at the BW and BW + 25% conditions only. These five participants (S1, S7, S8, S10, and S11) engaged in moderate amounts of exercise time per week and engaged in a multitude of exercise modalities that included a form of anaerobic conditioning and/or strength training (see **Table 1**). Furthermore, one participant (S3) had an "impaired" complexity at baseline (running at BW). Interestingly, this participant performed the least amount of exercise time per week and engaged in the least varied modes of exercise [see **Table 1**]. Thus, the movement poverty in terms of time and coordination diversity, may impact system adaptability as reflected in the "impaired" and "suboptimal" complexity during minimally perturbed steady-state behaviors. Moreover, the complexity outcomes demonstrated varying individual responses highlighting its potential utility as a mechanical "biomarker" of the current state of the locomotor system and training adaptation response. Future research should compare complexity of different fitness level groups (i.e., highly aerobic versus highly anaerobic fit individuals) during loaded ambulatory tasks to further elucidate characteristics of "optimal" performers.

The primary limitations of this study are its small, sex specific (female) sample and the number of consecutive data points (∼130). While this investigation cannot make inferences about sex specific responses to load carriage in the absence of a male cohort, females are an under represented population in load carriage literature (Loverro et al., 2019). Therefore, findings regarding motor variability, stride regulation and gait complexity of this study can only be generalized to healthy recruit-aged females (18–33 years old) whom are novices to load carriage and forced marching. Future research should compare males versus females and recruit versus experienced individuals (deployable soldiers) to determine if the unfamiliarity to the tasks and equipment were confounding the observed responses to load magnitude and locomotion pattern. Likewise, it is advised to perform fractal analysis with a minimum of 512 consecutive data points (Delignières et al., 2006), however, 128 consecutive strides has been determined to be within 6% of the actual scaling value (Hausdorff et al., 1997). In addition, performing steady-state behavior with load carriage while minimizing the effects of fatigue is difficult beyond several minute trials. Moreover, our findings on the effect of locomotion pattern on gait complexity are similar to investigations regarding imposed frequencies and complexity (Delignieres et al., 2004; Ducharme et al., 2018). Nevertheless, while not ideal for complexity, the ∼130 consecutive data points is a robust time-series for GEM decomposition (Dingwell et al., 2010) and provides the first quantitative data on load magnitude's influence on gait complexity. Lastly, upon the completion of the study we learned that one participant (S5) completed the experimental protocols with a distal avulsion of the semitendinosus. Interestingly, this participant exhibited "optimal" complexity for running at BW and BW + 25%. Although alone this data is inconclusive and may represent an isolated incident, but it does suggest that gait complexity of S_L and S_T may be an inappropriate factor to assess musculoskeletal health. The complexity of S_L and S_T specifically may only represent the global function of the locomotor system at achieving the task goal.

In conclusion, there are no interactive effects of load magnitude and locomotion pattern on motor variability, stride regulation and gait complexity. But load and locomotion do independently alter the function of the locomotor system. As load increases there is a reduction in relative variability (good:bad motor variability), gait complexity ($\alpha < 0.5$) and strides become more tightly controlled. FM further reduces gait complexity and mimics stride regulation strategies of BW + 45% load conditions. Moreover, despite more relative variability for FM compared to running, this appears to be a consequence of state-space exploration, as supported by the increased stride control/error correction and "suboptimal" complexity. While complexity of S_L and S_T may be indicative of locomotor system function in terms of achieving a task goal (maintaining horizontal velocity in the case of this investigation), the variability/complexity of these factors do not appear to represent the health of the musculoskeletal system (i.e., state of joint/tissue health and whether an injurious movement pattern is being used). Therefore, additional order parameters (different gait variables) should be investigated to identify a marker of global MSI risk. Likewise, research should be conducted with longer trials to confirm the complexity findings of this investigation and elucidate the role of fatigue. Soldiers ultimately operate

in dynamic environments with lots of perturbations under substantial load carriage where poor movement/slips, trips and fall can produce MSI or even death. The findings of this study indicate that locomotor system function is altered by FM and BW + 45% load, resulting in reduced motor variability and a system with less stability/adaptability that is potentially more susceptible to failure with additional perturbations.

DATA AVAILABILITY STATEMENT

The raw data supporting the conclusions of this article will be made available by the authors, upon reasonable request.

ETHICS STATEMENT

The studies involving human participants were reviewed and approved by the Institutional Review Board of University of Pittsburgh. The patients/participants provided their written informed consent to participate in this study.

AUTHOR CONTRIBUTIONS

KK, QM, NA, and CC analyzed the data. CC, WA, and KK designed the study and wrote the manuscript. KK, CJ, and DD were responsible for the data collection and data processing. RS, SG, GM, QM, SF, and WA contributed to writing and review and editing the manuscript. All authors contributed to the article and approved the submitted version.

FUNDING

This study was funded by the Freddie H. Fu award.

REFERENCES

Alexander, R. M. (1992). A model of bipedal locomotion on compliant legs. *Philos. Trans. R. Soc. Lond. B Biol. Sci.* 338, 189–198. doi: 10.1098/rstb.1992.0138

Al-Yahya, E., Dawes, H., Smith, L., Dennis, A., Howells, K., and Cockburn, J. (2011). Cognitive motor interference while walking: a systematic review and meta-analysis. *Neurosci. Biobehav. Rev.* 35, 715–728. doi: 10.1016/j.neubiorev.2010.08.008

Asay, J. L., Erhart-Hledik, J. C., and Andriacchi, T. P. (2018). Changes in the total knee joint moment in patients with medial compartment knee osteoarthritis over 5 years. *J. Orthop Res.* 36, 2373–2379. doi: 10.1002/jor.23908

Atlas Collaboration, Aad, G., Abbott, B., Abdallah, J., Abdel Khalek, S., Abdinov, O., et al. (2014). Measurement of the muon reconstruction performance of the ATLAS detector using 2011 and 2012 LHC proton-proton collision data. *Eur. Phys. J. C Part Fields* 74:3130.

Attwells, R. L., Birrell, S. A., Hooper, R. H., and Mansfield, N. J. (2006). Influence of carrying heavy loads on soldiers' posture, movements and gait. *Ergonomics* 49, 1527–1537. doi: 10.1080/00140130600757237

Baggaley, M., Esposito, M., Xu, C., Unnikrishnan, G., Reifman, J., and Edwards, W. B. (2020). Effects of load carriage on biomechanical variables associated with tibial stress fractures in running. *Gait Posture* 77, 190–194. doi: 10.1016/j.gaitpost.2020.01.009

Baida, S. R., Gore, S. J., Franklyn-Miller, A. D., and Moran, K. A. (2018). Does the amount of lower extremity movement variability differ between injured and uninjured populations? A systematic review. *Scand. J. Med. Sci. Sports* 28, 1320–1338. doi: 10.1111/sms.13036

Bak, P., and Paczuski, M. (1995). Complexity, contingency, and criticality. *Proc. Natl. Acad. Sci. U.S.A.* 92, 6689–6696. doi: 10.1073/pnas.92.15.6689

Bak, P., Tang, C., and Wiesenfeld, K. (1987). Self-organized criticality: an explanation of the 1/f noise. *Phys. Rev. Lett.* 59, 381–384. doi: 10.1103/physrevlett.59.381

Bakeman, R. (2005). Recommended effect size statistics for repeated measures designs. *Behav. Res. Methods* 37, 379–384. doi: 10.3758/bf03192707

Bent, L. R., Inglis, J. T., and McFadyen, B. J. (2004a). When is vestibular information important during walking? *J. Neurophysiol.* 92, 1269–1275. doi: 10.1152/jn.01260.2003

Bent, L. R., McFadyen, B. J., and Inglis, J. T. (2004b). Is the use of vestibular information weighted differently across the initiation of walking? *Exp. Brain Res.* 157, 407–416.

Bernstein, N. A. (1967). *The Coordination and Regulation of Movements*. London: Pergamon Press.

Birrell, S. A., Hooper, R. H., and Haslam, R. A. (2007). The effect of military load carriage on ground reaction forces. *Gait Posture* 26, 611–614. doi: 10.1016/j.gaitpost.2006.12.008

Bizzi, E., and Cheung, V. C. (2013). The neural origin of muscle synergies. *Front. Comput. Neurosci.* 7:51. doi: 10.3389/fncom.2013.00051

Black, D., Smith, B. A., Wu, J., and Ulrich, B. D. (2007). Uncontrolled manifold analysis of segmental angle variability during walking: preadolescents with and without down syndrome. *Exp. Brain Res.* 183, 511–521. doi: 10.1007/s00221-007-1066-1

Caballero, C., Davids, K., Heller, B., Wheat, J., and Moreno, F. J. (2019). Movement variability emerges in gait as adaptation to task constraints in dynamic environments. *Gait Posture* 70, 1–5. doi: 10.1016/j.gaitpost.2019.02.002

Cohen, J., Cohen, P., West, S. G., and Aiken, L. S. (2003). *Applied Multiple Regression/Correlation Analysis for the Behavioral Sciences*, 3rd Edn. New York, NY: Routledge.

Cusumano, J. P., and Dingwell, J. B. (2013). Movement variability near goal equivalent manifolds: fluctuations, control, and model-based analysis. *Hum. Mov. Sci.* 32, 899–923. doi: 10.1016/j.humov.2013.07.019

Davids, K., Glazier, P., Araujo, D., and Bartlett, R. (2003). Movement systems as dynamical systems: the functional role of variability and its implications for sports medicine. *Sports Med.* 33, 245–260. doi: 10.2165/00007256-200333040-00001

De Sanctis, P., Butler, J. S., Malcolm, B. R., and Foxe, J. J. (2014). Recalibration of inhibitory control systems during walking-related dual-task interference: a mobile brain-body imaging (MOBI) study. *Neuroimage* 94, 55–64. doi: 10.1016/j.neuroimage.2014.03.016

Delignieres, D., Lemoine, L., and Torre, K. (2004). Time intervals production in tapping and oscillatory motion. *Hum. Mov. Sci.* 23, 87–103. doi: 10.1016/j.humov.2004.07.001

Delignières, D., Ramdani, S., Lemoine, L., Torre, K., Fortes, M., and Ninot, G. (2006). Fractal analyses for 'short' time series: a re-assessment of classical methods. *J. Math. Psychol.* 50, 525–544. doi: 10.1016/j.jmp.2006.07.004

Delignières, D., and Torre, K. (2009). Fractal dynamics of human gait: a reassessment of Hausdorff et al. (1996)'s data. *J. Appl. Physiol.* 106, 1272–1279. doi: 10.1152/japplphysiol.90757.2008

Dingwell, J., John, J., and Cusumano, J. P. (2010). Do humans optimally exploit redundancy to control step variability in walking? *PLoS Comput. Biol.* 6:e1000856. doi: 10.1371/journal.pcbi.1000856

Dingwell, J., Salinas, M., and Cusumano, J. (2017). Increased gait variability may not imply impaired stride-to-stride control of walking in healthy older adults. *Gait Posture* 55, 131–137. doi: 10.1016/j.gaitpost.2017.03.018

Ducharme, S., Liddy, J. J., Haddad, J. M., Busa, M. A., Claxton, L. J., and Van Emmerik, R. E. (2018). Association between stride time fractality and gait adaptability during unperturbed and asymmetric walking. *Hum. Mov. Sci.* 58, 248–259. doi: 10.1016/j.humov.2018.02.011

Gates, D. H., and Dingwell, J. B. (2008). The effects of neuromuscular fatigue on task performance during repetitive goal-directed movements. *Exp. Brain Res.* 187, 573–585. doi: 10.1007/s00221-008-1326-8

Gelfand, I. M., and Latash, M. L. (1998). On the problem of adequate language in motor control. *Motor Control* 2, 306–313. doi: 10.1123/mcj.2.4.306

Gibson, J. J. (1966). *The Senses Considered as Perceptual Systems*. Boston, MA: Houghton Mifflin.

Gibson, J. J. (1979). *The Ecological Approach to Visual Perception*. Boston, MA: Houghton Mifflin.

Gisiger, T. (2001). Scale invariance in biology: Coincidence or footprint of a universal mechanism? *Biol. Rev. Camb. Philos. Soc.* 76, 161–209. doi: 10.1017/s1464793101005607

Goldberger, A., Peng, C. K., and Lipstiz, L. A. (2005). What is physiologic complexity and how does it change with aging and disease? *Neurobiol. Aging* 23, 23–26. doi: 10.1016/s0197-4580(01)00266-4

Hausdorff, J., Peng, C. K., Ladin, Z. V. I., Wei, J. Y., and Goldberger, A. L. (1995). Is walking a random walk? Evidence for long-range correlations in stride interval of human gait. *J. Appl. Physiol.* 349–358. doi: 10.1152/jappl.1995.78.1.349

Hausdorff, J. M. (2007). Gait dynamics, fractals and falls: finding meaning in the stride-to-stride fluctuations of human walking. *Hum. Mov. Sci.* 26, 555–589. doi: 10.1016/j.humov.2007.05.003

Hausdorff, J. M. (2009). Gait dynamics in Parkinson's disease: common and distinct behavior among stride length, gait variability, and fractal-like scaling. *Chaos* 19:026113. doi: 10.1063/1.3147408

Hausdorff, J. M., Mitchell, S. L., Firtion, R., Peng, C. K., Cudkowicz, M. E., Wei, J. Y., et al. (1997). Altered fractal dynamics of gait: reduced stride-interval correlations with aging and Huntington's disease. *J. Appl. Physiol.* 82, 262–269. doi: 10.1152/jappl.1997.82.1.262

Hausdorff, J. M., Purdon, P. L., Peng, C. K., Ladin, Z., Wei, J. Y., and Goldberger, A. L. (1996). Fractal dynamics of human gait: stability of long-range correlations in stride interval fluctuations. *J. Appl. Physiol.* 80, 1448–1457. doi: 10.1152/jappl.1996.80.5.1448

Hausdorff, J. M., Zemany, L., Peng, C., and Goldberger, A. L. (1999). Maturation of gait dynamics: stride-to-stride variability and its temporal organization in children. *J. Appl. Physiol.* 86, 1040–1047.

Hollands, M. A., and Marple-Horvat, D. E. (1996). Visually guided stepping under conditions of step cycle-related denial of visual information. *Exp. Brain Res.* 109, 343–356.

Huang, T., and Kuo, A. D. (2014). Mechanics and energetics of load carriage during human walking. *J. Exp. Biol.* 217, 605–613. doi: 10.1242/jeb.091587

Hunt, N., McGrath, D., and Stergiou, N. (2014). The influence of auditory-motor coupling on fractal dynamics in human gait. *Sci. Rep.* 4:5879.

Iyengar, N., Peng, C. K., Morin, R., Goldberger, A. L., and Lipsitz, L. A. (1996). Age-related alterations in the fractal scaling of cardiac interbeat interval dynamics. *Am. J. Physiol. Regul. Integr. Comp. Physiol.* 271, 1078–1084.

Jensen, A., Laird, M., Jameson, J. T., and Kelly, K. R. (2019). Prevalence of musculoskeletal injuries sustained during marine corps recruit training. *Mil. Med.* 184(Suppl. 1), 511–520. doi: 10.1093/milmed/usy387

Kim, Y., Tagawa, Y., Obinata, G., and Hase, K. (2011). Robust control of CPG-based 3D neuromusculoskeletal walking model. *Biol. Cybern.* 105, 269–282. doi: 10.1007/s00422-011-0464-4

Knapik, J. J., Reynolds, K. L., and Harman, E. (2004). Soldier load carriage: historical, physiological, biomechanical, and medical aspects. *Mil. Med.* 169, 45–56.

Krajewski, K. T., Dever, D. E., Johnson, C. C., Rawcliffe, A. J., Ahamed, N. U., Flanagan, S. D., et al. (2020). Load carriage magnitude and locomotion strategy alter knee total joint moment during bipedal ambulatory tasks in recruit-aged women. *J. Biomech.* 105:109772. doi: 10.1016/j.jbiomech.2020.109772

LaFiandra, M., Wagenaar, R. C., Holf, K. G., and Obusek, J. P. (2003). How do load carriage and walking speed influence trunk coordination and stride parameters? *J. Biomech.* 36, 87–95. doi: 10.1016/s0021-9290(02)00243-9

Latash, M. (2016). Biomechanics as a window into the neural control of movement. *J. Hum. Kinet.* 52, 7–20. doi: 10.1515/hukin-2015-0190

Latash, M., Levin, M. F., Scholz, J. P., and Schöner, G. (2010). Motor control theories and their applications. *Medicina* 46, 382–392. doi: 10.3390/medicina46060054

Latash, M., Scholz, J. P., and Schöner, G. (2002). Motor control strategies revealed in the structure of motor variability. *Exerc. Sports Sci. Rev.* 30, 26–31. doi: 10.1097/00003677-200201000-00006

Lenton, G., Doyle, T. L. A., Lloyd, D. G., Higgs, J., Billing, D., and Saxby, D. J. (2019). Lower-limb joint work and power are modulated during load carriage based on load configuration and walking speed. *J. Biomech.* 83, 174–180. doi: 10.1016/j.jbiomech.2018.11.036

Liew, B., Morris, S., and Netto, K. (2016). The effects of load carriage on joint work at different running velocities. *J. Biomech.* 49, 3275–3280. doi: 10.1016/j.jbiomech.2016.08.012

Lloyd, R. (2010). Kinetic changes associated with load carriage using two rucksack designs. *Ergonomics* 43, 1331–1341. doi: 10.1080/001401300421770

Lovalekar, M., Keenan, K. A., Beals, K., Nindl, B. C., Pihoker, A. A., Coleman, L. C., et al. (2020). Incidence and pattern of musculoskeletal injuries among women and men during marine corps training in sex-integrated units. *J. Sci. Med. Sport* 19, S1440–S2440.

Loverro, K., Hasselquist, L., and Lewis, C. L. (2019). Females and males use different hip and knee mechanics in response to symmertric military-relevant loads. *J. Biomech.* 95:109280. doi: 10.1016/j.jbiomech.2019.07.024

Marks-Tarlow, T. (1999). The self as a dynamical system nonlinear dynamics. *Psychol. Life Sci.* 3, 311–345.

Matthis, J. S., Barton, S. L., and Fajen, B. R. (2017). The critical phase for visual control of human walking over complex terrain. *Proc. Natl. Acad. Sci. U.S.A.* 114, E6720–E6729.

McGinnis, P., and Newell, K. M. (1982). Topological dynamics: a framework for describing movement and its constraints. *Hum. Mov. Sci.* 1, 289–305. doi: 10.1016/0167-9457(82)90017-3

Minassian, K., Hofstoetter, U. S., Dzeladini, F., Guertin, P. A., and Ijspeert, A. (2017). The human central pattern generator for locomotion: Does it exist and contribute to walking? *Neuroscientist* 23, 649–663. doi: 10.1177/1073858417699790

Molloy, J. M., Pendergrass, T. L., Lee, I. E., Chervak, M. C., Hauret, K. G., and Rhon, D. I. (2020). Musculoskeletal injuries and united states army readiness part I: overview of injuries and their strategic impact. *Mil. Med*. doi: 10.1093/milmed/usaa027

Moon, Y., Sung, J., An, R., Hernandez, M. E., and Sosnoff, J. J. (2016). Gait variability in people with neurological disorders: a systematic review and meta-analysis. *Hum. Mov. Sci.* 47, 197–208. doi: 10.1016/j.humov.2016.03.010

Mukherjee, M., and Yentes, J. M. (2018). Movement variability: a perspective on success in sports, health, and life. *Scand. J. Med. Sci. Sports* 28, 758–759. doi: 10.1111/sms.13038

Newell, K. M., and Vaillancourt, D. E. (2001). Dimensional change in motor learning. *Hum. Mov. Sci.* 20, 695–715. doi: 10.1016/s0167-9457(01)00073-2

Nordin, A., and Dufek, J. S. (2019). Reviewing the variability-overuse injury hypothesis: Does movement variability relate to landing injuries? *Res. Q. Exerc. Sport* 90, 190–205. doi: 10.1080/02701367.2019.1576837

Nourrit-Lucas, D., Tossa, A. O., Zelic, G., and Delignieres, D. (2015). Learning, motor skill, and long-range correlations. *J. Mot. Behav.* 47, 182–189. doi: 10.1080/00222895.2014.967655

Pacheco, M., and Newell, K. M. (2017). Search strategies in practice: Influence of information and task constraints. *Acta Psychol.* 182, 9–20. doi: 10.1016/j.actpsy.2017.11.004

Pandy, M. G., and Andriacchi, T. P. (2010). Muscle and joint function in human locomotion. *Annu. Rev. Biomed. Eng.* 12, 401–433. doi: 10.1146/annurev-bioeng-070909-105259

Peng, C., Mietus, J., Hausdorff, J. M., Havlin, S., Stanley, H. E., and Goldberger, A. L. (1993). Long-range anti-correlations and non-Gaussian behavior of the heartbeat. *Phys. Rev. Lett.* 70, 1343–1346. doi: 10.1103/physrevlett.70.1343

Peng, C. K., Havlin, S., Stanley, H. E., and Goldberger, A. L. (1995). Quantification of scaling exponents and crossove phenomena in nonstationary heartbeat time series. *Chaos* 5, 82–87. doi: 10.1063/1.166141

Peters, R. M., Dalton, B. H., Blouin, J. S., and Inglis, J. T. (2017). Precise coding of ankle angle and velocity by human calf muscle spindles. *Neuroscience* 349, 98–105. doi: 10.1016/j.neuroscience.2017.02.034

Ravi, D. K., Marmelat, V., Taylor, W. R., Newell, K. M., Stergiou, N., and Singh, N. B. (2020). Assessing the temporal organization of walking

variability: a systematic review and consensus guidelines on detrended fluctuation analysis. *Front. Physiol.* 11:562. doi: 10.3389/fphys.2020.00562

Richardson, J. T. E. (2011). Eta squared and partial eta squared as measures of effect size in educational research. *Educ. Res. Rev.* 6, 135–147. doi: 10.1016/j.edurev.2010.12.001

Roerdink, M., de Jonge, C. P., Smid, L. M., and Daffertshofer, A. (2019). Tightening up the control of treadmill walking: effects of maneuverability range and acoustic pacing on stride-to-stride fluctuations. *Front. Physiol.* 10:257. doi: 10.3389/fphys.2019.00257

Rossignol, S., Dubuc, R., and Gossard, J. P. (2006). Dynamic sensorimotor interactions in locomotion. *Physiol. Rev.* 86, 89–154. doi: 10.1152/physrev.00028.2005

Sánchez, C. C., Murillo, D. B., Davids, K., and Hernández, F. J. M. (2016). Variations in task constraints shape emergent performance outcomes and complexity levels in balancing. *Exp. Brain Res.* 234, 1611–1622. doi: 10.1007/s00221-016-4563-2

Seay, J., Fellin, R. E., Sauer, S. G., Frykman, P. N., and Bensel, C. K. (2014a). Lower extremity biomechanical changes associated with symmetrical torso loading during simulated marching. *Mil. Med.* 179, 85–91. doi: 10.7205/milmed-d-13-00090

Seay, J., Frykman, P. N., Sauer, S. G., and Gutekunst, D. J. (2014b). Lower extremity mechanics during marching at three different cadences for 60 minutes. *J. Appl. Biomech.* 30, 21–30. doi: 10.1123/jab.2012-0090

Sedighi, A., and Nussbaum, M. A. (2019). Exploration of different classes of metrics to characterize motor variability during repetitive symmetric and asymmetric lifting tasks. *Sci. Rep.* 9:9821.

Seifert, L., Button, C., and Davids, K. (2013). Key properties of expert movement systems in sport : an ecological dynamics perspective. *Sports Med.* 43, 167–178. doi: 10.1007/s40279-012-0011-z

Shafizadeh, M., Crowther, R., Wheat, J., and Davids, K. (2019). Effects of personal and task constraints on limb coordination during walking: a systematic review and meta-analysis. *Clin. Biomech.* 61, 1–10. doi: 10.1016/j.clinbiomech.2018.10.024

Simpson, K. M., Munro, B. J., and Steele, J. R. (2011). Effect of load mass on posture, heart rate and subjective responses of recreational female hikers to prolonged load carriage. *Appl. Ergon.* 42, 403–410. doi: 10.1016/j.apergo.2010.08.018

Simpson, R., Graham, S. M., Forida-James, G. D., Connaboy, C., Clement, R., and Jackson, A. S. (2010). Perceived exertion and heart rate models for estimating metabolic workload in elite British soldiers performing a backpack load-carriage task. *Appl. Physiol. Nutr. Metab.* 35, 650–656. doi: 10.1139/h10-053

Simpson, R. J., Graham, S. M., Connaboy, C., Clement, R., Pollonini, L., and Florida-James, G. D. (2017). Blood lactate thresholds and walking/running economy are determinants of backpack-running performance in trained soldiers. *Appl. Ergon.* 58, 566–572. doi: 10.1016/j.apergo.2016.04.010

Sporns, O., and Edelman, G. M. (1993). Solving Bernstein's problem: a proposal for the development of coordinated movement by selection. *Child Dev.* 64, 960–981. doi: 10.2307/1131321

Stadnitski, T. (2012). Measuring fractality. *Front. Physiol.* 3:127. doi: 10.3389/fphys.2012.00127

Taylor, N. A., Peoples, G. E., and Petersen, S. R. (2016). Load carriage, human performance, and employment standards. *Appl. Physiol. Nutr. Metab.* 41(6 Suppl. 2), S131–S147.

Telfer, S., Lange, M. J., and Sudduth, A. S. M. (2017). Factors influencing knee adduction moment measurement: a systematic review and meta-regression analysis. *Gait Posture* 58, 333–339. doi: 10.1016/j.gaitpost.2017.08.025

Terrier, P., and Dériaz, O. (2012). Persistent and anti-persistent pattern in stride-to-stride variability of treadmill walking: influence of rhythmic auditory cueing. *Hum. Mov. Sci.* 31, 1585–1597. doi: 10.1016/j.humov.2012.05.004

Terrier, P., Turner, V., and Schutz, Y. (2005). GPS analysis of human locomotion: further evidence for long-range correlations in stride-to-stride fluctuations of gait parameters. *Hum. Mov. Sci.* 24, 97–115. doi: 10.1016/j.humov.2005.03.002

Torre, K., and Balasubramaniam, R. (2009). Disentangling stability, variability and adaptability in human performance: focus on the interplay between local variance and serial correlation. *J. Exp. Psychol. Hum. Percept. Perform.* 37, 539–50. doi: 10.1037/a0020556

Torre, K., Delignières, D., and Lemoine, L. (2007). Detection of long-range dependence and estimation of fractal exponents through ARFIMA modelling. *Br. J. Math. Stat. Psychol.* 60, 85–106. doi: 10.1348/000711005x89513

Torre, K., Vergotte, G., Viel, É., Perrey, S., and Dupeyron, A. (2019). Fractal properties in sensorimotor variability unveil internal adaptations of the organism before symptomatic functional decline. *Sci. Rep.* 9:15736.

Turvey, M. (1990). Coordination. *Am. Psychol.* 45, 938–953.

Van Orden, G., Kloos, H., and Wallot, S. (2009). Living in the pink: intentionality wellbeing and complexity. *Handb. Philos. Sci.* 10, 639–689.

Van Orden, G. C., Holden, J. G., and Turvey, M. T. (2003). Self-organization of cognitive performance. *J. Exp. Psychol. Gen.* 132, 331–350.

Walsh, G. S., Low, D. C., and Arkesteijn, M. (2018). Effect of stable and unstable load carriage on walking gait variability, dynamic stability and muscle activity of older adults. *J. Biomech.* 73, 18–23. doi: 10.1016/j.jbiomech.2018.03.018

Warren, W. H., Kay, B. A., Zosh, W. D., Duchon, A. P., and Sahuc, S. (2001). Optic flow is used to control human walking. *Nat. Neurosci.* 4, 213–216. doi: 10.1038/84054

West, B. J., and Scafetta, N. (2003). Nonlinear dynamical model of human gait. *Phys. Rev. E Stat. Nonlin. Soft Matter Phys.* 67(5 Pt 1), 051917.

West, B. J., and Shlesinger, M. F. (1989). On the ubiquity of 1/f noise. *Int. J. Mod. Phys. B.* 3, 795–819.

Wills, J., Saxby, D. J., Lenton, G. K., and Doyle, T. L. A. (2019). Ankle and knee moment and power adaptations are elicited through load carriage conditioning in males. *J. Biomech.* 97:109341. doi: 10.1016/j.jbiomech.2019.109341

Willy, R. W., DeVita, P., Meardon, S. A., Baggaley, M., Womble, C. C., and Willson, J. D. (2019). Effects of load carriage and step length manipulation on Achilles tendon and knee loads. *Mil. Med.* 184, e482–e489.

Willy, R. W., Willson, J. D., Clowers, K., Baggaley, M., and Murray, N. (2016). The effects of body-borne loads and cadence manipulation on patellofemoral and tibiofemoral joint kinetics during running. *J. Biomech.* 49, 4028–4033. doi: 10.1016/j.jbiomech.2016.10.043

Woollacott, M., and Shumway-Cook, A. (2002). Attention and the control of posture and gait: a review of an emerging area of research. *Gait Posture* 16, 1–14. doi: 10.1016/s0966-6362(01)00156-4

Zabala, M. E., Favre, J., Scanlan, S. F., Donahue, J., and Andriacchi, T. P. (2013). Three-dimensional knee moments of ACL reconstructed and control subjects during gait, stair ascent, and stair descent. *J. Biomech.* 46, 515–520. doi: 10.1016/j.jbiomech.2012.10.010

Conflict of Interest: The authors declare that the research was conducted in the absence of any commercial or financial relationships that could be construed as a potential conflict of interest.

frontiers in Human Neuroscience

CASE REPORT
published: 25 September 2020
doi: 10.3389/fnhum.2020.549965

Effects of Multi-Muscle Electrical Stimulation and Stand Training on Stepping for an Individual With SCI

*Kamyar Momeni[1,2], Arvind Ramanujam[1], Manikandan Ravi[1], Erica Garbarini[1] and Gail F. Forrest[1,2]**

[1] Tim and Caroline Reynolds Center for Spinal Stimulation, Kessler Foundation, West Orange, NJ, United States,
[2] Department of Physical Medicine and Rehabilitation, Rutgers New Jersey Medical School, Newark, NJ, United States

The objective of this study was to evaluate the biomechanical, neural, and functional outcomes during a 10-min treadmill stepping trial before and after two independent interventions with neuromuscular electrical stimulation (ES) in an individual with spinal cord injury (SCI). In this longitudinal study, a 34-year-old male with sensory- and motor-complete SCI (C5/C6) underwent two consecutive interventions: 61 h of supine lower limb ES (ES-alone) followed by 51 h of ES combined with stand training (ST) using an overhead body-weight support (BWS) system (ST + ES). In post ES-alone (unloaded), compared to baseline, the majority (∼60%) of lower extremity muscles decreased their peak surface electromyography (sEMG) amplitude, while in post ST + ES (loaded), compared to post ES-alone, there was a restoration in muscle activation that endured the continuous 10-min stepping. Temporal α-motor neuron activity patterns were observed for the SCI participant. In post ST + ES, there were increases in spinal activity patterns during mid-stance at spinal levels L5–S2 for the right and left limbs. Moreover, in post ES-alone, trunk stability increased with excursions from the midline of the base-of-support (50%) to the left (44.2%; Baseline: 54.2%) and right (66.4%; baseline: 77.5%). The least amount of trunk excursion observed post ST + ES, from midline to left (43%; AB: 22%) and right (64%; AB: 64%). Overall, in post ES-alone, there were gains in trunk independence with a decrease in lower limb muscle activation, whereas in post ST + ES, there were gains in trunk independence and increased muscle activation in both bilateral trunk muscles as well as lower limb muscles during the treadmill stepping paradigm. The results of the study illustrate the importance of loading during the stimulation for neural and mechanical gains.

Keywords: spinal cord injury, multimuscle electrical stimulation, neuromuscular stimulation, stand training, locomotor training, body weight-supported training

OPEN ACCESS

Edited by:
Yury Ivanenko, Santa Lucia Foundation (IRCCS), Italy

Reviewed by:
Emilia Ambrosini, Politecnico di Milano, Italy
Kei Masani, University Health Network, Canada
Michael James MacLellan, University of Prince Edward Island, Canada

***Correspondence:**
Gail F. Forrest
gforrest@kesslerfoundation.org

Specialty section:
This article was submitted to Motor Neuroscience, a section of the journal Frontiers in Human Neuroscience

Received: *07 April 2020*
Accepted: *28 August 2020*
Published: *25 September 2020*

Citation:
Momeni K, Ramanujam A, Ravi M, Garbarini E and Forrest GF (2020) Effects of Multi-Muscle Electrical Stimulation and Stand Training on Stepping for an Individual With SCI. Front. Hum. Neurosci. 14:549965. doi: 10.3389/fnhum.2020.549965

INTRODUCTION

Motor-complete spinal cord injury (SCI) is associated with an inability to move below the level of a lesion resulting in skeletal unloading and rapid muscle atrophy (Spungen et al., 2003; Dudley-Javoroski and Shields, 2006; Momeni et al., 2019). The early musculoskeletal deterioration, while affecting both acute and chronic health conditions, can directly impact future functional mobility,

trunk independence, and independent standing or walking (Spungen et al., 2003; Gorgey and Dudley, 2007; Gorgey et al., 2012).

The combination of step and stand training protocols, such as locomotor training, and stand training (ST) alone have been extensively published to show improvements in seated balance, independent standing, gains in stepping and walking measures for individuals with a motor-incomplete SCI (Forrest et al., 2008b; Forrest et al., 2008a, 2012; Harkema et al., 2011, 2012b; Buehner et al., 2012). However, for individuals with complete lesions, these activity-based interventions do not seem to be sufficient for functional gains in the lower extremity (Qin et al., 2010), although several published studies do show the influence of activity-based therapies for positive lower extremity neurophysiological or neuromuscular modulations after having completed a large number of training sessions (Forrest et al., 2008b; Mitchell et al., 2015; Canton et al., 2016).

Previous studies on longitudinal applications of neuromuscular electrical stimulation (ES) for a single- or multimuscle-elicited contractions have shown a direct improvement in skeletal muscle size and strength, as well as body composition, metabolic profile, function, neuromuscular control, and reduction of fatigue in stimulated muscles (Mahoney et al., 2005; Sabatier et al., 2006; Gorgey et al., 2012, 2015; Ryan et al., 2013) for both chronic and acute SCI. Moreover, multimuscle ES of the lower and upper extremity have shown an improvement in muscle function even during activities of daily living (Popovic et al., 2006; Kapadia et al., 2014). When lower limb multimuscle ES is combined with ST and compared to lower limb multimuscle ES alone (without loading), there are increased gains in lower limb muscle hypertrophy (Forrest G. et al., 2009), trunk control, and trunk muscle activation during independent standing leading to independent standing postural balance. In the present investigation, we extend our earlier work (Momeni et al., 2019) to identify and characterize alterations in the neuromuscular, biomechanical, and functional adaptations during a treadmill stepping paradigm after ST combined with lower limb multi-muscle ES. Also, we will demonstrate the activity-dependent plasticity associated with loading during multimuscle ES compared to multimuscle ES alone (without loading). Loaded vs. unloaded training conditions accompanied the improved locomotion and dynamic posture, as observed in the individual with motor-complete SCI.

METHODS

An individual with chronic, motor-complete SCI (neurological level of injury at C5/C6) and an able-bodied (AB) individual participated in this study (**Table 1**). Neuromuscular and biomechanical assessments were completed for the participant with SCI: (1) prior to any intervention, (2) after 61 h of bilateral, lower limb ES in supine (ES-alone), and (3) after 51 h of dynamic ST combined with bilateral, lower limb ES (ST + ES). Similar biomechanical and neuromuscular assessments were also completed for AB at one time point, without any intervention.

TABLE 1 | Demographics of the participant with spinal cord injury (SCI) and the able-body control (AB).

Participant	Age (Year)	Height (cm)	Weight (kg)	TSI[a] (Months)	AIS[b]	Intervention (*h*)
SCI	34	180.3	66.4	19	A	61 (ES-alone) 51 (ST + ES)
AB	25	185.0	76.4	–	–	–

[a]Time since injury. [b]American Spinal Injury Association Impairment Scale from The International Standards for Neurological Classification of Spinal Cord Injury (ISNCSCI) (Marino et al., 2008; Schuld et al., 2016).

Training sessions occurred three to four times per week, each for a duration of 1 h (**Table 1**). All procedures were approved by the Kessler Foundation's Institutional Review Board. Informed consent was obtained before participation.

Training Protocol

Supine Electrical Stimulation (ES-Alone)

Neuromuscular electrical stimulation (ES) was applied in the supine position via bifurcated leads and self-adhesive reusable surface electrodes. Self-adhesive stimulation electrodes were placed over the motor points of bilateral upper-leg and lower-leg muscles: quadriceps muscle group (QUAD), hamstrings muscle group (HAM), gastrocnemius (GN), and tibialis anterior (TA). Two 5 × 10-cm oval electrodes were placed on each of the RF and BF muscles and two 5 × 5-cm square electrodes on each of the GN and TA muscles. Biphasic, square-wave electrical pulses were applied, using the Rehabilicare IF 3WAVE System (Compex Technologies Inc., New Brighton, MN, United States). Symmetrical 300-μs biphasic, square-wave pulses at 35 Hz were delivered over a duty cycle of 11 s on, 60 s off. Stimulation intensity was determined for each muscle and periodically adjusted throughout the interventions, based on participant's muscle response with a maximum amplitude of 100 mA. During the 11-s stimulation window in each cycle, stimulation pulses were applied to the lower-leg muscles first; then after 4 s, it was also applied to the upper-leg muscles for the remaining 7 s, creating a 7-s stimulation overlap between the upper- and lower-leg muscles in each cycle (Momeni et al., 2019).

Prior to training, the participant was acclimated to electrical stimulation during the process of determining the highest tolerable level of ES that produced both visible and palpable contractions in all muscles; these values were then recorded to be used and adjusted throughout the training.

Stand Training and Electrical Stimulation (ST + ES)

This is a combination of the multimuscle ES, mentioned above, and stand training, which involves a series of standardized dynamic tasks while standing using an overhead body-weight support (BWS) system (Robomedica®, Irvine, CA, United States). Training was divided into two different modes of stand training: stand adaptability (at higher percentage of BWS) and stand retraining (at lower percentage of BWS) (Harkema et al., 2012a). Stand adaptability training at higher percentage of BWS provided greater assistance with increased body weight assistance for an individual to complete the different stand training tasks

independently with less assistance from trainers. Stand retraining was performed with the minimum BWS (0%, if possible), with the trainers providing assistance during the stand training tasks, promoting weight bearing during standing. In addition to quiet standing as a task, other tasks were performed, such as lateral and anterior weight shifts, etc.

Further details of the stand training protocol are described in our previous work (Momeni et al., 2019). Once every 10 min throughout the training, the heart rate and blood pressure were monitored for the safety of the participant (Canton et al., 2016; Momeni et al., 2016).

Data Collection

Data were collected at baseline, post ES-alone intervention, and post ST + ES intervention. The participant performed a 10-min assisted-stepping session on a treadmill with a speed of 0.8 m/s and 60% BWS, but without use of ES; manual assistance at pelvis and bilateral knees was provided by trained therapists (Behrman et al., 2005). The AB participant performed two walking trials on the BWS treadmill: (1) with harness and 50% BWS and (2) without harness, both at a speed of 1.5 m/s to elicit bilateral muscle activations synonymous with walking (Anders et al., 2007).

Neuromuscular Data

Surface electromyography (sEMG) data were collected at 2,520 Hz using two EMG systems (MA-100 and MA-300, Motion Lab Systems Inc., Baton Rouge, LA, United States) and stainless steel, differential input design, and surface electrodes with an inter-electrode distance of 18 mm (Motion Lab Systems Inc., Baton Rouge, LA, United States). EMG electrodes were placed bilaterally on the following muscles: erector spinae T5 (SES), erector spinae T12 (IES), external obliques (EO), internal obliques (IO), gluteus maximus (GM), rectus femoris (RF), vastus lateralis (VL), biceps femoris (BF), tibialis anterior (TA), gastrocnemius (GN), and soleus (S). Electrode placement protocol has been explained in further detail elsewhere (Kendall et al., 2013; Momeni et al., 2019). Reference electrodes were placed on the clavicles.

Biomechanical/Kinematics Data

Kinematic data were collected at 60 Hz using a motion capture system (Vicon Motion Systems Ltd., Oxford Metrics, United Kingdom). Reflective markers were placed on specific anatomical landmarks according to the Vicon Plug-in Gait marker set.

Data Analysis

The first-, fifth-, and tenth-minute periods of the 10-min assisted-stepping trials were extracted for further analysis and are referred to as time periods (t_1, t_5, and t_{10}, respectively). Kinematic data were filtered using a low-pass (cut-off: 6 Hz) Butterworth filter (fourth order, zero lag). The bilateral heel and toe markers' 3-D coordinates were used to determine the instantaneous base of support (*BoS*), defined as the distance between the left and right heel markers, and gait cycle events (i.e., Heel strike and Toe off) for the stepping trials. Gait cycles were determined between consecutive ipsilateral heel strikes and time normalized. Trunk model (de Leva, 1996), using acromion and anterior superior iliac spine (ASIS) markers, determined: (i) sagittal plane excursion for trunk center-of-mass ($CoM_{T,AP}$), relative to left heel marker, normalized to mean step length (defined as the anterior–posterior distance between the bilateral heel markers at consecutive heel strikes), and duration of each gait cycle ($\widehat{CoM}_{T,AP}$) and ii) frontal plane excursion for trunk center-of-mass ($CoM_{T,ML}$), relative to left heel marker, normalized to the instantaneous width of BoS and duration of each gait cycle ($\widehat{\mathrm{CoM}}_{T,ML}$). Profiles were then averaged for the first minute of the stepping trial.

Quantification of sEMG was completed through custom-written programs, developed in MATLAB (MathWorks^{TM}, Natick, MA, United States). Surface EMG data were gain-normalized, full-wave rectified, and filtered using band-pass (20–150 Hz) and band-stop (60 ± 3 Hz) Butterworth filters (fourth order, zero lag) for further analysis. The onset and cessation of EMG bursts during each gait cycle were defined using the Teager–Kaiser energy operator (TKEO) as previously described (Solnik et al., 2010; Pilkar et al., 2012; Canton et al., 2016; Momeni et al., 2016). The TKEO measures instantaneous energy changes of a signal and amplifies the energy of the action potential spikes; therefore, it differentiates between the relaxed and contracted states of the muscle. Further, the TKEO output is derived from the instantaneous amplitude and frequency of the signal; hence, the TKEO conditioning flattens the low-frequency baseline during non-active periods, reduces false onset detection, and increases robustness of computerized methods (Solnik et al., 2010). To identify the onset and cessation of sEMG activation, the TKEO output for each muscle was used to calculate the baseline noise and establish a detection threshold of seven standard deviations above the calculated baseline.

Mean and peak burst amplitude (μV), and burst duration as a percentage of gait cycle (%GC) were calculated for each muscle. EMG variables were calculated for each gait cycle separately at three time periods, first-, fifth-, and tenth-minute (t_1, t_5, t_{10}), during the 10-min stepping trial at baseline, post ES-alone, and post ST + ES. Therefore, each mean EMG measure had three values at baseline, three at post ES-alone, and three at post ST + ES (**Table 2**).

Three measures of muscle co-contraction were calculated: co-excitation (CE), co-inhibition (CI), and co-activation (CA). CE was defined as the time period that two muscles were simultaneously active, relative to the total time either muscle was active during each gait cycle. CI was defined as the time period that two muscles were simultaneously inactive, relative to the total time either muscle was inactive, during each gait cycle. CA was defined as the mean of CE and CI, within each gait cycle. Values were: (i) averaged over multiple gait cycles for each given time period (t_1, t_5, and t_{10}) and (ii) presented as percentages of the gait cycle. An index value of 100% indicates complete CA, CE, or CI of activation, whereas a value of 0% indicates no CA, CE, or CI of activation (Johnson, 2003; Canton et al., 2016; Momeni et al., 2016).

For lower limb muscles, co-contraction (CA, CE, and CI) values were determined for the ipsilateral agonist/antagonist muscle pairings (i.e., RF/BF, RF/GM, VL/GM, VL/BF, TA/GN,

TABLE 2 | Burst duration, as a percentage of gait cycle (%GC), and mean EMG (μV) values for the left limb of the SCI participant.

	Muscle	BASELINE			ES-alone			ST + ES		
		1st min	5th min	10th min	1st min	5th min	10th min	1st min	5th min	10th min
BURST DURATION (%GC)	GM	12 ± 7	13 ± 6	10 ± 6	5 ± 3	6 ± 3	8 ± 4	9 ± 7	17 ± 6	14 ± 7
	BF	42 ± 11	29 ± 9	42 ± 12	34 ± 10	26 ± 17	34 ± 11	34 ± 7	25 ± 8	12 ± 6
	RF	70 ± 9	62 ± 9	52 ± 14	40 ± 9	50 ± 11	36 ± 9	28 ± 7	31 ± 7	29 ± 8
	VL	62 ± 11	39 ± 7	30 ± 12	28 ± 9	29 ± 11	15 ± 7	33 ± 7	31 ± 7	26 ± 7
	TA	60 ± 15	40 ± 9	46 ± 13	57 ± 9	45 ± 10	36 ± 10	42 ± 8	42 ± 11	20 ± 10
	GN	74 ± 7	64 ± 7	45 ± 7	14 ± 8	22 ± 10	25 ± 10	60 ± 7	68 ± 11	51 ± 8
	S	64 ± 8	58 ± 7	66 ± 9	82 ± 11	85 ± 10	63 ± 10	48 ± 6	68 ± 14	43 ± 6
	SES	55 ± 17	74 ± 19	74 ± 15	65 ± 18	60 ± 17	76 ± 19	58 ± 18	55 ± 14	70 ± 22
	IES	32 ± 14	77 ± 13	73 ± 13	85 ± 10	71 ± 16	90 ± 12	69 ± 13	83 ± 11	75 ± 13
	EO	43 ± 17	62 ± 20	75 ± 18	73 ± 16	67 ± 21	91 ± 14	23 ± 11	16 ± 7	15 ± 7
	IO	49 ± 17	74 ± 22	74 ± 16	51 ± 19	52 ± 18	54 ± 23	74 ± 19	61 ± 10	63 ± 19
MEAN EMG (μV)	GM	0.70 ± 0.06	0.62 ± 0.05	0.61 ± 0.04	0.76 ± 0.04	0.78 ± 0.04	0.76 ± 0.04	0.78 ± 0.06	0.71 ± 0.04	0.73 ± 0.05
	BF	1.24 ± 0.14	1.02 ± 0.11	0.89 ± 0.08	1.25 ± 0.07	1.64 ± 0.20	1.38 ± 0.14	1.12 ± 0.16	0.88 ± 0.08	0.82 ± 0.05
	RF	3.35 ± 0.49	2.68 ± 0.46	2.46 ± 0.52	1.88 ± 0.29	2.02 ± 0.35	1.93 ± 0.31	1.15 ± 0.13	1.47 ± 0.29	1.36 ± 0.19
	VL	2.97 ± 0.59	1.79 ± 0.43	1.22 ± 0.28	0.18 ± 0.03	0.17 ± 0.03	0.16 ± 0.02	1.76 ± 0.27	1.78 ± 0.40	1.18 ± 0.16
	TA	2.17 ± 0.53	1.49 ± 0.13	1.16 ± 0.11	1.93 ± 0.34	1.27 ± 0.17	1.15 ± 0.11	2.12 ± 0.28	1.60 ± 0.22	1.36 ± 0.13
	GN	5.83 ± 0.76	4.09 ± 0.33	3.35 ± 0.26	4.97 ± 0.42	3.29 ± 0.30	3.24 ± 0.21	4.10 ± 0.52	2.67 ± 0.29	2.09 ± 0.18
	S	6.52 ± 0.54	5.83 ± 0.46	5.20 ± 0.78	4.54 ± 0.94	3.71 ± 0.68	4.02 ± 0.44	7.75 ± 0.79	7.07 ± 1.12	6.38 ± 0.59
	SES	3.26 ± 0.32	2.99 ± 0.60	2.26 ± 0.36	37.72 ± 6.48	26.91 ± 5.24	1.36 ± 0.29	2.02 ± 0.32	1.61 ± 0.23	5.11 ± 1.53
	IES	24.07 ± 2.36	10.86 ± 1.60	9.66 ± 1.68	17.72 ± 2.37	14.77 ± 2.69	17.87 ± 4.75	36.54 ± 5.34	31.56 ± 5.42	30.64 ± 5.12
	EO	4.97 ± 0.65	6.48 ± 1.33	6.05 ± 1.09	3.00 ± 0.40	3.17 ± 0.58	4.19 ± 1.01	1.77 ± 0.21	1.68 ± 0.19	1.79 ± 0.22
	IO	3.40 ± 0.34	3.02 ± 0.61	2.29 ± 0.37	3.26 ± 0.47	2.80 ± 0.48	1.41 ± 0.28	25.49 ± 4.10	4.40 ± 0.45	3.05 ± 0.88

and TA/S) whereas for trunk muscles, co-contraction values were determined for the ipsilateral trunk muscle pairings (i.e., SES/IES and IO/EO). Each of the CA, CE, and CI values was calculated at t_1, t_5, and t_{10} periods of baseline, post ES-alone, and post ST + ES. Therefore, each muscle co-contraction pair had three values at baseline, three at post ES-alone, and three at post ST + ES. For instance, for the two shank muscle pairs (TA/GN and TA/S), there is a total of 12 indices available bilaterally for all time periods combined (i.e., 2 muscle pairs × 2 limbs × 3 time periods).

Statistical analyses were performed using IBM SPSS (v.26, IBM Corp., Armonk, NY, United States). Descriptive statistics include mean ± standard deviation. To compare each of these outcome measures derived from individual gait cycles (total of ∼30–40 gait cycles) for each time period, multiple paired *T*-tests were performed determining significant differences between consecutive time points (i.e., post ES-alone and baseline, post ST + ES and post ES-alone). Significance level was set at 0.05.

We generated spatiotemporal maps of the α-motorneuron (MN) activities during assisted stepping to distinguish the approximate location of ipsilateral MN pools in the rostrocaudal axis of the human spinal cord and to further determine the characteristics of the locomotion circuitry. EMG and kinematics data were used to construct maps of spinal MN activity according to myotomal charts of Kendall et al. (2005). These spinal localization charts were created based on anatomical and clinical data (Kendall et al., 2005); thus, it is assumed that our participants have the same spinal topography as the reference population. The recorded muscle activity patterns were weighed and mapped onto the approximate location of the ipsilateral spinal MN pools (Ivanenko et al., 2006). For each spinal segment, S_j, contributions of any number of rectified EMGs corresponding to that segment were weighed, separately, and then averaged:

$$S_j = \frac{\sum_{i=1}^{n_j} w_{ij}.EMG_i}{n_j} \quad (1)$$

where n_j is the total number of EMG signals corresponding to the *j*th spinal segment, and w_{ij} is the weighing coefficient for the *i*th muscle, within the *j*th spinal segment. Weighing coefficients are based on Kendall et al. (2005) reference segmental charts for all muscles, compiled by combining anatomical and clinical data from six sources; they assigned "X" to localizations agreed on by five or more sources and "x" to those agreed on by three to four sources. We have utilized Ivanenko's method (Ivanenko et al., 2006) that assigns a weighing coefficient of 1 and 0.5 to "X" and "x," respectively.

A total of 24 activation waveforms were derived based on the 24 anatomical vertebrate segments covering spinal levels C4 through S2, corresponding to the levels at which the motorneurons innervate the recorded muscles. Note – data were recorded from 22 bilateral muscles with the assumption that rectified EMG waveforms, utilized for generating maps, provide an indirect measure of each muscle's α-motorneurons' net activity in the spinal cord. To generate the smoothed spatiotemporal maps, filled contour plots were created from the mean of the activation waveform matrix across multiple time-normalized gait cycles, separated by stance and swing phases.

RESULTS

For the SCI participant, the linear envelope of the mean rectified sEMG profiles for t_1, t_5, and t_{10} at baseline, post ES-alone, and post ST + ES are shown in **Figure 1**. Profiles for the AB control during independent treadmill stepping are also shown in **Figure 1**.

Lower Extremity Muscle Activations

Mean Amplitude

In post ES-alone, compared to baseline measures, the mean amplitude (**Figure 1**) for bilateral S muscles decreased for t_1, t_5, and t_{10} ($p < 0.000$ bilaterally), except for right S muscle at t_1. In post ST + ES, compared to post ES-alone, the mean amplitudes for S muscles increased bilaterally in all time periods ($p < 0.000$ bilaterally).

Peak Amplitude

For all time periods (t_1, t_5, and t_{10}), peak EMG amplitudes (**Figure 2A**) for left RF ($p < 0.000$), VL ($p < 0.000$), GN ($p < 0.000$), and S ($p < 0.000$), and right RF ($p < 0.000$), BF ($p < 0.000$), TA ($p = 0.007$), GN ($p < 0.000$, except for t_{10}) decreased post ES-alone, compared to baseline. In post ST + ES, compared to ES-alone, peak EMG amplitudes for left VL ($p < 0.000$), TA ($p < 0.000$), S ($p < 0.000$) and for right BF ($p < 0.000$), TA ($p = 0.018$), S ($p < 0.000$), GN ($p < 0.000$) increased for all time periods.

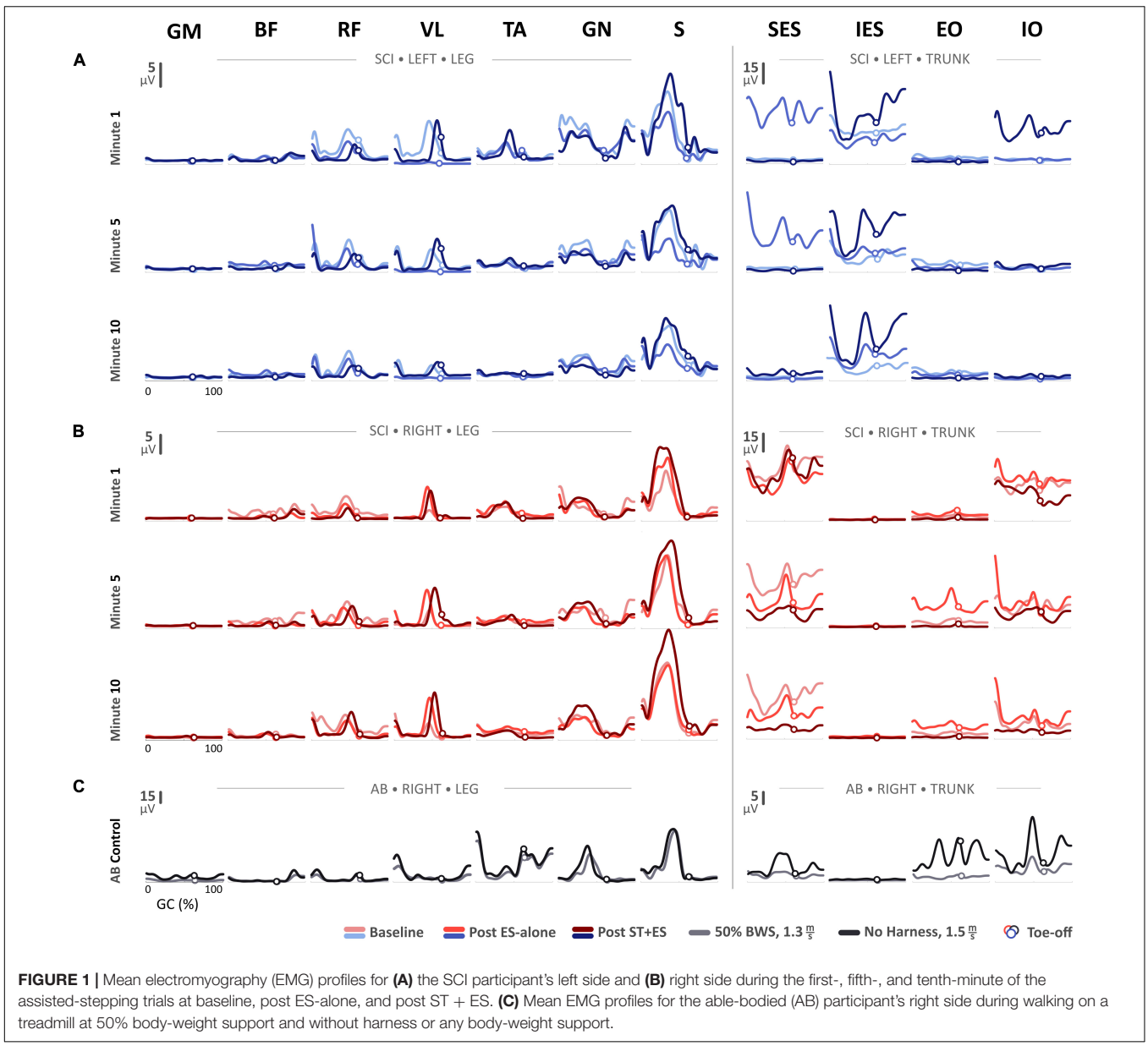

FIGURE 1 | Mean electromyography (EMG) profiles for **(A)** the SCI participant's left side and **(B)** right side during the first-, fifth-, and tenth-minute of the assisted-stepping trials at baseline, post ES-alone, and post ST + ES. **(C)** Mean EMG profiles for the able-bodied (AB) participant's right side during walking on a treadmill at 50% body-weight support and without harness or any body-weight support.

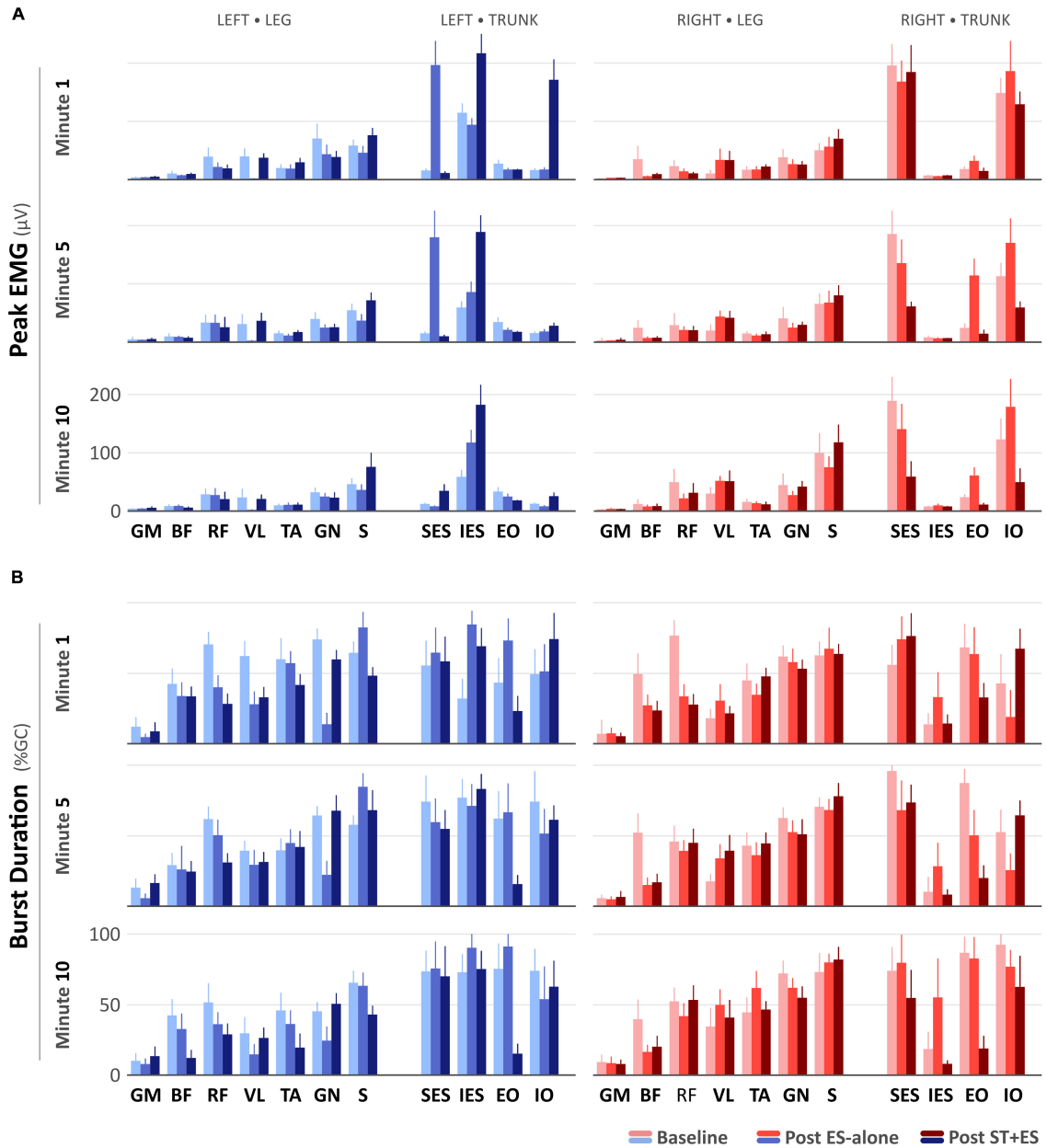

FIGURE 2 | (A) Peak electromyography (μV) and **(B)** burst duration (% Gait Cycle) values for the SCI participant during the first-, fifth-, and tenth-minute of the assisted-stepping trials at baseline, post ES-alone, and post ST + ES.

Burst Duration

In post ES-alone, compared to baseline, burst duration (**Figure 2B**) decreased bilaterally for RF ($p < 0.000$), BF ($p < 0.000$), GN ($p < 0.000$) muscles, and left VL ($p < 0.000$) for all time periods, while for bilateral S ($p < 0.014$) muscles, it decreased in two of six time periods (i.e., 2/6). In post ST + ES, compared to ES-alone, burst duration increased in seven different muscles, including left GM ($p < 0.000$), VL ($p < 0.000$), GN ($p < 0.000$), and right BF ($p = 0.036$), RF ($p < 0.000$), TA ($p < 0.000$), S ($p < 0.000$) in two of three time periods, while it decreased for left RF ($p < 0.000$), BF ($p = 0.001$), TA ($p < 0.000$), and S ($p < 0.000$) in all time periods (t_1, t_5, and t_{10}).

Trunk Muscle Activations

Mean Amplitude

In post ES-alone, compared to baseline, for all time periods (t_1, t_5, t_{10}), the mean amplitude (**Figure 1**) for left SES ($p < 0.000$), IES ($p < 0.000$), and right IO ($p < 0.000$) increased, while it decreased for right SES ($p < 0.000$). In post ST + ES, compared to ES-alone, the mean amplitude for left IES ($p < 0.000$) and IO ($p < 0.000$)

increased for t_1, t_5, and t_{10}, however, it decreased for right IO ($p < 0.000$). Bilateral SES ($p < 0.000$) amplitude also decreased in five of six time periods.

Peak Amplitude

In Post ES-alone, the peak EMG amplitude increased for left SES ($p < 0.000$), IES ($p < 0.000$), and right EO ($p < 0.000$), IO ($p < 0.000$); left EO ($p < 0.000$) increased in 11 of 12 time periods. Right SES ($p < 0.000$) peak EMG amplitude decreased for t_1, t_5, and t_{10}. In post ST + ES, compared to ES-alone, the peak EMG amplitude increased for left IES ($p < 0.000$) and IO ($p < 0.000$) for t_1, t_5, and t_{10}. Bilateral SES ($p < 0.000$) and right IO ($p < 0.000$) and EO ($p < 0.000$) decreased the peak EMG amplitude in 14 of 15 time periods (**Figure 2A**).

Burst Duration

In Post ES-alone, burst duration (**Figure 2B**) increased for bilateral IES ($p < 0.000$) and left EO ($p < 0.000$) in 10 of 12 time periods. In post ST + ES, compared to post ES-alone, burst duration increased for bilateral IO ($p < 0.000$, except the right IO at t_{10}) at each time period (t_1, t_5, and t_{10}). Burst duration decreased in all other muscles for t_1, t_5, and t_{10}.

Lower Extremity Muscle Co-contraction

In post ES-alone, 19 of 24 bilateral thigh agonist/antagonist CA indices increased significantly ($p < 0.015$) for all time periods (t_1, t_5, and t_{10}). CA indices for left VL/BF ($p < 0.015$, except at t_5) and right VL/GM ($p < 0.000$, except at t_1) significantly decreased. Bilateral shank (TA/GN, TA/S) agonist/antagonist CA decreased in 10 of 12 calculated indices ($p_{\text{LeftTA/GN}} < 0.009$ except at t_{10}, $p_{\text{RightTA/GN}} = 0.014$ only at t_1, $p_{\text{LeftTA/S}} < 0.000$ except at t_{10}, and $p_{\text{RightTA/S}} = 0.002$ only at t_5). In post ES-alone, 18 CE indices for left thigh and shank decreased significantly ($p < 0.024$). Nineteen (19 of 24) bilateral thigh and three (3 of 12) shank CI indices increased significantly ($p < 0.006$ and $p < 0.004$, respectively); three of 6 TA/S CI indices decreased ($p < 0.011$) (**Figure 3**).

In post ST + ES, 11 of 24 bilateral thigh CA indices decreased significantly over all time periods ($p < 0.029$). Bilateral shank muscle agonist/antagonist CA increased significantly in 9 of 12 calculated indices ($p < 0.014$). Seven (7 of 24) bilateral thigh CE indices decreased significantly ($p < 0.044$), while 8 of 12 shank CE indices increased ($p < 0.044$). Bilateral CI increased significantly in 9 of 24 thigh indices ($p < 0.029$) as well as 8 of 12 shank indices ($p < 0.043$), which includes significant increases in four of six bilateral TA/S CI indices ($p < 0.000$) (**Figure 3**).

Trunk Muscle Co-contraction

In post ES-alone, 6 of 12 CA indices increased bilaterally across all time periods (t_1, t_5, and t_{10}) ($p < 0.004$), while CE increased significantly in 6 of 12 ($p < 0.006$) and CI increased in 6 of 12 calculated indices ($p < 0.000$) (**Figure 3**). In post ST + ES, compared to ES-alone, 2 of 12 CA indices increased significantly ($p < 0.017$), while CE increased in 1 of 12 ($p < 0.000$) and CI increased in 6 of 12 calculated indices ($p < 0.015$) with four of six occurring in the t_{10} time period.

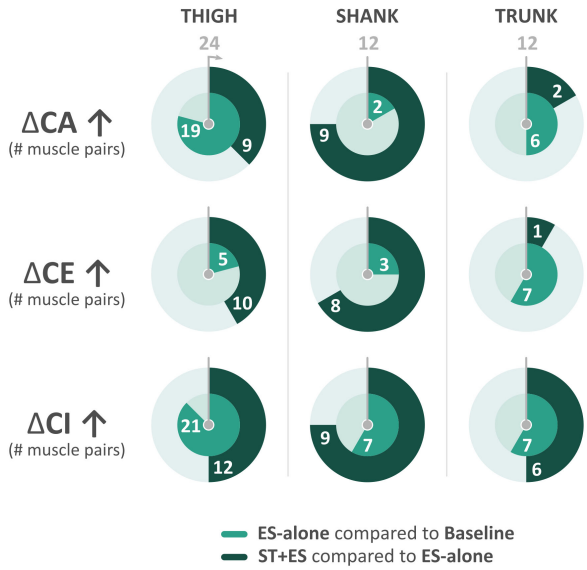

FIGURE 3 | Number of bilateral muscle pairs with a numerical increase in co-contraction measures (i.e., co-activation, co-excitation, and co-inhibition) across all time periods (t_1, t_5, and t_{10}) for electrical stimulation (ES)-alone relative to baseline and stand training (ST) + ES relative to ES-alone. Total number of muscle pairs across all time periods is 24 for the thigh, 12 for the shank, and 12 for the trunk.

TrunkCenter of Mass

For AB control, the $\widehat{CoM}_{\text{T}}$ trajectories are shown in **Figure 4**. $\widehat{CoM}_{\text{T,ML}}$ excursion during stepping ranged from 14.6 to 74.2% of *BoS* with left and right mid-stance occurring mediolaterally at 22.05 and 63.98%, respectively, about the midpoint of *BoS* (i.e., 50%). Mean step length ($\overline{SL}$) was 75.97 ± 0.96 cm, and mean BoS ($\overline{BoS}$) was 9.65 ± 1.47 cm throughout the trial.

For the SCI participant, baseline $\widehat{CoM}_{\text{T,ML}}$ trajectories ranged from 54.2 to 77.5% *BoS* with left and right mid-stance at 56.32 and 68.01%, respectively (**Figure 4**); post ES-alone, $\widehat{CoM}_{\text{T,ML}}$ excursion increased significantly ($p < 0.000$) and ranged from 42.2 to 66.4% of *BoS* with left and right mid-stance at 42.90 and 54.60%, respectively; in post ST + ES, $\widehat{CoM}_{\text{T,ML}}$ further increased (significant increase on the right side, $p < 0.000$) and ranged from 41.9 to 70.2% of *BoS* with left and right mid-stance at 42.64 and 64.16%, respectively. In post ES-alone, $\overline{SL}$ decreased from 57.21 ± 5.43 cm (baseline) to 51.78 ± 3.47 cm, and in post ST + ES, it increased to 61.55 ± 3.43 cm. Changes in $\overline{BoS}$ at post ES-alone, compared to baseline, were minimal from 23.97 ± 2.05 cm to 23.78 ± 2.57 cm, whereas in post ST + ES, there was an increase to 26.24 ± 3.14 cm. Note – these $\overline{SL}$ and $\overline{BoS}$ values are less than the AB values. The $\widehat{CoM}_{\text{T,AP}}$ ranges at baseline, post ES-alone, and post ST + ES were −35.8 to 61.6%, −38.9 to 65.5%, and −35.8 to 70.7% of SL, respectively, and similar to AB control $\widehat{CoM}_{\text{T,AP}}$ trajectories, which ranged from −42.7 to 66.0% of SL.

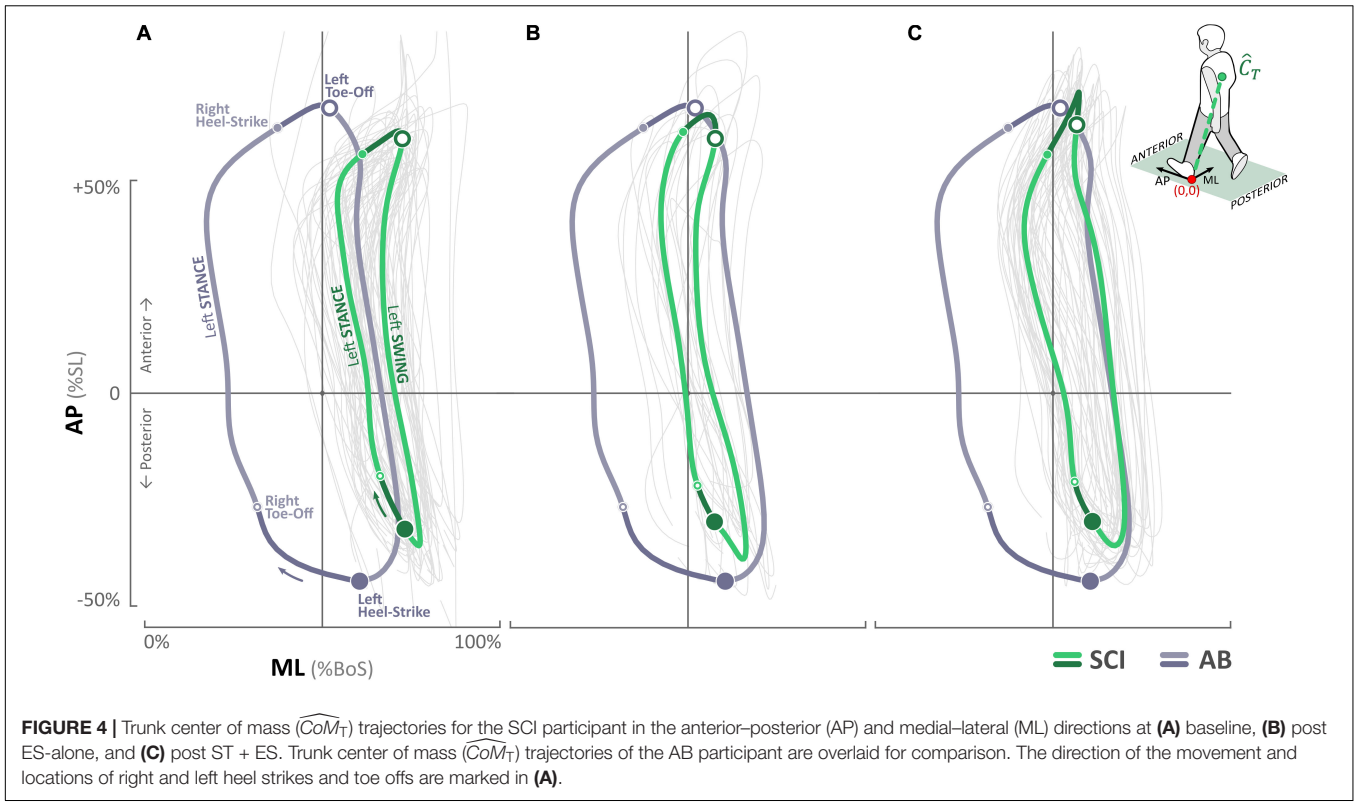

FIGURE 4 | Trunk center of mass ($\widehat{CoM_T}$) trajectories for the SCI participant in the anterior–posterior (AP) and medial–lateral (ML) directions at **(A)** baseline, **(B)** post ES-alone, and **(C)** post ST + ES. Trunk center of mass ($\widehat{CoM_T}$) trajectories of the AB participant are overlaid for comparison. The direction of the movement and locations of right and left heel strikes and toe offs are marked in **(A)**.

Spinal Motorneuron Activity Patterns

We used the recorded EMG data from 22 bilateral muscles to construct the spinal MN activity maps during assisted stepping for all time periods at baseline, post ES-alone, and post ST + ES. **Figure 5** illustrates the resulting maps of lumbosacral MN activity during t_1 of assisted stepping at baseline and post ES-alone and ST + ES interventions.

Observed bursts in the AB activity maps (**Figure 5D**) are consistent with previously published data on able-bodied individuals walking overground, with the exception of activity during mid-swing at S1-2 levels (Ivanenko et al., 2006). Temporal activation patterns are evident in all MN activity maps for the SCI participant (**Figures 5A–C**), however, there are apparent differences before and after interventions, compared to AB, especially during mid-swing at spinal levels L5–S2. Activation patterns for the SCI participant did show within-subject similarities, although in post ST + ES intervention, there were increases in spinal activation patterns during mid-stance at spinal levels L5–S2 for t_1, t_5, and t_{10} for the right limb and t_1 for the left limb, as noted for the AB participant.

DISCUSSION

In the current study, for an individual with SCI, we characterized the biomechanical, neural, and functional effects for longitudinal, multimuscle ES during dynamic loading (ST + ES) compared to unloaded (ES-alone) conditions during 10 min of continuous treadmill stepping. Data from the first, fifth, and tenth minutes (t_1, t_5, and t_{10}) of the 10-min condition identified the impact of the neural afferents associated with loading could influence locomotor outcome for muscle amplitude even after longitudinal stand training.

In post unloaded condition (ES-alone), compared to baseline, the majority (∼60%) of lower extremity muscle groups decreased their peak sEMG amplitude for all periods (t_1, t_5, and t_{10}) with no change in the level of muscle activation in the remaining 40% of lower limb muscles. However, in post loaded condition (ST + ES), compared to post unloaded condition (ES-alone), there was a restoration in muscle activation that endured the continuous 10-min stepping. Across 40% of the lower limb muscles, the increased range (20–95%) in peak muscle activation amplitude was in all periods (t_1, t_5, and t_{10}) especially for the knee extensors (VL, RF) and the ankle flexors and extensors (**Figure 2**); significantly, post ST + ES loaded condition restored a diminished left VL muscle activation amplitude.

Load Training Affects Spinal Excitability

After the unloaded training condition (ES-alone), compared to baseline, treadmill stepping evoked increased co-inhibition and lessened muscle amplitude responses for bilateral ankle flexors and extensors. However, these dampened sEMG responses were reversed during the 10-min stepping trial post loaded training condition (ST + ES), compared to ES-alone, for an increase in overall co-excitability (and amplitude) of the plantar flexor/extensor muscle pairs: TA/GN and TA/S (**Figure 3**).

Moreover, there appears to be a potential adaptation of spinal networks and muscle activation response due to stand training

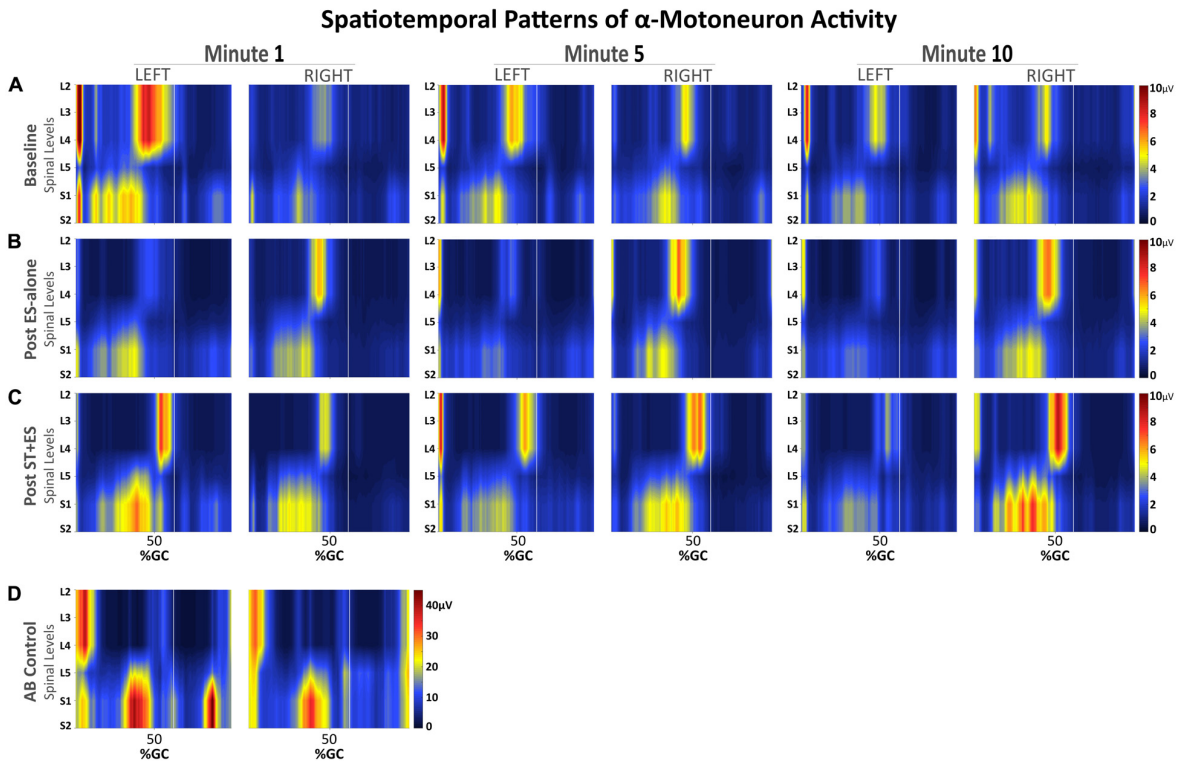

FIGURE 5 | Spatiotemporal patterns of α-motorneuron activation along the rostrocaudal axis of the spinal cord for the SCI participant **(A–C)** during assisted stepping on a treadmill with overhead body-weight support and for the able-bodied participant **(D)** during walking on a treadmill. Each segment on the vertical axis was reconstructed based on the recorded, non-normalized EMG signals from segmental localization charts (Kendall et al., 2005). Horizontal axis represents the time-normalized gait cycle with a vertical line that marks where the toe off occurs.

(Beres-Jones and Harkema, 2004; Ichiyama et al., 2008). Stand training, or loading, increased the afferent input (with ES) resulting in increased peak sEMG bursts and burst duration during the stance phase of stepping (**Figures 1**, **2** and **Table 2**). Specifically, peak sEMG occurred on peak load (**Figure 1**) at mid-stance for S, GN, and TA during weight-bearing stepping. Similar temporal sEMG responses for amplitude were seen in AB for GN and S muscles, except TA. TA activation bursts for AB occur at terminal swing and push-off at terminal stance (**Figure 1**). Similar spinal circuitry adaptations were reflected in left VL muscle activation. In post ES-alone, sEMG activation bursts for VL were diminished during 10-min stepping, only to be restored after longitudinal ST + ES load training (**Figure 1**).

Lack of weight bearing, or lack of afferent input, and conversely load training, or full weight bearing for afferent input, can have opposing effects on spinal networks and spinal excitability (Beres-Jones and Harkema, 2004; Forrest et al., 2008b). Beres-Jones and Harkema (2004) and Forrest et al. (2008a) established longitudinal, or even single-dose, step-training session resulted in greater sEMG amplitudes in GN, S, and TA during treadmill stepping for individuals with motor-complete injuries.

Our investigation shows a temporal coupling (i.e., phasing) of TA/GN sEMG amplitude during stepping (**Figure 1**), which is inappropriate for loading on the ipsilateral limb during stepping. The GN/S coupling is a more appropriate one during stepping. Forrest et al. (2008a) reported a similar co-contraction/co-excitation for the GN, S, and TA during loading after a high-dose locomotor training (LT) protocol for motor-complete SCI (Forrest et al., 2008b). After LT, the ankle joint at times would plantarflex on foot landing where the left TA had difficulty to concentrically contract against gravity to promote ankle dorsiflexion (Forrest et al., 2008b). In these experiments, the continued stepping with ankle plantarflexion at floor contact was likely to compromise afferent proprioceptive sensory input at foot floor contact and early stance and could have contributed partially to the co-contraction of the left TA and GN muscles. Beres-Jones and Harkema (2004) also suggested that the increased loading on the contralateral lower limb could have enhanced ipsilateral lower limb muscle activation; therefore, loading may not only facilitate ipsilateral extension but also may simultaneously facilitate contralateral flexion. Ultimately, the co-contraction of the left TA and the left GN needs further investigation (Beres-Jones and Harkema, 2004).

Trunk Muscle Activation and Center of Mass

At baseline, the $\widehat{CoM}_T$ data reflected an overall lack of decoupling for the cervical and thoracic trunk muscles during ipsilateral left and contralateral right leg swing during stepping;

the $\widehat{CoM}_{T,ML}$ trajectory projected beyond *BoS* midline (i.e., 50%). The lack of ipsilateral left trunk muscle activation combined with the stronger contralateral superior trunk muscles (SES) determined the overall path of the $\widehat{CoM}_{T,ML}$ at initial left toe-off (Ceccato et al., 2009). During right leg swing, especially at left mid-stance, there is a lack of contralateral trunk muscle bursts; the only activation of the right SES and right IO muscles provide trunk stabilization, resulting in a "pull" of the $\widehat{CoM}_{T,ML}$ further right of the *BoS* midline (Ceccato et al., 2009).

Lower Limb Multimuscle ES Affects Spinal Excitability

In post unloaded condition (ES-alone), the multimuscle ES of the lower limbs increased the neural control of trunk stability during continuous 10-min stepping. Specifically, during continuous 10-min stepping, the increased activation of the left SES and IES as the primary muscles stabilized the trunk during right swing, especially at left mid-stance (**Figure 4**). Overall, there was greater control of trunk $\widehat{CoM}_{T,ML}$ for more stabilized trunk $\widehat{CoM}_{T,ML}$ to decouple from leg movement during swing (compared to baseline); $\widehat{CoM}_{T,ML}$, trajectory was similar to AB trajectory.

Load Training and Lower Limb Multimuscle ES Affect Spinal Excitability

The greatest effect to trunk stability with the least amount of trunk excursion during continuous stepping resulted from the loaded condition combined with multimuscle ES (ST + ES) (**Figure 4**); trunk $\widehat{CoM}_{T,ML}$ excursions from the midline of *BoS* (50%) to the left (43%; AB: 22%) and right (64%; AB: 64%). Increased trunk stabilization during swing was due to the increase in the trunk neural adaptions during right swing. During right swing, especially at the left mid-stance, primary stabilizers for trunk control, left IES, and IO increased their amplitude and duration, concomitant to the decrease in right trunk muscles (SES, EO, and IO). The decrease in ipsilateral right trunk muscles are important to trunk stability during right swing (especially initial swing); they are known to provide a supportive, secondary role with a specific activation pattern occurring simultaneously with the main primary contralateral trunk stabilizers (Ceccato et al., 2009).

Previously, we have reported (Momeni et al., 2019) that ST + ES training for motor complete SCI increased neuromuscular and postural trunk control during standing, compared to post ES-alone and similar to the AB control during quiet standing. In addition, we reported gains in function that affected activities of daily living: (i) wheelchair transfers required less assistance, (ii) increased functional reach for improved seated balance, and (iii) increased independent seated trunk rotation ability. The current investigation extends previous findings to show that longitudinal stand training with components of stand retraining and stand adaptability can increase independent trunk control even in dynamic treadmill stepping conditions. In the unloaded condition (ES-alone), while there were gains in trunk stabilization during stepping (**Figure 4**), lower limb muscle activation decreased and co-inhibition increased during the continuous stepping (**Figure 3**).

With the addition of stand training to multimuscle ES, there was an increased longitudinal afferent input to the spinal network and increased excitability to normalize the trunk stability to resemble able-bodied trunk stability during stepping. Moraud et al. (2018) has suggested that these gains in postural control may also improve stepping quality in the lower extremity via the optimal medial–lateral trunk $\widehat{CoM}_{T}$ excursion assisting in preserving the muscle spindle feedback to the lower agonist/antagonist muscles in the lower limb during stepping (Moraud et al., 2018).

After the combined ST + ES training, lower limb muscle amplitude increased to enhance treadmill stepping for a continuous 10-min stepping trial (**Figure 5**). However, the increased co-excitation of the lower limb muscles (GN/TA) reflected an inappropriate intralimb stepping pattern. The observed inter-limb muscle activation spatial–temporal patterns and the spatial–temporal pattern of the α-motorneuron pool in the lumbosacral segment, especially the upper lumbar segment, for the SCI participant, are not fully representative of the AB's lumbosacral segment during terminal stance and terminal swing phases of stepping (**Figure 5**; Ivanenko et al., 2006); this is possibly because the stand training intervention was directed toward independent standing and not stepping. Using the α-motorneuron activity maps for this individual provides an approximate location of these motorneuron pools in the spinal cord (Yakovenko et al., 2002; Ivanenko et al., 2006). The maps, based on EMG profiles, do not directly represent individual contributions of muscles, but rather, they represent the organization of the spinal network and its motor output during stepping for this individual after the completion of the ES-alone and ST + ES interventions.

This preliminary case study is limited by the sample size of one, which makes it infeasible to obtain statistical significance in order to generalize its findings to the larger population. Future work needs to evaluate the intervention with a greater sample size for the effect of the intervention paradigm on trunk and lower limb gains. Another limitation of this study was the consecutive order of the interventions, without a washout period. Although this study focuses on the sequential changes and compares ST + ES only to ES-alone, a washout period would be preferable in future studies to avoid potential carryover effects comparing multiple interventions. Moreover, the therapists who performed the assisted stepping during data collection were not blinded to the type of intervention.

Overall, this study has shown, for one individual with SCI, an increase in dynamic postural stability and neural gains for integrated trunk and lower extremities after a dynamic standing intervention compared to an unloaded supine intervention for the same multimuscle ES protocol. The spinal neural networks and biomechanical adaptations reflected an increase in afferent input and spinal excitability (Edgerton and Roy, 2009) during training and the possible interactive neural control of trunk circuits

and lower limb during locomotion as described by Moraud et al. (2018). Further research should evaluate the influence of the proprioception, mediolateral trunk orientation, and trunk and lower limb motor pools on the neural and mechanical intersegmental relationship between trunk and lower extremity during locomotion, as well as how all these constraints influence or modulate the overall postural recovery during standing and locomotion.

DATA AVAILABILITY STATEMENT

The raw data supporting the conclusions of this article will be made available by the authors, without undue reservation, to any qualified researcher.

ETHICS STATEMENT

The studies involving human participants were reviewed and approved by the Kessler Foundation Institutional Review Board. The patients/participants provided their written informed consent to participate in this study.

AUTHOR CONTRIBUTIONS

GF and EG contributed to the conception and design of the study. KM and AR organized the database. KM performed the statistical analysis and wrote the first draft of the manuscript. GF and AR wrote sections of the manuscript. All authors contributed to manuscript revision, and read and approved the submitted version.

FUNDING

This research was supported by the Craig H. Neilson Foundation (191152) and NewJersey Commission on Spinal Cord Research (07-3063-SCR-E-0), both awarded to GF.

REFERENCES

Anders, C., Wagner, H., Puta, C., Grassme, R., Petrovitch, A., and Scholle, H.-C. (2007). Trunk muscle activation patterns during walking at different speeds. *J. Electromyogr. Kinesiol.* 17, 245–252. doi: 10.1016/j.jelekin.2006.01.002

Behrman, A. L., Lawless-Dixon, A. R., Davis, S. B., Bowden, M. G., Nair, P., Phadke, C., et al. (2005). Locomotor training progression and outcomes after incomplete spinal cord injury. *Phys. Ther.* 85, 1356–1371. doi: 10.1093/ptj/85.12.1356

Beres-Jones, J. A., and Harkema, S. J. (2004). The human spinal cord interprets velocity-dependent afferent input during stepping. *Brain* 127, 2232–2246. doi: 10.1093/brain/awh252

Buehner, J. J., Forrest, G. F., Schmidt-Read, M., White, S., Tansey, K., and Basso, D. M. (2012). Relationship between ASIA examination and functional outcomes in the neurorecovery network locomotor training program. *Arch. Phys. Med. Rehabil.* 93, 1530–1540. doi: 10.1016/j.apmr.2012.02.035

Canton, S., Momeni, K., Ramanujam, A., Garbarini, E., and Forrest, G. F. (2016). "Neuromotor response of the leg muscles following a supine, stand retraining with/without neuromuscular electrical stimulation training intervention for individuals with SCI: a case series," in *Proceedings of the 2016 38th Annual International Conference of the IEEE Engineering in Medicine and Biology Society (EMBC)* (Piscataway, NJ: IEEE), 3143–3146.

Ceccato, J.-C. C., de Sèze, M., Azevedo, C., and Cazalets, J.-R. R. (2009). Comparison of trunk activity during gait initiation and walking in humans. *PLoS One* 4:e8193. doi: 10.1371/journal.pone.0008193

de Leva, P. (1996). Adjustments to Zatsiorsky-Seluyanov's segment inertia parameters. *J. Biomech.* 29, 1223–1230. doi: 10.1080/02564602.1995.11416507

Dudley-Javoroski, S., and Shields, R. K. (2006). Assessment of physical function and secondary complications after complete spinal cord injury. *Disabil. Rehabil.* 28, 103–110. doi: 10.1080/09638280500163828

Edgerton, V. R., and Roy, R. R. (2009). Activity-dependent plasticity of spinal locomotion: implications for sensory processing. *Exerc. Sport Sci. Rev.* 37, 171–178. doi: 10.1097/JES.0b013e3181b7b932

Forrest, G., Angeli, C. A., Machin, D., Garbarini, E., Cirnigliaro, C., and Harkema, S. J. (2009). "Musculoskeletal changes following electrical stimulation and loading training paradigms," in *Proceedings of the Neuroscience Meeting Planner* Chicago, IL.

Forrest, G. F., Lorenz, D. J., Hutchinson, K., Vanhiel, L. R., Basso, D. M., Datta, S., et al. (2012). Ambulation and balance outcomes measure different aspects of recovery in individuals with chronic, incomplete spinal cord injury. *Arch. Phys. Med. Rehabil.* 93, 1553–1564. doi: 10.1016/j.apmr.2011.08.051

Forrest, G. F., Asselin, M., and Bond, L. (2008a). Locomotor training with incremental changes in velocity: muscle and metabolic responses. *Top. Spinal Cord Inj. Rehabil.* 14, 16–22. doi: 10.1310/sci1401-16

Forrest, G. F., Sisto, S. A., Barbeau, H., Kirshblum, S. C., Wilen, J., Bond, Q., et al. (2008b). Neuromotor and musculoskeletal responses to locomotor training for an individual with chronic motor complete AIS-B spinal cord injury. *J. Spinal Cord Med.* 31, 509–521. doi: 10.1080/10790268.2008.11753646

Gorgey, A. S., Dolbow, D. R., Dolbow, J. D., Khalil, R. K., and Gater, D. R. (2015). The effects of electrical stimulation on body composition and metabolic profile after spinal cord injury – Part II. *J. Spinal Cord Med.* 38, 23–37. doi: 10.1179/2045772314Y.0000000244

Gorgey, A. S., and Dudley, G. A. (2007). Skeletal muscle atrophy and increased intramuscular fat after incomplete spinal cord injury. *Spinal Cord* 45, 304–309. doi: 10.1038/sj.sc.3101968

Gorgey, A. S., Mather, K. J., Cupp, H. R., and Gater, D. R. (2012). Effects of resistance training on adiposity and metabolism after spinal cord injury. *Med. Sci. Sports Exerc.* 44, 165–174. doi: 10.1249/MSS.0b013e31822672aa

Harkema, S., Behrman, P. T. A., and Barbeau, H. (2011). *Locomotor Training*. Oxford: Oxford University Press.

Harkema, S. J., Schmidt-Read, M., Behrman, A. L., Bratta, A., Sisto, S. A., and Edgerton, V. R. (2012a). Establishing the neurorecovery network: multisite rehabilitation centers that provide activity-based therapies and assessments for neurologic disorders. *Arch. Phys. Med. Rehabil.* 93, 1498–1507. doi: 10.1016/j.apmr.2011.01.023

Harkema, S. J., Schmidt-Read, M., Lorenz, D. J., Edgerton, V. R., and Behrman, A. L. (2012b). Balance and ambulation improvements in individuals with chronic incomplete spinal cord injury using locomotor trainingbased rehabilitation. *Arch. Phys. Med. Rehabil.* 93, 1508–1517. doi: 10.1016/j.apmr.2011.01.024

Ichiyama, R. M., Courtine, G., Gerasimenko, Y. P., Yang, G. J., Van Den Brand, R., Lavrov, I. A., et al. (2008). Step training reinforces specific spinal locomotor circuitry in adult spinal rats. *J. Neurosci.* 28, 7370–7375. doi: 10.1523/JNEUROSCI.1881-08.2008

Ivanenko, Y. P., Poppele, R. E., and Lacquaniti, F. (2006). Spinal cord maps of spatiotemporal alpha-motoneuron activation in humans walking at different speeds. *J. Neurophysiol.* 95, 602–618. doi: 10.1152/jn.00767.2005

Johnson, T. D. (2003). A Bayesian change-point analysis of electromyographic data: detecting muscle activation patterns and associated applications. *Biostatistics* 4, 143–164. doi: 10.1093/biostatistics/4.1.143

Kapadia, N., Masani, K., Catharine Craven, B., Giangregorio, L. M., Hitzig, S. L., Richards, K., et al. (2014). A randomized trial of functional electrical stimulation for walking in incomplete spinal cord injury: effects on walking

competency. *J. Spinal Cord Med.* 37, 511–524. doi: 10.1179/2045772314Y.0000000263

Kendall, F., Provance, P., Rodgers, M., Romani, W., Florence, P. K., Patricia, G. P., et al. (2013). *Muscles: Testing and Function, with Posture and Pain*. Philadelphia, PA: Lippincott Williams & Wilkins.

Kendall, F. P., McCreary, E. K., Provance, P. G., Rodgers, M. M., and Romani, W. A. (2005). *Muscles: Testing and Function, with Posture and Pain*, 5th Edn. Philadelphia, PA: Lippincott Williams & Wilkins.

Mahoney, E. T., Bickel, C. S., Elder, C., Black, C., Slade, J. M., Apple, D., et al. (2005). Changes in skeletal muscle size and glucose tolerance with electrically stimulated resistance training in subjects with chronic spinal cord injury. *Arch. Phys. Med. Rehabil.* 86, 1502–1504. doi: 10.1016/j.apmr.2004.12.021

Marino, R. J., Jones, L., Kirshblum, S., Tal, J., and Dasgupta, A. (2008). Reliability and repeatability of the motor and sensory examination of the international standards for neurological classification of spinal cord injury. *J. Spinal Cord Med.* 31, 166–170. doi: 10.1080/10790268.2008.11760707

Mitchell, M. D., Yarossi, M. B., Pierce, D. N., Garbarini, E. L., and Forrest, G. F. (2015). Reliability of surface EMG as an assessment tool for trunk activity and potential to determine neurorecovery in SCI. *Spinal Cord* 53, 368–374. doi: 10.1038/sc.2014.171

Momeni, K., Canton, S., Ramanujam, A., Garbarini, E., and Forrest, G. F. (2016). "Effects of lower limb electrical stimulation on trunk stability in persons with SCI during walking: a case series," in *Proceedings of the 2016 38th Annual International Conference of the IEEE Engineering in Medicine and Biology Society (EMBC)* (Piscataway, NJ: IEEE), 6377–6380.

Momeni, K., Ramanujam, A., Garbarini, E. L., and Forrest, G. F. (2019). Multi-muscle electrical stimulation and stand training: effects on standing. *J. Spinal Cord Med.* 42, 378–386. doi: 10.1080/10790268.2018.1432311

Moraud, E. M., von Zitzewitz, J., Miehlbradt, J., Wurth, S., Formento, E., DiGiovanna, J., et al. (2018). Closed-loop control of trunk posture improves locomotion through the regulation of leg proprioceptive feedback after spinal cord injury. *Sci. Rep.* 8:76. doi: 10.1038/s41598-017-18293-y

Pilkar, R. B., Yarossi, M., and Forrest, G. (2012). "Empirical mode decomposition as a tool to remove the function electrical stimulation artifact from surface electromyograms: preliminary investigation," in *Proceedings of the Conf. Proc. Annu. Int. Conf. IEEE Eng. Med. Biol. Soc. IEEE Eng. Med. Biol. Soc. Annu. Conf.* (Piscataway, NJ: IEEE), 1847–1850.

Popovic, M. R., Thrasher, T. A., Adams, M. E., Takes, V., Zivanovic, V., and Tonack, M. I. (2006). Functional electrical therapy: retraining grasping in spinal cord injury. *Spinal Cord* 44, 143–151. doi: 10.1038/sj.sc.3101822

Qin, W., Bauman, W. A., and Cardozo, C. (2010). Bone and muscle loss after spinal cord injury: organ interactions. *Ann. N. Y. Acad. Sci.* 1211, 66–84. doi: 10.1111/j.1749-6632.2010.05806.x

Ryan, T. E., Brizendine, J. T., Backus, D., and McCully, K. K. (2013). Electrically induced resistance training in individuals with motor complete spinal cord injury. *Arch. Phys. Med. Rehabil.* 94, 2166–2173. doi: 10.1016/j.apmr.2013.06.016

Sabatier, M. J., Stoner, L., Mahoney, E. T., Black, C., Elder, C., Dudley, G. A., et al. (2006). Electrically stimulated resistance training in SCI individuals increases muscle fatigue resistance but not femoral artery size or blood flow. *Spinal Cord* 44, 227–233. doi: 10.1038/sj.sc.3101834

Schuld, C., Franz, S., Brüggemann, K., Heutehaus, L., Weidner, N., Kirshblum, S. C., et al. (2016). International standards for neurological classification of spinal cord injury: impact of the revised worksheet (revision 02/13) on classification performance. *J. Spinal Cord Med.* 39, 504–512. doi: 10.1080/10790268.2016.1180831

Solnik, S., Rider, P., Steinweg, K., DeVita, P., and Hortobágyi, T. (2010). Teager-Kaiser energy operator signal conditioning improves EMG onset detection. *Eur. J. Appl. Physiol.* 110, 489–498. doi: 10.1007/s00421-010-1521-8

Spungen, A. M., Adkins, R. H., Stewart, C. A., Wang, J., Pierson, R. N., Waters, R. L., et al. (2003). Factors influencing body composition in persons with spinal cord injury: a cross-sectional study. *J. Appl. Physiol.* 95, 2398–2407. doi: 10.1152/japplphysiol.00729.2002

Yakovenko, S., Mushahwar, V., Vanderhorst, V., Holstege, G., and Prochazka, A. (2002). Spatiotemporal activation of lumbosacral motoneurons in the locomotor step cycle. *J. Neurophysiol.* 87, 1542–1553. doi: 10.1152/jn.00479.2001

Conflict of Interest: The authors declare that the research was conducted in the absence of any commercial or financial relationships that could be construed as a potential conflict of interest.

frontiers in Human Neuroscience

MINI REVIEW
published: 23 October 2020
doi: 10.3389/fnhum.2020.568703

Brain Network Oscillations During Gait in Parkinson's Disease

Doris D. Wang[1] and Julia T. Choi[2]*

[1] Department of Neurological Surgery, University of California, San Francisco, San Francisco, CA, United States,
[2] Department of Applied Physiology and Kinesiology, University of Florida, Gainesville, FL, United States

Human bipedal walking is a complex motor task that requires supraspinal control for balance and flexible coordination of timing and scaling of many muscles in different environment. Gait impairments are a hallmark of Parkinson's disease (PD), reflecting dysfunction of cortico-basal ganglia-brainstem circuits. Recent studies using implanted electrodes and surface electroencephalography have demonstrated gait-related brain oscillations in the basal ganglia and cerebral cortex. Here, we review the physiological and pathophysiological roles of (1) basal ganglia oscillations, (2) cortical oscillations, and (3) basal ganglia-cortical interactions during walking. These studies extend a novel framework for movement of disorders where specific patterns of abnormal oscillatory synchronization in the basal ganglia thalamocortical network are associated with specific signs and symptoms. Therefore, we propose that many gait dysfunctions in PD arise from derangements in brain network, and discuss potential therapies aimed at restoring gait impairments through modulation of brain network in PD.

Keywords: locomotion, deep brain stimulation, basal ganglia, cerebral cortex, coherence, neurorehabilitation, closed-loop stimulation

OPEN ACCESS

Edited by:
Taiar Redha,
Université de Reims Champagne-Ardenne, France

Reviewed by:
Noman Naseer,
Air University, Pakistan
Judith Walters,
National Institute of Neurological Disorders and Stroke (NINDS), United States

****Correspondence:***
Doris D. Wang
doris.wang@ucsf.edu

Specialty section:
This article was submitted to Motor Neuroscience, a section of the journal Frontiers in Human Neuroscience

Received: *01 June 2020*
Accepted: *29 September 2020*
Published: *23 October 2020*

Citation:
Wang DD and Choi JT (2020) Brain Network Oscillations During Gait in Parkinson's Disease. Front. Hum. Neurosci. 14:568703. doi: 10.3389/fnhum.2020.568703

INTRODUCTION

Human gait requires the coordination of multiple brain areas to drive this complex and dynamic behavior. The supraspinal control of human locomotion begins in the cortical regions of supplemental motor area (SMA), premotor (PM) and primary motor (M1) cortices, where precise, intentional motor programs reach the basal ganglia for refinement, and then to the mesencephalic locomotor region (MLR), where cerebellar inputs join the MLR and descends to the medullary and pontine reticular formations to pass information to the spinal cord (Takakusaki, 2017). Disruptions in any part of this locomotion network can cause gait impairments. In the case of Parkinson's Disease (PD), lack of dopaminergic innervation to the striatum not only affects the basal ganglia, but also causes brain network dysfunctions in many nodes of the circuit involved in locomotion.

The ability to directly measure neural activity on the population level gives investigators a unique opportunity to study neuronal network functions and dysfunctions in disease states. Synchronized activity patterns driven by neural ensembles can be measured in the form of membrane potential oscillations, and are becoming increasingly recognized as a means to drive dynamic brain coordination (Llinas, 1988; Buzsaki and Draguhn, 2004). Neural networks can oscillate across many frequencies ranges, and different oscillatory bands have been associated with distinctive behavioral states (Csicsvari et al., 2003; Hammond et al., 2007). Brain oscillations are

important for nervous system functions because they provide key mechanisms for the encoding, storage, and processing of information across the neural network by biasing the probability of neuronal spiking activity (Llinas, 1988; Fries, 2005). These brain oscillations can be readily measured in the form of field potential by a wide variety of electrodes available for human clinical and research use, from local field potentials (LFP) recorded using depth electrodes penetrating the brain, electrocorticography (ECoG) potentials using electrode strip or grids placed over the surface of the brain, to electroencephalography (EEG) potentials using non-invasive scalp electrodes.

Using these methods over the past 15 years, researchers have developed a new framework for understanding neurological diseases resulting from disorders of network dynamics, or circuitopathies (Lozano and Lipsman, 2013). This work has generated a model for Parkinson's disease where specific signs and symptoms are related to specific abnormal oscillatory synchronization in the basal ganglia-thalamocortical network. Extending this framework, we propose that dysfunctional oscillations in locomotor network contribute to different aspects of gait impairments in Parkinson's disease. Here, we review recent evidence regarding the role of basal ganglia oscillations, cortical oscillations, and basal ganglia-cortical interactions during normal and abnormal gait in PD, and propose new therapeutic strategies to treat these circuitopathies to improve gait function in PD.

BASAL GANGLIA OSCILLATIONS DURING GAIT

Excessive basal ganglia oscillatory activity across different frequency bands have been associated with different motor signs of movement disorders. Increases in theta (4–8 Hz) and alpha (8–12 Hz) frequencies have been shown in the subthalamic nucleus (STN) of PD patients during resting tremor (Wang et al., 2005) and in the globus pallidus (GP) of patients with isolated dystonia at rest (Silberstein et al., 2003; Liu et al., 2008; Weinberger et al., 2012; Wang et al., 2018) and during phasic muscle contraction (Chen et al., 2006; Sharott et al., 2008). Elevated beta oscillations (13–30 Hz) and beta bursts (Tinkhauser et al., 2017b; Tinkhauser et al., 2018) has been observed in both the STN and GPi of PD patients at rest, which represents an akinesia state (Brown, 2003; Oswal et al., 2013; Wang et al., 2018). Additionally, narrowband gamma oscillations (60–80 Hz) has been found in the STN of PD patients with dopaminergic medication and during movement, and is associated with dyskinesia, a hyperkinetic state, in PD (Swann et al., 2016).

What happens to these oscillations during gait in PD? Normal upright walking consists alternating stance (foot is in contact with ground) and swing (foot is in the air) phase on each leg (**Figure 1A**); the left and right legs maintain reciprocal, out-phase-phase coordination that is critical for stable bipedal gait. Until recently, majority of LFP recordings are obtained from externalized DBS leads during the perioperative period via connection to an external amplifier, limiting patient mobility. Based on these limited stepping and walking tasks, several groups have reported alternating suppression of beta activity during stepping or gait in PD patients relative to the resting state. In a visually guided stepping task while sitting, alternating 20–30 Hz beta modulation was observed between left and right STN with gait cycle, and beta modulation increased with auditory cue (Fischer et al., 2018). Another study showed a suppression of beta power in the STN during both bicycling and walking, while this suppression was higher for bicycling (Storzer et al., 2017). Additionally, comparison between cued upper and lower extremity movements showed that there is greater movement-modulated desynchronization of high beta oscillations (24–31 Hz) for foot dorsi- and plantar-flexion compared to hand opening and closing (Tinkhauser et al., 2019). Now, with the availability of investigational neurostimulation devices with embedded sensing capabilities, new studies are shedding light on these basal ganglia oscillations change during gait in freely-moving PD patients. In a report of 10 patients implanted with such a bidirectional neurostimulator, it was found that high beta frequency power (20–30 Hz) and bilateral oscillatory connectivity are reduced during upright gait, as well as a reduction in overall high beta burst amplitude and burst lifetimes during gait compared to rest conditions (Hell et al., 2018; **Figure 1B**). However, not every study found decreased beta power during walking across all PD patients. Quinn et al. (2015) reported similar STN beta power during lying, sitting, standing, and forward walking for 14 akinetic-rigid (n = 7) and tremor-dominant (n = 7) PD patients, but only akinetic-rigid PD patients tended to exhibit beta desynchronization during walking, while tremor dominant patients did not. Another study found no difference in beta power, coherence, or cross-coupling during walking compared to sitting and standing; however, interhemispheric beta phase locking values decreased during walking compared to sitting and standing (Arnulfo et al., 2018). One explanation for this discrepancy on beta power among different studies is patient phenotypes, as akinetic-rigid PD patient could have greater gait-modulated beta changes (Quinn et al., 2015). Another explanation could be that since beta power appears to be modulated by phases of the gait cycle, averaging beta power for the duration of walking may not capture dynamic nature of this power modulation. Future studies characterizing the oscillatory changes during different phases of the gait cycle in different PD phenotypes will elucidate the dynamic control of gait within the basal ganglia.

Do these oscillatory changes represent physiological or pathological gait? In a study recording GPi LFP from patients with isolated dystonia without gait abnormalities, LFP power in the theta (4–8 Hz), alpha (8–12 Hz), and gamma (60–90 Hz) frequency bands was higher during walking on a treadmill than during either sitting or standing conditions, and beta (15–25 Hz) band was the only frequency that was down-regulated during walking (Singh et al., 2011). Subthalamic LFP also showed alpha, beta, and gamma frequency powers that are modulated and locked to the gait cycle (Hell et al., 2018). While in the latter study, the authors posit that these changes may be due to movement-induced artifacts, we believe these gait-cycle related oscillatory changes from the basal ganglia

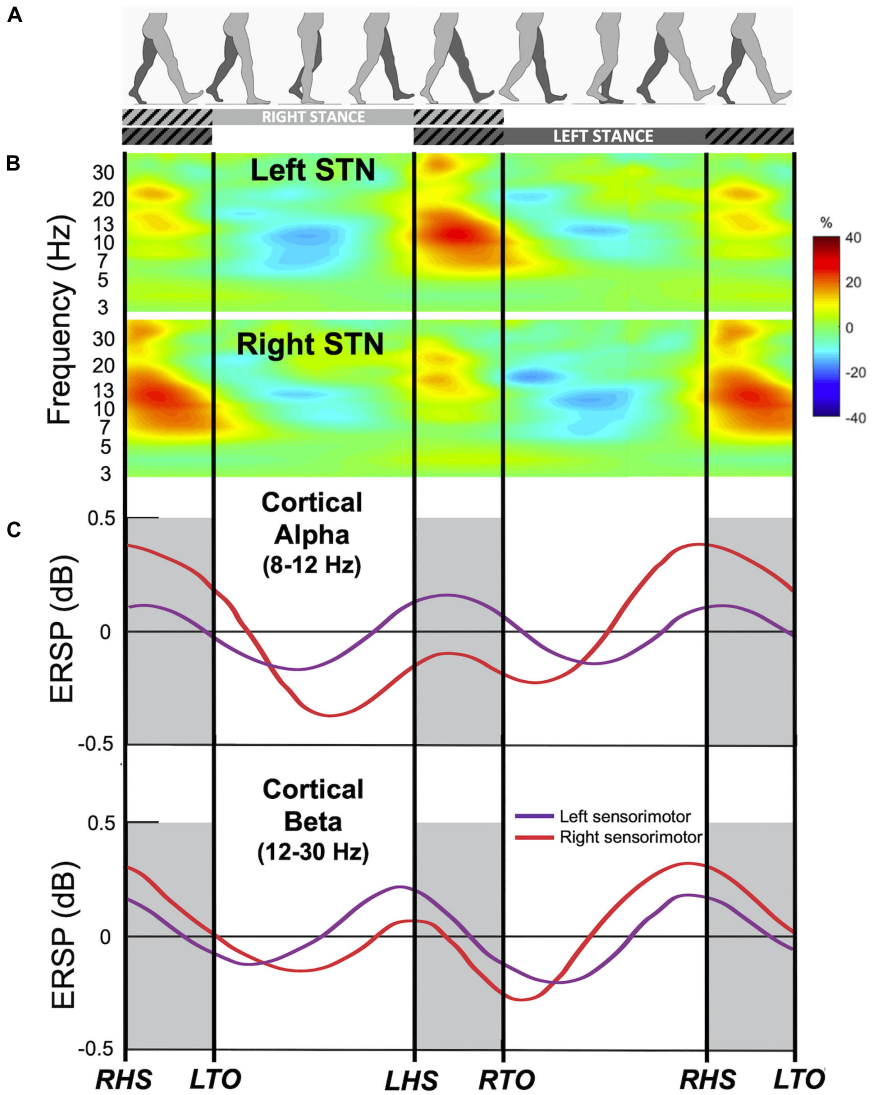

FIGURE 1 | Gait event-related spectral changes from the subthalamic nucleus (STN) and sensorimotor cortex. **(A)** Schematic of gait cycle events for the right (light gray) and left leg (dark gray) during walking. Hatched lines indicate double support period when both legs are in contact with the ground. **(B)** Group time-frequency spectral analysis of field potentials recorded from the bilateral STN of 10 freely walking PD patients aligned to the gait cycle. Upper panel: contralateral averaged signals (i.e., Left STN time locked to right leg events and vice versa) demonstrating event-related modulations in alpha and beta frequency bands during gait. Lower panel: ipsilateral averaged signals (i.e., right STN time locked to right leg events). Color bar indicate percent change relative to average gait baseline. Modified from Hell et al. (2018) with permission. **(C)** Gait event-related spectral perturbation recorded from EEG of 8 healthy individuals during treadmill walking. Upper panel: average of the alpha (8–12 Hz) band amplitude from the left sensorimotor cortex (purple) and right sensorimotor cortex (red) time-locked to the gait cycle. Bottom panel: average of the beta (12–30 Hz) band amplitude. ERSP, event-related spectral perturbation; RHS, right heel strike; RTO, right toe off; LHS, left heel strike; LTO, left toe off. Modified from Gwin et al. (2011) with permission.

represent physiological modulations during gait as similar patterns of activity have been observed in PD patients during intraoperative stepping tasks, as well as in freely moving dystonia patients without gait symptoms, using both recordings from externalized leads and implanted sensing devices. Additionally, there are differences within the oscillatory characteristics in PD patient during effective walking vs. pathological walking such as freezing of gait (FoG). Direct measurements of STN LFPs of PD patients demonstrated differences in beta frequency amplitude (Toledo et al., 2014; Hell et al., 2018) and alpha frequency entropy (Syrkin-Nikolau et al., 2017) between patients with or without FoG, with high beta amplitude and alpha entropy in freezers. Another measurement of beta frequency activity, beta burst duration, were also found to be prolonged during FoG episodes and shortened by DBS which improved gait (Anidi et al., 2018). Together, these data suggest that during normal walking, the human basal ganglia produces precisely timed modulation of low band frequency and beta frequency bands which are disrupted during pathological gait patterns seen in PD.

CORTICAL OSCILLATIONS DURING GAIT

The human motor cortex exhibits rhythmic EEG activity during walking that is coupled to the gait cycle (Gwin et al., 2011; Petersen et al., 2012). Electrocortical sources in the anterior cingulate, posterior parietal, and sensorimotor cortex showed increased alpha- and beta-band power during the double support period (near the end of stance phase of each leg when both feet are on the ground), and this pattern of alpha- and beta-band power fluctuations alternate between the left and right hemispheres by half a gait cycle (Gwin et al., 2011; **Figure 1C**). In addition, lower gamma band activity (25–40 Hz) in the premotor cortex shows desynchronization around the time of heel contact during robot assisted walking (Wagner et al., 2012). Synchronization in the 40–200 Hz during normal walking compared with standing has also been reported in 2 subjects utilizing ECoG over leg M1 (McCrimmon et al., 2018).

What is the functional role of these cortical oscillations during gait? In comparison to basal ganglia oscillations during gait, cortical oscillations show a similar pattern of alternation between the left and right hemispheres, as well as alpha and beta suppression during normal walking relative to rest. Cortical oscillations also show spectral power modulation that are associated with specific phases of the gait cycle, according to the specific task demands. Gait-modulated alternating suppression of alpha and beta oscillations likely exerts the similar effect as those involved with upper extremity tasks in order to suppress unwanted motor information and drive motor cortical activity in a spatiotemporal specific manner (Miller et al., 2007; Miller et al., 2010; Yanagisawa et al., 2012; Stolk et al., 2019). Increased activity in the anterior cingulate during double support period (when the leading leg contacts the ground) is thought to reflect error processing (Gwin et al., 2011). In general, a reduction in alpha- and beta-band power, along with greater theta power, in the sensorimotor cortex during more demanding walking tasks (e.g., walking on a balance beam, speed matching) is thought to reflect greater cortical involvement (Sipp et al., 2013; Bulea et al., 2015; Nordin et al., 2020). Distinct beta oscillations during gait adaptation (step shortening and lengthening) is thought to serve different motor and cognitive processes: motor cortical alpha- and beta-band power decrease is thought to reflect anticipatory processes and movement execution, while frontal beta-band activity increase is thought to reflect cognitive top-down control (e.g., motor inhibition during step shortening) (Wagner et al., 2016).

Additionally, oscillatory activity from the motor cortex may directly facilitate ankle dorsiflexors in swing phase, and ankle plantorflexors in stance phase, during treadmill walking (Petersen et al., 2012; Jensen et al., 2018, 2019). Corticomsucular coherence between Cz and the tibialis anterior muscle (ankle dorsiflexor) in the 24–40 Hz frequencies has been detected during the swing phase of treadmill walking, and the amount of beta and gamma coherence increases when stepping on virtual targets displayed on screen, indicating greater cortical involvement during precision stepping (Jensen et al., 2018; Spedden et al., 2019). The timing of motor cortex activity in relation to the step cycle suggests that the motor cortex is important for the execution of gait modifications, and groups of pyramidal tract neurons may control synergistic muscles that are simultaneously active at different phases of the gait cycle (Drew and Marigold, 2015). In contrast, modulation of the supplementary motor area, premotor cortex and posterior parietal cortex EEG occurs well in advance of visually guided modifications during treadmill walking (Nordin et al., 2019), and during the anticipatory postural adjustments for gait initiation (Varghese et al., 2016), consistent with their role in the planning of visually guided locomotion (Drew and Marigold, 2015).

How do these cortical oscillations change during gait in PD? One study showed a large increase in theta activity over the vertex (Cz electrode) during freezing compared to normal walking, as well as an increase in beta band activity in the parietal lead (Shine et al., 2014). Another study showed increased synchronization in the theta, alpha, beta and gamma bands between the left and right hemispheres during walking in PD compared to age-matched controls, and that hyper-synchronization in the frontal lobe is associated with freezing of gait (Miron-Shahar et al., 2019). This suggests that increased oscillatory synchronization in the both cerebral cortex and basal ganglia are associated with clinical features of gait disorders in PD. Several studies have also examined corticomuscular coherence during walking and cycling in PD (Yoshida et al., 2018; Gunther et al., 2019; Roeder et al., 2020). Subjects with PD and older age-matched participants did not show significant differences in corticomuscular coherence during double support phase in walking, nor bilateral cycling (Yoshida et al., 2018; Roeder et al., 2020). Together, these studies suggest abnormal cortical oscillations in PD does not affect the direct corticospinal drive to muscles during walking, but may impair walking via other indirect pathways (e.g., cortical-basal ganglia loop, cortico-brainstem). In the next section, we explore evidence how cortical-basal ganglia network changes are associated with gait disorders in PD.

BASAL GANGLIA-CORTICAL INTERACTIONS DURING GAIT

Because many of the motor symptoms in PD arise from pathological synchronization across different frequency ranges throughout the basal ganglia-cortical network, it is important to understand how cortical-subcortical structures interact during gait in PD, and how these interactions may be disrupted during abnormal gait. In a study that investigated 7 PD patients with bilateral STN DBS, 5 of which had FoG, investigators were able to simultaneously record subthalamic LFPs and scalp EEG during walking through a course that induced FoG episodes (Pozzi et al., 2019). Interestingly, the authors found no difference in STN low frequency (theta, alpha) and beta power, beta burst duration, or interhemispheric STN coupling between effective walking and FoG. However, during normal walking, the cortex and STN were synchronized in a low frequency band (4–13 Hz). FoG was characterized by low frequency cortical-subthalamic decoupling at the transition from normal walking into gait freezing, was sustained during the freezing episode,

and resolved with recovery of the effective walking pattern (Pozzi et al., 2019). This data suggests that during effective gait, cortical areas such as the SMA may be involved to produce normal gait patterns and transitions as a person is navigating through a path. Hypoactivation of cortical input may result in pathological oscillatory patterns in the basal ganglia that affect downstream locomotor regions. The specificity of cortical oscillatory changes during gait disorders in PD in relation to specific phases of the gait cycle has yet to be fully examined. Future studies focused on characterizing gait phase-specific cortical-basal ganglia oscillations in PD will provide a more complete understanding of the pathophysiology of PD gait.

NEW THERAPIES TO MODULATE BRAIN OSCILLATIONS DURING GAIT IN PD

While conventional continuous DBS therapy has been used to improve many motor symptoms of PD, it has not significantly improved all aspects of gait and postural control. For instance, stimulation of the substantia nigra and pedunculopontine nucleus tend to improve anticipatory posture adjustments and gait postural control while having no significant effect on gait parameters, whereas STN or GPi DBS improve gait parameters and have heterogenous effects on postural control during gait initiation (Collomb-Clerc and Welter, 2015).

One possible reason that conventional DBS therapy fails to significantly improve postural adjustments and gait disturbances is that standard therapeutic stimulation occurs in a constant, open-loop manner, and does not account for the recursive and dynamic nature of gait, as shown by the cyclic oscillatory change that occur during the normal gait cycle. Closed−loop, or adaptive, DBS is a promising therapy for improving gait and balance functions in PD. Adaptive DBS automatically adjusts stimulation parameters based on brain signals that reflect different clinical states and pathophysiology. For instance, prototypes of adaptive DBS have used amplitude of STN beta oscillations (Little et al., 2013) and beta bursts (Tinkhauser et al., 2017a) to increase stimulation to reduce akinesia in PD. Others have used narrow-band gamma activity in the motor cortex, a biomarker for dyskinesia, to reduce side effects associated with STN stimulation (Swann et al., 2018). Therefore, understanding the neural signatures of gait in Parkinson's disease – both in the cortex and in the basal ganglia – are critical for the development of better stimulation technologies.

Based on this principal, alternating DBS stimulation between the two hemispheres of the brain has been proposed as a potential therapy to improve gait functions in PD (Fischer et al., 2018). As presented earlier, alternating patterns of synchronized field potentials have been recorded from the motor cortical regions (Seeber et al., 2015; McCrimmon et al., 2018) and the basal ganglia (Singh et al., 2011; Fischer et al., 2018; Hell et al., 2018) in healthy subjects, as well as in PD and dystonia patients without gait impairments, during normal walking. A potential new therapy would be to use these physiological biomarkers or external kinematic sensors of gait as control signals to stimulate the locomotor centers during specific phases of the gait cycle (**Figure 2**). By decoding the physiological brain signals associated with gait control, we can then develop adaptive DBS to recapitulate these normal brain network dynamics to restore gait functions in PD patients. For instance, we can use high beta (24–31 Hz) desynchronization, which is associated with lower-limb movement and gait (Hell et al., 2018; Tinkhauser et al., 2019), to trigger stimulation during contralateral leg swing during the gait cycle. Another possibility is to used pathological oscillations associated with gait disorders, such as prolonged beta bursts, to trigger stimulation during freezing of gait episodes (Anidi et al., 2018) to abort or prevent these pathological gait patterns. With technological advances in DBS hardware design, now it may be possible to implement such adaptive stimulation paradigms using bidirectional DBS interfaces that has both sensing and stimulation capabilities. These novel platforms will be crucial in understanding the dynamic neural control of gait, and designing temporally-specific patterns of neuromodulation to improve gait.

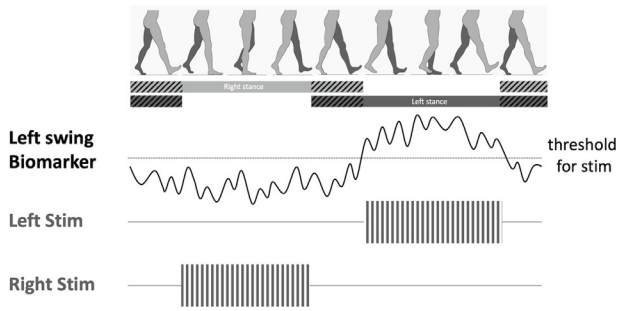

FIGURE 2 | Proposed adaptive deep brain stimulation (aDBS) paradigm. When a gait phase-specific biomarker is discovered (i.e., swing phase), a bidirectional DBS device can decode the features of the biomarker in real time, and trigger stimulation once threshold is reached. This aDBS paradigm would allow alternating stimulation between the two brain hemispheres in order to synchronize stimulation to the swing phase of the right leg.

CONCLUSION

Understanding brain oscillations during gait has theoretical significance because it will provide new mechanistic understanding of network dysfunctions during human locomotion in PD patients. Normal walking is associated with suppression of beta oscillations that exhibits a pattern of left-right alternation. Disorders of network dynamics in PD are manifested in elevated beta oscillations and excess interhemispheric phase locking during walking in PD patients with gait impairments. This new knowledge has tremendous translational potential as it will build a foundation for developing new neuromodulation therapies to improve gait in PD.

AUTHOR CONTRIBUTIONS

DW and JC contributed to the conceptual design, writing, editing, and generation of figures for this manuscript. All authors contributed to the article and approved the submitted version.

FUNDING

DW received grant support from the NINDS K12 NS080223 and the Burroughs Wellcome Fund Career Award for Medical Scientists.

SUPPLEMENTARY MATERIAL

The Supplementary Material for this article can be found online at: https://www.frontiersin.org/articles/10.3389/fnhum.2020.568703/full#supplementary-material

REFERENCES

Anidi, C., O'Day, J. J., Anderson, R. W., Afzal, M. F., Syrkin-Nikolau, J., Velisar, A., et al. (2018). Neuromodulation targets pathological not physiological beta bursts during gait in Parkinson's disease. *Neurobiol. Dis.* 120, 107–117. doi: 10.1016/j.nbd.2018.09.004

Arnulfo, G., Pozzi, N. G., Palmisano, C., Leporini, A., Canessa, A., Brumberg, J., et al. (2018). Phase matters: a role for the subthalamic network during gait. *PLoS One* 13:e0198691. doi: 10.1371/journal.pone.0198691

Brown, P. (2003). Oscillatory nature of human basal ganglia activity: relationship to the pathophysiology of Parkinson's disease. *Mov. Disord.* 18, 357–363. doi: 10.1002/mds.10358

Bulea, T. C., Kim, J., Damiano, D. L., Stanley, C. J., and Park, H. S. (2015). Prefrontal, posterior parietal and sensorimotor network activity underlying speed control during walking. *Front. Hum. Neurosci.* 9:247. doi: 10.3389/fnhum.2015.00247

Buzsaki, G., and Draguhn, A. (2004). Neuronal oscillations in cortical networks. *Science* 304, 1926–1929. doi: 10.1126/science.1099745

Chen, C. C., Kuhn, A. A., Trottenberg, T., Kupsch, A., Schneider, G. H., and Brown, P. (2006). Neuronal activity in globus pallidus interna can be synchronized to local field potential activity over 3-12 Hz in patients with dystonia. *Exp. Neurol.* 202, 480–486. doi: 10.1016/j.expneurol.2006.07.011

Collomb-Clerc, A., and Welter, M. L. (2015). Effects of deep brain stimulation on balance and gait in patients with Parkinson's disease: a systematic neurophysiological review. *Neurophysiol. Clin.* 45, 371–388. doi: 10.1016/j.neucli.2015.07.001

Csicsvari, J., Jamieson, B., Wise, K. D., and Buzsaki, G. (2003). Mechanisms of gamma oscillations in the hippocampus of the behaving rat. *Neuron* 37, 311–322. doi: 10.1016/s0896-6273(02)01169-8

Drew, T., and Marigold, D. S. (2015). Taking the next step: cortical contributions to the control of locomotion. *Curr. Opin. Neurobiol.* 33C, 25–33. doi: 10.1016/j.conb.2015.01.011

Fischer, P., Chen, C. C., Chang, Y. J., Yeh, C. H., Pogosyan, A., Herz, D. M., et al. (2018). Alternating modulation of subthalamic nucleus beta oscillations during stepping. *J. Neurosci.* 38, 5111–5121. doi: 10.1523/JNEUROSCI.3596-17.2018

Fries, P. (2005). A mechanism for cognitive dynamics: neuronal communication through neuronal coherence. *Trends Cogn. Sci.* 9, 474–480. doi: 10.1016/j.tics.2005.08.011

Gunther, M., Bartsch, R. P., Miron-Shahar, Y., Hassin-Baer, S., Inzelberg, R., Kurths, J., et al. (2019). Coupling between leg muscle activation and EEG during normal walking, intentional stops, and freezing of gait in parkinson's disease. *Front. Physiol.* 10:870. doi: 10.3389/fphys.2019.00870

Gwin, J. T., Gramann, K., Makeig, S., and Ferris, D. P. (2011). Electrocortical activity is coupled to gait cycle phase during treadmill walking. *Neuroimage* 54, 1289–1296. doi: 10.1016/j.neuroimage.2010.08.066

Hammond, C., Bergman, H., and Brown, P. (2007). Pathological synchronization in Parkinson's disease: networks, models and treatments. *Trends Neurosci.* 30, 357–364. doi: 10.1016/j.tins.2007.05.004

Hell, F., Plate, A., Mehrkens, J. H., and Botzel, K. (2018). Subthalamic oscillatory activity and connectivity during gait in Parkinson's disease. *Neuroimage Clin.* 19, 396–405. doi: 10.1016/j.nicl.2018.05.001

Jensen, P., Frisk, R., Spedden, M. E., Geertsen, S. S., Bouyer, L. J., Halliday, D. M., et al. (2019). Using Corticomuscular and Intermuscular Coherence to Assess Cortical Contribution to Ankle Plantar Flexor Activity During Gait. *J. Mot. Behav* 51, 668–680. doi: 10.1080/00222895.2018.1563762

Jensen, P., Jensen, N. J., Terkildsen, C. U., Choi, J. T., Nielsen, J. B., and Geertsen, S. S. (2018). Increased central common drive to ankle plantar flexor and dorsiflexor muscles during visually guided gait. *Physiol. Rep.* 6:e13598. doi: 10.14814/phy2.13598

Little, S., Pogosyan, A., Neal, S., Zavala, B., Zrinzo, L., Hariz, M., et al. (2013). Adaptive deep brain stimulation in advanced Parkinson disease. *Ann. Neurol.* 74, 449–457. doi: 10.1002/ana.23951

Liu, X., Wang, S., Yianni, J., Nandi, D., Bain, P. G., Gregory, R., et al. (2008). The sensory and motor representation of synchronized oscillations in the globus pallidus in patients with primary dystonia. *Brain* 131(Pt. 6), 1562–1573. doi: 10.1093/brain/awn083

Llinas, R. R. (1988). The intrinsic electrophysiological properties of mammalian neurons: insights into central nervous system function. *Science* 242, 1654–1664. doi: 10.1126/science.3059497

Lozano, A. M., and Lipsman, N. (2013). Probing and regulating dysfunctional circuits using deep brain stimulation. *Neuron* 77, 406–424. doi: 10.1016/j.neuron.2013.01.020

McCrimmon, C. M., Wang, P. T., Heydari, P., Nguyen, A., Shaw, S. J., Gong, H., et al. (2018). Electrocorticographic encoding of human gait in the leg primary motor cortex. *Cereb. Cortex* 28, 2752–2762. doi: 10.1093/cercor/bhx155

Miller, K. J., Leuthardt, E. C., Schalk, G., Rao, R. P., Anderson, N. R., Moran, D. W., et al. (2007). Spectral changes in cortical surface potentials during motor movement. *J. Neurosci.* 27, 2424–2432. doi: 10.1523/JNEUROSCI.3886-06.2007

Miller, K. J., Schalk, G., Fetz, E. E., den Nijs, M., Ojemann, J. G., and Rao, R. P. (2010). Cortical activity during motor execution, motor imagery, and imagery-based online feedback. *Proc. Natl. Acad. Sci. U.S.A.* 107, 4430–4435. doi: 10.1073/pnas.0913697107

Miron-Shahar, Y., Kantelhardt, J. W., Grinberg, A., Hassin-Baer, S., Blatt, I., Inzelberg, R., et al. (2019). Excessive phase synchronization in cortical activation during locomotion in persons with Parkinson's disease. *Parkinsonism. Relat. Disord.* 65, 210–216. doi: 10.1016/j.parkreldis.2019.05.030

Nordin, A. D., Hairston, W. D., and Ferris, D. P. (2019). Human electrocortical dynamics while stepping over obstacles. *Sci. Rep.* 9:4693.

Nordin, A. D., Hairston, W. D., and Ferris, D. P. (2020). Faster gait speeds reduce alpha and beta eeg spectral power from human sensorimotor cortex. *IEEE Trans. Biomed. Eng.* 67, 842–853. doi: 10.1109/TBME.2019.2921766

Oswal, A., Brown, P., and Litvak, V. (2013). Synchronized neural oscillations and the pathophysiology of Parkinson's disease. *Curr. Opin. Neurol.* 26, 662–670. doi: 10.1097/WCO.0000000000000034

Petersen, T. H., Willerslev-Olsen, M., Conway, B. A., and Nielsen, J. B. (2012). The motor cortex drives the muscles during walking in human subjects. *J. Physiol.* 590, 2443–2452. doi: 10.1113/jphysiol.2012.227397

Pozzi, N. G., Canessa, A., Palmisano, C., Brumberg, J., Steigerwald, F., Reich, M. M., et al. (2019). Freezing of gait in Parkinson's disease reflects a sudden derangement of locomotor network dynamics. *Brain* 142, 2037–2050. doi: 10.1093/brain/awz141

Quinn, E. J., Blumenfeld, Z., Velisar, A., Koop, M. M., Shreve, L. A., Trager, M. H., et al. (2015). Beta oscillations in freely moving Parkinson's subjects are attenuated during deep brain stimulation. *Mov. Disord.* 30, 1750–1758. doi: 10.1002/mds.26376

Roeder, L., Boonstra, T. W., and Kerr, G. K. (2020). Corticomuscular control of walking in older people and people with Parkinson's disease. *Sci. Rep.* 10:2980. doi: 10.1038/s41598-020-59810-w

Seeber, M., Scherer, R., Wagner, J., Solis-Escalante, T., and Muller-Putz, G. R. (2015). High and low gamma EEG oscillations in central sensorimotor areas are conversely modulated during the human gait cycle. *Neuroimage* 112, 318–326. doi: 10.1016/j.neuroimage.2015.03.045

Sharott, A., Grosse, P., Kuhn, A. A., Salih, F., Engel, A. K., Kupsch, A., et al. (2008). Is the synchronization between pallidal and muscle activity in primary dystonia due to peripheral afferance or a motor drive? *Brain* 131(Pt. 2), 473–484. doi: 10.1093/brain/awm324

Shine, J. M., Handojoseno, A. M., Nguyen, T. N., Tran, Y., Naismith, S. L., Nguyen, H., et al. (2014). Abnormal patterns of theta frequency oscillations during the

temporal evolution of freezing of gait in Parkinson's disease. *Clin. Neurophysiol.* 125, 569–576. doi: 10.1016/j.clinph.2013.09.006

Silberstein, P., Kuhn, A. A., Kupsch, A., Trottenberg, T., Krauss, J. K., Wohrle, J. C., et al. (2003). Patterning of globus pallidus local field potentials differs between Parkinson's disease and dystonia. *Brain* 126(Pt. 12), 2597–2608. doi: 10.1093/brain/awg267

Singh, A., Kammermeier, S., Plate, A., Mehrkens, J. H., Ilmberger, J., and Botzel, K. (2011). Pattern of local field potential activity in the globus pallidus internum of dystonic patients during walking on a treadmill. *Exp. Neurol.* 232, 162–167. doi: 10.1016/j.expneurol.2011.08.019

Sipp, A. R., Gwin, J. T., Makeig, S., and Ferris, D. P. (2013). Loss of balance during balance beam walking elicits a multifocal theta band electrocortical response. *J. Neurophysiol.* 110, 2050–2060. doi: 10.1152/jn.00744.2012

Spedden, M. E., Choi, J. T., Nielsen, J. B., and Geertsen, S. S. (2019). Corticospinal control of normal and visually guided gait in healthy older and younger adults. *Neurobiol. Aging* 78, 29–41. doi: 10.1016/j.neurobiolaging.2019.02.005

Stolk, A., Brinkman, L., Vansteensel, M. J., Aarnoutse, E., Leijten, F. S., Dijkerman, C. H., et al. (2019). Electrocorticographic dissociation of alpha and beta rhythmic activity in the human sensorimotor system. *eLife* 8:e48065. doi: 10.7554/eLife.48065

Storzer, L., Butz, M., Hirschmann, J., Abbasi, O., Gratkowski, M., Saupe, D., et al. (2017). Bicycling suppresses abnormal beta synchrony in the Parkinsonian basal ganglia. *Ann. Neurol.* 82, 592–601. doi: 10.1002/ana.25047

Swann, N. C., de Hemptinne, C., Miocinovic, S., Qasim, S., Wang, S. S., Ziman, N., et al. (2016). Gamma oscillations in the hyperkinetic state detected with chronic human brain recordings in parkinson's disease. *J. Neurosci.* 36, 6445–6458. doi: 10.1523/JNEUROSCI.1128-16.2016

Swann, N. C., de Hemptinne, C., Thompson, M. C., Miocinovic, S., Miller, A. M., Gilron, R., et al. (2018). Adaptive deep brain stimulation for Parkinson's disease using motor cortex sensing. *J. Neural Eng.* 15:046006. doi: 10.1088/1741-2552/aabc9b

Syrkin-Nikolau, J., Koop, M. M., Prieto, T., Anidi, C., Afzal, M. F., Velisar, A., et al. (2017). Subthalamic neural entropy is a feature of freezing of gait in freely moving people with Parkinson's disease. *Neurobiol. Dis.* 108, 288–297. doi: 10.1016/j.nbd.2017.09.002

Takakusaki, K. (2017). Functional neuroanatomy for posture and gait control. *J. Mov. Disord.* 10, 1–17. doi: 10.14802/jmd.16062

Tinkhauser, G., Pogosyan, A., Little, S., Beudel, M., Herz, D. M., Tan, H., et al. (2017a). The modulatory effect of adaptive deep brain stimulation on beta bursts in Parkinson's disease. *Brain* 140, 1053–1067. doi: 10.1093/brain/awx010

Tinkhauser, G., Pogosyan, A., Tan, H., Herz, D. M., Kuhn, A. A., and Brown, P. (2017b). Beta burst dynamics in Parkinson's disease OFF and ON dopaminergic medication. *Brain* 140, 2968–2981. doi: 10.1093/brain/awx252

Tinkhauser, G., Shah, S. A., Fischer, P., Peterman, K., Debove, I., Nygyuen, K., et al. (2019). Electrophysiological differences between upper and lower limb movements in the human subthalamic nucleus. *Clin. Neurophysiol.* 130, 727–738. doi: 10.1016/j.clinph.2019.02.011

Tinkhauser, G., Torrecillos, F., Duclos, Y., Tan, H., Pogosyan, A., Fischer, P., et al. (2018). Beta burst coupling across the motor circuit in Parkinson's disease. *Neurobiol. Dis.* 117, 217–225. doi: 10.1016/j.nbd.2018.06.007

Toledo, J. B., Lopez-Azcarate, J., Garcia-Garcia, D., Guridi, J., Valencia, M., Artieda, J., et al. (2014). High beta activity in the subthalamic nucleus and freezing of gait in Parkinson's disease. *Neurobiol. Dis.* 64, 60–65. doi: 10.1016/j.nbd.2013.12.005

Varghese, J. P., Merino, D. M., Beyer, K. B., and McIlroy, W. E. (2016). Cortical control of anticipatory postural adjustments prior to stepping. *Neuroscience* 313, 99–109. doi: 10.1016/j.neuroscience.2015.11.032

Wagner, J., Makeig, S., Gola, M., Neuper, C., and Muller-Putz, G. (2016). Distinct beta band oscillatory networks subserving motor and cognitive control during gait adaptation. *J. Neurosci.* 36, 2212–2226. doi: 10.1523/JNEUROSCI.3543-15.2016

Wagner, J., Solis-Escalante, T., Grieshofer, P., Neuper, C., Muller-Putz, G., and Scherer, R. (2012). Level of participation in robotic-assisted treadmill walking modulates midline sensorimotor EEG rhythms in able-bodied subjects. *Neuroimage* 63, 1203–1211. doi: 10.1016/j.neuroimage.2012.08.019

Wang, D. D., de Hemptinne, C., Miocinovic, S., Ostrem, J. L., Galifianakis, N. B., San Luciano, M., et al. (2018). Pallidal deep-brain stimulation disrupts pallidal beta oscillations and coherence with primary motor cortex in Parkinson's disease. *J. Neurosci.* 38, 4556–4568. doi: 10.1523/JNEUROSCI.0431-18.2018

Wang, S. Y., Aziz, T. Z., Stein, J. F., and Liu, X. (2005). Time-frequency analysis of transient neuromuscular events: dynamic changes in activity of the subthalamic nucleus and forearm muscles related to the intermittent resting tremor. *J. Neurosci. Methods* 145, 151–158. doi: 10.1016/j.jneumeth.2004.12.009

Weinberger, M., Hutchison, W. D., Alavi, M., Hodaie, M., Lozano, A. M., Moro, E., et al. (2012). Oscillatory activity in the globus pallidus internus: comparison between Parkinson's disease and dystonia. *Clin. Neurophysiol.* 123, 358–368. doi: 10.1016/j.clinph.2011.07.029

Yanagisawa, T., Yamashita, O., Hirata, M., Kishima, H., Saitoh, Y., Goto, T., et al. (2012). Regulation of motor representation by phase-amplitude coupling in the sensorimotor cortex. *J. Neurosci.* 32, 15467–15475. doi: 10.1523/JNEUROSCI.2929-12.2012

Yoshida, T., Masani, K., Zabjek, K., Popovic, M. R., and Chen, R. (2018). Dynamic cortical participation during bilateral, cyclical ankle movements: effects of Parkinson's disease. *PLoS One* 13:e0196177. doi: 10.1371/journal.pone.0196177

Conflict of Interest: DW receives consulting fees from Medtronic and Boston Scientific Inc.

The remaining author declares that the research was conducted in the absence of any commercial or financial relationships that could be construed as a potential conflict of interest.

frontiers in Bioengineering and Biotechnology

ORIGINAL RESEARCH
published: 29 October 2020
doi: 10.3389/fbioe.2020.552635

Ankle Push-Off Based Mathematical Model for Freezing of Gait in Parkinson's Disease

Midhun Parakkal Unni[1]*, *Prathyush P. Menon*[1]*, *Mark R. Wilson*[2] and *Krasimira Tsaneva-Atanasova*[1,3,4,5]

[1] Department of Mathematics, College of Engineering Mathematics and Physical Sciences, University of Exeter, Exeter, United Kingdom, [2] Sport & Health Sciences, University of Exeter, Exeter, United Kingdom, [3] Department of Bioinformatics and Mathematical Modelling, Institute of Biophysics and Biomedical Engineering, Bulgarian Academy of Sciences, Sofia, Bulgaria, [4] Living Systems Institute, University of Exeter, Exeter, United Kingdom, [5] EPSRC Centre for Predictive Modelling in Healthcare, University of Exeter, Exeter, United Kingdom

Freezing is an involuntary stopping of gait observed in late-stage Parkinson's disease (PD) patients. This is a highly debilitating symptom lacking a clear understanding of its causes. Walking in these patients is also associated with high variability, making both prediction of freezing and its understanding difficult. A neuromechanical model describes the motion of the mechanical (motor) aspects of the body under the action of neuromuscular forcing. In this work, a simplified neuromechanical model of gait is used to infer the causes for both the observed variability and freezing in PD. The mathematical model consists of the stance leg (during walking) modeled as a simple inverted pendulum acted upon by the ankle-push off forces from the trailing leg and pathological forces by the plantar-flexors of the stance leg. We model the effect on walking of the swing leg in the biped model and provide a rationale for using an inverted pendulum model. Freezing and irregular walking is demonstrated in the biped model as well as the inverted pendulum model. The inverted pendulum model is further studied semi-analytically to show the presence of horseshoe and chaos. While the plantar flexors of the swing leg push the center of mass (CoM) forward, the plantar flexors of the stance leg generate an opposing torque. Our study reveals that these opposing forces generated by the plantar flexors can induce freezing. Other gait abnormalities nearer to freezing such as a reduction in step length, and irregular walking patterns can also be explained by the model.

Keywords: Parkinson's disease, gait, chaos, neuro-mechanical model, modeling

OPEN ACCESS

Edited by:
Mario Bernardo-Filho,
Rio de Janeiro State University, Brazil

Reviewed by:
Chi-Wen Lung,
Asia University, Taiwan
Paulo Roberto Garcia Lucareli,
Universidade Nove de Julho, Brazil

***Correspondence:**
Midhun Parakkal Unni
mp603@exeter.ac.uk
Prathyush P. Menon
p.m.prathyush@exeter.ac.uk

Specialty section:
This article was submitted to Biomechanics, a section of the journal Frontiers in Bioengineering and Biotechnology

Received: *16 April 2020*
Accepted: *21 September 2020*
Published: *29 October 2020*

Citation:
Parakkal Unni M, Menon PP, Wilson MR and Tsaneva-Atanasova K (2020) Ankle Push-Off Based Mathematical Model for Freezing of Gait in Parkinson's Disease. Front. Bioeng. Biotechnol. 8:552635. doi: 10.3389/fbioe.2020.552635

1. INTRODUCTION

Parkinson's disease results from the loss of neurons in the substantia nigra pars compacta of the basal ganglia (BG) (Davie, 2008), which has projections toward the motor, and cognitive areas (Albin et al., 1989; Alexander and Crutcher, 1990). Freezing of gait (FoG) is a motor disability in PD patients where subjects experience an "episodic absence or marked reduction of forwarding progression of the feet despite the intention to walk" (Nutt et al., 2011, p 734). This debilitating symptom occurs during the late-stage PD (Giladi et al., 2001) and is known to be very difficult to predict and control. The physiology of this symptom is not yet established conclusively, consisting of both neural and mechanical components. A set of correlations between the neural inputs

(e.g., Dysfunction of Visuomotor and occipito-parietal pathways) and mechanical variables (e.g., gait pattern generation and automaticity) of PD-FoG have been studied (Heremans et al., 2013) but causality is not well-established. Apart from freezing, abnormal gait patterns in PD consists of high stride time variability with less reduction in stride length (Heremans et al., 2013). The relationship between these abnormalities and freezing is also not well-understood.

Gait has been studied fundamentally from two different perspectives. One that of robotics and control, and the second, biophysical. Mathematical models of passive gait have been studied extensively by several authors to understand their stability (e.g., Goswami et al., 1996; Manchester et al., 2011; Dai and Tedrake, 2013; Sadeghian and Barkhordari, 2020), and the effect of external conditions such as ramps (McGeer, 1990) and bifurcations has been investigated (e.g., Mahmoodi et al., 2013; Iqbal et al., 2014; Fathizadeh et al., 2018, 2019; Znegui et al., 2020). Impulsive dissipation at heel strike is studied for a multidimensional biped model in (Ros et al., 2015). There are other approaches to motor control using optimal control which demands an arbitrary or learned cost-functionals (e.g., Flash and Hogan, 1985; Pekarek et al., 2007; Parakkal Unni et al., 2017). These models are not sufficient to understand human locomotion in PD patients as these papers have focused on the stability behaviors and control of robots. Some of these cost functional/error minimization based models, even though they assume the existence of such a cost, have the advantage of being useful for extracting parameters easily from the data (Delp et al., 2007; Wu et al., 2019). However, they do not address explicitly how the external inputs result in high variability and freezing observed in PD gait (Heremans et al., 2013).

On the other hand, a biophysical model proposed in Taga (1995) considers the interaction with the Central Pattern Generators (CPG). The aim of the model is primarily to demonstrate walking as a stable limit cycle that emerges from the dynamic interaction between neural oscillation originating in CPG and the pendulum oscillation of body linkages, rather than involuntary stoppage of gait and variability. CPG-based complex model, which depends on several parameters such as the strength of neural connections, the magnitude of the coefficients in the rhythmic force controller, and strength of sensory inputs, has its significance. However, one drawback of such CPG-based complex model is often the dependence on an excessive number of parameters as described above to be determined for achieving a desired locomotor pattern over a large search space. To identify and tune such parameters for attaining involuntary freezing and variability of gait behavior for a wider population of patients is rather an arduous trial-and-error or learning and optimization based task. Involuntary stoppage of gait and variability is the key detail that is necessary to show the model's ability to display PD walking behavior. The effect of opposing forces generated by the plantar flexors observed in PD, as reported in Nieuwboer et al. (2004), is yet another detail for understanding the PD gait.

The model by Muralidharan et al. (2014) successfully captures the neural dynamics of basal ganglia (BG) but does not focus on the mechanics. A model which combines the chaotic region of the Lorentz system with the passive dynamic walker by Montazeri Moghadam et al. (2018), adds chaos externally, which makes it less relevant biophysically. However, these authors have established a need for explaining the variable nature of PD walking. As chaos is known to be absent in the basal ganglia (BG) of a PD patient (Mandali et al., 2015) the neuro-mechanical interactions need to be studied to find out its underpinnings. Another way to look at gait biophysically is through the equilibrium point hypothesis (Feldman, 1986; Duan et al., 1997), which suggests movements are the result of active changes in the equilibrium state of the motor system. Torque length characteristics of the muscles can be changed by a neural controller to achieve motion. It has been shown that the muscles act synergistically to reduce the variability in the targeted action. For example, the uncontrolled manifold hypothesis by Latash et al. (2002) explains the variability in muscle recruitment as "good" and "bad" regions of variability, depending on whether they achieve the targeted action or not. The muscle recruitments which achieve targeted action are considered "good" regions of variability, whereas the muscle recruitments which does not achieve targeted action are considered as "bad" regions of variability. The Equilibrium point approach (Feldman, 1986) makes the electromyogram (EMG) activity implicit. Another limitation of the equilibrium point hypothesis is in its difficulty in testing. The empirical determination of invariant characteristics (Sainburg, 2015) such as torque-length characteristics (Feldman, 1986) is necessary for validating the equilibrium point hypothesis. A way in which it is achieved is by asking the subjects "not to intervene" (Feldman, 1986; Sainburg, 2015) while doing a task such as unloading and assuming this results in stabilization of central commands to muscles (Sainburg, 2015). But this assumption is not necessarily true as there could be involuntary responses. The neuromuscular system is over-actuated with redundancies, as it contains more actuators than the degree of freedom. Use of muscle synergies (Latash, 2010) in models is one way to address redundancies. These models assume co-activation of a set of muscles as motor primitives to address the redundancy associated with muscle activation (Aoi et al., 2019; Tamura et al., 2020). The idea of muscle synergy is still debated and is considered difficult to refute by any empirical evidence or falsify (Popper, 2002; Olszewski and Sandroni, 2011) by some authors (Tresch and Jarc, 2009).

There is a need for a model to explain the empirical observations in PD gait, such as the high coefficient of variability and freezing near narrow passages (Snijders et al., 2008). Such a model will help in understanding the essential aspects of neural and mechanical systems contributing to PD gait, also shedding light into the future experimentations required. In this work, the relationships between the high variability and freezing will be studied by deriving a set of forces acting on the stance leg. They phenomenologically represent the EMG (Electromyogram) signals and therefore the activity of the CPGs. Kinetics of both swing leg and stance leg will be studied to better understand their roles under the action of these forces.

In summary, the model is built with two aims. The first aim is to explain the empirical observations that are seen in PD-Gait with a minimum number of variables. These include (1) a high coefficient of variation in PD subjects (Heremans et al.,

2013), (2) a pattern of reduction of step lengths before freezing (Nutt et al., 2011), (3) the ability of sensory and visual cues to help reduce freezing (Rochester et al., 2005; Young et al., 2014; Amini et al., 2019), (4) the difficulty of freezing prediction, and (5) the occurrence of freezing near obstacles and narrow passages (Snijders et al., 2008). Secondly, the model aims to show the role of the swing leg as a supplier of ankle push of force as well as one that determines the time of heel strike. Hence, a bipedal model and a reduced low dimensional model resembling an inverted pendulum are studied upon the action of the ankle push-off force. The movement of the CoM under the action of the ankle push-off force is depicted in **Figure 1**. Hence, the hypothesis investigated in this study is that the variability and the motor symptoms associated with PD (Heremans et al., 2013) can be explained by the experimentally observed premature activation of plantar flexors observed in PD (Nieuwboer et al., 2004).

2. MATERIALS AND METHODS—MODELING

2.1. Physiology

Walking is a complex process which involves the interaction of the brain, spinal cord and the musculoskeletal systems (Nutt et al., 2011). The typical gait cycle associated with walking involves "*stance*" and "*swing*" phases. The stance phase begins with a crucial heel strike phase, which is the initial contact that occurs instantaneously. As soon as the stance phase ends, the swing phase begins. The plantar flexor muscles of the trailing leg, supply energy to "push-off" the contra-lateral leading leg (Zelik and Adamczyk, 2016). Once the push-off occurs, the trailing leg enters the swing phase. The soleus and gastrocnemius muscles are the most notable plantar flexors, of which the significant role of the latter one in PD freezing/walking is established (Nieuwboer et al., 2004). Even though physiologically there is a non-linear relationship between the EMG signals and the torques generated (Genadry et al., 1988), a linear relationship can be assumed (Hof and Van Den Berg, 1977) between the envelope of the EMG (CPG firing) and the torques generated about the joint. Several other muscles are involved in walking, but the present study investigates only the effect of plantar flexors as these muscles supply most of the energy required for walking. In this work, the "freezing step" is defined as the step at which the legs do not have sufficient angular momentum to progress walking forward. When the physiology is modeled as an inverted pendulum-like system, the freezing results in backward motion of the stance leg. In a real-life scenario, this implies the patient either falls or stops movement. The remark 1 defines freezing and related terms used in this work.

REMARK 1. *In this study, "freezing" or "freezing event" is defined as the condition where there is no forward motion of the stance leg. "Freezing episode" is defined as the events happening in the time interval between the heels strike phase the freezing event. Hence, the "start of the freeze" is defined to be at the heel strike phase after which a freezing event occurs.*

Here, we carry out a systematic stability analysis, including unstable regimes, of the model in contrast to the stable limit cycle behavior studied in robotics (Grizzle et al., 2001) and passive walking dynamics literature (McGeer, 1990). Even though the complex freezing behavior can be explained through several possible routes (Nutt et al., 2011) (some of them purely based on neural control) an attempt is made here to explain it in the simplest possible way and to understand the effect of neuromuscular inputs in generating unstable and chaotic walking behavior as observed in PD (Heremans et al., 2013).

2.2. Dynamics of Walking

The dynamics of walking involves the coordinated action of neural input and muscles of the limbs. It consists in a continuous movement of the limbs as well as state reset at heel strike resulting

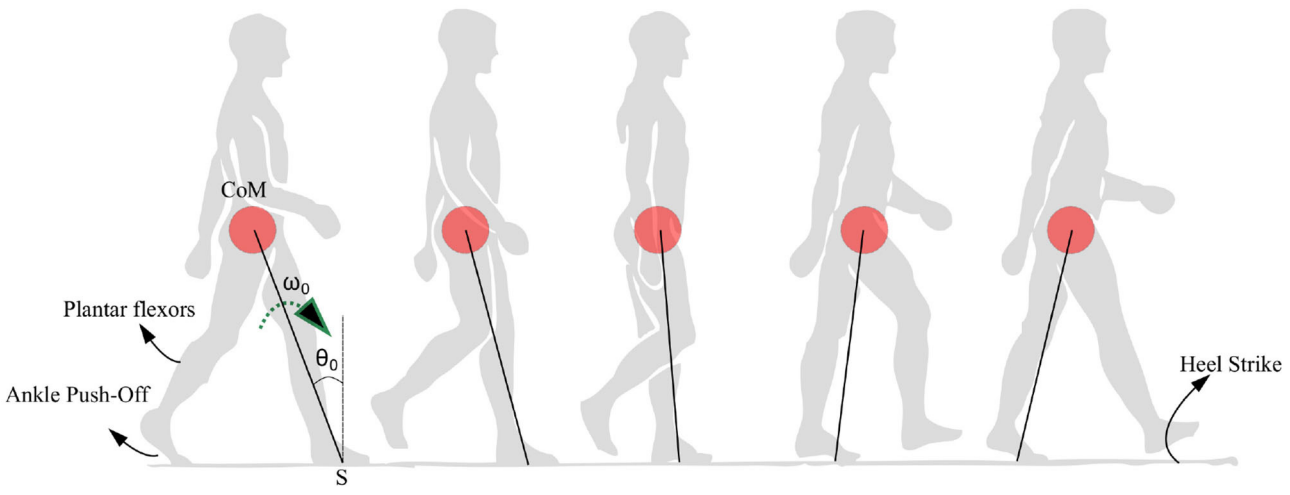

FIGURE 1 | Anatomical representation of the stance phase from the ankle push-off to the heel strike is shown. The position of the center of mass (CoM) is shown as a red circle which is assumed to be rotating with respect to a pivot point S. The location of the plantar flexors, approximate region generating ankle push-off force and heel strike region are noted. The initial angle and angular velocity are represented by θ_0 and ω_0, respectively.

in discrete dynamics (Sinnet et al., 2011). Plantar flexors of the swing leg supply the necessary torque to push the CoM forward. During walking, the CoM is supported by leg in stance phase for the majority of the time (80-90%) as the double support phase is approximately 10-20% of the overall gait cycle (Wahde and Pettersson, 2002; Kharb et al., 2011). The motion of the CoM with single support under the action of the plantar flexors is modeled in this work. The heel strike is modeled using discrete dynamics.

Traditionally the dynamics of walking is often modeled as biped model (Taga, 1995). In this section, a simplified biped model is presented. Further, a reduced, low dimensional, *inverted pendulum system* is considered as a special case relevant to PD. It is assumed that CoM is at the tip of the pendulum, and the links and the swing leg are massless. Therefore, the model generates the motion of the CoM of the human body. Running and jumping gaits are not considered in this model as the links are assumed to be rigid. It is also assumed that sufficient friction exists to avoid any slip. The angular displacements are assumed to be small enough (< 0.5 rad.) (Usherwood, 2005; Ranavolo et al., 2011; Polese et al., 2012) to allow for first/second-order approximations during the stance phase. Kane's method (Kane and Levinson, 1985) is used to derive the equations of motion (EoM). Kane's dynamical equation is of the form $\bar{F}_r + \bar{F}_r^* = 0$, where $\bar{F}_r$ and $\bar{F}_r^*$ represents generalized active forces and generalized inertia forces, respectively, as described in Kane and Levinson (1985) (chapter 6, page 159). The equations in the form necessary for simulation is obtained using python libraries, the details of which are given in Gede et al. (2013).

Symbols m_1, m_2 represent the mass of the body and swing leg, respectively, as shown in **Figure 2**. The length of both the legs is represented by l. The variables associated with the system are the components of the vector $x = [\theta_1, \theta_2, \omega_1, \omega_2]^T$ which

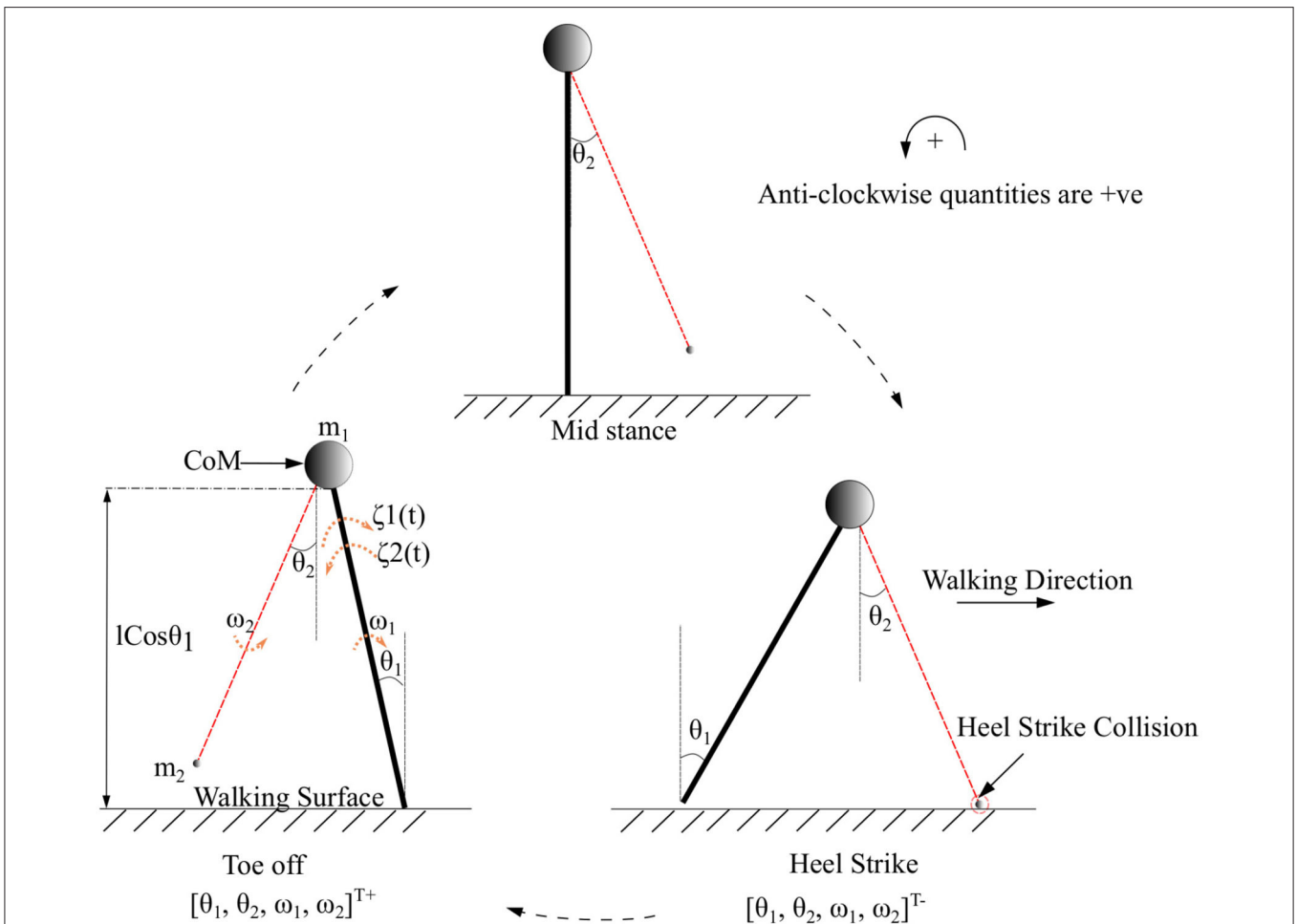

FIGURE 2 | The toe-off, mid stance, and heel strike instances of the two connected links of the biped with its CoM while walking in the forward direction. CoM indicated as a circle represents a point mass at the tip of the pendulum. The swing leg is indicated in red. The point of collision during a heel strike instance is circled in red. The terms θ_1 and θ_2 are the angles that the stance and swing legs subtend w.r.t. the vertical (in the inertial reference frame), respectively. The quantities ω_1, ω_2 and m_1, m_2 are the corresponding angular velocities and masses of the body and swing leg, respectively. The torques that are acting on the stance leg are indicated as $\zeta_1(t)$ (Ankle push-off force) and $\zeta_2(t)$ (Torque due to the activation of the plantar flexors of the stance leg). States immediately before and after heel strike is indicated with "-" and "+" superscripts, respectively.

are the angles and angular velocities (w.r.t inertial frame for stance leg and w.r.t. stance leg frame for swing leg) as indicated in **Figure 2**. There are two types of angular velocities. The one which corresponds to the rotation of the rigid body with respect to its center of rotation is called spin angular velocity and one which corresponds to the revolution of a point with respect to an origin is called orbital angular velocity. In this work, spin angular velocities with respect to the center of rotation of the rigid links are considered as they rotate about the center of rotation.

Hybrid systems (Lunze and Lamnabhi-Lagarrigue, 2009) are a class of dynamical systems, which exhibit both continuous states and discrete mode dynamics often associated with events such as resets, jumps, and switching. The continuous behavior is typically governed by a system of differential equations (similar to Equation 1) and the discrete part is governed by a vector-valued function (similar to Equation 2) (Lunze and Lamnabhi-Lagarrigue, 2009)(chapter 1). The transition between the discrete and continuous governing equations is determined by the state of the system in the overall phase space. The dynamics in this work is governed by the general hybrid dynamical system of the form,

$$\dot{x} = q(x),\ x^- \notin S \tag{1}$$

$$x^+ = \Delta(x^-),\ x^- \in S \tag{2}$$

where,

$$S := \{x \in \chi \mid g_{reset}(x) = 0\} \tag{3}$$

where, $q(x)$, $\Delta(x^-)$, and $g_{reset}(x)$ are continuous vector valued functions of x. In the absence of external torques acting on the leg, the term $q(x)$ is,

$$q(x) = \begin{bmatrix} \omega_1 \\ \omega_2 \\ \frac{1}{2l(m_1+m_2\sin^2(\theta_2))}\big(2gm_1\sin(\theta_1) - gm_2\sin(\theta_1+2\theta_2) \\ +gm_2\sin(\theta_1) + lm_2\omega_1^2\sin(2\theta_2) - 2lm_2\omega_2^2\sin(\theta_2)\big) \\ -\frac{\sin(\theta_2)}{l(m_1+m_2\sin^2(\theta_2))}\big(gm_1\cos(\theta_1) + gm_2\cos(\theta_1) \\ -l\omega_1^2(m_1+m_2) + lm_2\omega_2^2\cos(\theta_2)\big) \end{bmatrix} \tag{4}$$

The function, $\Delta(.)$ is the reset map, $\chi \subset \mathbb{R}^4$ the state space, and $g_{reset}(.)$ is the function that defines the heel strike. The set "S" defines a surface where the heel strikes the ground and the states change abruptly according to the reset map. The x^- and x^+ indicate the states immediately before and after the heel strike, respectively. The functions $\Delta(.)$ and $g_{reset}(.)$ are described in sequel.

As the body mass is considerably larger than the mass of the leg, the case where m_2 goes to 0 has only been considered. Further, small-angle approximation leads to the following equation for $\dot{\omega}_1$ and $\dot{\omega}_2$

$$\dot{\omega}_1 = g\frac{\theta_1}{l} \tag{5}$$

$$\dot{\omega}_2 = -\frac{(g - l\omega_1^2)\theta_2}{l} \tag{6}$$

The ankle push-off forces of the stance leg supply majority of the energy needed to propel the leg forward. When this neuromuscular forcing $\Gamma(t)$ is added to the stance leg, the Equation (5) becomes,

$$\dot{\omega}_1 := g\frac{\theta_1}{l} + \Gamma(t) \tag{7}$$

The forcing term $\Gamma(t)$ is derived in the following section.

2.3. Derivation of the Forcing Terms

The torques acting on the stance leg are derived in this section to generate the neuromuscular forcing term $\Gamma(t)$ for the stance leg. Torque produced by the plantar flexors on the trailing leg is defined as $G_r(t)$ and that on the leading leg as $G_l(t)$. These torques are assumed to be linearly related to the envelop of the EMG signals which are positive functions of time (Nieuwboer et al., 2004). The torque $G_r(t)$ generates the ankle push off force $F(t)$ and is assumed to be in phase with the heel strike. In the proposed model, the force $F(t)$ and the torque $G_l(t)$ are assumed to be

$$G_l(t) := \tau_l(\sin(2\pi f_{r_1}t + \phi) + 1) \tag{8}$$

$$F(t) := \tau_r(\sin(2\pi f_{r_2}t) + 1) \tag{9}$$

where τ_l and τ_r are constants. The variables, f_{r_1}, f_{r_2} and ϕ represent frequencies and the phase difference between torques on the leading and trailing leg, respectively. Both frequencies are assumed to be unity. The ankle push off torque acting on the leading leg (in stance phase) can be calculated using the free body diagram shown in **Figure 3**. The pivot points of the trailing leg and leading leg are "O" and "S," respectively. Trailing leg and leading leg subtends the same angle θ_1 w.r.t. the normal to the ground as the trailing leg and leading leg together with the ground is assumed to form an isosceles triangle. By balancing the moments about the point "S" in **Figure 3** yields,

$$I\dot{\omega}_1 = G_l(t) - lF(t)\sin(\theta_h) + mgl\sin(\theta_1) \tag{10}$$

When angle θ_1 is small ($\sin(\theta) \approx \theta$) and since $I = m_1l^2$, Equation (10) is rewritten as,

$$m_1l^2\dot{\omega}_1 = G_l(t) - lF(t)\sin(\theta_h) + m_1gl\theta_1 \tag{11}$$

Substituting $F(t)$ and $G_l(t)$ from Equation (8) and (9) in Equation (11), one obtains,

$$m_1l^2\dot{\omega}_1 = \tau_l(\sin(2\pi f_{r_1}t + \phi) + 1) - l\tau_r(\sin(2\pi f_{r_2}t) + 1)\sin(\theta_h) + m_1gl\theta_1 \tag{12}$$

Rearranging Equation (12), angular acceleration of the leading/stance leg is,

$$\dot{\omega}_1 = \frac{\overbrace{\tau_l(\sin(2\pi f_{r_1}t + \phi) + 1)}^{\text{Plantar flexors of the leading leg } (=\zeta_2(t))}}{l^2m_1} \tag{13}$$

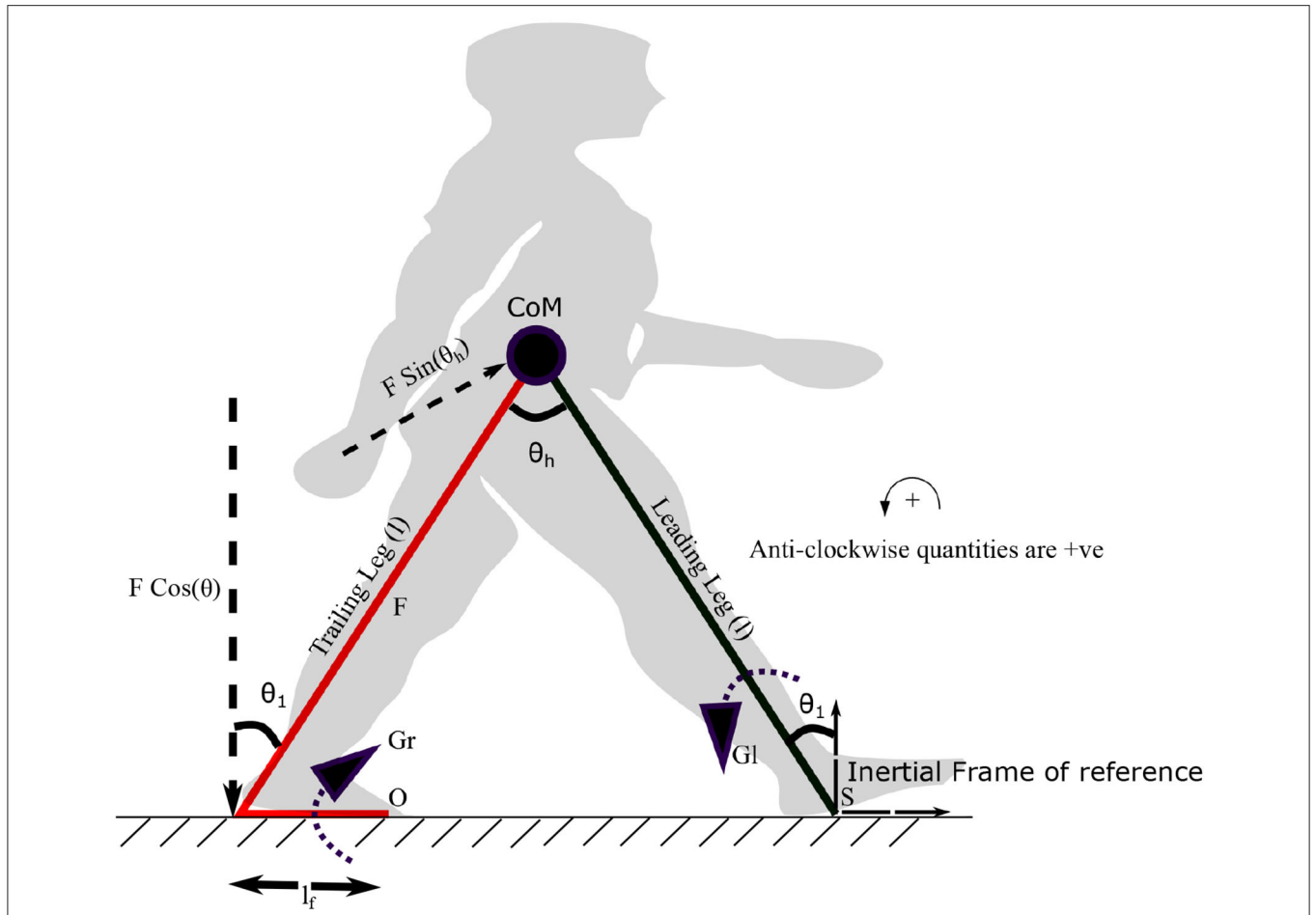

FIGURE 3 | The diagram visualizes the forces and moments on leading and trailing leg that enable the movement of the center of mass (CoM) forward. Symbols S and O indicate the points on leading and trailing leg about which the torques G_l and G_r are applied. G_r is the torque generated by the plantar flexors of the trailing leg, which results in a force F (ankle push-off) acting on the leading leg, about the point "S." The distance between the pivot point to the point of action of the force is l_f. The plantar flexors of the leading leg generate a torque G_l in the leading leg, in the opposite direction. The angle the leading leg subtends with the vertical axis at S is θ_1. θ_h represents the hip angle. The moments are balanced about "S" to get the equations of motion (EoM). An approximate position of the starting stance phase is shown in the background in gray color.

$$-\frac{\overbrace{\tau_r l \sin(\theta_h)(\sin(2\pi f_{r_2} t)+1)}^{\text{Ankle push off from trailing leg } (=\zeta_1(t))}}{l^2 m_1} + \overbrace{\frac{g\theta_1}{l}}^{Gravity} := \frac{\zeta_2(t)-\zeta_1(t)}{m_1 l^2} + \frac{g\theta_1}{l} \tag{14}$$

where $\Gamma(t) := \frac{(-\zeta_1(t)+\zeta_2(t))}{m_1 l^2}$ (as shown in **Figure 2**) is the time varying neuromuscular forcing.

The initial velocity of the swing leg is assumed to be constant in every step. As the mass m_2 is assumed to be zero, the corresponding angular momentum is also equal to zero. Therefore, the angular velocity of the stance leg is reset to conserve its angular momentum and the initial angular velocity of the swing leg after reset is assumed to be a positive constant to account for the impulse during the ankle push-off. This is a valid assumption as the definition of freezing in this work is independent of the swing leg movement. A reset is carried out when $\theta_1 + \theta_2 = 0$ and $\theta_1 < 0$. Using Equations (6) and (14), the equations of motion of a biped can be written as in Equations (1)–(2), where the functions $q(x)$, $\Delta(x)$, $g_{reset}(x)$ and the set S are written as follows,

$$q(x) := \begin{bmatrix} \omega_1 \\ \omega_2 \\ \frac{\zeta_2(t)-\zeta_1(t)}{m_1 l^2} + \frac{g\theta_1}{l} \\ -\frac{(g-l\omega_1^2)\theta_2}{l} \end{bmatrix} \tag{15}$$

$$\begin{aligned} S &:= \left\{ \left[\theta_1,\ \theta_2,\ \omega_1,\ \omega_2\right]^T \in \chi \mid g_{reset}\left(\left[\theta_1,\ \theta_2,\ \omega_1,\ \omega_2\right]^T\right) \right. \\ &= \left. 0 \wedge \theta_1 < 0 \right\}, \\ g_{reset}(.) &:= \theta_1 + \theta_2, \\ \Delta(.) &:= \left[-\theta_1,\ -\theta_2,\ \omega_1 \cos(\theta_h),\ \omega_2^0\right] \end{aligned} \tag{16}$$

with initial conditions $\omega_1(0) = \omega_1^0$, $\theta_1(0) = \theta_1^0$, $\omega_2(0) = \omega_2^0$, $\theta_2(0) = \theta_2^0$.

REMARK 2. *It may be noted that the torque generated by the plantar flexors is assumed to act about the point "O" as the pivot point. Balancing the moments due to the ankle push off force, $F(t)$ and $G_r(t)$ about the point O, the ankle push-off force can be determined in terms of $G_r(t)$ as,*

$$F(t) = \frac{G_r(t)}{l_f \cos(\theta_1)} \tag{17}$$

Here, the distance, l_f is taken between the heel to the pivot point on the foot for calculating the moments, as shown in ***Figure 3****. Therefore, implicitly, the following assumption has been made while prescribing $F(t)$.*

$$\frac{G_r(t)}{l_f \cos(\theta_1)} := \tau_r(\sin(2\pi f_{r_2} t) + 1) \tag{18}$$

2.4. Rationale for Using a Low Dimensional Model for Analysis

The angular velocity of the stance leg contributes directly to the angular acceleration of the swing leg. A higher absolute angular velocity of the stance leg leads to lower acceleration of the swing leg. However, the dynamics of the stance leg in Equation (14) is uncoupled from the dynamics of the swing leg, and hence resembles the dynamics of an "*inverted pendulum system*." It may be noted that the term "$l\omega_1^2$" can be approximated to a constant as in the physiological range of low angular velocities (especially in PD patients) $g >> l\omega_1^2$ (typically quantity $l\omega_1^2 = 0.448\ \text{m.rad}^2.s^{-2} = 0.7 \times 0.8^2$ is of order "0" while $g = 9.8\ \text{m.s}^{-2}$ is of order 1). This results in a condition where the swing leg acts independently to the stance leg, effectively determining the step length. Therefore, an inverted pendulum walking model for PD subjects is valid when constant step length is assumed. **Figure 1** depicts the physical rationale behind the use of an inverted pendulum model. The constant step length assumption is general enough to explain the variability in stepping as this leads to variability in stepping angular velocities rather than step lengths. In summary, in the following sections we present analysis of the stance phase walking model in light of the PD walking behavior at a constant step length. Physiologically, the hip applies torques on the swing leg and controls its initial angular velocity. The hip torques acting on the swing is not relevant in propelling the CoM forward, as most of the torque required for that is supplied by the ankle (Zelik and Adamczyk, 2016). Therefore, an assumption made on the swing leg angular velocity will not affect the applicability of the model to the freezing problem as freezing is related to the inability of the legs to propel the CoM forward in the case of walking. Hence, swing leg angular velocity is reset to ω_2^0 in every step. Furthermore, the low dimensional model helps to avoid making any assumptions on the initial angular velocity of the swing leg ω_2^0 as it doesn't involve a swing leg.

3. ANALYSIS OF THE REDUCED SYSTEM

When considered independently of the swing leg, the dynamics has states corresponding only to the stance leg, i.e., $x = [\theta_1,\ \omega_1]^T$. The terms defining the Equation (1)–(2) for the inverted pendulum case are given below.

$$q(.) := \begin{bmatrix} \omega_1 \\ \frac{\zeta_2(t)-\zeta_1(t)}{m_1 l^2} + \frac{g\theta_1}{l} \end{bmatrix} \tag{19}$$

$$S := \left\{ \left[\theta_1, \omega_1\right]^T \in \chi \mid g_{reset}\left(\left[\theta_1, \omega_1\right]^T\right) = 0 \right\} \tag{20}$$

$$g_{reset}(.) := \theta_1 - \theta_{reset} \tag{21}$$

$$\Delta(.) := \left[-\theta_1, \omega_1 \cos(\theta_h)\right]^T \tag{22}$$

As the inverted pendulum model is analyzed independently, θ_1, m_1, θ_1^0 and ω_1^0 will be referred here as θ, m, θ_0 and ω_0, respectively. These equations are solved to produce the motion trajectory during the stance phase of the stepping cycle. The sequence of model evolution is depicted in **Figure 4**, with the beginning and end of the stance positions, initial angular position (θ_0), initial angular velocity (ω_0) and the angle at reset (θ_{reset}). Step length is defined to be equal to $|\theta_{reset}|$ where $|.|$ denotes the absolute value.

3.1. Gait Cycle

The proposed model considers only the *"stance"* phase of the gait cycle. Therefore, "gait cycle" in this study has been defined as the process, where the model states evolve from an initial condition of a step ("double support phase") until the reset condition (where the heel of the swing leg is assumed to collide with the ground or "heel strike condition") is met and the initial condition of the next step is computed. Here, the state of the system moves through three different states (beginning of the *"stance"* (double support), end of the *"stance"* (before collision of the contra-lateral leg), heel strike (after collision of the contra-lateral leg) whose notations are given below (Equation 23) [1,2].

$$[\theta_0,\ \omega_0]^T \mapsto \underbrace{[\theta_0^-,\ \omega_0^-]^T}_{\text{Before collision}} \mapsto \underbrace{[\theta_0^+,\ \omega_0^+]^T}_{\text{After collision}} = [\theta_1,\ \omega_1]^T \tag{23}$$

Here $[\theta_0,\ \omega_0]^T$, $[\theta_0^-,\ \omega_0^-]^T$, $[\theta_0^+,\ \omega_0^+]^T$ correspond to the states at the initiation of the step, states at the end of the flow "immediately" before collision, and states "immediately" after collision, respectively. The states immediately after collision form the initial condition for the next step $[\theta_1,\ \omega_1]^T$. The superscripts ("-," "+") need not indicate the relative sizes of the states but the chronological order in which they appear, that is "-" superscript represent before collision variables and "+" represents after collision. But it should be noted that the transformation from $[\theta_0^-,\ \omega_0^-]^T$ to $[\theta_0^+,\ \omega_0^+]^T$ happens instantaneously in the model. Counterclockwise angles are defined as positive. In a typical walking simulation this results in $\theta^- < 0 < \theta^+$. That is, the

[1]Here $a \mapsto b$ indicates state a "maps to" state b after some time t where $t \geq 0$,

[2]$[x_1^-,\ x_2^-]^T$ and $[x_1,\ x_2]^{T-}$ are used interchangeably, where, x_1 and x_2 are components of some vector

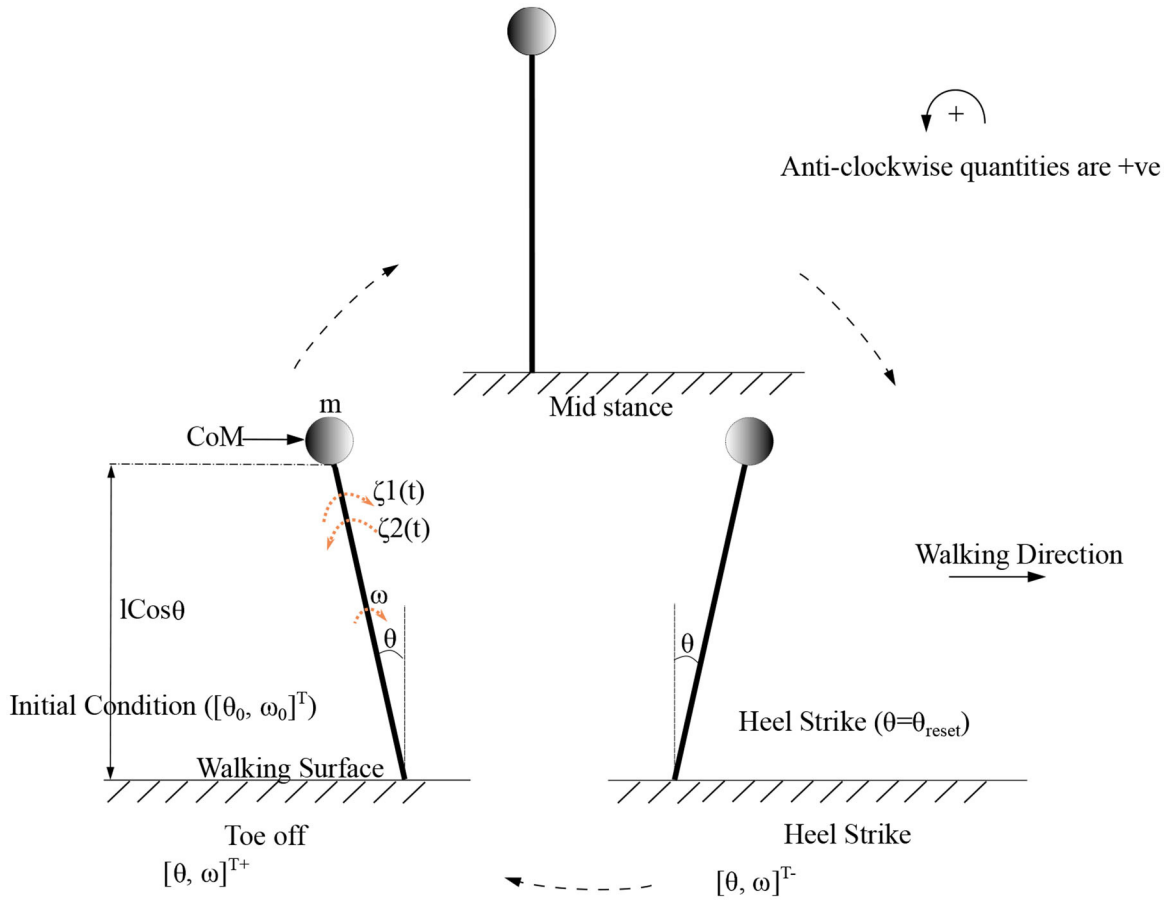

FIGURE 4 | Gait cycle for the low dimensional (*inverted pendulum system*) system is shown. Terms $[\theta_0, \omega_0]^T$ and $[\theta_0, \omega_0]^{T-}$ indicate the initial and final angular position and velocity of the leading/stance leg, respectively, at the beginning and end of the stance phase. θ_{reset} is the angular displacement at which the angle is reset. The CoM (center of mass) which is assumed to be acting as a point mass at the tip of the inverted pendulum is shown as a circle. States before and after heel strike is indicated with "-" and "+" superscripts, respectively.

stance phase ends at a negative value for the angle and resets to a positive value before beginning the next stance phase.

Subscripts (indicating the step number) will be dropped from before and after collision state symbols when the step number is not relevant for the derivation (Equation 24). The same superscript will be used while referring to other parameters which change during collision [3].

The states $[\theta,\ \omega]^T$ evolve as a function of time except at the collision point, where the same time point maps to two different state values. [4]

$$[\theta_n,\ \omega_n]^T \mapsto \underbrace{[\theta^-,\ \omega^-]^T}_{\text{Before collision}} \mapsto \underbrace{[\theta^+,\ \omega^+]^T}_{\text{After collision}} = [\theta_{n+1},\ \omega_{n+1}]^T \tag{24}$$

[3] p^- and p^+ refers to any parameter p before and after collision, respectively, in a particular step cycle.

[4] $\theta(t)$ and $\omega(t)$ are multi-valued functions at the point of collision.

3.2. Heel Strike Condition

A heel strike is defined as the state at which the swing leg (trailing leg) collides with the ground. This is modeled using an appropriate reset condition. At heel strike, both the angle and angular velocity are reset from the "before collision" to "after collision" state as described in Equation (24). The collision of the swing leg (trailing leg) at heel strike is modeled to be inelastic with angular momentum conserved. Therefore, the magnitudes of the angular momentum about the point of collision after and before collision are equated in the following way to generate the transition rule for angular velocity

$$lm(v^+ \sin(90)) = lm(v^- \sin(90 + \theta_h)) \tag{25}$$

$$lm(l\omega^+)1 = lm(l\omega^-)\cos(\theta_h) \tag{26}$$

$$\omega^+ = \omega^- \cos(\theta_h) \tag{27}$$

at the n^{th} iteration(step)

$$\omega_{n+1} = \omega_n^+ = \omega_n^- \cos(\theta_h) \tag{28}$$

where θ_h is the hip angle. The angle, on the other hand, will be reset from θ^- to $-\theta^-$. This results in the following transition rules at $\theta^- = \theta_{reset}$

$$\omega_n^+ = \omega_n^- \cos(\theta_h) \tag{29}$$
$$\theta_n^+ = -\theta_n^- \tag{30}$$

Rearranging we obtain $\Delta(.)$ as

$$\Delta\left(\left[\theta,\ \dot{\theta}\right]^{T-}\right) = \left[-\theta,\ \dot{\theta}\cos(\theta_h)\right]^T \quad . \tag{31}$$

3.3. Analytical and Numerical Solution of the Equations of Motion

The differential equation Equation (1), was solved using the definition of the vector field given in Equation (19) analytically to obtain the flows given below.

$$\begin{aligned}\theta(t) &= f_\theta(t,\ \omega_0,\ \theta_0) := N_1/D_1\\ \omega(t) &= f_\omega(t,\ \omega_0,\ \theta_0) = \frac{d}{dt}(f_\theta) := N_2/D_2\end{aligned} \tag{32}$$

where N_1, N_2, D_1, D_2 are given in **Supplementary Section 1**. The analytical solution is intended to be used for the bifurcation analysis as numerical solutions may not always be able to detect the chaotic behavior (Lozi, 2013). The analytical solution will therefore be used to generate the discrete map governing the motion in the following sections. A numerical solution of the Equations (1)–(2) using definitions given in Equations (19)–(22) with the appropriate reset conditions (in the physiological range) are solved to show the freezing behavior and dynamics in the phase plane. PD subjects freeze intermittently, and the amount of time the subject walks until the freeze is an important measure to quantify the transient walking behavior. A simulation for a 10 s- window is carried out for different values of the parameters τ_l and τ_r (for a constant initial condition). The total time for which transient walking behavior occurred is computed numerically as a function of the parameters τ_l and τ_r. Numerical methods are also used in solving boundary value problems to gain further insights into the system as given in the remark 3.

REMARK 3. *The parameters τ_l and τ_r determines the amount of energy supplied to the system apart from gravity. To understand how they influence the kinetic energy of the system, the difference in speed between the initial and final states are compared for the boundary value problem with boundary conditions $\theta_0 = 0$ rad. and $\theta_{0.5} = -0.1$ rad. with definitions given in Equations (19)–(22) unchanged. Here the boundary conditions are chosen from the physiological range.*

The quantities τ_l, τ_r, ω, ϕ, θ_{reset} and step length has units N m, N, rad. s^{-1}, rad., rad., and rad., respectively, when not specified.

3.4. Derivation of a Map to Describe Successive Stance Phases

The evolution of the flow (given by Equation 32) is terminated when the swing leg meets the ground. In other words, when there is sufficient energy in the system for forward motion, there exists a "reset time" $T(\theta_0,\ \omega_0)$ such that $f_\theta(T(\theta_0,\ \omega_0),\ \omega_0,\ \theta_0) = A_{reset}(\theta_0)$. Here, $A_{reset}(.)$ is a function of the joint angle and the ground that determines the angle of the stance leg while the foot strikes the ground. The arguments associated with the reset time $T(\theta_0,\ \omega_0)$ will be dropped and will be referred to as T from here on. Accounting the transition rules in Equation (29) for reset and conservation of angular momentum,
one defines[5]

$$\theta_1 = \theta^+(T) := -f_\theta(T,\ \omega_0,\ \theta_0) \tag{33}$$
$$\omega_1 = \omega^+(T) := f_\omega(T,\ \omega_0,\ \theta_0)\cos(\theta_h) \tag{34}$$

Following an induction hypothesis, for an arbitrary initial condition $(\theta_n,\ \omega_n)$ the map is

$$\theta_{n+1} = -f_\theta(T,\ \omega_n,\ \theta_n) \tag{35}$$
$$\omega_{n+1} = f_\omega(T,\ \omega_n,\ \theta_n)\cos(\theta_h) \tag{36}$$

The following definitions are made to make the notations compact for further analysis

$$\theta_{n+1} = \tilde{f}_\theta(T,\ \omega_n,\ \theta_n) := -f_\theta(T,\ \omega_n,\ \theta_n) \tag{37}$$
$$\omega_{n+1} = \tilde{f}_\omega(T,\ \omega_n,\ \theta_n) := f_\omega(T,\ \omega_n,\ \theta_n)\cos(\theta_h) \tag{38}$$

where $\tilde{f}_\omega(T,\ \omega_n,\ \theta_n,\ \phi)$ and $\tilde{f}_\theta(T,\ \omega_n,\ \theta_n,\ \phi)$ are T parametrized family of maps for $(\omega_n,\ \theta_n) \mapsto (\omega_{n+1},\ \theta_{n+1})$.

To investigate the condition of same step lengths and to generate a 1D map for further evaluation, $A_{reset}(\theta, t)$ is set to be θ_{reset}. Here θ_{reset} is an arbitrary angle in the physiological range at which the swing leg meets the ground. Then for an intermediate step, (when there is sufficient energy to move forward) there exists a $\tilde{T}$ s.t. $\tilde{f}_\theta(\tilde{T}(\theta_n,\ \omega_n),\ \omega_n,\ \theta_n) = \theta_n = -\theta_{reset}$. When there is not enough energy and therefore momentum to move forward, the model behavior is defined as freezing.

To find the $\tilde{T}$ at which θ_n maps to itself the following minimization problem is solved [6] using Newton's method (Wolfram Research Inc., 2019). This detects implicitly the time at which the swing leg collides with the ground.

$$\tilde{T}(\theta_n,\ \omega_n) := \arg\min_T(\tilde{f}_\theta(T,\ \omega_n,\ \theta_n,\ \phi) - \theta_n) \tag{39}$$

Substituting $\tilde{T}$ from Equation (39) in Equation (38) the following map is obtained.

$$\begin{aligned}\omega_{n+1} &= \tilde{f}_\omega(\tilde{T}(\theta_n,\ \omega_n),\ \omega_n,\ \theta_n)\\ &:= H(\omega_n) \text{ when } \theta_n = \theta_0\ \forall n \in \mathbb{N}\end{aligned}$$

When used as a 1D map,

$$\omega_{n+1} := \tilde{f}_\omega(\omega_n) \tag{40}$$

[5] Even though the symbol $\theta(T)$ is used at the point of collision, it may be noted that this is a one to many mapping and therefore is not a single valued function in the traditional sense of the word.

[6] The solution to this optimization problem may not always exist.

The argument $\tilde{T}$ in the function will be dropped from here-on. The function $\tilde{T}$ acts on the same input ω_n and $\theta_n = \theta_0$. This map has been analyzed to show the freezing behavior and variabilities associated with PD walking. The map has been analyzed for a particular parameter value to show the presence of horseshoe in the **Supplementary Section 2**.

REMARK 4. *Equations (1)–(2) represent a general hybrid system. When the hybrid bipedal system's solution is sought these equations are solved using the definitions given in Equations (15)–(16); and, Equations (19)–(22) are used for hybrid inverted pendulum system.*

4. RESULTS

Numerical simulation of the PD gait and associated freezing behavior is described in this section. The change in the angular velocity from negative to zero is a property of any solution containing freezing by definition. Typically in this model, the angular velocity changes to a positive value under the action of gravity during a freeze. The effect of variation of the parameters τ_l, τ_r, ϕ, θ_{reset} are also investigated. The work aims to show that, the two opposing torques modeled to be generated from the plantar flexors could elicit freezing and chaotic behavior. The ability of these torques to generate freezing behavior has been shown first in a simplified biped model described using Equations (15)–(16), and then in the inverted pendulum model generated by Equations (19)–(22). As argued previously the inverted pendulum dynamics sufficiently captures the PD walking scenario. The results are presented in the sequel to support this hypothesis. Also, walking is the process of moving the CoM by pushing the stance leg forward, and the inverted pendulum model helps to study the effect of the stance leg independent of other variables. A range of values for the constants τ_l, τ_r, and ϕ have been analyzed, such that the trend in behavior is clear to understand. The range in which the behavior of the map $\tilde{f}_\omega$ changes the number of periodic orbits from "0" to "more than one" in lower absolute value of angular velocity conditions, is given **Table 1**. Simulations are carried out to understand the behavior of the system over and above this range. But it may be noted that the maximum value of the torque for $l = 0.6$ m., $\theta_{reset} = -0.1$ rad. is approximately $0.23|\tau_r|$ N m and $2|\tau_l|$ N m in forward and backward directions, respectively. Hence, in this case, forward pushing plantar flexors has to generate 8.7 times the "premature activation of plantar flexors" to nullify the effect if the phase is matched exactly. Physiologically the minimum value of these torques is zero and the maximum is subject-specific.

TABLE 1 | Summary of qualitative behavior of the map.

No	Parameter	Range simulated	Figure no	Consequence of increasing the parameter
1	τ_l	[0, 5]	**Figure 10**	Increased τ_l results in the appearance of period 1-2-3 and higher orbits. This results in freezing at lower absolute angular velocity conditions
2	ϕ	[-6.28, -1.28]	**Figure 11**	Increase in ϕ results in the period doubling bifurcations as described in the **Figure 9**. When everything else remains constant a variation in ϕ results in freezing and high variability in walking.
3	τ_r	[30, 55]	**Figure 12A**	Increased τ_r results in disappearance of period 1-2-3 and higher orbits. This is one of the ways in which the patients get out of a freeze
4	θ_{reset}	[0.05, 0.15]	**Figure 12B**	Increased step length results in freezing region change its location on the map, from low initial absolute angular velocity to a higher absolute angular velocity initial conditions.

4.1. Freezing in a Biped Model

The hybrid system (Equations 1–2) defined by the Equations (15)–(16) are simulated numerically and the results are shown in **Figures 5A,B**. The figure shows normal walking for the first few steps and then freezing afterwards (highlighted). The gradual reduction in step length observed experimentally prior to freezing (Nutt et al., 2011) is also observed in the model.

There are two dissipative forces in this model; they are, the opposing torques due to the plantar flexors and the dissipation at the heel strike. Long-range walking will be achieved when the speed gain in every step compensate these two effects. The dissipative effect of the heel strike can't be controlled by the neuromuscular system, but the effect of plantar flexors can. **Figures 6A,B** illustrates the effect of the plantar flexors in this regard.

A simulation was carried out for a 10 s window and the time difference between, the start of the simulation and the time of the last heel strike before the freezing event (as defined in remark 1), has been computed. This is shown as a function of the parameters τ_l and τ_r in **Figure 6A**. The blue shades indicate eventual freezing and shorter walking time and the yellow region is the safer non-freezing region. There is an intermediate region of parameter τ_l and τ_r in which the walking happens without freezing in the 10 s window. A higher value of τ_l necessitates a higher τ_r for walking. But a very high τ_r doesn't necessarily produce balanced walking as it can result in a lack of coordination between the swing leg and the stance leg. Although the initial value problem (IVP) in **Figure 6A** and boundary value problem (BVP) in **Figure 6B** can't be directly compared, they show analogous qualitative results. That is, to achieve the same speed gain [or kinetic energy (KE) gain] a higher τ_l demands a higher τ_r. A key aspect of PD freezing is, therefore, the inability of the two plantar flexors to coordinate to produce the required energy. From an energy point of view, the role of the swing leg is mainly in the generation of ankle push

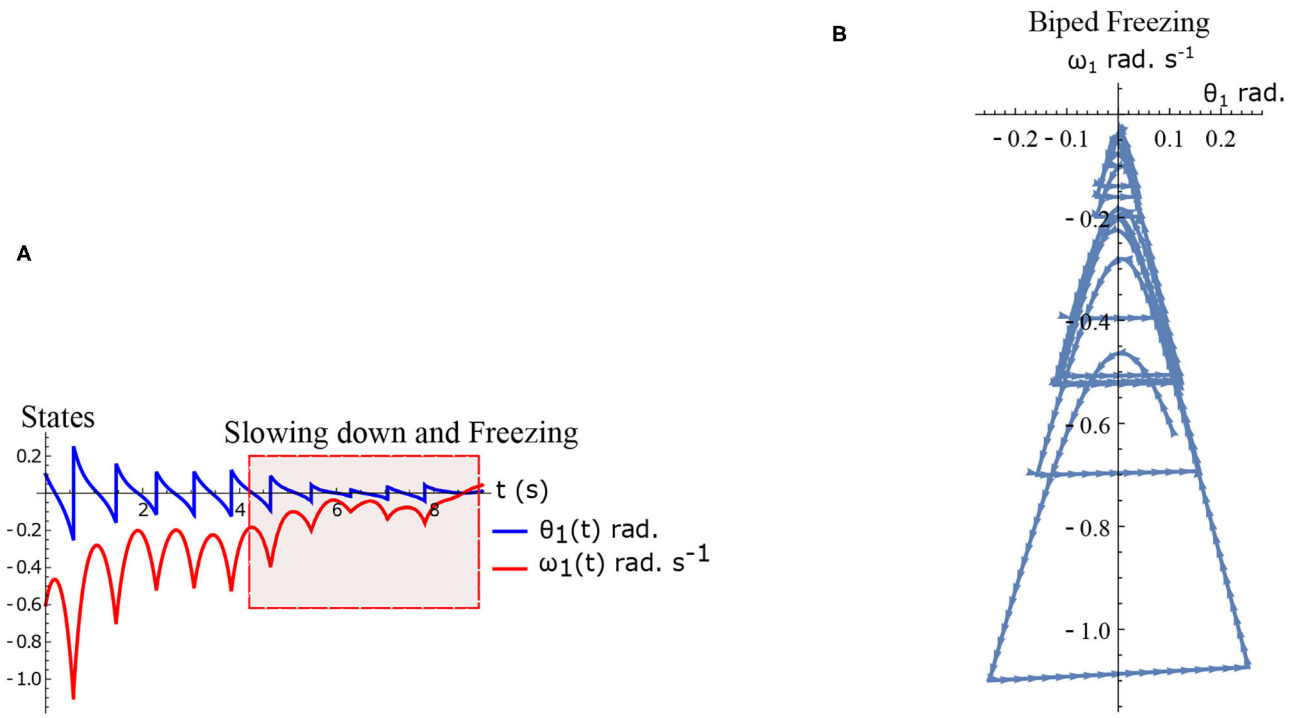

FIGURE 5 | Results of numerical simulation of the biped during freezing. Parameters are chosen to be $\tau_l = 2.3$ N m, $\tau_r = 15.74$ N, $\phi = -\pi/2$ rad. and initial conditions $\theta_2(0) = -0.1$ rad., $\theta_1(0) = 0.1$ rad., $\omega_2(0) = 2$ rad. s^{-1}, $\omega_1(0) = -0.6$ rad. s^{-1}. The change in the θ_{reset} in every step and gradual reduction in θ_1 nearer to a freezing event is evident. **(A)** Simulated time series of the states θ_1 and ω_1. Region of slowing down and freezing is highlighted **(B)** Shows numerical simulation of biped in the phase plane.

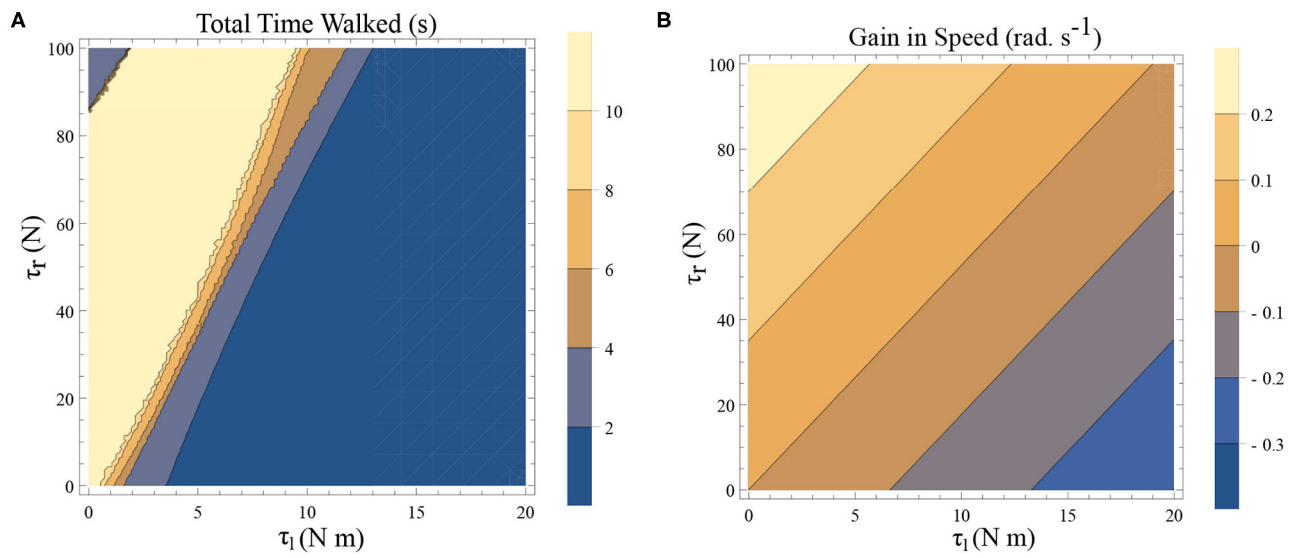

FIGURE 6 | (A) A simulation was carried out for a time window of 10 s, and the total time walked before freezing was computed. This time is plotted as a function of τ_l and τ_r. The initial conditions are set to be $\theta_2(0) = -0.1$ rad., $\theta_1(0) = 0.1$ rad., $\omega_2(0) = 1$ rad. s^{-1}, $\omega_1(0) = -0.6$ rad. s^{-1} and $\phi = -\pi/2$ rad. The yellow region forms the optimal region of the parameters τ_l, τ_r where walking is achieved. **(B)** Contour plot of the difference in speed($|\omega(0)| - |\omega(0.5)|$) as a function of τ_l and τ_r determined by solving a BVP numerically with $\theta_0^0 = 0$ and $\theta_1^{0.5} = -0.1$ rad. for the biped model with the other initial conditions being $\theta_2^0 = -0.1$ rad., $\omega_2^0 = 1$ (and $\phi = -\pi/2$ rad.). This illustrates a decrease in the speed and therefore kinetic energy when there is an increase in τ_l and a decrease in τ_r.

of force. In the following sections, the dynamics of the stance leg is studied independently using an inverted pendulum model, reducing the role of the swing only as a supplier of the ankle push-off force.

4.2. Freezing in an Inverted Pendulum Model

Freezing is defined as the condition where there is no more forward motion of the leg. Numerical simulation of such a scenario in the inverted pendulum model is shown in **Figure 7A** where there is a freezing episode after 18 s. A gradual reduction in step length observed in the biped model translate to the increased time taken in making the final few steps before freezing. The simulation in the phase plane for the last three steps is shown in **Figure 7B**. The dissipative torques due to the opposing plantar flexors act in the same way in the case of the inverted pendulum model. **Figures 8A,B** illustrate this similarity, where, an increased τ_r generates higher speed gains and, an elevated τ_l results in lower speed gains and lower total walk times. This is because increasing parameter τ_r heightens the forward ankle push-off while larger τ_l amplifies the dissipative torque. A key difference between the inverted pendulum model and the biped model is that a higher τ_r will not result in an imbalance in the former as there is no swing leg in that model, while there is a lack of balance in the latter. The contour plot of the speed differences as a function of τ_l and τ_r is shown in **Figure 8B**. The figure shows that a higher value of τ_l and a lower value of τ_r result in negative speed gain (reduction in KE). Numerical simulation of the total time of the walk, defined as the difference between the time in which the first step is taken and the last step before freezing in 10 s is shown in **Figure 8A**. More than 9 s of walking is indicative of the fact that there is no freezing in that parameter range in that time frame. A higher τ_r and lower τ_l results in better walking performance as in the case of a biped. Therefore, energetically, PD related behavior that is of interest is analogous in the case of inverted pendulum and biped model. Therefore, the analytical solution of the inverted pendulum model is investigated further to understand the consequence of the change in parameters τ_l, τ_r and ϕ. These parameters are controlled by the neural system while others such as mass of the body and length of the legs are not. The quantity θ_{reset} differentiates the inverted pendulum model from the biped model. Hence, the effect of this parameter is also studied.

4.3. Parameter Exploration of the Inverted Pendulum: Study of the Map $\tilde{f}_\omega$

The neural control on the muscles alters the magnitude and the phase of the control signals. Exploration of the parameters τ_l, τ_r, and ϕ, therefore, reflects the effect of the neural control on walking dynamics. One of the hypotheses that are investigated through the model is that of the generation of variability through the premature activation of the plantar flexors. We have quantified the phase difference of the "premature" activation using the parameter ϕ in the model. **Figure 9** shows the

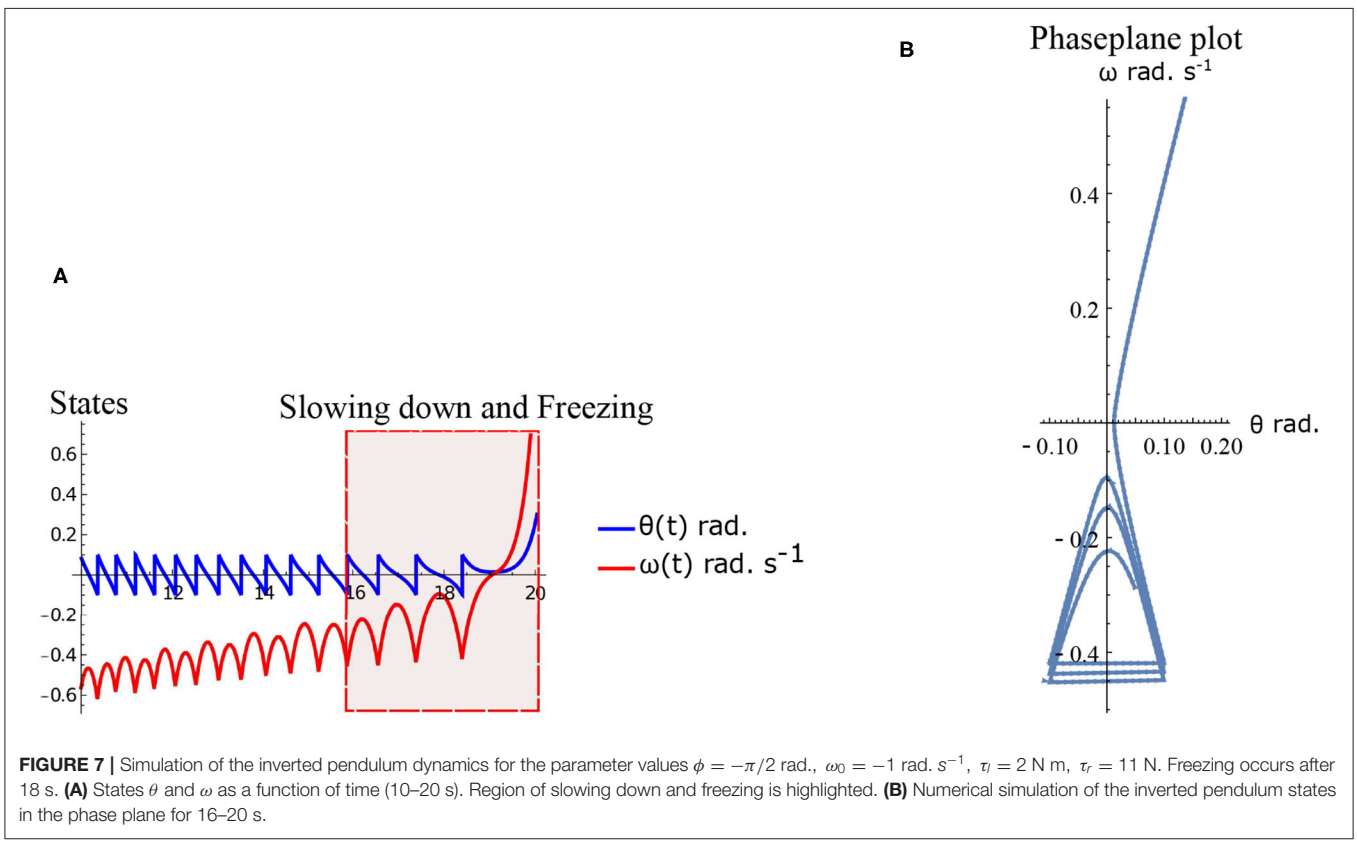

FIGURE 7 | Simulation of the inverted pendulum dynamics for the parameter values $\phi = -\pi/2$ rad., $\omega_0 = -1$ rad. s^{-1}, $\tau_l = 2$ N m, $\tau_r = 11$ N. Freezing occurs after 18 s. **(A)** States θ and ω as a function of time (10–20 s). Region of slowing down and freezing is highlighted. **(B)** Numerical simulation of the inverted pendulum states in the phase plane for 16–20 s.

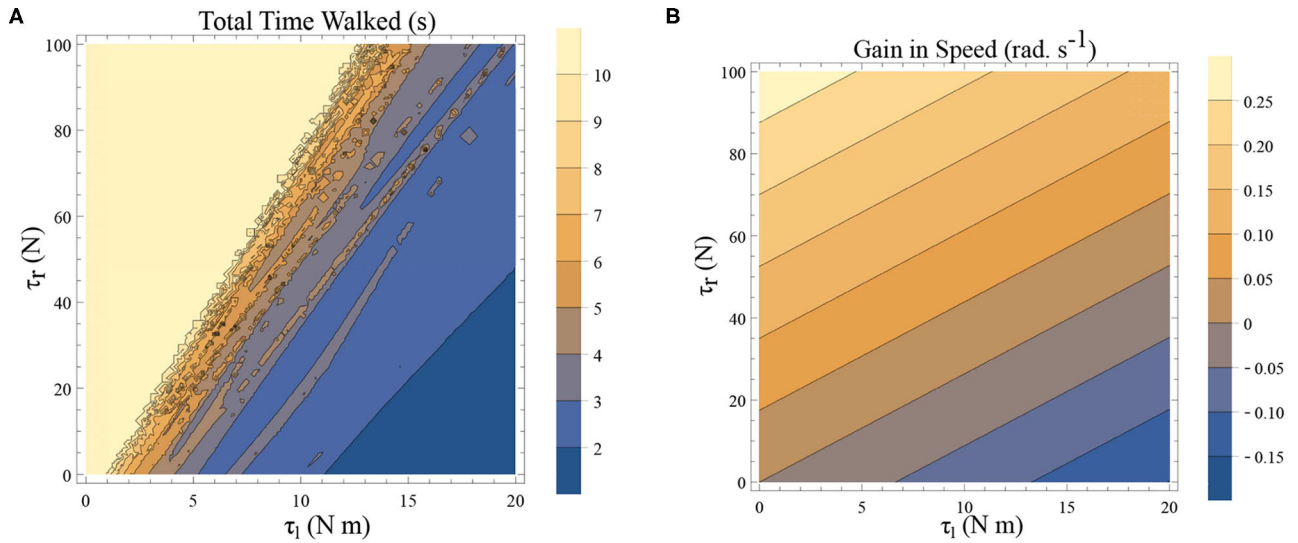

FIGURE 8 | (A) A simulation was carried out for a time window of 10 s, and the total time of walking before freezing was computed. This time is plotted as a function of τ_l and τ_r. The angle is reset when $\theta(t) = -0.1$ rad. and $\phi = -\pi/2$ rad. The colors indicate the duration of the walk (see the legend). **(B)** Contour plot of difference in speed ($|\omega(0)| - |\omega(0.5)|$) as a function of τ_l and τ_r determined by solving a BVP with $\theta_0 = 0$ rad. and $\theta_{0.5} = -0.1$ rad. (and $\phi = -\pi/2$ rad.) in Equation (1)–(2) using definitions in Equation (19)–(22). This illustrates a decrease in the speed and therefore KE when there is an increase in τ_l and a decrease in τ_r.

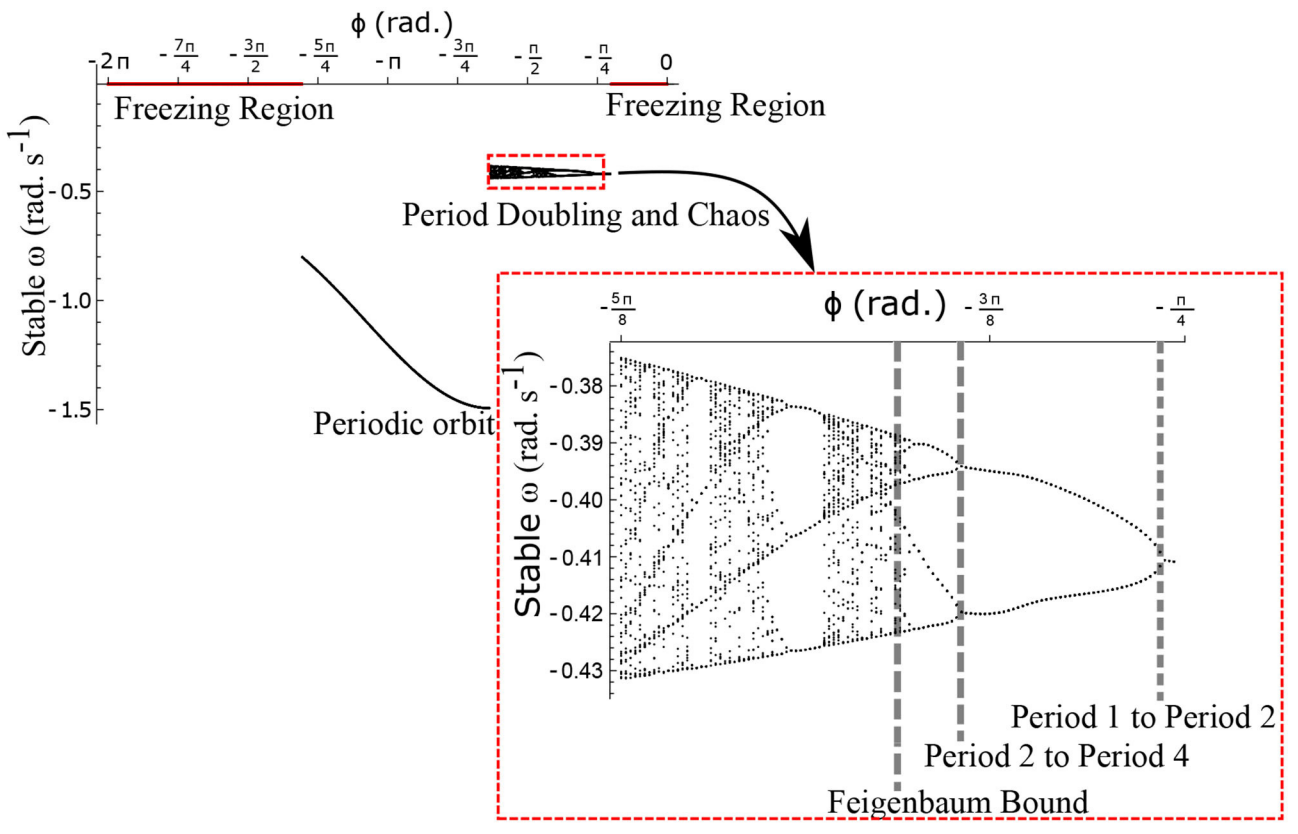

FIGURE 9 | Stable ω is shown as a function of the parameter ϕ for $\omega_0 = -0.433$ rad.s^{-1}, $\tau_l = 5$ N m, $\tau_r = 35$ N. The Feigenbaum bound was found to be at $\phi = -1.37$ rad. where walking becomes fully chaotic. The period-doubling cascade has been highlighted and enlarged. This chaotic region forms only a small part of the overall parameter space of ϕ. This region is sandwiched between the walking and the freezing regions indicated in red.

bifurcation diagram of the parameter ϕ in the range 0 to -2π for constant values of τ_l and τ_r. A period-doubling route to chaos can be observed when ϕ is varied between $-5\pi/8$ and $-\pi/4$. The map $\tilde{f}_\omega$ is iterated for 500 walking cycles and the last 50 walking cycles are used to compute the equilibrium points. The Feigenbaum bound is found to be at $\phi = -1.37$ rad. at which walking becomes fully chaotic. This indicates that the premature activation (or lack of coordination between the muscles) can generate highly variable behavior in the system despite deterministic neural signals. The region of chaotic ϕ is sandwiched between the periodic orbits and freezing region. This suggests a higher variability in walking likely arising from a shift in ϕ (early activation of plantar flexors) must be treated with caution. **Figure 9** shows the presence of chaos in the system for carefully selected parameter values. Its presence and stability are illustrated for other parameters values and initial conditions using a set of maps in **Figures 10–12B** and bifurcation diagrams in **Figures 13A–D**. A summary of the insights obtained from the maps are given in the **Table 1**. The presence of a period 3 orbit in a one-dimensional map is indicative of other periodic orbits and chaos. The presence of horseshoe in any of the period 1, 2,..., n maps also indicates chaos. An illustration of the presence of horseshoe for a set of parameter values is given in **Supplementary Section 2**. The intersection of the $\tilde{f}_\omega^1$, $\tilde{f}_\omega^2$, $\tilde{f}_\omega^3$ maps with $\omega_n = \omega_{n+1}$ indicate period 1, 2, 3 orbits, respectively. **Figures 10–12B** illustrate how the maps change with respect to the change of parameters.

Variation of the parameter τ_l or the magnitude of premature activation (as ϕ is set to -1.57 rad.) results in a set of rich dynamic behaviors as shown in **Figure 10**. The presence of the periodic orbits starts appearing approximately around $\tau_l \approx 3$ N m, where, the maps tangentially intersect the $\omega_n = \omega_{n+1}$ line. The intermittency thus generated could elicit a period of slow walking (as ω_n and ω_{n+1} are less than -0.5 rad. s^{-1}) as observed in PD. The period 3 orbits are generated upon a further increase in τ_l. As can be seen from the maps in **Figures 10–12B**, a higher initial value of ω_n (e.g., $\omega_n > 0.45$ rad. s^{-1} for $\tau_l \approx 3$ N m) results in a further increase in ω_{n+1} and gets attracted toward the periodic orbit of higher absolute value of angular velocity. This explains how swaying back and forth helps the PD patients in getting out of a freeze. Increasing τ_r results in almost opposite behavior as that of τ_l (**Figure 12A**). Varying ϕ can result in chaotic behavior as shown in **Figure 9**, and, **Figure 11** indicates the variation in the maps which leads to this behavior. The neural control of the activity of plantar flexors is not explicitly modeled here. However, coming out of freeze could be the result of an increase of τ_r or decrease τ_l or increased initial absolute angular velocity generated by swaying. A low absolute value of angular velocity (voluntary or involuntary) or decrease of τ_r or increase of τ_l results in freezing (angular velocity moving to the region where $\omega_n = 0$ rad. s^{-1}). This explains the higher chances of freezing episodes even when the subject reduces the velocity (voluntarily/involuntarily) near narrow passages. Increase in the step length or $|\theta_{reset}|$ results in freezing at comparatively higher absolute angular velocities (**Figure 12B**). But it may be noted that, typically, an increased step length is also associated with an increased absolute angular velocity due to inertia and therefore could be beneficial. There is likely an optimum step length for every subject as there is a trade-off between fatigue and initial angular velocity, which warrants further study.

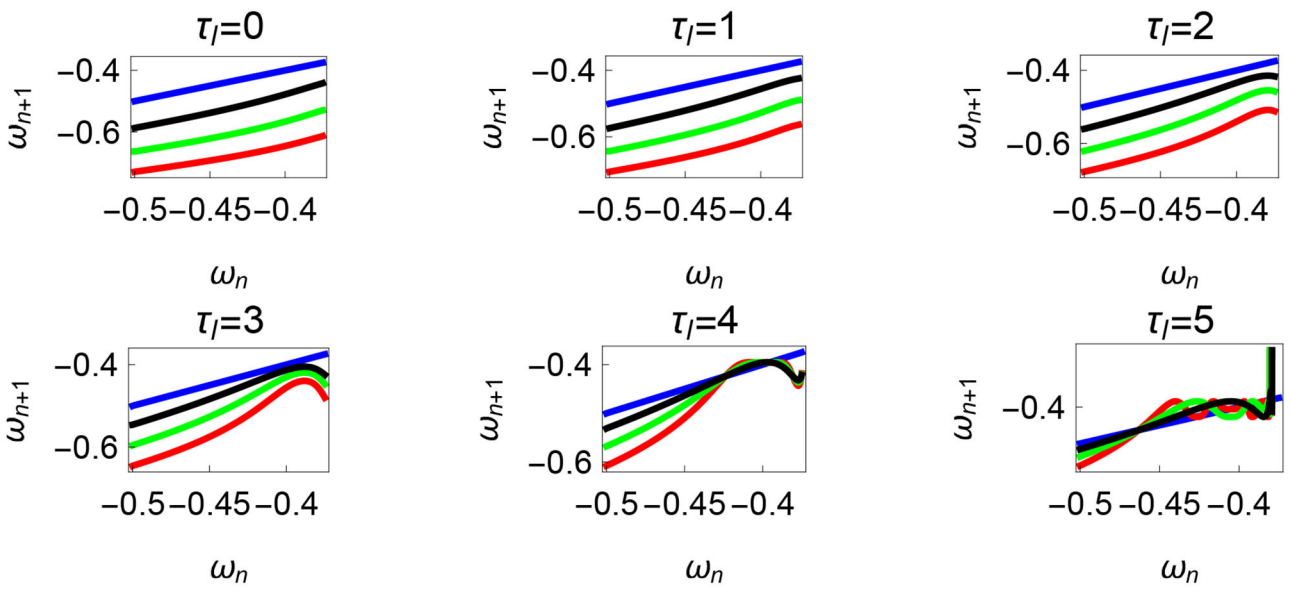

FIGURE 10 | Maps obtained by varying the parameter τ_l and fixing $\tau_r = 35$ N, $\phi = -1.57$ rad., $\theta_{reset} = -0.1$ rad. The black, green, and red curves represent $\tilde{f}_\omega^1$, $\tilde{f}_\omega^2$, $\tilde{f}_\omega^3$, respectively, and the $\omega_n = \omega_{n+1}$ is shown in blue. The curves intersect the blue line at a higher absolute value of angular velocity forming an attractor, this is not shown in the figure. There are no periodic orbits for the low velocity regimes for $\tau_l = 0 - 2$ N m but they appear afterwards. Units: τ_l, τ_r, ω, ϕ, θ_{reset} and step length has units N m, N, rad. s^{-1}, rad., rad., and rad., respectively, when not specified.

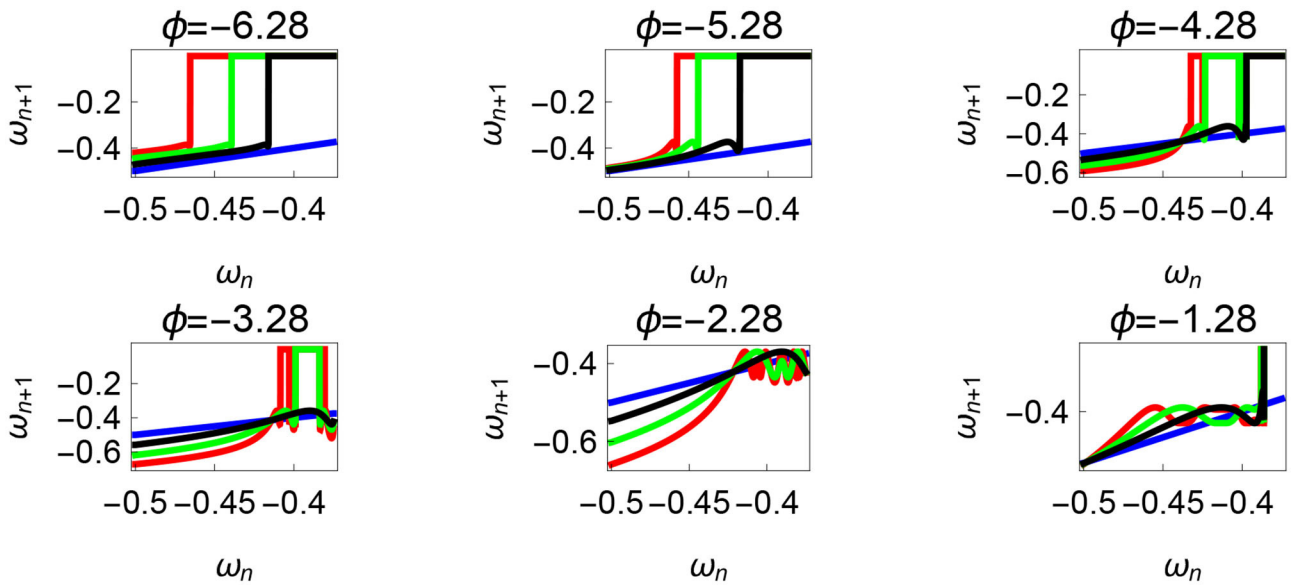

FIGURE 11 | Varying the parameter ϕ and fixing $\tau_r = 35$ N, $\tau_l = 5$ N m, $\theta_{reset} = -0.1$ rad. The black, green, and red curves represent $\tilde{f}^1_\omega$, $\tilde{f}^2_\omega$, $\tilde{f}^3_\omega$, respectively, and the $\omega_n = \omega_{n+1}$ is shown in blue. The curves intersect the blue line at a higher absolute value of angular velocity forming an attractor, this is not shown in the figure. Creation of the periodic orbits and its coexistence is observed. Units: τ_l, τ_r, ω, ϕ, θ_{reset} and step length has units N m, N, rad. s^{-1}, rad., rad., and rad., respectively, when not specified.

4.4. Bifurcations of the One Dimensional System for the Inverted Pendulum Model

Even though for most of the regions, the slope of the map in relation to the $\omega_n = \omega_{n+1}$ can be identified visually, the stability of the system is not explicitly studied in the previous section. The contour of $\tilde{f}^n_\omega(x,\ \tau_l,\ \tau_r, \phi) = x$ for n=1 and 3 are plotted for variation in parameters in **Figures 13**, **14**, respectively. The stability is computed by taking the derivatives (numerically) for the maps described in **Figures 10**–**12B**. These contours show how the points of intersection with $\omega_n = \omega_{n+1}$ line for the maps shown in **Figures 10**–**12B** change upon variation in parameters.

Period one orbits are the normal walking cycles. The existence of these orbits in both low and high angular velocity conditions and different parameter variations are shown in **Figure 13**. In **Figure 13A**, two fixed points comes closer to each other and completely vanish for high values of τ_l resulting in a complete lack of periodic solutions. Typically walking could be ascribed to the stable region for periodic orbits, but, when ω_0 is lower, and τ_l is non-zero, another periodic point emerges in the low-velocity regimes. This, therefore, results in slow-walking regions which under perturbations could lead to freezing. Also, at low-velocity regimes, the region is discontinuous and unstable for small perturbations of the parameter values or initial conditions. The stable periodic orbit moves to lower absolute value of angular velocities as τ_l is increased and eventually disappears.

The behavior observed while decreasing τ_r is analogous to increase in τ_l. **Figure 13B** illustrates how changing τ_r and ω_0 results in creation/destruction of the periodic orbits. It can be seen that at a sufficiently low value of τ_r the periodic orbit disappears. A higher value of τ_r results in the separation of the periodic orbits resulting in higher stable walking angular speeds. A similar behavior could be observed while decreasing τ_l in **Figure 13A**.

Initial angular velocity plays a major role in the behavior of the system. The effect of neural control parameters τ_l and τ_r in generating periodic behavior has been illustrated for lower and higher absolute angular velocity conditions in **Figures 13C,D**, respectively. In **Figure 13C**, the periodic orbit appears stable only for a tiny fraction of the parameters space. This is due to the highly discontinuous map shown previously. Conversely, at higher initial angular speeds the period one orbit is stable as shown in **Figure 13D**. It can be seen that an increase in τ_l moves the periodic orbit into an unstable region resulting in the possibility of a freeze. The presence of these orbits could only be seen in the low-velocity regions of the maps. Orbits of minimal period three indicate chaos and the presence of every other periodic orbits (Glendinning, 1994). The period 3 orbits for the variation of the parameters τ_l and τ_r is shown in the **Figure 14**. The Period 3 orbit is shown in blue and the period one in yellow.

5. DISCUSSION, SUMMARY, AND FUTURE WORK

Freezing of gait results from a complex set of interacting physiological systems which consist of the brain, spinal cord, musculoskeletal system and external disturbances (Nutt et al., 2011). The model explains how a lack of coordination between central pattern generators of the plantar flexors of the leading leg

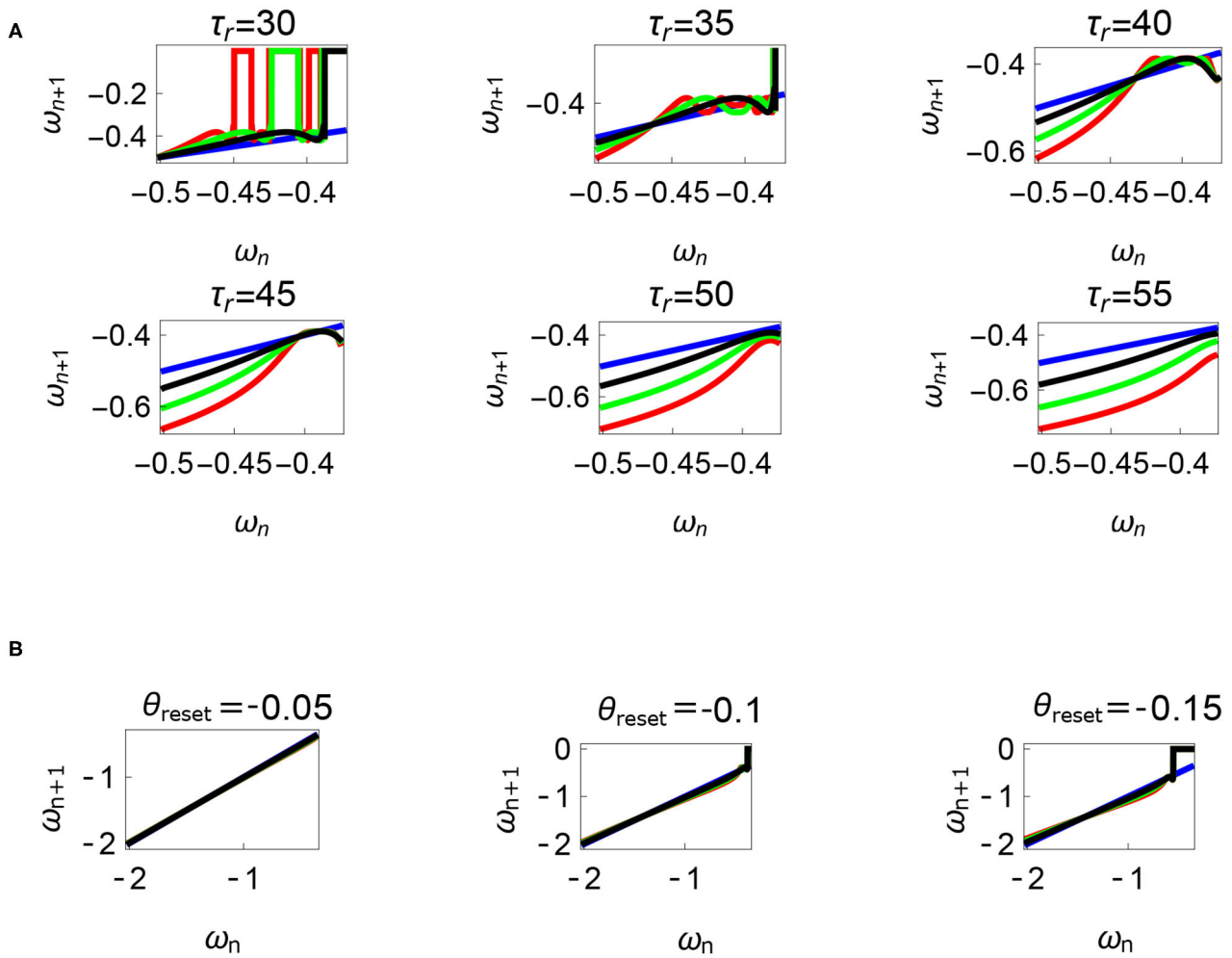

FIGURE 12 | Variations of the parameters τ_r and θ_{reset} are depicted in **Figures 12A,B**, respectively. Units: τ_l, τ_r, ω, ϕ, θ_{reset} and step length has units N m, N, rad. s^{-1}, rad., rad., and rad., respectively, when not specified. **(A)** Varying the parameter τ_r keeping $\tau_l = 5$ N m, $\phi = -1.57$ rad., $\theta_{reset} = -0.1$ rad. fixed. The black, green, and red curves represent $\tilde{f}^1_\omega$, $\tilde{f}^2_\omega$, $\tilde{f}^3_\omega$, respectively, and the $\omega_n = \omega_{n+1}$ is shown in blue. The curves intersect the blue line at a higher absolute value of angular velocity forming an attractor, this is not shown in the figure. Increasing τ_r has an analogous behavior as decreasing τ_l. **(B)** Varying the parameter θ_{reset} keeping $\tau_r = 35$ N, $\phi = -1.57$ rad., $\tau_l = 0.5$ N m. The black, green and red curves (overlapped) represent $\tilde{f}^1_\omega$, $\tilde{f}^2_\omega$, $\tilde{f}^3_\omega$, respectively, and the $\omega_n = \omega_{n+1}$ is shown in blue. The curves intersect at a high absolute value of angular velocity. The unstable region moving to the higher absolute value of angular velocities (moving to the left) can be observed while $|\theta_{reset}|$ is increased.

and trailing leg (Nieuwboer et al., 2004) could lead to freezing and variability of walking.

A model of the torques generated by the plantar flexors acting on the stance leg has been proposed, and its effect on a biped and a reduced inverted pendulum model has been studied. The pattern of freezing observed in the model matches well with the behavior observed experimentally[7] in Nutt et al. (2011) and **Figure 5A**). The equilibrium point description (Feldman, 1986; Sainburg, 2015) of the control of the muscles is avoided here and instead, we opted for an explicit control signal. However, variabilities in the "torque-length-characteristics" (Feldman, 1986) for a particular (set of) equilibrium point (points) can generate torques required for motion. Therefore, a parallel between the equilibrium point hypothesis of postural balance and our model can be drawn if the torques prescribed in the model are assumed to be the result of variabilities in the "torque-length-characteristics."

Chaotic regions are observed to be closer to those regions where freezing ensues. In the inverted pendulum model, these regions show up only at low absolute angular velocity initial conditions. This may explain why freezing is a "rarely" occurring intermittent condition. This also may explain why freezing happens near obstacles or narrow paths where the

[7]Here we are referring to the Figure 1 in Nutt et al. (2011). Source of the figure :https://pubmed.ncbi.nlm.nih.gov/21777828/#&gid=article-figures&pid=figure-1-uid-0

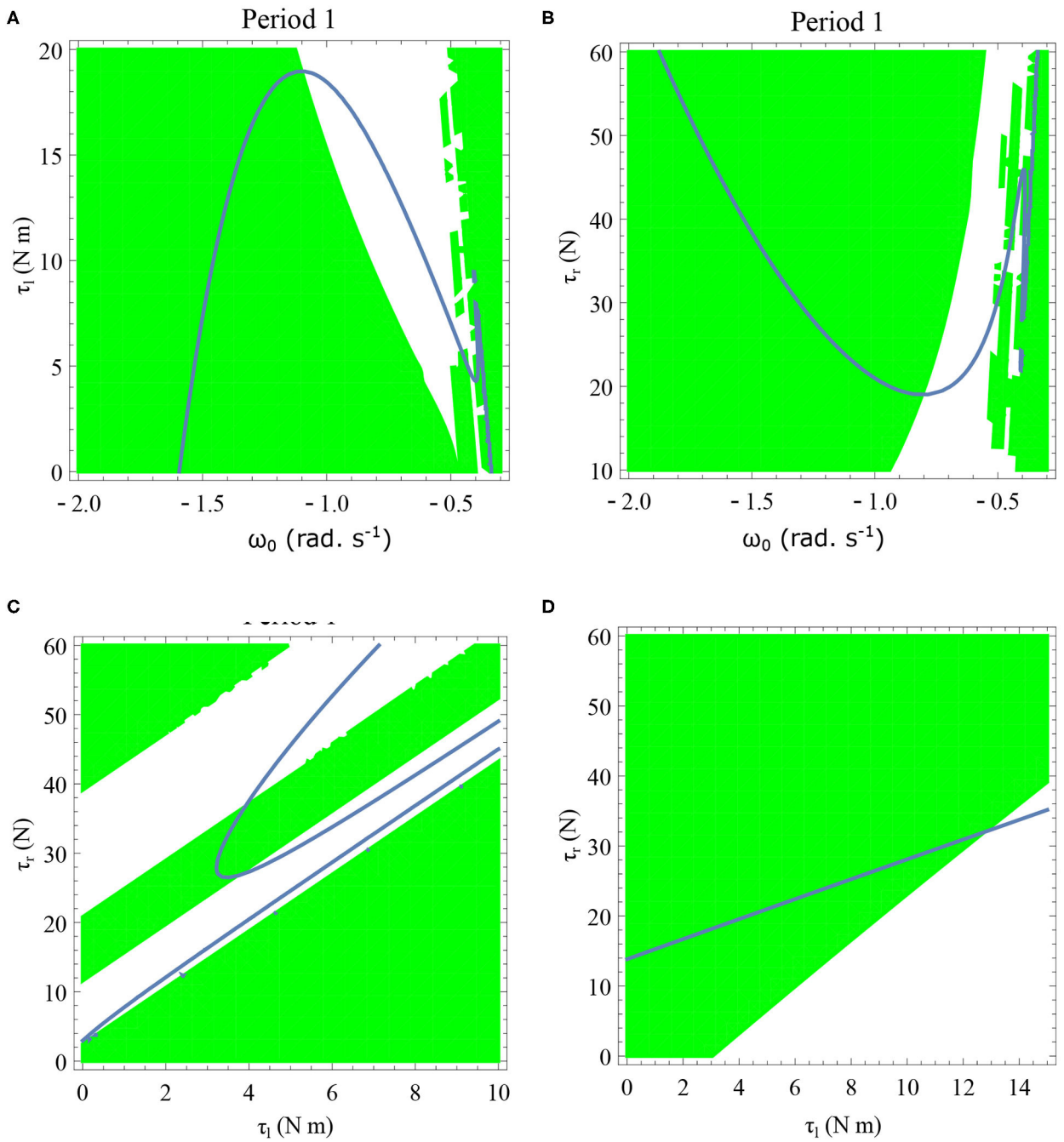

FIGURE 13 | Period one orbits are shown by varying τ_l and τ_r for two different values of initial angular velocities in **(C,D)**. Period one orbits found by varying τ_l and ω_0 is shown in **(A)**. Period one orbits found by varying $\tau_r$and ω_0 is shown in **(B)**. The parameter values used are given in the respective figures. The green region shows the stable region where $\dot{\tilde{f}}_\omega < 1$. The stable periodic regions are the ones where the green region overlap the curves of the periodic orbits. Units: τ_l, τ_r, ω, ϕ, θ_{reset} and step length has units N m, N, rad. s^{-1}, rad., rad., and rad., respectively, when not specified. **(A)** $\phi = -\pi/2$ rad., $\tau_r = 40$ N, $\theta_{reset} = -0.1$ rad. **(B)** $\phi = -\pi/2$ rad., $\tau_l = 5$ N m, $\theta_{reset} = -0.1$ rad. **(C)** $\phi = -\pi/2$ rad., $\omega_0 = -0.4$ rad. s^{-1}, $\theta_{reset} = -0.1$ rad. **(D)** $\phi = -\pi/2$ rad., $\omega_0 = -1$ rad. s^{-1}, $\theta_{reset} = -0.1$ rad.

subject voluntarily slows down to reduce the probability of collision. Obstacles could be either perceived or real. Hence, even though the pattern of freeze remains the same the causes could be varied. It might even be possible that the control of τ_l is driven by perceived obstacles or anxiety about the consequence of freezing (Ehgoetz Martens

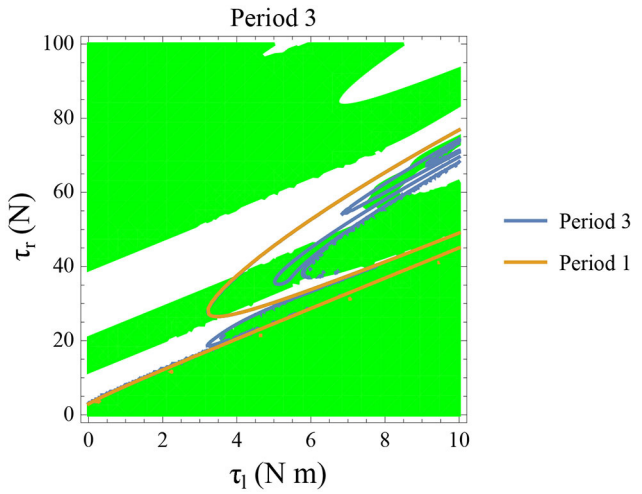

FIGURE 14 | Constant parameters used are $\phi = -\pi/2$ rad., $\omega_0 = -0.4$ rad. s^{-1}, and $\theta_{reset} = -0.1$ rad. The stable period 3 region is shown in green. The intersection of the period 3 orbits (in blue) and the stable regions form the region of stable period three orbits. The presence of period 3 orbits implies orbits of all other periods and therefore chaos.

et al., 2014; Martens et al., 2016). Increase in τ_l, therefore, could be thought to be indirectly influenced by anxiety and perceived obstacles. However, this hypothesis warrants further experimentation.

Varying the parameter step length which controls the stride length is observed to affect the maps and therefore the freezing regions. The results indicated that keeping the steps closer to each other such that $|\theta_{reset}|$ is minimized, is safer for the PD patient. The stability of the period 2 & 3 orbits are highly sensitive to small variations of parameters (ϕ, τ_r, τ_l) which are proposed to be the reason for sporadic variabilities in gait seen in PD subjects. We also hypothesize that stable low absolute angular velocity regions of the state space for some parameter values form a "cantor set" and necessitates further study.

It can be speculated that a reason for the observed help of auditory/sensory cues (Rochester et al., 2005; Young et al., 2014; Amini et al., 2019) in reducing instances of freezing, is by indirectly forcing PD patients to make shorter steps with lesser variability, thus reducing the possibility of moving into the freezing region of walking. Variability in the walking times observed in the Inverted pendulum model translates to variability in step lengths in the biped model. Biped model shows a more complicated dependence on the parameters to eventual freezing (**Figure 6A**). This dependence is also a function of the initial conditions and could be investigated further in future work along with detailed bifurcation analysis.

The CPG activity is controlled by feedback mechanisms with delays, noise and input from the brain (which in turn is affected by different factors, including emotional state). The ground and other environmental conditions also play a role in walking. These variabilities are not accounted for in our model, which represents a limitation of the study. Like any other studies which are based on a mathematical model and numerical simulations, our results and conclusions also might not necessarily represent the entire spectrum of patients. Further extensive patient-based studies are to be performed prior to use of these ideas for the treatment of PD gait. As future work, a more detailed model is planned to include these variabilities. The future models will be compared with the simpler versions to understand the minimum set of variables generating the abnormal walking behavior. The key aspects explained using the proposed model can be summarized as follows

1. The higher variability in PD patients could be the result of parameters being closer to the point of chaos. A further change of the parameters can result in freezing. Therefore, increased variability should be looked at with caution (clinically) and should be treated to reduce it. The difficulty in the prediction of freezing also owes to the horseshoe near the freezing regions.
2. The pattern of reducing the step-sizes before freezing has been shown to be the result of slowing down (**Figure 5A**). Voluntary/involuntary reduction in angular velocity (in absolute terms) near the obstacles makes the subject more susceptible to freezing and highly irregular walking.
3. One plausible reason why sensory cues such as auditory or visual cues help in freezing is by reducing step lengths. The proposed model shows that the reduction in step length helps in reducing freezing episodes at lower absolute value of angular velocity conditions as it moves the patient away from the freezing region. Further experimental study is needed to understand the clinical applicability.

DATA AVAILABILITY STATEMENT

The raw data supporting the conclusions of this article will be made available by the authors, without undue reservation, to any qualified researcher.

AUTHOR CONTRIBUTIONS

MP and PM have contributed in design, implementation, analysis and editing of the study and manuscript. KT-A has contributed to the design and analysis of the study and editing of the manuscript. MW has contributed to the design of the study and editing of the manuscript. All authors contributed to the article and approved the submitted version.

FUNDING

MP and KT-A have got funding support from EPSRC (Engineering and Physical Science Research Council) grant No EP/N014391/1 funding the Centre for Predictive Modelling in Healthcare at the University of Exeter. The EPSRC Centre for Predictive Modelling in Healthcare (CPMH) brings together a world-leading team of mathematicians, statisticians and

clinicians with a range of industrial partners, patients and other stakeholders to focus on the development of new methods for managing and treating chronic health conditions using predictive mathematical models. This unique approach is underpinned by the expertise and breadth of experience of the Centre's team and innovative approaches to both the research and translational aspects. As such the research presented in this manuscript has benefitted by the environment offered by the CPMH. MP has spent considerable time as part of the CPMH participating in various seminars, conferences and other activities contributed toward PhD. KT-A is the deputy director of CPMH.

ACKNOWLEDGMENTS

The authors would like to express their appreciation to Prof. Peter Ashwin for useful inputs and valuable comments. KT-A and MP gratefully acknowledge the financial support of the EPSRC via grant EP/N014391/1.

SUPPLEMENTARY MATERIAL

The Supplementary Material for this article can be found online at: https://www.frontiersin.org/articles/10.3389/fbioe.2020.552635/full#supplementary-material

REFERENCES

Albin, R. L., Young, A. B., and Penney, J. B. (1989). The functional anatomy of basal ganglia disorders. *Trends Neurosci*. 12, 366–375. doi: 10.1016/0166-2236(89)90074-X

Alexander, G. E., and Crutcher, M. D. (1990). Functional architecture of basal ganglia circuits: neural substrates of parallel processing. *Trends Neurosci*. 13, 266–271. doi: 10.1016/0166-2236(90)90107-L

Amini, A., Banitsas, K., and Young, W. R. (2019). Kinect4fog: monitoring and improving mobility in people with Parkinson's using a novel system incorporating the Microsoft Kinect V2. *Disabil. Rehabil. Assist. Technol*. 14, 566–573. doi: 10.1080/17483107.2018.1467975

Aoi, S., Ohashi, T., Bamba, R., Fujiki, S., Tamura, D., Funato, T., et al. (2019). Neuromusculoskeletal model that walks and runs across a speed range with a few motor control parameter changes based on the muscle synergy hypothesis. *Sci. Rep*. 9, 1–13. doi: 10.1038/s41598-018-37460-3

Dai, H., and Tedrake, R. (2013). "L2-gain optimization for robust bipedal walking on unknown terrain," in *2013 IEEE International Conference on Robotics and Automation* (Karlsruhe: IEEE), 3116–3123. doi: 10.1109/ICRA.2013.6631010

Davie, C. A. (2008). A review of Parkinson's disease. *Brit. Med. Bull*. 86:109–127. doi: 10.1093/bmb/ldn013

Delp, S. L., Anderson, F. C., Arnold, A. S., Loan, P., Habib, A., John, C. T., et al. (2007). Opensim: open-source software to create and analyze dynamic simulations of movement. *IEEE Trans. Biomed. Eng*. 54, 1940–1950. doi: 10.1109/TBME.2007.901024

Duan, X., Allen, R., and Sun, J. (1997). A stiffness-varying model of human gait. *Med. Eng. Phys*. 19, 518–524. doi: 10.1016/S1350-4533(97)00022-2

Ehgoetz Martens, K. A., Ellard, C. G., and Almeida, Q. J. (2014). Does anxiety cause freezing of gait in Parkinson's disease? *PLoS ONE* 9:e106561. doi: 10.1371/journal.pone.0106561

Fathizadeh, M., Mohammadi, H., and Taghvaei, S. (2019). A modified passive walking biped model with two feasible switching patterns of motion to resemble multi-pattern human walking. *Chaos Solitons Fractals* 127, 83–95. doi: 10.1016/j.chaos.2019.06.018

Fathizadeh, M., Taghvaei, S., and Mohammadi, H. (2018). Analyzing bifurcation, stability and chaos for a passive walking biped model with a sole foot. *Int. J. Bifurcat. Chaos* 28, 1850113. doi: 10.1142/S0218127418501134

Feldman, A. G. (1986). Once more on the equilibrium-point hypothesis (lambda model) for motor control. *J. Mot. Behav*. 18, 17–54. doi: 10.1080/00222895.1986.10735369

Flash, T., and Hogan, N. (1985). The coordination of arm movements: an experimentally confirmed mathematical model. *J. Neurosci*. 5, 1688–1703. doi: 10.1523/JNEUROSCI.05-07-01688.1985

Gede, G., Peterson, D. L., Nanjangud, A. S., Moore, J. K., and Hubbard, M. (2013). "Constrained multibody dynamics with python: from symbolic equation generation to publication," in *International Design Engineering Technical Conferences and Computers and Information in Engineering Conference, Vol. 55973* (Portland: American Society of Mechanical Engineers). doi: 10.1115/DETC2013-13470

Genadry, W., Kearney, R., and Hunter, I. (1988). Dynamic relationship between EMG and torque at the human ankle: variation with contraction level and modulation. *Med. Biol. Eng. Comput*. 26, 489–496. doi: 10.1007/BF02441916

Giladi, N., McDermott, M., Fahn, S., Przedborski, S., Jankovic, J., Stern, M., et al. (2001). Freezing of gait in PD prospective assessment in the datatop cohort. *Neurology* 56, 1712–1721. doi: 10.1212/WNL.56.12.1712

Glendinning, P. (1994). *Stability, Instability and Chaos: An Introduction to the Theory of Nonlinear Differential Equations*, Vol. 11. Cambridge University Press. doi: 10.1017/CBO9780511626296

Goswami, A., Thuilot, B., and Espiau, B. (1996). *Compass-Like Biped Robot Part I: Stability and Bifurcation of Passive Gaits*. Research Report RR-2996, INRIA.

Grizzle, J. W., Abba, G., and Plestan, F. (2001). Asymptotically stable walking for biped robots: analysis via systems with impulse effects. *IEEE Trans. Automat. Contr*. 46, 51–64. doi: 10.1109/9.898695

Heremans, E., Nieuwboer, A., and Vercruysse, S. (2013). Freezing of gait in Parkinson's disease: where are we now? *Curr. Neurol. Neurosci. Rep*. 13:350. doi: 10.1007/s11910-013-0350-7

Hof, A., and van den Berg, J. (1977). Linearity between the weighted sum of the EMGs of the human triceps surae and the total torque. *J. Biomech*. 10, 529–539. doi: 10.1016/0021-9290(77)90033-1

Iqbal, S., Zang, X., Zhu, Y., and Zhao, J. (2014). Bifurcations and chaos in passive dynamic walking: a review. *Robot Auton. Syst*. 62, 889–909. doi: 10.1016/j.robot.2014.01.006

Kane, T. R., and Levinson, D. A. (1985). *Dynamics, Theory and Applications*. McGraw Hill. Available online at: https://hdl.handle.net/1813/638

Kharb, A., Saini, V., Jain, Y., and Dhiman, S. (2011). A review of gait cycle and its parameters. *Int. J. Comput. Eng. Manage*. 13, 78–83. Available online at: https://www.ijcem.org/papers72011/72011_14.pdf

Latash, M. L. (2010). Motor synergies and the equilibrium-point hypothesis. *Motor Control* 14, 294–322. doi: 10.1123/mcj.14.3.294

Latash, M. L., Scholz, J. P., and Schoner, G. (2002). Motor control strategies revealed in the structure of motor variability. *Exerc. Sport Sci. Rev*. 30, 26–31. doi: 10.1097/00003677-200201000-00006

Lozi, R. (2013). "Can we trust in numerical computations of chaotic solutions of dynamical systems?" in *Topology and Dynamics of Chaos: In Celebration of Robert Gilmore's 70th Birthday* (World Scientific), 63–98. doi: 10.1142/9789814434867_0004

Lunze, J., and Lamnabhi-Lagarrigue, F. (2009). *Handbook of Hybrid Systems Control: Theory, Tools, Applications*. Cambridge: Cambridge University Press. doi: 10.1017/CBO9780511807930

Mahmoodi, P., Ransing, R., and Friswell, M. (2013). Modelling the effect of 'heel to toe' roll-over contact on the walking dynamics of passive biped robots. *Appl. Math. Model*. 37, 7352–7373. doi: 10.1016/j.apm.2013.02.048

Manchester, I. R., Tobenkin, M. M., Levashov, M., and Tedrake, R. (2011). Regions of attraction for hybrid limit cycles of walking robots. *IFAC Proc*. 44, 5801–5806. doi: 10.3182/20110828-6-IT-1002.03069

Mandali, A., Rengaswamy, M., Chakravarthy, V. S., and Moustafa, A. A. (2015). A spiking basal ganglia model of synchrony, exploration and decision making. *Front. Neurosci*. 9:191. doi: 10.3389/fnins.2015.00191

Martens, K. E., Hall, J. M., Gilat, M., Georgiades, M. J., Walton, C. C., and Lewis, S. (2016). Anxiety is associated with freezing of gait and attentional set-shifting in Parkinson's disease: a new perspective for early intervention. *Gait Post*. 49, 431–436. doi: 10.1016/j.gaitpost.2016.07.182

McGeer, T. (1990). Passive dynamic walking. *Int. J. Robot. Res*. 9, 62–82. doi: 10.1177/027836499000900206

Montazeri Moghadam, S., Sadeghi Talarposhti, M., Niaty, A., Towhidkhah, F., and Jafari, S. (2018). The simple chaotic model of passive dynamic walking. *Nonlinear Dyn*. 93, 1183–1199. doi: 10.1007/s11071-018-4252-8

Muralidharan, V., Balasubramani, P., Chakravarthy, S., Lewis, S. J. G., and Moustafa, A. (2014). A computational model of altered gait patterns in Parkinson's disease patients negotiating narrow doorways. *Front. Comput. Neurosci*. 7:190. doi: 10.3389/fncom.2013.00190

Nieuwboer, A., Dom, R., De Weerdt, W., Desloovere, K., Janssens, L., and Stijn, V. (2004). Electromyographic profiles of gait prior to onset of freezing episodes in patients with Parkinson's disease. *Brain* 127, 1650–1660. doi: 10.1093/brain/awh189

Nutt, J. G., Bloem, B. R., Giladi, N., Hallett, M., Horak, F. B., and Nieuwboer, A. (2011). Freezing of gait: moving forward on a mysterious clinical phenomenon. *Lancet Neurol*. 10, 734–744. doi: 10.1016/S1474-4422(11)70143-0

Olszewski, W., and Sandroni, A. (2011). Falsifiability. *Am. Econ. Rev*. 101, 788–818. doi: 10.1257/aer.101.2.788

Parakkal Unni, M., Sinha, A., Chakravarty, K., Chatterjee, D., and Das, A. (2017). Neuro-mechanical cost functionals governing motor control for early screening of motor disorders. *Front. Bioeng. Biotechnol*. 5:78. doi: 10.3389/fbioe.2017.00078

Pekarek, D., Ames, A. D., and Marsden, J. E. (2007). "Discrete mechanics and optimal control applied to the compass gait biped," in *2007 46th IEEE Conference on Decision and Control* (New Orleans, LA: IEEE), 5376–5382. doi: 10.1109/CDC.2007.4434296

Polese, J. C., Teixeira-Salmela, L. F., Nascimento, L. R., Faria, C. D. M., Kirkwood, R. N., Laurentino, G. C., et al. (2012). The effects of walking sticks on gait kinematics and kinetics with chronic stroke survivors. *Clin. Biomech*. 27, 131–137. doi: 10.1016/j.clinbiomech.2011.08.003

Popper, K. (2002). *Popper: The Logic of Scientific Discovery*. New York, NY: Routledge Classics.

Ranavolo, A., Conte, C., Iavicoli, S., Serrao, M., Silvetti, A., Sandrini, G., et al. (2011). Walking strategies of visually impaired people on trapezoidal-and sinusoidal-section tactile groundsurface indicators. *Ergonomics* 54, 246–256. doi: 10.1080/00140139.2010.548533

Rochester, L., Hetherington, V., Jones, D., Nieuwboer, A., Willems, A.-M., Kwakkel, G., et al. (2005). The effect of external rhythmic cues (auditory and visual) on walking during a functional task in homes of people with Parkinson's disease. *Arch. Phys. Med. Rehabil*. 86, 999–1006. doi: 10.1016/j.apmr.2004.10.040

Ros, J., Font-Llagunes, J. M., Plaza, A., and Kövecses, J. (2015). Dynamic considerations of heel-strike impact in human gait. *Multibody Sys. Dyn*. 35, 215–232. doi: 10.1007/s11044-015-9460-0

Sadeghian, H., and Barkhordari, M. (2020). Orbital analysis of passive dynamic bipeds; the effect of model parameters and stabilizing arm. *Int. J. Mech. Sci*. 178:105616. doi: 10.1016/j.ijmecsci.2020.105616

Sainburg, R. L. (2015). Should the Equilibrium Point Hypothesis (EPH) be considered a scientific theory? *Motor Control* 19, 142–148. doi: 10.1123/mcj.2014-0056

Sinnet, R. W., Powell, M. J., Shah, R. P., and Ames, A. D. (2011). A human-inspired hybrid control approach to bipedal robotic walking. *IFAC Proc*. 44, 6904–6911. doi: 10.3182/20110828-6-IT-1002.03802

Snijders, A. H., Nijkrake, M. J., Bakker, M., Munneke, M., Wind, C., and Bloem, B. R. (2008). Clinimetrics of freezing of gait. *Mov. Disord*. 23, S468–S474. doi: 10.1002/mds.22144

Taga, G. (1995). A model of the neuro-musculo-skeletal system for human locomotion. *Biol. Cybern*. 73, 97–111. doi: 10.1007/s0042200 50166

Tamura, D., Aoi, S., Funato, T., Fujiki, S., Senda, K., and Tsuchiya, K. (2020). Contribution of phase resetting to adaptive rhythm control in human walking based on the phase response curves of a neuromusculoskeletal model. *Front. Neurosci*. 14:17. doi: 10.3389/fnins.202 0.00017

Tresch, M. C., and Jarc, A. (2009). The case for and against muscle synergies. *Curr. Opin. Neurobiol*. 19, 601–607. doi: 10.1016/j.conb.2009.09.002

Usherwood, J. R. (2005). Why not walk faster? *Biol. Lett*. 1, 338–341. doi: 10.1098/rsbl.2005.0312

Wahde, M., and Pettersson, J. (2002). "A brief review of bipedal robotics research," in *Proceedings of the 8th UK Mechatronics Forum International Conference (Mechatronics 2002)*, 480–488. Available online at: http://www.me.chalmers.se/~mwahde/AdaptiveSystems/Publications/WahdePetterssonMech2002.pdf

Wolfram Research Inc. (2019). *Mathematica, Version 12.0*.

Wu, A. R., Simpson, C. S., van Asseldonk, E. H., van der Kooij, H., and Ijspeert, A. J. (2019). Mechanics of very slow human walking. *Sci. Rep*. 9, 1–10. doi: 10.1038/s41598-019-54271-2

Young, W. R., Rodger, M. W., and Craig, C. M. (2014). Auditory observation of stepping actions can cue both spatial and temporal components of gait in Parkinson's disease patients. *Neuropsychologia* 57, 140–153. doi: 10.1016/j.neuropsychologia.2014.03.009

Zelik, K. E., and Adamczyk, P. G. (2016). A unified perspective on ankle push-off in human walking. *J. Exp. Biol*. 219, 3676–3683. doi: 10.1242/jeb.1 40376

Znegui, W., Gritli, H., and Belghith, S. (2020). Design of an explicit expression of the Poincaré map for the passive dynamic walking of the compass-gait biped model. *Chaos Solitons Fractals* 130, 109436. doi: 10.1016/j.chaos.2019.109436

Conflict of Interest: The authors declare that the research was conducted in the absence of any commercial or financial relationships that could be construed as a potential conflict of interest.

frontiers in Bioengineering and Biotechnology

SYSTEMATIC REVIEW
published: 30 October 2020
doi: 10.3389/fbioe.2020.587680

Systematic Review of the Impact of Transcranial Direct Current Stimulation on the Neuromechanical Management of Foot and Ankle Physical Performance in Healthy Adults

Songlin Xiao[1], *Baofeng Wang*[1], *Xini Zhang*[1], *Junhong Zhou*[2,3]* *and Weijie Fu*[1,4]*

[1] School of Kinesiology, Shanghai University of Sport, Shanghai, China, [2] The Hinda and Arthur Marcus Institute for Aging Research, Hebrew SeniorLife, Boston, MA, United States, [3] Harvard Medical School, Boston, MA, United States, [4] Key Laboratory of Exercise and Health Sciences of Ministry of Education, Shanghai University of Sport, Shanghai, China

Objective: This study aims to review existing literature regarding the effects of transcranial direct current stimulation (tDCS) on the physical performances of the foot and ankle of healthy adults and discuss the underlying neurophysiological mechanism through which cortical activities influence the neuromechanical management of the physical performances of the foot and ankle.

Methods: This systematic review has followed the recommendations of the Preferred Reporting Items for Systematic reviews and Meta-Analyses. A systematic search was performed on PubMed, EBSCO, and Web of Science. Studies were included according to the Participants, Intervention, Comparison, Outcomes, and Setting inclusion strategy. The risk of bias was assessed through the Cochrane Collaboration tool, and the quality of each study was evaluated through the Physiotherapy Evidence Database (PEDro) scale.

Results: The electronic search resulted in 145 studies. Only eight studies were included after screening. The studies performed well in terms of allocation, blinding effectiveness, and selective reporting. Besides, the PEDro scores of all the studies were over six, which indicated that the included studies have high quality. Seven studies reported that tDCS induced remarkable improvements in the physical performances of the foot and ankle, including foot sole vibratory and tactile threshold, toe pinch force, ankle choice reaction time, accuracy index of ankle tracking, and ankle range of motion, compared with sham.

Conclusion: The results in these studies demonstrate that tDCS is promising to help improve the physical performances of the foot and ankle. The possible underlying mechanisms are that tDCS can ultimately influence the neural circuitry responsible for the neuromechanical regulation of the foot and ankle and then improve their physical performances. However, the number of studies included was limited and their sample sizes were small; therefore, more researches are highly needed to confirm the findings of the current studies and explore the underlying neuromechanical effects of tDCS.

Keywords: transcranial direct current stimulation, foot, ankle, physical performance, neural circuitry, neuromechanical management

OPEN ACCESS

Edited by:
Borja Sañudo,
Sevilla University, Spain

Reviewed by:
Maryam Zoghi,
La Trobe University, Australia
Chi-Wen Lung,
Asia University, Taiwan

***Correspondence:**
Weijie Fu
fuweijie@sus.edu.cn
Junhong Zhou
junhongzhou@hsl.harvard.edu

Specialty section:
This article was submitted to Biomechanics, a section of the journal Frontiers in Bioengineering and Biotechnology

Received: *27 July 2020*
Accepted: *09 October 2020*
Published: *30 October 2020*

Citation:
Xiao S, Wang B, Zhang X, Zhou J and Fu W (2020) Systematic Review of the Impact of Transcranial Direct Current Stimulation on the Neuromechanical Management of Foot and Ankle Physical Performance in Healthy Adults. Front. Bioeng. Biotechnol. 8:587680. doi: 10.3389/fbioe.2020.587680

INTRODUCTION

The functionality and physical performances of foot and ankle, including muscular strength, somatosensory function, and endurance, play a key role in locomotor control when standing, walking, jumping, and endurance running in everyday activities (Rodgers, 1988; Aagaard, 2018). In addition to the peripheral nervous system, the cortical functional networks of the brain have been linked to the formation and regulation of the physical performances of the foot and ankle (Noakes, 2011; Foerster et al., 2018a). A decrease in the excitability of cortical regions is associated with diminished biomechanical management of physical performance and increases the risk of injuries (e.g., chronic ankle inability) (Needle et al., 2017). Therefore, strategies designed to facilitate the neural circuitry of the brain have a great potential of improving the functional and physical performances of the foot and ankle.

One promising approach is transcranial direct current stimulation (tDCS). TDCS non-invasively modulates the excitability of brain regions by delivering low-amplitude current flow between two or more electrodes placed on the scalp (Nitsche and Paulus, 2000, 2001; Reardon, 2016). Anodal tDCS can increase cortical excitation through the tonic depolarization of the membrane resting potential, and cathodal tDCS may decrease cortical excitation by the hyperpolarization of the membrane resting potential (Stagg and Nitsche, 2011; Rahman et al., 2013). TDCS can enhance the cognitive–motor function and is beneficial for multiple neurological and psychiatric disorders (e.g., depression and Alzheimer's disease) (Kuo et al., 2014; Summers et al., 2016).

In recent years, researchers have explored the effects of tDCS on the physical performance of healthy individuals. Anodal tDCS applied over the primary motor cortex (M1) can improve multiple physical performances, such as balance control (Saruco, 2017; de Moura et al., 2019), pain perception (Vaseghi et al., 2014), muscle strength, and muscular endurance (Lattari et al., 2018; Vargas et al., 2018; Machado, S. et al., 2019). Specifically, tDCS designed to target the sensorimotor region has induced improvements in the physical performances of the foot and ankle of healthy adults (Devanathan and Madhavan, 2016; Zhou et al., 2018). For example, Zhou et al. (2018) observed that one session of tDCS targeting M1 has improved the vibrotactile sensation of the foot sole of healthy older adults when standing. These efforts have shed a light on a novel strategy for the enhancement of the physical performances of the foot and ankle by using tDCS to modulate the excitability of cortical brain regions. Considering the different methodologies and unpredicted effects, systematic review of published studies can provide valuable summaries of the effects of tDCS on the physical performances of the foot and ankle.

This study thus aims to systematically review available peer-reviewed publications to date on the effects of tDCS on the physical performances of the foot and ankle of healthy adults. We then further discuss the underlying neurophysiological mechanism through which cortical activities influence the neuromechanical management of physical performances of the foot and ankle. This review will provide the most recent achievements and a better understanding of research efforts in this direction to ultimately help optimize the implementation of tDCS to enhance the physical performances of the foot and ankle in the near future.

METHODS

The method of this review was designed following the recommendations of the Preferred Reporting Items for Systematic reviews and Meta-Analyses and the Cochrane Handbook for Systematic Reviews of Interventions (Moher et al., 2009; Cumpston et al., 2019).

Search Strategy

This systematic review conducted a comprehensive search of three databases, namely, PubMed, Web of Science, and EBSCO, up to May 2020. The search was performed using the terms "foot," "toe," and "ankle," which were separately combined with "transcranial direct current stimulation" or "tDCS" in all databases. Boolean operators "AND" and "OR" were used to combine keywords according to the recommendations of each database. All results found in the search were imported into the EndNote reference manager (EndNote X9, USA, Stanford) to gather together and automatically find out duplicate records.

Eligibility Criteria and Article Selection

The following inclusion criteria were applied based on the Participants, Intervention, Comparison, Outcomes, and Study design (Ferreira et al., 2019). (1) The participants were healthy adults with no history of musculoskeletal injury and overt neurological disease. (2) The intervention was tDCS, regardless of stimulation types, stimulus intensity, duration, and electrode location. (3) A comparison was with sham tDCS (i.e., placebo). (4) The primary outcomes were strength, perception, flexibility, or other related variables of the foot and ankle. (5) The study design was randomized, crossover, and sham-control designs. Animal studies and non-English studies were excluded. Reviews, case reports, letters, opinions, and conference abstracts were also excluded (**Figure 1**).

Two researchers independently evaluated the results of the search and resolved differences through discussion (SL and BF). The Abstracts and full texts of relevant articles were read thoroughly, and only those that met the eligibility criteria were selected. Then, the researchers further confirmed the selected articles and discussed possible disagreements; if any disagreement persisted, then a third researcher was consulted and judged the results (WJ).

Data Extraction

The original data of the included articles were summarized in Microsoft Excel (Microsoft Corporation, Redmond, WA, USA). The findings were divided into two categories, namely, the effects of tDCS on the physical performances of (1) the foot and (2) ankle, to facilitate the interpretation of the results. Besides, the following data were summarized: author, sample size, gender, age, anodal/cathodal location, electrode size, current intensity, duration, control, and main outcomes.

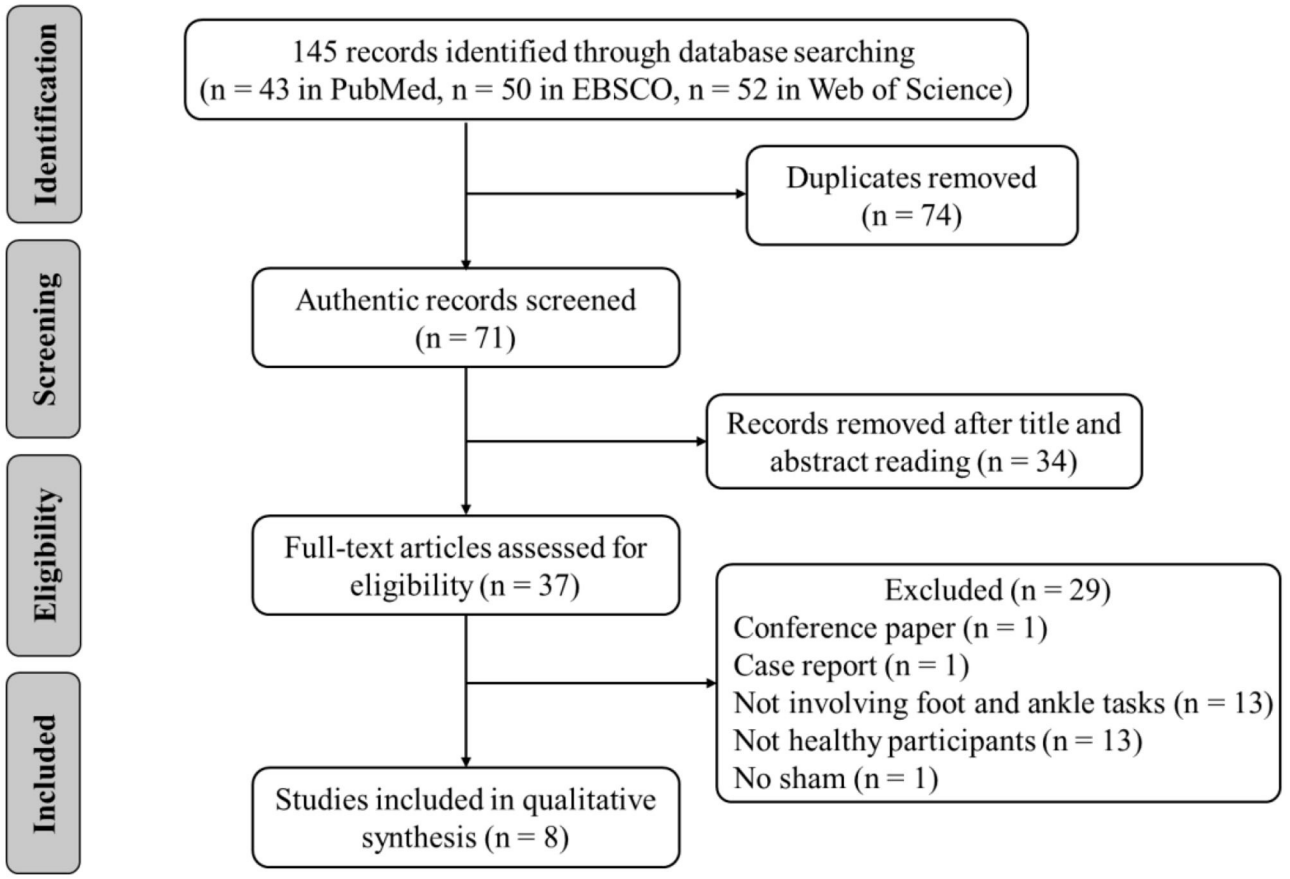

FIGURE 1 | Flow diagram of the search strategy.

Quality and Risk-of-Bias Assessments

The Physiotherapy Evidence Database (PEDro) scale was used to assess the quality of each study (Maher et al., 2003). Studies with a PEDro score of <6 were deemed as having low quality.

The risk of bias of each study was assessed using the Collaboration's "Risk of Bias" tool, version 5.2 based on the Cochrane Handbook for Systematic Reviews of Interventions (Cumpston et al., 2019). The risk of bias for each study was judged as "low," "high," or "unclear" risk of bias. The two researchers independently evaluated the PEDro score and risk of bias of each study; a third researcher was consulted to reach a final consensus if any disagreement persisted.

RESULTS

A total of 145 related articles were found in the databases (43 in PubMed, 50 in EBSCO, and 52 in Web of Science). Only eight articles were included for systematic review after removing duplicate articles and excluding irrelevant studies by reading the titles, Abstracts, and full texts. Four studies examined the effects of tDCS on foot physical performance (**Table 1**), and the other four studied its effects on ankle physical performance (**Table 3**).

Effects of tDCS on Foot Physical Performance

Four studies investigated the effect of tDCS on foot physical performance. Fifty-four participants, consisting of 52 males and 2 females, were recruited with an age of between 20 and 61 years (**Table 1**). A bias in gender was observed across these studies.

Only the immediate effects of one-session tDCS were examined in these studies. Three studies used conventional tDCS applied over the sensorimotor cortex with an electrode size of 35 cm^2 (Tanaka et al., 2009; Zhou et al., 2018; Yamamoto et al., 2020). One study used a 4 × 1 ring high-definition tDCS (HD-tDCS), in which the anodal electrode was placed over Cz and was surrounded by four cathodal electrodes with a size of 1 cm^2 (Xiao et al., 2020). Three studies applied the current intensity of 2 mA (Tanaka et al., 2009; Zhou et al., 2018; Xiao et al., 2020), and one study applied the intensity of 1.5 mA (Yamamoto et al., 2020). The duration of tDCS was 10 min in two studies (Tanaka et al., 2009; Yamamoto et al., 2020) and 20 min in the other two studies (Zhou et al., 2018; Xiao et al., 2020). The current density at the stimulation electrode was 0.043 or 0.057 mA/cm^2 with a total charge between 0.026 and 0.069 C/cm^2. Sham was used as a control in these studies, in which the placements of electrodes

TABLE 1 | The characteristics of studies investigating the effect of tDCS on foot physical performance.

Study	Sample	Gender	Age (years)	Drop-outs (N)	Design	Task	Cortical excitability examined	PEDro score
Yamamoto et al. (2020)	10	10 males	22–34	None	Crossover	Foot somatosensory tests	No	9
Xiao et al. (2020)	14	14 males	22.8 ± 1.2	None	Crossover	Foot flexor strength task	No	9
Zhou et al. (2018)	20	20 males	61 ± 4	None	Crossover	Foot sole vibratory sensation task	No	9
Tanaka et al. (2009)	10	8 males 2 females	20–35	3	Crossover	Toe pinch force task	No	6

TABLE 2 | Stimulation protocols and main outcomes of studies investigating the effect of tDCS on foot physical performance.

Study	Anodal/cathodal location	Electrode size (cm^2)	Current (mA)	Duration (min)	Total charge (C/cm^2)	Control	Main outcomes	Significant effect vs. sham
Yamamoto et al. (2020)	C: Left C3 R: Right supraorbital region	35	1.5	10	0.026	Sham: 30 s	↓ Tactile threshold of distal pulp of the hallux	c-tDCS > sham
Xiao et al. (2020)	A: Cz R: C3, C4, Fz, Pz	1	2.0	20	NR	Sham: 30 s	→ Foot flexor strength; ↓ ankle INV/DF kinesthesia threshold	Post- > pre- in the two conditions; ≠ between the conditions
Zhou et al. (2018)	A: Left C3 R: Right supraorbital region	35	2.0	20	0.069	Sham: 60 s	↓ Standing vibratory threshold of foot sole	a-tDCS > sham
Tanaka et al. (2009)	A and C: M1 ("hotspot" of the TA muscle) R: Right forehead	35	2.0	10	0.034	Sham: 30 s	↑ Toe pinch force	a-tDCS > sham

A, anodal; C, cathodal; R, reference electrode; M1, primary motor cortex; TA, tibialis anterior; a-tDCS, anodal transcranial direct current stimulation; c-tDCS, cathodal transcranial direct current stimulation; INV, inversion; DF, dorsiflexion; PEDro, Physiotherapy Evidence Database (PEDro) scale; ↓, denotes a decrease; →, denotes no significant change; ↑, denotes an increase; C3, C4, Cz, Fz, Pz: the electrodes placement of the 10/20 EEG system; NR, not reported.

TABLE 3 | The characteristics of studies investigating the effect of tDCS on ankle physical performance.

Study	Sample	Gender	Age (years)	Drop-outs (N)	Design	Task	Cortical excitability examined	PEDro score
Mizuno and Aramaki, (2017)	10	10 males	25 ± 3	2	Crossover	Passive dorsiflexion task	No	9
Devanathan and Madhavan, (2016)	14	6 males 8 females	20–32	None	Crossover	Ankle reaction time task	No	9
Sriraman et al. (2014)	12	4 males, 8 females	20–32	None	Crossover	Ankle motor task	Yes	6
Shah et al. (2013)	8	5 males, 3 females	18–26	None	Crossover	Ankle visuomotor task	Yes	6

were the same as real tDCS but the current was delivered in only the first 30 or 60 s of the stimulation (**Table 2**).

Several variables were assessed in these studies, including foot sole standing vibratory threshold, foot tactile threshold, foot flexor strength, and toe pinch force. Specifically, Zhou et al. (2018) observed that the standing vibratory threshold was decreased (i.e., better sensation) after anodal tDCS compared with sham. Yamamoto et al. (2020) examined the effects of cathodal tDCS designed to target the left motor area on foot tactile threshold and observed a significant decrease in the tactile threshold of the left center of the distal pulp of the hallux after cathodal tDCS compared with sham. One study showed that tDCS could improve toe pinch force (Tanaka et al., 2009). More recently, Xiao et al. (2020) found no significant differences in foot flexor strength between anodal HD-tDCS and sham stimulation.

Effects of tDCS on Ankle Physical Performance

Four studies examined the effects of tDCS on ankle physical performance. Forty-four participants, consisting of 25 males and 19 females, were recruited. The age of the participants was between 18 and 32 years (**Table 3**).

Only the immediate effects of one-session tDCS were examined in these studies. The target of tDCS was M1 in three studies (Sriraman et al., 2014; Devanathan and Madhavan, 2016; Mizuno and Aramaki, 2017), and the targets in the other study were M1 and the cerebellum (Shah et al., 2013). Three studies used transcranial magnetic stimulation to identify the area of M1 by hot spotting for the left tibialis anterior (TA) muscle (Shah et al., 2013; Sriraman et al., 2014; Devanathan and Madhavan, 2016), and one study placed the electrodes according to the 10/20 EEG system (Mizuno and Aramaki, 2017). The electrode sizes were between 8 and 35 cm^2 (Shah et al., 2013; Sriraman et al., 2014; Devanathan and Madhavan, 2016; Mizuno and Aramaki, 2017). Three studies applied the intensity of 1 mA for 15 min (Shah et al., 2013; Sriraman et al., 2014; Devanathan and Madhavan, 2016) and the other one used 2 mA for 10 min (Mizuno and Aramaki, 2017). The current density at the stimulation electrode was 0.057, 0.08, or 0.125 mA/cm^2 with a total charge between 0.034 and 0.113 C/cm^2. Sham was used as a control in these studies, in which the placement of electrodes was the same as real tDCS but the current was delivered in only the first 30 s of the stimulation.

For the excitability assessment induced by tDCS, one study showed that cerebellar cathodal and anodal tDCS increased the normalized motor-evoked potential (MEP) amplitudes for the TA muscle compared to the sham condition (Shah et al., 2013). The other study observed a trend toward a greater change in MEP amplitude during anodal tDCS compared to the pre-stimulation (Sriraman et al., 2014) (**Table 4**).

Ankle physical performance outcomes, including ankle reaction time, ankle range of motion, accuracy index for the ankle motor task, and passive kinesthesia thresholds, were measured in these studies. Devanathan and Madhavan (2016) observed that anodal tDCS could reduce the choice reaction time of ankle dorsiflexion compared with a sham condition. Mizuno and Aramaki (2017) observed that cathodal tDCS significantly increased ankle range of motion. Shah et al. (2013) and Sriraman et al. (2014) explored the effects of tDCS on ankle motor skill learning. The former found that anodal cerebellar, cathodal cerebellar, and anodal M1 tDCSs improved the target-tracking accuracy index of the ankle; and the latter similarly observed that tDCS increased motor performance during the practice of a skilled ankle motor task. Xiao et al. (2020) observed that anodal HD-tDCS decreased the passive kinesthesia thresholds of ankle inversion and dorsiflexion from pre- to post-stimulation, but no significant differences were observed between anodal and sham HD-tDCS.

Risk of Bias and Quality of Evidence

The summary risk of bias graph was illustrated in **Figure 2**. One study maintained a low risk of bias in all the domains evaluated (Xiao et al., 2020), whereas the other studies showed a certain high or uncertain risk in the risk-of-bias assessment. Regarding random sequence generation, all studies utilized randomization, but only one study sufficiently described the methods used for random sequence generation (Xiao et al., 2020). For blinding, five studies used a double-blind approach, one utilized single blinding, and the remaining described that no one noticed the difference between groups. Only two studies presented a high risk of incomplete outcome data. Three participants did not perform the hand pinch force task because of machine trouble and some other reasons in Tanaka et al. (2009). Two participants were excluded based on the results of the Smirnov–Grubbs rejection test by (Mizuno and Aramaki, 2017). Regarding selective reporting, all studies were deemed as having a low risk of bias. Besides, the PEDro scores of all the studies were over six, which indicated that all the included studies have high quality. Generally, the studies performed well in terms of allocation, blinding effectiveness, selective reporting, avoidance of order effects, maintenance of stimulation well-tolerated, and absence of side effects.

DISCUSSION

In this study, we systematically reviewed the literature reporting the effects of tDCS on the physical performances of the foot and ankle. Seven of the eight included studies showed improvements in the task performances of the foot and ankle, such as motor performance, motor learning skill, and somatosensory function, which suggests that tDCS is promising to help improve the physical performances of the foot and ankle. However, due to the small sample size, various tDCS parameters, etc., these findings still need to be examined and confirmed in future studies. We will thus discuss the underlying mechanism and outlook on the possible directions of futures studies.

Nowadays, the effectiveness of tDCS is gradually certified in improving physical performances (Vargas et al., 2018; Lattari et al., 2020a,b). The effects of tDCS on lower limb performance, especially the physical performances of the foot and ankle, are relatively understudied to date (Fleming et al., 2017). Applying tDCS over the foot and ankle area of the motor cortex is challenging because of its deep position in the interhemispheric fissure (Foerster et al., 2018b). However, an initial study exploring the effects of tDCS on lower limb M1 excitability reported that 10 min of 2 mA anodal conventional tDCS with an electrode size of 35 cm^2 can increase the corticospinal excitability of the leg area of the motor cortex as reflected by an increase in the amplitude of motor-evoked potentials of the TA muscle (Jeffery et al., 2007). In line with the aforementioned preliminary finding, subsequent studies have shown that tDCS can also modulate the excitability of the lower-limb area of the motor cortex and further alter the physical performances of the foot and ankle of healthy adults and thus has potential benefits on promoting the physical performances of the foot and ankle (Tanaka et al., 2009; Shah et al., 2013; Sriraman et al., 2014).

Notably, high variability in the effects of tDCS on these types of physical performances was observed (Angius et al., 2018). For

TABLE 4 | Stimulation protocols and main outcomes of studies investigating the effect of tDCS on ankle physical performance.

Study	Anodal/cathodal location	Electrode size (cm^2)	Current (mA)	Duration (min)	Total charge (C/cm^2)	Control	Main outcomes	Significant effect vs. sham
Mizuno and Aramaki, (2017)	A and C: Cz R: Center of the forehead	35	2.0	10	0.034	Sham: 30 s	↑ Ankle range of motion	c-tDCS > sham
Devanathan and Madhavan, (2016)	A: M1 ("hotspot" of the TA muscle) R: Right supraorbital region	12.5	1.0	15	0.072	Sham: 30 s	↓ Ankle dorsiflexion choice reaction time	a-tDCS > sham
Sriraman et al. (2014)	A: M1 ("hotspot" of the TA muscle) R: Right supraorbital region	8	1.0	15	0.113	Sham: 30 s	↑ Accuracy index of ankle tracking	a-tDCS > sham
Shah et al. (2013)	A and C: M1 ('hotspot' of the TA muscle), left cerebellum R: Right supraorbital region, left buccinator muscle	8	1.0	15	0.113	Sham: 30 s	↑ Accuracy index of ankle tracking	a-tDCS > sham cerebellar a-tDCS > sham cerebellar c-tDCS > sham

A, anodal; C, cathodal; R, reference electrode; M1, primary motor cortex; TA, tibialis anterior; a-tDCS, anodal transcranial direct current stimulation; c-tDCS, cathodal transcranial direct current stimulation; PEDro, Physiotherapy Evidence Database (PEDro) scale; ↓, denotes a decrease; ↑, denotes an increase; Cz, the electrodes placement of the 10/20 EEG system.

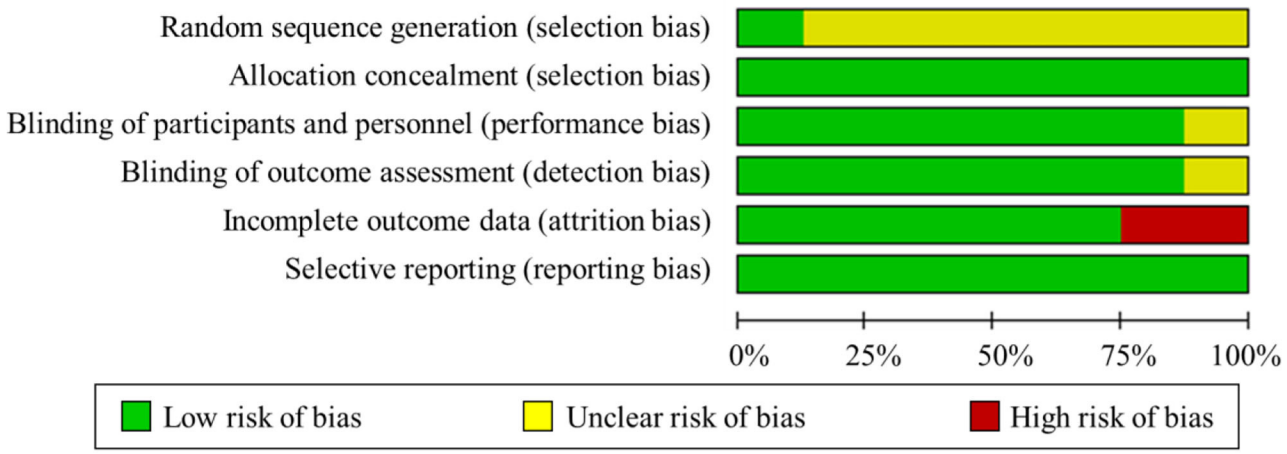

FIGURE 2 | Summary of risk-of-bias assessment.

example, anodal tDCS failed to enhance the muscle strength of the lower extremity of healthy participants, including knee extensor and foot flexor strength (Flood et al., 2017; Maeda et al., 2017; Xiao et al., 2020). The variability may have arisen from the variance in the characteristics of the participants, the design of study protocols, and tDCS montages. Specifically, the variance in experimental outcomes in response to tDCS was caused by several factors associated with high inter-individual variability, including the organization of local circuits, basal level of function, psychological state, level of neurotransmitters and receptor sensibility, baseline neurophysiological state, and genetic aspects (López-Alonso et al., 2015; Pellegrini et al., 2018a,b; Machado et al., 2019). In addition, those previous studies used different experimental designs and stimulation protocols (i.e., different montages), potentially contributing to the variance in the results or even the reversal effect (Datta et al., 2009; Angius et al., 2018; Machado, S. et al., 2019; Hassanzahraee et al., 2020; Pellegrini et al., 2020). For example, Hassanzahraee et al. (2020) observed the reversal of corticospinal excitability of anodal tDCS with a current intensity of 1.0 mA when the stimulation duration was over 26 min, which may provide certain implications for preventing excessive brain activation. Additionally, a "ceiling effect" may limit the benefit induced by tDCS in healthy adults (Zhou et al., 2018), that is, healthy participants can perform the task well at baseline; thus, the tDCS-induced improvement would be not as high as expected. Nevertheless, the main outcomes of these studies showed the potential of tDCS in enhancing the physical performances of the foot and ankle, yet its effectiveness

should be further confirmed in future studies with more rigorous study design and larger sample sizes.

These studies showed the potential of tDCS in enhancing the physical performances of the foot and ankle. However, the montages of tDCS (e.g., current intensity, duration, and electrode size) were inconsistent across the included studies. Specifically, three studies that investigated the effect of tDCS on foot physical performance used the conventional tDCS, which delivered a current of 1.5–2 mA via two large sponges (size: 35 cm^2). The total charge of received current on targets was between 0.026 and 0.069 C/cm^2, which can adequately induce variation in the response threshold of the stimulated neurons and change the electrical activity of the neurons (Fertonani and Miniussi, 2017). Thus, Zhou et al. (2018) found that 20 min of 2 mA tDCS applying over C3 can also improve foot somatosensory function. Similarly, among the studies investigating the effect of tDCS on ankle physical performance, four studies used the conventional tDCS delivering the current intensity between 1 and 2 mA via two large electrodes with different sizes (i.e., 8–35 cm^2). The total current charge was between 0.034 and 0.113 C/cm^2, and these studies showed that applying tDCS over M1 could increase ankle motor performance. However, this conventional tDCS may induce diffuse current flow on targets and the distribution of the induced electrical field may vary across participants. More importantly, the return of current in this conventional tDCS cannot be well-controlled, and may thus induce the inhibitory effects on the cortical regions next to the targeted area (To et al., 2016). For example, Zhou et al. (2018) targeted the primary sensory cortex (C3 area of 10/20 EEG template) using large sponge electrodes, and the excitability of the primary motor cortex (located anatomically next to the primary sensory cortex) may be inhibited, which may thus limit the effects of tDCS on the functional performance (e.g., they did not observe the significant improvement in the performance of timed-up-and-go test of mobility, though the foot-sole tactile sensation was improved). Besides, only one study using HD-tDCS observed a significant improvement in foot physical performance from pre- to post-stimulation, but not between anodal and sham HD-tDCS (Xiao et al., 2020). For anodal HD-tDCS, the anodal electrode was set at 2 mA, while the four return electrodes placed 3.5 cm apart from the anodal electrode were programmed to −0.5 mA. The previous study anticipated that −0.25 mA inhibitory input from the surrounding cortical areas may negate or override the focalized 1 mA current intensity over M1, which may influence overall M1 excitability (Pellegrini et al., 2020). Thus, the improvements in foot physical performance induced by anodal HD-tDCS may not be significant (Xiao et al., 2020). The applicable HD-tDCS protocol and its effectiveness should be further confirmed in future studies with more rigorous study design and larger sample size.

The mechanisms of tDCS in improving the physical performances of the foot and ankle are still uncertain (Angius et al., 2017). However, several possible explanations have been made. The modulation of the cortical excitability and the activation of the synaptic neuroplasticity of targeting brain regions play a key role in the regulation of neural circuits responsible for biomechanical management (Nitsche et al., 2008). Specifically, the current flow delivered by tDCS may augment active synaptic connections between the neuronal structures of cortical regions and thus may induce sustained changes in the neural activity of motor neurons. Such neuronal changes can improve the degree of the synchronous discharge of motor units, which influence the neural circuitry on the neuromechanical regulation of the foot and ankle and then improve their physical performance (Bindman et al., 1964; Dutta et al., 2015; Patel et al., 2019). TDCS can also induce an increase in cortico-muscular coherence, which is defined as the coherence mapping the synchrony between cortical neural activity and muscles (Chen C. et al., 2019). This occurrence may also support the aforementioned hypothesis of the underlying mechanism. Besides, the neuronal circuits involved in the regulation of motor tasks are likely active at a heightened state (Ziemann et al., 2004; Sriraman et al., 2014; Chen J. et al., 2019). The tDCS-induced improvements in physical performance and/or motor learning skills are commonly observed in the presence of activity-dependent modifications of synapses. Thus, the membrane shifting induced by anodal tDCS accessibly may shape synaptic plasticity and improve motor performance and learning (Sriraman et al., 2014). Sensory sensitivity depends on the degree of excitation in the somatosensory cortex and the integrity of the individual's neural circuitry (Fregni and Pascual-Leone, 2007). Wang et al. (2015) observed that anodal tDCS could modulate and augment cortical responsiveness to foot pressure stimuli in healthy adults by increasing the activation of the left posterior paracentral lobule (including the primary sensory cortex [S1]), and this tDCS-induced increase in cortical responsiveness to pressure stimuli may help the sensation of the lower limbs. Additionally, S1 is next to M1; therefore, tDCS targeting S1 may also increase the excitability of M1. Thus, improvements in sensory function may be attributed to the tDCS-induced activation of M1.

Interestingly, cathodal tDCS applied over the motor area also induced a positive effect on foot tactile sensation and ankle range of motion (Mizuno and Aramaki, 2017; Yamamoto et al., 2020). Cathodal tDCS usually decreases cortical excitability. By contrast, the administration of cathodal tDCS to the motor cortex of one hemisphere increases the excitability of the motor cortex of the other hemisphere in healthy participants (Schambra et al., 2003) and improves the physical performance of the ipsilateral foot (Yamamoto et al., 2020). Besides, an increase in ankle range of motion may be based on decreased pain perception secondary to the decreased excitability of the cerebral cortex caused by cathodal tDCS (Mizuno and Aramaki, 2017). Although anodal and cathodal tDCS maintain discrepant neurophysiological effects, both have shown benefits in improving the physical performance of the foot and ankle.

Multiple intermediate structural and functional levels between cortical regions and the foot and ankle in the regulatory pathway of the physical functions of the foot and ankle may mediate and integrate the effects of tDCS (Fertonani and Miniussi, 2017). These components are interconnected over multiple levels; therefore, tDCS that modulates neurons

close to the discharge threshold, which are potentially engaged in the execution of a specific task, may also regulate the functionality of multiple components (e.g., task-related networks and secondary-level neural circuitry) in the regulatory system (Siebner et al., 2009; Bikson et al., 2013; Miniussi et al., 2013; Luft et al., 2014). However, some improvements in performance have been noted without remarkable changes in corticospinal excitability (Abdelmoula et al., 2016; Angius et al., 2016). Thus, characterizing the multi-level components of the regulatory system of the foot and ankle's physical function in future studies using neuroimaging techniques will ultimately advance the understanding of the underlying mechanisms behind the ergogenic neuromechanical effects of tDCS on the foot and ankle, as well as the other parts of the body extremities.

The results of this systematic review should also be taken with caution since the included studies have some methodological limitations. First, the sample size of the included studies in this review is relatively small. Second, the selection of tDCS parameters varied across studies, and many of them lacked optimization. For example, two studies applied the conventional tDCS over the C3 area, which may not be the appropriate target for the control of the lower-extremity function (Zhou et al., 2018; Yamamoto et al., 2020). Thus, a standardized protocol of tDCS using a more rigorous study design and advanced neuro-modeling technique is highly demanded in future studies aiming at examining the effectiveness of tDCS on the physical performances of the foot and ankle. Besides, the neurophysiological mechanisms through which tDCS benefits the physical performance are still not fully understood. Only two studies measured the changes of cortical excitability within the tDCS targets (i.e., M1), but the "dose-response" effects of tDCS were not examined (Shah et al., 2013; Sriraman et al., 2014). Further studies are warranted to estimate the on-target "does" of tDCS (e.g., the normal component of the electric field within the tDCS targets) using neuro-modeling techniques with the brain magnetic resonance images of participants and correlate such dose to the observed functional improvements (Fischer et al., 2017). This will provide fundamental knowledge into the causal relationship between the tDCS-induced neurophysiological changes of cortical regions and the changes in behavior induced by tDCS. A bias in gender was observed in the studies investigated the effects of tDCS on foot sensory function and foot muscle strength. However, to date, no studies have examined how gender influences the tDCS-induced effects on foot physical performance, which is worthwhile to be explored in the future. Besides, much more numbers of studies generally demonstrated that tDCS can induce benefits to functional performance. However, potential publication bias should be noted, that is, studies with positive results are more preferred to be reported. Negative results on the efficacy of tDCS might be encouraged to be published to critique the implementation of tDCS, which will ultimately help optimize the protocol of tDCS intervention.

Research efforts on exploring the effects of tDCS on the physical performances of the foot and ankle have emerged recently, and a relatively limited number of studies ($n = 8$) was published. The current review was thus performed based upon this number of publications. Besides, this study only focused on the effect of tDCS on the physical performances of the foot and ankle of healthy adults; patients with diminished or impaired foot and ankle functionality should be taken into account in future studies.

CONCLUSION

Based on the existing studies, tDCS is promising to help improve the physical performances of the foot and ankle, such as motor performance, motor learning skill, and somatosensory function, which needs to be examined and confirmed in future studies. The underlying mechanism has been postulated that tDCS increased neuronal excitability of the targeted cortex and may potentially enhance the neuromechanical management of the physical performances of the foot and ankle. However, future studies with a larger sample size and a more rigorous experimental design (i.e., study protocol and tDCS montage) are warranted to confirm the findings of current studies and explore the neurophysiological and neuromechanical mechanisms of tDCS-induced improvements in the physical performances of the foot and ankle.

DATA AVAILABILITY STATEMENT

The original contributions presented in the study are included in the article/supplementary materials, further inquiries can be directed to the corresponding authors.

AUTHOR CONTRIBUTIONS

SX contributed to study design, data collection, drafting, and revising the manuscript. JZ and WF contributed to supervising study design, completing data analysis and interpretation, and revising the manuscript. BW and XZ revised the manuscript. All authors have read and approved the final version of the manuscript and agree with the order of the presentation of the authors.

FUNDING

This research was funded by the National Key Technology Research and Development Program of the Ministry of Science and Technology of China (2019YFF0302100, 2018YFF0300500), the National Natural Science Foundation of China (11772201, 119320131), Talent Development Fund of Shanghai Municipal (2018107), and the Dawn Program of Shanghai Education Commission, China (19SG47).

REFERENCES

Aagaard, P. (2018). Spinal and supraspinal control of motor function during maximal eccentric muscle contraction: effects of resistance training. *J. Sport Health Sci.* 7, 282–293. doi: 10.1016/j.jshs.2018.06.003

Abdelmoula, A., Baudry, S., and Duchateau, J. (2016). Anodal transcranial direct current stimulation enhances time to task failure of a submaximal contraction of elbow flexors without changing corticospinal excitability. *Neuroscience* 322, 94–103. doi: 10.1016/j.neuroscience.2016.02.025

Angius, L., Hopker, J., and Mauger, A. R. (2017). The ergogenic effects of transcranial direct current stimulation on exercise performance. *Front. Physiol.* 8:90. doi: 10.3389/fphys.2017.00090

Angius, L., Pageaux, B., Hopker, J., Marcora, S. M., and Mauger, A. R. (2016). Transcranial direct current stimulation improves isometric time to exhaustion of the knee extensors. *Neuroscience* 339, 363–375. doi: 10.1016/j.neuroscience.2016.10.028

Angius, L., Pascual-Leone, A., and Santarnecchi, E. (2018). Brain stimulation and physical performance. *Prog. Brain Res.* 240, 317–339. doi: 10.1016/bs.pbr.2018.07.010

Bikson, M., Name, A., and Rahman, A. (2013). Origins of specificity during tDCS: anatomical, activity-selective, and input-bias mechanisms. *Front. Hum. Neurosci.* 7:688. doi: 10.3389/fnhum.2013.00688

Bindman, L. J., Lippold, O. C., and Redfearn, J. W. (1964). The action of brief polarizing currents on the cerebral cortex of the rat (1) during current flow and (2) in the production of long-lasting after-effects. *J. Physiol.* 172, 369–382. doi: 10.1113/jphysiol.1964.sp007425

Chen, C., Fang, Y., Wang, X., Bao, S. C., Tang, Z., and Tong, R. K. (2019). Excitation comparison between multi-site stimulation using network-based tDCS and focal stimulation using high-definition tDCS. *Conf. Proc. IEEE Eng. Med. Biol. Soc.* 2019, 6884–6887. doi: 10.1109/EMBC.2019.8857287

Chen, J., Li, Y., Zhang, G., Jin, X., Lu, Y., and Zhou, C. (2019). Enhanced inhibitory control during re-engagement processing in badminton athletes: an event-related potential study. *J. Sport Health Sci.* 8, 585–594. doi: 10.1016/j.jshs.2019.05.005

Cumpston, M., Li, T., Page, M. J., Chandler, J., Welch, V. A., Higgins, J. P., et al. (2019). Updated guidance for trusted systematic reviews: a new edition of the Cochrane Handbook for Systematic Reviews of Interventions. *Cochrane Database Syst. Rev.* 10:Ed000142. doi: 10.1002/14651858.ED000142

Datta, A., Bansal, V., Diaz, J., Patel, J., Reato, D., and Bikson, M. (2009). Gyri-precise head model of transcranial direct current stimulation: improved spatial focality using a ring electrode versus conventional rectangular pad. *Brain Stimul.* 2, 201–207. doi: 10.1016/j.brs.2009.03.005

de Moura, M. C. D. S., Hazime, F. A., Marotti Aparicio, L. V., Grecco, L. A. C., Brunoni, A. R., and Hasue, R. H. (2019). Effects of transcranial direct current stimulation (tDCS) on balance improvement: a systematic review and meta-analysis. *Somatosens. Mot. Res.* 36, 122–135. doi: 10.1080/08990220.2019.1624517

Devanathan, D., and Madhavan, S. (2016). Effects of anodal tDCS of the lower limb M1 on ankle reaction time in young adults. *Exp. Brain Res.* 234, 377–385. doi: 10.1007/s00221-015-4470-y

Dutta, A., Krishnan, C., Kantak, S. S., Ranganathan, R., and Nitsche, M. A. (2015). Recurrence quantification analysis of surface electromyogram supports alterations in motor unit recruitment strategies by anodal transcranial direct current stimulation. *Restor. Neurol. Neurosci.* 33, 663–669. doi: 10.3233/RNN-140469

Ferreira, N. R., Junqueira, Y. N., Corrêa, N. B., Fonseca, E. O., Brito, N. B. M., Menezes, T. A., et al. (2019). The efficacy of transcranial direct current stimulation and transcranial magnetic stimulation for chronic orofacial pain: a systematic review. *PLoS ONE* 14:e0221110. doi: 10.1371/journal.pone.0221110

Fertonani, A., and Miniussi, C. (2017). Transcranial electrical stimulation: what we know and do not know about mechanisms. *Neuroscientist* 23, 109–123. doi: 10.1177/1073858416631966

Fischer, D. B., Fried, P. J., Ruffini, G., Ripolles, O., Salvador, R., Banus, J., et al. (2017). Multifocal tDCS targeting the resting state motor network increases cortical excitability beyond traditional tDCS targeting unilateral motor cortex. *Neuroimage* 157, 34–44. doi: 10.1016/j.neuroimage.2017.05.060

Fleming, M. K., Pavlou, M., Newham, D. J., Sztriha, L., and Teo, J. T. (2017). Non-invasive brain stimulation for the lower limb after stroke: what do we know so far and what should we be doing next? *Disabil. Rehabil.* 39, 714–720. doi: 10.3109/09638288.2016.1161835

Flood, A., Waddington, G., Keegan, R. J., Thompson, K. G., and Cathcart, S. (2017). The effects of elevated pain inhibition on endurance exercise performance. *PeerJ* 5:e3028. doi: 10.7717/peerj.3028

Foerster, Á., Dutta, A., Kuo, M. F., Paulus, W., and Nitsche, M. A. (2018a). Effects of anodal transcranial direct current stimulation over lower limb primary motor cortex on motor learning in healthy individuals. *Eur. J. Neurosci.* 47, 779–789. doi: 10.1111/ejn.13866

Foerster, Á., Rezaee, Z., Paulus, W., Nitsche, M. A., and Dutta, A. (2018b). Effects of cathode location and the size of anode on anodal transcranial direct current stimulation over the leg motor area in healthy humans. *Front. Neurosci.* 12:443. doi: 10.3389/fnins.2018.00443

Fregni, F., and Pascual-Leone, A. (2007). Technology insight: noninvasive brain stimulation in neurology-perspectives on the therapeutic potential of rTMS and tDCS. *Nat. Clin. Pract. Neurol.* 3, 383–393. doi: 10.1038/ncpneuro0530

Hassanzahraee, M., Nitsche, M. A., Zoghi, M., and Jaberzadeh, S. (2020). Determination of anodal tDCS duration threshold for reversal of corticospinal excitability: an investigation for induction of counter-regulatory mechanisms. *Brain Stimul.* 13, 832–839. doi: 10.1016/j.brs.2020.02.027

Jeffery, D. T., Norton, J. A., Roy, F. D., and Gorassini, M. A. (2007). Effects of transcranial direct current stimulation on the excitability of the leg motor cortex. *Exp. Brain Res.* 182, 281–287. doi: 10.1007/s00221-007-1093-y

Kuo, M. F., Paulus, W., and Nitsche, M. A. (2014). Therapeutic effects of non-invasive brain stimulation with direct currents (tDCS) in neuropsychiatric diseases. *Neuroimage* 85, 948–960. doi: 10.1016/j.neuroimage.2013.05.117

Lattari, E., Campos, C., Lamego, M. K., Legey, S., Neto, G. M., Rocha, N. B., et al. (2020a). Can transcranial direct current stimulation improve muscle power in individuals with advanced weight-training experience? *J. Strength Cond. Res.* 34, 97–103. doi: 10.1519/JSC.0000000000001956

Lattari, E., Oliveira, B. R. R., Monteiro Júnior, R. S., Marques Neto, S. R., Oliveira, A. J., Maranhão Neto, G. A., et al. (2018). Acute effects of single dose transcranial direct current stimulation on muscle strength: a systematic review and meta-analysis. *PLoS ONE* 13:e0209513. doi: 10.1371/journal.pone.0209513

Lattari, E., Rosa Filho, B. J., Fonseca Junior, S. J., Murillo-Rodriguez, E., Rocha, N., Machado, S., et al. (2020b). Effects on volume load and ratings of perceived exertion in individuals' advanced weight training after transcranial direct current stimulation. *J. Strength Cond. Res.* 34, 89–96. doi: 10.1519/JSC.0000000000002434

López-Alonso, V., Fernández-Del-Olmo, M., Costantini, A., Gonzalez-Henriquez, J. J., and Cheeran, B. (2015). Intra-individual variability in the response to anodal transcranial direct current stimulation. *Clin. Neurophysiol.* 126, 2342–2347. doi: 10.1016/j.clinph.2015.03.022

Luft, C. D., Pereda, E., Banissy, M. J., and Bhattacharya, J. (2014). Best of both worlds: promise of combining brain stimulation and brain connectome. *Front. Syst. Neurosci.* 8:132. doi: 10.3389/fnsys.2014.00132

Machado, D., Unal, G., Andrade, S. M., Moreira, A., Altimari, L. R., Brunoni, A. R., et al. (2019). Effect of transcranial direct current stimulation on exercise performance: a systematic review and meta-analysis. *Brain Stimul.* 12, 593–605. doi: 10.1016/j.brs.2018.12.227

Machado, S., Jansen, P., Almeida, V., and Veldema, J. (2019). Is tDCS an adjunct ergogenic resource for improving muscular strength and endurance performance? A systematic review. *Front. Psychol.* 10:1127. doi: 10.3389/fpsyg.2019.01127

Maeda, K., Yamaguchi, T., Tatemoto, T., Kondo, K., Otaka, Y., and Tanaka, S. (2017). Transcranial direct current stimulation does not affect lower extremity muscle strength training in healthy individuals: a triple-blind, sham-controlled study. *Front. Neurosci.* 11:179. doi: 10.3389/fnins.2017.00179

Maher, C. G., Sherrington, C., Herbert, R. D., Moseley, A. M., and Elkins, M. (2003). Reliability of the PEDro scale for rating quality of randomized controlled trials. *Phys. Ther.* 83, 713–721. doi: 10.1093/ptj/83.8.713

Miniussi, C., Harris, J. A., and Ruzzoli, M. (2013). Modelling non-invasive brain stimulation in cognitive neuroscience. *Neurosci. Biobehav. Rev.* 37, 1702–1712. doi: 10.1016/j.neubiorev.2013.06.014

Mizuno, T., and Aramaki, Y. (2017). Cathodal transcranial direct current stimulation over the Cz increases joint flexibility. *Neurosci. Res.* 114, 55–61. doi: 10.1016/j.neures.2016.08.004

Moher, D., Liberati, A., Tetzlaff, J., and Altman, D. G. (2009). Preferred reporting items for systematic reviews and meta-analyses: the PRISMA statement. *PLoS Med* 6:e1000097. doi: 10.1371/journal.pmed.1000097

Needle, A. R., Lepley, A. S., and Grooms, D. R. (2017). Central nervous system adaptation after ligamentous injury: a summary of theories, evidence, and clinical interpretation. *Sports Med.* 47, 1271–1288. doi: 10.1007/s40279-016-0666-y

Nitsche, M. A., Cohen, L. G., Wassermann, E. M., Priori, A., Lang, N., Antal, A., et al. (2008). Transcranial direct current stimulation: state of the art 2008. *Brain Stimul.* 1, 206–223. doi: 10.1016/j.brs.2008.06.004

Nitsche, M. A., and Paulus, W. (2000). Excitability changes induced in the human motor cortex by weak transcranial direct current stimulation. *J. Physiol.* 527, 633–639. doi: 10.1111/j.1469-7793.2000.t01-1-00633.x

Nitsche, M. A., and Paulus, W. (2001). Sustained excitability elevations induced by transcranial DC motor cortex stimulation in humans. *Neurology* 57, 1899–1901. doi: 10.1212/WNL.57.10.1899

Noakes, T. D. (2011). Time to move beyond a brainless exercise physiology: the evidence for complex regulation of human exercise performance. *Appl. Physiol. Nutr. Metab.* 36, 23–35. doi: 10.1139/H10-082

Patel, R., Ashcroft, J., Patel, A., Ashrafian, H., Woods, A. J., Singh, H., et al. (2019). The impact of transcranial direct current stimulation on upper-limb motor performance in healthy adults: a systematic review and meta-analysis. *Front. Neurosci.* 13:1213. doi: 10.3389/fnins.2019.01213

Pellegrini, M., Zoghi, M., and Jaberzadeh, S. (2018a). Biological and anatomical factors influencing interindividual variability to noninvasive brain stimulation of the primary motor cortex: a systematic review and meta-analysis. *Rev. Neurosci.* 29, 199–222. doi: 10.1515/revneuro-2017-0048

Pellegrini, M., Zoghi, M., and Jaberzadeh, S. (2018b). Cluster analysis and subgrouping to investigate inter-individual variability to non-invasive brain stimulation: a systematic review. *Rev. Neurosci.* 29, 675–697. doi: 10.1515/revneuro-2017-0083

Pellegrini, M., Zoghi, M., and Jaberzadeh, S. (2020). The effects of transcranial direct current stimulation on corticospinal and cortico-cortical excitability and response variability: conventional versus high-definition montages. *Neurosci Res.* doi: 10.1016/j.neures.2020.06.002. [Epub ahead of print].

Rahman, A., Reato, D., Arlotti, M., Gasca, F., Datta, A., Parra, L. C., et al. (2013). Cellular effects of acute direct current stimulation: somatic and synaptic terminal effects. *J. Physiol.* 591, 2563–2578. doi: 10.1113/jphysiol.2012.247171

Reardon, S. (2016). 'Brain doping' may improve athletes' performance: electrical stimulation seems to boost endurance in preliminary studies. *Nature* 531, 283–285. doi: 10.1038/nature.2016.19534

Rodgers, M. M. (1988). Dynamic biomechanics of the normal foot and ankle during walking and running. *Phys. Ther.* 68, 1822–1830. doi: 10.1093/ptj/68.12.1822

Saruco, E., et al., (2017). Anodal tDCS over the primary motor cortex improves motor imagery benefits on postural control: A pilot study. *Sci Rep.* 7:480.

Schambra, H. M., Sawaki, L., and Cohen, L. G. (2003). Modulation of excitability of human motor cortex (M1) by 1 Hz transcranial magnetic stimulation of the contralateral M1. *Clin. Neurophysiol.* 114, 130–133. doi: 10.1016/S1388-2457(02)00342-5

Shah, B., Nguyen, T. T., and Madhavan, S. (2013). Polarity independent effects of cerebellar tDCS on short term ankle visuomotor learning. *Brain Stimul.* 6, 966–968. doi: 10.1016/j.brs.2013.04.008

Siebner, H. R., Hartwigsen, G., Kassuba, T., and Rothwell, J. C. (2009). How does transcranial magnetic stimulation modify neuronal activity in the brain? Implications for studies of cognition. *Cortex* 45, 1035–1042. doi: 10.1016/j.cortex.2009.02.007

Sriraman, A., Oishi, T., and Madhavan, S. (2014). Timing-dependent priming effects of tDCS on ankle motor skill learning. *Brain Res.* 1581, 23–29. doi: 10.1016/j.brainres.2014.07.021

Stagg, C. J., and Nitsche, M. A. (2011). Physiological basis of transcranial direct current stimulation. *Neuroscientist* 17, 37–53. doi: 10.1177/1073858410386614

Summers, J. J., Kang, N., and Cauraugh, J. H. (2016). Does transcranial direct current stimulation enhance cognitive and motor functions in the ageing brain? A systematic review and meta- analysis. *Ageing Res. Rev.* 25, 42–54. doi: 10.1016/j.arr.2015.11.004

Tanaka, S., Hanakawa, T., Honda, M., and Watanabe, K. (2009). Enhancement of pinch force in the lower leg by anodal transcranial direct current stimulation. *Exp. Brain Res.* 196, 459–465. doi: 10.1007/s00221-009-1863-9

To, W. T., Hart, J., De Ridder, D., and Vanneste, S. (2016). Considering the influence of stimulation parameters on the effect of conventional and high-definition transcranial direct current stimulation. *Expert Rev. Med. Devices* 13, 391–404. doi: 10.1586/17434440.2016.1153968

Vargas, V. Z., Baptista, A. F., Pereira, G. O. C., Pochini, A. C., Ejnisman, B., Santos, M. B., et al. (2018). Modulation of isometric quadriceps strength in soccer players with transcranial direct current stimulation: a crossover study. *J. Strength Cond. Res.* 32, 1336–1341. doi: 10.1519/JSC.0000000000001985

Vaseghi, B., Zoghi, M., and Jaberzadeh, S. (2014). Does anodal transcranial direct current stimulation modulate sensory perception and pain? A meta-analysis study. *Clin Neurophysiol.* 125, 1847–1858.

Wang, Y., Hao, Y., Zhou, J., Fried, P. J., Wang, X., Zhang, J., et al. (2015). Direct current stimulation over the human sensorimotor cortex modulates the brain's hemodynamic response to tactile stimulation. *Eur. J. Neurosci.* 42, 1933–1940. doi: 10.1111/ejn.12953

Xiao, S., Wang, B., Zhang, X., Zhou, J., and Fu, W. (2020). Acute effects of high-definition transcranial direct current stimulation on foot muscle strength, passive ankle kinesthesia, and static balance: a pilot study. *Brain Sci.* 10:246. doi: 10.3390/brainsci10040246

Yamamoto, S., Ishii, D., Ichiba, N., Yozu, A., and Kohno, Y. (2020). Cathodal tDCS on the motor area decreases the tactile threshold of the distal pulp of the hallux. *Neurosci. Lett.* 719:133887. doi: 10.1016/j.neulet.2018.10.032

Zhou, J., Lo, O. Y., Lipsitz, L. A., Zhang, J., Fang, J., and Manor, B. (2018). Transcranial direct current stimulation enhances foot sole somatosensation when standing in older adults. *Exp. Brain Res.* 236, 795–802. doi: 10.1007/s00221-018-5178-6

Ziemann, U., Ilić, T. V., Pauli, C., Meintzschel, F., and Ruge, D. (2004). Learning modifies subsequent induction of long-term potentiation-like and long-term depression-like plasticity in human motor cortex. *J. Neurosci.* 24, 1666–1672. doi: 10.1523/JNEUROSCI.5016-03.2004

Conflict of Interest: The authors declare that the research was conducted in the absence of any commercial or financial relationships that could be construed as a potential conflict of interest.

frontiers in Sports and Active Living

ORIGINAL RESEARCH
published: 13 November 2020
doi: 10.3389/fspor.2020.596063

Modularity in Motor Control: Similarities in Kinematic Synergies Across Varying Locomotion Tasks

Bernd J. Stetter[1]*, *Michael Herzog*[1], *Felix Möhler*[1], *Stefan Sell*[1,2] and *Thorsten Stein*[1]

[1] Institute of Sports and Sports Science, Karlsruhe Institute of Technology, Karlsruhe, Germany, [2] Joint Center Black Forest, Hospital Neuenbuerg, Neuenbuerg, Germany

Kinematic synergies (kSYN) provide an approach to quantify the covariation of joint motions and to explain the mechanisms underlying human motor behavior. A low-dimensional control strategy by means of the activation of a moderate number of kSYN would simplify the performance of complex motor tasks. The purpose of this study was to examine similarities between the kSYN of varying locomotion tasks: straight-line walking, walking a 90° spin turn and walking upstairs. Task-specific kSYN were extracted from full body kinematic recordings of 13 participants by principal component analysis. The first five kSYN accounting for most of the variance within each task were selected for further analysis following previous studies. The similarities between the kSYN of the three different locomotion tasks were quantified by calculating cosine similarities (SIM), as a vector-based similarity measure ranging from 0 (no similarity) to 1 (high similarity), between absolute principal component loading vectors. A SIM between two kSYN > 0.8 was interpreted as highly similar. Two to three highly similar kSYN were identified when comparing two individual tasks with each other. One kSYN, primarily characterized by anteversion and retroversion of the arms and legs, were found to be similar in all three tasks. Additional kSYN that occurred between individual tasks reflected mainly an upwards/downwards movement of the body or a countercyclical knee flexion/extension. The results demonstrate that the three investigated locomotion tasks are characterized by kSYN and that certain kSYN repeatedly occur across the three locomotion tasks. PCA yields kSYN which are in descent order according to their amount of total variance accounted for. Referring to the placing of a kSYN within the order as priorization, we found a change in priorization of repeatedly occurring kSYN across the individual tasks. The findings support the idea that movements can be efficiently performed through a flexible combination of a lower number of control-relevant variables.

Keywords: motor coordination, movement organization, principal component analysis, full body kinematics, everyday locomotion tasks

OPEN ACCESS

Edited by:
Yury Ivanenko, Santa Lucia Foundation (IRCCS), Italy

Reviewed by:
Giovanna Catavitello, Catholic University of Louvain, Belgium
Naomichi Ogihara, The University of Tokyo, Japan

***Correspondence:**
Bernd J. Stetter
bernd.stetter@kit.edu

Specialty section:
This article was submitted to Biomechanics and Control of Human Movement, a section of the journal Frontiers in Sports and Active Living

Received: *18 August 2020*
Accepted: *07 October 2020*
Published: *13 November 2020*

Citation:
Stetter BJ, Herzog M, Möhler F, Sell S and Stein T (2020) Modularity in Motor Control: Similarities in Kinematic Synergies Across Varying Locomotion Tasks. Front. Sports Act. Living 2:596063. doi: 10.3389/fspor.2020.596063

INTRODUCTION

The true complexity of the control processes involved in ordinary human movements is masked by the ease of their execution (Wolpert et al., 2013). The human central nervous system (CNS) consists of billions of interconnected neurons, and the musculoskeletal system is composed of approximately 700 muscles and over 300 mechanical degrees of freedom (Bruton and O'Dwyer, 2018). This highly redundant motor system enables us to achieve movement in countless ways

(Bernstein, 1967), and one of the longstanding questions in motor control research is how the CNS resolves this redundancy. In addition, we learn an enormous number of skills, such as raising a hand or playing sports, in the course of our lives and even when the execution of such tasks seems to be easy, it requires a fine tuning of the CNS. This leads to another fundamental question of motor control research: namely, how this versatility is implemented in the CNS. Consequently, finding answers to these two questions through analyzing the coordination of human movements, has—besides other challenges such as dealing with non-linearities within the motor system (Franklin and Wolpert, 2011)—become a central issue in motor control research (e.g., Bizzi et al., 1991; Wolpert and Kawato, 1998; Scholz and Schöner, 1999; Todorov and Jordan, 2002; d'Avella et al., 2003; Daffertshofer et al., 2004; Lacquaniti et al., 2012).

A possible answer to the questions of how the CNS solves the challenge of versatility and redundancy could be through a modular control architecture (Wolpert and Kawato, 1998; d'Avella, 2016). Many daily tasks are not independent from each other and have certain similarities, e.g., walking straight ahead vs. walking in a curve. If motor skills are represented by a collection of compositional elements (Giszter, 2015; d'Avella, 2016) that act as building blocks for movement construction, one would assume that similar movement tasks (e.g., walking in a straight line vs. walking in a curve) are composed of similar elements, although these may be weighted differently during construction of movements.

Such compositional elements could have various forms (Giszter, 2015). Synergies have been proposed as one possibility for implementing the idea of a modular control architecture (Bizzi et al., 1991; Bruton and O'Dwyer, 2018). Synergies ensure organization by establishing working relationships and thus simplifying the control of movements in a highly redundant motor system (Bernstein, 1967; Bruton and O'Dwyer, 2018). Such synergies can either exist on a muscular (d'Avella et al., 2003) or kinematic level (Borghese et al., 1996; Catavitello et al., 2018) and they typically represent compositional elements working together to produce results not obtainable by any of the elements alone (McGowan et al., 2010; Wang et al., 2013; Tagliabue et al., 2015). There is a growing body of literature supporting the existence of synergies and demonstrating that multi-segmental movements are highly coupled and correlated for a variety of tasks (Kelso et al., 1983; Lacquaniti et al., 1986; Troje, 2002; Daffertshofer et al., 2004; Wang et al., 2013; Majed et al., 2017; Haid et al., 2018).

The use of principal component analysis (PCA) has been proven to be effective in reducing the redundancy of large kinematic datasets and has been shown to be a feasible approach to extract relevant hidden structures (Courtine et al., 2005; Wang et al., 2013; Majed et al., 2017; Zago et al., 2017b; Bruton and O'Dwyer, 2018). Such analysis performed on a full body kinematic dataset decomposes the complex movement pattern into its main kinematic synergies (kSYN) (Daffertshofer et al., 2004; Lamoth et al., 2009; Wang et al., 2013). The first several few principal components normally account for most of the variance in the original data, and can be interpreted as the kinematic elements by which the motor system organizes a movement (Wang et al., 2013). For example, most previous studies stated that the dimensionality of gait could be reduced to 3–5 kSYN (Courtine and Schieppati, 2004; Wang et al., 2013; Zago et al., 2017c). Within the last two decades, kSYN of whole body motion have been investigated for common locomotion tasks such as walking or running (Troje, 2002; Daffertshofer et al., 2004; Lamoth et al., 2009; Federolf et al., 2013); balance tasks (Federolf, 2016; Haid et al., 2018); and more complex movements such as contemporary dance (Hollands et al., 2004) or karate (Zago et al., 2017a). In the majority of the studies, redundancies and patterns of coordination were determined in order to gain insight into the movement control mechanisms (Wang et al., 2013).

One of the first studies investigating basic coordination patterns in straight-line walking and walking turns using PCA was done by Courtine and Schieppati (2004). Their findings indicated invariant coordination patterns among limb segments and the trunk during straight-line walking and walking turns. Furthermore, a turn-dependent tuning of the coordination patterns was observed depending on the walking direction of the body. Such adaptations are required to successfully turn, as the center of mass must be quickly halted and redirected over a relatively stable base of support (Dixon et al., 2013). The investigation of turning biomechanics showed changes in lower-limb joint kinematics and spatio-temporal differences for the two main turning strategies for 90° turns, namely spin turn and step turns (Taylor et al., 2005; Dixon et al., 2013). The spin turn is characterized by a change of direction toward the same side as the stance limb and has been postulated to be an economical turning strategy (Taylor et al., 2005; Dixon et al., 2013). Similarly, other frequently encountered locomotion tasks by humans in daily living, such as stair walking, are characterized by biomechanical changes in comparison to straight-line walking. Riener et al. (2002) described a greater knee angle and the change from heel contact to middle food contact while walking stairs and hypothesized that the participants switch their gait patterns. Whether such changes lead to a similar tuning of kSYN as proposed for walking turns has not been examined so far. Overall, differences in coordination due to changes in the locomotion task have not been studied extensively. A few studies analyzed similarities in whole body kSYN. Lamoth et al. (2009) examined whole body kinematics when comparing multi-segmental coordination and stride characteristics in walking and running. They highlighted that "walking and running entail similar, albeit speed- and gait-dependent, coordination structures." Their finding suggested that similar neural circuits in the spinal cord control the two locomotion tasks walking and running (Lamoth et al., 2009). d'Avella et al. (2003) came to a similar conclusion when they related muscle activity patterns to movement kinematics in frogs. They proposed the "existence of a substantial amount of shared structure in the control of different tasks" as well as "the existence of behavior-specific synergies." They concluded that mixing behavior-independent and behavior-specific modules allows for the execution of different, complex behaviors. Overall, the link between muscle synergies, kSYN and movement production can be described as follow: a certain set of muscle synergies are required to produce a movement and the consequence of activating muscle synergies leads to the activation of the associated kSYN. This leads to the assumption that the CNS

can benefit from a flexible combination of kSYN as supplements to muscular synergies for a range of similar movements.

Taken together, how and to what extend whole body kSYN are utilized across varying locomotion tasks has not yet been studied extensively. However, a deeper understanding on a cross-task use of whole body kSYN can help to better understand how the CNS takes advantage of a modular control architecture to efficiently solve the degrees of freedom problem in locomotion tasks. Therefore, the purpose of this study was to examine similarities in whole body kSYN between varying locomotion tasks by investigating straight-line walking, walking a 90° spin turn and walking upstairs. We expected that: (1) characteristic kSYN for the three tasks are identifiable and (2) certain kSYN repeatedly occur across the three tasks due to their similarity.

MATERIALS AND METHODS

Participants

Thirteen male volunteers (age 26.1 ± 2.9 years; height 178.7 ± 5.5 cm; body mass 78.4 ± 5.9 kg) participated in this study. All participants were physically active and had no known history of neurological or motor disorders or injuries over the last 6 months. The study was approved by the ethics committee of the Karlsruhe Institute of Technology. All participants were informed of the experimental procedures and gave informed written consent prior to study participation.

Data Acquisition

Full body kinematic data of straight-line walking (SW), walking a 90° spin turn (WT), and walking upstairs (WU), as tasks among the most common forms of human gait (Riener et al., 2002; Glaister et al., 2007), were collected using a marker-based motion capture system (Vicon Motion Systems Ltd., Oxford, UK) with a sampling rate of 200 Hz. Eighteen passive-reflective markers were placed bilaterally on the participants' forehead, shoulder, elbow, hand, pelvis, knee, ankle, heel, and forefoot following previous studies (Daffertshofer et al., 2004; Federolf et al., 2013). SW trials were collected while participants walked overground. For the WT trial, participants followed a path with a 90° curve to the right drawn on the ground. They were instructed to use a spin turn strategy, which means that they had to perform their first turning step with the left foot (Taylor et al., 2005). A staircase of seven steps was used to collect the WU trials. The stair tread had a height of 0.17 m, which is right in the middle of the DIN-normed range for stair treads (DIN 18065). All locomotion tasks were performed at a self-selected speed. Prior to the recording of one valid trial for each specific locomotion task, participants were given two to three practice trials per locomotion task.

Data Processing

Vicon Nexus software (V. 1.8.5, Oxford, UK) was used to produce gap-free 3D marker trajectories. Further data processing steps were carried out in Matlab (The MathWorks Inc., Natick, MA, USA). 3D marker trajectories were low-pass filtered (Butterworth 4th order) at a cut-off frequency of 15 Hz. Gait cycles for the left leg were identified by determining initial contact as the minimum of the vertical heel marker trajectories for SW and WT. The minimum of the forefoot marker was determined to identify gait cycles during WU, as the initial contact with the stair was made with the forefoot (Riener et al., 2002). Data were extracted from the gait cycle at the mid-point of the walkway, the turning step, in the middle of the three turning phases of approach, turning and departure (Dixon et al., 2013), and at the mid-point of the stairs as representative for SW, WT, and WU, respectively. Gait cycles were time-normalized to 100 data points. All marker coordinates were expressed relative to the horizontal position of the pelvis, i.e., the horizontal center of the pelvis markers was subtracted from all marker coordinates. To minimize the influence of anthropometric differences on the calculation of the kSYN, the mean over the analyzed period was subtracted and the marker trajectories were normalized to unit standard deviation (Daffertshofer et al., 2004). Based on the normalized marker trajectories, a movement data matrix was formed for each task. The dimension of the matrices was 1,300 (13 participants × 100 time points) × 54 (18 markers × 3D coordinates).

Extraction of Kinematic Synergies

kSYN for each task were extracted by applying PCA to the corresponding movement data matrices. PCA was performed using singular value decomposition. Each PCA yielded (i) principal component vectors PC_k, (ii) eigenvalues EV_k, and (iii) scores (Daffertshofer et al., 2004; Federolf et al., 2013; Wang et al., 2013). The PC_k indicate the directions of the largest variations in the movement data matrix. The eigenvalues indicate the fraction of the total variance accounted for by each PC_k. The scores contain the projections of the original movement data onto each PC_k. k denotes the order of the eigenvectors. The components, i.e., loadings of the PC_k, quantify the contribution of the original variables (1D marker coordinates) to a specific kSYN (Esbensen et al., 2002). A high loading value indicates that this variable strongly loads on a particular kSYN. Loadings were expressed as absolute values. To provide an intuitive interpretation of the kSYN, they were visualized as two-dimensional stick figures in the original marker coordinates (Federolf et al., 2012; Haid et al., 2018). This included the projection of individual scores on specific PC_k and the rescinding of the normalization (multiply by the standard deviation of the time series and add mean of the time series). Consequently, isolated deviations from the mean body position of an individual caused by a single kSYN could be represented graphically. **Figure 1** exemplifies the full movement as well as the first extracted kSYN of SW for one participant.

Similarity Analysis

The similarities between the first five kSYN according to their eigenvalues (Wang et al., 2013; Zago et al., 2017c) of the three different locomotion tasks were quantified using cosine similarity (SIM; Singh et al., 2018). SIM is a vector-based similarity measure ranging from 0 (no similarity) to 1 (high similarity), as long as all components of the vector are positive (Zhang, 2008). A SIM between two kSYN > 0.8 is interpreted as highly similar (Xiao et al., 2008; Song and Chen, 2013; Saito et al., 2018). The SIM

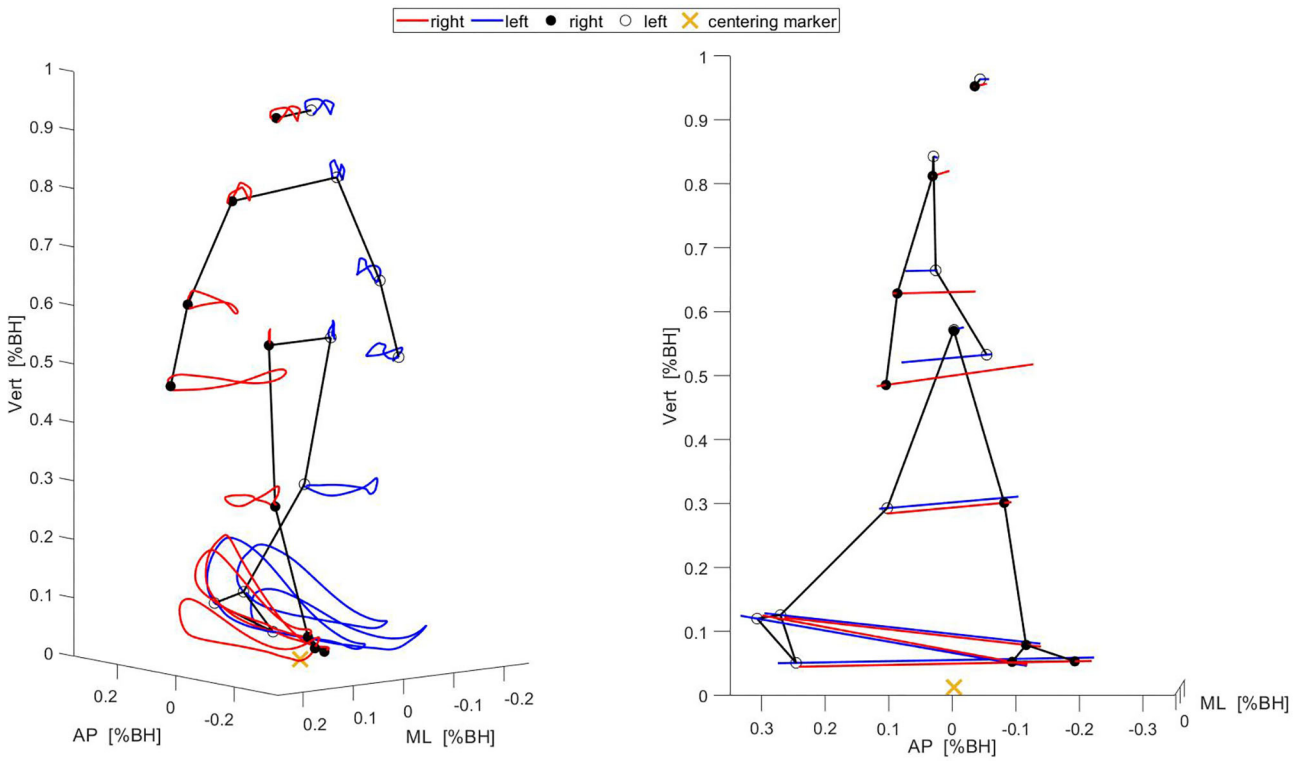

FIGURE 1 | Illustration of the full movement (Left) and the first kSYN (Right) of one gait cycle while the participant walked in a straight line. The stick figures show the marker positions at the beginning of the gait cycle. The red and blue lines show the marker trajectories over the whole gait cycle. AP, anterior-posterior; ML, medial-lateral; Vert, vertical; BH, body height.

between two kSYN is calculated as follows:

$$SIM\left(\overrightarrow{PC_n}, \overrightarrow{PC_m}\right) = \frac{\sum_{i=1}^{54} PC_{n,i} * PC_{m,i}}{\sqrt{\sum_{i=1}^{54} PC_{n,i}{}^2} * \sqrt{\sum_{i=1}^{54} PC_{m,i}{}^2}}$$

where $\overrightarrow{PC_n}$ and $\overrightarrow{PC_m}$ refer to the corresponding principal component loading vectors of the two kSYN under comparison, and *i* indicates the vector component. According to the equation, two kSYN were considered similar if the same variables load equally on both kSYN, and this is reflected in a high SIM value. SIM has been shown to produce high quality results across different fields (Lee et al., 2011; Xhafa et al., 2014).

RESULTS

Identified Kinematic Synergies

The aspects of the whole movement represented by each kSYN are listed in **Table 1** and visualized in the videos submitted as **Supplementary Materials**. Together, the first five kSYN explained 83.9, 91.1, and 86.5% of the variance in the kinematic data for SW, WT, and WU, respectively.

Similarities Between Kinematic Synergies

SW and WT showed two highly similar kSYN (**Table 1**): one between SW3 and WT3 (SIM = 0.89) and the second between SW1 and WT2 (SIM = 0.84). All other comparisons between SW and WT yielded SIM < 0.79.

SW and WU showed three highly similar kSYN (**Table 1**): one between SW1 and WU2 (SIM = 0.85), the second between SW2 and WU3 (SIM = 0.84), and the third between SW4 and WU5 (SIM = 0.83). All other comparisons between SW and WU yielded SIM < 0.77.

WU and WT showed two highly similar kSYN (**Table 1**): one between WU2 and WT2 (SIM = 0.86) and the second between WU1 and WT3 (SIM = 0.84). All other comparisons between WT and WU yielded SIM < 0.78.

Figure 2 illustrates similarities between the kinematic synergies of the three investigated locomotion tasks.

DISCUSSION

The current study examined similarities in kSYN across three common locomotion tasks: straight-line walking, walking a 90° spin turn and walking upstairs. Previous research in motor control has highlighted that the CNS organizes movement by flexible combinations of a low number of synergies (d'Avella, 2016; Lambert-Shirzad and van der Loos, 2017; Bruton and O'Dwyer, 2018). Based on the current literature, we expected that: (1) we could identify characteristic kSYN for the three tasks and (2) certain kSYN would repeatedly occur across the

TABLE 1 | Description of the first five kinematic synergies (kSYN) of the three different locomotion tasks.

kSYN	EV [%]	Characterization	SIM > 0.80
STRAIGHT-LINE WALKING (SW)			
SW1	37.0	Anteversion and retroversion of the arms and legs	WU2 (0.85), WT2 (0.84)
SW2	21.6	Countercyclical knee flexion/extension with countercyclical rising and lowering of the heels	WU3 (0.84)
SW3	15.9	Upwards/downwards movement of the body	WT3 (0.89)
SW4	5.4	Cyclical knee flexion/extension with anteversion/retroversion of the arm	WU5 (0.83)
SW5	4.0	Cyclical knee flexion/extension with hip flexion/extension	
WALKING 90° SPIN TURN (WT)			
WT1	43.1	Whole body rotation around the longitudinal axis	
WT2	23.3	Anteversion and retroversion of the arms and legs	SW1 (0.84), WU2 (0.86)
WT3	14.4	Upwards/downwards movement of the body with unilateral knee flexion	SW3 (0.89), WU1 (0.84)
WT4	8.1	Knee flexion of the swing leg with minor upper body rotation around the longitudinal axis	
WT5	2.2	Whole body rotation around the longitudinal axis with synchronous knee flexion/extension	
WALKING UPSTAIRS (WU)			
WU1	39.8	Upwards movement of the body with unilateral knee flexion	WT3 (0.84)
WU2	28.9	Anteversion and retroversion of the arms and legs	WT2 (0.86), SW1 (0.85)
WU3	9.6	Countercyclical knee flexion/extension with upwards movement of the body	SW2 (0.84)
WU4	4.5	Forward/backward leaning of the upper body	
WU5	3.7	Synchronous knee and arm flexion	SW4 (0.83)

The eigenvalues (EV) indicate the fraction of the total variance accounted for by each kSYN. The right-hand column shows the highly similar kSYN (cosine similarity (SIM) >0.80) across the different locomotion tasks.

three tasks due to the similarity of the locomotion involved. For this purpose, similarities in kSYN were compared across the three tasks. The study revealed that (1) the first five kSYN accounted for more than 83.9% of the total variance of each task and (2) two to three kSYN were in common across the three tasks, while other kSYN were task specific. Common kSYN across the three tasks predominantly represented the anteversion and retroversion of the arms and legs, the upwards/downwards movement of the body and flexion/extension movements of the knees. In consequence, the results confirm our hypotheses and help to gain a deeper understanding on the construction of locomotion movements.

Identification of Kinematic Synergies

Previous studies investigating whole body kinematics showed a reduction of control-relevant degrees of freedom via kSYN for various tasks including locomotion (Troje, 2002; Daffertshofer et al., 2004; Lamoth et al., 2009; Federolf et al., 2013), balance tasks (Federolf, 2016; Haid et al., 2018), and more complex movements (Hollands et al., 2004; Zago et al., 2017a). In line with related studies on whole body gait patterns for straight-line walking (Daffertshofer et al., 2004; Majed et al., 2017), we found a small number of compositional elements that described the essential features of gait: a combination of five kSYN explained 83.9% of the variance in the kinematic data. A comparable reduction to control relevant degrees of freedom during curved walking was reported by Courtine and Schieppati (2004) when they analyzed the limb segments and the trunk. Similarly, in an earlier study, Borghese et al. (1996) described the existence of laws of intersegmental coordination when investigating lower limb kinematics during walking. The authors observed regular loops on a plane for the elevation angles of the limb segment (pelvis, thigh, shank, and foot), despite large excursions of the individual angles, across six males. Lacquaniti et al. (2012) further reported in their review on patterned control of human locomotion that the so-called planar covariance corresponds with muscle activation patterns in order to simplify the problem of control of multi-segmental movements. Studies at the muscular level also suggest that movement tasks are performed using combined synergies (Cappellini et al., 2006; Bejarano et al., 2017; Bruton and O'Dwyer, 2018; Maguire et al., 2019). Additionally, animal studies support that the nervous system may use global variables having fewer degrees of freedom for controlling locomotion (Ivanenko et al., 2007; Catavitello et al., 2018). Catavitello et al. (2018) underlined the existence of kSYN when investigating the planar covariation of limb segment motion across a wide range of animals in a more recent study. The authors stated that kSYN lie at the interface between neural command signals and the mechanics of locomotion. A closer look at the first five kSYN of the three analyzed tasks (**Table 1**) highlights the phenomenon described by Daffertshofer et al. (2004) that these components reflect movements oscillating at either the stride frequency (e.g., arm and leg swing) or the second harmonic (i.e., movement components that oscillate at double frequency of the stride frequency, such as knee bending). Our finding supports the idea that the CNS may use kSYN as a possible implementation of the idea of a modular control architecture to deal with the large number of degrees of freedom of the motor system. Moreover, results are in line with the idea of mixing of behavior-independent and behavior-specific modules for the execution of different, complex behaviors, described by d'Avella et al. (2003).

Occurrence of Kinematic Synergies Across Locomotion Tasks

Regarding a cross-task use of kSYN, our findings show a change in the prioritization of similar kSYN. SW1, as the highest prioritized kSYN of SW, showed high similarity to WT2 and WU2, which is downstream of a presumably more task-specific kSYN, such as the body's rotation around the longitudinal axis for WT and the vertical displacement of the center of mass for WU. Interestingly, kSYN with high similarity

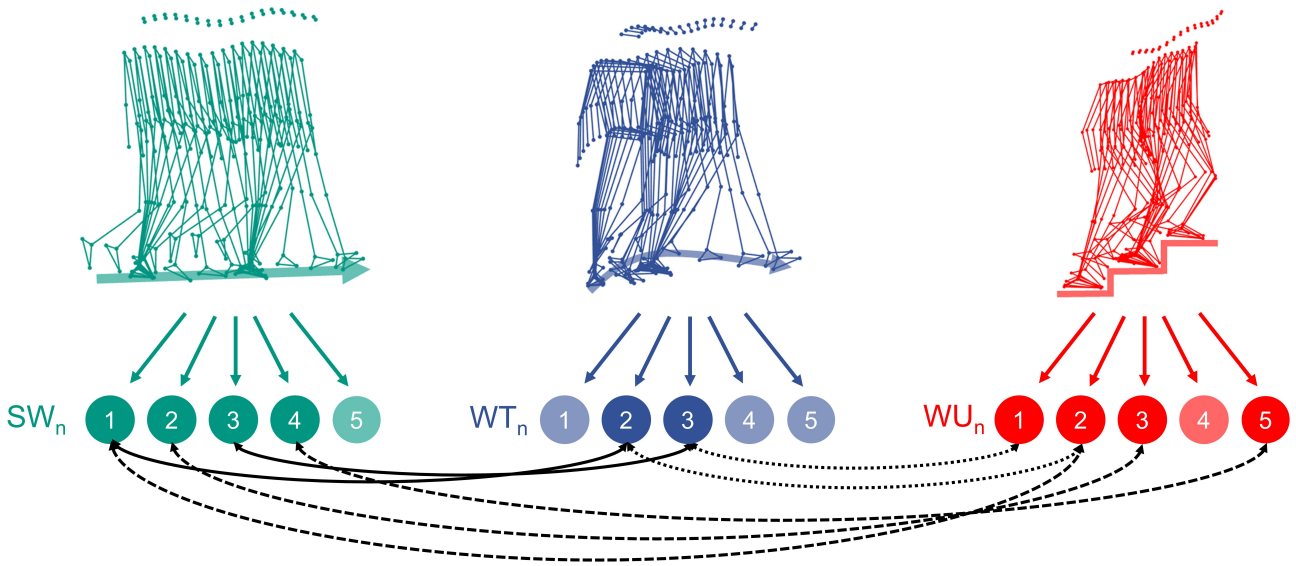

FIGURE 2 | Schematic representation of the three locomotion tasks (SW, straight-line walking; WT, walking 90° spin turn; WU, walking upstairs) and their decomposition into five main kinematic synergies. The black arrows highlight high similarities (cosine similarity >0.80) across the different locomotion tasks.

showed slight variations in their characteristic depending on the individual task. For example, the kSYN characterizing an upwards/downwards movement of the body with unilateral knee flexion in WT (WT3) was highly similar with the kSYN characterizing an upwards/downwards movement of the body in SW (SW3) and the kSYN characterizing an upwards movement of the body with unilateral knee flexion in WU (WU1). This finding indicates that the CNS has the capability to tune kSYN with the actual task requirements for a successful realization of the individual movement task.

The results of Lamoth et al. (2009) also indicate a cross-task use of kSYN. The authors concluded that walking and running entail similar kSYN (referred to in their study as coordinative structures), although these kSYN are speed- and gait-dependent. This finding is supported by similar phenomena at the muscular level during walking (Bejarano et al., 2017). Our findings suggest that, for movement construction in locomotion tasks, the CNS optimizes its kSYN selection: slightly adapt certain cross-task kSYN, reflected by a high SIM between tasks, and complement these by adding more task-specific kSYN to successfully realize the whole body movement.

The identified task-specific kSYN can be seen as a means to perform biomechanical subtasks (Maguire et al., 2019). Biomechanical subtasks of locomotion are, for example, generating body support and forward propulsion (McGowan et al., 2010). Previous research provides evidence that individual muscle synergies are associated with specific subtasks (McGowan et al., 2010; Maguire et al., 2019). This association between muscle synergies and specific subtasks is potentially reflected by the corresponding kSYN, which can be seen as representative for the biomechanical subtasks. For example, the kSYN characterizing the upwards/downwards movement of the body (SW3, WT3, and WU1) can be linked to the biomechanical subtask of generating body support. The result of combined activation of such functional units or referent coordinates form the whole movement for a specific motor task (Latash, 2020). Research on the origin of synergies and the linkage between kSYN and muscle synergies have produced results compatible with this idea (Tagliabue et al., 2015; Leo et al., 2016; Latash, 2020). Overall, the finding of this study—that pronounced kSYN repeatedly occur across the three investigated locomotion tasks—supports the idea that the CNS ensures movement organization by flexible combinations of a low number of synergies representing the idea of a modular control architecture.

The lower correlation between the kSYN in SW and WT (two kSYN with similar characteristics) compared to the relationships between the kSYN in SW and WU (three kSYN with similar characteristics) is possibly due to a greater asymmetry in the motion execution in WT. Asymmetries in WT are caused by rotation about the longitudinal axis and are characterized by different stride lengths (Orendurff et al., 2006). Comparable asymmetries are typically not present in WU (Andriacchi et al., 1980). Overall, it must be noted that the three investigated locomotion tasks can be performed with different strategies, e.g., walking a turn as a spin or step turn (Dixon et al., 2013) or walking upstairs using the step-over-step or step-by-step strategy (Reid et al., 2007), and at different velocities. Furthermore, turning is subdivided in three phases, namely approach, turning, and departure, that are characterized by biomechanical differences (Dixon et al., 2013). However, it remains unsolved how such differences in movement execution affect the kSYN structure and further research would be indispensable to obtain a more detailed understanding how the CNS can benefit from a flexible combination of kSYN.

Limitations

One consideration worth noting is that the kSYN were calculated based on single gait cycles per participant. Whether the incorporation of multiple trials per participant results in slightly different kSYN remains speculative and should be addressed in the future. The rather small and homogeneous group of participants consisting of 13 males potentially limits the outcome with respect to a general explanation for the mechanisms underlying human motor coordination. Nonetheless, future studies may benefit from the presented approach in this study. Whole body movements were reduced to five kSYN, which covered about 85–90% of the variance in the data. Thus, it can be assumed that the major part of relevant movement aspects is considered. Nonetheless, if the remaining 10–15% of the variance also contains relevant kSYN that could simplify the construction of various locomotion tasks cannot be answered. The investigation of higher order kSYN can be difficult, as such components rather represent movement components of the individual movement execution than common movement components across participants and they are more likely to be susceptible to noise (Federolf et al., 2012, 2014; Wang et al., 2013). Another limitation is that the qualitative descriptions of the kSYN represent subjective interpretations. As the interpretation of the kSYN depends on the decomposition method, this is a potential limitation of the study. The applied PCA approach is a linear decomposition method and the use of different matrix factorization methods could result in a different outcome (Lambert-Shirzad and van der Loos, 2017). In addition, when applying the PCA to marker coordinates, the complex, high-dimensional movements of all markers are transformed into a set of one-dimensional movement components (kSYN). These components of movements cannot necessarily be performed in an isolated form by humans, and instead result from a combination of actual movements (Federolf, 2016). Similarly, it must be mentioned that studies using matrix factorization methods to extract synergies reflect biomechanical constraints of the task and their link to underlying neural strategies of motor control has not been fully explored yet (Lambert-Shirzad and van der Loos, 2017). Finally, the extraction of kSYN using matrix factorization algorithms provide a descriptive model of covariations among segment movements.

Conclusion

In this study we reported on similarities between kSYN of varying tasks. This study demonstrated that SW, WT, and WU are characterized by kSYN and that certain kSYN repeatedly occur across the three locomotion tasks. In addition to a more detailed analysis of the relationship between kinematic and muscular synergies, future interventions should examine whether such synergies serve as a causal explanatory model. This means that, against the background of a modular control architecture, the ease of learning a task depends on its compatibility with existing synergies. The idea of a modular control architecture addresses an important issue on the interface of theory and practice. In the future, a clear understanding of the kSYN structure of everyday and sport movements could affect the design of neurorehabilitation programs or practice protocols in sport trough targeted exercises for regaining and improving motor function.

DATA AVAILABILITY STATEMENT

The raw data supporting the conclusions of this article will be made available by the authors, without undue reservation.

ETHICS STATEMENT

The studies involving human participants were reviewed and approved by ethics committee of the Karlsruhe Institute of Technology. The patients/participants provided their written informed consent to participate in this study.

AUTHOR CONTRIBUTIONS

BS, MH, SS, and TS were involved in the design of the study. BS and MH carried out all data collection and analysis. BS, MH, FM, and TS were involved in the interpretation and discussion of the results. BS took the lead in writing the manuscript. All authors provided critical feedback and contributed to the final manuscript.

FUNDING

This research did not receive any specific grant from funding agencies in the public, commercial, or not-for-profit sectors. We acknowledge support by the KIT-Publication Fund of the Karlsruhe Institute of Technology.

SUPPLEMENTARY MATERIAL

The Supplementary Material for this article can be found online at: https://www.frontiersin.org/articles/10.3389/fspor.2020.596063/full#supplementary-material

REFERENCES

Andriacchi, T. P., Andersson, G. B., Fermier, R. W., Stern, D., and Galante, J. O. (1980). A study of lower-limb mechanics during stair-climbing. *J. Bone Joint Surg. Am.* 62, 749–757. doi: 10.2106/00004623-198062050-00008

Bejarano, C. N., Pedrocchi, A., Nardone, A., Schieppati, M., Baccinelli, W., Monticone, M., et al. (2017). Tuning of muscle synergies during walking along rectilinear and curvilinear trajectories in humans. *Ann. Biomed. Eng.* 45, 1204–1218. doi: 10.1007/s10439-017-1802-z

Bernstein, N. (1967). The co-ordination and regulation of movements. *Science* 26, 415–416. doi: 10.1126/science.159.3813.415-a

Bizzi, E., Mussa-Ivaldi, F. A., and Giszter, S. (1991). Computations underlying the execution of movement: a biological perspective. *Science* 253, 287–291. doi: 10.1126/science.1857964

Borghese, N. A., Bianchi, L., and Lacquaniti, F. (1996). Kinematic determinants of human locomotion. *J. Physiol. 494(Pt* 3), 863–879. doi: 10.1113/jphysiol.1996.sp021539

Bruton, M., and O'Dwyer, N. (2018). Synergies in coordination: a comprehensive overview of neural, computational and behavioral approaches. *J. Neurophysiol.* 120, 2761–2774. doi: 10.1152/jn.00052.2018

Cappellini, G., Ivanenko, Y. P., Poppele, R. E., and Lacquaniti, F. (2006). Motor patterns in human walking and running. *J. Neurophysiol.* 95, 3426–3437. doi: 10.1152/jn.00081.2006

Catavitello, G., Ivanenko, Y., and Lacquaniti, F. (2018). A kinematic synergy for terrestrial locomotion shared by mammals and birds. *eLife* 7:e38190. doi: 10.7554/eLife.38190.028

Courtine, G., Roy, R. R., Hodgson, J., McKay, H., Raven, J., Zhong, H., et al. (2005). Kinematic and EMG determinants in quadrupedal locomotion of a non-human primate (Rhesus). *J. Neurophysiol.* 93, 3127–3145. doi: 10.1152/jn.01073.2004

Courtine, G., and Schieppati, M. (2004). Tuning of a basic coordination pattern constructs straight-ahead and curved walking in humans. *J. Neurophysiol.* 91, 1524–1535. doi: 10.1152/jn.00817.2003

Daffertshofer, A., Lamoth, C. J. C., Meijer, O. G., and Beek, P. J. (2004). PCA in studying coordination and variability: a tutorial. *Clin. Biomech.* 19, 415–428. doi: 10.1016/j.clinbiomech.2004.01.005

d'Avella, A. (2016). Modularity for motor control and motor learning. *Adv. Exp. Med. Biol.* 957, 3–19. doi: 10.1007/978-3-319-47313-0_1

d'Avella, A., Saltiel, P., and Bizzi, E. (2003). Combinations of muscle synergies in the construction of a natural motor behavior. *Nat. Neurosci.* 6, 300–308. doi: 10.1038/nn1010

Dixon, P. C., Stebbins, J., Theologis, T., and Zavatsky, A. B. (2013). Spatio-temporal parameters and lower-limb kinematics of turning gait in typically developing children. *Gait Posture* 38, 870–875. doi: 10.1016/j.gaitpost.2013.04.010

Esbensen, K. H., Guyot, D., Westad, F., and Houmoller, L. P. (2002). *Multivariate data analysis: in Practice: An Introduction to Multivariate Data Analysis and Experimental Design* (Oslo: CAMO), 19–75.

Federolf, P., Reid, R., Gilgien, M., Haugen, P., and Smith, G. (2014). The application of principal component analysis to quantify technique in sports. *Scand. J. Med. Sci. Sports* 24, 491–499. doi: 10.1111/j.1600-0838.2012.01455.x

Federolf, P., Tecante, K., and Nigg, B. (2012). A holistic approach to study the temporal variability in gait. *J. Biomech.* 45, 1127–1132. doi: 10.1016/j.jbiomech.2012.02.008

Federolf, P. A. (2016). A novel approach to study human posture control: "Principal movements" obtained from a principal component analysis of kinematic marker data. *J. Biomech.* 49, 364–370. doi: 10.1016/j.jbiomech.2015.12.030

Federolf, P. A., Boyer, K. A., and Andriacchi, T. P. (2013). Application of principal component analysis in clinical gait research: identification of systematic differences between healthy and medial knee-osteoarthritic gait. *J. Biomech.* 46, 2173–2178. doi: 10.1016/j.jbiomech.2013.06.032

Franklin, D. W., and Wolpert, D. M. (2011). Computational mechanisms of sensorimotor control. *Neuron* 72, 425–442. doi: 10.1016/j.neuron.2011.10.006

Giszter, S. F. (2015). Motor primitives—new data and future questions. *Curr. Opin. Neurobiol.* 33, 156–165. doi: 10.1016/j.conb.2015.04.004

Glaister, B. C., Bernatz, G. C., Klute, G. K., and Orendurff, M. S. (2007). Video task analysis of turning during activities of daily living. *Gait Posture* 25, 289–294. doi: 10.1016/j.gaitpost.2006.04.003

Haid, T. H., Doix, A.-C. M., Nigg, B. M., and Federolf, P. A. (2018). Age effects in postural control analyzed via a principal component analysis of kinematic data and interpreted in relation to predictions of the optimal feedback control theory. *Front. Aging Neurosci.* 10:22. doi: 10.3389/fnagi.2018.00022

Hollands, K., Daffertshofer, A., and Wing, A. M. (2004). "Principal components analysis of contemporary dance kinematics," in *Proceedings of the 3rd IEEE EMBSS UK & RI* (Southampton: University of Southampton).

Ivanenko, Y. P., Cappellini, G., Dominici, N., Poppele, R. E., and Lacquaniti, F. (2007). Modular control of limb movements during human locomotion. *J. Neurosci.* 27, 11149–11161. doi: 10.1523/JNEUROSCI.2644-07.2007

Kelso, S. J. A., Putnam, C. A., and Goodman, D. (1983). On the space-time structure of human interlimb co-ordination. *Quart. J. Exp. Psychol. Sect. A* 35, 347–375. doi: 10.1080/14640748308402139

Lacquaniti, F., Ivanenko, Y. P., and Zago, M. (2012). Patterned control of human locomotion. *J. Physiol.* 590, 2189–2199. doi: 10.1113/jphysiol.2011.215137

Lacquaniti, F., Soechting, J. F., and Terzuolo, S. A. (1986). Path constraints on point-to-point arm movements in three-dimensional space. *Neuroscience* 17, 313–324. doi: 10.1016/0306-4522(86)90249-6

Lambert-Shirzad, N., and van der Loos, H. F. M. (2017). On identifying kinematic and muscle synergies: a comparison of matrix factorization methods using experimental data from the healthy population. *J. Neurophysiol.* 117, 290–302. doi: 10.1152/jn.00435.2016

Lamoth, C. J. C., Daffertshofer, A., Huys, R., and Beek, P. J. (2009). Steady and transient coordination structures of walking and running. *Hum. Mov. Sci.* 28, 371–386. doi: 10.1016/j.humov.2008.10.001

Latash, M. L. (2020). On primitives in motor control. *Motor Control.* 24, 318–346. doi: 10.1123/mc.2019-0099

Lee, D., Park, J., Shim, J., and Lee, S.-G. (2011). Efficient filtering techniques for cosine similarity joins. *Information.* 14, 1265–90.

Leo, A., Handjaras, G., Bianchi, M., Marino, H., Gabiccini, M., Guidi, A., et al. (2016). A synergy-based hand control is encoded in human motor cortical areas. *eLife* 5:e13420. doi: 10.7554/eLife.13420

Maguire, C. C., Sieben, J. M., and de Bie, R. A. (2019). Movement goals encoded within the cortex and muscle synergies to reduce redundancy pre and post-stroke. *The relevance for gait rehabilitation and the prescription of walking-aids. A literature review and scholarly discussion. Physiother. Theory Pract.* 35, 1–14. doi: 10.1080/09593985.2018.1434579

Majed, L., Heugas, A. M., and Siegler, I. A. (2017). Changes in movement organization and control strategies when learning a biomechanically constrained gait pattern, racewalking: a PCA study. *Exp. Brain Res.* 235, 931–940. doi: 10.1007/s00221-016-4853-8

McGowan, C. P., Neptune, R. R., Clark, D. J., and Kautz, S. A. (2010). Modular control of human walking: adaptations to altered mechanical demands. *J. Biomech.* 43, 412–419. doi: 10.1016/j.jbiomech.2009.10.009

Orendurff, M. S., Segal, A. D., Berge, J. S., Flick, K. C., Spanier, D., and Klute, G. K. (2006). The kinematics and kinetics of turning: limb asymmetries associated with walking a circular path. *Gait Posture* 23, 106–111. doi: 10.1016/j.gaitpost.2004.12.008

Reid, S. M., Lynn, S. K., Musselman, R. P., and Costigan, P. A. (2007). Knee biomechanics of alternate stair ambulation patterns. *Med. Sci. Sports Exerc.* 39, 2005–2011. doi: 10.1249/mss.0b013e31814538c8

Riener, R., Rabuffetti, M., and Frigo, C. (2002). Stair ascent and descent at different inclinations. *Gait Posture* 15, 32–44. doi: 10.1016/S0966-6362(01)00162-X

Saito, A., Tomita, A., Ando, R., Watanabe, K., and Akima, H. (2018). Muscle synergies are consistent across level and uphill treadmill running. *Sci. Rep.* 8:5979. doi: 10.1038/s41598-018-24332-z

Scholz, J. P., and Schöner, G. (1999). The uncontrolled manifold concept: identifying control variables for a functional task. *Exp. Brain Res.* 126, 289–306. doi: 10.1007/s002210050738

Singh, R. E., Iqbal, K., and White, G. (2018). "Muscle synergy adaptation during a complex postural stabilization task," in *Advanced Systems for Enhancing Human Health: BioCAS 2018, Biomedical Circuits and Systems Conference: Cleveland, Ohio, USA, October 17-19, 2018* (Piscataway, NJ: *IEEE),* 1–4.

Song, S., and Chen, L. (2013). Efficient discovery of similarity constraints for matching dependencies. *Data Knowl. Eng.* 87, 146–166. doi: 10.1016/j.datak.2013.06.003

Tagliabue, M., Ciancio, A. L., Brochier, T., Eskiizmirliler, S., and Maier, M. A. (2015). Differences between kinematic synergies and muscle synergies during two-digit grasping. *Front. Hum. Neurosci.* 9:165. doi: 10.3389/fnhum.2015.00165

Taylor, M. J. D., Dabnichki, P., and Strike, S. C. (2005). A three-dimensional biomechanical comparison between turning strategies during the stance phase of walking. *Hum. Mov. Sci.* 24, 558–573. doi: 10.1016/j.humov.2005.07.005

Todorov, E., and Jordan, M. I. (2002). Optimal feedback control as a theory of motor coordination. *Nat. Neurosci.* 5, 1226–1235. doi: 10.1038/nn963

Troje, N. F. (2002). Decomposing biological motion: a framework for analysis and synthesis of human gait patterns. *J. Vis.* 2, 371–387. doi: 10.1167/2.5.2

Wang, X., O'Dwyer, N., and Halaki, M. (2013). A review on the coordinative structure of human walking and the application of principal component analysis. *Neural Regen. Res.* 8, 662–670. doi: 10.3969/j.issn.1673-5374.2013.07.011

Wolpert, D. M., Pearson, K. G., and Ghez, C. P. J. (2013). "The organization and planning of movement," in *Principles of Neural Science, 5th ed.* eds E. Kandel, J.

Schwartz, T. Jessell, S. Siegelbaum, and A. Hudspeth (New York, NY; London: McGraw-Hill Publishing), 743–767.

Wolpert, D. M., and Kawato, M. (1998). Multiple paired forward and inverse models for motor control. *Neural Netw.*11, 1317–1329. doi: 10.1016/S0893-6080(98)00066-5

Xhafa, F., Barolli, L., Barolli, A., and Papajorgji, P. (2014). *Modeling and Processing for Next-Generation Big-Data Technologies: With Applications and Case Studies*. Springer International Publishing. doi: 10.1007/978-3-319-09177-8

Xiao, C., Wang, W., Lin, X., and Yu, J. X. (2008). *Efficient Similarity Joins for Near Duplicate Detection*. Beijing: ACM. doi: 10.1145/1367497.1367516

Zago, M., Codari, M., Iaia, F. M., and Sforza, C. (2017a). Multi-segmental movements as a function of experience in karate. *J. Sports Sci.* 35, 1515–1522. doi: 10.1080/02640414.2016.1223332

Zago, M., Pacifici, I., Lovecchio, N., Galli, M., Federolf, P. A., and Sforza, C. (2017b). Multi-segmental movement patterns reflect juggling complexity and skill level. *Hum. Mov. Sci.* 54, 144–153. doi: 10.1016/j.humov.2017.04.013

Zago, M., Sforza, C., Bona, A., Cimolin, V., Costici, P. F., Condoluci, C., et al. (2017c). How multi segmental patterns deviate in spastic diplegia from typical developed. *Clin. Biomech.* 48, 103–109. doi: 10.1016/j.clinbiomech.2017.07.016

Zhang, J. (2008). *Visualization for Information Retrieval*. Berlin; Heidelberg: Springer-Verlag.

Conflict of Interest: The authors declare that the research was conducted in the absence of any commercial or financial relationships that could be construed as a potential conflict of interest.

frontiers in Human Neuroscience

ORIGINAL RESEARCH
published: 20 November 2020
doi: 10.3389/fnhum.2020.592021

Modification of Eye–Head Coordination With High Frequency Random Noise Stimulation

Yusuke Maeda[1], Makoto Suzuki[2]*, Naoki Iso[2], Takuhiro Okabe[2], Kilchoon Cho[2] and Yin-Jung Wang[3]*

[1] Department of Physical Therapy, School of Health Sciences at Odawara, International University of Health and Welfare, Kanagawa, Japan, [2] Faculty of Health Sciences, Tokyo Kasei University, Saitama, Japan, [3] Day-care Center, Yamagata, Japan

The vestibulo-ocular reflex (VOR) plays an important role in controlling the gaze at a visual target. Although patients with vestibular hypofunction aim to improve their VOR function, some retain dysfunction for a long time. Previous studies have explored the effects of direct current stimulation on vestibular function; however, the effects of random noise stimulation on eye–head coordination have not previously been tested. Therefore, we aimed to clarify the effects of high frequency noisy vestibular stimulation (HF-nVS) on eye–head coordination related to VOR function. Thirteen healthy young adult participants with no serious disease took part in our study. The current amplitude and density used were 0.4 mA and 0.2 mA/cm^2, respectively, with a random noise frequency of 100–640 Hz. The electrodes were located on both mastoid processes. The stimulus duration and fade in/out duration were 600 and 10 s, respectively. Subjects oscillated their head horizontally, gazing at the fixation point, at 1 Hz (0.5 cycles/s) for 30 repetitions. The coordination of eye–head movements was measured by eye-tracking and a motion capture system. Peak-to-peak angles for eye and head movement and deviation of the visual line from the fixation target revealed no significant differences between HF-nVS and sham. The lag time between the eye and head movement with HF-nVS post-stimulation was significantly shorter than that of the sham. We found that HF-nVS can reduce the lag time between eye and head movement and improve coordination, contributing to a clear retinal image. This technique could be applied as a form of VOR training for patients with vestibular hypofunction.

Keywords: **vestibulo-ocular reflex, eye–head coordination, fixation, lag time, high frequency noisy vestibular stimulation**

OPEN ACCESS

Edited by:
Yury Ivanenko,
Santa Lucia Foundation (IRCCS), Italy

Reviewed by:
Chris Dakin,
Utah State University, United States
Viviana Mucci,
Western Sydney University, Australia

****Correspondence:***
Yusuke Maeda
y.maeda@iuhw.ac.jp
Makoto Suzuki
maksuzu@gmail.com

Specialty section:
This article was submitted to Motor Neuroscience, a section of the journal Frontiers in Human Neuroscience

Received: *06 August 2020*
Accepted: *15 October 2020*
Published: *20 November 2020*

Citation:
Maeda Y, Suzuki M, Iso N, Okabe T, Cho K and Wang Y-J (2020) Modification of Eye–Head Coordination With High Frequency Random Noise Stimulation. Front. Hum. Neurosci. 14:592021. doi: 10.3389/fnhum.2020.592021

INTRODUCTION

When we look at an object in the world around us, eye–head coordination is vital to accurately identifying that object. The vestibulo-ocular reflex (VOR) functions to correct eye movements during head movement and leads to the stable and sharp foveal vision of the object (Chin, 2018). The vestibula, including three semicircular canals and otolith organs (utricle and saccule), can perceive angular velocity and the acceleration of the head (Yang et al., 2015). The VOR receives positional input from the vestibular afferents (Ischebeck et al., 2017, 2018) and sends signals to

the eye muscles and cerebellum, which send feedback signals to modulate or fine-tune the VOR (Wallace and Lifshitz, 2016). Thus, the position of the eyes affects the movement of the head.

It is well known that the vestibular nerves associated with both semicircular canals and otolith organs can be electrically stimulated (Fitzpatrick and Day, 2004; Uchino and Kushiro, 2011; Yang et al., 2015). Several previous studies applied a small direct current to the right and left mastoid processes behind the ear, and the firing rate of all vestibular afferents could be modified by the current (Fitzpatrick and Day, 2004; Uchino and Kushiro, 2011; Yang et al., 2015). Recently, Forbes et al. (2020) demonstrated that vestibular afferents were sensitive to alternating currents ranging randomly between low and high frequencies (0–300 Hz) known as Noisy Vestibular Stimulation, and the neck motor neurons were activated by vestibular stimulation. In addition, a review by Forbes et al. (2014) suggested that noisy vestibular stimulation with low to high frequencies and low amplitude could modify postural control. Moreover, some previous studies have applied low frequency with low amplitude (0–30 Hz and 0.3–0.5 mA, respectively) (Fujimoto et al., 2016; Wuehr et al., 2016) or low to high frequency with low amplitude noise vestibular stimulations (0.1–640 Hz and 0.4–1.0 mA, respectively) (Inukai et al., 2018) over the mastoid process. These studies suggested that noisy vestibular stimulation with low to high frequency with low amplitude improved walking performance (Wuehr et al., 2016) and standing balance (Fujimoto et al., 2016; Inukai et al., 2018). Meanwhile, to stimulate cortical neurons, a high frequency noise stimulation (100–640 Hz) can increase cortical excitation (Terney et al., 2008; Penton et al., 2018; Pavan et al., 2019). Specifically, high frequency random noisy stimulation between 100 and 640 Hz increased cortical neuron excitability, which lasted up to 60 min even after stimulation was stopped (Terney et al., 2008; Inukai et al., 2016). Others have demonstrated that high frequency noisy stimulation improves behavioral performance in visual detection and discrimination (Romanska et al., 2015; Campana et al., 2016; van der Groen and Wenderoth, 2016), perceptual learning (Fertonani et al., 2011; Camilleri et al., 2016; Moret et al., 2018), and arithmetic skills (Snowball et al., 2013; Pasqualotto, 2016; Popescu et al., 2016). In particular, the vestibular afferents were activated in response to high frequency noisy stimulation (Forbes et al., 2020). These results implied that the noise vestibular stimulation at high frequency might affect human behavior, mainly influenced by the vestibula.

Several studies (Uchino and Kushiro, 2011; Yang et al., 2015) and a review (Fitzpatrick and Day, 2004) have reported a direct current or step waveform that also alternates the direction of the current between step pulses. Although some studies have used noisy vestibular stimulation, they only assessed the activation of the vestibular afferents and neck motor neurons (Forbes et al., 2020), walking performance (Wuehr et al., 2016), and standing balance (Fujimoto et al., 2016; Inukai et al., 2018). The voluntary performance of eye–head coordination during high frequency and low amplitude noisy vestibular stimulation was not investigated. Therefore, although high frequency noisy vestibular stimulation (HF-nVS) can influence neural activity, it remains unclear whether eye–head coordination performance is affected by HF-nVS in the context of the VOR function. If, in addition to the knowledge provided by Forbes et al. (2020), the relationship between HF-nVS and eye–head coordination performance could be clarified, then we might understand better the nVS-induced modification processes for eye–head coordination and performance that occur in VOR functional modification. We, therefore, designed a paradigm involving eye–head coordination during HF-nVS. We predicted that if HF-nVS affects the VOR function, then HF-nVS should decrease the deviation from fixation targets and the time lag between the eye and head motions. We, therefore, investigated eye–head coordination during HF-nVS. Exploring how HF-nVS affects eye–head coordination tasks may have interesting implications for VOR training potential in behavioral science and neuroscience.

MATERIALS AND METHODS

Participants

Our target sample size was based on a 90% statistical power to detect changes in eye–head coordination with a 0.90 effect size and a two-sided α-level of 0.05. Inputting these parameters into the Hulley matrix (Hulley et al., 1988) yielded a sample size of 12. We recruited 13 healthy, neurologically intact subjects [two men and 11 women aged 21–48 years, mean ± standard deviation (SD): 33.4 ± 11.2 years] for the eye and head movement measurements. Screening for medication use and medical history was performed through an interview. Here, participants were also informed about the research, such as its purpose; procedures; duration of the experiment; potential risks, adverse effects, or discomfort that may occur; and the right to decline to participate in the study. None of the subjects took medications or had any psychiatric or neurological diseases. Our experimental procedures were approved by the Research Ethics Committee of the Tokyo Kasei University and performed following the principles of the Declaration of Helsinki. All subjects provided written informed consent prior to participation.

Recording of Reflexive Eye Movements

Each subject sat comfortably in front of a 0.5 cm diameter fixation target on the computer screen located 110 cm from the face at eye level (**Figure 1A**). Horizontal compensatory eye movement angles in response to sinusoidal horizontal head rotations were measured by an infrared camera (TalkEye Lite, Takei Scientific Instruments Co., Ltd., Tokyo, Japan) from the right eye during eye–head coordination tasks. The head rotation angle was recorded using the VICON motion capture system (Vicon Motion Systems, Ltd., Oxford, United Kingdom). Three infrared reflective markers (14 mm in diameter) were placed on the subject's forehead. The sampling frequency was 30 Hz for eye tracking and 100 Hz for motion capture, respectively.

In previous studies, the participant's head was passively turned approximately 5–15° at 0.1–33 s for VOR assessment (Halmagyi et al., 2017; Ischebeck et al., 2017, 2018). However, in daily living, when people actively turn their heads faster and wider and gaze at the fixation target, their eye movement can compensate for the head turn to maintain their gaze on

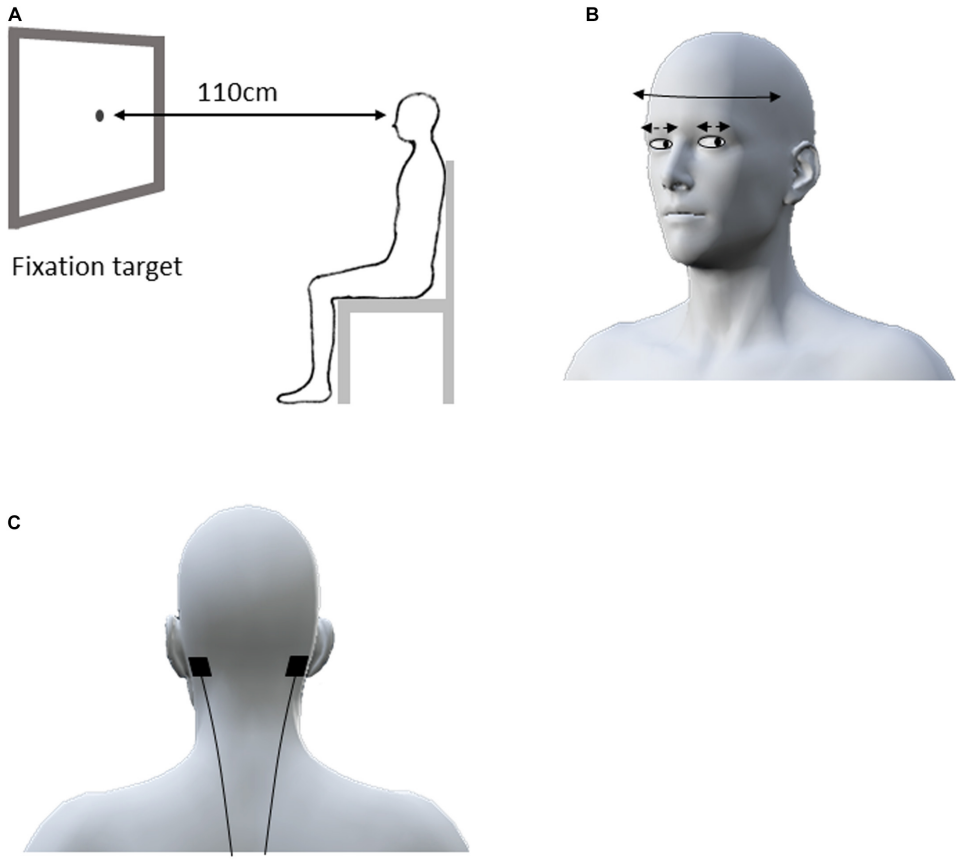

FIGURE 1 | Experimental design for the eye–head coordination task. The subject sat in front of a 0.5 cm fixation target on the computer screen located 110 cm from the face at eye level **(A)**. The subjects were asked to swing their head right and left alternately as far as possible for 30 s in accordance with the rhythm of a metronome at 1 Hz while staring at the fixation target **(B)**. During the eye–head coordination task, the electrodes for active and sham HF-nVS were positioned at either mastoid process **(C)**. HF-nVS, high frequency noise vestibular stimulation.

the target (Halmagyi et al., 2017). Therefore, in the eye–head coordination tasks of our study, each participant actively, widely, and horizontally performed head oscillations. Head oscillations occurred, with a gazing fixation point, at 1 Hz (0.5 cycles/s) for 30 repetitions. Specifically, to assess active eye–head coordination performance, we did not passively turn the participant's head, but rather, asked the participant to horizontally swing his/her head from right to left, as far as possible, for 30 s in accordance with the rhythm of a metronome, while staring at the fixation target (**Figure 1B**).

HF-nVS

Stimulation was delivered via a battery-driven electrical stimulator (DC-Stimulator Plus, Eldith, NeuroConn GmbH, Ilmenau, Germany) through 2.0 cm^2 conductive rubber electrodes with paste. For both active and sham HF-nVS, the electrodes were positioned according to the mastoid process (Fitzpatrick and Day, 2004; Uchino and Kushiro, 2011; Yang et al., 2015; Inukai et al., 2018) (**Figure 1C**). As previously described (Terney et al., 2008; Inukai et al., 2018; Brevet-Aeby et al., 2019; Donde et al., 2019; Moret et al., 2019; Forbes et al., 2020), noisy stimulation was administered using a device with a current density of 0.06–0.5 mA/cm^2. We then delivered electrical currents of 0.4 mA to 2.0 cm^2 via small electrodes to achieve a current density of 0.2 mA/cm^2 with alternating currents ranging randomly between 100 and 640 Hz (each frequency has equal power as white noise). For active HF-nVS, stimulus duration and fade in/out duration was 600 and 10 s. A previous study (Terney et al., 2008) applied an electrical current to a participant's skin for a short time, because the participant tended to perceive sensations, such as tingling, at the beginning of stimulation. Thus, in our study, for sham HF-nVS, the short-time stimulus and fade in/out durations were 60 and 10 s, respectively. After 60 s of stimulation, the stimulator was turned off, but electrodes were held at the mastoid process.

Experimental Procedure

The time path of the experimental procedure is schematically shown in **Figure 2**. The repeated-measurement design consisted of a cross-over, in which the two stimulus conditions for active and sham HF-nVSs were randomly performed with a break of at least 1 day in between. Participants experienced both active and sham HF-nVS conditions, and the starting condition was randomly assigned. The eye–head coordination tasks were

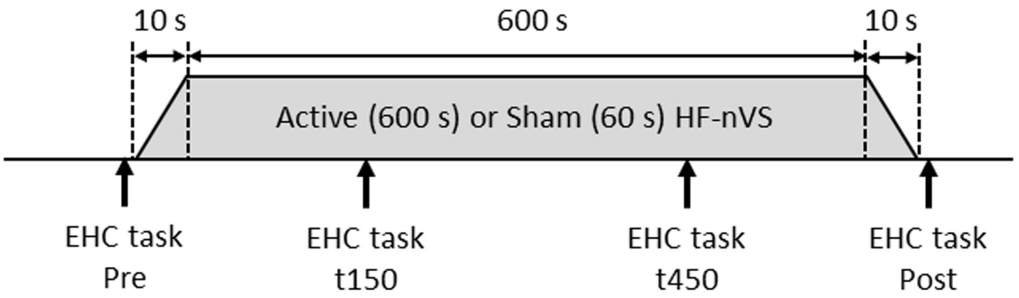

FIGURE 2 | Time course of the experimental procedure. For active HF-nVS, stimulus duration and fade in/out duration were 600 and 10 s. For sham HF-nVS, stimulus duration and fade in/out duration were 60 and 10 s. Each eye–head coordination task was conducted four times. EHC, eye–head coordination; HF-nVS, high frequency random noise stimulation; Pre, before stimulation beginning; t150, 150 s after the stimulation onset; t450, 450 s after the stimulation onset; Post, after the stimulation endpoint.

conducted before (Pre) stimulation, 150 s (t150) and 450 s (t450) after the onset of stimulation (i.e., 160 and 460 s including fade-in duration), and after (Post) the stimulation endpoint (i.e., 620 s after the stimulation beginning including fade in/out duration).

Data Analysis

All data were visually inspected and removed if contaminated by excessive noise, such as eye blinks. The blank cells produced by removing eye blinks were then linearly interpolated across the blank cells. Eye and head angle changes were then normalized to the difference from the initial angle of each participant, to eliminate inter-individual differences in initial eye and head positions. Next, data were up sampled to 300 Hz by cubic spline function to solve differences in sampling rates between the eye and head recordings.

To measure the deviation of the visual line from the fixation target, head angles were subtracted from eye angles. The absolute values of the visual line deviation were then calculated, resulting in a single number for each period (i.e., data sampled at 300 Hz for 30 s in Pre, t150, t450, and Post). The mean of the absolute values of visual line deviation in each Pre, t150, t450, or Post for each participant was used. Next, each participant's mean value in Pre was subtracted from the mean values in each t150, t450, or Post to provide normalized visual line deviation as an amount of change at t150, t450, and Post from Pre. To carefully assess intra- and inter-individual changes, differences in the normalized visual line deviations between active and sham HF-nVSs in t150, t450, and Post were analyzed by the permutated Brunner–Munzel test. The permutated Brunner–Munzel test, based on asymptotic permutational distribution, can compare small sample data, leading to a standard normal distribution and accurate *p-value* (Fagerland et al., 2011).

In addition, each subject's up-sampled data at 300 Hz of eye and head movements were normalized by linear transformation, and the data were expressed as Z scores (Aglioti et al., 2008) because peak-to-peak angles of eye and head movements were different between subjects. To quantify the time lag of compensatory eye movement in response to head movement, the time lag at minimum *r* value between up-sampled Z scores of eye and head movements was identified by cross-correlation function in each Pre, t150, t450, or Post because eye and head angles were expected to be in the opposite phase. After identifying time lag at minimum *r* value by cross-correlation function, the absolute values of the time lag were calculated. Each participant's time lag in Pre was then subtracted from the time lags in each t150, t450, or Post to provide the normalized time lag. Differences in the time lags between active and sham HF-nVSs in t150, t450, and Post were analyzed by the permutated Brunner–Munzel test. We defined statistical significance as $p < 0.05$. All statistical analyses were performed with R 3.5.2 software (R Foundation for Statistical Computing, Vienna, Austria).

RESULTS

All subjects completed all experimental conditions. No adverse HF-nVS-related effects occurred during the experiments. **Table 1** shows the peak-to-peak angles of the eye and head oscillations from subjects exposed to active or sham HF-nVS. Although both eye and head movements were sinusoidally and horizontally changed, peak-to-peak angles of eye movements were slightly smaller than those of the head. The absolute degree of the deviation of the visual line from the fixation target is shown in **Table 2**. Mean visual line deviations in the Pre, t150, t450, and Post were approximately 18.1°–22.1°. The visual line deviations normalized by subtraction of the Pre data from t150, t450, and Post were not significantly different between active and sham HF-nVSs (permuted Brunner–Munzel test, t150, $p = 0.977$; t450, $p = 0.977$; Post, $p = 0.935$; **Figure 3**). **Table 3** depicts the time lags and *r* values derived from the cross-correlation function. The *r* values of time lags were consistently negative and high across all experimental groups. The mean time lags in the Pre, t150, t450, and Post were approximately −0.88 to 0.52 s. The time lags normalized by subtraction of the Pre data from t150, t450, and Post were 0.050 ± 0.041, 0.063 ± 0.038, and 0.064 ± 0.034 s for sham HF-nVS, respectively, and were −0.005 ± 0.033, −0.0002 ± 0.039, and −0.069 ± 0.049 s for active HF-nVS, respectively. The permutated Brunner–Munzel test showed that there was a significantly smaller time lag for active HF-tRNS compared to sham HF-tRNS at Post (permuted

TABLE 1 | Peak-to-peak angles for eye and head movements.

	Conditions							
	Sham HF-nVS				Active HF-nVS			
Peak-to-peak angle (degree)	Pre	t150	t450	Post	Pre	t150	t450	Post
Eye	49.7 ± 1.1	45.1 ± 1.0	47.4 ± 0.9	48.7 ± 1.0	48.6 ± 0.9	47.2 ± 0.9	47.7 ± 1.0	47.7 ± 1.0
Head	39.9 ± 0.9	35.7 ± 0.8	37.9 ± 0.8	38.7 ± 0.9	39.0 ± 0.8	38.3 ± 0.8	39.0 ± 0.9	38.6 ± 0.8

Values are mean ± standard error of the mean.HF-nVS, high frequency noisy vestibular stimulation; Pre, before stimulation onset; t150, 150 s after stimulation onset; t450, 450 s after the stimulation onset; Post, after the stimulation endpoint.

TABLE 2 | The absolute degree of deviation of the visual line from the fixation target.

HF-nVS	Pre	t150	t450	Post
Sham	21.3 ± 0.06	17.9 ± 0.04	18.1 ± 0.05	18.7 ± 0.05
Active	19.3 ± 0.05	18.9 ± 0.05	22.1 ± 0.44	19.6 ± 0.05

Values are mean ± standard error of the mean.HF-nVS, high frequency noisy vestibular stimulation; Pre, before stimulation onset; t150, 150 s after stimulation onset; t450, 450 s after the stimulation onset; Post, after the stimulation endpoint.

Brunner–Munzel test, t150, $p = 0.204$; t450, $p = 0.222$; Post, $p = 0.030$; **Figure 4**).

DISCUSSION

To test the hypothesis that HF-nVS should decrease the deviation from the fixation target and the time lag between the eye and head motions, we measured changes in eye–head coordination related to the VOR function. Our results show that the normalized time lag of compensatory eye movement in response to head movement was smaller after active HF-nVS than after sham HF-nVS. The visual line deviation was not different between active and sham HF-nVSs. The normalized time lag between eye and head movements was significantly smaller after active HF-nVS and maintained a stable visual line deviation. This implies that HF-nVS affects eye–head coordination, reflecting the time lag between eye and head movements. This is the first systematic study to show that HF-nVS changes eye–head coordination.

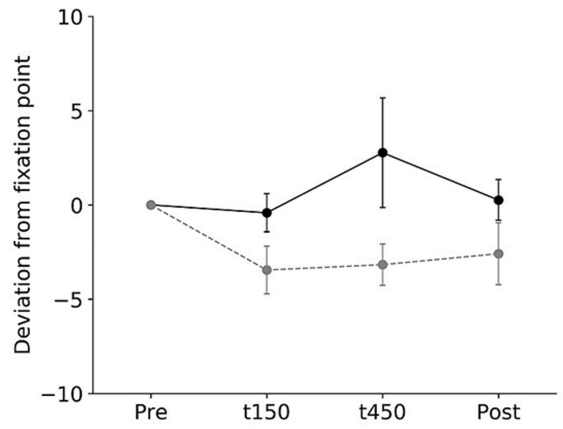

FIGURE 3 | Normalized visual line deviations during active and sham HF-nVSs. Black line and symbols denote active HF-nVS, and gray line and symbols denote sham HF-nVS. The symbols and bars denote the mean and standard error of the mean. The normalized visual line deviations for t150, t450, and Post were not significantly different between active and sham HF-nVS (permuted Brunner–Munzel test, t150, $p = 0.977$; t450, $p = 0.977$; Post, $p = 0.935$). HF-nVS, high frequency noisy vestibular stimulation; Pre, before stimulation onset; t150, 150 s after stimulation onset; t450, 450 s after the stimulation onset; Post, after the stimulation endpoint.

Corrective eye movement in response to head movements is essential for stabilizing foveal vision. The vestibular receptors of the inner ear are known to accurately detect movements of the head (Chin, 2018). The VOR receives input from the vestibular receptors, responding to movements of the head (Ischebeck et al., 2018). Electrical stimulation is a well-known procedure used to stimulate the vestibular system (Fitzpatrick and Day, 2004; Kim and Curthoys, 2004; Uchino and Kushiro, 2011; Yang et al., 2015; Fujimoto et al., 2016; Wuehr et al., 2016; Inukai et al., 2018). A small electrical direct current or step waveform applied to the mastoid process can modulate vestibular nerve activity (Fitzpatrick and Day, 2004; Uchino and Kushiro, 2011; Yang et al., 2015; Chin, 2018; Mackenzie and Reynolds, 2018). Recently, high frequency noisy stimulation has been found to apply to cortical (Terney et al., 2008) and vestibular neurons (Forbes et al., 2014, 2020; Inukai et al., 2018). Moreover, applying a noise small current with 0.05–20 Hz (the amplitude and density values were 10 mA and 0.6 mA/cm^2, respectively) (Mackenzie and Reynolds, 2018), 0–30 Hz (amplitude, 0.3–0.5 mA) (Fujimoto et al., 2016; Wuehr et al., 2016), and 0.1–640 Hz (the amplitude and density values were 0.4–1.0 mA and 0.2–0.5 mA/cm^2), respectively (Inukai et al., 2018), to the mastoid area alters ocular torsion response (Mackenzie and Reynolds, 2018), body sway response (Fujimoto et al., 2016; Inukai et al., 2018), and walking performance (Wuehr et al., 2016) related to the vestibular system. We observed that the time lag between eye and head movements was reduced after active HF-nVS over the mastoid process. This is a novel observation from our study.

TABLE 3 | Time lags and r values derived from the correlation function.

HF-nVS	Pre		t150		t450		Post	
	Time lag (s)	*r* value	Time lag (s)	*r* value	Time lag (s)	*r* value	Time lag (s)	*r* value
Sham	0.45 ± 0.02	−0.83 ± 0.05	0.50 ± 0.04	−0.79 ± 0.05	0.52 ± 0.04	−0.87 ± 0.04	0.52 ± 0.03	−0.85 ± 0.05
Active	0.51 ± 0.03	−0.88 ± 0.05	0.50 ± 0.02	−0.86 ± 0.05	0.51 ± 0.04	−0.78 ± 0.08	0.44 ± 0.04	−0.85 ± 0.06

Values are mean ± standard error of the mean.HF-nVS, high frequency noisy vestibular stimulation; Pre, before stimulation onset; t150, 150 s after stimulation onset; t450, 450 s after the stimulation onset.

In our study, one potential effect of a decreased time lag between eye and head movements by HF-nVS may be the stochastic resonance phenomenon. Stochastic resonance is a phenomenon in which the response of a system to an input signal benefits from the presence of noise (Gammaitoni et al., 1989; Collins et al., 1995; Gammaitoni, 1995; Gluckman et al., 1996; Moss et al., 2004; McDonnell and Abbott, 2009; Nobusako et al., 2018). Previous studies have noted that random noise stimulation could enhance the detection of weak stimuli or enhance the sensitivity of neurons to a weak stimulus related to the stochastic resonance phenomenon (Moss et al., 2004; Pavan et al., 2019). Because the effect of stochastic resonance is due to the improvement of signal detection in the presence of noise, stochastic resonance can provide noise benefits to some sensory and motor systems (Moss et al., 2004; McDonnell and Abbott, 2009; Nobusako et al., 2018). The effects of HF-nVS used in our study can be explained within the stochastic resonance framework, that is, the neural noise induced by HF-nVS could increase VOR function and improve eye–head coordination. However, further physiological and behavioral studies are required to understand the effects of HF-nVS on the VOR function.

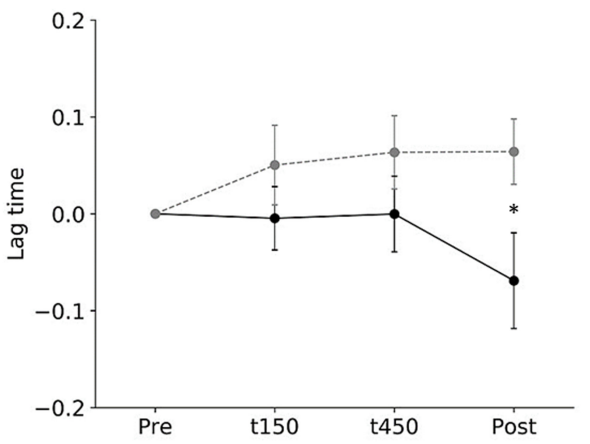

FIGURE 4 | The normalized root-mean-square values of time lags during active and sham HF-nVSs. Black line and symbols denote active HF-nVS, and gray line and symbols denote sham HF-nVS. The symbols and bars denote mean and standard error of the mean. The normalized root-mean-square values of time lags were significantly smaller for active HF-nVS than for sham HF-nVS at Post (permuted Brunner–Munzel test, t150, $p = 0.204$; t450, $p = 0.222$; Post, $p = 0.030$). HF-nVS, high frequency noisy vestibular stimulation; Pre, before stimulation onset; t150, 150 s after stimulation onset; t450, 450 s after the stimulation onset; Post, after the stimulation endpoint.

The small size of the electrodes results in more focused spatial stimulation of the mastoid areas, which may be related to the current densities. Although we used small electrodes and low current amplitude, the current density was not low (0.2 mA/cm^2) compared to previous studies (0.06–0.5 mA/cm^2) (Terney et al., 2008; Inukai et al., 2016, 2018; Brevet-Aeby et al., 2019; Donde et al., 2019; Moret et al., 2019; Forbes et al., 2020). In the present study, small electrodes with the optimal current density (0.2 mA/cm^2) for activating the VOR function were used. In the stochastic resonance phenomenon, a system is characterized by the output signal-to-noise ratio, which is defined as the ratio of the strength of the signal peak to the background noise at the input signal frequency (Collins et al., 1995; McDonnell and Abbott, 2009). Therefore, higher or lower current amplitude leads to a worse response of the system, including the low signal-to-noise ratio and disturbance of signal detection, whereas optimal current amplitude leads to an improved response of the system. In our study, HF-nVS could lead to eye–head coordination change including the VOR function related to optimal weak noise (i.e., optimal stimulus density in accordance with low current amplitude for small electrodes) in the stochastic resonance phenomenon (Moss et al., 2004). There is not, however, sufficient evidence to suggest that the current used in our study can reach the vestibular system. Although we expect that HF-nVS stimulates the vestibular system based on previous studies' stimulation intensities (Terney et al., 2008; Inukai et al., 2016, 2018; Brevet-Aeby et al., 2019; Donde et al., 2019; Moret et al., 2019; Forbes et al., 2020), we have to consider the potential for current spreading to nearby sites and complex structures of the inner ear. Therefore, further research is needed to simulate calculations on current spread by HF-nVS to the vestibula and other areas, such as the cerebellum, and to directly record changes in the VOR function related to HF-nVS by detailed physiological experiments.

In standard VOR assessments, the clinician turns the patient's head abruptly and unpredictably, roughly 15° in about 100 ms, and observes the compensatory eye movement response (Halmagyi et al., 2017). In another recent VOR assessment, Ischebeck et al. (2017, 2018) noted that the chair rotated for 33 s with an amplitude of 5.0° and a frequency of 0.16 Hz. This yielded five sinusoidal rotations of the chair with a peak velocity of 5.03°/s (Ischebeck et al., 2017, 2018). In our study, the participant was asked to hold their visual line to the fixation

target and horizontally rotate their head as far as possible with a beep rhythm of 1 Hz. These frequencies and ranges of head rotation were faster and further than those used in previous studies (Halmagyi et al., 2017; Ischebeck et al., 2017, 2018). As a result of the settings of this experiment, the mean (SD) peak-to-peak angles of eye and head oscillations were slightly larger than other studies, at around 40–50° (0.8–1.0°). Although we cannot explain the mechanism by which the visual line deviation was not different between active and sham HF-nVSs, one possibility is that a large variation in peak-to-peak movements for eye and head (from faster and bigger movements) might obscure the difference. Additionally, previous studies recorded inter-ocular asymmetry torsion movements (Severac Cauquil et al., 2003). Given that we recorded horizontal eye movement only, we were unable to detect this. Therefore, further research is needed to record more precisely not only horizontal but also torsion eye movements in response to head movement.

A potential limitation of our study is the sample size, which was estimated using Hulley's matrix method (Hulley et al., 1988). This method does not consider factors such as differences in age, sex, and baseline eye–head coordination performance and VOR function. Thus, a larger sample size is needed in further studies. These findings would be more widely representative with the addition of a detailed examination classifying participants by the above factors and the inclusion of a larger number of participants with normal VOR and VOR hypofunction.

FUTURE PERSPECTIVE

Compensatory eye movements in response to head motion ensure the stability of the gaze and clear vision during motion, which is necessary to perform the activities of daily living, including playing sports and other tasks. Our findings highlight the potential of HF-nVS as a form of VOR training for patients with vestibular hypofunction. Although we investigated whether eye–head coordination was affected by HF-nVS, future studies should assess eye–head coordination in patients with brain injuries and investigate changes in VOR function using HF-nVS.

CONCLUSION

In conclusion, our results show that by application of active HF-nVS, the time lag of eye and head movements was decreased compared by sham HF-nVS. Our results bring to light new ways of manipulating eye–head coordination with HF-nVS.

DATA AVAILABILITY STATEMENT

The original contributions presented in the study are included in the article/supplementary material. Further inquiries can be directed to the corresponding authors.

ETHICS STATEMENT

The studies involving human participants were reviewed and approved by the Research Ethics Committee of the Tokyo Kasei University. The patients/participants provided their written informed consent to participate in this study.

AUTHOR CONTRIBUTIONS

All persons who meet authorship criteria are listed as authors, and all authors certify that they have participated sufficiently in the work to take public responsibility for the content. YM and MS contributed to conception and design of study, analysis and/or interpretation of data, and drafting the manuscript. YM, MS, NI, TO, KC, and Y-JW contributed to acquisition of data.

FUNDING

This work was supported by a Grant-in-Aid for JSPS KAKENHI 18H03133 and the Comprehensive Research Project, Research Institute of Domestic Science, Tokyo Kasei University to MS.

REFERENCES

Aglioti, S. M., Cesari, P., Romani, M., and Urgesi, C. (2008). Action anticipation and motor resonance in elite basketball players. *Nat. Neurosci.* 11, 1109–1116. doi: 10.1038/nn.2182

Brevet-Aeby, C., Mondino, M., Poulet, E., and Brunelin, J. (2019). Three repeated sessions of transcranial random noise stimulation (tRNS) leads to long-term effects on reaction time in the Go/No Go task. *Neurophysiol. Clin.* 49, 27–32. doi: 10.1016/j.neucli.2018.10.066

Camilleri, R., Pavan, A., and Campana, G. (2016). The application of online transcranial random noise stimulation and perceptual learning in the improvement of visual functions in mild myopia. *Neuropsychologia* 89, 225–231. doi: 10.1016/j.neuropsychologia.2016.06.024

Campana, G., Camilleri, R., Moret, B., Ghin, F., and Pavan, A. (2016). Opposite effects of high- and low-frequency transcranial random noise stimulation probed with visual motion adaptation. *Sci. Rep.* 6:38919. doi: 10.1038/srep38919

Chin, S. (2018). Visual vertigo: Vertigo of oculomotor origin. *Med. Hypotheses* 116, 84–95. doi: 10.1016/j.mehy.2018.04.025

Collins, J. J., Chow, C. C., and Imhoff, T. T. (1995). Aperiodic stochastic resonance in excitable systems. *Phys. Rev. E Stat. Phys. Plasmas. Fluids Relat. Interdiscip. Top.* 52, R3321–R3324. doi: 10.1103/physreve.52.r3321

Donde, C., Brevet-Aeby, C., Poulet, E., Mondino, M., and Brunelin, J. (2019). Potential impact of bifrontal transcranial random noise stimulation (tRNS) on the semantic Stroop effect and its resting-state EEG correlates. *Neurophysiol. Clin.* 49, 243–248. doi: 10.1016/j.neucli.2019.03.002

Fagerland, M. W., Sandvik, L., and Mowinckel, P. (2011). Parametric methods outperformed non-parametric methods in comparisons of discrete numerical variables. *BMC Med. Res. Methodol.* 11:44. doi: 10.1186/1471-2288-11-44

Fertonani, A., Pirulli, C., and Miniussi, C. (2011). Random noise stimulation improves neuroplasticity in perceptual learning. *J. Neurosci.* 31, 15416–15423. doi: 10.1523/JNEUROSCI.2002-11.2011

Fitzpatrick, R. C., and Day, B. L. (2004). Probing the human vestibular system with galvanic stimulation. *J. Appl. Physiol.* 96, 2301–2316. doi: 10.1152/japplphysiol.00008.2004

Forbes, P. A., Kwan, A., Rasman, B. G., Mitchell, D. E., Cullen, K. E., and Blouin, J. S. (2020). Neural Mechanisms Underlying High-Frequency Vestibulocollic

Reflexes In Humans And Monkeys. *J. Neurosci.* 40, 1874–1887. doi: 10.1523/JNEUROSCI.1463-19.2020

Forbes, P. A., Siegmund, G. P., Schouten, A. C., and Blouin, J. S. (2014). Task, muscle and frequency dependent vestibular control of posture. *Front. Integr. Neurosci.* 8:94. doi: 10.3389/fnint.2014.00094

Fujimoto, C., Yamamoto, Y., Kamogashira, T., Kinoshita, M., Egami, N., Uemura, Y., et al. (2016). Noisy galvanic vestibular stimulation induces a sustained improvement in body balance in elderly adults. *Sci. Rep.* 6:37575. doi: 10.1038/srep37575

Gammaitoni, L. (1995). Stochastic resonance and the dithering effect in threshold physical systems. *Phys. Rev. E Stat. Phys. Plasmas. Fluids Relat. Interdiscip. Top.* 52, 4691–4698. doi: 10.1103/physreve.52.4691

Gammaitoni, L., Marchesoni, F., Menichella-Saetta, E., and Santucci, S. (1989). Stochastic resonance in bistable systems. *Phys. Rev. Lett.* 62, 349–352. doi: 10.1103/PhysRevLett.62.349

Gluckman, B. J., Netoff, T. I., Neel, E. J., Ditto, W. L., Spano, M. L., and Schiff, S. J. (1996). Stochastic Resonance in a Neuronal Network from Mammalian Brain. *Phys. Rev. Lett.* 77, 4098–4101. doi: 10.1103/PhysRevLett.77.4098

Halmagyi, G. M., Chen, L., Macdougall, H. G., Weber, K. P., Mcgarvie, L. A., and Curthoys, I. S. (2017). The Video Head Impulse Test. *Front. Neurol.* 8:258. doi: 10.3389/fneur.2017.00258

Hulley, S. B., Cummings, S. R., Browner, W. S., Grady, D. G., and Newman, T. B. (1988). *Designing clinical research*. Philadelphia: Lippincott Williams & Wilkins.

Inukai, Y., Otsuru, N., Masaki, M., Saito, K., Miyaguchi, S., Kojima, S., et al. (2018). Effect of noisy galvanic vestibular stimulation on center of pressure sway of static standing posture. *Brain Stimul.* 11, 85–93. doi: 10.1016/j.brs.2017.10.007

Inukai, Y., Saito, K., Sasaki, R., Tsuiki, S., Miyaguchi, S., Kojima, S., et al. (2016). Comparison of Three Non-Invasive Transcranial Electrical Stimulation Methods for Increasing Cortical Excitability. *Front. Hum. Neurosci.* 10:668. doi: 10.3389/fnhum.2016.00668

Ischebeck, B. K., De Vries, J., Janssen, M., Van Wingerden, J. P., Kleinrensink, G. J., Van Der Geest, J. N., et al. (2017). Eye stabilization reflexes in traumatic and non-traumatic chronic neck pain patients. *Muscul. Sci. Pract.* 29, 72–77. doi: 10.1016/j.msksp.2017.03.004

Ischebeck, B. K., De Vries, J., Van Wingerden, J. P., Kleinrensink, G. J., Frens, M. A., and Van Der Geest, J. N. (2018). The influence of cervical movement on eye stabilization reflexes: a randomized trial. *Exp. Brain Res.* 236, 297–304. doi: 10.1007/s00221-017-5127-9

Kim, J., and Curthoys, I. S. (2004). Responses of primary vestibular neurons to galvanic vestibular stimulation (GVS) in the anaesthetised guinea pig. *Brain Res. Bull.* 64, 265–271. doi: 10.1016/j.brainresbull.2004.07.008

Mackenzie, S. W., and Reynolds, R. F. (2018). Ocular torsion responses to sinusoidal electrical vestibular stimulation. *J. Neurosci. Methods* 294, 116–121. doi: 10.1016/j.jneumeth.2017.11.012

McDonnell, M. D., and Abbott, D. (2009). What is stochastic resonance? Definitions, misconceptions, debates, and its relevance to biology. *PLoS Comput. Biol.* 5:e1000348. doi: 10.1371/journal.pcbi.1000348

Moret, B., Camilleri, R., Pavan, A., Lo Giudice, G., Veronese, A., Rizzo, R., et al. (2018). Differential effects of high-frequency transcranial random noise stimulation (hf-tRNS) on contrast sensitivity and visual acuity when combined with a short perceptual training in adults with amblyopia. *Neuropsychologia* 114, 125–133. doi: 10.1016/j.neuropsychologia.2018.04.017

Moret, B., Donato, R., Nucci, M., Cona, G., and Campana, G. (2019). Transcranial random noise stimulation (tRNS): a wide range of frequencies is needed for increasing cortical excitability. *Sci. Rep.* 9:15150. doi: 10.1038/s41598-019-51553-7

Moss, F., Ward, L. M., and Sannita, W. G. (2004). Stochastic resonance and sensory information processing: a tutorial and review of application. *Clin. Neurophysiol.* 115, 267–281. doi: 10.1016/j.clinph.2003.09.014

Nobusako, S., Osumi, M., Matsuo, A., Fukuchi, T., Nakai, A., Zama, T., et al. (2018). Stochastic resonance improves visuomotor temporal integration in healthy young adults. *PLoS One* 13:e0209382. doi: 10.1371/journal.pone.0209382

Pasqualotto, A. (2016). Transcranial random noise stimulation benefits arithmetic skills. *Neurobiol. Learn. Mem.* 133, 7–12. doi: 10.1016/j.nlm.2016.05.004

Pavan, A., Ghin, F., Contillo, A., Milesi, C., Campana, G., and Mather, G. (2019). Modulatory mechanisms underlying high-frequency transcranial random noise stimulation (hf-tRNS): A combined stochastic resonance and equivalent noise approach. *Brain Stimul.* 12, 967–977. doi: 10.1016/j.brs.2019.02.018

Penton, T., Bate, S., Dalrymple, K. A., Reed, T., Kelly, M., Godovich, S., et al. (2018). Using High Frequency Transcranial Random Noise Stimulation to Modulate Face Memory Performance in Younger and Older Adults: Lessons Learnt From Mixed Findings. *Front. Neurosci.* 12:863. doi: 10.3389/fnins.2018.00863

Popescu, T., Krause, B., Terhune, D. B., Twose, O., Page, T., Humphreys, G., et al. (2016). Transcranial random noise stimulation mitigates increased difficulty in an arithmetic learning task. *Neuropsychologia* 81, 255–264. doi: 10.1016/j.neuropsychologia.2015.12.028

Romanska, A., Rezlescu, C., Susilo, T., Duchaine, B., and Banissy, M. J. (2015). High-Frequency Transcranial Random Noise Stimulation Enhances Perception of Facial Identity. *Cereb Cortex.* 25, 4334–4340. doi: 10.1093/cercor/bhv016

Severac Cauquil, A., Faldon, M., Popov, K., Day, B. L., and Bronstein, A. M. (2003). Short-latency eye movements evoked by near-threshold galvanic vestibular stimulation. *Exp. Brain Res.* 148, 414–418. doi: 10.1007/s00221-002-1326-z

Snowball, A., Tachtsidis, I., Popescu, T., Thompson, J., Delazer, M., Zamarian, L., et al. (2013). Long-term enhancement of brain function and cognition using cognitive training and brain stimulation. *Curr. Biol.* 23, 987–992. doi: 10.1016/j.cub.2013.04.045

Terney, D., Chaieb, L., Moliadze, V., Antal, A., and Paulus, W. (2008). Increasing human brain excitability by transcranial high-frequency random noise stimulation. *J. Neurosci.* 28, 14147–14155. doi: 10.1523/JNEUROSCI.4248-08.2008

Uchino, Y., and Kushiro, K. (2011). Differences between otolith- and semicircular canal-activated neural circuitry in the vestibular system. *Neurosci. Res.* 71, 315–327. doi: 10.1016/j.neures.2011.09.001

van der Groen, O., and Wenderoth, N. (2016). Transcranial Random Noise Stimulation of Visual Cortex: Stochastic Resonance Enhances Central Mechanisms of Perception. *J. Neurosci.* 36, 5289–5298. doi: 10.1523/JNEUROSCI.4519-15.2016

Wallace, B., and Lifshitz, J. (2016). Traumatic brain injury and vestibulo-ocular function: current challenges and future prospects. *Eye Brain* 8, 153–164. doi: 10.2147/EB.S82670

Wuehr, M., Nusser, E., Krafczyk, S., Straube, A., Brandt, T., Jahn, K., et al. (2016). Noise-Enhanced Vestibular Input Improves Dynamic Walking Stability in Healthy Subjects. *Brain Stimul.* 9, 109–116. doi: 10.1016/j.brs.2015.08.017

Yang, Y., Pu, F., Lv, X., Li, S., Li, J., Li, D., et al. (2015). Comparison of postural responses to galvanic vestibular stimulation between pilots and the general populace. *Biomed. Res. Int.* 2015:567690. doi: 10.1155/2015/567690

Conflict of Interest: The authors declare that the research was conducted in the absence of any commercial or financial relationships that could be construed as a potential conflict of interest.

frontiers in Physiology

ORIGINAL RESEARCH
published: 03 December 2020
doi: 10.3389/fphys.2020.609006

Limb-Specific Features and Asymmetry of Nerve Conduction Velocity and Nerve Trunk Size in Human

*Ayaka Nobue[1,2], Yoko Kunimasa[2], Hiromu Tsuneishi[2], Kanae Sano[1], Hiroyuki Oda[2] and Masaki Ishikawa[2]**

[1]Faculty of Health Sciences, Morinomiya University of Medical Sciences, Osaka, Japan, [2]Graduate School of Sport and Exercise Sciences, Osaka University of Health and Sport Sciences, Osaka, Japan

This study aimed to simultaneously examine the differences of human nerve conduction velocity (NCV) and nerve cross-sectional area (nCSA) between the upper and lower limbs and between different regions of the upper and lower limbs. Thirty healthy subjects volunteered for the study. NCV and nCSA of the ulnar and tibial nerves were measured with the dominant and non-dominant arms and the supporting and reacting legs using supramaximal electric stimulation and peripheral nerve ultrasonography at three regions for ulnar and tibial nerves, respectively. Supramaximal electric stimulation was superficially applied to the ulnar and tibial nerves at each point. These action potentials were recorded from the digiti minimi and soleus muscles for the ulnar and tibial nerves, respectively. Our results clearly showed that the NCV, nCSA, and circumference of the ulnar and tibial nerves were higher and greater in the lower limbs than in the upper limbs. The greater the circumference, the greater the nCSA for both the upper and lower limbs. However, unlike the upper limbs, the supporting leg did not have higher NCV than the reacting leg despite its greater circumference. Therefore, nCSA can be related to the circumference but not necessarily function for NCV developments of the lower limbs. These various aspects between the upper and lower limbs suggest that NCV does not depend on the nCSA sizes or upper and lower limb circumference; the results indicate the existence of limb-specific NCV but not nCSA developments.

Keywords: nerve conduction velocity (NCV), ultrasonography, peripheral nerve, electrical stimulation, rapid movement, reaction, nerve cross-sectional area

OPEN ACCESS

Edited by:
Borja Sañudo, Sevilla University, Spain

Reviewed by:
Rinaldo André Mezzarane, University of Brasilia, Brazil
Paul McCulloch, Midwestern University, United States

****Correspondence:***
Masaki Ishikawa
masaki@ouhs.ac.jp

Specialty section:
This article was submitted to Integrative Physiology, a section of the journal Frontiers in Physiology

Received: *22 September 2020*
Accepted: *11 November 2020*
Published: *03 December 2020*

Citation:
Nobue A, Kunimasa Y, Tsuneishi H, Sano K, Oda H and Ishikawa M (2020) Limb-Specific Features and Asymmetry of Nerve Conduction Velocity and Nerve Trunk Size in Human. Front. Physiol. 11:609006. doi: 10.3389/fphys.2020.609006

INTRODUCTION

The elucidation of the neuromuscular function of the human peripheral nervous system that enables rapid and accurate limb movements can be revealed by evaluating the morphology and functional characteristics of the peripheral nerves. Previous animal studies reported that trained mice had greater nerve axon diameter than the non-trained mice (Edds, 1950; Samorajski and Rolsten, 1975) and the peripheral nerve conduction velocity (NCV) was greater with the greater peripheral nerve axon diameter (Gasser and Grundfest, 1939; Hursh, 1939). In human,

however, the analysis of the peripheral nerve size *in vivo* is difficult and many reports are only available on human NCV. Kim et al. (2009a) and Pawlak and Kaczmarek (2010) reported that the NCV in the trained athletes was higher in the dominant than in the non-dominant upper limbs. Hatta et al. (1995) also reported that the NCV and dominant forearm circumference were faster and greater in badminton and kendo players than those in the healthy control subjects. Consequently, they imply that the developments of the human arm circumference and its muscle size would develop the human NCV. Therefore, high resolution imaging techniques of the peripheral nerve *in vivo* are expected to prove the above speculation.

The diameter size of the peripheral nerve fiber is very small (proximately 10–30 μmm). So far, the resolution of current *in vivo* human imaging technology cannot identify the cross-sectional area (CSA) of the nerve fibers. Therefore, the factors enhancing human NCV are not fully understood in the nerve fiber level. However, recent high-resolution imaging techniques of the peripheral nerve ultrasonography allow direct measurements of the cross-sectional area of the nerve trunk (nCSA), which is a bundle of various nerve fibers. Although there is no evidence for a correlation between nCSA and either axon diameter or NCV, this peripheral nerve ultrasonography combined with NCV calculation evoked by electrical stimulation makes it possible to further evaluate *in vivo* human peripheral nerve morphology and function.

Unlike the upper limbs, there have only been a few reports of NCV for the lower limbs, especially for a comparison of NCV for both the upper and lower limbs (Kim et al., 2009b). From the literature, the NCV of the upper limbs would be higher than that of the lower limbs (Mayer, 1963). However, the peripheral nerve ultrasonography showed that the lower limbs had greater nCSA than the upper limbs (Bedewi et al., 2017, 2018). These NCV and nCSA reports are not in line with the principle that the greater the peripheral nerve axon diameter, the higher the NCV (Edds, 1950; Samorajski and Rolsten, 1975). This conflict needs to be thoroughly examined during the simultaneous comparison between both human upper and lower limbs and at different regions because nCSA was not uniformly developed from the distal to proximal parts (Nobue and Ishikawa, 2015). The regional specificity of the nCSA developments and functions in both the upper and lower limbs also need to be fully discussed. In addition, the postural lower limb muscles had greater innervation ratio calculated by the number of muscle fibers dominated by axons than in the upper limb fine regulator muscles (Feinstein et al., 1955). Therefore, the branch unit of efferent nerve fibers in the greater innervation ratio muscle could be greater nerve axon size, and therefore, the lower limbs could have greater nCSA than the upper limbs. In this case, the simultaneous NCV measurements for both the upper and lower limbs together with nCSA measurements can solve the above-mentioned discrepancies and demonstrate the existence of the limb-specific NCV profiles.

The specificities of the lateral preference and dominancy of the upper limbs have been well examined but not in the lower limbs. McGrath et al. (2015) suggested the difficulty to discern the lateral preference and dominancy of the lower limbs. A previous human lower limb study (Kim et al., 2009b) found no differences in the NCV of the lower limbs between the dominant and non-dominant sides. Therefore, the lower limbs could have smaller differences in the nCSA and muscle sizes between the dominant and non-dominant sides than in the upper limbs. Therefore, unlike the upper limbs, the lateral preference and dominancy of the lower limbs may not exist.

Therefore, this study aimed to simultaneously examine the nCSA size of the upper and lower limb regions with the NCV of the ulnar and tibial nerves. Our hypotheses are as follows: (1) NCV, nCSA, and limb circumference are greater in the lower limbs than in the upper limbs. (2) The nCSA at any upper and lower limb region depends upon their circumferences. However, the lower limb shows no significant correlation between the size of the lower limb nCSA and its NCV as is the case with the previous upper limb study (Nobue and Ishikawa, 2015). Functionally, the proximal parts of the limbs have higher and thinner NCV and nCSA and *vice versa* than the distal parts. (3) Unlike the upper limbs, the NCV and nCSA of the lower limbs do not show any lateral preference despite the varying circumferences of both legs.

MATERIALS AND METHODS

Subjects

Thirty participants who have no history of any neurological, peripheral neuropathy, or other disorders of the upper and lower limbs, as well as no bilateral differences of the forearm and shank length, volunteered for this study [25 male and 5 female; age 19.8 ± 1.6 (18–25) years; body mass 65.5 ± 15.6 kg; height 172.0 ± 6.7 cm]. All subjects were competitive and active athletes who regularly attended local competitions for more than 6 years [tennis, baseball, track and field (sprint, javelin throw, high jump, hurdle, and decathlon), rugby, or soccer]. The dominant hand was confirmed by the Edinburgh Handedness Inventory (Oldfield, 1971), and the dominant (reacting) and non-dominant (supporting) legs were confirmed by the Waterloo Footedness Questionnaire (Elias et al., 1998). Informed consent was obtained before the experiment, which was conducted according to the guidelines of the Declaration of Helsinki and was approved by the Ethics Committee of the Osaka University of Health and Sport Sciences (authorization number 19-8).

Protocols

Firstly, the upper and lower limb circumferences were measured using a measuring tape. The nCSA of the ulnar and tibial nerves of the participants were measured by ultrasonography [Noblus, Hitachi Aloka Medical Ltd., a high-frequency (18 MHz) linear array ultrasound transducer; image resolution: 0.08 mm] in the sitting position with the forearm flexed at 120° and in the abdominal position, respectively. After the nCSA measurements, NCVs of the ulnar and tibial nerves were measured using the standard techniques of supramaximal

percutaneous stimulation with a constant current stimulator (DS7A, Digitimer Ltd., United Kingdom) and surface electrode recording (P-EMG plus, Oisaka Electronic Equipment, Japan) on each limb of each subject.

Measured Parameters

Nerve Cross-Sectional Area

The ulnar and tibial nerves were scanned at three regions in the upper and lower limbs, respectively (**Figures 1A,B**). In the upper limb, the first region was at 100 mm proximal point to the medial epicondyle of the humerus (UN_{prox}), the second region was at 30 mm distal point to the medial epicondyle of the humerus (UN_{mid}), and the third region was at 30 mm proximal point to the ulnar head (UN_{dis}). In the tibial nerves, the first region was at 100 mm proximal point to the popliteal fossa (TN_{prox}), the second region was at the popliteal fossa point (TN_{mid}), and the third region was at 50 mm proximal point to the soleus muscle belly (TN_{dis}). As mentioned above, the nCSA size, which is a bundle of nerve fibers was measured by the ultrasonographic images at each region of the ulnar and tibial nerves, respectively (Nobue and Ishikawa, 2015). From these ultrasonographic images, the boundary of the nerve circumference was traced, and the upper and lower limb nCSAs were separately analyzed at each point (UN_{prox}, UN_{mid}, and UN_{dis}; TN_{prox}, TN_{mid}, and TN_{dis}, respectively) by ImageJ software (ver 1.45 s, National Institutes of Health, Unites States). The mean upper and lower limb nCSAs were calculated by the measured three points at each limb, respectively. For the comparison between the different regions, the upper arm and forearm nCSAs were averaged by nCSA at UN_{prox} and UN_{mid} and at UN_{mid} and UN_{dis}, respectively. Moreover, the thigh and lower leg nCSAs were averaged by nCSA at TN_{prox} and TN_{mid} and at TN_{mid} and TN_{dis}, respectively.

Upper and Lower Limb Circumferences

The circumferences of the upper and lower limbs were measured around the maximal girth of the forearm and calf and at the measured nCSA points of UN_{prox}, UN_{mid}, UN_{dis}, TN_{prox}, TN_{mid}, and TN_{dis}, respectively (**Figures 1A,B**). The CSA for each arm and leg region was calculated from each circumference:

$$\text{CSA at each measured point} = \frac{1}{4\pi}\left(\textit{each circumference}\right)^2$$

The upper arm and forearm circumferences were averaged by circumferences at UN_{prox} and UN_{mid}, and at UN_{mid} and UN_{dis}, respectively. Furthermore, the thigh and lower leg circumferences were averaged by circumferences at TN_{prox} and TN_{mid}, and at TN_{mid} and TN_{dis}, respectively.

Motor Nerve Conduction Velocity

The motor response from each muscle was collected using the Signal software (Signal version 7.01, Cambridge Electronic Design Limited, United Kingdom) at a sampling rate of 10 kHz (Power 1,401, Cambridge Electronics Design Limited, United Kingdom). The compound muscle action potentials (CMAPs) were evoked by the electrical stimulation (DS7A, Digitimer Ltd., United Kingdom; 0.2 ms duration constant current square wave pulses) of the ulnar and tibial nerves starting from minimal and progressing to supramaximal stimuli intensity. As shown in **Figure 1A**, the CMAPs are evoked from the abductor digiti minimi muscle after electrical stimulation of ulnar nerve at the same nCSA measured points.

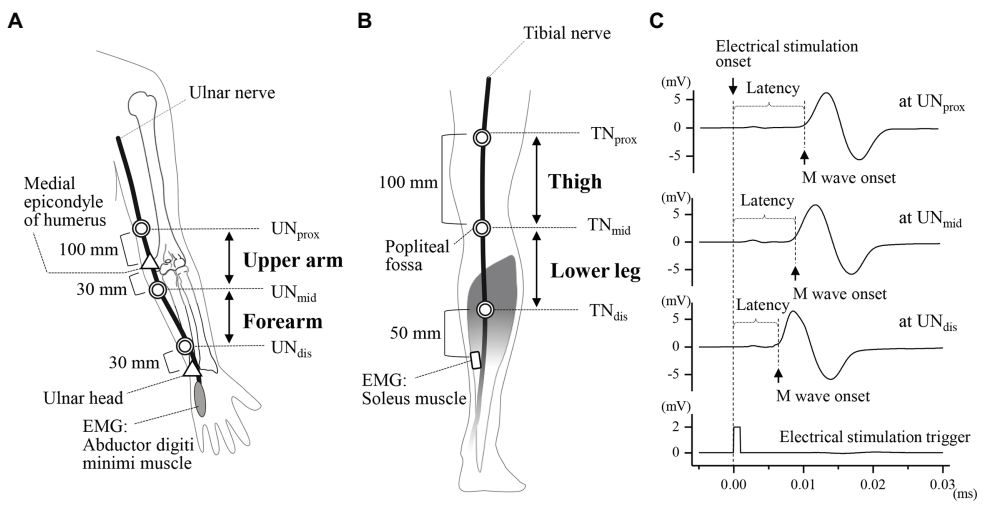

FIGURE 1 | The measurement setup for the ulnar and tibial nerves and the representative EMG responses with the compound muscle action potentials of the measured points of the cross-sectional area (CSA) and positions of nerve electrical stimulation of the ulnar and tibial nerves. **(A)** The measured positions of the circumstance, nerve cross-sectional area (nCSA), and electrical stimulation for the ulnar nerve: 100 mm proximal to the medial epicondyle of the humerus (UN_{prox}), 30 mm distal to the medial epicondyle of the humerus (UN_{mid}), and 30 mm proximal to the ulnar head (UN_{dis}). **(B)** The measured positions of the circumstance, nCSA and electrical stimulation for the tibial nerve: 100 mm proximal to the popliteal fossa (TN_{prox}), at the popliteal fossa (TN_{mid}), and 50 mm proximal to the soleus muscle (TN_{dis}). **(C)** The onset of the M wave was measured by the compound muscle action potential recorded from each stimulation point.

The active electrode was attached to the belly of the abductor digiti minimi muscle (the muscle innervated by the ulnar nerve) and a ground electrode was attached to the ulnar head. Examination was performed with the subjects sitting and the forearm flexed at 120°. Similarly, as shown in **Figure 1B**, the CMAPs are evoked from the soleus muscle after electrical stimulation of tibial nerve at the same nCSA measured points. The active electrode was attached to the belly of the soleus muscle (the muscle innervated by the tibial nerve) and a ground electrode was attached to the malleolus lateralis. Examination was performed with the subjects lying prone and the ankle in a neutral position. The stimulation regions for both upper and lower limbs were marked with an aqueous marker, and the distances between stimulation regions were measured using a measuring tape. The latency of the stimulus artifact at each point was detected as the onset of the M-wave (**Figure 1C**). NCV was calculated by dividing the distance between each stimulating point by the differences between the latency responses (Kimura, 2013). These values were used as follows:

Upper arm NCV of the ulnar nerve: the distance from UN_{prox} to UN_{mid}, the latency from UN_{prox} to UN_{mid}.

Forearm NCV of the ulnar nerve: the distance from UN_{mid} to UN_{dis}, the latency from UN_{mid} to UN_{dis}.

Upper limb NCV of the ulnar nerve: the average value of these above two NCVs.

Thigh NCV of the tibial nerve: the distance from TN_{prox} to TN_{mid}, the latency from TN_{prox} to TN_{mid}.

Lower leg NCV of the tibial nerve: the distance from TN_{mid} to TN_{dis}, the latency from TN_{mid} to TN_{dis}.

Lower limb NCV of the tibial nerve: the average value of these above two NCVs.

Skin and core body temperatures (around the soleus and abductor digiti minimi muscles) of each subject were monitored (CORE, greenTEG AG, Switzerland) at each trial to avoid the influence of temperature on NCV. During measurements, we confirmed that the skin and core body temperatures stayed constant at each subject.

Statistical Analyses

Results were presented as means ± standard deviations. For comparison between the upper and lower limbs, the mean maximal circumferences, NCVs and nCSA for each subject were averaged for the right and left arms and for the right and left legs, respectively. Prior to all statistical analyses for this comparison, the distribution of the variables was passed for normality. Thus, statistical analyses were performed using the paired *t*-test between the upper and lower limbs. For the lateral comparison, the variables were compared between dominant and non-dominant arms as well as between the supporting and reacting legs, respectively. For comparison between regions for each upper and lower limb, the variables were compared between forearm and upper arm and between thigh and lower leg, respectively. To consider the statistical test of interaction between these two comparisons, Mauchly's test of sphericity was performed on the data, and a two-way repeated-measures ANOVA (rmANOVA) was used to test for significance of the main effects of each parameter and interaction between lateral comparison as well as regions for the upper and lower limbs, respectively. When no transform was found that made the variable normally distributed, nonparametric Wilcoxon signed rank tests were used to test for differences between groups and the significance levels were Bonferroni corrected. The correlations between each parameter were evaluated using the Pearson's correlation coefficients after the distribution of the variables was passed for normality. The confidence level was set at $p < 0.05$ to determine statistical significances for all data. SPSS 25.0 software was used for statistical analyses.

RESULTS

For comparison between upper and lower limbs (averaged variables between lateral parts), **Table 1** shows the maximum circumference, NCV, and nCSA, respectively. The lower limb had significantly greater maximum circumferences, NCV, and nCSA than the upper limb, respectively ($p < 0.05$).

For the lateral comparison at upper limbs (averaged variables between upper arm and forearm), the maximum forearm circumferences, upper limb NCV, and upper limb nCSA were significantly greater in the dominant than in the non-dominant arms (264 ± 29 vs. 256 ± 31 mm, 56.7 ± 6.2 vs. 54.5 ± 4.0 m s^{-1}, and 6.9 ± 1.6 vs. 6.2 ± 1.2 mm, respectively: $p < 0.05$). For the lateral comparison at lower limbs (averaged variables between thigh and lower leg), the maximum lower leg circumference was greater in the supporting than in the reacting legs (376 ± 19 vs. 373 ± 18 mm, $p < 0.05$). The tibial nerve nCSA did not show any significant differences between the supporting and reacting legs (23.1 ± 4.7 vs. 23.6 ± 5.0 mm^2, respectively). However, the mean lower limb NCV was significantly lower in the supporting than in the reacting legs (55.7 ± 11.3 vs. 62.5 ± 10.7 m s^{-1}, $p < 0.05$).

More detail comparisons were performed for examining region and lateral specificities. In the circumference of the upper limb, the rmANOVA with lateral dominance and region as factors showed no interaction between all variables and revealed main effects of lateral dominance [$F_{(1,29)} = 19.54$, $p < 0.001$] and region [$F_{(1,29)} = 521.42$, $p < 0.001$], respectively (**Figure 2A**). In the ulnar NCV, the rmANOVA with lateral dominance and region as factors showed no interaction between

TABLE 1 | Comparison of the measured parameters for the upper and lower limbs.

	Upper limb Ulnar nerve	Lower limb Tibial nerve
Maximum circumferences (mm)	260 ± 30	374 ± 18*
Motor nerve conduction velocity (m s^{-1})	55.6 ± 4.3	59.1 ± 9.0*
Nerve cross-sectional area (mm^2)	6.6 ± 1.2	23.3 ± 4.1*

Values are expressed as means ± SD. The ulnar and tibial nCSAs were averaged by the three measured points for both the dominant and nondominant arms and for both the supporting and reacting legs, respectively.

**Shows significant differences between the upper and lower limbs ($p < 0.05$).*

all variables and revealed main effects of region [$F_{(1,29)}$ = 18.90, p < 0.001] but not lateral dominance [$F_{(1,29)}$ = 2.891, p = 0.100], respectively (**Figure 2B**). In the ulnar nCSA, the rmANOVA with lateral dominance and region as factors showed no interaction between all variables and revealed effects of lateral dominance [$F_{(1,29)}$ = 10.42, p = 0.003] and region [$F_{(1,29)}$ = 29.19, p < 0.001], respectively (**Figure 2C**).

In the circumference of the lower limb, the rmANOVA with lateral preference and region as factors showed no interaction between all variables and revealed main effects of region [$F_{(1,29)}$ = 295.83, p < 0.001] but not lateral preference [$F_{(1,29)}$ = 0.34, p = 0.564], respectively (**Figure 2D**). In the tibial NCV, the rmANOVA with lateral preference and region as factors showed no interaction between all variables and revealed effects of lateral preference [$F_{(1,29)}$ = 10.26, p = 0.003] and region [$F_{(1,29)}$ = 56.71, p < 0.001], respectively (**Figure 2E**). In the tibial nCSA, the rmANOVA showed no interaction between all variables and revealed with lateral preference and region as factors showed no interaction between all variables and revealed main effects of region [$F_{(1,29)}$ = 213.99, p < 0.001] but not lateral preference [$F_{(1,29)}$ = 3.526, p = 0.078], respectively (**Figure 2F**).

Figure 3 shows a semi-log plot of the nCSA at each region vs. the CSA calculated from its circumference at each region of the upper and lower limbs. According to the Pearson's correlation, the data of all limbs clearly follow a straight line, which indicates that all nCSA data of both limbs maintain a relatively constant value to its circumference (**Figure 3**; r = 0.90, p < 0.001), although the tibial nerve had a much greater nCSA than the ulnar nerve.

A further examination of the relationships between the ulnar NCV and nCSA at each region for the upper limbs showed

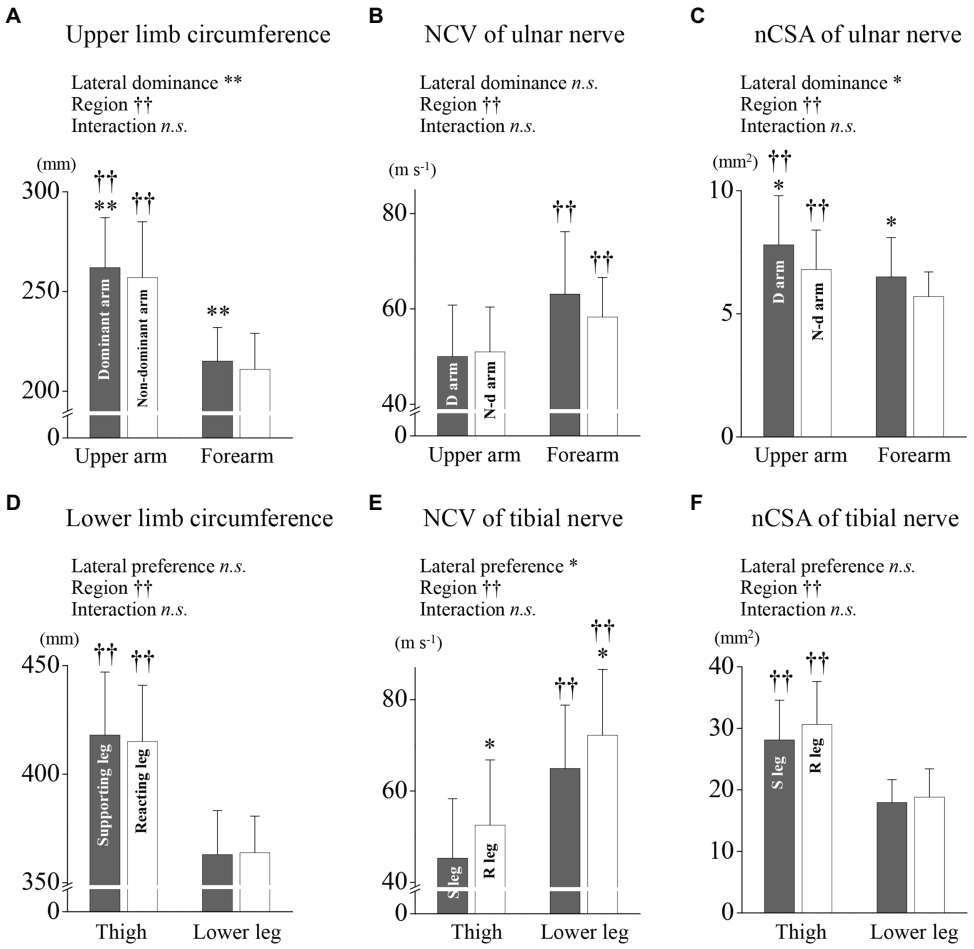

FIGURE 2 | Limb circumference, nerve conduction velocity (NCV), and nCSA nerve cross-sectional area for the upper and lower limbs. **(A)** The upper arm and forearm arm circumferences for the dominant and non-dominant arms are shown, respectively. **(B)** The ulnar NCV of the upper arm and forearm are shown for the dominant and non-dominant arms, respectively. **(C)** The ulnar nCSA of upper arm and forearm are shown for the dominant and non-dominant arms, respectively. **(D)** The thigh and lower leg circumferences for the supporting and reacting legs are shown, respectively. **(E)** The tibial NCV of the thigh and lower leg are shown for the supporting and reacting legs, respectively. **(F)** The tibial nCSA of the thigh and lower leg are shown for the supporting and reacting legs, respectively. *, †, and ns indicate repeated two-way ANOVA analysis showing the main effect of lateral dominance (preference), region and interaction. *, **, and †† are significantly higher values as compared with the others (*p < 0.01, **p < 0.001, ††p < 0.001, ns, not significant), respectively.

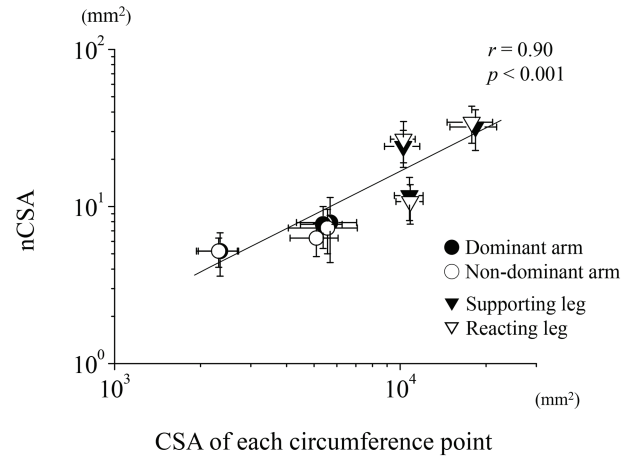

FIGURE 3 | Relationship between the nerve and CSA for the upper and lower limbs. Semi-log plots of nCSA and the estimated CSA of each circumference are plotted for both the upper and lower limbs.

no significant correlation for both dominant and non-dominant arms together, and for the dominant and non-dominant arms, respectively (**Figures 4A,B**). Similarly, at the lower limbs, no significant correlation was found between the tibial nerve NCV and nCSA (**Figures 4C,D**). In the upper limbs, positive correlations were found between the forearm nCSAs and the forearm circumferences (**Figure 5B**; $r = 0.41$, $p < 0.01$). In the lower limbs, a weak positive correlation was found between the lower leg nCSAs and their circumferences ($r = 0.28$, $p < 0.05$; **Figure 5D**).

DISCUSSION

Our results clearly showed that the lower limbs had higher and greater NCV, nCSA, and circumference than the upper limbs. However, NCV did not show any relationships with nCSA and circumference for both the upper and lower limbs. Unlike the upper limbs, the reacting leg had higher NCV than the supporting leg, despite the supporting leg having

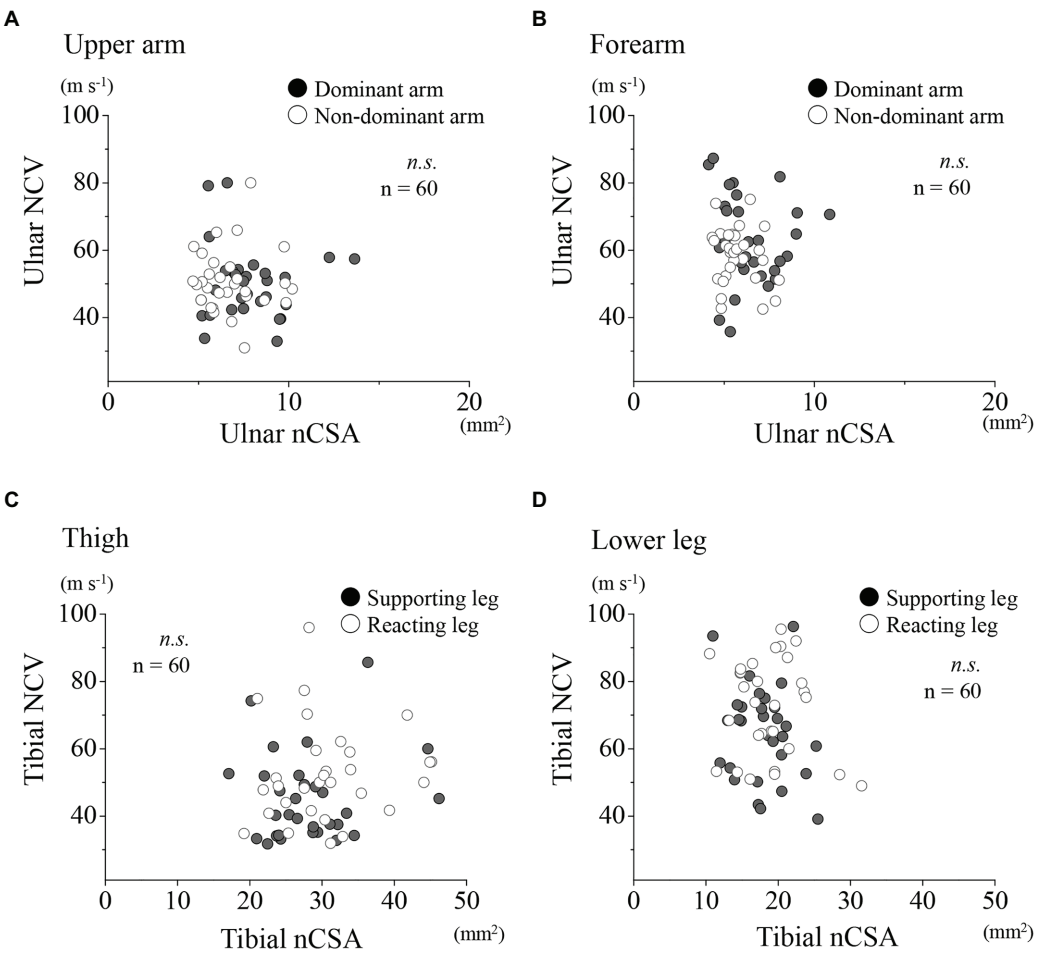

FIGURE 4 | Relationships between motor NCV and nCSA for the upper and lower limbs, respectively. Relationships between motor NCV and nCSA of the upper arm **(A)** and forearm **(B)** for the dominant (●) and non-dominant arms (○) as well as of the thigh **(C)** and lower leg **(D)** for the supporting (●) and reacting legs (○).

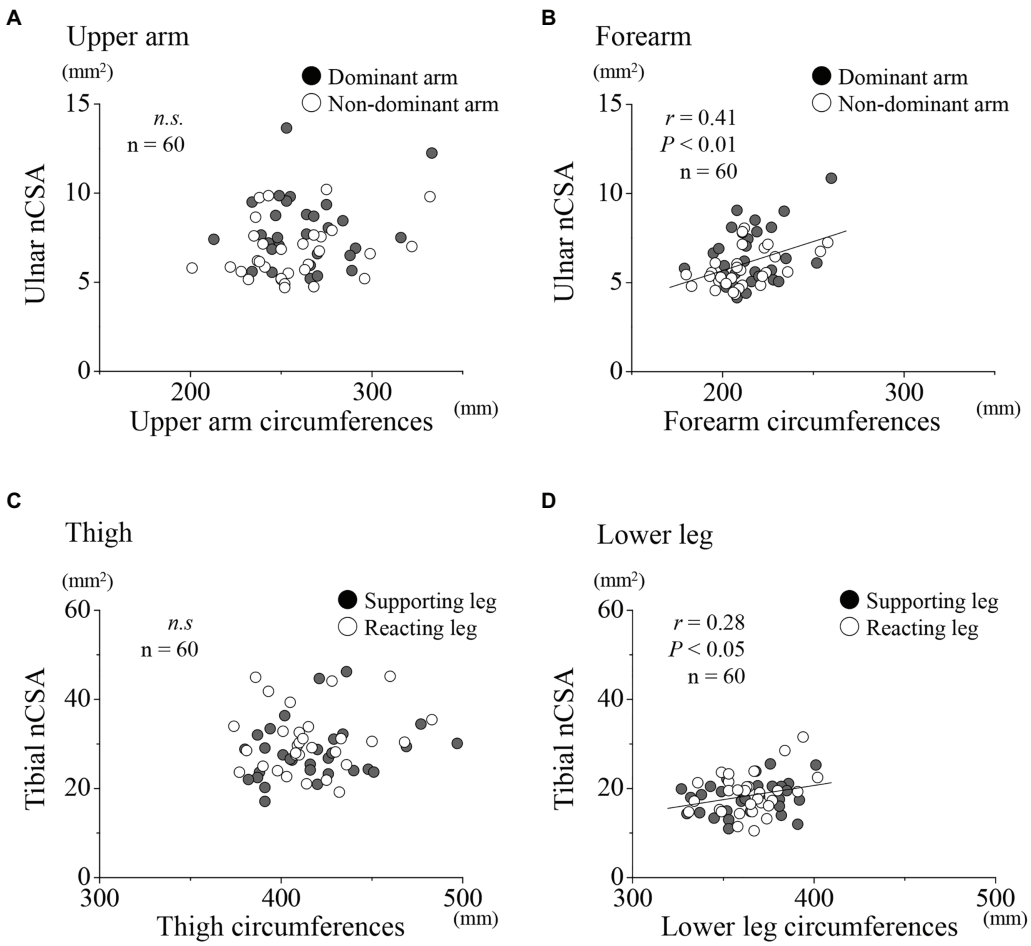

FIGURE 5 | Relationships between nCSA and circumferences for the upper and lower limbs, respectively. Relationships between nCSA of the upper arm **(A)** and forearm **(B)** for the dominant (●) and non-dominant arms (○) as well as of the thigh **(C)** and lower leg **(D)** for the supporting (●) and reacting legs (○).

greater circumference than the reacting leg. Therefore, the absolute nCSA size can be related to its circumference but not necessarily function to the NCV developments for the limbs. These varying aspects between the upper and lower limbs indicate the existence of limb-specific NCV developments but not nCSA developments.

Limb Specificity of Neuromuscular Features

As surmised by the reports of Bedewi et al. (2017, 2018), our results clearly confirmed that the lower limbs had an approximately 3.5 times greater human nCSA than the upper limbs, despite the lower limbs having approximately 1.4 times greater maximum circumference than the upper limbs. Additionally, the lower limbs NCV (59.1 ± 9.0 m s^{-1}) was greater than that in the upper limbs (55.6 ± 4.3 m s^{-1}). This result does not necessarily coincide with those of the previous study, which showed that the lower limbs had lower NCV (45.5 ± 3.8 m s^{-1}) than the upper limbs (58.9 ± 2.2 m s^{-1}; Mayer, 1963). This conflicting result could be related to the testing place of the leg muscles and nerves, which were much more distal in the previous study (abductor hallucis muscle and tibial nerve) than in the present study (soleus muscle and tibial nerve). Additionally, the NCV measured in the proximal part of the upper limb can be higher than that in the distal part (Trojaborg and Sindrup, 1969). Another possibility of the conflicting result is the influence of the tested subjects. The present study had active athletes as participants; however, those in the previous study were not (mentioned as just normal subjects). The NCV of the active athletes may be developed compared with the normal healthy subjects. When taken together, our results clearly showed that the lower limbs had greater and higher nCSA and NCV than the upper limbs. However, all nCSA data of each region in both the upper and lower limbs maintain a relatively constant value to its circumference and NCV did not show any relationships with nCSA for both the upper and lower limbs. Therefore, these aspects of NCV and nCSA between the upper and lower limbs indicate the existence of limb-specific NCV characteristics and non-limb-specific nCSA developments.

Lateral Preferences of Neuromuscular Features in the Upper and Lower Limbs

As shown by the previous study (Nobue and Ishikawa, 2015), the present study confirmed that the dominant arms had greater circumference and nCSA than the non-dominant arms. Furthermore, the dominant arm had higher NCV than the non-dominant arms. Therefore, the dominant upper limb can have greater and higher nCSA and NCV than the non-dominant upper limb, respectively. In the lower limbs, however, the supporting leg had lower NCV than the reacting leg. In addition, the nCSA cannot be necessarily high in the big supporting leg compared with the small reacting leg. In the reaction movements of the lower limbs, not only the reacting but also the opposite supporting legs work as the inherent functions of supporting the body weight prior to performing movements, which requires effective coordination between both legs (Promsri et al., 2020). Meanwhile, the reaction movements of the upper limbs could be focused by testing one arm but not another arm. Thereby, unlike the upper limbs, both lower limbs can have different functions to the reaction movements. Thus, the limb-specific function to quick response movements may lead to different results of lateral preferences of neuromuscular features for both the upper and lower limbs, respectively.

Region Specific of Peripheral Nerve Features

Trojaborg and Sindrup (1969) reported that NCV measured in the proximal part of upper limb was higher than that in the distal part. In this case, the nerve axon diameter may be possible to be greater in the proximal part than in the distal part due to the less nerve branching in the proximal part. However, there have not been any reports about the comparison of the nerve axon diameter at different regions. In the nCSA level of the present study, the nCSA in the proximal parts were greater than that in the distal parts for both the upper and lower limbs, depending on their circumferences (**Figures 2, 5**). However, the distal parts of both limbs had higher NCV than the proximal parts. These results were not in line with those of the upper limbs in the previous *in vivo* study (Trojaborg and Sindrup, 1969). Further examination of the region specific NCV and nerve size in both the upper and lower limbs are needed to solve this inconsistency. Taken together, the present study suggests that the nCSA at any regions in both the upper and lower limbs can be depended on their circumferences. In addition, our results imply the region-specificity in both the upper and lower limbs, where the distal parts of limbs can have higher NCV as well as thinner nCSA and *vice versa* than the proximal parts.

Methodological Limitations

The diameter size of the peripheral nerve fiber is proximately 10–30 μmm. So far, the resolution of current *in vivo* human imaging technology cannot identify an axon diameter of the nerve fibers. Therefore, in the present study, we have measured the size of the nerve trunk (nCSA), which is a bundle of nerve fibers, using peripheral nerve ultrasonography. In this size level, nCSA could contain a variety of fiber types, not only the efferent fibers but also afferent fibers. Therefore, further considerations in the diameter level of the myelinated nerve fibers and the distinction of the efferent fibers from different fiber types of mixed peripheral nerve should be given in future studies with more detail high-resolution ultrasonography. In this study, the subject was selected with no bilateral differences of the forearm and shank length and was recruited to minimize the effects of the different distances between the nodes of Ranvier in the myelinated axons. Further validation needs to expand the various subject groups.

CONCLUSION

Direct measurements of the human NCV and nCSA clearly showed the morphological and functional differences between the upper and lower limbs and between regions of both limbs. The different aspects between the upper and lower limbs and between regions suggest that NCV does not depend on either the nCSA sizes or circumference of both upper and lower limbs and indicate the existence of limb-specific NCV developments but not nCSA developments.

DATA AVAILABILITY STATEMENT

The original contributions presented in the study are included in the article/supplementary material, further inquiries can be directed to the corresponding author.

ETHICS STATEMENT

The studies involving human participants were reviewed and approved by the Human Ethics Committee of Osaka University of Health and Sport Sciences. The patients/participants provided their written informed consent to participate in this study.

AUTHOR CONTRIBUTIONS

AN, YK, KS, HO, and MI contributed to the study concept and design. AN, KS, HO, and MI contributed to methodological developments. AN, YK, and HT carried out the experiment, the data analysis, and interpretation. AN and MI co-wrote the paper. All authors contributed to the article and approved the submitted version.

FUNDING

This work was supported by Japan Society for Promotion of Science (KAKENHI) grant nos. 20K19499, 26702026, 15KK0261, 17H02156, and 18K10874.

REFERENCES

Bedewi, M. A., Abodonya, A., Kotb, M., Kamal, S., Mahmoud, G., Aldossari, K., et al. (2018). Estimation of ultrasound reference values for the lower limb peripheral nerves in adults: a cross-sectional study. *Medicine* 97:e0179. doi: 10.1097/MD.0000000000010179

Bedewi, M. A., Abodonya, A., Kotb, M., Mahmoud, G., Kamal, S., Alqabbani, A., et al. (2017). Estimation of ultrasound reference values for the upper limb peripheral nerves in adults: a cross-sectional study. *Medicine* 96:e9306. doi: 10.1097/MD.0000000000009306

Edds, M. V. Jr. (1950). Hypertrophy of nerve fibers to functionally overloaded muscles. *J. Comp. Neurol.* 93, 259–275. doi: 10.1002/cne.900930207

Elias, L. J., Bryden, M. P., and Bulman-Fleming, M. B. (1998). Footedness is a better predictor than is handedness of emotional lateralization. *Neuropsychologia* 36, 37–43. doi: 10.1016/s0028-3932(97)00107-3

Feinstein, B., Lindegard, B., Nyman, E., and Wohlfart, G. (1955). Morphologic studies of motor units in normal human muscles. *Acta Anat.* 23, 127–142. doi: 10.1159/000140989

Gasser, H. S., and Grundfest, H. (1939). Axon diameters in relation to the spike dimensions and the conduction velocity in mammalian a fibers. *Am. J. Phys.* 127, 393–414. doi: 10.1152/ajplegacy.1939.127.2.393

Hatta, A., Nishihira, Y., Takemiya, T., Shimoda, M., and Changming, L. (1995). Ulnar nerve conduction velocity in athletes: comparison between kendo, badminton, soft tennis players and nonathletes. *Adv. Exerc. Sports Physiol.* 2, 177–184.

Hursh, J. B. (1939). Conduction velocity and diameter of nerve fibers. *Am. J. Phys.* 127, 131–139. doi: 10.1152/ajplegacy.1939.127.1.131

Kim, S., Nishihira, Y., and Hatta, A. (2009b). Changes in the peripheral motor nerve conduction velocity and its distribution in the lower limbs with long-term exercise. *Adv. Exerc. Sports Physiol.* 15, 95–100.

Kim, S., Nishihira, Y., Higashiura, T., Hatta, A., Hayashi, Y., Hayashi, K., et al. (2009a). The effects of long-term exercise training on the motor nerve conduction velocity (MCV) in long-distance wheelchair athletes. *Jpn. Society Exerc. Sports Physiol.* 16, 17–24.

Kimura, J. (2013). *Electrodiagnosis in diseases of nerve and muscle: Principles and practice. 4th Edn.* Oxford: Oxford University Press.

Mayer, R. F. (1963). Nerve conduction studies in man. *Neurology* 13, 1021–1030. doi: 10.1212/wnl.13.12.1021

McGrath, T. M., Waddington, G., Scarvell, J. M., Ball, N. B., Creer, R., Woods, K., et al. (2015). The effect of limb dominance on lower limb functional performance--a systematic review. *J. Sports Sci.* 34, 289–302. doi: 10.1080/02640414.2015.1050601

Nobue, A., and Ishikawa, M. (2015). Relationship between the fascia size of ulnar nerve and the nerve conduction velocity in humans. *Jpn. J. Phys. Fitness Sports Med.* 64, 427–434. doi: 10.7600/JSPFSM.64.427

Oldfield, R. C. (1971). The assessment and analysis of handedness: the Edinburgh inventory. *Neuropsychologia* 9, 97–113. doi: 10.1016/0028-3932(71)90067-4

Pawlak, M., and Kaczmarek, D. (2010). Field hockey players have different values of ulnar and tibial motor nerve conduction velocity than soccer and tennis players. *Arch. Ital. Biol.* 148, 365–376. doi: 10.4449/aib.v148i4.1208

Promsri, A., Haid, T., Werner, I., and Federolf, P. (2020). Leg dominance effects on postural control when performing challenging balance exercises. *Brain Sci.* 10:128. doi: 10.3390/brainsci10030128

Samorajski, T., and Rolsten, C. (1975). Nerve fiber hypertrophy in posterior tibial nerves of mice in response to voluntary running activity during aging. *J. Comp. Neurol.* 159, 553–558. doi: 10.1002/cne.901590407

Trojaborg, W., and Sindrup, E. W. (1969). Motor and sensory conduction in different segments of the radial nerve in normal subjects. *J. Neurol. Neurosurg. Psychiatry* 32, 354–359. doi: 10.1136/jnnp.32.4.354

Conflict of Interest: The authors declare that the research was conducted in the absence of any commercial or financial relationships that could be construed as a potential conflict of interest.

frontiers in Human Neuroscience

ORIGINAL RESEARCH
published: 09 December 2020
doi: 10.3389/fnhum.2020.602595

Neuromechanical Assessment of Activated vs. Resting Leg Rigidity Using the Pendulum Test Is Associated With a Fall History in People With Parkinson's Disease

Giovanni Martino[1]*, *J. Lucas McKay*[1,2,3], *Stewart A. Factor*[3] and *Lena H. Ting*[1,4]

[1]W.H. Coulter Department of Biomedical Engineering, Georgia Institute of Technology, Emory University, Atlanta, GA, United States, [2]Department of Biomedical Informatics, Emory University, Atlanta, GA, United States, [3]Jean and Paul Amos PD and Movement Disorders Program, Department of Neurology, Emory University, Atlanta, GA, United States, [4]Department of Rehabilitation Medicine, Division of Physical Therapy, Emory University, Atlanta, GA, United States

Leg rigidity is associated with frequent falls in people with Parkinson's disease (PD), suggesting a potential role in functional balance and gait impairments. Changes in the neural state due to secondary tasks, e.g., activation maneuvers, can exacerbate (or "activate") rigidity, possibly increasing the risk of falls. However, the subjective interpretation and coarse classification of the standard clinical rigidity scale has prohibited the systematic, objective assessment of resting and activated leg rigidity. The pendulum test is an objective diagnostic method that we hypothesized would be sensitive enough to characterize resting and activated leg rigidity. We recorded kinematic data and electromyographic signals from rectus femoris and biceps femoris during the pendulum test in 15 individuals with PD, spanning a range of leg rigidity severity. From the recorded data of leg swing kinematics, we measured biomechanical outcomes including first swing excursion, first extension peak, number and duration of the oscillations, resting angle, relaxation index, maximum and minimum angular velocity. We examined associations between biomechanical outcomes and clinical leg rigidity score. We evaluated the effect of increasing rigidity through activation maneuvers on biomechanical outcomes. Finally, we assessed whether either biomechanical outcomes or changes in outcomes with activation were associated with a fall history. Our results suggest that the biomechanical assessment of the pendulum test can objectively quantify parkinsonian leg rigidity. We found that the presence of high rigidity during clinical exam significantly impacted biomechanical outcomes, i.e., first extension peak, number of oscillations, relaxation index, and maximum angular velocity. No differences in the effect of activation maneuvers between groups with clinically assessed low rigidity were observed, suggesting that activated rigidity may be independent of resting rigidity and should be scored as independent variables. Moreover, we found that fall history was more common among people whose rigidity was increased with a secondary task, as measured by biomechanical outcomes. We conclude that different

OPEN ACCESS

Edited by:
Borja Sañudo, Sevilla University, Spain

Reviewed by:
Noman Naseer, Air University, Pakistan
Charalambos Costas Charalambous, University of Nicosia, Cyprus

***Correspondence:**
Giovanni Martino
giovanni.martino@emory.edu

Specialty section:
This article was submitted to Motor Neuroscience, a section of the journal Frontiers in Human Neuroscience

Received: *03 September 2020*
Accepted: *16 November 2020*
Published: *09 December 2020*

Citation:
Martino G, McKay JL, Factor SA and Ting LH (2020) Neuromechanical Assessment of Activated vs. Resting Leg Rigidity Using the Pendulum Test Is Associated With a Fall History in People With Parkinson's Disease. Front. Hum. Neurosci. 14:602595. doi: 10.3389/fnhum.2020.602595

mechanisms contributing to resting and activated rigidity may play an important yet unexplored functional role in balance impairments. The pendulum test may contribute to a better understanding of fundamental mechanisms underlying motor symptoms in PD, evaluating the efficacy of treatments, and predicting the risk of falls.

Keywords: hyperreflexia, EMG, kinematics, dual-task, activation maneuver, biomechanics, hyper-resistance, neural control

INTRODUCTION

Rigidity is a cardinal feature of Parkinson's disease (PD) and its role in functional balance and gait impairment has been questioned (Wright et al., 2007; Franzén et al., 2009). Our recent work suggested that leg–but not arm, neck, or total–rigidity score is associated with frequent falls in people with PD (McKay et al., 2019). However, leg rigidity scores reflect a coarse and subjective categorization based on subitem 3.3 in the Movement Disorders Society Unified Parkinson's Disease Rating Scale (MDS-UPDRS). Rigidity is clinically described as a constantly increased resistance to a passive or externally induced motion throughout the range of movement (Fung and Thompson, 2002). Rigidity generally responds well to dopaminergic medication and surgical interventions (Xia, 2011), and a reduction in rigidity is taken as an indicator of successful treatment. Parkinsonian patients perceive rigidity as achiness and stiffness in the muscles and joints affected, which is also used as a metric for pain and impaired mobility.

Changes in the neural state can exacerbate rigidity (Hong et al., 2007; Mendonça and Jog, 2008; Powell et al., 2011), but such effects are quantified only at the lowest range of the MDS-UPDRS. In the MDS-UPDRS, a passive movement is imposed by an examiner and the perceived stiffness is rated with an ordinal score from 0 (absent rigidity) to 4 (severe rigidity) for each arm, leg, and neck. In the "resting rigidity" condition, the subject is asked to completely relax during the assessment (Webster and Mortimer, 1977). An activation maneuver (such as finger tapping) is used in the MDS-UPDRS to evaluate "activated rigidity" only if a person exhibits no resistance when relaxed; thus activation maneuver is mainly used in only at the mildest rigidity levels (Fung et al., 2000; Powell et al., 2011). Moreover, activated rigidity has not been systematically studied in the leg, although it could play a causal role in falls (McKay et al., 2019). Thus, more sensitive and objective methods for quantifying leg rigidity are necessary to enable associations between rigidity and other biomechanical or clinical outcomes.

Here, we proposed the use of the pendulum test to objectively characterize resting vs. activated rigidity based on biomechanical outcomes and electromyographic (EMG) recordings. Various methods have been proposed in the literature to objectively quantify rigidity in PD (Eisen, 1987; Andreeva and Khutorskaya, 1996; Kirollos et al., 1996; Patrick et al., 2001; Marusiak et al., 2010; Xia et al., 2011; Powell et al., 2012; Endo et al., 2015; Zetterberg et al., 2015), but the focus has been primarily on the upper limbs. Moreover, objective metrics have not been implemented in the clinical setting because of their complexity, need for expensive devices, and time involved. In contrast, the pendulum test is a diagnostic method that allows passive joint resistance to be objectively characterized based on the pattern of lower leg movement after release from the horizontal (Wartenberg, 1951). Assessment using the pendulum test is sensitive to standard clinical measurements of spasticity in children with cerebral palsy (Fowler et al., 2000; Fee and Miller, 2004; Szopa et al., 2014; Willaert et al., 2020), multiple sclerosis patients (Bianchi et al., 1999), and stroke survivors (Brown et al., 1988; Lin and Rymer, 1991; Bohannon et al., 2009; Kristinsdottir et al., 2020). The first swing excursion is the most sensitive outcome for spasticity severity (Fowler et al., 2000; Bohannon et al., 2009; Szopa et al., 2014; Willaert et al., 2020). However, other kinematic features of the pendulum test may also provide insight. These include reductions in the number and duration of the oscillations (Fowler et al., 2000; Szopa et al., 2014), in stiffness and damping coefficients estimated by inverse kinematics (Lin and Rymer, 1991; Fee and Miller, 2004), along with abnormal bursts of activation in the quadriceps and hamstrings (Lin and Rymer, 1991; Fowler et al., 2000; Kristinsdottir et al., 2020; Willaert et al., 2020). Furthermore, the use of a computational model associated with pendulum test data is capable of dissociating the contributions of abnormal muscle tone vs. abnormal reflex excitability to spasticity (De Groote et al., 2018), revealing new insights into physiological mechanisms of spasticity. In De Groote et al. (2018) we suggested that the abnormal limb motion in children with cerebral palsy results from the interactions between muscle tone and the resulting short-range stiffness, and force-dependent reflexes. In PD, marked reductions in leg swing velocity and resting angle have been observed (Brown et al., 1988) and attributed to increased damping in simulations (Le Cavorzin et al., 2003). However, these reductions have not been associated with the degree of leg rigidity.

The pendulum test may also be sufficiently sensitive to test the level of activated rigidity which we hypothesized could potentially increase the risk of falling during activities of daily living (ADL's). Several studies have shown that the presence of a secondary task or activation maneuver considerably enhances rigidity in people with PD (Kelly et al., 2012). The degree of the increase in parkinsonian rigidity with activation can differ from patient to patient and can be present in both on- and off- dopaminergic medication states (Fung et al., 2000; Hong et al., 2007; Shapiro et al., 2007; Powell et al., 2011). Also, different medications and dosages have been reported to have variable effects on both resting and activated rigidity (Webster and Mortimer, 1977; Kirollos et al., 1996; Relja et al., 1996; Krack et al., 2003; Shapiro et al., 2007), suggesting that different neural mechanisms could play a role in the manifestation of

parkinsonian rigidity. However, the difference between activated and resting rigidity and its relationship with the degree of severity of rigidity at rest or to other clinical outcomes in PD has not been explored before.

The objective of this study was to test whether the pendulum test would be an objective and sensitive test to quantify resting and activated rigidity in PD. We hypothesized that both resting and activated rigidity in PD alter pendulum test kinematics and EMG patterns. We predicted that the biomechanical outcomes of the pendulum test, namely first swing excursion, first extension peak, number and duration of the oscillations, resting angle, relaxation index, maximum and minimum angular velocity, would be associated with leg rigidity severity in people with PD. We further predicted that an activation maneuver would alter pendulum test outcomes, but that the effects would vary from an individual to the next. Finally, as an exploratory study, we tested whether the level of activated rigidity would be associated with fall history, which would be expected if activated rigidity were a potential cause of falls.

MATERIALS AND METHODS

Study Participants

We performed the pendulum test on 15 participants with PD. Participants were recruited from the cohort of an observational 1-year fall risk study (McKay et al., 2019). We included patients with a diagnosis of clinically defined PD who exhibited rigidity during MDS-UPDRS-III testing in the practically-defined "OFF" state (see below). Exclusion criteria were history of musculoskeletal and/or neurological disorders other than PD, inability to walk $\geq$3 m with or without assistance, and advanced stage dementia in which patients were unable to perform activities of daily living independently, signs of spasticity or paratonia at clinical examination. The sample size was selected to meet or exceed common recommendations of $\approx$10 cases/independent variable in regression analyses (Vittinghoff and McCulloch, 2007) and $\geq$12 cases/group in preclinical studies (Julious, 2005). PD participants were assessed in the practically defined OFF medication state, $\geq$12 h after their last dose of antiparkinsonian medications (Langston et al., 1992). Each participant's neurologist signed an OFF-medication clearance form before the patient was asked to withhold their medications for this experiment. All participants provided written informed consent before participation according to protocols approved by the Institutional Review Board of Emory University.

Lower limb rigidity was evaluated at the beginning of the experimental session by a trained examiner, following the MDS-UPDRS guidelines: rigidity in the lower extremities was tested by fully extending and flexing the knee with the patient sitting (0 = Absent, 1 = Slight or detectable only when activated by mirror or other movements, 2 = Mild to moderate, 3 = Marked, but the full range of motion easily achieved, 4 = Severe, range of motion achieved with difficulty). The participants were classified as "fallers" if they reported cases of falls in the 6 months before the data collection and were classified as "non-fallers" otherwise (McKay et al., 2019).

Pendulum Test

The pendulum test was performed with the subject sitting on a treatment table (**Figure 1A**) with the trunk inclined approximated 40° from the vertical to provide a comfortable starting position (Stillman and McMeeken, 1995). We designed a custom backrest that fits on a physical therapy table to control the posture of the participants. During the test, the examiner dropped the lower leg of the participant from the horizontal position with an extended knee joint; the lower leg was then allowed to swing freely under the influence of gravity. In each participant the pendulum test was assessed during four randomized different conditions: a baseline condition, with the subject completely relaxed and with the hands-on his/her lap, and while performing three different activation maneuvers (described below). The most rigid lower limb, as determined upon clinical examination, was assessed for each participant. Three trials were performed for each condition and a pause of 40 s was ensured between them to avoid fatigue due to the activation maneuvers. A total of 12 trials were recorded for each participant. We excluded the trials in which the participants were unable to relax, due to muscle activity that resulted in a non-monotonic exponential decrement of knee angle excursion. Specifically, using the following procedure: since the pattern of the knee angle during the pendulum test follows an exponential decrease of the peaks (**Figure 2A**), we excluded the trials in which the decrement from the i-th peak to i-th+1 was lower than the decrement from the i-th+1 to i-th+2 (**Figure 2B**). The same examiner carried out the test across all the sessions and participants.

Activation Maneuvers

We first identified which activation maneuver was most effective in increasing rigidity during the pendulum test. We tested the effect of three different activation maneuvers (**Figure 1A**): finger tapping, fist-clenching, and the Jendrassik maneuver. The rationale for the incorporation of an activation maneuver lies in that activation maneuver has been shown to enhance the degree of rigidity in PD patients (Matsumoto et al., 1963; Kelly et al., 2012). The finger tapping test is one of the standard activation maneuvers used to clinically evaluate rigidity in PD (Shimoyama et al., 1990; Martínez-Martín et al., 1994) and is indicated as one of the activation maneuvers used to assess rigidity in the UPDRS scale (Fahn and Elton, 1987). The second activation maneuver consists of a sustained clenching of the fists (Meara and Cody, 1992). As an alternative to finger tapping and clenching, the Jendrassik maneuver is a common clinical test where the patient interlocks the fingers of each hand in a hook-like fashion and isometrically pulls the hands apart as strongly as possible (Ertuglu et al., 2018).

Data Analysis

Joint kinematics were recorded using a motion capture analysis system (Vicon). Participants wore a 25-marker set according to a modified version of the Vicon's Plug-in Gait model (Welch and Ting, 2008). Kinematic data were filtered using a second order zero-lag low pass Butterworth with a cut-off frequency of 5 Hz to remove high-frequency recording artifacts (Stillman and McMeeken, 1995; Valle et al., 2006; Lotfian

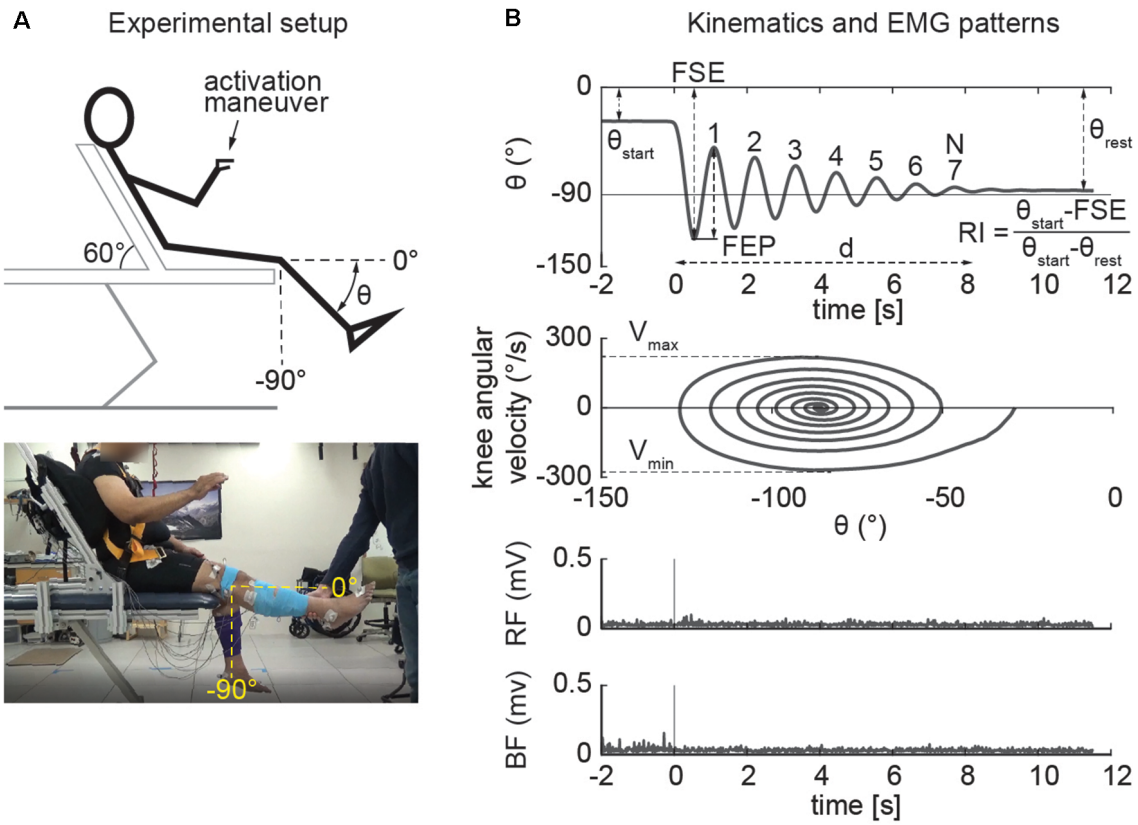

FIGURE 1 | Experimental setup and outcomes of the pendulum test. The example refers to the activated condition in which the participant performs finger tapping. The pendulum test was performed with the subject sitting on a treatment table with the trunk inclined approximated 60° from the horizontal to provide a comfortable starting position **(A)**. The swinging leg behaves as a damped pendulum, oscillating several times before coming to rest. First swing excursion (FSE), number (N) and duration (d) of the oscillations, first extension peak (FEP), resting angle (θ_{rest}), maximum (V_{max}), and minimum (V_{min}) angular velocity were assessed from kinematic data. The middle panels show the typical "whirlpool" pattern of angular velocity against angle data. EMG activity of rectus femoris (RF) and biceps femoris (BF) were also recorded in a subset of participants (bottom panel; **B**).

et al., 2016; Ferreira et al., 2020). Knee angles were taken by measuring the absolute angle of the leg segment in the sagittal plane. Biomechanical outcomes (**Figure 1B**) were then calculated including first swing excursion (FSE), first extension peak (FPE), number (N) and duration (d) of the oscillations, resting angle (θ_{rest}), relaxation index (RI), maximum (V_{max}) and minimum (V_{min}) angular velocity. The end of the oscillation was calculated by considering a cut-off of 3° toward extension (Fowler et al., 2000). These biomechanical outcomes were used in previous studies to describe the kinematic pattern of the leg during the pendulum test (Stillman and McMeeken, 1995; Fowler et al., 2000; Valle et al., 2006; Szopa et al., 2014; Lotfian et al., 2016; Whelan et al., 2018; Ferreira et al., 2020). In particular, maximum angular velocity and relaxation index (defined as the ratio between the starting angle and the resting angle of the knee) are reduced in PD (Brown et al., 1988). We also recorded EMG activity from biceps femoris (BF) and rectus femoris (RF) in a subset of participants (n = 10, **Table 1**). EMG data were collected at 1,200 Hz (Motion Lab Systems, Inc., Baton Rouge, LA, USA), high-pass filtered (35 Hz, third order zero-lag Butterworth filter) to remove motion artifact. The signal was then demeaned, rectified and low-pass filtered (40 Hz) to produce a linear envelope of the signal (Winter, 2009) as previously reported (Torres-Oviedo and Ting, 2007; Safavynia and Ting, 2013). We chose not to normalize data for within-subject interpretation of EMG activity (Powell et al., 2017).

Statistical Analysis

Participants were characterized in two groups as either low rigidity (leg rigidity score from 1 to 2) or high rigidity (leg rigidity score from 3 to 4). Differences in the central tendency of clinical and demographic variables between the low and high rigidity groups and between non-fallers and fallers were assessed with t-tests and Chi-squared tests as appropriate. Between-groups differences in averaged outcome measures taken during rest (FSE, FPE, N, d, θ_{rest}, RI, V_{max}, and V_{min}) were assessed with independent samples t-tests. Within-subject differences in averaged outcome measures (FSE, FPE, N, d, θ_{rest}, RI, V_{max}, and V_{min}) between the resting and activated states (i.e., changes from rest to activated) were assessed with paired-samples t-tests. Between-groups differences in the amount of change in each outcome measure between the resting and activated states were

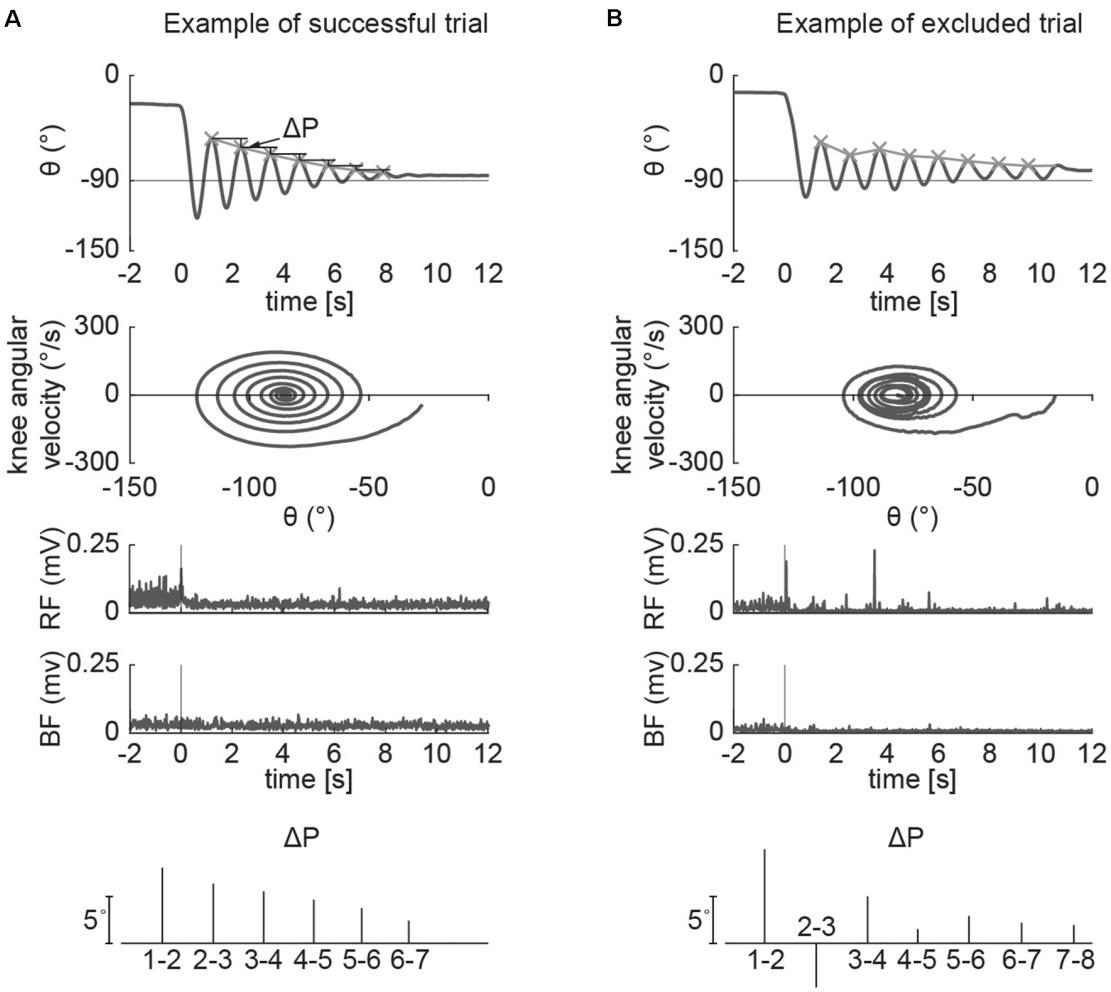

FIGURE 2 | Example of successful and excluded trials. The pattern of the knee angle during the pendulum test follows an exponential decrease of the peaks, while the phase plot of angular velocity against angular displacement follows a uniform "whirlpool" shape **(A)**. The voluntary input of the participant disrupts the uniform shape of the whirlpool and causes increased variations in limb excursion peak **(B)**. We excluded the trials in which the decrement from the i-th peak to i-th+1 is not greater than the following one.

assessed with independent samples t-tests. Cohen's *d* parameters (Cohen, 1992) were used to evaluate the effect size on outcome measures (**Table 4**). Due to the exploratory nature of the study, no corrections for multiple comparisons were used .

RESULTS

Fifteen participants with PD (11 males and four females, mean age 67 ± 10 years) enrolled in the study. Demographic and clinical characteristics are shown in **Table 1**. No significant differences in clinical or demographic characteristics were observed between the low and high rigidity groups (**Table 2**). Consistent with the previous report (McKay et al., 2018), some significant differences were observed between fallers and non-fallers on Sex, Total MDS-UPDRS-III score, rigidity score, and daily levodopa equivalent dose (LED, **Table 3**). We excluded from the analysis of all the trials in which the participants were unable to relax the leg during the test (**Figure 2**). Three subjects were unable to relax during the whole session and were excluded from further analysis. The number (mean ± SD) of successful trials among participants was 2 ± 1 during resting state, 1 ± 1 during finger tapping, 2 ± 1 during fist clenching, and 2 ± 1 during the Jendrassik maneuver. Initial analyses (one-way ANOVA, *post-hoc* Tukey–Kramer) identified no significant differences between the effects of the three different activation maneuvers on the biomechanical outcomes (all $p > 0.05$). Therefore we aggregated the results of all of the activated conditions.

Examples of Pendulum Test Kinematic Patterns

Different kinematic patterns of the pendulum test were observed across lower leg rigidity scores. For example, in a participant with slight leg rigidity (**Figure 3A**, score = 1/4) the leg oscillated

TABLE 1 | Demographic and clinical characteristics of the study participants.

ID	Age (year)	Sex	Analyzed leg side	MDS-UPDRS-III score (/132)	Leg rigidity score (/4)	Total rigidity score (/20)	Faller	Disease duration (year)	LED (mg)	EMG collected
PD01	62.5	M	R	33	1	3	N	8.5	700	N
PD02	58.3	M	L	43	3	10	N	7.3	0	N
PD03	66	F	R	23	3	7	N	2	300	N
PD04	47.4	M	L	37	4	16	Y	6.4	1,300	N
PD05	70	F	R	8	2	4	N	3.1	100	N
PD06	76	M	L	32	2	7	N	5	300	Y
PD07	64.2	M	L	33	3	6	Y	6.2	620	Y
PD08	70	M	R	52	2	7	Y	16	1,400	Y
PD09	71.1	M	L	20	1	3	N	1.1	532	Y
PD10	69.4	F	L	9	1	4	N	1.9	400	Y
PD11	55.4	M	L	28	2	6	Y	5.4	1,900	Y
PD12	81.2	M	L	38	3	7	Y	7.2	550	Y
PD13	51.4	M	R	65	2	10	Y	4.4	998	Y
PD14	72.3	F	R	28	2	5	N	5.3	700	Y
PD15	79.7	M	R	29	2	8	Y	1.7	300	Y
Mean (SD)	66.3 (9)			31.6 (15)	2.2 (0.8)	6.9 (3.2)		5.4 (3.6)	673 (506)	

TABLE 2 | Demographic and clinical characteristics of the study participants, overall and stratified on rigidity status.

	Low rigidity (*N* = 10)	High rigidity (*N* = 5)	Entire sample (*N* = 15)	*p*-value
Age (years)				0.442
Mean (SD)	68 (9)	63 (12)	66 (10)	
Range	51–80	47–81	47–81	
Sex				0.68
F	3 (30.0%)	1 (20.0%)	4 (26.7%)	
M	7 (70.0%)	4 (80.0%)	11 (73.3%)	
MDS-UPDRS-III				0.605
Mean (SD)	30 (17)	35 (7)	32 (15)	
Range	8–65	23–43	8–65	
Total rigidity†				0.189
Mean (SD)	4.0 (2.0)	6.0 (3.7)	4.7 (2.7)	
Range	2–8	3–12	2–12	
Faller				0.464
N	6 (60.0%)	2 (40.0%)	8 (53.3%)	
Y	4 (40.0%)	3 (60.0%)	7 (46.7%)	
PD Duration (years)				0.787
Mean (SD)	5.2 (4.8)	5.8 (2.2)	5.4 (3.7)	
Range	1.1–16.0	2.0–7.3	1.1–16.0	
LED (mg)				0.553
Mean (SD)	733 (558)	554 (482)	673 (524)	
Range	100–1,900	0–1,300	0–1,900	

† *Total rigidity omits leg rigidity score.*

four times, with a first swing excursion of greater than 100°, and negative peak angular speed of about −300°/s. A participant with mild to moderate rigidity (score = 2/4) exhibited a similar pattern (**Figure 3B**), with the leg oscillating five times before coming to rest. Although a participant with marked rigidity (**Figure 3C**, score = 3/4) also had about four-leg oscillations, the first swing excursion was smaller than participants with lower rigidity scores, near 90°, and negative peak angular speed of about −230°/s. In the participant with severe rigidity (**Figure 3D**, score = 4/4) no oscillations were observed, with the leg slowly lowering to a less vertical resting angle than other participants.

Low vs. High Rigidity Scores

We found differences in the biomechanical outcomes of the pendulum test between PD participants with low leg rigidity scores (1–2) and with high leg rigidity scores (3–4) during the resting condition (**Figure 4**). As rigidity increased there was a significant reduction of the first extension peak (**Figure 4B**, 58° ± 15 vs. 34° ± 23, $p = 0.042$), several oscillations (**Figure 4C**, 5 ± 1 vs. 3 ± 2, $p = 0.047$), relaxation index (**Figure 4E**, 1.5 ± 0.1 vs. 1.3 ± 0.2, $p = 0.013$) and maximum angular velocity (**Figure 4G**, 182°/s ± 35 vs. 105°/s ± 69, $p = 0.019$). Although not statistically significant, the first swing excursion showed also a trend toward reduction in the high rigidity group vs. the low rigidity group (**Figure 4A**, −97° ± 20 vs. −115° ± 11, $p = 0.051$). Furthermore, most of the individual values for both groups fell out of the range of the mean (±SD) of the biomechanical parameters (**Figure 4**, gray areas) estimated from previously reported pendulum test data in healthy subjects (Stillman and McMeeken, 1995).

TABLE 3 | Demographic and clinical characteristics of the study participants stratified on the prevalence of previous falls.

	Non-faller (*N* = 8)	Faller (*N* = 7)	*p*-value
Age (years)			0.454
Mean (SD)	68 (6)	64 (13)	
Range	58–76	47–81	
Sex			0.029
F	4 (50.0%)	0 (0.0%)	
M	4 (50.0%)	7 (100.0%)	
MDS-UPDRS-III			0.033
Mean (SD)	24.5 (12.1)	40.3 (13.5)	
Range	8–43	28–65	
Leg Rigidity			0.122
Mean (SD)	1.9 (0.8)	2.6 (0.8)	
Range	1–3	2–4	
Total Rigidity†			0.073
Mean (SD)	3.5 (1.8)	6.0 (3.1)	
Range	2–7	3–12	
Duration (years)			0.207
Mean (SD)	4.3 (2.7)	6.8 (4.5)	
Range	1.1–8.5	1.7–16.0	
LED (mg)			0.013
Mean (SD)	379 (257)	1,009 (562)	
Range	0–700	300–1,900	

†*Total rigidity omits leg rigidity score.*

Effects of Activation Maneuver

Individual differences in the effects of the activation maneuver were observed, even across participants with similar rigidity scores. For example, three individuals with the same rigidity score exhibited marked differences in whether and how biomechanical outcomes changed in the presence of an activation maneuver (**Figures 5A–C**, score = 2/2). Participant A (**Figure 5A**) exhibited eight oscillations of the leg during the resting condition and no changes in the kinematics during the activated condition, though increased BF tonic activity was observed before the movement. Although the other two participants with a leg rigidity score of 2 (**Figures 5B–C**) had a similar number of oscillations in the resting condition (N = 4) that was reduced during an activation maneuver (N = 3), they exhibited differences in other features of the pendulum test outcomes. During an activation maneuver in participant B (**Figure 5B**) first extension peak and maximum velocity decreased, tonic activity in both the RF and BF muscles increased, and reflexive activity in the BF was observed during the first knee extension. In Participant C (**Figure 5C**) a decrease in the first swing excursion, resting angle, and minimum and maximum angular velocity was observed during an activation maneuver, together with increased tonic activity in RF. Participant D had severe rigidity (**Figure 5D**) and did not exhibit any oscillations in either the resting or activated states, but angular velocity decreased in the presence of an activation maneuver. We also observed a change in resting angle after the end of the activation maneuver in the most severe subject (**Figure 5D**). We did not collect EMG data for participant D.

The changes in three biomechanical outcomes in the activation vs. resting state were found to have a distribution with a mean significantly different from zero, but the magnitude of this effect did not depend on the severity of leg rigidity (**Figure 6**). A one-sample t-test revealed a significant effect of activation on the first extension peak (**Figure 6B**, $-5.4° \pm 13.4$, $p = 0.018$), number of oscillations (**Figure 6C**, -0.8 ± 0.9, $p = 0.013$) and duration of the oscillations (**Figure 6D**, $-0.9\text{s} \pm 1.0$, $p = 0.013$). A two-sample t-test did not reveal any significant difference in the effect of activation maneuver on the biomechanical outcomes of the pendulum test when comparing the group with low rigidity (1–2) to the group with high rigidity (3–4; **Figure 6**, all $p > 0.05$).

Fallers vs. Non Fallers

In contrast, the effect of an activation maneuver on the biomechanical outcomes of the pendulum test was significantly different in non-fallers vs. fallers (**Figure 7**). In fallers compared to non-fallers, two-sample t-test revealed a significant decrease of first swing excursion (**Figure 7A**, $6.5° \pm 5.3$ vs. $-3.1° \pm 2.1$, $p = 0.002$), first extension peak (**Figure 7B**, $-13.1° \pm 14.9$ vs. $2.1° \pm 5.7$, $p = 0.026$), resting angle (**Figure 7F**, $2.6° \pm 3.6$ vs. $-1.2° \pm 1.4$, $p = 0.019$) and minimum angular velocity (**Figure 7H**, $27.0°/\text{s} \pm 35.1$ vs. $-10.4°/\text{s} \pm 30.1$, $p = 0.026$).

Non-parametric Tests Performed *Post hoc*

In addition to the statistical tests described above, we performed additional non-parametric tests *post hoc* to verify that the primary results were insensitive to departures from normality. We tested the distributions of each variable entered into analyses (eight outcomes in resting and eight change scores between resting and activated for 16 total) with Shapiro–Wilk tests. Of these, five Shapiro–Wilk tests were indicative of non-normality. For these, we repeated the analyses using Wilcoxon rank-sum tests. Overall, the results were similar, with only the first extension peak test being no longer statistically significant ($p = 0.106$) when performed non-parametrically.

DISCUSSION

Our results demonstrate that the pendulum test is an objective measure to assess both resting and activated lower leg rigidity in people with PD. Five biomechanical metrics (first swing excursion, first extension peak, number of oscillations, relaxation index, and maximum angular velocity) describing the oscillating pattern of the leg during the pendulum test were lower in those

TABLE 4 | Effect size using Cohen's *d* (Cohen, 1992).

	FSE	FEP	N	D	RI	θ_{rest}	V_{max}	V_{min}
Rest: high vs. low rigidity	−1.25	1.31	1.27	1.11	−0.87	1.68	1.57	−0.41
Δ Rest-activated: entire sample	−0.85	0.22	0.20	−0.10	−0.41	−0.27	2.13	1.49
Δ Rest-activated: high vs. low rigidity	−0.17	−0.49	−0.19	0.39	−0.04	−0.29	−2.42	−0.60
Δ Rest-activated: fallers vs. non-fallers	0.46	−1.14	−1.41	1.23	1.35	1.25	−0.83	−0.56

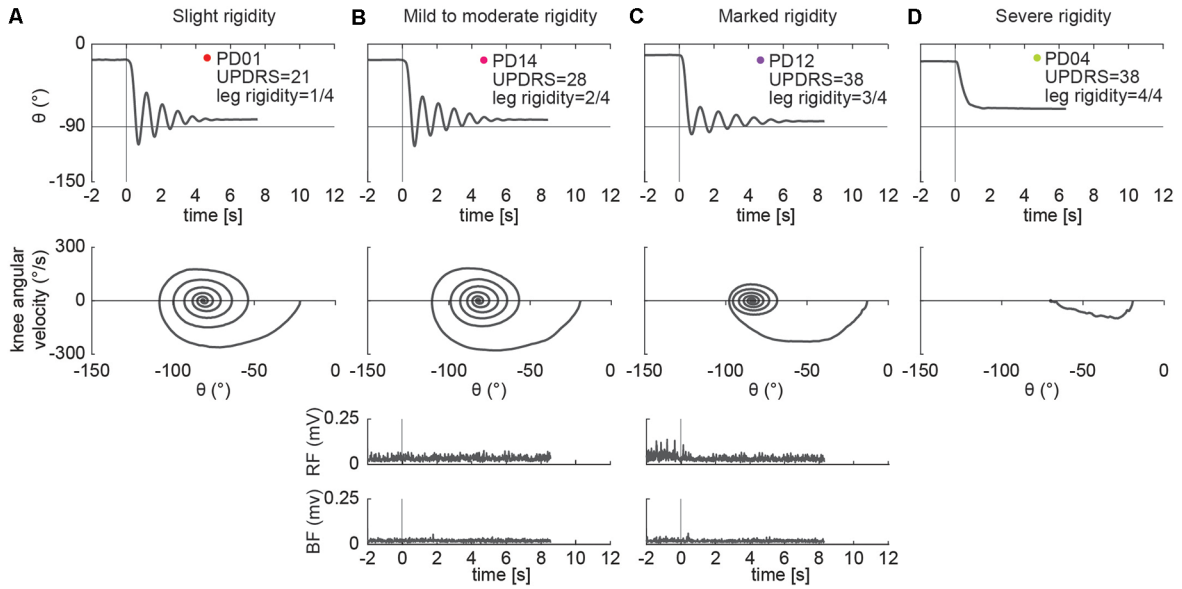

FIGURE 3 | Example of pendulum test kinematic traces and EMGs in four PD individuals with increasing levels of lower leg rigidity (as measured by following the UPDRS guidelines). Slight rigidity **(A)**. Mild to moderate rigidity **(B)**. Marked rigidity **(C)**. Severe rigidity **(D)**. No EMG was recorded in PD01 and PD04.

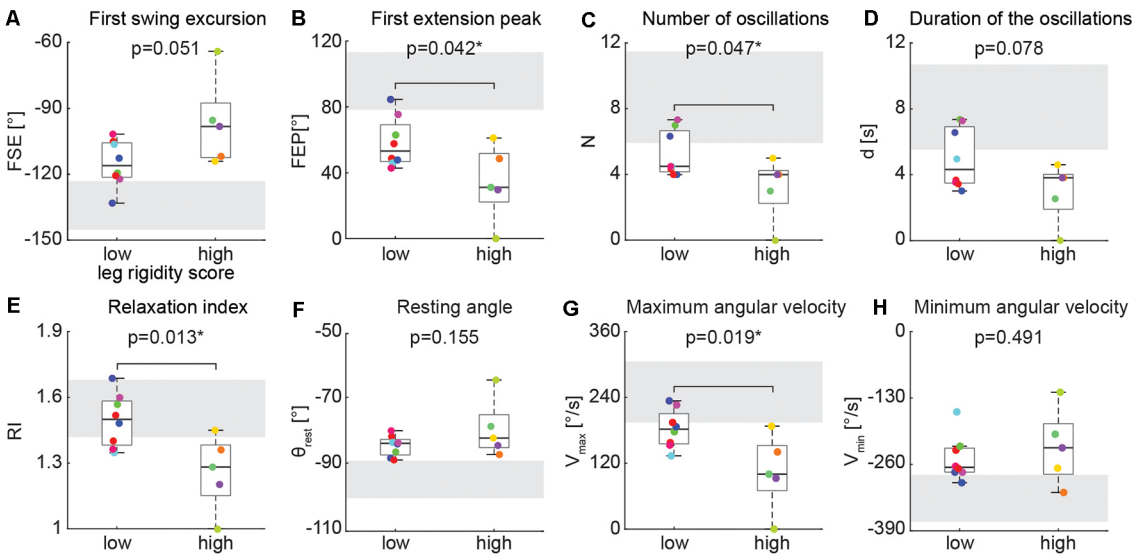

FIGURE 4 | Kinematic outcomes of the pendulum test in the baseline condition. First swing excursion (FSE; **A**), first extension peak (FPE; **B**), number (N; **C**) and duration (d; **D**) of the oscillations, resting angle (θ_{rest}; **E**), relaxation index (RI; **F**), maximum (V_{max}; **G**) and minimum (V_{min}; **H**) angular velocity. Subjects were grouped based on the rigidity score of the recorded leg: subjects with leg rigidity score from 1 to 2 (low rigidity, $n = 8$) and subjects with leg rigidity score from 3 to 4 (high rigidity, $n = 5$). Gray areas correspond to mean ± SD of biomechanical outcomes for healthy subjects estimated from Stillman and McMeeken (1995). Asterisks denote significant values ($p < 0.05$).

with higher leg rigidity scores, suggesting that a simple kinematic analysis of the pendulum test is sufficient to assess leg rigidity in PD. Further, in the presence of an activation maneuver, the pendulum test biomechanical outcomes were altered to a different extent among participants suggesting a sensitivity of the pendulum test to changes in rigidity. However, the effects of the activation maneuver on biomechanical outcomes were independent of the severity of leg rigidity scores at rest. On the contrary, individuals exhibiting an effect of the activation maneuver on biomechanical outcomes experience more falls in the preceding 6 months, suggesting that increased activated rigidity could be related to increased risk of falls and highlighting

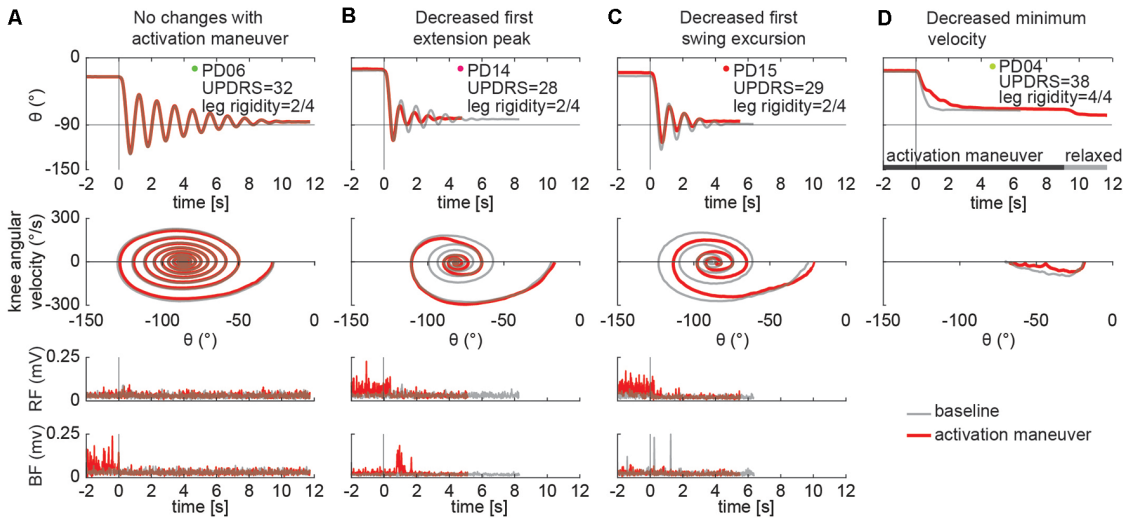

FIGURE 5 | Individual specific changes in the pattern of leg movement and EMG activity among PD subjects while performing an activation maneuver (AM). In subject PD06 we found no kinematic changes with an activation maneuver **(A)**. In subject PD14 we found a decrease in the first extension peak and of the number and duration of the oscillations during AM **(B)**. In subject PD15 we found a decrease in the first swing excursion and of the number and duration of the oscillations during AM **(C)**. In the subject with severe rigidity (PD04), we found a decrease in the angular velocity of the leg during AM. No EMG recorded in PD04 **(D)**.

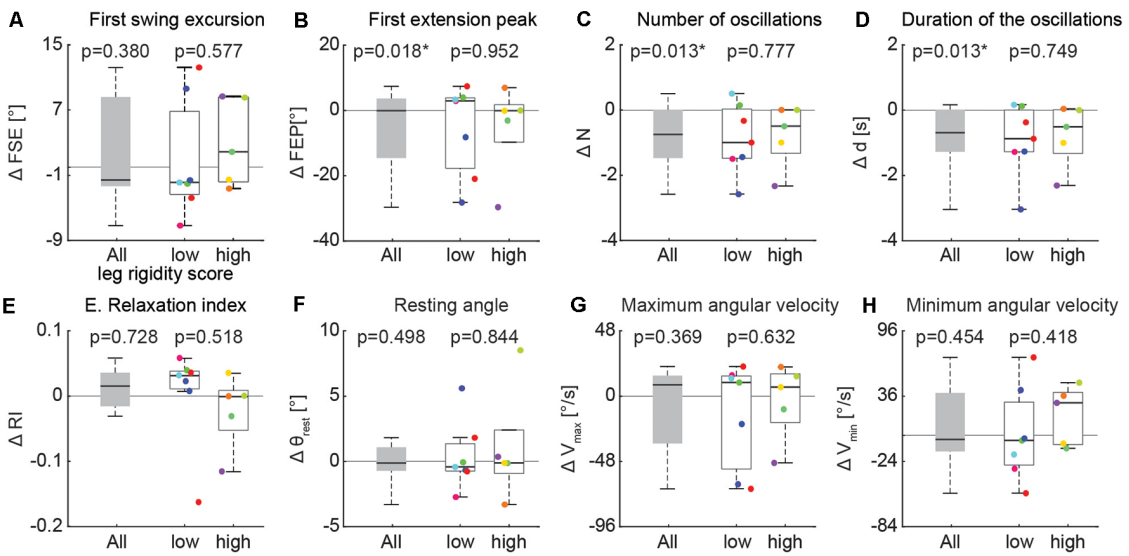

FIGURE 6 | Variation of kinematic outcomes of the pendulum test during an activation maneuver. First swing excursion (FSE; **A**), first extension peak (FPE; **B**), number (N; **C**) and duration (d; **D**) of the oscillations, resting angle (θ_{rest}; **E**), relaxation index (RI; **F**), maximum (V_{max}; **G**) and minimum (V_{min}; **H**) angular velocity. Each point represents the difference between the mean values of each outcome for one participant while performing an activation maneuver vs. the resting condition. Subjects were grouped based on the rigidity score of the recorded leg: subjects with leg rigidity score from 0 to 2 (low rigidity, $n = 7$) and subjects with leg rigidity score from 3 to 4 (high rigidity, $n = 5$). Asterisks denote significant values ($p < 0.05$).

the need to clinically evaluate activated rigidity independently from resting rigidity. Individual differences in the changes in biomechanics and muscle activity when performing the activation maneuver also suggest that there may be diverse underlying neural mechanisms at play that warrant further investigation. We conclude that activated rigidity may play an important yet unexplored role in fall risk in people with PD. The pendulum test may provide an important objective evaluation of resting and activated rigidity that may contribute to a better understanding of fundamental mechanisms underlying motor symptoms in PD and their fluctuations, evaluate the efficacy of treatments, and potentially reduce the risk of falls.

This is the first study to demonstrate that biomechanical outcomes of the pendulum test may be useful in objectively

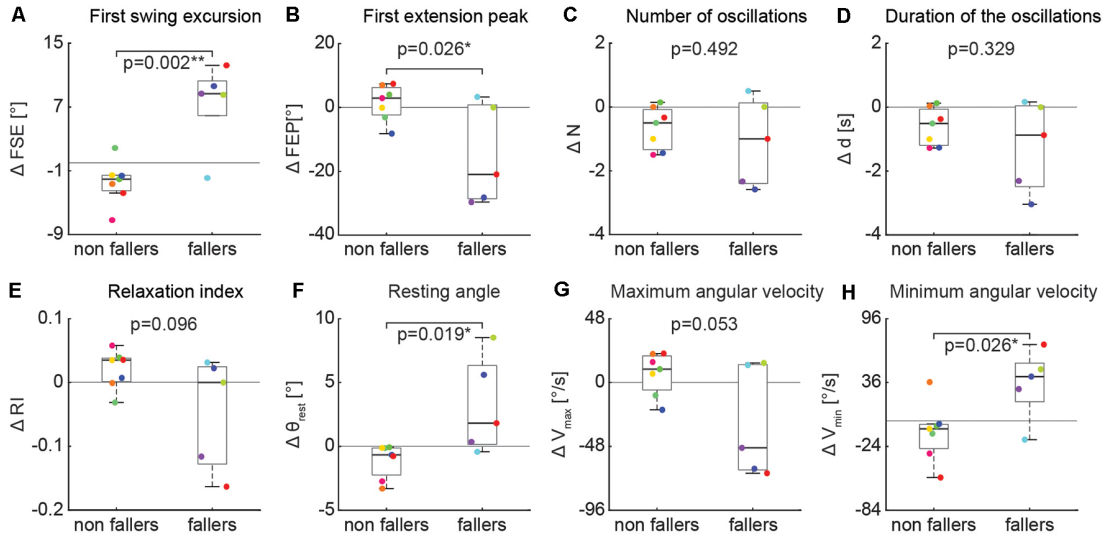

FIGURE 7 | Variation of kinematic outcomes of the pendulum test during an activation maneuver in non-fallers (n = 7) and fallers (n = 5). First swing excursion (FSE; **A**), first extension peak (FPE; **B**), number (N; **C**) and duration (d; **D**) of the oscillations, resting angle (θ_{rest}; **E**), relaxation index (RI; **F**), maximum (V_{max}; **G**) and minimum (V_{min}; **H**) angular velocity. Each point represents the difference between the mean values of each outcome for a participant while performing an activation maneuver vs. during the baseline condition. Asterisks denote significant values ($p < 0.05$).

assessing the severity of leg rigidity among PD participants. A few studies have described the abnormal pattern (i.e., reduced number of oscillations, maximum velocity and relaxation index) of the pendulum test in people with leg rigidity (Schwab, 1963; Brown et al., 1988; Le Cavorzin et al., 2003), but its relationship to the severity of rigidity has not been assessed previously. Here we found that the first extension peak, the number of oscillations, relaxation index, and maximum angular velocity were significantly decreased in PD people with marked rigidity compared to PD people with moderate rigidity. Further, we observed that our less rigid group had altered pendulum test kinematics concerning outcomes reported previously in healthy adults (Stillman and McMeeken, 1995), although some of the differences could be attributable to aging and require further exploration. In this pilot study, we focused on the differences in biomechanical outcomes between low and high rigidity groups, but larger studies will be required to assess the sensitivity, reliability, and repeatability to validate these measures for clinical assessment of rigidity and account for potential confounding factors (McKay et al., 2018).

The pendulum test has the potential to be an objective, simple, fast, practical, and affordable diagnostic method to evaluate rigidity. Expert neurologists can commit an error of up to 20% in assessing rigidity (Rizzo et al., 2016). Other instrumented clinical tests allow the evaluation of objective continuous parameters overcoming the limitations of the UPDRS rating scale (i.e., low resolution, inter-and intra- rater unreliability, ceiling effect), which include surface electromyography (Eisen, 1987; Andreeva and Khutorskaya, 1996), myometry (Marusiak et al., 2010), and/or torque measuring devices (Kirollos et al., 1996; Patrick et al., 2001; Endo et al., 2009; Xia et al., 2011; Powell et al., 2012; Zetterberg et al., 2015). However, to the best of our knowledge, all the methods previously proposed in the literature focused on the objective quantification of upper limb rigidity (Ferreira-Sánchez et al., 2020). The biomechanical outcomes of the pendulum test can be easily evaluated through simple observation of the leg swing or by using affordable devices equipped with gyroscope (Yeh et al., 2016) or simple video source (i.e., markerless motion capture, Mathis et al., 2018), making it feasible for standard clinical practice and telemedicine. For example, automated analysis of the pendulum test could be implemented into smartphones (Prince et al., 2018) whereas prior methods require expensive additional devices, data processing, and technical assistance (Ferreira-Sánchez et al., 2020).

This study supports the idea that resting and activated rigidity should be regarded as independent variables and scored separately (Fung et al., 2000). Currently, activation maneuvers are used in clinical evaluation only to detect rigidity at an early stage, or to bring rigidity into evidence if it does not manifest at rest. In this case, the UPDRS rating system assigns a score of 1, which is not dependent on the amount of rigidity elicited by the activation maneuver, and activated rigidity is not assessed if the resting rigidity is scored at a 1 or higher. Despite several studies quantifying the effect of an activation maneuver on rigidity (Fung et al., 2000; Hong et al., 2007; Powell et al., 2011), it is not clear whether the activated rigidity is greater in people with higher resting rigidity. Here, biomechanical outcomes revealed no differences in the effect of activation maneuvers between groups with clinically assessed low and high rigidity, suggesting that the effect of the activation maneuvers may be independent of rigidity severity at rest. Heterogeneity in the manifestation of activated rigidity may further provide insight into the varied mechanisms of motor impairment in people with PD. Several factors have been suggested to contribute to the rigidity (Berardelli et al., 1983;

van den Noort et al., 2017) including an increase in involuntary background activation (Marsden, 1982), changes in non-neural muscle tissue properties (Dietz et al., 1981), increased stretch reflexes (Tatton and Lee, 1975; Meara and Cody, 1993; Xia et al., 2016) and presence of shortening reaction (Lee et al., 2002; Xia et al., 2009). Furthermore, asymmetrical patterns of rigidity can be present among extensors and flexors (Meara and Cody, 1993; Xia et al., 2009). Although we recorded EMG activity only in a subsample of participants, our exploratory results suggest that increased tonic and reflex activity could be not mutually exclusive manifestations of rigidity. Indeed, while some individuals showed an increase of tonic activity in either flexors or extensors during an activation maneuver, others had an increase of muscle activity time-locked to the kinematic trajectories, consistent with reflexive activity.

Clinical assessment of activated rigidity—even when rigidity at rest is present—could help identify individuals with a higher risk of falls. The recently identified relationship between leg rigidity and falls in people with PD (McKay et al., 2019) highlights the need for more objective and continuous measures of leg rigidity (Ward et al., 1983). Here, we showed that the effects of the activation maneuver on pendulum test kinematics are greater in fallers compared to non-fallers, suggesting a potential role of activated rigidity in postural instability. Activated rigidity likely reflects a more realistic scenario of daily life, in which different concurrent tasks (such as talking or carrying an object) are performed during balance control. We found no significant difference among the tested activation maneuvers, supporting previous findings of the non-specificity of activation procedures (Hong et al., 2007). Moreover, several studies have shown that treatments can have a differential efficacy in reducing resting and activated rigidity (Webster and Mortimer, 1977; Caligiuri and Galasko, 1992; Kirollos et al., 1996; Krack et al., 2003; Shapiro et al., 2007). As such, the monitoring of activated rigidity could help predict the functional motor impairments arising during daily activities that may lead to falls, although this relationship is still unknown. The efficacy of treatments and rehabilitative interventions aimed at reducing rigidity should take into account individual responsiveness to both resting and activated rigidity. The pendulum test could help identify the extent to which multiple impaired physiological mechanisms manifest from patient to patient, representing a potential approach to understand the functional implications of resting and activated rigidity on movement.

This study had several limitations. First, the small sample size did not allow us to assess the sensitivity and validity of the pendulum test as a tool to measure the severity of resting and activated rigidity in PD. Increasing the cohort would also account for possible confounding factors such as the absence of women in the fallers group, and the difference in Total MDS-UPDRS-III score, rigidity score, and LED between the fallers and non-fallers groups. Second, we did not collect detailed information about the nature of the falls when reported retrospectively, which may be unreliable. However, studies have shown that falling frequency, situation (i.e., during sitting/standing, walking and turning), severity and direction could help in interpreting the mechanisms leading to falls in PD (Hiorth et al., 2013; Youn et al., 2017). Last, we collected EMG only in a subset of participants (n = 10, two of which were excluded from the analysis since they were unable to relax). This limited our ability to assess the neuropathological mechanisms that are mainly responsible for the abnormal pattern of the leg during the pendulum test in PD.

In conclusion, our results suggest that the biomechanical analysis of the pendulum test may provide an objective method to assess rigidity in people with PD that could be implemented into clinical practice. We also showed that the effect of an activation maneuver on pendulum test kinematics is variable across PD participants and independent from the leg rigidity score evaluated at rest, and thus should be scored separately. The importance of assessing activated rigidity is also highlighted by the increased effects of an activation maneuver in fallers compared to non-fallers PD groups. Further studies are necessary to elucidate the neurophysiological mechanisms of rigidity causing the abnormal pattern of the pendulum test in PD.

DATA AVAILABILITY STATEMENT

The raw data supporting the conclusions of this article will be made available by the authors, without undue reservation.

ETHICS STATEMENT

The studies involving human participants were reviewed and approved by Institutional Review Board of Emory University. The patients/participants provided their written informed consent to participate in this study. Written informed consent was obtained from the individual(s) for the publication of any potentially identifiable images or data included in this article.

AUTHOR CONTRIBUTIONS

LT and GM contributed to the conception of the study and wrote the original draft of the manuscript. GM, JM and LT contributed to the design of the experiments. GM performed the experiments and analyzed the data. GM and JM performed the statistical analysis. JM and SF provided clinical data. All authors contributed to the article and approved the submitted version.

FUNDING

This study was supported in part by National Institutes of Health grants R01HD046922, R01HD090642, K25HD086276, and the Sartain Lanier Family Foundation. JM has received research funding or support from the National Institutes of Health. SF has received research funding or support from Medtronics, Boston Scientific, Biohaven, Impax, Lilly, US World Meds, Sunovion Therapeutics, Vaccinex, Voyager, Jazz Pharmaceuticals, CHDI Foundation, Michael J. Fox Foundation, NIH (U10 NS077366), Parkinson Foundation. SF has received honoraria from Lundbeck, Sunovion, Biogen, Acadia, Impel, Acorda, CereSpir. SF has received royalties from Demos, Blackwell Futura, Springer for textbooks and Uptodate. LT has received research funding or support from the National Institutes of Health and the National Science Foundation.

REFERENCES

Andreeva, Y., and Khutorskaya, O. (1996). Application EMGs spectral analysis method for the objective diagnosis of different clinical forms of Parkinson's disease. *Electromyogr. Clin. Neurophysiol.* 36, 187–192.

Berardelli, A., Sabra, A. F., and Hallett, M. (1983). Physiological mechanisms of rigidity in Parkinson's disease. *J. Neurol. Neurosurg. Psychiatry* 46, 45–53. doi: 10.1136/jnnp.46.1.45

Bianchi, L., Monaldi, F., Paolucci, S., Iani, C., and Lacquaniti, F. (1999). Quantitative analysis of the pendulum test: application to multiple sclerosis patients treated with botulinum toxin. *Funct. Neurol.* 14, 79–92.

Bohannon, R. W., Harrison, S., and Kinsella-Shaw, J. (2009). Reliability and validity of pendulum test measures of spasticity obtained with the Polhemus tracking system from patients with chronic stroke. *J. Neuroeng. Rehabil.* 6:30. doi: 10.1186/1743-0003-6-30

Brown, R. A., Lawson, D. A., Leslie, G. C., MacArthur, A., MacLennan, W. J., McMurdo, M. E., et al. (1988). Does the Wartenberg pendulum test differentiate quantitatively between spasticity and rigidity? A study in elderly stroke and Parkinsonian patients. *J. Neurol. Neurosurg. Psychiatry* 51, 1178–1186. doi: 10.1136/jnnp.51.9.1178

Caligiuri, M. P., and Galasko, D. R. (1992). Quantifying drug-induced changes in parkinsonian rigidity using an instrumental measure of activated stiffness. *Clin. Neuropharmacol.* 15, 1–12. doi: 10.1097/00002826-199202000-00001

Cohen, J. (1992). A power primer. *Psychol. Bull.* 112, 155–159. doi: 10.1037/0033-2909.112.1.155

De Groote, F., Blum, K. P., Horslen, B. C., and Ting, L. H. (2018). Interaction between muscle tone, short-range stiffness and increased sensory feedback gains explains key kinematic features of the pendulum test in spastic cerebral palsy: a simulation study. *PLoS One* 13:e0205763. doi: 10.1371/journal.pone.0205763

Dietz, V., Quintern, J., and Berger, W. (1981). Electrophysiological studies of gait in spasticity and rigidity. Evidence that altered mechanical properties of muscle contribute to hypertonia. *Brain* 104, 431–449. doi: 10.1093/brain/104.3.431

Eisen, A. (1987). Electromyography in disorders of muscle tone. *Can. J. Neurol. Sci.* 14, 501–505. doi: 10.1017/s0317167100037999

Endo, T., Okuno, R., Yokoe, M., Akazawa, K., and Sakoda, S. (2009). A novel method for systematic analysis of rigidity in Parkinson's disease. *Mov. Disord.* 24, 2218–2224. doi: 10.1002/mds.22752

Endo, T., Yoshikawa, N., Fujimura, H., and Sakoda, S. (2015). Parkinsonian rigidity depends on the velocity of passive joint movement. *Parkinsons Dis.* 2015:961790. doi: 10.1155/2015/961790

Ertuglu, L. A., Karacan, I., Yilmaz, G., and Türker, K. S. (2018). Standardization of the Jendrassik maneuver in Achilles tendon tap reflex. *Clin. Neurophysiol. Pract.* 3, 1–5. doi: 10.1016/j.cnp.2017.10.003

Fahn, S., and Elton, R. L. (1987). "UPDRS program members. Unified Parkinson's disease rating scale," in *Recent Developments in Parkinson's Disease*, ed. S. Fahn (Florham, NJ: Macmillian Healthcare), 153–163.

Fee, J. W. Jr., and Miller, F. (2004). The Leg Drop Pendulum Test performed under general anesthesia in spastic cerebral palsy. *Dev. Med. Child Neurol.* 46, 273–281. doi: 10.1111/j.1469-8749.2004.tb00482.x

Ferreira, D. M., Liang, H., and Wu, J. (2020). Knee joint kinematics of the pendulum test in children with and without Down syndrome. *Gait Posture* 76, 311–317. doi: 10.1016/j.gaitpost.2019.12.025

Ferreira-Sánchez, M. D. R., Moreno-Verdú, M., and Cano-de-la-Cuerda, R. (2020). Quantitative measurement of rigidity in Parkinson's disease: a systematic review. *Sensors* 20:880. doi: 10.3390/s20030880

Fowler, E. G., Nwigwe, A. I., and Ho, T. W. (2000). Sensitivity of the pendulum test for assessing spasticity in persons with cerebral palsy. *Dev. Med. Child Neurol.* 42, 182–189. doi: 10.1017/s0012162200000323

Franzén, E., Paquette, C., Gurfinkel, V. S., Cordo, P. J., Nutt, J. G., and Horak, F. B. (2009). Reduced performance in balance, walking and turning tasks is associated with increased neck tone in Parkinson's disease. *Exp. Neurol.* 219, 430–438. doi: 10.1016/j.expneurol.2009.06.013

Fung, V. S., Burne, J. A., and Morris, J. G. (2000). Objective quantification of resting and activated parkinsonian rigidity: a comparison of angular impulse and work scores. *Mov. Disord.* 15, 48–55. doi: 10.1002/1531-8257(200001)15:1<48::aid-mds1009>3.0.co;2-e

Fung, V., and Thompson, P. (2002). *Rigidity and Spasticity.* Lippincott Williams and Wilkins. Available online at: https://digital.library.adelaide.edu.au/dspace/handle/2440/33112. Accessed January 15, 2019.

Hiorth, Y. H., Lode, K., and Larsen, J. P. (2013). Frequencies of falls and associated features at different stages of Parkinson's disease. *Eur. J. Neurol.* 20, 160–166. doi: 10.1111/j.1468-1331.2012.03821.x

Hong, M., Perlmutter, J. S., and Earhart, G. M. (2007). Enhancement of rigidity in Parkinson's disease with activation. *Mov. Disord.* 22, 1164–1168. doi: 10.1002/mds.21524

Julious, S. A. (2005). Sample size of 12 per group rule of thumb for a pilot study. *Pharm. Stat.* 4, 287–291. doi: 10.1002/pst.185

Kelly, V. E., Eusterbrock, A. J., and Shumway-Cook, A. (2012). A review of dual-task walking deficits in people with Parkinson's disease: motor and cognitive contributions, mechanisms, and clinical implications. *Parkinsons Dis.* 2012:918719. doi: 10.1155/2012/918719

Kirollos, C., Charlett, A., O'Neill, C. J., Kosik, R., Mozol, K., Purkiss, A. G., et al. (1996). Objective measurement of activation of rigidity: diagnostic, pathogenetic and therapeutic implications in parkinsonism. *Br. J. Clin. Pharmacol.* 41, 557–564. doi: 10.1046/j.1365-2125.1996.38313.x

Krack, P., Batir, A., Van Blercom, N., Chabardes, S., Fraix, V., Ardouin, C., et al. (2003). Five-year follow-up of bilateral stimulation of the subthalamic nucleus in advanced Parkinson's disease. *N. Engl. J. Med.* 349, 1925–1934. doi: 10.1056/NEJMoa035275

Kristinsdottir, K., Magnusdottir, G., Chenery, B., Gudmundsdottir, V., Gudfinnsdottir, H. K., Karason, H., et al. (2020). Comparison of spasticity in spinal cord injury and stroke patients using reflex period in pendulum test. *Eur. J. Transl. Myol.* 30:8907. doi: 10.4081/ejtm.2019.8907

Langston, J. W., Widner, H., Goetz, C. G., Brooks, D., Fahn, S., Freeman, T., et al. (1992). Core assessment program for intracerebral transplantations (CAPIT). *Mov. Disord.* 7, 2–13. doi: 10.1002/mds.870070103

Le Cavorzin, P., Carrault, G., Chagneau, F., Rochcongar, P., and Allain, H. (2003). A computer model of rigidity and related motor dysfunction in Parkinson's disease. *Mov. Disord.* 18, 1257–1265. doi: 10.1002/mds.10532

Lee, H.-M., Huang, Y.-Z., Chen, J.-J. J., and Hwang, I.-S. (2002). Quantitative analysis of the velocity related pathophysiology of spasticity and rigidity in the elbow flexors. *J. Neurol. Neurosurg. Psychiatry* 72, 621–629. doi: 10.1136/jnnp.72.5.621

Lin, D. C., and Rymer, W. Z. (1991). A quantitative analysis of pendular motion of the lower leg in spastic human subjects. *IEEE Trans. Biomed. Eng.* 38, 906–918. doi: 10.1109/10.83611

Lotfian, M., Mirbagheri, M. M., Kharazi, M. R., Dadashi, F., Nourian, R., Irani, A., et al. (2016). "Pendulum test measure correlates with gait parameters in children with cerebral palsy," in *38th Annual International Conference of the IEEE Engineering in Medicine and Biology Society (EMBC)*, (Orlando, FL), 1708–1711. doi: 10.1109/EMBC.2016.7591045

Marsden, C. D. (1982). The mysterious motor function of the basal ganglia: the Robert Wartenberg Lecture. *Neurology* 32, 514–539. doi: 10.1212/wnl.32.5.514

Martínez-Martín, P., Gil-Nagel, A., Gracia, L. M., Gómez, J. B., Martínez-Sarriés, J., and Bermejo, F. (1994). Unified Parkinson's Disease Rating Scale characteristics and structure. The Cooperative Multicentric Group. *Mov. Disord.* 9, 76–83. doi: 10.1002/mds.870090112

Marusiak, J., Kisiel-Sajewicz, K., Jaskólska, A., and Jaskólski, A. (2010). Higher muscle passive stiffness in Parkinson's disease patients than in controls measured by myotonometry. *Arch. Phys. Med. Rehabil.* 91, 800–802. doi: 10.1016/j.apmr.2010.01.012

Mathis, A., Mamidanna, P., Cury, K. M., Abe, T., Murthy, V. N., Mathis, M. W., et al. (2018). DeepLabCut: markerless pose estimation of user-defined body parts with deep learning. *Nat. Neurosci.* 21, 1281–1289. doi: 10.1038/s41593-018-0209-y

Matsumoto, K., Rossmann, F., Lin, T. H., and Cooper, I. S. (1963). Studies on induced exacerbation of Parkinsonian rigidity. *J. Neurol. Neurosurg. Psychiatry* 26, 27–32. doi: 10.1136/jnnp.26.1.27

McKay, J. L., Hackney, M. E., Factor, S. A., and Ting, L. H. (2019). Lower limb rigidity is associated with frequent falls in Parkinson's disease. *Mov. Disord. Clin. Pract.* 6, 446–451. doi: 10.1002/mdc3.12784

McKay, J. L., Lang, K. C., Ting, L. H., and Hackney, M. E. (2018). Impaired set shifting is associated with previous falls in individuals with and without

Parkinson's disease. *Gait Posture* 62, 220–226. doi: 10.1016/j.gaitpost.2018.02.027

Meara, R. J., and Cody, F. W. (1992). Relationship between electromyographic activity and clinically assessed rigidity studied at the wrist joint in Parkinson's disease. *Brain* 115, 1167–1180. doi: 10.1093/brain/115.4.1167

Meara, R. J., and Cody, F. W. (1993). Stretch reflexes of individual parkinsonian patients studied during changes in clinical rigidity following medication. *Electroencephalogr. Clin. Neurophysiol.* 89, 261–268. doi: 10.1016/0168-5597(93)90105-x

Mendonça, D. A., and Jog, M. S. (2008). Tasks of attention augment rigidity in mild Parkinson disease. *Can. J. Neurol. Sci.* 35, 501–505. doi: 10.1017/s0317167100009197

Patrick, S. K., Denington, A. A., Gauthier, M. J., Gillard, D. M., and Prochazka, A. (2001). Quantification of the UPDRS rigidity scale. *IEEE Trans. Neural Syst. Rehabil. Eng.*, 9, 31–41. doi: 10.1109/7333.918274

Powell, D., Hanson, N., Threlkeld, A. J., Fang, X., and Xia, R. (2011). Enhancement of parkinsonian rigidity with contralateral hand activation. *Clin. Neurophysiol.* 122, 1595–1601. doi: 10.1016/j.clinph.2011.01.010

Powell, D., Muthumani, A., and Xia, R.-P. (2017). Normalizing EMG to background muscle activation masks medication-induced reductions in reflex amplitudes in Parkinsonian rigidity. *J. Nat. Sci.* 3:e315. Available online at: http://www.jnsci.org/index.php?journal=nsci&page=article&op=view&path%5B%5D=315.

Powell, D., Threlkeld, A. J., Fang, X., Muthumani, A., and Xia, R. (2012). Amplitude- and velocity-dependency of rigidity measured at the wrist in Parkinson's disease. *Clin. Neurophysiol.* 123, 764–773. doi: 10.1016/j.clinph.2011.08.004

Prince, J., Arora, S., and de Vos, M. (2018). Big data in Parkinson's disease: using smartphones to remotely detect longitudinal disease phenotypes. *Physiol. Meas.* 39:044005. doi: 10.1088/1361-6579/aab512

Relja, M. A., Petravic, D., and Kolaj, M. (1996). Quantifying rigidity with a new computerized elbow device. *Clin. Neuropharmacol.* 19, 148–156. doi: 10.1097/00002826-199619020-00003

Rizzo, G., Copetti, M., Arcuti, S., Martino, D., Fontana, A., and Logroscino, G. (2016). Accuracy of clinical diagnosis of Parkinson disease: a systematic review and meta-analysis. *Neurology* 86, 566–576. doi: 10.1212/WNL.0000000000002350

Safavynia, S. A., and Ting, L. H. (2013). Long-latency muscle activity reflects continuous, delayed sensorimotor feedback of task-level and not joint-level error. *J. Neurophysiol.* 110, 1278–1290. doi: 10.1152/jn.00609.2012

Schwab, R. S. (1963). Evaluation and correlations of the wartenberg swing tests in Parkinson's disease. *Trans. Am. Neurol. Assoc.* 88, 270–274.

Shapiro, M. B., Vaillancourt, D. E., Sturman, M. M., Metman, L. V., Bakay, R. A. E., and Corcos, D. M. (2007). Effects of STN DBS on rigidity in Parkinson's disease. *IEEE Trans. Neural Syst. Rehabil. Eng.* 15, 173–181. doi: 10.1109/TNSRE.2007.896997

Shimoyama, I., Ninchoji, T., and Uemura, K. (1990). The finger-tapping test. A quantitative analysis. *Arch. Neurol.* 47, 681–684. doi: 10.1001/archneur.1990.00530060095025

Stillman, B., and McMeeken, J. (1995). A video-based version of the pendulum test: technique and normal response. *Arch. Phys. Med. Rehabil.* 76, 166–176. doi: 10.1016/s0003-9993(95)80026-3

Szopa, A., Domagalska-Szopa, M., Kidoń, Z., and Syczewska, M. (2014). Quadriceps femoris spasticity in children with cerebral palsy: measurement with the pendulum test and relationship with gait abnormalities. *J. Neuroeng. Rehabil.* 11:166. doi: 10.1186/1743-0003-11-166

Tatton, W. G., and Lee, R. G. (1975). Evidence for abnormal long-loop reflexes in rigid Parkinsonian patients. *Brain Res.* 100, 671–676. doi: 10.1016/0006-8993(75)90167-5

Torres-Oviedo, G., and Ting, L. H. (2007). Muscle synergies characterizing human postural responses. *J. Neurophysiol.* 98, 2144–2156. doi: 10.1152/jn.01360.2006

Valle, M. S., Casabona, A., Sgarlata, R., Garozzo, R., Vinci, M., and Cioni, M. (2006). The pendulum test as a tool to evaluate passive knee stiffness and viscosity of patients with rheumatoid arthritis. *BMC Musculoskelet. Disord.* 7:89. doi: 10.1186/1471-2474-7-89

van den Noort, J. C., Bar-On, L., Aertbeliën, E., Bonikowski, M., Braendvik, S. M., Broström, E. W., et al. (2017). European consensus on the concepts and measurement of the pathophysiological neuromuscular responses to passive muscle stretch. *Eur. J. Neurol.* 24:981–e38. doi: 10.1111/ene.13322

Vittinghoff, E., and McCulloch, C. E. (2007). Relaxing the rule of ten events per variable in logistic and Cox regression. *Am. J. Epidemiol.* 165, 710–718. doi: 10.1093/aje/kwk052

Ward, C. D., Sanes, J. N., Dambrosia, J. M., and Calne, D. B. (1983). Methods for evaluating treatment in Parkinson's disease. *Adv. Neurol.* 37, 1–7.

Wartenberg, R. (1951). Pendulousness of the legs as a diagnostic test. *Neurology* 1, 18–24. doi: 10.1212/wnl.1.1.18

Webster, D. D., and Mortimer, J. A. (1977). Failure of L-dopa to relieve activated rigidity in Parkinson's disease. *Adv. Exp. Med. Biol.* 90, 297–313. doi: 10.1007/978-1-4684-2511-6_21

Welch, T. D. J., and Ting, L. H. (2008). A feedback model reproduces muscle activity during human postural responses to support-surface translations. *J. Neurophysiol.* 99, 1032–1038. doi: 10.1152/jn.01110.2007

Whelan, A., Sexton, A., Jones, M., O'Connell, C., and McGibbon, C. A. (2018). Predictive value of the pendulum test for assessing knee extensor spasticity. *J. Neuroeng. Rehabil.* 15:68. doi: 10.1186/s12984-018-0411-x

Willaert, J., Desloovere, K., Van Campenhout, A., Ting, L. H., and De Groote, F. (2020). Movement history influences pendulum test kinematics in children with spastic cerebral palsy. *Front. Bioeng. Biotechnol.* 8:920. doi: 10.3389/fbioe.2020.00920

Winter, D. A. (ed.). (2009). "Kinesiological electromyography," in *Biomechanics and Motor Control of Human Movement* (Hoboken, NJ: John Wiley & Sons, Ltd.), 250–280.

Wright, W. G., Gurfinkel, V. S., Nutt, J., Horak, F. B., and Cordo, P. J. (2007). Axial hypertonicity in Parkinson's disease: direct measurements of trunk and hip torque. *Exp. Neurol.* 208, 38–46. doi: 10.1016/j.expneurol.2007.07.002

Xia, R. (2011). "Physiological and biomechanical analyses of rigidity in Parkinson's disease," in *Etiology and Pathophysiology of Parkinson's Disease*, ed. A. Q. Rana (Rijeka, Croatia: InTech), 485–506.

Xia, R., Muthumani, A., Mao, Z.-H., and Powell, D. W. (2016). Quantification of neural reflex and muscular intrinsic contributions to parkinsonian rigidity. *Exp. Brain Res.* 234, 3587–3595. doi: 10.1007/s00221-016-4755-9

Xia, R., Powell, D., Rymer, W. Z., Hanson, N., Fang, X., and Threlkeld, A. J. (2011). Differentiation between the contributions of shortening reaction and stretch-induced inhibition to rigidity in Parkinson's disease. *Exp. Brain Res.* 209, 609–618. doi: 10.1007/s00221-011-2594-2

Xia, R., Sun, J., and Threlkeld, A. J. (2009). Analysis of interactive effect of stretch reflex and shortening reaction on rigidity in Parkinson's disease. *Clin. Neurophysiol.* 120, 1400–1407. doi: 10.1016/j.clinph.2009.05.001

Yeh, C.-H., Hung, C.-Y., Wang, Y.-H., Hsu, W.-T., Chang, Y.-C., Yeh, J.-R., et al. (2016). Novel application of a Wii remote to measure spasticity with the pendulum test: proof of concept. *Gait Posture* 43, 70–75. doi: 10.1016/j.gaitpost.2015.10.025

Youn, J., Okuma, Y., Hwang, M., Kim, D., and Cho, J. W. (2017). Falling direction can predict the mechanism of recurrent falls in advanced Parkinson's disease. *Sci. Rep.* 7:3921. doi: 10.1038/s41598-017-04302-7

Zetterberg, H., Frykberg, G. E., Gäverth, J., and Lindberg, P. G. (2015). Neural and nonneural contributions to wrist rigidity in Parkinson's disease: an explorative study using the neuroflexor. *Biomed. Res. Int.* 2015:276182. doi: 10.1155/2015/276182

Conflict of Interest: The authors declare that the research was conducted in the absence of any commercial or financial relationships that could be construed as a potential conflict of interest.

frontiers in Bioengineering and Biotechnology

ORIGINAL RESEARCH
published: 13 January 2021
doi: 10.3389/fbioe.2020.574006

Control Modification of Grasp Force Covaries Agency and Performance on Rigid and Compliant Surfaces

Raviraj Nataraj[1,2]* *and Sean Sanford*[1,2]

[1] Movement Control Rehabilitation Laboratory, Stevens Institute of Technology, Hoboken, NJ, United States, [2] Department of Biomedical Engineering, Stevens Institute of Technology, Hoboken, NJ, United States

This study investigated how modifications in the display of a computer trace under user control of grasp forces can co-modulate agency (perception of control) and performance of grasp on rigid and compliant surfaces. We observed positive correlation ($p < 0.01$) between *implicit agency*, measured from time-interval estimation for intentional binding, and *grasp performance*, measured by force-tracking error, across varying control modes for each surface type. The implications of this work are design directives for cognition-centered device interfaces for rehabilitation of grasp after neurotraumas such as spinal cord and brain injuries while considering if grasp interaction is rigid or compliant. These device interfaces should increase user integration to virtual reality training and powered assistive devices such as exoskeletons and prostheses. The modifications in control modes for this study included changes in force magnitude, addition of mild noise, and a measure of automation. Significant differences ($p < 0.001$) were observed for each surface type across control modes with metrics for implicit agency, performance, and grasp control efficiency. Explicit agency, measured from user survey responses, did not exhibit significant variations in this study, suggesting implicit measures of agency are needed for identifying co-modulation with grasp performance. Grasp on the compliant surface resulted in greater dependence of performance on agency and increases in agency and performance with the addition of mild noise. Noise in conjunction with perceived freedom at a flexible surface may have amplified visual feedback responses. Introducing automation in control decreased agency and performance for both surfaces, suggesting the value in continuous user control of grasp. In conclusion, agency and performance of grasp can be co-modulated across varying modes of control, especially for compliant grasp actions. Future studies should consider reliable measures of implicit agency, including physiological recordings, to automatically adapt rehabilitation interfaces for better cognitive engagement and to accelerate functional outcomes.

Keywords: cognitive agency, hand grasp force, movement rehabilitation, visual feedback, precision pinch

OPEN ACCESS

Edited by:
Borja Sañudo,
University of Sevilla, Spain

Reviewed by:
Simone Tassani,
Pompeu Fabra University, Spain
Massimiliano Zingales,
University of Palermo, Italy

***Correspondence:**
Raviraj Nataraj
rnataraj@stevens.edu

Specialty section:
This article was submitted to Biomechanics, a section of the journal Frontiers in Bioengineering and Biotechnology

Received: *18 June 2020*
Accepted: *16 December 2020*
Published: *13 January 2021*

Citation:
Nataraj R and Sanford S (2021) Control Modification of Grasp Force Covaries Agency and Performance on Rigid and Compliant Surfaces. Front. Bioeng. Biotechnol. 8:574006. doi: 10.3389/fbioe.2020.574006

INTRODUCTION

The healthy hand is capable of exquisite grasp force control in manipulating objects during activities of daily living (Hubbard et al., 2009). Following neuromuscular traumas, such as spinal cord or brain injury, it is critical to rehabilitate grasp function for maintaining quality of life. Rehabilitation often involves physical therapy with repetitive task practice to reformulate neuromotor connections

(Shepherd, 2001). Advanced physical therapy may employ engaging platforms such as virtual reality (VR) (Sveistrup, 2004) or robotics (Saleh et al., 2017). Powered assistive devices may also be employed to restore function as with powered exoskeletons (Lucas et al., 2004; Heo et al., 2012; Nataraj and van den Bogert, 2017) or neuroprostheses that activate sensorimotor pathways (Marasco et al., 2018; Schofield et al., 2019) of the hand. The primary objective with assistive or rehabilitative technologies is to enhance control of the hand and increase functional ability to perform manual tasks. Improved motor control may be enacted from training the person to move better independently or with the assistance of a powered device. Regardless of the rehabilitation approach, the person should be cognitively engaged and integrated with the therapeutic platform or the assistive device (Moore and Fletcher, 2012; Nataraj, 2017; Nataraj et al., 2020a,b,c). Improved perception of involvement and control of movement should better ensure continued participation and positive functional outcomes (Doyle, 2002; Behrman et al., 2005).

Despite intuitive relation between cognitive integration to movement and greater functional performance, this concept has not been systematically investigated nor incorporated in standard rehabilitation protocols. True innovation in neuromotor rehabilitation would include methods that optimize user-device movement abilities while increasing user cognition of movement. Systematically identifying agency, perception of control, and adapting device control accordingly may produce more effective, cognition-driven rehabilitation. Methods that leverage cognitive factors, such as agency, may accelerate functional gains and increase clinical retention of such methods and devices, which depends on user perception of utility (Childress, 1973; Phillips and Zhao, 1993; Hughes et al., 2014).

Sense of agency, or the perception of control, has been studied in experimental constructs that relate actions to consequences (Moore and Haggard, 2008; Moore, 2016). These studies have investigated modulation of agency with external cues (Moore et al., 2009; Khalighinejad et al., 2017) and the existence of agency within human machine interfaces (Evans et al., 2015; Le Goff et al., 2018). Agency is naturally implicated with rehabilitation through perception of neuromuscular action and related functional consequences (Moore and Obhi, 2012). Agency contributes to the performance of functional movements such as reaching (Nataraj et al., 2020c,d) and is impaired in the presence of neurological disorders (Jeannerod, 2009; Ritterband-Rosenbaum et al., 2012). Agency can also be compromised during the use of powered assistive devices, such as exoskeletons (Hartigan et al., 2015) or sensorimotor prostheses (Antfolk et al., 2013; Hebert et al., 2013), due to distortions in embodiment (Kilteni et al., 2012; Caspar et al., 2015). It remains unclear how agency is related to functional performance of grasping, and how agency and performance may be modulated with varying levels of control. Establishing the connection between agency and grasp could inspire the development of rehabilitation platforms that leverage agency for more effective control of grasp. These platforms would utilize agency to maximize classical performance objectives such as minimal effort or better movement tracking (Nataraj and van den Bogert, 2017).

Implicit measures of agency may be best utilized for adapting rehabilitation paradigms for grasp since they are less prone to conscious response bias (Wegner, 2003; Saito et al., 2015) compared to explicit measures of agency, which require survey-type responses (Moore et al., 2012). Indirect markers of agency, such as intentional binding, may better explain underlying feelings of control that are sensitive to sensory cues (Moore and Fletcher, 2012) and during impaired function as with neuropathological grasp (Delevoye-Turrell et al., 2002). Intentional binding indicates how coupled in time one perceives a voluntary action to an expected sensory consequence (Haggard et al., 2002; Moore and Obhi, 2012). Time-interval estimation between action and consequence has become a standard to implicitly infer agency via intentional binding. In the seminal work (Haggard et al., 2002), participants judged the time duration between an action (keypress) and sensory consequence (sound tone). A perceptual shift toward time compression was observed when the action was voluntary (high agency) versus an involuntary twitch (low agency) from transcranial magnetic stimulation. Intentional binding has since been used to explore agency in various contexts, including the influence of sensorimotor processes on agency from internal predictions and external outcomes (Moore and Haggard, 2008; Frith and Haggard, 2018).

Time-interval estimation methods for implicit measurements of agency are well posed for rehabilitation training. These methods can quantify agency trial-to-trial and are classically used with sensory feedback experiments. These experiments are similar to motor rehabilitation protocols employing external reward and sensory cues through VR (Sveistrup, 2004; Saleh et al., 2017). Any programmable interface for rehabilitation training or assistive device tuning can potentially adapt parameters for greater agency. Parameters include feedback gains (Nataraj et al., 2010, 2012b; De Havas et al., 2018) or customized settings within training environments (Velazquez et al., 2008). Systematic and computational approaches to adapt user training through agency would readily apply to any advanced rehabilitation platform (VR, robotics) or powered assistive devices such as exoskeletons (Farris et al., 2013) and neuroprostheses (Nataraj et al., 2012a,b; Marasco et al., 2018). The objective of agency-based rehabilitation would be to leverage perception of control for more effective user performance of functional tasks involving hand grasp. However, it remains unclear if varying control modes can effectively co-modulate agency and performance of grasp.

In this study, we hypothesized that agency was positively related to performance of a grasp force task. To test this hypothesis, we varied the control of a grasp force trace that participants visually tracked to match a target ramp. Error to the ramp served as the primary performance metric. We sought to observe potential covariation of agency and grasp force performance across various control modes. The testing environment utilized a force-sensitive pinch apparatus to record forces that were visually projected under the terms of each control mode. Completion of the ramp signified an "action" to be coupled to sensory "consequences" (visual and sound events) from which users estimated lapsed time intervals to implicitly infer agency

via intentional binding. Each control mode defined the speed the force trace would move proportional to grasp force and if there existed a measure of noise or assisted automation. These control modes are consistent with parameters commonly adapted for powered devices such as setpoints for speed (Blaya and Herr, 2004; Wege et al., 2005), noise mitigation (Taylor et al., 2002; Agostini and Knaflitz, 2012), and automated assistance (Ronsse et al., 2011). These parameters can be tuned ad hoc (Terenzi, 1998) or identified through optimization of mechanical performance (e.g., effort, tracking) in a model system (Davoodi et al., 2007; Nataraj and van den Bogert, 2017). This study may newly inspire a cognitive basis from which to adapt such parameters in the rehabilitation of grasp performance.

The protocol in this grasp study was repeated for both a rigid and compliant surface. Compliance has been extensively considered for the object being grasped (Friedman and Flash, 2007; Nataraj et al., 2015) and in the design of robotic hands (Kazemi et al., 2012) that better mimic natural human grasp. As such, we sought to investigate how compliance may additionally affect the covariation of agency and performance across control modes. We hypothesized that compliant surfaces may induce higher agency due to the freedom to express more dexterous manipulation. Ultimately, we were able to observe how specific control modes may uniquely affect agency and performance of grasp against a rigid and compliant surface.

MATERIALS AND METHODS

The core experimental task involved participants controlling a visible trace to dynamically track a target ramp through precision pinch (index finger and thumb) grasp loading onto a force-sensitive pinch apparatus (**Figure 1**). Performance and agency were assessed across a variety of control modes for the force trace. An initial control mode, specified as "Baseline," translated grasp loads to changes in trace height at a fixed gain. This gain was ∼2 vertical inches on the screen per 1 N total force applied. Total force was computed as the sum of the 3D (x-y-z) force vector of the index finger to that of the thumb, or:

$$\text{Total force} = \sqrt{f_{x,\text{index}}^2 + f_{y,\text{index}}^2 + f_{z,\text{index}}^2} + \sqrt{f_{x,\text{thumb}}^2 + f_{y,\text{thumb}}^2 + f_{z,\text{thumb}}^2}.$$

Other control modes were modifications from "Baseline" that involved changes in gain magnitude (and required peak force), addition of noise, or inclusion of automation. Participants were asked to maximize tracking performance in matching the force trace to a target ramp. Additionally, participants were required to apply a peak force that exceeded the top of the ramp to complete grasp "action" for each trial. This action would subsequently initiate a sound beep as "consequence" from which participants estimated the time-interval between action and consequence to assess agency. Based on intentional binding, the more subjects underestimate the time-interval, i.e., compress their perception of time, they exhibit greater agency in coupling their actions to related consequences.

Participants

A total of 16 able-bodied volunteers (12 male, 4 female, 21 ± 3 years) were recruited to participate in this study. A power analysis for ANOVA at 95% suggested that seven-participant samples would show significant differences ($\alpha = 0.05$) in agency and grasp force performance across the tested control modes. Only right-handed participants were tested for right-hand grasp to avoid effects of hand dominance. All participants had normal or corrected-to-normal vision and did not report nor demonstrate a history of disease, injury or complications involving cognition or upper extremity function. All participants signed an informed consent form for this study approved by the Stevens Institutional Review Board.

Equipment (Hardware and Software)

A custom pinch apparatus (**Figure 2**) was constructed utilizing two 6-DOF load cells (Mini40, ATI Industrial Automation, Apex, NC, United States). The designated locations for applying pinch force included a surface for the index finger in parallel to a surface for the thumb. Both locations could accommodate surfaces as either a metal bar (rigid surface) or an elastic band (compliant surface). The band was set to provide approximately constant compliance of 1.5 N/cm normal to the surface. Data was acquired on a multi-input/output data acquisition system (PXIe-6363 with BNC interface, National Instruments, Austin, TX, United States). Force data was sampled at 100 Hz and processed in software developed in Simulink (Mathworks, Natick, MA, United States). The force trace was displayed in real-time on a 27-inch monitor (Dell P2717H).

Protocol

Participant Preparation

After arriving to the laboratory, participants were re-informed about consent and had their right-hand size measured. Hand size was measured as the maximum spread distance from tip of thumb to tip of index finger. The average hand size was 15 ± 1 cm. For each participant, the distance between the index and thumb pinch surfaces was set at one-third of their hand size. Each participant was seated with chair height adjusted so the grasping hand could be table-supported with shoulders comfortably level. The pinch apparatus was kept in place on the table surface with double-side adhesive tape. The apparatus was positioned directly in front of the participant midline and oriented 30-degrees so that the index finger surface was comfortably forward and leftward to the thumb while grasping (**Figure 2**). The distance between the participant and the apparatus was set for a comfortable reach when grasping. The monitor displaying the force trace and ramp was placed approximately at participant eye level at a distance 1.5 m from the head.

Force Grasp Task

The experimenter cued the participant to the start of each trial, at which time, the participant would move the hand from rest, palm-side down on the table, to place their index finger and thumb near, without contact, designated locations on grasp surfaces of the apparatus. Each trial with data capture was 10 s. At

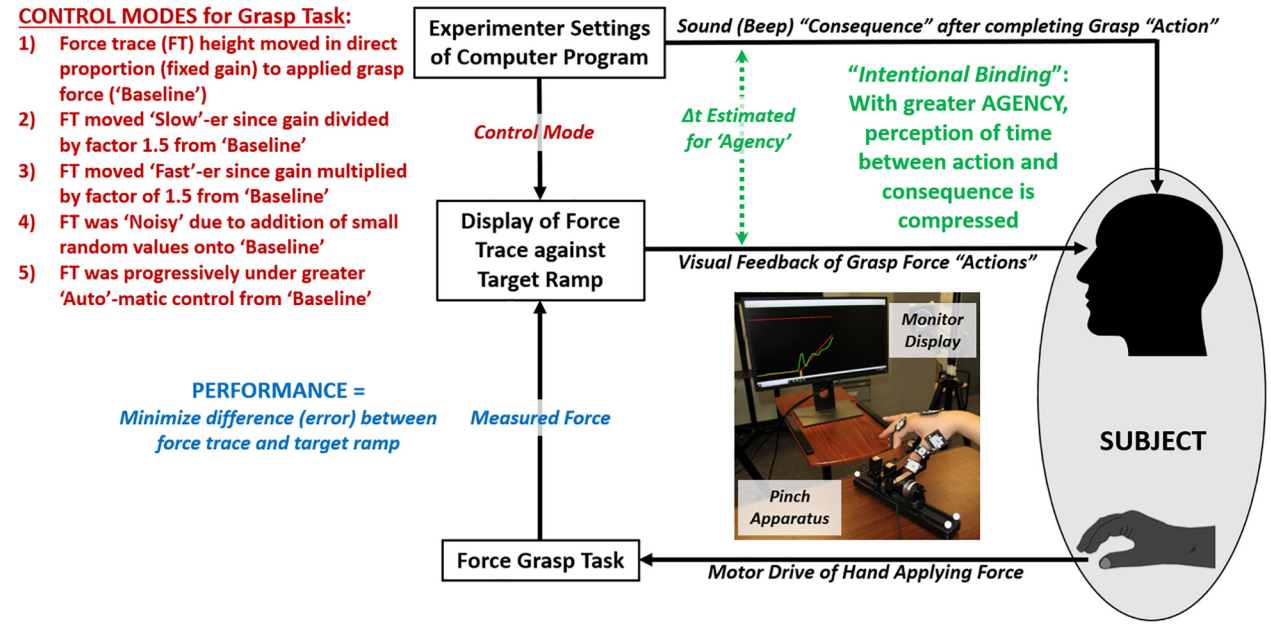

FIGURE 1 | Flow diagram of experiment of participant performing grasp force task to visually trace a target ramp under varying control modes while assessing performance and agency.

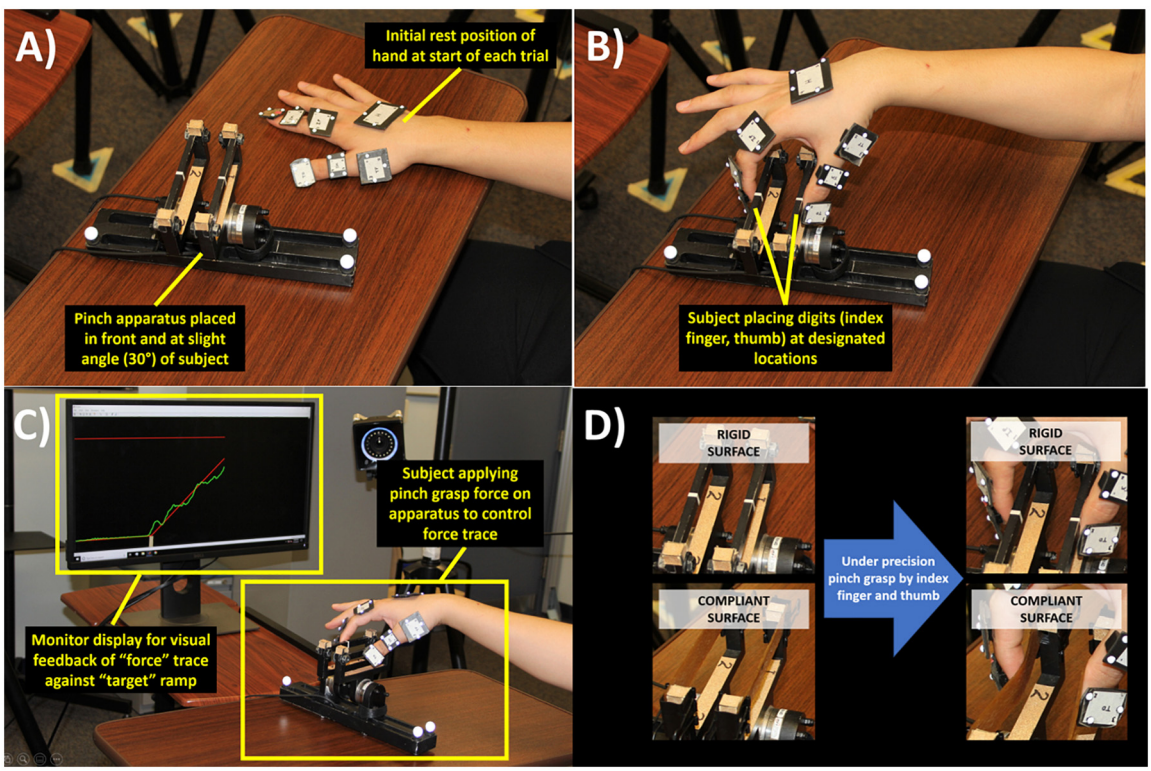

FIGURE 2 | Participant applied grasp force to pinch apparatus each trial. **(A)** Participant hand initially palm-down on table to start each trial. **(B)** After trial began, participant moved hand to contact index finger and thumb on designated locations of grasp surfaces on pinch apparatus. **(C)** Participant progressively applied grasp force to control height (up-down) of force trace to match ramp as trial progressed. **(D)** Protocol repeated for rigid and compliant grasp surfaces.

the start of each trial (t_{trial} = 0 s), the participant began to see real-time tracing of three lines. All three lines moved horizontally at a constant speed of 2.35 inches per second, computed as screen width divided by total trial time. The three lines (**Figure 3**) included: *(1) force trace (green line)* – the force trace height (upward vertical displacement) was under participant control and moved at fixed gain proportional to total grasp force. The force trace was additionally modified depending on the control mode applied. *(2) target performance trace (red line)* – this target trace was initially flat at height coincident with the force trace when no grasp forces were present. This target trace transitioned to a positive linear slope (ramp) from t_{trial} = 3 s to t_{trial} = 7 s. The ramp height grew at slope of ∼2 inches/sec over the 4-s ramp period. The bottom of the ramp coincided with zero force and the top with the target maximum force. *(3) target action trace (red line)* – this target trace was flat throughout the trial and

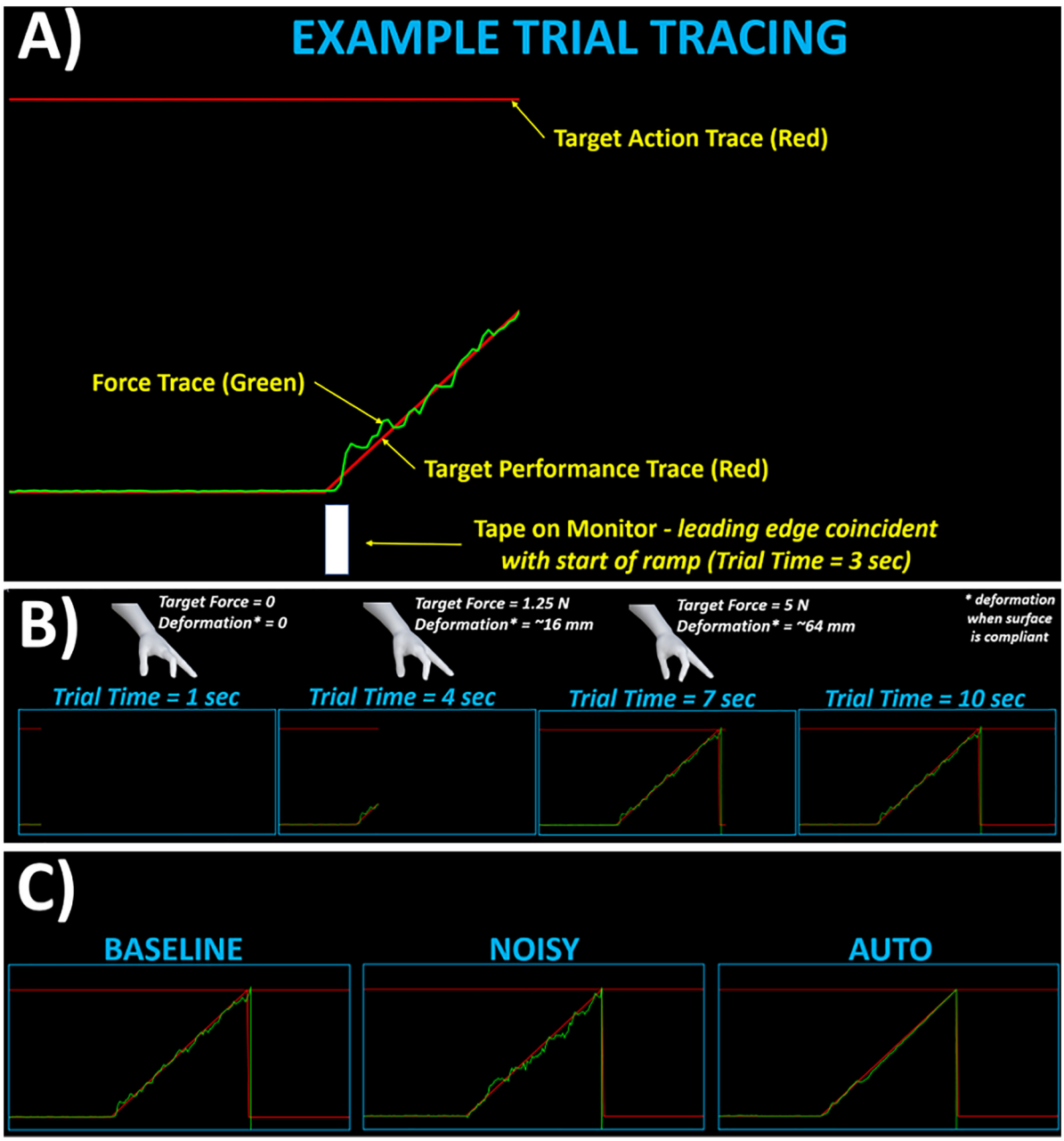

FIGURE 3 | Snapshots of real-time tracings shown for various trial cases. **(A)** Example depiction of force and target (action, performance) traces shown during ramp portion of trial. **(B)** Tracing shown at various progressive instances across the 10-s trial. Also shown are depictions of respective grasp postures and force-deformation moduli assuming a "compliant" grasp surface. **(C)** Representative final traces shown for trials with "Baseline", "Noisy", and "Auto" control modes.

remained at a height coincident with the target maximum force. This target maximum force was the same for all subjects since grasp forces were relatively low with maximum force around 5N. Variations in the maximum force were based on the specific control mode (described under "Varying control modes"). This target trace would meet the performance trace at the top of the ramp (t_{trial} = 7 s).

The performance objective of the participant was to apply grasp forces to match, as best to their ability, the green force trace with the target performance trace. The participant was cued as to when the ramp would start by a piece of tape at the monitor base whose starting edge was coincident to t_{trial} = 3 s. To successfully complete the trial and fulfill the agency objective, the participant needed to ensure the force trace crossed (contacted) the target action trace near (within 1 s) the top of the ramp. The crossing served as completion of the grasp "action" that then triggered a subsequent sound beep as "consequence" after some time-interval. The beep was moderately pitched with duration of 100 msec. The beep occurred at some time-interval between 100 and 1000 msec. The participant was asked to verbally estimate the time-interval to the best of their abilities after each beep. The participant was previously instructed that the time-interval was anywhere from 100 to 1000 msec in denominations of 100 msec. The actual time-intervals were always 100, 300, 500, 700, or 900 msec.

Varying Control Modes

All participants performed a block of trials of the grasp task for each of five different control modes, which were randomly presented. As previously described, the control modes examined in this study considered modifications in gain, addition of mild noise, and automation. The control modes were as follows:

(1) *Baseline* – The force trace magnitude (height) moved in direct proportion to the total grasp force applied at a gain of 2 in/N. The target maximum force associated with the top of the ramp at the end of 4-s period was 5 N. This control mode served as the template from which other control modes were modified.
(2) *Slow* – The force trace magnitude moved at a speed slower than "Baseline" for a given grasp load. Specifically, the gain was divided by 1.5 (reduced to 1.33 in/N) and the target maximum force consequently became 7.5 N. The participant needed to apply 50% more force on average than Baseline to accurately track the target ramp.
(3) *Fast* – The force trace magnitude moved at a speed faster than "Baseline" for a given grasp load. Specifically, the gain was multiplied by 1.5 (increased to 3 in/N) and the target maximum force consequently became 3.33 N. The participant needed to apply 33% less force on average than Baseline to accurately track the target ramp.
(4) *Noisy* – The force trace moved at the same speed as "Baseline" but was visually infected by mild noise. A small random value between (−0.5N, +0.5N) was added to each displayed instance of the force trace. This noise-level produced visible tremor that was noticeable but not distracting nor challenging in performing the grasp task.
(5) *Auto* – The force trace was progressively (linear with time) under greater automatic control. At the start-time of the ramp (t_{ramp} = 0, t_{trial} = 3 s), the participant controlled the force trace just as in "Baseline." Over the 4-s ramp period, the force trace with "Auto" control (FT_{auto}) was a weighted average between the participant's force trace with "Baseline" control (FT_{base}) and an optimal trace (FT_{opt}) that perfectly matches the ramp. The displayed force trace for "Auto" was given as: $FT_{auto} = \left(1 - \frac{t_{ramp}}{4}\right) \times FT_{base} + \left(\frac{t_{ramp}}{4}\right) \times FT_{opt}$. At t_{ramp} = 4 s, the force trace was guaranteed to match the top of the ramp and simultaneously match the target action line. This automated case was akin to user initiation of movement to trigger device assistance and auto-complete the movement (Farris et al., 2013).

Experimental Testing Blocks

Participants would perform a block of 20 consecutive trials for each of the five control modes. The first three trials of every block were "practice" with the time-interval between grasp action completion and the beep fixed at 1000 msec. The participant was aware these practice trials served to gain familiarity with the control mode and to re-calibrate their internal reference of a 1000 msec time-interval. The remaining 17 trials were used for agency and performance assessment with randomly presented time-intervals ranging from 100 to 900 msec with Gaussian distribution. Each participant was given up to 5 min between blocks to rest and complete a survey to rate their explicit subjective experience for the completed control mode. The trial-blocks for each of the control modes were conducted first for the rigid surface and then repeated for the compliant surface.

Surveys

For each trial-block, the participant was presented with a 1-statement survey to express their subjective perception of the control mode presented. Participants were asked to rate, on a 5-point Likert scale (−2 = strongly disagree, −1 = disagree, 0 = neutral, +1 = agree, +2 = strongly agree), to what extent the observed force trace movements reflected their intentions. The survey responses served as an explicit, or conscious, measure of agency (Moore et al., 2012) for comparison to the implicit measurements of agency.

Data and Statistical Analysis

There were four data variables serving as the primary metrics in this study as follows:

(1) *Implicit agency (msec)* was the underestimation in time-interval between "action" (completion of force ramp) and "consequence" (delayed sound beep) to signify greater intentional binding. This measurement was taken once with each trial.
(2) *Performance (N^{-1})* was the inverse of the grasp force error during the 4-s ramp period to signify greater force tracking. Each measurement was taken as the mean error per trial.
(3) *Control efficiency (sec^2/N^2)* was the normalization of performance by force acceleration (N/sec^2) to signify the error per unit acceleration effort to make corrections

in tracking a constant velocity ramp. This variable was computed concurrently with performance.

(4) *Explicit agency (Likert scale)* was the survey response score on subjective perception of control mode. This measurement was done once after each block of trials.

The analyses that were performed on the above metrics are as follows:

Analysis 1: A linear regression was applied to performance (*y*-axis) and implicit agency (*x*-axis) data to assess the dependence of performance on agency for each surface in the *aggregate* (across all control modes, subjects). The *F*-statistic and *p*-value were computed to refute the null hypothesis that the slope coefficient was equal to zero and suggest significant dependence of performance on implicit agency. ANCOVA was performed to assess significant difference in slopes between compliant and rigid surfaces and to determine if significant slopes were observable within each control mode, not just in the aggregate.

Analysis 2: We performed a repeated-measures two-way ANOVA (factors for surface-type and control mode) for each metric to observe main effects due to each factor and potential interactions between factors. For significant factors, *post hoc* pairwise comparisons were done with Bonferonni correction for multiple comparisons. For multiple comparisons, all reported *p*-values are scaled according to the number of comparisons such that first-level significance is always $p < 0.05$. *Post hoc* comparisons allowed for observation of specific simple effects to be considered for each pair of control modes within surface type.

Analysis 3: Finally, the mean variability (standard deviation) in the force profile in each of the three directional dimensions was compared between rigid and compliant surfaces to indicate the presence of any surface-unique directional sensitivities during grasp.

RESULTS

Analysis 1

The aggregate dependence of performance on agency across participant-averages for control modes is shown for each grasp surface in **Figure 4**. For both surfaces, there was a positive relationship between performance and agency indicated by a non-zero ($p < 0.001$) regression slope, however, the regression fit to both data sets was low ($R^2 < 0.20$). Dependence of performance on agency was greater (increased slope) for the compliant surface. The increased slope with compliant surface grasp was confirmed with an ANCOVA comparison (**Table 1B**, $p < 0.01$). ANCOVA did not reveal significant slope dependence within control modes (**Table 1A**). ANCOVA did demonstrate significant differences in the intercept parameters both within

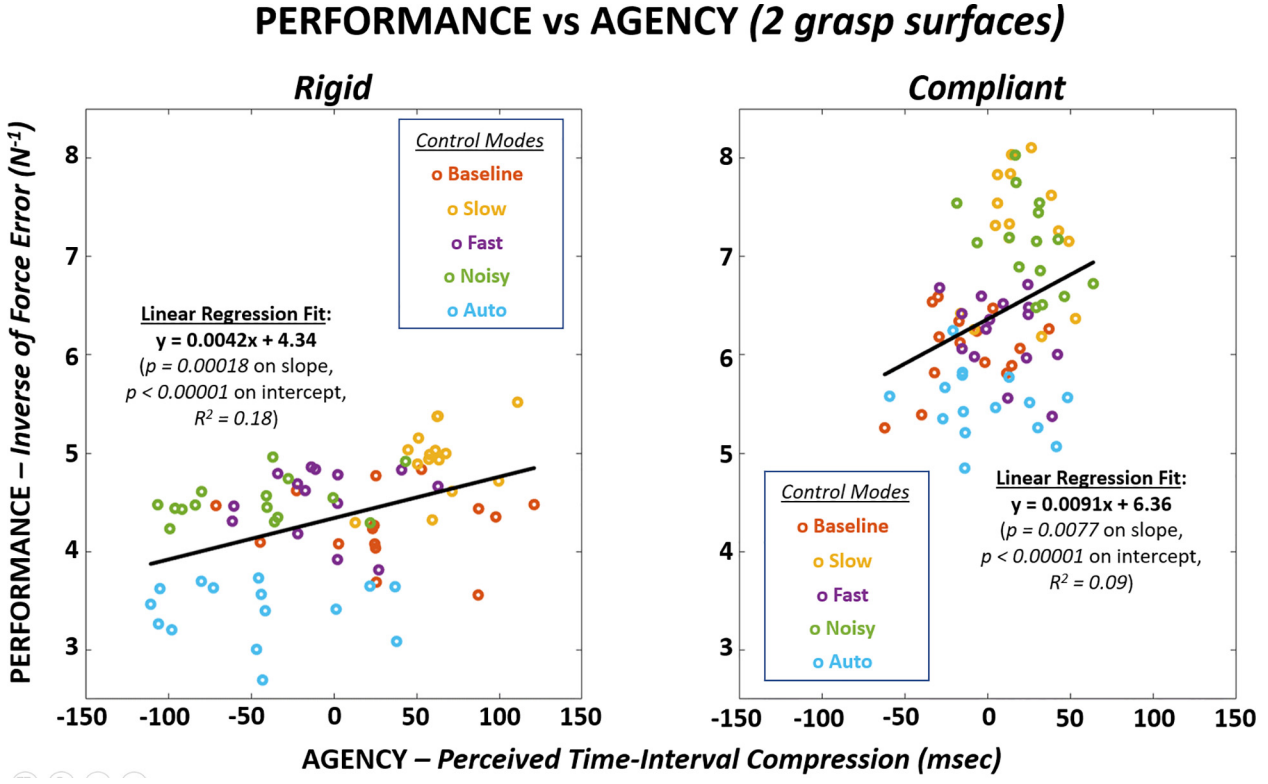

FIGURE 4 | Performance of precision pinch grasp displayed against implicit agency across control modes on both *rigid* (LEFT) and *compliant* (RIGHT) grasp surfaces. Each point indicates a participant-average for that control mode and surface. Performance positively measured as inverse of average tracking error to target force ramp. Implicit agency positively measured as underestimation of time-intervals between completion of ramp task and subsequent sound beep.

TABLE 1A | Linear regression results on slope (N^{-1} $msec^{-1}$) for each control mode and ANCOVA results across control modes for each surface.

	CONTROL MODE					ANCOVA	
SURFACE	**Baseline**	**Slow**	**Fast**	**Noisy**	**Auto**	***F*-statistic**	***p*-Value**
Rigid	−3E−04	7E−03	3E−04	2E−03	−1E−04	0.55	0.457
Compliant	4E−03	6E−04	−7E−03	−1E−02	−3E−03	1.3	0.278

TABLE 1B | Linear regression results on slope (N^{-1} $msec^{-1}$) in total (pooled) for each surface and ANCOVA results across both surfaces.

SURFACE		ANCOVA	
Rigid	**Compliant**	***F*-statistic**	***p*-Value**
0.0042	0.0091	3.04	**3E-03**

TABLE 1C | Linear regression results on intercept (N^{-1}) for each control mode and ANCOVA results across control modes for each surface.

	CONTROL MODE					ANCOVA	
SURFACE	**Baseline**	**Slow**	**Fast**	**Noisy**	**Auto**	***F*-statistic**	***p*-Value**
Rigid	4.27	4.52	4.54	4.60	3.40	64.9	**7.7E-61**
Compliant	6.12	7.22	6.29	7.41	5.50	97.3	**3.8E-72**

TABLE 1D | Linear regression results on intercept (N^{-1}) in total (pooled) for each surface and ANCOVA results across both surfaces.

SURFACE		ANCOVA	
Rigid	**Compliant**	***F*-statistic**	***p*-Value**
4.34	6.36	18.2	**2.3E-39**

Significant post hoc p-values (<0.05) bolded and reported with Bonferonni correction.

control modes and in the aggregate across surfaces (**Tables 1C,D**). Combined slope and intercept results suggest that independent regressions for control modes are parallel but different, and that intercept differences across control modes drive differences in aggregate slope.

Analysis 2

The two-way (factors of control mode, surface) ANOVA results for each of the primary metrics are shown in **Table 2**. A significant difference ($p < 0.001$) was observed with control mode for implicit agency, performance, and control efficiency. A significant difference ($p < 0.001$) was observed with surface for performance and control efficiency. In each case, the interaction term was significant and required an investigation of simple effects (i.e., hold one factor constant) and *post hoc* pairwise comparisons.

Several significant pairwise differences ($p < 0.0001$) were observed in *post hoc* across control modes for both implicit agency (**Figure 5** TOP and **Tables 3A–C**) and performance (**Figure 5** BOTTOM and **Tables 3D–F**). In the presence of significant interaction between surface and control mode, *unique* variations were observed across control modes based on surface for both implicit agency and performance. Performance was universally greater for the compliant surface than rigid surface. For the rigid surface, the highest agency and performance with significant pairwise differences ($p < 0.0001$) were observed for the "Slow" control mode. For the compliant surface, the highest agency and performance with significant pairwise differences ($p < 0.001$) were observed for the "Slow" and "Noisy" control modes.

Significant pairwise differences ($p < 0.0001$) were observed in control efficiency (**Figure 6** TOP and **Tables 4A–C**) across control modes for both rigid and compliant surfaces. Similar to performance, there was significant interactions between surface and control mode for control efficiency such that unique variations in efficiency across control modes were observed for each surface. Furthermore, performance efficiency was also universally greater for the compliant surface. The lowest control efficiency was observed with "Auto" control mode for both surfaces and with multiple significant ($p < 0.0001$) pairwise differences. Significant differences ($p < 0.05$) were not observed for explicit agency (**Figure 6** BOTTOM and **Table 4D**) except for the compliant surface which demonstrated one significant ($p < 0.05$) pairwise difference ("Baseline" greater than "Noisy"). As indicated from the two-way analysis, both surface effects and interaction with control modes were absent for explicit agency.

The shifts in metrics from rigid to compliant surfaces across control modes are explicitly shown in **Figure 7** and **Table 5**. significant differences ($p < 0.001$) were observed for all metrics except for explicit agency ($p > 0.05$). The largest shifts for implicit agency, performance, and efficiency were observed for the "Noisy" control mode.

TABLE 2 | Two-way ANOVA results for each metric over factors of control mode and surface.

	METRIC							
	Implicit agency		**Performance**		**Control efficiency**		**Explicit agency**	
FACTOR	***F*-statistic**	***p*-Value**	***F*-statistic**	***p*-Value**	***F*-statistic**	***p*-Value**	***F*-statistic**	***p*-Value**
Control mode	15.19	**1E-05**	76.8	**<1E-05**	16.4	**1E-05**	2.33	0.06
Surface	2.53	0.114	1054	**<1E-05**	2328	**1E-05**	∼0	∼1
Interaction	16.7	**1E-05**	6.7	**5E-05**	5.9	**2E-04**	0.73	0.57

Significant post hoc p-values (<0.05) bolded and reported with Bonferonni correction.

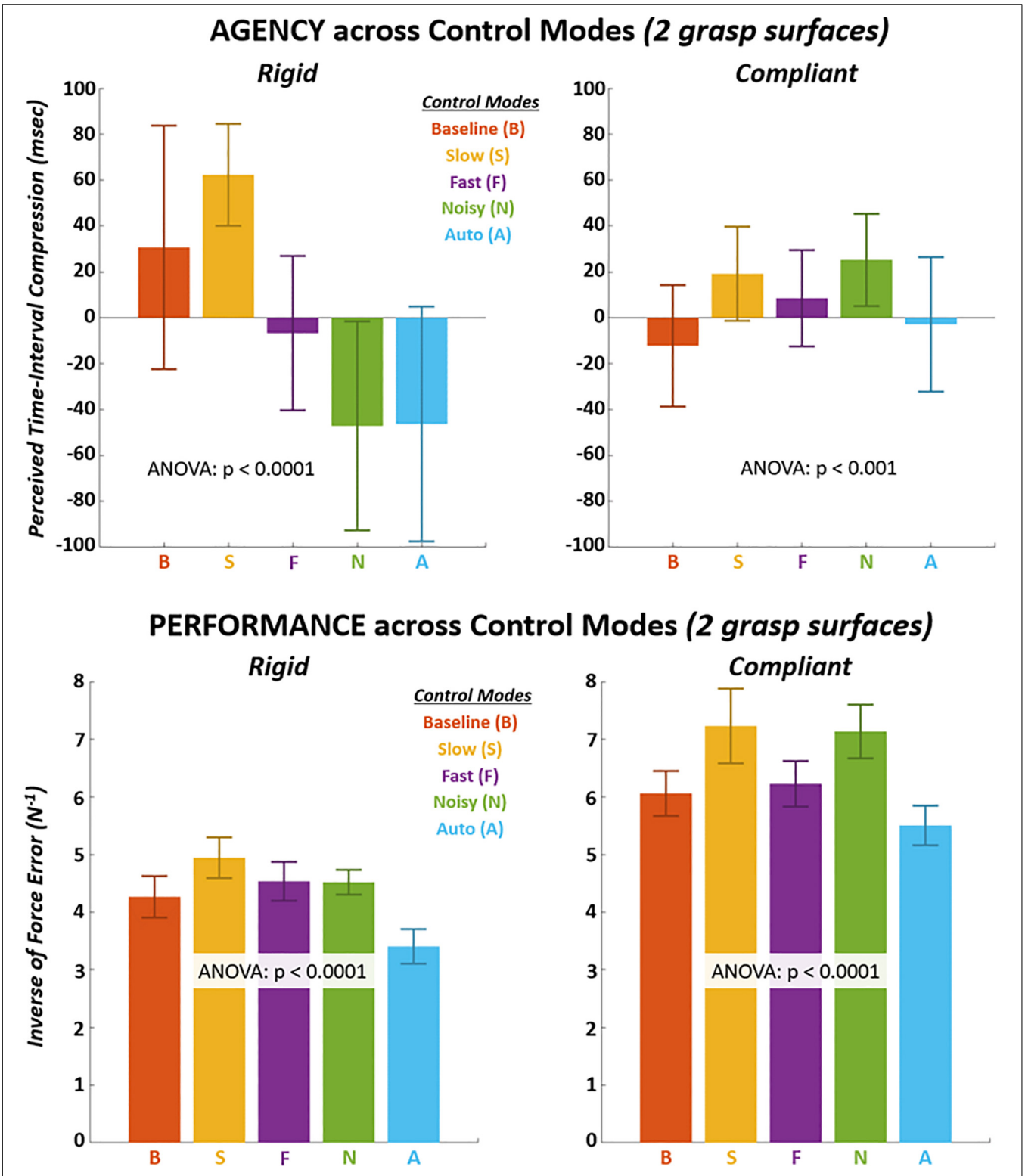

FIGURE 5 | TOP – Mean implicit agency shown for each control mode on each grasp surface. Implicit agency positively measured as underestimation of time-intervals between completion of ramp task and subsequent sound beep. BOTTOM – Mean performance shown for each control mode on each grasp surface. Performance positively measured as inverse of average tracking error to target force ramp.

TABLE 3A | Mean implicit agency (time-interval underestimation, *msec*) across control modes on rigid and compliant surfaces.

	CONTROL MODE					ANOVA		
SURFACE	**Baseline**	**Slow**	**Fast**	**Noisy**	**Auto**	***F*-statistic**	***p*-Value**	η^2
Rigid	31 ± 53	62 ± 22	−7 ± 34	−47 ± 45	−46 ± 51	18.9	1.4E-10	0.52
Compliant	−12 ± 27	19 ± 21	8 ± 21	25 ± 20	−3 ± 29	6.3	2.2E-04	0.26

TABLE 3B | *Post hoc* comparisons (*p*-values) for implicit agency across control modes on rigid surface.

	CONTROL MODE				
CONTROL MODE	**Baseline**	**Slow**	**Fast**	**Noisy**	**Auto**
Baseline	–	0.26	0.13	**4E-05**	**5E-05**
Slow	–	–	**3E-04**	**2E-08**	**2E-08**
Fast	–	–	–	0.08	0.09
Noisy	–	–	–	–	0.99

TABLE 3C | *Post hoc* comparisons (*p*-values) for implicit agency across control modes on compliant surface.

	CONTROL MODE				
CONTROL MODE	**Baseline**	**Slow**	**Fast**	**Noisy**	**Auto**
Baseline	–	**5E-03**	0.13	**5E-04**	0.82
Slow	–	–	0.73	0.96	0.09
Fast	–	–	–	0.32	0.69
Noisy	–	–	–	–	**0.02**

TABLE 3D | Mean performance (inverse force error, N^{-1}) across control modes on rigid and compliant surfaces.

	CONTROL MODE					ANOVA		
SURFACE	**Baseline**	**Slow**	**Fast**	**Noisy**	**Auto**	***F*-statistic**	***p*-Value**	η^2
Rigid	4.3 ± 0.36	4.9 ± 0.35	4.5 ± 0.34	4.5 ± 0.22	3.4 ± 0.30	48.9	1.4E-19	0.73
Compliant	6.1 ± 0.39	7.2 ± 0.64	6.2 ± 0.40	7.1 ± 0.47	5.5 ± 0.34	38.4	5.7E-17	0.69

TABLE 3E | *Post hoc* comparisons (*p*-values) for performance across control modes on rigid surface.

	CONTROL MODE				
CONTROL MODE	**Baseline**	**Slow**	**Fast**	**Noisy**	**Auto**
Baseline	–	**1E-06**	0.15	0.20	**1E-08**
Slow	–	–	**6E-03**	**4E-03**	**1E-08**
Fast	–	–	–	0.99	**1E-08**
Noisy	–	–	–	–	**1E-08**

TABLE 3F | *Post hoc* comparisons (*p*-values) for performance across control modes on compliant surface.

	CONTROL MODE				
CONTROL MODE	**Baseline**	**Slow**	**Fast**	**Noisy**	**Auto**
Baseline	–	**2E-08**	0.86	**2E-07**	**1E-02**
Slow	–	–	**8E-07**	0.98	**1E-08**
Fast	–	–	–	**8E-06**	**5E-04**
Noisy	–	–	–	–	**1E-08**

Significant post hoc p-values (<0.05) bolded and reported with Bonferonni correction.

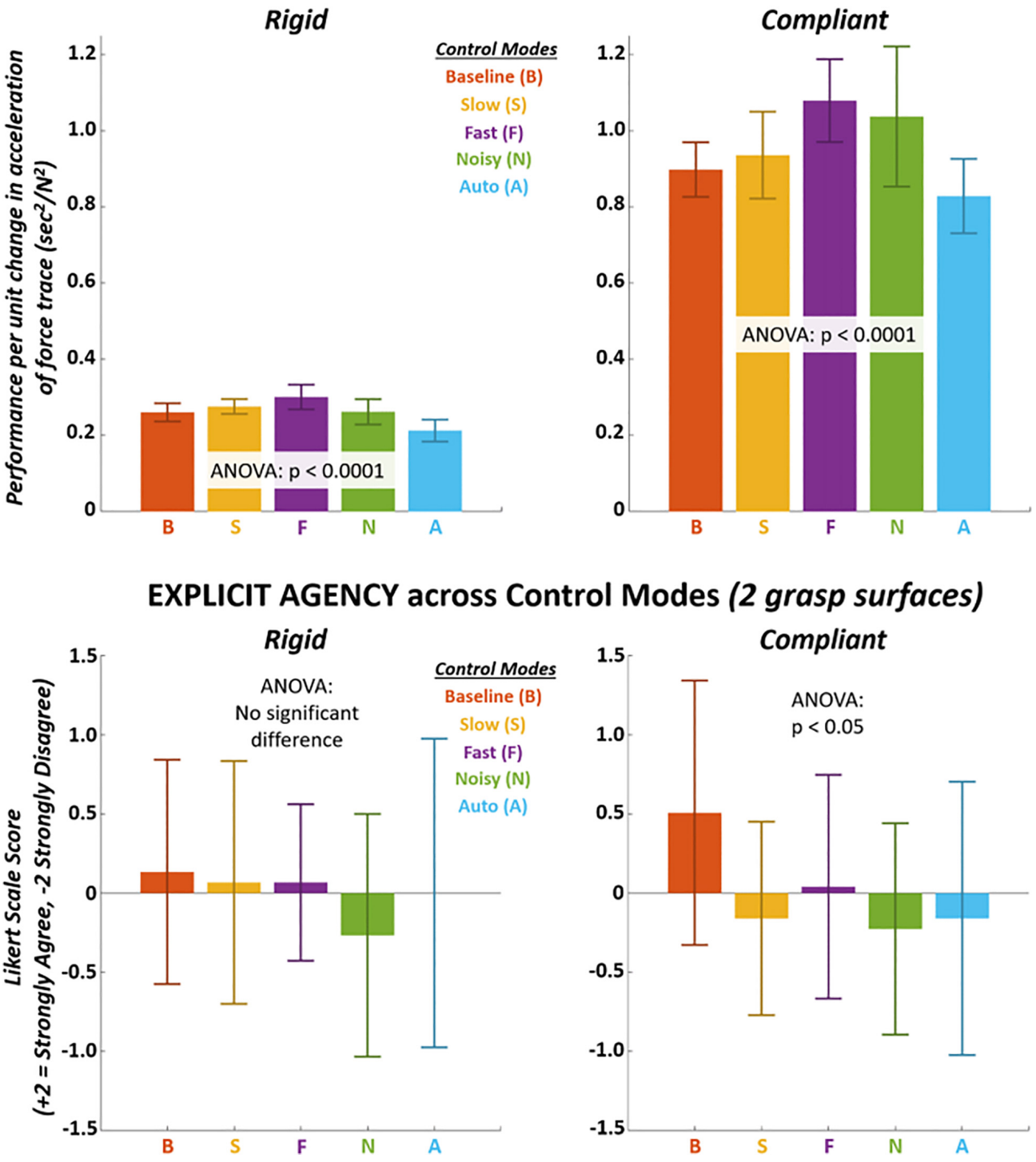

FIGURE 6 | TOP – Mean control efficiency shown for each control mode on each grasp surface. Control efficiency measured as performance normalized by acceleration (2nd derivative) of force trace. BOTTOM – Mean explicit agency shown for each control mode on each grasp surface. Explicit agency measured from survey response along *Likert scale: +2 strongly agree, +1 agree, 0 neutral, –1, disagree, –2 strongly disagree*. Survey asked participant to what extent they agreed that force trace movements reflected their intended actions after a trial-block for each control mode.

TABLE 4A | Mean control efficiency (sec^2/N^2) across control modes on rigid and compliant surfaces.

	CONTROL MODE					ANOVA		
SURFACE	**Baseline**	**Slow**	**Fast**	**Noisy**	**Auto**	***F*-statistic**	***p*-Value**	η^2
Rigid	0.26 ± 0.02	0.28 ± 0.02	0.30 ± 0.03	0.26 ± 0.03	0.21 ± 0.03	19.6	**7E-11**	0.53
Compliant	0.90 ± 0.07	0.94 ± 0.11	1.1 ± 0.11	1.0 ± 0.18	0.83 ± 0.10	10.7	**8E-07**	0.38

TABLE 4B | *Post hoc* comparisons (*p*-values) for control efficiency across control modes on rigid surface.

	CONTROL MODE				
CONTROL MODE	**Baseline**	**Slow**	**Fast**	**Noisy**	**Auto**
Baseline	–	0.59	**1E-03**	0.99	**1E-04**
Slow	–	–	0.12	0.67	**4E-07**
Fast	–	–	–	**3E-03**	**1E-08**
Noisy	–	–	–	–	**8E-05**

TABLE 4C | *Post hoc* comparisons (*p*-values) for control efficiency across control modes on compliant surface.

	CONTROL MODE				
CONTROL MODE	**Baseline**	**Slow**	**Fast**	**Noisy**	**Auto**
Baseline	–	0.91	**1E-03**	**2E-02**	0.52
Slow	–	–	**2E-02**	0.16	0.12
Fast	–	–	–	0.88	**3E-06**
Noisy	–	–	–	–	**1E-04**

TABLE 4D | Mean explicit agency (*Likert scale: +2 strongly agree to −2 strongly disagree*) across control modes on rigid and compliant surfaces.

	CONTROL MODE					ANOVA		
SURFACE	**Baseline**	**Slow**	**Fast**	**Noisy**	**Auto**	***F*-statistic**	***p*-Value**	η^2
Rigid	0.13 ± 0.71	0.07 ± 0.77	0.07 ± 0.49	−0.27 ± 0.77	0.0 ± 0.98	0.64	0.64	0.04
Compliant	0.51 ± 0.83	−0.16 ± 0.61	0.04 ± 0.71	−0.23 ± 0.67	−0.16 ± 0.86	2.5	**5E-02**	0.13

*Significant post hoc p-values (<0.05) bolded and reported with Bonferonni correction. Pairwise post hoc comparisons not reported for explicit agency **(D)** since neither main factor nor interaction demonstrated significant effect according to two-way ANOVA for this metric.*

Analysis 3

The mean absolute force profiles across a 10-s trial for a single digit are shown for each dimension and for rigid versus compliant surfaces in **Figure 8**. These mean force trajectories are taken across both digits and all subjects for the "Baseline" control mode. As expected, the greatest force was applied in the direction normal to the grasping surface. Significant differences ($p < 0.05$) in force variability (standard deviation) between surfaces were observed in the lateral and normal dimensions.

DISCUSSION

In this investigation of a precision grasp force task, we observed a positive relationship between implicit agency and performance and that both metrics can vary with modes of control. Furthermore, these general observations are consistent for grasp on either a rigid or compliant surface. While the positive dependence of performance on agency was significant and greater for the complaint surface, the regression fit was low. This suggests agency alone cannot "predict" performance and other explanatory variables are still needed. Furthermore, changes in control modes are required to elucidate this dependence, suggesting that agency can play a role in a dynamic framework for user-device adaptation. However, within a control mode whereby the user has presumably accommodated to a given condition (i.e., control mode), the performance-agency dependence may be diminished.

The dependence of performance on agency should motivate rehabilitation approaches that consider cognitive engagement beyond just entertainment and gamification (Sveistrup, 2004), but rather more efficient modes of physical therapy that restore neuromotor connectivity (Carter et al., 2012). Fostering motivation and engagement for greater participation is critical to ensure effective dosages of rehabilitation training (Hsieh et al., 2012; Stevenson et al., 2012). Our results additionally suggest that

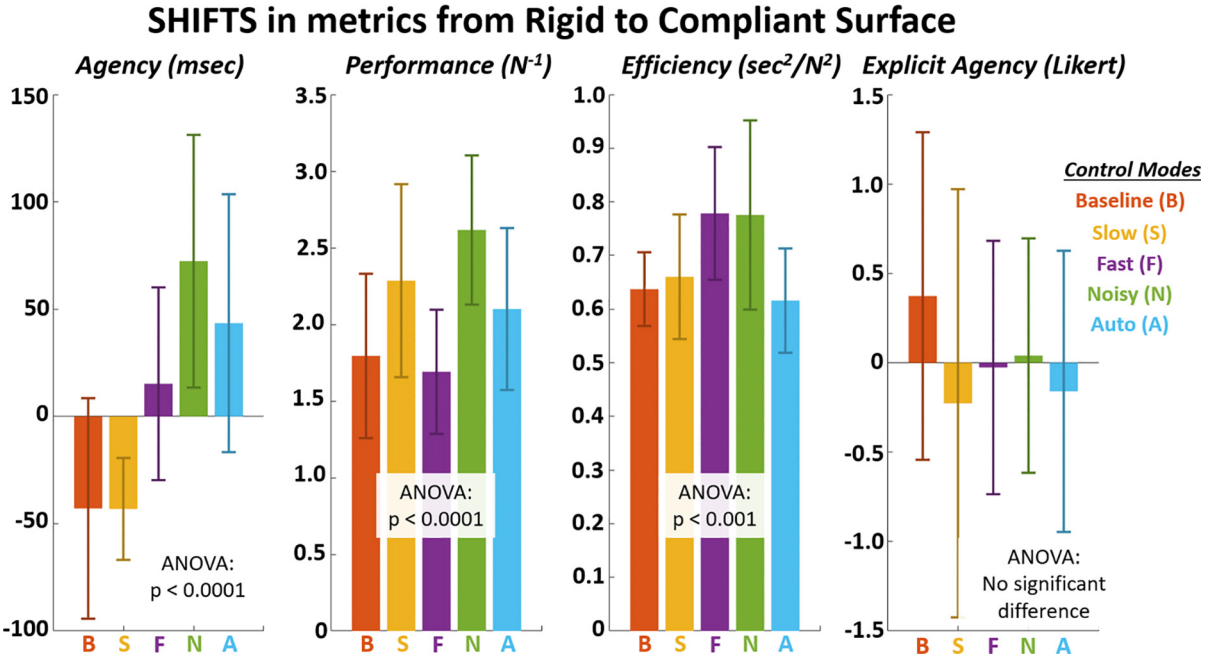

FIGURE 7 | Shifts in metrics across control modes from rigid to compliant grasp surface. The surface-control mode *interaction p*-values are as follows: implicit agency = 1E-05, performance = 5E-05, efficiency = 2E-04, explicit agency = 0.57.

TABLE 5 | Mean shifts from rigid to compliant surface for implicit agency (*msec*), performance (N^{-1}), efficiency (sec^2/N^2), and explicit agency (*Likert*).

	CONTROL MODE				
METRIC	**Baseline**	**Slow**	**Fast**	**Noisy**	**Auto**
Implicit agency	−43 ± 51	−43 ± 23	15 ± 45	72 ± 59	43 ± 60
Performance	1.8 ± 0.53	2.3 ± 0.63	1.7 ± 0.41	2.6 ± 0.49	2.1 ± 0.52
Efficiency	0.63 ± 0.07	0.66 ± 0.12	0.78 ± 0.12	0.78 ± 0.18	0.6 ± 0.10
Explicit agency	0.37 ± 0.91	−0.23 ± 1.2	−0.03 ± 0.71	0.04 ± 0.66	−0.16 ± 0.79

if cognition is systematically monitored and leveraged in real-time, the rehabilitation training sessions may further accelerate functional gains at a given level of participation.

Utilizing computerized interfaces, rehabilitation methods could readily leverage reliable, real-time cognitive measures with automated computational approaches. Optimization routines could be employed to systematically alter a VR training environment (Eddy and Lewis, 2002) with sensory feedback cues (visual, audio, haptic) that specifically enhance agency (Beck et al., 2017; Borhani et al., 2017; Wen et al., 2018). Presentation of avatars or goal-oriented tasks may be continually modified to elicit greater cognitive engagement while monitoring and promoting performance (Shin et al., 2014). Power-assistive exoskeletons and prosthetics driven by physiological commands (Lotte et al., 2012) may have input-output parameters [feedback gains, setpoint speeds, trajectories (Nataraj and van den Bogert, 2017)], customized to co-maximize agency and performance.

Virtual reality may be an appropriate platform to identify training settings and device parameters that maximize function and perception of control for rehabilitative and assistive interfaces (Sutcliffe and Kaur, 2000). Depending on the nature and extent of neuromuscular deficit, the training paradigm may be aimed toward either rehabilitating independent function or improving outcomes with a powered assistive device. In this study, VR training implications are specific to rehabilitation or powered assistance of hand grasp. Prevalent clinical populations include persons with impaired grasp due to hemiparesis, cervical-level spinal cord injury, or upper-limb amputation (Ma et al., 2014). In this study, we observed grasp movement training through a computerized interface with variations in control modes and surface types.

The factors of control modes and surface type demonstrated significant interaction in having significant effects on implicit agency, performance, and control efficiency. As such, it was necessary to observe simple effects with each factor while holding the other factor constant. Participants in this study demonstrated significantly greater hand grasp performance, efficiency of performance, and performance dependence on agency when grasping a compliant surface. Several investigations in hand grasp robotics employ algorithms that command actuation based on

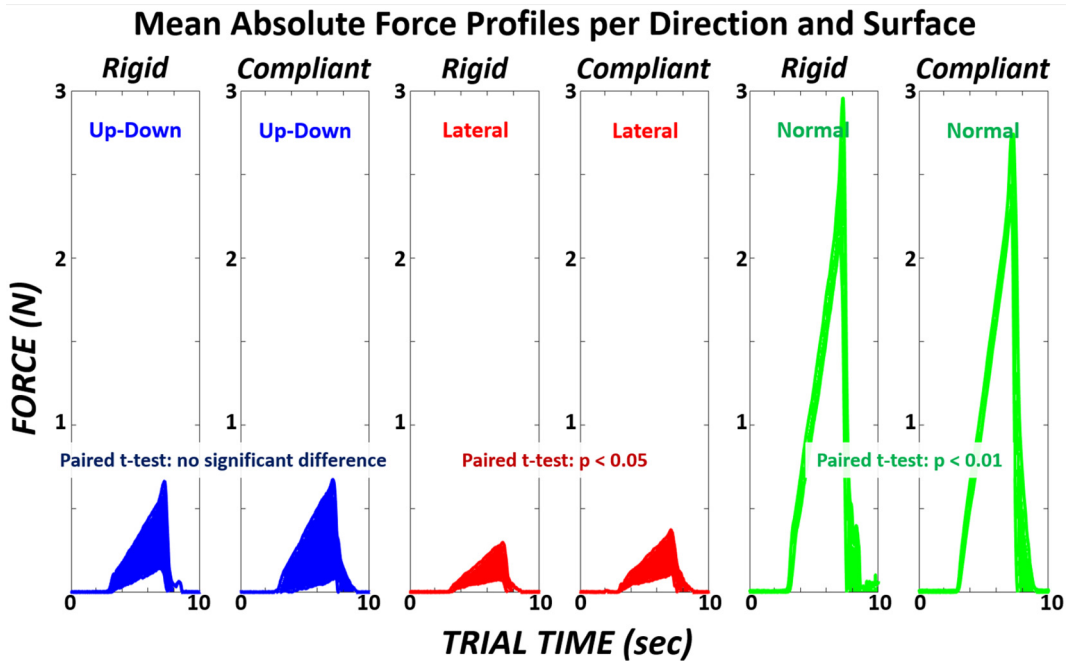

FIGURE 8 | Mean absolute force profile across the 10-s trial for a single digit shown in each dimension (*up-down, lateral, normal*) for rigid versus compliant surfaces. Profile thickness indicates ±1standard deviation. Paired *t*-test performed across the average variability (standard deviation) for each dimension during ramp period (t_{trial} = 3–7 s). The mean force variability in each dimension for the rigid surface was *0.294*, *0.098*, and *0.256 N*. The mean force variability in each dimension for the compliant surface was *0.291*, *0.142*, and *0.173 N*.

compliance (Cutkosky and Kao, 1989; Prattichizzo et al., 2012; Deimel and Brock, 2016). These approaches facilitate digit-level synergies that accommodate several degrees of freedom against a variety of grasp object sizes, shapes, hardness, and surface friction (Michelman and Allen, 1993; Kim et al., 2003; Dollar and Howe, 2006; Dollar et al., 2010). Our study suggests that compliance-based approaches are not only flexibly functional, but they may also encourage users to execute grasp with greater perception of control. While the shift in agency with compliant surfaces was negative for the "Baseline" and "Slow" modes of control, the largest singular shift was positive and observed with the "Noisy" mode.

Noise in sensory feedback can enhance functional performance (Priplata et al., 2002). However, visual noise is typically a distractor to impair performance (Vasilakos and Beuter, 1993; Baldassi et al., 2006). In our study, visual noise was relatively mild (magnitude <5% of target maximum force) and did not generate a significant change in performance from "Baseline" for the rigid surface. Visual noise did significantly reduce agency for the rigid surface, suggesting participants readily dissociated the visual noise from their own true actions (Miele et al., 2011). However, for the compliant surface, both agency and performance significantly increased from "Baseline." The increase in agency suggests participants perceptually embodied the noise of the trace into the actions of their own digits (Caspar et al., 2015). Facilitating body representation with complex visual feedback can enhance movement performance (Sanford et al., 2020). Furthermore, the inability to dissociate the noise may be explained by the increased uncertainty introduced with the compliant surface. However, this erroneous perception of control did not reduce performance, but rather enhanced it. It is conceivable that while the noise did not represent true actions, the compliant surface may have amplified participant perception of freedom to enact greater control. In turn, this enhanced perception may have effectively increased performance responsivity, akin to increasing feedback gains on true visual error (Wei et al., 2005).

Unlike "Noisy," the "Auto" control mode significantly reduced both performance and agency compared to "Baseline" across both surfaces. This finding suggests a sensitivity to gradual automation in grasp that reduced self-agency. The reduced perception of control appeared to reduce independent performance despite display of excellent performance with "Auto." We posit that this performance reduction was not due to conscious awareness of automation since no significant differences in explicit agency were observed. The major implication for assistive devices is the importance of continuous user control in restoration of hand grasp. Traditionally, users generate a command beyond a threshold, with electromyography (EMG) (Marasco et al., 2018) or mechanical switches (Farris et al., 2013), to trigger a "go" command to the movement device (Geethanjali, 2016). The device will then automatically complete a movement sequence, such as grasp closure (Hart et al., 1998) or a step (Hartigan et al., 2015), without further user input until movement completion. While efficient in executing preprogrammed functions, interfaces with greater automation may severely hinder sense of user

control and engagement to the device. More complex functions require nuanced user commands that may need to be identified through machine learning classification of EMG patterns (Zhou et al., 2017; Burns et al., 2019). However, even relatively simple tasks, such as ramped grasp force, may be benefited by more continuous user control to enhance agency and performance.

The "Slow" and "Fast" control modes effectively served as higher and lower grasp force ramps relative to "Baseline." Changes in visual display were effectively uniform once participants accommodated to the load rate required to accurately track the ramp. Since control modes were randomly presented and required grasp loads were relatively small, we do not attribute metric differences for these modes due to learning or fatigue. Participants demonstrated significant increase in agency and performance with "Slow" compared to "Baseline" suggesting greater engagement and capability with higher grasp force. Previous studies have suggested greater agency may be facilitated through greater effort (Demanet et al., 2013). It is not clear if an optimal force level exists for precision pinch from this study. Our objective only sought to specify a low force pinch task and subsequently identify the changes in performance and agency due to control modifications that include changes in force level, addition of noise, and level of automation.

The major limitation of this study was examination of only one level for each control mode type. This study prioritized initial identification of agency and performance across a variety of mode types and two grasp surfaces. For fully customized deployment of an assistive device, it would be necessary to tune across multiple levels of each control mode concurrently. Control settings such as force magnitude, noise amplitude and frequency, and degree of automation may be specified independently or in unique combinations. The next phase of this research should establish methods that efficiently identify device settings such as optimal feedback gains with selective sampling (Nataraj et al., 2014). Optimal parameters could be determined to not only minimize performance errors for better movement (Neptune, 1999; Xiang et al., 2010). But to maximize quantifiable metrics for cognition. Our study suggests implicit agency may be such as agency for greater user-device integration during rehabilitation practices. An assumption of this study was that gender does not affect grasp performance or agency. Gender-based differences for movement agency and precision grasp have not been well established, but not considering gender as a factor is a potential study limitation.

Future studies should also consider alternative measurements of agency. While explicit metrics for agency have been commonly utilized in other studies (Dewey and Knoblich, 2014), variability was too large to identify significant differences in this study. This study did demonstrate that an implicit measure of agency, time-interval estimation for intentional binding, had correlation to performance in the aggregate and could be modulated across control modes. It remains unclear if this metric has sufficient sensitivity and resolution for customization of rehabilitation programs and devices to individual users. Furthermore, requiring each user to provide a verbal estimate of time-intervals would be tedious and cognitively fatiguing while adapting the training interface. The user should be able to devote greater attention to operating the interface while implicit agency is passively measured.

Physiological measures such as EMG and brain electroencephalography (EEG) may be monitored to reflect changes in cognitive agency (Tsakiris et al., 2006; Kang et al., 2015; Beyer et al., 2017). These measures need to be validated as a reliable surrogate for implicit agency and device-based rehabilitation interfaces. Computational optimization tools may be employed to concurrently adapt the user-device interface based on dynamic features of real-time EEG and EMG to assess cognitive integration. To this end, probabilistic methods that evaluate embodied cognition (Ryu and Torres, 2018) may be especially appropriate to extract perceptual features from stochastic physiological signals such as EEG and EMG. Reliable and validated physiological measures for agency would facilitate autonomous adaptation of rehabilitation interfaces for greater cognition. Interfaces include VR-based training paradigms and powered assistive devices such as prosthetics and exoskeletons.

DATA AVAILABILITY STATEMENT

The underlying data supporting the conclusions of this article will be made available by the authors, without undue reservation.

ETHICS STATEMENT

The studies involving human participants were reviewed and approved by the Stevens Institutional Review Board. The patients/participants provided their written informed consent to participate in this study.

AUTHOR CONTRIBUTIONS

RN contributed to designing and developing the experiment, analyzing the data, writing and revising the manuscript, and directing the project. SS contributed to recruiting participants, performing the data collections, and revising the manuscript. Both authors contributed to the article and approved the submitted version.

FUNDING

New Jersey Health Foundation award PC 53-19 assisted with fees related to computer supplies used for data analysis.

ACKNOWLEDGMENTS

The authors would like to acknowledge Aniket Shah and Mingxiao Liu who both assisted with data collection and management. This work was made possible by support from the Schaefer School of Engineering and Science, at the Stevens Institute of Technology and Research grant (PC 53-19) from the New Jersey Health Foundation.

REFERENCES

Agostini, V., and Knaflitz, M. (2012). An algorithm for the estimation of the signal-to-noise ratio in surface myoelectric signals generated during cyclic movements. *IEEE Trans. Biomed. Eng.* 59, 219–225.

Antfolk, C., D'alonzo, M., Rosén, B., Lundborg, G., Sebelius, F., and Cipriani, C. (2013). Sensory feedback in upper limb prosthetics. *Expert Rev. Med. Devices* 10, 45–54. doi: 10.1586/erd.12.68

Baldassi, S., Megna, N., and Burr, D. C. (2006). Visual clutter causes high-magnitude errors. *PLoS Biol.* 4:e56. doi: 10.1371/journal.pbio.0040056

Beck, B., Di Costa, S., and Haggard, P. (2017). Having control over the external world increases the implicit sense of agency. *Cognition* 162, 54–60. doi: 10.1016/j.cognition.2017.02.002

Behrman, A. L., Lawless-Dixon, A. R., Davis, S. B., Bowden, M. G., Nair, P., Phadke, C., et al. (2005). Locomotor training progression and outcomes after incomplete spinal cord injury. *Phys. Ther.* 85, 1356–1371. doi: 10.1093/ptj/85.12.1356

Beyer, F., Sidarus, N., Bonicalzi, S., and Haggard, P. (2017). Beyond self-serving bias: diffusion of responsibility reduces sense of agency and outcome monitoring. *Soc. Cogn. Affect. Neurosci.* 12, 138–145. doi: 10.1093/scan/nsw160

Blaya, J. A., and Herr, H. (2004). Adaptive control of a variable-impedance ankle-foot orthosis to assist drop-foot gait. *IEEE Trans. Neural Syst. Rehab. Eng.* 12, 24–31. doi: 10.1109/tnsre.2003.823266

Borhani, K., Beck, B., and Haggard, P. (2017). Choosing, doing, and controlling: implicit sense of agency over somatosensory events. *Psychol. Sci.* 28, 882–893. doi: 10.1177/0956797617697693

Burns, M. K., Pei, D., and Vinjamuri, R. (2019). Myoelectric control of a soft hand exoskeleton using kinematic synergies. *IEEE Trans. Biomed. Circ. Syst.* 13, 1351–1361. doi: 10.1109/tbcas.2019.2950145

Carter, A. R., Shulman, G. L., and Corbetta, M. (2012). Why use a connectivity-based approach to study stroke and recovery of function? *Neuroimage* 62, 2271–2280. doi: 10.1016/j.neuroimage.2012.02.070

Caspar, E. A., Cleeremans, A., and Haggard, P. (2015). The relationship between human agency and embodiment. *Conscious. Cogn.* 33, 226–236. doi: 10.1016/j.concog.2015.01.007

Childress, D. S. (1973). Powered limb prostheses: their clinical significance. *IEEE Trans. Biomed. Eng.* BME-20, 200–207. doi: 10.1109/tbme.1973.324273

Cutkosky, M. R., and Kao, I. (1989). Computing and controlling compliance of a robotic hand. *IEEE Trans. Robot. Autom.* 5, 151–165. doi: 10.1109/70.88036

Davoodi, R., Urata, C., Hauschild, M., Khachani, M., and Loeb, G. E. (2007). Model-based development of neural prostheses for movement. *IEEE Trans. Biomed. Eng.* 54, 1909–1918. doi: 10.1109/tbme.2007.902252

De Havas, J., Ito, S., Haggard, P., and Gomi, H. (2018). Low gain servo control during the kohnstamm phenomenon reveals dissociation between low-level control mechanisms for involuntary vs. voluntary arm movements. *Front. Behav. Neurosci.* 12:113. doi: 10.3389/fnbeh.2018.00113

Deimel, R., and Brock, O. (2016). A novel type of compliant and underactuated robotic hand for dexterous grasping. *Int. J. Robot. Res.* 35, 161–185. doi: 10.1177/0278364915592961

Delevoye-Turrell, Y., Giersch, A., and Danion, J.-M. (2002). A deficit in the adjustment of grip force responses in schizophrenia. *Neuroreport* 13, 1537–1539. doi: 10.1097/00001756-200208270-00010

Demanet, J., Muhle-Karbe, P. S., and Lynn, M. T. Blotenberg, I and Brass, M. (2013). Power to the will: how exerting physical effort boosts the sense of agency. *Cognition* 129, 574–578.

Dewey, J. A., and Knoblich, G. (2014). Do implicit and explicit measures of the sense of agency measure the same thing? *PLoS One* 9:e110118. doi: 10.1371/journal.pone.0110118

Dollar, A. M., and Howe, R. D. (2006). A robust compliant grasper via shape deposition manufacturing. *IEEE/ASME Trans. Mechatronics* 11, 154–161. doi: 10.1109/tmech.2006.871090

Dollar, A. M., Jentoft, L. P., Gao, J. H., and Howe, R. D. (2010). Contact sensing and grasping performance of compliant hands. *Auton. Robots* 28, 65. doi: 10.1007/s10514-009-9144-9

Doyle, P. J. (2002). Measuring health outcomes in stroke survivors. *Arch. Phys. Med. Rehab.* 83, S39–S43.

Eddy, J., and Lewis, K. (2002). "Multidimensional design visualization in multiobjective optimization," in *Proceedings of the 9th AIAA/ISSMO Symposium on Multidisciplinary Analysis and Optimization*, (Atlanta, GA), 5621.

Evans, N., Gale, S., Schurger, A., and Blanke, O. (2015). Visual feedback dominates the sense of agency for brain-machine actions. *PLoS One* 10:e0130019. doi: 10.1371/journal.pone.0130019

Farris, R. J., Quintero, H. A., Murray, S. A., Ha, K. H., Hartigan, C., and Goldfarb, M. (2013). A preliminary assessment of legged mobility provided by a lower limb exoskeleton for persons with paraplegia. *IEEE Trans. Neural Syst. Rehab. Eng.* 22, 482–490. doi: 10.1109/tnsre.2013.2268320

Friedman, J., and Flash, T. (2007). Task-dependent selection of grasp kinematics and stiffness in human object manipulation. *Cortex* 43, 444–460. doi: 10.1016/s0010-9452(08)70469-6

Frith, C. D., and Haggard, P. (2018). Volition and the brain - revisiting a classic experimental study. *Trends Neurosci.* 41, 405–407. doi: 10.1016/j.tins.2018.04.009

Geethanjali, P. (2016). Myoelectric control of prosthetic hands: state-of-the-art review. *Med. Devices (Auckl.)* 9, 247. doi: 10.2147/mder.s91102

Haggard, P., Clark, S., and Kalogeras, J. (2002). Voluntary action and conscious awareness. *Nat. Neurosci.* 5, 382–385. doi: 10.1038/nn827

Hart, R. L., Kilgore, K. L., and Peckham, P. H. (1998). A comparison between control methods for implanted FES hand-grasp systems. *IEEE Trans. Rehab. Eng.* 6, 208–218. doi: 10.1109/86.681187

Hartigan, C., Kandilakis, C., Dalley, S., Clausen, M., Wilson, E., Morrison, S., et al. (2015). Mobility outcomes following five training sessions with a powered exoskeleton. *Top. Spinal Cord Inj. Rehab.* 21, 93–99. doi: 10.1310/sci2102-93

Hebert, J. S., Olson, J. L., Morhart, M. J., Dawson, M. R., Marasco, P. D., Kuiken, T. A., et al. (2013). Novel targeted sensory reinnervation technique to restore functional hand sensation after transhumeral amputation. *IEEE Trans. Neural Syst. Rehab. Eng.* 22, 765–773.

Heo, P., Gu, G. M., Lee, S.-j., Rhee, K., and Kim, J. (2012). Current hand exoskeleton technologies for rehabilitation and assistive engineering. *Int. J. Precis. Eng. Manuf.* 13, 807–824. doi: 10.1007/s12541-012-0107-2

Hsieh, Y.-w, Wu, C.-y., Lin, K.-c., Yao, G., Wu, K.-y, and Chang, Y.-j (2012). Dose–response relationship of robot-assisted stroke motor rehabilitation: the impact of initial motor status. *Stroke* 43, 2729–2734. doi: 10.1161/strokeaha.112.658807

Hubbard, I. J., Parsons, M. W., Neilson, C., and Carey, L. M. (2009). Task−specific training: evidence for and translation to clinical practice. *Occup. Ther. Int.* 16, 175–189. doi: 10.1002/oti.275

Hughes, A.-M., Burridge, J. H., Demain, S. H., Ellis-Hill, C., Meagher, C., Tedesco-Triccas, L., et al. (2014). Translation of evidence-based assistive technologies into stroke rehabilitation: users' perceptions of the barriers and opportunities. *BMC Health Serv. Res.* 14:124. doi: 10.1186/1472-6963-14-124

Jeannerod, M. (2009). The sense of agency and its disturbances in schizophrenia: a reappraisal. *Exp. Brain Res.* 192:527. doi: 10.1007/s00221-008-1533-3

Kang, S. Y., Im, C. H., Shim, M., Nahab, F. B., Park, J., Kim, D. W., et al. (2015). Brain networks responsible for sense of agency: an EEG study. *PLoS One* 10:e0135261. doi: 10.1371/journal.pone.0135261

Kazemi, M., Valois, J.-S., Bagnell, J. A., and Pollard, N. (2012). *Robust Object Grasping Using Force Compliant Motion Primitives," Robotics: Science and Systems (RSS)*. Sydney, NSW: MIT Press, 177–185.

Khalighinejad, N., Kunnumpurath, A., Bertini, C., Ladavas, E., and Haggard, P. (2017). Subliminal modulation of voluntary action experience: a neuropsychological investigation. *Cortex* 90, 58–70. doi: 10.1016/j.cortex.2017.02.012

Kilteni, K., Groten, R., and Slater, M. (2012). The sense of embodiment in virtual reality. *Presence Teleoperators Vir. Environ.* 21, 373–387. doi: 10.1162/pres_a_00124

Kim, B.-H., Yi, B.-J., Oh, S.-R., and Suh, I. H. (2003). Independent finger and independent joint-based compliance control of multifingered robot hands. *IEEE Trans. Robot. Autom.* 19, 185–199. doi: 10.1109/tra.2003.808846

Le Goff, K., Rey, A., Haggard, P., Oullier, O., and Berberian, B. (2018). Agency modulates interactions with automation technologies. *Ergonomics* 61, 1282–1297. doi: 10.1080/00140139.2018.1468493

Lotte, F., Faller, J., Guger, C., Renard, Y., Pfurtscheller, G., Lécuyer, A., et al. (2012). "Combining BCI with virtual reality: towards new applications and improved BCI," in *Towards Practical Brain-Computer Interfaces*, eds B. Allison, S. Dunne, R. Leeb, J Del R. Millán, and A. Nijholt (Heidelberg: Springer), 197–220. doi: 10.1007/978-3-642-29746-5_10

Lucas, L., DiCicco, M., and Matsuoka, Y. (2004). An EMG-controlled hand exoskeleton for natural pinching. *J. Robot. Mechatronics* 16, 482–488. doi: 10.20965/jrm.2004.p0482

Ma, V. Y., Chan, L., and Carruthers, K. J. (2014). Incidence, prevalence, costs, and impact on disability of common conditions requiring rehabilitation in the United States: stroke, spinal cord injury, traumatic brain injury, multiple sclerosis, osteoarthritis, rheumatoid arthritis, limb loss, and back pain. *Arch. Phys. Med. Rehab.* 95, 986–995. e1.

Marasco, P. D., Hebert, J. S., Sensinger, J. W., Shell, C. E., Schofield, J. S., Thumser, Z. C., et al. (2018). Illusory movement perception improves motor control for prosthetic hands. *Sci. Transl. Med.* 10:eaao6990. doi: 10.1126/scitranslmed.aao6990

Michelman, P., and Allen, P. (1993). "Compliant manipulation with a dextrous robot hand," in *Proceedings of the 1993 IEEE International Conference on Robotics and Automation*, (Atlanta, GA: IEEE), 711–716.

Miele, D. B., Wager, T. D., Mitchell, J. P., and Metcalfe, J. (2011). Dissociating neural correlates of action monitoring and metacognition of agency. *J. Cogn. Neurosci.* 23, 3620–3636. doi: 10.1162/jocn_a_00052

Moore, J., and Haggard, P. (2008). Awareness of action: inference and prediction. *Conscious. Cogn.* 17, 136–144. doi: 10.1016/j.concog.2006.12.004

Moore, J. W. (2016). What is the sense of agency and why does it matter? *Front. Psychol.* 7:1272. doi: 10.3389/fpsyg.2016.01272

Moore, J. W., and Fletcher, P. C. (2012). Sense of agency in health and disease: a review of cue integration approaches. *Conscious. Cogn.* 21, 59–68. doi: 10.1016/j.concog.2011.08.010

Moore, J. W., Middleton, D., Haggard, P., and Fletcher, P. C. (2012). Exploring implicit and explicit aspects of sense of agency. *Conscious. Cogn.* 21, 1748–1753. doi: 10.1016/j.concog.2012.10.005

Moore, J. W., and Obhi, S. S. (2012). Intentional binding and the sense of agency: a review. *Conscious. Cogn.* 21, 546–561. doi: 10.1016/j.concog.2011.12.002

Moore, J. W., Wegner, D. M., and Haggard, P. (2009). Modulating the sense of agency with external cues. *Conscious. Cogn.* 18, 1056–1064. doi: 10.1016/j.concog.2009.05.004

Nataraj, R. (2017). "Optimizing user integration for individualized rehabilitation," in *Biomimetic Prosthetics*, ed. R. Vinjamuri (London: IntechOpen).

Nataraj, R., Audu, M. L., Kirsch, R. F., and Triolo, R. J. (2010). Comprehensive joint feedback control for standing by functional neuromuscular stimulation—A simulation study. *IEEE Trans. Neural Syst. Rehab. Eng.* 18, 646–657. doi: 10.1109/tnsre.2010.2083693

Nataraj, R., Audu, M. L., and Li, Z.-M. (2015). Digit mechanics in relation to endpoint compliance during precision pinch. *J. Biomech.* 48, 672–680. doi: 10.1016/j.jbiomech.2014.12.040

Nataraj, R., Audu, M. L., and Triolo, R. J. (2012b). Center of mass acceleration feedback control of standing balance by functional neuromuscular stimulation against external postural perturbations. *IEEE Trans. Biomed. Eng.* 60, 10–19. doi: 10.1109/tbme.2012.2218601

Nataraj, R., Audu, M. L., and Triolo, R. J. (2012a). Center of mass acceleration feedback control of functional neuromuscular stimulation for standing in the presence of internal postural perturbations. *J. Rehab. Res. Dev.* 49:889. doi: 10.1682/jrrd.2011.07.0127

Nataraj, R., Audu, M. L., and Triolo, R. J. (2014). Modified Newton-Raphson method to tune feedback gains of control system for standing by functional neuromuscular stimulation following spinal cord injury. *Appl. Bion. Biomech.* 11, 169–174. doi: 10.1155/2014/634509

Nataraj, R., Hollinger, D., Liu, M., and Shah, A. (2020c). Disproportionate positive feedback facilitates sense of agency and performance for a reaching movement task with a virtual hand. *PLoS One* 15:e0233175. doi: 10.1371/journal.pone.0233175

Nataraj, R., Sanford, S., Liu, M., Walsh, K., Wilder, S., Santo, A., et al. (2020b). "Cognitive and physiological intent for the adaptation of motor prostheses," in *Advances in Motor Neuroprostheses*, ed. R. Vinjamuri (Cham: Springer), 123. doi: 10.1007/978-3-030-38740-2_8

Nataraj, R., Sanford, S., Shah, A., and Liu, M. (2020a). Agency and performance of reach-to-grasp with modified control of a virtual hand: implications for rehabilitation. *Front. Hum. Neurosci.* 14:126. doi: 10.3389/fnhum.2020.00126

Nataraj, R., Sanford, S., Shah, A., and Liu, M. (2020d). Agency and performance of reach-to-grasp with modified control of a virtual hand: implications for rehabilitation. *Front. Hum. Neurosci.* 14:126.

Nataraj, R., and van den Bogert, A. J. (2017). Simulation analysis of linear quadratic regulator control of sagittal-plane human walking—implications for exoskeletons. *J. Biomech. Eng.* 139:101009.

Neptune, R. R. (1999). Optimization algorithm performance in determining optimal controls in human movement analyses. *J. Biomech. Eng.* 121, 249–252. doi: 10.1115/1.2835111

Phillips, B., and Zhao, H. (1993). Predictors of assistive technology abandonment. *Assist. Technol.* 5, 36–45. doi: 10.1080/10400435.1993.10132205

Prattichizzo, D., Malvezzi, M., Gabiccini, M., and Bicchi, A. (2012). On the manipulability ellipsoids of underactuated robotic hands with compliance. *Robot. Auton. Syst.* 60, 337–346. doi: 10.1016/j.robot.2011.07.014

Priplata, A., Niemi, J., Salen, M., Harry, J., Lipsitz, L. A., and Collins, J. (2002). Noise-enhanced human balance control. *Phys. Rev. Lett.* 89:238101.

Ritterband-Rosenbaum, A., Christensen, M. S., and Nielsen, J. B. (2012). Twenty weeks of computer-training improves sense of agency in children with spastic cerebral palsy. *Res. Dev. Disabil.* 33, 1227–1234. doi: 10.1016/j.ridd.2012.02.019

Ronsse, R., Vitiello, N., Lenzi, T., Van Den Kieboom, J., Carrozza, M. C., and Ijspeert, A. J. (2011). Human–robot synchrony: flexible assistance using adaptive oscillators. *IEEE Trans. Biomed. Eng.* 58, 1001–1012. doi: 10.1109/tbme.2010.2089629

Ryu, J., and Torres, E. B. (2018). Characterization of sensory-motor behavior under cognitive load using a new statistical platform for studies of embodied cognition. *Front. Hum. Neurosci.* 12:116. doi: 10.3389/fnhum.2018.00116

Saito, N., Takahata, K., Murai, T., and Takahashi, H. (2015). Discrepancy between explicit judgement of agency and implicit feeling of agency: Implications for sense of agency and its disorders. *Conscious. Cogn.* 37, 1–7. doi: 10.1016/j.concog.2015.07.011

Saleh, S., Fluet, G., Qiu, Q., Merians, A., Adamovich, S. V., and Tunik, E. (2017). Neural patterns of reorganization after intensive robot-assisted virtual reality therapy and repetitive task practice in patients with chronic stroke. *Front. Neurol.* 8:452. doi: 10.3389/fneur.2017.00452

Sanford, S., Liu, M., Selvaggi, T., and Nataraj, R. (2020). Effects of visual feedback complexity on the performance of a movement task for rehabilitation. *J. Motor Behav.* 1–15. doi: 10.1080/00222895.2020.1770670

Schofield, J. S., Shell, C. E., Thumser, Z. C., Beckler, D. T., Nataraj, R., and Marasco, P. D. (2019). Characterization of the sense of agency over the actions of neural-machine interface-operated prostheses. *JoVE J. Vis. Exp.* 143:e58702.

Shepherd, R. B. (2001). Exercise and training to optimize functional motor performance in stroke: driving neural reorganization? *Neural Plast.* 8, 121–129. doi: 10.1155/np.2001.121

Shin, J.-H., Ryu, H., and Jang, S. H. (2014). A task-specific interactive game-based virtual reality rehabilitation system for patients with stroke: a usability test and two clinical experiments. *J. Neuroeng. Rehab.* 11:32. doi: 10.1186/1743-0003-11-32

Stevenson, T., Thalman, L., Christie, H., and Poluha, W. (2012). Constraint-induced movement therapy compared to dose-matched interventions for upper-limb dysfunction in adult survivors of stroke: a systematic review with meta-analysis. *Physiother. Can.* 64, 397–413. doi: 10.3138/ptc.2011-24

Sutcliffe, A. G., and Kaur, K. D. (2000). Evaluating the usability of virtual reality user interfaces. *Behav. Inform. Technol.* 19, 415–426. doi: 10.1080/014492900750052679

Sveistrup, H. (2004). Motor rehabilitation using virtual reality. *J. Neuroeng. Rehab.* 1:10.

Taylor, D. M., Tillery, S. I. H., and Schwartz, A. B. (2002). Direct cortical control of 3D neuroprosthetic devices. *Science* 296, 1829–1832. doi: 10.1126/science.1070291

Terenzi, S. (1998). Automatic tuning of myoelectric prostheses. *Development* 35, 294–304.

Tsakiris, M., Prabhu, G., and Haggard, P. (2006). Having a body versus moving your body: how agency structures body-ownership. *Conscious. Cogn.* 15, 423–432. doi: 10.1016/j.concog.2005.09.004

Vasilakos, K., and Beuter, A. (1993). Effects of noise on a delayed visual feedback system. *J. Theor. Biol.* 165, 389–407. doi: 10.1006/jtbi.1993.1196

Velazquez, H. F., Walter, R. S., Gruttadauria, M. K., Huelskamp, T. J., Gara, D. P., Lynch, W. M., et al. (2008). *Virtual reality system including personalized virtual environments* Google Patents US20080162261A1.

Wege, A., Kondak, K., and Hommel, G. (2005). "Mechanical design and motion control of a hand exoskeleton for rehabilitation," in *Proceedings of the IEEE*

International Conference Mechatronics and Automation, 2005, (Niagara Falls, Ont: IEEE), 155–159.

Wegner, D. M. (2003). The mind's best trick: how we experience conscious will. *Trends Cogn. Sci.* 7, 65–69. doi: 10.1016/s1364-6613(03)00002-0

Wei, Y., Bajaj, P., Scheidt, R., and Patton, J. (2005). "Visual error augmentation for enhancing motor learning and rehabilitative relearning," in *Proceedings of the 9th International Conference on Rehabilitation Robotics, ICORR 2005*, (Chicago, IL: IEEE), 505–510.

Wen, W., Brann, E., Di Costa, S., and Haggard, P. (2018). Enhanced perceptual processing of self-generated motion: evidence from steady-state visual evoked potentials. *Neuroimage* 175, 438–448. doi: 10.1016/j.neuroimage.2018.04.019

Xiang, Y., Arora, J. S., and Abdel-Malek, K. (2010). Physics-based modeling and simulation of human walking: a review of optimization-based and other approaches. *Struct. Multidiscipl. Optim.* 42, 1–23. doi: 10.1007/s00158-010-0496-8

Zhou, S., Yin, K., Liu, Z., Fei, F., and Guo, J. (2017). "sEMG-based hand motion recognition by means of multi-class adaboost algorithm," in *Proceedings of the 2017 IEEE International Conference on Robotics and Biomimetics (ROBIO)*, (Macau: IEEE), 1056–1061.

Conflict of Interest: The authors declare that the research was conducted in the absence of any commercial or financial relationships that could be construed as a potential conflict of interest.

frontiers in Human Neuroscience

OPINION
published: 13 January 2021
doi: 10.3389/fnhum.2020.622533

Novel Non-invasive Strategy for Spinal Neuromodulation to Control Human Locomotion

*Tatiana Moshonkina[1], Alexander Grishin[1], Irina Bogacheva[1], Ruslan Gorodnichev[2], Alexander Ovechkin[3,4], Ricardo Siu[3], V. Reggie Edgerton[5,6,7] and Yury Gerasimenko[1,8]**

[1] Pavlov Institute of Physiology, Russian Academy of Sciences, St. Petersburg, Russia, [2] Velikie Luki State Academy of Physical Education and Sports, Velikiye Luki, Russia, [3] Kentucky Spinal Cord Injury Research Center, Frazier Rehab Institute, University of Louisville Health, University of Louisville, Louisville, KY, United States, [4] Department of Neurological Surgery, University of Louisville, Louisville, KY, United States, [5] Department of Neurobiology, and Neurosurgery, University of California, Los Angeles, Los Angeles, CA, United States, [6] Institut Guttmann Hospital de Neurorehabilitació, Institut Universitari adscrit a la Universitat Autònoma de Barcelona, Barcelona, Spain, [7] Faculty of Science, The Center for Neuroscience and Regenerative Medicine, University of Technology Sydney, Ultimo, NSW, Australia, [8] Department of Physiology and Biophysics, University of Louisville, Louisville, KY, United States

Keywords: neuromodulation, paralysis, transcutaneous electrical spinal cord stimulation, humans, motor pools

OPEN ACCESS

Edited by:
Yury Ivanenko, Santa Lucia Foundation (IRCCS), Italy

Reviewed by:
Sukhvinder Kalsi-Ryan, University Health Network (UHN), Canada
Kristine C. Cowley, University of Manitoba, Canada

***Correspondence:**
Yury Gerasimenko
gerasimenko@infran.ru

Specialty section:
This article was submitted to Motor Neuroscience, a section of the journal Frontiers in Human Neuroscience

Received: *28 October 2020*
Accepted: *14 December 2020*
Published: *13 January 2021*

Citation:
Moshonkina T, Grishin A, Bogacheva I, Gorodnichev R, Ovechkin A, Siu R, Edgerton VR and Gerasimenko Y (2021) Novel Non-invasive Strategy for Spinal Neuromodulation to Control Human Locomotion. Front. Hum. Neurosci. 14:622533. doi: 10.3389/fnhum.2020.622533

INTRODUCTION

It is well-documented that neural control of stepping and standing can be generated in mammals within the spinal neuronal networks. Having a high level of automaticity, these locomotor-related neuronal circuits can produce a "stepping" movement pattern in the absence of input from the brain and/or peripheral afferent inputs. Recent observations have provided important insight into the properties of the spinal and supraspinal circuitry that are involved in movement control. We have shown that the spinal circuitry in mice, rats, cats, and humans can be neuromodulated to regain sensorimotor function after complete paralysis (Gerasimenko et al., 2008). We have also shown that with epidural spinal cord stimulation at the lumbar level, full weight-bearing standing, and voluntary movements of the lower limb can be recovered in humans with complete paralysis (Angeli et al., 2014). Altering spinal cord excitability enables voluntary movements after chronic complete paralysis in humans. Recent breakthrough studies reported that chronically paralyzed individuals regained the over-ground walking with balance assistance through interleaved continous lumbosacral (L1-S1) epidural stimulation and task specific locomotor training (Angeli et al., 2018; Gill et al., 2018).

We have developed a novel method of non-invasive transcutaneous spinal cord stimulation (scTS) which can modulate the excitability of spinal circuitry via electrodes placed on the skin overlying the cervical, lower thoracic, lumbosacral, and coccygeal vertebrae using a special form of electrical pulses delivered at a high frequency (Gerasimenko et al., 2015a). This methodology was able to neuromodulate the spinal locomotor networks such that involuntary stepping-like movements were induced in non-injured subjects when their legs were placed in a "gravity-neutral" apparatus (Gerasimenko et al., 2015b). In addition, our initial results with scTS show that this strategy can facilitate individuals having motor complete paralysis to generate rhythmic stepping patterns and non-repetitive voluntary movements (Gerasimenko Y. P. et al., 2015). The novel finding in this and ongoing studies is that specifically configured multisite stimulation can produce a more robust response when compared to the single site stimulation. Based on these findings, we developed a three-by-three multielectrode transcutaneous array that allows multiple sites to be modulated, thus, providing subject-specific options for controlling posture and locomotor behavior (Gerasimenko et al., 2015a). We observed that the effectiveness of inducing of involuntary stepping movements in a non-injured subject with legs placed in a "gravity-neutral" position during

spinal cord stimulation at one level (T11) with 3 interconnected electrodes (A,B,C) located at midline (B) and laterally (A and C) to the spinal cord vs. stimulation at 2 levels (T11 + L1) with electrodes (T11-ABC) + (L1-ABC) was different. The amplitude of knee displacement and surface electromyographic (sEMG) activity of leg muscles were significantly higher with multi-site stimulation at 2 levels than at one level (Gerasimenko et al., 2015b). Our preliminary data reveal that use of the multielectrode surface array can fine-tune the control of the locomotor behavior. Here we introduce a new strategy of spinal neuromodulation using the continuous stimulation of locomotor circuitry and the rhythmic stimulation of motor pools.

COMBINED ACTIVATION OF LOCOMOTOR CIRCUITRY AND MOTOR POOLS

This study is based on the concept of differential modulation of neuronal networks projecting to specific interneurons that coordinate the levels of recruitment of different combinations of motor pools throughout a step cycle. A novel approach of spatiotemporal spinal stimulation through rhythmic scTS coupled with continuous scTS to promote locomotor neural plasticity by activating regional spinal networks in a manner similar to that observed during normal gait has been suggested. The general idea is the use of continuous spinal stimulation to activate the locomotor networks in combination with rhythmic targeted activation of flexor and extensor motor pools of leg muscles in different phases of step cycle to further enable a stepping-like behavior. Recently it was shown that spatiotemporal epidural stimulation of flexor and extensor motor pools of left and right legs can facilitate swing or stance phases during the stepping cycle in chronic motor incomplete. Severely paralyzed (unable to walk over-ground) individuals recovered over-ground walking with balance assist (Wagner et al., 2018).

Our experimental paradigm included rhythmic scTS with two cathodes at each T11 and L1 delivered 2.5 cm lateral to the midline of the spine, and continuous scTS at T11 or L1 applied along the midline between the spinous processes (**Figure 1A**). ScTS was carried out with the electrical stimulator BioStim-5 (Cosyma INC). Stimulation was delivered using 2.5-cm-diameter round gel adhesive electrodes (Syrtenty Premium TENS) as cathodes, and two interconnected 5 × 9 cm^2 self-adhesive electrodes (Axelgaard, ValuTrode Cloth) placed over the iliac crests as anodes. The stimulation waveform consisted of monophasic rectangular 1.0-ms pulses at a frequency of 15 and 30 Hz, each pulse filled with a carrier frequency of 5 kHz.

In non-injured subjects ($N = 6$, 23.7 ± 2.3 years), stance and swing phases were detected by sensors-gyroscopes. Initiation of hip extension was the trigger for activation of extensor pools (L1) during stance phase, whereas the initiation of hip flexion was triggered for activation of flexor motor pools (T11) during swing phase (Grishin et al., 2020). During walking on treadmill, stimulation applied unilaterally at L1 during the stance phase with a frequency of 15 Hz increased the amplitude of movements in the hip joint, and significantly increased sEMG activity of the extensor muscles of the thigh and flexor muscles of the shank. Meanwhile, unilateral stimulation at T11 with a frequency of 30 Hz applied during the swing phase increased walking speed due to reduction of the stance phase duration. Additionally, the stimulation induced an increase in the amplitude of movements in the hip joint and the lifting of the knee as well as foot elevation. This was accompanied by an increase of sEMG activity in BF and TA muscles (**Figure 1B**). Combined spatiotemporal stimulation at L1 and T11 applied to stance and swing phases, correspondingly did not cause a change in the duration of the stepping cycle and the phases of the step, however, it changed the kinematic characteristics of movements. In the stance phase, the amplitude of movements in the hip joint increased. The amplitude of movements in the hip joint increased in the swing phase as well, but it also increased the lifting of the knee and foot elevation (**Figure 1B**). Additional continuous stimulation applied along the midline at T11 with frequency of 30 Hz facilitated the effect of rhythmic spatiotemporal stimulation. Thus, the data obtained shows that specifically configured multi-site scTS is able to selectively facilitate the activation of the motor pools of the lower extremities and control their activity to regulate the phases of the stepping cycle.

DISCUSSION

Our experience with multi-electrode epidural stimulation in mice, rats, and humans (Gerasimenko et al., 2008; Harkema et al., 2011; Angeli et al., 2014) indicate the potential to regain overground load-bearing stepping, as well as voluntary control of lower limb movements, using non-invasive neuromodulatory strategies. The main issue is to determine the potential of scTS applied to different sites of the spinal cord can provide spatiotemporal specificity of the locomotor network in a way that facilitates phase-specific flexor-extensor motor pool populations. Early, we demonstrated that transcutaneous electrical stimulation of rostral and caudal areas of lumbosacral enlargement resulted in a selective topographical recruitment of proximal and distal leg muscles based on their threshold intensity, maximal slope of the recruitment curves, and plateau point intensity and magnitude (Sayenko et al., 2018). Our data are generally consistent with previous reports and myotomal maps of the spinal cord and lumbosacral roots (Stewart, 1992; Ivanenko et al., 2006). It is well-known that the lumbosacral enlargement not only contains motor neuron pools projecting to proximal and distal leg muscles, but also encompasses neuronal networks controlling locomotion and standing. We demonstrated that epidural stimulation of the spinal rostral segments (L2) is more effective for inducing rhythmic movements, whereas stimulation of more caudal segments (S1–S2) allows for greater postural control (Angeli et al., 2014). During combined locomotor-specific scTS over the T11 at 30 Hz, with the postural-specific scTS over the L1 at 15 Hz, we observed the interplay of various stimulation characteristics in generation of continuous and alternating weight-bearing, and facilitation of body-weight transitions allowing effective stepping motions to be performed (Sayenko et al., 2018). These results suggest that stimulation

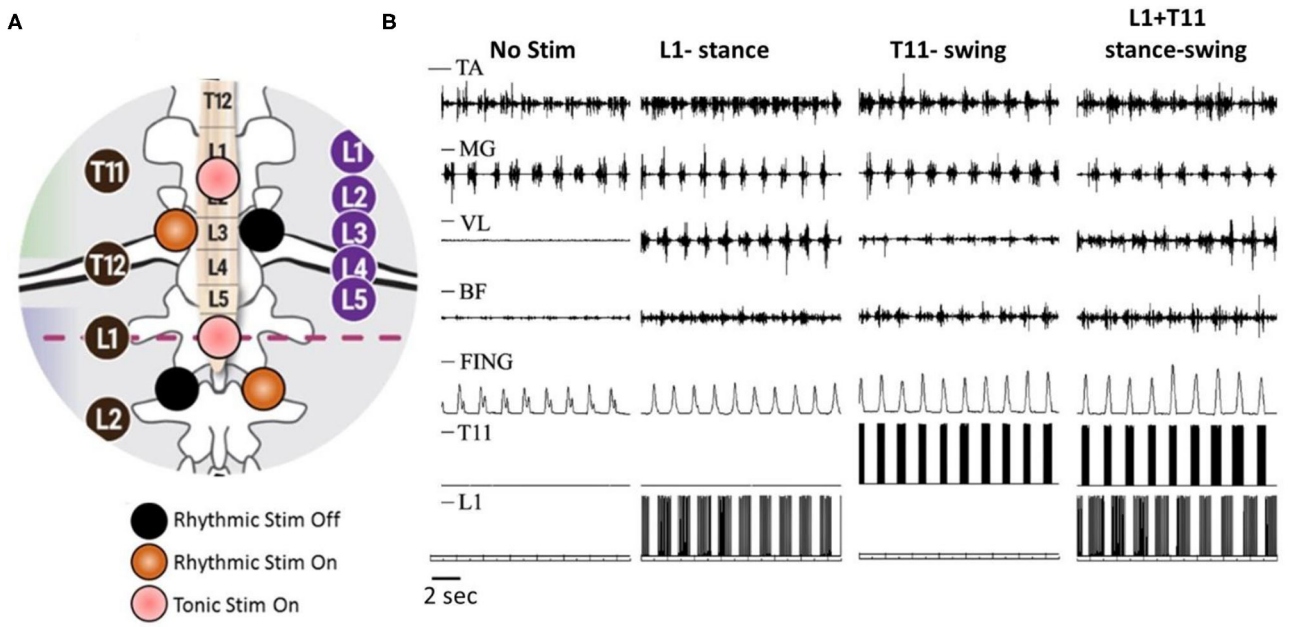

FIGURE 1 | Rhythmic and continues spinal cord transcutaneous stimulation paradigm. **(A)** Schematic localization of stimulation electrodes. Midline electrodes at T11 and L1 generate continuous stimulation at 30 Hz. Lateral electrode at T11 generate rhythmic stimulation at 30 Hz during swing phase and lateral electrode at L1 generate rhythmic stimulation at 15 Hz during stance phase. **(B)** Surface EMG activity of distal [tibialis ant. (TA) and medial gastrocnemius (MG)] and proximal [vastus lat. (VL) and biceps femoris (BF)] muscles as well as displacement of terminal poit (Fing) during walking on the treadmill without stimulation, with rhythmic stimulation of L1 at stance phase, with rhythmic stimulation of T11 at swing phase, and combined L1 and T11 stimulation applied to stance and swing phase, correspondingly.

of multiple spinal sites related to postural and locomotor circuitries activation might be complementary and thus can be a viable strategy to facilitate more effective stepping-like and postural movements.

Given the numerous observations of the different sources and techniques to gain access to the neurons that generate locomotor rhythms, it is not surprising that modulation of these neurons, commonly referred to as the locomotor central pattern generator, can be modulated electrically to different physiological states from multiple spinal segments, as well as multiple supraspinal sites. Although the rostral lumbar segments generate more robust pattern generation, neuromodulatory effects of stimulating at S1 was not expected to give the enhancement of the locomotor rhythms derived from the fictive locomotor patterns observed in the rodent neonatal preparation as reported in series of experiments by Lev-Tov and colleagues (Lev-Tov et al., 2000). For example, changes in the endogenous levels of cholinergic components in the sacral area with ascending projections via the ventral funiculus (Finkel et al., 2014) and Alpha-1 adrenoceptor agonists in this region have been observed to modulate the fictive locomotor output (Gabbay and Lev-Tov, 2004).

We have also shown that the rostral lumbar segments are the key controllers of hindlimb locomotor rhythmicity in the adult spinal rat (Gerasimenko et al., 2019). We observed that the rats with spinal cord transections at T8 and S1 remained capable of generating coordinated hindlimb locomotion when receiving epidural stimulation at L2. In contrast, minimal locomotion was observed when S1 stimulation was delivered after spinal cord transections at T8 and L2. These findings are compatible with work of others demonstrating the critical role of commissural neurons located in rostral lumbar segments supporting locomotor rhythm generation in response to bulbospinal activation of locomotion *in vitro* neonatal rat spinal cord (Cowley et al., 2009).

Shik hypothesized the role of propriospinal system in initiation of locomotion (Shik, 1997). It has been demonstrated that microstimulation of stepping strip in the dorsolateral funiculus (DLF) elicited stepping movements in mesencephalic cats (Kazennikov et al., 1983). According to these authors, neurons responding to stimulation of the stepping strip send their axons into the ventrolateral funiculus (VLF) near the gray matter. It has been suggested that excited fibers of DLF can activate hindlimb stepping indirectly through DLF -VLF propriospinal loops (Shik, 1997). Our data are consistent with suggestion about activation the locomotor-related neuronal network through DLF. We have demonstrated that after chronic local lesion of the dorsolateral column it was impossible to induce the locomotor activity in the cat by epidural stimulation of the spinal cord (Gerasimenko et al., 2002).Recently, neurotechnology that targets specific motor pools for restoration of walking in humans with spinal cord injury (SCI) was demonstrated. The authors delivered spatiotemporal epidural stimulation to specific flexor/extensor motor pools during specific phases of the locomotor cycle. Using this targeted neurotechnology, paralyzed chronic motor incomplete individuals were able to walk over-ground with balance assist (Wagner et al., 2018). The technology we describe here is able to target these motor pools similarly to restore walking without the need of surgical implantation.

Here we demonstrated that non-invasive preferential activation of spinal structures at specific segments is possible. According to the results presented on the **Figure 1B**, it is clear that lateral stimulation at T11 engaged the neural circuits controlling flexion, whereas lateral stimulation at L1 primarily recruited the circuits controlling extension during stepping. Spatiotemporal T11+L1 stimulation enhanced generation of motor patterns and enabled control of leg movements. We suggest that this non-invasive technology could be effective for neuromuscular control of postural and locomotor function in post-stroke subjects and in individuals with SCI.

AUTHOR CONTRIBUTIONS

The concept and design of this study were developed by YG. TM, AG, IB, RG, RS, and AO were involved in data acquisition, analysis, and interpretation. The manuscript draft written by YG and TM was critically revised and approved by all authors.

FUNDING

This research was funded in part by National Institutes of Health Grant 1R01 NS102920-01A1. The study was supported by National Technology Initiative Foundation (project #400-230).

REFERENCES

Angeli, C. A., Boakye, M., Morton, R. A., Vogt, J., Benton, K., Chen, Y., et al. (2018). Recovery of over-ground walking after chronic motor complete spinal cord injury. *N. Engl. J. Med.* 379, 1244–1250. doi: 10.1056/NEJMoa1803588

Angeli, C. A., Edgerton, V. R., Gerasimenko, Y. P., and Harkema, S. J. (2014). Altering spinal cord excitability enables voluntary movements after chronic complete paralysis in humans. *Brain* 137, 1394–1409. doi: 10.1093/brain/awu038

Cowley, K. C., Zaporozhets, E., Joundi, R. A., and Schmidt, B. J. (2009). Contribution of commissural projections to bulbospinal activation of locomotion in the *in vitro* neonatal rat spinal cord. *J. Neurophysiol.* 101, 1171–1178. doi: 10.1152/jn.91212.2008

Finkel, E., Etlin, A., Cherniak, M., Mor, Y., Lev-Tov, A., and Anglister, L. (2014). Neuroanatomical basis for cholinergic modulation of locomotor networks by sacral relay neurons with ascending lumbar projections. *J. Comp. Neurol.* 522, 3437–3455. doi: 10.1002/cne.23613

Gabbay, H., and Lev-Tov, A. (2004). Alpha-1 adrenoceptor agonists generate a "fast" NMDA receptor-independent motor rhythm in the neonatal rat spinal cord. *J. Neurophysiol.* 92, 997–1010. doi: 10.1152/jn.00205.2004

Gerasimenko, Y., Gorodnichev, R., Moshonkina, T., Sayenko, D., Gad, P., and Reggie Edgerton, V. (2015a). Transcutaneous electrical spinal-cord stimulation in humans. *Ann. Phys. Rehabil. Med.* 58, 225–231. doi: 10.1016/j.rehab.2015.05.003

Gerasimenko, Y., Gorodnichev, R., Puhov, A., Moshonkina, T., Savochin, A., Selionov, V., et al. (2015b). Initiation and modulation of locomotor circuitry output with multisite transcutaneous electrical stimulation of the spinal cord in noninjured humans. *J. Neurophysiol.* 113, 834–842. doi: 10.1152/jn.00609.2014

Gerasimenko, Y., Preston, C., Zhong, H., Roy, R. R., Edgerton, V. R., and Shah, P. K. (2019). Rostral lumbar segments are the key controllers of hindlimb locomotor rhythmicity in the adult spinal rat. *J. Neurophysiol.* 122, 585–600. doi: 10.1152/jn.00810.2018

Gerasimenko, Y., Roy, R. R., and Edgerton, V. R. (2008). Epidural stimulation: comparison of the spinal circuits that generate and control locomotion in rats, cats and humans. *Exp.Neurol.* 209, 417–425. doi: 10.1016/j.expneurol.2007.07.015

Gerasimenko, Y. P., Lu, D. C., Modaber, M., Zdunowski, S., Gad, P., Sayenko, D. G., et al. (2015) Noninvasive reactivation of motor descending control after paralysis. *J. Neurotrauma* 32, 1968–1980. doi: 10.1089/neu.2015.4008

Gerasimenko, Y. P., Makarovskii, A. N., and Nikitin, O. A. (2002). Control of locomotor activity in humans and animals in the absence of supraspinal influences. *Neurosci. Behav. Physiol.* 32, 417–423. doi: 10.1023/A:1015836428932

Gill, M. L., Grahn, P. J., Calvert, J. S., Linde, M. B., Lavrov, I. A., Strommen, J. A., et al. (2018). Neuromodulation of lumbosacral spinal networks enables independent stepping after complete paraplegia. *Nat. Med.* 24, 1677–1682. doi: 10.1038/s41591-018-0175-7

Grishin, A. A., Bobrova, E. V., Reshetnikova, V. V., et al. (2020). Sistema detektirovaniya faz shagatel'nogo tsikla i stimulyatsii spinnogo mozga kak instrument upravleniya lokomotsiyey cheloveka [A system for detecting the phases of the stepping cycle and stimulating the spinal cord as a tool for controlling human locomotion]. *Med. Tekh.* 323, 10–14.

Harkema, S., Gerasimenko, Y., Hodes, J., Burdick, J., Angeli, C., Chen, Y., et al. (2011). Effect of epidural stimulation of the lumbosacral spinal cord on voluntary movement, standing, and assisted stepping after motor complete paraplegia: a case study. *Lancet* 377, 1938–1947. doi: 10.1016/S0140-6736(11)60547-3

Ivanenko, Y. P., Poppele, R. E., and Lacquaniti, F. (2006). Spinal cord maps of spatiotemporal alpha-motoneuron activation in humans walking at different speeds. *J. Neurophysiol.* 95, 602–618. doi: 10.1152/jn.00767.2005

Kazennikov, O. V., Shik, M. L., and Iakovleva, G. V. (1983). Stepping movements caused by stimulation of the cat spinal cord dorsolateral funiculus. *Biull. Eksp. Biol. Med.* 96, 8–10. doi: 10.1007/BF00839814

Lev-Tov, A., Delvolvé, I., and Kremer, E. (2000). Sacrocaudal afferents induce rhythmic efferent bursting in isolated spinal cords of neonatal rats. *J. Neurophysiol.* 83, 888–894. doi: 10.1152/jn.2000.83.2.888

Sayenko, D. G., Rath, M., Ferguson, A. R., Burdick, J. W., Havton, L. A., Edgerton, V. R., et al. (2018). Self-assisted standing enabled by non-invasive spinal stimulation after spinal cord injury. *J. Neurotrauma* 36, 1435–1450. doi: 10.1089/neu.2018.5956

Shik, M. (1997). Recognizing propriospinal and reticulospinal systems of initiation of stepping. *Motor Control.* 1, 310–313. doi: 10.1123/mcj.1.4.310

Stewart, J. D. (1992). Electrophysiological mapping of the segmental anatomy of the muscles of the lower extremity. *Muscle Nerve* 15, 965–966.

Wagner, F. B., Mignardot, J. B., Le Goff-Mignardot, C. G., Demesmaeker, R., Komi, S., et al. (2018). Targeted neurotechnology restores walking in humans with spinal cord injury. *Nature* 563, 65–71. doi: 10.1038/s41586-018-0649-2

Conflict of Interest: YG researcher on the study team, hold shareholder interest in NeuroRecovery Technologies and Cosyma. He holds certain inventorship rights on intellectual property licensed by the regents of the University of California to NeuroRecovery Technologies and its subsidiaries. VE holds shareholder interest and certain inventor rights in NeuroRecovery Technologies and SpineX and holds certain inventorship rights on intellectual property licensed by The Regents of the University of California to NeuroRecovery Technologies and its subsidiaries.

The remaining authors declare that the research was conducted in the absence of any commercial or financial relationships that could be construed as a potential conflict of interest.

frontiers in Human Neuroscience

ORIGINAL RESEARCH
published: 04 February 2021
doi: 10.3389/fnhum.2020.622637

Neural Correlates of Knee Extension and Flexion Force Control: A Kinetically-Instrumented Neuroimaging Study

Dustin R. Grooms[1,2,3]*, *Cody R. Criss*[1,4], *Janet E. Simon*[1,2], *Adam L. Haggerty*[1,2] *and Timothy R. Wohl*[5,6]

[1]Ohio Musculoskeletal and Neurological Institute, Ohio University, Grover Center, Athens, OH, United States, [2]Division of Athletic Training, School of Applied Health Sciences and Wellness, College of Health Sciences and Professions, Ohio University, Grover Center, Athens, OH, United States, [3]Division of Physical Therapy, School of Rehabilitation and Communication Sciences, College of Health Sciences and Professions, Ohio University, Grover Center, Athens, OH, United States, [4]Translational Biomedical Sciences Program, Heritage College of Osteopathic Medicine, Ohio University, Athens, OH, United States, [5]Honors Tutorial College, Ohio University, Athens, OH, United States, [6]Division of Physical Therapy, School of Health and Rehabilitation Sciences, Ohio State University, Columbus, OH, United States

OPEN ACCESS

Edited by:
Taiar Redha,
Université de Reims Champagne-Ardenne, France

Reviewed by:
Roxana G. Burciu,
University of Delaware, United States
Nejc Sarabon,
University of Primorska, Slovenia

***Correspondence:**
Dustin R. Grooms
groomsd@ohio.edu

Specialty section:
This article was submitted to Motor Neuroscience, a section of the journal Frontiers in Human Neuroscience

Received: 28 October 2020
Accepted: 23 December 2020
Published: 04 February 2021

Citation:
Grooms DR, Criss CR, Simon JE, Haggerty AL and Wohl TR (2021) Neural Correlates of Knee Extension and Flexion Force Control: A Kinetically-Instrumented Neuroimaging Study. Front. Hum. Neurosci. 14:622637. doi: 10.3389/fnhum.2020.622637

Background: The regulation of muscle force is a vital aspect of sensorimotor control, requiring intricate neural processes. While neural activity associated with upper extremity force control has been documented, extrapolation to lower extremity force control is limited. Knowledge of how the brain regulates force control for knee extension and flexion may provide insights as to how pathology or intervention impacts central control of movement.

Objectives: To develop and implement a neuroimaging-compatible force control paradigm for knee extension and flexion.

Methods: A magnetic resonance imaging (MRI) safe load cell was used in a customized apparatus to quantify force (N) during neuroimaging (Philips Achieva 3T). Visual biofeedback and a target sinusoidal wave that fluctuated between 0 and 5 N was provided *via* an MRI-safe virtual reality display. Fifteen right leg dominant female participants (age = 20.3 ± 1.2 years, height = 1.6 ± 0.10 m, weight = 64.8 ± 6.4 kg) completed a knee extension and flexion force matching paradigm during neuroimaging. The force-matching error was calculated based on the difference between the visual target and actual performance. Brain activation patterns were calculated and associated with force-matching error and the difference between quadriceps and hamstring force-matching tasks were evaluated with a mixed-effects model ($z > 3.1$, $p < 0.05$, cluster corrected).

Results: Knee extension and flexion force-matching tasks increased BOLD signal among cerebellar, sensorimotor, and visual-processing regions. Increased knee extension force-matching error was associated with greater right frontal cortex and left parietal cortex activity and reduced left lingual gyrus activity. Increased knee flexion force-matching error was associated with reduced left frontal and right parietal region activity. Knee flexion

force control increased bilateral premotor, secondary somatosensory, and right anterior temporal activity relative to knee extension. The force-matching error was not statistically different between tasks.

Conclusion: Lower extremity force control results in unique activation strategies depending on if engaging knee extension or flexion, with knee flexion requiring increased neural activity (BOLD signal) for the same level of force and no difference in relative error. These fMRI compatible force control paradigms allow precise behavioral quantification of motor performance concurrent with brain activity for lower extremity sensorimotor function and may serve as a method for future research to investigate how pathologies affect lower extremity neuromuscular function.

Keywords: force sense, functional magnetic resonance imaging, quadriceps, hamstring, lower extremity, sensorimotor control

INTRODUCTION

Determining how the central nervous system regulates force is vital for understanding the neural control of biomechanical action. The integration of neuroimaging techniques with simultaneous biomechanical recording has allowed for concurrent capture of joint position and force with neural activity (Liu et al., 2000; Ward et al., 2008; Naufel et al., 2019). However, the majority of investigations have focused on the upper extremity and the primary motor cortex to elucidate the relationship between muscle force and neural activity (Georgopoulos et al., 1992; Ashe, 1997; Ward et al., 2008). Studies examining neural activity associated with lower extremity motor control have not quantified motor performance beyond movement timing (Luft et al., 2002; Kapreli et al., 2007; Grooms et al., 2019) or have been limited to electroencephalography paradigms, which provide excellent temporal resolution but lack the spatial resolution of functional magnetic resonance imaging (fMRI; Poortvliet et al., 2015). Prior work specific to fMRI has examined neural correlates of quadriceps force regulation in patients with knee osteoarthritis (Shanahan et al., 2015) using an isometric, force-matching paradigm, finding an anterior shift of the knee representation within the primary motor cortex in those with knee osteoarthritis. Various research groups have also employed cycle ergometers (Mehta et al., 2009), gait simulations (Jaeger et al., 2016), or leg press (Grooms et al., 2019) movement paradigms to quantify lower extremity movement with brain imaging. While these paradigms demonstrated success to activate the sensorimotor network and do so reliably, many fMRI lower extremity paradigms are metronome-paced and do not attempt to quantify motor performance (Luft et al., 2002; Kapreli et al., 2006). Therefore, the development of lower extremity paradigms that can concurrently measure neural activity *via* fMRI and biomechanical performance may offer more precise methods to investigate central strategies for force regulation, with implications for pathologies affecting sensorimotor control of the lower extremity (Hortobágyi et al., 2004; Ward et al., 2019).

Prior biomechanically isolated work has demonstrated force control deficits in a variety of orthopedic and neurological pathologies of the lower extremity (Hortobágyi et al., 2004; Docherty and Arnold, 2008; Telianidis et al., 2014) but a clear brain-behavioral interaction has yet to be established (Baumeister et al., 2011). Further, no study to our knowledge has attempted to contrast how the brain regulates force when engaged in knee extension (quadriceps-dominant activity) relative to knee flexion (hamstring-dominant activity). Unique deficits in quadriceps and hamstring function have been reported in a variety of orthopedic and neurological conditions, and the restoration of respective muscle and joint function is vital for the recovery and resumption of activities of daily living, adequate mobility, and mitigating the development of chronic conditions such as osteoarthritis (Manini et al., 2007; Manini and Clark, 2012; Tourville et al., 2014; Arhos et al., 2020). As lower extremity pathologies have been found to manipulate both quadriceps and hamstring muscle activity, timing, and function, determining the neural mechanisms for each is vital to better understand how lower extremity motor control is centrally governed (Telianidis et al., 2014; Abourezk et al., 2017; Blackburn et al., 2017; Hohmann et al., 2019). Isolating neural correlates of quadriceps and hamstring force generation and control may highlight central mechanisms for function following injury and permit the development of novel therapies that restore function. Therefore, our purpose was to: (1) develop and test a lower extremity neuroimaging paradigm for knee extension and flexion force control to better understand how the nervous system regulates lower extremity forces; and (2) determine differences between knee extension and flexion neural activity during a force control task.

MATERIALS AND METHODS

Participants

This study was approved by Ohio University's Institutional Review Board and all participants signed the informed consent document. We included female recreational athletes (at least 3 h of moderate to vigorous exercise per week, including 1 h of running, cutting, pivoting, or decelerating every week) aged 18–30 years. This population was selected for the following investigative work as they are at unique increased risk for noncontact knee injuries, whereby during athletics, exercise,

or activities of daily living that require rapid movement, sensorimotor control of the knee is compromised, resulting in positions that put excessive strain on the joint ligaments (Beynnon et al., 2014; Montalvo et al., 2019).

A sample size estimate was calculated based on effects reported by Shanahan et al. (2015) for the correlation to force-error, and Trinastic et al. (2010) for the contrast between movement conditions. For the force-error correlate analysis, an $r = 0.83$ was reported for the relationship between error and motor cortex peak activation location (Shanahan et al., 2015). A sample size estimate was calculated based on $r = 0.83$, $\alpha = 0.05$, and $1 - \beta = 0.8$ indicating a total sample size of 8 is required. For the motor condition analysis, the effect size between ankle plantarflexion and dorsiflexion was calculated as $d = 1.42$ (Trinastic et al., 2010). A sample size estimate was calculated based on $d = 1.42$, $\alpha = 0.05$, and $1 - \beta = 0.8$ resulting in needing a sample size of 7. Additionally, we modeled our study on previous literature of Newton et al. (2008) and Mehta et al. (2009) regarding paradigm development who enrolled 9 and 10 participants, respectively. Therefore, enrolling 15 participants provided adequate power for the proposed study. We enrolled 15 participants (15 F; age = 20.3 ± 1.2 years, height = 1.6 ± 0.10 m, and weight = 64.8 ± 6.4 kg) in this study. All participants were right leg dominant and met the exercise requirement criteria, as determined by the Marx Activity Rating Scale (**Table 1**; Marx et al., 2001).

We excluded participants who were contraindicated for fMRI (e.g., pregnancy, implanted metal devices, claustrophobia, and any other criteria as determined by the MRI operator), have a visual impairment, have a history of seizures or epilepsy, or have a history of surgery on the back, hip, leg, knee, etc. Other screening criteria included: primary sport, leg dominance, previous leg injury, medical history anxiety disorder, ADHD, depression, diabetic neuropathy, concussion or traumatic brain injury, cerebral palsy, balance disorder, vertigo, Parkinson's disease, multiple sclerosis, substance abuse or dependence, heart disease/defect, and prescription medication use within the 24 h before data collection. No individuals reported any of the previous medical conditions or consumed any medications impacting the data collection.

fMRI Data Collection

Data collection was completed in a single neuroimaging session (∼45 min including set-up, instruction, and scan time). During imaging, all participants wore standardized shorts and socks without shoes to reduce the possibility of altered skin tactile feedback. Participants also wore a splint to lock their right (dominant leg) ankle at neutral (∼90°) to minimize ankle movement throughout the scan. Headphone and hearing protection was provided for subject comfort and safety and to facilitate communication during scanning. While lying supine in the fMRI scanner, participants were strapped down to the table with four straps, one across the thighs at the mid-point between the greater trochanter and knee joint line, one across the hips at the anterior superior iliac spines, and two across the chest, from each shoulder to the pelvis at the iliac crest. The knee was fixed near terminal extension between 10° and 15° of flexion. Participants were also fitted with customized padding to reduce head motion. This padding was high-density MRI-safe foam that was inserted around the sides and top of the head to remove space between the skull and head coil. This was customized based on skull size, with those with larger skulls requiring less padding and smaller skulls requiring more padding.

TABLE 1 | Demographics and force error.

Data	Mean ± SD
Age (years)	20.3 ± 1.2
Height (m)	1.6 ± 0.10
Weight (kg)	64.8 ± 6.4
Activity level (Marx)	9.93 ± 5.50
Run	3.00 ± 0.85
Cut	2.07 ± 1.62
Decelerate	2.40 ± 1.64
Pivot	2.27 ± 1.49
Knee extension error (*N*)	1.068 ± 0.327
Knee flexion error (*N*)	0.999 ± 0.189

fMRI scans were collected with a 16-channel head coil. Before the functional data collection, a three-dimensional high-resolution T1-weighted image (repetition time (TR): 2,000 ms, echo time (TE): 4.58 ms, field of view: 256 × 256 mm; matrix: 256 × 256; slice thickness 1 mm, 176 slices, 8° flip-angle) was collected for image registration (∼8 min). fMRI collection parameters include 10 whole-brain gradient-echo-echo planar scans per block (four force-matching blocks, five rest blocks) acquired with a 3 s TR with anterior-posterior phase encoding and a 3.75 × 3.75 in-plane resolution, 5 mm slice thickness for 38 axial slices with a 35 ms TE, 90° flip angle, the field of view 240 mm and 64 × 64 matrix. Each functional force-matching run lasted 4 min and 30 s. fMRI measured regional brain activity during rest and motor control conditions, which were contrasted to isolate the regional brain activity to the isometric knee extension and flexion force-matching tasks.

The isometric force-matching motor task required the participant to either "kick up" or "press down" against a load cell (Biopac Systems Inc., TSD121B-MRI, 1,000 Hz sampling frequency) at the ankle (**Figure 1C**). Both knees rested upon a foam roller, while only the dominant, right leg was additionally strapped to a device against the load cell. Participants had to match their force output (visualized with biofeedback provided by MRI-safe virtual reality) with a sine wave that oscillated (1.2 Hz) from 0 to 5 N for 30 s with 30 s of rest for four total cycles, resulting in four force-matching blocks interspersed with five rest blocks of 30 s each (with the paradigm starting and ending with rest) for a total run time of 4 min and 30 s (**Figures 1A,B**). Standardized auditory cues informed participants when to begin and end force-matching. The force-matching error was calculated based on the difference between the visual target (sine wave) and actual performance (biofeedback). The force level for this study was low and we recruited a young active cohort to minimize the potential influence of fatigue; however, fatigue was monitored regularly and breaks were offered. No participants indicated fatigue or needed a break beyond the few minutes between scans.

Participants practiced the force-matching task for a full run with immediate examiner feedback if instructions were not

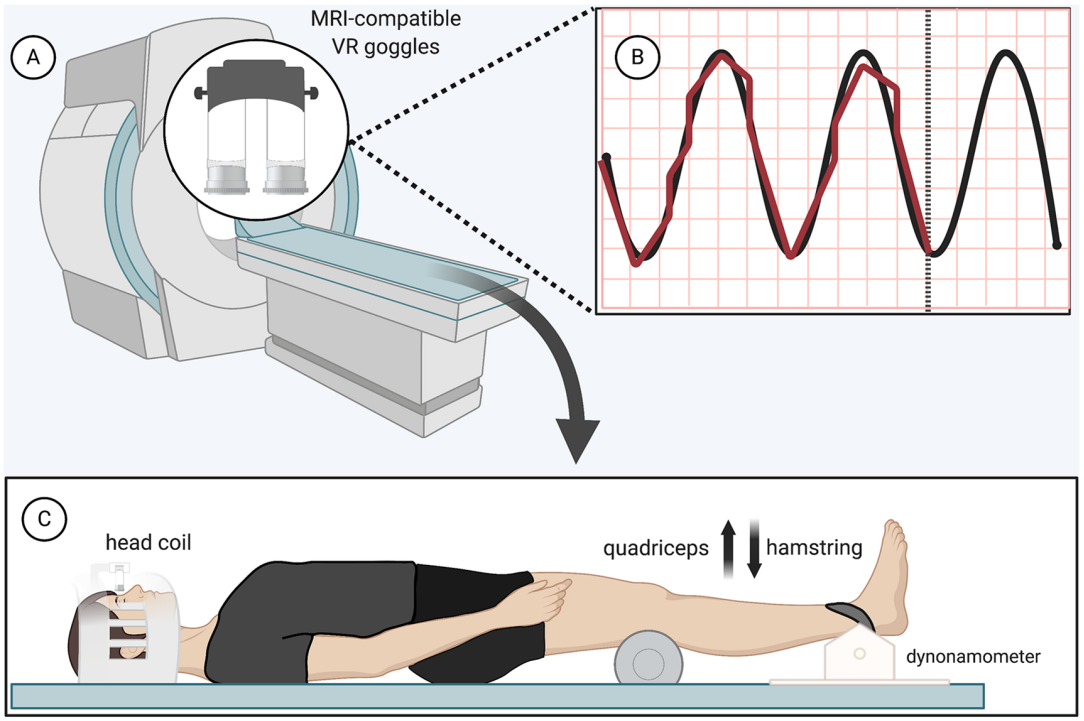

FIGURE 1 | Functional magnetic resonance imaging (fMRI) force-matching task—**(A)** magnetic resonance imaging (MRI)-compatible virtual reality display **(B)** black, Sinewave graph (0–5 N, 1.2 Hz); red, real-time display of participant force **(C)** load cell apparatus and patient position (participant restraints not pictured). Created with Biorender.

understood before completing the task during scanning. Also before data collection at the MRI, participants completed a mock MRI session where they familiarized themselves with the MRI environment, restraints to reduce head motion, and the lower extremity motor task. The participants were permitted to ask questions and practice the tasks with feedback from the experimenter. The practice session included three practice blocks (30 s each) of each force-matching task with examiner cueing to ensure the participant understood the task, followed by a complete run of each task with the same feedback and timing as during the actual MRI data collection session.

Error Calculation and Statistical Analysis

The force-matching error was recorded continuously throughout the force-matching tasks. For statistical analysis, error across the 30-s blocks was partitioned into 3-s intervals (the time interval for one sine wave). The first 3-s interval of each 30-s block was removed from the data analysis, as participants commonly required a few seconds to become acclimated to the task during the initiation of the movement block and thus, was shown to bias the overall average of the remaining nine intervals. The average error for each block was determined by the root mean square of the differential from target force to actual force on the remaining nine sets of 3-s intervals within each block, and the average error across the four blocks was computed for each participant for statistical analyses. Average knee extension and flexion force-matching error were compared with a paired samples *t*-test with an alpha set at 0.05.

fMRI Data and Statistical Analysis

The fMRI technique used in this study quantified the blood-oxygen-level-dependent (BOLD) signal *via* the hemodynamic response by contrasting the respective force-matching condition with interspersed rest conditions (Friston et al., 1995). We controlled for the additional sensory feedback of the strap across the shank by ensuring it was tightly pressed during both the rest and force-matching conditions, but the pressure of this tactile stimulus unavoidably changes with contraction and may thus contribute to the overall BOLD response. The BOLD response, quantified *via* fMRI collection and analysis, has been validated against direct neural recordings, demonstrating a very high correlation between blood flow and neural activity (Logothetis et al., 2001; Goense and Logothetis, 2008). The reliability of fMRI quantification of the BOLD signal is generally high and specific to knee movement and has high inter-session reliability (Newton et al., 2008; McGregor et al., 2012).

The fMRI statistical analyses were performed using the Oxford Centre for Functional MRI of the Brain Software Library (Smith et al., 2004; Jenkinson et al., 2012). Image analysis began with standard pre-statistic processing applied to individual data in the standardized FSL recommended order (Jenkinson et al., 2012), which included nonbrain removal, slice timing correction, standard motion correction, and realignment

parameters (three rotations and three translations) as covariates to limit confounding effects of head movement and spatial smoothing at 6 mm before statistical analysis (Jenkinson et al., 2002). One participant was removed from the knee extension force-matching analysis due to excessive head motion (>0.5 mm) and two removed from the knee flexion force-matching analysis, resulting in $n = 14$ for knee extension, $n = 13$ for knee flexion, and $n = 13$ for comparison between knee extension and knee flexion. High-pass temporal filtering at 90 Hz and time-series statistical analyses were carried out using a linear model with local autocorrelation correction. Functional images were co-registered with the respective high-resolution T1 image and the standard Montreal Neurological Institute template 152 using linear image registration. This registration process allowed data from each participant to be spatially aligned on a standardized brain template for comparison.

The subject-level analysis of knee sensorimotor control relative to rest was completed using a z score greater than 3.1 and a (corrected) cluster significance threshold of $\alpha < 0.05$. The cluster correction for multiple comparisons uses a variant of the Gaussian random field theory to decrease type I error in the statistical parametric mapping of imaging data by evaluating the activation not only at each voxel but also at the surrounding voxel cluster (as it is unlikely that the voxel tested and surrounding voxels are active above the threshold due to chance; Poldrack et al., 2011). The paired contrast between each individual's quadriceps vs. hamstring force control neural activity was performed with group z statistic images set at a threshold of z scores of greater than 3.1 and a corrected cluster significance level of $\alpha < 0.05$. As this was a brain activity correlate identification study, the effect size (r-value) of the relationship between brain activity and behavior are not reported to avoid circularity (voxel selection and magnitude estimation on the same data) and a follow-up validation study is required to estimate effect size with the identified regions from this work (Kriegeskorte et al., 2009, 2010).

RESULTS

Regional brain activation is reported as contralateral [indicating activation on the opposite side of the task, or the left hemisphere, as the task was always completed with the right (dominant) lower extremity] or ipsilateral (being the same side as the task, or the right hemisphere; **Tables 2–4**). Regions of brain activity are reported that were identified in FSLeyes based on peak-voxel with the Harvard-Oxford Cortical and Subcortical Structural Atlas (Desikan et al., 2006), Juelich Histological Atlas (Eickhoff et al., 2006, 2007) and the Cerebellar Atlas in MNI152 space after normalization with FNIRT (Diedrichsen et al., 2009) and with FSL tool atlasquery (Jenkinson et al., 2012). The atlasquery function from FSL utilizes the averaged probability across all voxels in the cluster to identify probabilistic anatomy across the cluster ensuring reporting of peak voxel location and overall cluster spatial representation.

Both knee extension and flexion force-matching tasks elicited increased bilateral BOLD signal among cerebellar, sensorimotor, and visual-processing regions (**Figures 2**, **4**). Increased knee extension force-matching error was associated with increased BOLD signal within the ipsilateral frontal cortex and contralateral parietal cortex and decreased contralateral BOLD signal within the lingual gyrus and intracalcarine cortex (**Figure 3**). Increased knee flexion force-matching error was related to decreased contralateral frontal and ipsilateral parietal region activity (**Figure 5**). Knee flexion force control had increased bilateral premotor, secondary somatosensory, and right anterior temporal activity relative to knee extension force control (**Figure 6**). Force-matching error performance was not statistically different between the knee extension and flexion tasks (**Table 1**). Head motion during the knee extension task was: 0.28 ± 0.17 mm absolute motion and 0.11 ± 0.10 mm relative motion. Head motion during the knee flexion task was: 0.22 ± 0.13 mm absolute motion and 0.10 ± 0.09 mm relative motion.

DISCUSSION

Lower extremity force control results in unique neural activation strategies depending on if engaging the quadriceps for knee extension or the hamstrings for knee flexion, with knee flexion requiring more sensorimotor neural activity for the same level of force generation and relative error. This paradigm allows precise behavioral quantification of motor performance concurrent with brain activity for lower extremity sensorimotor function, which may serve as a method for future research to investigate how pathologies or interventions affect lower extremity neuromuscular function.

Neural Correlates of Knee Extension Force Control

Knee extension force-matching had a neural activation pattern similar to prior reports of lower extremity knee-focused and quadriceps-dominant movements, with activation across the cortical and subcortical sensorimotor network (Luft et al., 2002; Kapreli et al., 2007). Quadriceps force error was associated with increased activity in frontal and parietal regions and associated with decreased crossmodal (Calvert, 2001) region activity (intracalcarine cortex and lingual gyrus) along the border of the occipital and parietal cortex.

Increased activation of frontal regions with increased error could indicate force control is more complex for those with a higher force-matching error, as previous research has identified an association between increased frontal activity with increased task complexity error (Schubotz and von Cramon, 2002; Mehta et al., 2012; Dunst et al., 2014). It is also possible that as a participant began to perform poorly and visualize their error, they engaged in more extensive or rapid recalibration to attempt to remain on target, requiring greater levels of attentive neural processing (Tracy, 2007; Tracy et al., 2007; Baweja et al., 2009). However, despite increased neural activity among attention and executive function-related brain regions, the relative error was higher which could also be simply a byproduct of more actively attending to their mismatched biofeedback and not secondary to employing a strategy to correct it (Tracy, 2007).

TABLE 2 | Regions of increased brain activity during the knee extension force-matching task.

Cluster index	Brain regions	Voxel count	*P*-value	Peak MNI voxel			*Z* stat-max
				x	*y*	*z*	
	Overall activation during knee extension force-matching						
6	B Precentral gyrus, Postcentral gyrus, Superior parietal lobule, Lateral occipital cortex	17,662	<0.00001	0	−34	56	10.1
5	B Precentral gyrus, Corticospinal tract, R Thalamus	1,567	<0.00001	10	−16	4	4.99
4	Corticospinal tract, L Thalamus	1,137	<0.00001	−8	−18	16	5.57
3	Precentral Gyrus, Inferior frontal gyrus, Premotor cortex	375	0.000116	−56	0	38	7.22
2	R Cerebellum VIIIA, VIIB, IX	284	0.000882	32	−50	−48	4.79
1	L Cerebellum VIIB, VIIIA, VIIIB, IX	182	0.0113	−20	−70	−44	6.26
	Neural activity increase associated with knee extension force error						
3	L Postcentral gyrus, Superior parietal lobule	206	0.00598	−20	−40	76	4.89
2	R Frontal pole	142	0.0344	30	52	20	5.02
1	R Middle frontal gyrus	130	0.0489	46	12	40	4.24
	Neural activity decrease associated with knee extension force error						
1	Intracalcarine cortex, Lingual gyrus	161	0.0201	−14	−82	10	4.68

Regions of brain activity are reported that were identified in FSLeyes with the Harvard-Oxford cortical and subcortical structural atlas, Julich histological atlas, and the Cerebellar atlas in MNI152 space after normalization with FNIRT by peak voxel and with FSL tool atlasquery. B, bilateral; L, left; R, right.

TABLE 3 | Regions of increased brain activity during the knee flexion force-matching task.

Cluster index	Brain regions	Voxel count	*P*-value	Peak MNI voxel			*Z* stat-max
				x	*y*	*z*	
	Overall activation during knee flexion force-matching						
3	B Postcentral gyrus, Precentral gyrus, Superior parietal lobule, Lateral occipital cortex, Supplementary motor cortex, Cingulate gyrus	16,647	<0.00001	−42	−78	−8	11.3
2	B Precentral gyrus, Supramarginal gyrus, Lateral occipital cortex, Lingual gyrus, Occipital fusiform gyrus, Cerebellum Right I-V, VIIB, VIIIA, Left VIIB, VIIIA	12,626	<0.00001	24	−70	−56	10.3
1	R Frontal pole, Frontal orbital cortex	189	0.008	26	34	−22	4.91
	Neural activity decrease associated with knee flexion force error						
2	R Precuneus, Postcentral gyrus, Posterior cingulate gyrus, Superior parietal lobule	257	0.00138	6	−40	50	5.91
1	L Frontal pole, Superior frontal gyrus, Middle frontal gyrus	215	0.00402	−36	30	40	5.25

Regions of brain activity are reported that were identified in FSLeyes with the Harvard-Oxford cortical and subcortical structural atlas, Julich histological atlas, and the cerebellar atlas in MNI152 space after normalization with FNIRT by peak voxel and with FSL tool atlasquery. There was no significant increased neural activity associated with knee flexion error. B, bilateral; L, left; R, right.

TABLE 4 | Regions of difference between knee extension and flexion force-matching.

Cluster index	Brain regions	Voxel count	*P*-value	Peak MNI voxel			*Z* stat-max
				x	*y*	*z*	
	Increased neural activity knee flexion > knee extension force control						
6	L Precentral and Postcentral gyrus	741	<0.00001	−62	−8	42	5.99
5	L Middle temporal gyrus, Angular gyrus, Inferior parietal lobule	259	0.00112	−62	−52	16	5.19
4	R Temporal pole	245	0.0016	44	22	−34	5.55
3	R Superior temporal gyrus, Supramarginal gyrus, Middle temporal gyrus	239	0.00187	48	−38	2	5.16
2	L Supplementary motor cortex, Paracingulate gyrus	194	0.00619	−6	10	48	4.44
1	B Corticospinal tract, L Thalamus	134	0.0354	−4	−10	−6	4.17

Regions of brain activity are reported that were identified in FSLeyes with the Harvard-Oxford cortical and subcortical structural atlas, Julich histological atlas, and the cerebellar atlas in MNI152 space after normalization with FNIRT by peak voxel and with FSL tool atlasquery. B, bilateral; L, left; R, right.

By contrast, those with less force-matching error had increased crossmodal visual-spatial and somatosensory region processing (or increased error had decreased relative activity), which may be involved in aligning and maintaining visual feedback with force regulation from peripheral afferent signals to minimize discrepancy. Previous work within the upper extremity has identified the lingual gyrus and intracalcarine regions to respond to congruent visual and somatosensory feedback (crossmodal; Driver and Spence, 1998; Macaluso et al., 2000). Further, extrastriate activity in the lingual gyrus and intracalcarine cortex has been implicated to be involved in body perception, and active during both visual and limb movements (Astafiev et al., 2004). Therefore, increased extrastriatal activity may correspond with a superior ability to align visual stimuli with proprioceptive afferent signals to minimize force-matching discrepancy. However, the increased

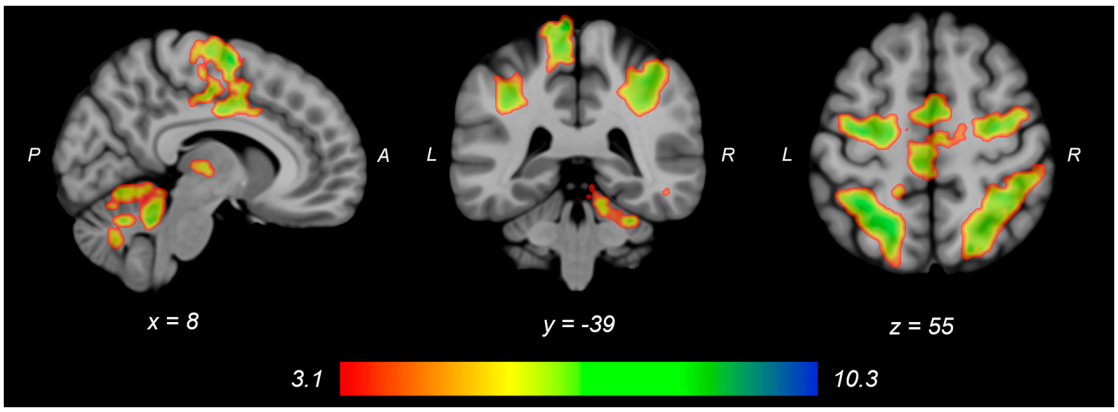

FIGURE 2 | Group average neural activity for knee extension force-matching from **Table 2**. P, posterior; A, anterior; L, left; R, right.

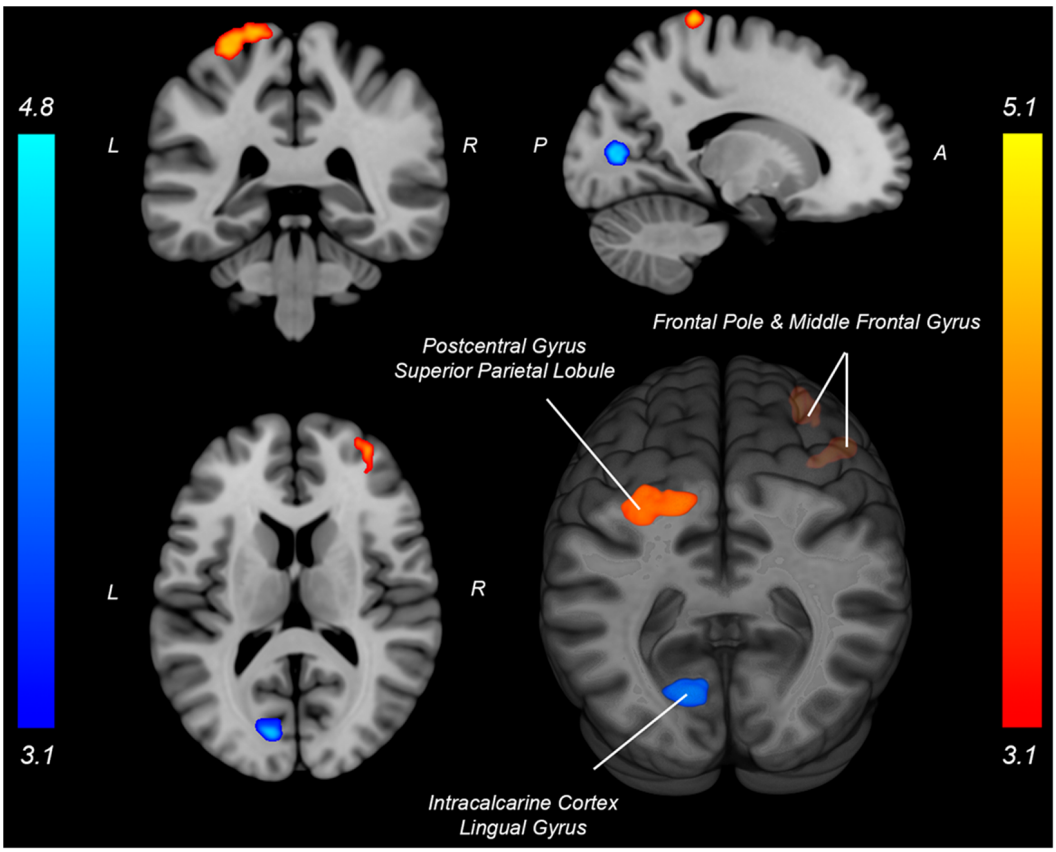

FIGURE 3 | Neural activity associated with knee extension force-matching error from **Table 2** (Red: brain activity positively associated with an error. Blue: brain activity negatively associated with an error). P, posterior; A, anterior; L, left; R, right.

extrastriatal activity could also be secondary to visualizing good performance *via* alignment of the target and participant force and not be the mechanism for reduced error. As intracalcarine cortex and lingual gyrus have greater levels of activity when such crossmodal stimuli are congruent compared to incongruent stimuli (e.g., spatial and temporal correspondence of visual presentation and tactile stimulation) and low error results in a visual stimulus that is congruent with proprioceptive sensed force generation and tactile cues (Driver and Spence, 1998; Macaluso et al., 2000).

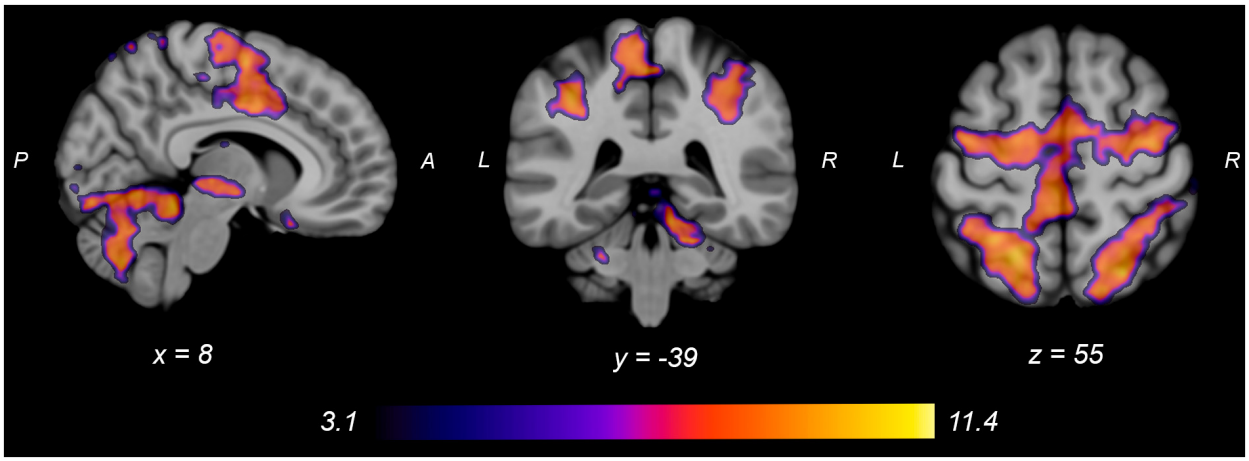

FIGURE 4 | Group average neural activity for knee flexion force-matching from **Table 3**. P, posterior; A, anterior; L, left; R, right.

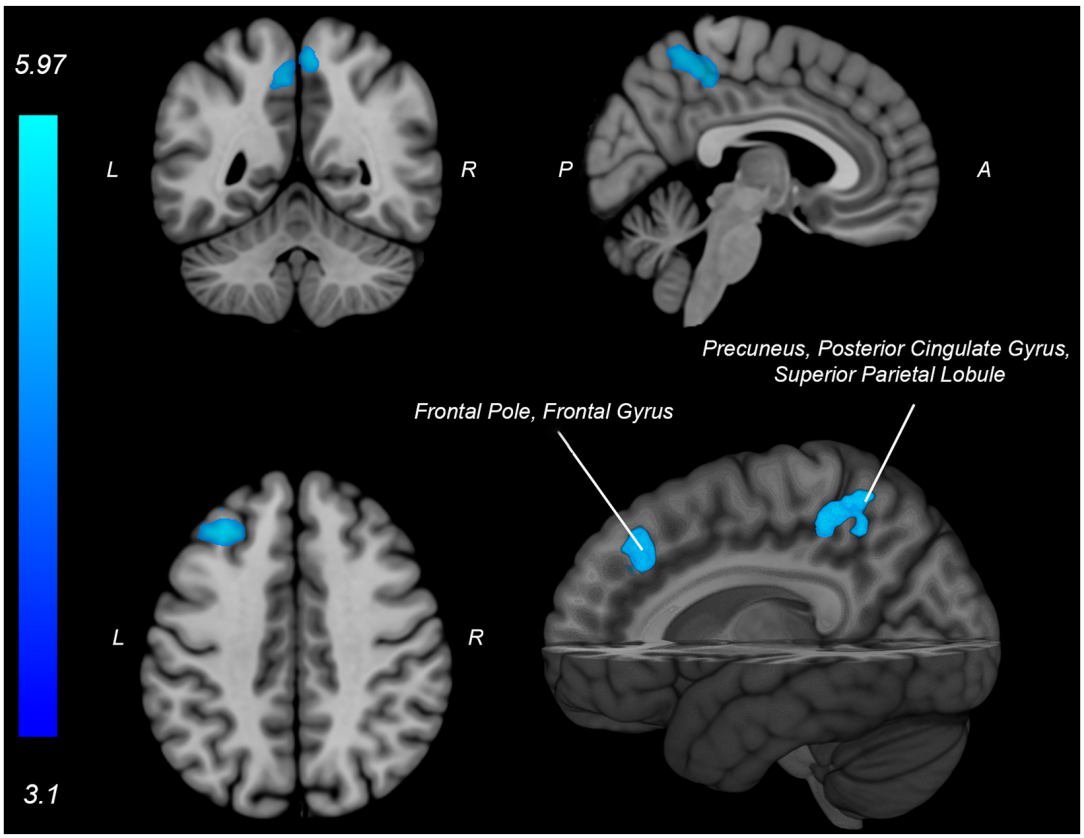

FIGURE 5 | Neural activity (blue) is negatively associated with knee flexion force-matching error from **Table 3**. P, posterior; A, anterior L, left; R, right.

Neural Correlates of Knee Flexion Force Control

The knee flexion force-matching task also had a neural activation pattern similar to prior lower extremity neuroimaging paradigms, with activation across the cortical and cerebellar sensorimotor network (Jaeger et al., 2014; Grooms et al., 2019). Knee flexion force error was associated with decreased activity in frontal and parietal regions, however, no increased neural activity was associated with knee flexion error. This contrasts with the knee extension force control error, which had increased

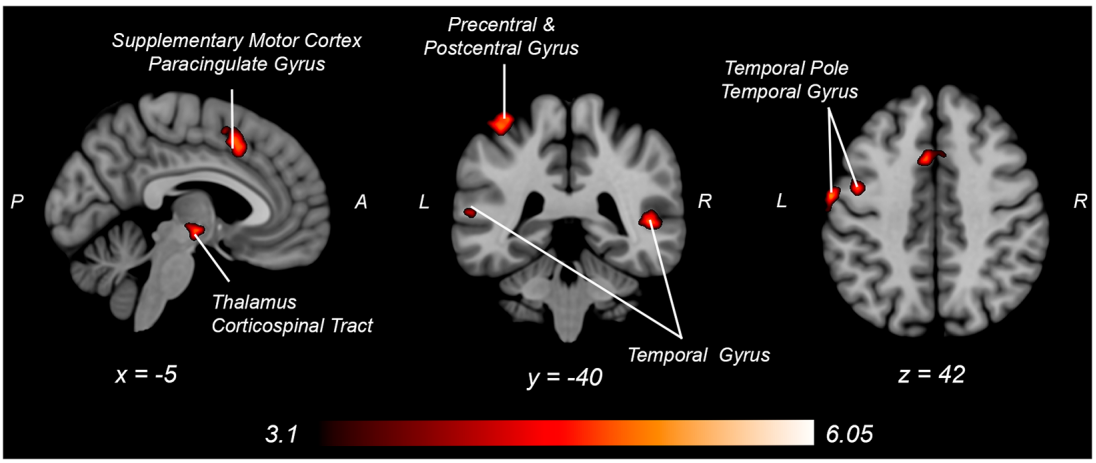

FIGURE 6 | Neural activity increases with knee flexion force matching relative to knee extension from **Table 4**. P, posterior; A, anterior L, left; R, right.

frontal and parietal lobe activity associated with increased force error.

This opposition may seem contradictory as one might expect more general alignment for the neural activity underlying force error between knee flexion and extension activities. However, the musculature enabling isolated knee flexion (primarily hamstring) vs. isolated knee extension (primarily quadriceps) have unique neural representation, peripheral nerve innervation, and spinal reflex structure (Jennings and Seedhom, 1994; Mrachacz-Kersting et al., 2006). Thus, the brain differences for error correction between knee extension and flexion may be secondary to mediation at the spinal level. The hamstrings are also typically weaker than the quadriceps (Wyatt and Edwards, 1981; Aagaard et al., 1995; Pincivero et al., 1997) and have a greater proprioceptive error (Relph and Herrington, 2016), potentially secondary to decreased relative cortical representation (Davies, 2020) and less muscle spindle innervation relative to the quadriceps (Banks, 2006).

Anecdotally, the participants in this study had a more difficult time learning how to perform the knee flexion task relative to the knee extension task as many needed more practice trials for the hamstring task than the quadriceps task to achieve reliable performance. The constrained action hypothesis posits that when you attend to a motor task, you constrain the automatic, implicit motor programs that would have otherwise facilitated the movement (Wulf et al., 2001; Kal et al., 2013; Vidal et al., 2018). However, if there is no automatic, implicit motor plan present to guide the movement, then attention to the motor task may improve performance. Therefore, the knee extension task may have been more "intuitive" (implicit) in this sample, contributing to decreased frontal cortex activity not constraining the automatic motor program and facilitating reduced extension error. Conversely, if the knee flexion task is anecdotally less implicit (lacking a well-established, implicit motor program), the association between increased frontal activity and improved performance for flexion may be attributable to the necessity of cognitive-attentive neural processes to drive the motor plan.

Neural Activity Differences Between Knee Extension and Flexion Force Control

Engaging in knee flexion force control required increased cortical and subcortical activation, including primary sensorimotor cortex, secondary motor cortex, temporal regions, parietal supramarginal gyrus, and corticospinal tract, whereas no brain regions had increased activity for relative knee extension force control. These findings may partially explain the apparent paradoxical similar activation pattern associated with increased knee extension force error, yet decreased knee flexion force error, as the knee flexion force-matching task required greater overall neural activity for similar force-matching performance. This could be secondary to the relatively greater demand on the hamstrings, as they are typically weaker than the quadriceps, requiring elevated neural activity to produce the same force level. Alternatively, the position of the knee may have influenced the result as a near-terminal extension may bias toward quadriceps shortened position and improved steadiness (Krishnan et al., 2011) compared to the hamstring position (lengthened). A likely neurophysiologic contributor is the relatively increased spinal reflexive innervation of the hamstring (Shahani and Young, 1971; Roy et al., 2014; Mackey et al., 2016) requiring increased cortical activity to overcome potential spinal inhibition. The increased knee flexor force-matching neural activity could also be secondary to the task being more atypical, as concentric precise force control of the hamstrings is not as common to be engaged during locomotion, where the quadriceps is primarily engaged in concentric positioning and the hamstrings act eccentrically to decelerate before heel strike. Thus, the nature of the concentric force matching task may result in increased activation for knee flexion that would not be the case with an eccentric force-matching task (Koohestani et al., 2020).

LIMITATIONS

This investigation was limited to a single joint position and an isometric contraction at a low force level, primarily to minimize head motion for fMRI. Possibly, synergist muscle groups that contribute to hip flexion or extension may reduce the ability to isolate the quadriceps for knee extension or the hamstring for knee flexion (though at the low force level required in this study, accessory muscle activity is unlikely), so future work may consider recording electromyography measures to ensure muscle group contributions. The force level was selected to ensure a sufficient fluctuation range to test force-sense but also keep head motion minimal. We used a low absolute value of 5 N, as opposed to a low relative force such as 5% of a maximal voluntary contraction. Prior works have employed both a ∼5 N absolute threshold (Newton et al., 2008) and similar relative thresholds (Shanahan et al., 2015). As our sample was homogeneous in terms of fitness, activity level, age, and BMI, there is a minimal indication the results would be different if scaled to a relative % for capability. Nonetheless, future work across varied samples may consider employing a relative metric for the force target. While we enrolled young and physically active females to better understand knee force control in this population at a unique high-risk for sensorimotor-related coordination errors that contribute to knee ligament injuries such as the anterior cruciate ligament, our participant selection criteria limit generalization to males or aging populations. Future investigations may consider heterogenous demographical recruitment of participants to increase generalizability or determine if changes in neural activity are present with various ages or pathological populations. Additionally, the use of a variety of joint angles and intensities may also highlight how limb position and magnitude plays a role in central mechanisms of force regulation.

CONCLUSION

This investigation employed a novel lower extremity force-matching neuroimaging-compatible paradigm to examine motor control of the knee extensors and flexors. The paradigm was found to activate the sensorimotor network with unique neural correlates to force-matching error across parietal and frontal regions. This paradigm may allow for future research to better understand the neural correlates of lower extremity neuromuscular control across varied pathologies or interventions. Specifically, this foundational work can support a future investigation into the unique contribution of the nervous system to lower extremity force regulation in pathologies that disrupt proprioception and sensorimotor function such as knee anterior cruciate ligament injury (Laboute et al., 2019), osteoarthritis (Shanahan, 2015), and patella-femoral pain (Te et al., 2017). As the evidence base for the role of the nervous system in these musculoskeletal conditions grows, the need for such paradigms that bridge neural activity and motor performance of the knee as described here are needed to provide pathology specific therapeutic targets (Silfies et al., 2017; Armijo-Olivo, 2018).

DATA AVAILABILITY STATEMENT

The raw data supporting the conclusions of this article will be made available by the authors, without undue reservation.

ETHICS STATEMENT

The studies involving human participants were reviewed and approved by Ohio University Institutional Review Board. The patients/participants provided their written informed consent to participate in this study.

AUTHOR CONTRIBUTIONS

DG, CC, and TW: conception. DG, CC, JS, and TW: experimental design and data analysis. DG, CC, AH, and TW: data collection. DG, CC, JS, AH, and TW: writing and review. All authors contributed to the article and approved the submitted version.

FUNDING

This study was supported by the US Department of Defense Congressionally Directed Medical Research Program Peer Reviewed Orthopaedic Research Program. Research Award (W81XWH-18-1-0707). Opinions, interpretations, conclusions, and recommendations are those of the author and are not necessarily endorsed by the Department of Defense.

REFERENCES

Aagaard, P., Simonsen, E. B., Trolle, M., Bangsbo, J., and Klausen, K. (1995). Isokinetic hamstring/quadriceps strength ratio: influence from joint angular velocity, gravity correction and contraction mode. *Acta Physiol. Scand.* 154, 421–427. doi: 10.1111/j.1748-1716.1995.tb09927.x

Abourezk, M. N., Ithurburn, M. P., McNally, M. P., Thoma, L. M., Briggs, M. S., Hewett, T. E., et al. (2017). Hamstring strength asymmetry at 3 years after anterior cruciate ligament reconstruction alters knee mechanics during gait and jogging. *Am. J. Sports Med.* 45, 97–105. doi: 10.1177/0363546516664705

Arhos, E. K., Thoma, L. M., Grindem, H., Logerstedt, D., Risberg, M. A., and Snyder-Mackler, L. (2020). Association of quadriceps strength symmetry and surgical status with clinical osteoarthritis 5 years after anterior cruciate ligament rupture. *Arthritis Care Res.* doi: 10.1002/acr.24479 [Epub ahead of print].

Armijo-Olivo, S. (2018). A new paradigm shift in musculoskeletal rehabilitation: why we should exercise the brain? *Braz. J. Phys. Ther.* 22, 95–96. doi: 10.1016/j.bjpt.2017.12.001

Ashe, J. (1997). Force and the motor cortex. *Behav. Brain Res.* 87, 255–269. doi: 10.1016/s0166-4328(97)00752-3

Astafiev, S. V., Stanley, C. M., Shulman, G. L., and Corbetta, M. (2004). Extrastriate body area in human occipital cortex responds to the performance of motor actions. *Nat. Neurosci.* 7, 542–548. doi: 10.1038/nn1241

Banks, R. W. (2006). An allometric analysis of the number of muscle spindles in mammalian skeletal muscles. *J. Anat.* 208, 753–768. doi: 10.1111/j.1469-7580.2006.00558.x

Baumeister, J., Reinecke, K., Schubert, M., and Weiss, M. (2011). Altered electrocortical brain activity after ACL reconstruction during force control. *J. Orthop. Res.* 29, 1383–1389. doi: 10.1002/jor.21380

Baweja, H. S., Patel, B. K., Martinkewiz, J. D., Vu, J., and Christou, E. A. (2009). Removal of visual feedback alters muscle activity and reduces force variability during constant isometric contractions. *Exp. Brain Res.* 197, 35–47. doi: 10.1007/s00221-009-1883-5

Beynnon, B. D., Vacek, P. M., Newell, M. K., Tourville, T. W., Smith, H. C., Shultz, S. J., et al. (2014). The effects of level of competition, sport, and sex on the incidence of first-time noncontact anterior cruciate ligament injury. *Am. J. Sports Med.* 42, 1806–1812. doi: 10.1177/0363546514540862

Blackburn, T., Pietrosimone, B., Goodwin, J., and Johnston, C. (2017). Quadriceps/Hamstrings co-activation during gait in individuals with anterior cruciate ligament reconstruction. *Osteoarthritis Cartilage* 25, S110–S111. doi: 10.1016/j.joca.2017.02.178

Calvert, G. A. (2001). Crossmodal processing in the human brain: insights from functional neuroimaging studies. *Cereb. Cortex* 11, 1110–1123. doi: 10.1093/cercor/11.12.1110

Davies, J. L. (2020). Using transcranial magnetic stimulation to map the cortical representation of lower-limb muscles. *Clin. Neurophysiol. Pract.* 5, 87–99. doi: 10.1016/j.cnp.2020.04.001

Desikan, R. S., Ségonne, F., Fischl, B., Quinn, B. T., Dickerson, B. C., Blacker, D., et al. (2006). An automated labeling system for subdividing the human cerebral cortex on MRI scans into gyral based regions of interest. *NeuroImage* 31, 968–980. doi: 10.1016/j.neuroimage.2006.01.021

Diedrichsen, J., Balsters, J. H., Flavell, J., Cussans, E., and Ramnani, N. (2009). A probabilistic MR atlas of the human cerebellum. *NeuroImage* 46, 39–46. doi: 10.1016/j.neuroimage.2009.01.045

Docherty, C. L., and Arnold, B. L. (2008). Force sense deficits in functionally unstable ankles. *J. Orthop. Res.* 26, 1489–1493. doi: 10.1002/jor.20682

Driver, J., and Spence, C. (1998). Attention and the crossmodal construction of space. *Trends Cogn. Sci.* 2, 254–262. doi: 10.1016/S1364-6613(98)01188-7

Dunst, B., Benedek, M., Jauk, E., Bergner, S., Koschutnig, K., Sommer, M., et al. (2014). Neural efficiency as a function of task demands. *Intelligence* 42, 22–30. doi: 10.1016/j.intell.2013.09.005

Eickhoff, S. B., Heim, S., Zilles, K., and Amunts, K. (2006). Testing anatomically specified hypotheses in functional imaging using cytoarchitectonic maps. *NeuroImage* 32, 570–582. doi: 10.1016/j.neuroimage.2006.04.204

Eickhoff, S. B., Paus, T., Caspers, S., Grosbras, M.-H., Evans, A. C., Zilles, K., et al. (2007). Assignment of functional activations to probabilistic cytoarchitectonic areas revisited. *NeuroImage* 36, 511–521. doi: 10.1016/j.neuroimage.2007.03.060

Friston, K. J., Frith, C. D., Turner, R., and Frackowiak, R. S. (1995). Characterizing evoked hemodynamics with fMRI. *NeuroImage* 2, 157–165. doi: 10.1006/nimg.1995.1018

Georgopoulos, A. P., Ashe, J., Smyrnis, N., and Taira, M. (1992). The motor cortex and the coding of force. *Science* 256, 1692–1695. doi: 10.1126/science.256.5064.1692

Goense, J. B. M., and Logothetis, N. K. (2008). Neurophysiology of the BOLD fMRI signal in awake monkeys. *Curr. Biol.* 18, 631–640. doi: 10.1016/j.cub.2008.03.054

Grooms, D. R., Diekfuss, J. A., Ellis, J. D., Yuan, W., Dudley, J., Foss, K. D. B., et al. (2019). A novel approach to evaluate brain activation for lower extremity motor control. *J. Neuroimaging* 29, 580–588. doi: 10.1111/jon.12645

Hohmann, E., Tetsworth, K., and Glatt, V. (2019). The hamstring/quadriceps ratio is an indicator of function in ACL-deficient, but not in ACL-reconstructed knees. *Arch. Orthop. Trauma Surg.* 139, 91–98. doi: 10.1007/s00402-018-3000-3

Hortobágyi, T., Garry, J., Holbert, D., and Devita, P. (2004). Aberrations in the control of quadriceps muscle force in patients with knee osteoarthritis. *Arthritis Rheum.* 51, 562–569. doi: 10.1002/art.20545

Jaeger, L., Marchal-Crespo, L., Wolf, P., Luft, A. R., Riener, R., Michels, L., et al. (2016). On the modulation of brain activation during simulated weight bearing in supine gait-like stepping. *Brain Topogr.* 29, 193–205. doi: 10.1007/s10548-015-0441-7

Jaeger, L., Marchal-Crespo, L., Wolf, P., Riener, R., Michels, L., and Kollias, S. (2014). Brain activation associated with active and passive lower limb stepping. *Front. Hum. Neurosci.* 8:828. doi: 10.3389/fnhum.2014.00828

Jenkinson, M., Bannister, P., Brady, M., and Smith, S. (2002). Improved optimization for the robust and accurate linear registration and motion correction of brain images. *NeuroImage* 17, 825–841. doi: 10.1016/s1053-8119(02)91132-8

Jenkinson, M., Beckmann, C. F., Behrens, T. E. J., Woolrich, M. W., and Smith, S. M. (2012). FSL. *NeuroImage* 62, 782–790. doi: 10.1016/j.neuroimage.2011.09.015

Jennings, A. G., and Seedhom, B. B. (1994). Proprioception in the knee and reflex hamstring contraction latency. *J. Bone Joint Surg. Br.* 76, 491–494. doi: 10.1302/0301-620x.76b3.8175863

Kal, E. C., van der Kamp, J., and Houdijk, H. (2013). External attentional focus enhances movement automatization: a comprehensive test of the constrained action hypothesis. *Hum. Mov. Sci.* 32, 527–539. doi: 10.1016/j.humov.2013.04.001

Kapreli, E., Athanasopoulos, S., Papathanasiou, M., Van Hecke, P., Kelekis, D., Peeters, R., et al. (2007). Lower limb sensorimotor network: issues of somatotopy and overlap. *Cortex* 43, 219–232. doi: 10.1016/s0010-9452(08)70477-5

Kapreli, E., Athanasopoulos, S., Papathanasiou, M., Van Hecke, P., Strimpakos, N., Gouliamos, A., et al. (2006). Lateralization of brain activity during lower limb joints movement. An fMRI study. *NeuroImage* 32, 1709–1721. doi: 10.1016/j.neuroimage.2006.05.043

Koohestani, M., Sharifnezhad, A., Abbasi, A., Javadi, A.-H., and Gokeler, A. (2020). Brain activation during maximum concentric and eccentric knee extension muscle contractions. *J. Brain Nerves* 2020, 1–6. doi: 10.31487/j.jbn.2020.01.05

Kriegeskorte, N., Lindquist, M. A., Nichols, T. E., Poldrack, R. A., and Vul, E. (2010). Everything you never wanted to know about circular analysis, but were afraid to ask. *J. Cereb. Blood Flow Metab.* 30, 1551–1557. doi: 10.1038/jcbfm.2010.86

Kriegeskorte, N., Simmons, W. K., Bellgowan, P. S. F., and Baker, C. I. (2009). Circular analysis in systems neuroscience: the dangers of double dipping. *Nat. Neurosci.* 12, 535–540. doi: 10.1038/nn.2303

Krishnan, C., Allen, E. J., and Williams, G. N. (2011). Effect of knee position on quadriceps muscle force steadiness and activation strategies. *Muscle Nerve* 43, 563–573. doi: 10.1002/mus.21981

Laboute, E., Verhaeghe, E., Ucay, O., and Minden, A. (2019). Evaluation kinaesthetic proprioceptive deficit after knee anterior cruciate ligament (ACL) reconstruction in athletes. *J. Exp. Ortop.* 6:6. doi: 10.1186/s40634-019-0174-8

Liu, J. Z., Dai, T. H., Elster, T. H., Sahgal, V., Brown, R. W., and Yue, G. H. (2000). Simultaneous measurement of human joint force, surface electromyograms, and functional MRI-measured brain activation. *J. Neurosci. Methods* 101, 49–57. doi: 10.1016/s0165-0270(00)00252-1

Logothetis, N. K., Pauls, J., Augath, M., Trinath, T., and Oeltermann, A. (2001). Neurophysiological investigation of the basis of the fMRI signal. *Nature* 412, 150–157. doi: 10.1038/35084005

Luft, A. R., Smith, G. V., Forrester, L., Whitall, J., Macko, R. F., Hauser, T.-K., et al. (2002). Comparing brain activation associated with isolated upper and lower limb movement across corresponding joints. *Hum. Brain Mapp.* 17, 131–140. doi: 10.1002/hbm.10058

Macaluso, E., Frith, C. D., and Driver, J. (2000). Modulation of human visual cortex by crossmodal spatial attention. *Science* 289, 1206–1208. doi: 10.1126/science.289.5482.1206

Mackey, A. S., Uttaro, D., McDonough, M. P., Krivis, L. I., and Knikou, M. (2016). Convergence of flexor reflex and corticospinal inputs on tibialis anterior network in humans. *Clin. Neurophysiol.* 127, 706–715. doi: 10.1016/j.clinph.2015.06.011

Manini, T. M., and Clark, B. C. (2012). Dynapenia and aging: an update. *J. Gerontol. A Biol Sci. Med. Sci.* 67A, 28–40. doi: 10.1093/gerona/glr010

Manini, T. M., Visser, M., Won-Park, S., Patel, K. V., Strotmeyer, E. S., Chen, H., et al. (2007). Knee extension strength cutpoints for maintaining mobility. *J. Am. Geriatr. Soc.* 55, 451–457. doi: 10.1111/j.1532-5415.2007.01087.x

Marx, R. G., Stump, T. J., Jones, E. C., Wickiewicz, T. L., and Warren, R. F. (2001). Development and evaluation of an activity rating scale for disorders of the knee. *Am. J. Sports Med.* 29, 213–218. doi: 10.1177/03635465010290021601

McGregor, K. M., Carpenter, H., Kleim, E., Sudhyadhom, A., White, K. D., Butler, A. J., et al. (2012). Motor map reliability and aging: a TMS/fMRI study. *Exp. Brain Res.* 219, 97–106. doi: 10.1007/s00221-012-3070-3

Mehta, J. P., Verber, M. D., Wieser, J. A., Schmit, B. D., and Schindler-Ivens, S. M. (2009). A novel technique for examining human brain activity associated with pedaling using fMRI. *J. Neurosci. Methods* 179, 230–239. doi: 10.1016/j.jneumeth.2009.01.029

Mehta, J. P., Verber, M. D., Wieser, J. A., Schmit, B. D., and Schindler-Ivens, S. M. (2012). The effect of movement rate and complexity on functional magnetic resonance signal change during pedaling. *Motor Control* 16, 158–175. doi: 10.1123/mcj.16.2.158

Montalvo, A. M., Schneider, D. K., Yut, L., Webster, K. E., Beynnon, B., Kocher, M. S., et al. (2019). "What's my risk of sustaining an ACL injury while playing sports?" A systematic review with meta-analysis. *Br. J. Sports Med.* 53, 1003–1012. doi: 10.1136/bjsports-2016-096274

Mrachacz-Kersting, N., Grey, M. J., and Sinkjær, T. (2006). Evidence for a supraspinal contribution to the human quadriceps long-latency stretch reflex. *Exp. Brain Res.* 168, 529–540. doi: 10.1007/s00221-005-0120-0

Naufel, S., Glaser, J. I., Kording, K. P., Perreault, E. J., and Miller, L. E. (2019). A muscle-activity-dependent gain between motor cortex and EMG. *J. Neurophysiol.* 121, 61–73. doi: 10.1152/jn.00329.2018

Newton, J. M., Dong, Y., Hidler, J., Plummer-D'Amato, P., Marehbian, J., Albistegui-Dubois, R. M., et al. (2008). Reliable assessment of lower limb motor representations with fMRI: use of a novel MR compatible device for real-time monitoring of ankle, knee and hip torques. *NeuroImage* 43, 136–146. doi: 10.1016/j.neuroimage.2008.07.001

Pincivero, D. M., Lephart, S. M., and Karunakara, R. G. (1997). Relation between open and closed kinematic chain assessment of knee strength and functional performance. *Clin. J. Sport Med.* 7, 11–16. doi: 10.1097/00042752-199701000-00003

Poldrack, R. A., Mumford, J. A., and Nichols, T. E. (2011). *Handbook of Functional MRI Data Analysis [Internet]*. Cambridge: Cambridge University Press.

Poortvliet, P. C., Tucker, K. J., Finnigan, S., Scott, D., Sowman, P., and Hodges, P. W. (2015). Cortical activity differs between position- and force-control knee extension tasks. *Exp. Brain Res.* 233, 3447–3457. doi: 10.1007/s00221-015-4404-8

Relph, N., and Herrington, L. (2016). The effects of knee direction, physical activity and age on knee joint position sense. *Knee* 23, 393–398. doi: 10.1016/j.knee.2016.02.018

Roy, F. D., Bosgra, D., and Stein, R. B. (2014). Interaction of transcutaneous spinal stimulation and transcranial magnetic stimulation in human leg muscles. *Exp. Brain Res.* 232, 1717–1728. doi: 10.1007/s00221-014-3864-6

Schubotz, R. I., and von Cramon, D. Y. (2002). A blueprint for target motion: fMRI reveals perceived sequential complexity to modulate premotor cortex. *NeuroImage* 16, 920–935. doi: 10.1006/nimg.2002.1183

Shahani, B. T., and Young, R. R. (1971). Human flexor reflexes. *J. Neurol. Neurosurg. Psychiatry* 34, 616–627. doi: 10.1136/jnnp.34.5.616

Shanahan, C. (2015). *Sensorimotor Changes in Knee Osteoarthritis: From Muscle Spindle Function to Brain Organisation and Activity*. Available online at: http://minerva-access.unimelb.edu.au/handle/11343/91673. Accessed November 2, 2018.

Shanahan, C. J., Hodges, P. W., Wrigley, T. V., Bennell, K. L., and Farrell, M. J. (2015). Organisation of the motor cortex differs between people with and without knee osteoarthritis. *Arthritis Res. Ther.* 17:164. doi: 10.1186/s13075-015-0676-4

Silfies, S. P., Vendemia, J. M. C., Beattie, P. F., Stewart, J. C., and Jordon, M. (2017). Changes in brain structure and activation may augment abnormal movement patterns: an emerging challenge in musculoskeletal rehabilitation. *Pain Med.* 18, 2051–2054. doi: 10.1093/pm/pnx190

Smith, S. M., Jenkinson, M., Woolrich, M. W., Beckmann, C. F., Behrens, T. E. J., Johansen-Berg, H., et al. (2004). Advances in functional and structural MR image analysis and implementation as FSL. *NeuroImage* 23, S208–S219. doi: 10.1016/j.neuroimage.2004.07.051

Te, M., Baptista, A. F., Chipchase, L. S., and Schabrun, S. M. (2017). Primary motor cortex organization is altered in persistent patellofemoral pain. *Pain Med.* 18, 2224–2234. doi: 10.1093/pm/pnx036

Telianidis, S., Perraton, L., Clark, R. A., Pua, Y.-H., Fortin, K., and Bryant, A. L. (2014). Diminished sub-maximal quadriceps force control in anterior cruciate ligament reconstructed patients is related to quadriceps and hamstring muscle dyskinesia. *J. Electromyogr. Kinesiol.* 24, 513–519. doi: 10.1016/j.jelekin.2014.04.014

Tourville, T. W., Jarrell, K. M., Naud, S., Slauterbeck, J. R., Johnson, R. J., and Beynnon, B. D. (2014). Relationship between isokinetic strength and tibiofemoral joint space width changes after anterior cruciate ligament reconstruction. *Am. J. Sports Med.* 42, 302–311. doi: 10.1177/0363546513510672

Tracy, B. L. (2007). Visuomotor contribution to force variability in the plantarflexor and dorsiflexor muscles. *Hum. Mov. Sci.* 26, 796–807. doi: 10.1016/j.humov.2007.07.001

Tracy, B. L., Dinenno, D. V., Jorgensen, B., and Welsh, S. J. (2007). Aging, visuomotor correction, and force fluctuations in large muscles. *Med. Sci. Sports Exerc.* 39, 469–479. doi: 10.1249/mss.0b013e31802d3ad3

Trinastic, J. P., Kautz, S. A., McGregor, K., Gregory, C., Bowden, M., Benjamin, M. B., et al. (2010). An fMRI study of the differences in brain activity during active ankle dorsiflexion and plantarflexion. *Brain Imaging Behav.* 4, 121–131. doi: 10.1007/s11682-010-9091-2

Vidal, A., Wu, W., Nakajima, M., and Becker, J. (2018). Investigating the constrained action hypothesis: a movement coordination and coordination variability approach. *J. Mot. Behav.* 50, 528–537. doi: 10.1080/00222895.2017.1371111

Ward, N. S., Swayne, O. B. C., and Newton, J. M. (2008). Age-dependent changes in the neural correlates of force modulation: an fMRI study. *Neurobiol. Aging* 29, 1434–1446. doi: 10.1016/j.neurobiolaging.2007.04.017

Ward, S. H., Perraton, L., Bennell, K., Pietrosimone, B., and Bryant, A. L. (2019). Deficits in quadriceps force control after anterior cruciate ligament injury: potential central mechanisms. *J. Athl. Train.* 54, 505–512. doi: 10.4085/1062-6050-414-17

Wulf, G., McNevin, N., and Shea, C. H. (2001). The automaticity of complex motor skill learning as a function of attentional focus. *Q. J. Exp. Psychol. A* 54, 1143–1154. doi: 10.1080/713756012

Wyatt, M. P., and Edwards, A. M. (1981). Comparison of quadriceps and hamstring torque values during isokinetic exercise. *J. Orthop. Sports Phys. Ther.* 3, 48–56. doi: 10.2519/jospt.1981.3.2.48

Conflict of Interest: The authors declare that the research was conducted in the absence of any commercial or financial relationships that could be construed as a potential conflict of interest.

frontiers in Sports and Active Living

ORIGINAL RESEARCH
published: 10 February 2021
doi: 10.3389/fspor.2020.610475

Accumulative Competitive Season Training Stress Affects Neuromuscular Function and Increases Injury Risk in Uninjured D1 Female Athletes

Troy M. Purdom[1]*, *Kyle S. Levers*[2], *Jacob Giles*[3], *Lindsey Brown*[3,4], *Chase S. McPherson*[3] *and Jordan Howard*[3]

[1] Department of Kinesiology, North Carolina Agriculture and Technical State University, Greensboro, NC, United States,
[2] Department of Exercise and Nutrition Sciences, George Washington University, Washington, DC, United States,
[3] Department of Health, Athletic Training, Recreation, and Kinesiology, Longwood University, Farmville, VA, United States,
[4] Department of Occupational Therapy, Virginia Common Wealth University, Richmond, VA, United States

OPEN ACCESS

Edited by:
Borja Sañudo,
Sevilla University, Spain

Reviewed by:
Gaspar Epro,
London South Bank University, United Kingdom
Francesco Di Nardo,
Marche Polytechnic University, Italy

***Correspondence:**
Troy M. Purdom
tpurdom@ncat.edu

Specialty section:
This article was submitted to Biomechanics and Control of Human Movement, a section of the journal Frontiers in Sports and Active Living

Received: *06 October 2020*
Accepted: *31 December 2020*
Published: *10 February 2021*

Citation:
Purdom TM, Levers KS, Giles J, Brown L, McPherson CS and Howard J (2021) Accumulative Competitive Season Training Stress Affects Neuromuscular Function and Increases Injury Risk in Uninjured D1 Female Athletes. Front. Sports Act. Living 2:610475. doi: 10.3389/fspor.2020.610475

Previous research has shown that acute competition training stress negatively affects neuromuscular function which can perpetuate a predisposition to injury. This study's aim was to investigate the effect of accumulated competition training stress effect on neuromuscular function and incidence of increased injury risk in uninjured female D1 soccer players. Neuromuscular function was evaluated in fifteen female division I soccer athletes who played >85% of competitive season competitions who were tested for mobility/stability, leg length symmetry, and vertical power at three different points across the competitive season (pre, mid, and post time blocks). Leg length symmetry was measured from the anterior superior iliac spine to the lateral malleolus prior to Y-balance testing. The Y-balance testing measures unilateral anterior, posteromedial, and posterolateral reach achieved in single leg stance using metrics that include L/R normalized composite reach (NCOMP), L/R normalized antiorior reach (NANT), and L/R NCOMP/NANT segmental differences across time. Injury risk was evaluated using validated objective criteria that included: (NCOMP total reach <94% of limb length*3), (NANT reach distance <84% leg length) along with NCOMP and NANT asymmetries >4.0. Maximal vertical power (MVP) was measured via vertical jump. Multiple repeated measures ANOVAs evaluated NCOMP, NANT, MVP, and leg length symmetry across time with LSD *post hoc* testing when relevant (X ± SD). A significant main effect was found [$F_{(1,\ 14)} = 62.92$, $p < 0.001$; $\eta^2 = 0.82$] with training stress and neuromuscular function without affecting maximal vertical power. Eighty percent of subject's bilateral NCOMP scores fell below the YBT reach standard at midseason (ES = 0.95, $p = 0.02$) while all subjects NANT reach distance remained below the reach threshold (ES = 0.74, $p = 0.003$) indicating a 6.5× and 2.5× greater injury risk, respectively. Competition stress affected neuromuscular function without affecting maximal power, which negatively impacted stability and increased injury risk.

Keywords: Y-balance, tonicity, mobility, stability, muscle tone, injury, peripheral nervous system, central nervous system

INTRODUCTION

Competitive athletes regularly endure high training loads that consist of repetitive exercise at high intensities, volumes, and frequencies with inadequate rest periods (Bengtsson et al., 2013; Dubois et al., 2018; Walker et al., 2019; Satkunskiene et al., 2020) that can perpetuate chronic fatigue and eventually injury (Silva et al., 2016; Jones et al., 2017). Furthermore, a dose response exists with increased frequency and duration further exacerbating the training stress throughout the competitive season (Bengtsson et al., 2013; Dubois et al., 2018; Caterisano et al., 2019; Satkunskiene et al., 2020). The high intensity, duration, and frequency of physical stress that collegiate athletes endure during training and competition can have residual effects (Bengtsson et al., 2013; Jones et al., 2017; Dubois et al., 2018; Walker et al., 2019; Satkunskiene et al., 2020) disrupting systematic neuromuscular function (Needle et al., 2014; Brownstein et al., 2017; Thomas et al., 2018; Satkunskiene et al., 2020) specifically, both central and peripheral fatigue for up to 72 and 48 h respectively (Brownstein et al., 2017; Thomas et al., 2018). Furthermore, the residual fatigue that competitive soccer athletes experience manifests as reduced performance prowess and increased injury rate when adequate recovery is not provided (Bengtsson et al., 2013; Silva et al., 2016; Dubois et al., 2018; Caterisano et al., 2019). In an 11 year retrospective study, competitive soccer matches where the team lost were significantly higher with <3 days of recovery while athletes with <4 days of recovery were shown to have increased rates of soft tissue injury (Bengtsson et al., 2013). Moreover, neuromuscular dysfunction due to cellular and tissue damage incurred during competition (Jones et al., 2017; Walker et al., 2019) has been shown to contribute to diminished neuromechanical function (Nédélec et al., 2012; Bengtsson et al., 2013; Brownstein et al., 2017; Satkunskiene et al., 2020) or stability (Plisky et al., 2006) that can manifest as a lower extremity injury (Plisky et al., 2006; Needle et al., 2014; Brazier et al., 2019; Higashihara et al., 2019).

Stability is contingent on motor control as a function of the afferent and efferent somatic nervous system function. Moreover, postural control relies on the integration from multiple control centers which include proprioception, visual cues, vestibular input, and planning (Needle et al., 2014). While sensory feedback is necessary for stability, motor control is largely a function of systematic neuromuscular function (Needle et al., 2014). Furthermore, postural control is highly contingent on the agonist/antagonist co-contraction to increase joint stiffness (Needle et al., 2014; Brazier et al., 2019) and is maintained through muscle tone, or low-level steady-state muscular contraction (Needle et al., 2014). Chronically stressing the nervous system can have negative impacts on neuromuscular function (Bengtsson et al., 2013; Buckthorpe et al., 2014; Brownstein et al., 2017; Thomas et al., 2018; Higashihara et al., 2019), affecting muscle tone and limiting mobility/stability due to hypertonic muscle spindles (afferent sensory network) that stimulate the reflex arc (Masi and Hannon, 2008; Needle et al., 2014; Stecco et al., 2014) and therefore muscle contraction (Bengtsson et al., 2013). For instance, while postural control is maintained by muscle tone, hypertonicity, or an abnormal increase in muscle tone with resistance to active movement can negatively affect joint stability (Needle et al., 2014). Furthermore, excessive hypertonicity can increase antagonist (opposing) muscle tone (Bengtsson et al., 2013; Needle et al., 2014; Stecco et al., 2014) which can limit joint range of motion and therefore mobility. Interestingly, increased joint stiffness may improve stability (Brazier et al., 2019) while failure to regulate stiffness can contribute to injury (Needle et al., 2014; Satkunskiene et al., 2020) through unfavorable motor control at specific joint centers.

Passive muscle tone is a neuromuscular function that provides low level resistance to stretch in an effort to maintain postural stability (equitable agonist/antagonist tension) (Masi and Hannon, 2008; Stecco et al., 2014; Higashihara et al., 2019). The degradation of motor control [balance] (Plisky et al., 2006) can occur acutely due to peripheral fatigue as a result of training stress (Brownstein et al., 2017; Satkunskiene et al., 2020) which can negatively affect postural stability. However, chronic training can influence the tissues surrounding the muscle (myofascial and connective tissue networks) which can negatively affect skeletal muscle function (Masi and Hannon, 2008; Nédélec et al., 2012; Needle et al., 2014; Stecco et al., 2014; Satkunskiene et al., 2020). Moreover, a peripheral complication of increased passive muscle tone is fascial rigidity which can hyper-stimulate the muscle spindle (Stecco et al., 2014), also known as hypertonicity (Needle et al., 2014). Fascial rigidity can create a positive feedback loop with the dysfunction of the muscle spindle (Plisky et al., 2006; Nédélec et al., 2012) hyperactivating passive muscle tone which reduces compliance of the antagonist muscle (Stecco et al., 2014). Therefore, reduced muscle compliance due to increased passive muscle tone can result in poor stability, and thus limit mobility (Plisky et al., 2006; Needle et al., 2014; Gonell et al., 2015). The negative effects of reduced muscle compliance can manifest as a reduction in stride length (Higashihara et al., 2019; Satkunskiene et al., 2020), postural degradation during high velocity movements (Masi and Hannon, 2008; Iwamoto et al., 2017) amongst other negative outcomes significantly affecting neuromechanical function during sport.

The high training loads collegiate soccer players experience across the competitive season without adequate recovery have demonstrated deleterious effects on neuromuscular function (Bengtsson et al., 2013; Brownstein et al., 2017; Satkunskiene et al., 2020) and therefore warrant periodic neuromuscular function evaluation (Gonell et al., 2015; Stiffler et al., 2017). A recent study detailing limitations of pre-season mobility/stability function to determine non-contact injuries across the season further suggests that periodic evaluation of neuromuscular function is necessary (Luedke et al., 2020). Specifically, validated measures of neuromuscular function can be used to monitor applied mobility-stability functionality (Plisky et al., 2006; Gonell et al., 2015; Stiffler et al., 2017) and maximal force/power production (Nédélec et al., 2012; Buckthorpe et al., 2014; Brownstein et al., 2017; Thomas et al., 2018). The Y-balance test (YBT) has been shown to be a valid method to evaluate stability asymmetries and therefore neuromuscular function in athletic populations (Plisky et al., 2006; Gonell et al., 2015; Giles et al., 2017; Stiffler et al., 2017), while maximal vertical power (MVP) is a valid method of measuring lower extremity maximal

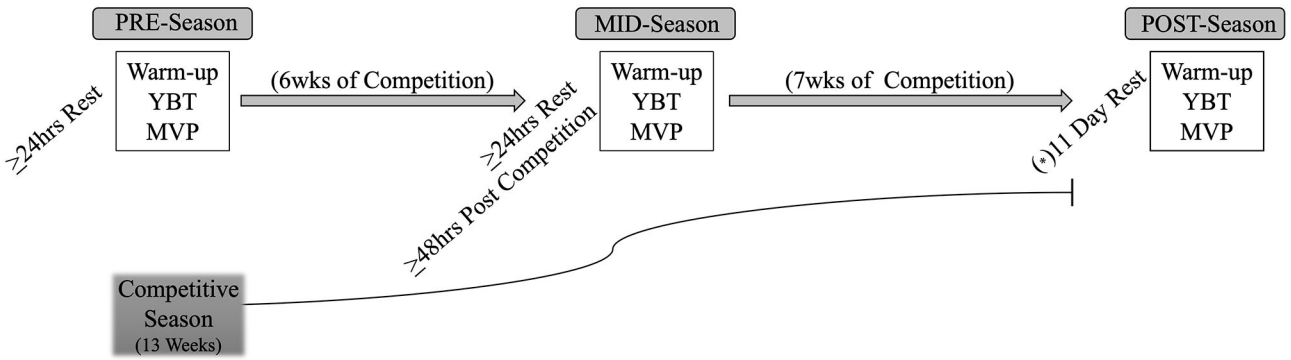

FIGURE 1 | Study timeline including data collection time blocks. (*) NCAA mandated post season discretionary period (NCAA D1 2018-2019 Manual) (The National Collegiate Athletic Association, 2018); POST season data was collected 11 days after the last competitive match. (YBT) y-balance Testing; (MVP) Maximal Vertical Power; (>)greater than or equal to.

force production (Canavan and Vescovi, 2004; Quagliarella et al., 2011; Buckthorpe et al., 2014; Thomas et al., 2018). Lower body asymmetry is defined as a discrepancy between the right and left (L/R) limb reach distance measured actively where passive measurement includes limb leg length, or the distance from the anterior superior iliac crest and lateral malleolus (Plisky et al., 2006). Anterior reach considers ankle dorsiflexion while posteromedial reach is a useful tool to identify ankle perturbation and therefore instability, specifically the anterior tibialis as well as lower extremity coordination (Plisky et al., 2006; Stiffler et al., 2017). The decrement in active single stance reach and therefore range of motion evaluated by the YBT can indicate a greater risk of injury (Plisky et al., 2006; Gonell et al., 2015; Stiffler et al., 2017) due to neuromuscular dysfunction (Masi and Hannon, 2008; Needle et al., 2014; Brownstein et al., 2017; Higashihara et al., 2019; Satkunskiene et al., 2020). Therefore, the aim of this study was to evaluate the effect of accumulative competitive season stress on neuromuscular function, specifically: measures of mobility/stability, asymmetry, and MVP in uninjured, high-minute Division I athletes.

MATERIALS AND METHODS

Exercise Design

Using a repeated measures design, this study investigated the impact of accumulated collegiate competitive season training stress on neuromuscular function in Division I female soccer players. Sample size was determined using a repeated measures a priori power analysis (G*Power, version 3.1.9.6) indicating a sample size of ($n = 9$) based upon $\eta^2 = 0.391$ from Satkunskiene et al. 2020 (Satkunskiene et al., 2020). Testing occurred at pre-designated testing blocks across the competitive season: pre-season (PRE), mid-season (MID) and post-season (POST) as shown in **Figure 1**. The PRE:MID season time points occurred six weeks apart while the MID:POST season time points were nine weeks apart. Division I NCAA compliance regulations have a seven day minimum discretionary rule preventing student athlete participation in, "all athletic related activities… beginning the day after… the last contest of the championship segment" (The National Collegiate Athletic Association, 2018). Therefore, POST season testing occurred 11 days after the final competitive match extending the POST testing block. No prescribed exercise occurred during the 11-day period between the last competition and POST time block and all testing was conducted with >24 h of rest and >48 h post competition.

Subjects

Twenty-nine Division I female soccer athletes initially enrolled in the study providing informed written consent approved by the university institutional review board and completed a health history questionnaire prior to participation. This study was conducted in accordance with the Declaration of Helsinki. Accumulation of competitive match stress paired with lack of adequate recovery have been shown to incur significant physiological stress that can accumulate (Bengtsson et al., 2013; Jones et al., 2017; Dubois et al., 2018; Walker et al., 2019; Satkunskiene et al., 2020) with deleterious effects that result in injury (Bengtsson et al., 2013; Needle et al., 2014; Caterisano et al., 2019). Therefore, the inclusion criteria consisted of high minute players with >5yrs competitive experience who incurred significant competition training stress by playing in >85% of competitive season games (>18/21) throughout the 13-week collegiate season, and had no significant injury preventing testing compliance. During the 13wk competitive season, subjects participated in concurrent training (mixed resistance and endurance training) sessions 4-5 days per week with a minimum of two matches per week, which has been shown to incur significant stress that can accumulate across the competitive season (Bengtsson et al., 2013; Jones et al., 2017; Dubois et al., 2018; Walker et al., 2019; Satkunskiene et al., 2020). Total weekly training volume throughout the competitive season could not exceed 20 h per NCAA Guidelines (The National Collegiate Athletic Association, 2018). However, the conference game schedule included ∼3 days recovery between matches, which has been shown to promote injury (Bengtsson et al., 2013). Of the 29 subjects who initially enrolled, three

TABLE 1 | Demographic information for subjects ($n = 15$) across all three time blocks (PRE, MID, POST).

	Age (years)	Height (cm)	Weight (kg)	%BF (%)	FFM (kg)	FM (kg)	Played/Total (Min)
PRE	19.5 ± 1.1	–	60.0 ± 5.1	18.7 ± 3.8	48.7 ± 3.7	11.3 ± 2.9	–
MID	19.6 ± 1.2	165.6 ± 4.3	60.7 ± 4.6	18.3 ± 3.2	49.5 ± 3.1	11.2 ± 2.6	481 ± 194/850
POST	19.6 ± 1.2	166.1 ± 5.2	60.3 ± 5.2	19.0 ± 3.0	48.8 ± 4.0	11.5 ± 2.3	1,251 ± 495/2,010

Data are presented as mean ± SD. PRE, pre-season; MID, midseason; POST, post-season. (Played/Total) ratio of competition minutes played to total competition minutes across 21 competitive season games. BF, body fat; FFM, fat free mass; FM, fat mass.

subjects voluntarily dropped from the study, two were excluded due to injury preventing testing, and nine excluded due to playing <85% of competitions throughout the competitive season. Thus, demographic information for 15 high minute uninjured Division I female soccer players included are shown in **Table 1**.

Each testing block began with subjects arriving to the laboratory having refrained from exercise for >24 h, avoiding stimulants/depressants including caffeine for >12 h, and fasted for >4 h. Height and weight were measured via electronic standiometer and scale (Seca Corp. Chino, CA, USA) while tissue density was measured by a trained researcher using handheld skinfold calipers (Beta Technology, Santa Cruz, CA, USA) and a three site skin fold method along with the Brozek equation to estimate body composition (American College of Sports Medicine, 2018). The subjects then completed a 5-min cycling aerobic warm-up prior to completing a standardized dynamic warm-up (20 m of high knees, butt kickers, and high bounds). Neuromuscular function was assessed with mobility/stability and joint symmetry utilizing a metric measuring tape and a YBT testing apparatus (Functional Movement Systems, Chatham, VA) by multiple trained researchers, which has been shown to have a high degree of interrater reliability (Shaffer et al., 2013). Joint symmetry was first evaluated by measuring leg lengths from the anterior superior iliac spine to the lateral malleolus followed by recording the best of three YBT attempts per side without shoes (Plisky et al., 2006; Gonell et al., 2015). The YBT measures anterior, posterolateral, and posteromedial reach distance by requiring the subject to maintain single leg stance while pushing the reach indicator with their non-stance foot in each of the three aforementioned directions (**Figure 2**). The stance foot and non-stance foot must remain in contact with the YBT apparatus at all times. The stance foot heel must not raise from the YBT apparatus while the toes of the non-stance foot maintain contact with the reach indicator until the subject can no longer progress the reach indicator or maintain balance. The subject must then return to the start position under control without touching the ground. Measures of the YBT are further discussed and shown below which include leg length symmetry (LLSYM) (difference between right and left leg lengths), the left-right (L/R) normalized composite reach (NCOMP), L/R normalized anterior reach (NANT), and L/R NCOMP/NANT segmental comparisons (Plisky et al., 2006; Gonell et al., 2015; Stiffler et al., 2017). Previous validated metrics that specify a predisposition to injury risk were identified as NCOMP reach deficiency (<94% leg length*3), NANT reach deficiency (<84% leg length) (Plisky et al., 2006; Stiffler et al., 2017), and/or L/R NCOMP/NANT (side-to-side comparison >4.0) (Plisky et al., 2006; Gonell et al., 2015; Stiffler et al., 2017). Therefore, NCOMP (%) and NANT (%) reach threshold values along with L/R side-to-side difference comparisons (absolute value) were used as injury risk indicators across time blocks.

YBT Measures:

- LLSYM = side-to-side comparison of anterior, superior iliac spine to lateral malleolus measured in millimeters (mm)
- NCOMP = [(ANT+PTL+PTM/leg length*3)*100] measured as a (%)
- NANT = [(ANT/ leg length)*100] measured as a (%)
- L/R NCOMP segmental comparisons (absolute value)
- L/R NANT segmental comparisons (absolute value)

Injury Risk Indicators:

- NCOMP reach deficiency (total reach <94% of limb length*3)
- NANT reach deficiency (anterior reach distance <84% leg length)
- L/R NANT side-to-side comparison >4.0 (absolute value)
- L/R NCOMP side-to-side comparison >4.0 (absolute value)

LLSYM: leg length symmetry; NCOMP: normalized composite score; ANT: anterior reach distance; PTL, post-eriorlateral reach distance; PTM, post-eriormedial reach distance; NANT, normalized anterior reach score.

After the warm-up protocol and YBT, MVP function was evaluated using vertical jump performance (Thomas et al., 2018) with a Vertec apparatus (Sports Imports, Columbus, OH) (Canavan and Vescovi, 2004; Quagliarella et al., 2011; Nédélec et al., 2012). Standing reach height was first measured prior to subjects completing three maximal effort countermovement jumps with a 60 s rest between attempts. Of the three maximal vertical jumps, the highest jump was recorded (Canavan and Vescovi, 2004). Vertical jump heights were converted to watts and therefore MVP using the Harman Formula: Power (watts) = [61.9*jump height (cm)] + [36.0*body mass (kg)] – 1,822] (Canavan and Vescovi, 2004; Quagliarella et al., 2011).

Statistical Analysis

Neuromuscular function was evaluated using MVP (watts) (Canavan and Vescovi, 2004; Quagliarella et al., 2011; Thomas et al., 2018) along with the YBT (NCOMP, NANT, LLSYM) (Plisky et al., 2006; Gonell et al., 2015). Two repeated

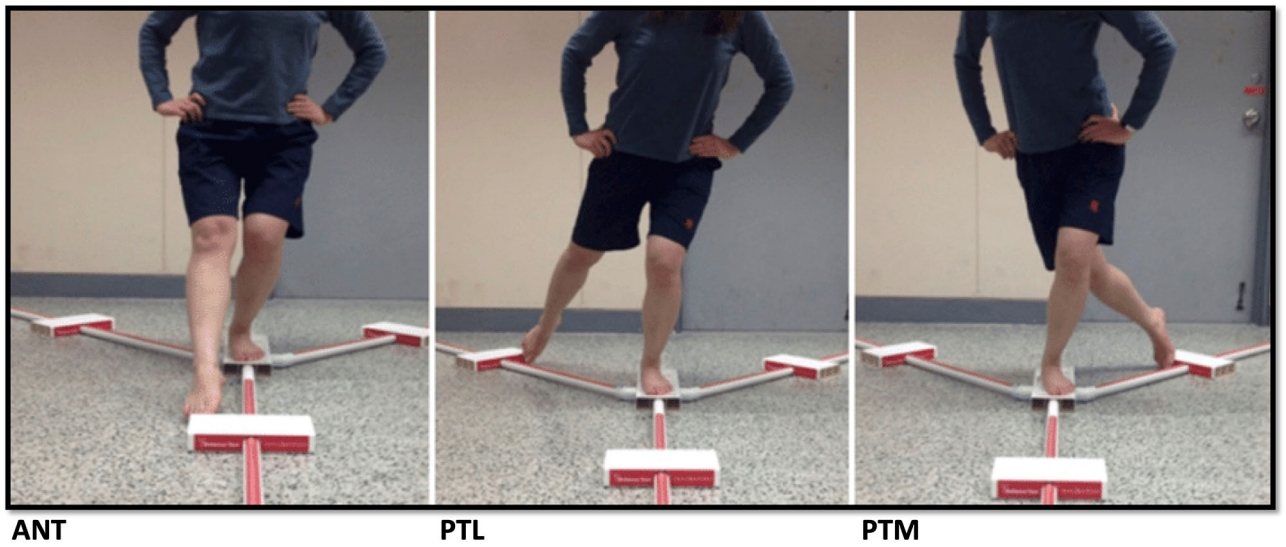

FIGURE 2 | Illustration of the single leg Y-balance test (YBT) in the anterior (ANT), posterior lateral (PTL), and posterior medial (PTM) directions. Injury risk indicators were NCOMP reach deficiency (total reach <94% of limb length*3), NANT reach deficiency (ANT reach distance <84% leg length), and segmental comparisons >4.0 (Plisky et al., 2006; Gonell et al., 2015; Stiffler et al., 2017).

measures analysis of variance (ANOVA) 4 × 3 statistical models (dependent variable × time) were used to analyze dependent variables. Metrics from the YBT and MVP were used comparatively to assess neuromuscular functional changes across the competitive season (PRE, MID, and POST time blocks): NCOMP L/R comparison difference (absolute value), NANT L/R comparison difference (absolute value), LLSYM, and MVP. The second ANOVA model compared left and right limb NCOMP reach distance as well as L/R limb NANT reach distance; both expressed as a percentage of leg length with the equations specified above across the competitive season using SPSS version 23 (IBM Corp, Armonk, NY). When statistical relevance was observed, the LSD *post hoc* test was used to evaluate pairwise comparisons. Significance was set at ($p < 0.05$) and all values are represented as (mean ± SD) and effect size (ES).

RESULTS

A significant main effect was observed [$F_{(1, 14)} = 62.29$, $p < 0.001$; $\eta^2 = 0.82$] with accumulated competition stress and neuromuscular function across time in both MID and POST timepoints in uninjured D1 female soccer players shown in **Table 2**. Pairwise comparisons revealed neuromuscular function was affected by accumulated competition training stress across the competitive season through a significant increase in L/R NCOMP segmental difference MID-POST (MID: 2.7 ± 1.9, POST: 4.6 ± 3.4; $p = 0.05$; ES = 0.69) without relevant differences in MVP shown in **Figure 3**. Left-right NCOMP and NANT reach distances were also impacted by competitive training stress across time [$F_{(1, 14)} = 2.79$, $p < 0.01$; $\eta^2 = 0.30$]. NCOMP and NANT reach distance for both legs decreased from PRE:MID, and then increased from MID:POST shown in **Figure 4**.

Table 2 details NANT and NCOMP comparisons across each time point. YBT measures indicate that neuromuscular function changed longitudinally with a ∼13% decrease in L/R NANT (ES = 0.83) PRE:MID before increasing 9.5% MID:POST (ES = 0.71). Longitudinal changes were further detailed with L/R NCOMP reach distance reducing ∼8% PRE:MID (ES = 0.86) and then increasing ∼8.5% (ES = 0.96). The accumulated training stress reduced bilateral NCOMP reach distance PRE:MID where 80% of subjects (12/15) had NCOMP reach distance scores below the YBT injury risk threshold (reach < 94% of 3× limb length) increasing injury risk by 6.5× (**Figure 4**). However, bilateral NCOMP reach distance returned above the risk threshold at POST with extended rest (11-days rest prior to POST-season testing). Furthermore, while 100% of the population was at a 2.5× increased injury risk (NANT reach <84% limb length) for both limbs throughout all three test blocks (entire competitive season) (**Figure 4**), bilateral NANT reach distance paralleled the NCOMP significant decrease PRE-MID that increased with significant rest MID:POST. No significant differences between MVP were observed throughout the competitive season indicating that maximal power production was unaffected by competitive season training stress ($p = 0.75$) (**Table 2**; **Figure 3**) with >24 h of rest and >48 h post competition.

DISCUSSION

The purpose of this study was to evaluate the accumulation of stress of the competitive season on neuromuscular function in Division I female soccer players. To our knowledge, this is the first study to evaluate the effects of accumulated competitive

TABLE 2 | Dependent variables are shown across all testing blocks (competitive season).

Dependent variables	PRE-season			MID-season			POST-season		
	LEFT	RIGHT	Abs DIFF	LEFT	RIGHT	Abs DIFF	LEFT	RIGHT	Abs DIFF
NANT (%)	67.5 ± 12.0∧	66.6 ± 11.5∧	3.7 ± 2.5	58.2 ± 8.3†∧	58.5 ± 9.0†∧	3.3 ± 2.1	64.6 ± 9.1*∧	64.5 ± 8.5*∧	4.6 ± 4.1*§
NCOMP (%)	96.6 ± 9.8	96.3 ± 10.9	2.9 ± 1.6	88.7 ± 7.3†#	88.8 ± 7.2†#	2.7 ± 1.9	96.2 ± 6.4*	97.9 ± 6.1*	4.6 ± 3.4*§
LLSYM L/R Diff (cm)	0.9 ± 0.2			1.0 ± 0.3			1.0 ± 0.2		
MVP (W)	392.2 ± 43.7			396.6 ± 43.5			403.6 ± 42.8		

*Data are presented as Mean ± SD. NCOMP- normalized composite reach score represented as a percent (%). NANT- normalized anterior reach score represented as a percent (%). LLSYM- leg length symmetry in centimeters (cm). MVP- maximal vertical power in watts (W). Abs Diff- Absolute left/right segmental difference (absolute value). (†) indicates a statistically significant change from PRE-season ($p < 0.05$). (*) indicates a statistically significant change from MID-season ($p < 0.05$). (∧)indicates failure to meet the NANT relative injury risk threshold = (ANT reach distance <84% of limb length). (#)indicates failure to meet the NCOMP relative injury risk threshold = [(ANT+PTL+PTM) <94% of (limb length*3)] (Plisky et al., 2006). ($) left/right difference exceeds 4.0 indicating increased injury risk (Plisky et al., 2006; Gonell et al., 2015; Stiffler et al., 2017).*

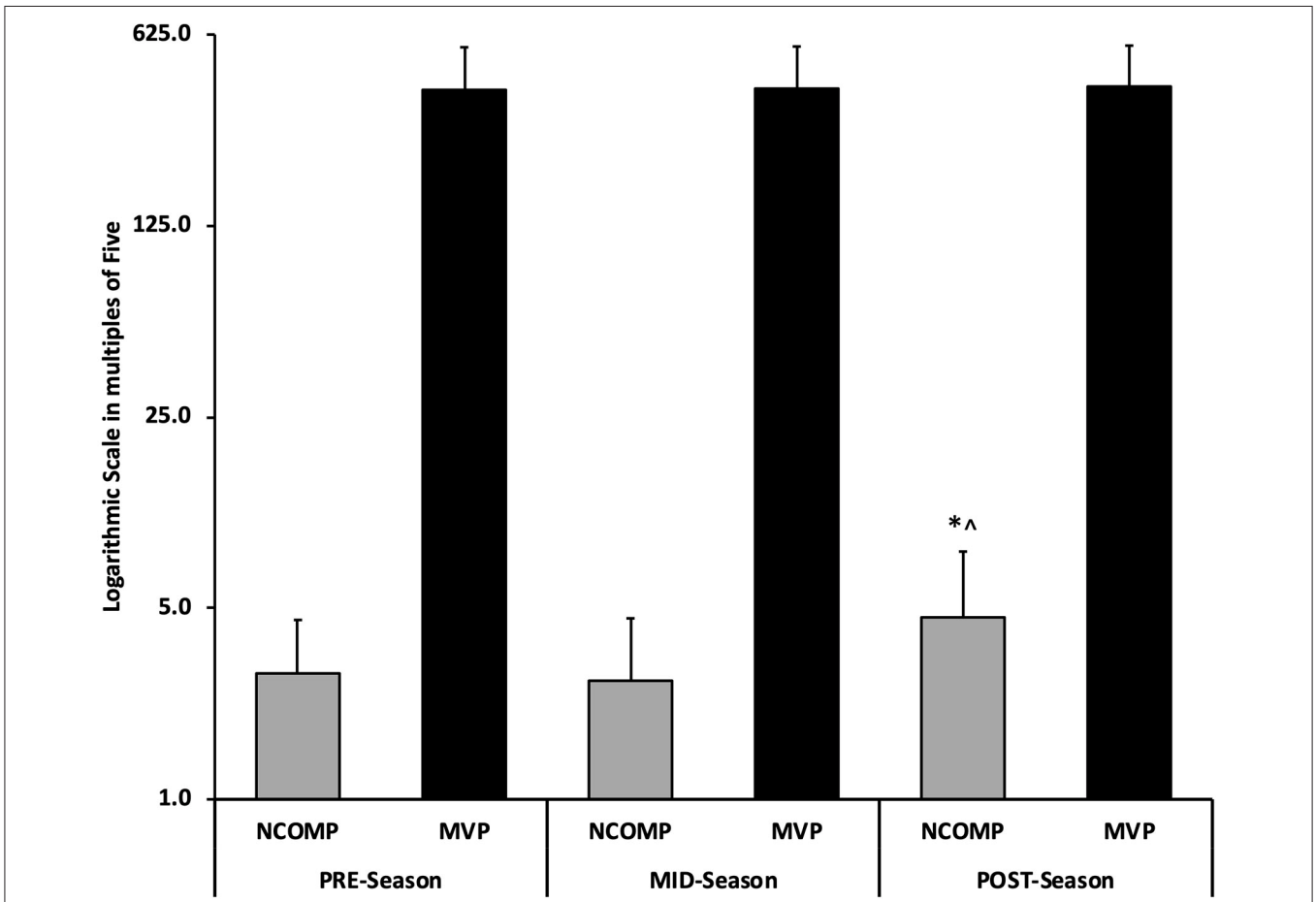

FIGURE 3 | Relationship between maximal vertical power (MVP) expressed in watts (W) and NCOMP left/right difference expressed as an (absolute value) across the competitive season (PRE, MID, POST time blocks). (NCOMP) normalized composite score, NCOMP = [(ANT+PTL+PTM/(leg length*3)]*100. (*) indicates a statistically significant change from MID season ($p < 0.05$). (∧) left/right NCOMP difference exceeds 4.0 indicating a 6.5x increase in injury risk (Plisky et al., 2006; Gonell et al., 2015; Stiffler et al., 2017).

season training stress effect on injury risk as it relates to applied neuromuscular function in uninjured female athletes. Previous research evaluated neuromuscular function acutely (Plisky et al., 2006; Buckthorpe et al., 2014; Gonell et al., 2015; Brownstein et al., 2017; Stiffler et al., 2017; Higashihara et al., 2019) and/or the efficacy of YBT performance and its efficacy to predict injury (Plisky et al., 2006; Shaffer et al., 2013; Gonell et al., 2015; Stiffler et al., 2017). This

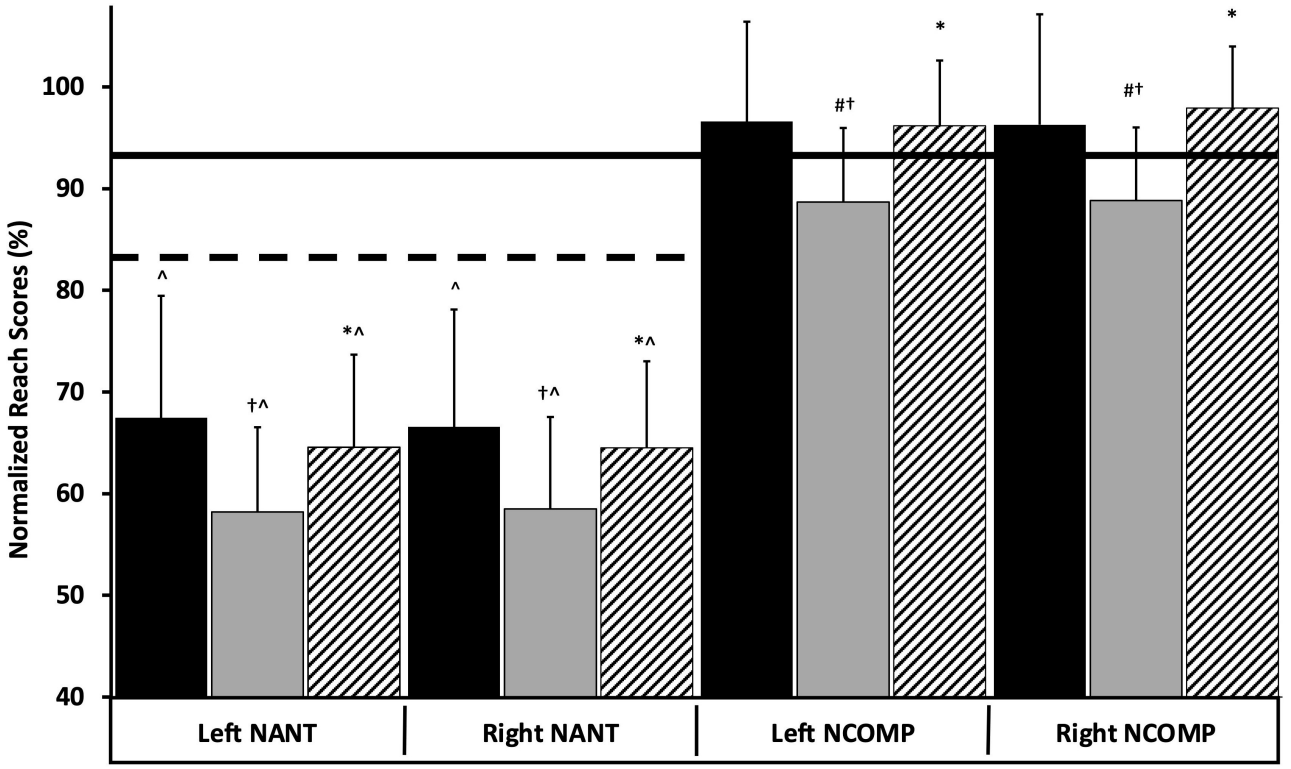

FIGURE 4 | Left and right normalized anterior reach (NANT) and normalized composite scores (NCOMP) scores expressed as percentages and displayed across the competitive season [PRE-season (black), MID-season (gray) POST-season (striped)]. (†) indicates a statistically significant change from PRE-season ($p < 0.05$). (*) indicates a statistically significant change from MID-season ($p < 0.05$). (#) indicates failure to meet the NCOMP relative injury risk threshold = [(ANT+PTL+PTM) <94% of (limb length*3)] which is visually represented by the solid horizontal line (Plisky et al., 2006). (∧) indicates failure to meet the NANT relative injury risk threshold = (ANT reach distance <84% of limb length), which is visually represented by the dashed horizontal line (Plisky et al., 2006; Gonell et al., 2015; Stiffler et al., 2017). ANT, anterior; PTL, posterior lateral; PTM, posterior medial.

study highlights the necessity to monitor the neuromuscular system's adaptive capacity to maintain mobility/stability despite continual high intensity, high volume competitive stress. The study sample, which was composed of high minute uninjured D1 female soccer athletes was shown to negatively respond to competitive season stress at both MID and POST time points with >24 h rest and >48 h post-competition without affecting MVP ($p = 0.75$). The accumulation of training stress on neuromuscular function was demonstrated with the decline in NCOMP/NANT reach distance performance across 6 weeks of competition (PRE:MID), which then increased MID:POST. This study demonstrates the sensitivity of the neuromuscular system to accumulated training stress and thus injury predisposition with and without adequate rest (POST season and MID season, respectively). Interestingly, despite seven weeks of additive competition stress (MID:POST), extended rest (11-days rest before POST testing; **Figure 1**) restored NCOMP/NANT reach distance to PRE values. However, NANT and NCOMP segmental comparisons increased MID:POST despite rest demonstrating the plasticity of competitive season stress on neuromuscular function.

Maximal vertical power was unaffected across the competitive season indicating that the cumulative stress of the competitive season had no significant impact on the neuromuscular system's ability to produce force within our population with >24 h of rest (**Figure 3**). Previous research found that neuromuscular function is affected by training stress that impacts voluntary maximal power (Brownstein et al., 2017; Thomas et al., 2018). However, neuromuscular function was shown to fully recover within 72 h after a single soccer match (Brownstein et al., 2017) which our results disagree. It is noteworthy that Brownstein et al. (2017) examined the acute effects of a single 90 min competitive soccer match on central and peripheral indices where this study focused on the accumulation of training stress across the competitive season (with >48 h of rest post-competition). Previous research show that the accumulation of competitive stress can have negative effects on performance and can perpetuate injury (Bengtsson et al., 2013; Silva et al., 2016; Jones et al., 2017; Dubois et al., 2018; Walker et al., 2019). Our findings indicate that MVP can maintain/recover within 24 h despite the accumulation of training stress incurred throughout the competitive season (Jones et al., 2017; Dubois et al., 2018; Walker et al., 2019; Satkunskiene et al., 2020), which disagrees with the current literature (Silva et al., 2016; Brownstein et al., 2017; Thomas et al., 2018). Interestingly, CNS activity specific to the motor cortex has been shown

adapt to fatigue which has previously been shown to occur acutely to maintain force production (Jiang et al., 2012). While significant changes in MVP were not observed in our population, movement quality decreased from PRE:MID and increased MID:POST (NCOMP/NANT reach distance) suggesting that chronic training stress and the negative indices of injury are perpetuated by mobility/stability disfunction without affecting MVP (**Figure 3**). Therefore, evaluating movement throughout the competitive season may be a more sensitive measure of chronic neuromuscular fatigue to assess injury risk, which can be a result of motor control degradation separate from the CNS. It is important to note that the degradation of motor control can manifest as a function of deteriorating PNS function: muscle tone, vestibular control, peripheral fatigue, etc. (Needle et al., 2014). However, our population is represented by uninjured athletes who maintained the ability to produce maximal force with diminished neuromuscular control that can facilitate greater injury predisposition among athletes (Brazier et al., 2019; Higashihara et al., 2019).

The YBT indices (NCOMP, NANT, LLSYM) observed across the competitive season to represent neuromuscular function have been shown to independently evaluate injury risk as they focus on different aspects of lower body neuromuscular integrity (Plisky et al., 2006; Gonell et al., 2015; Stiffler et al., 2017). Most apparent was the left and right NCOMP/NANT reach distance decreasing after 6 weeks of competition. More concerning was that 80% of the population (12/15 athletes) experienced a bilateral decline in NCOMP reach distance from PRE:MID dropping NCOMP reach distance below the risk threshold (<94% total reach distance) (**Figure 4**), which increased injury risk 6.5× MID season (Plisky et al., 2006; Gonell et al., 2015; Stiffler et al., 2017) (**Figure 4**). Additionally, bilateral NANT reach distance scored below the injury risk threshold (NANT reach <84% of limb length) over the entire competitive season, which further reduced and paralleled the significant NCOMP reach reduction PRE:MID ($p < 0.05$). The NCOMP and NANT reach distance reductions PRE:MID reinforce the effects of accumulated competitive season stress on the neuromuscular function (Bengtsson et al., 2013; Brownstein et al., 2017; Dubois et al., 2018; Satkunskiene et al., 2020). Increased passive muscle tone (Masi and Hannon, 2008) that disrupts the agonist/antagonist relationship (Iwamoto et al., 2017; Higashihara et al., 2019) can corrupt postural control and therefore limit mobility; a necessary function in competition. Interestingly, NCOMP reach distance increased MID:POST which would suggest restored neuromuscular function and decreased injury risk (Gonell et al., 2015; Stiffler et al., 2017). However, L/R asymmetry increased >4.0 (**Figure 3**; **Table 2**) over the same period indicating increased segmental neuromuscular dysfunction and therefore heightened injury risk (Plisky et al., 2006; Gonell et al., 2015). Left-right reach asymmetries are postulated to occur as a result of ankle dorsiflexion limitations as well as deficits in strength, flexibility, and motor control that inform injury risk (Needle et al., 2014; Stiffler et al., 2017). A limitation of this study was the delayed collection of the POST time block data and associated rest/recovery extension that occurred 11 days post-final match to comply with NCAA guidelines (The National Collegiate Athletic Association, 2018). However, while POST-season NCOMP/NANT reach distances increased to PRE-season values with extended rest, L/R NCOMP reach asymmetry increased MID:POST as a result training stress accumulation despite adequate recovery. These observations illustrate the plastic nature of unilateral NCOMP asymmetry to accumulated training stress after onset which can affect acceleration, deceleration, and lateral explosive movements perpetuating injury. While segmental changes paralleled each other in response to accumulated training stress across time in this study, evaluating dominant/non-dominant segmental neuromuscular responses to training stress could help describe the segmental differences that inform injury risk observed in this study and past research (Stiffler et al., 2017).

Normalized anterior reach (NANT) is shown to be an indicator of lower extremity mobility/stability while revealing potential limitations that preclude normal function and promote greater injury predisposition (Plisky et al., 2006; Gonell et al., 2015; Stiffler et al., 2017). Left-right NANT reach distance comparisons from PRE:MID season significantly decreased which promoted greater injury predisposition as a consequence to initiation of competitive season training stress. Furthermore, NANT asymmetry (absolute difference) increased by 28% beyond the 4.0 injury risk threshold (Plisky et al., 2006; Gonell et al., 2015; Stiffler et al., 2017) from MID to POST (**Figure 4**; **Table 2**) further demonstrating the plasticity of side-to-side asymmetries despite 11 days of rest. Comparatively, NANT reach decreased and then increased PRE-MID-POST with recovery illustrating the elasticity of reach distance to recovery. The average NANT decrement across the season was 24.6% below the aforementioned injury risk threshold. Aggregate data show that 100% of the population exhibited a >2.5× (Plisky et al., 2006; Gonell et al., 2015; Stiffler et al., 2017) elevated injury risk (NANT reach <84% limb length) (Plisky et al., 2006) for both limbs at all three time points (**Figure 4**) despite the increase in reach distance MID:POST. Practitioners should consider the sensitivity of adequate reach distance and side-to-side asymmetries to evaluate chronic neuromuscular fatigue. Therefore, the reach limitations observed in non-injured athletes can be an indicator of heightened passive muscle tone through amplified lower extremity neuromuscular agonist/antagonist activity restricting mobility (Needle et al., 2014; Iwamoto et al., 2017; Higashihara et al., 2019).

Greater co-contraction of ankle joint stabilizers are shown to limit range of motion in accelerated movement patterns in healthy subjects (Iwamoto et al., 2017). While the YBT utilizes slow, controlled movements to assess mobility and stability, previous research indicates that heightened muscular tonicity (abnormal increase in muscle activity) can be a limitation to mobility (Needle et al., 2014; Higashihara et al., 2019; Satkunskiene et al., 2020). The non-injured subjects in this study started the competitive season (PRE) with bilateral NANT reach limitations and a heightened injury predisposition that worsened PRE:MID and were restored MID:POST season. The results MID & POST occurred despite >24 h of rest prior to MID and a 11-day recovery prior to POST testing. While peripheral neural function including

muscle electrical activity (EMG) was not measured in this study, non-injured players that have compromised lower extremity mechanical function while maintaining MVP is suggestive of neuromuscular tone dysfunction that can perpetuate injury (Needle et al., 2014; Higashihara et al., 2019; Satkunskiene et al., 2020). Acknowledging that strength is a necessary component of stability (Needle et al., 2014; Stiffler et al., 2017), our population maintained peak power suggesting strength was not a limitation. Nevertheless, specific aspects of the YBT, namely NCOMP/NANT reach distance and symmetry should be monitored regularly as chronic training clearly affects neuromuscular function, particularly during periods of high training stress to help mitigate injury risk (Bengtsson et al., 2013; Silva et al., 2016; Satkunskiene et al., 2020).

Additional metrics of the YBT included LLSYM that was previously identified as an injury risk indicator (Plisky et al., 2006; Gonell et al., 2015; Stiffler et al., 2017). This study evaluated the chronic nature of competitive season stress with >24 h of rest which found no significant LLSYM changes. NCOMP and NANT metrics rather than pelvic dysfunction may be more sensitive indicators of chronic stress in collegiate female soccer players. However, past research has demonstrated that LLSYM and therefore pelvic symmetry dysfunction does occur in collegiate athletes (Giles et al., 2017). Notably, the effects of chronic training stress has been shown to reside for weeks after training cessation (Nédélec et al., 2012; Silva et al., 2016) despite reductions in training volume and intensity. However, pelvic dysfunction (LLSYM) has been previously shown to diminish in collegiate female soccer players with extended rest (9 weeks of recovery) (Giles et al., 2017). The residual effects of extended high-volume high-intensity training inherent to the competitive season has lasting effects on neuromuscular function that are best mitigated through adequate rest. While athletes' rest is regulated throughout the competitive season, suitable transition period management as well as pre-season preparation (Silva et al., 2016) is necessary to mitigate non-contact soft tissue injury (Plisky et al., 2006; Gonell et al., 2015; Stiffler et al., 2017; Higashihara et al., 2019).

Postural degradation has been shown to occur in heathy populations due to neuromuscular dysfunction (Masi and Hannon, 2008; Needle et al., 2014; Stecco et al., 2014; Higashihara et al., 2019) that contribute to injury (Plisky et al., 2006; Gonell et al., 2015; Stiffler et al., 2017; Higashihara et al., 2019). Our population consisted of uninjured healthy athletes with no apparent joint or mechanical dysfunction preventing testing. Therefore, alterations in neuromuscular function that manifest as a result of accumulated competitive season stress may explain degradation in mobility and stability (Plisky et al., 2006; Masi and Hannon, 2008; Brazier et al., 2019; Higashihara et al., 2019) while absent of power deficiencies that are necessary to perform. It is important to note that multiple systems contribute to stability, some of which were not tested. However apparent this limitation is, the fact remains that accumulated training stress (Jones et al., 2017; Dubois et al., 2018; Walker et al., 2019) has been shown to effect stability and mobility across the competitive season which should be further investigated with more stringent laboratory methodologies. Additional considerations are that bilateral movements such as running rely on reciprocal contributions of both limbs and are suggestive of normal function and therefore maintenance of performance. However, unilateral stability/mobility testing can expose masked neuromuscular dysfunction that can lead to limitations in joint stability and thus range of motion (Plisky et al., 2006) that promote injury risk. Therefore, the sensitivity of the YBT may be more relevant to evaluate changes in neuromuscular function rather than performance measures. Furthermore, the applied nature and objectivity along with the low cost and portability make the YBT a relevant objective field test for practitioners.

CONCLUSION

The accumulation of competitive season training stress was shown to affect neuromuscular function after 6 weeks and persist despite rest by impacting unilateral lower extremity stability. The NCOMP and NANT limitations observed are indictive of altered neuromuscular stability function and are more sensitive to the effects of accumulated training stress rather than power-based measures. Normalized composite scores measure anterior, posteriorlateral, and posteriormedial reach and are indicators of mobility/stability while anterior reach considers ankle dorsiflexion. The YBT through single limb loading stresses unilateral neuromechanical coordinated movement of the lower extremity exposing motor control deficiencies that limit range of motion. Throughout the competitive season, increased passive muscle tone may be the cause of the observed decrement in NANT/NCOMP reach paired with asymmetries within our population. Reach distance was shown to decrease and recover after rest. However, asymmetries persisted despite rest demonstrating the plasticity of accumulative competition training stress on neuromuscular function with recovery predisposing healthy, uninjured athletes to 6.5-fold greater injury risk. Furthermore, the degradation in postural control while maintaining maximal power can in turn lead to greater injury predisposition throughout the competitive season. These findings suggest that training stress over time absent adequate rest can negatively impact neuromuscular function and increase lower extremity injury risk due to less compliant tissues (elevated passive muscle tone). In summary, left and right NCOMP/NANT asymmetries and reach distances should be considered and monitored regularly when evaluating the impact of competitive season training stress as a means to reduce injury risk.

DATA AVAILABILITY STATEMENT

The raw data supporting the conclusions of this article will be made available by the authors, without undue reservation.

ETHICS STATEMENT

The studies involving human participants were reviewed and approved by Longwood University Institutional Review Board:

HHS IRB number: IRB00008677 FWA number: FWA00019433. The patients/participants provided their written informed consent to participate in this study.

AUTHOR CONTRIBUTIONS

TP and KL: Conceptualization and formal analysis. TP: Methodology and project administration. TP, JG, and KL: Writing. TP, KL, JG, CM, and LB: Data collection. All authors have read and agreed to the published version of the manuscript.

FUNDING

This manuscript was funded through North Carolina Agricultural and Technical State University.

ACKNOWLEDGMENTS

The authors would like to thank the Longwood University Department of Athletics, particularly Coach Dyer and Stoneman. Your commitment to the completion of this study had a tremendous contribution to this project's success.

REFERENCES

American College of Sports Medicine. (2018). in *ACSM's Guidelines for Exercise Testing and Prescription,* 10th ed, eds D. Reibe, J. Ehrman, G. Liguori, and M. Magal (Philadelphia: Wolters klywer/Lippincott Willimas). Ch. 4, p. 70–94.

Bengtsson, H., Ekstrand, J., and Hägglund, M. (2013). Muscle injury rates in professional football increase with fixture congestion: an 11-year follow-up of the UEFA Champions League injury study. *Br. J. Sports Med.* 47, 743–747. doi: 10.1136/bjsports-2013-092383

Brazier, J., Maloney, S., Bishop, C., Read, P., and Turner, A. (2019). Lower extremity stiffness: considerations for testing, performance enhancement, and injury risk. *J. Strength Cond. Res.* 33, 1156–1166.

Brownstein, C. G., Dent, J. P., Parker, P., Hicks, K. M., Howatson, G., Goodall, S., et al. (2017). Etiology and recovery of neuromuscular fatigue following competitive soccer match-play. *Front. Physiol.* 8:831. doi: 10.3389/fphys.2017.00831

Buckthorpe, M., Pain, M. T. G., and Folland, J. P. (2014). Central fatigue contributes to the greater reductions in explosive than maximal strength with high-intensity fatigue. *Exp. Physiol.* 99, 964–973. doi: 10.1113/expphysiol.2013.075614

Canavan, P. K., and Vescovi, J. D. (2004). Evaluation of power prediction equations: peak vertical jumping power in women. *Med. Sci. Sports Exerc.* 36, 1589–1593. doi: 10.1249/01.MSS.0000139802.96395.AC

Caterisano, A., Decker, D., Snyder, B., Feigenbaum, M., Glass, R., House, P., et al. (2019). CSCCa and NSCA joint consensus guidelines for transition periods: safe return to training following inactivity. *Strength Cond. J.* 41, 1–23. doi: 10.1519/SSC.0000000000000477

Dubois, R., Lyons, M., Paillard, T., Maurelli, O., and Prioux, J. (2018). Influence of weekly workload on physical, biochemical, and psychological characteristics in professional rugby union players over a competative season. *J. Strength Cond. Res.* 34, 527–545.

Giles, J., Purdom, T., Levers, K., Wetzel, D., Fry, N., and Brown, L. (2017). Using lower body mobility testing to evaluate detraining effect on muslce balance and joint symmetry in division i female soccer players. *J. Strength Cond. Res.* 31, S201–S202.

Gonell, A. C., Romero, J. A. P., and Soler, L. M. (2015). Relationship between the Y balance test scores and soft tissue injury incidence in a soccer team. *Int. J. Sports Phys. Ther.* 10, 955–66.

Higashihara, A., Ono, T., Tokutake, G., Kuramochi, R., Kunita, Y., Nagano, Y., et al. (2019). Hamstring muscles' function deficit during overground sprinting in track and field athletes with a history of strain injury. *J. Sports Sci.* 37, 2744–2750. doi: 10.1080/02640414.2019.1664030

Iwamoto, Y., Takahashi, M., and Shinkoda, K. (2017). Differences of muscle co-contraction of the ankle joint between young and elderly adults during dynamic postural control at different speeds. *J. Physiol. Anthropol.* 36, 1–9. doi: 10.1186/s40101-017-0149-3

Jiang, Z., Wang, X.-F., Kisiel-Sajewicz, K., Yan, J. H., and Yue, G. H. (2012). Strengthened functional connectivity in the brain during muscle fatigue. *Neuroimage* 60, 728–737. doi: 10.1016/j.neuroimage.2011.12.013.STRENGTHENED

Jones, C. M., Griffiths, P. C., and Millalieu, S. D. (2017). Training load and fatigue marker associations with injury and illness: a systematic review of longitudinal studies. *Sport. Med.* 47, 943–974. doi: 10.1007/s40279-016-0619-5

Luedke, L. E., Geisthardt, T. W., and Rauh, M. J. (2020). Y-balance test performance does not determine non-contact lower quadrant injury in collegiate american football players. *Sports* 8:27. doi: 10.3390/sports8030027

Masi, A. T., and Hannon, J. C. (2008). Human resting muscle tone (HRMT): narrative introduction and modern concepts. *J. Bodyw. Mov. Ther.* 12, 320–332. doi: 10.1016/j.jbmt.2008.05.007

Nédélec, M., McCall, A., Carling, C., Legall, F., Berthoin, S., and Dupont, G. (2012). Recovery in soccer: part 1. *Sport. Med.* 43, 9–22. doi: 10.1007/s40279-012-0002-0

Needle, A. R., Baumeister, J., Kaminski, T. W., Higginson, J. S., Farquhar, W. B., and Swanik, C. B. (2014). Neuromechanical coupling in the regulation of muscle tone and joint stiffness. *Scand. J. Med. Sci. Sport.* 24, 737–748. doi: 10.1111/sms.12181

Plisky, P. J., Rauh, M. J., Kaminski, T. W., and Underwood, F. B. (2006). Star excursion balance test as a predictor of lower extremity injury in high school basketball players. *J. Orthop. Sport. Phys. Ther.* 36, 911–919. doi: 10.2519/jospt.2006.2244

Quagliarella, L., Sasanelli, N., Belgiovine, G., and Moretti, L. (2011). Power output estimation in vertical jump performed by young male soccer players. *J. Strength Cond. Res.* 25, 1638–1646. doi: 10.1519/JSC.0b013e3181d85a99

Satkunskiene, D., da Silva, T. M., Kamandulis, S., Leite, N. M. C., Domeika, A., Mickevicius, M., et al. (2020). Effect of training and match loads on hamstring passive stiffness in professional soccer players. *J. Musculoskelet. Neuronal Interact.* 31, 1–12.

Shaffer, S. W., Teyhen, D. S., Lorenson, C. L., Warren, R. L., Koreerat, C. M., Straseske, C. A., et al. (2013). Y-balance test: a reliability study involving multiple raters. *Mil. Med.* 178, 1264–1270. doi: 10.7205/MILMED-D-13-00222

Silva, J. R., Brito, J., Akenhead, R., and Nassis, G. P. (2016). The transition period in soccer: a window of opportunity. *Sport. Med.* 46, 305–313. doi: 10.1007/s40279-015-0419-3

Stecco, A., Stecco, C., and Raghavan, P. (2014). Peripheral mechanisms contributing to spasticity and implications for treatment. *Curr. Phys. Med. Rehabil. Rep.* 2, 121–127. doi: 10.1007/s40141-014-0052-3

Stiffler, M. R., Bell, D. R., Sanfilippo, J. L., Hetzel, S. J., Pickett, K. A., and Heiderscheit, B. C. (2017). Star excursion balance test anterior asymmetry is associated with injury status in division I collegiate athletes. *J. Orthop. Sports Phys. Ther.* 47, 339–346. doi: 10.2519/jospt.2017.6974

The National Collegiate Athletic Association (2018). *NCAA 2018-2019 Division I Manual*. Indianapolis, IN.

Thomas, K., Brownstein, C. G., Dent, J., Parker, P., Goodall, S., and Howatson, G. (2018). Neuromuscular fatigue and recovery after heavy resistance, jump, and sprint training. *Med. Sci. Sports Exerc.* 50, 2526–2535. doi: 10.1249/MSS.0000000000001733

Walker, A. J., McFadden, B. A., Sanders, D. J., Rabideau, M. M., Hofacker, M. L., and Arent, S. M. (2019). Biomarker response to a competitive season in division i female soccer players. *J. Strength Cond. Res.* 33, 2622–2628. doi: 10.1519/JSC.0000000000003264

Conflict of Interest: The authors declare that the research was conducted in the absence of any commercial or financial relationships that could be construed as a potential conflict of interest.

frontiers in Human Neuroscience

ORIGINAL RESEARCH
published: 15 March 2021
doi: 10.3389/fnhum.2021.622825

A Neuromotor to Acoustical Jaw-Tongue Projection Model With Application in Parkinson's Disease Hypokinetic Dysarthria

Andrés Gómez[1,2], Pedro Gómez[2], Daniel Palacios[2,3], Victoria Rodellar[2], Víctor Nieto[2], Agustín Álvarez[2] and Athanasios Tsanas[1]*

[1] Old Medical School, Medical School, Usher Institute, University of Edinburgh, Edinburgh, United Kingdom, [2] NeuSpeLab, Center for Biomedical Technology, Universidad Politécnica de Madrid, Madrid, Spain, [3] Escuela Técnica Superior de Ingeniería Informática–Universidad Rey Juan Carlos, Móstoles, Spain

OPEN ACCESS

Edited by:
Yury Ivanenko, Santa Lucia Foundation (IRCCS), Italy

Reviewed by:
Jan Mucha, Brno University of Technology, Czechia
Juan Camilo Vasquez-Correa, University of Erlangen Nuremberg, Germany

***Correspondence:**
Pedro Gómez
pedro.gomezv@upm.es

Specialty section:
This article was submitted to Motor Neuroscience, a section of the journal Frontiers in Human Neuroscience

Received: *29 October 2020*
Accepted: *17 February 2021*
Published: *15 March 2021*

Citation:
Gómez A, Gómez P, Palacios D, Rodellar V, Nieto V, Álvarez A and Tsanas A (2021) A Neuromotor to Acoustical Jaw-Tongue Projection Model With Application in Parkinson's Disease Hypokinetic Dysarthria. Front. Hum. Neurosci. 15:622825. doi: 10.3389/fnhum.2021.622825

Aim: The present work proposes the study of the neuromotor activity of the masseter-jaw-tongue articulation during diadochokinetic exercising to establish functional statistical relationships between surface Electromyography (sEMG), 3D Accelerometry (3DAcc), and acoustic features extracted from the speech signal, with the aim of characterizing Hypokinetic Dysarthria (HD). A database of multi-trait signals of recordings from an age-matched control and PD participants are used in the experimental study.

Hypothesis: The main assumption is that information between sEMG and 3D acceleration, and acoustic features may be quantified using linear regression methods.

Methods: Recordings from a cohort of eight age-matched control participants (4 males, 4 females) and eight PD participants (4 males, 4 females) were collected during the utterance of a diadochokinetic exercise (the fast repetition of diphthong [al]). The dynamic and acoustic absolute kinematic velocities produced during the exercises were estimated by acoustic filter inversion and numerical integration and differentiation of the speech signal. The amplitude distributions of the absolute kinematic and acoustic velocities (AKV and AFV) are estimated to allow comparisons in terms of Mutual Information.

Results: The regression results show the relationships between sEMG and dynamic and acoustic estimates. The projection methodology may help in understanding the basic neuromotor muscle activity regarding neurodegenerative speech in remote monitoring neuromotor and neurocognitive diseases using speech as the vehicular tool, and in the study of other speech-related disorders. The study also showed strong and significant cross-correlations between articulation kinematics, both for the control and the PD

cohorts. The absolute kinematic variables presents an observable difference for the PD participants compared to the control group.

Conclusion: Kinematic distributions derived from acoustic analysis may be useful biomarkers toward characterizing HD in neuromotor disorders providing new insights into PD.

Keywords: speech kinematics, surface electromyography, neuromechanics, hypokinetic dysarthria, neuromotor disorders

INTRODUCTION

Background

Speech production is a dynamic neuromechanical activity which involves cognitive and neuromotor resources of extreme complexity, and which is not yet well understood (Duffy, 2013). The natural way in which it is acquired and used shades the sophisticated processes which are placed into work during its normal expression. Speech is instantiated in the linguistic neuromotor cortex (Demonet et al., 2005), and its execution demands the concourse of cognitive, neuromotor, neuromuscular, and musculoskeletal processes (Duffy, 2013). Through speech, thoughts and emotions are projected to the knowledge of others by cognitive-linguistic messages. These are programmed for their neuromotor expression by the activation, time-alignment and sensorimotor projection, extension, and strength of a large amount of diverse muscles and associated biomechanical structures. The neuromotor areas from the Central Nervous System (CNS), where planning, programming and control is provided are responsible of activating the respiratory, phonatory and articulatory muscular structures innervated by the Peripheral Nervous System (PNS), see Kandel et al. (2013). The resulting speech is a sequence of acoustic interactions between the glottal source signal and the vocal tract cavities, both driven by neuromotor impulses. This imprint conveys the cognitive-linguistic message. The alteration or dysfunction of any key vocal production mechanisms will result in a deficient production of speech known as a speech disorder. Among them, Motor Speech Disorders (MSD) are the result of dysfunctional neurologic structures involved in the planning, sequencing, activating, and monitoring the neuromuscular structures responsible of speech sound production, modulation and projection. One of the most active neuromuscular structures involved in speech production is the masseter-jaw-tongue complex, including part of the facial muscles and tissues attached to the mandible (Duffy, 2013). This structure is responsible for the production of open or closed, and front or back phonations perceptible in vowels and vowel-related sounds (Greenberg, 2004). Specifically, the quasi-steady positioning of this structure (for more than 30–50 ms) gives rise to vowel-like phonations, whereas its rapid movement is responsible for the acoustical representation of many consonant-like sounds. Neuromotor diseases affect the functional operation of this structure, and its central role in speech articulation suggests it could likely reflect key pathological changes reflected the neuromotor behavior. A well-known indicative neuromotor disorder known for its prevalence and social impact is Parkinson's Disease (PD), also known as shaking palsy. It is a well-known neurodegenerative disorder since it was first described by J. Parkinson (2002). Its etiology is unclear in most of the cases, but evidence is accumulated in the sense that it may be due to different dysfunctions taking place in the fine control of muscular actions in the interplay of the brain subsystems responsible of musculoskeletal control, as the hypothalamus, the cerebellum, the primary and secondary neuromotor control areas, and the frontal lobes (Brown et al., 2009). A compelling and comprehensive overall view is given in Duffy (2013): "*The motor system is present at all of the major anatomic levels of the nervous system and is directly responsible for all motor activity involving . . . to the planning, control, and execution of voluntary movement, including speech.*" It is a well-established fact that PD causes considerable alterations in speech and phonation (Ricciardi et al., 2016; Brabenec et al., 2017). Broadly speaking, speech alterations may be classified as dysphonia (on voice production), dysarthria (on speech articulation), dysprosody (on the fundamental frequency sequence), and dysfluency (on the rhythm and speech sequence of intersyllabic and intersegment blocks). These alterations are jointly referred to as Hypokinetic Dysarthria (HD). Harel B. et al. (2004) give a summary of the symptoms associated with HD "*Hypokinetic dysarthria, a speech disorder characterized by indistinctness of articulation, weakness of voice, lack of inflection, burst of speech, and hesitations and stoppages, is an integral part of the motoric changes in PD.*" In this same sense, there is "*compelling evidence to suggest that speech can help quantify not only motor symptoms... but generalized diverse symptoms in PD*" (Tsanas, 2012). Godino et al. (2017) stress the fact that "*The low levels of dopamine that appear in patients with PD lead to dysfunctions of the basal ganglia. . . These deficits negatively affect the three main anatomic subsystems involved in the speech production: respiration, phonation and articulation.*" A good description of the neuromotor systems involved in speech production, and how they may be affected by neurodegenerative diseases is to be found in Duffy (2013). Therefore, the search of neuromotor degenerative biomarkers in speech is to be concentrated on phonation (study of the glottal signals in terms of distortion and biomechanics), on speech articulation (study of acoustic and biomechanic clues as formants and jaw-tongue kinematics), on the prosodic flow (concentrated in the time evolution of the fundamental frequency and speech energy stability), and on fluency (syllabic and intersyllabic intervals, duration, stability, and fluctuation of the speaking rate). This is well documented in the work of Mekyska et al. (2015).

Moreover, speech can be used to investigate the nature and extent of vocal impairment in individuals who are at risk of developing PD and can provide a crucial opportunity to intervene in prodromal stages. For example, we have recently demonstrated some very compelling findings when comparing speech signals between a control group, people diagnosed with Sleep Behavior Disorder (SBD), which is among the strongest known predictors of PD risk, and a PD cohort (Arora et al., 2021). Furthermore, we have demonstrated that we can accurately telemonitor PD symptom severity using speech signals collected over the standard telephone network, thus alleviating the need for frequent physical patient visits to the clinic (Tsanas et al., 2021). The main compelling facts favoring speech-based PD biomarkers are the low cost of the required equipment, smart-phones and tablets being increasingly affordable and generally accessible devices, and the contact-less factor, which is particularly useful to facilitate remote studies. Summarizing, the acoustic markers induced by HD in PD speech allows to conclude that speech analysis might become a non-invasive and cost-effective tool to characterize and monitor PD. The role of speech as a possible biomarker in PD detection is well established in the state of the art research literature, with many studies discussing speech-based PD features sensitive to HD. In the present study the focus is placed on the study of acoustic and biomechanical clues, as formants, and jaw-tongue kinematics.

Previous Work

The number of studies focusing on the field of speech and neurodegenerative disorders has been consistently growing over the last 10–15 years, and for the sake of brevity only the most relevant ones will be mentioned in what follows. Brown et al. (2009) give a good description of the relationship between the premotor and motor cortex areas with speech production. Good descriptions of the neuromotor system of the phonation and articulation including neuromotor to muscular pathways affecting the larynx, pharynx, oral, and nasal cavities may be found in Jürgens (2002). Bourchard et al. (2016) offer a description of the relationship between simultaneously recorded neural activity and the kinematics of the lips, jaw, tongue, and larynx. An interesting review on neurophysiology of language may be found in Demonet et al. (2005). Relevant information on the neuromotor pathways on vocal control can be found in Goodman and Hasson (2017). A classical and detailed biomechanical description of tongue movement control may be found in Sanguinetti et al. (1997). The influence of PD on facial muscle sEMG is given in Wu et al. (2014), and for the articulatory and acoustic changes due to Amyotrophic Lateral Sclerosis (ALS) see Mefferd and Dietrich (2020). Relating acoustic features to articulation gesture the reader may see, Gerard et al. (2006), Buchaillard et al. (2009); Dromey et al. (2013). On diphthong articulation kinematics see Tasko and Greilick (2010); for tongue positioning during vowel articulation in speakers with dysartria see Yunusova et al. (2011); for tongue movements in speakers with ALS see Yunusova et al. (2012). For the use of speech signals from longitudinal assessment of PD we refer to Tsanas et al. (2011) and Tsanas (2012), and the specific ones by Green et al. (2013); Sapir (2014), Mekyska et al. (2015), or Brabenec et al. (2017). On PD and multiple sclerosis see Tjaden et al. (2013), for vowel articulation positions as a marker of neurodegenerative progress see Skodda et al. (2012).

Objectives

The present study builds on previous work to characterize the relationship between acoustic, 3D accelerometry traces, and electromyographical correlates of speech, in relation with the jaw-tongue structure when carrying on diadochokinetic exercises of clinical interest in neuromotor degenerative disorders as PD (Gómez et al., 2019a,b). We have three primary objectives in the study. Firstly, it is focused to evaluate the functional relationship between neuromotor action in the masseter derived from sEMG and 3Dacc with respect to the acoustic outcomes measured by the two first formants on signals produced both by male and female controls and PD participants exercising on a specific voiced diadochokinetic utterance (repeated sequence of [aI], according to the International Phonetic Alphabet, IPA, 2005). It is assumed that cross-correlations between sEMG, 3D acceleration, and acoustic features may help in determining the optimal time-delays to estimate the weights of projection models by linear regression methods. Secondly, we aim to explore the possibility of establishing inverse relationships between acoustic features and neuromotor activity estimated from sEMG measured on the masseter. Thirdly, we aim to establish whether there are notable differences between controls and PD participants in terms of the absolute kinematic behavior derived from the diadochokinetic exercise from the repetition of [aI] to define new HD biomarkers.

MATERIALS AND METHODS

Speech Neuromechanics

Speech is a complex activity which involves the coordinated joint action of respiration, phonation and articulation muscles, controlled by different cranial nerves (V, VII, IX, X, and XII) and phrenic nerves from the spinal cord, which are responsible for producing speech (Duffy, 2013). Motor activity related to speech is expressed by the cortical areas for motor speech planning and programming of the Central Nervous System (CNS) in Brodmann Area 4 (Primary Motor Cortex: PMC) located in the dorsal portion of the frontal lobe (see **Figure 1**). The programmed activity is transferred to the Peripheral Nervous System (PMS) by connections from the PMC, working in association with other motor areas (premotor cortex, supplementary motor area, posterior parietal cortex, and other subcortical brain regions, which play a role on motor planning and execution). The Upper Motor Neurons (UMNs) are neurons in the PMC, which together with other cortical areas connect with the Lower Motor Neurons (LMNs) in the PMS by the corticobulbar and corticospinal tracts. This is known as the direct pathway. LMNs are alpha-type motor neurons whose axons directly activate the muscles. The LMN and the muscle fibers it activates is known as the Motor Unit (MU). The MUs activating a given muscle, are known as the Final Common Pathways (FCPs). In the case of the masseter (the subject of the present study), the FCPs are grouped in

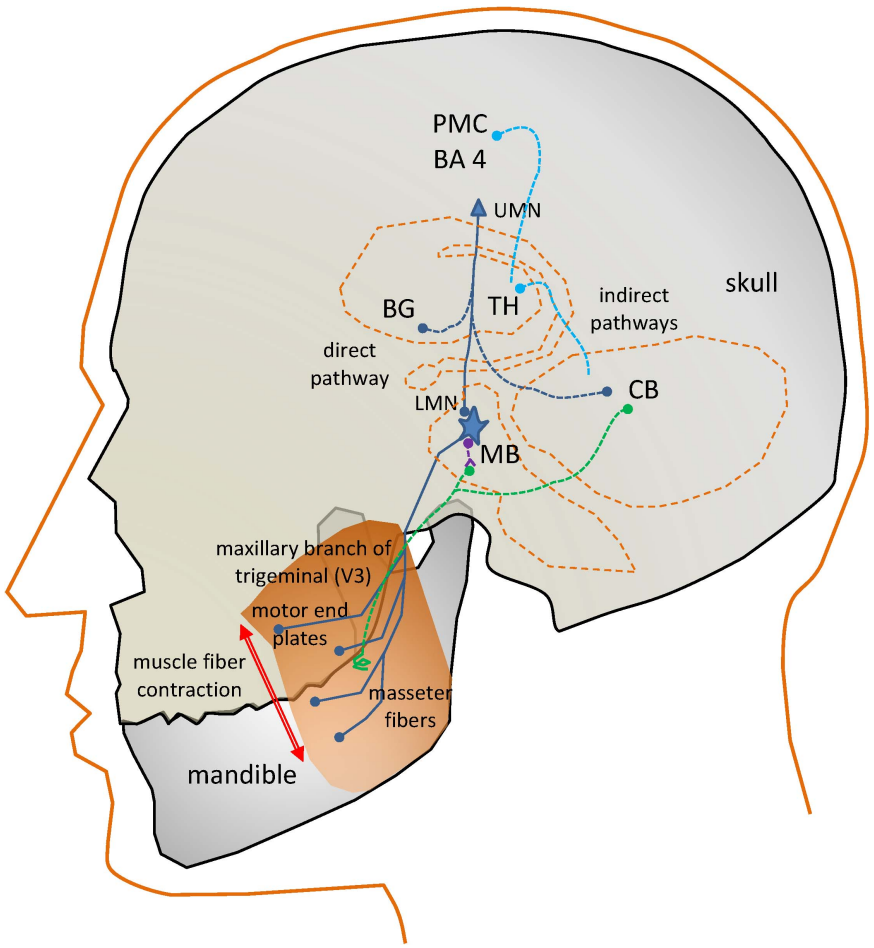

FIGURE 1 | Simplified view of the neural circuits involved in the action of the masseter neuromotor units. PM: Pre-motor Cortex (BA4, Brodmann's Area 4); UMN, Upper Motor Neuron; BG, Basal Ganglia; TH, Thalamus; CB, Cerebellum; LMN, Lower Motor Neuron; MB, Midbrain; dark blue, direct and final common pathways; light blue, indirect control pathways from CB and BG; green, sensory pathways; purple, inhibitory pathways.

the trigeminal maxillary branch, the third subdivision of the cranial nerve V (V3).

In the case of interest for the present study, the motor end plates of the FCPs innervate the masseter fibers producing the muscle contraction. The masseter activation is induced as well by indirect pathways. The fine control of a muscle movement requires some kind of feedback. This is provided by sensory pathways (in green) consisting in neurons activated by spindles (terminal sensors detecting fiber stretching) attached to the muscles, providing proprioceptive sensing to the LMNs in two ways. A direct feedback loop is provided by inhibitory interneurons (in purple). A more complex feedback loop connects sensor units with the Basal Ganglia (BG) and the Cerebellum (CB). These structures serve feedback information to the motor and frontal cortices, as well as to the LMN (blue lines). The BG control circuit assists the PMC in accurate and fine motor speech programming. The CB control circuit coordinates PMC motor planning from proprioceptive information.

Motor speech disorders are produced by specific problems affecting some of the described direct or indirect pathways of activation, or the muscle fibers. These disorders are commonly referred to as dysarthrias. In the case of PD, the speech disorder is known as HD, related with the pathological behavior of the complex BG control circuit. It will affect any or all the mentioned systems responsible for the neuromechanical control of speech: respiration, phonation, and articulation. The term "hypokinetic" refers to weak small range and rigid movement, giving the impression of flat, soft, and expressionless speech (Duffy, 2013). The activity of the BG control circuit is inhibitory on the PMC areas to modulate cortical activity. An excessive inhibition may result in HD. Most motor problems related with the BG motor circuit have to see with neurotransmitters. Specifically, dopaminergic deficits due to the progressive death of dopaminergic neurons in the substantia nigra *pars compacta* (located at the MB) are the main reason behind PD neuromotor symptoms: "*The substantia nigra is the origin of the nigrostriatal pathway, which travels to various structures within the basal ganglia. . . The dopamine deficiency in this nigrostriatal pathway and the basal ganglia account for most of the typical features of PD. Once the brain is no longer able to compensate for this*

dopamine loss, there are a number of effects which can occur. Typical symptoms include muscle rigidity, akinesia, bradykinesia, and tremor. . ." (Goberman and Coelho, 2002), more specifically "*The essential neuropathological changes in PD are a loss of melanine-containing dopaminergic neurons in the substantia nigra pars compacta. . . This results in a dysfunction of the basal ganglia circuitry, which is an integral part of cortico-basal ganglia-cortical loops that mediate motoric and cognitive functions*" (Harel B.T. et al., 2004).

In the present study, a biomechanical system of the jaw-tongue will be used, which may be modeled to estimate the neuromotor behavior of the system, and provide specific markers of proper or improper neuromotor activity. The selection of the masseter as the target muscle obey to the following reasons: it is a powerful muscle developing a strong sEMG when contracting, it is accessible (beneath the caudal section of the cheek), it may modify strongly the oral cavity when contracting or relaxing leaving a clear acoustic signature in formants, and its biomechanical activity is well understood. The study of the masseter neuromechanics is based on the electrical, dynamic, and kinematic activity of the muscle as a functional structure.

A Model Mediating Jaw Kinematics on Acoustic Features

The present study builds on a previous masseter-jaw-tongue biomechanical model (Gómez et al., 2019b), where the active contribution of other muscles (styloglossus, geniohyoid, intrinsic glossal, etc.) has not been taken into account, and the passive contribution of other tissues, as the oro-facial substructures are implicitly included in the inertial moment. The articulation gestures based on the masseter-jaw-tongue structure as considered in the present study are described as follows: the jaw (J) is fixed to the skull bone at fulcrum (F) as in a third-class lever system. The tongue (T) is a complex muscular and vascular structure supported on the jaw and the hyoid bone. Some other extrinsic muscles fix it to the cranial structure (mainly the styloglossus and geniohyoid). These muscles and the tissues surrounding the jaw will be considered part of the lumped equivalent of masses, forces and moments at the reference point of the jaw-tongue system P_{rJT}, defined at $\{x_r,y_r\}$, where forces acting on the system induce movements in the sagittal plane (x: horizontal, or rostral-caudal, y: vertical, or dorsal-ventral); these forces are f_m (exerted by the masseter), f_{sg} (by the styloglossus), f_{gi} (by the intrinsic glossus), f_h (by the geniohyoid), and f_g (gravity). Consequently, the P_{rJT} may be defined as a hypothetical point in the sagittal plane (x: caudal-rostral; y: dorsal-ventral) with static coordinates $\{x_r, y_r\}$ where the sum of dynamic and inertial forces is null. The force exerted by the masseter f_m will pull up the low mandible acting as a third-order lever with fulcrum at the maxillary attachment (F). In the present study we will not consider extrinsic actions other than by geniohyoid, and by the intrinsic glossus system, therefore, the only forces to be considered contributing to the lever momentum will be f_m, f_h, and f_g. The kinematic displacements experienced by P_{rJT} are given as $\{\Delta x_r \Delta y_r\}$. Lateral movements orthogonal to the sagittal plane are assumed small enough not to be considered (system with only two degrees of freedom). The functioning of the speech articulation neuromotor and biomechanical system is ilustrated **Figure 2**. Speech articulation is defined by the configuration of the articulation organs, such as the mandible, tongue, lips, and velo-pharyngeal tissues, among others of lesser interest for the present study (Dromey et al., 2013; Cattaneo and Pavesi, 2014; Whitfield and Goberman, 2014). Therefore, vowel articulation has been traditionally described in terms of the open-close gesture (also low-high attending to lower jaw position relative to upper jaw), the front-back gesture, and round-oval configurations (Dromey et al., 2013). These gestures determine certain acoustic features known as formants, which are defined as frequency positions where the harmonic structure of the vowel is especially enhanced, by means of the resonances of the Oro-Naso-Pharyngeal Tract (ONPT, see **Figure 2**). The open-close gesture, mainly dominated by the jaw, is affecting the first formant F_1. Pulling up the jaw by the masseter against gravity (f_m−f_g) is the dominant gesture in the phonation of high vowels as [i:] and [u:], whereas depressing the jaw under the force of gravity and the geniohyoid muscle action (f_h+f_g) is the gesture to phonate low vowel as [a:]. The front-back gesture is controlled also by the jaw position, although in high vowels like [i:] and [u:] the tongue position affects mainly the second formant F_2 (pushing the tongue forward is the gesture for [i:], pulling it back results in [u:]). Therefore, the articulation gesture of the jaw may be studied to relate articulatory gestures and acoustic features as the first two formants (F_1, F_2), as proposed in the Articulation Kinematic Model (AKM) shown in **Figure 2C**. The study is based on the dynamic tracking of the kinematic activity of the jaw-tongue reference point (P_{rJT}) by means of 3D accelerometry (3Dacc).

The articulation dynamics foresees that the resonant properties of the ONPT will change in time regarding the position of the P_{rJT} under the action of the forces mentioned, modifying, and producing dynamic changes in the first two formants$\{F_1, F_2\}$. From the perspective of speech production, the general problem of acoustic to articulatory inversion may be presented in general terms as the mapping A(**s**) = **F** (Ouni and Laprie, 2005), where **s** is the articulatory vector which presents the general shape of the vocal tract at a specific time instant for instance, the k parameters of an articulatory synthesis model, and **F** is the acoustics vector (typically the first m formants). A: **s**→**g** is a non-linear many-to-one mapping transforming the articulatory feature space **s** to the acoustic feature space **g**. In this sense, the inverse mapping presents several important problems: on the one hand the mapping A is non-linear, on the other hand, it is a many-to-one (Qin and Carreira-Perpiñán, 2007). Besides, **g** is an approximation to the values of the true resonances of the vocal tract, obtained usually from Linear Prediction Inverse Filtering (LPIF), and therefore, subject to strong assumptions on the representation of the real oro-naso-pharyngeal tract (ONPT) by a concatenation of rigid-wall cylindrical-tube sections on a straightened medial axis, the number of sections, depending on the sampling rate and the order of the LPIF (Deller et al., 1993). On the other hand, the feature vector **s** will depend on the specific generative model used. In many studies the seven following features are used: jaw position (high-low),

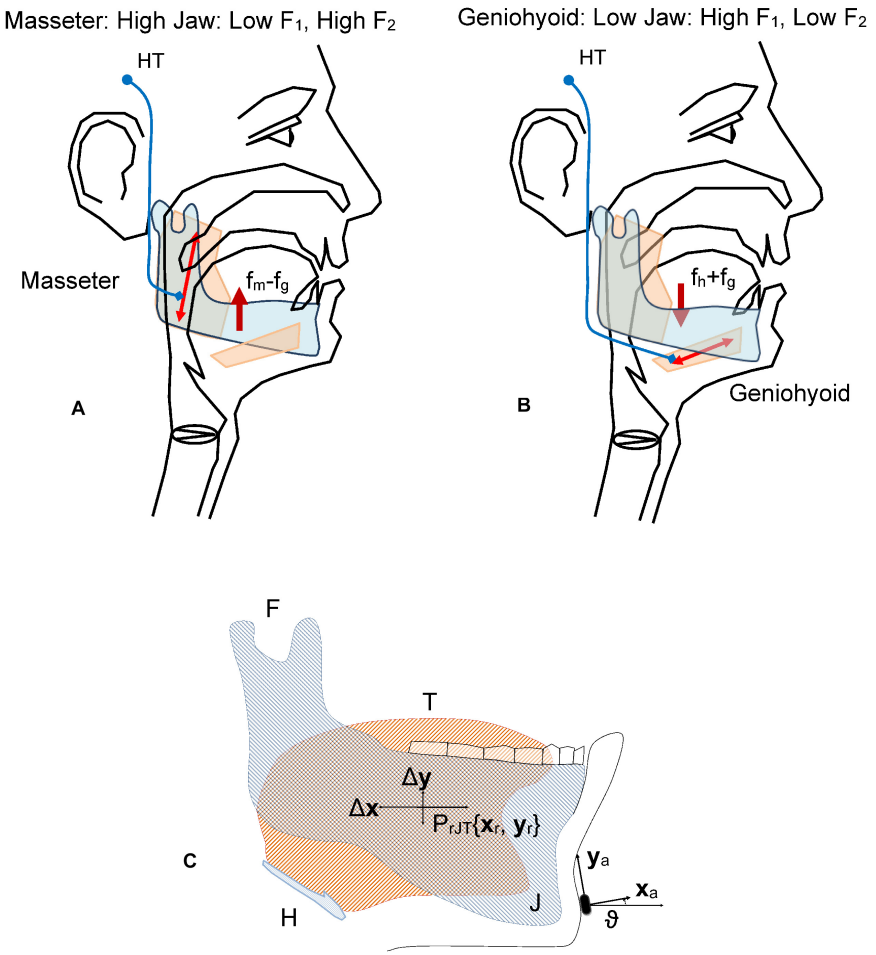

FIGURE 2 | Fundamentals of the jaw-tongue articulation. **(A)** Upper pulling (levator active against gravity, depressor inactive) As the jaw is high, the first formant F1 is low. **(B)** Lower pulling (depressor and gravity active, levator inactive) As the jaw is low the first formant is high. **(C)** Jaw-Tongue Biomechanical System. The jaw bone is represented in light gray; the tongue structure is represented in light orange. The point PrJT given by {xr, yr} is the reference point of the biomechanical system. HT, Hypothalamus; fm, force exerted by the masseter; fg, gravity force; fh, force exerted by the geniohyoid; F, attach joint of the jaw to the skull; H, hyoid bone; T, tongue (in orange); J, jaw (in gray).

tongue dorsum position (backward-forward), tongue dorsum shape (rounded-unrounded), tongue tip shape (up-down), lip height (open-close), lip protrusion (forward-backward), and larynx height (high-low). The solutions proposed are based on reproducing a reduced articulatory feature space **s** which may generate an approximation to the acoustic feature vector **g**, following an optimization process reducing the cost function $|\mathbf{g}\text{-}\mathbf{g}|$ to a minimum value. Several approaches are used such as codebook-based inversion, articulatory modeling, articulatory modeling, and statistical mapping (Sivaraman et al., 2019). The present study proposes a mapping model which is a simplification of the general one following several important assumptions:

- Only the vertical and horizontal components of the jaw-tongue position (high-low) are considered from the set of articulatory features s. These features are estimated using a 3D accelerometer fixed to the participant's chin. A transformation of coordinates from the 3D accelerometer to absolute ones in the sagittal plane is used (rotation and projection).
- The set of acoustic features is reduced to the first two formants F_1 and F_2.
- A kinematic-acoustic variable estimated from formant acoustics (AFV).
- A kinematic-dynamic variable estimated from jaw kinematics (AKV).
- A non-linear model projecting acoustic features to a kinematic-acoustic variable is proposed
- A linear model mapping acoustic features to dynamic variables is proposed.

Having these assumptions in mind, the present study is focused on the evaluation of a linear model on data produced by control and PD participants in the fast and repeated utterance of the diphthong [aI]. The reasons for selecting such

a diadochokinetic exercise are that, on the one hand this pattern ensures that the jaw-tongue system moves through a range where linearity governs the link between articulation and sound features "*For /aI/ the strength of the acoustic-kinematic association was robust across movements that differed in duration or displacements*" (Dromey et al., 2013). On the other hand, this exercise is mainly governed by the dynamic activity of the masseter, a very accessible facial muscle producing good sEMG recordings. Another important fact is that this exercise does not involve lip protrusion or rounding changes (Dromey et al., 2013). Therefore, the association between the jaw-tongue reference point movement may be associated with the first two formants in a one-to-one mapping. The complementary use of a 3D accelerometer on the jaw helps in providing a second assessment method to avail this association by an alternative acoustic-to-dynamic mapping.

The proposed model for projecting articulation kinematics to changes of the first two formants F_1 and F_2 can be described as:

$$\begin{bmatrix} \triangle F_1(t) \\ \triangle F_2(t) \end{bmatrix} = \begin{bmatrix} a_{11} & a_{12} \\ a_{21} & a_{22} \end{bmatrix} \begin{bmatrix} \triangle x_{\mathrm{r}}(t) \\ \triangle y_{\mathrm{r}}(t) \end{bmatrix} \tag{1}$$

where $\{a_{ij}\}$ are the parameters relating the dynamic changes of the formant values with the oscillations of the P_{rJT}. The utility of these relations is conditioned by the possibility of estimating the set of parameters $\{a_{ij}\}$ from the signals produced by a 3D accelerometer fixed on the chin of a participant under test, as shown in **Figure 2C**. The accelerometer reference axes are the chin-normal ($\boldsymbol{x}_a$) and tangential ($\boldsymbol{y}_a$), which will be changing following jaw displacements. The accelerometry signals may be transformed to the reference coordinates $\{x_r, y_r\}$ by means of a rotation in terms of ϑ, the angle between the axes $\boldsymbol{x}_a$ and $\boldsymbol{x}_r$. The set of parameters $\{a_{ij}\}$ relating acoustic features and articulation dynamics may be estimated by regression-based methods using specific repetitive diadochokinetic exercises, such as the repetition of the gliding sequence [. . .aIa. . .] as it will be shown in what follows. Assuming that (1) is time-invariant and invertible we would have:

$$\begin{bmatrix} dx_{\mathrm{r}}(t)/dt \\ dy_{\mathrm{r}}(t)/dt \end{bmatrix} = \begin{bmatrix} w_{11} & w_{12} \\ w_{21} & w_{22} \end{bmatrix} \begin{bmatrix} \partial F_1(t)/\partial t \\ \partial F_2(t)/\partial t \end{bmatrix} \tag{2}$$

where $\{w_{ij}\}$ are the coefficients of the transference matrix inverse $\boldsymbol{W} = \boldsymbol{A}^{-1}$:

$$\begin{bmatrix} w_{11} & w_{12} \\ w_{21} & w_{22} \end{bmatrix} = \begin{bmatrix} a_{11} & a_{12} \\ a_{21} & a_{22} \end{bmatrix}^{-1} \tag{3}$$

With these expressions in mind it will be possible to define the Absolute Formant Velocity (AFV) of the reference point (P_{rJT}) as:

$$|v_{\mathrm{f}}(t)| = \left[H_1 \left(\frac{dF_1(t)}{dt} \right)^2 + H_2 \left(\frac{dF_2(t)}{dt} \right)^2 + H_{12} \frac{dF_1(t)}{dt} \frac{dF_2(t)}{dt} \right]^{1/2} \tag{4}$$

where H_1, H_2 and H_{12} are quadratic forms of $\{w_{ij}\}$ (see Gómez et al., 2019b). Reliable estimates for $\{w_{ij}\}$ may be obtained from articulations involving changes in the positions of the reference point showing predictable dynamic changes, as in this and other diadochokinetic exercises. The AFV may be estimated in the following steps:

- Speech $s(t)$ is sampled at 50 kHz and 16 bits, down-sampled to 8 kHz and inverse filtered (Alku et al., 2019) to obtain a K-th order adaptive prediction vector $\{b_i\}$ representing the inverse vocal tract.
- The first two formants F_1 and F_2 are estimated by detecting the zeros of $B(z)$ in the complex plane:

$$B(z = z_{\mathrm{i}}) = 1 - \sum_{\mathrm{i}=1}^{\mathrm{k}} b_{\mathrm{i}} z_{\mathrm{i}}^{-\mathrm{i}} = 0;$$
$$z_{\mathrm{i}} = r_{\mathrm{i}} e^{j\varphi_{\mathrm{i}}};\ F_{\mathrm{i}} = \varphi_{\mathrm{i}}/(2\pi\tau);\ \varphi_{\mathrm{i}} \geq 0 \tag{5}$$

τ being the sampling rate in the time domain.

Similarly, an Absolute Kinematic Velocity (AKV) of the reference point may be derived from the normal and tangential acceleration components on the sagittal plane $\{a_{Xa}(t),\ a_{Ya}(t)\}$ measured directly by the 3D accelerometer as:

$$|v_{\mathrm{d}}(t)| = \left[\left(\int_{\zeta=0}^{t} a_{\mathrm{xd}}(\zeta)\, d\zeta \right)^2 + \left(\int_{\zeta=0}^{t} a_{\mathrm{yd}}(\zeta)\, d\zeta \right)^2 \right]^{1/2} \tag{6}$$

where $\{a_{xd}(t),\ a_{yd}(t)\}$ are the acceleration components in the sagittal plane rotated from the measurements recorded on the native accelerometer axes $\{a_{Xa}(t), a_{Ya}(t)\}$.

The estimation procedure of the AKV would involve the following steps:

- The acceleration component means $\{\hat{a}_{Xa}(t,W), \hat{a}_{Ya}(t,W)\}$ are used to estimate the 3D accelerometer angle ϑ on short time windows (W) to preserve time invariance. The acceleration components are rotated to the reference axes to produce $\{a_{xd}(t), a_{yd}(t)\}$.
- Rotated acceleration components are used to estimate the AKV following (6).

Distributions of Absolute Velocity Values

The probability distributions of both AFV and AKV from (4) and (6) are very relevant statistical descriptors of articulation kinematics. They can be directly estimated from their normalized amplitude histograms over bins between 0 and 20 (cm.s^{-1}) as:

- The speech signal is low-pass filtered to 4 kHz (antialiasing) and downsampled to 8 kHz. The 3D acceleration signals are low-pass filtered to 250 Hz and downsampled to 500 Hz.
- The first two formants are estimated every 2 ms on short time windows of 64 ms, equivalent to 512 samples with an overlap of 97% (62/64).
- The weights $\{w_{ij}\}$ are estimated from linear regression between dynamic displacements $\{\Delta x_r,\ \Delta y_r\}$ and formant deviations $\{\Delta F_1,\ \Delta F_2\}$. The quadratic coefficients H_1, H_2, and H_{12} are calculated from $\{w_{ij}\}$.
- The AFV ($|\ v_f(t)|$) is estimated from (4).

- The accelerations $\{a_{xd}(t), a_{yd}(t)\}$ are obtained by rotating the signals recorded by the 3D accelerometer downsampled to 500 Hz and integrated numerically. Detrend filtering must be used to avoid integration drifts.
- The AKV ($|\ v_d(t)|$) is estimated from (6).
- An N-bin histogram of counts by amplitudes is built from each participant's AFV and AKV. The interval covered for speeds is [0, $|\ v_r|_{max}$], with $|\ v_r|_{max}$ = 20 cm.s^{-1}, and N = 100, therefore each bin size is Δb_k = [$|\ v_r|_{max}$/N] = 0.2 cm.s^{-1} wide.
- The following histogram of counts is built for each bin $b_k = k \bullet \Delta b_k$:
  if $b_{k-1} \leq |\ v_r(t)| < b_k$ *then* $c_k = c_{k+1}$
  c_k being the number of counts for bin b_k.
- Count histograms c_k ($0 \leq k \leq$ N) are normalized to their total number of counts $C_T = \Sigma b_k$ ($0 \leq k \leq$ N), therefore they could be considered estimators of probability density functions $p_k = c_k/C_T$.

Thence $p(|\ v_{rk}|) = p_k$ will be an estimate of the AFV and AKV probability density functions. It has been proven that this feature is relevant in separating dysarthric from normative speech (Gómez et al., 2017).

Entropy-Based Detection

The AFV and AKV distribution show a two-degrees of freedom χ^2 behavior, therefore they are an estimation of the speaker's jaw mobility in terms of similarity with a certain "articulation temperature." The probability distributions may be used to estimate the divergence between utterances from different speakers in terms of entropy based metrics (Cover and Thomas, 2006) between two probability distributions (i, j) in terms Jensen-Shannon's Divergence (JSD) as:

$$D_{\mathrm{JSij}}\left\{p_{\mathrm{i}}\left(|v_{\mathrm{r}}|\right), p_{\mathrm{j}}\left(|v_{\mathrm{r}}|\right)\right\} = \frac{1}{2}D_{\mathrm{KL}}\left\{p_{\mathrm{i}}, p_{\mathrm{m}}\right\} + \frac{1}{2}D_{\mathrm{KL}}\left\{p_{\mathrm{j}}, p_{\mathrm{m}}\right\};$$
$$p_{\mathrm{m}} = \frac{p_{\mathrm{i}} + p_{\mathrm{j}}}{2} \tag{7}$$

where $p_i(v_r)$ and $p_j(v_r)$ are two distributions (either AFV or AKV) from two different participants, and D_{KL} is Kullback-Leibler's Divergence (Cover and Thomas, 2006):

$$D_{\mathrm{KLij}} = D_{\mathrm{KL}}\left\{p_{\mathrm{i}}\left(|v_{\mathrm{r}}|\right), p_{\mathrm{j}}\left(|v_{\mathrm{r}}|\right)\right\} = -\int_{\zeta=0}^{\infty} p_{\mathrm{i}}(\zeta) log\left[\frac{p_{\mathrm{i}}(\zeta)}{p_j(\zeta)}\right] d\zeta \tag{8}$$

The main advantage of JSD is that it is bounded and symmetrical ($D_{JSij} = D_{JSji}$). The AFV and AKV estimates from (4) and (6) and their normalized histograms were evaluated as described before. Two sets of distributions were produced, respectively, for the control participants (CP: p_{CP}) and the PD participants (PD: p_{PP}}. The average of the p_{CP} distributions was used as the control reference:

$$p_{\mathrm{CP}} = \frac{1}{k_{\mathrm{C}}}\sum_{\mathrm{i}=1}^{k_{\mathrm{C}}} p_{\mathrm{CPi}} \tag{9}$$

where k_C is the number of participants in the CP set separately for AFV and for AKV. The JSD between each participant in the sets CP and PD was estimated with respect to the average p_{CP}. Therefore, the divergences used in the present study are:

$$D_{\mathrm{JSf_{i\in CP}}} = D_{\mathrm{JS}}\left\{p_{\mathrm{if}}, p_{\mathrm{CPf}}\right\};\ D_{\mathrm{JSf_{i\in PD}}} = D_{\mathrm{JS}}\left\{p_{\mathrm{if}}, p_{\mathrm{CPf}}\right\};$$

$$D_{\mathrm{JSd_{i\in CP}}} = D_{\mathrm{JS}}\left\{p_{\mathrm{id}}, p_{\mathrm{CPd}}\right\};\ D_{\mathrm{JSd_{i\in PD}}} = D_{\mathrm{JS}}\left\{p_{\mathrm{id}}, p_{\mathrm{CPd}}\right\} \tag{10}$$

where the suffixes f and d specify JSDs estimated from AFV or AKV, respectively.

Masseter sEMG

The selection of the masseter as the reference muscle in studying the relationship of neuromotor activity and acoustic speech dynamics is based on the following reasons:

- The masseter changes the position of the jaw-tongue structure toward high and slightly forward positions when activated. Correspondingly, the vocal tract is modified from low-mid to high-front vocal resonances (Dromey et al., 2013). The relationship between neuromuscular action and acoustics seems to be quite direct.
- The masseter is a powerful muscle, its neuromotor activity induces strong sEMG signals on the back lower part of the cheek. Signal recording is feasible and very productive.
- The neuromotor pathways from the midbrain to the masseter are short and fast, the delays due to impulse propagation on the neural pathways, and the motor unit action potentials are small. This allows producing faster oscillation movements than other larger and more distant muscles, extending the high frequency limits of voluntary and involuntary tremor.

The procedure to record sEMG activity on the masseter is represented in **Figure 3** following the works of De Luca (1997) and Castroflorio et al. (2005).

The sEMG signal recorded is related with the summation of the MUAPs traveling along the muscle fibers on the muscle cell membranes as described in Martínez-Valdés et al. (2017):

$$s_{\mathrm{EMG}}(n) = \sum_{k} H(k) s_{\mathrm{MUAP}}(n-k)\, e(n) \tag{11}$$

where s_{EMG}(n) is the recorded sEMG signal, $H(k)$ is a transfer weight having into account skin and fat conductivity and time propagation effects, $s_{MUAP}(n)$ are the MUAPs traveling along the muscle fibers, $e(n)$ is the recording noise, and n is the time index (Farina and Merletti, 2001; Teklemariam et al., 2016). Concerning the dynamic action exerted by the muscle during activation it will be assumed that the force exerted by the muscle in the upper vertical direction $f_m(t)$ is a correlate of the sEMG recorded on the bulk of the masseter $s_m(t)$ (Roark et al., 2002; Lee, 2010) and therefore, it may be expressed as the joint action of these individual actions, therefore:

$$f_{\mathrm{m}}(t) = J_{\mathrm{m}} r_{\mathrm{m}}(t);\ J_{\mathrm{m}} = \frac{T_{\mathrm{m}}}{l_{\mathrm{m}} cos\vartheta};\ r_{\mathrm{m}}(t) = \int_{\zeta=0}^{t} |s_{\mathrm{m}}(\zeta)|\, d\zeta \tag{12}$$

where J_m is the mioelectric proportionality parameter when small oscillations are assumed, T_m is the angular neuromotor torque,

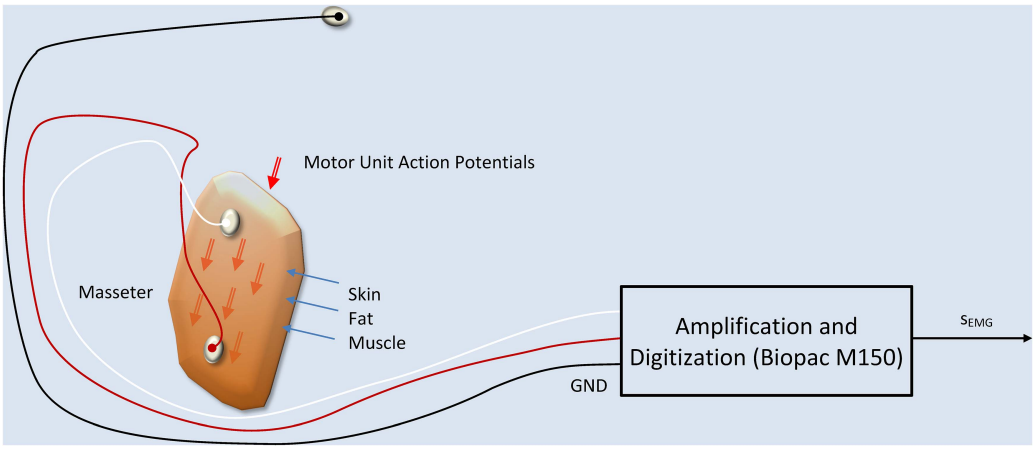

FIGURE 3 | sEMG production and recording model. The two active electrodes are fixed at both ends of the masseter muscle, on the skin, capturing a signal which is the additive composition of the Motor Unit Action Potentials (MUAPs) traveling along the muscle fibers. A ground electrode fixed at the forehead serves as a reference point. The equipment used in the recordings is a WiFi-connected electrode terminal unit which communicates the signals on a wireless link to a Biopac M150 recording system.

l_m is the effective jaw arm length (considering the jaw-tongue system as a lumped load), ϑ is the rotation angle (Hogan, 1984) and $r_m(t)$ is the integral of the rectified sEMG on the masseter. The sEMG is low-pass filtered at 250 Hz and downsampled to 500 Hz. Its rectified value is numerically integrated following (12). Detrending filtering must be used to avoid integration drifts. The reason behind force being related to the integral of the rectified sEMG, and not to sEMG, has to see with the way in which sEMG is recorded, using pairs of electrodes symmetrically placed at both sides of the neuromotor innervation zone on the muscle (see **Figure 3**), as suggested by the experts (De Luca, 1997; De Luca et al., 2010). The integral of the rectified sEMG will be referred in the sequel as the Electromyographic Correlate of the Masseter Force (ECMF).

Linear Regression-Based Statistical Mapping

The present study is intended to link the masseter neuromotor activity (estimated from the sEMG signal) with jaw-tongue kinematics (estimated from 3D accelerometry) and acoustic dynamics (estimated from the first two formants of voice). Cross-correlation (time lag correlation) is used to estimate the optimum time-lag alignment between two signals, determined by the maximum absolute values of Pearson's correlation coefficients. Linear regression between the aligned signals is used to estimate the weights of the corresponding projection model. Cross-correlation methods have been already used in acoustic-kinematic mapping are standard procedures (see Ouni and Laprie, 2005; Dromey et al., 2013; Mitra et al., 2017; Sivaraman et al., 2019). The aim of the present study is based on the inherent relationship between the masseter activity and jaw movement, to show that the front-to-end causality chain from Neuromotor Activity → Masseter sEMG → Vertical Force → Vertical Position → {ΔF1, ΔF2} may be quantitatively described by a simple model, and that the model parameters might be estimated in a first approximation by linear methods. Having in mind that the force exerted by the masseter could not be inferred directly, the present study opens the possibility of making this estimation possible relating acoustic features with neuromotor activity in an inverse relationship, using speech, sEMG and 3D accelerometry.

The methodology used is based on linear regression and cross-correlation on the mentioned signals and estimates, as represented in **Figure 4**.

The systemic approach is intended to establish the strength of the relationships in the cause-effect chain expressed by the following links: Neuromotor Activity → Masseter sEMG → Vertical Force → Vertical Position → $\{\Delta F_1, \Delta F_2\}$. In this problem s_{NA} is the ground truth (not directly observable), s_{EMG} is its observable correlate, and a_{cx} and a_{cy} are the observable dynamic correlates. The estimates of the acoustic accelerations a_{fx} and a_{fy} help in establishing a validation for the indirect estimation of kinematic variables directly from acoustics. These kinematic variables would allow estimating the neuromotor activity directly from acoustics using speech recordings from remote devices (Palacios et al., 2020).

Materials

Eight volunteering speakers (four males and four females) were recruited among PD participants from the APARKAM association of Alcorcón and Leganés, two cities in the southwest of the community of Madrid, Spain. The inclusion criteria were non having had a diagnosis of any laryngeal pathology, being in H&Y stage 2, and non-smokers. Another set of eight participants of both genders with not known laryngeal or neurological pathologies in a similar age range were selected to serve as controls. Their biometrical description is given in **Table 1**.

The study was approved by the Ethical Committee of Universidad Politécnica de Madrid, and the participants signed an informed consent. The experimentation protocols were

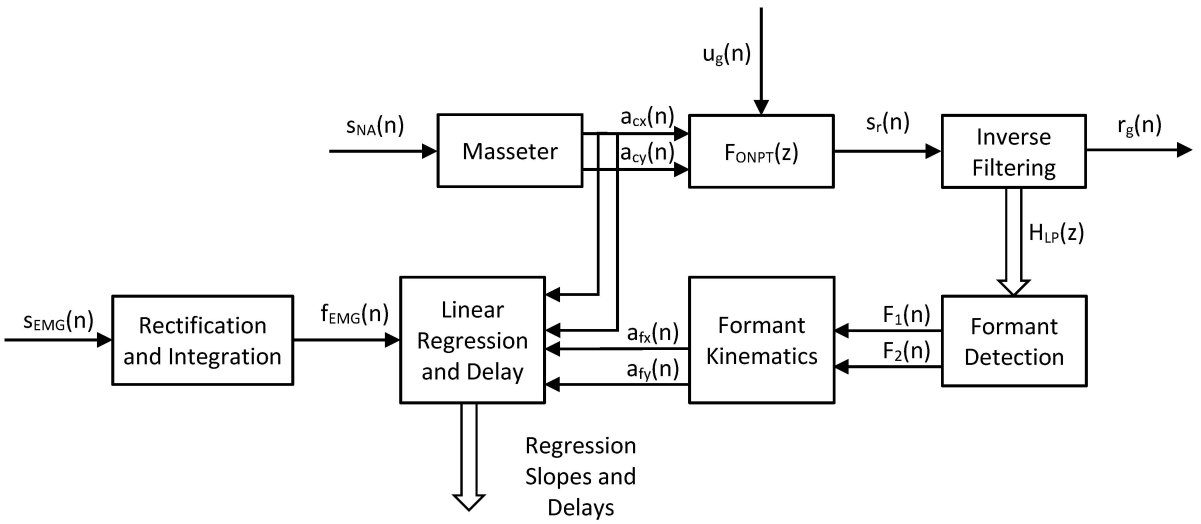

FIGURE 4 | Systemic view of the study. The neuromotor activity induced in the masseter sNA(n) produces accelerations in the horizontal and vertical directions of the jaw-tongue structure on the sagittal plane [acx(n) and acy(n)] which may be directly estimated from the 3D accelerometer. The dynamic action on this structure changes the configuration of the ONPT, and its filtering function FONPT(z). The radiated speech signal sr(n) is the result of filtering the glottal excitation ug(n) by the ONPT. The inverse filtering of speech reconstructs the inverse transfer function HLP(z), which is used to determine the first two formants F1(n) and F2(n). The dynamic behavior of the first two formants is used to indirectly estimate the correlates of the horizontal and vertical accelerations in the sagittal plane afx(n) and afy(n). Cross-correlation between dynamic and acoustic estimations of acceleration and force from sEMG measurements is used to optimally align formants and accelerations. Linear regression between dynamic and acoustic variables is used to estimate the model weights.

aligned with the Declaration of Helsinki. The data recording protocol consisted in the synchronous and simultaneous recording of voice, 3D accelerometry and sEMG as shown in **Figure 5**.

The speech samples were recorded at 50 kHz with16 bits resolution on a MOTU Traveler sound card by a wireless link, using a clip cardioid microphone (Audio Technica) at the speech therapist studio. No special soundproofing room was required due to the short distance to the microphone and its high directionality. The samples from the sEMG and the 3Dacc were recorded at 2.5 kHz. The five signal channels were acquired and digitized by a Biopac M150.

RESULTS

The methodology described refers to concurrent recording of speech, sEMG and 3D accelerometry. The results presented here refer to the use of rotated vertical accelerometry only with respect to the first and second formant oscillations. As an example, the corresponding records for the male participant CM_a when executing the diadochokinetic exercise of repeating [..*aI*..] are shown in **Figure 6**.

The ECMF, the rotated vertical acceleration (dynamic) and the vertical acceleration estimated from the first two formants (acoustic) are shown in detail in **Figure 7**.

The relationship between the vertical displacement Δy and the formant oscillations ΔF_1 and ΔF_2 may be studied using linear regression on the respective signals. The results are presented in **Figure 8**.

Other aspects of interest are the relationships between the ECMF and the vertical rotated accelerations measured by the accelerometer (dynamic) and estimated from formants (acoustic). As the relationship between these two variables is also of interest for the study the results are presented in **Figure 9**.

The results of similar evaluations for each participant in the study are given in **Table 2** for comparative purposes.

As HD is a manifestation of the neuromotor failure in responding to rapid movements, the concepts of absolute velocity

TABLE 1 | Participants' biometrical data.

Participant's code	Gender	Age	Condition	H&Y
CFa	F	67	C	
CFb	F	62	C	
CFc	F	66	C	
CFd	F	67	C	
CMa	M	69	C	
CMb	M	71	C	
CMc	M	68	C	
CMd	M	69	C	
PFa	F	73	P	2
PFb	F	66	P	2
PFc	F	65	P	2
PFd	F	70	P	2
PMa	M	69	P	2
PMb	M	73	P	2
PMc	M	72	P	2
PMd	M	69	P	2

defined in (4) and (6) may help in evaluating and quantifying this manifestation. The AKVs and AFVs from a control and a PD participant are represented in **Figure 10**.

The JSD of each participant with respect to the average distribution of the control participants p_{CP} defined in (9) to explain individual kinematics with respect to a common reference is given in **Table 3**.

The results from the PD cohort are compared with the ones from the control participants using three types of tests: Student's *t*-test, Kolmogorov-Smirnov (KS) and Mann-Whitney (MW). Previously, the results from each cohort have been tested for normality using the Lilliefors test. The normality hypothesis was not rejected for any of the cohorts (controls and PD). The results of the three tests are given at the bottom of the table. In this case, *t*-test and KS test rejected the null hypothesis of same means under a 0.05 significance level. MW test also rejected the null hypothesis of equal distributions from both cohort results under a 0.05 significance level.

DISCUSSION

Starting with the recordings from the example presented in **Figure 6** it may be seen that the sEMG shows spike-like bursts which correspond to muscle contractions during the articulation movements produced to utter the diadichokinetic exercise (a). The placement of the electrodes is of crucial importance, as well as cleaning the skin with deionized water or a soft de-makeup napkin prior to electrode placement. The ECMF, shown in (b) is well aligned with the rotated vertical acceleration given in (c). Both signals show similar oscillations, which presents narrow peaks, possibly due to the antagonist action of the geniohyoid muscle. The speech envelope (d) shows a larger intensity when the vocal opening is larger (lower sounds when the articulation moves to [*a*]) as the release of acoustic energy is larger during these intervals. It must be mentioned that formants do not arrive to extreme positions on the vowel triangle (→[a] and →[I]), swinging instead between a low and a high vowel, which can be described phonetically as [æ→I→æ]. In (e) the first two formants (in blue and red) show a counter-phase oscillation, which is delay-aligned with the acceleration. Similar plots were also produced from each participant.

Regarding **Figure 7**, it may be seen that the rotated vertical acceleration as measured by the accelerometer (b) shows a sharper behavior during vertical pull-ups when compared to the ECMF (a), although their positive peaks are well aligned. This may be due to the action of the antagonist muscles (mainly the geniohyoid), which apparently retain the vertical movement up to a point where they suspend the retention and a sharp vertical peak is released. The acoustical vertical acceleration (c) shows a smoother behavior, and although it is also aligned with (a) and (b) a small delay may be observed in the acoustical acceleration, due to the inertial response of the positioning of the jaw, which conditions the establishment of formants within some delay. An added factor to explain this delay is the time required for the acoustic wave to produce the sustained standing waves in the ONPT which are responsible of formants. These delays can be inferred from the regression study shown in **Figure 9**.

The results of applying linear regression are given in **Figure 8**, showing that the influence of the vertical displacement affects more the second formant than the first one (an oscillation of 2 mm produces a formant swing of almost 100 Hz on F_1, and about 200 Hz in F_2, peak-to-peak). The effect is reversed on each formant: whereas positive displacements in the vertical axis result in negative displacements on F_1, they induce a rise on F_2, as expected from the description given in **Figures 2A,B**). The correlation coefficients (Pearson and Spearman) are both large and significant. The delays suggest that the formants react to the vertical displacement with a delay between 14 and 18 ms. This delay is due to the inertial moment of the jaw-tongue structure, and to the time required for the formants to emerge acoustically as standing waves within the acoustical structures, a factor which is also regulated by the quality factors of the resonances, and ultimately on the energy losses caused by viscoelastic factors on the biological tissues, an interesting problem which would deserve further study.

Regarding the regression results shown in **Figure 9** between the ECMF and vertical acceleration A_{yd} measured from the accelerometer (a: dynamical) and A_{yf} from the indirect estimation on the first two formants (b: acoustical) it may be seen that there is a direct regression in both cases, showing large and significant correlation coefficients (Pearson). Nevertheless, the dynamical acceleration shows a small delay with respect to the ECMF (2 ms, which corresponds to a single sample interval at an effective sample frequency of 500 Hz). On its turn, the delay between the acoustical acceleration A_{yf} and the ECMF is of 32 ms. When checking the correlation between the dynamical and the acoustical acceleration estimates, a delay of 28 ms is observed in the second one with respect to the first one. The disagreement when considering the delays of both signals in regard to the ECMF is of 4 ms (2 sampling intervals at 500 ms), which could be attributed to small signal misalignment errors.

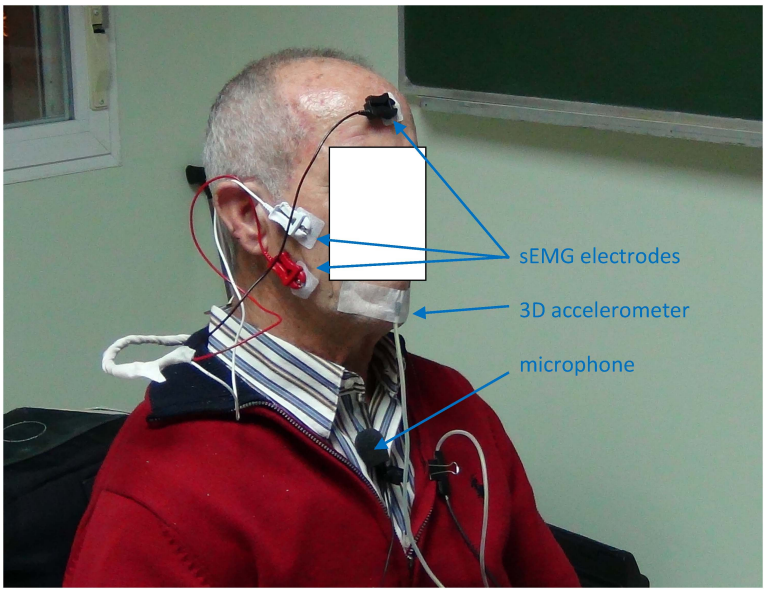

FIGURE 5 | Data recording from a normative male participant: a) the sEMG on the masseter muscle is taken by white and red contact electrodes on the masseter and a reference electrode (black) on the forefront; b) the 3D acceleration is acquired by a 3D accelerometer attached to the chin; the speech signal by a clip wireless cardioid microphone on the chest at 25 cm from the mouth. Jaw-fixed accelerometers are to be used only during signal recording to establish and validate a hands-off acoustic to kinematic projection model, to ultimate use only acoustic signals for at-home monitoring, producing indirect estimations of the neuromotor kinematic characteristics of the participant using the projection model resulting from the study. The participant consented the publication of this anonymized picture.

An exhaustive examination of the results presented in **Table 2** shows some interesting observations. For instance, the regression between the vertical displacement and the first formant oscillations (r_{21}) is the largest in absolute value for CMb, whereas PFb shows the smallest one. No significant difference is appreciated between control and PD participants in this respect. The gain factor a_{21} is the largest for PMb, whereas for CMa it is the smallest. In this case, this factor is significantly largest for PD participants than for controls, a fact that would require further study. The regression between the vertical displacement and the second formant oscillations (r_{22}) is the largest for CFa, and the smallest for PFb. No significant differences were found between control and PD participants. The smallest oscillation gain (a_{22}) was found for CFd, and the largest for PMb. In this case the estimations from controls and PD participants were also significant. The regression between ECMF and the dynamic vertical acceleration (r_{sd}) showed the largest value for PFc, and the smallest for PMb. No significant differences were observed between the two datasets. The oscillation gain (w_{sd}) produced rather disperse estimations in this case, the largest value is observed for CMc and the lowest for PFa. The regression results between ECMF and the vertical acoustic acceleration (r_{sf}) show the largest value for PFa, and the smallest one for PMb (negative in this case, a counter-intuitive result, possibly due to an inefficient small amplitude recording due to low conductance, this fact requiring a further study). No significant differences were found between the two datasets. The oscillation gain (w_{sf}) showed again a strong dispersion, and the singularity of PMb producing a large and negative value again. This dispersion in the values of w_{sd} and w_{sf} may be related with a less efficient recording of the sEMG in some cases, due to skin and fat conductance, as well as electrode placement. On its turn, the correlation between vertical dynamic and acoustic accelerations (r_{df}) showed large values, the difference between the largest (CMb) and the smallest (PFb) being relatively small. No significant differences were observed between the two datasets. Finally, the gain factor between both accelerations (w_{df}) showed the largest and lowest values for PMd and PFb. In this case, a significant difference was observed.

The results presented in **Figure 10** show that the distributions corresponding to the control participant extend to higher values of the absolute velocity (5–6 $cm.s^{-1}$) than the values from the PD participant, which barely extend to 3 $cm.s^{-1}$ (AKV) and do not surpass 1.5 $cm.s^{-1}$ (AFV). This may be an indication of hypokinetic behavior, compatible with HD. This same situation was present in all the PD participants tested, as showed in the results found in **Table 3**. The statistical relevance of this different behavior has been assessed by three statistical tests: *t*-test, Kolmogorov-Smirnov and Mann-Whitney. The rejection of the null hypothesis of equality of distributions may be interpreted in the sense that the sets of JSD from the control and PD participants come from different distributions and are separable based on the value of their respective JSDs. Therefore, the *p*-values of the tests avail a statistical differentiation between controls and patients using JSDs estimated from AKV (dynamic) as well as from AFV (acoustic).

As a general summary it may be said that the correlation studies on sEMG relative to A_{yd} and A_{yf} presented relevant results both for control and PD participants, which means that the disease in itself is not a differentiation factor regarding the association of myoelectric, dynamic, and acoustic signals,

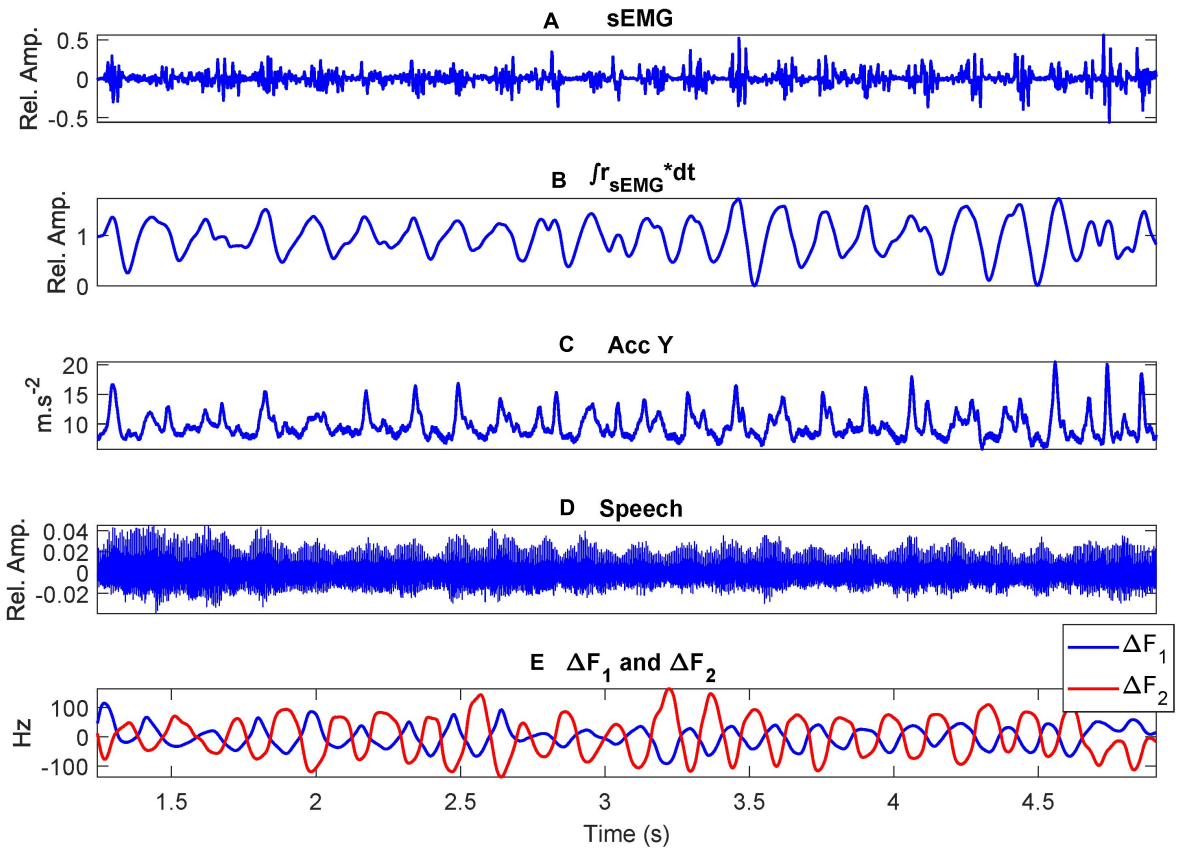

FIGURE 6 | Example recordings when uttering the repetition of [. . .al. . .] by a control participant (CMa): **(A)** the sEMG on the masseter muscle; **(B)** the ECMF; **(C)** acceleration on the vertical axis (sagittal plane); **(D)** speech signal; **(E)** first two formant oscillations (unbiased). Where (*) stands for the multiplication operation.

allowing to build chain models to infer the neuromotor activity in the masseter exclusively from acoustic estimates, therefore the assignment from acoustics to neuromotor (the objective of the present work) will work equivalently for both groups, allowing the design and use of an inverse model to project acoustic estimates to neuromotor ones.

Regarding the statistical tests reported on **Table 3**, a clear different behavior may be appreciated in the PD dataset with respect to the control dataset, as the JSDs of the PD dataset are larger to the average control distributions. The smallest JSDs are found in the control dataset, whereas the largest ones are found in the PD dataset. It may be seen also that the tests reject the null hypothesis of equal distributions between the control and PD participants' JSDs either estimated from dynamics (AKV) or from acoustics (AFV) under a 0.05 significance level. The differentiation between both groups is of most interest to assess HD by telemonitoring devices recording speech remotely. The validation of this possibility has been already studied using acoustic estimates only (Gómez et al., 2017, 2019a), but a wider study using both methods and ECMF is still pending.

The cross-correlation between the ECMF and the kinematic variables estimated also the delays for signal alignment. The following causes have been determined to explain the delays: the inertial dynamic behavior of the jaw-tongue structure, included in numerical integration (delay); the acoustic kinematic estimation, included in numerical differentiation (anticipation), and the most plausible hypothesis, yet to be tested, which would have to see with the time required for the standing waves in the resonances of the ONPT to attain enough intensity to create an emerging formant, and this process would have to see with the quality factor involved in the equivalent generating resonances, ultimately linked to the losses in the ONPT tissue walls (assumed to be rigid and non-viscous). This hypothesis may be checked tracking the pole positions after each time step (2 ms in the present study).

Apparently, the projection model for PD and control participants does not reveal strong differences as far as regression results show. On the contrary, the differentiation between both datasets is relevant in terms of absolute dynamic and acoustic kinematics. This observation must be taken with some precaution, given the important weaknesses and limitations affecting the study, among them the low number of participants studied, although a steady recruitment process is ongoing facing future studies. A non-deniable factor to be taken into account is the potential HD due to aging in the control group, as a confounding factor regarding neuromotor degeneration by disease. Another important limitation is that the low number of participants per gender did not allow a gender-separated study.

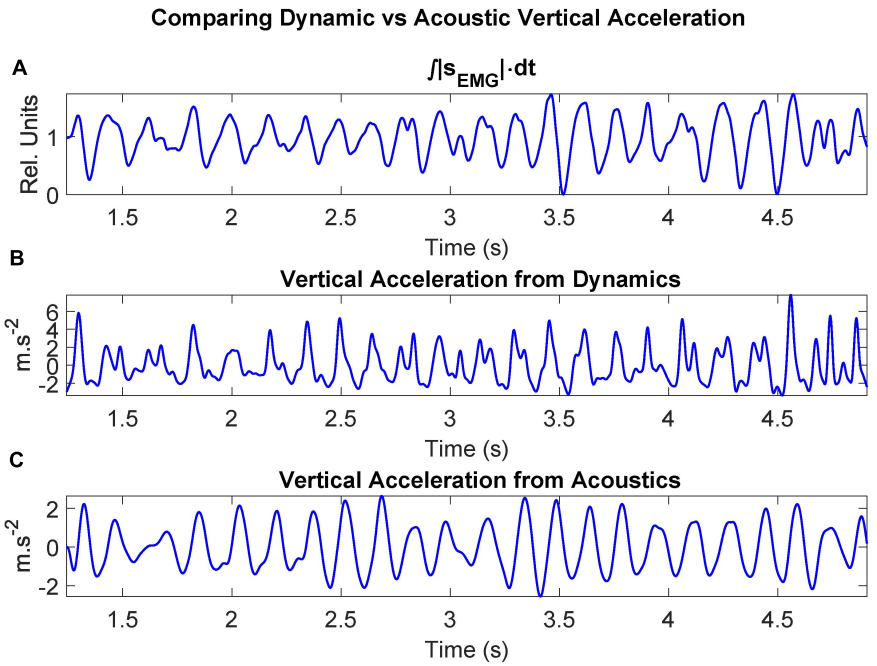

FIGURE 7 | Dynamic signals after processing recordings from the control participant CMa when uttering the repetition of [. . .al. . .]: **(A)** ECMF (proportional to the force exerted by the muscle); **(B)** acceleration on the vertical axis after rotation (sagittal plane); **(C)** vertical acceleration estimated from the first two unbiased formants.

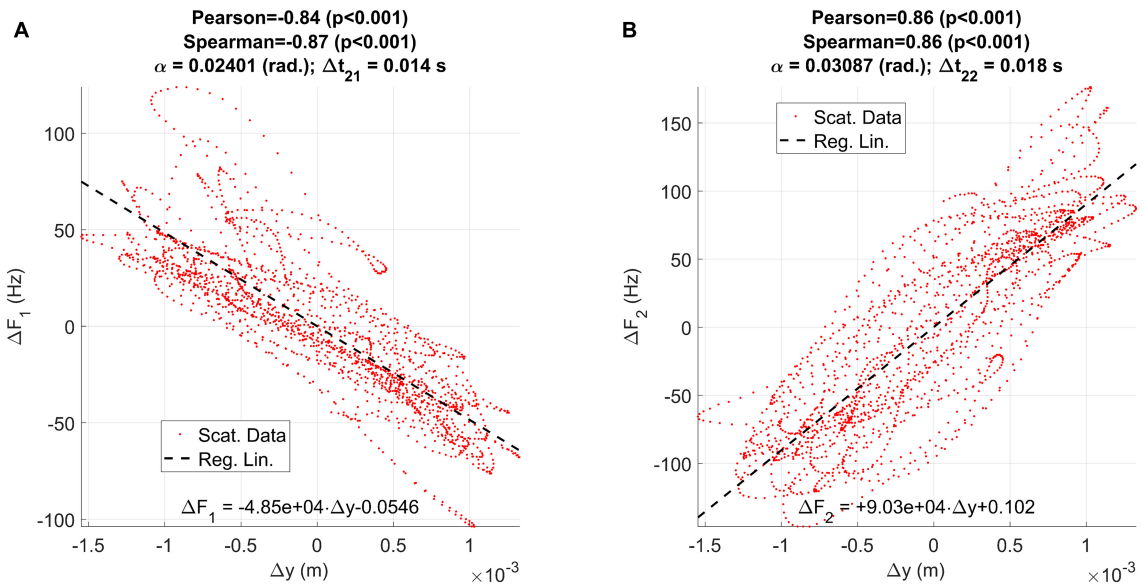

FIGURE 8 | Regression plots between the vertical displacement estimated from accelerometry (Δy) and the first two formant unbiased oscillations: **(A)** relative to ΔF1; **(B)** relative to ΔF2.

Another possible limiting fact is that all PD participants that have been recruited in the study were H&Y stage 2 and hence the generalization of our findings for different PD stages need to be evaluated in a follow-up study. This was a pragmatic constraint mandated by practical challenges in the recruitment. The study was conducted on members of PD associations in the southwest area of Madrid. These participants had been diagnosed and followed by the public healthcare system and accepted willingly and enthusiastically participating. However, for ethical reasons we could not test them in the OFF state. Therefore, participants in an early H&Y stage 1 did not manifest motor problems associated to speech quite clearly, and most of the recordings were not valid.

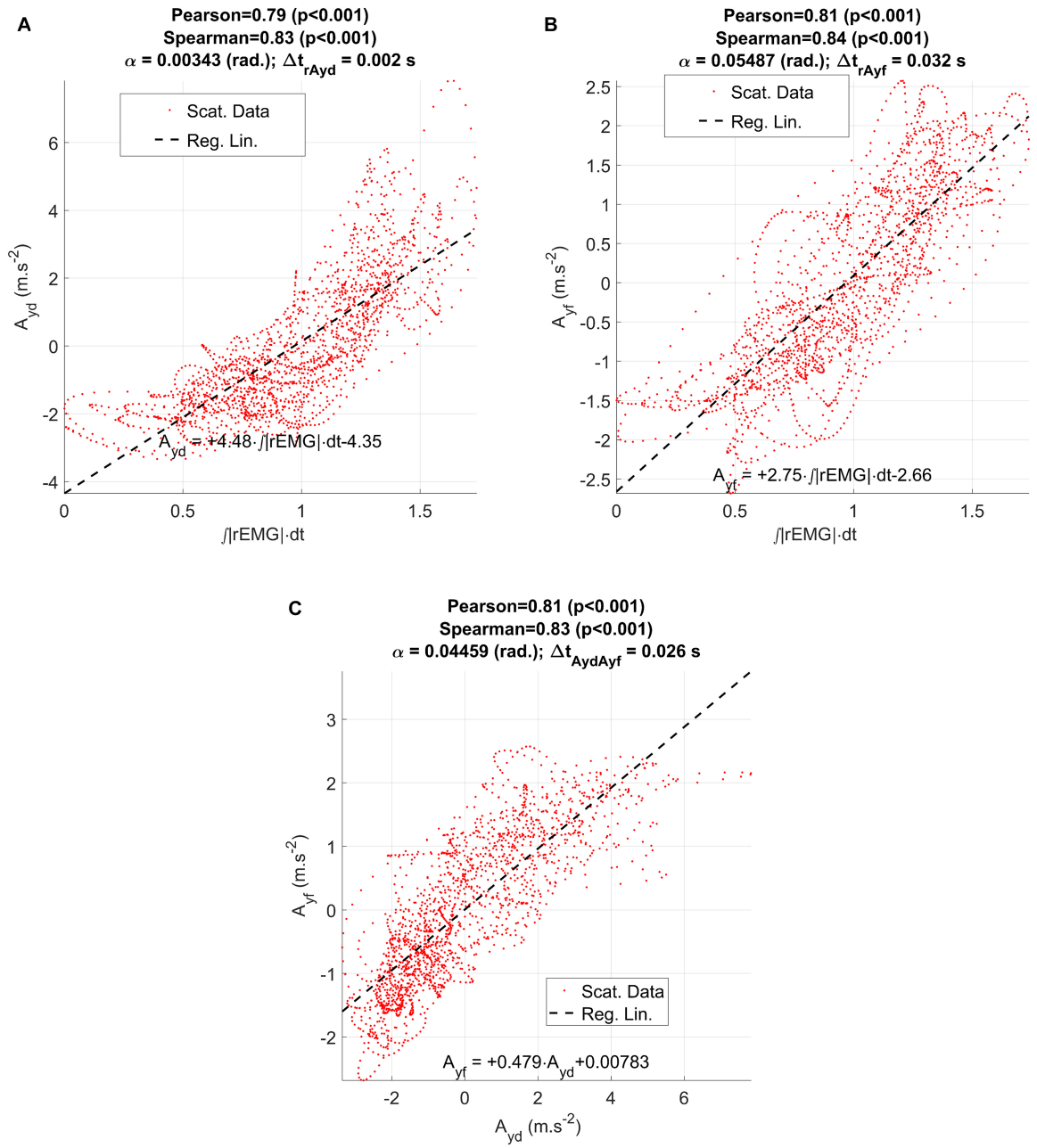

FIGURE 9 | Regression results between the ECMF and the estimated accelerations (dynamical and acoustical) from the participant CMa: **(A)** regression plot between the vertical dynamic acceleration (Ayd) and the ECMF; **(B)** regression plot between the vertical acoustic acceleration (Ayf) and the ECMF; **(C)** regression between the vertical dynamic and acoustic accelerations.

On the other hand, participants in more advanced PD (above state 2) suffered from other co-morbidities, ad it was challenging to recruit them for the needs of the study. Besides, we observed on the available participants in H&Y stage 3, that the recording session, although not lasting more than 25–30 min for a control participant, was for them an exhausting task. Indeed, most of the time was spent in the preparation of the face skin, fixing electrodes, accelerometer, and microphone. Recordings which would typically last 5–10 min for a control participant, almost doubled in these cases, due to misunderstanding of instructions, repetitions, and participants' fatigue.

The effects of choosing PD participants in H&Y stage 2 only, could be assessed observing if the estimations of each feature listed in **Table 2** differed significantly between HC and PD participants. If both distributions did not differ significantly between HC and PD participants in H&Y 2, possibly it could be expected that distributions from PD participants in H&Y < 2 would not differ significantly as well. Extrapolating

TABLE 2 | Linear regression results.

Participants	CFa	CFb	CFc	CFd	CMa	CMb	CMc	CMd	PFa	PFb	PFc	PFd	PMa	PMb	PMc	PMd
r_{21}	−0.9	−0.77	−0.79	−0.88	−0.84	−0.94	−0.92	−0.91	−0.93	−0.64	−0.85	−0.9	−0.86	−0.93	−0.81	−0.91
a_{21} (x10^3)	−55.5	−58.1	−76.1	−55	−44.8	−78.4	−94.8	−67.5	−205	−74.1	−95.9	−115	−145	−289	−185	−159
r_{22}	0.94	0.86	0.76	0.85	0.86	0.88	0.87	0.86	0.84	0.53	0.93	0.84	0.81	0.89	0.65	0.83
a_{22} (x10^3)	110	152	135	43.1	86.1	62.0	99.6	71.5	258	119	173	151	173	267	153	181
r_{sd}	0.7	0.78	0.83	0.66	0.79	0.58	0.53	0.71	0.74	0.78	0.81	0.86	0.6	0.49	0.63	0.84
w_{sd}	36.9	8.81	5.01	8.84	4.48	9.24	95.8	35.0	3.94	5.52	30.9	7.27	32.2	26.4	14.2	15.5
r_{sf}	0.72	0.8	0.79	0.69	0.81	0.53	0.59	0.74	0.84	0.79	0.82	0.76	0.67	−0.41	0.68	0.83
w_{sf}	20.4	5.05	3.4	4.9	2.77	4.06	44.9	15.9	0.75	0.96	14.1	3.67	8.15	−14.4	4.23	14.4
r_{df}	0.92	0.87	0.82	0.87	0.81	0.95	0.79	0.93	0.87	0.77	0.91	0.91	0.81	0.91	0.78	0.93
w_{df}	0.50	0.49	0.58	0.46	0.49	0.46	0.40	0.38	0.15	0.13	0.41	0.52	0.18	0.59	0.22	0.87

r_{21} and r_{22}: Pearson's correlation coefficients between vertical displacement and the first two formants; a_{21} and a_{22}: projection weights defined in expression (1); r_{sd}, and r_{sf}: Pearson's correlation coefficients between vertical accelerations estimated from dynamic and acoustic signals and the force estimated from the sEMG; r_{df}: Pearson's correlation coefficient between the vertical accelerations estimated from dynamic and acoustic signals; w_{sd}, w_{sf}: regression slopes between vertical displacement and the dynamic force estimated from the sEMG; w_{df}: regression slope between the vertical accelerations estimated from dynamic and acoustic signals.

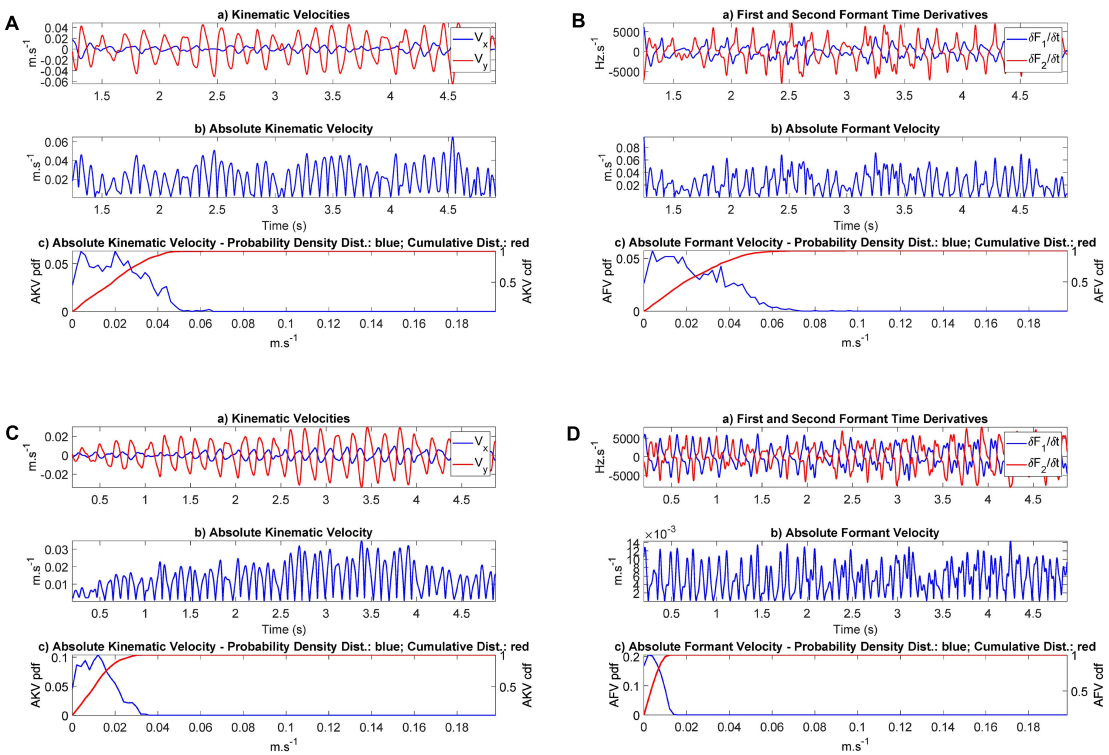

FIGURE 10 | Absolute Kinematic and Formant Velocities (AKV and AFV): **(A)** AKV from participant CMa; **(B)** AFV from participant CMa; **(C)** AKV from participant PMa; **(D)** AFV from the PD participant PMa. In each plot the subplot (a) represents the horizontal and vertical velocities or the corresponding formant derivatives in the time domain. The subplot (b) represents the instantaneous value of the absolute velocity. The subplot (c) gives the density distribution (in blue) and the accumulated distribution (in red). The range of the common scale of velocities goes from 0 to 20 cm.s^{-1}.

this observation to PD participants in H&Y > 2 is not possible considering the data available right now. The comparisons have been done using three statistical tests on the null hypothesis of equal distributions: a parametric *t*-test, and two non-parametric ones, Kolmogorov-Smirnov (KS), and Mann-Whitney (MW) on the correlation and model projection coefficients given in **Table 2** (10 features, one per row). We adjusted the significance level of 0.05 per each feature accordingly to Holm-Bonferroni's correction (Holm, 1979). The adjusted significance levels per feature (in parenthesis) were 0.0050 (1), 0.0056 (2), 0.0063 (3), 0.0071 (4), 0.0083 (5), 0.0100 (6), 0.0125 (7), 0.0167 (8), 0.0250 (9), 0.0500 (10). The sorted *p*-values per row (in parenthesis) were 0.0017 (4), 0.0064 (2), 0.1790 (8), 0.1966 (3), 0.4386 (10), 0.4881 (6), 0.5901 (7), 0.7176 (1), 0.7263 (5), 0.7832 (9). Therefore, the null hypothesis could only be rejected for feature a_{22} (4), because its *p*-value (0.0017) was under the lowest significance

level (0.0050). Comparing the results from the KS test in a similar way, the null hypothesis could only be rejected for feature a_{21} (p-value of 0.0014). The results from the MW test rejected the null hypothesis for both a_{21} and a_{22} (p-values of 0.0011), but not for the remnant features. The overall comparison results point to the global acceptance of the complementary hypothesis of equal means, except for the specific features a_{21} and a_{22}.

The effects of the H&Y stage choice could also be assessed observing if the JSD distances considered in **Table 3** differed significantly between HC and PD participants. As it may be seen, all the tests reject the null hypothesis of equal distributions of JSD scores respect to a significance level of 0.05, although the case of KS with JSD scores produced from the AKV distribution, is only slightly below the significance level (0.049). This means that probably this test (KS on JSD from AKV) would fail rejecting the null hypothesis for a set of PD participants in stage H&Y < 2. How the other tests would work under the same conditions is less predictable.

The unexplained contribution to the variance in linear regression results (in terms of $1-r^2$, where r is the respective correlation coefficient) by the effects of the ECMF on the vertical acceleration may be due to the action of the geniohyoid and other muscles contributing to the elevation and depression of the jaw-tongue system. The activity of the geniohyoid muscle in depressing the jaw-tongue structure has not been estimated in the present study. The inclusion of sEMG recording electrodes on geniohyoglossus muscle could complement it.

TABLE 3 | Results from JSD comparisons on the AKV and AFV distributions.

Participant's code	JSD/AKV	JSD/AFV
CFa	0.169	0.117
CFb	**0.091**	0.103
CFc	0.110	**0.091**
CFd	0.257	**0.227**
CMa	0.120	0.090
CMb	0.101	0.170
CMc	0.133	0.110
CMd	**0.283**	0.102
PFa	0.326	**0.597**
PFb	0.223	0.436
PFc	0.213	0.336
PFd	**0.124**	0.145
PMa	0.345	0.596
PMb	**0.453**	0.396
PMc	0.423	0.590
PMd	0.332	**0.120**
p-value t-Test	0.008	0.002
p-value KS	0.049	0.010
p-value MW	0.010	0.002

The mid and right columns give the JSDs of each participant with respect to the average AKV and AFV distributions of the control set, p_{PCd} and p_{PCf}, respectively. It may be seen that the JSDs of the PC participants are higher than the ones estimated on the control group. The p-values at the bottom of the table give the results of testing the JSDs from the PD set to the JSDs form the control participants. Values in bold specify the largest and smallest divergences with respect to the control averages.

There are several limitations affecting the present study, which have to be mentioned here. First of all, independent jaw-tongue movements are not analyzed, however, it must be stressed that the present study is mainly focused on proposing acoustic features which may be mapped to potential biomarkers of degenerative speech HD of neuromotor etiology, not on a general model in the sense of Ouni and Laprie (2005). Therefore, the proposed model does not cover the whole span of articulatory movements to acoustic features. Instead, reducing the movement space to vertical activity, helps in providing more accurate estimations of neuromotor activity on the masseter. A possible future extension of the study to independent tongue, jaw and lip movements would require monitoring the sEMG activity of other muscles, as the genio-hioglossus or the orbicular muscles. Besides, the model assumed linear relationship between formants and kinematics. Having in mind that the relationship with the biomarkers (acoustic and dynamic AKF and AKV) become non-linear, this is a necessary approach to allow a first conclusive study. Another important limitation is the small size of the dataset included in the study. This limitation will be removed when the pandemic conditions allow for the inclusion of more recordings. Once the projection model is validated using the multi-trait signals (speech, sEMG and 3DAcc) the detection properties of the proposed biomarkers (AKV and AFV) will be tested on larger PD speech databases (Sakar et al., 2013; Orozco-Arroyave et al., 2014), however, as they only contain speech data, we cannot use them for this validation phase, considering the novel direction that this work is proposing. Hopefully we will be able of using the projection model to produce the AKV and AFV biomarkers, to validate the statistical relevance of a speech-based home-monitoring approach on these databases and others recruited by our own using a tele-health platform (see Palacios et al., 2020). Another limiting factor is that PD participants were in a moderate stage of motor activity deterioration (H&Y stage 2). This limitation would require extending the analysis to PD participants across all stages to investigate the changes across the spectrum of the disease, from very early onset (HY stage 1) to very late PD stages.

Another important open issue is how speaker dependency and inter-speaker variability may affect absolute kinematic distributions as disease biomarkers. In this sense, it may be seen from the work of Dromey et al. (2013) that the variability of inter-speaker results for diphthong [aI] is the lowest from all diphthongs these authors have studied per class (control vs. PD participants). Moreover, it may be shown that the projection weights in **Table 2**, if normalized to the $[a_{ij}]$ vector norm as $\hat{a}_{ij} = a_{ij}/|a_{ij}|$ (see Gómez et al., 2021) do not show relevant inter-speaker variability per class. The way that inter-speaker variability may affect the absolute kinematic distributions (the proposed biomarkers), works different for controls than for PD participants, because these biomarkers are the normalized histogram distributions of the absolute kinematic velocities, and they only express if movement is more distributed toward low absolute velocities (hypokinetic), as is the case for the PD participant plotted in **Figures 10C,D** or if it spreads along low and high absolute velocities (normokinetic), as is the case for the control participant plotted in **Figures 10A,B**.

Therefore, inter-speaker variability is expressing if the speaker is hypokinetic or not, or to put it in other words, inter-speaker variability between controls and PD participants is an essential role of the proposed biomarkers, provided they are designed to differentiate hypokinetic from normokinetic speech. This separation is availed by the results shown in **Table 3**, where it may be seen that biomarker distributions (kinematic AKV, as well as acoustic AFV) from PD participants show larger distances (in terms of Jensen-Shannon Divergence) to distributions from control participants. Summarizing, the biomarkers proposed show an inter-speaker variability oriented to differentiate control participants from PD participants, in closed relationship with the second objective of the study as stated in section "Objectives."

CONCLUSION

This study presents a multi-trait evaluation of HD, including speech, 3D accelerometry and sEMG signal acquisition on the masseter. A cross-correlation signal alignment is carriend on these signals. A further regression analysis on the re-aligned acoustic formants, kinematic accelerations and dynamic-related electromyography signals allows the estimation of the projection model parameters. The projected acoustic-kinematic and dynamics-kinematics absolute movement distributions are used as HD biomarkers. An evaluation of these biomarkers in terms of Jensen-Shannon Divergence is conducted on data from control and PD participants, showing the capability of both biomarkers to detect HD in PD speech. The main findings derived from the study are the following:

- A multimodal framework for the assessment of the masseter's neuromotor activity based on sEMG, 3DAcc and speech, has been used on diadochokinetic exercises from PD and control participants.
- Large cross-correlations between the measured and estimated signals have been observed using linear regression on a small-size data sample of control and PD participants.
- The cross-correlation study did not show relevant differences between control and PD participants.
- The articulation kinematics estimated from 3D accelerometry and from acoustics showed a relevant similarity for all the participants included in the study.
- It was possible to differentiate the speech kinematic behavior of the control and PD participant sets used in this study, using absolute velocities (dynamic and acoustic) of the joint jaw-tongue reference point. Therefore, their amplitude distributions could be used as potential biomarkers of PD speech HD.

The findings of the current study are preliminary, given the limited sample size. We are currently extending our efforts toward the collection of a larger sample size and investigating how well the presented findings generalize across larger cohorts. The definition of an inverse model to infer neuromotor activity from acoustics is also a future objective. The inclusion of sEMG from other muscles active on the jaw-tongue articulation as the geniohyoid is also foreseen. A study regarding the delay on formant-estimated kinematics based on the non-linear properties of the ONPT is considered as well.

DATA AVAILABILITY STATEMENT

The raw data supporting the conclusions of this article will be made available by the authors, without undue reservation.

ETHICS STATEMENT

The studies involving human participants were reviewed and approved by the Comité de Ética de la Universidad Politécnica de Madrid. The patients/participants provided their written informed consent to participate in this study. Written informed consent was obtained from the individual(s) for the publication of any potentially identifiable images or data included in this article.

AUTHOR CONTRIBUTIONS

AG: manuscript preparation, model conceptual design, and implementation, instrumentation setup, and data recording. PG: research guidelines, manuscript preparation, and model implementation. DP and VR: data recording and manuscript preparation. VN: instrumentation design and setup and data recording. AÁ: data processing. AT: research guidelines and manuscript preparation. All authors contributed to the article and approved the submitted version.

FUNDING

This work was being funded by the grants TEC2016-77791-C4-4-R from the Government of Spain, and CENIE_TECA-PARK_55_02 INTERREG V-A Spain—Portugal (POCTEP).

ACKNOWLEDGMENTS

The authors wish to thank Asociación de Parkinson de Alcorcón y Móstoles (APARKAM), their members for their enthusiast collaboration, and to Azucena Balandín (director) and Zoraida Romero (speech therapist) for their help and advice.

REFERENCES

Alku, P., Murtola, T., Malinen, J., Kuortti, J., Story, B., Airaksinen, M., et al. (2019). OPENGLOT-An open environment for the evaluation of glottal inverse filtering. *Speech Commun.* 107, 38–47. doi: 10.1016/j.specom.2019.01.005

Arora, S., Lo, C., Hu, M., and Tsanas, A. (2021). Smartphone speech testing for symptom assessment in rapid eye movement sleep behavior disorder and Parkinson's disease. *IEEE Access* (in press).

Bourchard, K. E., Conant, D. F., Anumanchipalli, G. K., Dichter, B., Chaisanguanthum, K. S., Johnson, K., et al. (2016). High-Resolution,

non-invasive imaging of upper vocal tract articulators compatible with human brain recordings. *PLoS One* 11:e0151327. doi: 10.1371/journal.pone.0151327

Brabenec, L., Mekyska, J., Galaz, Z., and Rektorova, I. (2017). Speech Disorders in Parkinson's disease: early diagnostics and effects on medication in brain stimulation. *J. Neural Transm.* 124, 303–334. doi: 10.1007/s00702-017-1676-0

Brown, S., Laird, A. R., Pfordresher, P. Q., Thelen, S. M., Tourkeltaub, P., and Liotti, M. (2009). The somatotopy of speech: phonation and articulation in the human motor cortex. *Brain Cogn.* 70, 31–41. doi: 10.1016/j.bandc.2008.12.006

Buchaillard, S., Perrier, P., and Payan, Y. (2009). A biomechanical model of cardinal vowel production: muscle activations and the impact of gravity on tongue positioning. *J. Acoust. Soc. Am.* 126, 2033–2051. doi: 10.1121/1.3204306

Castroflorio, T., Farina, D., Bottin, A., Piancino, M. G., Bracco, P., and Merletti, R. (2005). Surface EMG of jaw elevator muscles: effect of electrode location and inter-electrode distance. *J. Oral Rehabil.* 32, 411–417. doi: 10.1111/j.1365-2842.2005.01442.x

Cattaneo, L., and Pavesi, G. (2014). The facial motor system. *Neurosci. Behav. Rev.* 38, 135–159. doi: 10.1016/j.neubiorev.2013.11.002

Cover, T. M., and Thomas, J. A. (2006). *Elements of Information Theory*. New York, NY: Wiley.

De Luca, C. J. (1997). The use of surface electromyography in biomechanics. *J. Appl. Biomech.* 13, 135–163. doi: 10.1123/jab.13.2.135

De Luca, C. J., Gilmore, L. D., Kuznetsov, M., and Roy, S. H. (2010). Filtering the surface EMG signal: movement artifact and baseline noise contamination. *J. Biomech.* 43, 1573–1579. doi: 10.1016/j.jbiomech.2010.01.027

Deller, J. R., Proakis, J. G., and Hansen, J. H. L. (1993). *Discrete-Time Processing of Speech Signals*. NewYork, NY: Macmillan.

Demonet, J. F., Thierry, G., and Cardebat, D. (2005). Renewal of the neurophysiology of language: functional neuroimaging. *Physiol. Rev.* 85, 49–95. doi: 10.1152/physrev.00049.2003

Dromey, C., Jang, G. O., and Hollis, K. (2013). Assessing correlations between lingual movements and formants. *Speech Commun.* 55, 315–328. doi: 10.1016/j.specom.2012.09.001

Duffy, J. R. (2013). *Motor Speech Disorders*. St. Louis, MO: Elsevier.

Farina, D., and Merletti, R. (2001). A novel approach for precise simulation of the EMG signal detected by surface electrodes. *IEEE Trans. Biomed. Eng.* 48, 637–646. doi: 10.1109/10.923782

Gerard, J. M., Perrier, P., and Payan, Y. (2006). "3D biomechanical tongue modeling to study speech production," in *Speech Production: Models, Phonetic Processes, and Techniques*, Chap. 6. eds J. Harrington and M. Tabain (New York, NY: Psychology Press), 85–102.

Goberman, A. M., and Coelho, C. (2002). Acoustic analysis of Parkinsonian speech I: speech characteristics and L-Dopa therapy. *Neurorehabilitation* 17, 237–246. doi: 10.3233/NRE-2002-17310

Godino, J. I., Shattuck-Hufnagel, S., Choi, J. Y., Moro, L., and Gómez, J. A. (2017). Towards the identification of Idiopathic Parkinson's Disease from the speech. New articulatory kinematic biomarkers. *PLoS One* 12:e0189583. doi: 10.1371/journal.pone.0189583

Gómez, A., Tsanas, A., Gómez, P., Palacios, D., Rodellar, V., and Álvarez, A. (2021). Acoustic to kinematic projection in Parkinson's Disease Dysarthria. *Biomed. Signal Process. Control* 66:102422.

Gómez, P., Gómez, A., Ferrández, J. M., Mekyska, J., Palacios, D., Rodellar, V., et al. (2019a). Neuromechanical modelling of articulatory movements from surface electromyography and speech formants. *Int. J. Neural Syst.* 29:1850039. doi: 10.1142/S0129065718500399

Gómez, P., Mekyska, J., Ferrández, J. M., Palacios, D., Gómez, A., Rodellar, V., et al. (2017). Parkinson disease detection form speech articulation neuromechanics. *Front. Neuroinformatics* 11:56. doi: 10.3389/fninf.2017.00056

Gómez, P., Mekyska, J., Gómez, A., Palacios, D., Rodellar, V., and Álvarez, A. (2019b). Characterization of Parkinson's disease dysarthria in terms of speech articulation kinematics. *Biomed. Signal Process. Control* 52, 312–320. doi: 10.1016/j.bspc.2019.04.029

Goodman, S. E., and Hasson, C. J. (2017). Elucidating sensorimotor control principles with myoelectric musculoskeletal models. *Front. Hum. Neurosci.* 11:531. doi: 10.3389/fnhum.2017.00531

Green, J. R., Yunusova, Y., Kuruvilla, M. S., Wang, J., Pattee, G. L., Synhorst, L., et al. (2013). Bulbar and speech motor assessment in ALS: challenges and future directions. *Amyotroph. Lateral Scler. Frontotemporal Degener.* 14, 494–500. doi: 10.3109/21678421.2013.817585

Greenberg, S. (2004). *Speech Processing in the Auditory System*. New York, NY: Springer.

Harel, B., Cannizzaro, M., and Snyder, P. J. (2004). Variability in fundamental frequency during speech in prodromal and incipient Parkinson's disease: a longitudinal case study. *Brain Cogn.* 56, 24–29. doi: 10.1016/j.bandc.2004.05.002

Harel, B. T., Cannizzaro, M. S., Cohen, H., Reilly, N., and Snyder, P. J. (2004). Acoustic characteristics of Parkinsonian speech: a potential biomarker of early disease progression and treatment. *J. Neurolinguistics* 17, 439–453. doi: 10.1016/j.jneuroling.2004.06.001

Hogan, N. (1984). Adaptive control of mechanical impedance by coactivation of antagonist muscles. *IEEE Trans. Aut. Cont.* 29, 681–690. doi: 10.1109/TAC.1984.1103644

Holm, S. (1979). A simple sequentially rejective multiple test procedure. *Scand. J. Stat.* 6, 65–70.

IPA (2005). *International Phonetic Association*. Available online at: https://www.internationalphoneticalphabet.org/ipa-charts/ipa-symbols-chart-complete/ (accessed January 08, 2021).

Jürgens, U. (2002). Neural pathways underlying vocal control. *Neurosci. Behav. Rev.* 26, 235–258. doi: 10.1016/S0149-7634(01)00068-9

Kandel, E., Schwartz, J. H., Jessell, T. M., Siegelbaum, S. A., and Hudspeth, A. J. (eds). (2013). *Principles of Neural Science*. New York, NY: McGraw- Hill.

Lee, K. S. (2010). Prediction of acoustic feature parameters using myoelectric signals. *IEEE Trans. Biomed. Eng.* 57, 1587–1595. doi: 10.1109/TBME.2010.2041455

Martínez-Valdés, E., Negro, F., Laine, C. M., Falla, D., Mayer, F., and Farina, D. (2017). Tracking motor units longitudinally across experimental sessions with high-density surface electromyography. *J. Physiol.* 595, 1479–1496. doi: 10.1113/JP273662

Mefferd, A. S., and Dietrich, M. S. (2020). Tongue- and jaw-specific articulatory changes and their acoustic consequences in talkers with dysarthria due to amyotrophic lateral sclerosis: effects of loud, clear, and slow speech. *J. Speech Lang. Hear. Res.* 63, 2625–2636. doi: 10.1044/2020_JSLHR-19-00309

Mekyska, J., Janousova, E., Gómez-Vilda, P., Smekal, Z., Rektorova, I., Eliasova, I., et al. (2015). Robust and complex approach of pathological speech signal analysis. *Neurocomputing* 167, 94–111. doi: 10.1016/j.neucom.2015.02.085

Mitra, V., Sivaraman, G., Nam, H., Espy-Wilson, C., Saltzman, E., and Tiede, M. (2017). Hybrid convolutional neural networks for articulatory and acoustic information based speech recognition. *Speech Commun.* 89, 103–112. doi: 10.1016/j.specom.2017.03.003

Orozco-Arroyave, J. R., Arias-Londoño, J. D., Vargas-Bonilla, J. F., González-Rátiva, M. C., and Nöth, E. (2014). "New Spanish speech corpus database for the analysis of people suffering from Parkinson's disease," in *Proceedings of the 9th Language Resources and Evaluation Conference, (LREC)*, Reykjavik, 342–347.

Ouni, S., and Laprie, Y. (2005). Modeling the articulatory space using a hypercube codebook for acoustic-to-articulatory inversion. *J. Acoust. Soc. Am.* 118, 444–460. doi: 10.1121/1.1921448

Palacios, D., Meléndez, G., López, A., Lázaro, C., Gómez, A., and Gómez, P. (2020). MonParLoc: a speech-based system for Parkinson's disease analysis and monitoring. *IEEE Access Early Access* 8, 188243–188255. doi: 10.1109/ACCESS.2020.3031646

Parkinson, J. (2002). An essay on the shaking palsy. *J. Neuropsychiatry Clin. Neurosci.* 14, 223–236. (Re-edited in Neuropsychiatry Classics from the 1817 original monograph with the same title by J. Parkinson, edited by Sherwood, Neely and Jones).

Qin, C., and Carreira-Perpiñán, M. A. (2007). "An empirical investigation of the non-uniqueness in the acoustic-to-articulatory mapping," in *Proceedings of the INTERSPEECH, August 27–31*, Antwerp, 74–77.

Ricciardi, L., Ebreo, M., Graziosi, A., Barbuto, M., Sorbera, C., Morgante, L., et al. (2016). Speech and gait in Parkinson's disease: when rhythm matters. *Parkinsonism Relat. Disord.* 32, 42–47.

Roark, R. M., Li, J. C. L., Schaefer, S. D., Adam, A., and De Luca, C. J. (2002). Multiple motor unit recordings of laryngeal muscles: the technique of vector laryngeal electromyography. *Laryngoscope* 112, 2196–2203. doi: 10.1097/00005537-200212000-00014

Sakar, B. E., Isenkul, M. E., Sakar, C. O., Sertbas, A., Gurgen, F., Delil, S., et al. (2013). Collection and analysis of a Parkinson speech dataset with multiple types of sound recordings. *IEEE J. Biomed. Health Inform.* 17, 828–834. doi: 10.1109/JBHI.2013.2245674

Sanguinetti, V., Laboissière, R., and Payan, Y. (1997). A control model of human tongue movements in speech. *Biol. Cybern.* 77, 11–22. doi: 10.1007/s004220050362

Sapir, S. (2014). Multiple factors are involved in the dysarthria associated with Parkinson's disease: a review with implications for clinical practice and research. *J. Speech Lang. Hear. Res.* 57, 1330–1343. doi: 10.1044/2014_JSLHR-S-13-0039

Sivaraman, G., Mitra, V., Nam, H., Tiede, M., and Espy-Wilson, C. (2019). Unsupervised speaker adaptation for speaker independent acoustic to articulatory speech inversion. *J. Acoust. Soc. Am.* 146, 316–329. doi: 10.1121/1.5116130

Skodda, S., Grönheit, W., and Schlegel, U. (2012). Impairment of vowel articulation as a possible marker of disease progression in Parkinson's disease. *PLoS One* 7:e32132. doi: 10.1371/journal.pone.0032132

Tasko, S. M., and Greilick, K. (2010). Acoustic and articulatory features of diphthong production: a speech clarity study. *J. Speech Lang. Hear. Res.* 53, 84–99. doi: 10.1044/1092-4388(2009/08-0124)

Teklemariam, A., Hodson-Tole, E. F., Reeves, N. D., Consten, N. P., and Cooper, G. (2016). A finite element model approach to determine the influence of electrode design and muscle architecture on myoelectric signal properties. *PLoS One* 11:e0148275. doi: 10.1371/journal.pone.0148275

Tjaden, K., Lam, J., and Wilding, G. (2013). Vowel acoustics in Parkinson's disease and multiple sclerosis: comparison of clear, loud, and slow speaking conditions. *J. Speech Lang. Hear. Res.* 56, 1485–1502. doi: 10.1044/1092-4388(2013/12-0259)

Tsanas, A. (2012). *Accurate Telemonitoring of Parkinson's Disease Symptom Severity Using Nonlinear Speech Signal Processing and Statistical Machine Leaning*. Ph.D. thesis, University of Oxford, Oxford.

Tsanas, A., Little, M. A., McSharry, P. E., and Ramig, L. O. (2011). Nonlinear speech analysis algorithms mapped to a standard metric achieve clinically useful quantification of average Parkinson's disease symptom severity. *J. R. Soc. Interface* 8, 842–855. doi: 10.1098/rsif.2010.0456

Tsanas, A., Little, M. A., and Ramig, L. O. (2021). Remote assessment of Parkinson's disease symptom severity using the simulated cellular mobile telephone network. *IEEE Access* 9, 11024–11036. doi: 10.1109/ACCESS.2021.3050524

Whitfield, J. A., and Goberman, A. M. (2014). Articulatory-acoustic vowel space: application to clear speech in individuals with Parkinson's disease. *J. Comm. Disord.* 51, 19–28. doi: 10.1016/j.jcomdis.2014.06.005

Wu, P., González, I., Patsis, G., Jiang, D., Sahli, H., Kerckhofs, E., et al. (2014). Objectifying facial expressivity assessment of Parkinson's patients: preliminary study. *Comput. Math. Methods Med.* 2014:427826. doi: 10.1155/2014/427826

Yunusova, Y., Green, J., Greenwood, L., Wang, J., Pattee, G. L., and Zinman, L. (2012). Tongue movements and their acoustic consequences in amyotrophic lateral sclerosis. *Folia Phoniatr. Logop.* 64, 94–102. doi: 10.1159/000336890

Yunusova, Y., Weismer, G. G., and Lindstrom, M. J. (2011). Classifications of vocalic segments from articulatory kinematics: healthy controls and speakers with Dysarthria. *J. Speech Lang. Hear. Res.* 54, 1302–1311. doi: 10.1044/1092-4388(2011/09-0193)

Conflict of Interest: The authors declare that the research was conducted in the absence of any commercial or financial relationships that could be construed as a potential conflict of interest.

frontiers in Bioengineering and Biotechnology

PERSPECTIVE
published: 16 March 2021
doi: 10.3389/fbioe.2021.624522

Could Gait Biomechanics Become a Marker of Atypical Neuronal Circuitry in Human Development?—The Example of Autism Spectrum Disorder

Marine Jequier Gygax[1], Anne M. Maillard[1] and Julien Favre[2]*

[1] Service des Troubles du Spectre de l'Autisme, Department of Psychiatry, Lausanne University Hospital, Lausanne, Switzerland, [2] Swiss BioMotion Lab, Department of Musculoskeletal Medicine, Lausanne University Hospital and University of Lausanne (CHUV-UNIL), Lausanne, Switzerland

This perspective paper presents converging recent knowledge in neurosciences (motor neurophysiology, neuroimaging and neuro cognition) and biomechanics to outline the relationships between maturing neuronal network, behavior, and gait in human development. Autism Spectrum Disorder (ASD) represents a particularly relevant neurodevelopmental disorder (NDD) to study these convergences, as an early life condition presenting with sensorimotor and social behavioral alterations. ASD diagnosis relies solely on behavioral criteria. The absence of biological marker in ASD is a main challenge, and hampers correlations between behavioral development and standardized data such as brain structure alterations, brain connectivity, or genetic profile. Gait, as a way to study motor system development, represents a well-studied, early life ability that can be characterized through standardized biomechanical analysis. Therefore, developmental gait biomechanics might appear as a possible motor phenotype and biomarker, solid enough to be correlated to neuronal network maturation, in normal and atypical developmental trajectories—like in ASD.

Keywords: autism, biomechanics, gait, neuronal circuit development, biomarker, walking, patterns, machine learning

OPEN ACCESS

Edited by:
Yury Ivanenko, Santa Lucia Foundation (IRCCS), Italy

Reviewed by:
Alessandro Crippa, Eugenio Medea (IRCCS), Italy
Jeff Eggleston, The University of Texas at El Paso, United States

****Correspondence:***
Marine Jequier Gygax
marine.jequier@chuv.ch

Specialty section:
This article was submitted to Biomechanics, a section of the journal Frontiers in Bioengineering and Biotechnology

Received: *31 October 2020*
Accepted: *19 February 2021*
Published: *16 March 2021*

Citation:
Jequier Gygax M, Maillard AM and Favre J (2021) Could Gait Biomechanics Become a Marker of Atypical Neuronal Circuitry in Human Development?—The Example of Autism Spectrum Disorder. Front. Bioeng. Biotechnol. 9:624522. doi: 10.3389/fbioe.2021.624522

INTRODUCTION

Although gait biomechanics during human development has been substantially studied, little is known about the neuronal correlates of this motor ability acquisition. As detailed by Dewolf et al. (2020b), emerging gait during early development requires successive interplays and activations of specific brain circuits. Therefore, one might wonder whether gait biomechanics could one day be seen as an expression of the maturation of brain functions.

A way to advance our knowledge in the field would be to study walking biomechanics in different developmental trajectories and correlate the biomechanical data with those assessing brain functions, such as neuroimaging and neuro-electrophysiology. In that perspective, as explained below, autism spectrum disorder (ASD) is a particularly interesting example of alternative brain development trajectory.

ASD is a neurodevelopmental disorder (NDD) related to subtle alterations in brain circuits and functions (Moyses-Oliveira et al., 2020; Shohat et al., 2020). These alterations result from genetics and epigenetics changes and might concern different cerebral regions and circuits (Esposito and Venuti, 2008). Despite current understanding, the diagnosis of ASD solely relies on the observation of clinical criteria according to the DSM-5 (Diagnostic and Statistical Manual of Mental Disorders, 5th edition) (Association, 2013; Lloyd et al., 2013). Particularly, core symptoms in ASD include deficits in social and communication skills, along with restricted interests and repetitive movements and actions. This fairly open set of behavioral criteria contribute to the high clinical heterogeneity in individuals receiving an ASD diagnosis. In spite of this heterogeneity, clinical scales, interview and age-adapted diagnostic tools allow ASD to be diagnosed in early development (18–24 months old). However, no reliable biological markers exist to support or confirm the clinical diagnosis of ASD, to establish a prognosis, or to follow the developmental trajectory. Furthermore, markers to distinguish different subgroups of ASD are still to be defined (Reichow et al., 2012; Studer et al., 2017). This absence of marker is clearly a major limitation to the advance of ASD research and therapeutic management.

Atypical sensory processing is highly prevalent in ASD (Ben-Sasson et al., 2019) and has been reported already in the first description of the disorder (Kanner, 1958b). Since then, ASD studies using clinical scores, questionnaires, and electrophysiology (Robertson and Baron-Cohen, 2017) have reported that the development of the sensory system is probably altered at different levels of processing, from sensory detection through multisensory integration. Alterations in sensory processing have notably been suggested to modify the perception of the environment and the way the individuals adapt their behavior with respect to the surroundings. Interestingly, during brain development, the sensory system matures "hand-in-hand" with the motor system, and sub-optimal functioning in one system has been shown to influence the other (Whyatt and Craig, 2013). A review on motor abilities in ASD using a computational approach suggested two possible origins of the atypical motor development: aberrant sensory noise and poor multisensory integration (Gowen and Hamilton, 2013). In this context, ASD appears particularly relevant to further explore the relationship between sensory and motor system developments. This idea is well supported by the literature review of Mosconi and Sweeney suggesting that sensory-motor dysfunction might be considered as primary features of ASD, assessable at a very young age, even before the behavioral core features of the diagnosis can be confirmed (Mosconi and Sweeney, 2015). In this prior review, the authors exposed how disrupted sensory-motor systems might participate to movement deficits in ASD and underlined the relevance to study motor control in this clinical population, with a possibility to use the motor signature to parse the clinical heterogeneity in ASD. Putting these considerations into practice points out to gait analysis. Indeed, walking is probably the most promising movement related to motor control to analyze for that purpose, as it represents the primary means of locomotion throughout human life, a major developmental milestone and a factor in social construct that can be described by standardized biomechanical measures.

Through a literature analysis, this paper aims at setting the basis for further research on the variability of motor control development, with the perspective to consider gait biomechanics as an expression of brain functions in different developmental trajectories. To illustrate our purpose, we use ASD as an example of atypical development.

MOTOR DEFICIT IN ASD

Alike sensory atypicalities, motor deficits were already reported in the first description of ASD, more than half a century ago (Kanner, 1958a,b). In recent years, different forms of motor impairment have been reported in about 80% of the school-aged children and adults diagnosed with ASD, mostly by case series or cross-sectional studies. Specifically, postural control deficit (Lim et al., 2017), stereotypies (purposeless repetitive movements) (Goldman et al., 2009; Uljarevic et al., 2017), clumsiness, coordination and manual praxis disorders (Weber, 1978; Barrow et al., 2011; Fournier et al., 2014; Kaur et al., 2018), increased joint mobility associated with hypotonia, and gait abnormalities (Shetreat-Klein et al., 2014), as young as 6 months after independent walking (Esposito and Venuti, 2008), have been observed in ASD. Furthermore, hypotonia, a characteristic that can be observed as early as 4–6 months of age, has been associated with autistic traits at 6 years in a longitudinal study (Serdarevic et al., 2017). Additionally, early gross motor developmental disorders have been associated with later ASD diagnosis and social communication deficits (Lloyd et al., 2013; LeBarton and Iverson, 2016). These consistent observations have even motivated some authors to claim that atypical neuro-motor development should be considered as "a putative endophenotype for ASD" (Esposito and Pasca, 2013), or at least as a core feature of the disorder (Teitelbaum et al., 1998; Rinehart et al., 2006; Dufek et al., 2017). Although it is clear that the motor system is altered in ASD, no specific developmental motor pattern has yet been identified, with the possible exception of the presence of dyspraxia in young adults (Dziuk et al., 2007; Kaur et al., 2018). Nevertheless, the recurrent observations of atypical motor development in ASD strongly support that more focused and objective assessments of the movement could highlight "bio-behavioral marker" (Anzulewicz et al., 2016). This possibility is particularly supported by prior works showing differences in upper limb kinematics (Crippa et al., 2015) and in micro-movements variability (Torres, 2013; Torres et al., 2013) between ASD and typically developing (TD) subjects.

Independent walking requires numerous processes like neurological development, musculo-skeletal maturation and experience accumulation, in order to be achieved between 12 and 18 months of age (Burnett and Johnson, 1971a,b; Forssberg, 1985; Thelen and Cooke, 1987; Ivanenko et al., 2007). Analyzing gait biomechanics seems particularly relevant to better understand ASD, and hopefully better manage this disorder in the future, because walking is a robust milestone of the neuro-motor system maturation. Furthermore, gait is a

movement that can be continuously observed lifelong. In that aspect, it could represent an indicator of the brain sensory-motor functions across development and provide an individual motor "signature" (Mosconi and Sweeney, 2015). An additional motivation to focus on walking comes from the tremendous knowhow in quantitative gait analysis, with well-established methods and prior uses in infants and children affected by different developmental disorders, like prematurity (Cahill-Rowley and Rose, 2016), cerebral palsy (Galli et al., 2010) and genetic syndrome (Naito et al., 2015), in addition to ASD, as detailed in the following paragraph.

In 2015, Kindregan et al. (2015), conducted a review on walking biomechanics in children with ASD and concluded to a more unstable gait in patients affected by ASD. Since the publication of the review by Kindregan et al., other studies analyzed gait biomechanics in children with ASD (Lim et al., 2016; Dufek et al., 2017; Eggleston et al., 2017, 2020; Hasan et al., 2017; Biffi et al., 2018; Manicolo et al., 2019). The results from these works and from the studies in the review by Kindregan et al. are summarized in **Figure 1**.

Unfortunately, while consistent in the observations of altered gait biomechanics in ASD, important methodological differences among studies prohibited the identification of specific biomechanical markers. This might come from limitations of prior gait studies displaying relatively small sample sizes and broad age-range in the cross-sectional studied cohorts, not taking into account the variability of gait during development (Hallemans et al., 2006). Furthermore, confounding factors such as ASD severity, attention deficit hyperactivity disorder (ADHD) comorbidity, medication, and obesity were most of the time not addressed, despite ASD movement patterns repeatedly reported as heterogeneous (Calhoun et al., 2011; Dufek et al., 2017; Eggleston et al., 2017). Nevertheless, gait biomechanics should not be viewed as a dead-end, but rather as a point in ASD research where a step toward large-scale studies has to be taken to allow compensating for the natural inter-individual variability, across ASD diagnosis and developmental trajectories. Recent results with other medical conditions have shown that applying machine learning methods on adequately-sized datasets could identify relevant gait patterns (Kwon et al., 2020), even when prior studies with smaller sample sizes reported rather inconsistent results (Mills et al., 2013; Favre and Jolles, 2016). Therefore, advanced statistical modeling or machine learning approaches could also certainly identify gait patterns specific to ASD. For instance, a statistical framework analysis applied to micro-movements during gait allowed distinguishing subjects with genetic syndrome, from subjects with ASD and controls (Torres et al., 2016). While identifying ASD-specific patterns will indisputably constitute a significant advance, it could be possible to go further by considering, not only the gait data, but also

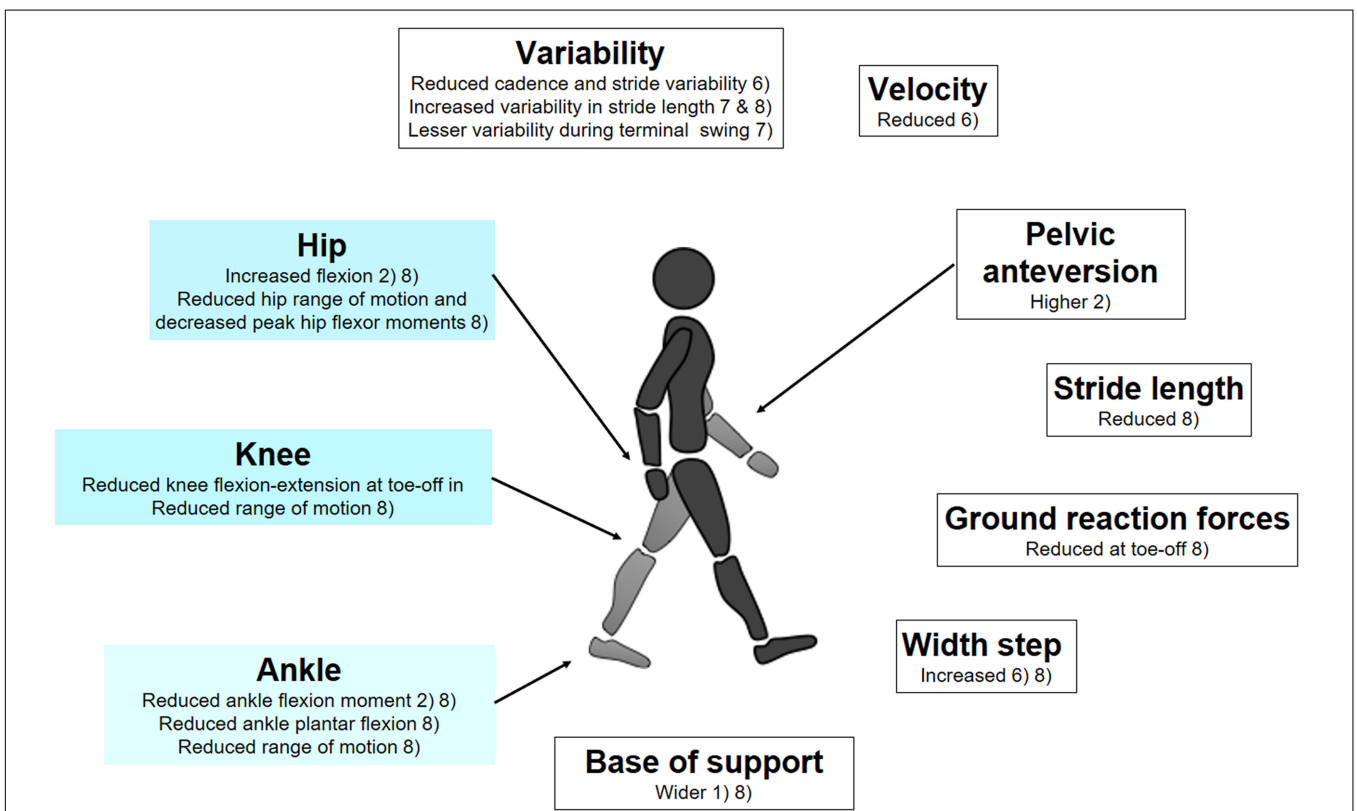

FIGURE 1 | Gait biomechanics data found in children with ASD, in comparison to control groups, matched for age and gender; (1) Manicolo et al. (2019); (2) Biffi et al. (2018); (3) Hasan et al. (2017); (4) Eggleston et al. (2017); (5) Dufek et al. (2017); (6) Lim et al. (2016)—CV Coefficient of variation; (7) Eggleston et al. (2020) (8) Kindregan et al. (2015)—review of 11 studies assessing gait biomechanics in children with ASD.

their relationships with complementary measures. For example, analyzing the associations between the structure of the knee joint and gait biomechanics offered interesting perspectives in the understanding of degenerative joint disease (Edd et al., 2018). In the case of ASD, it could be particularly valuable to bridge biomechanical and neural circuitry data, such as neuroimaging and electrophysiology.

GAIT BIOMECHANICS AND BRAIN NETWORKS MATURATION

In ASD, there are many brain structures thought to be involved in the behavioral semiology, and interestingly, many of these identified structures play a role in the motor system. Since more than a decade, the medial prefrontal cortex, has been recognized as "hub" central nervous system structure implicated in the semiology of autism at the integrative level of functional domains such as perception-sensation and motor skills (Shalom, 2009). Connections between the medial prefrontal cortex and basal ganglia support initiation and inhibition of voluntary movements (Canales and Graybiel, 2000) and are serving higher order cognitive functions in addition to motor control (Leisman et al., 2014). The basal ganglia are implicated not only in neural circuitry connecting sub-regions of prefrontal cortex, but also specific regions in cerebellum. The different neural systems known to present with modified structures and functions in ASD are also modulating afferent and efferent neural information at the level of the pons and the brain stem (for a review see Mosconi and Sweeney, 2015). The next paragraphs point out the role played in motor systems and social cognition by two brain structures – cerebellum and superior temporal sulcus (STS) and one well-described brain network, the default mode network (DMN).

Cerebellar structures and functions differ in ASD children and adult (for a review see Cook et al., 2013). Cerebellum is involved in movement control and in gait maturation, however, it is probably equivalently involved in emotion regulation and social cognition. In an extensive review on cerebellum, Van Overwalle et al. (2020) detailed how this brain structure is a core hub of brain networks involved in motor control and social cognition. It possesses important connections with cortical structure like the right superior temporal sulcus (STS) (Sokolov et al., 2014) involved in face and language processing in social context (Patel et al., 2019; Sato and Uono, 2019). In mouse models of ASD, manipulating circuitry linking prefrontal cortex to cerebellum allowed modulating repetitive motor behavior and social interest (Kelly et al., 2020). In adults with ASD, recognition of biological motion is preserved, but activation of STS during this task is not identical to controls (Alaerts et al., 2017), suggesting a variant recruitment of cerebral networks. An intact neural motor system is mandatory for perception-action coupling, as well as social understanding of the motor intentions, interpreted as visuo-motor resonance (Becchio and Castiello, 2012). These cognitive and somatosensory functions participate to the maturation of the body map representation already in infancy (Marshall and Meltzoff, 2020), and to reciprocal social cognition (Cook, 2016), which could not deploy without reliable sensory-motor system functioning.

Ontogenetically, gait is specific to human development (Forssberg, 1985). During gait development, spinal neural networks (Central Pattern Generators—CPG) are progressively modulated by supra-spinal brain structures. Spinal neural networks have mostly been studied in animal models, and their maturation requires the interplay of speed-dependant spinal interneurons (Deska-Gauthier et al., 2020) and activation/inactivation of sets of motor neurons (Ausborn et al., 2018). A detailed overview of the known and putative mechanisms is provided by Dewolf et al. (2020b). It shows also how little is known about the maturation of the cortical and sub-cortical brain structures leading to adult gait patterns, the timing of their activation, and their functions in this process (Petersen et al., 2010; Dewolf et al., 2020a,b). A recent human study suggested that functional connectivity maturation of the Default Mode Network (DMN) and related motor networks are correlated with walking skills at the age of 12 months. Walking skills was assessed by developmental clinical scale (including data about walking). This work also showed the progressive involvement of additional networks supporting the motor development, revealing possible neural mechanisms linking an early life motor behavior -the start of independent walking—to brain circuitry (Marrus et al., 2018). Interestingly, DMN is recognized for its role in self-referential processing (Raichle, 2015). Altered connectivity of the DMN and motor network have also been correlated to social deficits (Yerys et al., 2015; Nebel et al., 2016). Functional connectivity has been correlated to motor development in children born very preterm with NDD and brain structure maturation and motor skills have been shown to differ in these children compared to those born at term (Wheelock et al., 2018). To our knowledge, no such longitudinal studies combining motor system assessment and functional connectivity has been performed in a cohort of children with ASD.

To summarize, circuitry serving gait maturation and movement control in infants and toddlers most probably participates later to skills like language and higher cognitive function (Leisman et al., 2014), and could also represent a neuro-anatomical substrate to social cognition. Neuroimaging studies in cognitive development might gain from correlating data of standardized biomechanical assessment, like gait biomechanics, sensory-motor profiles and behavioral assessment. This might not only improve the understanding of the "neurophysiological signature" in ASD (Mosconi and Sweeney, 2015), but also help uncover neural substrate dedicated to gait maturation.

PERSPECTIVES

In order to use gait biomechanics as a marker of atypical development, it seems research should first focus on longitudinal studies assessing gait biomechanics in large datasets of typically developing children to establish normative data about motor phenotypes. It will require specific data analysis like dedicated statistical frameworks and machine learning methods. Improving

our knowledge on typically developing children would allow for comparison of motor development in ASD and other NDD.

Based on previous data, the developmental time-window, related to chronological age or developmental and cognitive milestones, might be crucial to identify specific movement patterns and related biomechanical characteristics in clinical research. As an early motor emerging skill, independent gait represents one of these specific developmental time-window. During the first months of independent walking, the maturation of kinetic and kinematic characteristics have been described, and might evolve progressively to an adult gait pattern (Hallemans et al., 2006; Ivanenko et al., 2007; Lacquaniti et al., 2012a). At early stage of development, gait is still not influenced by executive function, that are developing later and that are modulated by cultural environment (Cook, 2016). Additionally, gait represents a lifelong motor skill, easily reproducible and repetitively assessable, from very early life, to adulthood.

As seen, the maturation of independent walking requires the modulation of spinal neuronal networks by the cortico-spinal control. This could not be achieved without a high flexibility of the systems (Lacquaniti et al., 2012b). In ASD population, fragile sensory integration and limited flexibility might generate altered gait maturation in a specific way. ASD is a frequent neurodevelopmental lifelong condition, diagnosed very early in life.

For these different reasons, ASD represents a particularly relevant condition to study the relationships between gait biomechanics and brain circuits. Instrumented gait analysis could offer a possibility to obtain early quantitative data of affected motor patterns and might help identify early motor system traits specific to this disorder. As a standardized data of a motor phenotype, gait biomechanics might be correlated with brain structure and circuitry changes. In this perspective, the comparison of two different developmental trajectories—ASD vs. typically developing children – through biomechanics and brain connectivity, might offer the potential to bridge in a specific manner a clinical diagnosis relying on behavioral criteria, to brain structure and network maturation (**Figure 2**). It might also help further uncover the changes in neural mechanisms implicated in independent walking across development. Such approach is in line with recent concepts of research in mental disease and NDD, which promote the identification of behaviors that can be standardized, with a focus on "circuit-behavior relationships" (RDoc Research Domain Criteria; for details see Cuthbert, 2014; Mittal and Wakschlag, 2017).

To achieve this, gait biomechanics might be considered an estimation of brain functions during development. It should be integrated in clinical research study design combining multi-modal investigations, including neuroimaging, neurophysiology and behavioral assessment of ASD. Due to the interrelated nature of sensory and motor systems maturation, modifying the sensory environment during gait assessment might influence biomechanics in a way to uncover the flexibility of the sensory-motor system, essential to gait maturation. Eventually, if gait biomechanics could be identified as a motor biomarker of ASD, it will add criteria to distinguish population of patients, and orientate follow-up and therapies dedicated to enhancing

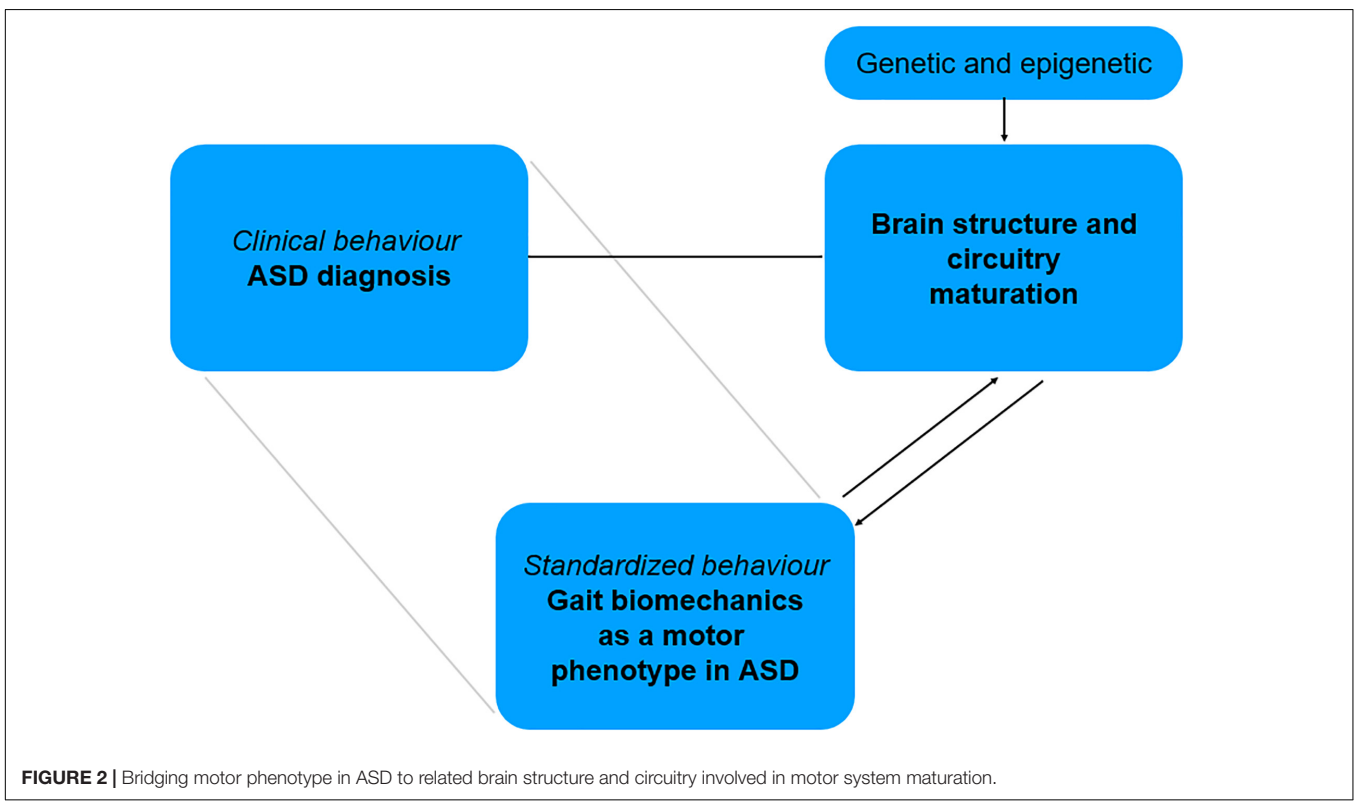

FIGURE 2 | Bridging motor phenotype in ASD to related brain structure and circuitry involved in motor system maturation.

sensory-motor functions. By considering the model of ASD as first step to extend our knowledge about using biomechanics as an expression of brain function, these paradigms could certainly be generalized to other NDD or diseases and offer new research perspectives.

DATA AVAILABILITY STATEMENT

The original contributions presented in the study are included in the article/supplementary material, further inquiries can be directed to the corresponding author/s.

AUTHOR CONTRIBUTIONS

MJ designed and wrote the article. AM participated to the writing. JF contributed to the design and participated to the writing. All authors contributed to the article and approved the submitted version.

FUNDING

This work was supported by the Hoffman Foundation.

REFERENCES

Alaerts, K., Swinnen, S. P., and Wenderoth, N. (2017). Neural processing of biological motion in autism: an investigation of brain activity and effective connectivity. *Sci. Rep.* 7:5612. doi: 10.1038/s41598-017-05786-z

Anzulewicz, A., Sobota, K., and Delafield-Butt, J. T. (2016). Toward the autism motor signature: gesture patterns during smart tablet gameplay identify children with autism. *Sci. Rep.* 6;31107. doi: 10.1038/srep31107

Association, A. P. (2013). , *Diagnostic and statistical manual of mental disorders: DSM-5*. Arlington, VA: American Psychiatric Association. doi: 10.1176/appi.books.9780890425596

Ausborn, J., Snyder, A. C., Shevtsova, N. A., Rybak, I. A., and Rubin, J. E. (2018). State-dependent rhythmogenesis and frequency control in a half-center locomotor CPG. *J. Neurophysiol.* 119, 96–117. doi: 10.1152/jn.00550.2017

Barrow, W. J., Jaworski, M., and Accardo, P. J. (2011). Persistent toe walking in autism. *J. Child Neurol.* 26, 619–621. doi: 10.1177/0883073810385344

Becchio, C., and Castiello, U. (2012). Visuomotor resonance in autism spectrum disorders. *Front. Integr. Neurosci.* 6:110. doi: 10.3389/fnint.2012.00110

Ben-Sasson, A., Gal, E., Fluss, R., Katz-Zetler, N., and Cermak, S. A. (2019). Update of a meta-analysis of sensory symptoms in ASD: a new decade of research. *J. Autism Dev. Disord.* 49, 4974–4996. doi: 10.1007/s10803-019-04180-0

Biffi, E., Costantini, C., Ceccarelli, S. B., Cesareo, A., Marzocchi, G. M., Nobile, M., et al. (2018). Gait pattern and motor performance during discrete gait perturbation in children with autism spectrum disorders. *Front. Psychol.* 9:2530. doi: 10.3389/fpsyg.2018.02530

Burnett, C. N., and Johnson, E. W. (1971a). Development of gait in childhood. I. Method. *Dev. Med. Child Neurol.* 13, 196–206. doi: 10.1111/j.1469-8749.1971.tb03245.x

Burnett, C. N., and Johnson, E. W. (1971b). Development of gait in childhood. II. *Dev. Med. Child Neurol.* 13, 207–215. doi: 10.1111/j.1469-8749.1971.tb03246.x

Cahill-Rowley, K., and Rose, J. (2016). Temporal-spatial gait parameters and neurodevelopment in very-low-birth-weight preterm toddlers at 18-22 months. *Gait Posture* 45, 83–89. doi: 10.1016/j.gaitpost.2016.01.002

Calhoun, M., Longworth, M., and Chester, V. L. (2011). Gait patterns in children with autism. *Clin. Biomech. (Bristol, Avon)* 26, 200–206. doi: 10.1016/j.clinbiomech.2010.09.013

Canales, J. J., and Graybiel, A. M. (2000). A measure of striatal function predicts motor stereotypy. *Nat. Neurosci.* 3, 377–383. doi: 10.1038/73949

Cook, J. (2016). From movement kinematics to social cognition: the case of autism. *Philos. Trans .R Soc. Lond B Biol. Sci.* 371:20150372. doi: 10.1098/rstb.2015.0372

Cook, J. L., Blakemore, S. J., and Press, C. (2013). Atypical basic movement kinematics in autism spectrum conditions. *Brain* 136, 2816–2824. doi: 10.1093/brain/awt208

Crippa, A., Salvatore, C., Perego, P., Forti, S., Nobile, M., Molteni, M., et al. (2015). Use of machine learning to identify children with autism and their motor abnormalities. *J. Autism. Dev. Disord.* 45, 2146–2156. doi: 10.1007/s10803-015-2379-8

Cuthbert, B. N. (2014). Research domain criteria: toward future psychiatric nosology. *Asian J. Psychiatr.* 7, 4–5. doi: 10.1016/j.ajp.2013.12.007

Deska-Gauthier, D., Borowska-Fielding, J., Jones, C. T., and Zhang, Y. (2020). The temporal neurogenesis patterning of spinal p3-v3 interneurons into divergent subpopulation assemblies. *J. Neurosci.* 40, 1440–1452. doi: 10.1523/JNEUROSCI.1518-19.2019

Dewolf, A. H., Ivanenko, Y. P., Mesquita, R. M., Lacquaniti, F., and Willems, P. A. (2020a). Neuromechanical adjustments when walking with an aiding or hindering horizontal force. *Eur. J. Appl. Physiol.* 120, 91–106. doi: 10.1007/s00421-019-04251-1

Dewolf, A. H., Sylos-Labini, F., Cappellini, G., Lacquaniti, F., and Ivanenko, Y. (2020b). Emergence of different gaits in infancy: relationship between developing neural circuitries and changing biomechanics. *Front. Bioeng Biotechnol.* 8:473. doi: 10.3389/fbioe.2020.00473

Dufek, J. S., Eggleston, J. D., Harry, J. R., and Hickman, R. A. (2017). A comparative evaluation of gait between children with autism and typically developing matched controls. *Med. Sci. (Basel)* 5:1. doi: 10.3390/medsci5010001

Dziuk, M. A., Gidley Larson, J. C., Apostu, A., Mahone, E. M., Denckla, M. B., and Mostofsky, S. H. (2007). Dyspraxia in autism: association with motor, social, and communicative deficits. *Dev. Med. Child. Neurol.* 49, 734–739. doi: 10.1111/j.1469-8749.2007.00734.x

Edd,]S. N., Omoumi, P., Andriacchi, T. P., Jolles, B. M., and Favre, J. (2018). Modeling knee osteoarthritis pathophysiology using an integrated joint system (IJS): a systematic review of relationships among cartilage thickness, gait mechanics, and subchondral bone mineral density. *Osteoarthritis Cartilage* 26, 1425–1437. doi: 10.1016/j.joca.2018.06.017

Eggleston, J. D., Harry, J. R., Cereceres, P. A., Olivas, A. N., Chavez, E. A., Boyle, J. B., et al. (2020). Lesser magnitudes of lower extremity variability during terminal swing characterizes walking patterns in children with autism. *Clin. Biomech. (Bristol, Avon)* 76:105031. doi: 10.1016/j.clinbiomech.2020.105031

Eggleston, J. D., Harry, J. R., Hickman, R. A., and Dufek, J. S. (2017). Analysis of gait symmetry during over-ground walking in children with autism spectrum disorder. *Gait Posture* 55, 162–166. doi: 10.1016/j.gaitpost.2017.04.026

Esposito, G., and Pasca, S. P. (2013). Motor abnormalities as a putative endophenotype for autism spectrum disorders. *Front. Integr. Neurosci.* 7:43. doi: 10.3389/fnint.2013.00043

Esposito, G., and Venuti, P. (2008). Analysis of toddlers' gait after six months of independent walking to identify autism: a preliminary study. *Percept Mot. Skills* 106, 259–269. doi: 10.2466/pms.106.1.259-269

Favre, J., and Jolles, B. M. (2016). Gait analysis of patients with knee osteoarthritis highlights a pathological mechanical pathway and provides a basis for therapeutic interventions. *EFORT Open Rev.* 1, 368–374. doi: 10.1302/2058-5241.1.000051

Forssberg, H. (1985). Ontogeny of human locomotor control. I. Infant stepping, supported locomotion and transition to independent locomotion. *Exp. Brain Res.* 57, 480–493. doi: 10.1007/BF00237835

Fournier, K. A., Amano, S., Radonovich, K. J., Bleser, T. M., and Hass, C. J. (2014). Decreased dynamical complexity during quiet stance in children with autism spectrum disorders. *Gait Posture* 39, 420–423. doi: 10.1016/j.gaitpost.2013.08.016

Galli, M., Cimolin, V., Rigoldi, C., Tenore, N., and Albertini, G. (2010). Gait patterns in hemiplegic children with cerebral palsy: comparison of right and left hemiplegia. *Res. Dev. Disabil.* 31, 1340–1345. doi: 10.1016/j.ridd.2010.07.007

Goldman, S., Wang, C., Salgado, M. W., Greene, P. E., Kim, M., and Rapin, I. (2009). Motor stereotypies in children with autism and other developmental

disorders. *Dev. Med. Child. Neurol.* 51, 30–38. doi: 10.1111/j.1469-8749.2008.03178.x

Gowen, E., and Hamilton, A. (2013). Motor abilities in autism: a review using a computational context. *J Autism Dev. Disord.* 43, 323–344. doi: 10.1007/s10803-012-1574-0

Hallemans, A., De Clercq, D., and Aerts, P. (2006). Changes in 3D joint dynamics during the first 5 months after the onset of independent walking: a longitudinal follow-up study. *Gait Posture* 24, 270–279. doi: 10.1016/j.gaitpost.2005.10.003

Hasan, C. Z. C., Jailani, R., Md Tahir, N., and Ilias, S. (2017). The analysis of three-dimensional ground reaction forces during gait in children with autism spectrum disorders. *Res. Dev. Disabil.* 66, 55–63. doi: 10.1016/j.ridd.2017.02.015

Ivanenko, Y. P., Dominici, N., and Lacquaniti, F. (2007). Development of independent walking in toddlers. *Exerc. Sport Sci. Rev.* 35, 67–73. doi: 10.1249/JES.0b013e31803eafa8

Kanner, L. (1958a). History and present status of childhood schizophrenia in the USA. *Z Kinderpsychiatr* 25, 138–149.

Kanner, L. (1958b). The specificity of early infantile autism. *Z Kinderpsychiatr* 25, 108–113.

Kaur, M., M Srinivasan, S., and N Bhat, A. (2018). Comparing motor performance, praxis, coordination, and interpersonal synchrony between children with and without autism spectrum disorder (ASD). *Res. Dev. Disabil.* 72, 79–95. doi: 10.1016/j.ridd.2017.10.025

Kelly, E., Meng, F., Fujita, H., Morgado, F., Kazemi, Y., Rice, L. C., et al. (2020). Regulation of autism-relevant behaviors by cerebellar-prefrontal cortical circuits. *Nat. Neurosci.* 23, 1102–1110. doi: 10.1038/s41593-020-0665-z

Kindregan, D., Gallagher, L., and Gormley, J. (2015). Gait deviations in children with autism spectrum disorders: a review. *Autism Res. Treat* 2015:741480. doi: 10.1155/2015/741480

Kwon, S. B., Ku, Y., Han, H. U., Lee, M. C., Kim, H. C., and Ro, D. H. (2020). A machine learning-based diagnostic model associated with knee osteoarthritis severity. *Sci. Rep.* 10:15743. doi: 10.1038/s41598-020-72941-4

Lacquaniti, F., Ivanenko, Y. P., and Zago, M. (2012a). Development of human locomotion. *Curr. Opin. Neurobiol.* 22, 822–828. doi: 10.1016/j.conb.2012.03.012

Lacquaniti, F., Ivanenko, Y. P., and Zago, M. (2012b). Patterned control of human locomotion. *J. Physiol.* 590, 2189–2199. doi: 10.1113/jphysiol.2011.215137

LeBarton, E. S., and Iverson, J. M. (2016). Gesture development in toddlers with an older sibling with autism. *Int. J. Lang. Commun. Disord.* 51, 18–30. doi: 10.1111/1460-6984.12180

Leisman, G., Braun-Benjamin, O., and Melillo, R. (2014). Cognitive-motor interactions of the basal ganglia in development. *Front. Syst. Neurosci.* 8:16. doi: 10.3389/fnsys.2014.00016

Lim, B. O., O'Sullivan, D., Choi, B. G., and Kim, M. Y. (2016). Comparative gait analysis between children with autism and age-matched controls: analysis with temporal-spatial and foot pressure variables. *J. Phys. Ther. Sci.* 28, 286–292. doi: 10.1589/jpts.28.286

Lim, Y. H., Partridge, K., Girdler, S., and Morris, S. L. (2017). Standing postural control in individuals with autism spectrum disorder: systematic review and meta-analysis. *J. Autism Dev. Disord.* 47, 2238–2253. doi: 10.1007/s10803-017-3144-y

Lloyd, M., MacDonald, M., and Lord, C. (2013). Motor skills of toddlers with autism spectrum disorders. *Autism* 17, 133–146. doi: 10.1177/1362361311402230

Manicolo, O., Brotzmann, M., Hagmann-von Arx, P., Grob, A., and Weber, P. (2019). Gait in children with infantile/atypical autism: age-dependent decrease in gait variability and associations with motor skills. *Eur. J. Paediatr. Neurol.* 23, 117–125. doi: 10.1016/j.ejpn.2018.09.011

Marrus, N., Eggebrecht, A. T., Todorov, A., Elison, J. T., Wolff, J. J., Cole, L., et al. (2018). Walking, gross motor development, and brain functional connectivity in infants and toddlers. *Cereb Cortex* 28, 750–763. doi: 10.1093/cercor/bhx313

Marshall, P. J., and Meltzoff, A. N. (2020). Body maps in the infant brain: implications for neurodevelopmental disabilities. *Dev. Med. Child Neurol.* 62, 778–783. doi: 10.1111/dmcn.14540

Mills, K., Hunt, M. A., and Ferber, R. (2013). Biomechanical deviations during level walking associated with knee osteoarthritis: a systematic review and meta-analysis. *Arthritis Care Res. (Hoboken)* 65, 1643–1665. doi: 10.1002/acr.22015

Mittal, V. A., and Wakschlag, L. S. (2017). Research domain criteria (RDoC) grows up: strengthening neurodevelopment investigation within the RDoC framework. *J. Affect. Disord.* 216, 30–35. doi: 10.1016/j.jad.2016.12.011

Mosconi, M. W., and Sweeney, J. A. (2015). Sensorimotor dysfunctions as primary features of autism spectrum disorders. *Sci. China Life Sci.* 58, 1016–1023. doi: 10.1007/s11427-015-4894-4

Moyses-Oliveira, M., Yadav, R., Erdin, S., and Talkowski, M. E. (2020). New gene discoveries highlight functional convergence in autism and related neurodevelopmental disorders. *Curr. Opin. Genet. Dev.* 65, 195–206. doi: 10.1016/j.gde.2020.07.001

Naito, M., Aoki, S., Kamide, A., Miyamura, K., Honda, M., Nagai, A., et al. (2015). Gait analysis in down syndrome pediatric patients using a sheet-type gait analyzer: pilot study. *Pediatr. Int.* 57, 860–863. doi: 10.1111/ped.12691

Nebel, M. B., Eloyan, A., Nettles, C. A., Sweeney, K. L., Ament, K., Ward, R. E., et al. (2016). Intrinsic visual-motor synchrony correlates with social deficits in autism. *Biol. Psychiatry* 79, 633–641. doi: 10.1016/j.biopsych.2015.08.029

Patel, G. H., Sestieri, C., and Corbetta, M. (2019). The evolution of the temporoparietal junction and posterior superior temporal sulcus. *Cortex* 118, 38–50. doi: 10.1016/j.cortex.2019.01.026

Petersen, T. H., Kliim-Due, M., Farmer, S. F., and Nielsen, J. B. (2010). Childhood development of common drive to a human leg muscle during ankle dorsiflexion and gait. *J. Physiol.* 588, 4387–4400. doi: 10.1113/jphysiol.2010.195735

Raichle, M. E. (2015). The brain's default mode network. *Annu. Rev. Neurosci.* 38, 433–447. doi: 10.1146/annurev-neuro-071013-014030

Reichow, B., Barton, E. E., Boyd, B. A., and Hume, K. (2012). Early intensive behavioral intervention (EIBI) for young children with autism spectrum disorders (ASD). *Cochrane Database Syst. Rev.* 10:CD009260. doi: 10.1002/14651858.CD009260.pub2

Rinehart, N. J., Tonge, B. J., Iansek, R., McGinley, J., Brereton, A. V., Enticott, P. G., et al. (2006). Gait function in newly diagnosed children with autism: cerebellar and basal ganglia related motor disorder. *Dev. Med. Child Neurol.* 48, 819–824. doi: 10.1017/S0012162206001769

Robertson, C. E., and Baron-Cohen, S. (2017). Sensory perception in autism. *Nat. Rev. Neurosci.* 18, 671–684. doi: 10.1038/nrn.2017.112

Sato, W., and Uono, S. (2019). The atypical social brain network in autism: advances in structural and functional MRI studies. *Curr. Opin. Neurol.* 32, 617–621. doi: 10.1097/WCO.0000000000000713

Serdarevic, F., Ghassabian, A., van Batenburg-Eddes, T., White, T., Blanken, L. M. E., Jaddoe, V. W. V., et al. (2017). Infant muscle tone and childhood autistic traits: a longitudinal study in the general population. *Autism. Res.* 10, 757–768. doi: 10.1002/aur.1739

Shalom, D. B. (2009). The medial prefrontal cortex and integration in autism. *Neuroscientist* 15, 589–598. doi: 10.1177/1073858409336371

Shetreat-Klein, M., Shinnar, S., and Rapin, I. (2014). Abnormalities of joint mobility and gait in children with autism spectrum disorders. *Brain Dev.* 36, 91–96.

Shohat, S., Amelan, A., and Shifman, S. (2020). Convergence and divergence in the genetics of psychiatric disorders from pathways to developmental stages. *Biol. Psychiatry* 89, 32–40. doi: 10.1016/j.biopsych.2020.05.019

Sokolov, A. A., Erb, M., Grodd, W., and Pavlova, M. A. (2014). Structural loop between the cerebellum and the superior temporal sulcus: evidence from diffusion tensor imaging. *Cereb Cortex* 24, 626–632. doi: 10.1093/cercor/bhs346

Studer, N., Gundelfinger, R., Schenker, T., and Steinhausen, H. C. (2017). Implementation of early intensive behavioural intervention for children with autism in Switzerland. *BMC Psychiatry* 17:34. doi: 10.1186/s12888-017-1195-4

Teitelbaum, P., Teitelbaum, O., Nye, J., Fryman, J., and Maurer, R. G. (1998). Movement analysis in infancy may be useful for early diagnosis of autism. *Proc. Natl. Acad. Sci. U S A.* 95, 13982–13987. doi: 10.1073/pnas.95.23.13982

Thelen, E., and Cooke, D. W. (1987). Relationship between newborn stepping and later walking: a new interpretation. *Dev. Med. Child Neurol.* 29, 380–393. doi: 10.1111/j.1469-8749.1987.tb02492.x

Torres, E. B. (2013). Atypical signatures of motor variability found in an individual with ASD. *Neurocase* 19, 150–165. doi: 10.1080/13554794.2011.654224

Torres, E. B., Brincker, M., Isenhower, R. W., Yanovich, P., Stigler, K. A., Nurnberger, J. I., et al. (2013). Autism: the micro-movement perspective. *Front. Integr. Neurosci.* 7:32. doi: 10.3389/fnint.2013.00032

Torres, E. B., Nguyen, J., Mistry, S., Whyatt, C., Kalampratsidou, V., and Kolevzon, A. (2016). Characterization of the statistical signatures of micro-movements underlying natural gait patterns in children with phelan McDermid syndrome: towards precision-phenotyping of behavior in ASD. *Front. Integr. Neurosci.* 10:22. doi: 10.3389/fnint.2016.00022

Uljarevic, M., Hedley, D., Alvares, G. A., Varcin, K. J., and Whitehouse, A. J. O. (2017). Relationship between early motor milestones and severity of restricted and repetitive behaviors in children and adolescents with autism spectrum disorder. *Autism Res.* 10, 1163–1168.

Van Overwalle, F., Manto, M., Cattaneo, Z., Clausi, S., Ferrari, C., Gabrieli, J. D. E., et al. (2020). Consensus paper: cerebellum and social cognition. *Cerebellum* 19, 833–868.

Weber, D. (1978). "Toe-walking" in children with early childhood autism. *Acta Paedopsychiatr* 43, 73–83.

Wheelock, M. D., Austin, N. C., Bora, S., Eggebrecht, A. T., Melzer, T. R., Woodward, L. J., et al. (2018). Altered functional network connectivity relates to motor development in children born very preterm. *Neuroimage* 183, 574–583. doi: 10.1016/j.neuroimage.2018.08.051

Whyatt, C., and Craig, C. (2013). Sensory-motor problems in Autism. *Front. Integr. Neurosci.* 7:51. doi: 10.3389/fnint.2013.00051

Yerys, B. E., Gordon, E. M., Abrams, D. N., Satterthwaite, T. D., Weinblatt, R., Jankowski, K. F., et al. (2015). Default mode network segregation and social deficits in autism spectrum disorder: evidence from non-medicated children. *Neuroimage Clin.* 9, 223–232. doi: 10.1016/j.nicl.2015.07.018

Conflict of Interest: The authors declare that the research was conducted in the absence of any commercial or financial relationships that could be construed as a potential conflict of interest.

frontiers in Human Neuroscience

ORIGINAL RESEARCH
published: 30 March 2021
doi: 10.3389/fnhum.2021.635611

Learned Overweight Internal Model Can Be Activated to Maintain Equilibrium When Tactile Cues Are Uncertain: Evidence From Cortical and Behavioral Approaches

*Olivia Lhomond[1], Benjamin Juan[1], Theo Fornerone[1], Marion Cossin[2], Dany Paleressompoulle[1], François Prince[2,3] and Laurence Mouchnino[1]**

[1] Aix-Marseille Université, CNRS, Laboratoire de Neurosciences Cognitives, FR 3C, Marseille, France, [2] Faculty of Medicine, Department of Surgery, Université de Montréal, Montreal, QC, Canada, [3] Institut National du Sport du Québec, Montreal, QC, Canada

OPEN ACCESS

Edited by:
Yury Ivanenko, Santa Lucia Foundation (IRCCS), Italy

Reviewed by:
Olivier Hue, Université du Québec à Trois-Rivières, Canada
Vassilia Hatzitaki, Aristotle University of Thessaloniki, Greece

***Correspondence:**
Laurence Mouchnino
laurence.mouchnino@univ-amu.fr

Specialty section:
This article was submitted to Motor Neuroscience, a section of the journal Frontiers in Human Neuroscience

Received: *30 November 2020*
Accepted: *01 March 2021*
Published: *30 March 2021*

Citation:
Lhomond O, Juan B, Fornerone T, Cossin M, Paleressompoulle D, Prince F and Mouchnino L (2021) Learned Overweight Internal Model Can Be Activated to Maintain Equilibrium When Tactile Cues Are Uncertain: Evidence From Cortical and Behavioral Approaches. Front. Hum. Neurosci. 15:635611. doi: 10.3389/fnhum.2021.635611

Human adaptive behavior in sensorimotor control is aimed to increase the confidence in feedforward mechanisms when sensory afferents are uncertain. It is thought that these feedforward mechanisms rely on predictions from internal models. We investigate whether the brain uses an internal model of physical laws (gravitational and inertial forces) to help estimate body equilibrium when tactile inputs from the foot sole are depressed by carrying extra weight. As direct experimental evidence for such a model is limited, we used Judoka athletes thought to have built up internal models of external loads (i.e., opponent weight management) as compared with Non-Athlete participants and Dancers (highly skilled in balance control). Using electroencephalography, we first (experiment 1) tested the hypothesis that the influence of tactile inputs was amplified by descending cortical efferent signals. We compared the amplitude of P1N1 somatosensory cortical potential evoked by electrical stimulation of the foot sole in participants standing still with their eyes closed. We showed smaller P1N1 amplitudes in the Load compared to No Load conditions in both Non-Athletes and Dancers. This decrease neural response to tactile stimulation was associated with greater postural oscillations. By contrast in the Judoka's group, the neural early response to tactile stimulation was unregulated in the Load condition. This suggests that the brain can selectively increase the functional gain of sensory inputs, during challenging equilibrium tasks when tactile inputs were mechanically depressed by wearing a weighted vest. In Judokas, the activation of regions such as the right posterior inferior parietal cortex (PPC) as early as the P1N1 is likely the source of the neural responses being maintained similar in both Load and No Load conditions. An overweight internal model stored in the right PPC known to be involved in maintaining a coherent representation of one's body

in space can optimize predictive mechanisms in situations with high balance constraints (Experiment 2). This hypothesis has been confirmed by showing that postural reaction evoked by a translation of the support surface on which participants were standing wearing extra-weight was improved in Judokas.

Keywords: balance control, cutaneous plantar inputs, EEG, parietal cortex, somatosensory processes, highly trained athletes

INTRODUCTION

Low confidence in relying on sensory cues to control the movement prompts the nervous system to increase the weighting of predictive mechanisms. According to current models of motor control, predictions from internal models are used to avoid instabilities due to feedback delays and uncertainty (Miall and Wolpert, 1996; Franklin and Wolpert, 2011; Crevecoeur et al., 2014). For example, to distinguish linear acceleration of the body from the gravitational acceleration, Merfeld et al. (1999) showed that an internal model that mimics physical principles is used to resolve the sensory ambiguity. In addition to the sensory ambiguity problem, using prediction from internal models might also be an adaptive behavior occurring when there is low confidence on sensory cues. For example, when wearing a 20 kg vest, a depressed sensory transmission occurred (Lhomond et al., 2016) likely due to foot deformation and skin compression provoked by increased pressure on the feet (Wright et al., 2012). The perceptual consequence of the high pressure exerted on the foot sole has been described by Wu and Madigan (2014) showing that the threshold to detect force applied to the foot sole while standing increased in obese participants relative to healthy individuals.

This change (i.e., increase) in the detection threshold may be the result of a depressed signal transmission to the cortex observed by Lhomond et al. (2016) as early as 50 ms after a tactile electrical stimulation. The early cortical response was associated with the enhancement of later neural responses to tactile stimulation. However, both these early and late neural responses remain non-optimal as shown by behavioral analyses. For instance, when standing still, the postural sway was increased when healthy individuals were loaded (Lhomond et al., 2016). This is not surprising as the increased postural sway is observed in overweight individuals (Hue et al., 2007; Gravante et al., 2003; Greve et al., 2007; Teh et al., 2006; Vela et al., 1998; Wearing et al., 2006). Faster sway was also observed by Simoneau and Teasdale (2015) and was interpreted as reflecting larger balance motor command variability.

In the present study, we investigate whether the brain uses an internal model of physical laws (gravitational and inertial forces) to help estimate body equilibrium when sensory feedback from the foot tactile receptors are altered by extra-weight. The efficacy of the prediction/estimation relies on the ability to activate accurate internal representation of the body position (and motion) relative to the environment. The difference between the brain's prediction of the consequence of the body motion and the actual motion constitutes an error signal; these sensory prediction errors drive the brain to adapt the internal model of how the loaded body motion is related to the sensory consequences (Wolpert et al., 1998a,b for review). Tactile perception may have a special role in body representation (Haggard et al., 2003), because the skin is at the interface between the body (i.e., the feet) and the outside world (i.e., supporting surface). Based on these studies, we sought to determine if the neural and behavioral responses to tactile stimulation are altered by the presence of an accurate internal model built up by training.

As direct experimental evidence for internal models is limited, we used Judoka athletes thought to have constructed internal models of external loads (i.e., opponent weight management). Therefore, it could be possible that the training of the Judokas based on the weight management of the opponent improves their ability to predict the motor and sensory consequences of a destabilization caused by an additional inertial load (Gandolfo et al., 1996; Kawato, 1999; Seidler et al., 2004). For instance, the movement of additional loads on the body is either voluntarily generated by the judoka or in reaction to the opponent's action. Therefore, most of the training contains carrying loads (opponent) in dynamic conditions and controlling forces applied in directions other than the vertical.

Using electroencephalography (experiment 1), we tested the hypothesis that the influence of tactile inputs was amplified by descending cortical efferent signals, by measuring the amplitude of the cortical response to the electric stimulation of the plantar sole (i.e., somatosensory-evoked potential (SEP) technique). We reasoned that the amplitude of this response should be a key variable for comparing the weighting of the foot cutaneous inputs between Judokas and Non-Athlete individuals. However, to disentangle changes in processing due to a specific overweight body internal model built up by Judokas' training or due to high-skill activity in balance control involving somatosensory afferents, we will use a "sham" group of Dancers trained in contemporary dance technique (i.e., barefoot training as in Judokas' training). We reasoned that in Judokas the tactile-related SEP should be enhanced by cortical mechanisms aiming to compensate the depressed signal transmission due to the added weight (Lhomond et al., 2016). Alternatively, in Non-Athlete participants and Dancers the SEP should decrease due to the absence of cortical influence, that is, in absence of training in weight management. The Judokas' training would build up an overweight-body internal model that should optimize the predictive mechanisms when loaded as compared to Non-Athlete participants. We focused our analyses on the right temporoparietal region (i.e., rTPJ), a pivotal region for processing body motion relative to the gravitational field (see Pfeiffer et al., 2014, for a review). This region showed an important role for processing information from different sensory modalities into an

accurate perception of upright (Kheradmand et al., 2015). We predict that the rTPJ will show greater activity in Judokas with the added weight during natural standing.

According to current conceptions of motor control, the brain uses internal models to capture the relationship between the context in which the movement is produced and the effect of the motor commands on the moving body (Wolpert et al., 1995; Wolpert and Flanagan, 2001). The use of internal models for voluntary movement has been also extended to reflex control and specifically to the long latency reflexes of about 45-100 ms postperturbation (Kurtzer et al., 2008). Therefore, these models should also contribute to adapting postural reactions to a body movement not voluntarily produced (i.e., evoked by a translation of the support, Experiment 2). One of the goals of this study was to determine whether altered postural reaction in response to a perturbation can be explained by internal models built up during the judokas' specific training as compared to Non-athlete participants. Postural reaction evoked by a translation of the support surface on which participants are standing wearing extra-weight should be improved in judokas.

MATERIALS AND METHODS

Experiment 1

Participants and Tasks

In Experiment 1, 14 highly trained male Judokas (black belt grade, mean age: 20 ± 3 years; mean height: 178 ± 10 cm; mean weight: 74 ± 10 kg) and 14 Non-Athlete participants (mean age: 25 ± 4 years; mean height: 172 ± 7 cm; mean weight: 70 ± 10 kg) participated in the experiment. A "sham" group of 5 highly trained Dancers (mean age: 25 ± 6 years; mean height: 171 ± 0.1 cm; mean weight: 58 ± 14 kg) was also tested. All participants gave their written informed consent to take part in this study, which conforms to the standards set in the Declaration of Helsinki. Participants were requested to stand upright, barefoot with their arms alongside their body and to keep their eyes closed in two conditions: i) Load, participants were standing while wearing a 20 kg weighted vest representing an increased weight of 26 ± 4% for the Judokas and 27 ± 4% for the Non-Athletes (**Figure 1A**) ii) No Load, without extra weight. As a result, the mean body mass index (BMI) increased from healthy weight to mild obesity for both groups (from 23.7 ± 2.3 kg/m^2 and 23.8 ± 2.8 kg/m^2 to 29.9 ± 2.2 kg/m^2 and 30.1 ± 2.9 kg/m^2 for the Judokas and Non-Athletes, respectively). For both conditions, particular attention was paid to maintain the self-selected foot position constant (i.e., feet shoulder-width apart before each trial) by marking the feet position on the platform on which they are standing. Each participant performed 15 trials in each condition for a total of 60 stimulations. The conditions were presented in block; half of the participants performed the Load condition first while the other half started with the No Load condition.

Stimulating System

The plantar sole of the left foot was stimulated four times (i.e., St1, St2, St3 and St4) with 500 ms between each stimulation in a recording trial which lasted 5 seconds. The stimulus was delivered by an isolated bipolar constant current stimulator (DS5 Digitimer, Welwyn Garden City, UK); the cathode was located under the metatarsal region and the anode underneath the heel (5 × 9 cm electrodes, Fyzea Optimum Electrodes). The stimulation consisted of a single rectangular 10 ms pulse. We used the technique of Mouchnino et al. (2015) who showed that stimulation of the plantar sole skin above the perceptual threshold and below the motor threshold, stimulates the plantar sole as a whole rather than targeting a specific portion of the foot. The stimulation intensity was determined as follows: for each participant while in a quiet standing position, we first found the lowest intensity which resulted in a constant perception of the stimulation. This perceptual threshold was determined, and the stimulation intensity was set at 25% higher than the threshold value. The threshold value showed a main group effect ($F_{2,30}$ = 5.93; p = 0.006); *post hoc* analyses showed that the perceptual threshold of both Judokas and Dancers was higher as compared to Non-Athletes. The high perceptual threshold, which is similar (p = 0.62) for the two high-skilled populations may be the consequence of the greater thickness of the foot sole likely due to barefoot training (8.6 ± 1.3 mA, 8 ± 1.9 mA and 6.9 ± 1 mA for the Judokas, Dancers and Non-Athletes, respectively).

Electrophysiological Recordings and Analyses

Participants were fitted with a 64 Ag/AgCl surface electrodes embedded on an elastic cap ActiveTwo system, BioSemi, Netherlands or Geodesic 64-channel EEG sensor net (GSN64; Electrical Geodesics Inc., Eugene, OR, United States). The EEG was sampled at a rate of 1000 Hz. We performed data pre-processing with BrainVision Analyzer 2 (Brain Products, Germany). The EEG signals were filtered off-line with i) a 40 Hz 24 dB/octave high cut-off filters. ii) a 0.1 Hz 12 dB/octave low cut-off filters and iii) a 50 Hz notch filter when necessary. Somatosensory evoked potentials (SEPs) were obtained by averaging, for each participant and condition, all synchronized epochs relative to the electrical stimulus. The average amplitude of the 150 ms pre-stimulus epoch served as baseline. We measured the SEPs over the Cz electrode as this electrode overlays the sensorimotor cortices and on the homunculus, the feet are located on the inner surface of the longitudinal fissure. A small positive component (P1) was followed by a prominent negative deflection (N1) (**Figure 2A**). Thereafter, a late positive component (P2) followed by negativity (N2). The early P1N1 peak latencies were comparable to latencies evoked by stimulating the sural nerve (Altenmüller et al., 1995; Duysens et al., 1995). The fact that the sural nerve is predominantly a cutaneous nerve (Burke et al., 1981) suggests that P1N1 originates mainly from cutaneous input. The amplitude of the early P1N1 and late P2N2 SEP were measured peak-to-peak.

To estimate the neural sources of the SEPs, we used dynamic statistical parametric mapping (dSPM) implemented in the Brainstorm software (Tadel et al., 2011, freely available at http://neuroimage.usc.edu/brainstorm). We used the data from all sensors processed and averaged for each participant, condition and electrode. The forward model was computed using a three-shell sphere boundary element model (BEM) on the

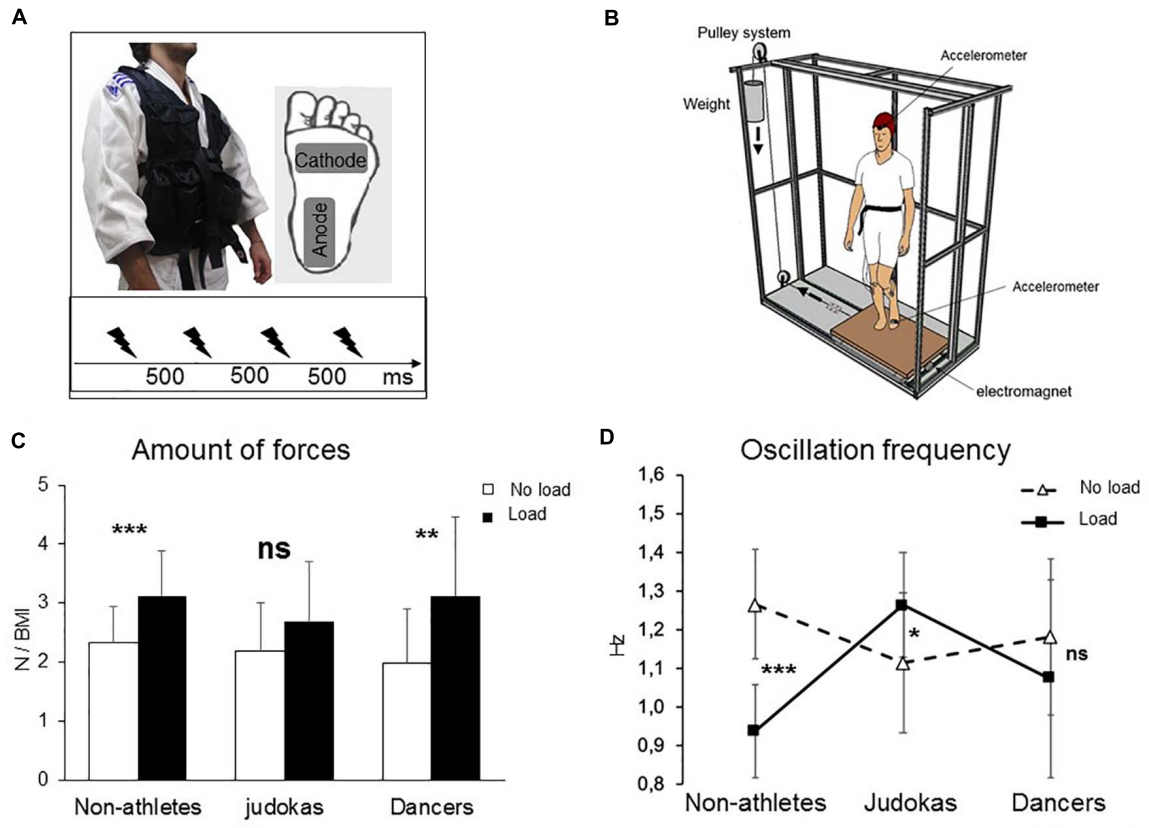

FIGURE 1 | (A) Experimental set up for the electroencephalographic experiment. Insert depicts the workout vest worn by the participants (Judokas, Non-Athletes and Dancers); the added weight was distributed on the front and back of this vest. Position of the stimulation electrodes underneath the left foot and time-intervals between stimulations. **(B)** Experimental set up for the behavioral perturbation experiment 2. The platform translated to the right participant side by means of a pulley system. **(C)** Mean integral of the forces in all directions normalized relative to the BMI for Non-Athletes, Judokas and Dancers (error bars are standard deviation across participants) (**$p < 0.005$; ***$p < 0.001$ and ns: not significant). **(D)** Oscillation frequencies for Non-Athletes, Judokas and Dancers (error bars are standard error of the mean).

anatomical MRI brain MNI Colin27 template (15000 vertices), a predominant volume conductor model (Mosher et al., 1999; Huang et al., 2016). The cortical sources were searched at both the early and late components for each condition.

Behavioural Recordings and Analyses

Participants stood, on a 46.4 × 50.8 cm force platform (AMTI OR6-6, Watertown, MA, United States). Ground reaction forces and moments were recorded at a sampling rate of 1000 Hz and used to analyse body sway along the anteroposterior (AP) and mediolateral (ML) directions. After applying a 10 Hz 4th order Butterworth filter, data were normalized relative to the BMI of each participant. Computing the integral of horizontal forces overtime provides a mean to assess balance control as the shear forces were a technique to maintain balance (King and Zatsiorsky, 2002). For each trial, the integrals for forward, backward, rightward and leftward horizontal forces were computed after de-biasing the signal with a baseline computed during 1s from the recording onset. We computed the integral of a 2s time-window which encompassed the four stimulation periods.

Experiment 2

Participants and Tasks

To assess the behavioral consequence of the neural mechanisms reported in the first experiment, we perturbed the equilibrium of standing participants while standing still. A total of 13 healthy Judokas (mean age: 22 ± 9 years; mean height: 175 ± 7 cm; mean weight: 70 ± 8 kg) and 14 healthy participants (mean age: 23 ± 3 years; mean height: 173 ± 7 cm; mean weight: 68 ± 14 kg) participate in the second experiment. No difference was found between group's BMI ($t_{26} = 0.04$; $p = 0.96$). Seven Judokas and 1 Non-Athlete participated in both experiments on separate occasions. The participants were requested to stand upright barefoot with their arms alongside their body and to keep their eyes closed during the trial. Each participant performed 40 trials per conditions for a total of 80 trials.

Stimulating Systems and Behavioural Recordings and Analyses

Body translation was produced by placing the force platform on two aluminum guiding rails (Bosh Rexroth) with a ball bearing system to reduce friction. A cable attached to the platform ran

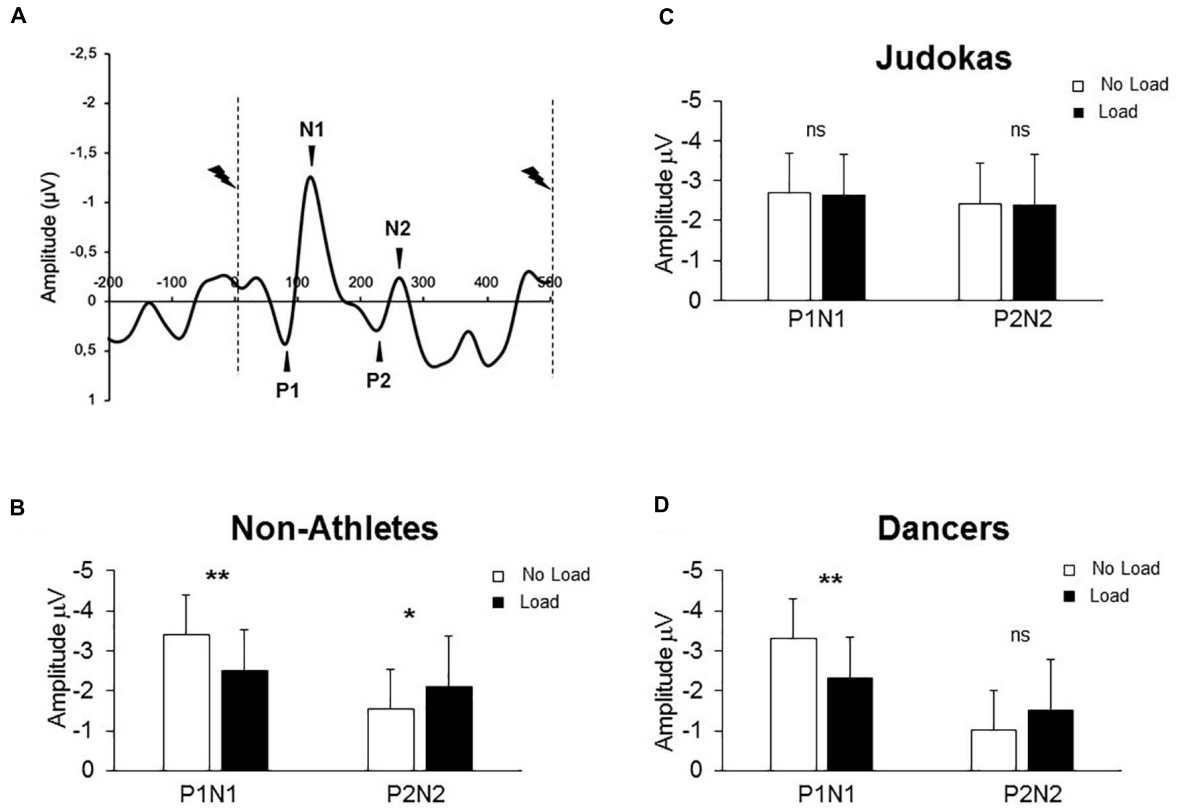

FIGURE 2 | (A) Grand average SEP for all Non-Athletes recorded at Cz in both conditions (Control and Loaded). Dashed lines indicate the moment of the stimulation. **(B) (**Non-Athletes) **(C)** (Judokas) and **(D)** (Dancers): Mean for the 60 stimulations of the early and late SEPs amplitudes for each group (error bars are standard deviation across participants) (**$p < 0.005$; *$p < 0.05$ and ns: not significant).

laterally through a pulley system with a 1.5 kg load fixed to its extremity (**Figure 1B**). The platform was held stationary by an electromagnet fixed on the opposite side to the cable attachment. The platform accelerated very slightly to the right without endangering the participants' equilibrium under the influence of the load only when the restraining electromagnet was deactivated. The lateral translation used in the current study generated a peak acceleration of 7.3 ± 9 cm.s^{-2} with the latency of 142 ± 56 ms which was well below that reported evoking a proximal hip postural reaction (13.5 cm.s^{-2}, Henry et al., 1998). The average acceleration of the platform translation lasted 725 ms and did not vary from trial-to-trial within participants.

Head acceleration was recorded by using a triaxial accelerometer (Model 4630: Measurement Specialties, United States) placed on the forehead. The head acceleration and its latency were analysed in the ML direction (i.e., direction of the platform displacement). For each trial, acceleration signals were filtered with a 10 Hz 4th order Butterworth filter, de-biased and normalized relative to the BMI of each participant (i.e., including participants' weight and height). The integrals for rightward and leftward acceleration were calculated during a 5s period. This was done to assure that at onset of the platform translation, the raw head acceleration signal was below the vestibular threshold (0.048 m.s^{-2}) as reported by Gianna et al. (1996) for similar acceleration profile, so that the translation resulted in a change in the somatosensory cues from the soles of the feet without modifying vestibular inputs. Afterwards, the lateral body tilt that followed stimulated vestibular receptors as confirmed by head acceleration and most likely proprioceptive afferents.

Statistical Analyses

In experiment 1, the SEPs and behavioral data were submitted to repeated-measures analysis of variance (ANOVA) designed with conditions (No Load and Load) and SEP component (early and late responses to tactile stimulation) and Judokas, Non-Athletes and Dancers as a group factor. We also conducted paired t-test for the statistical source estimation maps for contrasts (i.e., Loaded minus No Load conditions). In experiment 2, the data were submitted to an ANOVA design with conditions with the Judokas and Non-Athletes as a group factor. For experiments 1 and 2, significant effects were further analyzed with HSD Tukey test *post hoc* analysis. Since the sample size of the Dancer group was small, partial Eta-Squared values for the effect size were given for the ANOVA. Eta-Squared (η_P^2) value of 0.52 can be interpreted as 52 percent of variance that is associated with each of the main effect (Lakens, 2013). The level of significance was set at 5% for all analyses.

Results Experiment 1

Behavioral Measures of Postural Oscillations

To assess postural stability, the average of the integral of ML and AP forces overtime was computed and normalized to the BMI (**Figure 1C**). The ANOVA revealed a main condition effect (Load, No Load) ($F_{1,28} = 30.7$, $p < 0.001$, $\eta_P^2 = 0.52$). *Post hoc* analyses showed that in the Non-Athletes' group, the amount of forces was higher in the Load than in the No Load conditions ($p = 0.004$) as for the Dancers' group ($p = 0.018$). Interestingly, the Judokas were impervious to influence from the additional weight ($p = 0.22$).

Examination of the frequency of force oscillations (**Figure 1D**) reveals an interaction between the group and condition ($F_{1,28} = 32$; $p < 0.0001$, $\eta_P^2 = 0.69$). In Non-Athletes, *post hoc* analysis revealed a significant decrease in the Load condition compared to the No Load condition ($p = 0.0001$) likely due to additional inertia that tends to slow down the body oscillations. On the contrary, in Judokas, a significant increase of the frequency was observed compared to the No Load condition ($p = 0.022$); this likely allowed a rapid correction to the postural sway excursion due to the additional weight. No significant difference was observed in the Dancers' group ($p = 0.61$).

Somatosensory Evoked Potentials

Figure 2A shows typical EEG signals recorded during quiet standing in the Non-Athletes' group. The results showed a significant interaction between components (early and late) condition (No Load, Load) and group (Non-Athletes, Judokas and Dancers) on the SEP amplitude ($F_{2,30} = 13.8$; $p < 0.0001$, $\eta_P^2 = 0.47$). *Post hoc* analyses confirmed that in the Non-Athlete group (**Figure 2B**) the early P1N1 SEP had a smaller amplitude in the Load compared to the No Load condition while the late P2N2 SEP showed greater amplitude in the Load condition ($p < 0.0001$ and $p = 0.028$, for early and late SEP respectively). In contrast in Judokas (**Figure 2C**), the early P1N1 or late P2N2 SEP is maintained at an equivalent value in both conditions ($p > 0.05$). In Dancers (**Figure 2D**), solely the early SEP had a smaller amplitude in the Load compared to the No Load condition ($p = 0.014$) whereas the late SEP was unchanged ($p > 0.05$).

A main group effect was observed on the P1 latency ($F_{2,30} = 3.78$; $p = 0.034$, $\eta_P^2 = 0.20$); the early SEP latency was shorter in the Non-Athletes than in Judokas' group ($p = 0.033$). No difference was observed between both highly trained groups ($p = 0.96$). The latencies did not show any effect of the condition ($F_{1,30} = 1.11$, $p = 0.29$, see **Table 1** for all latencies). Overall these results confirm that training solely on equilibrium maintenance (i.e., Dance training) may not counteract the effect of extra-weight.

Source Localisation

In order to highlight the sources of the early and late neural responses to tactile stimulation in the Judokas and Non-Athlete groups, we computed the statistical source maps in two 100 ms time windows encompassing the P1N1 and P2N2 components. Remarkably, in both groups (Judokas and Non-Athletes) the statistical source maps revealed as early as the P1N1 component an increase of the superior parietal cortex (BA7) in the Load relative to No Load condition (**Figures 3A,B**). In Judokas (**Figure 3B**) the increase activation of the superior PPC area mainly in the right hemisphere is associated with an increase activation of the right inferior PPC, extrastriate body area (EBA), middle temporal gyrus (MTg) and of the prefrontal and premotor areas localized bilaterally in the Load as compared to the No Load condition. Later during the P2N2 in Non-Athlete participants in the Load condition, significantly greater activation of the inferior PPC and of the prefrontal and, of the rostral and dorsal regions of the anterior cingulate cortex (ACC) bilaterally (**Figure 3A**; the left internal view was not shown) was observed relative to the No Load condition.

Experiment 2: Postural Reaction Evoked by Platform Translation

When the rightward platform translation starts, the ground reaction forces increased in the opposite direction before actively reversing the forces to preserve equilibrium (i.e., postural reaction, **Figure 4A**). The latency of the peak of these shear forces and its amplitude were analyzed (**Figures 4B,C**). The time at which the forces subsequently reversed direction (i.e., postural reaction latency) was similar in both conditions ($F_{1,26} = 0.13$; $p = 0.71$) with no condition * group interaction ($F_{1,26} = 0.81$; $p = 0.37$; overall mean 460 ± 50 ms). The ANOVA showed a main condition effect on the amplitude reached by the force ($F_{1,26} = 15.22$; $p = 0.0006$). However, the condition * group interaction that failed to reach the significant level ($F_{1,26} = 3.45$; $p = 0.07$) showed that in the Non-Athletes' group, the peak amplitude was higher in Load as compared to No Load condition ($p = 0.002$) whereas in the Judokas no differences were observed between conditions ($p = 0.48$).

We have been interested in the amount of head acceleration in reaction to the perturbation as an index for body sway in the frontal plane (i.e., perturbed plane, **Figures 4A,D**). The results showed a significant main effect of condition on the head ML acceleration (normalization with respect to the BMI) to the left side ($F_{1,26} = 6.34$ $p = 0.018$). The head acceleration was smaller in the Load than in the No Load conditions likely due to the stabilizing effect of the mass inertia (**Figure 4D**). No group effect was observed ($F_{1,26} = 0.008$; $p = 0.92$) on the amount of head acceleration.

DISCUSSION

The aim of this study was to determine if the neural and behavioral responses to tactile stimulation are altered by a specific training in weight management under high balance constraints. First, we have confirmed what has been observed previously (Lhomond et al., 2016) in Non-Athletes and extended to the Dancers. In these two groups as compared to the No Load condition, the Load condition showed a depressed early neural response to tactile stimulation. Remarkably and also in accordance to Lhomond et al.'s (2016) study, this decrease was associated with an increase in the late sensory processes

TABLE 1 | Latencies and amplitude of the early and late SEPs (mean and standard deviation) in control as compared with Loaded condition for Non-Athletes, Judokas and Dancers (***$p < 0.001$, **$p < 0.01$; *$p < 0.05$).

Non-Athletes								
	No load				**Load**			
	P1N1		**P2N2**		**P1N1**		**P2N2**	
Latency	47 ± 11 ms	93 ± 15 ms	171 ± 40 ms	208 ± 40 ms	51 ± 10 ms	87 ± 18 ms	175 ± 40ms	215 ± 45ms
Amplitude	−3,39 ± 1,57 μV		−1,54 ± 0,84 μV		−2,50 ± 1,17 μV***		−2,10 ± 1,12 μV*	
Judokas								
	No load				**Load**			
	P1N1		**P2N2**		**P1N1**		**P2N2**	
	59 ± 10ms	95 ± 14ms	164 ± 36ms	220 ± 34ms	62 ± 13ms	99 ± 16ms	167 ± 23ms	224 ± 20ms
	−2,70 ± 1,28 μV		−2,43 ± 1,04 μV		−2,64 ± 1,65 μV		−2,4 ± 1,47 μV	
Dancers								
	No load				**Load**			
	P1N1		**P2N2**		**P1N1**		**P2N2**	
Latency	60 ± 17ms	102 ± 11ms	154 ± 29ms	178 ± 42ms	58 ± 14ms	96 ± 15ms	145 ± 29ms	175 ± 34ms
Amplitude	−3,91 ± 1,83 μV		−0,77 ± 0,68 μV		−2,68 ± 1,38 μV*		−1,03 ± 0,28 μV	

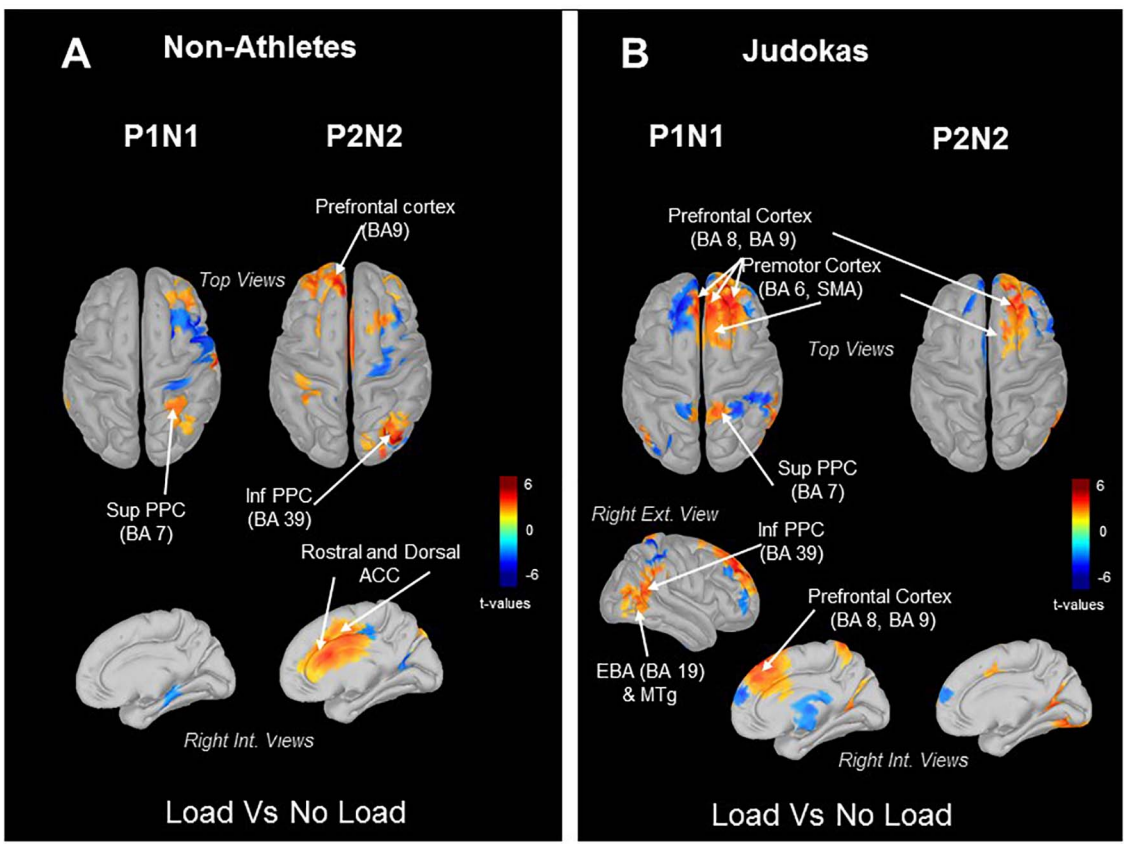

FIGURE 3 | Topographic maps (dSPM) computed from all trials. Significant *t*-values ($p \leq 0.05$, $n = 14$) of the source localization (Loaded minus Control condition) were shown at different timing to assess the dynamic of these activities during the Early SEP and Late SEP. Panel **(A)** in Judokas and panel **(B)** in Non-Athletes.

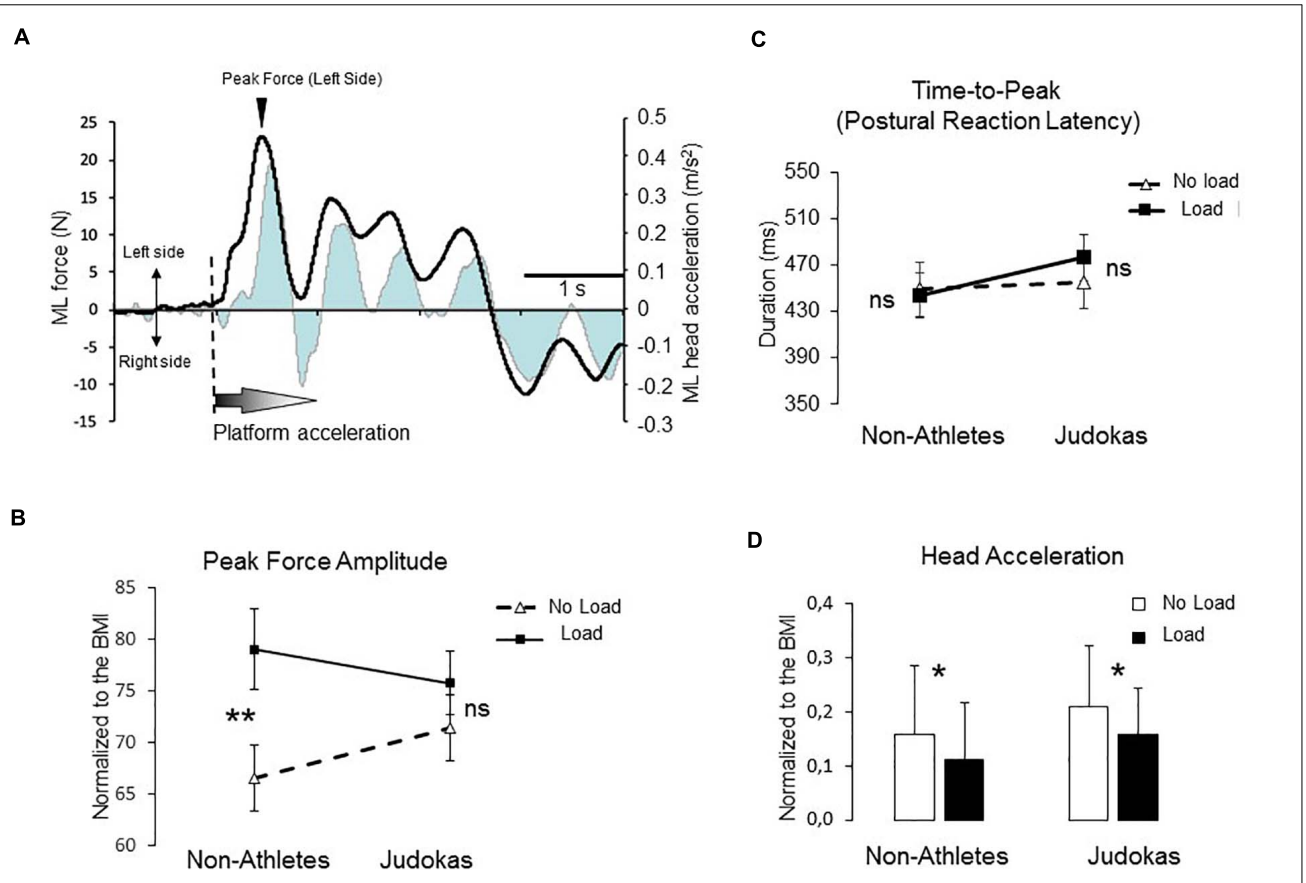

FIGURE 4 | (A) The illustration represents the mean mediolateral force (black line) superimposed on the lateral head acceleration (gray line) for one participant. **(B)** Amplitude of the peak force for Non-Athletes and Judokas (error bars are standard error of the mean) (**$p < 0.005$ and ns: not significant) **(C)** Duration between the onset of the translation and the force peak (i.e., postural reaction latency) in Non-Athletes and Judokas (error bars are standard error of the mean) (ns: not significant) **(D)** Integrals of head acceleration during a 2-s period for Non-Athletes and Judokas normalized to the BMI (*$p < 0.05$).

(i.e., P2N2 SEP). Both mechanisms are, however, functionally non-optimal as shown by increased postural oscillations in the Load condition for Non-Athletes and Dancers. More importantly in the Judoka's group, the neural early response to tactile stimulation was impervious to the Load condition. This suggests that the brain can selectively increase the functional gain of sensory inputs, during challenging equilibrium tasks when tactile inputs were mechanically depressed by wearing a weighted vest. From a behavioral perspective, stability was preserved in Load as compared to No Load conditions in Judokas either in conditions with a stationary supporting surface (Experiment 1) or after platform translation (Experiment 2). On the contrary, Non-Athlete participants increased the amount of force applied to the ground to stay upright (Experiment 1) and the lateral force before reversing their direction to return close to the original equilibrium position (Experiment 2).

An important result of the present study is that the early response to cutaneous stimulation (P1N1 SEP) whether it was decreased (in Non-Athletes and Dancers) or not (in Judokas) was associated with increase activation of the superior PPC (i.e., BA 7) in the Load condition. Increasing the pressure under the feet may have stimulated a population of neurons responsive to somatosensory inputs (Padberg et al., 2009) in the anterior pulvinar nucleus of the thalamus which projects to parietal areas 5 and 7 (i.e., superior PPC; Pons and Kaas, 1985; Gharbawie et al., 2010). This direct thalamocortical projection to the superior PPC could be activated when compression under the skin of the feet increases due to the loading. Indeed, the superior parietal lobule (e.g., PEc and PE areas in the macaque brain), which is an important node for sensorimotor integration, receives strong afferents from regions of the thalamus where legs are represented (Chung et al., 1986; Impieri et al., 2018). Although the same increase of activation is observed in the Load condition in both Non-Athletes and Judokas, the different responses to tactile stimulation can be explained by the presence (Judokas) or not (Non-Athletes) of a parallel distributed processing within the cerebral cortex. For instance, increase activities in the prefrontal cortex (PFC), premotor cortex, inferior PPC, EBA and MTg in the Load condition were observed in Judokas.

In Judokas, in the Load condition the PFC come into play as early as the P1N1. This is consistent with the involvement of the PFC when balance requires a high attention level in order

to trigger the adapted postural reactions. For instance, Basso Moro et al. (2014) showed that the PFC increases its activity in quiet standing participants asked to maintain their 'virtual" equilibrium viewing a virtual swing board susceptible to external destabilizing perturbations. Previously, Slobounov et al. (2000, 2005) proposed the existence of specialized neural detectors of imbalance. They reported an increase of power of the gamma band frequency (30–50 Hz) over the PFC about 200 ms before an avatar shifted from a stable to an unstable posture leading to fall. More specifically the link between PFC activation and the amplitude of the cortical response to tactile stimulation can be described as spatial attention. Indeed, spatial attention to a stimulus (here tactile) enhances the response to the stimulus as reported by Chen et al. (2008) for primary visual areas. The attentional gain operating at cortical level may have counteracted the depressed transmission of tactile inputs due to increase pressure on the mechanoreceptors embedded in the foot sole. For example, this cortical modulation has been reported to maximize the quality of the tactile feedback and improves tactile perception prior to foot contact during locomotion (Duysens et al., 1995 and Dietz et al., 1985).

In addition, there is growing evidence that the frontoparietal cortical network strongly lateralized to the right hemisphere observed in Judokas is recruited for spatial attention when information about the direction of motion is known in advance (see for review Corbetta and Shulman, 2002). Indeed expectation for the pressures motion under the feet when wearing the weighted vest has been learned during the Judokas' training. For instance, the movement of additional loads on the body is either voluntarily generated by the judoka or in reaction to the opponent's action. Therefore most of the training contains carrying loads (opponent) in dynamic conditions and applied in directions other than the vertical.

Expected tactile stimuli (e.g., location, features) elicit greater neural activity in several cortical areas involved in the dorsal frontoparietal network, than unexpected stimuli as in Non-Athletes in the Load condition. These results suggest that Judokas have built up an internal representation of the somatosensory disturbance due to the added weight on the body as it is evidenced by the high balance stability observed in Judokas in the Load condition (Experiment 1) and by the fact that the lateral force before triggering the postural reaction in response to the platform translation was impervious to the load condition (Experiment 2). The fact that at least two representations (normal weighted and overweighed representations) cohabit is in line with evidence that representations of the self are malleable rather than fixed (see for review Apps and Tsakiris, 2014).

Our results highlight the well-known role of the right parietal areas (inf PPC and EBA) in building up, storing and updating a body representation in space (Wolpert et al., 1998a,b; Tsakiris et al., 2008; Pfeiffer et al., 2014). For example, the disruption of the rTPJ and specifically the BA 39 area (see MNI coordinates, Tsakiris et al., 2008) suggested that the rTPJ is actively involved in maintaining a coherent sense of one's body distinct from the external world. An efferent signal from the right PPC could have allowed the integration of tactile cues with proprioceptive localization of body parts in space leading to the remapping of tactile stimulation into an external reference frame (Azañón et al., 2010; Kammers et al., 2006). This is in line with Fabre et al.'s (2020b) study showing that obese individuals improved the sensory processes used in the setting of the anticipatory postural adjustments prior to step initiation after following a program targeting different dimensions of the body internal representation (e.g., proprioceptive training, dance and dance-like training, physical activity and mindfulness-Based Stress Reduction and relaxing session) and not weight loss.

One could argue that the early cortical response to the tactile stimulation observed in Judokas reflected the acquisition of high-level motor skill in balance control. It is noteworthy, however, that even though the Dancers (Perrin et al., 2002; see Bläsing et al., 2012 and Fabre et al., 2020a for reviews) like the Judokas (Taskin et al., 2015) were highly trained in balance control they showed similar neural and behavioral responses to the Non-Athletes' group in the Load condition. It rules out the possibility that early neural modulation reflects solely a learned motor skill in balance control. One could argue that both behavioral and cortical response in dancers might be attributed to their small sample size and/or to the fact that the weight they carried was heavier relative to their body weight than judoka's. However, the similarities in both behavior and cortical activities between the Non-athlete group and the dancers (corroborated by high Eta-squared values), does not support this limitation. Rather, we hypothesize that the sensorimotor changes observed in judokas and not in dancers, which enhanced relevant foot cutaneous information were linked to a modified body representation or a more efficient use of this representation.

Finally, the fact that in Judokas, premotor areas are also engaged in this frontoparietal network shows the close functional linkage between the stimulus- and response-selection signals. In support of this close connection, we have recently demonstrated (Lhomond et al., 2019) that premotor (i.e., SMA) was at the origin of the upregulating cutaneous inputs (when mechanically depressed by added weight) to restore the level of sensory afferents to make it suitable for setting the anticipatory adjustments prior to step initiation. The relationship between relevant sensory inputs and motor activity is evidenced by the fact that Judokas increased their frequency of postural oscillations in the Load as compared to the No Load condition. This enhancement of the frequency is likely actively triggered because due to the added mass the frequency should mechanically decrease as observed in Non-Athletes. In addition, this could explain that the amplitude of the destabilization (i.e., peak force, **Figure 4B**) following the platform translation (experiment 2) before the postural reaction is triggered, were not affected by the Load condition in Judokas. By contrast, the delayed postural responses (larger amplitudes of destabilization) in the Load condition observed in Non-Athletes may be the consequence of a compensation that comes later (i.e., P2N2). The greater activation in the Load condition during the late P2N2 component (**Figure 3A**) of the right inferior PPC and the dorsal and rostral cingulate cortices (ACC) of both hemispheres is consistent with the fact that the motor commands issued from the ACC may have increased due to the load management. This is possible by the existence of direct bilateral connections of this motor area of

the medial wall with the spinal cord and the primary motor cortex (He et al., 1995; Dum et al., 2016).

Our study is the first to explore the cortical activity relative to a judo training which permits to develop some abilities in postural stability during a task requiring a high level of balance control in load condition. Our results showed that the Judokas use internal model of the extra weight built during their training to help estimate body equilibrium when sensory feedback from the foot tactile receptors is altered by extra loads. Judo is one of the Paralympic disciplines that include visually impaired athletes. One particular interesting application of this study is how visually impaired Judokas used the sensory feedback from their feet in order to maintain balance and execute accurate movement carrying extra weight. Considering this study as a translational research and applying knowledge for example, to military purpose when the weight the soldiers carry is heavy is, however, premature. The results of this study may be dependent on the duration of the 'over-weighted balance training' targeting internal body representation improvement. So far, there are no scientific guidelines concerning the optimal duration and intensity of exercises with dynamic external load.

DATA AVAILABILITY STATEMENT

The raw data supporting the conclusions of this article will be made available by the authors, without undue reservation.

ETHICS STATEMENT

Ethical review and approval was not required for the study on human participants in accordance with the local legislation and institutional requirements. The patients/participants provided their written informed consent to participate in this study.

AUTHOR CONTRIBUTIONS

OL, FP, and LM contributed to the design, data collection and analyses, and writing of the manuscript. BJ, TF, MC, and DP contributed to the set up design, data collection, and results analyses. All authors contributed to the article and approved the submitted version.

FUNDING

This study was funded by the Scientific Research and Innovation program of the DGA.

ACKNOWLEDGMENTS

We thank Franck Buloup for developing the software Docometre used for data acquisition and Dany Paleressompoulle for developing the set up used for the experiment.

REFERENCES

Altenmüller, E., Berger, W., Prokop, T., Trippel, M., and Dietz, V. (1995). Modulation of sural nerve somatosensory evoked potentials during stance and different phases of the step-cycle. *Electroencephalogr. Clin. Neurophysiol. Evoked Potentials* 96, 516–525. doi: 10.1016/0013-4694(95)00093-e

Apps, M. A. J., and Tsakiris, M. (2014). The free-energy self: a predictive coding account of self-recognition. *Neurosci. Biobehav. Rev.* 41, 85–97. doi: 10.1016/j.neubiorev.2013.01.029

Azañón, E., Longo, M. R., Soto-Faraco, S., and Haggard, P. (2010). Report the posterior parietal cortex remaps touch into external space. *Curr. Biol.* 20, 1304–1309. doi: 10.1016/j.cub.2010.05.063

Basso Moro, S., Bisconti, S., Muthalib, M., Spezialetti, M., Cutini, S., Ferrari, M., et al. (2014). A semi-immersive virtual reality incremental swing balance task activates prefrontal cortex: a functional near-infrared spectroscopy study. *Neuroimage* 85, 451–460. doi: 10.1016/j.neuroimage.2013.05.031

Bläsing, B., Calvo-Merino, B., Cross, E. S., Jola, C., Honisch, J., and Stevens, C. J. (2012). Neurocognitive control in dance perception and performance. *Acta Psychol.* 139, 300–308. doi: 10.1016/j.actpsy.2011.12.005

Burke, D., Skuse, N. F., and Lethlean, A. K. (1981). Cutaneous and muscle afferent components of the cerebral potential evoked by electrical stimulation of human peripheral nerves. *Electroencephalogr. Clin. Neurophysiol.* 51, 579–588. doi: 10.1016/0013-4694(81)90202-9

Chen, Y., Martinez-Conde, S., Macknik, S. L., Bereshpolova, Y., Swadlow, H. A., and Alonso, J.-M. (2008). Task difficulty modulates the activity of specific neuronal populations in primary visual cortex. *Nat. Neurosci.* 11, 974–982. doi: 10.1038/nn.2147

Chung, J. M., Lee, K. H., Surmeier, D. J., Sorkin, L. S., Kim, J., and Willis, W. D. (1986). Response characteristics of neurons in the ventral posterior lateral nucleus of the monkey thalamus. *J. Neurophysiol.* 56, 370–390. doi: 10.1152/jn.1986.56.2.370

Corbetta, M., and Shulman, G. L. (2002). Control of goal-directed and stimulus-driven attention in the brain. *Nat. Rev. Neurosci.* 3, 201–215. doi: 10.1038/nrn755

Crevecoeur, F., Scott, S. H., Thonnard, J., Lefevre, P., and Valero-Cuevas, F. (2014). Beyond muscles stiffness: importance of state-estimation to account for very fast motor corrections Valero-Cuevas FJ, ed. *PLoS Comput. Biol.* 10:e1003869. doi: 10.1371/journal.pcbi.1003869

Dietz, V., Quintern, J., and Berger, W. (1985). Afferent control of human stance and gait: evidence for blocking of group I afferents during gait. *Exp. Brain Res.* 61, 153–163. doi: 10.1007/BF00235630

Dum, R. P., Levinthal, D. J., and Strick, P. L. (2016). Motor, cognitive, and affective areas of the cerebral cortex influence the adrenal medulla. *Proc. Natl. Acad. Sci. U.S.A.* 113, 9922–9927. doi: 10.1073/pnas.1605044113

Duysens, J., Tax, A. A. M., Nawijn, S., Berger, W., Prokop, T., and Altenmuller, E. (1995). Gating of sensation and evoked-potentials following foot stimulation during human gait. *Exp. Brain Res.* 105, 423–431.

Fabre, M., Blouin, J., and Mouchnino, L. (2020a). Enhancing the internal representation of the body through sensorimotor training in sports and dance improves balance control. *Res. Invest. Sports Med.* 6, 474–476. doi: 10.31031/RISM.2020.06.000629

Fabre, M., Chavet, P., Fornerone, T., Juan, B., Abossolo, O., Pardo, F., et al. (2020b). Somatosensory cortical facilitation during step preparation restored by an improved body representation in obese patients. *Gait Posture* 80, 246–252. doi: 10.1016/j.gaitpost.2020.06.002

Franklin, D. W., and Wolpert, D. M. (2011). Computational mechanisms of sensorimotor control. *Neuron* 72, 425–442. doi: 10.1016/j.neuron.2011.10.006

Gandolfo, F., Mussa-Ivaldi, F. A., and Bizzi, E. (1996). Motor learning by field approximation. *Neurobiology* 93, 3843–3846. doi: 10.1073/pnas.93.9.3843

Gharbawie, O. A., Stepniewska, I., Burish, M. J., and Kaas, J. H. (2010). Thalamocortical connections of functional zones in posterior parietal cortex and frontal cortex motor regions in New World monkeys. *Cereb Cortex* 20, 2391–2410. doi: 10.1093/cercor/bhp308

Gianna, C., Heimbrand, S., and Gresty, M. (1996). Thresholds for detection of motion direction during passive lateral whole-body acceleration in normal subjects and patients with bilateral loss of labyrinthine function. *Brain Res. Bull.* 40, 443–447. doi: 10.1016/0361-9230(96)00140-2

Gravante, G., Russo, G., Pomara, F., and Ridola, C. (2003). Comparison of ground reaction forces between obese and control young adults during quiet standing on a baropodometric platform. *Clin. Biomech.* 18, 780–782. doi: 10.1016/s0268-0033(03)00123-2

Greve, J., Alonso, A., Bordini, A. C. P. G., and Camanho, G. L. (2007). Correlation between body mass index and postural balance. *Clinics* 62, 717–720. doi: 10.1590/s1807-59322007000600010

Haggard, P., Taylor-Clarke, M., and Kennett, S. (2003). Tactile perception, cortical representation and the bodily self. *Curr. Biol.* 13, R170–R173.

He, S. Q., Dum, R. P., and Strick, P. L. (1995). Topographic organization of corticospinal projections from the frontal lobe: motor areas on the medial surface of the hemisphere. *J. Neurosci.* 15:3284. doi: 10.1523/JNEUROSCI.13-03-00952.1993

Henry, S. M., Fung, J., and Horak, F. B. (1998). EMG responses to maintain stance during multidirectional surface translations. *J. Neurophysiol.* 80, 1939–1950. doi: 10.1152/jn.1998.80.4.1939

Huang, Y., Parra, L. C., and Haufe, S. (2016). The New York head—a precise standardized volume conductor model for EEG source localization and tES targeting. *Neuroimage* 140, 150–162. doi: 10.1016/j.neuroimage.2015.12.019

Hue, O., Simoneau, M., Marcotte, J., Berrigan, F., Doré, J., Marceau, P., et al. (2007). Body weight is a strong predictor of postural stability. *Gait Posture* 26, 32–38. doi: 10.1016/j.gaitpost.2006.07.005

Impieri, D., Gamberini, M., Passarelli, L., Rosa, M. G. P., and Galletti, C. (2018). Thalamo-cortical projections to the macaque superior parietal lobule areas PEc and PE. *J. Comp. Neurol.* 526, 1041–1056. doi: 10.1002/cne.24389

Kammers, M. P. M., van der Ham, I. J. M., and Dijkerman, H. C. (2006). Dissociating body representations in healthy individuals: differential effects of a kinaesthetic illusion on perception and action. *Neuropsychologia* 44, 2430–2436. doi: 10.1016/j.neuropsychologia.2006.04.009

Kawato, M. (1999). Internal models for motor control and trajectory planning. *Curr. Opin. Neurobiol.* 9, 718–727. doi: 10.1016/s0959-4388(99)00028-8

Kheradmand, A., Lasker, A., and Zee, D. S. (2015). Transcranial magnetic stimulation (TMS) of the supramarginal gyrus: a window to perception of upright. *Cereb. Cortex* 25, 765–771. doi: 10.1093/cercor/bht267

King, D. L., and Zatsiorsky, V. M. (2002). Periods of extreme ankle displacement during one-legged standing. *Gait Posture* 15, 172–179. doi: 10.1016/s0966-6362(01)00189-8

Kurtzer, I. L., Pruszynski, J. A., and Scott, S. H. (2008). Long-latency reflexes of the human arm reflect an internal model of limb dynamics. *Curr. Biol.* 18, 449–453. doi: 10.1016/j.cub.2008.02.053

Lakens, D. (2013). Calculating and reporting effect sizes to facilitate cumulative science: a practical primer for t-tests and ANOVAs. *Front. Psychol.* 4:863. doi: 10.3389/fpsyg.2013.00863

Lhomond, O., Teasdale, N., Simoneau, M., and Mouchnino, L. (2016). Neural consequences of increasing body weight: evidence from somatosensory evoked potentials and the frequency-specificity of brain oscillations. *Front. Hum. Neurosci.* 10:318. doi: 10.3389/fnhum.2016.00318

Lhomond, O., Teasdale, N., Simoneau, M., and Mouchnino, L. (2019). Supplementary motor area and superior parietal lobule restore sensory facilitation prior to stepping when a decrease of afferent inputs occurs. *Front. Neurol.* 9:1132. doi: 10.3389/fneur.2018.01132

Merfeld, D. M., Zupan, L., and Peterka, R. J. (1999). Humans use internal models to estimate gravity and linear acceleration. *Nature* 398, 615–618. doi: 10.1038/19303

Miall, R. C., and Wolpert, D. M. (1996). Forward models for physiological motor control. *Neural Netw.* 9, 1265–1279. doi: 10.1016/s0893-6080(96)00035-4

Mosher, J. C., Leahy, R. M., and Lewis, P. S. (1999). EEG and MEG: forward solutions for inverse methods. *IEEE Trans. Biomed. Eng.* 46, 245–259. doi: 10.1109/10.748978

Mouchnino, L., Fontan, A., Tandonnet, C., Perrier, J., Saradjian, A. A. H., Blouin, J., et al. (2015). Facilitation of cutaneous inputs during the planning phase of gait initiation. *J. Neurophysiol.* 114, 301–308. doi: 10.1152/jn.00668.2014

Padberg, J., Cerkevich, C., Engle, J., Rajan, A. T., Recanzone, G., Kaas, J., et al. (2009). Thalamocortical connections of parietal somatosensory cortical fields in macaque monkeys are highly divergent and convergent. *Cereb Cortex* 19, 2038–2064. doi: 10.1093/cercor/bhn229

Perrin, P., Deviterne, D., Hugel, F., and Perrot, C. (2002). Judo, better than dance, develops sensorimotor adaptabilities involved in balance control. *Gait Posture* 15, 187–194. doi: 10.1016/s0966-6362(01)00149-7

Pfeiffer, C., Serino, A., and Blanke, O. (2014). The vestibular system: a spatial reference for bodily self-consciousness. *Front. Integr. Neurosci.* 8:31. doi: 10.3389/fnint.2014.00031

Pons, T. P., and Kaas, J. H. (1985). Connections of area 2 of somatosensory cortex with the anterior pulvinar and subdivisions of the ventroposterior complex in macaque monkeys. *J. Comp. Neurol.* 240, 16–36. doi: 10.1002/cne.902400103

Seidler, R., Noll, D., and Thiers, G. (2004). Feedforward and feedback processes in motor control. *Neuroimage* 22, 1775–1783. doi: 10.1016/j.neuroimage.2004.05.003

Simoneau, M., and Teasdale, N. (2015). Balance impairment in obese individuals is caused by larger balance motor commands variability. *Gait Posture* 41, 203–208. doi: 10.1016/j.gaitpost.2014.10.008

Slobounov, S., Hallett, M., Stanhope, S., and Shibasaki, H. (2005). Role of cerebral cortex in human postural control: an EEG study. *Clin. Neurophysiol.* 116, 315–323. doi: 10.1016/j.clinph.2004.09.007

Slobounov, S., Tutwiler, R., Slobounova, E., Rearick, M., and Ray, W. (2000). Human oscillatory brain activity within gamma band (30–50 Hz) induced by visual recognition of non-stable postures. *Cogn. Brain Res.* 9, 177–192. doi: 10.1016/s0926-6410(99)00055-5

Tadel, F., Baillet, S., Mosher, J. C., Pantazis, D., and Leahy, R. M. (2011). Brainstorm: a user-friendly application for MEG/EEG analysis. *Comput. Intell. Neurosci.* 2011:879716. doi: 10.1155/2011/879716

Taskin, C., Karakoc, O., Sanioglu, A., and Taskin, M. (2015). Investigation of postural balance control in judo and handball players. *Turk. J. Sport Exerc.* 17, 92–95. doi: 10.15314/tjse.2015112544

Teh, E., Teng, L. F., Acharya, U. R., Ha, T. P., Goh, E., and Min, L. C. (2006). Static and frequency domain analysis of plantar pressure distribution in obese and non-obese subjects. *J. Bodyw. Mov. Ther.* 10, 127–133. doi: 10.1016/j.jbmt.2005.07.004

Tsakiris, M., Costantini, M., and Haggard, P. (2008). The role of the right temporo-parietal junction in maintaining a coherent sense of one's body. *Neuropsychologia* 46, 3014–3018. doi: 10.1016/j.neuropsychologia.2008.06.004

Vela, S. A., Lavery, L. A., Armstrong, D. G., and Anaim, A. A. (1998). The effect of increased weight on peak pressures: implications for obesity and diabetic foot pathology. *J. Foot Ankle Surg.* 37, 416–420. doi: 10.1016/s1067-2516(98)80051-3

Wearing, S. C., Hennig, E. M., Byrne, N. M., Steele, J. R., and Hills, A. P. (2006). The biomechanics of restricted movement in adult obesity. *Obes. Rev.* 7, 13–24. doi: 10.1111/j.1467-789x.2006.00215.x

Wolpert, D. M., and Flanagan, J. R. (2001). Motor prediction. *Curr. Biol.* 11, R729–R732.

Wolpert, D. M., Ghahramani, Z., and Jordan, M. I. (1995). An internal model for sensorimotor integration. *Science* 269, 1880–1882. doi: 10.1126/science.7569931

Wolpert, D. M., Goodbody, S. J., and Husain, M. (1998a). Maintaining internal representations: the role of the human superior parietal lobe. *Nat. Neurosci.* 1, 529–533. doi: 10.1038/2245

Wolpert, D. M., Miall, R. C., and Kawato, M. (1998b). Internal models in the cerebellum. *Trends Cogn. Sci.* 2, 338–347. doi: 10.1016/s1364-6613(98)01221-2

Wright, W. G., Ivanenko, Y. P., and Gurfinkel, V. S. (2012). Foot anatomy specialization for postural sensation and control. *J. Neurophysiol.* 107, 1513–1521. doi: 10.1152/jn.00256.2011

Wu, X., and Madigan, M. L. (2014). Impaired plantar sensitivity among the obese is associated with increased postural sway. *Neurosci. Lett.* 583, 49–54. doi: 10.1016/j.neulet.2014.09.029

Conflict of Interest: The authors declare that the research was conducted in the absence of any commercial or financial relationships that could be construed as a potential conflict of interest.

frontiers in Bioengineering and Biotechnology

ORIGINAL RESEARCH
published: 01 April 2021
doi: 10.3389/fbioe.2021.635661

Toward Predicting Motion Sickness Using Virtual Reality and a Moving Platform Assessing Brain, Muscles, and Heart Signals

*Marco Recenti[1†], Carlo Ricciardi[1,2†], Romain Aubonnet[1], Ilaria Picone[1,2], Deborah Jacob[1], Halldór Á. R. Svansson[1], Sólveig Agnarsdóttir[1], Gunnar H. Karlsson[1], Valdís Baeringsdóttir[1], Hannes Petersen[3,4] and Paolo Gargiulo[1,5]**

[1] Institute of Biomedical and Neural Engineering, Reykjavik University, Reykjavík, Iceland, [2] Department of Advanced Biomedical Sciences, University Hospital of Naples "Federico II", Naples, Italy, [3] Department of Anatomy, University of Iceland, Reykjavík, Iceland, [4] Akureyri Hospital, Akureyri, Iceland, [5] Department of Science, Landspitali University Hospital, Reykjavík, Iceland

Motion sickness (MS) and postural control (PC) conditions are common complaints among those who passively travel. Many theories explaining a probable cause for MS have been proposed but the most prominent is the sensory conflict theory, stating that a mismatch between vestibular and visual signals causes MS. Few measurements have been made to understand and quantify the interplay between muscle activation, brain activity, and heart behavior during this condition. We introduce here a novel multimetric system called BioVRSea based on virtual reality (VR), a mechanical platform and several biomedical sensors to study the physiology associated with MS and seasickness. This study reports the results from 28 individuals: the subjects stand on the platform wearing VR goggles, a 64-channel EEG dry-electrode cap, two EMG sensors on the gastrocnemius muscles, and a sensor on the chest that captures the heart rate (HR). The virtual environment shows a boat surrounded by waves whose frequency and amplitude are synchronized with the platform movement. Three measurement protocols are performed by each subject, after each of which they answer the Motion Sickness Susceptibility Questionnaire. Nineteen parameters are extracted from the biomedical sensors (5 from EEG, 12 from EMG and, 2 from HR) and 13 from the questionnaire. Eight binary indexes are computed to quantify the symptoms combining all of them in the Motion Sickness Index (I_{MS}). These parameters create the MS database composed of 83 measurements.All indexes undergo univariate statistical analysis, with EMG parameters being most significant, in contrast to EEG parameters. Machine learning (ML) gives good results in the classification of the binary indexes, finding random forest to be the best algorithm (accuracy of 74.7 for I_{MS}). The feature importance analysis showed that muscle parameters are the most relevant, and for EEG analysis, beta wave results were the most important. The present work serves as the first step in identifying the key physiological

OPEN ACCESS

Edited by:
Borja Sañudo,
University of Seville, Spain

Reviewed by:
Andreia S. P. Sousa,
Polytechnic Institute of Porto, Portugal
Chun-Shu Wei,
National Chiao Tung University, Taiwan
Frederic Merienne,
ParisTech École Nationale Supérieure d'Arts et Métiers, France

***Correspondence:**
Paolo Gargiulo
paologar@landspitali.is;
paolo@ru.is

[†] These authors have contributed equally to this work and share first authorship

Specialty section:
This article was submitted to Biomechanics, a section of the journal Frontiers in Bioengineering and Biotechnology

Received: 30 November 2020
Accepted: 05 February 2021
Published: 01 April 2021

Citation:
Recenti M, Ricciardi C, Aubonnet R, Picone I, Jacob D, Svansson HÁR, Agnarsdóttir S, Karlsson GH, Baeringsdóttir V, Petersen H and Gargiulo P (2021) Toward Predicting Motion Sickness Using Virtual Reality and a Moving Platform Assessing Brain, Muscles, and Heart Signals. Front. Bioeng. Biotechnol. 9:635661. doi: 10.3389/fbioe.2021.635661

factors that differentiate those who suffer from MS from those who do not using the novel BioVRSea system. Coupled with ML, BioVRSea is of value in the evaluation of PC disruptions, which are among the most disturbing and costly health conditions affecting humans.

Keywords: motion sickness, postural control, sea sickness, virtual reality, machine learning, heart rate, electroencephalogram – EEG, electromyography – EMG

INTRODUCTION

Postural control (PC) is a central nervous system (CNS) feedback control system that governs human upright stance and gives a platform for locomotion and task-driven behavior, as well as several autonomic responses. The PC system works on a subconscious level and is based on continuous CNS input from visual, vestibular, proprioceptive, and somatosensory receptors Massion (1994). The CNS then processes this information to direct (efferent signals) both somatic (muscular) and autonomic (blood pressure etc.) responses. The PC system can be disturbed in two ways: the first one is a disease disruption (lost function) at all levels, and the second is a physiological "overstimulation" (increased function), which gives rise to motion sickness (MS).

State of the Art

Motion sickness is experienced by those who passively travel and is more common in women and at a young age. Although there are great individual differences, sex and age are both predictors of MS and motion sickness susceptibility (MSS) in general populations, probably due to gene–environment interaction Golding (2006a).

In addition, MS and MSS also fluctuate across age, i.e., in general, humans from 2 years of age begin to feel motion sick during traveling, peaking at 13 years of age and declining postpubertal (Bos et al., 2007; Huppert et al., 2019).

One of the best-known manifestations of MS is seasickness Petersen (2012). Due to modern technology, humans have faced new MS situations such as spaceflights [space sickness Crampton (1990)] or when playing computer games, including the phenomenon of "cybersickness" in virtual reality (VR) environments LaViola (2000). MS is a polysymptomatic disorder, where the primary symptoms are nausea and vomiting, but sweating, facial pallor, increased salivation, drowsiness, and dizziness are also frequent Golding (2006a). There is varying susceptibility among the general population, but all those with a fully or partially functional vestibular system can experience MS. Females report higher incidence in MS history (higher frequency and severity of symptoms) and are more susceptible to seasickness, simulator sickness, and visually induced MS than males of the same age (Flanagan et al., 2005; Lawther and Griffin, 1988; Turner, 1999).

Two main theories regarding the pathogenesis of MS exist. The "sensory conflict theory" (SCT) Reason (1978) states that MS is caused by conflict between visual, vestibular, and/or somatosensory inputs. In the case of passive travel, such as being a passenger in a car or on a ship, the physical motion perceived by the vestibular system does not match the expected signals from the visual system. Sensory conflict can also occur due to a purely visual stimulus, as can be experienced by people during VR simulations who may perceive a visual movement, but vestibular signals do not match this. Recent studies report possible "sensory conflict neurons" in the brainstem and cerebellum (Oman and Cullen, 2014; Cohen et al., 2019) and also brain networks that mediate nausea and vomiting Yates et al. (2014b), which appear to further support the sensory conflict theory. A second theory of pathogenesis in MS is the "postural control theory" Riccio and Stoffregen (1991). It states that prolonged postural instability precedes the subjective symptoms of MS, i.e., that MS is directly brought on by an inability to control the posture during motion rather than a detection of any sensory conflict. The ability to remain bipedal/upright is crucial to human survival and MS appears to be closely linked to postural instability; studies have shown that greater postural instability or increased body sway correlates with greater MSS (Cobb, 1999; Tal et al., 2010).

Regardless of the underlying pathophysiology, CNS adaptive signals as well as efferent signals involved in the corrective processes, preceding and during MS, are measurable via various methods. Some studies have looked into possible correlations between MS levels and physiological biosignals such as electroencephalography (EEG), electrogastrography (EGG), electro-oculography (EOG), skin conductivity, heart rate (HR), blood pressure, body temperature, and cerebral blood oxygen demand visualized in functional magnetic resonance imaging. Relationships between the levels of MS experienced by subjects have been demonstrated in various EEG, EGG, and eye movement studies. Koohestani et al. (2019) give an overview of objective biosignal measures in MS research. Objective kinematic measures such as center of pressure (COP) are also documented as having relationships to MS levels in the literature (Thurrell and Bronstein, 2002; Weech et al., 2018) as well as spectral characteristics of spontaneous sway, which have been measured as a possible objective measurement for a predictive MS parameter Laboissière et al. (2015).

Abbreviations: ADA-B, ada-boosting; AUCROC, area under the curve receiver operating characteristics; CNS, central nervous system; EEG, electroencephalography; EGG, electrogastrography; EMG, electromyography; EOG, electro-oculography; GB, gradient boosting tree; HR, heart rate; I_{Dizz}, dizziness and vertigo index; I_{Fatig}, fatigue index; I_{GenDis}, general discomfort index; I_{Head}, head index; I_{MS}, motion sickness index; I_{NM}, neurological/muscle strain index; I_{PV}, physiological/vegetative index; I_{Stom}, stomach-related index; KNN, K nearest neighbor; LG, low gamma; ML, machine learning; MLP, multilayer perceptron; MS, motion sickness; MSS, motion sickness susceptibility; MSSQ, motion sickness susceptibility questionnaire; PC, postural control; PSD, power spectral density; RF, random forests; SCT, sensory conflict theory; SVM, support vector machine; VR, virtual reality.

Objective measures can be useful for tracking the onset of MS, as it may be possible to use biosignals to predict the likelihood of the subject experiencing MS. Therefore, a subject's MSS can be linked to measurable physiological or kinematic parameters in some cases by correlating the objective measurements with a standardized subjective MSS test/experienced MS level test. This is crucial for all further genetic studies on MS.

Motion sickness susceptibility is generally assessed by means of a questionnaire: subjective reporting of experienced levels of typical MS symptoms during biosignal measurement is a method used extensively in recent experimental studies (Kennedy et al., 1993; Golding, 2016; Mazloumi Gavgani et al., 2018). Correlation of various biosignals and subjective reporting of MS levels is a task to which machine learning (ML) is actively contributing. EEG has been used as a technique to correlate biosignal measurements with MS levels in multiple subjects using ML for VR-related MS Li et al. (2020). Ko et al. (2011) used neural network ML algorithms to estimate patient's MS level based on the EEG power spectra from possible stimulated brain areas. Li et al. (2019) also studied EEG, COP, and head and waist motion markers correlated to a subjective MS questionnaire using ML following visually induced MS. Wang et al. (2019) used postural difference measures pre- and post-visually induced MS calculated with a deep long short term memory model. These studies used visually induced MS exclusively for estimating physiological response in virtual environments. Hell and Argyriou (2018) also used ML to predict MS using a VR rollercoaster simulation tool and a neural network architecture predicting MS and the intensity of roller coasters in order to improve the gaming experience.

Scientific Goal and Proposed Experiment

In this paper, we present the results from the first study using a new seasickness measurement platform called BioVRSea. This system is a sailing simulator that records, in synchronized fashion, heart, muscle, and brain signals (**Figure 1**). The participants wear the VR goggles showing a rough sea scenario. The movement of the ship on the waves in the VR scenario is coupled to the moving platform and the frequency and amplitude of the VR wave motion is synchronized with the platform motion. Subjective and objective MS levels are assessed by a questionnaire while biosensors measure EEG, electromyography (EMG), and HR of the subject. The creation of a database allows the implementation of various statistical and ML algorithms with the aim of correlating the biometric results with new indexes that combine the various symptoms of MS, having as main novelty the EEG application and interpretation in association with VR and moving platform inducing MS, linked to other biosignals.

MATERIALS AND METHODS

The biosensors used in this study are 64-channel EEG, 2-channel EMG, and HR chest monitor.

This first study is based on data acquired from 28 subjects (age: 23.8 ± 1.2), 22 women and 6 men (ethic approval by the Icelandic Bioethics Commission – Number: VSN-20-101 – May 2020). Each participant is measured three times (except one subject who underwent only two protocols) using different protocols based on the amplitude and frequency of the simulated waves. From each protocol, we extract 19 parameters associated with HR, EEG, and EMG signals. Moreover, after every protocol, the

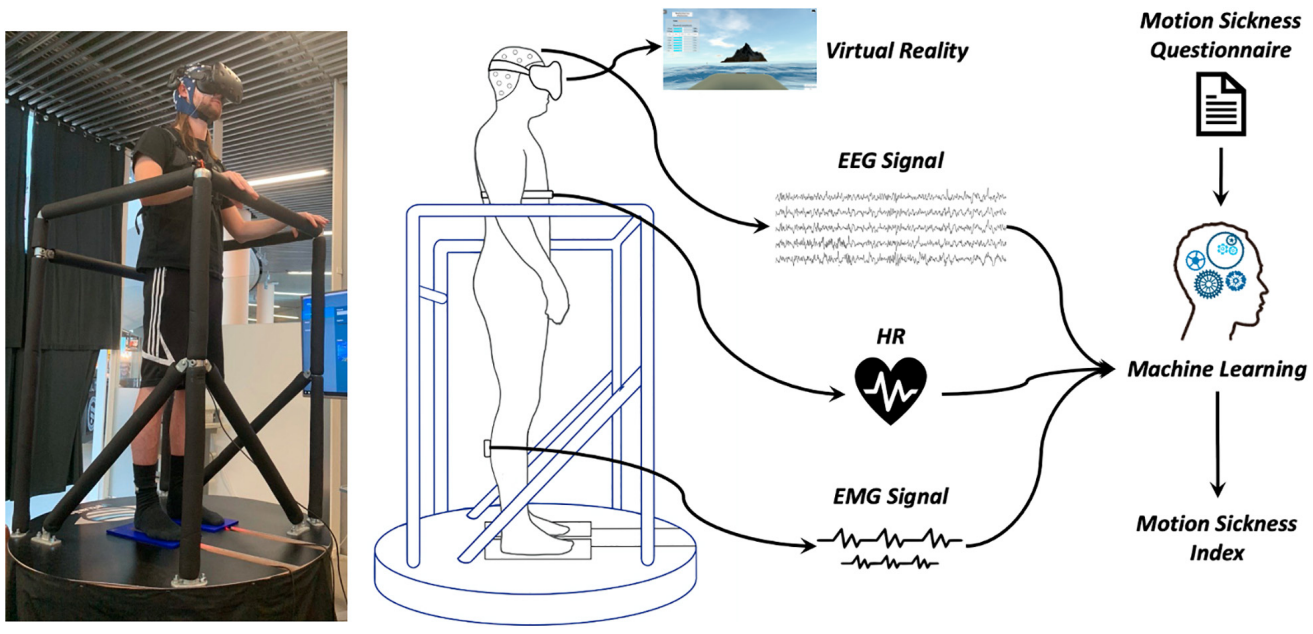

FIGURE 1 | BioVRSea structure: the moving platform, shown in a photo with a subject on the left, is combined with a rough sea VR scenario and with EEG, EMG, and HR bio-signal acquisition.

subject answers the Motion Sickness Susceptibility Questionnaire (MSSQ) Golding (2006b) based on the self-evaluation of 13 different neurophysiological conditions. A total of 83 datasets [(28 × 3) - 1] constitute the final database of our study.

BioVRSea Measurement's Protocols

The VR software (Virtualis, VR, France) dynamically visualizes a virtual environment as if the subject is out on the open sea on a little boat. A moving platform (Virtualis VR, France) mimics the waves according to the simulated environment (**Figure 1**). The operator can set frequency (between 0.5 and 3 Hz) and amplitude of the waves (from 0 to 2). During the simulation, we vary the amplitude of the platform movements from 0% up to 100%. The platform allows fast (tailored) movements in 0°−45°−90°−135°−180°−225°−270°−315°−360° (linear acc. not available) coupled to synchronized visual VR movements.

Three different protocols are implemented in this study (**Figure 2**):

- 0 Hz, null wave amplitude. Sea simulation is not performed during this protocol. The subject remains in an upright position on the platform for 60 s, observing mountains surrounded by lights in a dark environment through the goggles.
- 1 Hz, and wave amplitude = 0.6. This sea simulation protocol is divided into four parts, 30 s each with different platform movement amplitudes: 25, 50, 75, and again 25%. Total time: 120 s.
- 3 Hz, and wave amplitude = 0.5. This sea simulation protocol is divided into four parts, 30 s each with different platform movement amplitudes: 25, 50, 75, and again 25%. Total time: 120 s.

The first protocol mentioned (0 Hz) is the non-movable (platform stable) pre-test (baseline) sampling where the subjects can relax. This is done before the other two protocols (1 and 3 Hz) where the subjects during the movements have to grab onto the protection bars that they have in front. The eyes must be opened during all the three protocols.

The selection of these frequencies was based on two main reasons. The first reason is to only act upon one of MS etiologic theory: multiple theories have been listed to explain MS, and the SCT is easily the leading perspective. Frequencies below 1 Hz are not considered because they might act upon the additional Postural Instability Theory, which is rooted in perception of lower <0.5 Hz frequencies Riccio and Stoffregen (1991). The second reason is to ensure that an easy scenario (1 Hz) is available to reduce the risk of falling, as well as a harder one (3 Hz) to ensure sufficient movement to trigger MS.

Data Acquisition

During each protocol, heart, muscle, and brain data are acquired using the following technologies:

- HR is measured using a heart chest sensor (Polar Electro, Kempele, Finland, sampling frequency of 1,000 Hz).
- Muscle electrical activities from the lower limbs are acquired using two wireless EMG sensors (sampling frequency of 1,600 Hz) placed on the gastrocnemius of each leg (Kiso ehf, Reykjavik, Iceland).
- Brain electrical activity is measured using a 64-channel dry electrode cap (sampling frequency of 500 Hz) from AntNeuro, Hengelo, Netherlands.

Feature Extraction

Electromyography data processing was performed using Matlab_2020b (MathWorks Inc., Natick, Massachusetts, United States). The EMG signal was filtered with a 50th-order FIR bandpass filter with cutoff frequencies at 40 and 500 Hz.

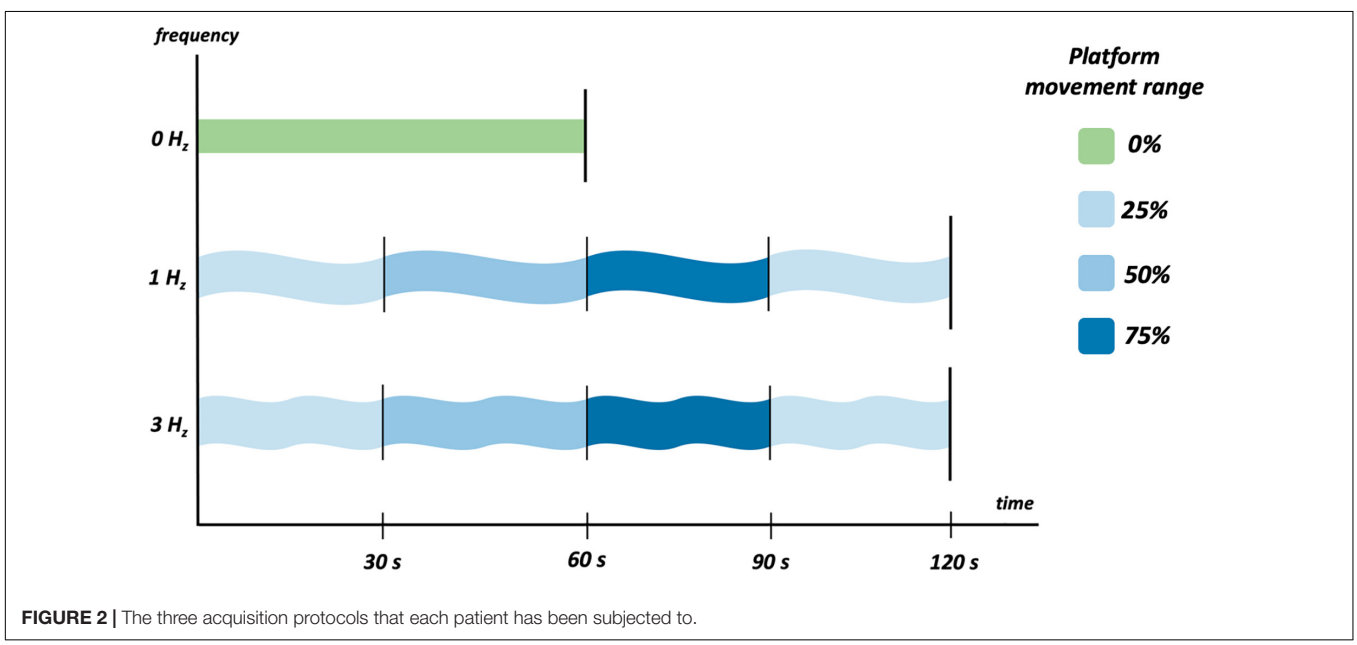

FIGURE 2 | The three acquisition protocols that each patient has been subjected to.

A fast Fourier transform was then used to obtain the frequency spectrum. The relative power spectral density (PSD) was then calculated for five frequency bands, equally distributed from 40 to 500 Hz, resulting in five parameters per leg. Finally, the integral of the rectified EMG signal for each leg was calculated and divided by the sample size, resulting in one parameter per leg. A total of 12 EMG-related features is thus computed.

The EEG was recorded using a 64-dry electrode channel system with an EOG electrode placed below the right eye and a ground electrode placed on the left side of the neck. Data pre-processing and analysis were performed with Brainstorm Tadel et al. (2011) and Matlab_2020b.

The data were re-referenced using the common average reference. A high-pass and a low-pass filter were set, respectively, from 0.1 and 40 Hz. Bad channels were manually removed when EEG voltage was higher than 300 μV. If more than 20% of the channels showed too much noise or incorrect signal, the whole trial was rejected. The signals were digitized in segments of 30 s, within 1-Hz and 3-Hz protocols. DC offset correction was performed, and baseline correction was applied using the 0-Hz segment. Channels marked as bad were removed and interpolated. Individual trials were visually inspected and rejected when indicative of excessive muscle activity, eye movements, or other artifacts.

The PSD was computed for each epoch with Welch's method, with the following frequency bands: delta (0.5–4 Hz), theta (4–8 Hz), alpha (8–13 Hz), beta (13–35 Hz), and low gamma (LG) (35–40 Hz). The relative power of each band was then computed and averaged across all channels, obtaining a total of five EEG-related features.

Finally, from the HR signal, we calculate two features: HR average and standard deviation.

This results in a total of 19 biometric features for each acquisition protocol (**Table 1**).

Table 2 shows the objective physiological measurement differences for all the subjects between the first static protocol and the other two, the light one (1 Hz) in green and the hard one (3 Hz) in red. The arrows show how the values of the single EEG, EMG, and HR data rise or fall during the protocols. For example, it is possible to notice how the EMG values for both legs at low frequencies increase for the most patients, while they decrease at high frequencies. On the opposite, the EEG values do not follow such a regular trend.

TABLE 1 | Description of the 19 biometric parameters that compose the database.

Biometric parameter	Description
EEG – Delta	Relative power spectra between frequency band 0.5–4 Hz
EEG – Theta	Relative power spectra between frequency band 4–8 Hz
EEG – Alpha	Relative power spectra between frequency band 8–13 Hz
EEG – Beta	Relative power spectra between frequency band 13–35 Hz
EEG – LG	Relative power spectra between frequency band 35–40 Hz
EMG – L area	Integral of the rectified EMG signal of left gastrocnemius divided by the sample size
EMG – R area	Integral of the rectified EMG signal of right gastrocnemius divided by the sample size
EMG – L 40-132	Left gastrocnemius relative PSD in the 40–132 Hz frequency band
EMG – L 132-224	Left gastrocnemius relative PSD in the 132–224 Hz frequency band
EMG – L 224-316	Left gastrocnemius relative PSD in the 224–316 Hz frequency band
EMG – L 316-408	Left gastrocnemius relative PSD in the 316–408 Hz frequency band
EMG – L 408-500	Left gastrocnemius relative PSD in the 408–500 Hz frequency band
EMG – R 40-132	Right gastrocnemius relative PSD in the 40–132 Hz frequency band
EMG – R 132-224	Right gastrocnemius relative PSD in the 132–224 Hz frequency band
EMG – R 224-316	Right gastrocnemius relative PSD in the 224–316 Hz frequency band
EMG – R 316-408	Right gastrocnemius relative PSD in the 316–408 Hz frequency band
EMG – R 408-500	Right gastrocnemius relative PSD in the 408–500 Hz frequency band
HR average	Heart rate average
HR std	Heart rate standard deviation

Motion Sickness Questionnaire and Relative Indexes

At the end of every protocol the subjects were asked to fill out a questionnaire regarding their MS symptoms. The questionnaire is based on the MSSQ proposed by Golding (2006b). The subjects must give a score between zero and two for 13 typical MS symptoms: general discomfort, dizziness and vertigo, stomach awareness, sweating, nausea, salivation, burping, headache, fullness of head, blurred vision, fatigue, eye strain, and difficulty focusing.

We define a total of eight binary indexes considering the MSSQ answers.

General discomfort (I_{GenDis}, 1st) and Dizziness and Vertigo (I_{Dizz}, 2nd) are considered as independent and individual indexes. Stomach awareness, sweating, nausea, salivation, and burping are considered together as stomach-related to create the Stomach-related Index (I_{Stom}, 3rd). Headache, fullness of head, and blurred vision together produce the Head Index (I_{Head}, 4th) while fatigue, eye strain, and difficulty focusing contribute to the Fatigue Index (I_{Fatig}, 5th). I_{Stom}, I_{Fatig}, and I_{Head} are computed as binary indexes following these steps: first, we compute the average from the individual responses of each index; second, we calculate the maximum among the averages; and third, we divide the cohort into two groups (below and above 1/3 of the maximum). For I_{GenDis} and I_{Dizz}, we apply only steps 2 and 3 using the direct response instead of the average.

Moreover, we established two more indexes, Physiological/Vegetative Index (I_{PV}, 6th) and Neurological/Muscle Strain Index (I_{NM}, 7th). I_{PV} is based on the previously outlined steps from the responses from

TABLE 2 | Difference of the objective brain, muscle, and health bio measurements between the first static protocol and the light (1 Hz – green) and the hard one (3 Hz – red) for all the patients (the one that did not perform the 3-Hz protocol is not included).

PATIENT ID	1	2	3	4	5	6	7	8	9	10	11	12	13	14	15	16	17	18	19	20	21	22	23	24	25	26	27
EEG – Delta	↓	↓	↓	↓	↓	↓	↓	↓	↓	↑	↑	↑	↑	↑	↓	↑	↑	↑	↑	↑	↓	↓	↓	↓	↓	↓	↓	↓	↓	↑	↓	↓	↓	↑	↑	↓	↑	↓	↓	↓	↓	↑	↑
EEG – Theta	↑	↑	↑	↑	↑	↓	↑	↑	↓	↓	↓	↓	↓	↓	↑	↓	↓	↓	↓	↓	↓	↓	↓	↓	↓	↓	↓	↓	↓	↑	↑	↓	↓	↑	↓	↑	↓	↓	↓	↓	↑	↓	↓	↓	↓
EEG – Alpha	↑	↑	↑	↑	↑	↑	↑	↑	↑	↓	↓	↓	↓	↓	↑	↓	↓	↓	↓	↓	↓	↓	↓	↑	↓	↑	↓	↓	↓	↓	↓	↑	↑	↑	↑	↑	↑	↑	↑	↓	↑	↑	↑	↓	↓	↑	↓	↑	↓	↑	↓	↓	↓
EEG – Beta	↑	↑	↑	↑	↑	↑	↑	↑	↑	↑	↓	↓	↑	↑	↓	↓	↓	↑	↑	↑	↑	↓	↓	↑	↑	↑	↑	↓	↑	↑	↑	↑	↑	↑	↑	↑	↑	↑	↑	↑	↓	↓	↓	↑	↓	↑	↑	↑	↑	↑	↑
EEG – LG	↑	↑	↑	↑	↑	↑	↑	↑	↑	↑	↓	↑	↑	↑	↑	↑	↓	↓	↑	↑	↑	↑	↑	↑	↑	↑	↑	↑	↑	↑	↑	↑	↑	↑	↑	↑	↑	↑	↑	↑	↓	↓	↑	↑	↑	↑	↑	↓	↑	↑	↑	↑	↑
EMG – L area	↑	↑	↑	↑	↑	↑	↑	↑	↑	↑	↑	↑	↑	↑	↑	↑	↑	↑	↑	↑	↑	↑	↑	↑	↑	↑	↑	↑	↑	↑	↑	↑	↑	↑	↑	↑	↑	↑	↑	↑	↑	↑	↑	↑	↑	↑	↑	↑	↑	↑	↑	↑	↑
EMG – R area	↑	↑	↑	↑	↑	↑	↑	↑	↑	↑	↑	↑	↑	↑	↑	↑	↑	↑	↑	↑	↑	↑	↑	↑	↑	↑	↑	↑	↑	↑	↑	↑	↑	↑	↑	↑	↑	↑	↑	↑	↓	↑	↑	↑	↑	↑	↑	↑	↑	↑	↑	↑	↑
EMG – L 40-132	↑	↑	↑	↑	↑	↑	↑	↑	↑	↑	↑	↑	↑	↑	↑	↑	↑	↑	↑	↑	↑	↑	↑	↑	↑	↑	↑	↑	↑	↑	↑	↑	↑	↑	↑	↑	↑	↑	↑	↑	↓	↓	↑	↑	↑	↑	↑	↑	↑	↑	↑	↓	↑	↑	↑
EMG – L 132-224	↓	↓	↓	↑	↓	↓	↓	↓	↓	↓	↓	↓	↑	↓	↓	↓	↓	↓	↑	↓	↓	↓	↓	↓	↓	↓	↓	↓	↓	↑	↑	↑	↓	↓	↓	↓	↓	↓	↓	↓	↑	↑	↓	↑	↓	↓	↓	↓	↓	↓	↓	↓	↓	↓	↓
EMG – L 224-316	↓	↓	↓	↓	↓	↓	↓	↓	↓	↓	↓	↓	↓	↓	↓	↓	↓	↓	↑	↓	↓	↓	↓	↓	↓	↓	↓	↓	↓	↑	↑	↓	↓	↓	↓	↓	↓	↓	↓	↓	↑	↓	↓	↓	↓	↓	↓	↓	↓	↓	↓	↓	↓	↓
EMG – L 316-408	↓	↓	↓	↓	↓	↓	↓	↓	↓	↓	↓	↓	↓	↓	↓	↓	↓	↓	↑	↓	↓	↓	↓	↓	↓	↓	↓	↓	↓	↑	↑	↓	↓	↓	↓	↓	↓	↓	↓	↓	↑	↓	↓	↓	↓	↓	↓	↓	↓	↓	↓	↓	↓	↓
EMG – L 408-500	↓	↓	↓	↓	↓	↓	↓	↓	↓	↓	↓	↓	↓	↓	↓	↓	↓	↓	↑	↓	↓	↓	↓	↓	↓	↓	↓	↓	↓	↑	↑	↓	↓	↓	↓	↓	↓	↓	↓	↓	↑	↓	↓	↓	↓	↓	↓	↓	↓	↓	↓	↓	↓	↓
EMG – R 40-132	↑	↑	↓	↑	↑	↑	↑	↑	↑	↑	↑	↑	↑	↑	↑	↑	↑	↑	↑	↑	↑	↑	↑	↑	↑	↑	↑	↑	↑	↑	↑	↑	↑	↑	↑	↑	↑	↑	↑	↑	↓	↓	↑	↑	↑	↑	↑	↑	↑	↑	↑	↑	↑
EMG – R 132-224	↑	↓	↓	↓	↓	↓	↑	↑	↓	↓	↓	↓	↓	↓	↓	↓	↓	↓	↓	↑	↑	↓	↓	↓	↓	↑	↓	↓	↓	↓	↑	↓	↓	↓	↓	↓	↓	↑	↑	↑	↑	↓	↓	↑	↓	↑	↓	↓	↓	↓	↓	↓	↓
EMG – R 224-316	↓	↓	↑	↓	↓	↓	↓	↓	↓	↓	↓	↓	↓	↓	↓	↓	↓	↓	↓	↓	↓	↓	↑	↓	↓	↓	↓	↓	↓	↓	↓	↓	↓	↓	↓	↓	↓	↓	↓	↓	↑	↑	↓	↓	↓	↓	↓	↓	↓	↓	↓	↓	↓
EMG – R 316-408	↓	↓	↑	↓	↓	↓	↓	↓	↓	↓	↓	↓	↓	↓	↓	↓	↓	↓	↓	↑	↓	↓	↓	↓	↓	↓	↓	↓	↓	↓	↓	↑	↓	↓	↓	↓	↓	↑	↓	↓	↓	↓	↓	↓	↓	↓	↓	↓	↓	↑	↓	↓	↓
EMG – R 408-500	↓	↓	↑	↓	↓	↓	↓	↓	↓	↓	↓	↓	↓	↓	↓	↓	↓	↓	↓	↑	↓	↓	↓	↓	↓	↓	↓	↓	↓	↓	↓	↑	↓	↓	↓	↓	↓	↑	↓	↓	↓	↓	↓	↓	↓	↓	↓	↓	↓	↑	↓	↓	↓
HR average	↑	↑	↑	↑	↑	↑	↑	↑	↓	↓	↑	↑	↑	↑	↑	↑	↑	↑	↑	↑	↑	↑	↑	↑	↑	↓	↑	↑	↑	↓	↑	↑	↑	↓	↓	↓	↑	↑	↓	↑	↑	↑	↑	↑	↑	↑	↑	↑	↓	↓	↓	↑	↑	↑
HR std	↓	↑	↑	↑	↓	↓	↑	↑	↑	↑	↑	↑	↑	↑	↓	↑	↑	↓	↑	↑	↑	↑	↑	↑	↑	↑	-	↑	↑	↑	↑	↑	-	↑	↑	↑	↑	↑	↑	↓	↑	↑	↑	↑	↓	↓	↑	↑	↑	↓	↓	↑	↓	↓

The up arrows show an increase, and the down arrows show a decrease.

sweating, salivation, nausea, burping, stomach awareness, and general discomfort conditions. Similarly, the I_{NM} is based on fatigue, eye strain, difficulty focusing, headache, fullness of head, blurred vision, and again general discomfort conditions.

The last index is called Motion Sickness Index (I_{MS}, 8th), and it is based on the weighted sum SumMS of all the MSSQ answers (Eq. 1) and steps 2 and 3.

$$SumMS = (0,2 \cdot GenDisc + 0,2 \cdot Dizz\&Vert + 0,2 \cdot \sum(StomAwe, Nausea, Sweat, Saliv, Burp) + 0,2 \cdot \sum(Fatigue, EyeStr, DiffFocus) + 0,2 \cdot \sum(Headache, FullHead, BlurrVis)) \quad (1)$$

In **Table 3**, it is possible to see the percentage of MSSQ answers and indexes for the entire cohort. It is possible to identify general discomfort, sweating, nausea, and vertigo as the most significant indexes with over 20% of responses being 2, which is the highest possible value. Salivation and burping, conversely, are the least significant with a percentage lower than 5% providing a response of value 2.

Table 4, similarly to **Table 2**, shows the increase or decrease of the value of the subjective given answer to the questionnaire using the colored arrows. It is possible to see that some patients, like numbers 10, 11, 14, and 22, have an increase of the symptom for both the 1-Hz and the 3-Hz protocols while others do not show any significant difference. Subject number 16 shows an increase only with the 3-Hz protocol, confirming the strong influence of the wave frequency on the body.

Statistical Analysis

All the parameters extracted from EEG, EMG, and HR underwent a non-parametric statistical univariate explorative analysis in order to understand whether there was a statistically different grouping by I_{GenDis}, I_{Dizz}, I_{Stom}, I_{Head}, I_{Fatig}, I_{PV}, I_{NM}, and I_{Ms}. All the indexes underwent univariate statistical analysis through the Mann–Whitney test.

ML Tool and Algorithms

The ML analysis was performed by using KNIME Analytics Platform (v. 4.2.0), which is a well-known platform in the field of biomedical studies, as it is considered the best choice for advanced users of ML Tougui et al. (2020) Several studies have been performed in clinical settings: for radiomics studies in oncology (Ricciardi et al., 2019; Romeo et al., 2020), for fetal monitoring (Improta et al., 2019; Ricciardi et al., 2020b), for investigating some relationships in ophthalmology (D'Addio et al., 2019; Improta et al., 2020), and in cardiology Ricciardi et al. (2020a).

The following algorithms were implemented through the platform: Random Forests (RF), Gradient Boosting tree (GB), Ada-Boosting of decision tree (ADA-B), Support Vector Machine (SVM), K Nearest Neighbor (KNN), and Multilayer Perceptron (MLP). The first three are based on a structure made up of nodes (starting point of the tree, which indicates an attribute), leaves (the question to be answered, which is the final label), and branches (connecting the nodes) and showed good results in different studies (Recenti et al., 2020; Ricciardi et al., 2020c). There are many criteria for splitting up the records: the gain ratio was used in this study Safavian and Landgrebe (1991). RF and GB are two empowered versions of the decision tree; they apply the ensemble learning methods of randomization, bagging, and boosting to make the weak learner stronger (Breiman, 2001; Friedman, 2001). SVM and KNN are two instance-based algorithms (Keller et al., 1985; Suykens and Vandewalle, 1999); the former assigns the class to the test data based on their distance from similar training data while the latter is capable of solving problems that have to do with overfitting, small datasets, and non-linear and/or high-dimensional data; it can also be used for both classification and regression. It aims to find the best hyperplane that divides the dataset into two classes. MLP consists of a form of neural network with an input layer, one or more hidden layers, and an output layer. The training is usually achieved by using the algorithm backpropagation of errors or some of its variants Riedmiller and Braun (1993).

TABLE 3 | Percentage of the MSSQ answers for each symptom, and percentage of zeros and ones for the eight computed indexes.

MSSQ Symptoms	0 (%)	1 (%)	2 (%)	Index	0 (%)	1 (%)	Index	0 (%)	1 (%)	Index	0 (%)	1 (%)
Gen. Discomfort	43.4	30.1	26.5	I_{GenDis}	43.4	56.6						
Sweating	43.4	32.5	24.1									
Salivation	79.5	15.7	4.8				I_{PV}	63.9	36.1			
Nausea	61.4	14.5	24.1	I_{Stom}	62.6	37.4						
Burping	94.0	6.0	0.0									
Stomach Awern.	66.3	18.1	15.7									
Fatigue	67.5	16.3	13.2							I_{MS}	61.4	38.6
Eye Strain	53.8	26.9	19.2	I_{fatig}	56.6	43.4						
Diff. Focusing	62.7	22.9	14.5									
Headache	55.4	25.3	19.3				I_{NM}*	59.0	41.0			
Full. Of Head	63.9	22.9	13.2	I_{Head}	57.8	42.2						
Blurr. Vision	61.4	26.5	12.0									
Dizziness - Vertigo	54.2	24.1	21.7	I_{Dizz}	54.2	45.8						

I_{NM} includes also General Discomfort.

TABLE 4 | Difference of the subjective MS symptoms between the first static protocol and the light (1 Hz – green) and the hard (3 Hz – red) for all the patients (the one that did not perform the 3-Hz protocol is not included).

Patient Id	1	2	3	4	5	6	7	8	9	10	11	12	13	14	15	16	17	18	19	20	21	22	23	24	25	26	27
Gen. Discomfort	←	–	→	←	→	←	–	←	←	←	←	–	–	←	–	–	–	–	–	←	←	←	–	←	→	–	←
Sweating	–	–	←	←	–	←	←	–	←	←	←	–	–	←	–	–	–	–	–	←	–	–	–	←	–	–	–
Salivation	–	–	–	–	–	–	–	–	–	–	–	–	–	–	←	–	–	–	–	←	←	←	–	←	←	←	←
Nausea	←	–	–	←	←	←	←	←	←	←	←	←	←	←	←	←	→	←	←	←	←	←	←	←	←	←	←
Burping	–	–	–	–	–	–	–	–	–	–	–	–	–	–	–	–	–	–	–	–	–	–	–	–	–	–	–
Stomach Awern.	–	–	–	–	–	–	–	–	–	–	–	–	–	–	–	–	–	–	–	–	–	–	–	–	–	–	–
Fatigue	–	–	–	–	–	–	→	–	→	–	–	–	–	–	←	–	←	←	←	←	←	←	←	←	→	←	←
Eye Strain	–	–	–	–	←	–	–	–	–	–	–	–	–	–	–	–	–	–	–	←	←	←	–	←	←	←	←
Diff. Focusing	–	–	–	–	–	–	–	–	–	–	–	–	–	–	–	–	–	–	–	←	←	←	–	←	←	←	←
Headache	←	–	←	←	←	←	←	←	←	←	←	←	←	←	←	←	←	←	←	←	←	←	←	←	←	←	←
Full. Of Head	–	–	–	–	–	–	–	–	–	–	–	–	–	–	–	–	–	–	–	–	–	–	–	–	–	–	–
Blurr. Vision	–	–	–	–	–	–	–	–	–	–	–	–	–	–	–	–	–	–	–	–	–	–	–	–	–	–	–
Dizziness – Vert.	–	–	–	–	–	–	–	–	–	–	–	←	–	–	–	–	–	–	→	–	–	–	–	–	←	–	–

The up arrows show an increase, and the down arrows show a decrease.

The most employed evaluation metrics were used to assess the performance of the algorithms into the classifications tasks: accuracy, sensitivity, specificity, and Area Under the Curve Receiver Operating Characteristics (AUCROC) Hossin and Sulaiman (2015). All these metrics were computed using the K-Fold Cross Validation Kohavi (1995) with k = 10 using 10 different seeds. This means that the database is divided into 10 groups and each of them is used in turn as the test group while the other nine are used for the training of the model. Using 10 different seeds allows the creation of different 10-fold divisions, which allows a better exploration of the database and achieving the best results.

RESULTS

Statistical Analysis Results

Table 5 shows the results of the statistical tests that assess the significance of the 19 parameters with the eight binary MSSQ indexes. Interestingly, only 4 out of 19 parameters never show a significance.

The EEG Beta and LG showed significance only for the individuals suffering from headache, fullness of head, and blurred vision (I_{Head}), while no other significances were found for an EEG parameter.

The amplitude/area of EMG on both sides achieved a significance for all the conditions except for General Discomfort (I_{GenDis}). Similarly, excluding a few cases, the power spectrum of the EMG obtained a significance for almost all the conditions except in the band of 132–224 for the left side, which is never significant.

The HR Average was significant according to all indexes excluding I_{Stom}, I_{Fatig}, and I_{Head} while HR std showed statistical significance only according to I_{GenDis}.

The I_{GenDis} index was the index that showed the least number of significances for the analyzed parameters; only EMG – R 40–132 and 132–4 Hz and HR parameters achieved significant results according to this index. On the other hand, I_{Head}, I_{Dizz}, and I_{NM} were the indexes according to which the biometric parameters show the greatest number of significant results (respectively, 13 and 12).

Finally, 11 out of 19 parameters show a significant result according to the overall I_{MS}: 10 EMG-related features, 1 HR-related feature, and no EEG feature.

ML Results

The ML analysis focuses on the binary classification of physiological, neurological, and general MS conditions based on the MSSQ responses. We performed the classification of the following index previously defined:

(1) The Physiological/Vegetative Index (I_{PV}),
(2) The Neurological/Muscle Strain Index (I_{NM}),
(3) The MS Index (I_{MS}).

We assessed these conditions using six different algorithms, finding RF to yield the best results (**Table 6**).

As regards I_{PV} and I_{NM}, the RF was the best algorithm for classifying both indexes; an accuracy of 75.9% with an AUCROC of 0.815 was achieved for I_{PV} while an accuracy of 79.5% with an AUCROC of 0.832 was obtained. The highest sensitivity (85.0%) was obtained by the ADA-B for the physiological index, while the highest sensitivity was achieved by RF (74.4%). As regards the neurological index, the best sensitivity (80.0%) was achieved by the ADA-B while the best specificity (83.3%) was obtained by RF. The MLP was the worst algorithm to perform both the classifications since it reached the lowest accuracy (respectively, 49.4 and 45.8%) while the lowest AUCROC was reached by KNN for the physiological index (0.573) and by SVM for the neurological index (0.590).

The feature importance analysis (**Figure 3**) shows that parameters extracted from EMG were the most important ones by far for the classification of both indexes. The first EEG-based features can be found in the 5th place in the ranking while the first HR-based features can be found after the 10th place. Moreover, it has to be highlighted that the top three features in **Figure 3** for these indexes are all statistically significant also in the previous univariate analysis (**Table 5**).

Concerning I_{MS}, the overall model for the indexes is good enough considering accuracies greater than 70.0%, AUCROC greater than 0.800, and the number of trials (equal to 83) that does not allow us to analyze a large dataset; indeed, a greater number of subjects would allow the improvement of the evaluation metrics of the models.

The feature importance analysis (**Figure 3** and **Table 7**) highlighted novel results for I_{MS}: the seasickness can be strongly linked to features extracted from EMG (the top two were area and frequency analysis in the range 40–132) and HR-based (average and standard deviation were at the third and fourth place). On the other hand, another important and surprising result is the low importance of all the features extracted from the EEG, they were below the seventh place in the final ranking (this also for the other indexes except EEG-Beta which is quite relevant for I_{PV} and I_{NM}). This can be explained by the fact that a dry cap EEG was used for the acquisition. More noise was detected and led to a lower signal quality. Channels had to be rejected and could not be interpolated, leading to an averaged PSD on less channels. This can be one of the reasons of the low significance related to EEG features.

DISCUSSION

Postural control is central in governing upright posture in humans. PC failure is dual, firstly pathological disruption leading to clinical difficulties where symptoms of vertigo, dizziness, imbalance, and falling are prominent Dakin and Bolton (2018).

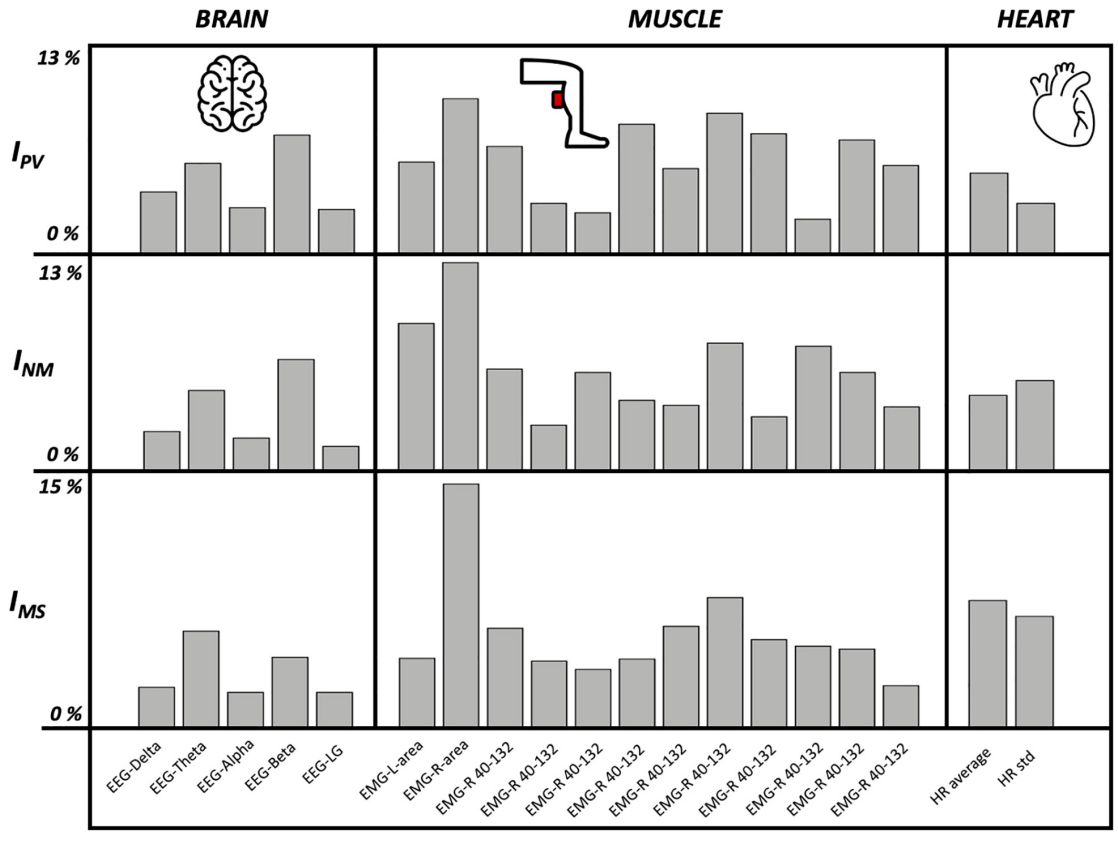

FIGURE 3 | Brain, muscle, and heart feature importance for I_{PV}, I_{NM}, and I_{MS} using Random Forest algorithm.

Secondly, an overstimulation of the PC system may precipitate a series of symptoms of discomfort known as MS Golding (2016). As in PC diseases, there are many objective measurements to be used in the diagnosis of these diseases. On the other hand, there are limited ways to objectively measure MS. Questionnaires are used to evaluate the incidence of subjective symptoms associated with MS, most often nausea, pallor, vomiting, sweating, headache, lightheadedness, and body discomfort Balk et al. (2013). There is an urgent need for objective measurement to evaluate MS, as it threatens human well-being when one is situated in a motion-rich environment. It is also critical to objectively distinguish people into MS-prone and non-MS-prone individuals. This is possible using questionnaires Golding (2006b), but having an objective way to discriminate these two groups is of great value when comes to genetic research.

In this study, we use the BioVRSea research setup and focus on EEG, EMG, and HR bio-signals associated with subjective MS symptoms. Our EEG-coupled results show significant difference in brain neural networking in individuals indicating subjective symptoms of headache, fullness of the head, and blurred vision (I_{Head}). In an earlier study, we showed that open eyes trials reflect a greater number of significant differences in EEG absolute spectral power across all bands during both adaptation and habituation. This suggests that following both acute and prolonged proprioceptive perturbation, cortical activity may be up-regulated with the availability of visual feedback Barollo et al. (2020). These results generally support our prior hypothesis that the visual recognition of instability may play a critical role in governing cortical processes requisite for PC Edmunds et al. (2019). These results underline the importance of visual information in PC and simultaneously open up the VR afferent link in PC perturbations. Being able to couple these subjective symptoms, i.e., headache, fullness of the head, and blurred vision, to objective intracranial activity is crucial in clinical context and opens up ways for VR-coupled biosignal evaluation of PC pathologies Maire et al. (2017). This is in keeping with many other studies performed on motion and CNS triggers of head-related symptoms. Jang et al. (2020) identified that the alpha band was linked to VR sickness, with a decrease of the absolute power during the experiment, followed by an increase during the recovery, highlighting a negative correlation with the MSSQ score. Kim et al. (2005) detected that in the case of cybersickness, the severity of the symptoms was positively correlated with the delta wave, and negatively with the beta waves. It is interesting to see that, in our study, despite the low significance of EEG regarding the different indexes chosen, the power associated to the beta band is the parameter presenting the most importance in I_{PV} and I_{NM}. This corroborates the fact that beta band is related to MS symptoms and is a feature that should be investigated in MS studies. Our results do not enable to drawing of hypotheses regarding the other power bands.

Our observations have indicated that definite vection does not necessarily result in visually induced MS (you can have very compelling vection but no visually induced MS), but at the same time, most participants who get sick also report vection. Our intentions are to verify the relationship between MS and visually induced MS, although there are some participants that get sick on the platform but never experience MS in the real world. They probably have not experienced enough rough waters and therefore we do not expect false positive/negative.

To be able to evaluate the relationship between BioVRSea biosignals and subjective MS symptoms, the use of ML was

TABLE 5 | Significance of the 19 biometric parameters calculated with the univariate statistical analysis (Mann–Whitney test) for all the eight indexes.

	I_{GenDis}	I_{Stom}	I_{Fatig}	I_{Head}	I_{Dizz}	I_{PV}	I_{NM}	I_{MS}
EEG – Delta	0.734	0.903	0.790	0.383	0.841	0.529	0.993	0.667
EEG – Theta	0.934	0.880	0.388	0.613	0.400	0.927	0.184	0.181
EEG – Alpha	0.713	0.865	0.769	0.620	0.577	0.560	0.971	0.888
EEG – Beta	0.393	0.510	0.236	0.050*	0.194	0.105	0.130	0.335
EEG – LG	0.508	0.247	0.229	0.029*	0.070	0.087	0.081	0.217
EMG – L area	0.114	**0.001*** **	0.004**	**0.001*** **	**0.001*** **	**0.001*** **	**0.001*** **	**0.001*** **
EMG – R area	0.157	0.004**	**0.001*** **	**0.001*** **	**0.001*** **	0.004**	**0.001*** **	**0.001*** **
EMG – L 40–132	0.274	0.029*	0.006**	**0.001*** **	**0.001*** **	0.040*	0.004**	0.011**
EMG – L 132–224	0.941	0.492	0.274	0.079	0.165	0.444	0.285	0.449
EMG – L 224–316	0.247	0.031*	0.006**	**0.001*** **	**0.001*** **	0.090	0.010**	0.013**
EMG – L 316–408	0.236	0.025*	0.012**	0.003**	**0.001*** **	0.043*	0.003**	0.011**
EMG – L 408–500	0.286	0.023*	0.029*	0.003**	**0.001*** **	0.032*	0.002**	0.009**
EMG – R 40–132	0.040*	0.006**	0.003**	**0.001*** **	**0.001*** **	0.002**	**0.001*** **	0.008**
EMG – R 132–224	0.044*	0.027*	0.051*	0.035*	0.015**	0.005**	0.008**	0.100
EMG – R 224–316	0.079	0.026*	0.012**	0.007**	0.002**	0.037*	0.007**	0.040*
EMG – R 316–408	0.139	0.030*	0.006**	**0.001*** **	**0.001*** **	0.039*	0.003**	0.012**
EMG – R 408–500	0.118	0.020*	0.003**	**0.001*** **	**0.001*** **	0.018*	**0.001*** **	0.003**
HR average	**0.001*** **	0.219	0.082	0.314	0.012**	0.037*	0.010**	0.042*
HR std	0.040*	0.451	0.213	0.149	0.251	0.264	0.249	0.136

*Significant at 0.05. **Significant at 0.01. ***Significant at 0.001.

TABLE 6 | Evaluation metrics after the classification ML analysis for I_{PV}, I_{NM}, and I_{MS}.

Index	Algorithms	Accuracy	Sensitivity	Specificity	AUCROC
I_{PV}	RF	**75.9**	77.5	74.4	**0.815**
	GB	74.7	75.0	74.4	0.705
	ADA-B	**75.9**	85.0	67.4	**0.781**
	SVM	60.2	62.5	58.1	0.603
	KNN	57.8	60.0	55.8	0.573
	MLP	49.4	77.5	23.3	0.642
I_{NM}	RF	**79.5**	74.3	83.3	**0.832**
	GB	69.9	71.4	68.8	0.711
	ADA-B	73.5	80.0	68.8	0.746
	SVM	60.2	51.4	66.7	0.590
	KNN	67.5	65.7	68.8	0.694
	MLP	45.8	80.0	20.8	0.737
I_{MS}	RF	**74.7**	59.4	84.3	**0.801**
	GB	72.3	68.8	74.5	**0.803**
	ADA-B	71.1	71.9	70.6	**0.765**
	SVM	55.4	43.8	62.7	0.532
	KNN	67.5	59.4	72.5	0.670
	MLP	53.0	40.6	60.8	0.681

The bold values are the most significant values in the evaluation metrics that describe the results of the ML classification for I_{PV}, I_{NM}, and I_{MS} using the listed algorithms.

TABLE 7 | Feature importance (%) for IPV, INM, and IMS using Random Forest algorithm.

	I_{FV}	I_{NM}	I_{MS}
EEG – Delta	3.74	2.37	2.47
EEG – Theta	5.46	4.84	5.87
EEG – Alpha	2.78	1.97	2.16
EEG – Beta	7.18	6.71	4.29
EEG – LG	2.68	1.48	2.16
EMG – L area	5.56	8.88	4.23
EMG – R area	**9.39**	12.54	**14.77**
EMG – L 40–132	6.51	6.12	6.04
EMG – L 132–224	3.07	2.76	4.06
EMG – L 224–316	2.49	5.92	3.56
EMG – L 316–408	**7.85**	4.24	4.18
EMG – L 408–500	5.17	3.95	6.16
EMG – R 40–132	**8.52**	7.7	**7.9**
EMG – R 132–224	7.28	3.26	5.36
EMG – R 224–316	2.11	7.5	4.96
EMG – R 316–408	6.9	5.92	4.78
EMG – R 408–500	5.36	3.85	2.57
HR average	4.89	4.54	**7.72**
HR std	3.07	5.43	6.76

The bold values are the three most important values of the features importance (%) for each of the indexes considered (I_{FV}, I_{NM}, and I_{MS}) using the random forest algorithm.

necessary. This study clearly shows the benefit of ML; indeed, it allowed us to achieve two aims: first, the possibility to model several biometric parameters extracted from three types of signals (EEG, EMG, and HR) in order to be able to classify/distinguish patients suffering from seasickness according to these features; second, the feature importance analysis allowed us to further confirm the statistical results by ranking the features according to their contribution to the classification task. Moreover, as regards the ML models, the RF was the most reliable among all the implemented ones (**Table 6**).

The amplitude of the EMG signals in both legs showed significant difference regarding all conditions except general discomfort (I_{GenDis}). That indicates that almost all subjective symptoms of MS showed correlation with changes in EMG. This is in context with the fact that all human efforts initiated to prevent falls, i.e., acute or long-term vertigo and dizziness, are mediated through postural stabilizing muscles Perrin et al. (2018). Some studies used EMG measurements to analyze the behavior related to MS, with sensors placed on the abdominal muscles Shafeie et al. (2013) and EMG combined with cervical vestibular myogenic potential to study the effect of scopolamine for the seasickness treatment Tal et al. (2016). As far as we know, no study found significance related to EMG in the lower limbs to quantify MS. This is an important piece of information regarding our BioVRSea research setup and is a promising single tool to objectively extract MS sufferers. On the other hand, this is not surprising as the prime effector in PC is aimed at muscles maintaining the upright posture and simultaneously avoiding falls. Our BioVRSea research setup might answer several clinical questions related to strategies used to prevent falls in patients with PC pathologies.

The HR parameters were significantly associated with the symptom of General Discomfort (I_{GenDis}). The General Discomfort symptom is general in its nature and does not specifically point to MS. On the other hand, the triggered MS discomfort relates to an escalated sense of generalized panic in severe MS conditions, which is well capable of creating extreme cardiovascular deviations Yates et al. (2014a). This is expected as HR is probably the best-known biosignal associated with numerous physical as well as pathological conditions, particularly of a PC nature.

These results can be used to have quite a whole vision of the body reaction to induced MS. This total vision can be used to help the pathological patients and the people that are more prone to MS planning an eventual rehabilitative therapy. Future ideas are to use more physiological measurements like blood oxygenation, skin sweating, and force used on the legs for the equilibrium. All these actual and future body parameters coupled with the BioVRSea system and ML are of value in further evaluation of PC disruptions, which are probably the most disturbing and costly health conditions affecting humans.

Limitations

Of course, the study has some limitations. The first is the small number of subjects that limits also the possibility of obtaining higher evaluation metrics in the ML analysis. The second is the type of population that has been analyzed in this research because it was limited regarding age and health status; all the subjects were young and healthy. Further studies could increase the number of subjects, which would allow improvements in the performance of ML and include in the population more diverse subjects. We use dry electrodes for the EEG acquisition resulting in high noise signal, which we believe has limited the value of the associated EEG parameters in both statistical significance and ML. The use of a wet cap EEG for further acquisitions is a potential improvement.

Of course, the VR view that the investigated individual visualizes standing on a virtual small vessel is not a true scenario of working environment at sea but is nevertheless capable of creating MS sensation at least in experienced sailors (verbal statements after being on platform).

DATA AVAILABILITY STATEMENT

The raw data supporting the conclusions of this article will be made available by the authors, without undue reservation.

ETHICS STATEMENT

The studies involving human participants were reviewed and approved by the Icelandic Bioethics Committee – Number: VSN-20-101. The patients/participants provided their written informed consent to participate in this study.

AUTHOR CONTRIBUTIONS

MR, CR, RA, HP, and PG wrote the manuscript. MR and CR conceived the acquisition protocols and conducted the acquisitions with HS, SA, and GK. MR and CR conceived and computed the eight indexes with the support of PG. RA and GK performed the EEG analysis. HS, SA, and VB performed the EMG analysis. CR performed the machine learning analysis. IP performed the univariate statistical analysis. MR designed the tables and the figures and formatted the manuscript; **Figure 1** is created by VB and MR. DJ reviewed and made additions to the manuscript. HP contributed to the medical knowledge. HP and PG conceived the original idea of quantifying motion sickness using bionsensors and virtual reality. PG coordinated the work. All authors contributed to the article and approved the submitted version.

FUNDING

This study was funded by Landspitali University Hospital, Reykjavik (Number: A-2020-054).

ACKNOWLEDGMENTS

The authors would like to thank the students of the course "Medical Technology and Bio-signals 2020" of the BA studies in Biomedical Engineering in Reykjavik University who contributed to the acquisition of the database and inspiring the present work. The authors would also like to thank Samherji hf. Akureyri Iceland for support and Virtualis VR, France and his president Frank Assaban for the precious collaboration.

REFERENCES

Balk, S. A., Bertola, M. A., and Inman, V. W. (2013). "Simulator sickness questionnaire: twenty years later," in *Proceedings of the 7th International Driving Symposium on Human Factors in Driver Assessment, Training, and Vehicle Design: Driving Assessment*, New York, NY, 257–263.

Barollo, F., Frioriksdottir, R., Edmunds, K. J., Karlsson, G. H., Svansson, H. A., Hassan, M., et al. (2020). Postural control adaptation and habituation during vibratory proprioceptive stimulation: an HD-EEG investigation of cortical recruitment and kinematics. *IEEE Trans. Neural. Syst. Rehabil. Eng.* 28, 1381–1388. doi: 10.1109/TNSRE.2020.2988585

Bos, J. E., Damala, D., Lewis, C., Ganguly, A., and Turan, O. (2007). Susceptibility to seasickness. *Ergonomics* 50, 890–901. doi: 10.1080/00140130701245512

Breiman, L. (2001). Random forests. *Mach. Learn.* 45, 5–32.

Cobb, S. V. G. (1999). Measurement of postural stability before and after immersion in a virtual environment. *Appl. Ergon.* 30, 47–57. doi: 10.1016/s0003-6870(98)00038-6

Cohen, B., Dai, M., Yakushin, S. B., and Cho, C. (2019). The neural basis of motion sickness. *J. Neurophysiol.* 121, 973–982. doi: 10.1152/jn.00674.2018

Crampton, G. H. (1990). *Motion and Space Sickness*. Boca Raton, FL: CRC Press.

D'Addio, G., Ricciardi, C., Improta, G., Bifulco, P., and Cesarelli, M. (2019). "Feasibility of machine learning in predicting features related to congenital nystagmus," in *XV Mediterranean Conference on Medical and Biological Engineering and Computing – MEDICON 2019. MEDICON 2019. IFMBE Proceedings*, Vol. 76, eds J. Henriques, N. Neves, and P. de Carvalho (Cham: Springer).

Dakin, C. J., and Bolton, D. A. (2018). Forecast or fall: prediction's importance to postural control. *Front. Neurol.* 9:924. doi: 10.3389/fneur.2018.00924

Edmunds, K. J., Petersen, H., Hassan, M., Yassine, S., Olivieri, A., Barollo, F., et al. (2019). Cortical recruitment and functional dynamics in postural control adaptation and habituation during vibratory proprioceptive stimulation. *J. Neural Eng.* 16:026037. doi: 10.1088/1741-2552/ab0678

Flanagan, M. B., May, J. G., and Dobie, T. G. (2005). Sex differences in tolerance to visually-induced motion sickness. *Aviat. Space Environ. Med.* 76, 642–646.

Friedman, J. H. (2001). Greedy function approximation: a gradient boosting machine. *Ann. Stat.* 29:1189–1232.

Golding, J. F. (2006a). Motion sickness susceptibility. *Auton. Neurosci.* 129, 67–76. doi: 10.1016/j.autneu.2006.07.019

Golding, J. F. (2006b). Predicting individual differences in motion sickness susceptibility by questionnaire. *Pers. Individ. Diff.* 41, 237–248. doi: 10.1016/j.paid.2006.01.012

Golding, J. F. (2016). *Motion Sickness. In Handbook of Clinical Neurology*, Vol. 137. Amsterdam: Elsevier, 371–390.

Hell, S., and Argyriou, V. (2018). "Machine learning architectures to predict motion sickness using a virtual reality rollercoaster simulation tool," in *Proceedings of the 2018 IEEE International Conference on Artificial Intelligence and Virtual Reality (AIVR)*, (Piscataway, NJ: IEEE), 153–156.

Hossin, M., and Sulaiman, M. N. (2015). A review on evaluation metrics for data classification evaluations. *Int. J. Data Mining Knowl. Manag. Process* 5:1.

Huppert, D., Grill, E., and Brandt, T. (2019). Survey of motion sickness susceptibility in children and adolescents aged 3 months to 18 years. *J. Neurol.* 266, 65–73. doi: 10.1007/s00415-019-09333-w

Improta, G., Ricciardi, C., Amato, F., D'Addio, G., Cesarelli, M., and Romano, M. (2019). "Efficacy of machine learning in predicting the kind of delivery by cardiotocography," in *Proceedings of the Mediterranean Conference on Medical and Biological Engineering and Computing*, (Cham: Springer), 793–799. doi: 10.1007/978-3-030-31635-8_95

Improta, G., Ricciardi, C., Cesarelli, G., D'Addio, G., Bifulco, P., and Cesarelli, M. (2020). Machine learning models for the prediction of acuity and variability of eye-positioning using features extracted from oculography. *Health Technol.* 10, 961–968. doi: 10.1007/s12553-020-00449-y

Jang, K. M., Shin Woo, Y., and Kyoon Lim, H. (2020). "Electrophysiological changes in the virtual reality sickness: EEG in the VR sickness," in *Proceedings of the 25th International Conference on 3D Web Technology*, (Cham: Springer), 1–4.

Keller, J. M., Gray, M. R., and Givens, J. A. (1985). A fuzzy k-nearest neighbor algorithm. *IEEE Trans. Syst. Man Cybernet.* 15, 580–585.

Kennedy, R. S., Lane, N. E., Berbaum, K. S., and Lilienthal, M. G. (1993). Simulator sickness questionnaire: an enhanced method for quantifying simulator sickness. *Int. J. Aviation Psychol.* 3, 203–220. doi: 10.1207/s15327108ijap0303_3

Kim, Y. Y., Kim, H. J., Kim, E. N., Ko, H. D., and Kim, H. T. (2005). Characteristic changes in the physiological components of cybersickness. *Psychophysiology* 42, 616–625.

Ko, L. W., Wei, C. S., Jung, T. P., and Lin, C. T. (2011). "Estimating the level of motion sickness based on EEG spectra," in *Proceedings of the International Conference on Foundations of Augmented Cognition*, (Berlin: Springer), 169–176. doi: 10.1007/978-3-642-21852-1_21

Kohavi, R. (1995). A study of cross-validation and bootstrap for accuracy estimation and model selection. *Ijcai* 14, 1137–1145.

Koohestani, A., Nahavandi, D., Asadi, H., Kebria, P. M., Khosravi, A., Alizadehsani, R., et al. (2019). A knowledge discovery in motion sickness: a comprehensive literature review. *IEEE access* 7, 85755–85770. doi: 10.1109/access.2019.2922993

Laboissière, R., Letievant, J. C., Ionescu, E., Barraud, P. A., Mazzuca, M., and Cian, C. (2015). Relationship between spectral characteristics of spontaneous postural sway and motion sickness susceptibility. *PLoS One* 10:e0144466. doi: 10.1371/journal.pone.0144466

LaViola, J. J. Jr. (2000). A discussion of cybersickness in virtual environments. *ACM Sigchi Bull.* 32, 47–56. doi: 10.1145/333329.333344

Lawther, A., and Griffin, M. J. (1988). A survey of the occurrence of motion sickness amongst passengers at sea. *Aviat. Space Environ. Med.* 59, 399–406.

Li, X., Zhu, C., Xu, C., Zhu, J., Li, Y., and Wu, S. (2020). VR motion sickness recognition by using EEG rhythm energy ratio based on wavelet packet transform. *Comput. Methods Programs* 188:105266. doi: 10.1016/j.cmpb.2019.105266

Li, Y., Liu, A., and Ding, L. (2019). Machine learning assessment of visually induced motion sickness levels based on multiple biosignals. *Biomed. Signal Process. Control* 49, 202–211. doi: 10.1016/j.bspc.2018.12.007

Maire, R., Mallinson, A., Ceyte, H., Caudron, S., Van Nechel, C., Bisdorff, A., et al. (2017). Discussion about visual dependence in balance control: european society for clinical evaluation of balance disorders. *J. Int. Adv. Otol.* 13, 404–406. doi: 10.5152/iao.2017.4344

Massion, J. (1994). Postural control system. *Curr. Opin. Neurobiol.* 4, 877–887.

Mazloumi Gavgani, A., Walker, F. R., Hodgson, D. M., and Nalivaiko, E. (2018). A comparative study of cybersickness during exposure to virtual reality and "classic" motion sickness: are they different? *J. Appl. Physiol.* 125, 1670–1680. doi: 10.1152/japplphysiol.00338.2018

Oman, C. M., and Cullen, K. E. (2014). Brainstem processing of vestibular sensory exafference: implications for motion sickness etiology. *Exp. Brain Res.* 232, 2483–2492. doi: 10.1007/s00221-014-3973-2

Perrin, P., Mallinson, A., Van Nechel, C., Peultier-Celli, L., Petersen, H., Magnusson, M., et al. (2018). Defining clinical-posturographic and intra-posturographic discordances: what do these two concepts mean? *J. Int. Adv. Otol.* 14, 127–129. doi: 10.4324/9780429484803-8

Petersen, H. (2012). Seasickness. *Laeknabladid* 98, 653–659.

Reason, J. T. (1978). Motion sickness adaptation: a neural mismatch model. *J. R. Soc. Med.* 71, 819–829. doi: 10.1177/014107687807101109

Recenti, M., Ricciardi, C., Monet, A., Jacob, D., Ramos, J., Gìslason, M., et al. (2020). Predicting body mass index and isometric leg strength using soft tissue distributions from computed tomography scans. *Health Technol.* 11, 239–249. doi: 10.1007/s12553-020-00498-3

Ricciardi, C., Edmunds, K. J., Recenti, M., Sigurdsson, S., Gudnason, V., Carraro, U., et al. (2020a). Assessing cardiovascular risks from a mid-thigh CT image: a tree-based machine learning approach using radiodensitometric distributions. *Sci. Rep.* 10:2863.

Ricciardi, C., Improta, G., Amato, F., Cesarelli, G., and Romano, M. (2020b). Classifying the type of delivery from cardiotocographic signals: a machine learning approach. *Comput. Methods Programs* 196:105712. doi: 10.1016/j.cmpb.2020.105712

Ricciardi, C., Jónsson, H. Jr., Jacob, D., Improta, G., Recenti, M., Gíslason, M. K., et al. (2020c). Improving prosthetic selection and predicting BMD from biometric measurements in patients receiving total hip arthroplasty. *Diagnostics* 10:815. doi: 10.3390/diagnostics10100815

Ricciardi, C., Renato, C., Giuseppe, C., Lorenzo, U., Giovanni, I., Domenico, S., et al. (2019). "Distinguishing Functional from Non-functional Pituitary Macroadenomas with a Machine Learning Analysis," in *Proceedings of the XV Mediterranean Conference on Medical and Biological Engineering and Computing – MEDICON 2019. MEDICON 2019. IFMBE Proceedings*, Vol. 76, eds J. Henriques, N. Neves, and P. de Carvalho (Cham: Springer).

Riccio, G. E., and Stoffregen, T. A. (1991). An ecological theory of motion sickness and postural instability. *Ecol. Psychol.* 3, 195–240. doi: 10.1207/s15326969eco0303_2

Riedmiller, M., and Braun, H. (1993). "A direct adaptive method for faster backpropagation learning: the RPROP algorithm," in *Proceedings of the IEEE International Conference on Neural Networks*, (Piscataway, NJ: IEEE), 586–591.

Romeo, V., Cuocolo, R., Ricciardi, C., Ugga, L., Cocozza, S., Verde, F., et al. (2020). Prediction of tumor grade and nodal status in oropharyngeal and oral cavity squamous-cell carcinoma using a radiomic approach. *Anticancer. Res.* 40, 271–280. doi: 10.21873/anticanres.13949

Safavian, S. R., and Landgrebe, D. (1991). A survey of decision tree classifier methodology. *IEEE Trans. Syst. Man Cybernet.* 21, 660–674. doi: 10.1109/21.97458

Shafeie, M., Zolfaghari, N., and McConville, K. M. V. (2013). "Abdominal muscle behavior and motion sickness during paired visual input with roll motion," in *Proceedings of the 2013 6th International Conference on Human System Interactions (HSI)*, (Piscataway, NJ: IEEE), 247–251.

Suykens, J. A., and Vandewalle, J. (1999). Least squares support vector machine classifiers. *Neural Process. Lett.* 9, 293–300.

Tadel, F., Baillet, S., Mosher, J. C., Pantazis, D., and Leahy, R. M. (2011). Brainstorm: a user-friendly application for MEG/EEG analysis. *Comput. Intellig. Neurosci.* 2011:879716.

Tal, D., Bar, R., Nachum, Z., Gil, A., and Shupak, A. (2010). Postural dynamics and habituation to seasickness. *Neurosci. Lett.* 479, 134–137. doi: 10.1016/j.neulet.2010.05.044

Tal, D., Shemy, S., Kaminski-Graif, G., Wiener, G., and Hershkovitz, D. (2016). Vestibular evoked myogenic potentials and motion sickness medications. *Clin. Neurophysiol.* 127, 2350–2354. doi: 10.1016/j.clinph.2016.03.010

Thurrell, A., and Bronstein, A. (2002). Vection increases the magnitude and accuracy of visually evoked postural responses. *Exp. Brain Res.* 147, 558–560. doi: 10.1007/s00221-002-1296-1

Tougui, I., Jilbab, A., and El Mhamdi, J. (2020). Heart disease classification using data mining tools and machine learning techniques. *Health Technol.* 10, 1137–1144. doi: 10.1007/s12553-020-00438-1

Turner, M. (1999). Motion sickness in public road transport: passenger behaviour and susceptibility. *Ergonomics* 42, 444–461. doi: 10.1080/001401399185586

Wang, Y., Chardonnet, J. R., and Merienne, F. (2019). "VR sickness prediction for navigation in immersive virtual environments using a deep long short term memory model," in *Proceedings of the 2019 IEEE Conference on Virtual Reality and 3D User Interfaces (VR)*, (Piscataway, NJ: IEEE), 1874–1881.

Weech, S., Moon, J., and Troje, N. F. (2018). Influence of bone-conducted vibration on simulator sickness in virtual reality. *PLoS One* 13:e0194137. doi: 10.1371/journal.pone.0194137

Yates, B. J., Bolton, P. S., and Macefield, V. G. (2014a). Vestibulo-sympathetic responses. *Compr. Physiol.* 4, 851–887. doi: 10.1002/cphy.c130041

Yates, B. J., Catanzaro, M. F., Miller, D. J., and McCall, A. A. (2014b). Integration of vestibular and emetic gastrointestinal signals that produce nausea and vomiting: potential contributions to motion sickness. *Exp. Brain Res.* 232, 2455–2469. doi: 10.1007/s00221-014-3937-6

Conflict of Interest: The authors declare that the research was conducted in the absence of any commercial or financial relationships that could be construed as a potential conflict of interest.

frontiers in Human Neuroscience

ORIGINAL RESEARCH
published: 09 April 2021
doi: 10.3389/fnhum.2021.548558

Electroencephalography as a Biomarker for Functional Recovery in Spinal Cord Injury Patients

Marcel Simis[1], Deniz Doruk Camsari[2,3], Marta Imamura[1], Thais Raquel Martins Filippo[4], Daniel Rubio De Souza[1], Linamara Rizzo Battistella[1] and Felipe Fregni[3]*

[1] Hospital das Clinicas HCFMUSP, Faculdade de Medicina, Universidade de São Paulo, São Paulo, Brazil, [2] Department of Psychiatry and Psychology, Mayo Clinic, Rochester, MN, United States, [3] Neuromodulation Center, Spaulding Rehabilitation Hospital, Harvard Medical School, Boston, MA, United States, [4] Universidade Paulista and Universidade Nove de Julho, São Paulo, Brazil

Background: Functional changes after spinal cord injury (SCI) are related to changes in cortical plasticity. These changes can be measured with electroencephalography (EEG) and has potential to be used as a clinical biomarker.

Method: In this longitudinal study participants underwent a total of 30 sessions of robotic-assisted gait training (RAGT) over a course of 6 weeks. The duration of each session was 30 min. Resting state EEG was recorded before and after 30-session rehabilitation therapy. To measure gait, we used the Walking Index for Spinal Cord Injury Scale, 10-Meter- Walking Test, Timed-Up-and-Go, and 6-Min-Walking Test. Balance was measured using Berg Balance Scale.

Results: Fifteen participants with incomplete SCI who had AIS C or D injuries based on American Spinal Cord Injury Association Impairment Scale classification were included in this study. Mean age was 35.7 years (range 17–51) and the mean time since injury was 17.08 (range 4–37) months. All participants showed clinical improvement with the rehabilitation program. EEG data revealed that high beta EEG activity in the central area had a negative correlation with gait (p = 0.049; β coefficient: −0.351; and adj-R^2: 0.23) and balance (p = 0.043; β coefficient: −0.158; and adj-R^2:0.24) measured at baseline, in a way that greater high beta EEG power was related to worse clinical function at baseline. Moreover, improvement in gait and balance had negative correlations with the change in alpha/theta ratio in the parietal area (Gait: p = 0.049; β coefficient: −0.351; adj-R^2: 0.23; Balance: p = 0.043; β coefficient: −0.158; and adj-R^2: 0.24).

Conclusion: In SCI, functional impairment and subsequent improvement following rehabilitation therapy with RAGT correlated with the change in cortical activity measured by EEG. Our results suggest that EEG alpha/theta ratio may be a potential surrogate marker of functional improvement during rehabilitation. Future studies are necessary to improve and validate these findings as a neurophysiological biomarker for SCI rehabilitation.

Keywords: spinal cord injury, electroencephalography, rehabilitation, biomarkers, neuroplasticity

OPEN ACCESS

Edited by:
Borja Sañudo,
Sevilla University, Spain

Reviewed by:
Giorgio Scivoletto,
Santa Lucia Foundation (IRCCS), Italy
Carmelo Chisari,
Pisana University Hospital, Italy

****Correspondence:***
Marcel Simis
marcelsimis@gmail.com

Specialty section:
This article was submitted to Motor Neuroscience, a section of the journal Frontiers in Human Neuroscience

Received: *02 April 2020*
Accepted: *16 March 2021*
Published: *09 April 2021*

Citation:
Simis M, Doruk Camsari D, Imamura M, Filippo TRM, Rubio De Souza D, Battistella LR and Fregni F (2021) Electroencephalography as a Biomarker for Functional Recovery in Spinal Cord Injury Patients. Front. Hum. Neurosci. 15:548558. doi: 10.3389/fnhum.2021.548558

INTRODUCTION

Spinal cord injury (SCI) is one of the most important causes of permanent disability with a major social and economic impact on the affected population. Patients with SCI have a higher mortality risk, which can be 28.8 times greater than the reference population (Leite et al., 2019). The worldwide prevalence of SCI is estimated to be 440 to 526 per million people, with an incidence rate varying from 13.0 per million to 163.4 per million people and reaching 220.0 per million people in under-developed countries (Kang et al., 2018).

Rehabilitative therapies in SCI have significantly improved over the past decades with the development of better rehabilitation protocols and new technologies such as robotic-assisted gait training (RAGT). Despite these advances, there are still a significant number of patients with severe impairment who fail to show any significant improvement with these interventions (Scivoletto et al., 2011; Nam et al., 2017). Understanding the mechanisms of functional recovery in SCI and developing surrogate markers of treatment response are crucial for the development of innovative approaches and tailored treatments for SCI patients. New evidence suggests that neuroplasticity has an essential role in restoring sensory, motor and autonomic functions, by the reorganization of circuits at the level of the SCI, and in the cortical areas of the brain (Liu et al., 2012). Both adaptive and maladaptive neuroplasticity in SCI have been previously investigated using different neuroimaging techniques and quantitative electroencephalography (qEEG).

Studies with functional Magnetic Resonance Imaging suggest that SCI patients have alterations of functional connectivity in different areas of the encephalon, including the primary motor cortex (M1), the premotor cortex (PMC), the supplementary motor area (SMA), the thalamus (TH), the cerebellum, and the right orbitofrontal cortex (OFC). These changes are thought to be related to functional and structural reorganization following the injury to efferent and afferent neural pathways (Athanasiou et al., 2017) and have been shown continue to evolve over time following the injury (Hawasli et al., 2018). Moreover, it is suggested that SCI patients with poorer recovery have decreased functional connectivity between the primary motor cortex and other higher order motor areas such as SMA and PMC as compared to the patients with good recovery (Hou et al., 2016).

Another instrument to study cortical networks is qEEG due to its accessibility, relatively low-cost application and high temporal resolution as compared to other neuroimaging techniques. QEEG measures have been investigated in numerous neuropsychiatric conditions to guide or predict treatment response. Another two important areas where qEEG have provided important insights into are human learning (Etnier et al., 1996; Smith et al., 1999; Kiefer et al., 2014) and cognition (Trammell et al., 2017).

Studies in SCI have so far shown decreased EEG alpha power, lower peak frequencies, and higher beta power in SCI subjects (Tran et al., 2004; Herbert et al., 2007; Doruk et al., 2017). Additional findings in SCI included abnormal or absence of somatosensory- evoked potentials (Lewko et al., 1995; Cheliout-Heraut et al., 1998; Spiess et al., 2008; Kuhn et al., 2012), altered event- related synchronization-desynchronization (Muller-Putz et al., 2007; Gourab, 2010; Cremoux et al., 2013; Müller-Putz and Kaiser, 2014), and cortical network changes (Mattia et al., 2006; De Vico Fallani et al., 2007, 2008; Mattia et al., 2009). A longitudinal study evaluating the event-related desynchronization (ERD) over the motor cortex within the first months following the injury showed that alpha and beta ERD evolution after SCI is negatively correlated with the clinical progression of the patients (Lopez-Larraz et al., 2015).

Advances in signal analysis methods have made it possible to use qEEG to index changes in M1, somatosensory cortex and in the parietal cortex that might be related to the adaptive and maladaptive reorganization of the neural networks after SCI. In a recent EEG study, analysis of functional connectivity within the sensorimotor networks during multiple motor imagery tasks showed that SCI patients had decreased connectivity within the sensorimotor network. SCI patients also had increased local processing during the late stages of imagery tasks which was attributed to adaptive compensatory mechanisms and plastic changes following injury (Athanasiou et al., 2018). In another study, compared to healthy controls, subjects with tetraplegia showed enlargement of functional networks and differences in functional interactions within these networks while performing an attempted movement (Mattia et al., 2009).

Current evidence suggests that EEG can be a useful tool to evaluate functional impairment and neuroplastic changes related to SCI. Previous studies have shown that qEEG measures may also be useful in predicting motor recovery following robot assisted rehabilitation in other conditions such as stroke (Trujillo et al., 2017). However, there is a lack of longitudinal studies that correlate changes in EEG with functional improvement after rehabilitation therapy in SCI. Therefore, in this study we aimed to identify the longitudinal changes in brain activity measured by EEG that are related to the functional improvement in SCI patients who have received rehabilitation therapy.

We hypothesized that an injury to corticomotor and somatosensory pathways would lead to neuroplastic changes in the central and parietal areas of the cortex that can be indirectly measured by the changes in neural oscillations at the alpha and beta frequencies measured by EEG. Based on the previous studies, we mainly focused on the brain activity in the alpha and beta frequency bands as these would be the most relevant EEG measures related to motor function and functional recovery. Other EEG bandwidths and alpha/theta ratio were tested in an exploratory analysis (Tran et al., 2004; Herbert et al., 2007; Doruk et al., 2017).

MATERIALS AND METHODS

This study was approved by the Ethics Committee for Analysis of Research Projects of University of São Paulo Medical School.

Sample Characteristics

This study included 15 participants with incomplete SCI admitted to the Institute of Physical Medicine and Rehabilitation (IMREA) of University of São Paulo. Written informed consent was obtained from each participant. The inclusion criteria were:

(1) diagnosis of incomplete SCI (rated as AIS C or D in American Spinal Cord Injury Association Impairment (ASIA) scale), (2) age between 16 and 70, and (3) one to 36 months after the injury.

The exclusion criteria were: (1) having cardiac pacemaker, (2) unstable angina or other decompensated heart disease, (3) chronic obstructive pulmonary disease, (4) dysreflexia of autonomic system, (5) tracheostomy, (6) presenting deformity and stiffness of the hip joint, knee (20° or more of flexion) and ankle (10 or more plantar flexion), (7) restricted range of motion, (8) lack of cardiovascular conditioning or disabling fatigue, (9) body weight greater than 135 kg, (10) body height greater than 2 meters, (11) leg length difference greater than 2 cm, (12) osteoporosis, (13) instable fracture in lower extremity, and (14) presence of decubitus ulcer of lower extremity.

Rehabilitation Program

Participants went through the IMREA rehabilitation program, for about 8 weeks, consisted of six weekly sessions of 60 min of physical therapy, occupational therapy, and physical fitness, as well as two weekly 60-min sessions of nursing, nutrition, psychology and social work. For locomotion therapy, the Lokomat system (Hocoma AG, Switzerland), which is a RAGT, was used. A trained therapist conducted all sessions.

The Lokomat therapy was performed five times a week over a course of 6 weeks (for a total of 30 sessions). Each session lasted for 30 min. The training load and speed were gradually increased based on tolerability. The supporting body starts with 50% of the patient body weight, and it decreased by 10% every 2 weeks. The Lokomat guiding force varied between 90–75%, based on the patient's capacity to perform active movements. The progression of gait speed was adjusted during the training period based on the tolerance level of the participant. The treatment was combined with the conventional gait therapy without the use of the suspension device used in gait training.

Demographic and Clinical Variables

Information on age, gender, time since the injury, level of the lesion, and medication use was obtained from all subjects. Participants were classified according to the ASIA to determine the ASIA Impairment Scale (AIS). Participants were categorized into AIS "C" or "D," depending on their ability to move at least half of the key muscles below the single neurological level, with adequate strength or not.

To measure gait, we used the Walking Index for Spinal Cord Injury (WISCI II) Scale, 10-Meter- Walking Test (10MWT), Timed-Up-and-Go (TUG), and 6-Min-Walking Test (6MWT; Ditunno et al., 2000; van Hedel et al., 2005; Bohannon, 2006; Jackson et al., 2008). Individuals without walking ability were scored a speed value of 0 m/s. To measure balance, we used Berg Balance Scale (BBS; Berg et al., 1989). The evaluations were performed by the same rater at the baseline (i.e., prior to any Lokomat training), and after 30 sessions of training. Participants could use assistive devices and braces during the tests, but not harness systems, parallel bars or other support systems.

Electroencephalography

Resting-state electroencephalography (EEG) was recorded for 20 min using a 128-channel EEG cap with active electrodes (Acti-Champs, PyCorder, Brainvision LLC®). The acquisition was performed before and after 30-session rehabilitation therapy. All recordings were obtained eyes closed. The EEG data were analyzed visually by an EEG expert clinical neurophysiologist to exclude the existence of epileptiform discharges.

For the offline analysis, we used a high-pass filter of 1 Hz and low-pass filter of 40 Hz, followed by manual artifact detection and rejection by a blinded assessor. Then, the data were exported and analyzed offline with EEGLab (Delorme and Makeig, 2004) and MATLAB (MATLAB R2012a, The MathWorks Inc. Natick, MA, United States, 2000).

The artifact-free data was processed using Fast Fourier transformation (averaged windows of 5 s with 50% overlap) to calculate power (μV^2) for the following EEG bands: theta (4–8 Hz) and alpha (8–13 Hz) and the sub-bands: low alpha (8–10 Hz), high alpha (10–13 Hz), low beta (13–20 Hz), and high beta (21–30 Hz). Electrodes representing cortical areas were selected and averaged over for the following regions: frontal (F1, F2, F3, F4, F5, F6, AF3, AF4, FC3, and FC4), central (C1, C2, C3, C4, C5, and C6), parietal (P1, P2, P3, P4, P5, and P6), temporal (T1, T2, T3, T4, T5, T6, T7, T8, T9, and T10), and occipital (O1, O2, and Oz) areas.

Statistical Analysis

Functional Outcomes

Due to our small sample size, a non-parametric test (Wilcoxon Signed Rank) was performed to compare pre- and post-treatment gait and balance measures (WISC, 10MWT, 6MWT, TUG, and BBS). Data were expressed as mean and standard deviation for the analysis. Participants who could not perform the tests were not included in the analyses. For the demographic and clinical characteristics gender, AIS classification (C or D) and level of injury (cervical or bellow cervical) were treated as binary variable; and time since lesion (in months) and age (in years) as continuous variables. We conducted univariate analysis to assess the relationship between functional outcomes and demographic/clinical characteristics.

Functional Outcomes and EEG

Functional outcomes as a predictor of baseline EEG

First, the normality of EEG data was tested using histograms. After confirming that the data have approximately normal distribution, we conducted separate univariate linear regression analyses where the independent variable was one of the functional outcomes (WISCI or BBS measured at baseline) and the dependent variable was the baseline EEG power [separately for each frequency bands (e.g., alpha, low beta), or the alpha/theta power ratio (alpha/theta)] to assess if there is any association between functional outcomes and EEG measures at baseline. Each dependent EEG variable tested one at a time. The initial analyses were performed only for the average of central electrodes (related to primary motor cortex) and parietal electrodes (related to primary somatosensory cortex), since our hypothesis was that

the expected EEG changes would be secondary to the lesion in the corticomotor and somatosensory pathways, and therefore, these areas would be the most likely to show alterations in EEG activities related to functional outcomes.

To test for the hypothesis that baseline EEG measures can predict functional improvement, we performed analyses where the independent variable was the improvement of WISCI or BSS calculated as the difference between post-rehabilitation – pre-rehabilitation, (ΔWISCI or ΔBSS) and the dependent variable was the baseline EEG power.

Functional outcomes as a predictor of change in EEG

To test the hypothesis that the change in brain activity measured by EEG (ΔEEG) is related to functional improvement (ΔWISCI or ΔBSS), we tested univariate models where the change in EEG activity [calculated as the difference between post-rehabilitation – pre-rehabilitation, (ΔEEG)] in specific cortical areas and in each frequency band (e.g., central alpha power post-rehabilitation minus central alpha power pre-rehabilitation) was the dependent variable, and the improvement of WISCI or BBS (ΔWISCI or ΔBSS) was the independent variable.

To test the specificity of the cortical area for the significant EEG variables, we also tested other brain regions (frontal, temporal and occipital; besides central and parietal). These other cortical areas were only tested for the EEG variables that were significant in the initial analyses since the analyses were hypothesis-driven. For the statistical analyses, we used Stata Statistical Software 15 (StataCorp LLC), and the significant level was p-value < 0.05.

RESULTS

Fifteen participants with incomplete SCI who had had AIS C or D injuries based on ASIA classification were included in this study. Mean age was 35.7 years (range 17–51) and the mean time since injury was 17.08 (range 4–37) months. Lesion levels of were cervical ($n = 11$), lumbar ($n = 1$), and thoracic ($n = 3$). Participants were taking medications due to clinical comorbidities, including chronic pain, depression, urinary incontinence, and spasticity. One of the participants did not have an EEG recording at baseline and was excluded from the analysis.

Functional Outcomes

Functional Outcomes

The analyses of functional change (pre vs. post-treatment) showed significant improvement of gait measured by the scales WISCI ($p = 0.009$), 6MWT ($p = 0.029$), and TUG ($p = 0.037$), but the improvement was not significant for 10MWT ($p = 0.093$). There was also a statistically significant improvement for balance measured by BBS ($p = 0.007$). Because of the absence of a control group, it was not possible to state that the improvement was related to intervention. Due to severe gait impairment, 5 of 14 could not perform the test 6MWT, 10MWT, and TUG, and were excluded from the analyses. **Table 1** summarizes the results.

Functional Outcomes as a Predictor of EEG Variables

Baseline EEGs

For the selected cortical areas (central and parietal), only high beta power in the central area had a normal distribution and was considered in this analysis. Baseline high beta EEG power in the central area (average of central electrodes) was predicted by the baseline measurements of WISCI ($p = 0.010$; β coefficient: −0.003; and adj-R^2: 0.39) and BBS ($p = 0.012$; β coefficient: −0.001; and adj-R^2: 0.31).

Although our hypothesis was related to central and parietal areas, we tested other cortical areas for the same EEG variables to test whether the results were specific to these brain regions or represents a more global change in brain activity. Results are summarized in **Table 2**.

Changes in EEGs [Post-Rehabilitation – Pre-Rehabilitation, (ΔEEG)]

In the central area, ΔEEG for all bands had a normal distribution. In the parietal area, only Δ alpha/theta had a normal distribution and was considered in this analysis. Gait improvement measured by WISCI (Δ WISCI) had a negative correlation with the change in alpha/theta ratio in the parietal area ($p = 0.049$; β coefficient: −0.351; and adj-R^2: 0.23). The improvement in balance (Δ BBS) had a negative correlation with the change in alpha/theta ratio in the parietal area ($p = 0.043$; β coefficient: −0.158; and adj-R^2:0.24). Results are summarized in **Table 3**.

The significant results in the parietal area (mentioned above) were also tested for frontal, temporal and occipital areas. None of the other cortical areas was found significant, suggesting the high specificity of the relationship between functional improvement and the EEG signal in the parietal area. Moreover, we did not find a prognostic EEG biomarker since none of the independent variable were significant for the analysis in which

TABLE 1 | Improvement in functional outcomes.

	Pre mean (±SD)	Post mean (±SD)	*p*-value
WISCI	9.4 (8.1)	11.3 (8.2)	***p* = 0.009***
6MWT (m)	137.9 (105.3)	194.4 (105.4)	***p* = 0.029***
10MWT (s)	40 (47.9)	30.6 (35.1)	$p = 0.093$
TUG (s)	52.1 (54.0)	40.6 (62.5)	***p* = 0.037***
BBS	24.9 (20.4)	29 (22.5)	***p* = 0.007***

SD: standard deviation; Asterisks represent p-values smaller than 0.05.

TABLE 2 | Baseline EEG predicted by functional outcomes.

Power bandwidth High beta	WISCI *p*-value	BBS *p*-value
Frontal	**0.025***	0.067
Temporal	0.980	0.234
Central	**0.010***	**0.012***
Parietal	0.785	0.744
Occipital	0.286	0.435

Asterisks represent p-values smaller than 0.05.

TABLE 3 | Changes in EEG predicted by improvement in functional outcomes.

Δ Power bandwidth	Δ WISCI		Δ BBS	
	Central	Parietal	Central	Parietal
Δ Theta	0.960	NT	0.900	NT
Δ Alpha	0.082	NT	0.053	NT
Δ Low alpha	0.147	NT	0.061	NT
Δ High alpha	0.052	NT	0.131	NT
Δ Low beta	0.263	NT	0.941	NT
Δ High beta	0.694	NT	0.851	NT
Δ Alpha/Theta	0.071	**0.049***	0.095	**0.043***

NT: Not tested (since it was not normally distributed); Asterisks represent p- values smaller than 0.05.

dependent variable was the baseline EEG power to predict the functional improvement.

DISCUSSION

Clinical and Functional Outcomes

We found significant clinical improvement with the rehabilitation program, with the mean gain of 1.9 (SD:2.6) in WISCI and the mean gain of 4.1 (SD:5.7) in BBS. The training was well tolerated, and there were no adverse events.

EEG Activity at Baseline Related to Functional Impairment at Baseline

High beta EEG activity in the central area had a negative correlation with gait and balance measured at baseline, in a way that greater high beta EEG power was related to worse clinical function. This relation was also significant in the frontal area, but not in parietal, temporal, or occipital areas. Beta oscillations have been associated with GABAergic activity in inhibitory interneurons and pyramidal neurons and are thought to reflect plastic changes in neural networks (Whittington et al., 2000; Rossiter et al., 2014). In a study comparing chronic SCI patients with age and sex matched, able-bodied control group, authors found consistently decreased alpha wave (8–13 Hz) and increased beta wave activity (13–30 Hz) in the SCI group (Herbert et al., 2007). Similarly, studies in stroke patients also showed a relation between increased beta wave activity and poor motor function (Simis et al., 2015; Thibaut et al., 2017). Our results are also supported by another study from our group, with a larger and different sample of incomplete SCI patients, in which we also found that greater high beta EEG power at baseline was negatively correlated with baseline gait function (Simis et al., 2020). Additionally, in that study, functional improvement was associated with greater baseline high beta power and greater decrease in high beta power after interventions. Even though we did not find any significant correlation between functional improvement and change in high beta power in the present study, this might be due to a type II error, considering our small sample size.

Overall, our results are in line with the literature and suggest that the correlation between baseline high beta EEG activity and poor functional impairment might be an indirect biomarker of adaptive/maladaptive changes and cortical reorganization within the corticomotor networks following SCI.

Changes in EEG Activity (Post-Rehabilitation – Pre-Rehabilitation) Related to Functional Improvement

Change in alpha/theta activity ratio in the parietal area was negatively correlated with the improvement of gait (p = 0.049; adj-R^2: 0.23) and balance (p = 0.043; adj-R^2:0.24).

How alpha oscillations are generated remains unclear. Different models have been proposed including the cortical generation of the rhythms; TH as the pacemaker of the alpha rhythm (Bollimunta et al., 2011), or a more complex circuit (cortico-thalamo-cortical and intra-cortical circuits) associated with feedforward circuits that regulate alpha activity (Hindriks and van Putten, 2013). Previous studies comparing SCI participants with able-bodied controls showed that SCI participants have decreased alpha and increased beta activity in the cortex, with a larger difference in central, parietal and occipital areas. Besides, SCI subjects were consistently found to have lower peak frequencies than controls (Tran et al., 2004; Herbert et al., 2007). These EEG changes have been explained by the concept of thalamocortical dysrhythmia (TCD), which is the shift in the dominant spectral power to slower frequencies as a result of the deafferentation of excitatory input over TH (Llinas et al., 1999; Llinas and Steriade, 2006; Hirata and Castro-Alamancos, 2010). In our results, the negative correlation between functional improvement and alpha/theta ratio could be seen as contradictory, since it goes in the same direction of the TCD. On the other hand, it is important to note that in our results changes in alpha power was not correlated with functional improvement; but only its relation to theta power was, which is further discussed below. One explanation for why we did not see a direct correlation within the alpha band after rehabilitation might be explained by the disruption or the reorganization of the networks associated with motor learning, yet, in the absence of a control group this interpretation remains to be further explored.

The generation of theta oscillations has been related to structures in the hippocampus (hippocampal theta rhythm) and extra hippocampal (septal complex, entorhinal cortex, and pedunculopontine tegmentum). The functions of theta oscillation are not fully understood but are probably related to memory formation, sleep, and arousal (Hasselmo, 2005; Pignatelli et al., 2012). It is proposed that theta is promoted in the brainstem by GABAergic projection, from the neurons in *nucleus incertus* and *ventral tegmental nucleus of Gudden*, to the frontal cortex and nucleus accumbens. This circuit regulates the activity of thalamocortical neurons. It is suggested that GABAergic inputs to thalamic relay nuclei maintain tonic inhibition, which suppress unimportant information and unnecessary motor activity. On the other hand, when high attention is required, there is a decrease of this tonic inhibitory input allowing the enhanced arousal/attention and sensorimotor transmission, facilitating the motor response (Brown and McKenna, 2015). Therefore, the improvement of gait and balance may be related

to the downregulation of this circuity (hence decrease in theta oscillations), which reflects as a decrease in alpha/theta activity in the parietal area. However, due to the absence of control group, it is not possible conclude whether these changes are solely related to motor recovery or RAGT, or both. It is possible that the EEG changes is associated to motor skill acquisition related to the therapy sessions, which may be present in subjects without SCI.

POSSIBLE CLINICAL APPLICATIONS

Our results suggest that EEG measures such as alpha/theta ratio might be a potential biomarker to determine treatment response and functional recovery in SCI patients and individualize rehabilitation therapies based neurophysiologic evidence. Additionally, these biomarkers can be potentially used as surrogate outcomes of patient's clinical progression and to define discharge criteria from therapy. Moreover, it may be used to guide new rehabilitation therapies such as brain-computer-interface training and non-invasive brain stimulation techniques.

Even though we did not find any direct relationship between baseline EEG measures and functional outcomes, baseline EEG biomarkers have been implicated in the literature as a potential biomarker of treatment response in variety of neuropsychiatric diseases, such as multiple sclerosis (Tramonti et al., 2019) and depression (Olbrich and Arns, 2013) and therefore could play an important role in clinical practice. Further studies with larger sample sizes are needed to explore the potential use of baseline EEG measures as a predictor of treatment response in SCI.

LIMITATIONS

The study had a small sample size with participants with different lesion levels and time since injury. Additionally, participants were taking medications that can influence EEG activity, which we were unable to control in our multivariate models due to our low sample size. Therefore, our results need to be confirmed in larger cohorts. Moreover, the results need to be carefully interpreted due to the absence of a control group. Another limitation is that EEG measures used in this study provides only an indirect measure of cortical activity and may not be sufficient to identify more local changes in the cortical structures. Future studies employing more advanced EEG analyses techniques to analyze the effects of rehabilitation techniques are needed to confirm our results. On the other hand, the use of simple and well-established methods (such as EEG power) can be more easily translated into clinical practice once proven to be accurate surrogate markers of brain activity in SCI.

CONCLUSION

In SCI, functional impairment and subsequent improvement following rehabilitation therapy with RAGT correlated with the change in cortical activity measured by EEG. Our results suggest that EEG alpha/theta ratio may be a potential surrogate marker of functional improvement during rehabilitation. Future studies are necessary to improve and validate these findings as a neurophysiological biomarker for SCI rehabilitation.

DATA AVAILABILITY STATEMENT

The raw data supporting the conclusions of this article will be made available by the authors, without undue reservation.

ETHICS STATEMENT

The studies involving human participants were reviewed and approved by Ethics Committee for Analysis of Research Projects (CAPPesq) of University of São Paulo Medical School. The patients/participants provided their written informed consent to participate in this study.

AUTHOR CONTRIBUTIONS

MS, TF, DR, LB, MI, and FF contributed conception and design of the study. MS, TF, DR, LB, and MI contributed for data the acquisition. MS and DD organized the database. MS and DD performed the statistical analysis. MS wrote the first draft of the manuscript. FF and DD wrote sections of the manuscript. All authors contributed to manuscript revision, read and approved the submitted version.

FUNDING

This work was supported by grants from the Naval International Cooperative Opportunities in Science and Technology – Office of Naval Research Global (NICOP-ONRG N62909-16-1-2096). The researchers received support from the São Paulo Research Foundation (FAPESP- SPEC, grant #2017/12943-8). The work received a support from Núcleo de Apoio a Pesquisa-Núcleo de Estudos Avançados em Reabilitação (NAP-NEAR).

ACKNOWLEDGMENTS

Authors are grateful to Margarida H. Miyazaki, executive director of IMREA, Mariane Tateishi and Katia Lina Miyahara, Clinical Director of IMREA, for the great support of the hospital. Besides, Renato Anghinah for EEG support and Artur dos Santos for assistance with study monitoring.

REFERENCES

Athanasiou, A., Klados, M. A., Pandria, N., Foroglou, N., Kavazidi, K. R., Polyzoidis, K., et al. (2017). A systematic review of investigations into functional brain connectivity following spinal cord injury. *Front. Hum. Neurosci.* 11:517. doi: 10.3389/fnhum.2017.00517

Athanasiou, A., Terzopoulos, N., Pandria, N., Xygonakis, I., Foroglou, N., Polyzoidis, K., et al. (2018). Functional brain connectivity during multiple motor imagery tasks in spinal cord injury. *Neural Plast.* 2018:9354207.

Berg, K., Wood-Dauphinee, S. L., Williams, J. I., and Gayton, D. (1989). Measuring balance in the elderly: preliminary development of an instrument. *Physiother. Can.* 41, 304–311. doi: 10.3138/ptc.41.6.304

Bohannon, R. W. (2006). Reference values for the timed up and go test: a descriptive meta-analysis. *J. Geriatr. Phys. Ther.* 29, 64–68. doi: 10.1519/00139143-200608000-00004

Bollimunta, A., Mo, J., Schroeder, C. E., and Ding, M. (2011). Neuronal mechanisms and attentional modulation of corticothalamic alpha oscillations. *J. Neurosci.* 31, 4935–4943. doi: 10.1523/jneurosci.5580-10.2011

Brown, R. E., and McKenna, J. T. (2015). Turning a negative into a positive: ascending GABAergic control of cortical activation and arousal. *Front. Neurol.* 6:135. doi: 10.3389/fneur.2015.00135

Cheliout-Heraut, F., Loubert, G., Masri-Zada, T., Aubrun, F., and Pasteyer, J. (1998). Evaluation of early motor and sensory evoked potentials in cervical spinal cord injury. *Neurophysiol. Clin.* 28, 39–55. doi: 10.1016/s0987-7053(97)89577-9

Cremoux, S., Tallet, J., Berton, E., Dal Maso, F., and Amarantini, D. (2013). Motor-related cortical activity after cervical spinal cord injury: multifaceted EEG analysis of isometric elbow flexion contractions. *Brain Res.* 1533, 44–51. doi: 10.1016/j.brainres.2013.08.008

De Vico Fallani, F., Astolfi, L., Cincotti, F., Mattia, D., Marciani, M. G., Salinari, S., et al. (2007). Cortical functional connectivity networks in normal and spinal cord injured patients: evaluation by graph analysis. *Hum. Brain Mapp.* 28, 1334–1346. doi: 10.1002/hbm.20353

De Vico Fallani, F., Sinatra, R., Astolfi, L., Mattia, D., Cincotti, F., Latora, V., et al. (2008). Community structure of cortical networks in spinal cord injured patients. *Annu. Int. Conf. IEEE Eng. Med. Biol. Soc.* 2008, 3995–3998.

Delorme, A., and Makeig, S. (2004). EEGLAB: an open source toolbox for analysis of single-trial EEG dynamics including independent component analysis. *J. Neurosci. Methods* 134, 9–21. doi: 10.1016/j.jneumeth.2003.10.009

Ditunno, J. F. Jr., Ditunno, P. L., Graziani, V., Scivoletto, G., Bernardi, M., Castellano, V., et al. (2000). Walking index for spinal cord injury (WISCI): an international multicenter validity and reliability study. *Spinal Cord* 38, 234–243. doi: 10.1038/sj.sc.3100993

Doruk, D., Moreno-Duarte, I., Morales-Quezada, L., and Fregni, F. (2017). Investigation of neural markers in chronic pain in spinal cord injury: a TMS and EEG preliminary study and a brief systematic review. *Princ. Pract. Clin. Res.* 3, 1–10.

Etnier, J. L., Whitwer, S. S., Landers, D. M., Petruzzello, S. J., and Salazar, W. (1996). Changes in electroencephalographic activity associated with learning a novel motor task. *Res. Q. Exerc. Sport* 67, 272–279. doi: 10.1080/02701367.1996.10607954

Gourab, K. S. B. (2010). Changes in movement-related beta-band EEG signals in human spinal cord injury. *Clin. Neurophysiol.* 121, 2017–2023. doi: 10.1016/j.clinph.2010.05.012

Hasselmo, M. E. (2005). What is the function of hippocampal theta rhythm?–Linking behavioral data to phasic properties of field potential and unit recording data. *Hippocampus* 15, 936–949. doi: 10.1002/hipo.20116

Hawasli, A. H., Rutlin, J., Roland, J. L., Murphy, R. K. J., Song, S. K., Leuthardt, E. C., et al. (2018). Spinal cord injury disrupts resting-state networks in the human brain. *J. Neurotrauma* 35, 864–873. doi: 10.1089/neu.2017.5212

Herbert, D., Tran, Y., Craig, A., Boord, P., Middleton, J., and Siddall, P. (2007). Altered brain wave activity in persons with chronic spinal cord injury. *Int. J. Neurosci.* 117, 1731–1746. doi: 10.1080/00207450701242826

Hindriks, R., and van Putten, M. J. (2013). Thalamo-cortical mechanisms underlying changes in amplitude and frequency of human alpha oscillations. *Neuroimage* 70, 150–163. doi: 10.1016/j.neuroimage.2012.12.018

Hirata, A., and Castro-Alamancos, M. A. (2010). Neocortex network activation and deactivation states controlled by the thalamus. *J. Neurophysiol.* 103, 1147–1157. doi: 10.1152/jn.00955.2009

Hou, J., Xiang, Z., Yan, R., Zhao, M., Wu, Y., Zhong, J., et al. (2016). Motor recovery at 6 months after admission is related to structural and functional reorganization of the spine and brain in patients with spinal cord injury. *Hum. Brain Mapp.* 37, 2195–2209. doi: 10.1002/hbm.23163

Jackson, A. B., Carnel, C. T., Ditunno, J. F., Read, M. S., Boninger, M. L., Schmeler, M. R., et al. (2008). Outcome measures for gait and ambulation in the spinal cord injury population. *J. Spinal Cord Med.* 31, 487–499. doi: 10.1080/10790268.2008.11753644

Kang, Y., Ding, H., Zhou, H., Wei, Z., Liu, L., Dayu, P., et al. (2018). Epidemiology of worldwide spinal cord injury: a literature review. *Neurorestoratology* 6, 1–9. doi: 10.2147/jn.s143236

Kiefer, A. W., Gualberto Cremades, J., and Myer, G. D. (2014). Train the brain: novel electroencephalography data Indicate links between motor learning and brain adaptations. *J. Nov. Physiother.* 4:198.

Kuhn, F., Halder, P., Spiess, M. R., Schubert, M., and Em-Sci Study Group (2012). Oneyear evolution of ulnar somatosensory potentials after trauma in 365 tetraplegic patients: early prediction of potential upper limb function. *J. Neurotrauma* 29, 1829–1837. doi: 10.1089/neu.2011.2277

Leite, V. F., Souza, D. R., Imamura, M., and Battistella, L. R. (2019). Post-discharge mortality in patients with traumatic spinal cord injury in a Brazilian hospital: a retrospective cohort. *Spinal Cord* 57, 134–140. doi: 10.1038/s41393-018-0183-y

Lewko, J. P., Tarkka, I. M., and Dimitrijevic, M. R. (1995). Neurophysiological assessment of the motor and sensory spinal pathways in chronic spinal cord injury. *Restor. Neurol. Neurosci.* 7, 225–234. doi: 10.3233/rnn-1995-7405

Liu, J., Yang, X., Jiang, L., Wang, C., and Yang, M. (2012). Neural plasticity after spinal cord injury. *Neural Regen. Res.* 7, 386–391.

Llinas, R. R., Ribary, U., Jeanmonod, D., Kronberg, E., and Mitra, P. P. (1999). Thalamocortical dysrhythmia: a neurological and neuropsychiatric syndrome characterized by magnetoencephalography. *Proc. Natl. Acad. Sci. U.S.A.* 96, 15222–15227. doi: 10.1073/pnas.96.26.15222

Llinas, R. R., and Steriade, M. (2006). Bursting of thalamic neurons and states of vigilance. *J. Neurophysiol.* 95, 3297–3308. doi: 10.1152/jn.00166.2006

Lopez-Larraz, E., Montesano, L., Gil-Agudo, A., Minguez, J., and Oliviero, A. (2015). Evolution of EEG motor rhythms after spinal cord injury: a longitudinal study. *PLoS One* 10:e0131759. doi: 10.1371/journal.pone.0131759

Mattia, D., Cincotti, F., Astolfi, L., de Vico Fallani, F., Scivoletto, G., Marciani, M. G., et al. (2009). Motor cortical responsiveness to attempted movements in tetraplegia: evidence from neuroelectrical imaging. *Clin. Neurophysiol.* 120, 181–189. doi: 10.1016/j.clinph.2008.09.023

Mattia, D., Cincotti, F., Mattiocco, M., Scivoletto, G., Marciani, M. G., and Babiloni, F. (2006). Motor-related cortical dynamics to intact movements in tetraplegics as revealed by high-resolution EEG. *Hum. Brain Mapp.* 27, 510–519. doi: 10.1002/hbm.20195

Müller-Putz, G. R., and Kaiser, V. (2014). Changes in movement-related betaband EEG signals in human spinal cord injury. *J. Neural. Eng.* 11, 2017–2023.

Muller-Putz, G. R., Zimmermann, D., Graimann, B., Nestinger, K., Korisek, G., and Pfurtscheller, G. (2007). Event-related beta EEG-changes during passive and attempted foot movements in paraplegic patients. *Brain Res.* 1137, 84–91.

Nam, K. Y., Kim, H. J., Kwon, B. S., Park, J. W., Lee, H. J., and Yoo, A. (2017). Robot-assisted gait training (Lokomat) improves walking function and activity in people with spinal cord injury: a systematic review. *J. Neuroeng. Rehabil.* 14:24.

Olbrich, S., and Arns, M. (2013). EEG biomarkers in major depressive disorder: discriminative power and prediction of treatment response. *Int. Rev. Psychiatry* 25, 604–618.

Pignatelli, M., Beyeler, A., and Leinekugel, X. (2012). Neural circuits underlying the generation of theta oscillations. *J. Physiol. Paris* 106, 81–92.

Rossiter, H. E., Davis, E. M., Clark, E. V., Boudrias, M. H., and Ward, N. S. (2014). Beta oscillations reflect changes in motor cortex inhibition in healthy ageing. *Neuroimage* 91, 360–365.

Scivoletto, G., Tamburella, F., Laurenza, L., Foti, C., Ditunno, J. F., and Molinari, M. (2011). Validity and reliability of the 10-m walk test and the 6-min walk test in spinal cord injury patients. *Spinal Cord* 49, 736–740.

Simis, M., Doruk, D., Imamura, M., Anghinah, R., Morales-Quezada, L., Fregni, F., et al. (2015). Neurophysiologic predictors of motor function in stroke. *Restor. Neurol. Neurosci.* 34, 45–54.

Simis, M., Uygur-Kucukseymen, E., Pacheco-Barrios, K., Battistella, L. R., and Fregni, F. (2020). Beta-band oscillations as a biomarker of gait recovery in spinal cord injury patients: a quantitative electroencephalography analysis. *Clin. Neurophysiol.* 131, 1806–1814.

Smith, M. E., McEvoy, L. K., and Gevins, A. (1999). Neurophysiological indices of strategy development and skill acquisition. *Brain Res. Cogn. Brain Res.* 7, 389–404.

Spiess, M., Schubert, M., Kliesch, U., Em-Sci Study group, and Halder, P. (2008). Evolution of tibial SSEP after traumatic spinal cord injury: baseline for clinical trials. *Clin. Neurophysiol.* 119, 1051–1061.

Thibaut, A., Simis, M., Battistella, L. R., Fanciullacci, C., Bertolucci, F., Huerta-Gutierrez, R., et al. (2017). Using brain oscillations and corticospinal excitability to understand and predict post-stroke motor function. *Front. Neurol.* 8:187. doi: 10.3389/fneur.2017.00187

Trammell, J. P., MacRae, P. G., Davis, G., Bergstedt, D., and Anderson, A. E. (2017). The relationship of cognitive performance and the theta-alpha power ratio is age-dependent: an EEG study of short term memory and reasoning during task and resting-state in healthy young and old adults. *Front. Aging Neurosci.* 9:364. doi: 10.3389/fnagi.2017.00364

Tramonti, C., Imperatori, L. S., Fanciullacci, C., Lamola, G., Lettieri, G., Bernardi, G., et al. (2019). Predictive value of electroencephalography connectivity measures for motor training outcome in multiple sclerosis: an observational longitudinal study. *Eur. J. Phys. Rehabil. Med.* 55, 743–753.

Tran, Y., Boord, P., Middleton, J., and Craig, A. (2004). Levels of brain wave activity (8-13 Hz) in persons with spinal cord injury. *Spinal Cord* 42, 73–79.

Trujillo, P., Mastropietro, A., Scano, A., Chiavenna, A., Mrakic-Sposta, S., Caimmi, M., et al. (2017). Quantitative EEG for predicting upper limb motor recovery in chronic stroke robot-assisted rehabilitation. *IEEE Trans. Neural Syst. Rehabil. Eng.* 25, 1058–1067.

van Hedel, H. J., Wirz, M., and Dietz, V. (2005). Assessing walking ability in subjects with spinal cord injury: validity and reliability of 3 walking tests. *Arch. Phys. Med. Rehabil.* 86, 190–196.

Whittington, M. A., Traub, R. D., Kopell, N., Ermentrout, B., and Buhl, E. H. (2000). Inhibition-based rhythms: experimental and mathematical observations on network dynamics. *Int. J. Psychophysiol.* 38, 315–336.

Conflict of Interest: The authors declare that the research was conducted in the absence of any commercial or financial relationships that could be construed as a potential conflict of interest.

frontiers in Human Neuroscience

ORIGINAL RESEARCH
published: 16 April 2021
doi: 10.3389/fnhum.2021.639773

Effects of Perturbation Velocity, Direction, Background Muscle Activation, and Task Instruction on Long-Latency Responses Measured From Forearm Muscles

*Jacob Weinman, Paria Arfa-Fatollahkhani, Andrea Zonnino, Rebecca C. Nikonowicz and Fabrizio Sergi**

Human Robotics Laboratory, Department of Biomedical Engineering, University of Delaware, Newark, DE, United States

OPEN ACCESS

Edited by:
Mario Bernardo-Filho, Rio de Janeiro State University, Brazil

Reviewed by:
Renato Naville Watanabe, Federal University of ABC, Brazil
Mariagiovanna Cantone, Sant'Elia Hospital, Italy

***Correspondence:**
Fabrizio Sergi
fabs@udel.edu

Specialty section:
This article was submitted to Motor Neuroscience, a section of the journal Frontiers in Human Neuroscience

Received: *09 December 2020*
Accepted: *15 March 2021*
Published: *16 April 2021*

Citation:
Weinman J, Arfa-Fatollahkhani P, Zonnino A, Nikonowicz RC and Sergi F (2021) Effects of Perturbation Velocity, Direction, Background Muscle Activation, and Task Instruction on Long-Latency Responses Measured From Forearm Muscles. Front. Hum. Neurosci. 15:639773. doi: 10.3389/fnhum.2021.639773

The central nervous system uses feedback processes that occur at multiple time scales to control interactions with the environment. The long-latency response (LLR) is the fastest process that directly involves cortical areas, with a motoneuron response measurable 50 ms following an imposed limb displacement. Several behavioral factors concerning perturbation mechanics and the active role of muscles prior or during the perturbation can modulate the long-latency response amplitude (LLRa) in the upper limbs, but the interactions among many of these factors had not been systematically studied before. We conducted a behavioral study on thirteen healthy individuals to determine the effect and interaction of four behavioral factors – background muscle torque, perturbation direction, perturbation velocity, and task instruction – on the LLRa evoked from the flexor carpi radialis (FCR) and extensor carpi ulnaris (ECU) muscles after velocity-controlled wrist displacements. The effects of the four factors were quantified using both a 0D statistical analysis on the average perturbation-evoked EMG signal in the period corresponding to an LLR, and using a timeseries analysis of EMG signals. All factors significantly modulated LLRa, and their combination nonlinearly contributed to modulating the LLRa. Specifically, all the three-way interaction terms that could be computed without including the interaction between instruction and velocity significantly modulated the LLR. Analysis of the three-way interaction terms of the 0D model indicated that for the ECU muscle, the LLRa evoked when subjects are asked to maintain their muscle activation in response to the perturbations was greater than the one observed when subjects yielded to the perturbations ($p < 0.001$), but this effect was not measured for muscles undergoing shortening or in absence of background muscle activation. Moreover, higher perturbation velocity increased the LLRa evoked from the stretched muscle in presence of a background torque ($p < 0.001$), but no effects of velocity were measured in absence of background torque. Also, our analysis identified

significant modulations of LLRa in muscles shortened by the perturbation, including an interaction between torque and velocity, and an effect of both torque and velocity. The time-series analysis indicated the significance of additional transient effects in the LLR region for muscles undergoing shortening.

Keywords: stretch reflex, long latency responses, motor neurophysiology, electromyography, robotics

INTRODUCTION

Countering unexpected and unpredictable loads is a ubiquitous occurrence of everyday life. Humans can precisely perform movements and interact with the environment even in the presence of these external perturbations. These mechanical perturbations require the nervous system to induce a compensatory action in order to ensure the task success. An important component of the compensatory actions produced by the central nervous system is the long-latency response (LLR). In upper limb muscles, the LLR is evident as the burst of muscle activity occurring 50–100 ms following a limb displacement. Accordingly, this event occurs between the fastest nervous system response, i.e., the short-latency reflex (SLR) occurring within 20–50 ms, and the delayed voluntary reaction which begins 100 ms after the imposed perturbation (Hammond, 1956; Lee and Tatton, 1975; Kurtzer, 2015).

After a seminal study by Hammond in 1956 (Hammond, 1956), several investigators have utilized a limb perturbation paradigm to investigate the physiological mechanisms subserving the muscle stretch responses to the externally applied loads (Allum, 1975; Crago et al., 1976; Evarts and Granit, 1976; Thomas et al., 1977; Kurtzer, 2015; Zonnino et al., 2019). In these paradigms, the muscle responses including the LLRs are recorded through surface electromyography (EMG) activity evoked in the muscle stretched by an imposed angular joint displacement induced by a mechanical perturbation of known and controllable characteristics (Rothwell et al., 1980; Tarkka and Larsen, 1987; Cody and Plant, 1989; Matthews, 1989, 1993; Noth et al., 1991; Kurtzer, 2015).

There is a body of evidence supporting the practical importance of muscle stretch responses – specifically the LLR component – in the neurological research. Previous studies showed that LLR can be considered as the primary outcome measure in various rehabilitation and robot-aided training protocols for several neurological diseases including stroke, Parkinson's disease (PD), spinal cord injury, and cerebellar ataxia (Sinkjær and Hayashi, 1989; Hayashi et al., 2001; Trumbower et al., 2013; Mirbagheri et al., 2015; Banks et al., 2019; Deneri et al., 2020). One recent study in 2019 (Banks et al., 2019), distinguished LLR as a promising physiological marker of walking dysfunction in chronic stroke. Trumbower et al., also demonstrated that there is a bilateral impaired regulation of the LLR during tasks which require increased stability in both the paretic and non-paretic upper limbs of stroke survivors (Trumbower et al., 2013). Moreover, previous studies on Parkinson's disease reported that LLR might be a useful objective physiological measure of muscle stiffness and rigidity in PD patients (Sinkjær and Hayashi, 1989; Hayashi et al., 2001).

Several behavioral factors are known to affect the amplitude of LLRs, including the neuromechanical state of the muscle prior perturbation (i.e., muscle length and activation) (Bedingham and Tatton, 1984; Calancie and Bawa, 1985), the direction of perturbation (i.e., whether the perturbation stretches or shortens the muscle) (Miscio et al., 2001; Lewis et al., 2004, 2010), the kinematic features of the applied perturbation (i.e., perturbation velocity, duration, amplitude, velocity profile) (Lee and Tatton, 1982; Lewis et al., 2005; Schuurmans et al., 2009), and the instructions provided to participants as to how to respond to the applied perturbations (Miscio et al., 2001; Lewis et al., 2006; Kurtzer et al., 2014).

Although investigators mostly focused on studying LLR features in stretched muscles, there is evidence of EMG activity evoked in the muscle shortened by the applied perturbation (Miscio et al., 2001; Lewis et al., 2004). Specifically, an increase in the EMG activity of the extensor carpi radialis (ECR) muscle which was shortened due to the applied wrist extension perturbation was documented in a study conducted in 2004 (Lewis et al., 2004). Although the shortened muscle response was smaller in amplitude than the one evoked in the stretched (flexor) muscle, both had two separate components of SLR and LLR with a similar onset timing. Another study also observed a similarly timed, low-amplitude EMG response with an onset of about 50 ms, evoked in the ECR muscle in response to a rapid wrist extension (Miscio et al., 2001). The authors suggest that part of the measured effects may be due to cross-talk (a volume-conducted response from the stretched muscle). However, because significant perturbation-evoked responses were measured in muscles undergoing shortening even using intramuscular EMG (Lewis et al., 2010), it may be reasonable that LLR are evoked in muscles subject to both a shortening and a stretching perturbation.

Studies also examined the effects of background muscle activation prior to the imposed perturbation on the LLR amplitude. In general, an increase in background activation results in an increase in the magnitude of muscle activity in both the proximal and distal muscles of the upper limbs (Bedingham and Tatton, 1984; Miscio et al., 2001; Pruszynski et al., 2009). Affecting the background motoneuron pool excitability, pre-existing background muscle activation is thought to reflect an automatic adjustment mechanism, known as the automatic gain component of the LLR (Bedingham and Tatton, 1984; Matthews, 1986; Miscio et al., 2001; Pruszynski et al., 2009).

Several studies quantified the effects of the kinematic features of the applied perturbation on the LLR amplitude (Lee and Tatton, 1975, 1982; Lewis et al., 2005, 2006; Schuurmans et al., 2009). It is generally accepted that the LLR amplitude increases as a function of the velocity of the applied perturbations

(Tatton and Bawa, 1979; Bedingham and Tatton, 1984). In the common ramp-and-hold perturbation paradigms, which are conducted at constant velocity, perturbation duration may also play a factor when the duration of the perturbation is within the range of neuromuscular delays expected for the LLR. However, the details of the interaction between perturbation velocity and duration in modulating LLR amplitude are not yet completely understood. A study by Lewis et al. showed that LLR amplitudes of the biceps brachii undergoing stretch are modulated by velocity in all conditions, but the slope of the relationship is also modulated by duration (Lewis et al., 2005). Yet, the range of velocities and durations that modulate the response in such a way is likely limited. In fact, we know that for FCR, a very high velocity and short duration (<40 ms) perturbation is not sufficient to evoke a long-latency response, whereas a perturbation of low velocity and long duration (>60 ms) generates well-developed LLRs (Lee and Tatton, 1982).

Task instruction also plays a key role in modulation of the LLR response. Accumulating evidence shows that the temporal overlap of two different responses including a task-dependent response and an automatic response results in the task-dependent change in LLR amplitude (Rothwell et al., 1980; Lewis et al., 2006; Pruszynski et al., 2011). The task-dependent response is larger when participants attempt to counter a perturbation than yield to the perturbation (Calancie and Bawa, 1985; Miscio et al., 2001; Lewis et al., 2006; Kurtzer et al., 2014). Participants can be instructed to respond to the perturbation in different ways: they can be asked to relax immediately following the perturbation (Miscio et al., 2001) — a condition referred to as "yield"; to maintain the background torque and avoid a voluntary response to the perturbation (Calancie and Bawa, 1985) — a condition referred to as "Do Not Intervene"; or to explicitly compensate by activating their muscles in the opposite direction of the perturbation (Lewis et al., 2006), or to compensate cued by a visual feedback of the hand position (Kurtzer et al., 2014) — conditions referred to as "Resist." In conditions where the subject was instructed to counter the stretch, LLR amplitude typically increased compared to a control condition, demonstrating that the LLR can be modulated to functionally adapt to the task at the upper limb (Crago et al., 1976; Colebatch et al., 1979; Rothwell et al., 1980). However, the 'yield' or the 'DNI' instructions were never directly compared, with the exception of one study (Calancie and Bawa, 1985), which only recruited two individuals. Because the state of the muscle in the "yield" and the "DNI" conditions is fundamentally different, it would be useful to quantify the differential effects of these two conditions on the evoked LLR.

Gathered together, several factors concerning the mechanics of the applied perturbations and the active role of muscles prior or during the perturbation can modulate the amplitude of long-latency responses in the upper limbs. Hence, it is of a paramount importance to study how the interaction of these factors would affect the muscle stretch responses in a single study. However, the majority of previous studies has systematically studied only one or two of the factors modulating LLRa, with the interaction between perturbation velocity and task instruction studied in Lewis et al. (2006), the interaction between perturbation velocity and background torque studied in Bedingham and Tatton (1984), and the interaction between task instruction and background torque studied in Calancie and Bawa (1985). One previous study (Miscio et al., 2001) has studied the effects of three of the factors highlighted above (i.e., task instructions, perturbation direction, and torque), though not with a full factorial design capable of quantifying the interactions among all factors. As such, to the best of our knowledge, no previous study conducted a full factorial design capable of quantifying the effects of and the interactions among all combinations of four factors known to modulate LLR amplitude, i.e., task instructions, perturbation duration, background torque, and perturbation velocity.

The goal of this study is to determine the effects of and the interactions among several experimental factors modulating the LLR amplitude during ramp-and-hold perturbation. Specifically, the goal of this study is to establish the effect and interaction of background muscle torque, perturbation direction, perturbation velocity, and task instruction on the LLR amplitude evoked from the flexor carpi radialis (FCR) and extensor carpi ulnaris (ECU) muscles following the application of controlled angular displacements of the wrist in both the extension and flexion directions.

MATERIALS AND METHODS

Thirteen healthy individuals were recruited to participate in this study (protocol approved by the University of Delaware Institutional Review Board, protocol no. 1097082-6). Subjects – age (mean ± s.d.: 24 ± 3 years) were naïve to the purpose of the study and free from known neurological or orthopedic disorders affecting arm function. Subjects were exposed to an experiment that aimed to quantify the amplitude of long-latency responses via the recording of EMG activity from a wrist flexor and extensor pair, the flexor carpi radialis (FCR) and extensor carpi ulnaris (ECU). These responses were evoked by flexion or extension perturbations applied by a robot to a subject's wrist in various conditions.

Materials

The equipment used for this experiment is shown in **Figure 1**, and includes several components, described below in detail.

Perturbation Robot

A custom-developed robot, the MR-StretchWrist, was used to apply perturbations to subject's wrists. The MR-StretchWrist is a 1-degree of freedom robot that can provide wrist flexion and extension between −45 to 45 degrees (Zonnino et al., 2019). The robot employs an ultrasonic piezoelectric motor (EN6060, Shinsei Motor Inc., Japan) that can provide 500 mNm of torque and can move at velocities of up to 900 degrees/second.

To provide torque for sufficient muscle stretch within the desired time of 50 ms, a capstan transmission with a 3:1 gear ratio was included in the design. The capstan drive contains two pulleys with different diameters connected via a microfiber braided line (SpiderWire Stealth SPW-0039, 0.4 mm diameter braided fishing line). The cable is wrapped around each pulley

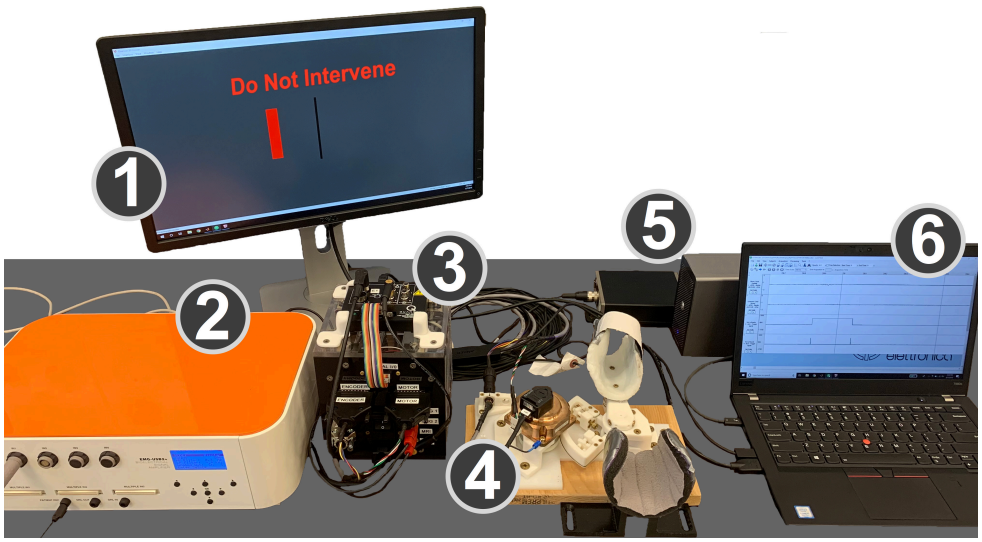

FIGURE 1 | Experimental setup. (1) Monitor displaying the GUI that cued subjects to the desired level of wrist flexion or extension torque and provides task instructions. (2) EMG amplifier. (3) Control box with the power supply, motor driver, and data acquisition board. (4) MR-StretchWrist robot. (5) Force sensor preamplifier box and analog/digital I/O device for force sensor data. (6) Laptop running EMG collection software, Simulink, and real-time QUARC software.

multiple times to ensure zero slippage. The capstan transmission is an ideal candidate for this application because it has no backlash, low friction, and high bandwidth.

Measurement of the wrist flexion/extension angle was obtained using an incremental encoder (resolution: 0.09 deg) placed on the motor shaft, with a resulting resolution in measuring the wrist flexion/extension angle of 0.03 deg.

EMG Amplifier and Electrodes

Electromyography data was recorded with an OTBioelettronica EMG-USB2+ amplifier (OTBioelettronica s.r.l., Torino, Italy), using OTBiolab Software (OTBioelettronica s.r.l., Torino, Italy). Disposable Silver/Silver chloride surface electrodes with conductive gel (HEX Dual Electrodes, Noraxon USA, Scottsdale, AZ, United States) were placed on the skin of the subject. A moistened conductive band was wrapped around the wrist, ensuring contact with the radial and ulnar stylar processes, to serve as a reference electrode. Bipolar cables were attached to the disposable electrodes and connected to the amplifier.

Force Measurement

An ATI Mini 27 Ti force sensor integrated in the MR-StretchWrist is used to measure the wrist flexion/extension torque (Full-scale Load (FSL): 2 Nm, Resolution: 0.5 mNm, Measurement uncertainty: 1.5% of FSL). Transducer signals are processed by a preamplifier box (ATI Industrial Automation, Apex, NC, United States), and digitized by an analog/digital I/O device (PCIe-6321, National Instruments, Austin, TX, United States) connected to a laptop.

Control Software

Software for robot position control, perturbation timing, and for the graphical user interface was developed in Matlab and Simulink, and executed in real-time (sample rate: 1 kHz) using the QUARC real-time control software (Quanser, Markham, ON, Canada). Encoder data were acquired using the Q2 USB data acquisition board (DAQ).

Methods

EMG Electrode Positioning

To determine the location of the electrodes to measure activity of the FCR and ECU, manual palpations were performed on the right arm of the subjects. Repeated wrist flexion during palpation while the wrist was in its neutral position aided in locating the FCR. Similarly, repeated wrist extension in this same orientation aided in locating the ECU. Points parallel to the muscle's fibers were drawn 3 cm apart. The skin was then prepped with 70% isopropyl alcohol wipes and the application a thin layer of conductive skin prep gel (Nuprep, Weaver and Co., Aurora, CO, United States).

Experimental Procedures

In this study, subjects were seated with their forearms resting in a stationary support connected to a normal desk, with the forearm extending anteriorly in front of the body. Their hand was strapped inside of a mold such that their wrist was in a semiprone/neutral condition, and any static wrist flexion/extension torque (range: 0 – 2 Nm) would be supported by the mold with little deflections. A GUI was shown on a computer screen indicating the amount of wrist flexion/extension torque to apply. After the subject reached the appropriate torque

target, and maintained it within a 50 mNm range for 0.4 to 0.8 s, the robot perturbed the wrist in the direction that would stretch the agonist muscle with respect to the cued torque (i.e., if the background torque was flexion, the perturbation was wrist extension). Perturbations were applied for a duration of 200 ms in all conditions, so to avoid undesired oscillations of the EMG signal due to impact dynamics arising from the abrupt end of a perturbation. After each wrist perturbation, the robot halted for 1 second before returning to the neutral position for the following perturbation. Numerous conditions were studied in this protocol, defined by factorial combinations of four factors: (1) perturbation velocity, (2) perturbation direction, (3) background torque, (4) task instructions.

Perturbation velocity assumed three levels: 50, 125, and 200 deg/s. Perturbation direction assumed two levels: wrist flexion or wrist extension. Background torque was set to either 0 or 200 mNm. Task instruction assumed two levels: "yield" (Y) and "do not intervene" (DNI). In the Y condition, subjects were told to not provide any resistance after the perturbation and yield (i.e., relax) to the movement. In the DNI condition, subjects were told to continue applying the same amount of torque that they were applying prior to perturbation. These two instructions are fundamentally the same in the absence of a background torque.

Ten trials per condition (combination of each level of velocity, direction, background torque, instruction) were collected, resulting in each experiment consisting of a total of 240 perturbations. The order in which conditions were applied was randomly generated by the Simulink and MATLAB files. Furthermore, the time between the end of the prior perturbation and the start of the next perturbation cue was randomized between 3 and 7 s.

EMG Processing

Pre-processing of the raw EMG data was conducted using Matlab code (Matlab 2017a, MathWorks, Natick, MA, United States). After on-board analog amplification (gain = 2000, amplifier settings: low-pass cut-off frequency: 0.3 Hz, high-pass cut-off frequency: 4.4 kHz), data were sampled at 10240 Hz. A band-pass filter, a 4th order Butterworth filter (f_{LP} = 250 Hz and f_{HP} = 20 Hz), was used to remove low frequency noise related to movement artifacts and high frequency noise related to intrinsic measurement noise. Matlab's *filtfilt* function was used to obtain a filtered waveform without any phase shift of the signal. The filtered waveform was then rectified. Digital outputs produced by the DAQ board (Q2-USB, Quanser, Markham, ON, Canada) were sent to the EMG amplifier to identify instants of perturbation onset, used for segmentation of the EMG signal into 200 ms long timeseries, one for each perturbation, each starting at the time of perturbation onset. EMG tracks were shifted in time such that t = 0 ms corresponded to the instant of arrival of the pulse.

The amplitude of the segmented EMG signal measured during a perturbation was normalized by the average magnitude of the rectified EMG signal measured from that same muscle during agonist background contractions preceding all perturbations. This procedure allowed us to conduct group analysis of normalized EMG data. With this procedure, an EMG signal of unitary magnitude indicated that the rectified EMG signal measured during each perturbation had the same amplitude of the average EMG signal generated by that muscle for a 200 mNm isometric torque. Units of the normalized EMG timeseries are referred to as normalized units (nu).

These procedures resulted in 10 segmented timeseries extracted from each subject per combination of conditions (velocity, direction, torque, instruction). Long-latency response amplitude (LLRa), defined as the average signal of the EMG tracks in the [50 100] ms interval, was calculated for each perturbation for both muscles, and indexed as a function of subject, repetition, and combination of experimental conditions. The subject-specific average of LLRa for each combination of perturbation conditions was used as the outcome measure for the 0-D statistical analysis.

Repeated measurements from each subject were averaged to yield the timeseries with average rectified EMG response for each subject $EMG_{sub,v,d,t,inst}$ used for the 1-D statistical analysis. Group averages $\overline{EMG}_{v,d,t,i}$ and corresponding standard deviations $\bar{s}_{v,d,t,i}$ were then calculated for display purposes.

Statistical Analysis

Two four-way full factorial linear mixed model ANOVAs were conducted using the subject-specific average LLRa measured for FCR and ECU, respectively, as outcome measure. The four factors included in the ANOVA were perturbation velocity (0, 125, 200 deg/s), background torque (0, 200 mNm), instruction (yield, do not intervene), and perturbation direction (stretch vs. shorten), defined based on the effect that the perturbation would have on the length of each muscle. As an example, a flexion perturbation would correspond to the "stretch" level for ECU, and the "shorten" level for FCR. Statistical analysis was conducted using JMP, and all variables were coded as nominal variables, with the default conditions of 50 deg/s for velocity, 0 mNm for background torque, yield for instruction, non-stretch for perturbation direction. JMP Pro Version 14 (SAS Institute Inc., Cary, NC, United States) was used for this analysis.

The linear mixed model included 16 terms for fixed effects (4 main effects, 6 two-way interactions, 4 three-way interactions, one four-way interaction term, and an intercept), plus an additional set of offset variables for random subject-specific effects. The Satterthwaite method was used to determine the number of degrees of freedom in the model. All terms are reported if their estimated effect is significant at the type I error rate α = 0.05. In those cases, Tukey HSD *post hoc* tests were also used to determine pairs of levels with significant differences.

A 1-D ANOVA was also conducted on the timeseries of rectified EMG signal ($EMG_{sub,v,d,t,i}$) measured during the post-perturbation interval comprised between 0 and 200 ms using the spm1d software (Pataky et al., 2015, 2016). 1-D statistical analysis models are useful to analyze the effects of the experimental conditions on the perturbation-induced muscle response without prior hypotheses on the specific time interval where an effect is expected (Pataky et al., 2015, 2016). While with the 0D analysis we restricted our focus on the time interval ensuing the perturbation comprised between 50 and 100 ms (thus obtaining a scalar, or 0D, outcome measure), with the 1D model we sought to determine whether there is an effect on the timeseries of

measured EMG amplitudes associated with all the experimental conditions, and their combinations, *at any time point* in the post-perturbation interval comprised between 0 and 200 ms. As such, the 1-D ANOVA is useful to establish effects of all factors and their interaction at multiple time-points, but controlling for the multiple comparisons resulting from this type of analysis.

Because the current version of the spm1D Matlab software only allows to build full factorial models with a maximum of three main effects, we broke each four-way model into two three-way models and performed our analysis using the spm1d function *anova3rm*. Each model included the factors speed, background torque, and instruction, with one model including LLRs measured during stretch, and the other model including LLRs measured during shortening. This setup allowed us to study the effects and interaction of all factors studies in the 0D analysis, with the exception of all terms involving perturbation direction. Given the software limitations, we chose to exclude perturbation direction from this analysis as it was an effect that had been largely neglected by most other studies.

The 1-D analysis was implemented as a mixed model ANOVA for measurements collected at all time points, which controls for the associated multiple comparisons using random field theory (Pataky et al., 2016). As such, the output of the 1D ANOVA procedure is a time-series of F scores for all main effects and their interaction, combined with the identification of time intervals where those effects are significant at $\alpha = 0.05$, corrected for the multiple comparisons performed at multiple time points. When an effect or an interaction was significant during the LLR time-window (i.e., from 50 to 100 ms after perturbation onset), we conducted *post hoc* tests to determine pairs of levels with significant modulation in EMG signal.

RESULTS

Of the 13 participants recruited for this study, data sets of 2 subjects for ECU and 3 subjects for FCR were excluded from analyses due to poor EMG recordings. Therefore, statistical analysis was performed on data collected on $n = 11$ individuals for the ECU muscle, and $n = 10$ individuals for the FCR muscle. Timeseries extracted in the different experimental conditions for the ECU muscle are shown in **Figures 2**, **3**. Similar representations are provided for the FCR muscle in **Supplementary Figures 1, 2** of the **Supplementary Materials**.

0-D Analysis

The linear mixed model computed an adjusted R^2 of 0.627 for FCR, and an adjusted R^2 of 0.788 for ECU. The model reported a significant effect of all four main factors. However, since all factors are involved in several two- and three-way interactions, only the interactions will be analyzed and discussed below. Results are presented below as least square means ± standard error (LLRa) or difference in least square means ± standard error

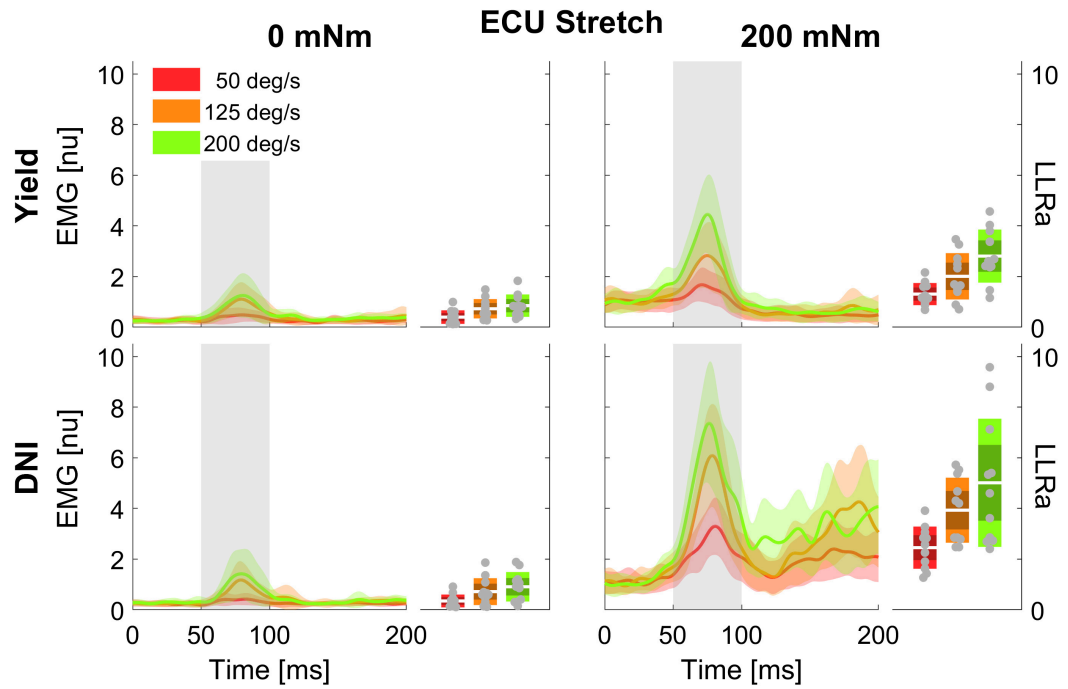

FIGURE 2 | Time series of EMG signal (left half-panels) and LLRa (boxplot in the right half-panels) from all subjects resulting with perturbations in the flexion direction (stretching the ECU muscle). Color indicates the speed of the perturbation (red = 50 deg/s, orange = 125 deg/s, green = 200 deg/s), with the line indicating the mean and the shaded area indicating the ± 1 s.d. region. Panels in different rows include measurements at two levels of task instruction – Yield (top), and DNI (bottom); columns include measurements at two levels of background torque – 200 mNm (right), and 0 mNm (left). In the boxplots, darker shades represent 1 standard deviation from the mean, and lighter shades indicate the 95% confidence interval.

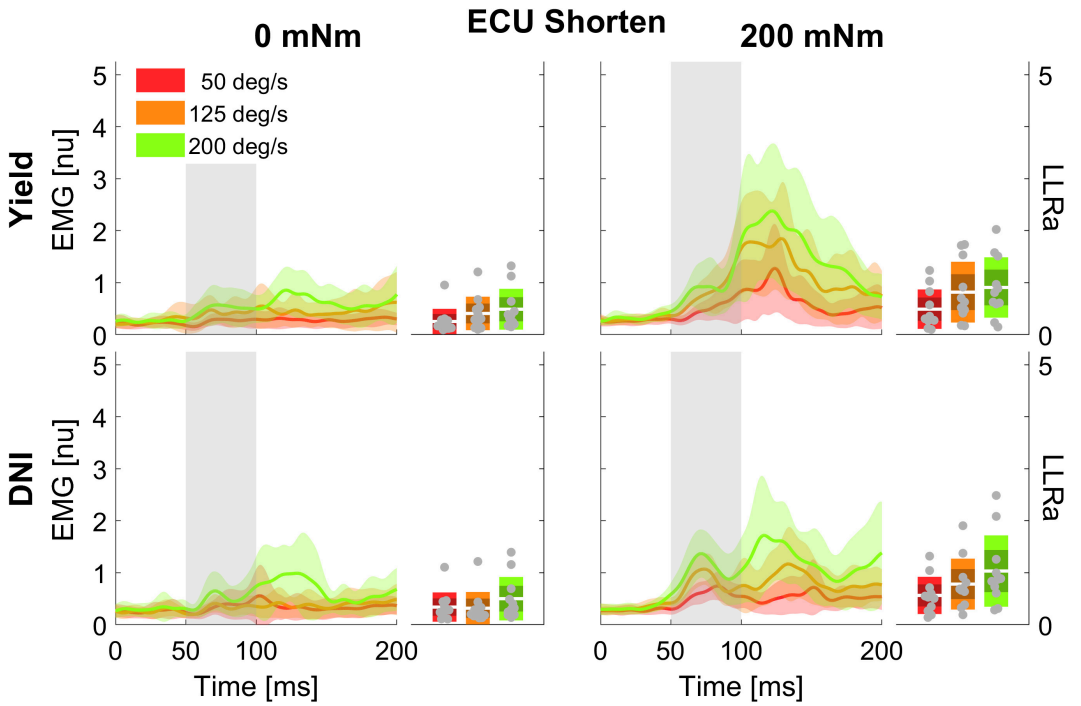

FIGURE 3 | Time series of EMG signal and LLRa from all subjects resulting with perturbations in the extension direction (shortening the ECU muscle).

(ΔLLRa) in units of the outcome measure, i.e., normalized units (nu). A report including the significant fixed effects from the linear mixed model ANOVA is provided below in **Tables 1**, **2**.

A significant three-way interaction between perturbation direction, instruction, and torque was measured for the ECU muscle (**Figure 4**). A significant effect of instruction or perturbation direction on LLRa was observed only in presence of a background torque for both muscles. In presence of background torque, the LLRa associated with stretch perturbations was greater than the LLRa associated with shortening perturbation both when task instructions were DNI (LLRa — Stretch DNI: 3.80 ± 0.17 nu, Shorten DNI: 0.79 ± 0.17 nu, $p < 0.001$), and when task instructions were to yield (LLRa — Stretch Y: 2.04 ± 0.17 nu, Shorten Y: 0.74 ± 0.17 nu, $p < 0.001$). In presence of background torque and muscle stretch, LLRa was greater in the DNI condition compared to yield (ΔLLRa — DNI vs. Y: 1.76 ± 0.16 nu, $p < 0.001$).

A significant three-way interaction between perturbation direction, torque, and velocity was measured for the ECU muscle (**Figure 5**). A significant effect of perturbation velocity or direction was observed only in presence of a background torque. In presence of background torque, the LLRa associated with stretch perturbations was greater

TABLE 1 | Significant main effects and interactions for ECU LLRa.

Fixed Effect	N. param.	D.F. Num.	D.F. Den.	Prob > F
Direction	1	1	230	**< 0.001**
Instruction	1	1	230	**< 0.001**
Torque	1	1	230	**< 0.001**
Velocity	1	1	230	**< 0.001**
Direction*Instruction	1	1	230	**< 0.001**
Direction*Torque	1	1	230	**< 0.001**
Direction*Velocity	2	2	230	**< 0.001**
Instruction*Torque	1	1	230	**< 0.001**
Torque*Velocity	2	2	230	**< 0.001**
Direction*Instruction*Torque	1	1	230	**< 0.001**
Direction*Torque*Velocity	2	2	230	**0.006**

A total of 11 effects are presented. Bold is used when p < 0.05.

TABLE 2 | Main effects and interactions for FCR LLRa.

Fixed Effect	N. param.	D.F. Num.	D.F. Den.	Prob > F
Direction	1	1	207	**< 0.001**
Instruction	1	1	207	**0.016**
Torque	1	1	207	**< 0.001**
Velocity	1	1	207	**< 0.001**
Direction*Torque	1	1	207	**< 0.001**
Direction*Velocity	2	2	207	**< 0.001**
Instruction*Torque	1	1	207	**0.005**
Direction*Instruction	1	1	207	0.13
Torque*Velocity	2	2	207	0.16
Direction*Instruction*Torque	1	1	207	0.055
Direction*Torque*Velocity	2	2	207	0.66

*Of the 11 effects listed from **Table 1**, the FCR LLRa shares 7 significant effects. Bold is used when p < 0.05.*

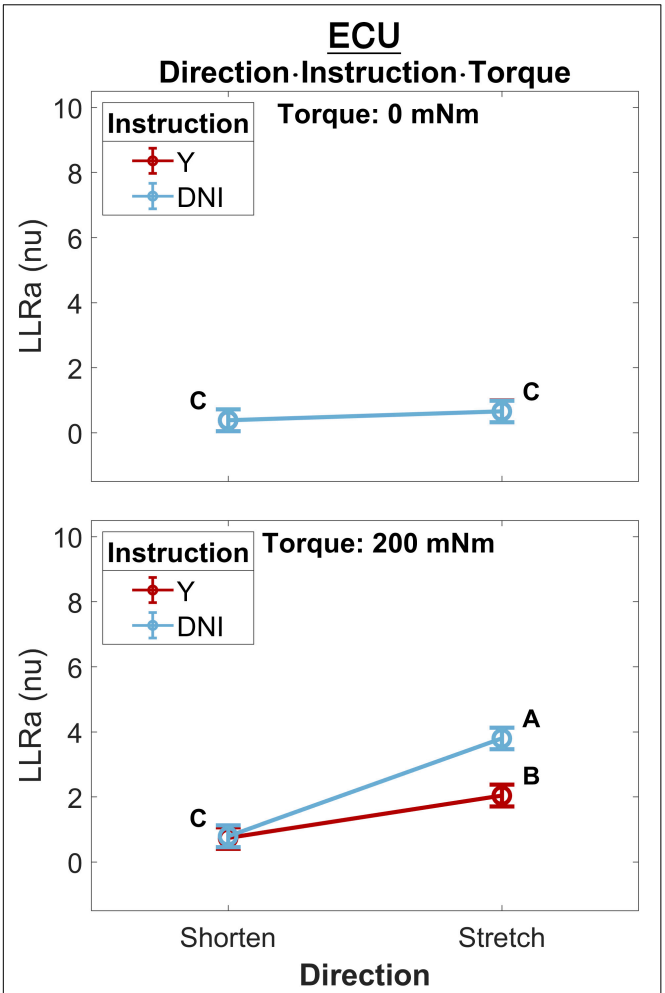

FIGURE 4 | Least square means (mean displayed with a circle and whisker extending to ± one standard error of the mean) for the significant three-way interaction between perturbation direction, instruction, and torque, conducted for the ECU muscle. Plots are split by torque level – 0 mNm (top), 200 mNm (bottom). Line colors indicate instruction, and different levels of perturbation direction are displayed along the x axis. Letters on the plots are representative of *post hoc* Tukey HSD tests; pairs of elements that do not share a letter are significantly different.

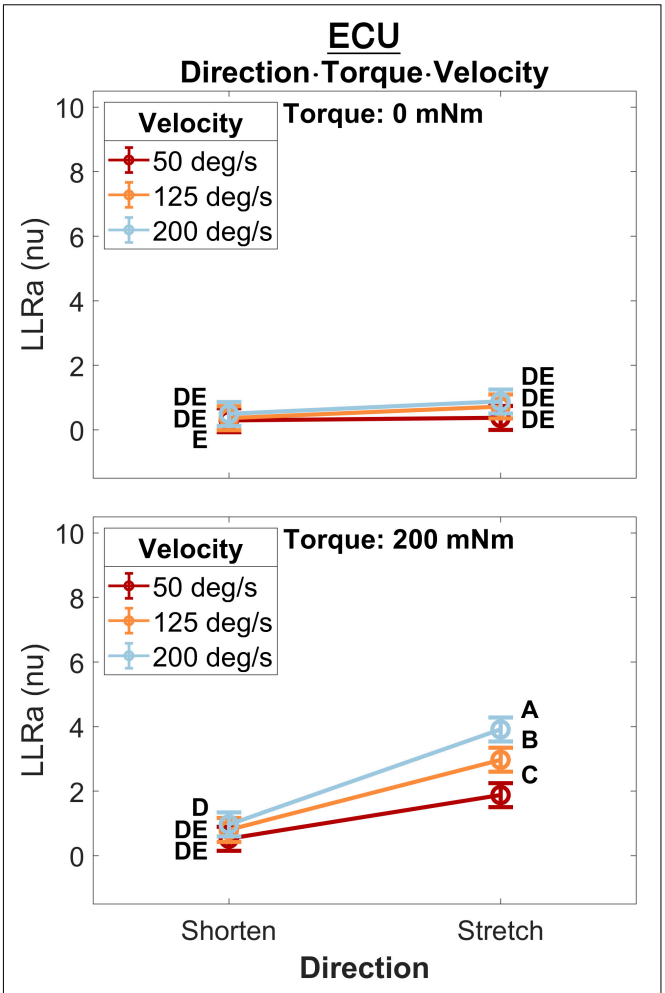

FIGURE 5 | Least square means for the significant three-way interaction between perturbation direction, velocity, and torque, conducted for the ECU. Plots are split by torque level – 0 mNm (top), 200 mNm (bottom) – line color indicates velocity, and different levels of perturbation direction are displayed along the x axis.

than the LLRa associated with shortening perturbations at all velocities (200 deg/s: Stretch: 3.91 ± 0.19 nu, Shorten: 0.97 ± 0.19 nu, $p < 0.001$; 125 deg/s: Stretch: 2.97 ± 0.19 nu, Shorten: 0.80 ± 0.19 nu, $p < 0.001$; 50 deg/s: Stretch: 1.88 ± 0.19 nu, Shorten: 0.53 ± 0.19 nu, $p < 0.001$). In presence of background torque and for perturbations that stretched the muscle, LLRa increased with velocity (ΔLLRa 200-125 deg/s: 0.94 ± 0.20 nu, $p < 0.001$; ΔLLRa 125-50 deg/s: 1.09 ± 0.20 nu, $p < 0.001$). Instead, no velocity-dependent effect was measured for perturbations shortening the muscle.

Five two-way interaction terms were significant for ECU, while three terms were significant for FCR. Three terms were common to both muscles and are described next.

The interaction between instruction and torque resulted from a greater increase in LLRa measured in the DNI conditions compared to the yield conditions measured in the presence of a background torque for both muscles (**Figure 6**). In the presence of background torque, LLRa measured during the DNI condition was significantly greater than LLRa measured in the Y condition (FCR LLRa — DNI: 3.67 ± 0.53 nu, Y: 2.39 ± 0.53 nu, $p = 0.001$; ECU LLRa — DNI: 2.30 ± 0.15 nu, Y: 1.40 ± 0.15 nu, $p < 0.001$). There was no difference in LLRa measured in absence of background torque between the two instructions (FCR LLRa — DNI: 1.12 ± 0.53 nu, Y: 1.22 ± 0.53 nu, $p = 0.990$; ECU LLRa — DNI: 0.52 ± 0.15 nu, Y: 0.52 ± 0.15 nu, $p = 1$). Significant differences between torque levels were measured in both the FCR and ECU for both instructions (FCR ΔLLRa — DNI: 2.55 ± 0.34 nu, $p < 0.001$, Y: 1.16 ± 0.34 nu, $p = 0.004$; ECU ΔLLRa —

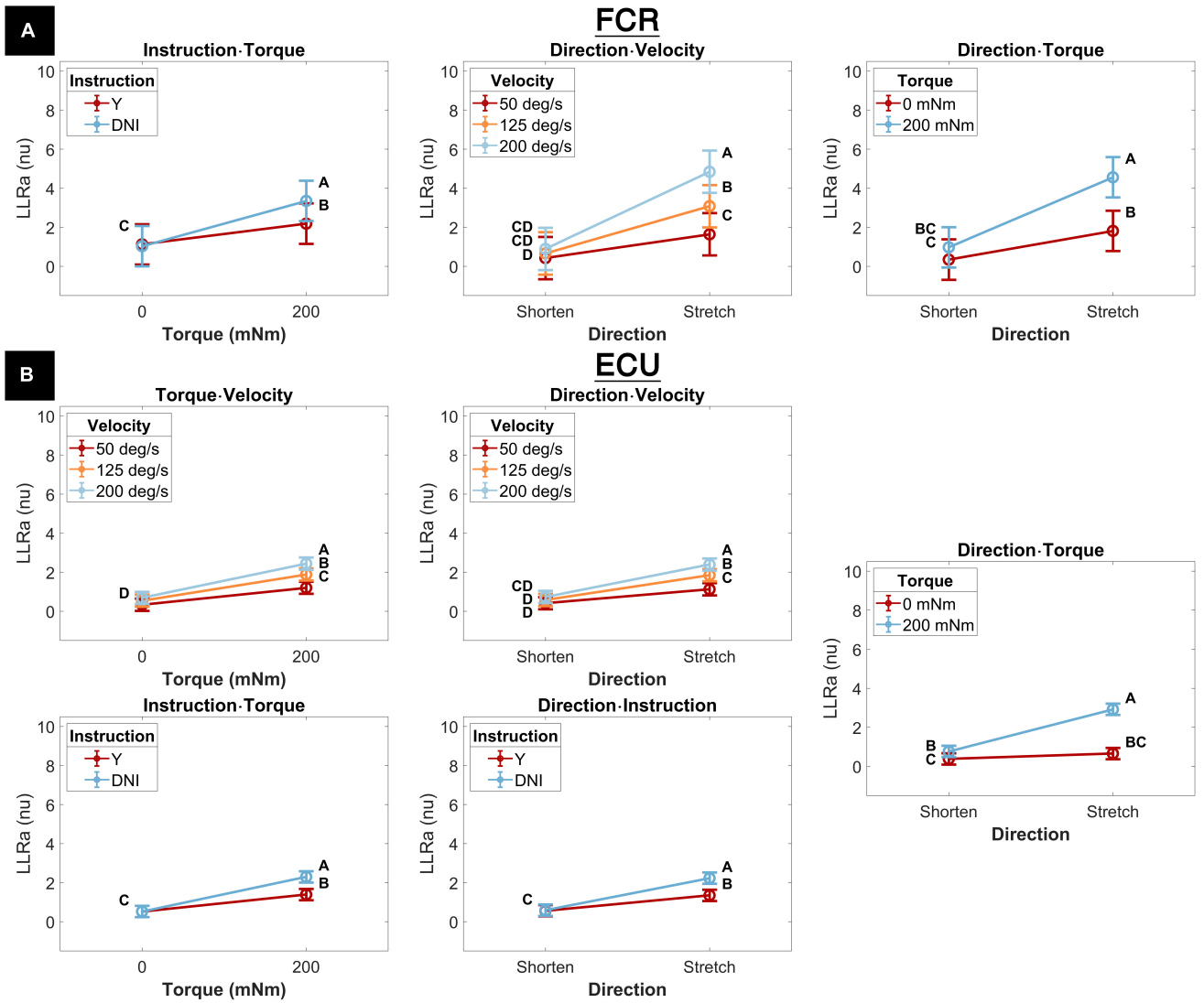

FIGURE 6 | Least square means for all significant two-way interactions for both the FCR **(A)** and the ECU **(B)**. Letters on the plots are representative *post hoc* Tukey HSD tests; pairs of elements that do not share a letter are significantly different. *Post hoc* tests are, and the corresponding letter notation are separate for each panel.

DNI: 1.77 ± 0.11 nu, $p < 0.001$, Y: 0.87 ± 0.11 nu, $p < 0.001$).

The interaction between perturbation direction and velocity resulted from a greater increase in LLRa measured when muscles are stretched by a perturbation compared to when they are shortened measured at higher velocities (**Figure 6**). LLRa measured during stretch were significantly greater at higher velocities (FCR LLRa — 200 deg/s: 5.31 ± 0.56 nu, 125 deg/s: 3.37 ± 0.56 nu, 50 deg/s 1.79 ± 0.56 nu, 200-125 deg/s $p < 0.001$, 125-50 deg/s $p = 0.003$; ECU LLRa — 200 deg/s: 2.40 ± 0.16 nu, 125 deg/s 1.85 ± 0.16 nu, 50 deg/s 1.13 ± 0.16 nu, 200-125 deg/s $p = 0.002$, 125-50 deg/s $p < 0.001$), while there was no significant effect of velocity during perturbations where the muscle was shortened. The increase in LLRa between shorten and stretch conditions was greater at higher velocities (FCR ΔLLRa — 50 deg/s: 1.34 ± 0.42 nu, 125 deg/s 2.66 ± 0.42 nu, 200 deg/s 4.35 ± 0.42 nu, 200-125 deg/s $p = 0.005$, 200-50 deg/s $p < 0.001$, 125-50 deg/s $p = 0.026$; ECU ΔLLRa — 50 deg/s: 0.71 ± 0.14 nu, 125 deg/s 1.27 ± 0.14 nu; 200 deg/s 1.66 ± 0.14 nu, 200-125 deg/s $p = 0.047$, 200-50 deg/s $p < 0.001$, 125-50 deg/s $p = 0.006$).

The significant interaction between perturbation direction and torque resulted from the greater increase in LLRa associated with stretch perturbations compared to shortening measured in presence of background torque (**Figure 6**). LLRa associated with stretch perturbations were greater than those associated with shortening in presence of background torque (FCR ΔLLRa — 0 mNm: 1.62 ± 0.34 nu, 200 mNm: 3.95 ± 0.34 nu, $p < 0.001$; ΔLLRa ECU — 0 mNm: 0.27 ± 0.11 nu, 200 mNm: 2.15 ± 0.11 nu, $p < 0.001$). LLRa measured in presence of background torque were greater than in absence of background torque for both muscles when they were stretched (FCR ΔLLRa stretch: 3.02 ± 0.34 nu, $p < 0.001$; ECU ΔLLRa stretch:

2.26 ± 0.11 nu, $p < 0.001$), but only for ECU when shortened (FCR ΔLLRa shorten: 0.69 ± 0.34 nu, $p = 0.180$; ECU ΔLLRa shorten: 0.38 ± 0.11 nu, $p = 0.006$).

Two two-way interaction terms were significant only for the ECU muscle. One term, the interaction between torque and velocity, resulted from a greater increase in LLRa associated with higher velocity perturbations measured in the presence of a background torque (**Figure 6**). The change in LLRa associated with the two levels of background torque increased at greater velocities (ΔLLRa — 200 deg/s: 1.75 ± 0.14 nu, 125 deg/s: 1.34 ± 0.14 nu, 50 deg/s: 0.87 ± 0.14 nu, 200-125 deg/s $p = 0.040$, 200-50 deg/s $p < 0.001$, 125-50 deg/s $p = 0.0181$). LLRa measured in presence of background torque was significantly different for each velocity level and increased with greater velocity (ΔLLRa — 200-50 deg/s: 1.24 ± 0.14 nu, $p < 0.001$, 200-125 deg/s: 0.56 ± 0.14 nu $p = 0.001$, 125-50 deg/s: 0.68 ± 0.14 nu $p < 0.001$).

The second two-way interaction term significant only for the ECU muscle was the interaction between perturbation direction and instruction. This term resulted from a greater increase in LLRa measured in the DNI condition compared to yield condition measured when muscles are stretched (**Figure 6**). When muscles were stretched, LLRa associated with the DNI conditions were larger than the yield condition (LLRa — DNI: 2.23 ± 0.15 nu, Y: 1.35 ± 0.15 nu, $p = 0.001$), while no significant difference between instruction conditions was measured when muscles were shortened. A significant increase in LLRa was measured in both instruction conditions when muscles were stretched compared to shortened, but this increase was greater in the DNI condition compared to the yield condition (ΔLLRa — DNI: 1.64 ± 0.11 nu; Y: 0.79 ± 0.11 nu, $p < 0.001$).

The model returned a significant effect of each of the four factors, i.e., perturbation direction, instruction, background torque, and velocity. For the effect of perturbation direction, stretched muscles resulted in a significantly larger LLR amplitude than those of shortened muscles (FCR LLRa — stretch: 3.49 ± 0.50 nu, shorten: 0.71 ± 0.50 nu, $p < 0.001$; ECU LLRa — stretch: 1.79 ± 0.13 nu, shorten: 0.58 ± 0.13 nu, $p < 0.001$). With respect to the significant effect of instruction, the DNI condition resulted in larger LLR amplitudes compared to the yield condition for both the FCR and ECU (FCR LLRa — DNI: 2.39 ± 0.50 nu, yield: 1.81 ± 0.50 nu, $p = 0.016$; ECU LLRa — DNI: 1.41 ± 0.13 nu, yield: 0.96 ± 0.13 nu, $p < 0.001$). The presence of background torque at 200 mNm resulted in a significantly larger LLR amplitude compared to the absence of background torque for both muscles (FCR LLRa — 200 mNm: 3.03 ± 0.50 nu, 0 mNm: 1.17 ± 0.50 nu, $p < 0.001$; LLRa ECU — 200 mNm: 1.84 ± 0.13 nu, 0 mNm: 0.52 ± 0.13 nu, $p < 0.001$). The significant effect of velocity resulted from higher velocities associated with larger LLRas for both muscles (FCR LLRa — 50 deg/s: 1.12 ± 0.52 nu, 125 deg/s: 2.04 ± 0.52 nu, 200 deg/s: 3.14 ± 0.52 nu; ECU LLRa — 50 deg/s: 0.77 ± 0.14 nu, 125 deg/s: 1.21 ± 0.14 nu, 200 deg/s: 1.56 ± 0.14 nu). Tukey HSD *post hoc* analysis indicated that all velocity levels are significantly different from one another for both muscles. (FCR — 200-125 deg/s: $p < 0.001$, 125-50 deg/s: $p = 0.006$; ECU — 200-125 deg/s: $p = 0.002$, 125-50 deg/s: $p < 0.001$).

1D Analysis

The results of the 1D ANOVA are represented in terms of a timeseries of F scores, shown in **Figures 7**, **8** for the ECU and FCR, respectively. For effects and interactions that have significant upcrossings within the LLR region, *post hoc* 1D t-tests were used to further break down the effects.

The three-way interaction between instruction, torque, and velocity was not significant within the LLR for both muscles and both directions, however, there is a narrow significant upcrossing during the SLR for ECU Stretch (25.8 to 28.3 ms, peak $F_{2,20} = 11.495$).

The two-way interaction between instruction and torque is significant within the LLR region for both directions of the ECU muscle, but not for the FCR muscle. Within the LLR region, there are significant upcrossings for ECU during both muscle shortening and stretching (ECU Stretch: 52.6 to 70.0 ms, local peak in LLR region $F_{1,10} = 26.152$; ECU Shorten: 62.2 to 66.8 ms, peak $F_{1,10} = 37.434$). There are also significant upcrossings within the voluntary region for the stretch of the ECU and FCR (ECU Stretch: 148.6 to 200 ms, peak $F_{1,10} = 26.152$; FCR Stretch: 183.0 to 196.0 ms, 199.3 to 200 ms, peak $F_{1,10} = 27.377$).

The two-way interaction between instruction and torque measured for the ECU muscle is broken down in the 1D *post hoc* t-tests to analyze the measured effect at all time points, as shown in **Figure 9**. Analysis of *post hoc* tests highlights how the DNI has positive or negative effect on the amplitude of processed EMG recordings at different time points, and the effect differs as a function of stretch and background torque condition. When the ECU was stretched, the normalized EMG signal in DNI was greater than yield within the LLR and voluntary regions in the presence of background torque, (ECU Stretch: 49.1 to 200 ms, peak $T = 13.703$, **Figure 9B**, center). No significant change in EMG signal was measured in absence of background torque as a function of task instructions (**Figure 9B**, left). As a result, the change in EMG signal measured between the DNI and Y condition was greater in presence of background torque than in absence only after the delay similar to that considered for forearm LLRs (ECU Stretch: 38.7 ms to 200 ms, peak $\Delta T = 14.450$, peak in the LLR region $\Delta T = 9.397$, **Figure 9B**, right). When the ECU was shortened, EMG recordings measured in presence of background torque in the DNI condition were greater than those measured in the yield condition in the initial part of LLR, but then EMG recordings measured during DNI were smaller than yield at a later time in the LLR time period (ECU Shorten: 57.7 to 77.0 ms, local peak $T = 4.470$, 94.6 ms to 129.5 ms, local peak $T = -3.925$, **Figure 9A**, center). Instead, no significant change in EMG signal was measured in absence of background torque as a function of task instructions (**Figure 9A**, left). The change in T scores between torque levels for the shortened condition also indicated significant upcrossings in the LLR and voluntary regions (ECU Shorten: 54.2 to 73.5 ms, local peak $\Delta T = 4.961$, 92.5 to 132.9 ms, local peak $T = -5.461$, **Figure 9A**, right).

The two-way interaction between torque and velocity is significant in the LLR region for the ECU when stretched and for the FCR when it is both shortened and stretched. For both the ECU and FCR there is a significant upcrossing within the LLR region (ECU Stretch: 52.6 to 74.7 ms, peak $F_{2,20} = 19.872$; FCR

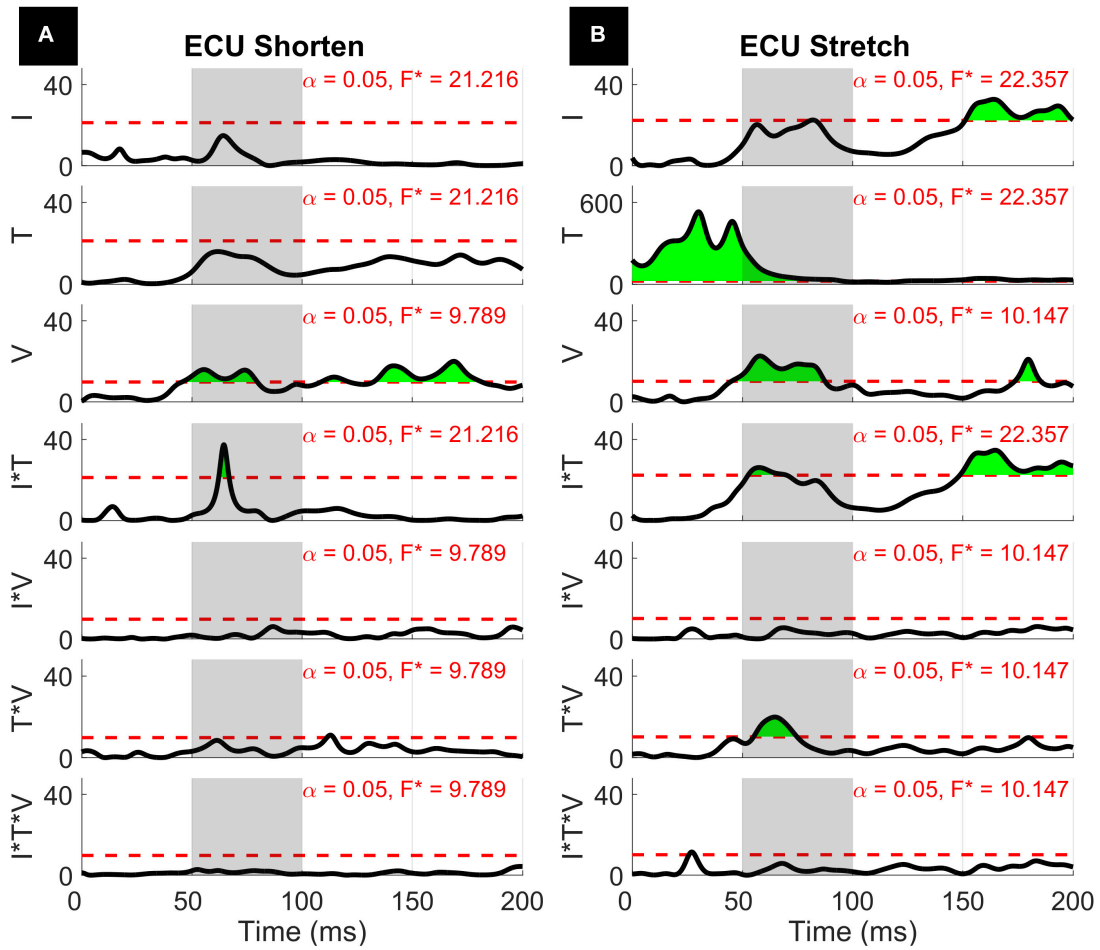

FIGURE 7 | Results of the 1D 3-way ANOVA for the shortened **(A)** and stretched **(B)** states of the ECU. Curves are a time-series of *F* scores for the effect of a factor or of an interaction of factors on the outcome measure. The dashed red line indicates the critical *F*-value for that main effect or interaction. Regions in green indicate significant upcrossings. The shaded gray region is representative of the LLR (50 to 100 ms).

Shorten: 47.9 to 65.8 ms, peak $F_{2,20}$ = 22.421; FCR Stretch: 58.0 to 68.6 ms, peak $F_{2,20}$ = 19.244).

The two-way interaction between torque and velocity for muscle and perturbation direction is broken down in 1D *post hoc* tests for ECU Stretch, FCR Shorten, and FCR Stretch (**Figures 10–12**). For the stretch of the ECU (**Figure 10**), significant upcrossings were present in *post hoc* tests comparing EMG signals measured at different velocity levels and at multiple torque levels, primarily during the LLR time period. Analysis of the timeseries of t-scores demonstrate that EMG signal increases with velocity and with background torque, and that the region where such an increase is measured largely overlaps with the expected latency of a LLR. The largest upcrossing was measured for the 200-50 deg/s comparison in presence of a background torque (40.8 to 98.1 ms, peak T = 10.202, **Figure 10**, center row, center column). Upcrossings within the LLR region were also measured for the 200-50 deg/s *t*-test in the absence of background torque, the 200-125 deg/s *t*-test in the presence of background torque, and the 125-50 degree/second *t*-test in both torque conditions. Significant upcrossings were measured within the LLR region for the 200-50 deg/s comparison and the 200-125 degrees/second comparison (Δ200-50 deg/s: 56.4 to 73.8 ms, peak ΔT = 5.915, **Figure 10** center row, right column, Δ200-125 deg/s: 56.0 to 62.7 ms, peak ΔT = 4.304, **Figure 10**, top row, right column). The significance of the between-torque condition difference of the t-scores resulting from comparing pairs of velocity levels indicates that background torque differentially modulates the velocity dependence of EMG signals.

Qualitatively similar results were measured for the stretch of FCR (**Figure 11**). Significant upcrossings were measured for *t*-test comparisons mostly during the LLR time period. The largest t-scores were generated for the 200-50 deg/s *t*-test in the presence of background torque (23.7 to 80.9 ms, peak T = 12.856, **Figure 11** center row, center column). Significant upcrossings were also present for the 200-125 deg/s *t*-test in presence of background torque, 200-50 degree/second *t*-test in the absence of background torque, the 200-125 deg/s *t*-test in both torque conditions, and the 125-50 deg/s *t*-test in both torque conditions. One significant upcrossing was measured for the between-torque

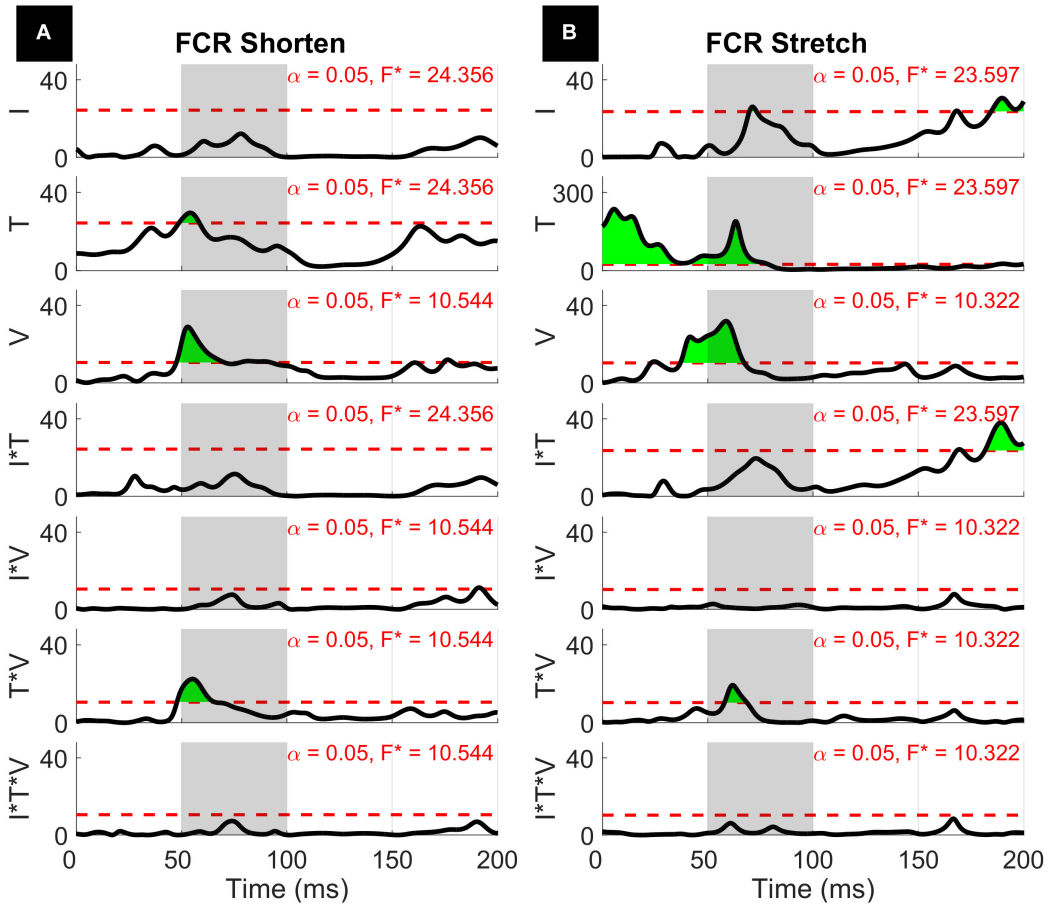

FIGURE 8 | Results of the 1D 3-way ANOVA for the shortened **(A)** and stretched **(B)** states of the FCR.

condition difference of t-scores resulting from comparing pairs of velocity conditions (Δ200-50 deg/s: 57.9 to 64.0 ms, peak ΔT = 4.604, **Figure 11** center row, right column).

For FCR responses measured during muscle shortening (**Figure 12**), significant upcrossings were present in *t*-test comparisons between velocity levels in the presence of background torque. Like in the previous conditions, the largest t-scores were generated for the 200-50 degree/second *t*-test in the presence of background torque (46.0 to 93.3 ms, peak T = 8.601, **Figure 12** center row, center column). There are also smaller, significant upcrossing for this *t*-test in the voluntary region (149.1 to 165.1 ms, 187.9 to 200 ms). Significant upcrossings were also present for the 200-125 deg/s *t*-test in presence of background torque, 200-50 degree/second *t*-test in the absence of background torque, and the 125-50 degree/second *t*-test in both torque conditions. Significant upcrossings within the LLR region were calculated for difference between *t*-tests of different background torque levels (Δ200-50 deg/s: 48.7 to 63.2 ms, peak ΔT = 6.587, **Figure 12** center row, right column, Δ200-125 deg/s: 50.6 to 59.2 ms, peak ΔT = 5.176, **Figure 12**, top row, right column). Such differential effect of background torque at multiple velocities on EMG signal collected from a muscle under shortening was only observed for the ECU muscle in the 0D analysis (**Figure 5**, significant difference between conditions A – background torque: 0 mNm and velocity: 50 deg/s — and B – background torque: 200 mNm and velocity: 200 deg/s).

The two-way interaction between instruction and velocity is only significant for the shortened state of the FCR during a narrow time window outside of the LLR region (189.8 to 193.1 ms, peak $F_{2,20}$ = 10.959).

With respect to the main effects, both the FCR and ECU had significant upcrossings within the LLR region. The main effect of instruction was significant within the LLR region for the stretch of the FCR and ECU only for a very short time period (FCR stretch: 69.8 to 73.2 ms, local peak $F_{1,10}$ = 26.080; ECU stretch: 81.1 to 82.8 ms, local peak $F_{1,10}$ = 22.546) and has upcrossings within the voluntary region for both the stretch of the FCR and ECU (FCR Stretch: 184.6 to 200 ms, peak $F_{1,10}$ = 30.620; ECU Stretch: 151.1 to 200 ms, peak $F_{1,10}$ = 32.771). There were otherwise no significant upcrossings for the effect of instruction for the shortened state of the muscles.

DISCUSSION

In the present study, we aimed to investigate the effects of and the interactions among four behavioral factors in modulating the LLR amplitude (LLRa) evoked from FCR and

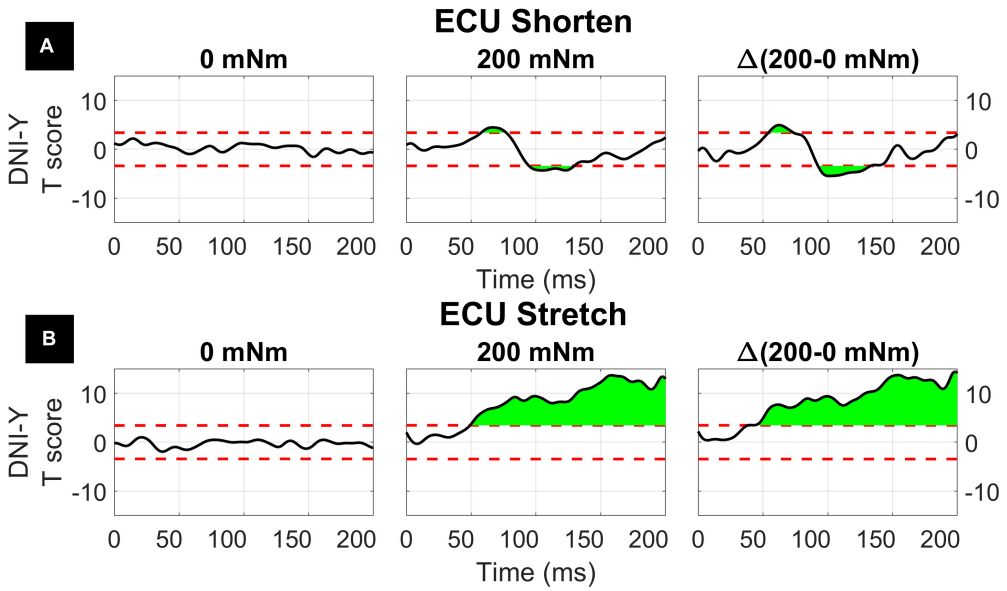

FIGURE 9 | Results of the 1D *t*-tests for the interaction between task instruction and torque for the shortened **(A)** and stretched **(B)** states of the ECU. Plots indicate the statistical score of 1D paired *t*-tests between the DNI and yield instructions and split in columns by torque level. Plots in the right column report the difference between the *T*-scores in the second and first column's tests, used to demonstrate interaction between these factors. The dashed red line indicates the Bonferroni-adjusted critical T values and regions in green indicate significant upcrossings.

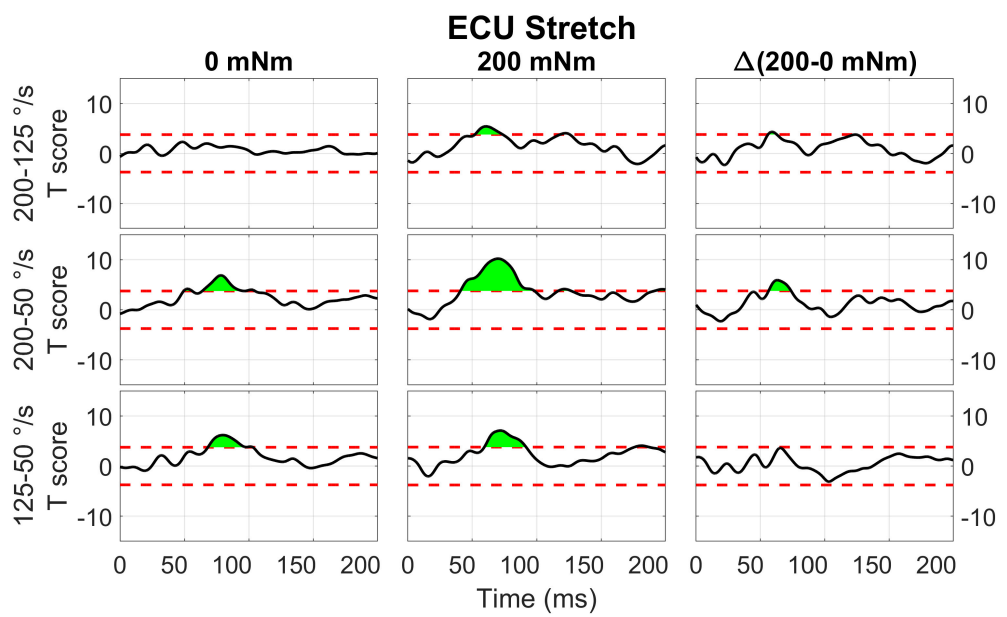

FIGURE 10 | Results of the 1D *t*-tests of the interaction between torque and velocity for the stretched state of the ECU. Plots in different rows indicate the statistical score of 1d paired *t*-tests between the velocity levels (200-125, 200-50, 125-50 deg/s) and columns indicate different torque levels. Plots in the right column report the difference between the *T*-scores in the second and first column's tests, used to demonstrate interaction between these factors. The dashed red line indicates the Bonferroni-adjusted critical *T*-values and regions in green indicate significant upcrossings.

ECU muscles during ramp-and-hold perturbations applied to the wrist joint. The four behavioral factors studied in this work were perturbation direction (stretch vs. shorten), background muscle activation (0 vs. 200 mNm of joint torque requiring agonist muscle activity), perturbation velocity (50, 125, and 200 deg/s), and task instructions (yield vs DNI). In line with previous studies (Lee and Tatton, 1982; Bedingham and Tatton, 1984; Calancie and Bawa, 1985; Miscio et al., 2001;

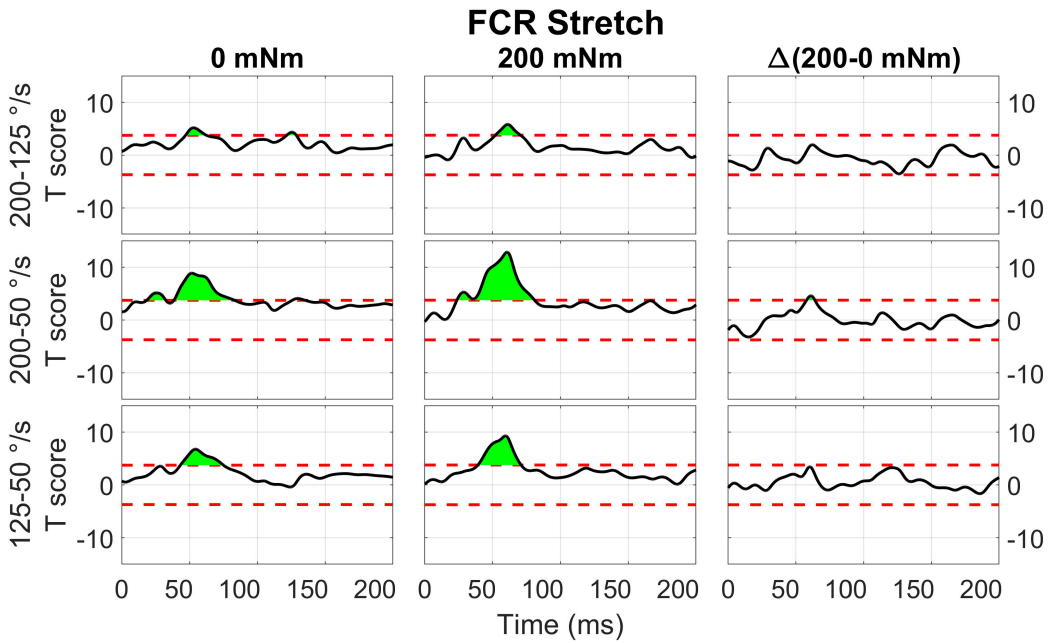

FIGURE 11 | Results of the 1D *t*-tests of the torque and velocity interaction for the stretched state of the FCR.

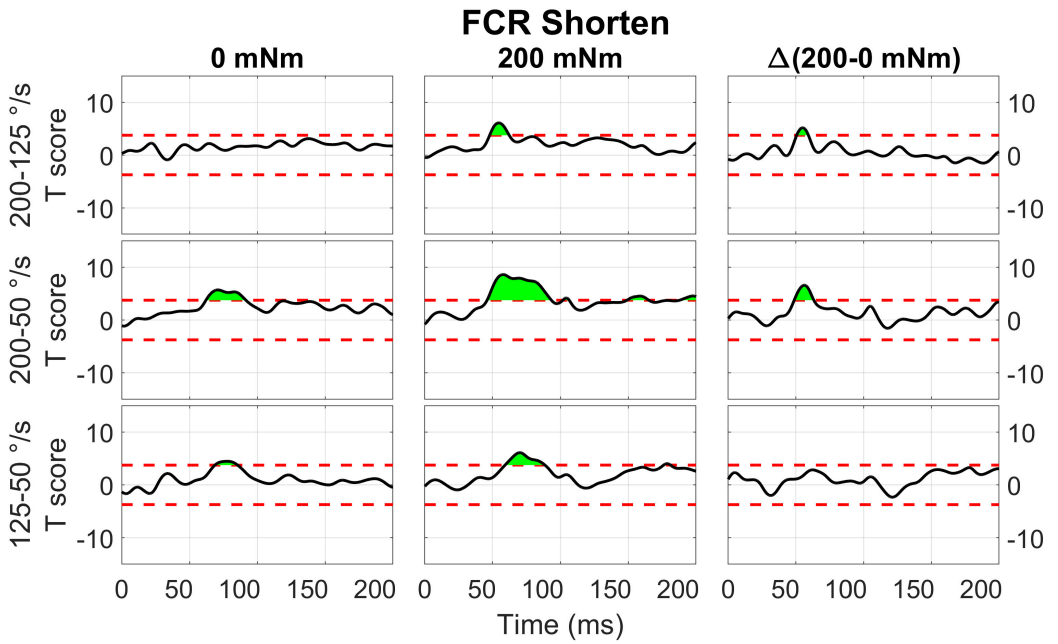

FIGURE 12 | Results of the 1D *t*-tests of the torque and velocity interaction for the shortened state of the FCR.

Lewis et al., 2004, 2005, 2006, 2010; Schuurmans et al., 2009; Kurtzer et al., 2014), we observed that all factors modulate the LLRa in the FCR and ECU muscles. However, given the use of full factorial design involving all combinations of the four factors, we were able to study higher-order interactions among the four behavioral factors. Moreover, the use of a 1D analysis of stretch-evoked EMG data allowed us to establish the effects of the behavioral factors on EMG amplitude at multiple timepoints in the post-perturbation period, without restricting the analysis to a-priori selected time windows where a modulation would be expected.

In line with previous studies (Tatton and Bawa, 1979; Bedingham and Tatton, 1984), our findings demonstrated that perturbation velocity significantly modulates LLRa, as larger

LLRa resulted from perturbations with 200 deg/s velocity compared to the 125 and 50 deg/s velocity conditions, while the 50 deg/s perturbation velocity evoked the lowest LLRa. Note that given the chosen task design, where perturbations are applied for a constant duration (200 ms), perturbation velocity and displacement are associated, so the measured effect could be due to the fact that the joint is subject to a greater displacement in the higher velocity conditions. From studies that systematically spanned a set of perturbation velocity and durations (Lee and Tatton, 1982; Lewis et al., 2005; Schuurmans et al., 2009), we know that total joint displacement is the primary contributor to LLRs, with perturbations at high velocity but brief duration not generating significant LLRa. In our experience, the execution of LLRa studies on perturbation durations that require stopping the limb within the [50 100] ms interval proved to be challenging, as in preliminary data we observed the occurrence of motion artifacts associated with the oscillations induced by the manipulator stopping. For this reason, we decided to focus on perturbations of longer duration (200 ms), which allowed to completely avoid those artifacts.

Results also revealed a significant increase in LLRa when a 200 mNm background torque was applied prior to the perturbations in comparison to the perturbations with no background torque. Pre-existing background muscle activation is thought to reflect an automatic adjustment mechanism, known as the automatic gain component of LLR (Bedingham and Tatton, 1984; Matthews, 1986; Miscio et al., 2001; Pruszynski et al., 2009).

Task instruction also significantly modulated the LLR in this study. The majority of previous studies examined the 'yield' or 'DNI' instruction with a 'resist' or 'compensate' instruction (Miscio et al., 2001; Lewis et al., 2006; Kurtzer et al., 2014). However, no prior study tested whether the 'yield' and 'DNI' task instruction differentially modulate the LLRa, with the exception of one study by Calancie and Bawa (1985) who recruited only two healthy individuals. Our findings showed that larger LLRs were evoked when participants attempt keep constant the muscles' activation state (i.e., DNI), compared to when they are asked to yield to the perturbations, which is justifiable in accordance to the evidence that the temporal overlap of two different responses including a task-dependent response and an automatic response results in the task-dependent change in LLR amplitude (Rothwell et al., 1980; Lewis et al., 2006; Pruszynski et al., 2011).

Also, in line with a few previous studies quantifying LLR from both stretched and shortened muscles (Miscio et al., 2001; Lewis et al., 2004), the above-mentioned modulations had more prominent effects on the LLRa evoked from the muscle stretched in response to the perturbations vs. the shortened muscle, however several significant effects of the behavioral factors were also measured in muscles undergoing shortening (see below for details).

With our full factorial design, we were able to observe more granular modulations of the LLR response induced by the four behavioral factors reported above. Specifically, significant results were observed for all the three-way interaction terms that can be computed without including the interaction between instruction and velocity, as detailed below.

Perturbation Direction, Task Instruction and Background Torque

As illustrated in **Figure 4**, perturbation direction did not affect the LLRa evoked from the perturbations with no background torque (i.e., the LLR measured during perturbations shortening the muscle were of similar amplitude as the one measured during perturbations stretching the muscle). This finding is in contrast with a previous study by Miscio et al. (2001), which demonstrated that there would be a lower LLRa evoked from the shortened muscle in comparison to the LLRa evoked from the stretched muscle even in absence of background muscle activity. In addition, task instruction did not modulate the LLRa evoked in absence of background torque. This result is expected and serves as a validation of the pursued experimental design, as in this case the behavior elicited in the Y and DNI conditions is expected to be identical.

Results from the perturbations with 200 mNm background torque showed a significant difference between LLRa evoked from stretched muscle in the Y and DNI task instructions. Larger LLRa was detected from perturbations when participants were instructed to maintain their level of activation (DNI) after the perturbation, compared to when they were instructed to yield to the displacement. In contrast, task instructions did not modulate the LLRa evoked from the shortened muscle neither in presence of a 200mNm background torque. Also, the LLRa for shortened muscle was significantly lower than the LLRa for stretched muscle in both instruction conditions. This interaction is also consistently reported also in the 1D analysis (**Figure 9**).

In agreement with this result, Miscio et al. (2001) also reported a smaller LLRa for shortened muscle in comparison to the stretched muscles when there was a 10% maximum voluntary contraction (MVC) background torque and subjects were instructed to not intervene to the perturbations. However, their task instructions did not include a 'yield' condition for comparison. The EMG activity recorded from the shortened muscle in the previous study was interpreted as a volume conducted response based on their direct nerve stimulation results. Besides, their regression analysis showed a positive correlation between the area of FCR stretch response and the low-level activity recorded from the shortened antagonist muscle (ECR) ($r^2 =$ 0.59). Instead, our data supports a differential modulation of the response for the stretched and shortened muscles between different levels of task instructions, suggesting that the source of the observations may not be due to cross-talk, but to true physiological decoupling of the muscle responses.

Perturbation Direction, Background Torque, Perturbation Velocity

Results of the 0D analysis (**Figure 5**) support a significant interaction between the effects of torque and velocity on the LLRa evoked from perturbations stretching the ECU muscle, but not from perturbations shortening the ECU muscle. In support of this observation, the 1D analysis (**Figure 10**) revealed a significant interaction between torque and velocity on the LLRa for ECU muscle only under stretching, but not under shortening. For

the FCR muscle, the interaction was significant in response to the both stretching and shortening perturbations, though the differential effects of background activity are smaller, and last for a smaller duration for this muscle (**Figures 11**, **12**). The smaller size and duration of the effects of torque and velocity, combined with the greater between-subject variability of FCR data might be a possible reason why the 0D analysis did not detect a significant effect of this interaction term for the FCR muscle.

Previous studies also demonstrated a significant effect of the interaction between perturbation torque and velocity on the LLRa evoked from the stretched muscle (Bedingham and Tatton, 1984). However, based on our literature review, no prior study evaluated this interaction for the muscle subject to a perturbation that shortened the muscle. Berardelli et al. (Berardelli and Hallett, 1984), reported that background torque and velocity would increase the amplitude of the EMG activity evoked from the shortened tibialis anterior muscle with a latency within 100–150 ms, but no interaction analysis was conducted in that study.

For both muscles, perturbation direction did not modulate the LLRa elicited by any velocity condition in absence of background torque. However, Miscio et al. (2001), observed lower LLRa for the shortened muscle compared with the stretched muscle which were perturbed with 500 deg/s velocity with no background torque. It might be possible that higher perturbation velocities are needed to differentiate the long latency stretch response of the agonist and antagonist muscles when there is no background activity. Moreover, to the best of our knowledge, our study is the first study comparing the effects of different perturbation velocities on the LLRa between the shortened and stretched upper limbs' muscles, and the first to observe an interaction between background torque and velocity in the LLRa of a muscle undergoing shortening, an effect that was visible for the FCR muscle.

Interaction Between Task Instruction and Velocity

No analysis has revealed any interaction between the task instruction and perturbation velocity. The majority of previous work studied the interaction between perturbation velocity with perturbation duration and amplitude (Lee and Tatton, 1982; Lewis et al., 2005, 2006; Schuurmans et al., 2009). Among them, Lewis et al. (Lewis et al., 2006), was the only study that examined the interaction between task instruction and perturbation velocity. In contrast to our results, they reported a significant interaction, which resulted in a greater facilitation in the LLRa evoked from the Biceps brachii muscle, for the 'Flex' instructed perturbations with a 90 degree/s velocity. In their 'Flex' instruction, subjects were instructed to flex their elbows as soon as possible in response to the perturbation, a condition which wasn't included in our experiment. Hence, it is possible that countering perturbations applied to the proximal upper limb joints (such as the elbow) would elicit a different modulation in the LLR from the one observed here for forearm muscles.

Similarity of the Effects Between FCR and ECU

Some of the interaction terms were only significant for ECU, and not for FCR. Specifically, no three-way interaction term was significant for the FCR muscle (as opposed to two terms significant for FCR), and two of the five two-way interactions significant for the ECU muscle were not significant for FCR. Overall, the mismatch of results between the two muscles is primarily due to larger variability of the measurements obtained for the FCR muscle compared to the ECU muscle, while all effects were generally in the same direction for both muscles. In many cases, in fact, the magnitude of measured modulations in LLRa (expressed in normalized units, so roughly comparable between muscles) was actually larger for the FCR muscle than for the ECU muscle. However, the standard error of the mean estimated by the mixed model was several times larger for the FCR muscle compared to the ECU muscle.

As an example, the term corresponding to the three-way interaction between direction, instruction, and torque was close to the conventional type-I error rate for the FCR muscle (p = 0.055). Further inspection of the parameter estimates corresponding to that interaction term shows that the mean difference in LLRa measured between Y and DNI conditions was slightly larger in the FCR muscle than it was for the ECU muscle under stretch (FCR LLRa – DNI: 6.05 ± 0.58 nu, Y: 3.95 ± 0.58 nu; ECU LLRa – DNI: 3.80 ± 0.17 nu, Y: 2.04 ± 0.17 nu), while smaller effects were measured in the shorten condition (FCR LLRa – DNI: 1.28 ± 0.58 nu, Y: 0.83 ± 0.58 nu; ECU LLRa – DNI: 0.78 ± 0.17 nu, Y: 0.73 ± 0.17 nu) for both muscles. Yet, the four-fold larger s.e.m. measured for the FCR prevented this effect from becoming significant.

0D vs. 1D Analysis

To the best of our knowledge, this study is the first to apply a mixed-model 1D analysis to the timeseries of EMG signals measured in response to velocity-controlled perturbations. 1D analyses are used to quantify if and when a timeseries is significantly modulated by an experimental factor, without a-priori hypotheses on the duration of this modulation, or on the time window where such a modulation is expected. Typically, reflex studies use 0D variables such as the average of the rectified signal in a pre-defined time window (Kurtzer et al., 2008), or the cumulative sum of the rectified EMG signal within a region of supra-threshold response (Brinkworth and Türker, 2003) – the latter definition allowing to explicitly account for a combined measure of amplitude and duration of a reflex response.

A shortcoming of using 0D datapoints generated from a 1D data set is the possibility for false positives. It has been indicated that the false positive rate of the 0D data is greater than the desired false positive rate of $\alpha = 0.05$ when using noisy outcome measures such as peak in an interval (Pataky et al., 2016), and that this may be the case also in presence of smoothing (Pataky et al., 2015, 2016). Less noisy outcome measures such as the mean EMG signal in a pre-defined time window are not likely to result in limited control of the false positive rate of inference

tests. However, the main advantage of using a 1D analysis for the study of stretch reflexes is the fact that the 1D analysis gives a more granular insight on the shape of the waveform (e.g., one peak, two peaks) which can be masked by the operation of averaging necessary for the creation of a 0D dataset. Moreover, the 1D analysis allows to test hypothesis on whether an effect is *only* present in a specific time-region, while controlling for the type-I error rate of inferential statements.

As an example, our 0D analysis showed that, in presence of background activation, there is an effect of task instruction on the LLRa measured from the ECU when stretched, but no effect measured when the muscle is shortened (**Figure 4**). However, a closer inspection on this modulation is provided by the *post hoc t*-tests presented in **Figure 9**. It is true that the difference between rectified EMG signal measured in the DNI and Y condition for the ECU under stretch is greater in the 200 mNm condition, reflecting a larger signal measured in the DNI condition (**Figure 9**, center). However, the same contrast plot extracted from the ECU during shortening perturbations highlights the presence of a biphasic response, where the DNI condition results in an early increase in EMG signal in the LLR time window, followed by a decrease in EMG signal. The average of the positive and negative changes is likely the reason why the same effect could not be captured using the 0D analysis.

Also, insight from a 1D analysis provides information about the *gradient in timing* resulting from different behavioral factors. Specifically, the effect of instruction is usually visible later than the one of velocity and torque, which have upcrossings in SLR and early LLR (**Figures 7**, **8**). Instruction has a narrow region of significant main effects in the late LLR period (70 to 73 ms for FCR stretch, 81 to 83 ms for ECU stretch), with significant upcrossings in the voluntary period. Velocity conditions are significant in the early to mid LLR period (FCR stretch ∼40 to 70 ms, ECU stretch ∼45 to 90 ms, FCR shorten ∼50 to 90 ms, ECU shorten ∼45 to 80 ms), all having significant peaks near 60 ms. The 1D analysis allowed us to deduct the presence of a 10 to 20 ms delay between the significant peaks due to instruction versus velocity. The time frame of these significant peaks are comparable with previous findings and the identification of two distinct peaks within the LLR period, named M2 and M3 in the literature. However, it is difficult to compare the exact timing in absolute terms since "latency" in the literature is often defined relative to the onset of EMG activity (Lee and Tatton, 1982; Calancie and Bawa, 1985; Miscio et al., 2001; Lewis et al., 2006; Kurtzer et al., 2014).

Yet, the results of the 0D and 1D analyses do not perfectly overlap. This is in part also due to limitations in the current version of the software used for the analysis. The spm1D MATLAB package allows up to three input conditions, as seen through its anova3rm function. To analyze the four conditions studied, two analyses per muscle were conducted when in the shortened and stretched conditions. As such, none of the three-way interactions that were significant in the 0D analysis could be studied in the same form using the 1D analysis. Another limitation of the 1D analysis is related to its limited statistical power. Because of the large number of datapoints included in the analysis, and the fact that the EMG signal is somewhat noisy and composed of multiple resolution elements in a time window of 200 ms following a perturbation, 1D analyses afford a reduced statistical power compared to a 0D analysis that only looks at the average within a pre-defined time window (Pataky et al., 2015).

Study Limitations

The sample size available for this study is in line with the one used in previous behavioral experiments with LLR of forearm muscles (Miscio et al., 2001; Pruszynski et al., 2009; Lewis et al., 2010) in terms of number of subjects recruited. The number of datapoints collected from each subject is also in line with most previous studies, with 240 datapoints per subject collected. However, given the need to estimate a larger number of model terms, a larger sample size would have allowed more precise estimation of all model effects and reduced the variance of the outcomes between the different muscles and the different statistical analysis techniques pursued.

The estimate of the effects of background torque is potentially confounded by the fact that we only applied perturbations in one direction, and the direction was predictable only in the 200 mNm condition. Specifically, in the 200 mNm condition, we applied perturbations that would stretch the agonist muscle, and as such the direction was predictable by the subject. Instead, in the 0 mNm condition, perturbations were applied in a random direction, not predictable by the subject. As such, the coefficients estimated for the two levels of the factor background torque might be different also simply because in the 200 mNm condition, subjects were able to predict perturbation direction, while in the rest condition, they were unable to do so. It is possible that prior knowledge of perturbation direction modulates the LLRa. As such, it is possible that our model estimated the compound effect of two distinct factors: a factor due to muscle pre-load, and another factor due to knowledge of the perturbation direction. This ambiguity could be addressed in future studies by applying perturbations that either stretch or shorten agonist muscles after pre-load.

CONCLUSION

In summary, this study has quantified the effect of four behavioral factors – background torque, task instruction, perturbation velocity and direction – on the long-latency response (LLR) amplitude evoked from the FCR and ECU muscles during ramp-and-hold perturbations applied to the wrist joint in the flexion and extension direction. Our analysis demonstrated that all of those factors modulate LLRa, and that their combination nonlinearly contribute to modulating the LLRa. Specifically, all the three-way interaction terms that can be computed without including the interaction between instruction and velocity significantly modulated the LLR. The interaction analysis suggested that higher background torque augmented the LLRa evoked from the stretched muscle when subjects are asked to maintain their muscle activation in response to the perturbations.

Besides, higher perturbation velocity increased the LLRa evoked from the stretched muscle in presence of a background torque. Also, our analysis identified significant modulations of LLRa also in muscles shortened by the perturbation, including an interaction between torque and velocity, and an effect of both torque and velocity. While a lot of the behavioral factors listed above nonlinearly contribute to modulating LLRa, we observed that the effects of task instruction and velocity do not combine more than linearly to modulate the LLRa.

DATA AVAILABILITY STATEMENT

The raw data supporting the conclusions of this article have been uploaded on a zenodo repository, https://zenodo.org/record/4641292#.YGEzVC2cZTZ.

ETHICS STATEMENT

The studies involving human participants were reviewed and approved by The University of Delaware Institutional Review Board, protocol no. 1097082-6. The patients/participants provided their written informed consent to participate in this study.

AUTHOR CONTRIBUTIONS

JW supported development of stimulus hardware and protocol, performed data collection and analysis, and contributed to manuscript writing. PA-F supported data analysis and manuscript writing. AZ developed stimulus hardware and protocol and supported data collection and analysis. RN supported manuscript writing. FS developed the study design, supervised data collection and analysis, manuscript writing. All authors reviewed and approved the manuscript in its current form.

FUNDING

Research reported in this publication was supported by the National Institute of Neurological Disorders and Stroke of the National Institutes of Health under award number R21NS111310. The content is solely the responsibility of the authors and does not necessarily represent the official views of the National Institutes of Health. Additional support was provided by the University of Delaware Research Foundation grant no. 16A01402, by ACCEL NIGMS IDeA grant no. U54-GM104941.

ACKNOWLEDGMENTS

We thank all our participants for their participation in this research.

SUPPLEMENTARY MATERIAL

The Supplementary Material for this article can be found online at: https://www.frontiersin.org/articles/10.3389/fnhum.2021.639773/full#supplementary-material

REFERENCES

Allum, J. H. J. (1975). Responses to load disturbances in human shoulder muscles: the hypothesis that one component is a pulse test information signal. *Exp. Brain Res.* 22, 307–326.

Banks, C. L., Little, V. L., Walker, E. R., and Patten, C. (2019). Lower extremity long-latency reflexes differentiate walking function after stroke. *Exp. Brain Res.* 237, 2595–2605. doi: 10.1007/s00221-019-05614-y

Bedingham, W., and Tatton, W. G. (1984). Dependence of EMG responses evoked by imposed wrist displacements on pre-existing activity in the stretched muscles. *Can. J. Neurol. Sci.* 11, 272–280. doi: 10.1017/s0317167100045534

Berardelli, A., and Hallett, M. (1984). Shortening reaction of human tibialis anterior. *Neurology* 34, 242–245. doi: 10.1212/wnl.34.2.242

Brinkworth, R. S. A., and Türker, K. S. (2003). A method for quantifying reflex responses from intra-muscular and surface electromyogram. *J. Neurosci. Methods* 122, 179–193. doi: 10.1016/S0165-0270(02)00321-7

Calancie, B., and Bawa, P. (1985). Firing patterns of human flexor carpi radialis motor units during the stretch reflex. *J. Neurophysiol.* 53, 1179–1193. doi: 10.1152/jn.1985.53.5.1179

Cody, F. W., and Plant, T. (1989). Electromyographic reflexes evoked in human wrist flexors by tendon extension and by displacement of the wrist joint. *J. Physiol.* 411, 379–392.

Colebatch, J. G., Gandevia, S. C., McCloskey, D. I., and Potter, E. K. (1979). Subject instruction and long latency reflex responses to muscle stretch. *J. Physiol.* 292, 527–534. doi: 10.1113/jphysiol.1979.sp012869

Crago, P. E., Houk, J. C., and Hasan, Z. (1976). Regulatory actions of human stretch reflex. *J. Neurophysiol.* 39, 925–935. doi: 10.1152/jn.1976.39.5.925

Deneri, E., Tilek, N., Çoban, A., and Tataroğlu, C. (2020). Long latency reflexes in patients with postural instability and ataxia. *Neurol. Sci. Neurophysiol.* 37, 164–169. doi: 10.4103/nsn.nsn_44_20

Evarts, E. V., and Granit, R. (1976). Relations of reflexes and intended movements. *Prog. Brain Res.* 44, 1–14. doi: 10.1016/s0079-6123(08)60719-0

Hammond, P. H. (1956). The influence of prior instruction to the subject on an apparently involuntary neuro-muscular response. *J. Physiol.* 132, 17–18.

Hayashi, R., Hashimoto, T., Tada, T., and Ikeda, S. (2001). Relation between changes in long-latency stretch reflexes and muscle stiffness in Parkinson's disease–comparison before and after unilateral pallidotomy. *Clin. Neurophysiol.* 112, 1814–1821.

Kurtzer, I., Crevecoeur, F., and Scott, S. H. (2014). Fast feedback control involves two independent processes utilizing knowledge of limb dynamics. *J. Neurophysiol.* 11568, 1631–1645. doi: 10.1152/jn.00514.2013

Kurtzer, I. L. (2015). Long-latency reflexes account for limb biomechanics through several supraspinal pathways. *Front. Integr. Neurosci.* 8:99. doi: 10.3389/fnint.2014.00099

Kurtzer, I. L., Pruszynski, J. A., and Scott, S. H. (2008). Long-latency reflexes of the human arm reflect an internal model of limb dynamics. *Curr. Biol.* 18, 449–453. doi: 10.1016/j.cub.2008.02.053

Lee, R., and Tatton, W. (1982). Long latency reflexes to imposed displacements of the human wrist: dependence on duration of movement. *Exp. Brain Res.* 45, 207–216.

Lee, R., and Tatton, W. G. (1975). Motor responses to sudden limb displacements in primates with specific CNS lesions and in human patients with motor system disorders. *Can. J. Neurol. Sci.* 2, 285–293. doi: 10.1017/s0317167100020382

Lewis, G. N., MacKinnon, C. D., and Perreault, E. J. (2006). The effect of task instruction on the excitability of spinal and supraspinal reflex pathways

projecting to the biceps muscle. *Exp. Brain Res.* 174, 413–425. doi: 10.1007/s00221-006-0475-x

Lewis, G. N., MacKinnon, C. D., Trumbower, R., and Perreault, E. J. (2010). Co-contraction modifies the stretch reflex elicited in muscles shortened by a joint perturbation. *Exp. Brain Res.* 207, 39–48. doi: 10.1007/s00221-010-2426-9

Lewis, G. N., Perreault, E. J., and MacKinnon, C. D. (2005). The influence of perturbation duration and velocity on the long-latency response to stretch in the biceps muscle. *Exp. Brain Res.* 163, 361–369. doi: 10.1007/s00221-004-2182-9

Lewis, G. N., Polych, M. A., and Byblow, W. D. (2004). Proposed cortical and sub-cortical contributions to the long-latency stretch reflex in the forearm. *Exp. Brain Res.* 156, 72–79. doi: 10.1007/s00221-003-1767-z

Matthews, P. B. (1986). Obseravtions on the automatic compensation of reflex gain on varying the pre-existing level of motor discharge in man. *J. Physiol.* 374, 73–90. doi: 10.1113/jphysiol.1986.sp016066

Matthews, P. B. (1989). Long-latency stretch reflexes of two intrinsic muscles of the human hand analysed by cooling the arm. *J. Physiol.* 419, 519–538. doi: 10.1113/jphysiol.1989.sp017884

Matthews, P. B. (1993). Interaction between short-and long-latency components of the human stretch reflex during sinusoidal stretching. *J. Physiol.* 462, 503–527. doi: 10.1113/jphysiol.1993.sp019566

Mirbagheri, M. M., Kindig, M. W., and Niu, X. (2015). Effects of robotic-locomotor training on stretch reflex function and muscular properties in individuals with spinal cord injury. *Clin. Neurophysiol.* 126, 997–1006. doi: 10.1016/j.clinph.2014.09.010

Miscio, G., Pisano, F., Del Conte, C., Pianca, D., Colombo, R., and Schieppati, M. (2001). The shortening reaction of forearm muscles: the influence of central set. *Clin. Neurophysiol.* 112, 884–894. doi: 10.1016/S1388-2457(01)00468-0

Noth, J., Schwarz, M., Podoll, K., and Motamedi, F. (1991). Evidence that low-threshold muscle afferents evoke long-latency stretch reflexes in human hand muscles. *J. Neurophysiol.* 65, 1089–1097. doi: 10.1152/jn.1991.65.5.1089

Pataky, T. C., Vanrenterghem, J., and Robinson, M. A. (2015). Zero- vs. one-dimensional, parametric vs. non-parametric, and confidence interval vs. hypothesis testing procedures in one-dimensional biomechanical trajectory analysis. *J. Biomech.* 48, 1277–1285. doi: 10.1016/j.jbiomech.2015.02.051

Pataky, T. C., Vanrenterghem, J., and Robinson, M. A. (2016). The probability of false positives in zero-dimensional analyses of one-dimensional kinematic, force and EMG trajectories. *J. Biomech.* 49, 1468–1476. doi: 10.1016/j.jbiomech.2016.03.032

Pruszynski, J. A., Kurtzer, I., Lillicrap, T. P., and Scott, S. H. (2009). Temporal evolution of "automatic gain-scaling." *J. Neurophysiol.* 102, 992–1003. doi: 10.1152/jn.00085.2009

Pruszynski, J. A., Kurtzer, I., and Scott, S. H. (2011). The long-latency reflex is composed of at least two functionally independent processes. *J. Neurophysiol.* 106, 449–459. doi: 10.1152/jn.01052.2010

Rothwell, J. C., Traub, M. M., and Marsden, C. D. (1980). Influence of voluntary intent on the human long-latency stretch reflex. *Nature* 286, 496–498. doi: 10.1038/286496a0

Schuurmans, J., De Vlugt, E., Schouten, A. C., Meskers, C. G. M., De Groot, J. H., and Van Der Helm, F. C. T. (2009). The monosynaptic Ia afferent pathway can largely explain the stretch duration effect of the long latency M2 response. *Exp. Brain Res.* 193, 491–500. doi: 10.1007/s00221-008-1647-7

Sinkjær, T., and Hayashi, R. (1989). Regulation of wrist stiffness by the stretch reflex. *J. Biomech.* 22, 1133–1140. doi: 10.1016/0021-9290(89)90215-7

Tarkka, I. M., and Larsen, T. A. (1987). Changes of electrically elicited reflexes in hand and forearm muscles in man. *Am. J. Phys. Med.* 66, 308–314. doi: 10.1097/00002060-198710000-00010

Tatton, W. G., and Bawa, P. (1979). Input-output properties of motor unit responses in muscles stretched by imposed displacements of the monkey wrist. *Exp. Brain Res.* 37, 439–457.

Thomas, J. S., Brown, J., and Lucier, G. E. (1977). Influence of task set on muscular responses to arm perturbations in normal subjects and Parkinson pateints. *Exp. Neurol.* 55, 618–628. doi: 10.1016/0014-4886(77)90288-6

Trumbower, R. D., Finley, J. M., Shemmell, J. B., Honeycutt, C. F., and Perreault, E. J. (2013). Bilateral impairments in task-dependent modulation of the long-latency stretch reflex following stroke. *Clin. Neurophysiol.* 124, 1373–1380. doi: 10.1016/j.clinph.2013.01.013

Zonnino, A., Farrens, A. J., Ress, D., and Sergi, F. (2019). "StretchfMRI: a novel technique to quantify the contribution of the reticular formation to long-latency responses via fMRI," in *IEEE 16th International Conference on Rehabilitation Robotics (ICORR), Toronto, ON*, (Piscataway, NJ: IEEE), 1247–1253. doi: 10.1109/ICORR.2019.8779451

Conflict of Interest: The authors declare that the research was conducted in the absence of any commercial or financial relationships that could be construed as a potential conflict of interest.

frontiers in Physiology

REVIEW
published: 28 April 2021
doi: 10.3389/fphys.2021.623893

Bone-to-Brain: A Round Trip in the Adaptation to Mechanical Stimuli

Laura Gerosa[1]* *and Giovanni Lombardi*[2,3]

[1] Gruppo San Donato Foundation, Milano, Italy, [2] Laboratory of Experimental Biochemistry & Molecular Biology, IRCCS Istituto Ortopedico Galeazzi, Milano, Italy, [3] Department of Athletics, Strength and Conditioning, Poznań University of Physical Education, Poznań, Poland

Besides the classical ones (support/protection, hematopoiesis, storage for calcium, and phosphate) multiple roles emerged for bone tissue, definitively making it an organ. Particularly, the endocrine function, and in more general terms, the capability to sense and integrate different stimuli and to send signals to other tissues, has highlighted the importance of bone in homeostasis. Bone is highly innervated and hosts all nervous system branches; bone cells are sensitive to most of neurotransmitters, neuropeptides, and neurohormones that directly affect their metabolic activity and sensitivity to mechanical stimuli. Indeed, bone is the principal mechanosensitive organ. Thanks to the mechanosensing resident cells, and particularly osteocytes, mechanical stimulation induces metabolic responses in bone forming (osteoblasts) and bone resorbing (osteoclasts) cells that allow the adaptation of the affected bony segment to the changing environment. Once stimulated, bone cells express and secrete, or liberate from the entrapping matrix, several mediators (osteokines) that induce responses on distant targets. Brain is a target of some of these mediator [e.g., osteocalcin, lipocalin2, sclerostin, Dickkopf-related protein 1 (Dkk1), and fibroblast growth factor 23], as most of them can cross the blood-brain barrier. For others, a role in brain has been hypothesized, but not yet demonstrated. As exercise effectively modifies the release and the circulating levels of these osteokines, it has been hypothesized that some of the beneficial effects of exercise on brain functions may be associated to such a bone-to-brain communication. This hypothesis hides an interesting clinical clue: may well-addressed physical activities support the treatment of neurodegenerative diseases, such as Alzheimer's and Parkinson's diseases?

Keywords: osteokines, exercise, biomechanical stimulation, mechanosensing, blood-brain barrier, neurodegenerative diseases

OPEN ACCESS

Edited by:
Taiar Redha, Université de Reims Champagne-Ardenne, France

Reviewed by:
Alvaro Reischak-Oliveira, Federal University of Rio Grande do Sul, Brazil
Nathalie Bravenboer, VU University Medical Center, Netherlands

***Correspondence:**
Laura Gerosa
laura.gerosa@grupposandonato.it

Specialty section:
This article was submitted to Integrative Physiology, a section of the journal Frontiers in Physiology

Received: *30 October 2020*
Accepted: *06 April 2021*
Published: *28 April 2021*

Citation:
Gerosa L and Lombardi G (2021) Bone-to-Brain: A Round Trip in the Adaptation to Mechanical Stimuli. Front. Physiol. 12:623893. doi: 10.3389/fphys.2021.623893

INTRODUCTION

In the last few years, a role for bone tissue in homeostasis has emerged as it solves fundamental functions in the body. Indeed, beyond providing mechanical support and protection to the body and solving important roles in hematopoiesis, calcium storage, ion homeostasis, and phosphate metabolism, additional functions have been described (Calvi et al., 2003; Bergwitz and Juppner, 2010). As a mechanosensitive organ, bone is a dynamic player in biomechanics

and body-environment relation and nervous system communication for establishing functional sensing and motor behavior. Indeed, bone and nervous system communicate with each other through a bidirectional connection. Thus, bone emerges as a complex peripheral element able to communicate not only with peripheral organs but also with brain both indirectly, through the peripheral nervous system (PNS), and directly, by releasing molecules able to cross the blood brain barrier (BBB) and to act at the brain level. Noteworthy, recent findings demonstrate that bone acts also as an endocrine tissue, dynamically responsive to internal and external stimuli (Cappariello et al., 2016). It actively communicates with other organs, thus becoming a fundamental key player in the circuit, whose goal is to adapt the body to specific environment. Further, bone, through its endocrine function, regulates whole body homeostasis, energy metabolism, fertility, at least in males, and, as recently established, cognitive functions (Takeda et al., 2002; Yadav et al., 2009; Oury et al., 2011, 2013).

With this review, we want to highlight the importance of the communication between bone and the nervous system, with particular emphasis on the contribution of this relation during mechanical stimulation. In the first part, we will describe the bony elements that act as mechanosensors and the way they respond to stimuli. We than describe how nervous system and bone are connected and communicate with each other to regulate bone homeostasis and bone remodeling depending on biomechanical stimulation it receives. We will first describe how the brain communicate with bone. Finally, although the current little knowledge, we will focus on the bone-to-brain communication based on the new findings on the bone-derived molecules potentially involved in this axis.

A deepen knowledge of the bidirectional communication system between bone and brain is of fundamental interest to address the investigation on the mechanisms underlying bone response and adaption to biomechanical stimuli. It would also help in the search for new targets of proper therapeutic interventions aimed at restoring or ameliorating the adaptive response, especially for those pathologies (e.g., osteoporosis, bone fragility, etc.) that impairs this circuit, but it may also help at improving conditions affecting the nervous system. Thus, our final goal is to bring out the bone and the molecules that it releases as putative therapeutic targets for neurological pathologies that may be also characterized by bone defects, as osteoporosis, bone fragility and increased fracture risk.

BIOMECHANICAL STIMULATION AND MECHANOSENSING IN BONE

Biomechanical stimulation of bone is fundamental to regulate bone homeostasis, guiding resident cells to adaptation, maintenance, and repair, but also to adapt the entire body to the changing environment.

It is well known that bone is not a static element, but it is able to remodel its cellular components and its entire structure according to the different stimulation it receives, from static or simple movements to the physical activity-generated multidirectional stresses (Duncan and Turner, 1995). There is a finely regulated process that maintain an equilibrium between bone resorption and bone formation that is fundamental for bone homeostasis that is regarded as bone remodeling. This process is mediated by osteoclasts and osteoblasts, which are responsible for bone resorption and for extracellular matrix (ECM) deposition and bone formation, respectively (Parfitt, 2000; Florencio-Silva et al., 2015; Owen and Reilly, 2018). Noteworthy, osteoclasts derive from precursor cells of the monocyte lineage and their differentiation process is mainly stimulated by the activation of receptor activator of nuclear factor κB (RANK) by the RANK ligand (RANKL) expressed and released by stromal cells and osteoblasts, other than immune cells (Suda et al., 1999). On the contrary, osteoprotegerin (OPG), a decoy receptor for RANKL, that is expressed by osteoblasts and osteocytes, interferes with RANKL–RANK binding, thereby inhibiting osteoclasts differentiation and, consequently, bone resorption (Simonet et al., 1997).

The activity of osteoclasts and osteoblasts and, hence, the overall bone remodeling, are regulated by mechanical stimuli (loading and exercises), but also by endocrine and paracrine signals (David et al., 2007; Sen et al., 2011). In this context, external stimuli corresponding to body stationary or moving in the space, converge in the biomechanical stimulation of those bony elements called mechanosensors. These mechanosensors are, for definition, able to sense and respond to biophysical factors in the environment. Indeed, the skeleton must remodel itself to accommodate functional demands (e.g., change in loading intensity and/or direction) (Thompson et al., 2012). In case of chronic intense physical activity (i.e., loading), bones become larger and stronger; on the contrary, a reduction in loading intensity (i.e., bed rest, immobilization) corresponds to enhanced bone resorption that hesitates in reduced bone strength and mass and increased fracture risk.

Bone is a mechanosensitive organ in which at least four elements are considered the mechanosensory elements that collaborate with each other to regulate bone modeling and remodeling. These elements correspond to the main cell types resident into the bone tissue: i.e., osteocytes, osteoblasts, osteoclasts, and osteoprogenitor cells (mesenchymal stem cell, MSC). An important consequence of mechanical stimulation is an indirect regulation of osteoclasts function and of their recruitment through the expression of RANKL by osteoprogenitor cells (Yasuda et al., 1998). Osteoprogenitor cells and pre-osteoblastic cells, located within the bone marrow and in the periosteum, which are mechanically active environment, respond to mechanical stimuli through the regulation of their proliferation, differentiation, and commitment, and, thus, modulating osteoblastogenesis (David et al., 2007; Sen et al., 2011). Further, even if osteocytes are considered the main principal mechanoresponsive elements in bone, it has been demonstrated that also osteoblasts are able to respond to mechanical stimuli (Xiao and Quarles, 2015). Thus, mechanostimuli regulate directly and indirectly all these cells since each of them could respond to mechanical stimulation by modulating pathways that bring to the co-regulation of the other actors.

Osteocytes as the Main Bone Mechanosensory Elements

Osteocytes are the most abundant cells present in the bone tissue and are considered the main cell types that respond to mechanical stimulation, regulating mechanosensing, and mechanotransduction (Thompson et al., 2012). Further, osteocytes solve two other important roles: they regulate bone homeostasis throughout the regulation of osteoclast and osteoblast activity, and they act as endocrine elements by secreting hormone-like mediators that affect the functioning of cells in bone as well as in other tissues and organs (Chen et al., 2015; Robling and Bonewald, 2020).

These functions are facilitated by their peculiar morphology that allows a direct contacting with other bone cells as well as a direct connection with the interstitial fluid and, hence, with blood. Indeed, these cells are star-shaped cells embedded into the mineralized ECM of bone with prolongations developed within a lacuno-canalicular system (LCS) that put in communication each osteocyte with several other osteocytes and osteoblasts and osteoclasts and also with complex structures such as bone marrow and blood vessels. Further, LCS is filled by an interstitial fluid, that surrounds osteocytes' body and prolongations that is in equilibrium with the plasma and exposes osteocytes to blood-brought factors derived from distal organs. Thanks to the dynamics governing the fluid movement within the LCS, osteocytes are principally stimulated by shear stress and sense different concentrations of the soluble mediators transported by the fluid (Bonewald, 2017). Osteocytes integrate these inputs and generate chemical signals that coordinate the proper response of the other bone cells. The perception of mechanical stimuli results in the regulation of osteoblast and osteoclast functions thereby influencing bone formation and resorption. Osteocytes may sense mechanical stimuli thanks to multiple mechanosensitive structures, such as cytoskeleton, dendritic processes, integrin-based focal adhesions, connexin-based intercellular junctions, primary cilium, ion channels, and ECM (Dallas et al., 2013; Qin et al., 2020; Robling and Bonewald, 2020).

During mechanotransduction, in osteocytes, the first event that occurs is the increase in intracellular calcium, that derives not only from the external compartment, but also from internal stores, such as those in endoplasmic reticulum (ER) (Lewis et al., 2017). After this first event, several pathways are activated and intervene into the regulation of bone homeostasis.

Wnt/β-Catenin

Mechanical stimulation activates the canonical Wnt pathway and influences osteocytes regulation of bone formation during load (Galli et al., 2012; Holguin et al., 2016). Typically, in unloaded state osteocytes secretes inhibitors of the Wnt pathway, namely sclerostin and Dickkopf-related protein 1 (Dkk1), thus favoring osteoclastogenesis. Under loading, instead, the osteocytic expression of sclerostin and Dkk1 is inhibited and, consequently, the Wnt ligands are able to activate this pathway, which, in mature osteoblasts, leads to a direct stimulation of osteoblastogenesis and osteoblast migration, as marked by the expression of the tardive differentiation marker osteopontin (OPN), and inhibition of osteoclastogenesis throughout the release of OPG (Galea et al., 2017). On one hand, the Wnt-induced OPG blocks the RANKL-RANK interaction and inhibits the differentiation of osteoclasts while, on the other hand, OPN prevents bone resorption since it is an activator of osteoblastogenesis with positive role for bone formation in a mechanically stimulated environment (Morinobu et al., 2003).

Focal Adhesions

Focal adhesions (FAs) are networks of proteins that dynamically connect the ECM to the intracellular actin cytoskeleton. Thus, extracellular fluid movements are transmitted inside the cells through these membrane proteins anchored to ECM (Chen et al., 2003). Integrins and adhesome proteins are the principal elements that cooperate in focal adhesions leading, in osteocytes, to a mechanosensory response. These protein complexes represent important mechanosensors in osteocytes and regulate skeletal development but also bone mechanobiology (Salter et al., 2001).

Apoptosis and Senescence

Appropriate mechanical stimulation prevents osteocytes apoptosis. Mechanical stimulation, indeed, promotes Erk activation supporting osteocytes survival, but, if the loading is too high, it induces damages and, in turn, promotes osteocytes apoptosis (Plotkin et al., 2005; Cardoso et al., 2009). Thus, only an appropriate loading (in terms of intensity and duration) prevents osteocytes senescence and improves their viability.

Sclerostin

As reported above, this is an antagonist of Wnt-β catenin signaling that stimulates bone resorption and inhibits bone formation (Li et al., 2005). It has been found high in circulation of subjects during prolonged bed rest and immobilization (Spatz et al., 2015). Thus, a proper mechanostimulation, consequently, to correct exercising, could downregulate the circulating levels of sclerostin, thereby inhibiting bone resorption process.

YAP/TAZ

These proteins are two proto-oncogenes that act as mechanosensors and mechanotransducers in different cell types (Dupont et al., 2011). In osteocytes these proteins translocate into the nucleus following mechanical stimulation transduced by both FAs linked with F-actin and by piezo ion channel activated after mechanical stimulation of membrane (Li et al., 2019). This translocation activates several pathways that stimulate bone formation and maintenance of bone mechanical properties, even if the precise mechanism that determines the nuclear translocation of YAP/TAZ is not well defined (Kegelman et al., 2018, 2020).

A schematic representation of the mechanosensing and mechanosensory pathways in osteocyte are represented in **Figure 1**.

Bidirectional Connections Between Brain and Bone

In the first part of this review, we have briefly illustrated the complex mechanosensing strategies occurring in bone

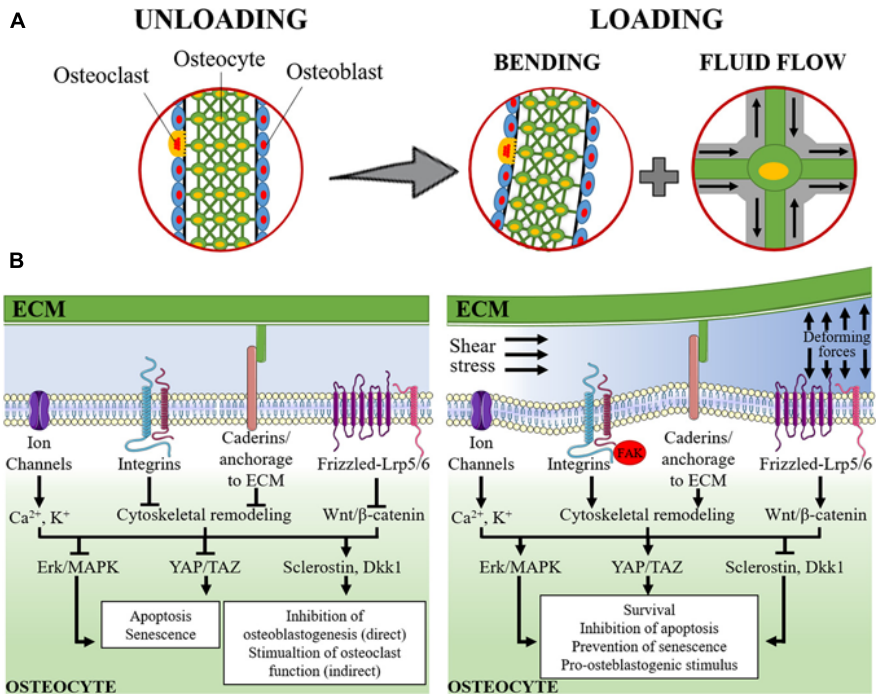

FIGURE 1 | Schematic representation of mechanosensing in osteocytes. **(A)** The lacuno-canalicular system is schematically modeled with osteocytes (green cells) that take contact with adjacent osteocytes, within the bone matrix, and with osteoblasts (light blue cells) and osteoclasts (yellow cells) on the surface of the bone segment. On the left, it is represented the rest status (unloading). On the right it is represented the loading condition: the applied forces cause the bending of the bony segment while, within the lacuno-canalicular system, the interstitial fluid is redistributed and its flow submits osteocytes to shear stress and change in extracellular pressure. **(B)** The signaling pathways activated under unloading (left) and loading (right) conditions are schematically represented. During unloading, pro-apoptotic and pro-senescence pathways are activated (consequently to the inhibition of Erk/MAPK and YAP/TAZ) together with the induction of sclerostin and Dickkopf-related protein 1 (Dkk1). These latter mediators are released into the intercellular fluid and reach osteoblasts and pre-osteoblasts where they exert their anti-osteoblastogenic effects, thereby, indirectly favoring the osteoclast function. During loading, the applied forces and the intra-canalicular fluid shear stress cause the deformation of the osteocyte plasma membrane and of the extracellular matrix (ECM). This results in: (i) perturbation of the electrolyte homeostasis (Ca^{2+} and K^{+}); (ii) activation of cadherin and integrin-mediated signaling and the associated focal adhesion kinase (FAK) pathway that result into the remodeling of the cytoskeleton; and (iii) activation of the Wnt/β-catenin signaling. The downstream signaling determines the activation of Erk/MAPK and YAP/TAZ that, together with the inhibition of the expression of sclerostin and Dkk1, result into the stimulation of osteocyte survival, inhibition of apoptosis and prevention of senescence and, in turn, a support to osteoblastogenesis and osteoblast function.

and how much dynamic is this organ in order to actively respond to biomechanical stimuli and, consequently, to allow the body to adapt to the changing environment. Further, we will go deeper into the complexity of bone mechanosensing, highlighting the existing relationship with the nervous system. Indeed, besides the direct regulation of bone metabolism, homeostasis and remodeling that occur at the bone cell level, depending on the received mechanical stimuli received from bone fluid movements, skeletal muscle traction and ground/impact reactions, another important mechanism controlling bone response and metabolism involves the nervous system.

Bone can be regulated both directly by PNS and indirectly by central nervous system (CNS). However, it has recently emerged a strong two-way interaction between bone and brain, that could be defined as bone-brain axis: not only brain regulates bone (efferent pathway), but also bone can communicate to the brain (afferent pathway) through the release of molecules, i.e., osteokines, that can act in the brain and, indeed, have been found in brain (Brazill et al., 2019; Millar et al., 2019).

In addition to the soluble mediators, other routes of inter-organ cross-talk exist. An intriguing, and increasingly studied, path is represented by the extracellular vesicles (EVs) and their cargo. EVs are cell-derived membrane vesicles, differing in size, biogenesis and membrane protein profile [i.e., exosomes, microvesicles (MVs), apoptotic bodies]. Exosomes and MVs are involved in paracrine and endocrine intercellular communication. They are actively released from the source cell and selectively loaded with specific components sorted from the cytosol, to reach a target cell in which the vesicle content elicits a biological response. EVs mediate the direct transfer of the contained information into the target cell and the EV-mediated information transfer is implicated in several diseases (Faraldi et al., 2020). There are evidence about an EV-mediated crosstalk between brain and bone, although this field still needs to be fully depicted.

We will firstly describe how nervous system can communicate with bone, mechanisms whose functioning are well known, to then move to the more innovative bone-to-brain view that, however, still needs deeper investigations.

BRAIN-TO-BONE COMMUNICATION

Direct Regulation of Bone by the Peripheral Nervous System: Bone Innervation

The autonomous nervous system is known to regulate the peripheral functions prompt to maintain body homeostasis and to initiate the adaptive response to various stress, including the biomechanical stimulation. It acts through two antagonistic system: the parasympathetic nervous system, which favors the "rest and digest" response; and the sympathetic nervous system, that is responsible for the "fight or flight" response.

Noteworthy, the parasympathetic nervous system acts through the release of acetylcholine (ACh), a neurotransmitter that activates both muscarinic and nicotinic cholinergic receptors, while sympathetic nerves release norepinephrine (NE), a neurotransmitter that acts via α- and β- adrenergic receptors (α-AR and β-AR) expressed by pre-synaptic and post-synaptic terminals, respectively.

During the last years, the development of new techniques led to the demonstration that bone is a highly innervated organ from both sympathetic and sensory neurons, thus showing that bone is physically related to the PNS (Mach et al., 2002). Interestingly, histological analyses showed high densities of nerves, belonging to the autonomous branch, in areas of high osteogenic activity. Further, immunocytochemistry experiments have successfully demonstrated the presence of receptors for neural peptides on bone cells (Elefteriou, 2005). Finally, the importance of the brain-bone connection has been further supported by the identification of neural tracts between femoral bone marrow and the CNS using retrograde trans-synaptic signaling (Denes et al., 2005).

Parasympathetic Innervation of Bone

Nicotinic acetylcholine receptor (nAChR) subunits are expressed by osteoclasts and differentiating and mature osteoblasts (Mandl et al., 2016). Further, transcript of muscarinic AChR type M1, M2, and M4 have been found in immature and differentiated osteoblasts (Sato et al., 2010). Transcripts of both AChR types have been detected in murine osteocyte-like MLO-Y4 and their levels are modulated by ACh, but the precise pathways activated by ACh in these cells are still unknown (Ma et al., 2014). Besides AChRs, osteoblasts express the machinery to synthesize ACh, but the functional role of this presence remains unknown (En-Nosse et al., 2009). The expression of both nicotinic and muscarinic ACh receptors on osteoblasts, osteocytes, and osteoclasts suggests that these cells are directly regulated by the parasympathetic nervous system. It has been observed both *in vitro* and *in vivo* experiments that activation of nAChR inhibits RANKL-dependent osteoclastogenesis, even if more experiments are needed to better elucidate the specific role on bone homeostasis of the different subunits of nAChRs since some results are contradictory (Mandl et al., 2016). Further, it has been observed that agonists of nAChR increase osteoclasts apoptosis and restrain bone resorption (Bajayo et al., 2012). All these evidences suggest that parasympathetic nervous system inhibits bone resorption and, thus, promotes bone formation (**Table 1**).

Sympathetic Innervation of Bone

Sympathetic action on bone remodeling could be hypothesized after the observation of very low levels of mRNA of α-ARs in osteoblasts and osteoclasts and higher levels of β-ARs. Consequently, β-ARs may be the main AR to mediate the action of sympathetic nerves in bone (Khosla et al., 2018). Further, β-ARs have been also found in osteocyte-like MLO-Y4 cells (Yao et al., 2017). Osteoblasts and osteoclasts express the β-2AR, but the biological relevance of the action of these receptors on osteoclasts is still not known. What is known is that the stimulation of β-2AR leads to increased osteoclasts formation, impairs osteoblasts functions and, consequently, increases bone loss. The inhibition of these receptors, on the contrary, leads to enhanced bone formation (Elefteriou, 2008). Moreover, stimulation of β-ARs in osteocyte-like MLO-Y4 cells affects osteoclastogenesis by increasing the RANKL-to-OPG ratio (Yao et al., 2017; Liang et al., 2018).

In summary, the regulation of bone remodeling by the autonomous nervous system results in the promotion of bone formation by the parasympathetic system and, conversely, in favoring bone resorption by sympathetic nervous system (**Table 1**).

Sensory Innervation of Bone

Besides the parasympathetic and sympathetic activities in bone, it has been shown that sensory nerves are important for bone

TABLE 1 | Peripheral nervous system to bone communication.

Nervous system branch	Neurotransmitter	Receptor	Target cell	Main action
Parasympathetic	ACh	nAChR	Osteoblast	Inhibition of
		mAChR	Osteoclast	bone resorption
Sympathetic	NE	αAR	Osteoblast	Promotion of
		βAR	Osteoclast	bone resorption
Sensory	CgRP	CgRPR	Osteoblast	Promotion of bone formation
	SP	SPR	Osteoclast	
	Sem3A	Nrp1, Plxna1, 2, 3		

Ach, acetylcholine; nAChR, nicotinic acetylcholine receptor; mAChR, muscarinic acetylcholine receptor; NE, norepinephrine; αAR, alpha adrenergic receptor; βAR, beta adrenergic receptor; CgRP, calcitonin gene-related peptide; SP, substance P; Sem3A, semaphorin 3A; CgRPR, calcitonin gene-related peptide receptor; SPR, substance P receptor; Nrp1, sema3A receptor; Plxnal1, 2, 3, sema3A co-receptors.

formation and solve fundamental roles in their response to mechanical loading. The sensory innervation represents the third arm of the autonomous system involved in the regulation of bone remodeling. The existence of such innervation in bone has been demonstrated through the detection of sensory fibers in bone and also of calcitonin gene-related peptide (CGRP) and substance P (SP), which are neuropeptide released by sensory fibers and acting as neurotransmitters (Mach et al., 2002). The receptors for these neuropeptides have also been detected in osteoblasts and osteoclasts (Kodama et al., 2017). Low amounts of NK1-R, a SP receptor, have been detected in osteocytes, however, the specific function in these cells is still unknown (Goto et al., 1998). CGRP and SP stimulate proliferation and activity of osteoblasts, thus influencing bone formation. Specifically, CGRP stimulates bone formation induced by mechanical loading (Ma et al., 2013; Sample et al., 2014). A role for the sensory nervous system in bone remodeling, as promoter for bone formation, has been demonstrated, too, through denervation studies and investigation on the bidirectional communication between sensory neurons and osteoblasts in co-culture systems (Ding et al., 2010; Kodama et al., 2017). In particular, co-culture experiments lead to the observation that sensory neurons release glutamate and SP that act on osteoblasts, while osteoblasts release ATP that acts on sensory neurons (Kodama et al., 2017).

Other important neuropeptides, known to regulate bone homeostasis, are semaphorins. Particularly, sema3A, released by sensory fibers, plays a role in the regulation of bone remodeling, by promoting bone mass gain and dendritic osteocyte elongation, by acting on Nrp1 receptor and Plxna1, 2, 3 co-receptors. Indeed, it has been shown that mice knockout for sema3A experienced a decrease in bone mass and, consequently, to a reduction in bone formation (Fukuda et al., 2013; Niimura et al., 2016) (**Table 1**). Further, sema3A deficiency in osteocytes leads to severe osteopenia, in aged mice, since it promotes osteocyte survival (Hayashi et al., 2019).

Indirect Regulation of Bone by Central Nervous System: Neuroendocrine Signaling

To date, it is known that bone metabolism and remodeling are regulated not only by the PNS but also by CNS through the action of several molecules as neurohormones, neuropeptides and neurotransmitters.

Neurohormones That Regulate Bone Metabolism

The principal mechanism of regulation of the peripheral functions by the CNS is mediated through the release of neurohormones by the hypothalamus that stimulate hormone release from the pituitary gland. Osteoblasts and osteoclasts, but not osteocytes, express different receptors for these hormones and it has been demonstrated that some of these regulate skeletal integrity favoring either bone resorption or bone formation (**Table 2**).

Both the follicle-stimulating hormone (FSH) and the thyroid-stimulating hormone (TSH) regulate directly bone remodeling. *In vitro* and *in vivo* experiments showed that FSH stimulates formation and function of osteoclasts, promoting bone resorption, by acting through a FSH receptor expressed on the plasma membrane of osteoclasts and their precursors (Sun et al., 2006; Robinson et al., 2010). On the contrary, TSH sustains bone integrity by stimulating osteoblasts functioning and inhibiting osteoclasts activity by acting directly through the TSH receptors expressed by these cells (Abe et al., 2003; Baliram et al., 2013). On one hand, TSH limits bone loss by decreasing osteoclastogenesis and, on the other hand, it restores bone mass by promoting osteoblastogenesis. Further, TSH can suppress osteoblasts differentiation. These pleiotropic actions define TSH as a single and independent molecule that regulate bone remodeling acting on both bone formation and bone resorption (Abe et al., 2003; Sampath et al., 2007; Baliram et al., 2011).

The expression of prolactin receptors has been detected in osteoblasts, but not in osteoclasts, and it has been demonstrated that prolactin contributes to the regulation of bone homeostasis by inhibiting osteoblastic proliferation and bone mineralization (Seriwatanachai et al., 2008, 2009). The indirect prolactin-dependent promotion of bone resorption may be responsible for the mobilization of calcium from bone to be used for milk secretion during lactation.

Adrenocorticotrophic hormone (ACTH) binds to melanocortin receptor family 2 (MC2R) that is expressed by osteoblastic cells and its expression is high at sites of active bone deposition, thus suggesting a role in the promotion of bone formation through the stimulation of osteoblasts proliferation (Zhong et al., 2005; Tourkova et al., 2017).

The growth hormone (GH) stimulates bone gain both indirectly, by stimulating insulin-like growth factors (IGFs) that regulates skeletal development, and directly, by acting on bone cells (DiGirolamo et al., 2007; Dobie et al., 2014).

TABLE 2 | Brain to bone communication: neurohormones.

Neurohormone	Target cell in bone	Main action
FSH	Osteoclast	Stimulation of osteoclastogenesis and osteoclast function
	Osteoclast precursors	
TSH	Osteoblast	Independent regulation of bone formation and bone resorption
	Osteoclast	
Prolactin	Osteoblast	Inhibition of osteoblast proliferation and bone mineralization
ACTH	Osteoblast	Promotion of osteoblast proliferation
GH	Osteoblast	Promotion of bone formation
AVP/ADH	Osteoblast	Inhibition of osteoblastogenesis
	Osteoclast	Stimulation of osteoclastogenesis
OT	Osteoblast	Stimulation of osteoblastogenesis
	Osteoclast	Inhibition of osteoclast activity
Melatonin	Osteoblast	Promotion of osteoblasts differentiation
	Osteoclast	Promotion of osteogenesis

FSH, follicle-stimulating hormone; TSH, thyroid-stimulating hormone; ACTH, adrenocorticotropic hormone; GH, growth hormone; AVP/ADH, arginine-vasopressin/antidiuretic hormone; OT, oxytocin.

TABLE 3 | Brain to bone communication: neuropeptides.

Neuropeptide	Target cell in bone	Main action
NPY	Osteoblast (Y1 receptor)	Inhibition of osteoblasts function (Y1)
	Hypothalamus (Y2 receptor)	Anti-osteogenic effects (Y2)
AgRP	Osteoblast and osteoclast (throughout the sympathetic nervous system)	Stimulation of osteoblasts activity
CART	No evidences for direct role on bone cells	Stimulation of bone mass gain
Melanocortin	Hypothalamus (MC4R)	Stimulation bone formation
	Osteoblast (MC4R)	
	Osteoblast and osteoclast (MCRs)	
Neuromedin U	Central action–mediated by leptin	Inhibition of bone mass gain
VIP	Osteoblast	Anti-resorptive effect
	Osteoclast	

NPY, neuropetide Y; AgRP, agouti-related protein; CART, cocaine/amphetamine-related transcript; MC4R, melanocortin 4 receptor; MCRs, melanocortin receptors; VIP, vasoactive intestinal peptide.

Arginine-vasopressin (AVP, also known as antidiuretic hormone, ADH) and oxytocin (OT) regulate bone metabolism by acting in opposite ways: AVP impairs osteoblastogenesis and induces osteoclastogenesis by directly acting on AVP receptors expressed in both osteoblasts and osteoclasts; on the contrary, OT promotes osteoblastogenesis and inhibits osteoclast activity by acting on OT receptors expressed in osteoblasts and osteoclasts (Tamma et al., 2013; Sun et al., 2016).

Finally, the expression of the melatonin receptors have been observed in both osteoblasts and osteoclasts and it has been demonstrated that melatonin regulates bone homeostasis by promoting osteoblast differentiation and osteoblastogenesis (Roth et al., 1999; Zhang et al., 2010). Defective melatonin signaling has been associated with impaired osteoblast function and development of scoliosis (Akoume et al., 2019).

Neuropeptides That Regulate Bone Metabolism

Bone homeostasis and remodeling are also under the direct control of several neuropeptides released by hypothalamus (**Table 3**).

Neuropeptide Y (NPY) has been demonstrated to play important peripheral roles. It is produced centrally in the arcuate nucleus (ARC) of the hypothalamus and regulates bone homeostasis with site-specific effects in periphery (Baldock et al., 2009). Both NPY and the relative Y1 receptors have been found in cells of the osteoblastic lineage. Peripherally NPY exerts catabolic effects in bone through the inhibition of osteoblasts activity and interacts with mechanical signals to integrate the osteoblasts regulation with the local environmental loading status. Specifically, this interconnection and local effects of NPY are mediated by osteocytes which produces local NPY that affects osteoblast activity after mechanical stimuli (Igwe et al., 2009). Noteworthy, the actions of this neuropeptide in bone homeostasis are exerted not only peripherally on Y1 receptors expressed by osteoblasts, but also throughout a central signaling, on CNS throughout the Y2 receptors (Shi et al., 2011; Lee N. J. et al., 2015). In particular, it has been observed that, when activated, Y2 receptors, present in hypothalamic NPY-expressing neurons, elicit anti-osteogenic effects on trabecular but not on cortical bone (Shi et al., 2010). Interestingly, pre-osteocytes and osteocytes express NPY, as demonstrated in neonatal calvaria, and its expression was reduced in response to fluid shear stress. The treatment of calvaria osteoblasts with NPY decreased the intracellular levels of cyclic AMP (cAMP) and limits the expression of the markers of osteoblast differentiation (e.g., osteocalcin (OCN), bone sialoproteins, and dentin matrix acidic phosphoprotein 1-DMP1) (Igwe et al., 2009).

Agouti-related peptide (AgRP) acts through the sympathetic nervous system on bone metabolism. Increased neuronal AgRP activity downregulates the sympathetic tone favoring bone mass gain throughout the enhancement of the osteoblast activity (Kim et al., 2015; Shi et al., 2017).

Cocaine amphetamine regulated transcript (CART) is a neuropeptide precursor protein highly expressed in the hypothalamus, but also peripherally. It has been observed that while low hypothalamic CART expression is associated with increased bone resorption, through the induction of higher levels of RANKL, elevated CART expression resulted an increase in bone mass (Elefteriou et al., 2005).

The melanocortin peptides bind to five different G protein-coupled receptors and they sustain osteo-positive effects by binding to melanocortin 4 receptor (MC4R), which is highly expressed in the hypothalamus (Farooqi et al., 2000). Melanocortin receptor MC4R have been found in mouse periosteum and rat osteoblasts suggesting a direct role for melanocortin in bone development and metabolism (Dumont et al., 2005). Further, other melanocortin receptors have been detected in both osteoblasts and osteoclasts (Zhong et al., 2005). Melanocortin agonists stimulate osteoblast proliferation in *in vitro* models. Further, knock out mice for MC4R experience increase bone mass due to reduced osteoclasts number (Elefteriou, 2005), suggesting that melanocortin promotes bone formation throughout the regulation of the proliferation rate of both osteoblasts and osteoclasts.

Another neuropeptide that regulates bone mass is neuromedin U that elicits bone resorption through a leptin-mediated pathway, acting preferentially at the CNS level rather than peripherally (Sato et al., 2007).

The vasoactive intestinal peptide (VIP) acts through sympathetic and parasympathetic nerve fibers. It is frequently released together with ACh by parasympathetic terminals at the bony periosteum level and, mainly, in the epiphysis. It acts directly on osteoblasts and osteoclasts by binding to its G protein-coupled receptors and exerts an anti-resorptive effect (Togari et al., 1997). It has been shown that VIP inhibits RANKL expression in osteoblasts, while it suppresses RANK in osteoclasts, and, in parallel, induces OPG expression in osteoblast (Mukohyama et al., 2000; Juarranz et al., 2005).

Neurotransmitters That Regulate Bone Metabolism

Bone homeostasis and bone remodeling are regulated also by neurotransmitters released by CNS, such as serotonin, glutamate,

and dopamine (**Table 4**). Indeed, bone cells express receptors for these neurotransmitters. Osteoblasts, osteocytes, and osteoclasts express different subtypes of G protein-coupled receptors for serotonin. Particularly, osteocyte-like MLO-Y4 cells express the serotonin receptors 5-HT1A and 5-HT2A, but also the serotonin transporter (5-HTT) and the enzyme involved in serotonin synthesis, thus being an important component of the serotonin system in bone (Bliziotes et al., 2006). Interestingly, the precise mechanism of action of serotonin in regulating bone cells activity is still under investigation and it is supposed that it acts differently depending on its origin: gut-derived serotonin decreases osteoblast proliferation, while serotonin derived from CNS enhances bone formation (Cui et al., 2011; Park et al., 2018).

Osteoblasts and osteoclasts express glutamate receptors, in particular the *N*-methyl-D-aspartate (NMDA) type is quantitatively the most represented (Chenu et al., 1998; Gu et al., 2002). The role of glutamate in bone is interesting and highly complex, since the active glutamate derives both centrally and peripherally and its action involves different cells. On one hand, there is glutamate innervation at the bone levels near bone cells expressing glutamate receptors (i.e., osteoblasts and osteoclasts) but, on the other hand, the entire osteoblasts population expresses the set of components for a regulated release of glutamate (Hinoi et al., 2002; Bhangu, 2003). However, different researches have demonstrated that glutamate inhibits osteoclasts activity and promotes osteoblasts functions (Taylor, 2002; Morimoto et al., 2006). Noteworthy, both the glutamate transporter, GLAST, and the glutamate receptors respond to mechanical loading. *In vivo* studies demonstrated that mechanical load regulates the expression of GLAST and glutamate receptors in bone (Mason et al., 1997; Ho et al., 2005). Interestingly, it has been hypothesized that osteocytes are the first responders to mechanical load in bone. Indeed, after some days of mechanical loading, GLAST protein was undetectable in osteocytes, while its expression increases in osteoblasts (Mason et al., 1997).

Dopamine is another important central neurotransmitter that also affects bone homeostasis. It acts through dopamine receptor (DR)-1, -2, -3, and -5 and enhances osteoblastic proliferation and bone mineralization and suppresses osteoclastogenesis (Hanami et al., 2013; Lee D. J. et al., 2015; Wang et al., 2020). Modulation of dopamine levels as therapeutic interventions for those pathologies featured by a dysregulation of dopamine levels [e.g., Alzheimer disease (AD), Parkinson disease (PD)] could interferes with bone mass (Chen et al., 2016).

Adipose Tissue and Skeletal Muscles As Two Intermediates in Bone-Brain Axis

Beside a direct brain-to-bone axis, these two organs may communicate throughout an indirect crosstalk involving mediators expressed and released by a third tissue. Adipose tissue and skeletal muscles are, actually, two important organs able to integrate stimuli of different nature (biomechanical and biochemical) and to release mediators (e.g., myokines and adipokines) having effects all over the body and, hence, also in bone either directly or throughout the mediation of the nervous system.

Hormones Released by Adipocytes: Adipokines

Actually, among several adipokines, there are two main hormones, released by adipocytes, that act on CNS to regulate bone metabolism and remodeling.

Leptin is released by adipocytes in response to insulin stimulation and glucose uptake, which correspond to anabolic state (Barr et al., 1997; Mueller et al., 1998) and binds receptors located in the CNS involved in the regulation of appetite and energy metabolism. In addition, it binds on receptors located at the hypothalamic level that regulate bone metabolism through the activation of the SNS. Hence, leptin-regulated neural pathways control both aspects of bone remodeling (Takeda et al., 2002; Elefteriou et al., 2005).

Adiponectin also regulates bone metabolism by acting on neurons of locus coeruleus, decreases the sympathetic tone and, therefore, increases bone mass (Kajimura et al., 2013). It is important to note that OCN, a bone-derived hormone whose functions will be discussed below, stimulates the release of adiponectin by adipocytes (Hill et al., 2014; Otani et al., 2015). Thus, it could be considered the existence of an indirect way by which bone, acting through the peripheral adipose tissues and then, through the CNS, regulates its own remodeling.

Hormones Released by Skeletal Muscle Cells: Myokines

It is known that skeletal muscles, during their activity (i.e., contraction), release molecules, the so called myokines, that act on other tissues, with a hormone-like activity, to mediate adaptive responses (Gomarasca et al., 2020).

Irisin, one of the more recently identified myokines, is a circulating hormone-like mediator that is released by skeletal muscles during and after exercises (Bostrom et al., 2012; Wrann et al., 2013; Lombardi et al., 2016). It regulates energy metabolism,

TABLE 4 | Brain to bone communication: neurotransmitters.

Neurotransmitter	Receptor	Target cell in bone	Main action
Serotonin	GPCRs for serotonin	Osteoblast	Central serotonin: enhancement of bone formation
		Osteoclast	Peripheral serotonin: inhibition of osteoblast proliferation
Glutamate	NMDA receptors	Osteoblast	Stimulation of osteoblasts differentiation and function
		Osteoclast	Inhibition of osteoclasts activity
Dopamine	DR-1, DR-2, DR-3, and DR-5	Osteoblast	Stimulation of bone formation and mineralization
		Osteoclast	Inhibition of osteoclastogenesis

GPCRs, G protein-coupled receptors; NMDA, n-methyl-D-aspartate; DR, dopamine receptor.

by stimulating the usage of energy substrates to release heat, and acts not only on skeletal muscles, but also on adipose tissue, bone, and brain. In bone, irisin mediates anabolic effects and acts by stimulating osteoblasts activity and reducing the number of osteoclasts (Colaianni et al., 2015), thus promoting bone formation. If, on one hand, its circulating levels are increased by physical exercise, on the other hand, it is decreased in bone metabolic dysfunction, as in osteoporosis (Anastasilakis et al., 2014). In brain, irisin is expressed in Purkinje neurons of the rat and mouse cerebellum and it is necessary for the proper neural differentiation of embryonic stem cells (Forouzanfar et al., 2015). Further, it may have neuroprotective effects after ischemic stroke and, by acting on hippocampus, it may rescue synaptic plasticity and memory impairment in AD (Asadi et al., 2018; Lourenco et al., 2019; Martinez Munoz et al., 2018). Irisin could be an interesting therapeutic target in osteoporotic traits associated to neurodegenerative disorders, based on its pro-anabolic effects, and in view of the fact that its circulating levels could be increased by physical exercise. However, it is not yet known if peripheral irisin, released by the skeletal muscle, can act directly on CNS, a condition that implies the crossing of the BBB, where it may regulate, among the other effects, bone remodeling after exercise.

BONE-TO-BRAIN COMMUNICATION

It has been shown that osteocytes release EVs, throughout a calcium-dependent mechanism, and that these EVs contain, among the others, RANKL, OPG, and sclerostin. This mechanism is supposed to represent a way by which the osteocyte response to mechanical loading may be transmitted to other tissues/organs, as demonstrated by *ex vivo* studies of intact bone that showed an enhanced release of EVs following mechanical stimulation (Morrell et al., 2018). However, very little is known about the central role of the bone-derived mediators. For instance, the precise mechanism by which bone-derived mediators may cross the BBB is not well known and it is still under investigation.

It has been shown that low bone density (BMD) and osteoporosis may associate with dementia and AD in postmenopausal women (Tan et al., 2005; Loskutova et al., 2009). Further, low BMD and BMD loss are risk factors for osteoporosis and AD and is an early risk factor for dementia. Women with high levels of hip bone loss have an increased probability to develop cognitive dementia compared to women with limited loss. In addition, looking at this point from another point of view, it has been shown that high lean body mass is associated with lower risk of cognitive impairment or dementia (Burns et al., 2010; Friedman et al., 2010; Basgoz et al., 2020).

The serum level of several bone-derived mediators has been found modulated in patient affected by bone diseases, as osteoporosis, but also in the case of neurodegenerative diseases, such as AD [e.g., OCN, OPN, sclerostin (Yuan et al., 2019), Dkk-1 (Huang et al., 2018), and lipocalin 2 (Song and Kim, 2018)] and PD [e.g., bone morphogenic protein 2 (Goulding et al., 2020), OCN (Shan et al., 2019)]. Interestingly, in AD, PD, as well as in other neurodegenerative diseases, osteopenia and osteoporosis are often comorbidities (Roos, 2014; Binks and Dobson, 2016). Thus, these molecules might be considered as relevant therapeutic targets in pathological conditions affecting the CNS featured by bone dysmetabolism. Indeed, by acting peripherally, with addressed exercise programs, it may be possible to modulate the levels of these proteins with potential beneficial effects on CNS, other than on bone (Lee et al., 2019).

In this last part of the review, we will discuss the current knowledge around the established and the putative actions of bone-derived molecules in the nervous system, highlighting how their exercise-induced modulation may potentially benefit both organs (**Table 5**).

Osteocalcin

Osteocalcin, also known as bone γ-carboxyglutamic acid protein (BGLAP), is a bone derived protein mainly released by osteoblasts, and usually measured at the serum level as an indicator of bone formation (Hauschka et al., 1989). It is firstly produced as a pre-pro-peptide that become mature after the carboxylation of the three glutamic acid residues (Glu → Gla). Once OCN is mature and carboxylated it is released in the extracellular space to be incorporated into the bone ECM where it binds to hydroxyapatite (Poser et al., 1980; Malashkevich et al., 2013). In circulation there are several forms of OCN comprising the fully carboxylated (cOCN), the fully uncarboxylated (ucOCN) and the intermediate mono- and bi-carboxylated ones, together with several cleavage products, due to the susceptibility to enzymatic fragmentation, especially of the under-carboxylated forms (Lombardi et al., 2015).

Several studies in mice have shown a biological role for OCN, and mainly for ucOCN form, in metabolism. It has been shown that OCN regulates glucose metabolism, stimulates insulin release from islets, affects fertility and production of sex steroid hormones (Patti et al., 2013). Further, it has been reported to act on adipocytes where it stimulates the release of adiponectin (Kanazawa, 2015). Testis, skeletal muscles, liver, blood vessels, and small intestine have been identified as other targets of OCN activity. Actually, despite the evidence in rodents, and also in *in vitro* cell systems, such roles in humans have not been established and, also, current evidences indicate that the endocrine functions of OCN may be relegated to a mild, and possibly indirect, modulation (Lombardi et al., 2015).

During recent years, a new role emerged for OCN related to the nervous system, in rodents. Indeed, in mice OCN has been indicated as necessary for both brain development and function (Oury et al., 2013; Khrimian et al., 2017).

An *in vivo* mouse model of OCN−/− demonstrated a significant passivity, compared to the wild type (WT) counterpart, and the utility of OCN to correct brain development and cognition (Oury et al., 2013). Adult OCN−/− mice developed abnormalities in brain structures and alterations in neurotransmitter levels, impairment in learning and memory, and anxious-depressive phenotype. Further, after birth, mice with a complete deletion of OCN showed the same, or at least similar although less severe, phenotypic alterations, with the exception of brain morphological abnormalities, observed in adult OCN−/− mice. Intraventricular administration of OCN, in these mice, restored the normal phenotype and corrected

TABLE 5 | Bone to brain communication: hormones and peptides.

Bone-derived mediator	Cells source in bone and brain	Exercise-related modifications	Main actions	
OCN	Osteoblast	↑ Circulating levels by aerobic exercises (mice and human)	BONE	cOCN binds to hydroxyapatite in bone ECM and regulates mineralization
		↑ ucOC by endurance non-weight bearing activities		Marker of bone formation
		↑ cOC by endurance weight bearing/impact activities		
			BRAIN	*Mouse*
				Able to cross the BBB
				Regulation of neurotransmitters synthesis in different brain areas
				Necessary for both brain development and functioning
				Regulation of learning, memory, and cognitive functions
				Human
				Correlation between plasma level of OCN and global cognition in women
				Low level of OCN correlates with brain microstructural changes
				The OCN form active in human brain is unknown
LCN2	Osteoblast (at least the 50% of circulating LCN2)	↓ by physical exercises	BONE	Promotion of osteoclastogenesis
		↑ by bed resting		Inverse correlation between LCN2 and BMD, in women
			BRAIN	*Mouse*
				Able to cross the BBB
				Act on hypothalamic MC4R to regulate appetite response
				Increased during metabolic inflammation and acts on hippocampus to modulate inflammation
sclerostin	Osteocyte	↓ by mechanical loading	BONE	Inhibition of osteoblastogenesis through inhibition of Wnt/β-catenin pathway and stimulation of RANKL release
		↑ by bed resting/immobilization	BRAIN	Potential regulation of neuronal function, through Wnt/β-catenin, possibly in neurodegenerative diseases
				Not known if able to cross the BBB
Dkk1	Osteoblast, osteocyte	↓ by chronic exercise (serum levels)	BONE	Inhibition of osteoblastogenesis through inhibition of Wnt/β-catenin pathway
			BRAIN	*Mouse*
				Upregulated in transgenic AD mice
				Contributes to impairment in LTP, learning and memory
				Human
				Upregulated in AD patients
				Circulating Dkk1 inversely correlates with cognitive performances in elderly women
				Not known if able to cross the BBB

(Continued)

TABLE 5 | Continued

Bone-derived mediator	Cells source in bone and brain	Exercise-related modifications	Main actions	
FGF23	Osteocyte, Osteoblasts, expressed in specific brain areas (hypothalamus, hippocampus, cortex and in cerebrospinal fluid)	↑ in unloading	BONE	Inhibition of osteoblastic activity
				Stimulation of osteoclast-mediated bone resorption
			BRAIN	Not known if able to cross the BBB (evidence for other FGF proteins)
				KO mice have impairment hippocampal cognitive functions
				Not yet well known the role in brain
OPN	Osteoblast	↓ by acute exercise in weight loss program	BONE	Stimulation of bone resorption and demineralization
				Negative correlation with BMD
			BRAIN	Highly expressed in brain sections of PD patients
				High serum level in AD patients
				Regulation of reparative processes in neurodegenerative disorders
RANKL	Osteoblast, immune cells	↓ by acute exercise	BONE	Stimulation of osteoclastogenesis and osteoclast function
			BRAIN	Highly expressed in hypothalamus and involved in the regulation of body temperature and fever; involvement in depressive disorders
BMPs	Osteoblast (synthesis), Osteoclasts (resorption dependent release from ECM)	↑ acute exercise	BONE	Stimulation of bone formation
				Modulation of osteogenesis following mechanical stimulation
			BRAIN	Involved in neurogenesis during embryonic phase and in adulthood
BDNF	CNS, PNS, osteoblasts, and chondrocytes	↑ acute exercise	BONE	Beneficial effects on bone cells, in particular promotion of proliferation and differentiation of MSC into osteoblasts
				Conditional KO in brain mice develops bone defects
			BRAIN	Support to synaptic plasticity, neurodevelopment, and neuronal differentiation
				Reduced circulating levels in AD and PD patients
IGF-1	Osteoblasts, chondrocytes In brain both during embryogenesis and in adulthood (cerebellum, olfactory bulb, hippocampus)	↑ by acute exercise	BONE	Stimulation of bone formation through stimulation of chondrocytes proliferation and osteoblasts differentiation
		↓ by chronic exercises		Decreased serum levels with age and in patients affected by osteoporosis
			BRAIN	Involvement in neurodevelopment and plasticity
				Involvement in aging-associated neurodegenerative disorders

OCN, osteocalcin; LCN2, lipocalin2; Dkk1, dickkopf-related protein 1; LTP, long term potentiation; FGF23, fibroblast growth factor 23; KO, knockout; OPN, osteopontin; BMD, bone mineral density; RANKL, receptor activator of nuclear factor κB ligand; BMPs, bone-morphogenic proteins; ECM, extracellular matrix; BDNF, brain-derived neurotrophic factor; CNS, central nervous system; PNS, peripheral nervous system; IGF-1, insulin-like growth factor 1.

anxiety and memory deficits (Oury et al., 2013). Experiments on this mouse model suggested that OCN may be necessary to reduce age-related cognitive impairment (Villeda et al., 2014). Interestingly, the circulating levels of OCN and cognitive functions strongly inversely correlate with age, suggesting that OCN may be necessary to contain the cognitive decline associated with aging.

Noteworthy, recent papers indicate that OCN can cross the BBB and, once in the CNS, it regulates neuronal functions, acting directly in brainstem, midbrain, and hippocampus to influence the synthesis of several neurotransmitters. It has been observed that, in OCN−/− mice, peripherally administrated ucOCN crosses the BBB and localizes at the brain level, while the cOCN form passes throughout the BBB less efficiently (Shan et al., 2019). Centrally, OCN stimulates the synthesis of monoamine neurotransmitters, including serotonin, dopamine, and noradrenaline, and inhibits the synthesis of γ-aminobutyric acid (GABA), that is the principal inhibitory neurotransmitter. Thus, OCN released from bone, cross the BBB and may have effects on the regulation of learning, memory, and cognitive functions (Oury et al., 2013).

Only recent clinical researches have been investigating on how peripheral level of OCN may put into correlation bone metabolism, and cognitive functions. It has been demonstrated a positive correlation between plasma OCN, executive functioning, and global cognition, but not with episode memory in women (Bradburn et al., 2016). Interestingly, no such correlation has been observed in men, suggesting the potential existence of gender differences in cognitive performance. Further, it has been reported that low levels of OCN correlate with brain microstructural changes observed with magnetic resonance imaging in middle-aged women (Puig et al., 2016).

Effects of Exercise

Circulating level of OCN increases after a single bout of endurance exercise in mice and, possibly, in humans (Mera et al., 2016), concomitantly to the increased glucose uptake by skeletal muscles and the reduction of circulating insulin concentrations. In particular, it has been observed that, in mice, this exercise-related increase of circulating OCN was associated with an increased bone resorption rate (Mera et al., 2016). Thus, aerobic exercise increases circulating levels of OCN, in mice, that may act through the IL-6/gpr130 axis to improve energy metabolism and cognition. In human, aerobic, and combined aerobic-resistance exercises increase serum level of OCN (Chahla et al., 2015; Mohammad Rahimi et al., 2020). These findings lead to the hypothesis that the induction of OCN release may associate with the preventive effect of exercise on dementia. However, additional studies are needed to better understand which form of OCN actually stimulates brain functions and to clarify which kind of exercise modulate a specific form of OCN. This would be of particular interest in the case of prescription of physical activity to specific cohorts of patients with the aim of ameliorating cognitive defects. At this purpose, it has been demonstrated that different kind of physical activity may associate with the relative prevalence of certain forms of OCN. During a 3-weeks stage race, professional cyclists, who underwent to strenuous activity in absence of loading, experienced a decrease in total circulating OCN without any change in the levels of ucOCN (i.e., decreased cOCN) in association with a stimulation of osteoclast activity (Lombardi et al., 2012b). On the contrary, male mountain ultra-marathoners, who are chronically subjected to strenuous activity associated with a high level of load, experienced circulating cOCN levels comparable to those recorded in their sedentary counterparts but halved ucOCN levels. Noteworthy, although a mountain ultra-marathon acutely induces a decrease in the circulating levels of bone formation markers, it causes a further decrease in ucOCN levels (Sansoni et al., 2017).

Lipocalin2

Lipocalin2 is a glycoprotein that regulates several functions and, among them neutrophil response to pathogens (it is also known as neutrophil gelatinase-associated lipocalin), regulation of oxidative stress in kidney tubule cells, modulation of insulin release and energy metabolism. It has been recently discovered that, in normal conditions, at least 50% of circulating lipocalin2 (LCN2) is produced released by osteoblasts and this fraction is able to cross the BBB and to act in the hypothalamus. Indeed, throughout the generation of a mouse model lacking Lcn2 specifically in osteoblasts, Lcn2osb−/− (Mosialou et al., 2017), it has been demonstrated that osteoblasts are the cells that contribute LCN2 levels sufficient to regulate appetite and glucose metabolism, at least in basal states. This hypothesis has been further supported by the observation coming from several studies performed on mouse model in which the LCN2 was deleted from the germline cells. However, different studies have led to controversial results. Indeed, metabolic inflammation, has been closely associated with an increase of LCN2 suggesting a role of this hormone as pro-diabetic and pro-obesogenic. On the contrary, other studies evidenced an opposite role for LCN2, highlighting its functions as anti-diabetic and anti-obesogenic.

The increase of LCN2 during metabolic inflammation has been observed not only peripherally but also in the CNS and, particularly, in the hippocampus where it may solve a role in the modulation of inflammation (Bhusal et al., 2019). Interestingly, both peripheral and central administration of LCN2 reduce food intake and gain of body weight.

Lipocalin2 can cross the BBB and acts in hypothalamus where it activates neurons in the paraventricular nucleus. Further, series of molecular and biochemical studies showed that LCN2 activates the MC4R pathway, by directly binding to MC4R.

Regulation of appetite mediated by bone-derived LCN2 provides a feedback mechanism to the well-established central control of bone mass and therefore further illustrates how important is the cross-talk between bone and the brain.

Effects of Exercise

During bed rest, healthy volunteers experienced a time-dependent increase of circulating LCN2 levels. Further, LCN2 expression in bone was increased in mice subjected to mechanical unloading by tail suspension, or botulin toxin A-induced muscle paralysis, or in dystrophic mice, compared their normal

loading/healthy counterparts. However, in these mice, exercise counteracted LCN2 increase (Rucci et al., 2015).

Sclerostin

Sclerostin is a glycoprotein released by osteocytes that inhibits osteoblastogenesis through inhibition of Wnt-β catenin pathway and, hence sustains osteoclast-mediated bone resorption also throughout the concomitant induction of RANKL in osteoblasts (Li et al., 2005). Sclerostin is encoded by the *SOST* gene and its production is regulated by different factors, including mechanical stimulation. Indeed, it has been reported that mechanical loading decreases *SOST* transcription in osteocytes and, consequently, increases bone formation. Immobilization is associated with decreased BMD and increased serum sclerostin in animal models and humans (Robling et al., 2008; Spatz et al., 2013). However, the action of sclerostin within the skeleton is thought to reflect the local action of sclerostin released by osteocytes, while the amount of circulating sclerostin does not always reflect bone density. Indeed, the relationship between circulating sclerostin and bone formation is not simple and far from clear and, hence, further explorations of this aspect are required. Deficient sclerostin production in human causes sclerosteosis and Van Buchem disease both characterized by increase in bone mineral density (Brunkow et al., 2001; Balemans et al., 2002).

It has been demonstrated that sclerostin binds to the low-density lipoprotein-receptor-related protein-5 and -6 (LRP5/6) and inhibits the Wnt signaling (Li et al., 2005). Among the pleiotropic action of this pathway, Wnt signaling regulates synaptic plasticity and memory, and it has been linked to the pathogenesis neurodegenerative disorders, such as AD (Wan et al., 2014; Libro et al., 2016; Tapia-Rojas and Inestrosa, 2018). The hypothesis is that sclerostin could be involved in the regulation of this pathway in neurodegenerative diseases, however, it has not been yet demonstrated whether sclerostin is able to cross the BBB, or not. Other studies are necessary to understand if and how the modulation of the circulating levels of sclerostin (for instance, throughout specific exercise programs) can affect Wnt signaling in brain.

Effects of Exercise

Acute physical activity represents an important inhibitory stimulus for sclerostin (Lombardi et al., 2017). However, when this activity is performed in absence of load, especially when at high intensity, as in cycling, it may increase and associates to a state of stimulated bone resorption (Grasso et al., 2015). However, in professional athletes, who are chronically submitted to high-training workloads, at rest this stimulus is attenuated maybe due to negative feedback mechanism (Lombardi et al., 2012a) or dependently to the whole bone mass.

Dickkopf-Related Protein 1

Dickkopf-related protein 1 protein is highly express in bone tissue, particularly it was first detected in osteoblasts and osteocytes, and it is secreted within the bone microenvironment (Li et al., 2006). Similarly to sclerostin, it has a role in bone mechanotransduction, and by binding to LRP6, it antagonizes Wnt/β-catenin pathway, thus inhibiting osteoblastogenesis, thus, favoring bone resorption (Li et al., 2006; Pinzone et al., 2009).

Notably, as mentioned above, Wnt signaling is fundamental for several functions, including regulation of synaptic plasticity, neuronal development, and functions, and its deregulation is associated with neurodegenerative disorders, such as AD.

Interestingly, Dkk1 protein has been found to be overexpressed in the brain of AD patients and transgenic-AD mice. In subsequent studies, investigating its specific role in neurodegeneration, demonstrated that the overexpression of Dkk1 protein in hippocampal mice causes impairment in long-term potentiation, learning and memory (Purro et al., 2012). Further, *in vivo* studies in rat and mouse and *in vitro* on neuronal cultures indicated that increased Dkk1 protein expression may contribute to cell death in cerebral ischemia, epilepsy, and neurodegenerative diseases (Cappuccio et al., 2005; Busceti et al., 2007; Mastroiacovo et al., 2009; Rosi et al., 2010). An interesting study measured peripheral Dkk1 levels in elderly women with memory concerns, in order to investigate a potential role as biomarker for Dkk1. This study revealed an inverse correlation between Dkk1 and cognitive performances but did not determine whether the serum level of Dkk1 corresponded to its brain level (Ross et al., 2018).

What is not clear is whether circulating Dkk1, released within bone microenvironment, can cross the BBB and can mediate this putative effect or, instead, a neural release of Dkk1 is responsible for the phenotypic findings.

Effects of Exercise

Dickkopf-related protein 1 serum level are decreased by long-term exercise (Kim et al., 2017), while during bed rest, exercise does not impede the unloading-associated increase in serum levels of sclerostin and Dkk1 (Belavy et al., 2016).

Fibroblast Growth Factor 23

Fibroblast Growth Factor 23 is mostly expressed by bone osteoblasts and osteocytes even if its expression has been detected in small amounts also in some brain areas, such as hypothalamus, hippocampus, and cortex (Liu et al., 2006; Yoshiko et al., 2007) and it has also been detected in the cerebrospinal fluid (CSF) (Kunert et al., 2017). However, the majority of circulating fibroblast growth factor 23 (FGF23) derives from osteocytes (Feng et al., 2006). When unstimulated (i.e., unloaded) osteocytes expresses FGF23, together with sclerostin and Dkk1. This response on one hand, inhibits osteoblast synthetic activity and differentiation, thus, favoring osteoclast-mediated bone resorption, on the other side make the other organs aware about the increased circulating load of bone catabolic products (e.g., calcium and phosphorous). Indeed, FGF23 acts on the kidney tubule where it stimulates the excretion of phosphorous in urine and also regulates vitamin D metabolism (Lombardi et al., 2014).

Despite the reported expression and detection in brain, definitive roles for FGF23 in brain functioning have not yet been established.

In vitro, murine hippocampal neurons treated with medium enriched with FGF23 show a less complex morphology (Hensel et al., 2016). A recent paper using a FGF23 knockout mouse model has demonstrated an impairment of hippocampal-dependent cognitive functions without any structural brain alterations (Laszczyk et al., 2019).

Interestingly, there are various papers that demonstrate that all the compounds belonging to the FGF family can cross the BBB and, consequently, it has been hypothesized a similar feature for FGF23 (Cuevas et al., 1998; Hsuchou et al., 2013).

Effects of Exercise

Serum levels of FGF23 decrease in mice subjected to both acute and chronic physical exercises and this is in accordance with FGF23 role on skeletal mineralization (Li et al., 2016). During a 3-weeks stage race in cyclists, who experience strenuous skeletal muscle activity in absence of load, FGF23 serum levels increased in association to enhanced osteoclast activity and parallel rise in serum phosphorous level (Lombardi et al., 2014). However, another study performed on rats demonstrated no changes in FGF23 serum levels after peak power and endurance training, demonstrating that further studies are necessary to better investigate on FGF23 serum level modulation after physical activity (Buskermolen et al., 2019).

OTHER MEDIATORS IN THE BRAIN-BONE-BRAIN CROSS-TALK

There are several key molecules that are expressed and exert functions on both brain and bone. Thus, in the absence of specific studies, it is difficult to understand if these molecules act only locally or if bone derived molecules could cross the BBB and act also in brain or *vice versa*. Among these molecules one can account irisin (whose roles have been discussed above), OPN, RANKL, bone morphogenic protein (BMP), brain-derived neurotrophic factor (BDNF), and IGF-1.

Osteopontin

Osteopontin is a bone-derived glycoprotein that is expressed also by other different tissues and organs and is a known mediator of the osteo-immune crosstalk (Lanteri et al., 2012). Evidences indicate that OPN is also expressed in the brain. In bone it is present in the ECM and promotes bone resorption supporting bone demineralization by anchoring osteoclasts to bone mineral matrix (Reinholt et al., 1990; Singh et al., 2018). It has been observed that patients with high serum level of OPN have low BMD (Filardi et al., 2019).

In brain it seems to protect neurons and regulate repair processes in various brain disorders and neurodegenerative diseases (Kaleta, 2019). Interestingly, OPN protein levels were found high in patient with AD in both CSF and plasma, and more elevated in newly diagnosed AD compared to chronic patients (Comi et al., 2010; Sun et al., 2013). It has also been found highly expressed in brain sections of subjects affected by PD (Maetzler et al., 2007).

Receptor Activator of Nuclear Factor κB

Receptor activator of nuclear factor κB ligand, as mentioned above, binds RANK expressed on osteoclasts and osteoclasts precursors and activates their differentiation into mature resorbing cells (Liu and Zhang, 2015). It is expressed in various tissues including bone and brain.

In bone, it favors bone resorption process, and it is an established therapeutic target for in the treatment of osteoporosis. Indeed, anti-RANKL antibody, that blocks RANKL–RANK binding, is currently successfully used as an anti-resorptive treatment.

In brain, RANKL is highly express in the hypothalamus and its function is to control the central regulation of body temperature and fever, in females (Hanada et al., 2009). Interestingly, the treatment with anti-RANKL in mice affected by chronic social defeat stress and depression-like syndrome ameliorates the phenotypes, suggesting a putative novel therapeutic use of anti-RANKL antibodies in human depression (Zhang et al., 2020).

Bone Morphogenic Proteins

Bone morphogenic proteins (BMPs) are growth factors belonging to the largest transforming growth factor β (TGFβ) superfamily and are expressed by different tissues, including bone and brain. These proteins are extracellular multifunctional cytokines that could be sequestered in the ECM during its deposition. Indeed, in ECM there is a high concentration of BMP ligands and also of antagonists of BMPs that inhibit their activity through transmembrane serine/threonine kinase receptors. Hence, the action of BMPs entrapped in ECM is finely regulated by agonists or antagonists (Weiss and Attisano, 2013).

In bone, BMPs stimulate skeletal growth, promoting bone formation and remodeling. BMPs signaling is modulated by different mechanostimuli leading to a specific BMP action. Since sequestered in ECM, BMPs are in a dynamically active space responding to different mechanical stimuli. For instance, fluid shear stress determines an immediate increase of BMPs signaling, consequent to their release from ECM, that stimulates osteocytes and osteoblasts (Schreivogel et al., 2019). Thus, mechanically modulated BMPs affect osteogenesis. However, it is important to keep in mind that several other molecules exist that are intermediates between mechanosensing and BMPs signaling (da Silva Madaleno et al., 2020). The mechanosensitive growth factor MGF24E is one of these molecules; it stimulates SMAD phosphorylation and the expression of osteogenic genes, finally increasing bone mineral density (Deng et al., 2015). This consideration is important in view of therapeutic approaches whose aim is to stimulate bone regeneration through the modulation of BMPs levels.

It is known that in adult brain, exists a niche that hosts neural stem cells the subgranular zone of the hippocampal dentate gyrus, where adult neurogenesis persists. As described above adult neurogenesis could be stimulated by physical activity, since it stimulates bone molecules that consequently could act in brain. BMPs in brain are involved in neurogenesis both in embryonic stages and in adulthood, by acting at that level (Gobeske et al., 2009; Armenteros et al., 2018; Jovanovic et al., 2018).

Thus, these molecules could be considered as novel therapeutic targets for those pathologies in which bone loss associates to the neurodegenerative disorder, since they may stimulate both neurogenesis and bone anabolism.

Brain-Derived Neurotrophic Factor

Brain-derived neurotrophic factor is a neurotrophic factor that is released by CNS and PNS. Further, it could be expressed and released by other tissues, such as bone. In brain, it solves several roles, including support to synaptic plasticity, neurodevelopment, and neuronal differentiation. It has been observed that its levels are reduced in patients affected by neurodegenerative diseases, such as AD and PD (Mattson, 2008).

As mentioned above, BDNF and its receptors are also expressed in osteoblasts and chondrocyte. *In vitro* experiments showed the beneficial effects of BDNF on bone cells promoting differentiation of MSC into osteoblasts (Kauschke et al., 2018), while conditional knockout mice for BDNF in brain displayed defects in bone, including high bone mass and longer femurs (Camerino et al., 2012).

Insulin-Like Growth Factor 1

Insulin-Like Growth Factor 1 (IGF-1) is a hormone structurally similar to insulin, which is primarily synthetized in liver following GH signaling (Laviola et al., 2008). Besides liver, it is synthesized in other tissues, including bone and brain. IGF-1 signaling is central to pathways that promote cell growth and survival, maturation, and proliferation, allowing for tissue growth and renewal. Indeed it is highly express in all neuroephitelial cell type during embryogenesis and in adulthood in those brain areas where persist neurogenesis (cerebellum, olfactory bulb, and hippocampus) (Bach et al., 1991; Bartlett et al., 1991; Bondy et al., 1992).

In bone it stimulates chondrocyte proliferation and osteoblast differentiation, thus promoting bone formation. Indeed, it has been found that IGF-1 serum levels are decreased with age and in patients with osteoporosis (Yakar et al., 2002; Rosen, 2004; Wrigley et al., 2017).

In brain IGF-1 has roles in neurodevelopment both prenatally and in the early post-natal period, and in plasticity and remodeling throughout the life. Noteworthy, this hormone is involved in neuropsychiatric and neurodegenerative disorders associated with aging (Cohen et al., 2009; Bozdagi et al., 2013; Shcheglovitov et al., 2013; Gontier et al., 2015).

CONCLUSION

Brain Diseases: Biomechanical Intervention as a Support to the Therapy

Different studies have demonstrated that there is a strong correlation between cognitive impairment and bone diseases. Impaired cognitive functions and neurodegeneration, indeed, are often associated with defects in bone (Roos, 2014; Binks and Dobson, 2016), while therapeutic strategies addressed at improving bone status (e.g., exercise training) associate with lower risk of cognitive impairment or dementia (Lee et al., 2019).

Brain and neurodegenerative diseases, independently from the involvement of skeletal muscles, associate with a limited physical activity behavior that results in an impaired bone function (i.e., osteopenia and osteoporosis). However, exercise would have a beneficial effect on bone function, and beside the positive impact on brain function dependent upon the improvement in energy metabolism, bone (and skeletal muscle)-derived mediators may act on, and positively affect, central PNSs. These bone-derived mediators can be induced by specifically addressed exercise training. Thereby, taking advantage of the existing connection between bone and brain, a novel view is emerging about the possibility to improve brain functions throughout the stimulation of bone metabolism.

It has been shown that low bone density (BMD) and osteoporosis may associate with dementia and AD in postmenopausal women (Filardi et al., 2019; Kaleta, 2019). Further, low BMD and BMD loss are risk factors for osteoporosis and AD and is an early risk factor for dementia. Women with high levels of hip bone loss have an increased probability to develop cognitive dementia compared to women with limited loss. In addition, looking at this point from another point of view, it has been shown that high lean body mass is associated with lower risk of cognitive impairment or dementia (Maetzler et al., 2007; Comi et al., 2010; Sun et al., 2013).

It is well known that physical activity decreases the risk for several diseases and improves the quality of life. Several studies have shown that physical exercise could prevent or even ameliorate cognitive impairment and dementia conditions, but also can bring benefits to memory and brain functions (Hillman et al., 2008; Heisz et al., 2015). Besides exercise, also healthy lifestyle, such as good eating habits, and adequate sleep time, prevent dementia. The prevention of dementia throughout physical activity has been demonstrated by a study that showed that exercise could promote the transcription of those genes that regulate the production of free radical scavenging enzymes and preventing free radical-mediated damage to neurons (Simioni et al., 2018; De la Rosa et al., 2020). Further, it has been observed that exercising ameliorates the cognitive functions by improving hippocampal volume and increasing mitochondria biogenesis in neurons, thus, favoring the energy metabolism in neurons (Olson et al., 2006; Fabel et al., 2009; Steiner et al., 2011).

It has been recently proposed that the improvement in brain functions consequent to physical exercise could be associated with the activity of molecules released by bone in response to the biomechanical stimulation. And, indeed, it is known that huge amounts of mediators are released in the bloodstream after exercises and most of them have specific positive effects on neurogenesis, angiogenesis, synaptic plasticity, and hippocampal dendritic spine densities, as well as in maintaining and improving the cognitive function (Katsimpardi et al., 2014; Heisz et al., 2017).

As describe in detail above, the circulating levels of bone-derived molecules, i.e., osteokines, change depending on the loading status and condition. LCN2 peripheral levels are inversely associated with the exercising status: less exercise corresponds to high level of LCN2 and, consequently, to reduce the brain-determined caloric intake. OCN circulating levels

are also modulated by exercises highlighting its potentially therapeutic modulation for improving age-related cognitive decline, preventing anxiety and depression, and preventing neurodegeneration in those pathologies affected by neuronal loss, as PD and AD.

Regulation of sclerostin and Dkk1 circulating levels by exercise is important for regulation of bone remodeling. Circulating sclerostin levels seem to inversely correlate with physical exercise, decreasing after mechanical stimuli to inhibit bone resorption. It emerges an important role of Wnt signaling in bone remodeling and this pathway is highly modulated by loading and unloading (Robling and Turner, 2009; Duan and Bonewald, 2016; Galea et al., 2017). Thus, pharmacotherapy targeting Wnt/β-catenin signaling may be useful in combination with load bearing exercise programs.

IGF-1 and BDNF are two neurotrophins that potentially could be used as biomarkers for recovery of patient suffering of ischemic stroke or other neurodegenerative pathologies, but the precise molecular mechanisms by which their levels can be regulated by physical activity are not definitively understood (Carro et al., 2000; Trejo et al., 2001; Huang et al., 2014; Maass et al., 2016).

Importantly, physical exercise improves cognitive functions by producing positive benefits whose impact may be further enhanced throughout the combination with a specific cognitive training. Indeed, synergistic effects of physical and cognitive exercises on memory function and serum levels of neurotrophic molecules, particularly of IGF-1 and BDNF, have been described in young adults and their levels were associated with positive results in those subjects experiencing the better responses to exercises (Heisz et al., 2017).

Future Perspectives

With this review we have highlighted the emerging aspects of the complex interconnection that exists between bone and brain. From this overview, it emerges a dynamic role of bone as a mechanosensor and endocrine organ, able to respond to mechanostimulation throughout the release of molecules whose function is to coordinate a proper adoptive response to the changing environmental situations. Physical exercise, indeed, perturbs bone homeostasis and stimulates bone response by determining benefit for the bone itself and, directly or indirectly, for the brain. However, if, from one hand, the knowledge of the biological role of some mediators in the context of the brain-to-brain crosstalk are somehow advanced, for others mediators such a function has been just hypothesized and, however, far to be demonstrated. As a matter of fact, the presentation of these factor results imbalanced.

As described above, patients affected by both brain diseases very often experience also bone metabolic dysfunctions. Exploiting the influence of bone on brain, novel therapeutic interventions, possibly exercise-based adjuvant strategies to the standard pharmacological and psychiatric treatments, may be adopted to treat neurological pathologies. Such strategies should be addressed at modulating the circulating level of specific bone-derived molecules, throughout specific exercise programs, in order to obtain positive effects also at the central level. Such an approach, however, in order to be effective needs a further and deep investigation of the mechanisms underlying the bone-to-brain axis and the future researches should answer to the following questions: which kind of stimulus can specifically modulate the expression of a given mediator?; is this mediator able to cross the BBB? and in which measure?; how does this mediator act in brain?

AUTHOR CONTRIBUTIONS

LG and GL drafted the manuscript and critically revised the manuscript. Both authors contributed to the article and approved the submitted version.

FUNDING

This work has been funded by the Italian Ministry of Health ("Ricerca Corrente" program).

REFERENCES

Abe, E., Marians, R. C., Yu, W., Wu, X. B., Ando, T., Li, Y., et al. (2003). TSH is a negative regulator of skeletal remodeling. *Cell* 115, 151–162. doi: 10.1016/s0092-8674(03)00771-2

Akoume, M. Y., Elbakry, M., Veillette, M., Franco, A., Nada, D., Labelle, H., et al. (2019). A Differential Hypofunctionality of Galphai Proteins Occurs in Adolescent Idiopathic Scoliosis and Correlates with the Risk of Disease Progression. *Sci. Rep.* 9:10074. doi: 10.1038/s41598-019-46325-2

Anastasilakis, A. D., Polyzos, S. A., Makras, P., Gkiomisi, A., Bisbinas, I., Katsarou, A., et al. (2014). Circulating irisin is associated with osteoporotic fractures in postmenopausal women with low bone mass but is not affected by either teriparatide or denosumab treatment for 3 months. *Osteoporos Int.* 25, 1633–1642. doi: 10.1007/s00198-014-2673-x

Armenteros, T., Andreu, Z., Hortiguela, R., Lie, D. C., and Mira, H. (2018). BMP and WNT signalling cooperate through LEF1 in the neuronal specification of adult hippocampal neural stem and progenitor cells. *Sci. Rep.* 8:9241. doi: 10.1038/s41598-018-27581-0

Asadi, Y., Gorjipour, F., Behrouzifar, S., and Vakili, A. (2018). Irisin Peptide Protects Brain Against Ischemic Injury Through Reducing Apoptosis and Enhancing BDNF in a Rodent Model of Stroke. *Neurochem. Res.* 43, 1549–1560. doi: 10.1007/s11064-018-2569-9

Bach, M. A., Shen-Orr, Z., Lowe, W. L. Jr., Roberts, C. T. Jr., and LeRoith, D. (1991). Insulin-like growth factor I mRNA levels are developmentally regulated in specific regions of the rat brain. *BrainRes. Mol. Brain Res.* 10, 43–48. doi: 10.1016/0169-328x(91)90054-2

Bajayo, A., Bar, A., Denes, A., Bachar, M., Kram, V., Attar-Namdar, M., et al. (2012). Skeletal parasympathetic innervation communicates central IL-1 signals regulating bone mass accrual. *Proc. Nat. Acad. Sci. USA* 109, 15455–15460. doi: 10.1073/pnas.1206061109

Baldock, P. A., Lee, N. J., Driessler, F., Lin, S., Allison, S., Stehrer, B., et al. (2009). Neuropeptide Y knockout mice reveal a central role of NPY in the coordination of bone mass to body weight. *PLoS One* 4:e8415. doi: 10.1371/journal.pone.0008415

Balemans, W., Patel, N., Ebeling, M., Van Hul, E., Wuyts, W., Lacza, C., et al. (2002). Identification of a 52 kb deletion downstream of the SOST gene in patients with van Buchem disease. *J. Med. Genet.* 39, 91–97. doi: 10.1136/jmg.39.2.91

Baliram, R., Chow, A., Huber, A. K., Collier, L., Ali, M. R., Morshed, S. A., et al. (2013). Thyroid and bone: macrophage-derived TSH-beta splice variant increases murine osteoblastogenesis. *Endocrinology* 154, 4919–4926. doi: 10.1210/en.2012-2234

Baliram, R., Latif, R., Berkowitz, J., Frid, S., Colaianni, G., Sun, L., et al. (2011). Thyroid-stimulating hormone induces a Wnt-dependent, feed-forward loop for osteoblastogenesis in embryonic stem cell cultures. *Proc. Nat. Acad. Sci. USA* 108, 16277–16282. doi: 10.1073/pnas.1110286108

Barr, V. A., Malide, D., Zarnowski, M. J., Taylor, S. I., and Cushman, S. W. (1997). Insulin stimulates both leptin secretion and production by rat white adipose tissue. *Endocrinology* 138, 4463–4472. doi: 10.1210/endo.138.10.5451

Bartlett, W. P., Li, X. S., Williams, M., and Benkovic, S. (1991). Localization of insulin-like growth factor-1 mRNA in murine central nervous system during postnatal development. *Dev. Biol.* 147, 239–250. doi: 10.1016/s0012-1606(05)80021-1

Basgoz, B., Ince, S., Safer, U., Naharci, M. I., and Tasci, I. (2020). Low bone density and osteoporosis among older adults with Alzheimer's disease, vascular dementia, and mixed dementia: A Cross-sectional Study With Prospective Enrollment. *Turk J. Phs. Med. Rheabil.* 66, 193–200. doi: 10.5606/tftrd.2020.3803

Belavy, D. L., Baecker, N., Armbrecht, G., Beller, G., Buehlmeier, J., Frings-Meuthen, P., et al. (2016). Serum sclerostin and DKK1 in relation to exercise against bone loss in experimental bed rest. *J. Bone Miner Metab.* 34, 354–365. doi: 10.1007/s00774-015-0681-3

Bergwitz, C., and Juppner, H. (2010). Regulation of phosphate homeostasis by PTH, vitamin D, and FGF23. *Ann. Rev. Med.* 61, 91–104. doi: 10.1146/annurev.med.051308.111339

Bhangu, P. S. (2003). 'Pre-synaptic' vesicular glutamate release mechanisms in osteoblasts. *J. Musculoskelet. Neuronal. Interact.* 3, 17–29.

Bhusal, A., Rahman, M. H., Lee, W. H., Bae, Y. C., Lee, I. K., and Suk, K. (2019). Paradoxical role of lipocalin-2 in metabolic disorders and neurological complications. *Biochem. Pharmacol.* 169:113626. doi: 10.1016/j.bcp.2019.113626

Binks, S., and Dobson, R. (2016). Risk Factors, Epidemiology and Treatment Strategies for Metabolic Bone Disease in Patients with Neurological Disease. *Curr. Osteoporos. Rep.* 14, 199–210. doi: 10.1007/s11914-016-0320-5

Bliziotes, M., Eshleman, A., Burt-Pichat, B., Zhang, X. W., Hashimoto, J., Wiren, K., et al. (2006). Serotonin transporter and receptor expression in osteocytic MLO-Y4 cells. *Bone* 39, 1313–1321. doi: 10.1016/j.bone.2006.06.009

Bondy, C., Werner, H., Roberts, C. T. Jr., and LeRoith, D. (1992). Cellular pattern of type-I insulin-like growth factor receptor gene expression during maturation of the rat brain: comparison with insulin-like growth factors I and II. *Neurosci.* 46, 909–923. doi: 10.1016/0306-4522(92)90193-6

Bonewald, L. F. (2017). The Role of the Osteocyte in Bone and Nonbone Disease. *Endocrinol. Metab. Clin. North Am.* 46, 1–18. doi: 10.1016/j.ecl.2016.09.003

Bostrom, P., Wu, J., Jedrychowski, M. P., Korde, A., Ye, L., Lo, J. C., et al. (2012). A PGC1-alpha-dependent myokine that drives brown-fat-like development of white fat and thermogenesis. *Nature* 481, 463–468. doi: 10.1038/nature10777

Bozdagi, O., Tavassoli, T., and Buxbaum, J. D. (2013). Insulin-like growth factor-1 rescues synaptic and motor deficits in a mouse model of autism and developmental delay. *Mol. Autism.* 4:9. doi: 10.1186/2040-2392-4-9

Bradburn, S., McPhee, J. S., Bagley, L., Sipila, S., Stenroth, L., Narici, M. V., et al. (2016). Association between osteocalcin and cognitive performance in healthy older adults. *Age Ageing* 45, 844–849. doi: 10.1093/ageing/afw137

Brazill, J. M., Beeve, A. T., Craft, C. S., Ivanusic, J. J., and Scheller, E. L. (2019). Nerves in Bone: Evolving Concepts in Pain and Anabolism. *J. Bone Miner Res.* 34, 1393–1406. doi: 10.1002/jbmr.3822

Brunkow, M. E., Gardner, J. C., Van Ness, J., Paeper, B. W., Kovacevich, B. R., Proll, S., et al. (2001). Bone dysplasia sclerosteosis results from loss of the SOST gene product, a novel cystine knot-containing protein. *Am. J. Hum. Genet.* 68, 577–589. doi: 10.1086/318811

Burns, J. M., Johnson, D. K., Watts, A., Swerdlow, R. H., and Brooks, W. M. (2010). Reduced lean mass in early Alzheimer disease and its association with brain atrophy. *Archiv. Neurol.* 67, 428–433. doi: 10.1001/archneurol.2010.38

Busceti, C. L., Biagioni, F., Aronica, E., Riozzi, B., Storto, M., Battaglia, G., et al. (2007). Induction of the Wnt inhibitor, Dickkopf-1, is associated with neurodegeneration related to temporal lobe epilepsy. *Epilepsia* 48, 694–705. doi: 10.1111/j.1528-1167.2007.01055.x

Buskermolen, J., van der Meijden, K., Furrer, R., Mons, D. J., van Essen, H. W., Heijboer, A. C., et al. (2019). Effects of different training modalities on phosphate homeostasis and local vitamin D metabolism in rat bone. *PeerJ.* 7:e6184. doi: 10.7717/peerj.6184

Calvi, L. M., Adams, G. B., Weibrecht, K. W., Weber, J. M., Olson, D. P., Knight, M. C., et al. (2003). Osteoblastic cells regulate the haematopoietic stem cell niche. *Nature* 425, 841–846. doi: 10.1038/nature02040

Camerino, C., Zayzafoon, M., Rymaszewski, M., Heiny, J., Rios, M., and Hauschka, P. V. (2012). Central depletion of brain-derived neurotrophic factor in mice results in high bone mass and metabolic phenotype. *Endocrinology* 153, 5394–5405. doi: 10.1210/en.2012-1378

Cappariello, A., Ponzetti, M., and Rucci, N. (2016). The "soft" side of the bone: unveiling its endocrine functions. *Horm. Mol. Biol. Clin. Invest.* 28, 5–20. doi: 10.1515/hmbci-2016-0009

Cappuccio, I., Calderone, A., Busceti, C. L., Biagioni, F., Pontarelli, F., Bruno, V., et al. (2005). Induction of Dickkopf-1, a negative modulator of the Wnt pathway, is required for the development of ischemic neuronal death. *J. Neurosci.* 25, 2647–2657. doi: 10.1523/JNEUROSCI.5230-04.2005

Cardoso, L., Herman, B. C., Verborgt, O., Laudier, D., Majeska, R. J., and Schaffler, M. B. (2009). Osteocyte apoptosis controls activation of intracortical resorption in response to bone fatigue. *J. Bone Miner. Res.* 24, 597–605. doi: 10.1359/jbmr.081210

Carro, E., Nunez, A., Busiguina, S., and Torres-Aleman, I. (2000). Circulating insulin-like growth factor I mediates effects of exercise on the brain. *J. Neurosci.* 20, 2926–2933.

Chahla, S. E., Frohnert, B. I., Thomas, W., Kelly, A. S., Nathan, B. M., and Polgreen, L. E. (2015). Higher daily physical activity is associated with higher osteocalcin levels in adolescents. *Prev. Med. Rep.* 2, 568–571. doi: 10.1016/j.pmedr.2015.06.017

Chen, C. S., Alonso, J. L., Ostuni, E., Whitesides, G. M., and Ingber, D. E. (2003). Cell shape provides global control of focal adhesion assembly. *Biochem. Biophys. Res. Commun.* 307, 355–361. doi: 10.1016/s0006-291x(03)01165-3

Chen, C. Y., Lane, H. Y., and Lin, C. H. (2016). Effects of Antipsychotics on Bone Mineral Density in Patients with Schizophrenia: Gender Differences. *Clin. Psychopharmacol. Neurosci.* 14, 238–249. doi: 10.9758/cpn.2016.14.3.238

Chen, H., Senda, T., and Kubo, K. Y. (2015). The osteocyte plays multiple roles in bone remodeling and mineral homeostasis. *Med. Mol. Morphol.* 48, 61–68. doi: 10.1007/s00795-015-0099-y

Chenu, C., Serre, C. M., Raynal, C., Burt-Pichat, B., and Delmas, P. D. (1998). Glutamate receptors are expressed by bone cells and are involved in bone resorption. *Bone* 22, 295–299. doi: 10.1016/s8756-3282(97)00295-0

Cohen, E., Paulsson, J. F., Blinder, P., Burstyn-Cohen, T., Du, D., Estepa, G., et al. (2009). Reduced IGF-1 signaling delays age-associated proteotoxicity in mice. *Cell* 139, 1157–1169. doi: 10.1016/j.cell.2009.11.014

Colaianni, G., Cuscito, C., Mongelli, T., Pignataro, P., Buccoliero, C., Liu, P., et al. (2015). The myokine irisin increases cortical bone mass. *Proc. Nat. Acad. Sci. USA* 112, 12157–12162. doi: 10.1073/pnas.1516622112

Comi, C., Carecchio, M., Chiocchetti, A., Nicola, S., Galimberti, D., Fenoglio, C., et al. (2010). Osteopontin is increased in the cerebrospinal fluid of patients with Alzheimer's disease and its levels correlate with cognitive decline. *J. Alzheimer. Dis.* 19, 1143–1148. doi: 10.3233/JAD-2010-1309

Cuevas, P., Carceller, F., Munoz-Willery, I., and Gimenez-Gallego, G. (1998). Intravenous fibroblast growth factor penetrates the blood-brain barrier and protects hippocampal neurons against ischemia-reperfusion injury. *Surg. Neurol.* 49, 77–83. doi: 10.1016/s0090-3019(97)00193-6

Cui, Y., Niziolek, P. J., MacDonald, B. T., Zylstra, C. R., Alenina, N., Robinson, D. R., et al. (2011). Lrp5 functions in bone to regulate bone mass. *Nat. Med.* 17, 684–691. doi: 10.1038/nm.2388

da Silva Madaleno, C., Jatzlau, J., and Knaus, P. (2020). BMP signalling in a mechanical context - Implications for bone biology. *Bone* 137:115416. doi: 10.1016/j.bone.2020.115416

Dallas, S. L., Prideaux, M., and Bonewald, L. F. (2013). The osteocyte: an endocrine cell . and more. *Endocrine Rev.* 34, 658–690. doi: 10.1210/er.2012-1026

David, V., Martin, A., Lafage-Proust, M. H., Malaval, L., Peyroche, S., Jones, D. B., et al. (2007). Mechanical loading down-regulates peroxisome proliferator-activated receptor gamma in bone marrow stromal cells and favors osteoblastogenesis at the expense of adipogenesis. *Endocrinology* 148, 2553–2562. doi: 10.1210/en.2006-1704

De la Rosa, A., Olaso-Gonzalez, G., Arc-Chagnaud, C., Millan, F., Salvador-Pascual, A., Garcia-Lucerga, C., et al. (2020). Physical exercise in the prevention and treatment of Alzheimer's disease. *J. Sport Health Sci.* 9, 394–404. doi: 10.1016/j.jshs.2020.01.004

Denes, A., Boldogkoi, Z., Uhereczky, G., Hornyak, A., Rusvai, M., Palkovits, M., et al. (2005). Central autonomic control of the bone marrow: multisynaptic tract tracing by recombinant pseudorabies virus. *Neurosci* 134, 947–963. doi: 10.1016/j.neuroscience.2005.03.060

Deng, M., Liu, P., Xiao, H., Zhang, Y., Wang, Y., Zhao, J., et al. (2015). Improving the osteogenic efficacy of BMP2 with mechano growth factor by regulating the signaling events in BMP pathway. *Cell Tissue Res.* 361, 723–731. doi: 10.1007/s00441-015-2154-3

DiGirolamo, D. J., Mukherjee, A., Fulzele, K., Gan, Y., Cao, X., Frank, S. J., et al. (2007). Mode of growth hormone action in osteoblasts. *J. Biol. Chem.* 282, 31666–31674. doi: 10.1074/jbc.M705219200

Ding, Y., Arai, M., Kondo, H., and Togari, A. (2010). Effects of capsaicin-induced sensory denervation on bone metabolism in adult rats. *Bone* 46, 1591–1596. doi: 10.1016/j.bone.2010.02.022

Dobie, R., MacRae, V. E., Huesa, C., van't Hof, R., Ahmed, S. F., and Farquharson, C. (2014). Direct stimulation of bone mass by increased GH signalling in the osteoblasts of Socs2-/- mice. *J. Endocrinol.* 223, 93–106. doi: 10.1530/JOE-14-0292

Duan, P., and Bonewald, L. F. (2016). The role of the wnt/beta-catenin signaling pathway in formation and maintenance of bone and teeth. *Int. J. Cel. Biochem. Cell Biol.* 77, 23–29. doi: 10.1016/j.biocel.2016.05.015

Dumont, L. M., Wu, C. S., Tatnell, M. A., Cornish, J., and Mountjoy, K. G. (2005). Evidence for direct actions of melanocortin peptides on bone metabolism. *Peptides* 26, 1929–1935. doi: 10.1016/j.peptides.2004.12.034

Duncan, R. L., and Turner, C. H. (1995). Mechanotransduction and the functional response of bone to mechanical strain. *Calcif Tissue Int.* 57, 344–358. doi: 10.1007/BF00302070

Dupont, S., Morsut, L., Aragona, M., Enzo, E., Giulitti, S., Cordenonsi, M., et al. (2011). Role of YAP/TAZ in mechanotransduction. *Nature* 474, 179–183. doi: 10.1038/nature10137

Elefteriou, F. (2005). Neuronal signaling and the regulation of bone remodeling. *Cell Mol. Life Sci.* 62, 2339–2349. doi: 10.1007/s00018-005-5175-3

Elefteriou, F. (2008). Regulation of bone remodeling by the central and peripheral nervous system. *Archiv. Biochem. Biophys.* 473, 231–236. doi: 10.1016/j.abb.2008.03.016

Elefteriou, F., Ahn, J. D., Takeda, S., Starbuck, M., Yang, X., Liu, X., et al. (2005). Leptin regulation of bone resorption by the sympathetic nervous system and CART. *Nature* 434, 514–520. doi: 10.1038/nature03398

En-Nosse, M., Hartmann, S., Trinkaus, K., Alt, V., Stigler, B., Heiss, C., et al. (2009). Expression of non-neuronal cholinergic system in osteoblast-like cells and its involvement in osteogenesis. *Cell Tissue Res.* 338, 203–215. doi: 10.1007/s00441-009-0871-1

Fabel, K., Wolf, S. A., Ehninger, D., Babu, H., Leal-Galicia, P., and Kempermann, G. (2009). Additive effects of physical exercise and environmental enrichment on adult hippocampal neurogenesis in mice. *Front. Neurosci.* 3:50. doi: 10.3389/neuro.22.002.2009

Faraldi, M., Gomarasca, M., Perego, S., Sansoni, V., Banfi, G., and Lombardi, G. (2020). Effect of collection matrix, platelet depletion, and storage conditions on plasma extracellular vesicles and extracellular vesicle-associated miRNAs measurements. *Clin. Chem. Lab. Med.* 2020:1296. doi: 10.1515/cclm-2020-1296

Farooqi, I. S., Yeo, G. S., Keogh, J. M., Aminian, S., Jebb, S. A., Butler, G., et al. (2000). Dominant and recessive inheritance of morbid obesity associated with melanocortin 4 receptor deficiency. *J. Clin. Invest.* 106, 271–279. doi: 10.1172/JCI9397

Feng, J. Q., Ward, L. M., Liu, S., Lu, Y., Xie, Y., Yuan, B., et al. (2006). Loss of DMP1 causes rickets and osteomalacia and identifies a role for osteocytes in mineral metabolism. *Nat. Genet.* 38, 1310–1315. doi: 10.1038/ng1905

Filardi, T., Carnevale, V., Massoud, R., Russo, C., Nieddu, L., Tavaglione, F., et al. (2019). High serum osteopontin levels are associated with prevalent fractures and worse lipid profile in post-menopausal women with type 2 diabetes. *J. Endocrinol. Invest.* 42, 295–301. doi: 10.1007/s40618-018-0914-0

Florencio-Silva, R., Sasso, G. R., Sasso-Cerri, E., Simoes, M. J., and Cerri, P. S. (2015). Biology of Bone Tissue: Structure, Function, and Factors That Influence Bone Cells. *BioMed. Res. Int.* 2015, 421746. doi: 10.1155/2015/421746

Forouzanfar, M., Rabiee, F., Ghaedi, K., Beheshti, S., Tanhaei, S., Shoaraye Nejati, A., et al. (2015). Fndc5 overexpression facilitated neural differentiation of mouse embryonic stem cells. *Cell Biol. Int.* 39, 629–637. doi: 10.1002/cbin.10427

Friedman, S. M., Menzies, I. B., Bukata, S. V., Mendelson, D. A., and Kates, S. L. (2010). Dementia and hip fractures: development of a pathogenic framework for understanding and studying risk. *Geriatr. Orthop. Surg. Rehabil.* 1, 52–62. doi: 10.1177/2151458510389463

Fukuda, T., Takeda, S., Xu, R., Ochi, H., Sunamura, S., Sato, T., et al. (2013). Sema3A regulates bone-mass accrual through sensory innervations. *Nature* 497, 490–493. doi: 10.1038/nature12115

Galea, G. L., Lanyon, L. E., and Price, J. S. (2017). Sclerostin's role in bone's adaptive response to mechanical loading. *Bone* 96, 38–44. doi: 10.1016/j.bone.2016.10.008

Galli, C., Piemontese, M., Lumetti, S., Manfredi, E., Macaluso, G. M., and Passeri, G. (2012). The importance of WNT pathways for bone metabolism and their regulation by implant topography. *Eur. Cell Mater* 24, 46–59. doi: 10.22203/ecm.v024a04

Gobeske, K. T., Das, S., Bonaguidi, M. A., Weiss, C., Radulovic, J., Disterhoft, J. F., et al. (2009). BMP signaling mediates effects of exercise on hippocampal neurogenesis and cognition in mice. *PLoS One* 4:e7506. doi: 10.1371/journal.pone.0007506

Gomarasca, M., Banfi, G., and Lombardi, G. (2020). Myokines: The endocrine coupling of skeletal muscle and bone. *Adv. Clin. Chem.* 94, 155–218. doi: 10.1016/bs.acc.2019.07.010

Gontier, G., George, C., Chaker, Z., Holzenberger, M., and Aid, S. (2015). Blocking IGF Signaling in Adult Neurons Alleviates Alzheimer's Disease Pathology through Amyloid-beta Clearance. *J. Neurosci.* 35, 11500–11513. doi: 10.1523/JNEUROSCI.0343-15.2015

Goto, T., Yamaza, T., Kido, M. A., and Tanaka, T. (1998). Light- and electron-microscopic study of the distribution of axons containing substance P and the localization of neurokinin-1 receptor in bone. *Cell Tissue Res.* 293, 87–93. doi: 10.1007/s004410051100

Goulding, S. R., Sullivan, A. M., O'Keeffe, G. W., and Collins, L. M. (2020). The potential of bone morphogenetic protein 2 as a neurotrophic factor for Parkinson's disease. *Neural. Regen Res.* 15, 1432–1436. doi: 10.4103/1673-5374.274327

Grasso, D., Corsetti, R., Lanteri, P., Di Bernardo, C., Colombini, A., Graziani, R., et al. (2015). Bone-muscle unit activity, salivary steroid hormones profile, and physical effort over a 3-week stage race. *Scand. J. Med. Sci. Sport* 25, 70–80. doi: 10.1111/sms.12147

Gu, Y., Genever, P. G., Skerry, T. M., and Publicover, S. J. (2002). The NMDA type glutamate receptors expressed by primary rat osteoblasts have the same electrophysiological characteristics as neuronal receptors. *Calcif Tissue Int.* 70, 194–203. doi: 10.1007/s00223-001-2004-z

Hanada, R., Leibbrandt, A., Hanada, T., Kitaoka, S., Furuyashiki, T., Fujihara, H., et al. (2009). Central control of fever and female body temperature by RANKL/RANK. *Nature* 462, 505–509. doi: 10.1038/nature08596

Hanami, K., Nakano, K., Saito, K., Okada, Y., Yamaoka, K., Kubo, S., et al. (2013). Dopamine D2-like receptor signaling suppresses human osteoclastogenesis. *Bone* 56, 1–8. doi: 10.1016/j.bone.2013.04.019

Hauschka, P. V., Lian, J. B., Cole, D. E., and Gundberg, C. M. (1989). Osteocalcin and matrix Gla protein: vitamin K-dependent proteins in bone. *Physiol Rev.* 69, 990–1047.

Hayashi, M., Nakashima, T., Yoshimura, N., Okamoto, K., Tanaka, S., and Takayanagi, H. (2019). Autoregulation of Osteocyte Sema3A Orchestrates Estrogen Action and Counteracts Bone Aging. *Cell Metab.* 29, 627–37e5. doi: 10.1016/j.cmet.2018.12.021

Heisz, J. J., Clark, I. B., Bonin, K., Paolucci, E. M., Michalski, B., Becker, S., et al. (2017). The Effects of Physical Exercise and Cognitive Training on Memory and Neurotrophic Factors. *J. Cogn. Neurosci.* 29, 1895–1907. doi: 10.1162/jocn_a_01164

Heisz, J. J., Vandermorris, S., Wu, J., McIntosh, A. R., and Ryan, J. D. (2015). Age differences in the association of physical activity, sociocognitive engagement, and TV viewing on face memory. *Health psychol.* 83–88. doi: 10.1037/hea0000046

Hensel, N., Schon, A., Konen, T., Lubben, V., Forthmann, B., Baron, O., et al. (2016). Fibroblast growth factor 23 signaling in hippocampal cells: impact on

neuronal morphology and synaptic density. *J. Neurochem.* 137, 756–769. doi: 10.1111/jnc.13585

Hill, H. S., Grams, J., Walton, R. G., Liu, J., Moellering, D. R., and Garvey, W. T. (2014). Carboxylated and Uncarboxylated Forms of Osteocalcin Directly Modulate the Glucose Transport System and Inflammation in Adipocytes. *Hormone. Metab. Res.* 46, 341–347. doi: 10.1055/s-0034-1368709

Hillman, C. H., Erickson, K. I., and Kramer, A. F. (2008). Be smart, exercise your heart: exercise effects on brain and cognition. *Nat. Rev. Neurosci.* 9, 58–65. doi: 10.1038/nrn2298

Hinoi, E., Fujimori, S., Takarada, T., Taniura, H., and Yoneda, Y. (2002). Facilitation of glutamate release by ionotropic glutamate receptors in osteoblasts. *Biochem. Biophys. Res. Commun.* 297, 452–458. doi: 10.1016/s0006-291x(02)02223-4

Ho, M. L., Tsai, T. N., Chang, J. K., Shao, T. S., Jeng, Y. R., and Hsu, C. (2005). Down-regulation of N-methyl D-aspartate receptor in rat-modeled disuse osteopenia. *Osteoporos. Int.* 16, 1780–1788. doi: 10.1007/s00198-005-1928-y

Holguin, N., Brodt, M. D., and Silva, M. J. (2016). Activation of Wnt Signaling by Mechanical Loading Is Impaired in the Bone of Old Mice. *J. Bone Miner. Res.* 31, 2215–2226. doi: 10.1002/jbmr.2900

Hsuchou, H., Pan, W., and Kastin, A. J. (2013). Fibroblast growth factor 19 entry into brain. *Fluids Barriers CNS* 10:32. doi: 10.1186/2045-8118-10-32

Huang, T., Larsen, K. T., Ried-Larsen, M., Moller, N. C., and Andersen, L. B. (2014). The effects of physical activity and exercise on brain-derived neurotrophic factor in healthy humans: A review. *Scand J. Med. Sci. Sport* 24, 1–10. doi: 10.1111/sms.12069

Huang, Y., Liu, L., and Liu, A. (2018). Dickkopf-1: Current knowledge and related diseases. *Life Sci.* 209, 249–254. doi: 10.1016/j.lfs.2018.08.019

Igwe, J. C., Jiang, X., Paic, F., Ma, L., Adams, D. J., Baldock, P. A., et al. (2009). Neuropeptide Y is expressed by osteocytes and can inhibit osteoblastic activity. *J. Cell Biochem.* 108, 621–630. doi: 10.1002/jcb.22294

Jovanovic, V. M., Salti, A., Tilleman, H., Zega, K., Jukic, M. M., Zou, H., et al. (2018). BMP/SMAD Pathway Promotes Neurogenesis of Midbrain Dopaminergic Neurons In Vivo and in Human Induced Pluripotent and Neural Stem Cells. *J. Neurosci.* 38, 1662–1676. doi: 10.1523/JNEUROSCI.1540-17.2018

Juarranz, Y., Abad, C., Martinez, C., Arranz, A., Gutierrez-Canas, I., Rosignoli, F., et al. (2005). Protective effect of vasoactive intestinal peptide on bone destruction in the collagen-induced arthritis model of rheumatoid arthritis. *Arthritis. Res. Ther.* 7, R1034–R1045. doi: 10.1186/ar1779

Kajimura, D., Lee, H. W., Riley, K. J., Arteaga-Solis, E., Ferron, M., Zhou, B., et al. (2013). Adiponectin regulates bone mass via opposite central and peripheral mechanisms through FoxO1. *Cell Metabol.* 17, 901–915. doi: 10.1016/j.cmet.2013.04.009

Kaleta, B. (2019). The role of osteopontin in kidney diseases. *Inflamm. Res.* 68, 93–102. doi: 10.1007/s00011-018-1200-5

Kanazawa, I. (2015). Osteocalcin as a hormone regulating glucose metabolism. *World J. Diabetes* 6, 1345–1354. doi: 10.4239/wjd.v6.i18.1345

Katsimpardi, L., Litterman, N. K., Schein, P. A., Miller, C. M., Loffredo, F. S., Wojtkiewicz, G. R., et al. (2014). Vascular and neurogenic rejuvenation of the aging mouse brain by young systemic factors. *Science* 344, 630–634. doi: 10.1126/science.1251141

Kauschke, V., Gebert, A., Calin, M., Eckert, J., Scheich, S., Heiss, C., et al. (2018). Effects of new beta-type Ti-40Nb implant materials, brain-derived neurotrophic factor, acetylcholine and nicotine on human mesenchymal stem cells of osteoporotic and non osteoporotic donors. *PLoS One* 13:e0193468. doi: 10.1371/journal.pone.0193468

Kegelman, C. D., Coulombe, J. C., Jordan, K. M., Horan, D. J., Qin, L., Robling, A. G., et al. (2020). YAP and TAZ Mediate Osteocyte Perilacunar/Canalicular Remodeling. *J. Bone Miner Res.* 35, 196–210. doi: 10.1002/jbmr.3876

Kegelman, C. D., Mason, D. E., Dawahare, J. H., Horan, D. J., Vigil, G. D., Howard, S. S., et al. (2018). Skeletal cell YAP and TAZ combinatorially promote bone development. *FASEB J.* 32, 2706–2721. doi: 10.1096/fj.201700872R

Khosla, S., Drake, M. T., Volkman, T. L., Thicke, B. S., Achenbach, S. J., Atkinson, E. J., et al. (2018). Sympathetic beta1-adrenergic signaling contributes to regulation of human bone metabolism. *J. Clin. Invest.* 128, 4832–4842. doi: 10.1172/JCI122151

Khrimian, L., Obri, A., Ramos-Brossier, M., Rousseaud, A., Moriceau, S., Nicot, A. S., et al. (2017). Gpr158 mediates osteocalcin's regulation of cognition. *J. Exp. Med.* 214, 2859–2873. doi: 10.1084/jem.20171320

Kim, J. G., Sun, B. H., Dietrich, M. O., Koch, M., Yao, G. Q., Diano, S., et al. (2015). AgRP Neurons Regulate Bone Mass. *Cell Rep.* 13, 8–14. doi: 10.1016/j.celrep.2015.08.070

Kim, T. H., Chang, J. S., Park, K. S., Park, J., Kim, N., Lee, J. I., et al. (2017). Effects of exercise training on circulating levels of Dickkpof-1 and secreted frizzled-related protein-1 in breast cancer survivors: A pilot single-blind randomized controlled trial. *PLoS One* 12:e0171771. doi: 10.1371/journal.pone.0171771

Kodama, D., Hirai, T., Kondo, H., Hamamura, K., and Togari, A. (2017). Bidirectional communication between sensory neurons and osteoblasts in an in vitro coculture system. *FEBS Lett.* 591, 527–539. doi: 10.1002/1873-3468.12561

Kunert, S. K., Hartmann, H., Haffner, D., and Leifheit-Nestler, M. (2017). Klotho and fibroblast growth factor 23 in cerebrospinal fluid in children. *J. Bone Miner. Metab.* 35, 215–226. doi: 10.1007/s00774-016-0746-y

Lanteri, P., Lombardi, G., Colombini, A., Grasso, D., and Banfi, G. (2012). Stability of osteopontin in plasma and serum. *Clin. Chem. Lab. Med.* 50, 1979–1984. doi: 10.1515/cclm-2012-0177

Laszczyk, A. M., Nettles, D., Pollock, T. A., Fox, S., Garcia, M. L., Wang, J., et al. (2019). FGF-23 Deficiency Impairs Hippocampal-Dependent Cognitive Function. *eNeuro* 6:2019. doi: 10.1523/ENEURO.0469-18.2019

Laviola, L., Natalicchio, A., Perrini, S., and Giorgino, F. (2008). Abnormalities of IGF-I signaling in the pathogenesis of diseases of the bone, brain, and fetoplacental unit in humans. *Am. J. Physiol. Endocrinol. Metabm.* 295, E991–E999. doi: 10.1152/ajpendo.90452.2008

Lee, D. J., Tseng, H. C., Wong, S. W., Wang, Z., Deng, M., and Ko, C. C. (2015). Dopaminergic effects on in vitro osteogenesis. *Bone Res* 3, 15020. doi: 10.1038/boneres.2015.20

Lee, N. J., Nguyen, A. D., Enriquez, R. F., Luzuriaga, J., Bensellam, M., Laybutt, R., et al. (2015). NPY signalling in early osteoblasts controls glucose homeostasis. *Mol. Metab.* 4, 164–174. doi: 10.1016/j.molmet.2014.12.010

Lee, T. H., Formolo, D. A., Kong, T., Lau, S. W., Ho, C. S., Leung, R. Y. H., et al. (2019). Potential exerkines for physical exercise-elicited pro-cognitive effects: Insight from clinical and animal research. *Int. Rev. Neurobiol.* 147, 361–395. doi: 10.1016/bs.irn.2019.06.002

Lewis, K. J., Frikha-Benayed, D., Louie, J., Stephen, S., Spray, D. C., Thi, M. M., et al. (2017). Osteocyte calcium signals encode strain magnitude and loading frequency in vivo. *Proc. Nat. Acad. Sci. USA* 114, 11775–11780. doi: 10.1073/pnas.1707863114

Li, D. J., Fu, H., Zhao, T., Ni, M., and Shen, F. M. (2016). Exercise-stimulated FGF23 promotes exercise performance via controlling the excess reactive oxygen species production and enhancing mitochondrial function in skeletal muscle. *Metabol. Clin. Exp.* 65, 747–756. doi: 10.1016/j.metabol.2016.02.009

Li, J., Sarosi, I., Cattley, R. C., Pretorius, J., Asuncion, F., Grisanti, M., et al. (2006). Dkk1-mediated inhibition of Wnt signaling in bone results in osteopenia. *Bone* 39, 754–766. doi: 10.1016/j.bone.2006.03.017

Li, X., Han, L., Nookaew, I., Mannen, E., Silva, M. J., Almeida, M., et al. (2019). Stimulation of Piezo1 by mechanical signals promotes bone anabolism. *eLife* 8:49631. doi: 10.7554/eLife.49631

Li, X., Zhang, Y., Kang, H., Liu, W., Liu, P., Zhang, J., et al. (2005). Sclerostin binds to LRP5/6 and antagonizes canonical Wnt signaling. *J. Biol. Chem.* 280, 19883–19887. doi: 10.1074/jbc.M413274200

Liang, H., Zeng, Y., Feng, Y., Wu, H., Gong, P., and Yao, Q. (2018). Selective beta2-adrenoreceptor signaling regulates osteoclastogenesis via modulating RANKL production and neuropeptides expression in osteocytic MLO-Y4 cells. *J. Cell Biochem.* 2018:27998. doi: 10.1002/jcb.27998

Libro, R., Bramanti, P., and Mazzon, E. (2016). The role of the Wnt canonical signaling in neurodegenerative diseases. *Life Sci.* 158, 78–88. doi: 10.1016/j.lfs.2016.06.024

Liu, S., Zhou, J., Tang, W., Jiang, X., Rowe, D. W., and Quarles, L. D. (2006). Pathogenic role of Fgf23 in Hyp mice. *Am. J. Physiol. Endocrinol. Metab.* 291, E38–E49. doi: 10.1152/ajpendo.00008.2006

Liu, W., and Zhang, X. (2015). Receptor activator of nuclear factor-kappaB ligand (RANKL)/RANK/osteoprotegerin system in bone and other tissues (review). *Mol. Med. Rep.* 11, 3212–3218. doi: 10.3892/mmr.2015.3152

Lombardi, G., Barbaro, M., Locatelli, M., and Banfi, G. (2017). Novel bone metabolism-associated hormones: the importance of the pre-analytical phase for understanding their physiological roles. *Endocrine* 56, 460–484. doi: 10.1007/s12020-017-1239-z

Lombardi, G., Corsetti, R., Lanteri, P., Grasso, D., Vianello, E., Marazzi, M. G., et al. (2014). Reciprocal regulation of calcium-/phosphate-regulating hormones in cyclists during the Giro d'Italia 3-week stage race. *Scand J. Med. Sci. Sport* 24, 779–787. doi: 10.1111/sms.12080

Lombardi, G., Lanteri, P., Colombini, A., Mariotti, M., and Banfi, G. (2012a). Sclerostin concentrations in athletes: role of load and gender. *J. Biol. Regul. Homeost Agents* 26, 157–163. Epub 2012/04/06. doi: 18 [pii].,

Lombardi, G., Lanteri, P., Graziani, R., Colombini, A., Banfi, G., and Corsetti, R. (2012b). Bone and energy metabolism parameters in professional cyclists during the Giro d'Italia 3-weeks stage race. *PLoS One* 7:e42077. doi: 10.1371/journal.pone.0042077

Lombardi, G., Perego, S., Luzi, L., and Banfi, G. A. (2015). four-season molecule: osteocalcin. Updates in its physiological roles. *Endocrine* 48, 394–404.

Lombardi, G., Sanchis-Gomar, F., Perego, S., Sansoni, V., and Banfi, G. (2016). Implications of exercise-induced adipo-myokines in bone metabolism. *Endocrine* 54, 284–305.

Loskutova, N., Honea, R. A., Vidoni, Brooks, W. M., and Burns, J. M. (2009). Bone density and brain atrophy in early Alzheimer's disease. *J. Alzheimer. Dis.* 18, 777–785. doi: 10.3233/JAD-2009-1185

Lourenco, M. V., Frozza, R. L., de Freitas, G. B., Zhang, H., Kincheski, G. C., Ribeiro, F. C., et al. (2019). Exercise-linked FNDC5/irisin rescues synaptic plasticity and memory defects in Alzheimer's models. *Nat. Med.* 25, 165–175. doi: 10.1038/s41591-018-0275-4

Ma, W., Zhang, X., Shi, S., and Zhang, Y. (2013). Neuropeptides stimulate human osteoblast activity and promote gap junctional intercellular communication. *Neuropeptides* 47, 179–186. doi: 10.1016/j.npep.2012.12.002

Ma, Y., Li, X., Fu, J., Li, Y., Gao, L., Yang, L., et al. (2014). Acetylcholine affects osteocytic MLO-Y4 cells via acetylcholine receptors. *Mol. Cell Endocrinol.* 384, 155–164. doi: 10.1016/j.mce.2014.01.021

Maass, A., Duzel, S., Brigadski, T., Goerke, M., Becke, A., Sobieray, U., et al. (2016). Relationships of peripheral IGF-1, VEGF and BDNF levels to exercise-related changes in memory, hippocampal perfusion and volumes in older adults. *NeuroImage* 131, 142–154. doi: 10.1016/j.neuroimage.2015.10.084

Mach, D. B., Rogers, S. D., Sabino, M. C., Luger, N. M., Schwei, M. J., Pomonis, J. D., et al. (2002). Origins of skeletal pain: sensory and sympathetic innervation of the mouse femur. *Neurosci* 113, 155–166. doi: 10.1016/s0306-4522(02)00165-3

Maetzler, W., Berg, D., Schalamberidze, N., Melms, A., Schott, K., Mueller, J. C., et al. (2007). Osteopontin is elevated in Parkinson's disease and its absence leads to reduced neurodegeneration in the MPTP model. *Neurobiol. Dis.* 25, 473–482. doi: 10.1016/j.nbd.2006.10.020

Malashkevich, V. N., Almo, S. C., and Dowd, T. L. X. - (2013). ray crystal structure of bovine 3 Glu-osteocalcin. *Biochemistry* 52, 8387–8392. doi: 10.1021/bi4010254

Mandl, P., Hayer, S., Karonitsch, T., Scholze, P., Gyori, D., Sykoutri, D., et al. (2016). Nicotinic acetylcholine receptors modulate osteoclastogenesis. *Arthritis Res. Ther.* 18:63. doi: 10.1186/s13075-016-0961-x

Martinez Munoz, I. Y., Camarillo Romero, and Garduno Garcia, J. J. (2018). Irisin a Novel Metabolic Biomarker: Present Knowledge and Future Directions. *Int. J. Endocrinol.* 2018:7816806. doi: 10.1155/2018/7816806

Mason, D. J., Suva, L. J., Genever, P. G., Patton, A. J., Steuckle, S., Hillam, R. A., et al. (1997). Mechanically regulated expression of a neural glutamate transporter in bone: a role for excitatory amino acids as osteotropic agents? *Bone* 20, 199–205. doi: 10.1016/s8756-3282(96)00386-9

Mastroiacovo, F., Busceti, C. L., Biagioni, F., Moyanova, S. G., Meisler, M. H., Battaglia, G., et al. (2009). Induction of the Wnt antagonist, Dickkopf-1, contributes to the development of neuronal death in models of brain focal ischemia. *J. Cereb. Blood Flow Metab.* 29, 264–276. doi: 10.1038/jcbfm.2008.111

Mattson, M. P. (2008). Glutamate and neurotrophic factors in neuronal plasticity and disease. *Ann. NY Acad. Sci.* 1144, 97–112. doi: 10.1196/annals.1418.005

Mera, P., Laue, K., Ferron, M., Confavreux, C., Wei, J., Galan-Diez, M., et al. (2016). Osteocalcin Signaling in Myofibers Is Necessary and Sufficient for Optimum Adaptation to Exercise. *Cell Metab.* 23, 1078–1092. doi: 10.1016/j.cmet.2016.05.004

Millar, S. A., Anderson, S. I., and O'Sullivan, S. E. (2019). Osteokines and the vasculature: a review of the in vitro effects of osteocalcin, fibroblast growth factor-23 and lipocalin-2. *PeerJ.* 7:e7139. doi: 10.7717/peerj.7139

Mohammad Rahimi, G. R., Bijeh, N., and Rashidlamir, A. (2020). Effects of exercise training on serum preptin, undercarboxylated osteocalcin and high molecular weight adiponectin in adults with metabolic syndrome. *Exp. Physiol.* 105, 449–459. doi: 10.1113/EP088036

Morimoto, R., Uehara, S., Yatsushiro, S., Juge, N., Hua, Z., Senoh, S., et al. (2006). Secretion of L-glutamate from osteoclasts through transcytosis. *EMBO J.* 25, 4175–4186. doi: 10.1038/sj.emboj.7601317

Morinobu, M., Ishijima, M., Rittling, S. R., Tsuji, K., Yamamoto, H., Nifuji, A., et al. (2003). Osteopontin expression in osteoblasts and osteocytes during bone formation under mechanical stress in the calvarial suture in vivo. *J. Bone Miner. Res.* 18, 1706–1715. doi: 10.1359/jbmr.2003.18.9.1706

Morrell, A. E., Brown, G. N., Robinson, S. T., Sattler, R. L., Baik, A. D., Zhen, G., et al. (2018). Mechanically induced Ca(2+) oscillations in osteocytes release extracellular vesicles and enhance bone formation. *Bone Res.* 6:6. doi: 10.1038/s41413-018-0007-x

Mosialou, I., Shikhel, S., Liu, J. M., Maurizi, A., Luo, N., He, Z., et al. (2017). MC4R-dependent suppression of appetite by bone-derived lipocalin 2. *Nature* 543, 385–390. doi: 10.1038/nature21697

Mueller, W. M., Gregoire, F. M., Stanhope, K. L., Mobbs, C. V., Mizuno, T. M., Warden, C. H., et al. (1998). Evidence that glucose metabolism regulates leptin secretion from cultured rat adipocytes. *Endocrinology* 139, 551–558. doi: 10.1210/endo.139.2.5716

Mukohyama, H., Ransjo, M., Taniguchi, H., Ohyama, T., and Lerner, U. H. (2000). The inhibitory effects of vasoactive intestinal peptide and pituitary adenylate cyclase-activating polypeptide on osteoclast formation are associated with upregulation of osteoprotegerin and downregulation of RANKL and RANK. *Biochem. Biophys. Res. Commun.* 271, 158–163. doi: 10.1006/bbrc.2000.2599

Niimura, M., Sato, T., Enoki, Y., Okubo, M., Kokabu, S., Takeda, S., et al. (2016). Semaphorin 3A Promotes Dendrite Elongation of Osteocytes in Association with Down-regulation of CDK6. *In Vivo* 30, 231–236.

Olson, A. K., Eadie, B. D., Ernst, C., and Christie, B. R. (2006). Environmental enrichment and voluntary exercise massively increase neurogenesis in the adult hippocampus via dissociable pathways. *Hippocampus* 16, 250–260. doi: 10.1002/hipo.20157

Otani, T., Mizokami, A., Hayashi, Y., Gao, J., Mori, Y., Nakamura, S., et al. (2015). Signaling pathway for adiponectin expression in adipocytes by osteocalcin. *Cell Signal.* 27, 532–544. doi: 10.1016/j.cellsig.2014.12.018

Oury, F., Khrimian, L., Denny, C. A., Gardin, A., Chamouni, A., Goeden, N., et al. (2013). Maternal and offspring pools of osteocalcin influence brain development and functions. *Cell* 155, 228–241. doi: 10.1016/j.cell.2013.08.042

Oury, F., Sumara, G., Sumara, O., Ferron, M., Chang, H., Smith, C. E., et al. (2011). Endocrine regulation of male fertility by the skeleton. *Cell* 144, 796–809. doi: 10.1016/j.cell.2011.02.004

Owen, R., and Reilly, G. C. (2018). In vitro Models of Bone Remodelling and Associated Disorders. *Front. Bioeng. Biotechnol.* 6:134. doi: 10.3389/fbioe.2018.00134

Parfitt, A. M. (2000). The mechanism of coupling: a role for the vasculature. *Bone* 26, 319–323. doi: 10.1016/S8756-3282(00)80937-0

Park, K. R., Kim, E. C., Hong, J. T., and Yun, H. M. (2018). Dysregulation of 5-hydroxytryptamine 6 receptor accelerates maturation of bone-resorbing osteoclasts and induces bone loss. *Theranostics* 8, 3087–3098. doi: 10.7150/thno.24426

Patti, A., Gennari, L., Merlotti, D., Dotta, F., and Nuti, R. (2013). Endocrine actions of osteocalcin. *Int. J. Endocrinol.* 2013:846480. doi: 10.1155/2013/846480

Pinzone, J. J., Hall, B. M., Thudi, N. K., Vonau, M., Qiang, Y. W., Rosol, T. J., et al. (2009). The role of Dickkopf-1 in bone development, homeostasis, and disease. *Blood* 113, 517–525. doi: 10.1182/blood-2008-03-145169

Plotkin, L. I., Mathov, I., Aguirre, J. I., Parfitt, A. M., Manolagas, S. C., and Bellido, T. (2005). Mechanical stimulation prevents osteocyte apoptosis: requirement of integrins, Src kinases, and ERKs. *Am. J. Physiol. Cell Physiol.* 289, C633–C643. doi: 10.1152/ajpcell.00278.2004

Poser, J. W., Esch, F. S., Ling, N. C., and Price, P. A. (1980). Isolation and sequence of the vitamin K-dependent protein from human bone. Undercarboxylation of the first glutamic acid residue. *J. Biol. Chem.* 255, 8685–8691. Epub 1980/09/25.,

Puig, J., Blasco, G., Daunis-i-Estadella, J., Moreno, M., Molina, X., Alberich-Bayarri, A., et al. (2016). Lower serum osteocalcin concentrations are associated with brain microstructural changes and worse cognitive performance. *Clin. Endocrinol.* 84, 756–763. doi: 10.1111/cen.12954

Purro, S. A., Dickins, E. M., and Salinas, P. C. (2012). The secreted Wnt antagonist Dickkopf-1 is required for amyloid beta-mediated synaptic loss. *J. Neurosci.* 32, 3492–3498. doi: 10.1523/JNEUROSCI.4562-11.2012

Qin, L., Liu, W., Cao, H., and Xiao, G. (2020). Molecular mechanosensors in osteocytes. *Bone Res.* 8:23. doi: 10.1038/s41413-020-0099-y

Reinholt, F. P., Hultenby, K., Oldberg, A., and Heinegard, D. (1990). Osteopontin–a possible anchor of osteoclasts to bone. *Proc. Nat. Acad. Sci. USA* 87, 4473–4475. doi: 10.1073/pnas.87.12.4473

Robinson, L. J., Tourkova, I., Wang, Y., Sharrow, A. C., Landau, M. S., Yaroslavskiy, B. B., et al. (2010). FSH-receptor isoforms and FSH-dependent gene transcription in human monocytes and osteoclasts. *Biochem. Biophys. Res. Commun.* 394, 12–17. doi: 10.1016/j.bbrc.2010.02.112

Robling, A. G., and Bonewald, L. F. (2020). The Osteocyte: New Insights. *Ann. Rev. Physiol.* 82, 485–506. doi: 10.1146/annurev-physiol-021119-034332

Robling, A. G., and Turner, C. H. (2009). Mechanical signaling for bone modeling and remodeling. *Crit. Rev. Eukariot. Gene Expr.* 19, 319–338. doi: 10.1615/critreveukargeneexpr.v19.i4.50

Robling, A. G., Niziolek, P. J., Baldridge, L. A., Condon, K. W., Allen, M. R., Alam, I., et al. (2008). Mechanical stimulation of bone in vivo reduces osteocyte expression of Sost/sclerostin. *J. Biol. Chem.* 283, 5866–5875. doi: 10.1074/jbc.M705092200

Roos, P. M. (2014). Osteoporosis in neurodegeneration. *J. Trace Elem. Med. Biol.* 28, 418–421. doi: 10.1016/j.jtemb.2014.08.010

Rosen, C. J. (2004). Insulin-like growth factor I and bone mineral density: experience from animal models and human observational studies. *BestPract. Res. Clin. Endcorinol. Metab.* 18, 423–435. doi: 10.1016/j.beem.2004.02.007

Rosi, M. C., Luccarini, I., Grossi, C., Fiorentini, A., Spillantini, M. G., Prisco, A., et al. (2010). Increased Dickkopf-1 expression in transgenic mouse models of neurodegenerative disease. *J. Neurochem.* 112, 1539–1551. doi: 10.1111/j.1471-4159.2009.06566.x

Ross, R. D., Shah, R. C., Leurgans, S., Bottiglieri, T., Wilson, R. S., and Sumner, D. R. (2018). Circulating Dkk1 and TRAIL Are Associated With Cognitive Decline in Community-Dwelling, Older Adults With Cognitive Concerns. *J. Gerontol. A Biol. Sci. Med. Sci.* 73, 1688–1694. doi: 10.1093/gerona/glx252

Roth, J. A., Kim, B. G., Lin, W. L., and Cho, M. I. (1999). Melatonin promotes osteoblast differentiation and bone formation. *J. Biol. Chem.* 274, 22041–22047. doi: 10.1074/jbc.274.31.22041

Rucci, N., Capulli, M., Piperni, S. G., Cappariello, A., Lau, P., Frings-Meuthen, P., et al. (2015). Lipocalin 2: a new mechanoresponding gene regulating bone homeostasis. *J. Bone Miner Res.* 30, 357–368. doi: 10.1002/jbmr.2341

Salter, D. M., Millward-Sadler, S. J., Nuki, G., and Wright, M. O. (2001). Integrin-interleukin-4 mechanotransduction pathways in human chondrocytes. *Clin. Orthopaed. Relat. Res.* 391, S49–S60. doi: 10.1097/00003086-200110001-00006

Sampath, T. K., Simic, P., Sendak, R., Draca, N., Bowe, A. E., O'Brien, S., et al. (2007). Thyroid-stimulating hormone restores bone volume, microarchitecture, and strength in aged ovariectomized rats. *J. Bone Miner Res.* 22, 849–859. doi: 10.1359/jbmr.070302

Sample, S. J., Heaton, C. M., Behan, M., Bleedorn, J. A., Racette, M. A., Hao, Z., et al. (2014). Role of calcitonin gene-related peptide in functional adaptation of the skeleton. *PLoS One* 9:e113959. doi: 10.1371/journal.pone.0113959

Sansoni, V., Vernillo, G., Perego, S., Barbuti, A., Merati, G., Schena, F., et al. (2017). Bone turnover response is linked to both acute and established metabolic changes in ultra-marathon runners. *Endocrine* 56, 196–204. doi: 10.1007/s12020-016-1012-8

Sato, S., Hanada, R., Kimura, A., Abe, T., Matsumoto, T., Iwasaki, M., et al. (2007). Central control of bone remodeling by neuromedin U. *Nat. Med.* 13, 1234–1240. doi: 10.1038/nm1640

Sato, T., Abe, T., Chida, D., Nakamoto, N., Hori, N., Kokabu, S., et al. (2010). Functional role of acetylcholine and the expression of cholinergic receptors and components in osteoblasts. *FEBS Lett.* 584, 817–824. doi: 10.1016/j.febslet.2010.01.001

Schreivogel, S., Kuchibhotla, V., Knaus, P., Duda, G. N., and Petersen, A. (2019). Load-induced osteogenic differentiation of mesenchymal stromal cells is caused by mechano-regulated autocrine signaling. *J. Tissue Eng. Regen. Med.* 13, 1992–2008. doi: 10.1002/term.2948

Sen, B., Xie, Z., Case, N., Styner, M., Rubin, C. T., and Rubin, J. (2011). Mechanical signal influence on mesenchymal stem cell fate is enhanced by incorporation of refractory periods into the loading regimen. *J. Biomech.* 44, 593–599. doi: 10.1016/j.jbiomech.2010.11.022

Seriwatanachai, D., Krishnamra, N., and van Leeuwen, J. P. (2009). Evidence for direct effects of prolactin on human osteoblasts: Inhibition of cell growth and mineralization. *J. Cell Biochem.* 107, 677–685. doi: 10.1002/jcb.22161

Seriwatanachai, D., Thongchote, K., Charoenphandhu, N., Pandaranandaka, J., Tudpor, K., Teerapornpuntakit, J., et al. (2008). Prolactin directly enhances bone turnover by raising osteoblast-expressed receptor activator of nuclear factor kappaB ligand/osteoprotegerin ratio. *Bone* 42, 535–546. doi: 10.1016/j.bone.2007.11.008

Shan, C., Ghosh, A., Guo, X. Z., Wang, S. M., Hou, Y. F., Li, S. T., et al. (2019). Roles for osteocalcin in brain signalling: implications in cognition- and motor-related disorders. *Mol. Brain* 12:23. doi: 10.1186/s13041-019-0444-5

Shcheglovitov, A., Shcheglovitova, O., Yazawa, M., Portmann, T., Shu, R., Sebastiano, V., et al. (2013). SHANK3 and IGF1 restore synaptic deficits in neurons from 22q13 deletion syndrome patients. *Nature* 503, 267–271. doi: 10.1038/nature12618

Shi, Y. C., Lin, S., Castillo, L., Aljanova, A., Enriquez, R. F., Nguyen, A. D., et al. (2011). Peripheral-specific y2 receptor knockdown protects mice from high-fat diet-induced obesity. *Obesity* 19, 2137–2148. doi: 10.1038/oby.2011.99

Shi, Y. C., Lin, S., Wong, I. P., Baldock, P. A., Aljanova, A., Enriquez, R. F., et al. (2010). NPY neuron-specific Y2 receptors regulate adipose tissue and trabecular bone but not cortical bone homeostasis in mice. *PLoS One* 5:e11361. doi: 10.1371/journal.pone.0011361

Shi, Z., Madden, C. J., and Brooks, V. L. (2017). Arcuate neuropeptide Y inhibits sympathetic nerve activity via multiple neuropathways. *J. Clin. Invest.* 127, 2868–2880. doi: 10.1172/JCI92008

Simioni, C., Zauli, G., Martelli, A. M., Vitale, M., Sacchetti, G., Gonelli, A., et al. (2018). Oxidative stress: role of physical exercise and antioxidant nutraceuticals in adulthood and aging. *Oncotarget* 9, 17181–17198. doi: 10.18632/oncotarget.24729

Simonet, W. S., Lacey, D. L., Dunstan, C. R., Kelley, M., Chang, M. S., Luthy, R., et al. (1997). Osteoprotegerin: a novel secreted protein involved in the regulation of bone density. *Cell* 89, 309–319. doi: 10.1016/s0092-8674(00)80209-3

Singh, A., Gill, G., Kaur, H., Amhmed, M., and Jakhu, H. (2018). Role of osteopontin in bone remodeling and orthodontic tooth movement: a review. *Progr. Orthodont* 19:18. doi: 10.1186/s40510-018-0216-2

Song, J., and Kim, O. Y. (2018). Perspectives in Lipocalin-2: Emerging Biomarker for Medical Diagnosis and Prognosis for Alzheimer's Disease. *Clin. Nutr. Res.* 7, 1–10. doi: 10.7762/cnr.2018.7.1.1

Spatz, J. M., Ellman, R., Cloutier, A. M., Louis, L., van Vliet, M., Suva, L. J., et al. (2013). Sclerostin antibody inhibits skeletal deterioration due to reduced mechanical loading. *J. Bone Miner Res.* 28, 865–874. doi: 10.1002/jbmr.1807

Spatz, J. M., Wein, M. N., Gooi, J. H., Qu, Y., Garr, J. L., Liu, S., et al. (2015). The Wnt Inhibitor Sclerostin Is Up-regulated by Mechanical Unloading in Osteocytes in Vitro. *J. Biol. Chem.* 290, 16744–16758. doi: 10.1074/jbc.M114.628313

Steiner, J. L., Murphy, E. A., McClellan, J. L., Carmichael, M. D., and Davis, J. M. (2011). Exercise training increases mitochondrial biogenesis in the brain. *J. Appl. Physiol.* 111, 1066–1071. doi: 10.1152/japplphysiol.00343.2011

Suda, T., Takahashi, N., Udagawa, N., Jimi, E., Gillespie, M. T., and Martin, T. J. (1999). Modulation of osteoclast differentiation and function by the new members of the tumor necrosis factor receptor and ligand families. *Endocrine Rev.* 20, 345–357. doi: 10.1210/edrv.20.3.0367

Sun, L., Peng, Y., Sharrow, A. C., Iqbal, J., Zhang, Z., Papachristou, D. J., et al. (2006). FSH directly regulates bone mass. *Cell* 125, 247–260. doi: 10.1016/j.cell.2006.01.051

Sun, L., Tamma, R., Yuen, T., Colaianni, G., Ji, Y., Cuscito, C., et al. (2016). Functions of vasopressin and oxytocin in bone mass regulation. *Proc. Nat. Acad. Sci. USA* 113, 164–169. doi: 10.1073/pnas.1523762113

Sun, Y., Yin, X. S., Guo, H., Han, R. K., He, R. D., and Chi, L. J. (2013). Elevated osteopontin levels in mild cognitive impairment and Alzheimer's disease. *Mediat. Inflamm.* 2013:615745. doi: 10.1155/2013/615745

Takeda, S., Elefteriou, F., Levasseur, R., Liu, X., Zhao, L., Parker, K. L., et al. (2002). Leptin regulates bone formation via the sympathetic nervous system. *Cell* 111, 305–317.

Tamma, R., Sun, L., Cuscito, C., Lu, P., Corcelli, M., Li, J., et al. (2013). Regulation of bone remodeling by vasopressin explains the bone loss in hyponatremia. *Proc. Nat. Acad. Sci. USA* 110, 18644–18649. doi: 10.1073/pnas.1318257110

Tan, Z. S., Seshadri, S., Beiser, A., Zhang, Y., Felson, D., Hannan, M. T., et al. (2005). Bone mineral density and the risk of Alzheimer disease. *Archiv. Neurol.* 62, 107–111. doi: 10.1001/archneur.62.1.107

Tapia-Rojas, C., and Inestrosa, N. C. (2018). Loss of canonical Wnt signaling is involved in the pathogenesis of Alzheimer's disease. *Neural. Regen Res.* 13, 1705–1710. doi: 10.4103/1673-5374.238606

Taylor, A. F. (2002). Osteoblastic glutamate receptor function regulates bone formation and resorption. *J. Musculoskelet. Neuronal. Interact.* 2, 285–290.

Thompson, W. R., Rubin, C. T., and Rubin, J. (2012). Mechanical regulation of signaling pathways in bone. *Gene* 503, 179–193. doi: 10.1016/j.gene.2012.04.076

Togari, A., Arai, M., Mizutani, S., Mizutani, S., Koshihara, Y., and Nagatsu, T. (1997). Expression of mRNAs for neuropeptide receptors and beta-adrenergic receptors in human osteoblasts and human osteogenic sarcoma cells. *Neurosci. Lett.* 233, 125–128. doi: 10.1016/s0304-3940(97)00649-6

Tourkova, I. L., Liu, L., Sutjarit, N., Larrouture, Q. C., Luo, J., Robinson, L. J., et al. (2017). Adrenocorticotropic hormone and 1,25-dihydroxyvitamin D3 enhance human osteogenesis in vitro by synergistically accelerating the expression of bone-specific genes. *Lab. Invest.* 97, 1072–1083. doi: 10.1038/labinvest.2017.62

Trejo, J. L., Carro, E., and Torres-Aleman, I. (2001). Circulating insulin-like growth factor I mediates exercise-induced increases in the number of new neurons in the adult hippocampus. *J. Neurosci.* 21, 1628–1634.

Villeda, S. A., Plambeck, K. E., Middeldorp, J., Castellano, J. M., Mosher, K. I., Luo, J., et al. (2014). Young blood reverses age-related impairments in cognitive function and synaptic plasticity in mice. *Nat. Med.* 20, 659–663. doi: 10.1038/nm.3569

Wan, W., Xia, S., Kalionis, B., Liu, L., and Li, Y. (2014). The role of Wnt signaling in the development of Alzheimer's disease: a potential therapeutic target? *BioMed. Res. Int.* 2014:301575. doi: 10.1155/2014/301575

Wang, C. X., Ge, X. Y., Wang, M. Y., Ma, T., Zhang, Y., and Lin, Y. (2020). Dopamine D1 receptor-mediated activation of the ERK signaling pathway is involved in the osteogenic differentiation of bone mesenchymal stem cells. *Stem Cell Res. Ther.* 11:12. doi: 10.1186/s13287-019-1529-x

Weiss, A., and Attisano, L. (2013). The TGFbeta superfamily signaling pathway. *Wiley Interdiscip. Rev. Dev. Biol.* 2, 47–63. doi: 10.1002/wdev.86

Wrann, C. D., White, J. P., Salogiannnis, J., Laznik-Bogoslavski, D., Wu, J., Ma, D., et al. (2013). Exercise induces hippocampal BDNF through a PGC-1alpha/FNDC5 pathway. *Cell Metabol.* 18, 649–659. doi: 10.1016/j.cmet.2013.09.008

Wrigley, S., Arafa, D., and Tropea, D. (2017). Insulin-Like Growth Factor 1: At the Crossroads of Brain Development and Aging. *Front. Cell Neurosci.* 11:14. doi: 10.3389/fncel.2017.00014

Xiao, Z., and Quarles, L. D. (2015). Physiological mechanisms and therapeutic potential of bone mechanosensing. *Rev. Endocrine Metab. Disorders* 16, 115–129. doi: 10.1007/s11154-015-9313-4

Yadav, V. K., Oury, F., Suda, N., Liu, Z. W., Gao, X. B., Confavreux, C., et al. (2009). A serotonin-dependent mechanism explains the leptin regulation of bone mass, appetite, and energy expenditure. *Cell* 138, 976–989. doi: 10.1016/j.cell.2009.06.051

Yakar, S., Rosen, C. J., Beamer, W. G., Ackert-Bicknell, C. L., Wu, Y., Liu, J. L., et al. (2002). Circulating levels of IGF-1 directly regulate bone growth and density. *J. Clin. Invest.* 110, 771–781. doi: 10.1172/JCI15463

Yao, Q., Liang, H., Huang, B., Xiang, L., Wang, T., Xiong, Y., et al. (2017). Beta-adrenergic signaling affect osteoclastogenesis via osteocytic MLO-Y4 cells' RANKL production. *Biochem. Biophys. Res. Commun.* 488, 634–640. doi: 10.1016/j.bbrc.2016.11.011

Yasuda, H., Shima, N., Nakagawa, N., Yamaguchi, K., Kinosaki, M., Mochizuki, S., et al. (1998). Osteoclast differentiation factor is a ligand for osteoprotegerin/osteoclastogenesis-inhibitory factor and is identical to TRANCE/RANKL. *Proc. Nat. Acad. Sci. USA* 95, 3597–3602. doi: 10.1073/pnas.95.7.3597

Yoshiko, Y., Wang, H., Minamizaki, T., Ijuin, C., Yamamoto, R., Suemune, S., et al. (2007). Mineralized tissue cells are a principal source of FGF23. *Bone* 40, 1565–1573. doi: 10.1016/j.bone.2007.01.017

Yuan, J., Meloni, B. P., Shi, T., Bonser, A., Papadimitriou, J. M., Mastaglia, F. L., et al. (2019). The Potential Influence of Bone-Derived Modulators on the Progression of Alzheimer's Disease. *J. Alzheimer. Dis.* 69, 59–70. doi: 10.3233/JAD-181249

Zhang, J., Fujita, Y., Chang, L., Pu, Y., Qu, Y., Wang, S., et al. (2020). Beneficial effects of anti-RANKL antibody in depression-like phenotype, inflammatory bone markers, and bone mineral density in male susceptible mice after chronic social defeat stress. *Behav. Brain. Res.* 379:112397. doi: 10.1016/j.bbr.2019.112397

Zhang, L., Su, P., Xu, C., Chen, C., Liang, A., Du, K., et al. (2010). Melatonin inhibits adipogenesis and enhances osteogenesis of human mesenchymal stem cells by suppressing PPARgamma expression and enhancing Runx2 expression. *J. Pineal. Res.* 49, 364–372. doi: 10.1111/j.1600-079X.2010.00803.x

Zhong, Q., Sridhar, S., Ruan, L., Ding, K. H., Xie, D., Insogna, K., et al. (2005). Multiple melanocortin receptors are expressed in bone cells. *Bone* 36, 820–831. doi: 10.1016/j.bone.2005.01.020

Conflict of Interest: The authors declare that the research was conducted in the absence of any commercial or financial relationships that could be construed as a potential conflict of interest.

frontiers in Human Neuroscience

ORIGINAL RESEARCH
published: 10 May 2021
doi: 10.3389/fnhum.2021.637157

Muscle Synergies in Children Walking and Running on a Treadmill

*Margit M. Bach, Andreas Daffertshofer and Nadia Dominici**

Department of Human Movement Sciences, Faculty of Behavioural and Movement Sciences, Amsterdam Movement Sciences & Institute for Brain and Behavior Amsterdam, Vrije Universiteit Amsterdam, Amsterdam, Netherlands

Muscle synergies reflect the presence of a common neural input to multiple muscles. Steering small sets of synergies is commonly believed to simplify the control of complex motor tasks like walking and running. When these locomotor patterns emerge, it is likely that synergies emerge as well. We hence hypothesized that in children learning to run the number of accompanying synergies increases and that some of the synergies' activities display a temporal shift related to a reduced stance phase as observed in adults. We investigated the development of locomotion in 23 children aged 2–9 years of age and compared them with seven young adults. Muscle activity of 15 bilateral leg, trunk, and arm muscles, ground reaction forces, and kinematics were recorded during comfortable treadmill walking and running, followed by a muscle synergy analysis. We found that toddlers (2–3.5 years) and preschoolers (3.5–6.5 years) utilize a "walk-run strategy" when learning to run: they managed the fastest speeds on the treadmill by combining double support (DS) and flight phases (FPs). In particular the activity duration of the medial gastrocnemius muscle was weakly correlated with age. The number of synergies across groups and conditions needed to cover sufficient data variation ranged between four and eight. The number of synergies tended to be smaller in toddlers than it did in preschoolers and school-age children but the adults had the lowest number for both conditions. Against our expectations, the age groups did not differ significantly in the timing or duration of synergies. We believe that the increase in the number of muscle synergies in older children relates to motor learning and exploration. The ability to run with a FP is clearly associated with an increase in the number of muscle synergies.

Keywords: children, locomotion, development, muscle synergies, treadmill, running

OPEN ACCESS

Edited by:
Yury Ivanenko, Santa Lucia Foundation (IRCCS), Italy

Reviewed by:
Shinya Aoi, Kyoto University, Japan
Tetsuro Funato, The University of Electro-Communications, Japan
Vincent C. K. Cheung, The Chinese University of Hong Kong, China

***Correspondence:**
Nadia Dominici
n.dominici@vu.nl

Specialty section:
This article was submitted to Motor Neuroscience, a section of the journal Frontiers in Human Neuroscience

Received: *02 December 2020*
Accepted: *08 April 2021*
Published: *10 May 2021*

Citation:
Bach MM, Daffertshofer A and Dominici N (2021) Muscle Synergies in Children Walking and Running on a Treadmill. Front. Hum. Neurosci. 15:637157. doi: 10.3389/fnhum.2021.637157

INTRODUCTION

Muscle synergies reflect a common neural input to multiple muscles easing the control of complex motor tasks like locomotion (Bernstein, 1967; Bizzi and Cheung, 2013). The central nervous system can activate large groups of muscles by small sets of descending neural signals at specific moments during the gait cycle (d'Avella et al., 2003; Ting and Macpherson, 2005; Bizzi and Cheung, 2013).

Abbreviations: AD, anterior deltoid; BB, biceps brachii; BF, biceps femoris; BR, brachioradialis; ES, erector spinae; F_v, vertical ground reaction forces; FWHM, full-width at half-maximum; GM, gluteus maximus; GT, greater trochanter; HS, heel strike; LD, latissimus dorsi; LE, lateral epicondyle; LM, lateral malleolus; MG, medial gastrocnemius; NMF, non-negative matrix factorization; PC, principal component; PCA, principal component analysis; PD, posterior deltoid; RF, rectus femoris; TA, tibialis anterior; TB, triceps brachii; TFL, tensor fascia latae; TO, toe-off; TRAP, trapezius; VMO, vastus medialis.

When children develop walking skills, the number of muscle synergies that accompany the cyclic movement of the lower extremities increases (Dominici et al., 2011). In neonates, two muscle synergies are present resembling the reflexive stepping pattern seen at birth, while in toddlers two additional are present, i.e., a total of four synergies can be observed that persist to and during adulthood (Dominici et al., 2011; Sylos-Labini et al., 2020). The shape of the synergies' waveforms evolves from wide, sinusoidal shapes to more focal ones with shorter activation duration from toddlers, to preschoolers and adults (Dominici et al., 2011). Here, we ask whether there is similar change in the number of synergies and the shape of their waveforms during the development of running. Is it generally true that an immature locomotor pattern is represented by fewer muscle synergies and less focal activation peaks?

Running may be defined as having a flight phase (FP) in contrast to walking where there is a double support phase (DS). Infants without independent walking experience toddling on a treadmill but with body-weight support show a shift from DS to FP at speeds of around 0.75 m/s (Vasudevan et al., 2016). Children, at the age of 6–18 years can run with FP though seemingly only in about 90% of the strides (Rozumalski et al., 2015). Given the relatively rare presence of FP, one may expect that children learning to run employ a so-called *walk-run strategy*, i.e., a mixture of DS and FP.

Running in adults differs from walking in that the activation timing changes in several muscles, amplitudes increase, or activation profiles may alter all together (Cappellini et al., 2006; Ivanenko et al., 2008; Hagio et al., 2015; Yokoyama et al., 2016). Muscle synergy analysis revealed, in particular, a shift in timing that is related to the activation of the calf muscles in line with a shorter stance phase in running compared to walking (Cappellini et al., 2006). One may ask whether such a pattern is also present in children during the development and maturation of running. In fact, already without running, the peak medial gastrocnemius activity of children at the age of 7–9 years does shift to earlier in the gait cycle during walking from 45% at comfortable speeds to 25% at fast speeds (Tirosh et al., 2013). Yet, it seems that the medial gastrocnemius muscle is pivotal for the development of walking as its full-width half-maximum (FWHM) decreases with age in typically developing children aged 1–12 years (Cappellini et al., 2016). The FWHM is a measure of the duration of the peak activation and any reduction of this measure suggests an increased ability to contract the muscle. But how do all these changes relate to (the emergence of) the aforementioned, common neural input?

We sought to answer these questions by investigating the development of both walking and running in children aged 2–9 years old. Using electromyographic (EMG) signals from 15 bilateral leg, trunk, and arm muscles, we extracted muscle synergies and related their number and waveforms with the ability to run with a FP. We expected the youngest children to make use of the afore-introduced walk-run strategy. We also hypothesized that the pivotal role of the medial gastrocnemius muscle extends to the development of running and expected its FWHM to reduce with increasing age for both walking and running. If this assumption holds, this would imply a (gradual) maturation of muscle synergies toward resemblance of adult patterns by means of an increased number of synergies accompanied by a temporal shift related to a reduced stance phase. To anticipate, we failed to find support for some of these hypotheses.

MATERIALS AND METHODS

Participants

Thirty healthy participants were included in this study (23 children aged 2–9 years old and 7 young adults; see **Table 1**) with exclusion of those with known developmental disease or neurological disorders. Participant groups were selected based on the ability to manage the speeds on a treadmill with FP ($\sim$ running, see below): toddlers (range: 25.7–40.4 months), preschoolers (range: 59.0–75.0 months), school-age (range: 78.4–106.1 months), and adults (range: 22–28 years).

Adult participants and guardians/parents of the children provided written informed consent in compliance with the Declaration of Helsinki. Ethical approval was given by The Scientific and Ethical Review Board of the Faculty of Behavioral and Movement Sciences, Vrije Universiteit Amsterdam, Netherlands (file number: VCWE-2016-149R1).

Setup

Participants were instructed to walk or run on the treadmill (Motek Medical BV, Culemborg, Netherlands) at a comfortable speed. Each of these conditions was repeated until a minimum of 20 consecutive strides had been recorded, where possible (Oliveira et al., 2014). When more than twenty gait cycles were recorded, the middle twenty cycles were chosen for analysis.

Walking and running were practiced and comfortable speeds were first determined by starting at a slow pace that was increased in steps of 0.1 km/h until the participant reported a comfortable speed. In two instances, participants were unable/unwilling to continue after practicing and we included the data recorded during these familiarization trials for analysis (one for walking and another for running).

Children participants wore a full-body climbing harness (CAMP Bambino Full Body Harness, CAMP USA, CO, United States) modified to also have a secure attachment point on the back at all times when on the treadmill. All participants wore own shoes for the duration of the experiment.

Data Acquisition

Behavior

Vertical, mediolateral, and anteroposterior ground reaction forces were sampled at 1 kHz for every trial via the two force plates in the instrumented treadmill.

Foot switches (piezo-resistive pressure sensitive sensors: Zerowire; Cometa, Bareggio, Italy) were placed on the skin on the heel and the head of the first metatarsal underneath the foot and were secured with tape; shoes and socks were placed over the foot switches. Foot switch data were sampled at 2 kHz.

Kinematic data were recorded bilaterally using an active marker system (Optotrak motion system, NDI Measurement

TABLE 1 | Participant characteristics [Mean (SD)].

	Toddlers	Pre-schoolers	School-age	Adults
Age	35.3 (5.6) months	66.1 (6.5) months	92.9 (9.5) months	24.15 (2.5) years
Gender (m/f)	2/3	3/3	6/6	4/3
Height (cm)	96.2 (2.8)	117.2 (7.7)	130.2 (6.8)	178.7 (5.7)
Weight (kg)	15.0 (2.0)	20.8 (3.3)	25.4 (4.9)	71.3 (8.3)

Sciences, Ontario, Canada) and sampled at 100 Hz. Two cameras were placed diagonally behind the treadmill and one was placed diagonally in front on the right-hand side of the participant. Single markers were attached to the right head of 5th metatarsal, right lateral malleolus (LM), right lateral femoral epicondyle (LE), and right greater trochanter (GT), right and left calcaneus, right and left glenohumeral joint, right and left lateral humeral epicondyle, and right and left ulnar styloid. Here, kinematic and foot switch data merely served for step detection in the case the vertical ground reaction data were unreliable.

Electrophysiology

Bipolar EMG signals were recorded with a wireless system (Mini wave plus, Zerowire; Cometa, Bareggio, Italy; sampled at 2 kHz after online band-pass filtering between 10 and 500 Hz) using pediatric Ag-AgCl pre-gelled EMG disk-electrodes for children (inter-electrode distance: 19 mm: DuoTrode, Myotronics, Kent, WA, United States) and pre-gelled Ag-AgCl electrodes for adults (BlueSensor H5; Ambu, Ballerup, Denmark). Skin was cleaned with alcohol and excess hair was removed prior to electrode placement on the bulk of the muscle belly parallel to the muscle fiber direction, conform SENIAM recommendations (Hermens et al., 1999).

We targeted the following 16 bilateral muscles: tibialis anterior (TA), gastrocnemius medialis (MG), biceps femoris (BF), vastus medialis oblique (VMO), rectus femoris (RF), tensor fascia latae (TFL), adductor longus, gluteus maximus (GM), erector spinae—L2 level (ES), latissimus dorsi (LD), deltoid—anterior part (AD), deltoid—posterior part (PD), trapezius—descending part (TRAP), triceps brachii (TB), biceps brachii (BB), and brachioradialis (BR). Adductor longus was, on the basis of the quality of the recorded muscle activity, excluded for all participants for further analysis leaving 15 bilateral muscles.

A single participant was recorded in a different lab using a slightly different setup. The kinematics was measured at 100 Hz using a passive marker system (Vicon Motion Systems Ltd., Oxford, United Kingdom). The reflective markers (14 mm in diameter) were placed bilaterally in the same positions as the other participants. Twelve cameras were placed around the ceiling of the room. The treadmill (Motek Medical BV, Amsterdam, Netherlands), measured only vertical ground reaction forces. The EMG protocol and equipment did not differ from the other participants.

Data Analysis

Behavior

While step events were mainly detected based on the vertical ground reaction forces (F_v), they were supplemented with the events detected from the heel markers and foot switches when F_v data were not sufficient for the event detection. The F_v were filtered with a Savitzky-Golay filter (3rd order, 121 framelength; Savitzky and Golay, 1964). Heel strike (HS) and toe-off (TO) were defined as the first sample crossing the threshold [mean (F_v)/10]. First and last HS and TO were excluded for further analysis. Heel markers were used to detect step events from the kinematics (Roerdink et al., 2008). The foot switch detection was based on an on/off algorithm. Foot switch data and kinematic data were re-sampled to 1 kHz for this application. All events were visually verified. The FP and DS were determined for up to twenty strides for every participant and condition.

All behavioral data were time-normalized to the right HS. Based on HS and TO, the percentage stance and swing of each gait cycle were determined. Velocity was normalized to leg length yielding the walking Froude number (Alexander and Jayes, 1983)

$$Fr = \frac{v^2}{g \times l}$$

where, v denotes stride speed as measured by the treadmill (m/s), g represents the gravitational constant (9.81 ms^{-2}) and l is the leg length (m) as the combined measured distance of thigh (GT-LE) and shank (LE-LM). Normalizing to the walking Froude number is considered suitable when comparing gait patterns at different speeds in participants of different size (Ivanenko et al., 2004a).

Electrophysiology

Electromyographic data were visually inspected and artifacts were removed using a custom-written burst-detection algorithm. EMG data were high-pass (2nd order bi-directional Butterworth filter at 20 Hz; De Luca et al., 2010; Willigenburg et al., 2012) and notch filtered (bi-directional stop notch filter around k·50 Hz, k = 1,. . .,10, with half-bandwidth of 0.5 Hz). Subsequently, EMG data were rectified using the modulus of the analytic signal and finally low-pass filtered (bidirectional 2nd order filter at 10 Hz) to obtain the corresponding EMG envelopes (Oliveira et al., 2016). These envelopes were time-normalized to 200 samples per gait cycle. Right-side EMG signals were normalized to the right HS and left-side EMG normalized to the left HS.

To characterize differences in the duration of EMG activity, we computed the FWHM. The FWHM was calculated as the number of samples exceeding each cycle's half maximum, after subtracting the cycle's minimum. We determined FWHM for each condition as the grand average within groups and across right and left side and expressed it as a percentage of the gait cycle. While we determined FWHM for every muscle per group, in view of our hypothesis we also expressed FWHM of the MG muscle as a function of age. Moreover, we estimated the phase shift τ between

the walking and running mean activity patterns of the MG muscle (Ivanenko et al., 2004b) using the cross-correlation. The cross-correlation was computed as (Nelson-Wong et al., 2009):

$$R_{\alpha\beta}(\Delta) = \frac{\int \alpha(t) \times \beta(t+\Delta)dt}{\sqrt{\int \alpha^2(t)dt \times \int \beta^2(t)dt}}$$

where α and β denote the two mean-subtracted waveforms during walking and running and refers to a time lag between the two. Then, the maximum correlation peak was determined as well as its corresponding time lag τ. Positive τ values indicate a lag of the MG signal during walking relative to running. To ease interpretation, we expressed the time lag τ in percent of the gait cycle.

For the subsequent synergy analysis, the concatenated EMG envelopes [concatenation leads to higher reconstruction accuracy (RA); Oliveira et al., 2014] were amplitude normalized to the mean value for every individual muscle (Halaki and Gi, 2012; Torricelli et al., 2014; Goudriaan et al., 2018). To increase the signal-to-noise ratio for the synergy analysis, the muscle synergy analysis was performed on each participant side (Clark et al., 2010), and thus, EMG envelopes were concatenated in a (15 muscles) × (20 strides × 200 samples) matrix for every condition and side for each participant. To ease comparison of our experimental findings with the literature, we also performed the muscle synergy analysis on only the lower limb muscles (TA, MG, BF, VMO, RF, TFL, GM, and ES), which resulted in an (8 muscles) × (20 strides × 200 samples) matrix for each participant, condition, and side (see **Supplementary Material 1** for details).

For dimensionality reduction we first employed a principal component analysis (PCA) on the mean-centered data (Boonstra et al., 2015). The appropriate number of muscle synergies was determined as the minimum number required to explain 80% of the variance. Then, a rank-reduced data set was reconstructed and the mean was added back. Subsequently, we employed non-negative matrix factorization (NMF) as a decomposition tool (Lee and Seung, 1999; Tresch et al., 2006; Dominici et al., 2011; Steele et al., 2015; Rabbi et al., 2020) to identify the relevant muscle synergies. Similar to PCA, NMF is an optimization method but is supplemented by the constraint that both the extracted weighting coefficients and activation waveforms are non-negative. This accounts for the constructive (non-negative) superposition of neural and muscle activations. Following the conventional NMF approach, weightings W and activation waveforms C were estimated by minimizing the Frobenius norm between (rank-reduced) envelope data E and the sum of synergies ($W \times C$, i.e., weightings × waveforms):

$$\| E - (W \times C) \|_F = \min$$

E denotes the aforementioned data, i.e., it resembles an $m \times t$ matrix (m = 15 muscles and t = 20 strides × 200 samples), the weighting coefficients W comprise an $m \times n$ matrix (n = number of synergies), and C contains the activation waveforms ($m \times t$ matrix) (Lee and Seung, 1999). We employed a multiplicative algorithm (Berry et al., 2007, implemented in Matlab, The Mathworks, Natick, MA, United States ver. 2019b; 200 replicates, 3,000 iterations, convergence threshold 10^{-6} and termination tolerance 10^{-8}) that requires an a-priori choice of the number of muscle synergies. Capitalizing on the optimized Frobenius norm, we also estimated the RA following (Zandvoort et al., 2019; Kerkman et al., 2020) that is defined as

$$RA = 1 - \frac{\| E - (W \times C) \|_F}{\| E \|_F}$$

In addition, we verified that the selected number of synergies adequately reconstruct the activity of each muscle by computing the RA per muscle, condition, and participant side.

The output of the NMF is (pseudo-)random for every optimization run. Hence, we ordered the outcomes by their correlation across participants. To do so, a separate NMF analysis was carried out on the grand-average of the adult data and the waveforms were arranged based on the timing of the main peaks of the activation pattern (Cappellini et al., 2006; Santuz et al., 2020). Subsequently, this serve as a "model-order" for the outputs of the NMF from all other participants which were then correlated to that model-order and ranked based on the largest Pearson correlation coefficient.

Finally, we determined the FWHM of every activation waveform for each participant side and the time lag τ between walking and running activation waveforms.

Statistics

Descriptive statistics included the calculation of the mean and standard deviation (SD).

Behavior

To test for effects of *age* on FP and for effects of *age* and *condition* (levels: instructed walking and running) on DS, we used two linear regression models. Next to main effects, the second one also served to identify interactions *age* × *condition*. The significance threshold was set to $\alpha = 0.05$.

Group differences in stance duration, stride duration, and Froude values were assessed using Kruskal–Wallis tests for every condition (with corresponding Bonferroni correction for multiple comparison); note that Kolmogorov-Smirnov tests revealed significant deviations from normality arguably due to small group sizes, which let us choose for non-parametric testing. Only p-values below 0.01 were considered significant in order to correct for the multiple corrections.

Electrophysiology

Along the same lines of the behavioral data, the time lag between walking and running and the FWHM of muscle activations and the waveforms of the muscle synergies were compared non-parametrically for every condition (Kruskal–Wallis tests with Bonferroni correction). Moreover, we detailed the age-dependency of the MG's FWHM by fitting exponentially saturating functions. To quantify the corresponding goodness-of-fit we report the adjusted R^2-value unless specified otherwise.

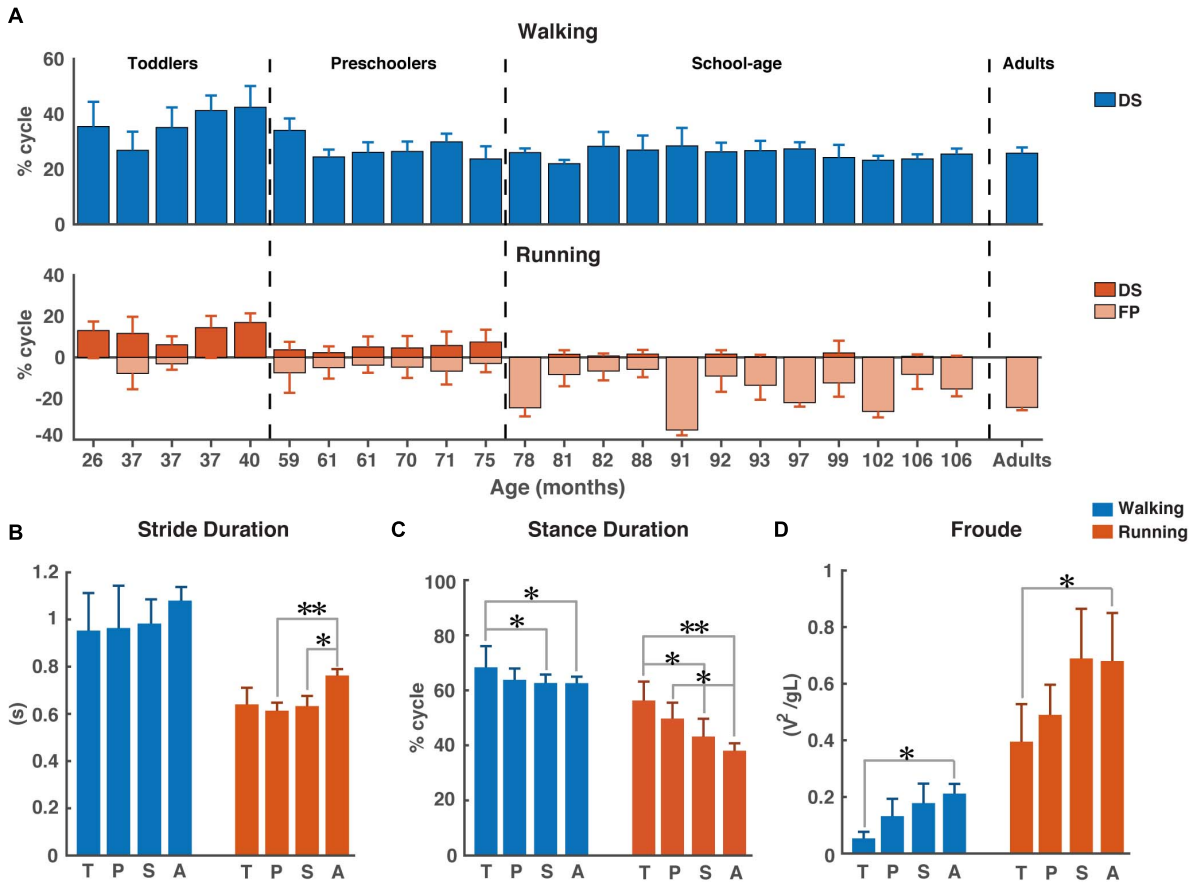

FIGURE 1 | Temporal gait parameters. **(A)** Percentage double support and flight phase during walking (blue) and running (red). Flight phase is depicted with negative numbers. Vertical dotted lines separate the different groups: Toddlers, Preschoolers, School-age, and Adults, **(B)** Stride duration for walking and running, **(C)** Stance duration for walking and running, and **(D)** Froude number for walking and running. DS, double support; FP, flight phase; s, seconds; T, toddlers; P, preschoolers; S, school-age; A, adults; V, velocity, g, gravitational constant; L, leg length. *$p < 0.01$ and **$p < 0.001$.

RESULTS

We failed to record the aimed-for minimum of 20 strides for all participants (between 14 and 20 strides were analyzed). All the children in the toddler group were assisted with handhold by either a researcher or their parent/guardian ($N = 5$). Yet, we are confident that this did not affect the level of body-weight support during locomotion as we verified the level of vertical ground reaction forces via the toddler's body weight (range of body-weight support was 0–7%). The conditions referred to in the following are the instructed conditions.

Behavioral Results

As expected, the young children in this study used a combination of DS and FP when running on a treadmill (see **Figure 1A**). For FP there was a significant main effect of *age* ($p < 0.001$) and the FP increased with increasing age. A similar significance could be established for the main effect of *age* on DS ($p < 0.001$) but, opposite to FP, DS decreased with increasing age. And, there was a significant main effect of *condition* on DS ($p < 0.001$), which turned out to be smaller during running than during walking. Moreover, we found a significant *age* × *condition* interaction effect on DS ($p = 0.0012$); see **Table 2** for overview.

We could not establish significant differences in stride duration between *groups* for walking, while during running stride duration of preschoolers and the school-age group differed significantly from that of the adults ($p = 0.0008$, $p = 0.0061$, respectively, **Figure 1B**). We also found a significant difference in stance duration between the toddlers and both the school-age

TABLE 2 | Linear regression estimates.

	Factor	Estimate	SE	*t*	*p*-value
DS	Intercept	29.59	0.39	74.95	0
	Age	−0.02	0.00	−6.31	4×10^{-10}
	Condition running	−22.79	0.55	−41.20	$<2 \times 10^{-16}$
	Age: Condition running	−0.01	0.00	−3.25	0.0012
FP	Intercept	3.95	0.59	6.82	2×10^{-11}
	Age	0.07	0.00	19.73	$<2 \times 10^{-16}$

DS, double support phase; FP, flight phase; SE, standard error; t, t-statistic.

group and the adults, both during walking ($p = 0.0072$, $p = 0.0077$, respectively) and running ($p = 0.0045$, $p = 0.0003$, respectively). And, the stance duration of preschoolers differed significantly from that in the adults for running ($p = 0.0095$); see **Figure 1C**.

The aforementioned differences are particularly interesting since for dimensionless speed we only found significant differences between toddlers and adults during walking ($p = 0.0027$) and between toddlers and adults during running ($p = 0.0061$); see **Figure 1D**.

Electrophysiology

The ensemble-averaged EMGs of all muscles depicted in **Figure 2A** appeared consistent with those reported in the literature for school-age and adult participants (e.g., Cappellini et al., 2006, 2018; Tirosh et al., 2013; Rozumalski et al., 2017).

During walking, lower leg activity had about the same overall modulation across groups with wider peaks of activity in the toddler group that was reduced in the older groups. Activity patterns in arm muscles were relatively flat during the gait cycle across all groups, while trunk muscles showed a clear modulation with increasing intensity in all the groups, but the adults. The gluteus maximus activity showed only a single major peak in the beginning of the stance phase in the toddlers, while in adults two isolated peaks were present with the additional one being early swing, in agreement with earlier reports (Olree and Vaughan, 1995; Cappellini et al., 2006, 2016; Dominici et al., 2011; Kerkman et al., 2020). Likewise, the erector spinae activity showed a single, prolonged activation peak for about 50% of the gait cycle in the toddlers, whereas in adults we could observe two distinct peaks.

During running, EMG activity increased in all muscles, but most pronounced in the adults' lower extremities. In the toddlers, the EMG patterns of upper trunk muscles largely agreed with those of the other groups, but peak activity was less pronounced. A clear pattern of activation in arm muscles was visible in all groups except toddlers with more consistent EMG activity in the adults. The upper trunk (TRAP and PD) muscles changed from a pattern with two negligible peaks to a pattern with two prominent ones. The lower trunk muscle (ES) changed from a unimodal pattern with a small burst of activity during heel strike to a prominent bimodal pattern with bursts of activity in early stance and mid-swing (**Figure 2A**).

As expected, the most notable differences between the two conditions (instructed walking vs. running) were found in the time lag of peak activity of the calf muscle (MG) toward earlier in the gait cycle during running. The toddlers displayed a significantly smaller shift than the adults ($p = 0.0071$) and, when looking at all groups, there was a clear trend of shift increase with increasing age. The time lag in the toddler group had a mean ($\pm$SD) of $8.8 \pm 8.0\%$ of the gait cycle, where the others' time lags were $16.3 \pm 5.7\%$, $18.5 \pm 7.8\%$, and $20.5 \pm 7.1\%$ (for preschoolers, school-age, and adults, respectively); cf. **Figure 2B**.

For the MG's FWHM we found a decreasing function of age for both instructed walking and running conditions with goodness-of-fit values of $R^2 = 0.26$ and $R^2 = 0.30$, respectively (**Figures 2C,D**).

Last but not least, we found significant differences in the FWHM between groups for eight muscles in the walking condition and six muscles in the running condition (**Figure 2E**). In the lower leg muscles, we found significant differences between the toddler group and the adults (TA: $p = 0.00012$, MG: $p = 0.00011$, BF: $p < 0.00006$) for walking (MG: $p = 0.0017$, BF: $p = 0.0018$) and for running; between the preschoolers and the adults in the TA muscle during walking ($p = 0.0064$) and the MG and BF muscles during running ($p = 0.0009$, $p = 0.00017$, respectively); and between school-age and adults in the BF muscle during running ($p = 0.0048$). In the upper leg muscles the only differences were found in the walking condition between the preschoolers and the adults in the RF, TFL, and GM muscles ($p = 0.0021$, $p = 0.0097$, and $p = 0.009$, respectively). In the lower trunk muscles the ES muscle was significantly different between toddlers and the school-age group, toddlers and adults, the preschoolers and the adults, and finally the school-age children and the adults for walking ($p = 0.002$, $p < 0.00001$, $p = 0.0001$, $p = 0.0085$, respectively) but also the toddlers and preschoolers were significantly different from the adults ($p = 0.0071$, $p = 0.0024$, respectively) during running. The LD was significantly different between all children groups and the adults for walking ($p < 0.00001$, $p = 0.0056$, and $p = 0.0006$, respectively) and between the preschoolers and adults for running ($p = 0.0054$). In the upper trunk muscles the only differences were visible in the running condition with significant differences between the school-age group and adults in AD ($p = 0.00026$), and the toddlers as well as the preschoolers were significant different from the adults in TRAP ($p = 0.0004$, $p = 0.0053$, respectively). No significant differences were found in the arm muscles for any condition.

Number of Synergies

The results for the analysis involving all muscles are illustrated in **Figure 3**. Across participant sides and conditions, PCA revealed that four to eight components were needed to explain 80% of the variance with the highest numbers needed for the walking condition compared to the running condition (**Figure 3A**). In the toddlers walking, 70% of the group required six synergies (range: five-seven), while in the preschoolers and the school-age groups, the majority required seven synergies (50% and 55%, respectively, range: four-seven and five-eight, respectively), and finally in the adult group five-six synergies were needed with 72% requiring five synergies. For running, 80% of the toddlers required six synergies (range: five-six), in the preschoolers 50% of them required six synergies (range: five-seven), and school-age group there was an almost even distribution between participants requiring six and seven synergies (40%, respectively, range: four-seven synergies), whereas in the adults five synergies explained the variance of the data for 70% of the participants, with a range of four-five. After NMF, the percentage of RA remained approximately 70% across groups and conditions (**Figure 3B**) and RA across single muscles exceeded 70% as a group average across conditions.

The results of the lower limb analysis and the number of synergies extracted can be found in **Supplementary Material 1**. Between two and five synergies were needed to explain the variance across all participants and conditions with the majority

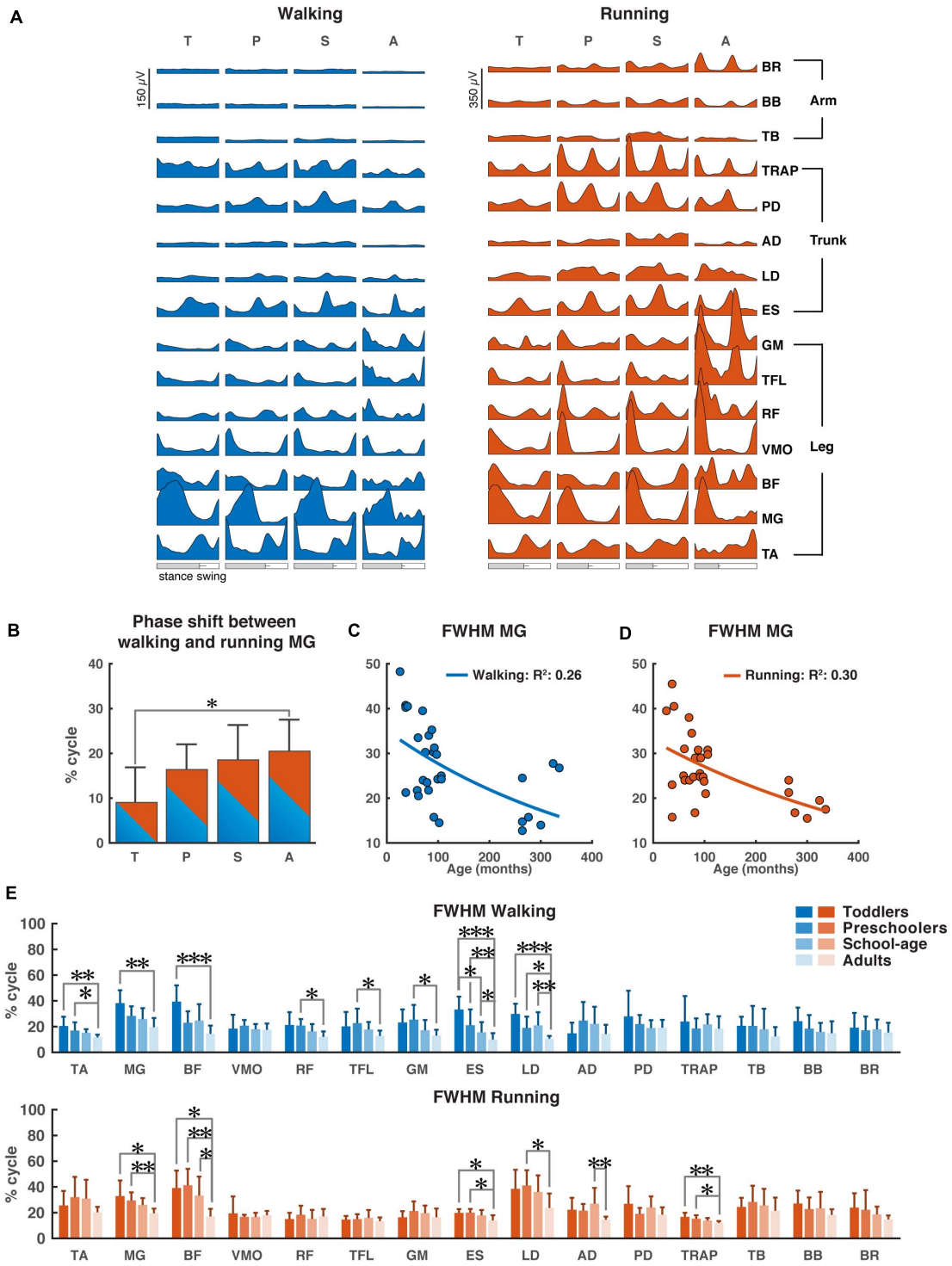

FIGURE 2 | Characteristics of EMG signals. **(A)** Grand averages of 15 EMG activity patterns for walking (blue) and running (red) for all four groups, data are plotted vs. normalized gait cycle, relative duration of stance varied across groups, a bar indicates an amount of variability in the stance phase duration across groups. **(B)** Phase shift between the peak activation of medial gastrocnemius (MG) for walking and running for each group, positive value indicates a lag of walking signal relative to running signal. **(C,D)** Full-width half-maximum (FWHM) of the MG activity as a function of age for walking **(C)** and running **(D)**. Continuous lines represent exponential fittings, note the decrease in values with age. **(E)** FWHM of all muscles (means + SD) for the four groups. TA, tibialis anterior; MG, medial gastrocnemius; BF, biceps femoris; VMO, vastus medialis oblique; RF, rectus femoris; TFL, tensor fascia latae; GM, gluteus maximus; ES, erector spinae; LD, latissimus dorsi; AD, anterior deltoid; PD, posterior deltoid; TRAP, trapezius; TB, triceps brachii; BB, biceps brachii; BR, brachioradialis; T, toddlers; P, preschoolers; S, school-age; A, adults; FWHM, full-width half-maximum. *$p < 0.01$, **$p < 0.001$, and ***$p < 0.0001$.

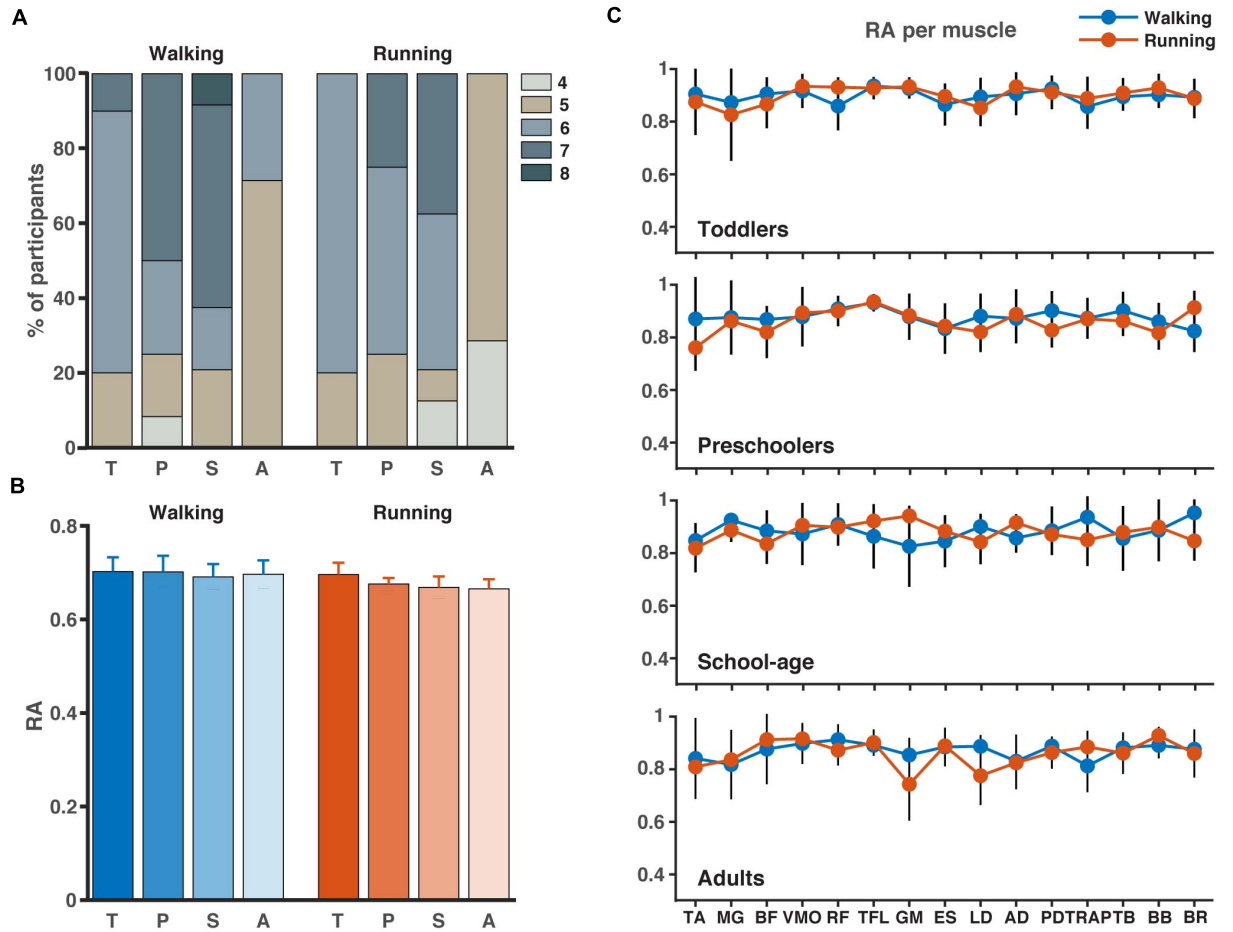

FIGURE 3 | Number of synergies and accuracy. **(A)** Number of synergies needed to account for the cycle-to-cycle variability of EMG activity during walking and running for each group as determined by principal component analysis PCA (>80% of variance). **(B)** The corresponding reconstruction accuracy (RA) after rank-reduction with PCA followed by NMF. **(C)** The RA (mean SD) for each muscle and condition (blue = walking, red = running). TA, tibialis anterior; MG, medial gastrocnemius; BF, biceps femoris; VMO, vastus medialis oblique; RF, rectus femoris; TFL, tensor fascia latae; GM, gluteus maximus; ES, erector spinae; LD, latissimus dorsi; AD, anterior deltoid; PD, posterior deltoid; TRAP, trapezius; TB, triceps brachii; BB, biceps brachii; BR, brachioradialis; T, toddlers; P, preschoolers; S, school-age; A, adults.

of the participants requiring four synergies during walking and the majority requiring three during running. Similarly, to the full-body analysis, the percentage RA on the lower limb analysis varied around 70%.

Structure of Muscle Synergies

Based on the number of muscle synergies identified per participant in the previous section, the activation waveforms and corresponding weighting coefficients were grouped; cf. **Figure 4**. Every waveform showed a peak at a specific moment during the gait cycle. In **Figure 4**, the first waveform for all groups represented the loading response around the foot contact moment. On average, the lower limb muscles among others, the BF, VMO, and GM largely contributed to the first synergy during walking and running in the toddlers, while for the older children and the adults VMO contributed more to it. The second waveform peaked at mid-stance and due to the relatively shorter stance phase for running compared to walking, this pattern was shifted to earlier in the gait cycle during running compared to walking. As expected, this waveform was mostly influenced by the MG (Cappellini et al., 2006). The third waveform peaked prior to foot off in the walking condition across groups, and after foot-off for the running condition except for the toddler group, where it peaked around the foot-off event. This synergy was primarily influenced by the ES and the other trunk and arm muscles during walking and running. The fourth waveform reached its maximum at the early swing and was dominated by the TA muscle, presumably because the foot needs to clear the floor at this moment in the gait cycle, whereas the fifth waveform peaked at the end of swing in preparation for the foot contact. Higher order waveforms, if present, were more variable between participants and less defined when it comes to the main peak: the fifth synergy was not dominated by any particular muscles but predominantly influenced by the trunk and arm muscles, and this applies also to the sixth, seventh, and eighth synergies when present across groups.

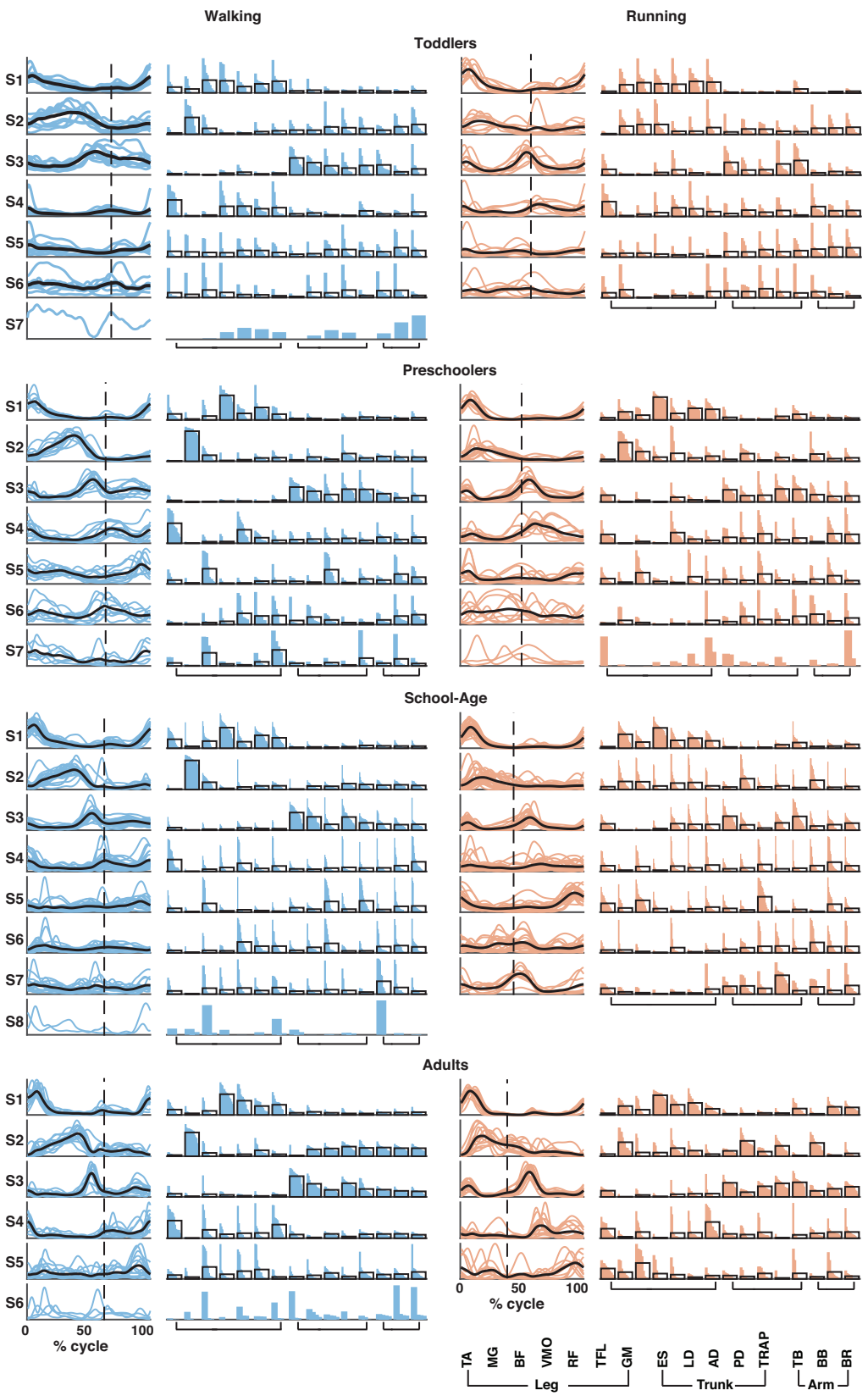

FIGURE 4 | Continued

FIGURE 4 | Muscle synergy structure for the four groups for walking (left; in blue**)** and running (right; in red). Vertical dotted line in activation timing plots represents the end of the stance phase. Each colored line represents a participant side, leading to one line for right side and one line for left side for each participant resulting in a total of (n = 10) for the toddler group, (n = 12) for the preschoolers, (n = 24) for the school-age group, and (n = 14) for the adult group. Black lines represent the mean. Y-axis is in arbitrary units. In the weighting plots, each colored bar represents the weighting coefficient for one participant side, the weightings are ordered based on their size. The black outlines represent the mean for the group. TA, tibialis anterior; MG, gastrocnemius medialis; BF, biceps femoris; VMO, vastus medialis oblique; RF, rectus femoris; TFL, tensor fascia latae; GM, gluteus maximus; ES, erector spinae; LD, latissimus dorsi; AD, anterior deltoid; PD, posterior deltoid; TRAP, trapezius; TB, triceps brachii; BB, biceps brachii; and BR, brachioradialis.

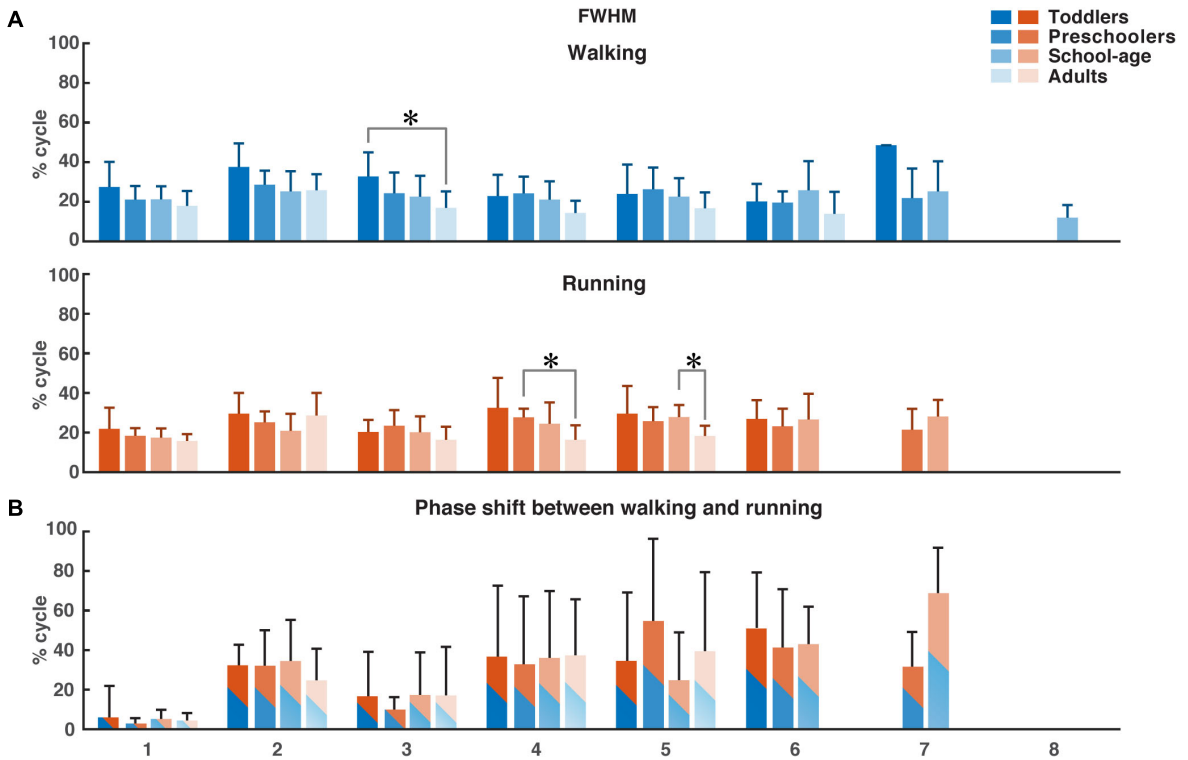

FIGURE 5 | FWHM of consistent activation waveforms and phase shift between walking and running activation waveforms. **(A)** FWHM of all waveforms as a function of the percentage of the gait cycle for each group. Color-coding refer to the groups. **(B)** Phase shift as a function of the gait cycle, determined using the cross-covariance between the waveforms for walking and running. Means and standard deviations are given per group. FWHM, full-width half-maximum. *$p < 0.01$.

Using FWHM for the temporal activation waveforms (**Figure 5**), we found a significant difference between the toddler group and adult group in the third waveform in walking (p = 0.0013). For running, the only significant differences were found in waveform four between the preschoolers and adults (p = 0.0084) and in waveform five between the school-age group and the adults (p = 0.0074). There was a trend toward a larger FWHM in the younger groups for waveform two in walking, and a trend toward a reduction in the FWHM in running with increasing age, but with a similar duration of the FWHM in the adult group compared to the toddlers in running. There were no significant differences between groups for the phase shift of the activation waveforms between walking and running due to the large variabilities between participant sides.

Previous findings in adults from Cappellini et al. (2006) showed a characteristic time lag in the temporal activation pattern corresponding to the second synergy (weighted primarily on the calf muscles) to an early moment in the gait cycle in running compared to walking. We found a similar phase shift in all groups but no significant differences between the four groups.

DISCUSSION

Children make use of a walk-run strategy when learning to run. A weak exponential relationship between age and the FWHM of the MG muscle for both walking and running indicates this muscle to be important for development. We found a varying number of synergies between participant sides when investigating the muscle synergies during comfortable walking and running in 15 leg, trunk, and arm muscles in four age groups. It seems that a smaller number of synergies are active in the toddler group and adult groups compared to the preschoolers and school-age groups. Despite tendencies to wider activation patterns in the youngest groups, there were few significant differences between the groups. Yet, we did not find any significant differences in time

lags between activation patterns between walking and running across the four groups.

Behavioral Results

We found very similar stride duration and normalized speed across groups, with only few significant differences. However, we found several significant differences in the stance duration across groups in the running condition (**Figure 1C**). This difference in stance duration appears correlated to the split of the groups, which was based on the ability to manage the running condition with a FP; cf. **Figure 1A**. Here it seems that a longer stance duration with decreasing age is directly related to the reduced ability to run with a FP.

There are two traditional ways of defining running: having a FP or the kinetic and potential energies of the center of mass being in-phase. Here, we argue that all children were running despite the lack of a FP. That is, they did not have a FP in the instructed running conditions, but their double support phases differ from the double support phases observed during walking (see, e.g., **Table 2**). Hence, we refer to this as making use of a "walk-run strategy." Our previous research into the development of mature running patterns revealed that even in young children walking and running are distinguishable from each other and that a multitude of kinetic and kinematic parameters can serve to discriminate between immature and mature gait patterns (Bach et al., 2021).

Muscle Activity

Tirosh et al. (2013) found that the difference of the peak MG activation for children aged 7–9 years old was around 20% of the gait cycle between walking at comfortable and fast speeds. In this study we found a shift of around 9% of the gait cycle for the toddlers (2–3.5 years), increasing to around 16% for preschoolers (3.5–6.5 years) and 19% for school-age (6.5–9 years). Put differently, the shift between walking and running in our oldest children group was comparable to what Tirosh et al. (2013) found in their study between walking and fast walking. The fast walking speed in the study of Tirosh et al. (2013) were of similar speed as the comfortable running speeds in this study for the oldest children (0.65–0.75 Froude vs. 0.75 Froude in our study).

To test the hypothesis of the existence of a walk-run strategy, we examined the EMG patterns in the children for four types of locomotion: prescribed running with only FP, prescribed running with only DS, prescribed running with a mix of FP and DS within the gait cycle, and prescribed walking (see **Supplementary Material 2**). We found that the EMG patterns corresponding to the prescribed running condition are more similar to each other despite the lack of FP in terms of amplitude and pattern compared to the EMG patterns of the walking condition.

Number of Synergies

When employing the NMF algorithm, certain *post hoc* decisions have to be made, the most important being the number of synergies to run the NMF algorithm over. The most common methods to determine this number is to either apply a threshold or to calculate the "best-linear-fit" (e.g., Cheung et al., 2005; d'Avella et al., 2006). The thresholds are applied to the centered R^2-value (e.g., Delis et al., 2014; Oliveira et al., 2016; Singh et al., 2018; Booth et al., 2019; Santuz et al., 2020; Short et al., 2020), the uncentered R^2-value (e.g., Torres-Oviedo et al., 2006; Kim et al., 2018; Steele et al., 2019), and the RA based on Frobenius norm (Zandvoort et al., 2019; Kerkman et al., 2020). Here, we opted for a different approach in that we first applied a PCA algorithm to the data as the outcome of the PCA is more likely to converge. After applying the PCA with a set threshold of 80% of the variance of the data explained, the data was reconstructed and after this, the NMF algorithm was applied. One may argue that continuing with the PCA rank-reduced data set would be sufficient for a muscle synergy analysis. Following this route, however, may hamper the physiological interpretation of the outcome due to negative weightings and the interpretation of them. When applying NMF, the outcome is constrained to be positive which corresponds to the summation of muscle contractions which by hypothesis are always positive. We confirmed that applying PCA followed by NMF did not greatly influence the amount of signal content lost and as such is a sound approach for the determination of muscle synergies during locomotion tasks.

We hypothesized the muscle synergies for running to "gradually" mature by means of an increased number of synergies. Our data, however, did not reveal this. Instead, we found an increase in the number of synergies with age but with a much larger number of synergies across children groups compared to the adults with a relatively larger number of synergies in the older children compared to the youngest children. Combined with what is known from motor learning and the variability we maintain in the data by concatenating across strides, the large range of synergies needed across groups and conditions to explain the variance of the data seems related to motor learning and optimizing the locomotion pattern. This is also visible in the relatively larger percentage of participant sides in the preschoolers and school-age groups needing more than six synergies in the walking condition and in the same two groups in the running condition. The relatively larger number of synergies required to explain the same variation could be due to exploration and motor learning where the lack of this increase in the toddler group could be due to the use of a "simpler" locomotor strategy to manage the tasks (Dominici et al., 2010). Adults have fine-tuned their locomotion patterns and thus we see a comparatively low number of synergies across all participant sides and conditions. The duration of the peaks of the activation patterns computed using the FWHM confirm this finding, that we consider a trend toward activation bursts for all synergies and conditions compared to the adults, who have indeed the same number of synergies as the toddlers. Another reason for the different number of synergies across groups could be due to splitting of synergies, also known as fractionization. It has been found that children aged 3–5 years, all with the ability to run over ground with a FP, show synergies that later split into more synergies for novice adult runners (Cheung et al., 2020). Likewise, the study also showed that from sedentary adults to elite adult runners, a merging of synergies occurred, which suggests that with experience, a smaller number of synergies are needed

as a larger number of muscles is represented in each synergy. That is confirmed with the findings of this study. We found an increase in number of synergies from the toddlers to the school-age group, and a subsequent decrease of the number of synergies in the adult group.

Structure of Muscle Synergies

We focused the analysis on all 15 muscles recorded from the lower limb, trunk, and upper limb, but also carried out an analysis on a subset of these muscles in order to confirm the findings from the literature where the main focus is often on the lower limb muscles (**Supplementary Material 1**). We found that the number of synergies across groups were much lower and comparable to what has previously been found in walking in children and adults (e.g., Dominici et al., 2011; Oliveira et al., 2016; Hinnekens et al., 2020; Mileti et al., 2020; Sylos-Labini et al., 2020) where four synergies is one of the most common findings. The activation patterns and the weighting coefficients were also comparable to what has previously been found in literature. The FWHM had smaller variability within groups which suggests that the variability we observed in the full-body analysis was due to the larger set of muscles and the possible larger contribution of the trunk and arm muscles to the waveforms.

In the synergy results of the full-body analysis there was large variability in the activation patterns and the weightings within groups. These large variabilities were participant-specific and we hypothesized that they may be related to motor-learning: children are exploring their own abilities to be able to run on a treadmill. In the adult patterns, there were a few outliers in every synergy in both activation patterns and weightings, but in general, the results were robust across participants.

There were significant differences in especially the stance duration between groups influencing the appearance of the muscle synergies. The FWHM of the synergies that appeared not significantly different between groups as a function of the full gait cycle might be considered different when identifying the relatively longer stance duration in the toddler group as running. Yet, there were fewer significant differences in the FWHM when expressed as a function of the stance duration (see **Supplementary Material 3**). Despite the relative differences in the stance duration for especially running, this suggests that the FWHM of the synergies did not depend on the duration of the stance phase and that differences between groups did not increase when taking the altered stance duration into account.

In the EMG signals the phase shift of the peak MG muscle activity was significantly smaller in the toddler group compared to the other groups. We expected that this would also be visible in the synergy analysis. However, we do not find any statistically significant differences in the phase shift between groups for the activation pattern (S2), commonly reported to relate to the shank muscles. In the walking conditions, the MG muscle activity clearly dominated the second synergy. In the running conditions, however, the MG muscle activity was frequently split between the first and the second synergy. This might explain why the influence of the shift in the single muscle analysis did not come to the fore in the synergy analysis.

Limitations

One limitation in this study is the large gap in age between the participant of 40 and 59 months where, for several reasons, it was not possible to recruit and measure any children. We do not expect having this data would have changed the outcomes significantly, but it would have given a larger insight into the development of running on a treadmill in this age as well.

All children in the toddler group were assisted not only with the harness during treadmill locomotion but also with handhold from either a researcher or their parent/guardian. This did not apply to any children in any of the other groups. We verified with the recorded ground reaction forces that there were no added effects of handhold compared to the harness but the effect is present in the arm muscles on the side of the handhold as there will be less muscle activity compared to the other side. We indirectly corrected for this in the analysis by normalizing the muscle activity, not to the maximum activation for that particular muscle, but to the mean activity of that muscle. By normalizing to the mean activity of all muscles, we ensured that even muscles with low activity would not dominate the muscle synergy analysis.

Finally, all conditions referred to in this study are the prescribed conditions. This means, that the participant themselves confirmed the recorded speed was comfortable walking or running speed for them. We confirm in the Froude values that there are only significant differences between the walking speed for the toddler and adult group and the running speed between the toddler and school-age group. We also confirm that there are significant differences between the prescribed walking and running conditions for all groups ($p = 0.0039$, $p = 0.009$, $p = 3.2{\cdot}10^{-5}$, $p = 0.0017$, respectively).

Conclusion

Children follow a walk-run strategy when learning to run on a treadmill. Older children incorporate exploratory muscle synergies when "optimizing" their walking and running pattern on the treadmill whereas the youngest children below 3.5 years of age make use of a "simpler" motor control pattern trending toward larger bursts of activation. We believe that the increase in the number of muscle synergies for individual participant sides relates to motor learning and exploration.

DATA AVAILABILITY STATEMENT

The datasets generated for this study are available on request to the corresponding author.

ETHICS STATEMENT

The studies involving human participants were reviewed and approved by the Scientific and Ethical Review Board of the Faculty of Behavioral Movement Sciences, Vrije Universiteit Amsterdam, Netherlands (file number: VCWE-2016-149R1). Written informed consent to participate in this study was

provided by the adult participants or the legal guardian/next of kin of the children participants.

AUTHOR CONTRIBUTIONS

MB and ND conceived and designed research. MB conducted experiments. MB, AD, and ND analyzed the data. The first draft of the manuscript was written by MB and all authors commented on previous versions of the manuscript. All authors read and approved the final manuscript.

FUNDING

This project has received funding from the European Research Council (ERC) under the European Union's Horizon 2020 Research and Innovation Program under grant agreement no. 715945 Learn2Walk and from the Dutch Organization for Scientific Research (NWO) VIDI grant (016.156.346 FirSTeps).

ACKNOWLEDGMENTS

We would like to thank Annike Bekius and Jennifer N. Kerkman with their help during data acquisition and all participants for their participation in the study.

SUPPLEMENTARY MATERIAL

The Supplementary Material for this article can be found online at: https://www.frontiersin.org/articles/10.3389/fnhum.2021.637157/full#supplementary-material

REFERENCES

Alexander, R. M., and Jayes, A. S. (1983). A dynamic similarity hypothesis for the gaits of quadrupedal mammals. *J. Zool.* 201, 135–152.

Bach, M. M., Daffertshofer, A., and Dominici, N. (2021). The development of mature gait patterns in children during walking and running. *Eur. J. Appl. Physiol.* 121, 1073–1085. doi: 10.1007/s00421-020-04592-2

Bernstein, N. (1967). *The Co-Ordination and Regulation of Movements*. Pergamon: Oxford.

Berry, M. W., Browne, M., Langville, A. N., Pauca, V. P., and Plemmons, R. J. (2007). Algorithms and applications for approximate nonnegative matrix factorization. *Comput. Stat. Data Anal.* 52, 155–173. doi: 10.1016/j.csda.2006.11.006

Bizzi, E., and Cheung, V. C. (2013). The neural origin of muscle synergies. *Front. Comput. Neurosci.* 7:51. doi: 10.3389/fncom.2013.00051

Boonstra, T. W., Danna-Dos-Santos, A., Xie, H. B., Roerdink, M., Stins, J. F., and Breakspear, M. (2015). Muscle networks: connectivity analysis of EMG activity during postural control. *Sci. Rep.* 5:17830. doi: 10.1038/srep17830

Booth, A. T. C., van der Krogt, M. M., Harlaar, J., Dominici, N., and Buizer, A. I. (2019). Muscle synergies in response to biofeedback-driven gait adaptations in children with cerebral palsy. *Front. Physiol.* 10:1208. doi: 10.3389/fphys.2019.01208

Cappellini, G., Ivanenko, Y. P., Martino, G., MacLellan, M. J., Sacco, A., Morelli, D., et al. (2016). Immature spinal locomotor output in children with cerebral palsy. *Front. Physiol.* 7:478. doi: 10.3389/fphys.2016.00478

Cappellini, G., Ivanenko, Y. P., Poppele, R. E., and Lacquaniti, F. (2006). Motor patterns in human walking and running. *J. Neurophysiol.* 95, 3426–3437. doi: 10.1152/jn.00081.2006

Cappellini, G., Sylos-Labini, F., MacLellan, M. J., Sacco, A., Morelli, D., Lacquaniti, F., et al. (2018). Backward walking highlights gait asymmetries in children with cerebral palsy. *J. Neurophysiol.* 119, 1153–1165. doi: 10.1152/jn.00679.2017

Cheung, V. C. K., Cheung, B. M. F., Zhang, J. H., Chan, Z. Y. S., Ha, S. C. W., Chen, C. Y., et al. (2020). Plasticity of muscle synergies through fractionation and merging during development and training of human runners. *Nat. Commun.* 11:4356. doi: 10.1038/s41467-020-18210-4

Cheung, V. C., d'Avella, A., Tresch, M. C., and Bizzi, E. (2005). Central and sensory contributions to the activation and organization of muscle synergies during natural motor behaviors. *J. Neurosci.* 25, 6419–6434. doi: 10.1523/JNEUROSCI.4904-04.2005

Clark, D. J., Ting, L. H., Zajac, F. E., Neptune, R. R., and Kautz, S. A. (2010). Merging of healthy motor modules predicts reduced locomotor performance and muscle coordination complexity post-stroke. *J. Neurophysiol.* 103, 844–857. doi: 10.1152/jn.00825.2009

d'Avella, A., Portone, A., Fernandez, L., and Lacquaniti, F. (2006). Control of fast-reaching movements by muscle synergy combinations. *J. Neurosci.* 26, 7791–7810. doi: 10.1523/JNEUROSCI.0830-06.2006

d'Avella, A., Saltiel, P., and Bizzi, E. (2003). Combinations of muscle synergies in the construction of a natural motor behavior. *Nat. Neurosci.* 6, 300–308. doi: 10.1038/nn1010

De Luca, C. J., Gilmore, L. D., Kuznetsov, M., and Roy, S. H. (2010). Filtering the surface EMG signal: movement artifact and baseline noise contamination. *J. Biomech.* 43, 1573–1579. doi: 10.1016/j.jbiomech.2010.01.027

Delis, I., Panzeri, S., Pozzo, T., and Berret, B. (2014). A unifying model of concurrent spatial and temporal modularity in muscle activity. *J. Neurophysiol.* 111, 675–693. doi: 10.1152/jn.00245.2013

Dominici, N., Ivanenko, Y. P., Cappellini, G., d'Avella, A., Mondi, V., Cicchese, M., et al. (2011). Locomotor primitives in newborn babies and their development. *Science* 334, 997–999. doi: 10.1126/science.1210617

Dominici, N., Ivanenko, Y. P., Cappellini, G., Zampagni, M. L., and Lacquaniti, F. (2010). Kinematic strategies in newly walking toddlers stepping over different support surfaces. *J. Neurophysiol.* 103, 1673–1684. doi: 10.1152/jn.00945.2009

Goudriaan, M., Shuman, B. R., Steele, K. M., Van den Hauwe, M., Goemans, N., Molenaers, G., et al. (2018). Non-neural muscle weakness has limited influence on complexity of motor control during gait. *Front. Hum. Neurosci.* 12:5. doi: 10.3389/fnhum.2018.00005

Hagio, S., Fukuda, M., and Kouzaki, M. (2015). Identification of muscle synergies associated with gait transition in humans. *Front. Hum. Neurosci.* 9:48. doi: 10.3389/fnhum.2015.00048

Halaki, M., and Gi, K. (2012). "Chapter 7 normalization of EMG signals: to normalize or not to normalize and what to normalize to?" in *Computational Intelligence in Electromyography Analysis – A Perspective on Current Applications and Future Challenges*, ed. G. R. Naik (Rijeka: InTech), 175–194.

Hermens, H. J., Freriks, B., Merletti, R., Stegeman, D., Blok, J., Rau, G., et al. (1999). European recommendations for surface electromyography. *Roessingh Res. Dev.* 8, 13–54.

Hinnekens, E., Berret, B., Do, M. C., and Teulier, C. (2020). Modularity underlying the performance of unusual locomotor tasks inspired by developmental milestones. *J. Neurophysiol.* 123, 496–510. doi: 10.1152/jn.00662.2019

Ivanenko, Y. P., Cappellini, G., Poppele, R. E., and Lacquaniti, F. (2008). Spatiotemporal organization of alpha-motoneuron activity in the human spinal cord during different gaits and gait transitions. *Eur. J. Neurosci.* 27, 3351–3368. doi: 10.1111/j.1460-9568.2008.06289.x

Ivanenko, Y. P., Dominici, N., Cappellini, G., Dan, B., Cheron, G., and Lacquaniti, F. (2004a). Development of pendulum mechanism and kinematic coordination from the first unsupported steps in toddlers. *J. Exp. Biol.* 207(Pt 21), 3797–3810. doi: 10.1242/jeb.01214

Ivanenko, Y. P., Poppele, R. E., and Lacquaniti, F. (2004b). Five basic muscle activation patterns account for muscle activity during human locomotion. *J. Physiol.* 556(Pt 1), 267–282. doi: 10.1113/jphysiol.2003.057174

Kerkman, J. N., Bekius, A., Boonstra, T. W., Daffertshofer, A., and Dominici, N. (2020). Muscle synergies and coherence networks reflect different modes of

coordination during walking. *Front. Physiol.* 11:751. doi: 10.3389/fphys.2020.00751

Kim, Y., Bulea, T. C., and Damiano, D. L. (2018). Children with cerebral palsy have greater stride-to-stride variability of muscle synergies during gait than typically developing children: implications for motor control complexity. *Neurorehabil. Neural Repair* 32, 834–844.

Lee, D. D., and Seung, H. S. (1999). Learning the parts of objects by non-negative matrix factorization. *Nature* 401, 788–791. doi: 10.1038/44565

Mileti, I., Serra, A., Wolf, N., Munoz-Martel, V., Ekizos, A., Palermo, E., et al. (2020). Muscle activation patterns are more constrained and regular in treadmill than in overground human locomotion. *Front. Bioeng. Biotechnol.* 8:581619. doi: 10.3389/fbioe.2020.581619

Nelson-Wong, E., Howarth, S., Winter, D. A., and Callaghan, J. P. (2009). Application of autocorrelation and cross-correlation analyses in human movement and rehabilitation research. *J. Orthop. Sports Phys. Ther.* 39, 287–295. doi: 10.2519/jospt.2009.2969

Oliveira, A. S., Gizzi, L., Farina, D., and Kersting, U. G. (2014). Motor modules of human locomotion: influence of EMG averaging, concatenation, and number of step cycles. *Front. Hum. Neurosci.* 8:335. doi: 10.3389/fnhum.2014.00335

Oliveira, A. S., Gizzi, L., Ketabi, S., Farina, D., and Kersting, U. G. (2016). Modular control of treadmill vs overground running. *PLoS One* 11:e0153307. doi: 10.1371/journal.pone.0153307

Olree, K. S., and Vaughan, C. L. (1995). Fundamental patterns of bilateral muscle activity in human locomotion. *Biol. Cybern.* 73, 409–414. doi: 10.1007/BF00201475

Rabbi, M. F., Pizzolato, C., Lloyd, D. G., Carty, C. P., Devaprakash, D., and Diamond, L. E. (2020). Non-negative matrix factorisation is the most appropriate method for extraction of muscle synergies in walking and running. *Sci. Rep.* 10:8266. doi: 10.1038/s41598-020-65257-w

Roerdink, M., Coolen, B. H., Clairbois, B. H., Lamoth, C. J., and Beek, P. J. (2008). Online gait event detection using a large force platform embedded in a treadmill. *J. Biomech.* 41, 2628–2632. doi: 10.1016/j.jbiomech.2008.06.023

Rozumalski, A., Novacheck, T. F., Griffith, C. J., Walt, K., and Schwartz, M. H. (2015). Treadmill vs. overground running gait during childhood: a qualitative and quantitative analysis. *Gait Posture* 41, 613–618. doi: 10.1016/j.gaitpost.2015.01.006

Rozumalski, A., Steele, K. M., and Schwartz, M. H. (2017). Muscle synergies are similar when typically developing children walk on a treadmill at different speeds and slopes. *J. Biomech.* 64, 112–119. doi: 10.1016/j.jbiomech.2017.09.002

Santuz, A., Brull, L., Ekizos, A., Schroll, A., Eckardt, N., Kibele, A., et al. (2020). Neuromotor dynamics of human locomotion in challenging settings. *iScience* 23:100796. doi: 10.1016/j.isci.2019.100796

Savitzky, A., and Golay, M. J. E. (1964). Smoothing and differentiation of data by simplified least squares procedures. *Anal. Chem.* 36, 1627–1639. doi: 10.1021/ac60214a047

Short, M. R., Damiano, D. L., Kim, Y., and Bulea, T. C. (2020). Children with unilateral cerebral palsy utilize more cortical resources for similar motor output during treadmill gait. *Front. Hum. Neurosci.* 14:36. doi: 10.3389/fnhum.2020.00036

Singh, R. E., Iqbal, K., White, G., and Hutchinson, T. E. (2018). A systematic review on muscle synergies: from building blocks of motor behavior to a neurorehabilitation tool. *Appl. Bionics Biomech.* 2018:3615368. doi: 10.1155/2018/3615368

Steele, K. M., Munger, M. E., Peters, K. M., Shuman, B. R., and Schwartz, M. H. (2019). Repeatability of electromyography recordings and muscle synergies during gait among children with cerebral palsy. *Gait Posture* 67, 290–295. doi: 10.1016/j.gaitpost.2018.10.009

Steele, K. M., Tresch, M. C., and Perreault, E. J. (2015). Consequences of biomechanically constrained tasks in the design and interpretation of synergy analyses. *J. Neurophysiol.* 113, 2102–2113. doi: 10.1152/jn.00769.2013

Sylos-Labini, F., La Scaleia, V., Cappellini, G., Fabiano, A., Picone, S., Keshishian, E. S., et al. (2020). Distinct locomotor precursors in newborn babies. *Proc. Natl. Acad. Sci. U.S.A.* 117, 9604–9612. doi: 10.1073/pnas.1920984117

Ting, L. H., and Macpherson, J. M. (2005). A limited set of muscle synergies for force control during a postural task. *J. Neurophysiol.* 93, 609–613. doi: 10.1152/jn.00681.2004

Tirosh, O., Sangeux, M., Wong, M., Thomason, P., and Graham, H. K. (2013). Walking speed effects on the lower limb electromyographic variability of healthy children aged 7-16 years. *J. Electromyogr. Kinesiol.* 23, 1451–1459. doi: 10.1016/j.jelekin.2013.06.002

Torres-Oviedo, G., Macpherson, J. M., and Ting, L. H. (2006). Muscle synergy organization is robust across a variety of postural perturbations. *J. Neurophysiol.* 96, 1530–1546. doi: 10.1152/jn.00810.2005

Torricelli, D., Pajaro, M., Lerma, S., Marquez, E., Martinez, I., Barroso, F., et al. (2014). "Modular control of crouch gait in spastic cerebral palsy," in *Proceedings of the XIII Mediterranean Conference on Medical and Biological Engineering and Computing 2013*, ed. L. Roa Romero (Cham: Springer), 1718–1721.

Tresch, M. C., Cheung, V. C., and d'Avella, A. (2006). Matrix factorization algorithms for the identification of muscle synergies: evaluation on simulated and experimental data sets. *J. Neurophysiol.* 95, 2199–2212. doi: 10.1152/jn.00222.2005

Vasudevan, E. V., Patrick, S. K., and Yang, J. F. (2016). Gait transitions in human infants: coping with extremes of treadmill speed. *PLoS One* 11:e0148124. doi: 10.1371/journal.pone.0148124

Willigenburg, N. W., Daffertshofer, A., Kingma, I., and van Dieen, J. H. (2012). Removing ECG contamination from EMG recordings: a comparison of ICA-based and other filtering procedures. *J. Electromyogr. Kinesiol.* 22, 485–493. doi: 10.1016/j.jelekin.2012.01.001

Yokoyama, H., Ogawa, T., Kawashima, N., Shinya, M., and Nakazawa, K. (2016). Distinct sets of locomotor modules control the speed and modes of human locomotion. *Sci. Rep.* 6:36275. doi: 10.1038/srep36275

Zandvoort, C. S., van Dieen, J. H., Dominici, N., and Daffertshofer, A. (2019). The human sensorimotor cortex fosters muscle synergies through cortico-synergy coherence. *Neuroimage* 199, 30–37. doi: 10.1016/j.neuroimage.2019.05.041

Conflict of Interest: The authors declare that the research was conducted in the absence of any commercial or financial relationships that could be construed as a potential conflict of interest.

frontiers in Human Neuroscience

ORIGINAL RESEARCH
published: 24 May 2021
doi: 10.3389/fnhum.2021.669059

In-Bed Sensorimotor Rehabilitation in Early and Late Subacute Stroke Using a Wearable Elbow Robot: A Pilot Study

Mei Zhen Huang[1], *Yong-Soon Yoon*[2], *Jisu Yang*[3], *Chung-Yong Yang*[1,4] *and Li-Qun Zhang*[1,5,6]*

[1]Department of Physical Therapy and Rehabilitation Science, School of Medicine, University of Maryland, Baltimore, MD, United States, [2]Department of Rehabilitation Medicine, Presbyterian Medical Center, Jeonbuk, South Korea, [3]Department of Neuroscience and Behavioral Biology, College of Arts and Sciences, Emory University, Atlanta, GA, United States, [4]Department of Physical Medicine and Rehabilitation, The Seum Hospital, Jeonbuk, South Korea, [5]Department of Orthopaedics, University of Maryland, Baltimore, MD, United States, [6]Department of Bioengineering, University of Maryland, College Park, MD, United States

OPEN ACCESS

Edited by:
Taiar Redha,
Université de Reims Champagne-Ardenne, France

Reviewed by:
Noureddin Nakhostin Ansari,
Tehran University of Medical Sciences, Iran
Augusto Fusco,
Fondazione Policlinico Universitario A. Gemelli IRCCS, Italy

***Correspondence:**
Li-Qun Zhang
l-zhang@som.umaryland.edu

Specialty section:
This article was submitted to Motor Neuroscience, a section of the journal Frontiers in Human Neuroscience

Received: 17 February 2021
Accepted: 13 April 2021
Published: 24 May 2021

Citation:
Huang MZ, Yoon Y-S, Yang J, Yang C-Y and Zhang L-Q (2021) In-Bed Sensorimotor Rehabilitation in Early and Late Subacute Stroke Using a Wearable Elbow Robot: A Pilot Study. Front. Hum. Neurosci. 15:669059. doi: 10.3389/fnhum.2021.669059

Objects: To evaluate the feasibility and effectiveness of in-bed wearable elbow robot training for motor recovery in patients with early and late subacute stroke.

Methods: Eleven in-patient stroke survivors (male/female: 7/4, age: 50.7 ± 10.6 years, post-stroke duration: 2.6 ± 1.9 months) received 15 sessions of training over about 4 weeks of hospital stay. During each hourly training, participants received passive stretching and active movement training with motivating games using a wearable elbow rehabilitation robot. Isometric maximum muscle strength (MVC) of elbow flexors and extensors was evaluated using the robot at the beginning and end of each training session. Clinical measures including Fugl-Meyer Assessment of upper extremity (FMA-UE), Motricity Index (MI) for upper extremities, Modified Ashworth Scale (MAS) were measured at baseline, after the 4-week training program, and at a 1-month follow-up. The muscle strength recovery curve over the training period was characterized as a logarithmic learning curve with three parameters (i.e., initial muscle strength, rate of improvement, and number of the training session).

Results: At the baseline, participants had moderate to severe upper limb motor impairment {FMA-UE [median (interquartile range)]: 28 (18–45)} and mild spasticity in elbow flexors {MAS [median (interquartile range)]: 0 (0–1)}. After about 4 weeks of training, significant improvements were observed in FMA-UE (p = 0.003) and MI (p = 0.005), and the improvements were sustained at the follow-up. The elbow flexors MVC significantly increased by 1.93 Nm (95% CI: 0.93 to 2.93 Nm, p = 0.017) and the elbow extensor MVC increased by 0.68 Nm (95% CI: 0.05 to 1.98 Nm, p = 0.036). Muscle strength recovery curve showed that patients with severe upper limb motor impairment had a greater improvement rate in elbow flexor strength than those with moderate motor impairment.

Conclusion: In-bed wearable elbow robotic rehabilitation is feasible and effective in improving biomechanical and clinical outcomes for early and late subacute stroke in-patients. Results from the pilot study suggested that patients with severe upper limb motor impairment may benefit more from the robot training compared to those with moderate impairment.

Keywords: stroke rehabilitation, robot, recovery time course, upper limbs, subacute stroke

INTRODUCTION

Stroke is the leading cause of long-term disability among adults in the United States (Virani et al., 2020) and worldwide (Johnson et al., 2016). More than 795,000 people suffer a stroke in the United States each year (Virani et al., 2020), and nearly three-quarters of all strokes occur in people over the age of 65 (Virani et al., 2020). With an ever-increasing elderly population, the stroke will continue to be a major health issue (Virani et al., 2020). Up to 70% of stroke survivors have hemiparesis affecting the upper extremity and about two-thirds of the stroke survivors demonstrate a long-term reduction in upper limb motor function (Kwakkel et al., 2003; Lee et al., 2015), which restrict their ability to perform everyday activities, reduce productivity, and limit social activities (Buma et al., 2013; Lee et al., 2015; Johnson et al., 2016; Virani et al., 2020). Improving upper limb function is a core element of stroke rehabilitation needed to maximize patient outcomes and reduce disability.

The first few months post-stroke are critical for motor recovery (O'dwyer et al., 1996; Kwakkel et al., 2003; Krakauer, 2006; Mirbagheri et al., 2009; Lee et al., 2015; Winstein et al., 2016; Kundert et al., 2019), when neural circuits reorganization, including spontaneous recovery and learning–dependent processes, dominate during the acute and subacute stages (Kwakkel et al., 2003; Krakauer, 2006; Lee et al., 2015). However, multiple studies worldwide have shown that for hospitalized stroke patients, 50–70% of the daytime they were inactive in their ward (Bernhardt et al., 2004; Lang et al., 2007; West and Bernhardt, 2012; Luker et al., 2015), and the time to receive physical therapy and occupational therapy was estimated to be less than 3 h per day (Bernhardt et al., 2004; West and Bernhardt, 2012). The duration of the therapeutic session was about 30 min, while the repetition for passive and active movement in the upper limb was about 33–50 (Lang et al., 2009). Moreover, observation showed that affected upper extremity use is minimal (3.3 ± 1.8 h) during the inpatient rehabilitation stay (Lang et al., 2007). Patients with severe motor impairment may have few engagements in the physical activity and intervention for the affected limb (Luker et al., 2015). However, it has been widely recognized that the effective way to promote neuroplasticity and functional motor recovery poststroke is intensive treatments (Buma et al., 2013) through specific functional (Van Peppen et al., 2004) and repetitive motor tasks (French et al., 2016). Apparently, most of the current inpatient stroke rehabilitation interventions cannot provide the desired training.

Over the past two decades, rehabilitation robots, with the capability to increase the number of movement repetitions in a given time compared to conventional therapy and provide individualized foundational tasks without requiring constant therapist involvement, have gained much attention in stroke rehabilitation (Volpe et al., 2000; Veerbeek et al., 2017). Moreover, robotic devices may also provide a timely quantitative and sensitive evaluation of the biomechanical performance of the patients (Ren et al., 2017), which can aid clinicians to manage the rehabilitation program and optimize the treatment goals for individual patients.

Despite increasing literature were presented, the effectiveness of robotics for rehabilitation in upper limb motor poststroke rehabilitation remains inconclusive (Bertani et al., 2017; Veerbeek et al., 2017; Ferreira et al., 2018; Mehrholz et al., 2018; Chien et al., 2020). Robotic therapy adjunct to standard-intensity conventional therapy was more beneficial than standard intensity conventional therapy alone (Bertani et al., 2017; Veerbeek et al., 2017; Ferreira et al., 2018; Mehrholz et al., 2018). However, the meta-analysis also suggested that under similar training intensity, the improvement of upper limb function was comparable between robotic therapy and conventional therapy for stroke survivors (Veerbeek et al., 2017; Ferreira et al., 2018; Chien et al., 2020). It should be noted that those meta-analysis results derived in the aggregate of the general stroke population may not provide the best evidence of practice for stroke survivors with different levels of impairments (Winstein et al., 2016). Recent robotic rehabilitation studies reported that chronic stroke survivors with moderate deficits achieved greater improvement in motor function from robot-assisted upper limb training than those with mild motor deficits (Hsieh et al., 2012; Takahashi et al., 2016; Takebayashi et al., 2020). Therefore, stratification of stroke participants based on the impairment level is important in terms of estimating the recovery pattern and prognostication of outcomes (Veerbeek et al., 2017). Moreover, research in robotic training in early stroke rehabilitation is still scarce, particularly for the elbow joint. Elbow extension/flexion is essential for upper limb function such as reaching and grasping, while the elbow joint is also the most common and long-lasting affected post-stroke (Roby-Brami et al., 2003). To our knowledge, there is a lack of available exoskeleton robots targeting the elbow joint for in-bed stroke rehabilitation. Most of the existing exoskeleton robots are complex and expensive (Veerbeek et al., 2017) that limits their application in the in-patient clinical setting. Meanwhile, an end-factor controlled robot may not be suitable for subacute patients with moderate and severe upper limb control. As an alternative, a portable exoskeleton elbow robot would be beneficial for in-patient upper limb rehabilitation. Motivated by the unmet need, we have developed a wearable elbow robot that can provide both passive stretching and active game-based training. The active and passive robotic training

modalities have been suggested to be feasible and effective in ankle rehabilitation post-stroke (Ren et al., 2017).

The purpose of the present study was to conduct in-patient rehabilitation training on subacute stroke survivors with moderate and severe upper limb motor impairment using a wearable elbow rehabilitation robot. We aimed to: (1) evaluate the feasibility and effectiveness of a wearable elbow robotic device in subacute stroke in-bed training; and (2) investigate the active motor recovery patterns of stroke survivors with severe and moderate levels of motor impairments. It was assumed that: (1) a 4-week in-bed robot-guided training would improve elbow biomechanical properties and motor function; (2) patients with different motor impairment levels at the baseline would have different motor recovery patterns.

MATERIALS AND METHODS

Participants

Patients with early subacute (7 days to 3 months post-stroke) and late subacute (3–6 months) stroke were enrolled in this study (Bernhardt et al., 2017). Inclusion criteria were: (1) age of 18–79 years old; (2) first episode of stroke verified through computed tomography or magnetic resonance imaging; (3) within 6 months post-stroke with impaired elbow motor function (grading of hemiplegic elbow joint Medical Research Council <4), (4) absence of any medical contraindication to exercise; (5) no gross visuospatial or visual field deficits which interfered with feedback training using a computer monitor; (6) the ability to understand and follow oral instructions (follow direction by order obey ≥ 1 step); and (7) medically stable.

Exclusion criteria were: (1) traumatic brain injury; (2) subarachnoid hemorrhage or lacunar infarct without apparent hemiplegia or hemiparesis; (3) previous upper limb amputation; (4) previous musculoskeletal problems on the impaired side including severe arthropathy, arthritis, or complicated orthopedic surgery on either side; (5) other degenerative neurologic problems such as Parkinsonism, Alzheimer's dementia, or known other dementia; (6) skin lesion, acute infection on application site of the robotic arm; and (7) multiple stroke with neurological sequelae. The study was carried out in conformity with the Declaration of Helsinki; all patients gave their informed consent to participate in the study, which had been approved by the local scientific and ethics committees.

The Wearable Elbow Robot Device

A wearable elbow robot (Rehabtek LLC, Linthicum Heights, MD, USA) with audiovisual feedback was used for the in-bed elbow movement training (**Figure 1A**). The exoskeleton robot included the upper arm and forearm braces, a servomotor (EC-4 poles, 120W, Maxon Powermax, Sachseln, Switzerland) with a gearhead (GP32C, ratio 86:1, Maxon Powermax, Sachseln, Switzerland) and a bevel gear with a ratio of 3:1. The driving linkage was connected to the forearm brace through a force sensor (MLP-50, nonlinearity 0.05 lb, Transducer Techniques, Temecula, CA, USA) to determine the elbow joint torque. The output axis of the bevel gear was aligned with the elbow flexion axis and flexed/extended the elbow joint through the force sensor and forearm brace.

The wearable robot was designed to provide passive stretching, game-based active movement training with the assist-as-needed scheme, and evaluation of biomechanical properties, including muscle strength and elbow range of motion. The wearable robot was interfaced through a touchscreen computer for display and user interface (**Figure 1B**). The user interface allowed adjustment of the applied torque value, movement velocity, and difficulty levels of the active movement games, such as assistance or resistance level (i.e., assisted-as-needed scheme) according to the patient's ability.

Elbow Robot Training Set-Up and Procedures

Patients lay supine in bed and wore the wearable robot on the paretic arm, with the shoulder at about 30-degree flexion and 15-degree abduction. The elbow robot was carefully mounted on the affected elbow with the brace adjusted to align the elbow flexion axis along with the wearable robot output axis (**Figure 1A**). The computer monitor was put in front of the patient with height and angle adjusted for proper viewing (**Figure 1B**). To determine a safe range of robot movement, the operator manually moved the elbow to its end of flexion/extension within the tolerance of patients.

The training procedures are shown in **Figure 2**. Each training session typically consisted of passive intelligent stretching of the elbow (15 min), active-assisted and/or resisted movement training through movement gameplay (15 min), and passive intelligent stretching for cool down (15 min). Elbow active range of motion (ROM) and maximum isometric voluntary contraction (MVC) of elbow flexors and extensors were measured before and after each session of training. The training protocol would be adjusted individually to accommodate the condition of patients with severe hemiplegia including more passive stretching and less active movement training while therapy intensity was maintained $\sim$150 repetitions of elbow flexion/extension passively or actively.

During the passive intelligent stretching, the forearm was passively moved by the robot in the sagittal plane at 30–40°/s. As the resistance may increase near the extreme positions of the elbow joint, the robot gradually slowed down to stretch the muscle-tendon complex slowly and safely (Ren et al., 2017). Once a predefined peak resistance torque (e.g., 5 Nm) was reached, the elbow joint was held at the extreme position for 10 s to allow soft tissue stress relaxation (Ren et al., 2017). During stretching, the patient was instructed to relax, feel the stretch but not to react to it (Ren et al., 2017). If the patient reacted to the stretching with high resistance, the robot would stop if a resistance torque limit was reached or reverse the direction of movement if resistance torque was beyond the limit (Ren et al., 2017).

Two types of active movement training were completed by the participants by voluntarily flexing and extending their elbow to play various movement games under real-time feedback, in which the robot could provide assistance after the patients tried but could not finish the movement task, or the robot provided resistance to challenge the patients if they could move the

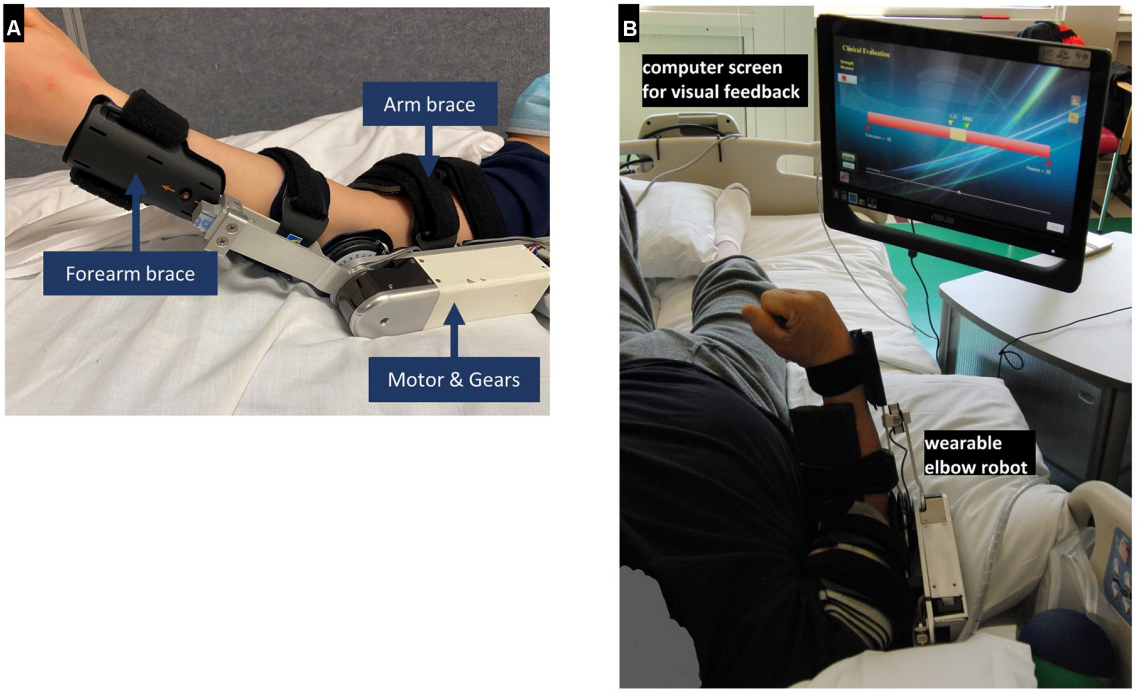

FIGURE 1 | (A) The wearable elbow robot used for training. **(B)** Clinical in-bed setup using the wearable rehabilitation robot. It is worn by a patient on the elbow for controlled passive stretching and active movement training with robotic assistance or resistance or with real-time feedback during training. A force sensor was used to detect the elbow flexion and extension torque.

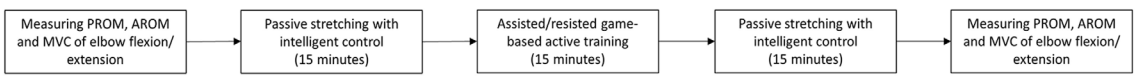

FIGURE 2 | Elbow robot training procedure.

elbow to the target positions in the gameplay. Robot assistance during patient's active movement training helped the patients reach the target and kept them engaged, while robot resistance continued challenging the patients to generate muscle strength (Waldman et al., 2013; Ren et al., 2017). The choice of assistive or resistive type of active movement training was dependent on the patient's severity of elbow impairment. For patients at the early stage of recovery with little elbow movement capability, the wearable rehabilitation robot constrained the joint at an isometric condition and the patient's potential re-emerging force-generation was detected sensitively by the wearable robot, and shown in real-time to the patient through visual feedback as a yellow bar on the computer monitor to guide the patient to generate the desired joint torque output (**Figure 1B**).

Participants received four sessions per week during their about 4-week hospital stay, for a total of about 15 sessions. The training protocol would be adjusted individually to accommodate the condition of patients with severe hemiplegia including more passive stretching, and less active movement training while therapy intensity was maintained ∼150 repetitions of elbow flexion/extension passively or actively. In addition to the robotic training, all the patients also received their regular inpatient rehabilitation including physical therapy and occupational therapy.

Outcome Evaluation

Biomechanical outcome measures were conducted immediately before and after the robotic training, including muscle strength measured as a maximum isometric voluntary contraction (MVC) of elbow flexors and extensors. During the measurement, the wearable robot was locked at the 90° elbow flexion and the participant was encouraged to extent and flex his or her elbow maximally. Each measure was done three times with a rest break of 30–60 s to minimize fatigue. The measured data were saved in the robot computer and the averaged value of the three assessments was taken as the corresponding outcome measure.

Clinical outcome measures, including upper limb motor recovery, muscle strength, and spasticity, were made on all the participants before and after all the robot-aided training (i.e., about 4 weeks from baseline) and 4 weeks after the completion of the training.

Fugl-Meyer Assessment of upper extremity (FMA-UE) was used to evaluate motor recovery (maximum score of 66) with a higher score indicating better motor recovery (Gladstone et al., 2002). The cut-off score for severe, moderate, and mild upper limb motor impairment is suggested to be 26 and 53 (Woodbury et al., 2013). Muscle strength was also evaluated using Motricity Index for the upper extremities (MI). As a valid muscle strength evaluation scale of stroke recovery in the first 6 months post-stroke, MI assessed the muscle strength of shoulder abduction, elbow flexion, and pinch grip. The total score ranges from 0 to 99, with a higher score corresponding to better muscle strength (Bohannon, 1999).

Spasticity of the elbow flexors and extensors was evaluated using the Modified Ashworth Scale (MAS). Considering the 1+ score is not ordinal, the scores of 0, 1, 1+, 2, 3, and 4 were adjusted to 0–5 ordinal scores in further analysis, with a higher value indicating more severe muscle spasticity (Pandyan et al., 1999a; Ansari et al., 2008).

Data Analysis

The normality of variables was checked using the Shapiro-Wilk test. Due to the small sample size, non-parametric analysis was used for the study. For all outcome variables, the group mean and standard deviation or median and inter-quartile range (IQR) at pre-and post-training, and follow-up were calculated. For the clinical outcome measures, the Friedman test was used to test whether the change between pre-, post-, and follow-up was statistically significant. Paired comparisons using the Wilcoxon signed-rank test were made between pre-and post-training conditions and between pre-and follow-up with Bonferroni adjustment. All statistical analyses were performed using the SPSS statistical software (Version 26, IBM, Armonk, NY, USA). The statistical significance was set at $p < 0.05$.

Furthermore, for MVC of elbow flexors and extensors, measured before and after each of the treatment sessions, improvement curves over sessions based on a logarithmic fitting equation as below (Kwakkel et al., 2006; Langhorne et al., 2011; Chen et al., 2018):

$$y = a \times ln(x) + b$$

where x is the number of the training session, y is the MVC value, a denotes the rate of improvement and b indicates the initial muscle strength of the patient. The coefficient of determination (R^2) was calculated to assess the goodness of fit.

RESULTS

Participants

Eleven patients (mean age ± SD: 50.7 ± 10.6 years) with moderate to severe upper limb motor impairment [FMA-UE, median (IQR): 28 (14–45)] at subacute stroke stage (post-stroke duration: 2.6 ± 1.9 months) completed the training during their hospital stay of 28 days on average (range: 24–30 days). **Table 1** summarizes the characteristics of each participant at the baseline. Three and eight patients were with severe and moderate upper limb motor impairment, respectively, at the baseline.

Feasibility

We applied the robot training in accordance with their routine in-patient treatment schedule and there was no dropout in the patients. Mild skin compression due to robot fixation and muscle soreness were reported by six patients after the first session of training, but this symptom was relieved within 24 h after onset of the symptoms. In general, the in-bed elbow robot training was well-tolerated by the participants without other adverse events. Every participant was able to complete the 50-min training and reported satisfaction with passive stretching and occasionally mild fatigue following the active movement when asked by the researchers. Except one patient, who was discharged after 13-sessions of training, the other 10 patients completed 15 sessions of training. Due to the researcher applied assistance to patients during the muscle strength testing, the biomechanical measures for three patients were excluded from the analysis. Thus, in the following in-session and curve-fitting analysis, biomechanical data for eight patients over 13 sessions were included.

Biomechanical Outcomes

Improvements After the 3–4 Week Training Program

After 3–4 week of training during the hospital stay, the MVC of elbow flexors significantly increased by 1.93 Nm (95% CI: 0.93 to 2.93 Nm, $p = 0.017$) and the MVC of elbow extensors significantly increased by 0.68 Nm (95% CI: 0.05 to 1.98 Nm, $p = 0.036$; **Figure 3**).

In-Session Changes Over the 4-Week Training Program

Each session of robot-guided training-induced changes in the MVC of elbow flexors and extensors, as indicated by the pre-and post-session dot plots over 13 sessions are shown in **Figure 3**. These recovery curves showed overall improvement in the patients' motor control ability over 13 training sessions, as well as the improved performance due to each training session, as shown by the differences between the pre-and post-session improvement curves (the blue and red curves respectively). We plot the overall change for eight patients with biomechanical measures, and further plot the recovery curve for patients with moderate upper limb motor impairment (FMA-UE motor >26, $n = 5$) and severe motor impairment (FMA-UE motor ≤26, $n = 2$). Overall, the improvement rate derived from the post-session measures was larger than the pre-session measures for both elbow flexion MVC (**Figure 4A**) and extension MVC (**Figure 4B**), which was related to the improvement induced by each training session. For the elbow flexors (**Figure 4C**), overall, patients with severe motor impairment had a lower initial performance value (pre: $b = 2.898$; post: $b = 2.693$) than those with moderate motor impairment (pre: $b = 3.873$; post: $b = 4.551$), and the post-session improvement rate was larger in the severe motor impairment group ($a = 0.865$) compared to the moderate motor impairment group ($a = 0.323$).

Patient No. 11 with very severe motor impairment (FMA-UE = 5) at baseline was unable to generate active elbow movement in the first five sessions of training. His recovery curve was discontinuous due to the important zero to non-zero motor output change and was modeled separately (**Figure 5**).

TABLE 1 | Characteristics of the patients at the baseline[a].

Patient	Sex	Age (years)	Stroke duration (months)	Stroke type	Lesion area	Hemiplegic side	Dominant hand	FMA-UE	MAS of flexors	MAS of extensors	Motricity index
1	Female	62	3	Infract	Temporal lobe	Left	Right	45	1	0	62.5
2	Male	63	2	Hemorrhage	Frontal lobe, cerebellum	Right	Right	14	1	0	25.5
3	Female	57	2	Hemorrhage	Thalamus	Right	Right	49	0	0	64
4	Female	39	5	Hemorrhage	Temporal lobe	Right	Right	37	0	0	65
5	Male	54	3	Hemorrhage	Brain stem	Right	Right	28	1	0	42.5
6	Male	44	6	Infract	Frontal lobe, basal ganglia	Left	Right	7	0	0	63.5
7	Female	52	1	Hemorrhage	Basal ganglia	Right	Right	30	1	0	30
8	Female	56	1	Infract	Thalamus, basal ganglia	Left	Right	26	0	0	52
9	Female	71	3	Hemorrhage	Thalamus, basal ganglia	Left	Right	28	0	1	57.5
10	Male	45	2	Infract	Frontal lobe, basal ganglia	Right	Right	52	0	1	62
11	Male	37	1	Infract	Frontal, temporal, and parietal lobe	Left	Right	5	0	0	N/A
Mean	Male: $n = 7$; Female: $n = 4$	50.7	2.6	Infarct: $n = 5$; Hemorrhage: $n = 6$		Left: $n = 5$; Right: $n = 6$	Right: $n = 11$	28[b]	0[b]	0[b]	52.5
SD		10.6	1.9					14–45[b]	0–1[b]	0–0[b]	14.0

[a]*FMA-UE, Fugl-Meyer Assessment-Upper Extremities; MAS, Modified Ashworth Scale; N/A, not applicable to conduct.* [b]*Median (inter-quartile range); SD, standard deviation.*

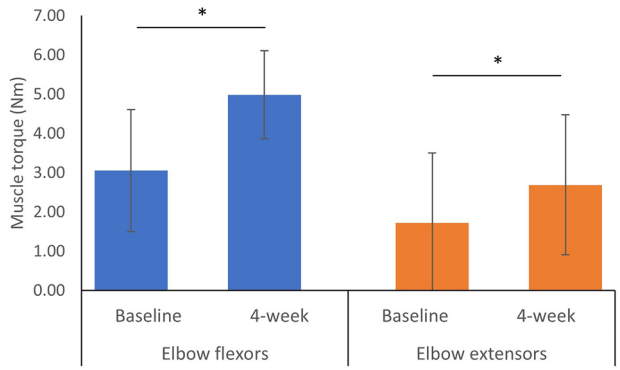

FIGURE 3 | Maximum isometric voluntary contraction at baseline and 4-week after the training program[a]. [a]Error bars represent standard deviation. *Indicates a significant difference between two measured time points from Wilcoxon Signed Ranks Test $p < 0.05$.

Clinical Outcomes

The clinical measures were conducted before and after 15 sessions of training (except for one patient discharged after 13 sessions of training), and 4 weeks after the termination of training. After 4 weeks of training, significant improvements were observed in FMA-UE ($p = 0.003$) and Motricity Index ($p = 0.005$; **Table 2**), and the improvements sustained at the follow-up ($p < 0.05$). However, no significant differences were observed between the post-training and 4-week follow-up. In addition, subscale value of FMA are presented in **Table 2**. Generally, participants showed improvement in movement, while no significant change was observed in coordination. There was no significant change of muscle spasticity measured by MAS between the baseline, post-training, and follow-up sessions.

DISCUSSION

Our findings suggest that the in-bed wearable elbow robotic rehabilitation training is feasible in early and late subacute stroke survivors with moderate to severe upper limb motor impairment. Over the 4 weeks of training, participants made consistent improvements on elbow biomechanical and clinical outcomes, while the recovery curve showed that patients with severe motor impairment may have a greater rate of improvement compared to those with moderate motor impairment. The current findings address the valuable application of in-bed rehabilitation robotic training for subacute stroke survivors with its advantages in quantifying and monitoring the motor recovery and delivery of the individualized intervention, though our results must

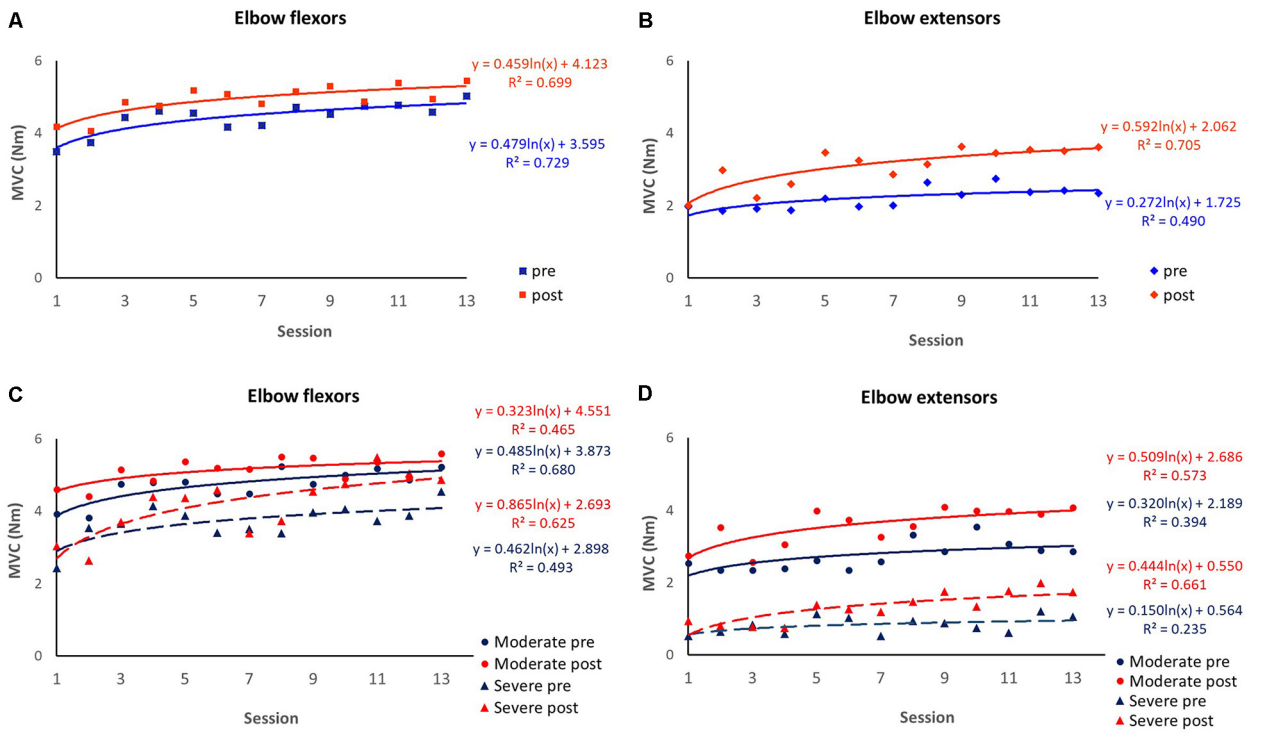

FIGURE 4 | Session-by-session pre-and post-session maximum isometric voluntary contraction (MVC). Improvement curves across the 13 sessions are fitted with logarithmic function $y = a \times \ln(x) + b$, where x is the number of the training session, y is the MVC value, a denotes the rate of improvement and b indicates the initial performance capability level of the patients. The coefficient of determination (R^2) was calculated to assess the goodness of fit. **(A)** MVC of elbow flexors over eight patients. **(B)** MVC of elbow extensors over eight patients. **(C)** MVC of elbow flexors over patients with severe motor impairment ($n = 2$) and moderate motor impairment ($n = 6$). **(D)** MVC of elbow extensors over patients with severe motor impairment ($n = 2$) and moderate motor impairment ($n = 6$).

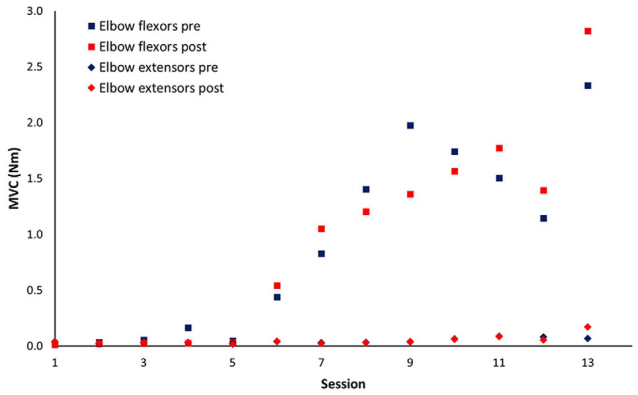

FIGURE 5 | Session-by-session pre-and post-session maximum isometric voluntary contraction (MVC) for patient No.11. This patient started to develop elbow flexors voluntary contraction after five sessions of training.

be interpreted with obvious caution given the absence of a control group.

The wearable elbow robot training combined with both passive and active movement has several unique features. First, the intelligent control algorithm provides a forceful while safe stretching to the upper limb muscles, which can prevent muscle contracture and joint stiffness (Ren et al., 2017; Salazar et al., 2019). Also, the strong stretching may enhance somatosensory input that helps drive neural reorganization (Behm et al., 2016). Second, an assisted-as-needed scheme was applied in the active movement training, which would be particularly useful for the subacute stroke survivors with moderate to severe motor impairment that has limited capability to generate active movement. If the patient could generate active arm movement, the robot would provide resistance that further enhances the movement control; if the patient could initiate movement but with difficulty to complete the required movement, the robot would help the patient to finish the rest of the movement; or if the patient was unable to generate active movement, the robot would assist the patient to passively move the arm to the desired position. Indeed, applying passive movement before clinical recovery has been proven that can elicit cortical activation patterns that may be critical for the restoration of motor function (Matteis et al., 2003). The robotic assistance would progressively reduce through the training that further promotes motor learning (Winstein et al., 2016). Third, the robot with a highly sensitive force sensor can discern the emergence of the subtle change of tiny movement. For patients, this subtle movement change was further augmented and displayed on the computer screen to provide real-time visual feedback that motivates and guides the patient to improve joint torque generation (Ren et al., 2017). For clinicians, the detection by the robot could provide essential information to optimize the treatment goal and assist rehabilitation plan. In **Figure 5**, the patient was unable to generate active muscle strength in elbow flexors until after five sessions of training, and this slight change was successfully detected by the robot.

Utilizing the robot, immediate biomechanical measures can be made before and after each training session, and further plot a recovery curve of the biomechanical outcome change (**Figure 4**). Though we can observe fluctuation of performance that may occur between sessions, overall, the patients demonstrated an improving trend over the training sessions. However, fluctuation patterns may imply that for longitudinal intervention trials, the multiple-session assessment may provide a better estimation of participants' condition than a single-session assessment. Furthermore, consistent with previous clinical trials (Takahashi et al., 2016; Takebayashi et al., 2020), our stratified recovery curve informed that patients with severe motor impairment were likely to benefit more from robotic training compared to those with moderate motor impairment. We believe this recovery could provide important information to guide the clinical application of robot training (Veerbeek et al., 2017). First, the recovery curve can assist clinicians to estimate the recovery pattern of the patients, thus optimizing the treatment plan; second, with a larger sample size to plot the recovery curve, we may be able to estimate the minimal training sessions to achieve the desired outcome, which may assist Medicare policymaking.

A limitation of the present study is the lack of a control group to isolate the effect of spontaneous motor recovery. However, we applied the clinical measures including FMA-UE and Motricity Index (MI) for upper limb muscle strength at baseline, immediately after the intervention program, and 1-month after the termination of the program, which could serve as a self-control comparison (**Table 2**). Immediately after the training program, the median score of FMA-UE significantly

TABLE 2 | Clinical measures at baseline, post-training and follow-up[a].

	Baseline		Post-training		Follow-up		*p*-value	
	Median	IQR	Median	IQR	Median	IQR	Pre-post	Pre-follow-up
FMA-UE	28	14–37	42	19–51	51	36–53	0.003*	0.005*
Shoulder/elbow	17	14–26	28	19–30	29	18–32	0.008*	0.008*
Wrist	5	2–6	7	4–9	7	6–9	0.007*	0.005*
Hand	6	2–8	9	4–12	11	7–12	0.005*	0.005*
Coordination	0	0–2	2	0–4	2	2–5	0.068	0.041*
Motricity index	60	40–64	70	60–71	70	60–73	0.005*	0.005*
MAS elbow flexors	0	0–1	0	1–1	0	0.5–1	0.083	0.157
MAS elbow extensors	0	0–0	0	0–1	0	0–1	0.564	0.414

[a]*FMA-UE, Fugl-Meyer Assessment-Upper Extremities; IQR, inter-quartile range; MAS, Modified Ashworth Scale. *Statistically significant difference using Wilcoxon signed rank test, $p < 0.05$.*

increased to 14, which is larger than 9, the minimal clinically important difference (MCID) value of FMA-UE for subacute poststroke patients (Narayan Arya et al., 2011). After a 1-month follow-up, there were significant changes in the FMA-UE and MI. Collectively, the outcome of clinical measures could further support the effectiveness of in-bed wearable training in the improvement of upper limb motor limb function and minimize the confounding of spontaneous recovery.

There are limitations to the study. First, patients in the study also received routine in-patient rehabilitation, which could contribute to their improvement. However, this study demonstrated the feasibility to incorporate the in-bed robot training with routine inpatient rehabilitation training, which may not focus on sensorimotor rehabilitation. Anecdotally, the patients enjoyed the robot training and were highly motivated. However, we did not have a treatment satisfaction rating using the Likert system to evaluate patients' responses, which should be adopted in future studies. Second, patients in the present study had mild or absent elbow spasticity which may limit the generalizability of the study. The mild or absent elbow spasticity would be due to most of the patients being at the early subacute stage (7 days to 3 months post-stroke; Bernhardt et al., 2017) that spasticity had not been developed yet (Wissel et al., 2013). In fact, one patient 1-month post-stroke with zero MAS at the elbow showed wrist spasticity of two at the follow-up and two other early subacute patients showed an increase of MAS from zero at the baseline to one at post-training. Also, the forceful passive elbow stretching by the robot might help control spasticity (Ren et al., 2017). Nonetheless, appropriate quantification of spasticity is important. MAS may not be a valid and ordinal level measure of muscle spasticity (Pandyan et al., 1999b). Future studies can consider using the modified Modified Ashworth Scale, which has been suggested to be better inter-rater and intra-session reliability than the MAS to measure spasticity (Ansari et al., 2006, 2009). Also, Brunnstrom recovery stages (BRS) can be used to evaluate the changes of muscle tone, synergistic movements, and active isolated movement (Naghdi et al., 2010). Third, only a small number of in-patients participated in the study. The goodness-of-fit value for curve fitting was thus relatively low. In the future, a strictly designed randomized control trial with a large sample size with different motor impairment levels is needed.

In conclusion, the above study demonstrated the feasibility of using in-bed wearable elbow robot-aided rehabilitation training in subacute stroke survivors with moderate to severe upper limb motor impairment. Furthermore, robotic therapy may result in significant improvement across biomechanical and clinical measures. The recovery curve generated from the robot biomechanical measures could provide useful information to guide the clinical applications of robot-aided training. Patients with severe motor impairment may benefit more from the robot training compared to those with less severe impairment.

DATA AVAILABILITY STATEMENT

The raw data supporting the conclusions of this article will be made available by the authors, without undue reservation.

ETHICS STATEMENT

The studies involving human participants were reviewed and approved by the ethics committee of Presbyterian Medical Center, Jeonbuk, South Korea. The patients/participants provided their written informed consent to participate in this study.

AUTHOR CONTRIBUTIONS

All authors listed have made a substantial, direct and intellectual contribution to the work, and approved it for publication.

FUNDING

This study was supported in part by the National Institute on Disability, Independent Living, and Rehabilitation Research (NIDILRR, grant: 90BISB0001 and 90DP0099). The first author MH was supported by a NIDILRR postdoctoral training grant (90AR5028).

REFERENCES

Ansari, N. N., Naghdi, S., Arab, T. K., and Jalaie, S. (2008). The interrater and intrarater reliability of the Modified Ashworth Scale in the assessment of muscle spasticity: limb and muscle group effect. *NeuroRehabilitation* 23, 231–237. doi: 10.3233/nre-2008-23304

Ansari, N. N., Naghdi, S., Hasson, S., Mousakhani, A., Nouriyan, A., and Omidvar, Z. (2009). Inter-rater reliability of the Modified Modified Ashworth Scale as a clinical tool in measurements of post-stroke elbow flexor spasticity. *NeuroRehabilitation* 24, 225–229. doi: 10.3233/NRE-2009-0472

Ansari, N. N., Naghdi, S., Moammeri, H., and Jalaie, S. (2006). Ashworth Scales are unreliable for the assessment of muscle spasticity. *Physiother. Theory Pract.* 22, 119–125. doi: 10.1080/09593980600724188

Behm, D. G., Blazevich, A. J., Kay, A. D., and Mchugh, M. (2016). Acute effects of muscle stretching on physical performance, range of motion and injury incidence in healthy active individuals: a systematic review. *Appl. Physiol. Nutr. Metab.* 41, 1–11. doi: 10.1139/apnm-2015-0235

Bernhardt, J., Dewey, H., Thrift, A., and Donnan, G. (2004). Inactive and alone: physical activity within the first 14 days of acute stroke unit care. *Stroke* 35, 1005–1009. doi: 10.1161/01.STR.0000120727.40792.40

Bernhardt, J., Hayward, K. S., Kwakkel, G., Ward, N. S., Wolf, S. L., Borschmann, K., et al. (2017). Agreed definitions and a shared vision for new standards in stroke recovery research: the stroke recovery and rehabilitation roundtable taskforce. *Int. J. Stroke* 12, 444–450. doi: 10.1177/1747493017711816

Bertani, R., Melegari, C., Maria, C., Bramanti, A., Bramanti, P., and Calabrò, R. S. (2017). Effects of robot-assisted upper limb rehabilitation in stroke patients: a systematic review with meta-analysis. *Neurol. Sci.* 38, 1561–1569. doi: 10.1007/s10072-017-2995-5

Bohannon, R. W. (1999). Motricity index scores are valid indicators of paretic upper extremity strength following stroke. *J. Physical Therapy Sci.* 11, 59–61. doi: 10.1589/jpts.11.59

Buma, F., Kwakkel, G., and Ramsey, N. (2013). Understanding upper limb recovery after stroke. *Res. Neurol. Neurosci.* 31, 707–722. doi: 10.3233/RNN-130332

Chen, K., Xiong, B., Ren, Y., Dvorkin, A. Y., Gaebler-Spira, D., Sisung, C. E., et al. (2018). Ankle passive and active movement training in children with acute brain injury using a wearable robot. *J. Rehabil. Med.* 50, 30–36. doi: 10.2340/16501977-2285

Chien, W. T., Chong, Y. Y., Tse, M. K., Chien, C. W., and Cheng, H. Y. (2020). Robot-assisted therapy for upper-limb rehabilitation in subacute stroke patients: a systematic review and meta-analysis. *Brain Behav.* 10:e01742. doi: 10.1002/brb3.1742

Ferreira, F. M. R. M., Chaves, M. E. A., Oliveira, V. C., Van Petten, A. M. V. N., and Vimieiro, C. B. S. (2018). Effectiveness of robot therapy on body function and structure in people with limited upper limb function: a systematic review and meta-analysis. *PLoS One* 13:e0200330. doi: 10.1371/journal.pone.0200330

French, B., Thomas, L. H., Coupe, J., Mcmahon, N. E., Connell, L., Harrison, J., et al. (2016). Repetitive task training for improving functional ability after stroke. *Cochrane Database Syst. Rev.* 4:CD006073. doi: 10.1002/14651858.CD006073.pub2

Gladstone, D. J., Danells, C. J., and Black, S. E. (2002). The fugl-meyer assessment of motor recovery after stroke: a critical review of its measurement properties. *Neurorehabil. Neural Repair* 16, 232–240. doi: 10.1177/1545968302401105171

Hsieh, Y.-W., Wu, C.-Y., Lin, K.-C., Yao, G., Wu, K.-Y., and Chang, Y.-J. (2012). Dose-response relationship of robot-assisted stroke motor rehabilitation: the impact of initial motor status. *Stroke* 43, 2729–2734. doi: 10.1161/STROKEAHA.112.658807

Johnson, W., Onuma, O., Owolabi, M., and Sachdev, S. (2016). Stroke: a global response is needed. *Bull. World Health Organ.* 94:634. doi: 10.2471/BLT.16.181636

Krakauer, J. W. (2006). Motor learning: its relevance to stroke recovery and neurorehabilitation. *Curr. Opin. Neurol.* 19, 84–90. doi: 10.1097/01.wco.0000200544.29915.cc

Kundert, R., Goldsmith, J., Veerbeek, J. M., Krakauer, J. W., and Luft, A. R. (2019). What the proportional recovery rule is (and is not): methodological and statistical considerations. *Neurorehabil. Neural Repair* 33, 876–887. doi: 10.1177/1545968319872996

Kwakkel, G., Kollen, B., and Twisk, J. (2006). Impact of time on improvement of outcome after stroke. *Stroke* 37, 2348–2353. doi: 10.1161/01.STR.0000238594.91938.1e

Kwakkel, G., Kollen, B. J., Van Der Grond, J., and Prevo, A. J. (2003). Probability of regaining dexterity in the flaccid upper limb: impact of severity of paresis and time since onset in acute stroke. *Stroke* 34, 2181–2186. doi: 10.1161/01.STR.0000087172.16305.CD

Lang, C. E., Macdonald, J. R., Reisman, D. S., Boyd, L., Kimberley, T. J., Schindler-Ivens, S. M., et al. (2009). Observation of amounts of movement practice provided during stroke rehabilitation. *Arch. Phys. Med. Rehabil.* 90, 1692–1698. doi: 10.1016/j.apmr.2009.04.005

Lang, C. E., Wagner, J. M., Edwards, D. F., and Dromerick, A. W. (2007). Upper extremity use in people with hemiparesis in the first few weeks after stroke. *J. Neurol. Phys. Therapy* 31, 56–63. doi: 10.1097/NPT.0b013e31806748bd

Langhorne, P., Bernhardt, J., and Kwakkel, G. (2011). Stroke rehabilitation. *The Lancet* 377, 1693–1702. doi: 10.1016/S0140-6736(11)60325-5

Lee, K. B., Lim, S. H., Kim, K. H., Kim, K. J., Kim, Y. R., Chang, W. N., et al. (2015). Six-month functional recovery of stroke patients: a multi-time-point study. *Int. J. Rehabil. Res.* 38:173. doi: 10.1097/MRR.0000000000000108

Luker, J., Lynch, E., Bernhardsson, S., Bennett, L., and Bernhardt, J. (2015). Stroke survivors' experiences of physical rehabilitation: a systematic review of qualitative studies. *Arch. Phys. Med. Rehabil.* 96, 1698–1708.e1610. doi: 10.1016/j.apmr.2015.03.017

Matteis, M., Vernieri, F., Troisi, E., Pasqualetti, P., Tibuzzi, F., Caltagirone, C., et al. (2003). Early cerebral hemodynamic changes during passive movements and motor recovery after stroke. *J. Neurol.* 250, 810–817. doi: 10.1007/s00415-003-1082-4

Mehrholz, J., Pohl, M., Platz, T., Kugler, J., and Elsner, B. (2018). Electromechanical and robot-assisted arm training for improving activities of daily living, arm function and arm muscle strength after stroke. *Cochrane Database Syst. Rev.* 9:CD006876. doi: 10.1002/14651858.CD006876.pub5

Mirbagheri, M. M., Tsao, C., and Rymer, W. Z. (2009). Natural history of neuromuscular properties after stroke: a longitudinal study. *J. Neurol. Neurosurg Psychiatry* 80, 1212–1217. doi: 10.1136/jnnp.2008.155739

Naghdi, S., Ansari, N. N., Mansouri, K., and Hasson, S. (2010). A neurophysiological and clinical study of Brunnstrom recovery stages in the upper limb following stroke. *Brain Inj.* 24, 1372–1378. doi: 10.3109/02699052.2010.506860

Narayan Arya, K., Verma, R., and Garg, R. (2011). Estimating the minimal clinically important difference of an upper extremity recovery measure in subacute stroke patients. *Top. Stroke Rehabil.* 18, 599–610. doi: 10.1310/tsr18s01-599

O'dwyer, N. J., Ada, L., and Neilson, P. D. (1996). Spasticity and muscle contracture following stroke. *Brain* 119, 1737–1749. doi: 10.1093/brain/119.5.1737

Pandyan, A. D., Johnson, G. R., Price, C. I., Curless, R. H., Barnes, M. P., Rodgers, H., et al. (1999a). A review of the properties and limitations of the Ashworth and modified Ashworth Scales as measures of spasticity. *Clin. Rehabil.* 13, 373–383. doi: 10.1191/026921599677595404

Pandyan, A. D., Johnson, G. R., Price, C. I., Curless, R. H., Barnes, M. P., Rodgers, H., et al. (1999b). A review of the properties and limitations of the Ashworth and modified Ashworth Scales as measures of spasticity. *Clin. Rehabil.* 13, 373–383. doi: 10.1191/026921599677595404

Ren, Y., Wu, Y., Yang, C., Xu, T., Harvey, R. L., Zhang, L., et al. (2017). Developing a wearable ankle rehabilitation robotic device for in-bed acute stroke rehabilitation. *IEEE Trans. Neural Syst. Rehabil. Eng.* 25, 589–596. doi: 10.1109/TNSRE.2016.2584003

Roby-Brami, A., Feydy, A., Combeaud, M., Biryukova, E., Bussel, B., Levin, M., et al. (2003). Motor compensation and recovery for reaching in stroke patients. *Acta Neurol. Scand.* 107, 369–381. doi: 10.1034/j.1600-0404.2003.00021.x

Salazar, A. P., Pinto, C., Mossi, J. V. R., Figueiro, B., Lukrafka, J. L., Pagnussat, A. S., et al. (2019). Effectiveness of static stretching positioning on post-stroke upper-limb spasticity and mobility: systematic review with meta-analysis. *Ann. Phys. Rehabil. Med.* 62, 274–282. doi: 10.1016/j.rehab.2018.11.004

Takahashi, K., Domen, K., Sakamoto, T., Toshima, M., Otaka, Y., Seto, M., et al. (2016). Efficacy of upper extremity robotic therapy in subacute poststroke hemiplegia: an exploratory randomized trial. *Stroke* 47, 1385–1388. doi: 10.1161/STROKEAHA.115.012520

Takebayashi, T., Takahashi, K., Domen, K., and Hachisuka, K. (2020). Impact of initial flexor synergy pattern scores on improving upper extremity function in stroke patients treated with adjunct robotic rehabilitation: a randomized clinical trial. *Top. Stroke Rehabil.* 27, 516–524. doi: 10.1080/10749357.2020.1738660

Van Peppen, R. P., Kwakkel, G., Wood-Dauphinee, S., Hendriks, H. J., Van Der Wees, P. J., Dekker, J., et al. (2004). The impact of physical therapy on functional outcomes after stroke: what's the evidence? *Clin. Rehabil.* 18, 833–862. doi: 10.1191/0269215504cr843oa

Veerbeek, J. M., Langbroek-Amersfoort, A. C., Van Wegen, E. E., Meskers, C. G., and Kwakkel, G. (2017). Effects of robot-assisted therapy for the upper limb after stroke: a systematic review and meta-analysis. *Neurorehabil. Neural Repair* 31, 107–121. doi: 10.1177/1545968316666957

Virani, S. S., Alonso, A., Benjamin, E. J., Bittencourt, M. S., Callaway, C. W., Carson, A. P., et al. (2020). Heart disease and stroke statistics—2020 update: a report from the American Heart Association. *Circulation* 141, E139–E596. doi: 10.1161/CIR.0000000000000757

Volpe, B., Krebs, H., Hogan, N., Edelstein, L., Diels, C., Aisen, M., et al. (2000). A novel approach to stroke rehabilitation: robot-aided sensorimotor stimulation. *Neurology* 54, 1938–1944. doi: 10.1212/wnl.54.10.1938

Waldman, G., Yang, C.-Y., Ren, Y., Liu, L., Guo, X., Harvey, R. L., et al. (2013). Effects of robot-guided passive stretching and active movement training of ankle and mobility impairments in stroke. *NeuroRehabilitation* 32, 625–634. doi: 10.3233/NRE-130885

West, T., and Bernhardt, J. (2012). Physical activity in hospitalised stroke patients. *Stroke Res. Treat.* 2012:813765. doi: 10.1155/2012/813765

Winstein, C. J., Stein, J., Arena, R., Bates, B., Cherney, L. R., Cramer, S. C., et al. (2016). Guidelines for adult stroke rehabilitation and recovery: a guideline for healthcare professionals from the American Heart Association/American Stroke Association. *Stroke* 47, e98–e169. doi: 10.1161/STR.0000000000000098

Wissel, J., Manack, A., and Brainin, M. (2013). Toward an epidemiology of poststroke spasticity. *Neurology* 80, S13–S19. doi: 10.1212/WNL.0b013e3182762448

Woodbury, M. L., Velozo, C. A., Richards, L. G., and Duncan, P. W. (2013). Rasch analysis staging methodology to classify upper extremity movement impairment after stroke. *Arch. Phys. Med. Rehabil.* 94, 1527–1533. doi: 10.1016/j.apmr.2013.03.007

Conflict of Interest: L-QZ has an ownership in Rehabtek LLC, which received U.S. federal fundings in developing the rehabilitation robot used in this study.

The remaining authors declare that the research was conducted in the absence of any commercial or financial relationships that could be construed as a potential conflict of interest.

frontiers in Physiology

ORIGINAL RESEARCH
published: 12 July 2021
doi: 10.3389/fphys.2021.647603

Connectomics of Bone to Brain—Probing Physical Renderings of Cellular Experience

Melissa L. Knothe Tate[1], Abhilash Srikantha[2], Christian Wojek[2] and Dirk Zeidler[3]*

[1] Blue Mountains World Interdisciplinary Innovation Institute, Sydney, NSW, Australia, [2] Corporate Research and Technology, Carl Zeiss AG, Oberkochen, Germany, [3] Carl Zeiss MultiSEM GmbH, Oberkochen, Germany

"Brainless" cells, the living constituents inhabiting all biological materials, exhibit remarkably *smart*, i.e., stimuli-responsive and adaptive, behavior. The emergent spatial and temporal patterns of adaptation, observed as changes in cellular connectivity and tissue remodeling by cells, underpin neuroplasticity, muscle memory, immunological imprinting, and sentience itself, in diverse physiological systems from brain to bone. Connectomics addresses the direct connectivity of cells and cells' adaptation to dynamic environments through manufacture of extracellular matrix, forming tissues and architectures comprising interacting organs and systems of organisms. There is imperative to understand the physical renderings of cellular experience throughout life, from the time of emergence, to growth, adaptation and aging-associated degeneration of tissues. Here we address this need through development of technological approaches that incorporate cross length scale (nm to m) structural data, acquired via multibeam scanning electron microscopy, with machine learning and information transfer using network modeling approaches. This pilot case study uses cutting edge imaging methods for nano- to meso-scale study of cellular inhabitants within human hip tissue resected during the normal course of hip replacement surgery. We discuss the technical approach and workflow and identify the resulting opportunities as well as pitfalls to avoid, delineating a path for cellular connectomics studies in diverse tissue/organ environments and their interactions within organisms and across species. Finally, we discuss the implications of the outlined approach for neuromechanics and the control of physical behavior and neuromuscular training.

Keywords: connectomics, imaging, machine learning, cell, cell memory, cellular epidemiology

OPEN ACCESS

Edited by:
Taiar Redha,
Université de Reims Champagne-Ardenne, France

Reviewed by:
Michael B. Morris,
The University of Sydney, Australia
Navid Rabiee,
Sharif University of Technology, Iran

****Correspondence:***
Melissa L. Knothe Tate
knothetate@gmail.com;
proftate.bmwi3@gmail.com

Specialty section:
This article was submitted to Integrative Physiology, a section of the journal Frontiers in Physiology

Received: *30 December 2020*
Accepted: *10 June 2021*
Published: *12 July 2021*

Citation:
Knothe Tate ML, Srikantha A, Wojek C and Zeidler D (2021) Connectomics of Bone to Brain—Probing Physical Renderings of Cellular Experience. Front. Physiol. 12:647603. doi: 10.3389/fphys.2021.647603

INTRODUCTION

Cells of the human body populate their habitat through division, starting with two cells at conception and expanding to over 70 trillion cells over the course of a lifetime (Knothe Tate, 2017). Throughout the lifespan of the organism they inhabit, cells memorialize the biophysical and chemical stimuli they experience via gene expression of structural proteins created from molecular building blocks, e.g., amino acids. In this way, cells encode an organism's and their own experiences

in the physical world, by creating and adapting tissues, throughout life. Just as punch cards encode the recursive logic of textile weaves created with weaving looms (where card holes allow passage of hooks and the fibers they shuttle), genes encode and translate the arrangement of amino acids comprising elastin, collagen and other structural proteins making up tissue weaves (Knothe Tate, 2017, 2020; Ng et al., 2017a,b). A major barrier to understanding the emergent behavior that underpins this tissue genesis and adaptation is the lack of methods to image and analyze cellular connectivity across length and time scales.

The manuscript proposes a paradigm shifting approach to understand the cellular underpinnings of diseases as different as osteoarthritis and early onset dementia in bone and brain. We know as biologists that cells manufacture, remodel and adapt tissues throughout life (Knothe Tate et al., 2016a; Putra et al., 2019). The tissues render physically the collective cellular experience, reflected in architectures (bones) and memories (brain) which themselves exhibit *emergent properties* (Knothe Tate, 2020). These emergent properties cannot simply be deduced from the individual parts, which themselves do not exhibit such properties; rather, these emergent properties arise from spatial and temporal arrangements among multiple parts, e.g., memories that are physically encoded in neurons are not observable in single neurons but rather emerge from the spatial arrangement and temporal behavior of interacting neurons in the brain. A pathological example of emergence would be disease emergence, e.g., of osteoarthritis in the musculoskeletal system or early onset dementia in the brain, which cannot be predicted based on the occurrence of a single sick cell but rather at the stage of loss in function or loss in return to homeostasis due to emergence of disease amongst groups of cells that interact.

The elucidation of such disease emergence represents a currently untenable yet compelling research problem. On the one hand, the lack of methods to probe and understand emergent behavior of inhabitant cells within their complex ecosystems presents a hurdle to understanding and fundamental discoveries. On the other hand, the role of cell populations and the loss of their connectivity in disease progression has been stymied by the tradeoff between achieving sufficient resolution across vastly different length and time scales, e.g., single field of view and single time point images (nano- to microscale for electron to optical microscopy), and other imaging modalities that enable high temporal albeit less spatial resolution (MRI). Rapid advances in the field seek to overcome this current hurdle. To address each of these points, workflows are needed to render and analyze vast amounts of imaging data from nano- to meso-length scales. The manuscript describes that process and sets a path forward.

The neuroscience community refers to the totality of cellular connections and their three-dimensional (3D) networks, e.*g.*, in the brain, as the *connectome* and the process of rendering, analyzing and understanding the connectome as *connectomics* (Seung, 2012; Jbabdi and Behrens, 2013; Blakely, 2021). A recently integrated biosystems engineering, imaging and analysis platform enables a connectomics approach to map cellular connectivity across organs as diverse as brain and bone (Eberle et al., 2015; Knothe Tate et al., 2016c, 2019; Pereira et al., 2016). Tested in mouse brains (Mikula et al., 2012; Lichtman et al., 2014; Hayworth et al., 2015; Mikula and Denk, 2015; Swanson and Lichtman, 2016; Hayworth et al., 2020; Günther et al., 2021) and in our own pilot studies of the human hip (Eberle et al., 2015; Pereira et al., 2016; Knothe Tate, 2017), as well as validated through the delineation of standardized protocols and workflows (Ngo et al., 2019), these biosystems engineering approaches may find future applications relevant for every organ of the body.

Here, key enabling steps are described for quantifying relationships and connectivity between cells in different disease states. Specifically, we test machine learning algorithms with cellular network maps of the human hip to elucidate the role of cell networks in organ and organism (patho)physiology throughout life (**Figure 1**). This approach may pave the way for next generation theranostics, i.e., enabling prediction of emergent cell scale pathology, including disease detection as well as treatment, well before permanent damage occurs at tissue and organ length scales. Based on the results of this pilot study, we assess opportunities and identify potential pitfalls of the integrated imaging, modeling and machine learning approaches.

Datasets Rendered as Cellular Networks in Maps of Human Tissue

Human tissue samples from the femoral neck and head of patients undergoing total hip replacement were obtained with Institutional Review Board Approval (Cleveland Clinic IRB12-335). Samples were prepared for electron microscopy (EM) using a published protocol (Ngo et al., 2019) developed to enable fixation and polymethyl methacrylate embedding and electron microscopy of mesoscopic samples which exceed the typical diffusion path lengths for mm-sized electron microscopy samples.

Samples were first etched (to expose cells just below the block face surface) and imaged using multi-beam Scanning Electron Microscopy, to achieve nano- to meso-scale renderings of cellular inhabitants (mainly osteocytes with some red blood cells visible in resulting images). Based on this protocol, carbon coating provided sufficient contrast to visualize osteocytes exposed by chemical etching on the surface of the sample block. Although not used for the current study, sequential layers of cellular networks could be revealed by reiterating the etching and imaging steps, resulting in a volume of tissue with fully rendered three dimensional (3D) cellular network.

Three datasets were acquired using three generations of multibeam Scanning Electron Microscopes (mSEM) to image three different samples, starting with a 61 beam prototype at 12 nm pixel size and ending with a state-of-the-art commercial system (Zeiss mSEM 505) (**Table 1**).

In our first pilot study (Knothe Tate et al., 2016c; Pereira et al., 2016), we tested the feasibility of using the Google Maps API platform to stitch and render the maps in a way that would be accessible to, as well as navigable and quantitatively

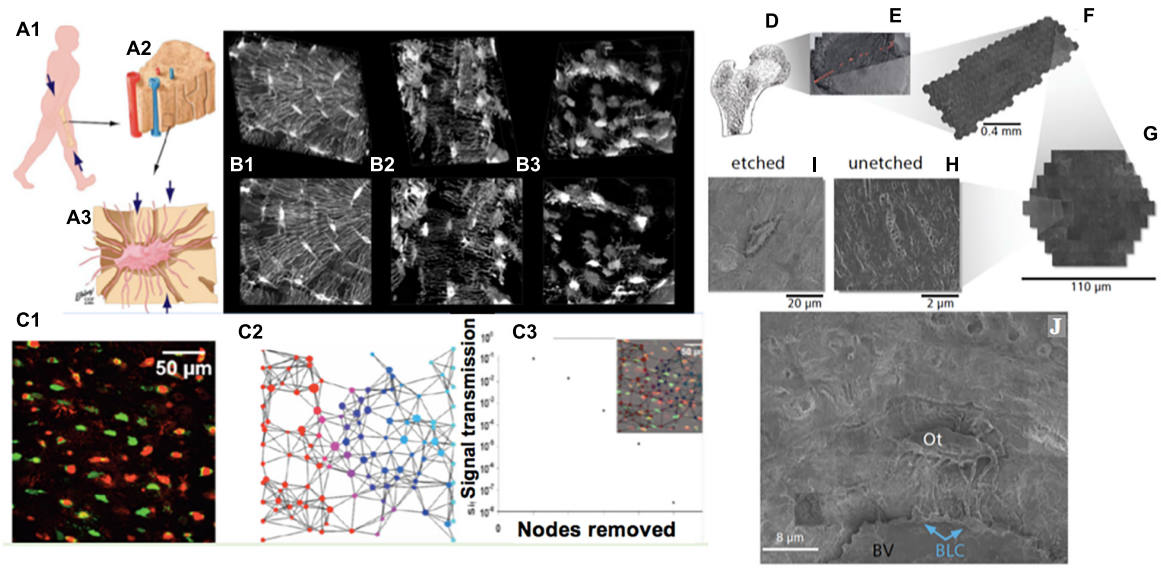

FIGURE 1 | Imaging cellular networks and environments across length scales, from nano to meso, using cross length scale imaging (multi-beam scanning electron microscopy) of the cellular inhabitants of the human femoral neck, i.e., osteocytes, as a case study. **(A)** Organism **(A1)** to tissue **(A2)** to cellular (osteocyte, **A3**) length scales demonstrating the most prevalent cellular inhabitants of bone, osteocytes. During development, cells manufacture the tissues comprising the femoral head and neck (proximal femur, **A1,D**); the cellular inhabitants of bone, cartilage and other tissues model (during growth) and remodel (enabling adaptation) the respective tissues of their local environment through up- and down-regulation of structural protein transcription, and secretion into the extracellular matrix. **(B)** The cellular network of bone's resident osteocytes changes throughout life, in health and disease (**B1**: healthy, **B2,B3**: diseased). **(B,C)** The loss in network connectivity reflects the health status of the cells (**C1**, **live** and **dead** osteocytes visualized using an ethidium bromide assay) as well as the patency of the network (**C2**—stochastic network model with nodes representing cells**, C3**—calculation of loss in information transfer with loss in network nodes**)**; loss of viable cells within the network results in loss in network connectivity and subsequent diminished information transfer capacity across and within the network. **(D–J)** mSEM imaging, combined with image stitching and Google Maps API geonavigation applications, enables high resolution imaging of inhabitant cells within tissues, as well navigation and analysis of single cells and their complex networks, seamlessly across length scales (**D,** femoral head and neck; **E,** section through the femoral head created by stitching together of many images, comprising arrays; **F**, of hexagons; **G**, themselves made of arrays of electron beams). Rather than using single electron beams as in traditional electron microscopy, mSEM uses arrays of 61 and more beams **(F,G)** to capture large areas of tissue (mesoscale, **E**) with nanoscale resolution **(H–J)**. Through inorganic and organic etching procedures adapted from atomic force microscopy, the third dimension of cellular networks may be captured **(H,I)** and the local and global environment of tissues' cellular inhabitants (Ot, Osteocyte; BLC, Bone Lining Cell) can be explored within tissue contexts (BV, upper half of oval Blood Vessel, above which bony matrix is seen). Images adapted and used with permission (**A,** Knothe Tate et al., 2010; **B,** Knothe Tate et al., 2002; **C,** Anderson et al., 2008; **D–J,** Knothe Tate et al., 2016c).

analyzable, by scientists and the lay public alike. The resulting data set was annotated using Google Maps' pins to mark manually viable and *pyknotic* cells (necrotic and apoptotic cells are typically identified by condensation of the chromatin and fragmentation of the nucleus, defining *pyknotic*). As a surrogate identification factor (classifier for machine learning implementation), osteocytes with less than three visible processes were identified visually and manually pinned as *pyknotic*, indicated by a red pin. Osteocytes with more than three visible processes were identified visually and manually pinned as *viable*, indicated by a green pin. The manual process took several weeks for the 1st generation dataset (**Table 1**). Full details of this process are described in previous publications (Knothe Tate et al., 2016c; Pereira et al., 2016).

TABLE 1 | Dataset metrics from three generations of mSEM maps from three different human hip samples obtained with IRB approval.

Data metrics	1st generation (gen)[#]	2nd gen[+]	3rd gen
Total area imaged (mm^2)	5.69	13.1	1,810
Total images in area	54,717	100,589	7,335,982
Multibeam FOVs	897	1649	120,262
Pixels (megapixels)	75,276	857,086	1.07×10^{10}
Size (Terabytes)	0.08	0.87	10.98

FOVs refers to Fields of View. See links for navigable, rendered maps comprising each dataset:
[#]https://www.mechbio.org/sites/mechbio/files/maps5/index.html (Knothe Tate et al., 2016c).
[+]https://www.mechbio.org/sites/mechbio/files/maps7/index.html user: mechbio, password: #google-maps.

Automation of Landmark Identification Using the You Only Look Once Machine Learning Algorithm

Increasing dataset sizes necessitated development of objective, automated methods for identification and quantification of cells, an ideal application for machine learning approaches. To this end, we implemented the so-called "You Only Look Once" (YOLO) machine learning algorithm (Redmon et al., 2015), using the previously marked datasets as training data (**Figures 2A,B**).

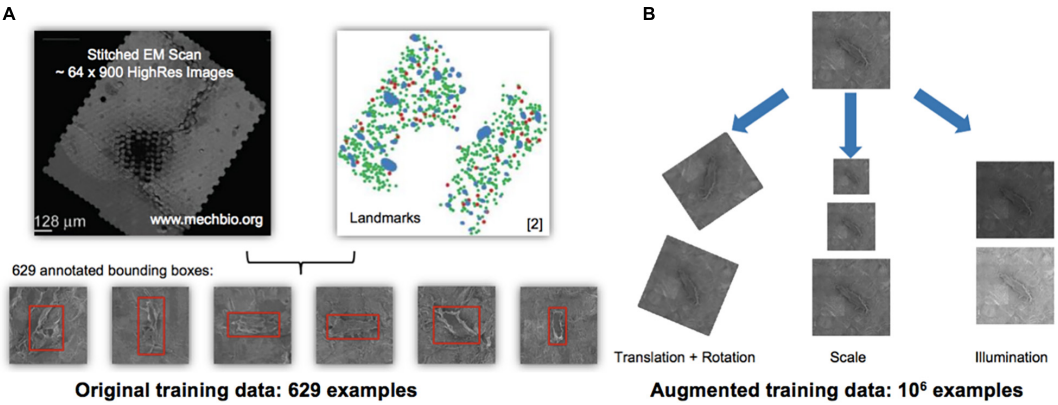

FIGURE 2 | Automated detection algorithm to classify osteocytes using manual methods and the You Only Look Once algorithm (YOLO; Redmon et al., 2015). **(A,B)** Training and testing data for the machine learning algorithm using the 1st generation mSEM map. The manually acquired training data set, comprising 629 examples of osteocytes (**A**—stitched electron microscopy scan on left and manually located and "pinned," using Google Maps API, osteocytes, where green indicates viable and red marks pyknotic), was scaled up to an augmented training set of 10^6 examples **(B)** using digital permutations of translation and rotation, scale and illumination. From the augmented dataset, 75% of the data was used for training and 25% of the data was used for testing of the YOLO algorithm, all using the data from the 1st generation map. The algorithm was then run independently on the 2nd (**Figure 3**) and 3rd generation maps. Note: the red bounding boxes **(A)** indicate detected cells prior to classification, i.e., not indicative of cells' health status.

Seventy five percent of the augmented dataset was used to train the model and 25% of the data were set aside to test the model. The You Only Look Once machine learning algorithm was applied to detect cells on all datasets (**Figure 2C**). The image processing was simple and straightforward. The YOLO detection system resizes the input image to 448 × 448, runs a single convolutional network on the image, and thresholds the resulting detections by the model's confidence.

In summary, we acquired three datasets rendering osteocyte networks in tissues of the femoral head. The different datasets include data from different samples imaged using new generations of mSEM and associated increasing computational capacity. The first data set included 5.69 mm^2 tissue and over 50,000 images (0.08 terabyte), with manual identification of 629 osteocytes taking several weeks' time. To enable automated, rapid detection of osteocytes and in consideration of the increasing size and complexity of the datasets enabled through advances in the mSEM instrument and parallel computational advances (second and third generations) over the past decade (from an advanced prototype to a commercial system), we applied a machine learning algorithm to detect osteocytes based on the You Only Look Once (YOLO) convolutional neural network described originally by Redmon et al. (2015). The YOLO algorithm is faster and more efficient than typical classifier-based algorithms. YOLO "looks at an image once" (thus the acronym) to predict the presence of objects and their locations. The image is divided into an S × S grid in which bounding boxes and confidence scores for object detection within bounding boxes are calculated. The confidence scores give a quantitative probability of how similar the predicted box detecting an object is with the training data (ground truth). The higher the confidence score, the more accurate the prediction (Redmon et al., 2015; Shivaprasad, 2019).

We applied the machine learning approach to second and third generation maps, with the third data set comprising 1,810 mm^2 tissue and over 7,000,000 images (10.98 TB), identifying a total of 206,180 osteocytes in 100 h on a graphics processing unit (GPU, GeForce GTX 1080 graphics card enabled) compared to the manual pinning method of our previously published work (Knothe Tate et al., 2016c) that identified 629 osteocytes manually over several weeks. The algorithm performance currently exceeds 92% accuracy for osteocyte detection and classification, based on the accuracy of detecting the 629 original cells using the trained procedure.

Osteocyte coordinates can be extracted from the YOLO classified image set, enabling high throughput analyses of massive datasets, which in the future could include other cellular inhabitants of tissues including blood cells, immune cells, chondrocytes, etc. While the method shows great promise for automated detection of cells, the greatest limitation of the method is the definition of appropriate and unbiased classifiers. The definition of osteocytes as pyknotic and viable based on the number of cell processes was shown to be flawed in a parallel study testing the assumption using biochemical based viability measures (Anastopolous and Knothe Tate, 2021). Not only did the method not account for empty osteocyte lacunae that appeared as "ghost osteocytes" (resin filled empty lacunae) but also osteocyte process number has not been tied inextricably to cell viability. Multimodal imaging methods and assays using iodine to stain nuclear material demonstrate that better descriptors of cell health are needed (Anastopolous and Knothe Tate, 2021).

With these limitations in mind, the technological approach provides novel opportunities for a new field of cellular epidemiology, where emergent changes in cell health may in the future be used to predict disease outbreaks and prevent disease transmission, much like they are used at the length scale of human inhabitants of geographically defined environments (Knothe Tate et al., 2016c; Dong et al., 2019). The described

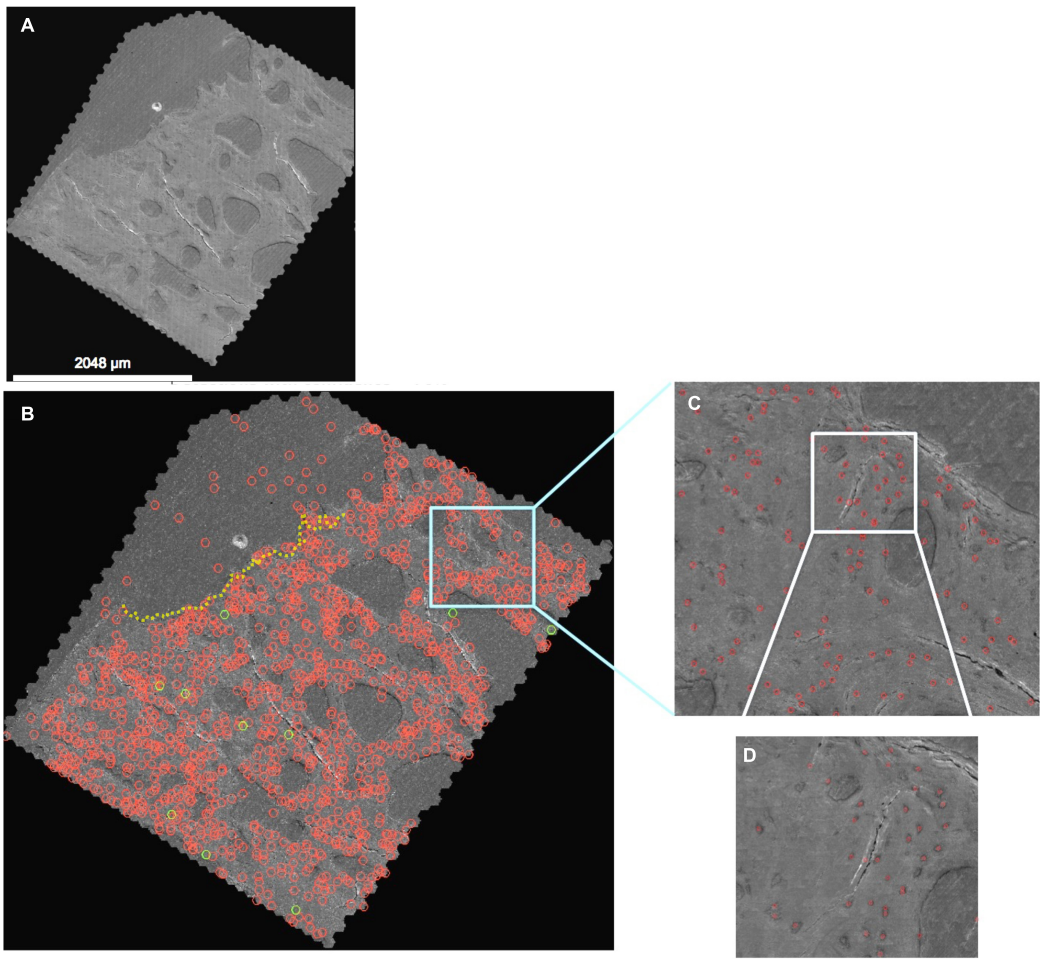

FIGURE 3 | Automated detection algorithm applied to the 2nd generation map **(A)**, where detections with greater than 70% confidence (quantitative prediction of match to "ground truth" defined by training data) are depicted. **(B)** The entire map, depicting higher resolution details at increasing levels of zoom **(C,D)** in the Google Maps API. Note: the red circles indicate detected cells which are changed to green when the classifier (three or more processes) is met. Red circles above the dotted yellow line delineating the edge of the tissue surface (**B**, upper corner) are cells, vessels and artifacts outside of the femoral head and neck tissue. The map depicted here can be navigated and explored like Google Maps at http://www.mechbio.org/sites/mechbio/files/maps7/index.html to access the map, type in user: mechbio, password: #google-maps.

workflow and data analytics pipeline enables acquisition, preparation, and imaging of tissue and organ samples, as well as post-imaging rendering of and analysis of cellular networks from different tissues across length scales, of nano- to meso-length scales.

Implications for Understanding Neuromechanics and the Control of Physical Behavior and Neuromuscular Training

In addition to its obvious application for development of next generation materials, devices and diagnostics, this disruptive biosystems engineering platform provides a novel tool for elucidating the relationship between neural and musculoskeletal connectomics, movement, navigation and memory (Epstein et al., 2017; Knothe Tate, 2017). The loss in connectivity observed in the dendritic osteocyte network of aging and diseased bone is similar to that of the brain cells in aging individuals and patients with early onset dementia (Huang et al., 2015; Knothe Tate and Fath, 2016; Knothe Tate et al., 2016c; Pereira et al., 2016; Rossini et al., 2020). The possibility that movement and geographical maps are encoded not only in the brain but also in the musculoskeletal tissues is tantalizing. The technological platform here provides a means by which networks within tissues and organs of different systems within individual organisms can be studied, from cellular to whole being contexts. This is expected to lead to discovery of novel mechanisms underpinning motor neural circuitry and biomechanical action. Just as dogs and other mammals train their neural networks in their sleep, running and jumping across virtual dream terrains, perhaps the physical experience of life itself is encoded in our cells, the structural proteins our cells manufacture via gene expression and secrete to form our

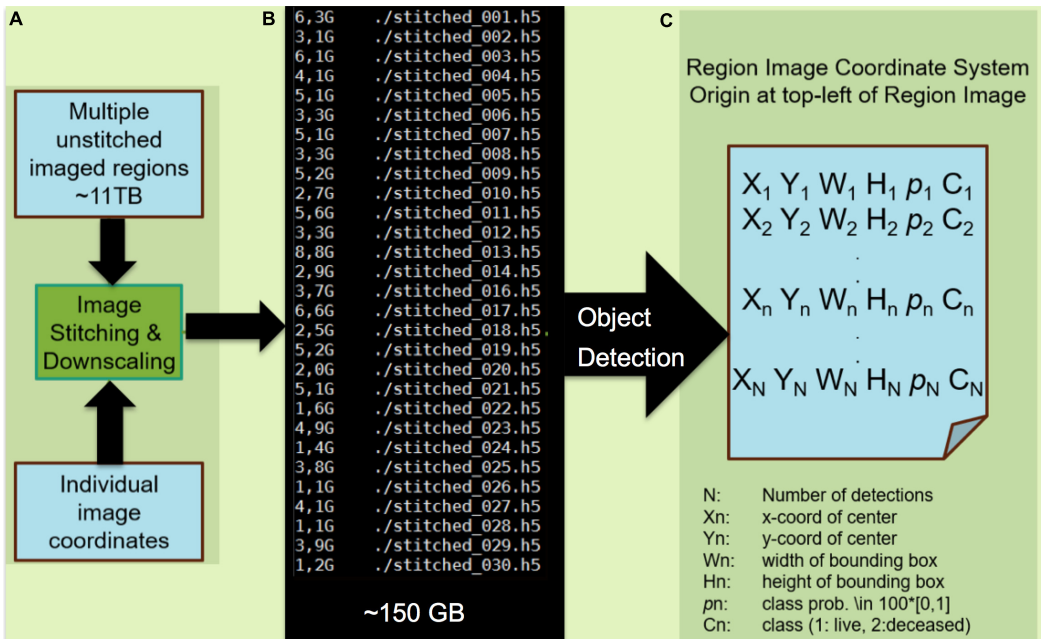

FIGURE 4 | Processing of images and application of the machine learning classification algorithm. **(A)** Module A preprocesses the mSEM output by stitching individual images into region-wide panoramas by the virtue of recorded image coordinates. In the interest of computational efficiency, the resulting image is down-scaled such that individual cells occupy *circa* 200 × 200 pixels. Here, the 11TB mSEM output from the 3rd generation map is stitched into 30 image regions amounting to 150 GB of data after downscaling. **(B)** Module B applies the pretrained object detector. **(C)** The output is a file listing that includes the location of each detected cell as a bounding box (X,Y,W,H), class (viable/pyknotic, annotated as "deceased") and associated confidence *p*. Each of N detections results in a set of five predictions for each corresponding bounding box, including the x and y coordinates of the center of the bounding box (X_n,Y_n), width and height of the bounding box (W_n,H_n), and the confidence of the detection (p_n where a confidence or probability of 0 means no object was detected and 1.0 means a perfect match with "ground truth"). The object is then further classified as live or deceased (C_n). The object detector is pretrained using 600 living and 50 pyknotic examples (Knothe Tate et al., 2016b) and took 12 h to train on a single graphics processing unit (GTX1080). The testing phase on the 150 GB dataset lasted 100 h. Note: modules A and B can be combined into a single module.

tissues, as well as the adaptation of our tissues throughout life (Knothe Tate, 2020).

MATERIALS AND METHODS

Sample Preparation

Tissues were fixed in a combination of 4% formaldehyde and 2.5% paraformaldehyde in 0.2 M cacodylate buffer. Tissues were then embedded in poly(methyl methacrylate) under vacuum (Ngo et al., 2019). Following this, the sample was precision CNC-milled and etched using 0.02 M hydrochloric acid and 10% sodium hypochlorite to remove organic and inorganic top layer, in order to reveal cellular material (Reilly et al., 2001; Knapp et al., 2002). The sample was then carbon coated and placed under a vacuum, preparing for mSEM imaging. Imaging was performed on the 61-beam Zeiss MultiSEM 505-prototype at 12 nm pixel size.

Identification of Relevant Landmarks, Creation of Training Datasets

Manual marking of landmarks was described in a previous paper (Knothe Tate et al., 2016c) and the thereby identified 629 osteocytes were used as the basis for a training and testing data set (**Figure 2**).

Machine Learning Approach Using the You Only Look Once (YOLO) Algorithm

The "You Only Look Once" (YOLO) neural network automated object detection algorithm (Redmon et al., 2015; *described further for the layperson in* Shivaprasad, 2019) was applied to facilitate rapid throughput diagnostic assessment of imaging datasets while mitigating the effects of observer bias. An image is first divided into a grid, where each grid cell predicts bounding boxes for objects. Then probability-based confidence scores are calculated for the bounding boxes; the confidence score compares how close the predicted bounding box and object therein matches the known objects and bounding boxes defined by the training data set, or "ground truth." To prevent multiple detections of the same object, the bounding box with highest confidence greater than 0.5 (which would be 50% chance of matching the training data point) is selected from overlapping bounding boxes; referred to as non-max suppression, this process results in highest confidence for model predictions per object detected and maximizes accuracy of the model.

Initially, YOLO was trained for automated osteocyte detection, using 629 annotated cells, which were further

augmented to 10^6 examples through variation by rotation, scale and contrast (**Figure 2**). Unseen images were then processed with YOLO and automatically detected objects were identified and marked by bounding boxes. The success of the YOLO algorithm has been proven for detecting osteocytes in the 2nd generation map within 100 h of testing. A straight-forward approach to improve the detector performance includes collection of more than 1,000 false- and missed-detections (**Figure 4**) to obtain a more representative training dataset.

DATA AVAILABILITY STATEMENT

The original contributions presented in the study are included in the article/supplementary material, further inquiries can be directed to the corresponding author/s.

ETHICS STATEMENT

The studies involving human participants were reviewed and approved by the Cleveland Clinic Institutional Review Board.

AUTHOR CONTRIBUTIONS

MK and DZ conceived the work. The specimens were collected and prepared for imaging by MK with assistance from the Cleveland Clinic and Zeiss teams. Image acquisition was carried out by the Zeiss Team, led by DZ and MK in the Demonstration Labs at Carl Zeiss Microscopy GmbH in Oberkochen. The machine learning algorithm was developed and tested by AS and CW. The manuscript was written by MK and was revised and approved of by all coauthors. All authors contributed to the article and approved the submitted version.

FUNDING

This work was supported in part through the National Health and Medical Research Council (Development Grant), Paul Trainor Foundation and the Alexander von Humboldt Foundation, and in kind support of Carl Zeiss Microscopy AG.

ACKNOWLEDGMENTS

We express our appreciation to Ulf Knothe, M.D., D.Sc., for his invaluable role in acquiring specimens through the Cleveland Clinic (IRB), and Tomasz Garbowski for his mSEM expertise as well as Carl Zeiss Microscopy GmbH, for in kind use of their mSEM microscope and infrastructure. We acknowledge with appreciation colleagues and trainees for myriad contributions to this ongoing research project. T. Garbowski from the Zeiss Team provided invaluable assistance in acquiring images at the Zeiss Demonstration Labs.

REFERENCES

Anastopolous, S., and Knothe Tate, M. L. (2021). Unleashing The Power Of Multimodal Imaging To Assess Cell Survival In Tissues Of The Osteoarthritic Hip. *Orthop. Res. Soc. Meeting* 64:2406.

Anderson, E. J., Kreuzer, S. M., Small, O., and Knothe Tate, M. L. (2008). Pairing computational and scaled physical models to determine permeability as a measure of communication in micro- and nano-scale pericellular spaces. *Microfluidics Nanofluid.* 4, 193–204.

Blakely, T. (2021). *A Browsable Petascale Reconstruction of the Human Cortex*. Available online at: https://ai.googleblog.com/2021/06/a.browstable-petascale-reconstruction-at.html (accessed June, 2021).

Dong, E., Du, H., and Gardner, L. (2019). An interactive web-based dashboard to track COVID-19 in real time. *Lancet Infect. Dis.* 20, 533–534. doi: 10.1016/S1473-3099(20)30120-1

Eberle, A.-L., Mikula, S., Schalek, R., Lichtman, J., Knothe Tate, M. L., and Zeidler, D. (2015). High-resolution, high-throughput imaging with a multiple beam scanning electron microscope. *J. Microscopy* 259, 114–120. doi: 10.1111/jmi.12224

Epstein, R. A., Patai, E. Q., Julian, J. B., and Spiers, H. J. (2017). The cognitive map in humans: Spatial navigation and beyond. *Nat. Neurosci.* 20, 1504–1513. doi: 10.1038/nn.4656

Günther, A., Dedek, K., Haverkamp, S., Irsen, S., Briggman, K. L., and Mouritsen, H. (2021). Double cones and the diverse connectivity of photoreceptors and bipolar cells in an Avian Retina. *J. Neurosci.* 41, 5015–5028. doi: 10.1523/JNEUROSCI.2495-20.2021

Hayworth, K. J., Peale, D., Januszewski, M., Knott, G. W., Lu, Z., Xu, C. S. et al. (2020). Gas cluster ion beam SEM for imaging of large tissue samples with 10 nm isotropic resolution. *Nat. Methods* 17, 68–71 doi: 10.1038/s41592-019-0641-2

Hayworth, K. J., Xu, C. S., Lu, Z., Knott, G. W., Fetter, R. D., Tapia, J. C., et al. (2015). Ultrastructurally smooth thick partitioning and volume stitching for large-scale connectomics. *Nat. Methods* 12, 319–322. doi: 10.1038/nmeth.3292

Huang, S.-W., Wang, W.-T., Chou, L.-C., Liao, C.-D., Liou, T.-H., and Lin, H.-W. (2015). Osteoarthritis increases the risk of dementia: a nationwide cohort study in Taiwan. *Sci. Rep.* 5:10145. doi: 10.1038/srep10145

Jbabdi, S., and Behrens, T. E. (2013). Long-range connectomics. *Ann. N Y. Acad. Sci.* 1305, 83–93. doi: 10.1111/nyas.12271

Knapp, H. F., Reilly, G. C., Stemmer, A., Niederer, P., and Knothe Tate, M. L. (2002). Development of preparation methods for and insights obtained from Atomic Force Microscopy of fluid spaces in cortical bone. *Scanning* 24, 25–33. doi: 10.1002/sca.4950240104

Knothe Tate, M. L. (2017). "Navigation of bee brains to human hips - microscopy and the modern Magellans," in *A new age in scanning electron microscopy: Applications in the life sciences* (Washington, DC: AAAS), 19–23.

Knothe Tate, M. L. (2020). Advanced design and manufacture of mechanoactive materials - inspired by skin, bones and skin-on-bones. *Front. Bioeng. Biotechnol.* 8:845. doi: 10.3389/fbioe.2020.00845

Knothe Tate, M. L., and Fath, T. (2016). The only constant is change: next generation medical devices for physical and mental health. *Adv. Healthc. Mat.* 5, 1840–1843.

Knothe Tate, M. L., Detamore, M., Capadona, J., Wooley, A., and Knothe, U. (2016c). Engineering and Commercialization of Human-Device Interfaces, from Bone to Brain. *Biomaterials* 95, 35–46. doi: 10.1016/j.biomaterials.2016.03.038

Knothe Tate, M. L., Falls, T., Mishra, S., and Atit, R. (2010). Engineering an ecosystem: taking cues from nature's paradigm to build tissue in the lab and the body. *Fields Instit. Mathemat. Biol. Monogr. Ser. N. Perspect. Mathemat. Biol.* 57, 113–134.

Knothe Tate, M. L., Gunning, P. W., and Sansalone, V. (2016a). Emergence of form from function - mechanical engineering approaches to probe the role of stem cell mechanoadaptation in sealing cell fate. *Bioarchitecture* 6:1229729. doi: 10.1080/19490992.2016.1229729

Knothe Tate, M. L., Tami, A. E. G., Bauer, T. W., and Knothe, U. (2002). Micropathoanatomy of Osteoporosis - Indications for a Cellular Basis of Bone Disease. *Adv. Osteopor. Fracture Manage.* 2, 9–14.

Knothe Tate, M. L., Zeidler, D., Nathanson, A., Ngo, L., Garbowski, T., Srikantha, A., et al. (2019). Diagnostics of the future for musculoskeletal connectomics – from nano to mesoscale and prototype to pipeline. *Trans. Arth. Res. Soc.* 62:2046.

Knothe Tate, M. L., Zeidler, D., Pereira, A. F., Hageman, D., Garbowski, T., Mishra, S., et al. (2016b). Organ-to-Cell-Scale Health Assessment Using Geographical Information System Approaches with Multibeam Scanning Electron Microscopy. *Adv. Healthc. Mat.* 5, 1581–1587. doi: 10.1002/adhm.201600026

Lichtman, J. W., Pfister, H., and Shavit, N. (2014). The big data challenges of connectomics. *Nat. Neurosci.* 17, 1448–1454.

Mikula, S., and Denk, W. (2015). High-resolution whole-brain staining for electron microscopic circuit reconstruction. *Nat. Methods* 12, 541–546.

Mikula, S., Binding, J., and Denk, W. (2012). Staining and embedding the whole mouse brain for electron microscopy. *Nat. Methods* 9, 1198–1201. doi: 10.1038/nmeth.2213

Ng, J., Kilbreath, S., Kersch, M., and Knothe Tate, M. L. (2017a). Establishing the Basis for Mechanobiology-Based Physical Therapy Protocols to Potentiate Cellular Healing and Tissue Regeneration. *Front. Physiol. Exerc. Physiol.* 2017:00303. doi: 10.3389/fphys.2017.00303

Ng, J., Knothe, L., Whan, R., Knothe, U., and Knothe Tate, M. L. (2017b). Scale-up of Nature's Tissue Weaving Algorithms to Engineer Advanced Functional Materials. *Sci. Rep.* 7:40396. doi: 10.1038/srep40396

Ngo, L., Nathanson, A., Garbowski, T., Knothe, U., Zeidler, D., and Knothe Tate, M. L. (2019). Sample preparation protocol enabling nano-to-mesoscopic mapping of cellular connectomes and their habitats in human tissues and organs. *Bio-protocol* 9:e3298. doi: 10.1101/533448

Pereira, A. F., Hageman, D. J., Garbowski, T., Riedesel, C., Knothe, U., Zeidler, D., et al. (2016). 'Creating High-Resolution Multiscale Maps of Human Tissue Using Multi-beam SEM'. *PLoS Comp. Biol.* 12:e1005217. doi: 10.1371/journal.pcbi.1005217

Putra, V. D. L., Song, M. J., McBride-Gagyi, S., Chang, H., Poole, K., Whan, R., et al. (2019). Mechanomics approaches to understand cell behavior in context of tissue neogenesis, during prenatal development and postnatal healing. *Front. Cell Dev. Biol.* 7:354. doi: 10.3389/fcell.2019.00354

Redmon, J., Divvala, S., Girshick, R., and Farhadi, A. (2015). *You Only Look Once: Unified, Real-Time Object Detection*. New Jersey, NJ: IEEE. doi: 10.1109/CVPR.2016.91

Reilly, G., Knapp, H., Stemmer, A., Niederer, P., and Knothe Tate, M. L. (2001). Investigation of the morphology of the lacunocanalicular system of cortical bone using atomic force microscopy. *Ann. Biomed. Eng.* 29, 1074–1081. doi: 10.1114/1.1424910

Rossini, P. M., Miraglia, F., Alú, F., Cotelli, M., Ferreri, F., De Iorio, R., et al. (2020). Neurophysiological hallmarks of neurodegenerative cognitive decline: the study of brain connectivity as a biomarker of early dementia. *J. Pers. Med.* 10:34. doi: 10.3390/jpm1002 0034

Seung, S. (2012). *Connectome - How the Brain's Wiring Makes us Who We Are*. Boston: Mariner Books.

Shivaprasad, P. (2019). *A Comprehensive Guide To Object Detection Using YOLO Framework — Part 1*. Toronto: towardsdatascience.

Swanson, L. W., and Lichtman, J. W. (2016). From Cajal to connectome and beyond. *Annu. Rev. Neurosci.* 39, 197–216. doi: 10.1146/annurev-neuro-071714-0333954

Conflict of Interest: Zeiss provided in kind support for this project, which is of a fundamental and translational nature. AS and CW were employed by Zeiss AG. DZ was employed by Carl Zeiss MultiSEM GmbH.

The remaining author declares that the research was conducted in the absence of any commercial or financial relationships that could be construed as a potential conflict of interest.

frontiers in Human Neuroscience

SYSTEMATIC REVIEW
published: 01 September 2021
doi: 10.3389/fnhum.2021.620573

The Effect of Repetitive Transcranial Magnetic Stimulation on Lower-Limb Motor Ability in Stroke Patients: A Systematic Review

Huiliu Fan[1], *Yang Song*[1,2,3], *Xuanzhen Cen*[1,2,3], *Peimin Yu*[1], *István Bíró*[2,3] *and Yaodong Gu*[1]*

[1] Faculty of Sports Science, Ningbo University, Ningbo, China, [2] Doctoral School of Safety and Security Sciences, Obuda University, Budapest, Hungary, [3] Faculty of Engineering, University of Szeged, Szeged, Hungary

Repetitive transcranial magnetic stimulation (rTMS) is fundamental in inducing neuroplastic changes and promoting brain function restoration. Nevertheless, evidence based on the systematic assessment of the implication of rTMS in stroke patients is inadequate. This study aimed to evaluate the value of rTMS in the treatment of lower-limb motor dysfunction in stroke patients via gait characteristics. The electronic literature search was performed in ScienceDirect, Google Scholar, and PubMed databases using "repetitive transcranial magnetic stimulation," "gait," and "stroke" between 2000 and 2020. By screening all the identified studies, a total of 10 studies covering 257 stroke patients were included by matching the inclusion criteria, involving both rTMS with high (≥5 Hz) and low frequency (<5 Hz). Despite the limited study number and relatively high risk of bias, the results of this review primarily confirmed the enhancing effects of rTMS on the lower-limb motor ability (e.g., gait and balance) of stroke patients. In addition, 15- to 20-min course of rTMS for 2 to 3 weeks was found to be the most common setting, and 1 Hz and 10 Hz were the most commonly used low and high frequencies, respectively. These results might have significant clinical applications for patients with weakened lower-limb mobility after a stroke. Nevertheless, more rigorous studies in this field are much warranted.

Systematic Review Registration: https://inplasy.com/, identifier INPLASY2021 80079.

Keywords: stroke, systematic review, walking, balance, repetitive transcranial magnetic stimulation

OPEN ACCESS

Edited by:
Taiar Redha,
Université de Reims Champagne-Ardenne, France

Reviewed by:
Nejc Sarabon,
University of Primorska, Slovenia
Massimo Venturelli,
University of Verona, Italy
Sanjay Kumar,
Oxford Brookes University, United Kingdom

***Correspondence:**
Yaodong Gu
guyaodong@nbu.edu.cn

Specialty section:
This article was submitted to Motor Neuroscience, a section of the journal Frontiers in Human Neuroscience

Received: *23 October 2020*
Accepted: *12 August 2021*
Published: *01 September 2021*

Citation:
Fan H, Song Y, Cen X, Yu P, Bíró I and Gu Y (2021) The Effect of Repetitive Transcranial Magnetic Stimulation on Lower-Limb Motor Ability in Stroke Patients: A Systematic Review. Front. Hum. Neurosci. 15:620573. doi: 10.3389/fnhum.2021.620573

INTRODUCTION

Stroke is an acute syndrome of clinical signs of focal (or global) disturbance of cerebral function, which can even lead to death (Wolfe, 2000). Disability is a common complication for patients who have survived a stroke. There are also some secondary changes in the skeletal muscles of stroke patients, including the reduced muscle mass as well as increased intramuscular fat (Scherbakov et al., 2013), which may further reduce the muscle strength and gait independence (Akazawa et al., 2017; Naoki et al., 2018). Eventually, these results would seriously influence the life quality of these patients (Wade et al., 1992). According to previous studies, nearly 50% of stroke patients would suffer from hemiparesis as well as 30% of them are unable to walk without assistance (Kelly-Hayes et al., 2003). Previous studies have also found that stroke patients walked slower compared to healthy individuals, and it can also be distinguished by the higher falling cadence, prolonged

gait cycle, temporal gait asymmetry, and also increased double support phase after stroke (Von Schroeder et al., 1995; Patterson et al., 2008).

It was indicated that gait performance is an important index to evaluate lower extremity motor function recovery post-stroke (Barroso et al., 2017). Most stroke patients would obtain a certain degree of walking ability improvement after normal rehabilitation treatment, but most of them are accompanied by the abduction and external rotation of the hip joint, hyperextension of the knee joint, foot drop, varus, and short support time of the affected side, resulting in the gait abnormity (Byun et al., 2011). Evaluating the gait biomechanics of stroke patients has been applied to predict the improvement in functional ability after interventions (Kim and Eng, 2004). It also plays an important role in making rehabilitation strategies and monitoring its impact (Barroso et al., 2017). For example, the symmetry of the center of foot pressure in stroke patients is closely related to the degree of lower limb dysfunction, limb balance ability, stride speed, and body stability, which can reflect the degree of lower extremity function recovery and walking quality in stroke patients (Chen et al., 2007; Patterson et al., 2008).

Repetitive transcranial magnetic stimulation (rTMS), one of the brain stimulation techniques without any trauma, can be used to induce neuroplastic changes as well as promote brain function restoration (Clément et al., 2018). For the different brain functions, different intensities, frequencies, stimulation positions, and coil directions of rTMS need to be adjusted to achieve good therapeutic effects (Mansur et al., 2005; Machado et al., 2008). Previous research has proved that using rTMS can stimulate the representative brain areas of lower limb movement and further help patients improve motor function (Chieffo et al., 2014; Sasaki et al., 2016). For example, three weeks of high-frequency deep rTMS has a favorable influence on long-term improvements in the motor function of the lower extremity after stroke, and it could last for more than a month since the treatment finished (Chieffo et al., 2014). rTMS combined with traditional physiotherapy and occupational therapy can achieve a better rehabilitation effect on promoting motor function recovery (Cha and Kim, 2017). Besides, rTMS combined with repetitive transcranial electrical stimulation also contributed to the motor function recovery in stroke patients, which is more effective than combined limb function training (Attal et al., 2016). Tung et al. (2019) has already reviewed the short-term beneficial effects of rTMS on the post-stroke recovery of lower limb motor function, and the safety of applying rTMS has been further affirmed. Nevertheless, there is quite limited evidence based on the systematic assessment of the implication of rTMS in stroke patients up to now, let alone any conclusions regarding the better setting of rTMS interventions (e.g., frequency and duration) that could contribute to more benefit.

Therefore, the aim of this study was to primarily review and summarize the value of rTMS in the treatment of lower extremity motor dysfunction in stroke subjects via gait characteristics, and then try to find out the appropriate rTMS setting that may contribute to more benefits. The review could provide specific knowledge for researchers and clinicians on the use of rTMS in patients.

METHODS

Search Strategy

The search strategy was applied to find out all the relevant published literature on the influence of rTMS on lower limb motor dysfunction in stroke patients. The extensive systematic search for all electronic publications from 2000 to 15 February 2020 was conducted using three databases including ScienceDirect, Google Scholar, and PubMed. The English-language literature search employed the following search words: "repetitive transcranial magnetic stimulation" AND "gait" AND "stroke". The citation snowballing method was applied to identify other potentially relevant studies in the reference list of all eligible articles (Song et al., 2020). And these studies that have been accidentally overlooked were searched in other electronic databases to get available full-text by entering the specific information of authors and article titles.

In order to ensure a rigorous searching process, two researchers independently searched and assessed the retrieved literature. Any disagreements of inclusion (if existed) would be resolved with the third author.

Eligibility Criteria

After deleting duplicate articles, the retrieved articles were screened first by titles then assessed by abstracts and full-text to meet the following eligibility criteria in accordance with the PICOS standard. (1) participants/patients, participants who have been diagnosed with stroke were included in this study, and there is no restriction on age, sex, and ethnicity; (2) Interventions, studies where participants received rTMS interventions or rTMS interventions combined with traditional physiotherapy and occupational therapy were included; (3) comparison, there is no limitation regarding the control interventions; (4) outcome, the main outcomes that collected from these included studies was the change of gait characteristics after interventions; (5) study design, English papers that published on peer-reviewed journals were covered, however, conference abstracts, review articles, book chapters, case reports, etc., were not included in this review.

Data Extraction

For each published literature, the following information was extracted and summarized, and verified by two authors independently, characteristics of studies (i.e., authors and year), characteristics of subjects (i.e., sample size, age, gender, time post stroke, and treatment state), experimental design (i.e., coil type, intervention, control, and parameters), and primary outcomes. Mendeley software (Elsevier Ltd., Amsterdam, Netherlands) was applied to organize published literature and create citations. Any disagreements were handled by discussing or consulting with another author.

Study Quality Assessment

According to the Cochrane Risk of Bias Assessment Tool, two researchers independently evaluated the quality of these included studies. More specifically, seven following aspects were assessed, (1) random sequence generation; (2) allocation concealment; (3)

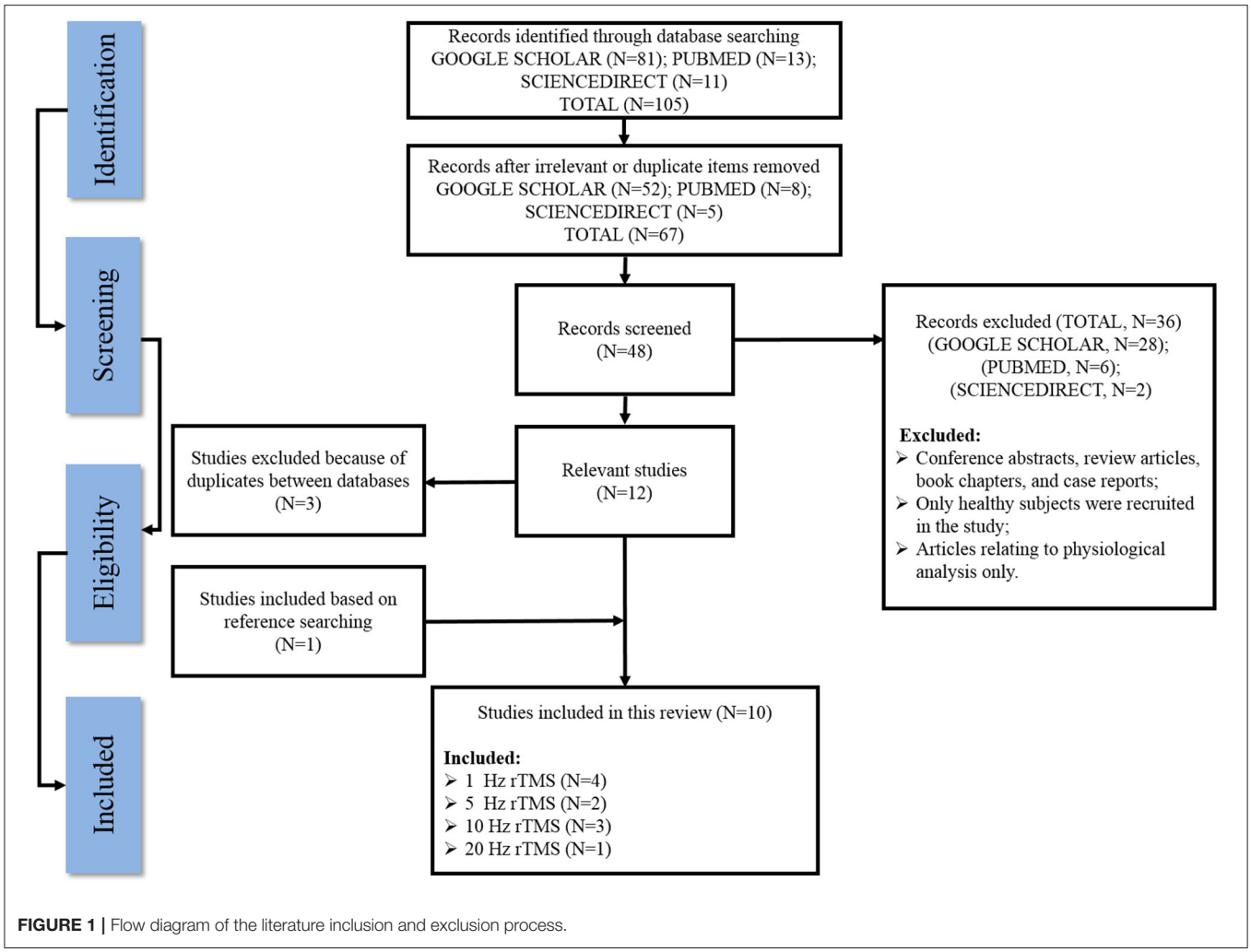

FIGURE 1 | Flow diagram of the literature inclusion and exclusion process.

blinding of participants and personnel; (4) blinding of outcome assessment; (5) incomplete outcome data; (6) selective reporting; (7) other biases. Any disagreements were handled by discussing or consulting with another author.

RESULTS

Search Results

Figure 1 outlines a flow diagram illustrating the search history and selection protocol. The literature search produced a total of 105 records from three electronic databases (SCIENCEDIRECT, GOOGLE SCHOLAR, and PUBMED) and they were reduced to 67 after removing all the irrelevant/duplicate articles. Based on the eligibility criteria, 28 articles from GOOGLE SCHOLAR, six articles from PubMed, and two articles from SCIENCEDIRECT were excluded as potentially inappropriate for the current study. One additional article was included after checking the reference lists of the eligible articles, while three articles were removed owing to duplicates between these databases. Finally, a total of 10 articles that met the inclusion standard were included in the present systematic review.

Study Quality

The quality of all included studies was evaluated in terms of risk of bias, and the results were presented in **Figure 2**; **Table 1**. Firstly, it is always not possible to completely blind the participants and personnel to allocation and outcome. Thus, the following two aspects, blinding of participants and personnel and blinding of outcome assessment, contributed to the main sources of risk of bias. Furthermore, of all the 10 studies included in this review, only half of them presented the detailed methods of group randomization and used the allocation concealment, which further lowered the study quality. Nevertheless, a low risk of bias of the incomplete outcome data, selective reporting, and other biases domains was found in most studies.

The Basic Characteristics of Included Studies

Tables 2, **3** summarized the basic characteristics of all the included studies. Of all the included studies published from 2000 to 2020, 257 stroke patients were covered in these studies, with the age ranged from less than 18 to 80 years old. The stimulus interventions can be classified as low-frequency (defined

TABLE 1 | Risk of bias evaluation of included studies.

Trials	Random Sequence Generation	Allocation Concealment	Blinding of Participants and Personnel	Blinding of Outcome Assessment	Incomplete Outcome Data	Selective Reporting	Other Bias
Chieffo et al. (2014)	Unclear	Unclear	High	High	Low	Low	Low
Kim et al. (2014)	Unclear	High	High	High	Low	Low	Low
Rastgoo et al. (2016)	High	Unclear	High	High	Low	Low	Low
Choi et al. (2016)	Low	Low	High	High	Low	Low	Low
Wang et al. (2019)	Low	Low	High	High	High	Low	Low
Kakuda et al. (2013)	Low	High	High	High	High	Low	Low
Elkholy et al. (2014)	Low	Unclear	High	High	Low	Low	Low
Wang et al. (2012)	Unclear	Low	High	High	Low	Low	Low
Goh et al. (2020)	Unclear	Low	High	High	Low	Low	Low
Ji et al. (2016)	Low	Low	High	High	Low	Low	Low

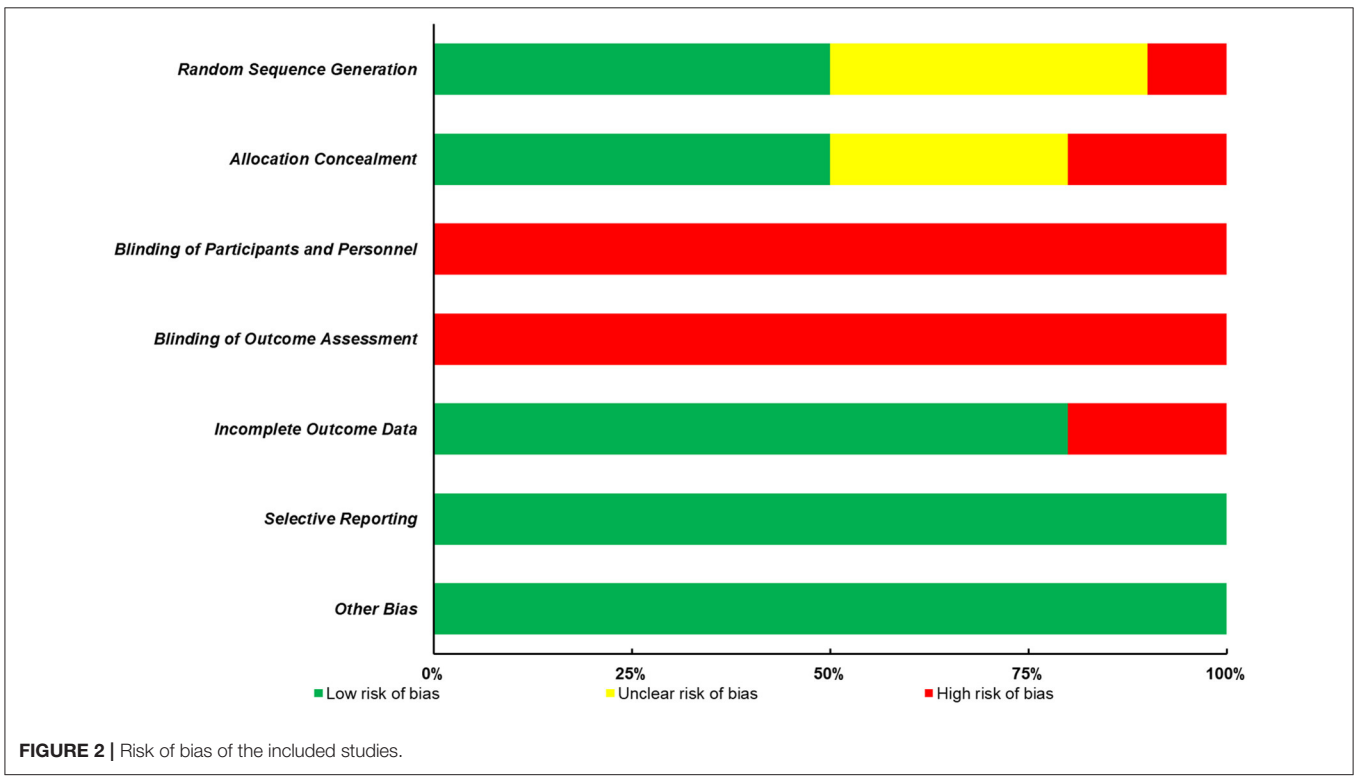

FIGURE 2 | Risk of bias of the included studies.

as <5 Hz) and high-frequency (defined as more than 5 Hz) based on the summary, with 1 Hz being the most commonly used low frequency and 10 Hz being the most commonly used high frequency. The duration of the intervention varied from 1 week to 6 weeks, with 2 to 3 weeks being the most common setting.

The main findings of these included studies were further presented in the following two sections, (1) Effects of low-frequency stimulus; (2) Effects of high-frequency stimulus.

Effects of Low-Frequency Stimulus

Four studies that investigated the effects of low-frequency stimulus on lower-limb motor dysfunction of stroke patients were included in this review. Wang et al. (2012) first started trials on these patients. Subjects received rTMS or sham rTMS (1 Hz) followed by task-specific training for 2 weeks in total. The results demonstrated that real rTMS combined with task-oriented treatment significantly improved the motor control and walking ability of the stroke patients when compared to pre-intervention and sham rTMS + task-oriented treatment. Two subsequent studies based on a similar rTMS intervention (rTMS with 1 Hz frequency) also reported some positive results. Elkholy et al. (2014) compared the effects of low-frequency rTMS with conventional physical therapy on muscle tone, walking cadence, walking speed, and sensorimotor recovery of stroke patients. Subjects were required to receive 20-min rTMS 3 sessions per week for 6 weeks. They found that rTMS significantly improved

TABLE 2 | The basic characteristics of the included studies.

Trials	Sample size (N)	Gender M/F	Age (years) /time Post-Stroke (months)	Treatment State	Intervention	Coil type	Control	Experimental Design	Outcome Parameters
1. Low-frequency rTMS									
Elkholy et al. (2014)	N: 30	16/14	rTMS: 44.06 ± 3.71/ 2.53 ± 0.52 CON: 45.66 ± 4.27/ 2.533 ± 0.516	Cerebrovascular accident	rTMS + physical therapy	Double-cone coil	Physical therapy	Frequency: 1 Hz Duration: 20 min x 3 sessions per week, 6 weeks	1. Muscle tone 2. Walking cadence 3. Walking speed 4. Sensorimotor recovery
Kim et al. (2014)	N: 32 rTMS: 22 CON: 10	rTMS: 11/11 CON: 6/4	rTMS: 67.4 ± 7.8/0.52 ± 0.42 CON: 64.8 ± 11.7/0.49 ± 0.16	First-ever ischemic cerebellar/brain stem stroke	rTMS	Figure-of-eight coil	Sham rTMS	Frequency: 1 Hz Duration: 15 min x 5 sessions, 5 days	1. Walking ability 2. Balance
Rastgoo et al. (2016)	N: 20 rTMS: 10 CON: 10	rTMS: 8/2 CON: 8/2	rTMS: 54.6 ± 11.75/30.2 ± 18.3 CON: 49.7 ± 11/27.4 ± 20.1	First-ever stroke resulted in unilateral hemiparesis	rTMS	Figure-of-eight coil	Sham rTMS	Frequency: 1 Hz Duration: 20 min x 5 sessions, 5 days	1. Muscle spasticity 2. Walking ability 3. Lower limb functions
Wang et al. (2012)	N: 24 rTMS: 12 CON: 12	rTMS: 7/5 CON: 8/4	rTMS: 64.90 ± 12.37/22.08 ± 13.92 CON: 62.98 ± 10.88/12.00 ± 14.76	Unilateral hemiparesis secondary to cerebrovascular accident	rTMS + task-oriented treatment	Figure-of-eight coil	Sham rTMS + task-oriented treatment	Frequency: 1 Hz Duration: 10 min x 10 sessions, 2 weeks	1. Motor performance 2. Walking performance
2. High-frequency rTMS									
Chieffo et al. (2014)	N: 10 rTMS: 10 CON: 10	NA	62.2 ± 10.23/21 ± 7.29	First-ever stroke in the middle cerebral artery	rTMS	H-coil	Sham rTMS	Frequency: 20 Hz Duration: 30 min x 10 sessions, 3 weeks	1. Lower limb functions 2. Walking ability
Choi et al. (2016)	N: 30 rTMS: 15 CON: 15	rTMS: 14/1 CON: 13/2	rTMS: 67.1 ± 3.8/49.6 ± 28.3 CON: 68.7 ± 5.2/44.0 ± 29.9	Chronic stroke in in the middle cerebral artery	rTMS	Figure-of-eight coil	Sham rTMS	Frequency: 10 Hz Duration: 10 min x 10 sessions, 2 weeks	1. Balance
Goh et al. (2020)	N: 15	10/5	57.7 ± 9.7/ 22.8 ± 16.7	First-ever left hemispheric stroke	rTMS	Double-cone coil	NA	Frequency: 5 Hz Duration: 16 min x 3 sessions, 7 ± 2days	1. Gait speed
Ji et al. (2016)	N: 30 rTMS: 15 CON: 15	rTMS: 8/7 CON: 9/6	rTMS: 53.80 ± 8.07/1.80 ± 0.77 CON: 56.33 ± 10.98/1.66 ± 0.61	Ischemic and hemispheric stroke	rTMS	Figure-of-eight coil	Sham rTMS	Frequency: 10 Hz Duration: 15 min x 5 sessions per week, 4 weeks	1. Static balance 2. Dynamic balance
Kakuda et al. (2013)	N: 19	10/9	56.2 ± 11.9/61.0 ± 26.1	A single symptomatic supratentorial stroke	rTMS + mobility training	Double-cone coil	NA	Frequency: 10 Hz Duration: 20 min x 20 sessions, 13 days	1. Walking velocity 2. Lower limb functions
Wang et al. (2019)	N: 14 rTMS: 8 CON: 6	rTMS: 7/1 CON: 4/2	rTMS: 53.5 ± 13.7/31.8 ± 24.0 CON: 54.7 ± 12.2/25.3 ± 15.7	Unilateral hemiparesis secondary to stroke	rTMS	Figure-of-eight coil	Sham rTMS	Frequency: 5 Hz Duration: 15 min x 3 sessions per week, 3 weeks	1. Walking speed 2. Gait symmetry 3. Lower limb functions 4. Muscle activity

N, number; M, male; F, female; rTMS, repetitive transcranial magnetic stimulation; CON, control interventions; NA, not available.

TABLE 3 | The primary outcomes of the included studies.

Trials	Primary outcomes
Low-frequency rTMS	
Elkholy et al. (2014)	rTMS significantly improved all the parameters of the stroke patients when compared to the pre-intervention and control groups.
Kim et al. (2014)	Real rTMS intervention significantly improved the walking ability and balance of the stroke patients when compared to pre-intervention and sham stimulation.
Rastgoo et al. (2016)	Real rTMS intervention significantly improved the muscle spasticity and motor function of the stroke patients when compared to pre-intervention and sham stimulation.
Wang et al. (2012)	Real rTMS + task-oriented treatment significantly improved the motor control and walking ability of the stroke patients when compared to pre-intervention and sham rTMS + task-oriented treatment.
High-frequency rTMS	
Chieffo et al. (2014)	Real rTMS intervention significantly improved the lower limb functions of the stroke patients when compared to pre-intervention and sham stimulation.
Choi et al. (2016)	Real rTMS intervention significantly improved the balance function of the stroke patients when compared to pre-intervention and sham stimulation.
Goh et al. (2020)	rTMS significantly improved the dual-task gait speed, but not the single-task gait speed of the stroke patients, when compared to pre-intervention.
Ji et al. (2016)	Real rTMS intervention significantly improved both the static and dynamic balance of the stroke patients when compared to pre-intervention and sham rTMS.
Kakuda et al. (2013)	rTMS + mobility training significantly improved walking velocity and lower limb functions of the stroke patients when compared to pre-intervention.
Wang et al. (2019)	Real rTMS intervention significantly improved the walking speed, gait asymmetry, and motor function of the stroke patients when compared to pre-intervention and sham stimulation.

rTMS, repetitive transcranial magnetic stimulation.

all the parameters of the stroke patients when compared to the pre-intervention and control groups. Kim et al. (2014) also demonstrated that 15-min real rTMS intervention for five consecutive days significantly improved the walking ability and balance of the stroke patients. Finally, Rastgoo et al. (2016) further confirmed the effects of low-frequency rTMS on stroke patients using a similar intervention setting with Kim et al. (2014). They indicated that real rTMS intervention significantly improved the muscle spasticity and motor function of the stroke patients when compared to pre-intervention and sham stimulation.

Effects of High-Frequency Stimulus

More than half of the included studies (6 out of 10 trials) investigated the effects of high-frequency rTMS on the lower-limb motor ability of stroke patients. Specifically, rTMS at a frequency of 5 Hz was applied in two studies, rTMS at a frequency of 10 Hz were applied in three studies, and the remaining one study applied rTMS at a frequency of 20 Hz.

Two recent studies focused on the effects of rTMS (5 Hz). Wang et al. (2019) found that 15-min real rTMS intervention at three sessions per week for 3 weeks significantly improved the walking speed, gait asymmetry, and motor function of the stroke patients when compared to pre-intervention and sham stimulation. Goh et al. (2020) further confirmed the effects of rTMS on gait speed after the subjects taking part in a 16-min real rTMS intervention for three sessions during 1 week. In terms of the rTMS at a frequency of 10 Hz, positive effects were found in all the three studies although there are some methodological differences. Kakuda and his colleague first start the trial in 2013. Subjects were required to receive a 20-min rTMS and specific mobility training for 20 sessions during 13 days, and they found that rTMS + mobility training significantly improved walking velocity and lower limb functions of the stroke patients when compared to pre-intervention. In 2016, both Choi et al. (2016) and Ji et al. (2016) investigated the effects of rTMS on the balance of stroke patients using a similar intervention setting, and they demonstrated that real rTMS intervention significantly improved the balance function of the stroke patients when compared to pre-intervention and sham stimulation. In addition, Chieffo et al. (2014) compared the effects of 30-min real rTMS intervention (20 Hz) for 10 sessions during 3 weeks with sham rTMS on lower limb functions and walking ability of stroke patients. The results indicated that the real rTMS intervention significantly improved the lower limb functions of the stroke patients when compared to pre-intervention and sham stimulation.

DISCUSSION

This study primarily reviewed and summarized evidence from previous research articles investigating the effects of rTMS on lower limb motor ability of stroke patients, with the further aim to find out the appropriate rTMS setting that may contribute to more beneficial results.

According to the eligibility criteria, 10 studies that covered 257 stroke patients were included in this systematic review. Although the risk of bias is relatively high, the results of this review primarily confirmed that rTMS has a positive effect on the lower limb motor ability of stroke patients. To be more specific, both low-frequency rTMS (<5 Hz) and high-frequency rTMS (≥ 5 Hz) added benefits to the muscle function, walking

ability, and balance of stroke patients. In terms of the appropriate setting of rTMS, it was found that 15- to 20-min course of rTMS for 2 to 3 weeks was the most common one. In addition, the results of this review also found that 1 Hz and 10 Hz were the most commonly used low and high frequencies, respectively. Nevertheless, only 10 studies were included, which may weaken the validity of the findings in this review. More rigorous trials in this field are warranted for further verification. Regarding the frequency of rTMS, it is also suggested that future studies should investigate the effects of different frequencies of rTMS on the lower limb motor ability of stroke patients. In addition, there are two included studies investigating the effects of combination intervention (e.g., rTMS combined with task-oriented training or rTMS combined with mobility training) on stroke patients, and they also found some positive results (Wang et al., 2012; Kakuda et al., 2013). However, neither of them was compared with the single rTMS intervention, thus whether a better effect exists is still unclear and is worth studying.

The underlying mechanism by which rTMS can add help to the recovery of lower limb motor ability of stroke patients has been widely speculated. It was found that stroke disrupts the balance of activity in the two brain hemispheres (Wang et al., 2019). The hypothesis of interhemispheric competition holds that the motor cortex of the uninfluenced hemisphere is inhibited, while the motor cortex of the affected hemisphere is exaggerated (Wang et al., 2019). Therefore, the reduction of competition between cerebral hemispheres after stroke is considered to be a potential mechanism for functional improvement after stroke (Nowak et al., 2009). rTMS is one of the non-invasive methods to stimulate nerve cells in the superficial brain zones (Barker, 1991). It has been proven that rTMS through the brain can regulate cortical excitability and cortical restoration, with the influence mainly relying on the different frequencies of the stimulation (Chen and Seitz, 2001). Low-frequency rTMS may initiate a short-term decline in cortical excitability of the affected hemisphere, such as motor evoked potential. The inhibition of cerebellar excitability brought by rTMS with low frequency may further improve the ability to adapt to learning in the process of conventional stroke rehabilitation, thereby better-improving walking ability (Wang et al., 2012; Elkholy et al., 2014; Kim et al., 2014; Rastgoo et al., 2016). On the other hand, rTMS with high frequency enhances the amplitude of motor evoked potential and cortical excitability of the uninfluenced hemisphere, potentially reduced the competition and gradually help to improve the motor ability of stroke patients (Kakuda et al., 2013; Chieffo et al., 2014; Choi et al., 2016; Ji et al., 2016; Wang et al., 2019; Goh et al., 2020).

Some limitations that existed in this review need to be addressed. For example, although the citation snowballing method was applied to identify relevant studies in the reference list of all eligible articles, only three databases were used in this study for searching the relevant published literature, which may accidentally leave out some studies. In addition, the small sample size and relatively high risk of bias of these included studies may potentially weaken the validation of these findings.

CONCLUSIONS

In conclusion, the results of this systematic review primarily confirmed the positive effects of rTMS on the lower limb motor ability (e.g., gait and balance) of stroke patients. It was also found that 15- to 20-min course of rTMS for 2 to 3 weeks was the most common one, and 1 Hz and 10 Hz were the most commonly used low and high frequencies, respectively. These results have significant clinical applications for patients with weakened lower-limb mobility after a stroke. Research related to rTMS either on gait or balance is in a fledging period, more rigorous studies are ought to be focused on this field.

DATA AVAILABILITY STATEMENT

The original contributions presented in the study are included in the article/supplementary material, further inquiries can be directed to the corresponding author.

AUTHOR CONTRIBUTIONS

HF, YS, XC, and PY conceived the presented idea, developed the framework, and wrote the manuscript. IB and YG provided critical feedback and contributed to the final version. All authors were involved in the final direction of the paper, contributed to the final version of the manuscript, and have read and agreed to the published version of the manuscript.

FUNDING

This study was sponsored by the Major Program of the National Social Science Foundation of China (Grant No. 19ZDA352), National Key R&D Program of China (2018YFF0300903), and K. C. Wong Magna Fund in Ningbo University.

REFERENCES

Akazawa, N., Kazuhiro, H., Naomi, O., Kimiyuki, T., Atsushi, H., and Hideki, M. (2017). Relationships between muscle mass, intramuscular adipose and fibrous tissues of the quadriceps, and gait independence in chronic stroke survivors: a cross-sectional study. *Physiotherapy* 104, 438–445. doi: 10.1016/j.physio.2017.08.009

Attal, N., Samar, S. A., Ciampi, D. A. D., Alaa, M., Sophie, B., Frédérique, J., et al. (2016). Repetitive transcranial magnetic stimulation and transcranial direct current stimulation in neuropathic pain due to radiculopathy. *Pain* 157,1224–1231. doi: 10.1097/j.pain.0000000000000510

Barker, A. T. (1991). An introduction to the basic principles of magnetic nerve stimulation. *J. Clin. Neurophysiol.* 8, 26–37. doi: 10.1097/00004691-199101000-00005

Barroso, F. O., Diego, T., Francisco, M., Alguacil-Diego, I. M., Roberto, C., Cristina, S., et al. (2017). Combining muscle synergies and biomechanical analysis to assess gait in stroke patients. *J. Biomech.* 63, 98–103. doi: 10.1016/j.jbiomech.2017.08.006

Byun, S., Jung, T., Kim, C., and Lee, Y. (2011). Effects of the sliding rehabilitation machine on balance and gait in chronic stroke patients – a controlled clinical trial. *Clin. Rehabil.* 25, 408–415. doi: 10.1177/0269215510385850

Cha, H. G., and Kim, M. K. (2017). Effects of strengthening exercise integrated repetitive transcranial magnetic stimulation on motor function recovery in subacute stroke patients: a randomized controlled trial. *Technol. Health Care* 25, 1–9. doi: 10.3233/THC-171294

Chen, C-Y., Hong, P. W-H., Chen, C-L., Chou, S. W., Wu, C-Y., et al. (2007). Ground reaction force patterns in stroke patients with various degrees of motor recovery determined by plantar dynamic analysis. *Chang. Gung. Med. J.* 30, 62–72.

Chen, R., and Seitz, R. J. (2001). Changing cortical excitability with low-frequency magnetic stimulation. *Neurology* 57, 379–380. doi: 10.1212/WNL.57.3.379

Chieffo, R., De Prezzo, S., Houdayer, E., Nuara, A., Di Maggio, G., Coppi, E., et al. (2014). Deep repetitive transcranial magnetic stimulation with H-coil on lower limb motor function in chronic stroke: a pilot study. *Arch. Phys. Med. Rehabil.* 95, 1141–1147. doi: 10.1016/j.apmr.2014.02.019

Choi, C. M., Kim, J. H., Lee, J. K., Lee, B. Y., Kee, H. S., Jung, K. I., et al. (2016). Effects of repetitive transcranial magnetic stimulation over trunk motor spot on balance function in stroke patients. *Ann. Rehabil. Med.* 40, 826–834. doi: 10.5535/arm.2016.40.5.826

Clément, N., Emmanuelle, D., Gregory, S., Annick, R., Elise, L., Sonia, D., et al. (2018). Effects of low- and high-frequency repetitive transcranial magnetic stimulation on long-latency auditory evoked potentials. *Neurosci. Lett.* 686, 198–204. doi: 10.1016/j.neulet.2018.09.002

Elkholy, S. H., Atteya, A. A., Hassan, W. A., Sharaf, M., and Gohary, A. M. E. (2014). Low rate Repetitive Transcranial Magnetic Stimulation (rTMS) and gait rehabilitation after stroke. *Int. J. Neurorehabilitation* 1:109. doi: 10.4172/2376-0281.10001109

Goh, H. T., Connolly, K., Hardy, J., McCain, K., and Walker-Batson, D. (2020). Single session of repetitive transcranial magnetic stimulation to left dorsolateral prefrontal cortex increased dual-task gait speed in chronic stroke: a pilot study. *Gait Posture* 78, 1–5. doi: 10.1016/j.gaitpost.2020.02.020

Ji, S. G., Shin, Y. J., and Kim, M. K. (2016). The effects of repetitive transcranial magnetic stimulation on balance ability in acute stroke patients. *Korean Soc. Phys. Med.* 11, 11–17. doi: 10.13066/kspm.2016.11.3.11

Kakuda, W., Abo, M., Watanabe, S., Momosaki, R., Hashimoto, G., Nakayama, Y., et al. (2013). High-frequency rTMS applied over bilateral leg motor areas combined with mobility training for gait disturbance after stroke: a preliminary study. *Brain Inj.* 27, 1080–1086. doi: 10.3109/02699052.2013.794973

Kelly-Hayes, M., Beiser, A., Kase, C. S., Scaramucci, A., D'Agostino, R. B., and Wolf, P. A. (2003). The influence of gender and age on disability following ischemic stroke: the Framingham study. *J. Stroke Cerebrovasc. Dis.* 12, 119–126. doi: 10.1016/S1052-3057(03)00042-9

Kim, C. M., and Eng, J. J. (2004). Magnitude and pattern of 3D kinematic and kinetic gait profiles in persons with stroke: relationship to walking speed. *Gait Posture* 20, 140–146. doi: 10.1016/j.gaitpost.2003.07.002

Kim, W. S., Jung, S. H., Oh, M. K., Min, Y. S., Lim, J. Y., and Paik, N. J. (2014). Effect of repetitive transcranial magnetic stimulation over the cerebellum on patients with ataxia after posterior circulation stroke: a pilot study. *J. Rehabil. Med.* 46, 418–423. doi: 10.2340/16501977-1802

Machado, S., Bittencourt, J., Minc, D., Cláudio, E. P., and Riberio, P. (2008). Therapeutic applications of repetitive transcranial magnetic stimulation in clinical neurorehabilitation. *Funct. Neurol.* 23, 113–122.

Mansur, C. G., Fregni, F., Boggio, P. S., Riberto, M., Gallucci-Neto, J., Santos, C. M., et al. (2005). A sham stimulation-controlled trial of rTMS of the unaffected hemisphere in stroke patients. *Neurology* 64, 1802–1804. doi: 10.1212/01.WNL.0000161839.38079.92

Naoki, A., Kazuhiro, H., Naomi, O., Kimiyuki, T., Hideki, M., and Masaki, M. (2018). Muscle mass and intramuscular fat of the quadriceps are related to muscle strength in non-ambulatory chronic stroke survivors: a cross-sectional study. *PLoS ONE* 13:e0201789. doi: 10.1371/journal.pone.0201789

Nowak, D. A., Grefkes, C., Ameli, M., and Fink, G. R. (2009). Interhemispheric competition after stroke: brain stimulation to enhance recovery of function of the affected hand. *Neurorehabil. Neural Repair* 23, 641–656. doi: 10.1177/1545968309336661

Patterson, K. K., Parafianowicz, I., Danells, C. J., Closson, V., Verrier, M. C., Staines, W. R., et al. (2008). Gait asymmetry in community-ambulating stroke survivors. *Arch. Phys. Med. Rehabil.* 89, 304–310. doi: 10.1016/j.apmr.2007.08.142

Rastgoo, M., Naghdi, S., Ansari, N. N., Olyaei, G., Jalaei, S., Forogh, B., et al. (2016). Effects of repetitive transcranial magnetic stimulation on lower extremity spasticity and motor function in stroke patients. *Disabil. Rehabil.* 38, 1918–1926. doi: 10.3109/09638288.2015.1107780

Sasaki, N., Abo, M., Hara, T., Yamada, N., Niimi, M., and Kakuda, W. (2016). High-frequency rTMS on leg motor area in the early phase of stroke. *Acta Neurol. Belg.* 117, 189–194. doi: 10.1007/s13760-016-0687-1

Scherbakov, N., Haehling, S., Anker, S. D., Dirnagl, U., and Doehner, W. (2013). Stroke induced sarcopenia: muscle wasting and disability after stroke. *Int. J. Cardiol.* 170, 89–94. doi: 10.1016/j.ijcard.2013.10.031

Song, Y., Sun, D., István, B., Thirupathi, A., Liang, M., Teo, E. C., et al. (2020). Current evidence on traditional Chinese exercise for cancers: a systematic review of randomized controlled trials. *Int. J. Env. Res. Public Health* 17:5011. doi: 10.3390/ijerph17145011

Tung, Y.-C., Lai, C.-H., Liao, C.-D., Huang, S.-W., Liou, T.-H., and Chen, H.-C. (2019). Repetitive transcranial magnetic stimulation of lower limb motor function in patients with stroke: a systematic review and meta-analysis of randomized controlled trials. *Clin. Rehabil.* 33, 1102–1112. doi: 10.1177/0269215519835889

Von Schroeder, H. P., Coutts, R. D., Lyden, P. D., Billings, E., and Nickel, V. L. (1995). Gait parameters following stroke: a practical assessment. *J. Rehabil. Res. Dev.* 32, 25–31.

Wade, D. T., Collen, F. M., Robb, G. F., and Warlow, C. P. (1992). Physiotherapy intervention late after stroke and mobility. *BMJ Clin. Res.* 304, 1179–1180. doi: 10.1136/bmj.304.6835.1179-c

Wang, R. Y., Tseng, H. Y., Liao, K. K., Wang, C. J., Lai, K. L., and Yang, Y. R. (2012). rTMS combined with task-oriented training to improve symmetry of interhemispheric corticomotor excitability and gait performance after stroke: a randomized trial. *Neurorehabil. Neural Repair* 26, 222–230. doi: 10.1177/1545968311423265

Wang, R. Y., Wang, F. Y., Huang, S. F., and Yang, Y. R. (2019). High-frequency repetitive transcranial magnetic stimulation enhanced treadmill training effects on gait performance in individuals with chronic stroke: a double-blinded randomized controlled pilot trial. *Gait Posture* 68, 382–387. doi: 10.1016/j.gaitpost.2018.12.023

Wolfe, C. D. (2000). The impact of stroke. *Br. Med. Bull.* 56, 275–286. doi: 10.1258/0007142001903120

Conflict of Interest: The authors declare that the research was conducted in the absence of any commercial or financial relationships that could be construed as a potential conflict of interest.

frontiers in Sports and Active Living

REVIEW
published: 14 October 2021
doi: 10.3389/fspor.2021.753062

Clarifying the Biomechanical Concept of Coordination Through Comparison With Coordination in Motor Control

Arata Kimura, Toshiharu Yokozawa and Hiroki Ozaki*

Department of Sports Research, Japan Institute of Sports Sciences, Tokyo, Japan

Coordination is a multidisciplinary concept in human movement science, particularly in the field of biomechanics and motor control. However, the term is not used synonymously by researchers and has substantially different meanings depending on the studies. Therefore, it is necessary to clarify the meaning of coordination to avoid confusion. The meaning of coordination in motor control from computational and ecological perspectives has been clarified, and the meanings differed between them. However, in biomechanics, each study has defined the meaning of the term and the meanings are diverse, and no study has attempted to bring together the diversity of the meanings of the term. Therefore, the purpose of this study is to provide a summary of the different meanings of coordination across the theoretical landscape and clarify the meaning of coordination in biomechanics. We showed that in biomechanics, coordination generally means the relation between elements that act toward the achievement of a motor task, which we call biomechanical coordination. We also showed that the term coordination used in computational and ecological perspectives has two different meanings, respectively. Each one had some similarities with biomechanical coordination. The findings of this study lead to an accurate understanding of the concept of coordination, which would help researchers formulate their empirical arguments for coordination in a more transparent manner. It would allow for accurate interpretation of data and theory development. By comprehensively providing multiple perspectives on coordination, this study intends to promote coordination studies in biomechanics.

Keywords: biomechanics, conceptual analysis, coordination, motor control, performance enhancement

OPEN ACCESS

Edited by:
Yury Ivanenko,
Santa Lucia Foundation (IRCCS), Italy

Reviewed by:
Tetsuro Funato,
The University of Electro-Communications, Japan
Giovanna Catavitello,
Catholic University of Louvain, Belgium

****Correspondence:***
Arata Kimura
arata.kimura@jpnsport.go.jp

Specialty section:
This article was submitted to Biomechanics and Control of Human Movement, a section of the journal Frontiers in Sports and Active Living

Received: *04 August 2021*
Accepted: *16 September 2021*
Published: *14 October 2021*

Citation:
Kimura A, Yokozawa T and Ozaki H (2021) Clarifying the Biomechanical Concept of Coordination Through Comparison With Coordination in Motor Control. Front. Sports Act. Living 3:753062. doi: 10.3389/fspor.2021.753062

INTRODUCTION

Coordination is one of the central concepts in human movement science, especially in the field of biomechanics and motor control. Then, is there a common idea of coordination in these fields? Even though we believe there are more similarities than most people appreciate, there may be differences as well. Therefore, this study will focus on the denotation and connotation of coordination in these fields.

Biomechanics is a field that aims to identify the function of elements (e.g., muscles, joint movements) involved in achieving motor tasks. This identification is expected to provide information on improving movement and making it safer. However, because the musculoskeletal

system is highly interconnected and integrated, it is almost impossible to identify the function of each element in isolation during a whole-body movement. Therefore, coordination between elements should be taken into account (Winter, 2009). In recent years, there has been a growing interest in coordination, as seen by the addition of a chapter regarding coordination in a well-known textbook on biomechanics, which was not included in the first edition (Winter, 2009; Robertson et al., 2013).

In terms of coordination, one central question in motor control is how a large number of degrees of freedom in the human body become organized (Bernstein, 1967). The human body has ∼300 joints and 800 muscles, which combined bring about changes in the overall movement of the body. For the production of a successful movement, it is believed that the different degrees of freedom at each spatiotemporal scale should be coordinated. This issue has been examined from multiple perspectives in motor control, the most typical of which are computational and ecological perspectives (Bruton and O'dwyer, 2018; Profeta and Turvey, 2018). The computational perspective is a branch of motor control that views the brain as a computational machine and attempts to understand how the central nervous system (CNS) processes information to move the body. The researchers in a computational perspective conclude that a large number of degrees of freedom are coordinated by the control of the CNS (d'Avella and Bizzi, 1998; Saltiel et al., 2001; d'Avella et al., 2003). The ecological perspective is a branch of motor control that attempts to understand human movement through the interaction between the human body and its surrounding environment, situation, and context, without giving the CNS a privileged status. The researchers in the ecological perspective conclude that coordination takes place without intervention by an external directing control, such as the CNS (Kugler et al., 1980; Turvey, 1990, 2007); thus, the coordination between a large number of degrees of freedom is not pre-designed but emerges spontaneously.

It turns out that the term coordination has been examined in a variety of contexts. Such a term tends to be often not used synonymously and has different meanings because the meaning of a concept is context-dependent. Using ambiguously defined terms may lead to communicative conflicts and misunderstandings. Therefore, clarification of the meaning of terms is necessary to avoid confusion. Previous studies clarified the meaning of coordination in motor control in terms of computational and ecological perspectives and indicated that the meanings differed between them (Bruton and O'dwyer, 2018; Profeta and Turvey, 2018). However, in biomechanics, each study has defined the meaning of the term and the meanings are diverse, but no study has attempted to bring together the diversity of meanings of the term. Therefore, the meaning of coordination in biomechanics remains ambiguous and it may prevent the progress of coordination studies in biomechanics.

The purpose of this study is to provide a summary of the different meanings of coordination across the theoretical landscape and clarify the meaning of coordination in biomechanics. Through this, we intend to establish a biomechanical perspective on coordination. In the present study, we emphasize coordination in terms of biomechanics, but we believe that this study has implications for various other related fields. Although coordination has been studied in various fields, researchers in different fields are not yet aware of each other's work. Therefore, this study will focus on summarizing the basic findings commonly shared in each field rather than summarizing the latest findings. We thought that we should first summarize the basic findings of each field and then combine these findings in order to help researchers in the various fields. We hope to enhance our understanding of each other's work and suggest useful directions for future progress.

The remaining of this paper consists of five sections. Section Meaning of coordination in biomechanics deals with coordination in biomechanics. Section Meaning of coordination in motor control relates to the coordination used in motor control, particularly from computational and ecological perspectives. Section Comparison across fields focuses on the similarities and differences in the meaning of coordination between biomechanical and computational perspectives, and biomechanical and ecological perspectives. Section Some topics to be discussed presents some topics for further study regarding coordination in biomechanics. Finally, Section Conclusion provides the significance of this study.

MEANING OF COORDINATION IN BIOMECHANICS

The term coordination is not used synonymously and has substantially different meanings in biomechanics. There are at least two different meanings of coordination. One views coordination as the relation between elements to achieve a common task goal. The other views coordination as an interrelation of multiple elements and does not explicitly include acting toward a common goal. In this section, we discuss the different meanings of coordination in more detail.

Functional Relationships for the Achievement of a Motor Task

The most prominent definition of coordination relates to the functional relationships between elements for the achievement of a motor task. Zatsiorsky and Prilutsky (2012) defined muscle coordination as the distribution of muscle activation or force among individual muscles to produce a given motor task. Winter (2009) used the term synergy rather than coordination and defined synergy as elements collaborating toward a common goal. Zajac et al. (2002) also defined the term synergy as co-acting elements to achieve a task goal that is unobtainable by one element alone. These definitions commonly imply that coordination or synergy means the relation between elements to achieve a motor task, called biomechanical coordination in this study.

To form an image, the meaning of biomechanical coordination is illustrated using quiet standing with both legs. In quiet standing, the center of mass (COM) should be kept within the base of support to maintain posture (Shumway-Cook and Horak, 1986; Kuo, 1995; Hof et al., 2005). In other words, keeping the COM within the base of support is a functional

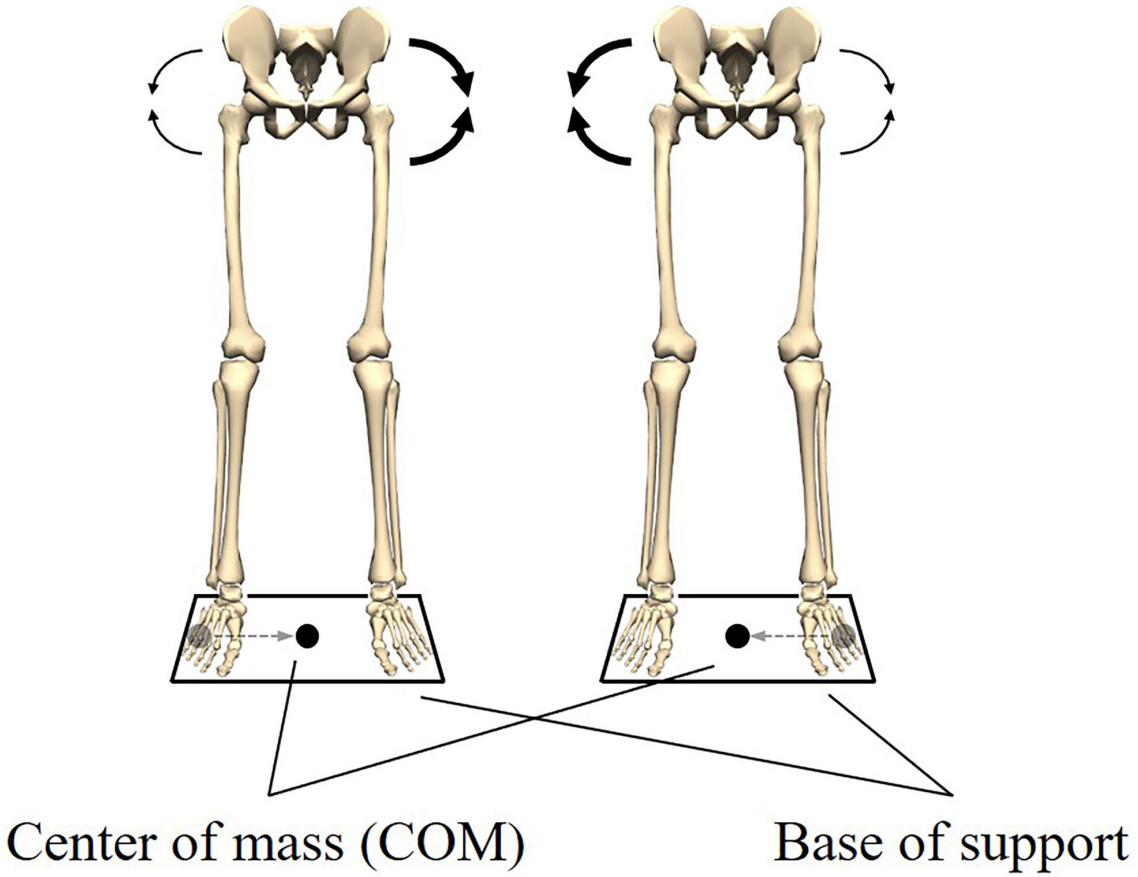

FIGURE 1 | Postural stability in the left-right direction during quiet standing. Keeping the center of mass (COM) within the base of support is a functional requirement to maintain quiet standing. The functional requirement is met by the coordination of the left and right hip abductors/adductors moments. When the COM is located at the left end of the base of support, the right abductor moment increases and the left abductor moment decreases. Also, when the COM is located at the right end of the base of support, the left abductor moment increases and the right abductor moment decreases. This relationship between the moments allows the COM to be kept within the base of support.

requirement to maintain quiet standing. Here, for the sake of simplicity, we focus only on the position of the COM in the left-right direction. Using two force platforms and performing inverse dynamics, it was found that the position of the COM was controlled by the left and right hip abductor/adductor moments (Winter et al., 1996). Furthermore, the left and right hip abductor/adductor moments were exactly equal in magnitude and 180° out of phase (Winter et al., 1996). These results indicated that an increased abductor moment on one side was accompanied by decreased abductor moments on the contralateral side (**Figure 1**). The relationship between these moments led to a stable left-right balance and quiet standing was maintained. It can, thus, be concluded that these moments were coordinated.

As the definition suggests, biomechanical coordination has a fairly inclusive meaning. Therefore, several terms are similar to biomechanical coordination: "cooperation," "collaboration," and "compensation." These terms, of course, have broader meanings. For instance, cooperation usually implies association for common benefit; collaboration often connotes working together to achieve something; compensation usually implies the correction of loss. Although these words have their own connotations, an important part of each involves the relation between elements to achieve a common goal. It is sometimes useful to consider all these terms as different forms of biomechanical coordination.

To identify biomechanical coordination, at least the following two factors should be met, as also noted by Latash and Zatsiorsky (2015). First, the elements must be related rather than independent, i.e., the elements have to do something together. Second, the related elements act toward meeting the functional requirements. Even if elements are related, they are not coordinated if they do not act toward meeting the functional requirements. Also, even if each element acts toward meeting the functional requirements, they are not coordinated if they are not related.

Interrelation of Multiple Elements

Human body segments are mechanically linked by joints; therefore, the motion of one segment can be affected by the motion of other segments. Thus, it has been suggested that biomechanical analysis should consider the interrelation between segments rather than looking only at the kinematics of a single joint (Glazier and Robins, 2012; Glazier, 2017). Several studies have examined coupling, which provides a measure of the relative timing and magnitude of the motion between segments or joints (Heiderscheit et al., 2002; Ferber et al., 2005; Wilson et al., 2008). Coupling is used when, for example, the hip joint flexes or extends simultaneously with knee flexion or extension, referred to as hip-knee joint coupling. It is quantitatively evaluated by vector coding and relative phase analysis (Wheat and Glazier, 2006). Some studies refer to the interrelation of multiple elements as coordination, which is synonymous with coupling (Tepavac and Field-Fote, 2001; Abbasi et al., 2020; Acasio et al., 2021). However, coupling is different from biomechanical coordination. The fundamental difference is whether it includes meeting functional requirements. Coupling does not explicitly include meeting functional requirements and, therefore, may be irrelevant with regards to the achievement of a motor task.

Some studies used the term coordination to refer to muscle activation pattern (Prilutsky and Gregor, 2000; Larivière and Arsenault, 2008; Donath et al., 2015). The muscle activation pattern is defined as the repeated or regular way in which the muscle activates during a movement. Donath et al. (2015) examined the effects of aging and intense exercise on muscle activation patterns. Importantly, as with coupling, the muscle activation pattern does not explicitly include meeting functional requirements. In other words, patterned muscle activity does not necessarily act toward meeting functional requirements. However, confusingly, there are cases where the patterned muscle activity acts toward meeting the functional requirements. For example, during pedaling, the plantar flexors (gastrocnemius and soleus) and dorsiflexor (tibialis anterior) muscles show simultaneous activation, resulting in ankle stabilization (Raasch and Zajac, 1999; So et al., 2005). This stabilization increases the efficiency of energy transfer to the pedal and leads to pedal acceleration, which is a functional requirement of pedaling. Therefore, the relation between the plantar flexors and the dorsiflexor is interpreted as coordinating to meet the functional requirement of accelerating the pedal. Here, it is important to distinguish between the fact that the muscles show patterned activation and the fact that these muscles act toward meeting the functional requirements. This distinction avoids confusion between muscle activation patterns and biomechanical coordination.

Bottom Line

When one term has multiple meanings, it can become confusing as in the case of coordination. We aimed to eliminate this confusion by clarifying the meaning of coordination in biomechanics. This required a conceptual analysis, which revealed that the coordination had at least two different meanings. The first refers to multiple elements related to achieving a common purpose, often referred to as synergy. The second refers to the interrelated elements. The former and the latter are distinctly different; the former requires that the interrelated elements act to meet functional requirements, while the latter does not. We believe that the careful application of this kind of analysis is relevant for the eradication of misunderstandings.

MEANING OF COORDINATION IN MOTOR CONTROL

Computational Perspective

Coordination Related to Removing Redundancy

It is widely acknowledged that the human body has a greater number of degrees of freedom than necessary to successfully perform motor tasks (Bernstein, 1967). For example, for reaching a target in the two-dimensional space, the number of arm joint rotations is typically three (shoulder, elbow, and wrist joints). Thus, the position of the hand is determined by the combination of the three joint angles. However, the position of the hand is a single point in the two-dimensional space. Thus, there is not just one, but an infinite number of combinations of joint angles to determine the position of the hand. It is believed that the CNS is always faced with the problem of choosing a certain combination from an infinite number of possibilities (Franklin and Wolpert, 2011). This is known as the motor redundancy problem (Bernstein, 1967). When the brain is viewed as a computational machine, the need to instantly determine a certain combination from an infinite number of possibilities indicates that the CNS is required to perform an enormous amount of computation. The question of how the CNS deals with this problem has attracted the interest of researchers.

The CNS is believed to address the problem by adopting a strategy to reduce the enormous amount of computation. The CNS does not control muscles individually but rather controls them *via* synergy which is a neural module that activates multiple muscles simultaneously (Saltiel et al., 2001; d'Avella et al., 2003; Chiovetto et al., 2013; Kuppuswamy and Harris, 2014) (**Figure 2**). One muscle can be part of multiple muscle synergies and one synergy can activate multiple muscles. This control strategy allows the CNS to reduce the number of degrees of freedom requiring control, thereby reducing the amount of computation. Then, the CNS can instantly determine a certain combination even in an infinite number of possibilities. In this context, the terms synergy and coordination have often been used synonymously (Bizzi et al., 2008; d'Avella and Lacquaniti, 2013).

The presence of synergy is shown using measured experimental data. A method for identifying synergy has been used to measure electromyographic signals of a large number of muscles and applies matrix factorization techniques (Tresch et al., 1999, 2006; d'Avella et al., 2003, 2006; Hart and Giszter, 2004; Ivanenko et al., 2004; Ting and Macpherson, 2005; Tresch and Jarc, 2009; Cheung et al., 2012). Ivanenko et al. (2004) demonstrated that the muscle activation of 12–16 ipsilateral leg and trunk muscles could be reduced to five basic independent components during walking. Additionally, d'Avella et al. (2006) identified four or five synergies in up to 19 arm muscles'

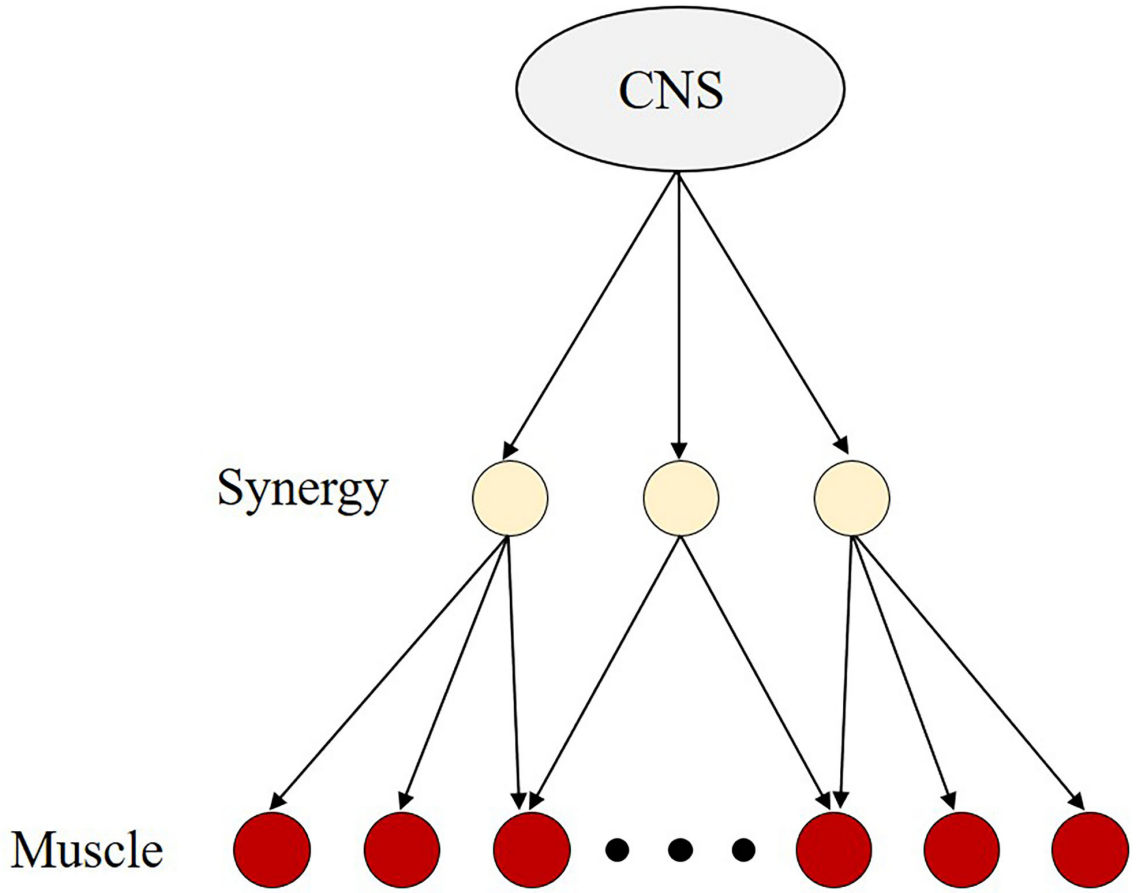

FIGURE 2 | The concept of the muscle synergy hypothesis. Because the human body has a greater number of degrees of freedom to successfully perform the motor task, it is believed that the central nervus system (CNS) is always faced with the problem of choosing a certain combination from an infinite number of possibilities. It implies that the CNS needs to perform a large amount of computation. To address this problem, CNS is believed to adopt a control strategy that reduces the number of degrees of freedom requiring control, i.e., the muscle synergy hypothesis. The muscle synergy hypothesis is based on the assumption that the CNS controls synergies composed of multiple muscles, rather than individual muscles separately. With this control strategy, the CNS may be less computationally demanding than when controlling individual muscles.

activities in pointing movements. These studies concluded that muscle activation patterns were captured by a small number of time-varying synergies, suggesting that the CNS exploited this low dimensionality to simplify control.

Some researchers argue that muscle synergy reflects the basic aspects of muscle activation, but this argument has been criticized because there is a lack of direct evidence for the neural implementation of muscle synergy in the CNS (Hart and Giszter, 2010; Overduin et al., 2012; Cheung and Seki, 2021). This criticism suggests that muscle synergy is likely an artifact that relies on certain assumptions employed by the algorithm for separating the activations of the synergy. However, recent electrophysiological experiments have provided evidence that the activations of muscle synergy are expressions of neural activity (Hart and Giszter, 2010; Yakovenko et al., 2011; Overduin et al., 2012; Takei et al., 2017; Yaron et al., 2020). During voluntary hand movements, the muscle fields of premotor interneurons in the primate cervical spinal cord were not uniformly distributed across the hand muscles but rather distributed as clusters corresponding to muscle synergy. Using frog spinal cords, Hart and Giszter (2010) demonstrated that premotor interneurons have divergent output projections to motoneurons of muscles that match the muscle synergies identified from the electromyography of motor behaviors. These findings directly support the idea that muscle synergy is not an artifact but reflects the basic aspects of muscle activation.

Breaking Away From the View of Coordination as a Relation That Eliminates Redundancy

A different definition of synergy (often referred to as coordination) was provided at the end of the last century (Gelfand and Latash, 1998) and was later sophisticated by Latash and colleagues (Latash et al., 2007; Latash, 2012). They deviated from the view of synergy as a relation between elements to solve the computational problem on the CNS. Latash and colleagues described synergy as not related to a reduction of the

amount of computation in the CNS. According to this view, it is assumed that the CNS does not produce a single optimal solution but provides families of combinations between elements that can achieve the motor task with acceptable accuracy. If the CNS determines a single solution from an infinite number of possibilities, an enormous amount of computation is required. Therefore, it is natural to assume that CNS will reduce the amount of computation. However, if the CNS provides a family of combinations that can achieve the motor task, the amount of computation required would be reduced. Therefore, there will be no need to eliminate the extra degrees of freedom. Latash and colleagues argue that having extra degrees of freedom than necessary means abundance, not redundancy (Latash et al., 2002; Gera et al., 2010; Latash, 2018). This abundance leads to multiple variations of the combinations between elements to achieve the motor task and is believed to allow for the flexibility to deal with unexpected perturbations applied to one or a few of the elements.

Latash and colleagues believe that the CNS does not strictly control individual joint movements, but focuses on control that minimizes variability in the outcome of motor tasks (in the case of a reaching task, the position of the hand). The CNS does not specify a precise pattern of joint movement that would lead to the desired outcome of motor tasks, but rather organizes the movement such that, if a certain joint movement introduces an error into the desired outcome, other joint movements compensate to minimize the original error. They defined the term synergy as a neural organization that ensures task-specific covariation of elements to contribute to the achievement of a motor task.

Synergy has often been examined by uncontrolled manifold (UCM) analysis (Scholz and Schöner, 1999; Scholz et al., 2000; Latash et al., 2001; Domkin et al., 2002, 2005; Krishnamoorthy et al., 2003; Tseng et al., 2003; Yang and Scholz, 2005) (**Figure 3**). This analysis determined the solution space of the motor task, which is a subspace related to achieving the motor task in the state space. The solution space is referred to as the uncontrolled manifold. The variables in the state-space can be divided into two orthogonal components. One component lies parallel to the solution manifold (||UCM), indicating that it does not deviate from the solution space. The other component lies perpendicular to the solution manifold (⊥UCM) and represents the configuration of variables away from the solution space. If the variability of ||UCM is higher than that of ⊥UCM when the same motor task is repeated, the variables are co-varied to achieve the motor task. In the study of Scholz et al. (2000), for instance, participants performed shooting with a laser pistol at a target. As a result, the seven joint angles of the arms co-varied to keep the orientation of the gun relative to the target invariant.

The UCM analysis is supposed to reflect a control hypothesis, i.e., the CNS controls variables that affect the achievement of a task (⊥UCM) and relatively does not control variables that do not affect the achievement of a task (|| UCM). In other words, the CNS selectively controls the variables that are not along the direction to the UCM. The presence of this control strategy has also been supported theoretically (Todorov and Jordan, 2002; Todorov, 2004; Diedrichsen, 2007; Liu and Todorov, 2007); the optimal feedback control model proposed by Todorov and Jordan (2002) does not act to correct movements in directions that have no bearing on the achievement of the motor task. The result is thought to suggest that the emergence of coordination reflects the operation of the control laws.

Ecological Perspective

Self-Organized Coordination

Like the computational perspective, one of the most prominent issues in the ecological perspective is how the human body organizes the extra degree of freedom (Kay, 1988; Turvey, 1990; Van Emmerik et al., 2004). Coordination between elements may address this issue. This was first realized by Bernstein (1967), who believed that overcoming redundant degrees of freedom was the core of motor control. According to Bernstein, coordination was the reduction of a large number of degrees of freedom involved in a particular movement to a small number of variables. In the computational perspective, coordination is sometimes defined as the relation between elements that reduce the number of degrees of freedom controlled by the CNS. However, in the ecological perspective, the term coordination is defined differently than in the computational perspective. The coordination defined in the ecological perspective removes the need to consider the CNS even though it is associated with a reduction in the number of degrees of freedom (Vereijken et al., 1992; Turvey, 2007). The coordination between elements is not pre-programmed in the CNS but is a temporary functional grouping of elements that emerges without input from a controller *via* self-organizing processes. In this study, such coordination is called self-organized coordination. Self-organization is a process in which the order emerges solely from the interactions between elements and their surrounding environment, situation, and context (Haken, 2006). These interactions are performed without any external control.

Self-organized coordination has been investigated using periodic movements. The experimental window into self-organized coordination was a paradigm introduced by Kelso et al. (1981), Kelso (1984). Kelso's original experiments dealt with rhythmical finger movement in a transverse plane (i.e., abduction/adduction) and required participants to oscillate their index fingers to the frequency of a metronome in one of two patterns, in-phase or anti-phase. In the in-phase pattern, both fingers move symmetrically (i.e., homologous muscle groups contracting simultaneously). In the anti-phase pattern, both fingers move asymmetry (i.e., homologous muscle groups contracting in an alternating fashion). These experiments showed that when participants began to oscillate their index fingers in the anti-phase pattern and the frequency of the metronome was gradually increased, the phase pattern became unstable and, at a critical frequency, suddenly changed to an in-phase pattern (**Figure 4**). These results are also supported by a theoretical model, the Haken-Kelso-Bunz (HKB) model (Haken et al., 1985). The experimental and model-based analyses showed the following two main findings. First, a single parameter, frequency, could manipulate the phase transition generated by the two-finger movement. Second, the instability or variability of the phase pattern promoted the spontaneous phase transition. This implies that the variability may be informative, not meaningless.

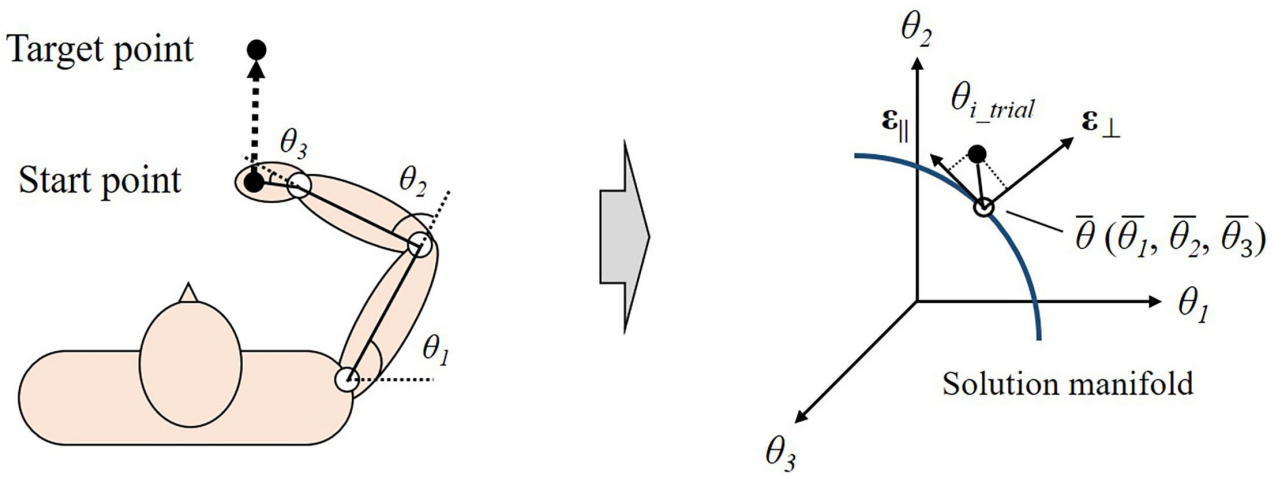

FIGURE 3 | Overview of uncontrolled manifold (UCM) analysis in multidimensional space during reaching task. The state space is spanned by three variables (joint angles: θ_1, θ_2, θ_3). The blue nonlinear line shows the solution manifold, the set of variables that achieve the task result with zero error. In a repetition of reaching task, the UCM analysis decomposed the variables of each trial (θ_{i_trial}) into two components around the average (θ). One component lies parallel to the solution manifold ($\varepsilon_{||}$) and the other component lies perpendicular to the solution space ($\varepsilon_{\perp}$).

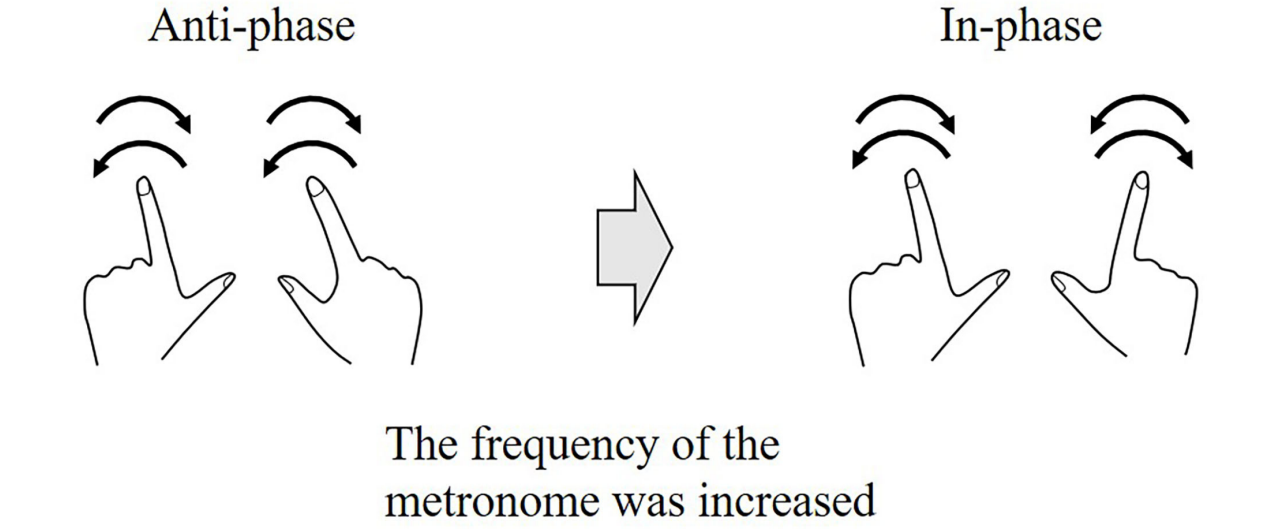

FIGURE 4 | Phase transition during a rhythmical finger movement task. The experiment required participants to oscillate their index fingers to the frequency of the metronome in either in-phase or anti-phase. The participants oscillate their index fingers in the anti-phase pattern at a low frequency, and as the frequency was gradually increased, the phase pattern switches to an in-phase pattern at a certain critical frequency. This switching of the phase pattern is called a phase transition.

Coordination as a Correction of the Deviations in Elements

Insights gained from the ecological perspective have been successfully applied to a variety of fields. In particular, they have influenced the way that scientists view movement variability during repetition of a motor task (Hamill et al., 1999; Davids et al., 2003; Bartlett et al., 2007; Stergiou and Decker, 2011; Preatoni et al., 2013). According to traditional theory, movement variability was thought to be due to noise in the CNS. Thus, it was suggested that movement variability may emerge as an unwanted source of error that should be eliminated or reduced (Fitts, 1954; Schmidt et al., 1979; Harris and Wolpert, 1998; Van Beers et al., 2002). However, today, it is thought that movement variability does not only include an unwanted source of error (Müller and Sternad, 2003, 2004, 2009; Cohen and Sternad, 2009; Sternad, 2018). For example, in the reaching movement, the joint angles are slightly different in every trial. Despite this, the hand reaches the desired position and the reaching task is successful in every trial. It can therefore be expected that the joint angles are related such that the deviations in joint angles are canceled out, leading to a relatively invariant final hand position (Müller and Sternad, 2003). This relation between joint angles is

sometimes termed coordination. Coordination means a relation that is beneficial to the achievement of a motor task and it differs from self-organized coordination.

The presence of the coordination was first suggested by Bernstein's observation of hammering on an anvil (Bernstein, 1967). The participants were fully trained and had repeated the same movements hundreds of times a day for years. Nevertheless, he noticed that variability in the trajectory of the hammer tip in a series of strikes was smaller than the variability of the individual joint movements of the subject's arm holding the hammer; a famous phrase to describe this is "repetition without repetition." Therefore, he suggested that the joints were not acting independently, but functionally linked to correct each other's errors. However, this was only suggestive and not conclusive. The variability in the spatial position of the tip of the hammer cannot be compared to the degree of reproducibility of the joint angle because these variables have different units. One way to solve this problem is covariation by randomization (CR) analysis (Kudo et al., 2000; Müller and Sternad, 2003, 2004; Verrel et al., 2010, 2012a,b) (**Figure 5**). CR analysis assesses coordination among joint angles by comparing the outcome of performance (e.g., the trajectory of the tip of the hammer) between the original and decorrelated data in a repetitive motor task. Decorrelated data are produced by randomly reordering joint angles across trials, thereby removing all possible correlations among them. Then, the decorrelated data are substituted into a forward dynamics model to determine the variability of the performance outcome. Thus, coordination is present when the variability of the performance outcome is higher for the decorrelated data than for the original data.

COMPARISON ACROSS FIELDS

Biomechanics—Computational Perspective

Biomechanical coordination is the relation between elements that act toward meeting functional requirements and is examined to identify the function of elements involved in a particular movement (**Table 1**). On the other hand, coordination in the computational perspective sometimes means the relation between elements that reduce the number of degrees of freedom to solve a computational problem on the CNS and is examined to understand the control mechanism of the CNS (**Table 1**). Coordination was found to have different meanings. The finding leads to insights that biomechanical coordination is not necessarily related to reducing the CNS computation. For example, left and right hip abductor/adductor moments are coordinated to maintain a quiet standing, but this is not necessarily related to the reduction in the CNS computation. There may be cases where biomechanical coordination results in the reduction of the CNS computation, but that is not always the case.

The meaning of coordination and the aim of studying coordination differ between biomechanics and motor control from the computational perspective, but it does not mean that these two fields are unrelated. Understanding the control mechanisms of the CNS, the aim of the computational perspective study, requires taking into account the biomechanics of the musculoskeletal system (Tytell et al., 2011). This is because there is no one-to-one correspondence between a neural command and the resulting movement (Zatsiorsky and Prilutsky, 2012). Even if the same neural command is input, the output movement differs depending on the current state of the musculoskeletal system (e.g., current joint angles and corresponding muscle moment arms, muscle lengths, and velocities). In addition, the state of the musculoskeletal system is physically determined by the behavior of neural circuits. These facts show that human movement is generated by the interaction between the behavior of neural circuits and the biomechanics of the musculoskeletal system. Thus, biomechanics and the computational perspective are closely related.

Latash and colleagues do not agree with the view that coordination is the relation between elements to reduce the number of degrees of freedom. Instead, they view coordination as a neural organization that ensures task-specific covariation of elements that contribute to the achievement of the motor task (**Table 1**). Such a covariation that contributes to the achievement of the motor task appears to be similar to biomechanical coordination. It may be the reason why UCM analysis is used not only in motor control but also in biomechanical studies (Verhoeven and Newell, 2016; Iino et al., 2017; Tokuda et al., 2018; Möhler et al., 2019, 2020). Verhoeven and Newell (2016) investigated the coordination between joint movements for the success of a basketball free-throw task using UCM analysis. They revealed that successfully controlling the trial-to-trial variability of release parameters (i.e., release position, angle, and speed) along the solution manifold and the coordination of postural control between joint movements changed as a function of skill level. It should be noted that the coordination used in these kinds of studies eliminates the consideration of the control by the CNS, while coordination as presented by Latash and colleagues considers the control of CNS.

Biomechanics—Ecological Perspective

The prominent issue in the ecological perspective is how humans organize the extra degrees of freedom. The key concept for this is self-organized coordination, which is a temporary functional grouping of elements that emerges without input from a controller, such as the CNS (**Table 1**). Each element becomes functionally linked to behave as a task-specific unit, which reduces the number of degrees of freedom. It was found that biomechanical coordination and self-organized coordination have different meanings. This implies that even though self-organized coordination occurs between elements, it does not indicate that these elements act toward achieving a motor task. This can be explained using the rhythmical finger movement in a transverse plane example. This task required participants to oscillate their index fingers in anti-phase at the same frequency as a metronome. However, as the frequency of the metronome gradually increased, phase transition occurred at a certain critical frequency. This phase transition means that the purpose of the task is not achieved. Thus, the index fingers do not

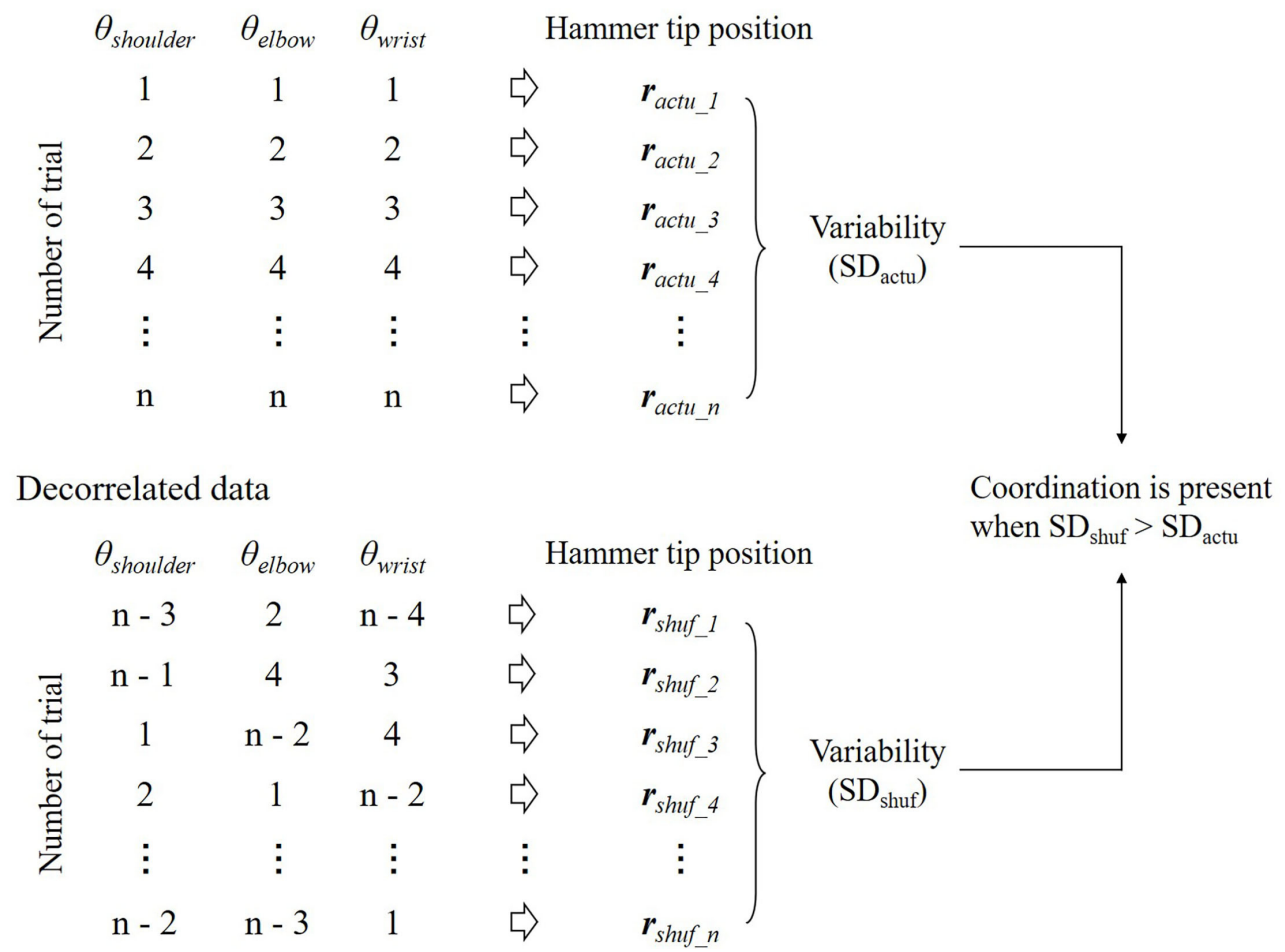

FIGURE 5 | Illustration of the covariation by randomization (CR) analysis. All variables are randomly shuffled across trials to produce decorrelated data. This procedure allows for removing any correlation between variables within a trial. The decorrelated data are substituted into a forward dynamics model to determine the performance outcome and the standard deviation (SD) after the random shuffle (SD_{shuf}). If SD_{shuf} is higher than the variability of the performance outcome for the original data (SD_{actu}), the coordination between variables is present to reduce the variability of the performance outcome.

behave to achieve a motor task, although it is considered self-organized coordination.

Some researchers use the term coordination to mean covariation between elements that are beneficial to the achievement of a motor task (Müller and Sternad, 2003, 2004) (**Table 1**). These researchers are influenced by the notion that movement variability includes not only a meaningless but also a functional component. However, in the past, biomechanics researchers did not tend to consider movement variability as an important topic worthy of research attention (Glazier et al., 2006). This idea was derived from an implicit assumption commonly held by biomechanics researchers, namely that human movements were highly consistent when the same motor task was repeated (Glazier et al., 2006; Bartlett et al., 2007). Therefore, trial-to-trial variability was typically deemed to have negligible practical significance. However, even elite athletes show a certain amount of variability in movements (Davids et al., 2003), thus, this assumption is not valid. The trial-to-trial movement variability is not negligible, but rather noteworthy. Currently, the ecological perspective has been incorporated into biomechanics and it is accepted that variability has a functional component.

Since the idea of ecological perspective has been incorporated into biomechanics, the methods used in ecological perspective could be applied to biomechanics. However, simply applying the methods would be insufficient. Biomechanics researchers are interested in determining certain elements related to the achievement of a motor task (Lees, 1999); for this, the relation between the outcome of a performance (e.g., ball location, speed, etc. in throwing) and the individual elements (e.g. joint angle, angular velocity, etc.) are often examined (Chow and Mindock, 1999; Hughes and Bartlett, 2002; Chow and Knudson, 2011).

TABLE 1 | Meaning of coordination in each field.

Field	Meaning of coordination
Biomechanics	Relation that act toward meeting functional requirements Winter, 2009
Computational perspective	Relation that reduce the number of degrees of freedom to solve a computational problem on the CNS d'Avella et al., 2003
	Neural organization that ensures task-specific covariation of elements that contribute to the achievement of the motor task Latash et al., 2007
Ecological perspective	Self-organizing relation between elements that reduce degrees of freedom Turvey, 2007
	Relation that is beneficial to the achievement of a motor task Müller and Sternad, 2003

The meaning of coordination and synergy within a field is similar although coordination is sometimes referred to as synergy.

Therefore, in biomechanics, it is valuable to examine which joint movements are coordinated for the achievement of a motor task. This cannot be addressed by simply using the methods employed in the ecological perspective, such as CR analysis. This is because CR analysis only shows the presence or absence of coordination to achieve the motor task and thus, does not provide information regarding which elements are coordinated. Applying methods from other related fields to biomechanics may require improvements of the methods to increase suitability for biomechanics (Kimura et al., 2021).

SOME TOPICS TO BE DISCUSSED

Coordination is a growing interest in the field of biomechanics. This may be due to the idea that coordination is a fundamental concept for understanding what we perceive as the most basic of movements, such as locomotion, as well as complex movements in sports situations. In this study, we reviewed the main aspects of coordination in various fields and tried to clarify what coordination is in biomechanics. In this section, we present some topics to further promote coordination studies in biomechanics.

Analytical Methods and Results Interpretation

Many methods have emerged to quantitatively evaluate coordination. UCM, principal component analysis (PCA) (Borghese et al., 1996; Bianchi et al., 1998; Ivanenko et al., 2007, 2008), CR, and relative phase (RP) analysis (Jeka et al., 1993; Kelso et al., 2001; Mechsner et al., 2001) are commonly used in motor control studies. Some of these methods are used in biomechanics. Worth mentioning is that the interpretation of the results differs depending on the study, even though the same method is used. Some studies interpreted the results obtained from UCM analysis as the CNS controlling variables that affect task achievement ($\perp$UCM) and relatively not controlling variables that do not affect task achievement ($\parallel$ UCM) (Scholz and Schöner, 1999; Scholz et al., 2000; Latash et al., 2002; Tseng et al., 2003; Domkin et al., 2005; Schöner and Scholz, 2007). Scholz and Schöner (1999) concluded that, for the task of sit-to-stand, CNS predominantly controlled the position of the center of mass rather than the hand or head. Whereas, other studies interpreted that the results obtained from the UCM analysis indicated that the variables were related to achieving the motor task (Iino et al., 2017; Möhler et al., 2019; DiCesare et al., 2020). Iino et al. (2017) concluded that, for table tennis, the joint angles are related such that deviations in joint angles are canceled out to stabilize the racket angles at ball impact. The difference between these interpretations is whether the studies intended to understand the control of the CNS. The latter interpretation did not aim to understand the control of the CNS and therefore did not discuss the CNS even though they used UCM analysis. Failure to understand the differences in interpretation of results may lead to misunderstanding within the literature. Therefore, it is necessary to clarify not only the meaning of the concepts but also how to interpret the results.

Links Between Biomechanics and Other Fields

Empirical examinations in biomechanics have focused on the analysis of elements that are related to the performance outcome (Chow and Mindock, 1999; Hughes and Bartlett, 2002; Chow and Knudson, 2011). These examinations enable coaches to know which elements to focus on (Chow and Knudson, 2011). As Glazier indicated, it is not enough for the biomechanical examination to analyze the correlations between performance outcomes and individual elements, but it is also necessary to analyze how the performance outcomes are produced by considering the interrelation between variables (Glazier and Robins, 2012; Glazier, 2017). However, biomechanical research has rarely considered interrelations and tends to describe what happens without explaining how performance outcomes are produced (McGarry, 2009; Glazier and Robins, 2012). These indications imply the importance of considering coordination in biomechanics. Indeed, while coaching focuses on a single part of the body, coaches know that changing the movement of one part affects the movement of other parts of the body. Therefore, to gain insights with practical implications, it is necessary to understand the fundamental relationship between a single focal movement and its relation to other movements.

The approach of focusing on interrelation is the main feature of network science (Newman, 2010). Network science is a field that studies networks of physical and biological phenomena, using methods including graph theory from mathematics and statistical mechanics from physics. In recent years, the theories and methods of network science have been applied not only to physics and biology but also to clinical biomechanics (Murphy et al., 2018). Murphy et al. (2018) viewed the musculoskeletal system as a network structure, composed of bones and the

muscles that link them, and examined the clinical connections between structure and muscle injury. When a certain muscle is injured, other muscles may also be injured *via* compensatory mechanisms of the body (Colné and Thoumie, 2006). The effect of a certain muscle injury on the whole musculoskeletal system depends on how interconnections of the musculoskeletal system are structured. Therefore, it is believed that understanding these interconnections will help us to know which muscles are most at risk of secondary injury due to compensatory changes caused by focal injuries, thereby informing a more comprehensive approach to rehabilitation. In the future, it will be useful to explore the applicability of network science not only to clinical biomechanics but also to biomechanics with the aim of performance enhancement.

CONCLUSION

Even though the term coordination has different meanings, few studies have summarized these meanings as we have. Therefore, it appears that the meaning of coordination has not been accurately understood. The present analysis of this study is not complete because it does not cover all of the literature, but we believe that it has organized the various theoretical standpoints on coordination and contributed to a more accurate understanding of coordination.

By mapping out several ideas regarding coordination, we hope that researchers will be able to make a conscious commitment to theoretical standpoints. Above all, we hope that this study will help researchers formulate their empirical arguments for coordination in a more transparent manner to improve the discussion. An inaccurate understanding of a concept may lead to errors in the interpretation of data and theory development. Finally, this study may help promote coordination studies in biomechanics.

AUTHOR CONTRIBUTIONS

AK was responsible for the conceptualization, investigation, writing—original draft, writing—review and editing, visualization, and funding acquisition. TY and HO were responsible for the visualization, writing—original draft, and writing—review and editing. All authors approved the final version of this manuscript.

FUNDING

AK is supported by a grant from the Tateisi Science and Technology Foundation. The grant number is 2201007.

ACKNOWLEDGMENTS

The authors would like to thank members of the Japan Institute of Sports Sciences for the helpful comments.

REFERENCES

Abbasi, A., Yazdanbakhsh, F., Tazji, M. K., Aghaie Ataabadi, P., Svoboda, Z., Nazarpour, K., et al. (2020). A comparison of coordination and its variability in lower extremity segments during treadmill and overground running at different speeds. *Gait Post.* 79, 139–144. doi: 10.1016/j.gaitpost.2020.04.022

Acasio, J. C., Nussbaum, M. A., and Hendershot, B. D. (2021). Trunk-pelvic coordination during unstable sitting with varying task demand: a methodological study. *J. Biomech.* 118:110299. doi: 10.1016/j.jbiomech.2021.110299

Bartlett, R., Wheat, J., and Robins, M. (2007). Is movement variability important for sports biomechanists? *Sport. Biomech.* 6, 224–243. doi: 10.1080/14763140701322994

Bernstein, N. A. (1967). *The Co-ordination and Regulation of Movements*. Oxford: Pergamon Press.

Bianchi, L., Angelini, D., Orani, G. P., and Lacquaniti, F. (1998). Kinematic coordination in human gait: relation to mechanical energy cost. *J. Neurophysiol.* 79, 2155–2170. doi: 10.1152/jn.1998.79.4.2155

Bizzi, E., Cheung, V. C. K., d'Avella, A., Saltiel, P., and Tresch, M. (2008). Combining modules for movement. *Brain Res. Rev.* 57, 125–133. doi: 10.1016/j.brainresrev.2007.08.004

Borghese, N. A., Bianchi, L., and Lacquaniti, F. (1996). Kinematic determinants of human locomotion. *J. Physiol.* 494, 863–879. doi: 10.1113/jphysiol.1996.sp021539

Bruton, M., and O'dwyer, N. (2018). Synergies in coordination: a comprehensive overview of neural, computational, and behavioral approaches. *J. Neurophysiol.* 120, 2761–2774. doi: 10.1152/jn.00052.2018

Cheung, V. C., Turolla, A., Agostini, M., Silvoni, S., Bennis, C., Kasi, P., et al. (2012). Muscle synergy patterns as physiological markers of motor cortical damage. *Proc. Natl. Acad. Sci. U. S. A.* 109, 14652–14656. doi: 10.1073/pnas.1212056109

Cheung, V. C. K., and Seki, K. (2021). Approaches to revealing the neural basis of muscle synergies: a review and a critique. *J. Neurophysiol.* 125, 1580–1597. doi: 10.1152/jn.00625.2019

Chiovetto, E., Berret, B., Delis, I., Panzeri, S., and Pozzo, T. (2013). Investigating reduction of dimensionality during single-joint elbow movements: a case study on muscle synergies. *Front. Comput. Neurosci.* 7:11. doi: 10.3389/fncom.2013.00011

Chow, J. W., and Knudson, D. V. (2011). Use of deterministic models in sports and exercise biomechanics research. *Sport. Biomech.* 10, 219–233. doi: 10.1080/14763141.2011.592212

Chow, J. W., and Mindock, L. (1999). Discus throwing performances and medical classification of wheelchair athletes. *Med. Sci. Sports Exerc.* 31, 1272–1279. doi: 10.1097/00005768-199909000-00007

Cohen, R. G., and Sternad, D. (2009). Variability in motor learning: relocating, channeling and reducing noise. *Exp. Brain Res.* 193, 69–83. doi: 10.1007/s00221-008-1596-1

Colné, P., and Thoumie, P. (2006). Muscular compensation and lesion of the anterior cruciate ligament: Contribution of the soleus muscle during recovery from a forward fall. *Clin. Biomech.* 21, 849–859. doi: 10.1016/j.clinbiomech.2006.04.002

d'Avella, A., and Bizzi, E. (1998). Low dimensionality of supraspinally induced force fields. *Proc. Natl. Acad. Sci. U. S. A.* 95, 7711–7714. doi: 10.1073/pnas.95.13.7711

d'Avella, A., and Lacquaniti, F. (2013). Control of reaching movements by muscle synergy combinations. *Front. Comput. Neurosci.* 7:42. doi: 10.3389/fncom.2013.00042

d'Avella, A., Saltiel, P., and Bizzi, E. (2003). Combinations of muscle synergies in the construction of a natural motor behavior. *Nat. Neurosci.* 6, 300–308. doi: 10.1038/nn1010

d'Avella, A., Portone, A., Fernandez, L., and Lacquaniti, F. (2006). Control of fast-reaching movements by muscle synergy combinations. *J. Neurosci.* 26, 7791–7810. doi: 10.1523/JNEUROSCI.0830-06.2006

Davids, K., Glazier, P., Araujo, D., and Bartlett, R. (2003). Movement systems as dynamical systems. *Sport. Med.* 33, 245–260. doi: 10.2165/00007256-200333040-00001

DiCesare, C. A., Bonnette, S., Myer, G. D., and Kiefer, A. W. (2020). Differentiating successful and unsuccessful single-leg drop landing performance using uncontrolled manifold analysis. *Motor Control* 24, 75–90. doi: 10.1123/mc.2017-0076

Diedrichsen, J. (2007). Optimal task-dependent changes of bimanual feedback control and adaptation. *Curr. Biol.* 17, 1675–1679. doi: 10.1016/j.cub.2007.08.051

Domkin, D., Laczko, J., Djupsjöbacka, M., Jaric, S., and Latash, M. L. (2005). Joint angle variability in 3D bimanual pointing: uncontrolled manifold analysis. *Exp. Brain Res.* 163, 44–57. doi: 10.1007/s00221-004-2137-1

Domkin, D., Laczko, J., Jaric, S., Johansson, H., and Latash, M. L. (2002). Structure of joint variability in bimanual pointing tasks. *Exp. Brain Res.* 143, 11–23. doi: 10.1007/s00221-001-0944-1

Donath, L., Kurz, E., Roth, R., Zahner, L., and Faude, O. (2015). Different ankle muscle coordination patterns and co-activation during quiet stance between young adults and seniors do not change after a bout of high intensity training. *BMC Geriatr.* 15, 1–8. doi: 10.1186/s12877-015-0017-0

Ferber, R., Davis, I. M., and Williams, D. S. (2005). Effect of foot orthotics on rearfoot and tibia joint coupling patterns and variability. *J. Biomech.* 38, 477–483. doi: 10.1016/j.jbiomech.2004.04.019

Fitts, P. M. (1954). The information capacity of the human motor system in controlling the amplitude of movement. *J. Exp. Psychol.* 47, 381–391. doi: 10.1037/h0055392

Franklin, D. W., and Wolpert, D. M. (2011). Computational mechanisms of sensorimotor control. *Neuron* 72, 425–442. doi: 10.1016/j.neuron.2011.10.006

Gelfand, I. M., and Latash, M. L. (1998). On the problem of adequate language in motor control. *Motor Control* 2, 306–313. doi: 10.1123/mcj.2.4.306

Gera, G., Freitas, S., Latash, M. L., Monahan, K., Schöner, G., and Scholz, J. P. (2010). Motor abundance contributes to resolving multiple kinematic task constraints. *Motor Control* 14, 83–115. doi: 10.1123/mcj.14.1.83

Glazier, P., Wheat, J., Pease, D., and Bartlett, R. (2006). "The interface of biomechanics and motor control: Dynamic systems theory and the functional role of movement variability", in *Movement System Variability*, eds K. Davids, S. Bennett, and K. M. Newell (Champaign, IL: Human Kinetics), 49–72.

Glazier, P. S. (2017). Toward a grand unified theory of sports performance. *Hum. Mov. Sci.* 56, 139–156. doi: 10.1016/j.humov.2015.08.001

Glazier, P. S., and Robins, M. T. (2012). Comment on "Use of deterministic models in sports and exercise biomechanics research" by Chow and Knudson (2011). *Sport. Biomech.* 11, 120–122. doi: 10.1080/14763141.2011.650189

Haken, H. (2006). *Information and Self-organization: A Macroscopic Approach to Complex Systems*. Berlin: Springer.

Haken, H., Kelso, J. S., and Bunz, H. (1985). A theoretical model of phase transitions in human hand movements. *Biol. Cybern.* 51, 347–356. doi: 10.1007/BF00336922

Hamill, J., Van Emmerik, R. E., Heiderscheit, B. C., and Li, L. (1999). A dynamical systems approach to lower extremity running injuries. *Clin. Biomech.* 14, 297–308. doi: 10.1016/S0268-0033(98)90092-4

Harris, C. M., and Wolpert, D. M. (1998). Signal-dependent noise determines motor planning. *Nature* 394, 780–784. doi: 10.1038/29528

Hart, C. B., and Giszter, S. F. (2004). Modular premotor drives and unit bursts as primitives for frog motor behaviors. *J. Neurosci.* 24, 5269–5282. doi: 10.1523/JNEUROSCI.5626-03.2004

Hart, C. B., and Giszter, S. F. (2010). A neural basis for motor primitives in the spinal cord. *J. Neurosci.* 30, 1322–1326. doi: 10.1523/JNEUROSCI.5894-08.2010

Heiderscheit, B. C., Hamill, J., and Van Emmerik, R. E. (2002). Variability of stride characteristics and joint coordination among individuals with unilateral patellofemoral pain. *J. Appl. Biomech.* 18, 110–121. doi: 10.1123/jab.18.2.110

Hof, A. L., Gazendam, M. G. J., and Sinke, W. E. (2005). The condition for dynamic stability. *J. Biomech.* 38, 1–8. doi: 10.1016/j.jbiomech.2004.03.025

Hughes, M. D., and Bartlett, R. M. (2002). The use of performance indicators in performance analysis. *J. Sports Sci.* 20, 739–754. doi: 10.1080/026404102320675602

Iino, Y., Yoshioka, S., and Fukashiro, S. (2017). Uncontrolled manifold analysis of joint angle variability during table tennis forehand. *Hum. Mov. Sci.* 56, 98–108. doi: 10.1016/j.humov.2017.10.021

Ivanenko, Y. P., Cappellini, G., Dominici, N., Poppele, R. E., and Lacquaniti, F. (2007). Modular control of limb movements during human locomotion. *J. Neurosci.* 27, 11149–11161. doi: 10.1523/JNEUROSCI.2644-07.2007

Ivanenko, Y. P., d'Avella, A., Poppele, R. E., and Lacquaniti, F. (2008). On the origin of planar covariation of elevation angles during human locomotion. *J. Neurophysiol.* 99, 1890–1898. doi: 10.1152/jn.01308.2007

Ivanenko, Y. P., Poppele, R. E., and Lacquaniti, F. (2004). Five basic muscle activation patterns account for muscle activity during human locomotion. *J. Physiol.* 556, 267–282. doi: 10.1113/jphysiol.2003.057174

Jeka, J. J., Kelso, J. S., and Kiemel, T. (1993). Pattern switching in human multilimb coordination dynamics. *Bull. Math. Biol.* 55, 829–845. doi: 10.1016/S0092-8240(05)80191-0

Kay, B. A. (1988). The dimensionality of movement trajectories and the degrees of freedom problem: a tutorial. *Hum. Mov. Sci.* 7, 343–364. doi: 10.1016/0167-9457(88)90016-4

Kelso, J. S. (1984). Phase transitions and critical behavior in human bimanual coordination. *Am. J. Physiol.* 246, R1000–R1004. doi: 10.1152/ajpregu.1984.246.6.R1000

Kelso, J. S., Fink, P. W., DeLaplain, C. R., and Carson, R. G. (2001). Haptic information stabilizes and destabilizes coordination dynamics. *Proc. R. Soc. B Biol. Sci.* 268, 1207–1213. doi: 10.1098/rspb.2001.1620

Kelso, J. S., Holt, K. G., Rubin, P., and Kugler, P. N. (1981). Patterns of human interlimb coordination emerge from the properties of non-linear, limit cycle oscillatory processes: theory and data. *J. Mot. Behav.* 13, 226–261. doi: 10.1080/00222895.1981.10735251

Kimura, A., Omura, L., Yoshioka, S., and Fukashiro, S. (2021). Identifying coordination between joint movements during a throwing task with multiple degrees of freedom. *Hum. Mov. Sci. In press.* doi: 10.1016/j.humov.2021.102799

Krishnamoorthy, V., Latash, M. L., Scholz, J. P., and Zatsiorsky, V. M. (2003). Muscle synergies during shifts of the center of pressure by standing persons. *Exp. Brain Res.* 152, 281–292. doi: 10.1007/s00221-003-1574-6

Kudo, K., Tsutsui, S., Ishikura, T., Ito, T., and Yamamoto, Y. (2000). Compensatory coordination of release parameters in a throwing task. *J. Mot. Behav.* 32, 337–345. doi: 10.1080/00222890009601384

Kugler, P. N., Kelso, J. S., and Turvey, M. T. (1980). 1 on the concept of coordinative structures as dissipative structures: I. theoretical lines of convergence. *Adv. Psychol.* 1, 3–47. doi: 10.1016/S0166-4115(08)61936-6

Kuo, A. D. (1995). An optimal control model for analyzing human postural balance. *IEEE Trans. Biomed. Eng.* 42, 87–101. doi: 10.1109/10.362914

Kuppuswamy, N., and Harris, C. M. (2014). Do muscle synergies reduce the dimensionality of behavior?. *Front. Comput. Neurosci.* 8:63. doi: 10.3389/fncom.2014.00063

Larivière, C., and Arsenault, A. B. (2008). On the use of EMG-ratios to assess the coordination of back muscles. *Clin. Biomech.* 23, 1209–1219. doi: 10.1016/j.clinbiomech.2008.09.001

Latash, M. L. (2012). The bliss (not the problem) of motor abundance (not redundancy). *Exp. Brain Res.* 217, 1–5. doi: 10.1007/s00221-012-3000-4

Latash, M. L. (2018). Abundant degrees of freedom are not a problem. *Kinesiol. Rev.* 7, 64–72. doi: 10.1123/kr.2017-0058

Latash, M. L., Scholz, J. F., Danion, F., and Schöner, G. (2001). Structure of motor variability in marginally redundant multifinger force production tasks. *Exp. Brain Res.* 141, 153–165. doi: 10.1007/s002210100861

Latash, M. L., Scholz, J. P., and Schöner, G. (2002). Motor control strategies revealed in the structure of motor variability. *Exerc. Sport Sci. Rev.* 30, 26–31. doi: 10.1097/00003677-200201000-00006

Latash, M. L., Scholz, J. P., and Schöner, G. (2007). Toward a new theory of motor synergies. *Motor Control* 11, 276–308. doi: 10.1123/mcj.11.3.276

Latash, M. L., and Zatsiorsky, V. (2015). *Biomechanics and Motor Control: Defining Central Concepts*. New York, NY: Academic Press.

Lees, A. (1999). Biomechanical assessment of individual sports for improved performance. *Sport. Med.* 28, 299–305. doi: 10.2165/00007256-199928050-00001

Liu, D., and Todorov, E. (2007). Evidence for the flexible sensorimotor strategies predicted by optimal feedback control. *J. Neurosci.* 27, 9354–9368. doi: 10.1523/JNEUROSCI.1110-06.2007

McGarry, T. (2009). Applied and theoretical perspectives of performance analysis in sport: scientific issues and challenges. *Int. J. Perform. Anal. Sport* 9, 128–140. doi: 10.1080/24748668.2009.11868469

Mechsner, F., Kerzel, D., Knoblich, G., and Prinz, W. (2001). Perceptual basis of bimanual coordination. *Nature* 414, 69–73. doi: 10.1038/35102060

Möhler, F., Marahrens, S., Ringhof, S., Mikut, R., and Stein, T. (2020). Variability of running coordination in experts and novices: a 3D uncontrolled manifold analysis. *Eur. J. Sport Sci.* 20, 1187–1196. doi: 10.1080/17461391.2019.1709561

Möhler, F., Ringhof, S., Debertin, D., and Stein, T. (2019). Influence of fatigue on running coordination: a UCM analysis with a geometric 2D model and a subject-specific anthropometric 3D model. *Hum. Mov. Sci.* 66, 133–141. doi: 10.1016/j.humov.2019.03.016

Müller, H., and Sternad, D. (2003). A randomization method for the calculation of covariation in multiple nonlinear relations: illustrated with the example of goal-directed movements. *Biol. Cybern.* 89, 22–33. doi: 10.1007/s00422-003-0399-5

Müller, H., and Sternad, D. (2004). Decomposition of variability in the execution of goal-oriented tasks: three components of skill Improvement. *J. Exp. Psychol. Hum. Percept. Perform.* 30, 212–233. doi: 10.1037/0096-1523.30.1.212

Müller, H., and Sternad, D. (2009). "Motor learning: changes in the structure of variability in a redun-dant task", in *Progress in Motor Control—A Multidisciplinary Perspective*, ed D.Sternad (New York, NY: Springer), 439–456.

Murphy, A. C., Muldoon, S. F., Baker, D., Lastowka, A., Bennett, B., Yang, M., et al. (2018). Structure, function, and control of the human musculoskeletal network. *PLoS Biol.* 16:1,e2002811. doi: 10.1371/journal.pbio.2002811

Newman, M. E. J. (2010). *Networks: An Introduction. Oxford: Oxford University Press*. doi: 10.1093/acprof:oso/9780199206650.001.0001

Overduin, S. A., d'Avella, A., Carmena, J. M., and Bizzi, E. (2012). Microstimulation activates a handful of muscle synergies. *Neuron* 76, 1071–1077. doi: 10.1016/j.neuron.2012.10.018

Preatoni, E., Hamill, J., Harrison, A. J., Hayes, K., van Emmerik, R. E. A., Wilson, C., et al. (2013). Movement variability and skills monitoring in sports. *Sport. Biomech.* 12, 69–92. doi: 10.1080/14763141.2012.738700

Prilutsky, B. I., and Gregor, R. J. (2000). Analysis of muscle coordination strategies in cycling. *IEEE Trans. Rehabil. Eng.* 8, 362–370. doi: 10.1109/86.867878

Profeta, V. L., and Turvey, M. T. (2018). Bernstein's levels of movement construction: a contemporary perspective. *Hum. Mov. Sci.* 57, 111–133. doi: 10.1016/j.humov.2017.11.013

Raasch, C. C., and Zajac, F. E. (1999). Locomotor strategy for pedaling: muscle groups and biomechanical functions. *J. Neurophysiol.* 82, 515–525. doi: 10.1152/jn.1999.82.2.515

Robertson, D. G. E., Caldwell, G. E., Hamill, J., Kamen, G., and Whittlesey, S. (2013). *Research Methods in Biomechanics*. Champaign: Human Kinetics.

Saltiel, P., Wyler-Duda, K., d'Avella, A., Tresch, M. C., and Bizzi, E. (2001). Muscle synergies encoded within the spinal cord: Evidence from focal intraspinal NMDA iontophoresis in the frog. *J. Neurophysiol.* 85, 605–619. doi: 10.1152/jn.2001.85.2.605

Schmidt, R. A., Zelaznik, H., Hawkins, B., Frank, J. S., and Quinn Jr, J. T. (1979). Motor-output variability: a theory for the accuracy of rapid motor acts. *Psychol. Rev.* 86, 415–451. doi: 10.1037/0033-295X.86.5.415

Scholz, J. P., and Schöner, G. (1999). The uncontrolled manifold concept: Identifying control variables for a functional task. *Exp. Brain Res.* 126, 289–306. doi: 10.1007/s002210050738

Scholz, J. P., Schöner, G., and Latash, M. L. (2000). Identifying the control structure of multijoint coordination during pistol shooting. *Exp. Brain Res.* 135, 382–404. doi: 10.1007/s002210000540

Schöner, G., and Scholz, J. P. (2007). Analyzing variance in multi-degree-of-freedom movements: uncovering structure versus extracting correlations. *Motor Control* 11, 259–275. doi: 10.1123/mcj.11.3.259

Shumway-Cook, A., and Horak, F. B. (1986). Assessing the influence of sensory interaction on balance. *Suggestion from the field. Phys. Ther.* 66, 1548–1550. doi: 10.1093/ptj/66.10.1548

So, R. C., Ng, J. K. F., and Ng, G. Y. (2005). Muscle recruitment pattern in cycling: A Review. *Phys. Ther. Sport* 6, 89–96. doi: 10.1016/j.ptsp.2005.02.004

Stergiou, N., and Decker, L. M. (2011). Human movement variability, nonlinear dynamics, and pathology: is there a connection? *Hum. Mov. Sci.* 30, 869–888. doi: 10.1016/j.humov.2011.06.002

Sternad, D. (2018). It's not (only) the mean that matters: variability, noise and exploration in skill learning. *Curr. Opin. Behav. Sci.* 20, 183–195. doi: 10.1016/j.cobeha.2018.01.004

Takei, T., Confais, J., Tomatsu, S., Oya, T., and Seki, K. (2017). Neural basis for hand muscle synergies in the primate spinal cord. *Proc. Natl. Acad. Sci. U. S. A.* 114, 8643–8648. doi: 10.1073/pnas.1704328114

Tepavac, D., and Field-Fote, E. C. (2001). Vector coding: A technique for quantification of intersegmental coupling in multicyclic behaviors. *J. Appl. Biomech.* 17, 259–270. doi: 10.1123/jab.17.3.259

Ting, L. H., and Macpherson, J. M. (2005). A limited set of muscle synergies for force control during a postural task. *J. Neurophysiol.* 93, 609–613. doi: 10.1152/jn.00681.2004

Todorov, E. (2004). Optimality principles in sensorimotor control. *Nat. Neurosci.* 7, 907–915. doi: 10.1038/nn1309

Todorov, E., and Jordan, M. I. (2002). Optimal feedback control as a theory of motor coordination. *Nat. Neurosci.* 5, 1226–1235. doi: 10.1038/nn963

Tokuda, K., Anan, M., Takahashi, M., Sawada, T., Tanimoto, K., Kito, N., et al. (2018). Biomechanical mechanism of lateral trunk lean gait for knee osteoarthritis patients. *J. Biomech.* 66, 10–17. doi: 10.1016/j.jbiomech.2017.10.016

Tresch, M. C., Cheung, V. C., and d'Avella, A. (2006). Matrix factorization algorithms for the identification of muscle synergies: evaluation on simulated and experimental data sets. *J. Neurophysiol.* 95, 2199–2212. doi: 10.1152/jn.00222.2005

Tresch, M. C., and Jarc, A. (2009). The case for and against muscle synergies. *Curr. Opin. Neurobiol.* 19, 601–607. doi: 10.1016/j.conb.2009.09.002

Tresch, M. C., Saltiel, P., and Bizzi, E. (1999). The construction of movement by the spinal cord. *Nat. Neurosci.* 2, 162–167. doi: 10.1038/5721

Tseng, Y. W., Scholz, J. P., Schöner, G., and Hotchkiss, L. (2003). Effect of accuracy constraint on joint coordination during pointing movements. *Exp. Brain Res.* 149, 276–288. doi: 10.1007/s00221-002-1357-5

Turvey, M. T. (1990). Coordination. *Am. Psychol.* 45, 938–953. doi: 10.1037/0003-066X.45.8.938

Turvey, M. T. (2007). Action and perception at the level of synergies. *Hum. Mov. Sci.* 26, 657–697. doi: 10.1016/j.humov.2007.04.002

Tytell, E. D., Holmes, P., and Cohen, A. H. (2011). Spikes alone do not behavior make: why neuroscience needs biomechanics. *Curr. Opin. Neurobiol.* 21, 816–822. doi: 10.1016/j.conb.2011.05.017

Van Beers, R. J., Baraduc, P., and Wolpert, D. M. (2002). Role of uncertainty in sensorimotor control. *Philos. Trans. R. Soc. B Biol. Sci.* 357, 1137–1145. doi: 10.1098/rstb.2002.1101

Van Emmerik, R. E., Rosenstein, M. T., Mcdermott, W. J., and Hamill, J. (2004). A nonlinear dynamics approach to human movement. *J. Appl. Biomech.* 20, 396–420. doi: 10.1123/jab.20.4.396

Vereijken, B., Emmerik, R. E., Whiting, H. T. A., and Newell, K. M. (1992). Free (z) ing degrees of freedom in skill acquisition. *J. Mot. Behav.* 24, 133–142. doi: 10.1080/00222895.1992.9941608

Verhoeven, F. M., and Newell, K. M. (2016). Coordination and control of posture and ball release in basketball free-throw shooting. *Hum. Mov. Sci.* 49, 216–224. doi: 10.1016/j.humov.2016.07.007

Verrel, J., Lövdén, M., and Lindenberger, U. (2010). Motor-equivalent covariation stabilizes step parameters and center of mass position during treadmill walking. *Exp. Brain Res.* 207, 13–26. doi: 10.1007/s00221-010-2424-y

Verrel, J., Lövdén, M., and Lindenberger, U. (2012a). Older adults show preserved equilibrium but impaired step length control in motor-equivalent stabilization of gait. *PLoS ONE* 7:e52024. doi: 10.1371/journal.pone.0052024

Verrel, J., Pradon, D., and Vuillerme, N. (2012b). Persistence of motor-equivalent postural fluctuations during bipedal quiet standing. *PLoS ONE* 7:e4831. doi: 10.1371/journal.pone.0048312

Wheat, J. S., and Glazier, P. S. (2006). "Measuring coordination and variability in coordination", in *Movement System Variability*, eds K. Davids, S. Bennett, and K. M. Newell (Champaign, IL: Human Kinetics), 167–181. doi: 10.5040/9781492596851.ch-009

Wilson, C., Simpson, S., Van Emmerik, R., and Hamill, J. (2008). Coordination variability and skill development in expert triple jumpers. *Sport. Biomech.* 7, 2–9. doi: 10.1080/14763140701682983

Winter, D. A. (2009). *Biomechanics and Motor Control of Human Movement*. New Tork: John Wiley and Sons.

Winter, D. A., Prince, F., Frank, J. S., Powell, C., and Zabjek, K. F. (1996). Unified theory regarding A/P and M/L balance in quiet stance. *J. Neurophysiol.* 75, 2334–2343. doi: 10.1152/jn.1996.75.6.2334

Yakovenko, S., Krouchev, N., and Drew, T. (2011). Sequential activation of motor cortical neurons contributes to intralimb coordination during reaching in the cat by modulating muscle synergies. *J. Neurophysiol.* 105, 388–409. doi: 10.1152/jn.00469.2010

Yang, J. F., and Scholz, J. P. (2005). Learning a throwing task is associated with differential changes in the use of motor abundance. *Exp. Brain Res.* 163, 137–158. doi: 10.1007/s00221-004-2149-x

Yaron, A., Kowalski, D., Yaguchi, H., and Seki, K. (2020). Forelimb force direction and magnitude independently controlled by spinal modules in the macaque. *Proc. Natl. Acad. Sci. U. S. A.* 117, 27655–27666. doi: 10.1073/pnas.1919253117

Zajac, F. E., Neptune, R. R., and Kautz, S. A. (2002). Biomechanics and muscle coordination of human walking: Part I: introduction to concepts, power transfer, dynamics and simulations. *Gait Posture* 16, 215–232. doi: 10.1016/S0966-6362(02)00068-1

Zatsiorsky, V. M., and Prilutsky, B. I. (2012). *Biomechanics of Skeletal Muscles*. Urbana: Human Kinetics.

Conflict of Interest: The authors declare that the research was conducted in the absence of any commercial or financial relationships that could be construed as a potential conflict of interest.

Advantages of publishing in Frontiers

OPEN ACCESS
Articles are free to read for greatest visibility and readership

FAST PUBLICATION
Around 90 days from submission to decision

HIGH QUALITY PEER-REVIEW
Rigorous, collaborative, and constructive peer-review

TRANSPARENT PEER-REVIEW
Editors and reviewers acknowledged by name on published articles

Frontiers
Avenue du Tribunal-Fédéral 34
1005 Lausanne | Switzerland

Visit us: www.frontiersin.org
Contact us: frontiersin.org/about/contact

REPRODUCIBILITY OF RESEARCH
Support open data and methods to enhance research reproducibility

DIGITAL PUBLISHING
Articles designed for optimal readership across devices

FOLLOW US
@frontiersin

IMPACT METRICS
Advanced article metrics track visibility across digital media

EXTENSIVE PROMOTION
Marketing and promotion of impactful research

LOOP RESEARCH NETWORK
Our network increases your article's readership